TURBINES COMPRESSORS AND FANS

SECOND EDITION

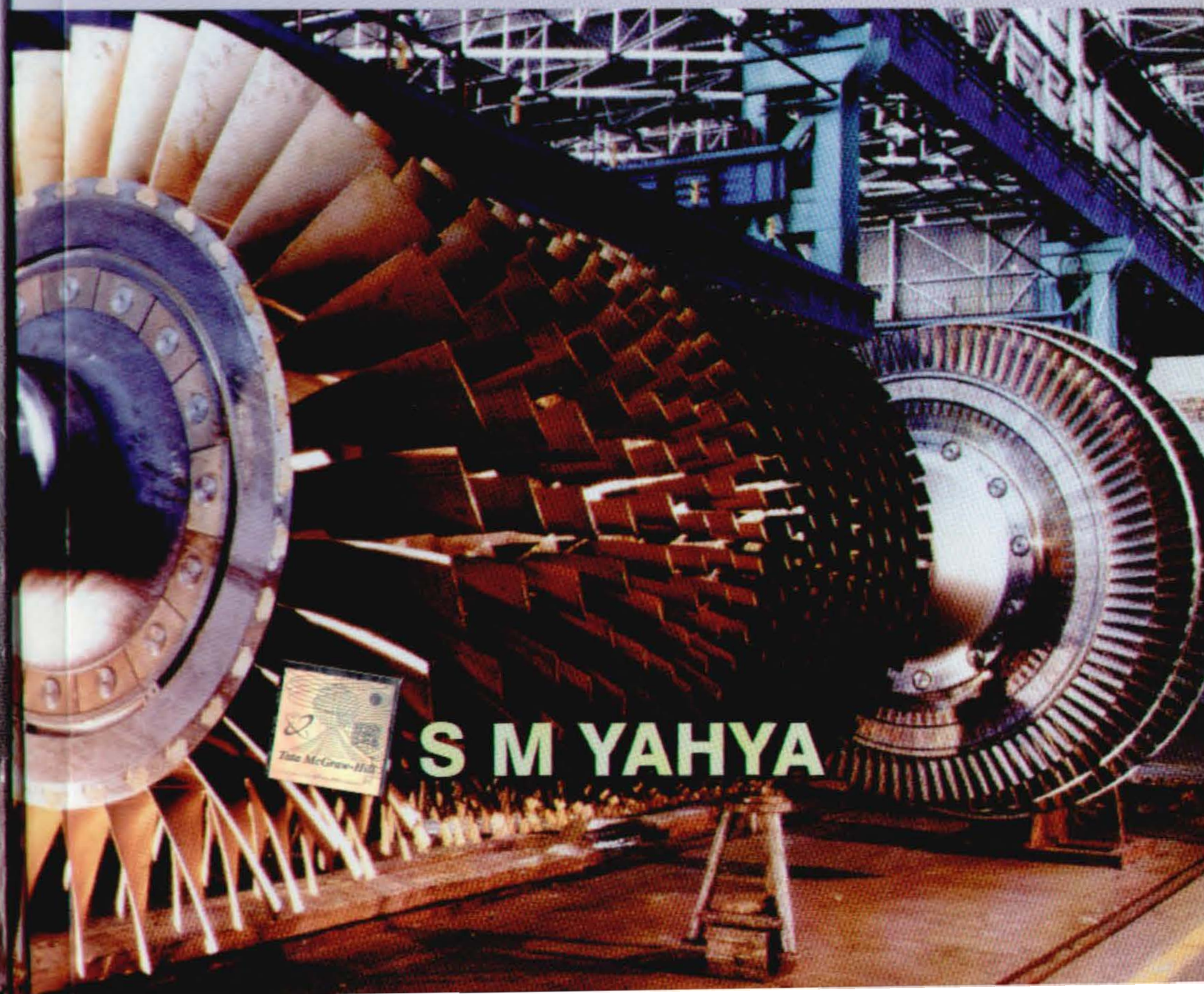

S M YAHYA

TATA McGRAW HILL

TURBINES COMPRESSORS AND FANS

SECOND EDITION

YAHYA

TURBINES
COMPRESSORS AND FANS

SECOND EDITION

TURBINES COMPRESSORS AND FANS

SECOND EDITION

S M YAHYA
Emeritus Fellow
Indian Institute of Technology
New Delhi

Tata McGraw-Hill Publishing Company Limited
NEW DELHI

McGraw-Hill Offices

New Delhi New York St Louis San Francisco Auckland Bogotá Caracas
Kuala Lumpur Lisbon London Madrid Mexico City Milan Montreal
San Juan Santiago Singapore Sydney Tokyo Toronto

Tata McGraw-Hill

*A Division of The **McGraw-Hill** Companies*

Third reprint 2003
RZLQCRMDRQBDZ

Cover Photographs: Courtesy NTPC and BHEL

ISBN 0-07-042039-4

Published by Tata McGraw-Hill Publishing Company Limited,
7 West Patel Nagar, New Delhi 110 008, typeset in Times at Tej Composers,
WZ-391, Madipur New Delhi 110 063, and printed at
Rashtriya Printers M-135, Panchsheel Garden,
Naveen Shahdara, Delhi 110 032

Foreword to the First Edition

It is gratifying to note that in this book unified treatment and dimensional analysis have been duly emphasized in the initial chapters of the book, although its title projects specific types of turbomachinery. Such a unified treatment generally broadens the horizon and facilitates horizontal transfer of knowledge and experience. Another significant aspect is the use of SI units throughout the book. This should form a pace-setter for having all other technical books with SI units.

After covering the essential aero-thermodynamic principles of turbomachinery, the author deals separately with a chapter on cascades which have formed the basis for the optimum selection of aerodynamic geometry of blades. This is a very welcome feature of the book. A subject of topical interest dealing with "High Temperature Turbines" has been covered by devoting to it a full chapter.

Although classical turbomachines continue to play a major role in the energy sector, a class of machines called wind turbines are gaining importance due to the renewable nature of wind energy. It is but appropriate that the book closes with a chapter on wind energy and turbines giving it a measure of completeness commensurate with the title.

The value of the book is enhanced by the numerous illustrations and a balanced emphasis on various topics covered in the book. Principal technical data of modern aviation gas turbines such as that for the supersonic aircraft Concorde and RB-199, specifications of the turbine and compressor blade profiles and some wind turbines form other distinguishing features of the work. This book will be a valuable addition to the existing books in turbomachinery which are primarily directed towards the course work of students. Moreover, the book introduces the reader to the current research areas in turbomachinery. The author's extensive experience in teaching and research has been truly reflected in this book. A detailed topic-wise bibliography containing over 800 references will be a valuable source of information for the researchers.

This book would be equally helpful to practising engineers who desire to initiate themselves professionally in the field of turbomachinery.

Pramod A Paranjpe
Head, Propulsion Division
National Aeronautical Laboratory
Bangalore, India

Preface to the Second Edition

The first edition of this book has been serving students and practising engineers since 1983. Last few decades have seen striking developments in turbine power plants employing combined cycle and solar energy. Therefore, to put the role of turbomachines in the present perspective two new chapters on Combined Cycle Plants (Chap. 5) and Solar Turbine Plants (Chap. 17) have been added.

The basic aim of the book remains the same of dealing with the individual turbomachine and its role in the power plant. In view of this, topics such as optimization of the combined cycle and optics in the solar turbine power plants have not been included.

The errors occurring in the earlier edition have been weeded out. Several solved and unsolved examples and questions have been added to enrich the content. Some sections in the chapters have been modified. Additional references have also been included to enhance the Bibliography.

It is hoped that the new edition will have enlarged audience from the academic institutions, the industry and R&D organizations.

Attention to errors and suggestions for improvement will be gratefully acknowledged.

S M YAHYA

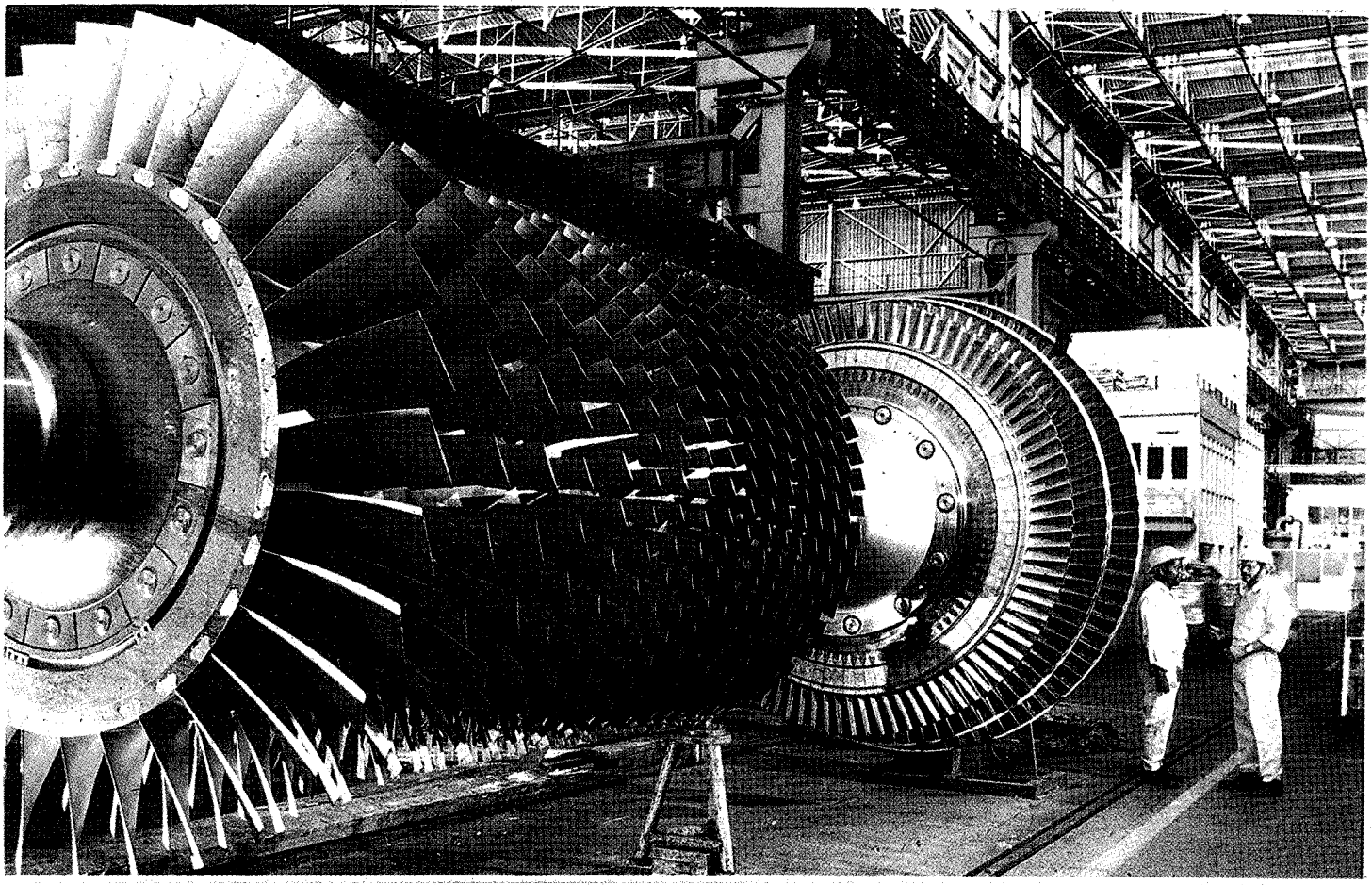

Compressor and gas turbine rotors under assembly at BHEL-Hyderabad, India *(Courtesy:* BHEL, India)

Preface to the First Edition

Recent emphasis on energy problems has generated renewed interest in turbines, compressors and fans. Steam and gas turbines develop the bulk of power required for land and air applications. Similarly, fans, blowers and compressors are some of the major power-absorbing machines in industry. The wind turbine or windmill has reappeared on the power-generation scene. Therefore, at this time a book wholly in SI units dealing with this class of machines is badly needed by students, teachers and practising engineers.

The basic principle of working of these machines is the same—the energy level of a continuously flowing fluid is changed by the action of a rotating element, the rotor. The theoretical treatment of such machines requires the knowledge of both fluid dynamics and thermodynamics: therefore, some fundamental problems in thermodynamics and fluid dynamics common to these machines have been covered in separate chapters in the beginning. They provide the important link between the engineering sciences and an important class of machines (turbomachines) used in a variety of industrial, power generation and aircraft propulsion fields.

The overall performance and the importance of a given machine is better appreciated when its role in relation to other components in the plant is understood. Therefore, chapters on gas and steam turbine plants which employ these machines have also been included and placed in the earlier part of the book.

A short chapter on dimensional analysis prepares the reader to proceed to the analysis of particular types of machines. In this the various quantities that affect the design and performance of turbomachines are identified and discussed. A brief discussion on various dimensionless parameters is also given.

Chapters 1 to 6 deal with the various kinds of turbines, compressors and fans in a general way. The later chapters deal with the aero-thermodynamic aspects of particular kinds of thermal turbomachines in greater depth. Therefore, theoretical details and physical explanation of individual

machines are given in separate chapters on turbines, compressors and fans which constitute the main body of this volume. Velocity triangles and enthalpy-entropy diagrams have been frequently used in these chapters to explain the various kinematic and thermodynamic aspects of these machines.

Chapter 7 on cascades acquaints the reader with the geometries of blades and blade rows in different types of turbomachine stages. This also focuses attention on the practical aspects of turbomachines. Various types of wind tunnels employed for cascade testing are described here.

Chapter 8 deals with the conventional axial-flow turbine stages. Some unconventional turbines used in aerospace applications like partial admission and cooled turbines are also covered in Chapters 8 and 9 respectively.

The treatment of axial compressor stages in Chapter 10 is on the same lines as discussed in the earlier chapters for axial turbine stages.

Both centrifugal compressors and radial turbines form a separate group of turbomachines employing a different technology. These machines have been discussed in Chapter 11 and 12. Here the tangential direction is taken as the reference direction in velocity triangles for the stages. This is in marked contrast to the treatment for axial stages where the axial direction has been taken as the reference direction.

Fans and blowers on account of their low pressures (expressed in millimetres of water gauge instead of bar) are also a separate class of turbomachines. Therefore, instead of combining them with the compressor stages they are separately discussed in Chapters 13 and 14.

Chapter 15 deals briefly with the salient features of wind turbines. Some general aspects of wind energy have also been included here.

Only SI units have been used in this book. Generally bar and millibar have been used as units for pressure; their relationship to N/m^2, kN/m^2 and MN/m^2 is given in an appendix.

Useful references for further reading are given in the Select Bibliography at the end of the book.

The material covered in this volume will be useful in the study of subjects on steam and gas turbines, aircraft propulsion, thermal power plants, thermal turbomachines, fluid machinery and energy studies. Therefore, besides students and teachers, design engineers in the areas of power plants, aerospace, supercharged IC engines, industrial fans, blowers and compressors should also find this book useful.

S M YAHYA

Acknowledgements

It is gratefully acknowledged that the material throughout the book is based on the ideas and concepts already developed over the years by numerous authors and researchers, some of whose publications are reported at the end of the book. Formal reference of many laws and theories that are now of a classical nature has not been given. I regret if any acknowledgement that is due has been missed out or found inadequate. The needful will be done if attention to this is drawn.

I am grateful to The Roll-Royce Ltd, Turbounion Ltd, United Technologies, Pratt and Whitney Aircraft Company, National Thermal Power Corporation and Bharat Heavy Electricals Ltd., for supplying useful information material for inclusion in this book. Institution of Mechanical Engineers, American Society of Mechanical Engineers and the Pergamon Press gave permission for using some material from their publications which is gratefully acknowledged.

I am indebted to the Indian Institute of Technology, Delhi for the financial assistance towards some expenditures incurred in the preparation of the first edition.

Thanks are also due to the staff of the Tata McGraw-Hill Publishing Company for their great help and expertise in publishing this book.

Finally, I am grateful to my wife, Shakila, and children, Nasreen, Asma, Yasmeen and Tariq, who, unmindful of my neglect of them because of this book, gave me moral support and comforting moments.

S M YAHYA

Contents

Chapter 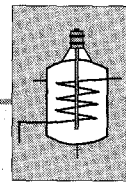 1

Introduction

Turbines and compressors are now being used in electric power generation, aircraft propulsion and a wide variety of medium and heavy industries. Small and heavy-duty fans and blowers cover a wide range of industrial applications. Axial fans (propellers) are used for propelling small low-speed aircraft, while large jet airliners employ axial-ducted fans in their comparatively new turbo-fan concept.

Though the steam turbine was perfected much earlier than the gas turbine engine, the last four decades have seen almost parallel developments in aeroengines and steam turbine power plants. As a result today on the one hand we have the jumbo jets and their high thrust engines in the aeronautical field, while on the other there are giant steam turbine plants operating in the "superthermal power stations". These developments suggest that the 2000 MW steam turbine plants will be operating in many countries in the 21st century; along with this the "super jumbo jet" airliners will also be flying between the major cities of the world.

1.1 Turbomachines

Turbines, compressors and fans are all members of the same family of machines called turbomachines. A turbomachine[1,2,5,11] is a power or head generating machine which employs the dynamic action of a rotating element, the rotor; the action of the rotor changes the energy level of the continuously flowing fluid through the turbomachine. Before discussing other aspects of turbomachines, they are compared here with the positive displacement machines. This will help in understanding the special features of turbines, compressors and fans.

Positive displacement machines (both engines and compressors as shown in Figs. 1.1 to 1.4), especially of the reciprocating type are inherently low speed machines on account of mechanical and volumetric efficiency considerations. In contrast to this the majority of turbomachines run at comparatively higher speeds without any mechanical problems. The volumetric efficiency of turbomachines is close to hundred per cent.

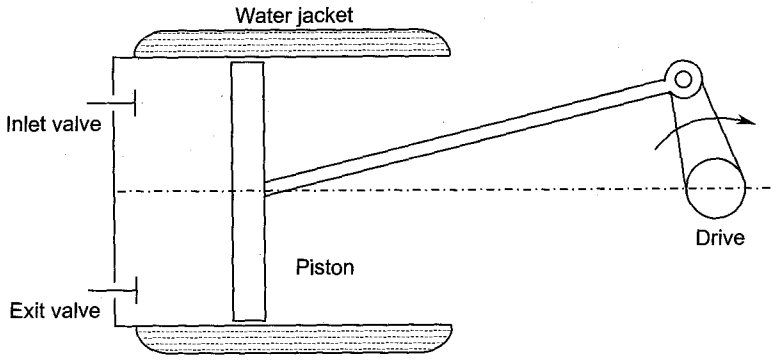

Fig. 1.1 Reciprocating compressor

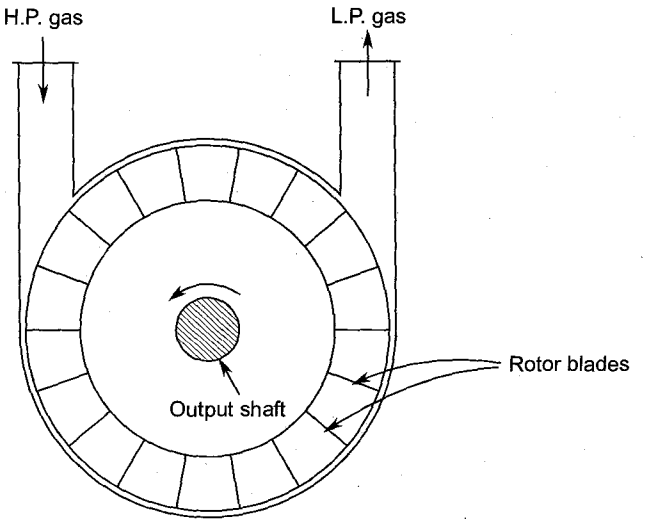

Fig. 1.2 Drag turbine (positive displacement machine)

If a reciprocating engine is stopped, the working gas trapped inside the cylinder stays there in the same state in which it was at the time of stoppage of the engine piston. This is possible if the cylinder is perfectly insulated from the surroundings and there is no leakage.

Now consider the state of the gas in a turbine whose motion is stopped. The gas will experience changes in its state dictated by the surroundings. This is an important feature which distinguishes turbomachines from positive displacement machines.

On account of much lower speeds, a reciprocating compressor can theoretically be made to work isothermally. Cylinder jacket cooling and intercooling with multi-stage compression help in achieving isothermal compression. On the other hand, the high speed turbocompressor is an adiabatic machine; the same is true for other turbomachines.

A reciprocating or positive displacement machine, due to its low speed and limited displacement can only handle smaller flow rates of fluids through it. While on account of much higher rotor and fluid velocities the flow rates in turbomachines are much larger compared to positive displacement machines.

Figure 1.3 shows a rotary positive displacement compressor (two-lobe Roots blower). Two symmetrical lobes rotate in opposite directions in a casing composed of two semi-circular ends separated by a parallel section. The lobe profiles are designed to give conjugate motion of the two rotors/lobes. The two lobes do not drive one another like toothed wheels. A small clearance between the lobe surfaces provides a contactless conjugate motion. Therefore, the rotors are driven by the timing gears located outside the casing.

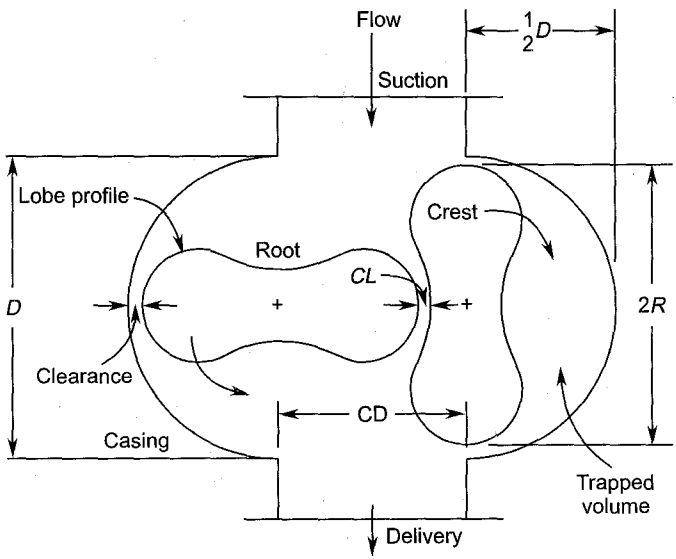

Fig. 1.3 Two-lobe compressor/Roots blower

Rotation of the lobes provides the suction, compression and discharge processes at both the ends of the casing. Note that the compression process is not a continuous adiabatic process.

Such a positive displacement machine is a cross between the reciprocating machine and a turbo compressor. Therefore, it combines the advantages of both the reciprocating device and a turbomachine.

Another positive rotary displacement device (rotary piston engine) is shown in Fig. 1.4. This is the well known Wankel engine which combines the advantages of the reciprocating internal combustion engine and the gas turbine. In this device a rotor resembling an equilateral

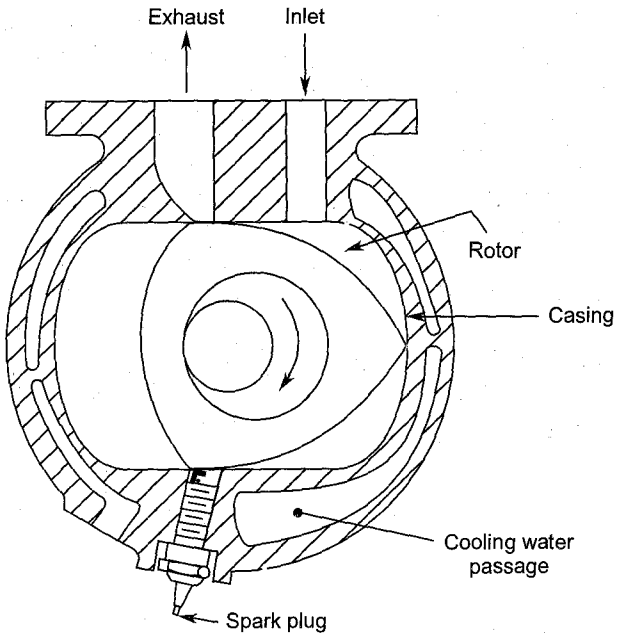

Fig. 1.4 Rotary piston Wankel engine

triangle rotates inside an epitrochoidal casing; the geometry of the triangular rotor is such that its apexes are always in contact with the inner surface of the casing during rotation. The volume of the fluid (air-fuel mixture or the products of combustion) between a face of the rotor and the casing varies during one revolution of the rotor and the processes of suction, compression, expansion and exhaust are executed as in the conventional reciprocating engine.

1.2 Turbines

The power generating turbomachines decrease the head or energy level of the working fluids passing through them. These machines are called turbines, e.g. steam, gas, hydro, wind and solar turbines. They are coupled to power absorbing machines, such as electric generators, pumps, compressors, etc.

1.3 Pumps and Compressors

The head or pressure producing machines increase the energy level (pressure or head) of the fluids passing through them. These machines are known as pumps, compressors (or turbocompressors), fans, blowers and propellers. They are driven by prime movers such as turbines and

electric motors for supplying the power required to increase the energy level of the fluid.

1.4 Fans and Blowers

A fan continuously moves a mass of air, gas or vapour at the desired velocity by the action of its rotor. For achieving this objective there is a slight increase in the gas pressure across the fan rotor. However, the main aim of a fan is to move a gas without an appreciable increase in its pressure. The total pressure developed by fans is of the order of a few millimetres of water gauge (W.G.).

A blower which is also sometimes referred to as a fan develops an appreciable rise in pressure of the gas flowing through it. This pressure rise is required to overcome pressure losses of the gas during its flow through various passages. In some applications such as power plant boilers and mine ventilation system the pressures developed by the blowers are more than 1600 mm W.G.. Some low-pressure turbo-compressors are also called blowers or turboblowers.

In contrast to fans and blowers, the pressures developed by the compressors are from moderate to high. Therefore, the pressure rise through the compressors is expressed in terms of pressure ratio.

1.5 Compressible Flow Machines

The pressure, temperature and density changes occurring in fluids passing through steam and gas turbines, and compressors are appreciable. A finite change in the temperature of the working fluid is a typical characteristic of this class of machines which distinguishes them from other turbo-machines. This class of machines with predominantly compressible flows are referred to as compressible flow or thermal turbomachines.[14] They are characterized by higher temperatures and peripheral speeds of the rotor.

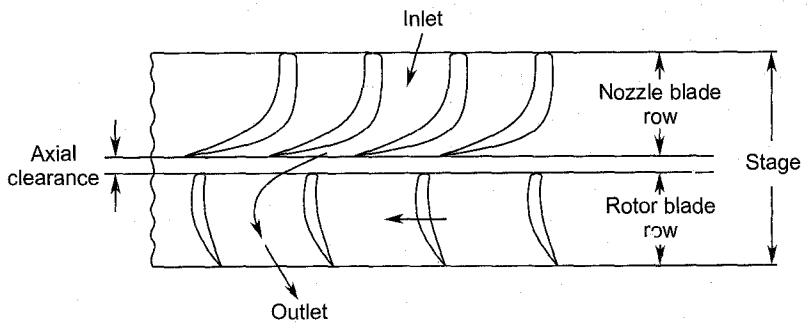

Fig. 1.5 An axial turbine stage

Therefore, their design and operation are influenced by compressible flows, high temperature and speed problems.

1.6 Incompressible Flow Machines

Hydraulic pumps and turbines are examples of turbomachines working with a liquid. The fluid or water is incompressible giving a constant volume flow rate for a given mass flow rate in steady operation. Water and air are considered here as typical working fluids in turbomachines handling liquids and gases. The density of water is about 800 times that of atmospheric air. Therefore, the force required to accelerate a given quantity of water is much larger compared to that required for air. This factor largely accounts for much lower fluid and rotor velocities in hydro-turbomachines.

Turbomachines dealing with gases over a small pressure difference also behave as incompressible flow machines. This is because of negligible changes in the temperature and density of the fluid across the machine. Fans, low pressure blowers, airscrews and windmills are examples of such machines.

Thus a majority of incompressible flow machines work near ambient conditions and are comparatively low speed and low temperature machines. This makes their running and maintenance much easier compared to thermal turbomachines.

1.7 Turbine, Compressor and Fan Stages

A stage of a turbomachine generally consists of a ring of moving blades along with a ring of fixed blades.

A turbine stage as shown in Fig. 1.5 is made up of a ring of fixed nozzle blades followed by the rotor blade ring. However a nozzleless stage with only the rotor is also possible and is often employed in an inward flow radial turbine.

A compressor or a blower stage consists of a rotor followed by a diffuser blade ring. The first stage of a multi-stage compressor or a single stage compressor may also consist of a ring of inlet guide vanes (IGV) upstream of the rotor as shown in Fig. 1.6.

The principal element in a turbomachine stage is the rotor which performs the basic function of transfer of energy. Therefore, a single rotor on its own may also form a stage in a turbine, compressor or fan. Unenclosed fans are examples of such stages.

In radial machines a scroll or volute casing also forms a part of the stage.

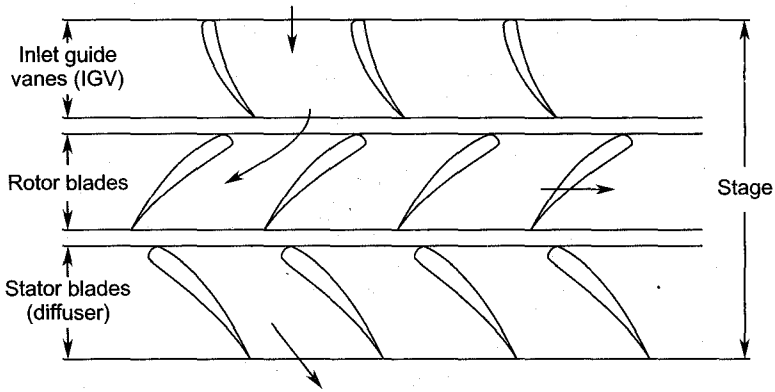

Fig. 1.6 An axial compressor stage

1.8 Extended Turbomachines

Most of the turbomachines are enclosed in casings which guide a finite flow through them. This category includes steam and gas turbines, compressors and ducted fans. In contrast to these enclosed machines, aircraft propellers and windmills are open and interact with an "infinite sea" of air. These machines are called extended turbomachines. Figures 1.7 and 1.8 show these machines and their applications. The air screw accelerates the atmospheric air rearward, thus moving the aircraft forward.

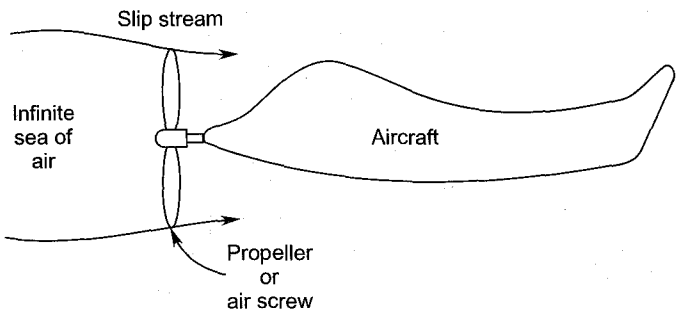

Fig. 1.7 An aircraft propeller (extended turbomachine)

The windmill or the wind turbine transfers the wind energy to the aerogenerator. This prime mover has also been used to drive pumps and other devices.

1.9 Axial Stages

In an axial flow turbomachine or its stage (Fig. 1.9) the radial component of the fluid velocity is negligible. The change in radius between the entry

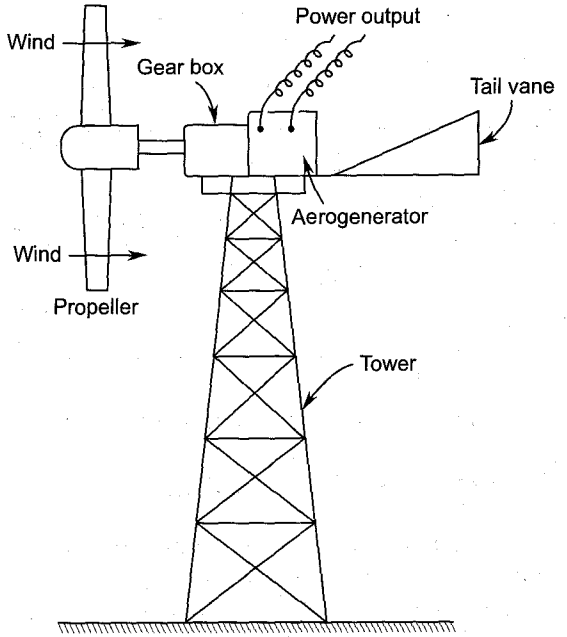

Fig. 1.8 A windmill (extended turbomachine)

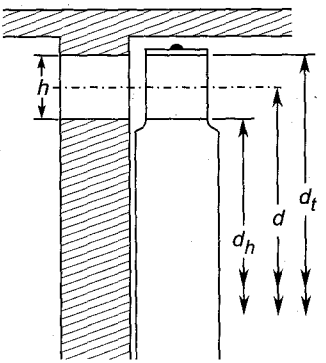

Fig. 1.9 An axial turbomachine

and exit of the stage is small. The through flow in such machines mainly occurs in the axial direction, hence the term "axial stage".

An axial machine can be easily connected with other components. For example in a gas turbine plant this configuration offers mechanically and aerodynamically a convenient connection between the compressor, combustion chamber and turbine.

For the same reason, axial stages are widely employed in multi-stage turbomachines. Such a stage is ideally suited for high flow rates.

The area of cross-section available to the flow in an axial stage is

$$A_x = \frac{\pi}{4}(d_t^2 - d_h^2) = \pi dh \tag{1.1}$$

Suitable values of the hub and tip diameters can be chosen to provide the required area. For aircraft propulsion, the axial flow configuration of compressors and turbines has a special advantage of low frontal area, resulting in a lower aircraft drag.

The turning of the fluid in axial stages is not too severe and the length of the blade passages is short. This leads to lower aerodynamic losses and higher stage efficiencies.

On account of the individual blade root fixtures, the rotor of an axial stage has limited mechanical strength. This restricts the maximum permissible peripheral speed of the rotor.

1.10 Radial Stages

In the radial stage of a turbomachine the through flow of the fluid occurs mainly in the radial direction, i.e. perpendicular to the axis of rotation. Therefore, the change of radius between the entry and exit of the stage is finite. This causes a finite change in the energy level of the fluid due to the centrifugal energy.

A radial turbomachine may be inward-flow type or outward-flow type. Since the purpose of compressors, blowers, fans and pumps is to increase the energy level of the fluid, they are of the outward-flow radial type as shown in Fig. 1.10. Radial gas turbines are mostly of the inward flow type as shown in Fig. 1.11; the fluid transfers its centrifugal energy to the rotor in flowing from a larger to a smaller radius. The Ljungstrom steam turbine (Fig. 1.12) is a double rotation outward flow radial turbine. The outward-flow configuration is chosen here to accommodate the large volume flow rate of the rapidly expanding steam.

Referring to Fig. 1.10, the areas of cross-section at various stations in a centrifugal compressor stage are given by

$$A_i = \frac{\pi}{4}(d_t^2 - d_h^2) = \pi dh \tag{1.2}$$

$$A_1 = \pi d_1 b_1 \tag{1.3}$$

$$A_2 = \pi d_2 b_2 \tag{1.4}$$

For given impeller and shaft diameters and change of radius from entry to exit the area at the entry to the stage is restricted by Eq. (1.2). At this station a compressible fluid has the largest volume requiring a correspondingly large area. Conversely, the same is true for an inward flow gas turbine (Fig. 1.11). On account of this, radial flow stages do not

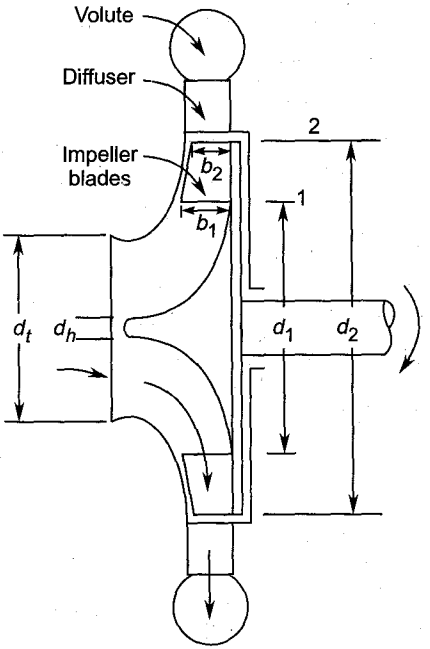

Fig. 1.10 A centrifugal compressor stage

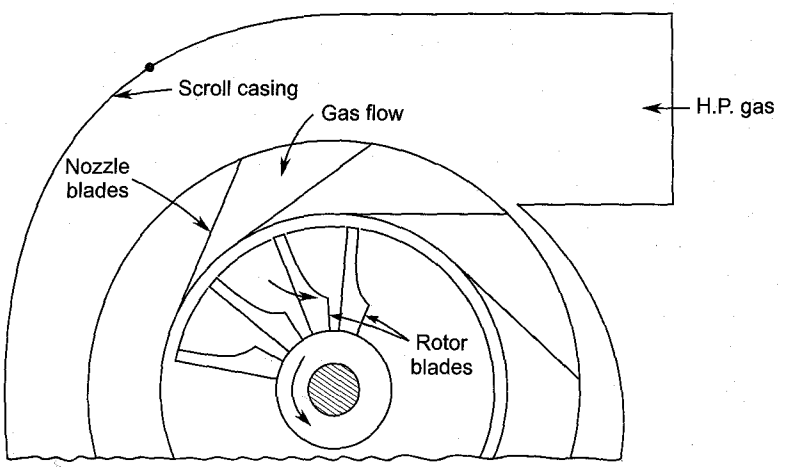

Fig. 1.11 An inward-flow radial turbine stage

offer the best geometrical configuration for high flow rates. In radial flow stages the flow invariably turns through 90° traversing a much longer blade passage compared to that in the axial types. This leads to comparatively higher losses and lower efficiencies. In a multi-stage radial machine the flow is required to change its direction drastically several times in long interconnecting flow passages. This is obviously an

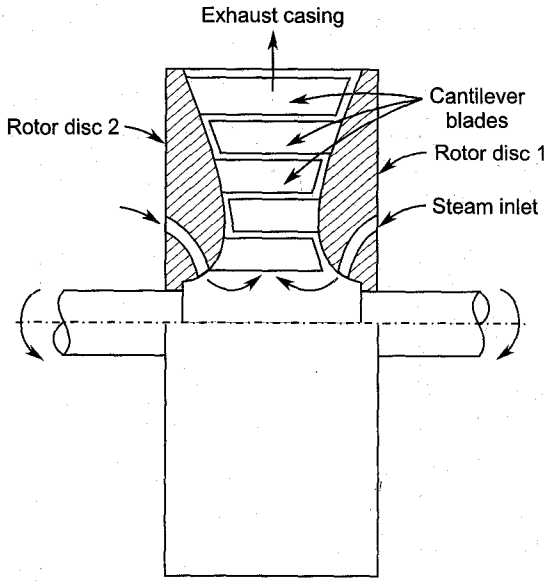

Fig. 1.12 An outward-flow radial turbine (Ljungstrom turbine)

undesirable feature both mechanically and aerodynamically. Therefore, a majority or radial machines are single-stage machines; very few multi-stage radial machines employ more than three stages.

Since the power developed is proportional to the mass flow rate, and the number of stages that can be employed is much smaller compared to axial machines, radial flow machines are not suited for large power requirements.

Radial stages employ 'one piece' rotors in which the blades are an integral part of the main body. This makes a radial rotor mechanically stronger than an axial type in which the blades are separately fixed. Therefore, radial machines can employ higher peripheral speeds.

On account of higher peripheral speeds and additional change in the energy level of the fluid caused due to centrifugal energy, much higher values of the pressure ratio per stage are obtained in the radial stage compared to the axial type.

Radial flow compressors and turbines for large power and thrust requirements have a larger overall diameter of the aeroengine, leading to an unacceptably large frontal area. Therefore, radial machines are unsuitable for the propulsion of large aircrafts.

1.11 Mixed Flow Stages

For certain requirements, the flow in a turbine, pump or blower stage is partly radial and partly axial. Such a stage is known as a mixed

flow stage; it combines the advantages of both the axial and radial types.

The flow at the exit of a mixed flow machine (Fig. 1.13) has finite components in both radial and axial directions. In this type of a pump the head generated due to centrifugal energy is a considerable proportion of the total head generated in the stage.

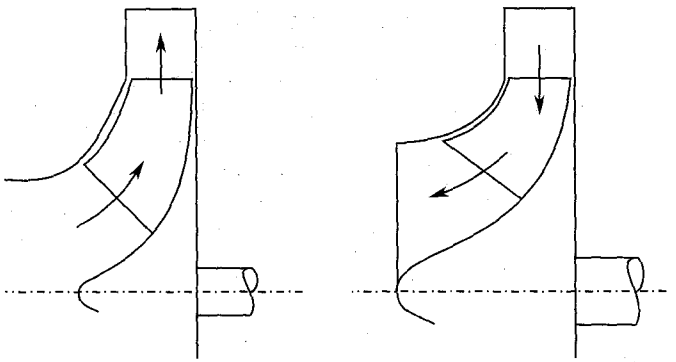

(a) Mixed flow pump or blower (b) Mixed flow turbine

Fig. 1.13 Mixed flow machines

The mixed flow configuration has been widely used in hydraulic pumps and turbines. This type has also been found adventageous in some blowers but it has yet to make its appearance in compressible flow turbo-machines, viz. steam and gas turbines and compressors.

1.12 Impulse Stages

Machines in which there is no change of static or pressure head of the fluid in the rotor are known as impulse machines. The rotor blades only cause energy transfer without any energy transformation. The energy transformation from pressure or static head to kinetic energy or vice versa takes place only in fixed blades. For example, the transfer of kinetic energy of a high velocity fluid to the rotor in an impulse turbine occurs only due to the impulsive action of the fluid on the rotor. An impulse turbine stage is shown in Fig. 1.14. Since the rotor blade passages in an impulse turbine do not cause any acceleration of the fluid, the chances of its separation due to boundary layer growth on the blade surfaces are greater. On account of this, the rotor blade passages of the impulse machine suffer greater losses giving lower stage efficiencies.

Some examples of impulse machines are the paddle wheel, Pelton wheel and Curtis steam turbine.

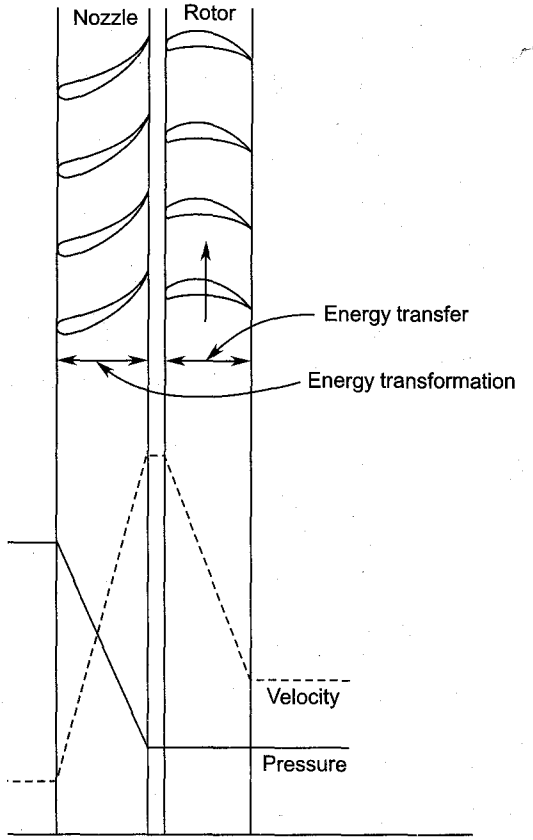

Fig. 1.14 An impulse turbine stage

1.13 Reaction Stages

The degree of reaction of a turbomachine stage is defined as the ratio of the static or pressure head change occurring in the rotor to the total change across the stage.

Turbomachines or their stages in which changes in static or pressure head occur both in the rotor and stator blade passages are known as reaction machines or stages. Here the energy transformation occurs both in fixed as well as moving blades. The rotor experiences both energy transfer and transformation. Therefore, reaction turbines are expected to be more efficient on account of the continuously accelerating flow and lower losses.

Some examples of reaction machines are Hero's turbine, the lawn sprinkler and Parson's steam turbine. Pressure and velocity changes through a reaction turbine stage are shown in Fig. 1.15.

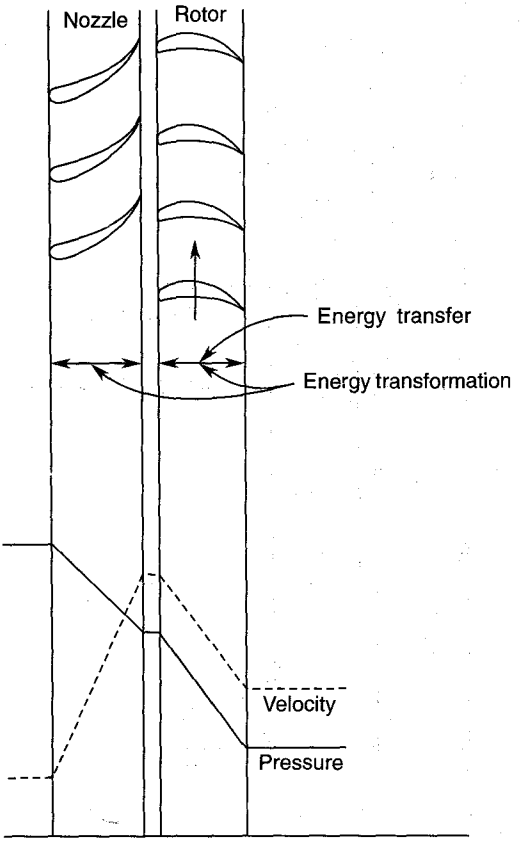

Fig. 1.15 A reaction turbine stage

A 50% or half degree reaction machine has some special characteristics. Axial flow turbines and compressors with 50% reaction have symmetrical blades in their rotors and stators as shown in Figs. 1.16 and 1.17. It may be noted that the velocity triangles at the entry and exit of a 50% stage are also symmetrical.

1.14 Variable Reaction Stages

In large axial machines the blade lengths are considerable and there are large changes in the peripheral speeds from the hub to the tip of the rotor. The flow parameters in such stages or machines experience appreciable variation along the blade height (spanwise direction). Under these conditions it is not possible to maintain a given degree of reation constant throughout the blade height. For example, if the rotor blade section at the blade root is purely impulse, other sections at higher radii will have a progressively increasing degree of reaction. Thus in a long blade of an axial

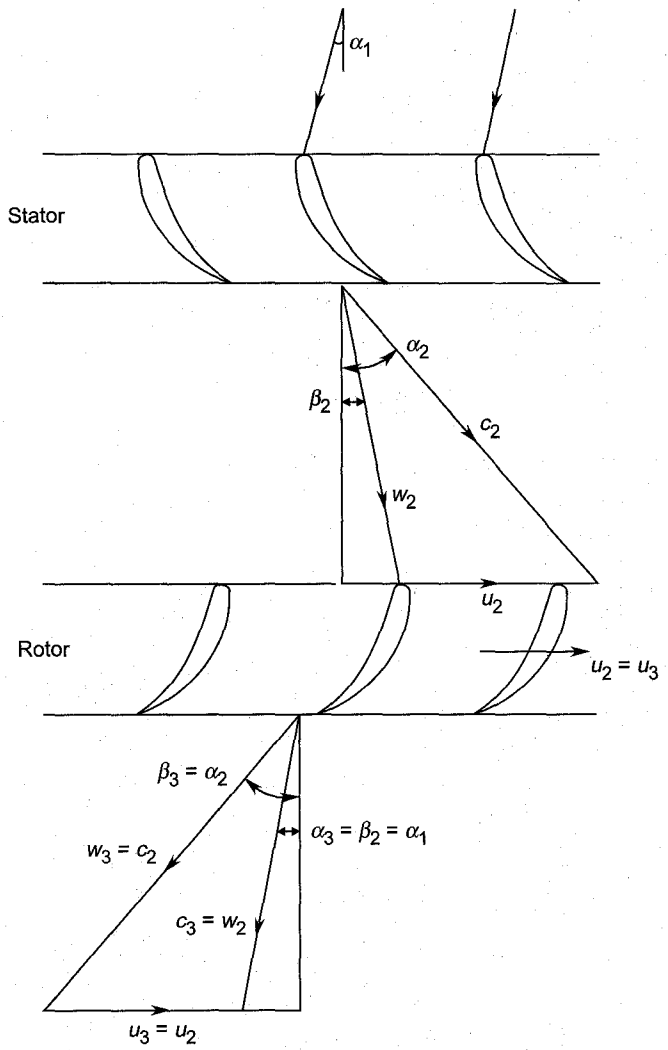

Fig. 1.16 A 50% reaction turbine stage

flow turbine, compressor or fan stage, the degree of reaction is variable from hub to tip; this leads to the employment of twisted blades.

1.15 Multi-stage Machines

It will be seen later that for a given rotor speed only a limited change in the energy level of the fluid can occur in a turbomachine stage. This holds equally for turbines, compressors, pumps and blowers. Therefore, in applications where a large change in the energy level is required, more stages are employed.

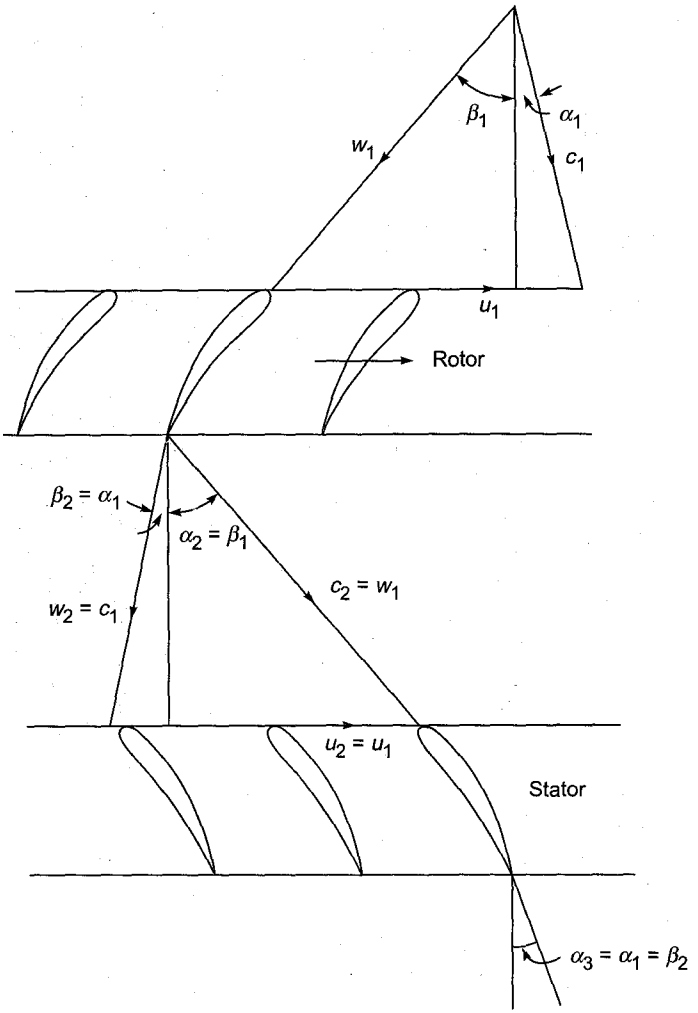

Fig. 1.17 A 50% reaction compressor stage

Multi-stage machines may employ only impulse or reaction stages or a combination of these. Impulse machines may utilize a large pressure drop in several pressure stages or a high kinetic energy in a number of velocity stages; a combination of pressure and velocity stages in impulse machines is also employed. In certain compressor applications it is profitable to use axial and radial stages in the same machine. Different stages may be mounted on one or more shafts.

In large steam turbines the difference of steam pressure between the boiler and the condensor is very large. If this was to be utilized in a single stage, a rotor of an impracticably large diameter at a very high speed would have to be used. This would create, besides manufacturing difficulties, serious strength and bearing problems.

Gas turbine plants, on account of the comparatively lower values of the pressure ratio employed, have a smaller number of stages.

A multi-stage arrangement is also employed for high pressure compressors and blowers. The flow in the stages of these machines is decelerating and demands a gentle compression over a small pressure rise. This becomes necessary to prevent high losses associated with boundary layer separation in an adverse pressure gradient. Thus a high pressure producing turbomachine has a much larger number of stages compared to an equivalent power producing machine.

1.16 Stage Velocity Triangles

The flow geometry at the entry and exit of a turbomachine stage is described by the velocity triangles at these stations. A minimum number of data on velocity vectors and their directions are required to draw a complete set of velocity triangles.

All types of turbomachines have a finite cross-section at the entry and exit. Therefore, the magnitudes of velocity vectors and their directions vary over these sections. Because of this, an infinite number of velocity triangles would be required to fully describe the flow. This is obviously not possible. On the other hand, a single pair of velocity triangles will only represent A one-dimensional flow through the stage.

In view of this, mean values of velocity vectors and their directions are defined for blade rows of given geometries and flow conditions. These values make it possible to draw the mean velocity triangles for the stage.

The velocity triangles for a turbomachine contain, besides the peripheral velocity (u) of the rotor blades both the absolute (c) and relative (w) fluid velocity vectors. These velocities are related by the following well known vector equation:

Absolute velocity vector = peripheral velocity vector + relative velocity vector

$$\boldsymbol{c} = \boldsymbol{u} + \boldsymbol{w} \tag{1.5}$$

This simple relation is frequently used and is very useful in drawing the velocity triangles for turbomachines. For instance, velocity triangles of Figs. 1.16 and 1.17 have been drawn using this relation. The angles are from the axial direction (the reference direction). For axial machines, $u_1 = u_2 = u_3 =$ constant.

1.17 Design Conditions

Like other machines, turbomachines are also designed for some prescribed running conditions at which they should have high or maximum

efficiency. The design conditions, among other things, fix the geometry of the flow; at the design point operation of a turbomachine there is some correspondence between the blade angles and the mean fluid angles. The ratio of the peripheral velocity of the rotor to some fluid velocity is also fixed by design conditions.

Aerodynamic or aerothermodynamic design conditions should fully take into account the strength considerations, ease in manufacture, material and economic aspects.

1.18 Off-design Conditions

Off-design running conditions of a turbomachine may arise due to changes in the rotational speed, flow rate, load or boundary conditions. Along with high performance at the design point, it is desirable that a turbomachine does not suffer from very poor performance at off-design conditions. Poor performance results from changed velocity triangles of the stage or stages; the flow deviates from the optimum conditions giving lower efficiency.

Some off-design conditions may be prohibitive on account of break-down of the stable flow conditions as in compressors, fans and blowers. In such machines the surge line determines the range of stable operation.

1.19 Applications

Some important applications for turbines, compressors and fans are briefly described here. Numerous other general and special applications can be found in the vast amount of literature available on these machines.

1.19.1 Power Generation

Applications of turbomachines in the power industry are well-known. The bulk of thermal and hydropower is generated by the base load steam and hydro turbines.

Electric power is also generated by some big and small gas turbine power plants. Peak load power stations are now using 'retired' aeroengines for their gas turbine plants. Low cooling water requirements and the ability to start in a short time make them superior to steam turbines in some situations.

Combined gas and steam turbine power plants are also now employed for bulk power generation (base load) on account of their higher overall efficiencies.

Wind energy in high velocity wind regions of the world is being utilized in various ways through windmills or wind turbines. Such

turbines are a great asset in isolated areas which are far away from other sources of energy.

Large fans and blowers are used for developing the draught required in the boilers of steam power plants. The cooling of turbo-generators is also achieved by employing circulating fans.

1.19.2 Aircraft Propulsion

Though the gas turbine engine has been used for automobiles, marine propulsion and railway traction, its major thrust has been in the field of aircraft propulsion. While high rotational speeds at the gas turbine output shaft lead to difficult mechanical problems in a large number of applications, it is not a serious drawback in turbo-jet engines; here the gas turbine is only used to provide the jet-thrust. The smaller and low speed aircrafts employ the shaft power for driving the airscrews or propellers through reduction gears.

1.19.3 Industrial

Small steam turbine drives are ideal for many industrial applications on account of their considerable simplicity and ease in achieving variable speed. Large pumps, blowers and compressors can be coupled direct to the driving turbine shafts.

High pressure multi-stage centrifugal pumps and compressors are widely used in petro-chemical industries.

Industrial furnaces employ fans and blowers of various sizes for producing the required draught.

1.19.4 Miscellaneous

Small gas turbines are ideally suited for many auxiliary drives. They are used to drive turbo-pumps and generators in underwater vehicles, aircrafts, rockets and missiles. Some micro-turbines running on the astronauts waste heat have been developed for spacecrafts. Such turbines have diameters of the order of 15 mm and speeds in the range of 100-400 thousand rpm.

The drills used by dental and orthopaedic surgeons are driven by tiny air-turbines. The low temperature expanded air is used for cooling the drilled area. High speed small radial turbines are also frequently used in cryogenic engineering.

Small fans are used for cooling electrical and optical equipments. Often, the presence of these fans is discovered when a piece of equipment stops functioning properly due to lack of adequate cooling.

Notation for Chapter 1

A	Area of cross-section
b	Blade width
c	Absolute velocity of the fluid
d	Rotor diameter
h	Blade height
u	Peripheral or tangential velocity of rotor blades
w	Relative velocity of the fluid
W.G.	Water gauge

Greek Symbols

α	direction of the absolute velocity vector
β	Direction of the relative velocity vector

Subscripts

1	Entry to the turbine nozzles or compressor rotor
2	Exit of the turbine nozzles or compressor rotor
3	Exit of the turbine rotor or compressor stator
h	Hub
t	Tip
x	Axial

QUESTIONS

1.1 Define a turbomachine. What are the main differences between incompressible and compressible flow machines?

1.2 Describe two industrial applications for each of the following machines: gas turbines, gas compressors and low pressure fans. Explain their roles in the overall systems with the aid of sketches.

1.3 Sketch a typical impulse gas turbine stage. Show the velocity triangles at the entry and exit of the rotor for design conditions. Draw the off-design velocity triangles when the turbine overspeeds.

1.4 Show the arrangement of blades in an axial compressor with two stages. Show graphically the variation of static pressure and absolute velocity through the machine. Why is this type of compressor more suitable for a turbo-jet engine?

1.5 Describe with the aid of illustrative sketches the working of a centrifugal compressor stage. State three advantages of such a machine over an axial type.

1.6 Sketch a drag pump and a turbine. Are these turbomachines? Give reasons.

1.7 What is an extended turbomachine? Give three examples and sketches of such machines. What are the salient features which differentiate these machines from the enclosed type?

1.8 Explain briefly why hydro-turbomachines are low-speed machines compared to steam and gas turbines. Why is the power developed per stage much greater for hydro-turbines relative to steam and gas turbines?

1.9 What is a mixed flow turbomachine? Sketch such stages for a turbine and blower; show the directions of absolute fluid velocities at the entry and exit.

1.10 What are the advantages of double rotation turbomachines? Show the arrangements employed for double rotation axial turbines and compressors.

1.11 State three features of turbomachines which distinguish them from other machines. Which of the following machines are turbomachines: windmill, Wankel engine, hydraulic dynamometer, gear pump, turbocharger, dragpump and lobe compressor?

1.12 Draw a sketch of a two-stage axial flow compressor showing the rotor and stator blade rows. Show the variation of pressure and velocity of the gas through the stages.

1.13 Why radial gas turbines and compressors are not suitable for large power applications?

1.14 Explain briefly why reciprocating compressors and engines are unsuitable for high flow rates and power.

1.15 Describe the working of a Wankel engine.

Chapter 2

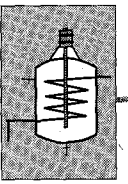

Thermodynamics

Thermodynamic and aerodynamic analyses of turbines, compressors, fans and blowers require the relations between force, mass and velocity. The following laws are frequently used in dealing with problems of design and operation of these machines.

1. First law of thermodynamics—energy equation in its various forms.
2. Second law of thermodynamics—entropy and loss relations.
3. Law of conservation of mass—continuity relations.
4. Newton's second law of motion—momentum equation.

2.1 Basic Definitions and Laws

Some important definitions used in the analysis of compressible flow turbomachines are stated here before discussing the various aero-thermodynamic aspects of these machines. Others can be found in standard textbooks[19-28] on thermodynamics.

2.1.1 System

An arbitrary collection of matter having a fixed identity is known as a system. All things outside the system are referred to as surroundings. An imaginary surface which separates the system from its surroundings is known as the boundary.

2.1.2 Closed System

A closed system has a fixed quantity of matter (fluid or gas). There is no inflow or outflow of matter to and from a closed system; however, a closed system can interact with its surroundings through work and heat transfers. The boundaries of a closed system containing the fixed mass of matter can change. Expanding gas in an internal combustion engine is one such example.

2.1.3 Open System (Control Volume)

A system is open when there is a continuous flow of matter through it. Such a system is also referred to as a control volume. It has a fixed space but does not contain a fixed mass of matter; instead there is a continuous flow of mass through it. The identity of the matter occupying the control volume varies with time.

The surface which surrounds a control volume is referred to as the control surface.

2.1.4 State

The state of a system is its condition which is defined by its properties.

2.1.5 Process

A process is a change or a series of changes in the state of the system.

2.1.6 Cycle

When the initial and final states of a system experiencing a series of processes are identical, it is said to execute a cycle.

2.1.7 Pressure

Pressure at a point surrounded by an infinitesimal area ΔA is the force per unit area. This is given by

$$p = \lim_{\Delta A \to \Delta A_c} \left(\frac{\Delta F}{\Delta A} \right) \tag{2.1}$$

(Here subscript c refers to the continuum.)

The unit of pressure in SI units is

$$\text{Pascal} = \text{N/m}^2$$

2.1.8 Density

The density of a medium is the mass of the matter (gas) per unit volume. This is given by

$$\rho = \lim_{\Delta V \to \Delta V_c} \left(\frac{\Delta m}{\Delta V} \right) \tag{2.2}$$

Density is expressed in kg/m^3.

2.1.9 Temperature

When two systems in contact with each other are in thermal equilibrium, the property common to both the systems having the same value is called temperature. Thus temperature is a measure of the thermal potential of a system.

2.1.10 Energy

Energy is the capacity of doing work. The state of a system can be changed by adding or extracting energy.

Heat and work are also different forms of energy in transit. They are not contained in any system.

Heat is the form of energy which transfers between two systems by virtue of the temperature difference between them. Heat transfer to or from a system changes its state.

Work is done by a system on its surroundings when they are moved through a distance by the action of a force. This is exerted by the system on the surroundings in the direction of displacement of the surroundings. The magnitude of mechanical work is given by

$$\text{Work} = \text{force} \times \text{distance in the direction of force}$$

Both heat and work are path functions and depend on the type of process. Therefore, they are not properties of a system. Energy, heat and work are all expressed in joules (J), kilojoules (kJ) or newton metres (N m).

2.1.11 First Law of Thermodynamics

The first law of thermodynamics states that when a system executes a cyclic process, the algebraic sum of the work transfers is proportional to the algebraic sum of the heat transfers.

$$\oint dW \propto \oint dQ$$

$$\oint dW = J \oint dQ$$

When heat and work terms are expressed in the same units, the above relation is written as

$$\oint dQ - \oint dW = 0 \tag{2.3}$$

It can be shown that the quantity $(dQ - dW)$ is independent of the path of the process; hence it represents a change in the property of the system. This property is referred to as "energy", denoted here by the symbol E. Thus

$$dE = dQ - dW \tag{2.4}$$

Equation (2.4) for the two states of a system can be written as

$$E_2 - E_1 = Q - W$$

$$Q = W + (E_2 - E_1) \tag{2.5}$$

Heat transfer = work + change in energy

2.1.12 Specific Heats of Gases

The specific heat of a gas is the heat carrying capacity in a process. It is the amount of heat that is required to raise the temperature of a unit mass of the gas by one degree.

Two different types of specific heats are used in the analysis of compressible flow machines: specific heats at constant volume and constant pressure.

The specific heat at constant volume (c_v) is the amount of heat required to raise the temperature of a unit mass of the gas by one degree at constant volume. It is given by

$$c_v = \left(\frac{\partial q}{\partial T}\right)_v = \left(\frac{\partial u}{\partial T}\right)_v \tag{2.6}$$

The specific heat at constant pressure (c_p) is the amount of heat required to raise the temperature of a unit mass of the gas by one degree at constant pressure. It is given by

$$c_p = \left(\frac{\partial q}{\partial T}\right)_p = \left(\frac{\partial h}{\partial T}\right)_p \tag{2.7}$$

The specific heats of real gases vary with temperature.

$$c_p,\ c_v = f(T) \tag{2.8}$$

The ratio (γ) of the two specific heats defined above is an important parameter in compressible flow problems of turbomachines.

$$\gamma = \frac{c_p}{c_v} \tag{2.9}$$

Values of γ for some commonly used gases and vapours in engineering applications are:

1.4 (air), 1.264 – 1.4 (superheated steam), 1.67 (helium) 1.13 – 1.30 (Freon – 21) and 1.33 (products of combustion).

2.1.13 Internal Energy

The internal energy of a gas is the energy stored in it by virtue of its molecular motion. If it is assumed that the internal energy of a perfect gas

is zero at the absolute zero temperature, its value at a temperature T is given by

$$u = c_v T \tag{2.10}$$

2.1.14 Enthalpy

The heat supplied to or rejected by a system at constant pressure is the change of enthalpy during the process. The value of enthalpy at a given state is given by

$$h = u + pv = u + \frac{p}{\rho} \tag{2.11a}$$

and for a perfect gas

$$h = c_p T \tag{2.11b}$$

2.1.15 Ideal Gas

An ideal gas obeys Boyle's and Charle's law, i.e.

$$(pv)_T = \text{const. (Boyle's law)} \tag{2.12}$$

$$\left(\frac{v}{T}\right)_p = \text{const. (Charle's law)} \tag{2.13}$$

Thus an ideal gas obeys the simple equation of state

$$pv = RT \tag{2.14}$$

or

$$p = \rho RT \tag{2.15}$$

The two specific heats and the gas constant for an ideal gas are related by the following equation:

$$c_p - c_v = R \tag{2.16}$$

Putting Eq. (2.9) in Eq. (2.16), we get

$$c_v = \frac{1}{\gamma - 1} R \tag{2.17}$$

$$c_p = \frac{\gamma}{\gamma - 1} R \tag{2.18}$$

2.1.16 Perfect Gas

A perfect gas or a calorically ideal gas is an ideal gas whose specific heats remain constant at all temperatures.

$$\frac{d}{dT}(c_v) = 0 \tag{2.19}$$

c_v = constant with temperature

$$\frac{d}{dT}(c_p) = 0 \tag{2.20}$$

c_p = constant with temperature

The analyses of compressible flow machines given in this book assume perfect gas relations.

2.1.17 Semi-perfect Gas

A semi-perfect gas is an ideal gas whose specific heats vary with temperature.

$$c_v = f(T) \tag{2.21a}$$

$$u_2 - u_1 = \int_1^2 c_v \, dT \tag{2.21b}$$

$$c_p = f(T) \tag{2.22a}$$

$$h_2 - h_1 = \int_1^2 c_p \, dT \tag{2.22b}$$

2.1.18 Real Gas

The real gas behaviour deviates from that of an ideal gas. It does not obey the equation of state [Eqs. (2.14), (2.15), etc.]. Different equations of state are used for real gases. Some of them are the equations of Van der Waals, Berthelot and Beattie-Bridgeman.

2.1.19 Second Law of Thermodynamics

The second law of thermodynamics has been enunciated in a number of ways. Some of them are as follows:

(a) *Clausius statement:* Heat cannot, on its own, flow from a body at lower temperature to a body at higher temperature.

(b) *Kelvin-Planck's statement:* It is impossible to construct a heat engine which performs a complete cycle and delivers work exchanging heat from a single source.

The following relations are derived from the second law of thermodynamics:

Definition of entropy

$$S_2 - S_1 = \int_1^2 \frac{dQ_R}{T} \tag{2.23}$$

Clausius inequality

$$\oint \frac{dQ}{T} \leq 0 \tag{2.24}$$

In any irreversible process

$$S_2 - S_1 > \int_1^2 \frac{dQ}{T} \tag{2.25}$$

In an irreversible adiabatic process

$$S_2 - S_1 > 0 \tag{2.26}$$

In any reversible cycle

$$\oint \frac{dQ_R}{T} = 0 \tag{2.27}$$

In an isentropic or reversible adiabatic process

$$S_2 - S_1 = 0 \tag{2.28}$$

2.1.20 Reversible Process

A process is reversible if the system and its surroundings can be restored to their initial states by reversing the process. A reversible process in a flow machine is possible only in the absence of fluid friction and heat transfer with finite temperature difference. Since these conditions are impossible to achieve in actual processes, all real flows in turbines, compressors, fans and blowers are irreversible. The reversible process is used only as an "ideal reference process" for comparison with its equivalent actual process.

2.1.21 Irreversible Process

A process that does not satisfy the above conditions of a reversible process is an irreversible process.

2.1.22 Adiabatic Process

When there is no heat transfer between the system and the surroundings during a process, it is known as an adiabatic process.

All the turbomachines discussed in this book are assumed to experience only adiabatic processes.

2.1.23 Isentropic Process

An adiabatic process in which there is no change in entropy is known as a reversible adiabatic or isentropic process. This is governed by the following relations:

$$pv^{\gamma} = \text{const.} \tag{2.29}$$

$$\frac{T_1}{T_2} = \left(\frac{p_1}{p_2}\right)^{\frac{\gamma-1}{\gamma}} = \left(\frac{v_2}{v_1}\right)^{\gamma-1} = \left(\frac{\rho_1}{\rho_2}\right)^{\gamma-1} \tag{2.30}$$

$$Tds = dh - vdp = dh - \frac{1}{\rho}\, dp = 0 \tag{2.31}$$

2.1.24 Non-flow Process

A process occurring in a closed system is a non-flow process. One such example is shown in Fig. 2.1. It represents the expansion of a fixed mass of gas inside the cylinder of a reciprocating engine.

The work done in an infinitesimal non-flow process is given by

$$dw_{nfp} = p\ dv \tag{2.32a}$$

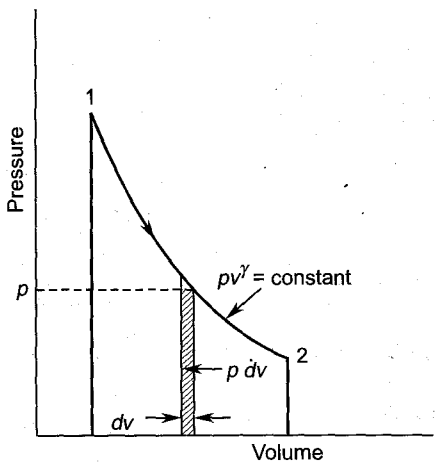

Fig. 2.1 Expansion work in a closed system (non-flow process)

The work done between the two states 1 and 2 is

$$w_{nfp} = \int_1^2 p\ dv \tag{2.32b}$$

For an adiabatic process, assuming perfect gas relations

$$w_{nfp} = \frac{1}{\gamma - 1}\ (p_1 v_1 - p_2 v_2) \tag{2.33a}$$

or $$w_{nfp} = c_v\ (T_1 - T_2) \tag{2.33b}$$

or $$w_{nfp} = u_1 - u_2 \tag{2.33c}$$

2.1.25 Flow Process

A process occurring in an open system or through a control volume is a flow process. Flows occurring in all turbomachines are flow processes.

Figure 2.2 represents such a process. The infinitesimal work done in a reversible process is given by

$$dw_{fp} = -\, v\, dp \tag{2.34a}$$

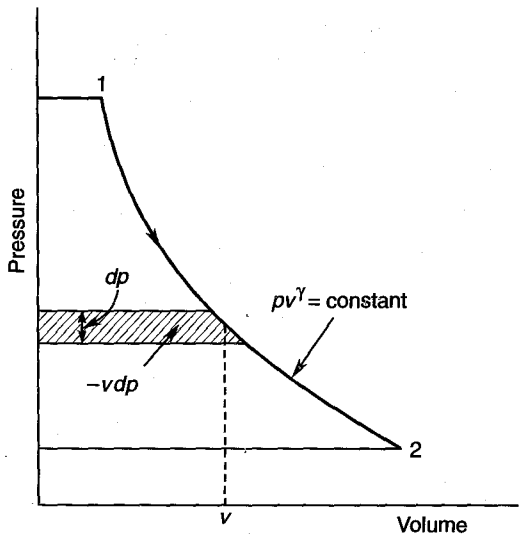

Fig. 2.2 Expansion work in an open system (flow process)

For a finite process

$$w_{fp} = -\int_1^2 v\, dp \tag{2.34b}$$

For an adiabatic process in a perfect gas,

$$w_{fp} = \frac{\gamma}{\gamma - 1}(p_1 v_1 - p_2 v_2) \tag{2.35a}$$

or
$$w_{fp} = c_p (T_1 - T_2) \tag{2.35b}$$

or
$$w_{fp} = h_1 - h_2 \tag{2.35c}$$

2.1.26 Availability

The part of heat energy that is available for conversion into work is called 'available energy'. In a heat engine cycle available part of the energy (heat) supplied is the maximum possible value of the work output; the

actual work is always less than this value. The availability (A) depends on the states of both the system and the surroundings (environment); this is given by

$$A = (H - H_0) - T_0 (S - S_0) \tag{2.36a}$$

For unit mass of the working fluid (gas, steam, etc)

$$a = (h - h_0) - T_0 (s - s_0) \tag{2.36b}$$

Here, properties with subscript 'o' such as H_0, T_0, S_0 refer to the surroundings.

In a steady flow process the maximum value of the obtainable work is given by

$$W_{max} = W_{rev} = A_1 - A_2 \tag{2.37}$$

The minimum value of the energy (heat) rejected is the unavailable energy. It is given by

$$B = T_0 (S_2 - S_1) \tag{2.38a}$$

$$b = T_0 (s_2 - s_1) \tag{2.38b}$$

Maximum work obtainable between two equilibrium states is equal to the change in the Gibbs function; this is defined as

$$G = H - TS = U + pV - TS \tag{2.39}$$

$$W_{max} = G_1 - G_2 = (H_1 - H_2) - T_0 (S_2 - S_1) \tag{2.40}$$

Application of eqn. (2.36b) for the two states in a steady flow process gives

$$\begin{aligned} a_1 &= (h_1 - h_0) - T_0 (s_1 - s_0) \\ a_2 &= (h_2 - h_0) - T_0 (s_2 - s_0) \\ w_{max} &= w_{rev} = a_1 - a_2 \\ &= (h_1 - T_0 s_1) - (h_2 - T_0 s_2) \\ &= (h_1 - h_2) - T_0 (s_2 - s_1) \end{aligned} \tag{2.41}$$

2.2 Energy Equation

The energy equation [Eq. (2.5)] derived from the first law of thermodynamics in Sec. 2.1.11 is

$$Q = W + (E_2 - E_1)$$

For applications in turbomachines, the energy terms will include internal energy, gravitational potential energy and kinetic energy. Other forms of energy which can be included but are not relevant here are strain energy, magnetic energy, etc.

$$E = U + m (gZ) + \frac{1}{2} mc^2 \tag{2.42}$$

$$dE = dU + m(g\ dZ) + m\ d\left(\frac{1}{2}c^2\right) \tag{2.43}$$

The change in the energy in a finite process between two states is given by

$$E_2 - E_1 = (U_2 - U_1) + m\ g\ (Z_2 - Z_1) + \frac{1}{2}m(c_2^2 - c_1^2) \tag{2.44}$$

Substituting Eq. (2.44) in Eq. (2.5) a general form of the energy equation is obtained

$$Q = W + (U_2 - U_1) + m\ g(Z_2 - Z_1) + \frac{1}{2}m(c_2^2 - c_1^2) \tag{2.45}$$

Dividing throughout by m,

$$q = w + (u_2 - u_1) + g(Z_2 - Z_1) + \frac{1}{2}(c_2^2 - c_1^2) \tag{2.46}$$

2.2.1 Steady-flow Energy Equation

For steady flow processes through turbomachines, the work term in Eqs. (2.45) and (2.46) contains shaft work and flow work. Thus,

$$W = W_s + (p_2V_2 - p_1V_1) \tag{2.47}$$

Substituting Eq. (2.47) in Eq. (2.45) and rearranging, we get

$$Q = W_s + (U_2 + p_2V_2) - (U_1 + p_1V_1) + mg(Z_2 - Z_1) + \frac{1}{2}m(c_2^2 - c_1^2)$$

Writing enthalpy H for the quantity $U + pV$.

$$H_1 + m\ g\ Z_1 + \frac{1}{2}mc_1^2 + Q = H_2 + mg\ Z_2 + \frac{1}{2}mc^2{}_2 + W_s \tag{2.48}$$

In terms of specific quantities,

$$h_1 + g\ Z_1 + \frac{1}{2}\ c_1^2 + q = h_2 + g\ Z_2 + \frac{1}{2}\ c_2^2 + w_s \tag{2.49}$$

Equation (2.48) or (2.49) is the steady flow energy equation for a control volume or an open system. This will now be rewritten for processes in various turbomachines and their components.

2.2.2 Hydro-turbomachines

In hydro-turbomachines

$$\rho = \frac{1}{v} = \text{const.}$$

$$u_1 \approx u_2$$

$$q \approx 0$$

Therefore, from Eq. (2.49), shaft work is given by

$$w_s = g\,(Z_1 - Z_2) + \frac{1}{2}(c_1^2 - c_2^2) + (p_1 - p_2)v \qquad (2.50)$$

In a stationary component, such as guide blades or draught tubes, shaft work is absent. Therefore, Eq. (2.50) gives

$$c_2^2 - c_1^2 = 2g\,(Z_1 - Z_2) + (p_1 - p_2)v \qquad (2.51)$$

2.2.3 Compressible Flow Machines

Most of the compressible flow turbomachines, such as turbines, compressors and blowers are adiabatic machines, i.e. $q \approx 0$. In these machines the change in potential energy $(Z_1 - Z_2)g$ is negligible as compared to changes in enthalpy $(h_1 - h_2)$ and kinetic energy$(c_1^2/2 - c_2^2/2)$.

Therefore, Eq. (2.49) yields

$$h_1 + \frac{1}{2}\,c_1^2 = h_2 + \frac{1}{2}\,c_2^2 + w_s \qquad (2.52)$$

The shaft work is given by

$$w_s = \left(h_1 + \frac{1}{2}c_1^2\right) - \left(h_2 + \frac{1}{2}c_2^2\right)$$

If the entry and exit velocities are small or the difference between them is negligible, then shaft work is given by the difference between the static enthalpies at the two states

$$w_s = h_1 - h_2 \qquad (2.53)$$

2.2.4 Energy Transformation

As pointed out earlier, energy transfer (shaft work input or output) in a turbomachine stage is possible only in the rotor, whereas energy transformation can occur both in moving and fixed blades. A special application of the energy equation is in the stationary components of turbines, compressors and blowers. These components are nozzle blade rings, diffusers and volute casings. The shaft work is absent in these components and the flow is almost adiabatic ($q \approx 0$). Therefore, Eq. (2.52) gives

$$h_1 + \frac{1}{2}\,c_1^2 = h_2 + \frac{1}{2}\,c_2^2 = \text{const.} \qquad (2.54)$$

2.2.5 Stagnation Enthalpy

In an adiabatic energy transformation process if the initial state is represented by h, T, c, etc. and the final gas velocity is zero, the resulting

value of the enthalpy ($h_2 = h_0$) has a special significance. Under these conditions, Eq. (2.54) yields

$$h_0 = h + \frac{1}{2} c^2 \tag{2.55}$$

Since the gas is stagnant or stationary in the final state, the quantity (h_0) in Eq. (2.55) is known as the stagnation enthalpy. This can now be defined as the enthalpy of a gas or vapour when it is adiabatically decelerated to zero velocity. It may be observed that the definition of stagnation enthalpy in Eq. (2.55) is only another form of the energy equation.

2.2.6 Stagnation Temperature

For a perfect gas, a stagnation temperature is defined through stagnation enthalpy. From Eq. (2.55),

$$c_p T_0 = c_p T + \frac{1}{2} c^2$$

$$T_0 = T + \frac{c^2}{2c_p} \tag{2.56}$$

T_0 is known as the stagnation temperature, T is the static temperature and $c^2/2c_p$ is the velocity temperature (T_c)

$$T_c = \frac{c^2}{2c_p} \tag{2.57}$$

$$T_0 = T + T_c \tag{2.58}$$

Equation (2.56) can be used to obtain an important relation for compressible flow machines

$$\frac{T_0}{T} = 1 + \frac{c^2}{2c_p T}$$

Using Eq. (2.18),

$$\frac{T_0}{T} = 1 + \frac{c^2}{\frac{2\gamma}{\gamma - 1} RT}$$

The velocity of sound in a gas at a local temperature T is given by

$$a = \sqrt{\gamma R T} \tag{2.59}$$

The Mach number of the flow is defined as the ratio of the local velocity of the gas and the local velocity of sound

$$M = \frac{c}{a} = \frac{c}{\sqrt{\gamma R T}} \tag{2.60}$$

Therefore,

$$\frac{T_0}{T} = 1 + \left(\frac{\gamma - 1}{2}\right)\left(\frac{c^2}{a^2}\right)$$

$$\frac{T_0}{T} = 1 + \left(\frac{\gamma - 1}{2}\right) M^2 \tag{2.61}$$

2.2.7 Stagnation Velocity of Sound

Stagnation values of various flow parameters are used as reference values in the analysis of compressible flow machines. Therefore, an expression for the stagnation velocity of sound is derived here.

By definition,

$$a_0 = \sqrt{\gamma R T_0} \tag{2.62}$$

Substituting for R,

$$a_0 = \sqrt{(\gamma - 1)\, c_p T_0} \tag{2.63}$$

Since $c_p T_0 = h_0$

$$a_0 = \sqrt{(\gamma - 1)\, h_0} \tag{2.64}$$

2.2.8 Stagnation Pressure

The pressure of a gas or fluid which is obtained by decelerating it in a reversible adiabatic (isentropic) process to zero velocity is known as the stagnation pressure.

The ratio of the stagnation and static pressures can be obtained from Eq. (2.61)

$$\frac{p_0}{p} = \left(\frac{T_0}{T}\right)^{\frac{\gamma}{\gamma - 1}} \tag{2.65a}$$

$$\frac{p_0}{p} = \left(1 + \frac{\gamma - 1}{2} M^2\right)^{\frac{\gamma}{\gamma - 1}} \tag{2.65b}$$

When the pressure changes are small, the process can be assumed to be incompressible ($\rho \approx$ constant). Then the stagnation pressure can be determined from the Bernoulli equation

$$p_0 = p + \frac{1}{2} \rho c^2 \tag{2.66}$$

This has been further discussed in Sec. 6.5.

2.2.9 Stagnation Density

The density of a stationary gas or vapour is the stagnation density. For a perfect gas its value at known values of stagnation temperature and pressure is given by

$$\rho_0 = \frac{p_0}{RT_0} \tag{2.67}$$

For an isentropic process from Eq. (2.30),

$$\frac{\rho_0}{\rho} = \left(\frac{T_0}{T}\right)^{\frac{1}{\gamma-1}}$$

$$\frac{\rho_0}{\rho} = \left(1+\frac{\gamma-1}{2}M^2\right)^{\frac{1}{\gamma-1}} \tag{2.68}$$

2.2.10 Stagnation State

The concept of a reference state of the gas in compressible flow machines is very useful. The stagnation state of a gas is often used as a reference state. A state defined by the stagnation temperature and pressure is the "stagnation state" of the gas. This state is obtained by decelerating a gas isentropically to zero velocity.

It should be observed that it is necessary here to qualify the deceleration process as an isentropic process. This was not necessary in defining stagnation enthalpy and temperature.

2.3 ADIABATIC FLOW THROUGH NOZZLES

A majority of steam and gas turbine stages have nozzle blade rings. The rotor blade passages of reaction turbines also behave as nozzle blade passages. The thermodynamic analysis[107] is the same for different types of nozzles irrespective of their geometrical configurations.

Figure 2.3 shows the isentropic (reversible adiabatic) and adiabatic processes through a nozzle between states 1 and 2. For a perfect gas, the temperature variations are identical with enthalpy variations. Therefore, the ordinate represents either temperature or enthalpy.

The entry conditions are represented by the pressure p_1, temperature T_1, enthalpy h_1, velocity c_1, etc. The stagnation values of various parameters can be determined by the various relations discussed earlier. Therefore, the stagnation point O_1 can be fixed. Thus the quantities p_{01}, T_{01} and h_{01} are also known.

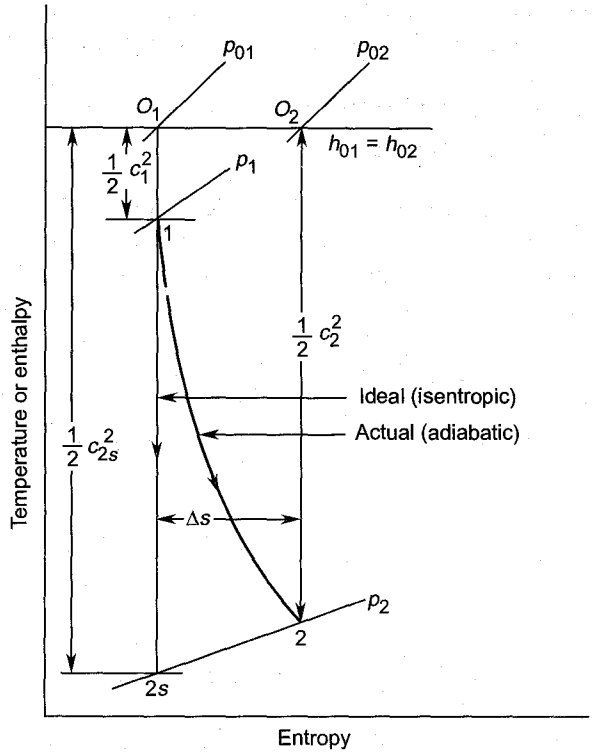

Fig. 2.3 Expansion processes in a nozzle

The final state point after isentropic expansion to pressure p_2 is $2s$. The gas velocity that would be obtained in this process would be c_{2s}. This is the ideal gas velocity and is given by

$$c_{2s}^2 = 2(h_{01} - h_{2s}) \tag{2.69a}$$

For perfect gases,

$$c_{2s}^2 = 2\ c_p(T_{01} - T_{2s}) \tag{2.69b}$$

The actual process occurring in the nozzle is the irreversible adiabatic process (1-2) leading to an increase in entropy (Δs). Thus the actual state point at the end of the process is 2 with pressure p_2, temperature T_2 and enthalpy h_2.

Since shaft work is absent here, stagnation enthalpy remains constant ($h_{01} = h_{02}$) as shown in Fig. 2.3. This enables the determination of actual velocity c_2 at the end of the expansion.

$$c_2^2 = 2(h_{02} - h_2) \tag{2.70a}$$

or

$$c_2^2 = 2c_p(T_{02} - T_2) \tag{2.70b}$$

The actual velocity c_2 is obviously lesser than the isentropic velocity c_{2s}. It is also observed that the irreversible adiabatic flow experiences an

increase in entropy Δs and a decrease in the stagnation pressure $\Delta p_0 = p_{01} - p_{02}$. This is a manifestation of the irreversibility due to losses.

2.3.1 Nozzle Efficiency for Large Pressure Ratio

The function of a nozzle is to transform the energy of the expanding gas into kinetic energy. Therefore, the nozzle efficiency should be a measure of the efficiency of this transformation. The following definition serves this purpose:

$$\eta_N = \frac{\text{actual change in the kinetic energy}}{\text{ideal change in the kinetic energy}}$$

For the energy transformation, the following relation can be written from Fig. 2.3.

$$h_{01} = h_{02} = h_1 + \frac{1}{2} c_1^2 = h_{2s} + \frac{1}{2} c_{2s}^2 = h_2 + \frac{1}{2} c_2^2 \qquad (2.71)$$

This gives

$$\text{Actual change in the kinetic energy} = \frac{1}{2}(c_2^2 - c_1^2) = h_1 - h_2$$

$$\text{Ideal change in the kinetic energy} = \frac{1}{2}(c_{2s}^2 - c_1^2) = h_1 - h_{2s}$$

Therefore,

$$\eta_N = \frac{c_2^2 - c_1^2}{c_{2s}^2 - c_1^2} = \frac{h_1 - h_2}{h_1 - h_{2s}} \qquad (2.72)$$

2.3.2 Nozzle Velocity Coefficient

In a large number of applications the gas or steam enters the nozzles from a large space. Therefore, the enthalpy at the beginning of the expansion process is considered as h_{01} instead of h_1 and the efficiency is defined in a slightly different way by the following relation:

$$\eta'_N = \frac{\text{K.E. of the actual jet at exit}}{\text{K.E. of the ideal jet at exit}} = \frac{h_{01} - h_2}{h_{01} - h_{2s}} \qquad (2.73)$$

Substituting Eq. (2.71) into Eq. (2.73),

$$\eta'_N = \left(\frac{c_2}{c_{2s}}\right)^2 = C_N^2 \qquad (2.74)$$

Equation (2.74) gives a simple relation between the nozzle velocity coefficient [9] and the nozzle efficiency[286].

If the kinetic energy term at the entry, being negligibly small, is ignored, Eq. (2.72) reduces to Eq. (2.74).

2.3.3 Nozzle Efficiency for Small Pressure Ratio

Equation (2.72) can be rewritten in the following form:

$$\eta_N = \frac{(h_1 - h_{2s}) - (h_2 - h_{2s})}{h_1 - h_{2s}}$$

$$\eta_N = 1 - \frac{h_2 - h_{2s}}{h_1 - h_{2s}} \tag{2.75}$$

In this equation, $(h_2 - h_{2s})$ is the enthalpy loss due to irreversible flow. For isentropic flow, Eq. (2.31) gives

$$\int_{h_1}^{h_{2s}} dh = \int_{p_1}^{p_2} \frac{dp}{\rho}$$

If the change in pressure is small, the flow can be considered as incompressible ($\rho \approx$ constant). Therefore,

$$h_1 - h_{2s} = \frac{1}{\rho}(p_1 - p_2) \tag{2.76}$$

Now $h_2 - h_{2s} = (h_1 - h_{2s}) - (h_1 - h_2)$

Substituting for $(h_1 - h_{2s})$ and $(h_1 - h_2)$, we get

$$h_2 - h_{2s} = \frac{1}{\rho}(p_1 - p_2) - \frac{1}{2}(c_2^2 - c_1^2)$$

$$h_2 - h_{2s} = \frac{1}{\rho}\left\{\left(p_1 + \frac{1}{2}\rho c_1^2\right) - \left(p_2 + \frac{1}{2}\rho c_2^2\right)\right\}$$

Using Eq. (2.66), we get

$$h_2 - h_{2s} = \frac{1}{\rho}(p_{01} - p_{02}) \tag{2.77}$$

Substituting Eqs. (2.76) and (2.77) in Eq. (2.75)

$$\eta_N = 1 - \frac{p_{01} - p_{02}}{p_1 - p_2} \tag{2.78}$$

Here $\Delta p_0 = p_{01} - p_{02}$ is the stagnation pressure loss across the nozzle due to irreversible flow through a pressure drop of

$$\Delta p = p_1 - p_2$$

2.3.4 Efficiency of a Two-dimensional Nozzle

Expressions for nozzle efficiency in the earlier sections have been written for uniform properties over the entry and exit sections of the nozzle. But this one-dimensional flow pattern is far from the actual flow pattern occurring at these sections. The inlet and exit areas are large and the properties vary considerably over these sections. Therefore, the following method[286] is adopted to define nozzle efficiency:

Figure 2.4 shows the cross-section of an elemental jet in the two-dimensional flow field at the exit of a nozzle.

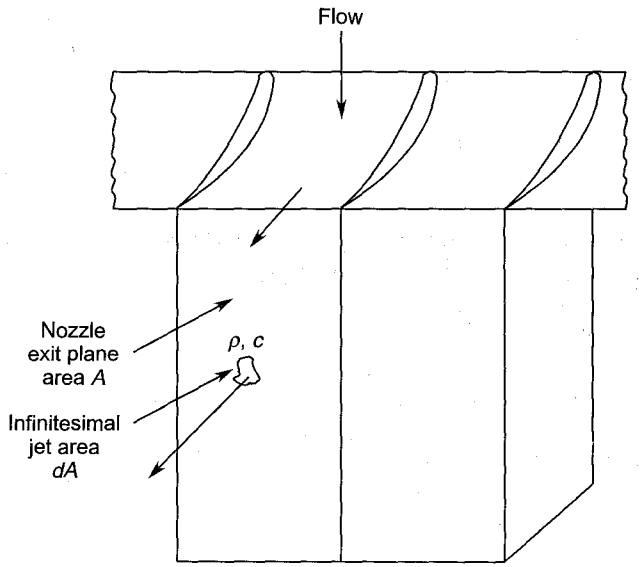

Fig. 2.4 Two-dimensional nozzle

The mass flow-rate through this jet of cross-section dA is

$$d\dot{m} = \rho\, c\, dA$$

For the entire exit section,

$$\dot{m} = \int_{A_2} \rho\, c\, d\, A \tag{2.79}$$

The force exerted by the elemental jet on a surface perpendicular to its axis is equal to the momentum lost in this direction.

$$dF = c\, d\dot{m} = \rho\, c^2\, dA$$

For the entire exit section the total force is

$$F = \int_{A2} \rho\, c^2\, d\, A \tag{2.80}$$

A truly one-dimensional jet with the same flow-rate and force has a uniform velocity c_{av}. Its magnitude, by employing Eqs. (2.79) and (2.80) is given by

$$c_{av} = \frac{F}{\dot{m}} = \frac{\int_{A2} \rho c^2 \, dA}{\int_{A2} \rho c \, dA} \tag{2.81}$$

The isentropic velocity at the exit remains the same (c_{2s}) as before. Therefore, the nozzle velocity coefficient for the two-dimensional nozzle is

$$C_N'' = \frac{\int_{A2} \rho c^2 \, dA}{c_{2s} \int_{A2} \rho c \, dA} \tag{2.82}$$

The kinetic energy of the actual elemental jet is

$$\frac{1}{2} \, d\dot{m} \, c^2 = \frac{1}{2} \, \rho \, c^3 \, dA$$

This, on integration over the entire exit section, gives:

Actual kinetic energy of the jet at exit

$$= \int_{A2} \frac{1}{2} \rho c^3 \, dA \tag{2.83}$$

The kinetic energy of the ideal jet at the exit is

$$\frac{1}{2} \, \dot{m} c_{2s}^2 = \frac{1}{2} \, c_{2s}^2 \int_{A2} \rho c \, dA \tag{2.84}$$

Substituting Eqs. (2.83) and (2.84) into Eq. (2.73) we get

$$\eta_N'' = \frac{\int_{A2} \rho c^3 \, dA}{c_{2s}^2 \int_{A2} \rho c \, dA} \tag{2.85}$$

Here it should be noted that

$$\eta_N'' \neq C_N''^2$$

If the flow is assumed to be one-dimensional, Eqs. (2.82) and (2.85) reduce to Eq. (2.74).

2.4 Adiabatic Flow Through Diffusers

Diffusers bring about the transformation of kinetic energy of gases into a static pressure rise. Such a transformation process occurs in the fixed blade rings downstream of a compressor rotor.

Figure 2.5 shows the reversible and irreversible adiabatic processes in a diffuser. The entry conditions are represented by p_1, h_1, T_1, c_1, etc.; the stagnation point O_1 can be determined from these values. Therefore, the values of the stagnation enthalpy (h_{01}) and pressure (p_{01}) are also known.

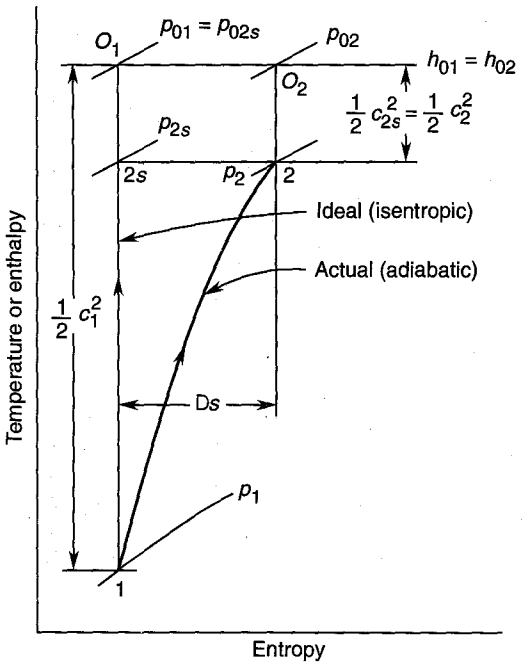

Fig. 2.5 Compression processes in a diffuser

The pressure obtained at the end of a reversible adiabatic (isentropic) diffusion process is p_{2s}. There is no change in entropy and loss of stagnation pressure.

$$\Delta s = 0$$

$$p_{01} = p_{02s}$$

The stagnation enthalpy remains constant.

$$h_{01} = h_{02s}$$

$$h_1 + \frac{1}{2}c_1^2 = h_{2s} + \frac{1}{2}c_{2s}^2 \qquad (2.86)$$

c_{2s} is the velocity at the end of the isentropic diffusion.

The actual process is irreversible adiabatic. This must be accompanied by a stagnation pressure loss and an increase in entropy. The final state in

such a process is represented by point 2. This is fixed by assuming the same change in kinetic energy, *i.e.*

$$\frac{1}{2}(c_1^2 - c_{2s}^2) = \frac{1}{2}(c_1^2 - c_2^2)$$

$$c_2 = c_{2s}$$

The irreversible diffusion on account of losses must give a lower static pressure at the end of the process. This is seen in Fig. 2.5. The stagnation enthalpy remains constant,

$$h_{01} = h_{02} = h_{02s}$$

$$h_2 = h_{2s}$$

$$\Delta p_0 = p_{01} - p_{02}$$

2.4.1 Diffuser Efficiency for Small Pressure Rise

For small rise in static pressure, the flow in the diffuser can be considered incompressible ($\rho \approx$ constant).

For incompressible isentropic process 1 – 2*s*,

$$p_{01} = p_{02s}$$

$$p_1 + \frac{1}{2}\rho c_1^2 = p_{2s} + \frac{1}{2}\rho c_{2s}^2$$

Therefore, the pressure rise is given by

$$(\Delta p)_s = p_{2s} - p_1 = \frac{1}{2}\rho (c_1^2 - c_{2s}^2) \tag{2.87}$$

For the actual state point 2,

$$p_{02} = p_2 + \frac{1}{2}\rho c_2^2 \tag{2.88}$$

Therefore, the pressure rise in the actual process is given by

$$(\Delta p)_a = p_2 - p_1$$

or
$$(\Delta p)_a = \left(p_{02} - \frac{1}{2}\rho c_2^2\right) - \left(p_{01} - \frac{1}{2}\rho c_1^2\right)$$

or
$$(\Delta p)_a = \frac{1}{2}\rho (c_1^2 - c_2^2) - (p_{01} - p_{02}) \tag{2.89}$$

But $\frac{1}{2}\rho (c_1^2 - c_2^2) = \frac{1}{2}\rho (c_1^2 - c_{2s}^2)$

Therefore, Eqs. (2.87) and (2.89) give

$$(\Delta p)_a = (\Delta p)_s - \Delta p_0 \tag{2.90}$$

The diffuser efficiency is defined by

$$\eta_D = \frac{\text{static pressure rise in the actual process}}{\text{static pressure rise in the isentropic process}}$$

$$\eta_D = \frac{(\Delta p)_a}{(\Delta p)_s} = \frac{p_2 - p_1}{p_{2s} - p_1} \tag{2.91}$$

Substituting from Eq. (2.90), Eq. (2.91) becomes

$$\eta_D = 1 - \frac{\Delta p_0}{(\Delta p)_s} \tag{2.92}$$

From Eq. (2.86), we get

$$(\Delta h)_s = h_{2s} - h_1 = \frac{1}{2}\,(c_1^2 - c_{2s}^2)$$

However, for an isentropic process

$$(\Delta h)_s = \frac{(\Delta p)_s}{\rho}$$

Therefore,

$$\eta_D = 1 - \frac{\Delta p_0}{\rho (\Delta h)_s} \tag{2.93}$$

Equations (2.87) and (2.91) give

$$\eta_D = \frac{2\,(p_2 - p_1)}{\rho\,(c_1^2 - c_2^2)} \tag{2.94}$$

The quantities that can be measured are Δp_0 and $(\Delta p)_a$. Therefore, an expression for diffuser efficiency in terms of these quantities is more useful.

Rewriting Eq. (2.91) with the help of Eq. (2.90)

$$\eta_D = \frac{(\Delta p)_a}{(\Delta p)_a + \Delta p_0}$$

$$\eta_D = \frac{1}{1 + \Delta p_0/(\Delta p)_a}$$

$$\eta_D = \frac{1}{1 + (p_{01} - p_{02})/(p_2 - p_1)} \tag{2.95}$$

2.4.2 Pressure Recovery Coefficient for Small Pressure Rise

A diffuser converts kinetic energy of the gas into static pressure through an area change in its passage. The pressure rise in a reversible

diffuser for a given velocity at entry is an explicit function of its area ratio

$$A_r = \frac{A_2}{A_1} \tag{2.96}$$

Continuity for incompressible flow gives

$$\rho A_1 c_1 = \rho A_2 c_{2s}$$

$$\Delta s = 0$$

$$\frac{c_1}{c_2} = \frac{c_1}{c_{2s}} = A_r \tag{2.97}$$

Equation (2.87) gives

$$p_{2s} - p_1 = \frac{1}{2} \rho c_1^2 \left(1 - \frac{c_{2s}^2}{c_1^2}\right)$$

The pressure recovery coefficient is defined by

$$C_{ps} = \frac{p_{2s} - p_1}{\frac{1}{2} \rho c_1^2} = 1 - \frac{c_{2s}^2}{c_1^2} \tag{2.98}$$

Introducing the area ratio from Eq. (2.97), the ideal or isentropic pressure recovery coefficient is

$$C_{ps} = 1 - \frac{1}{A_r^2} \tag{2.99}$$

The actual pressure recovery will be lower than this ideal value

$$C_{pa} = \frac{p_2 - p_1}{\frac{1}{2} \rho c_1^2} \tag{2.100}$$

$$C_{pa} = \frac{(p_{2s} - p_1) - \Delta p_0}{\frac{1}{2} \rho c_1^2}$$

$$= C_{ps} - \frac{\Delta p_0}{\frac{1}{2} \rho c_1^2} \tag{2.101}$$

Equations (2.91) and (2.100) yield

$$C_{pa} = \frac{\eta_D (p_{2s} - p_1)}{\frac{1}{2} \rho c_1^2}$$

or

$$C_{pa} = \eta_D \times C_{ps}$$

$$\eta_D = \frac{C_{pa}}{C_{ps}} \tag{2.102}$$

Thus diffuser efficiency can also be defined as the ratio of the actual and ideal coefficients of pressure recovery.

2.4.3 Diffuser Efficiency for Large Pressure Rise

For a large pressure rise through a diffuser, the density change is appreciable and the flow is compressible.

Therefore,

$$c_{2s} \neq c_2$$

However, their values are still governed by the energy equation [Eq. (2.86)],

Figure 2.6 shows the ideal and actual diffusion processes to the same final pressure (p_2). The ideal or isentropic process gives the same pressure

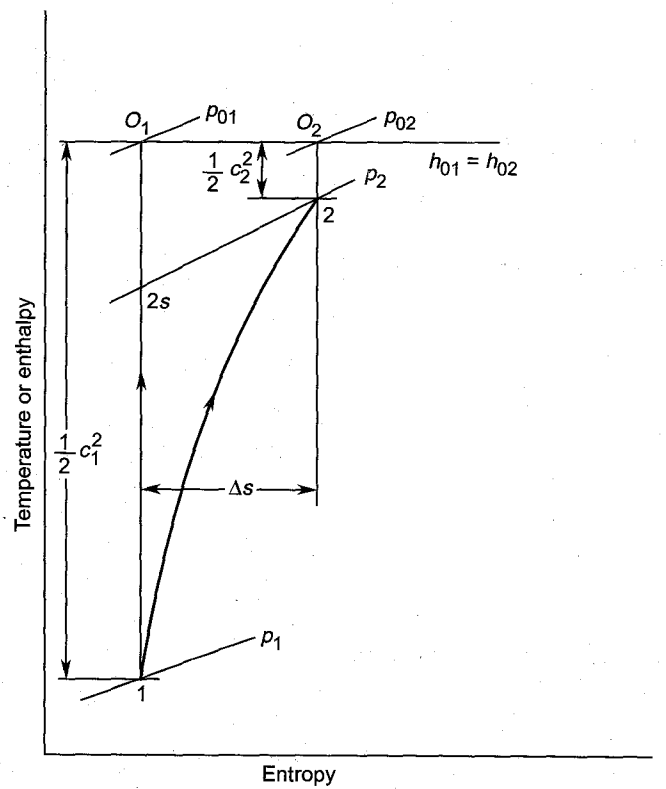

Fig. 2.6 Compression processes in a diffuser

rise $(p_2 - p_1)$ for a smaller change in kinetic energy $(c_1^2/2 - c_{2s}^2/2)$. In the actual process the corresponding change in the kinetic energy is $(c_1^2/2 - c_2^2/2)$. Therefore, the diffuser efficiency is defined by

$$\eta'_D = \frac{\text{change of kinetic energy in the ideal process}}{\text{change of kinetic energy in the actual process}}$$

$$\eta'_D = \frac{c_1^2 - c_{2s}^2}{c_1^2 - c_2^2} \tag{2.103}$$

Rewriting the energy equation [Eq. (2.86)] for the processes shown in Fig. 2.6, we have

$$h_1 + \frac{1}{2} c_1^2 = h_{2s} + \frac{1}{2} c_{2s}^2 = h_2 + \frac{1}{2} c_2^2$$

$$\frac{1}{2} (c_1^2 - c_{2s}^2) = h_{2s} - h_1$$

$$\frac{1}{2} (c_1^2 - c_2^2) = h_2 - h_1$$

Substituting these values in Eq. (2.103),

$$\eta'_D = \frac{h_{2s} - h_1}{h_2 - h_1} \tag{2.104}$$

For incompressible flow, this expression can be reduced to the expressions derived in Eqs. (2.91) to (2.95). For instance, Eq. (2.94) is derived here from Eq. (2.104).

For incompressible and isentropic process $1 - 2s$,

$$\int_1^{2s} dh = \frac{1}{\rho} \int_1^{2s} dp$$

$$h_{2s} - h_1 = \frac{1}{\rho} (p_2 - p_1)$$

Therefore, from Eq. (2.104),

$$\eta'_D = \frac{2 (p_2 - p_1)}{\rho (c_1^2 - c_2^2)}$$

which is Eq. (2.94).

2.5 Work and Efficiencies in Turbine Stages

Work and efficiency expressions [11] are developed here for expansion in the turbine stages. Energy equation in its various forms and the concepts

discussed for nozzles will be employed here also. However, an important difference on account of the presence of shaft work must be remembered.

Figure 2.7 shows some properties of a gas (or vapour) at the entry and exit of a turbine or turbine stage. On account of the expanding flow, the low pressure side of the turbine casing is shown larger than the high pressure side (Fig. 2.7); the converse is true for compressors.

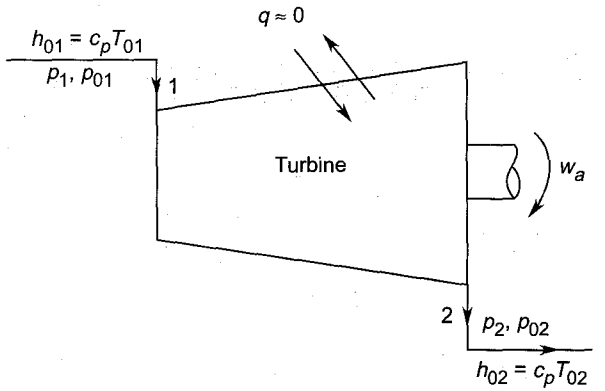

Fig. 2.7 Expansion in a turbine

The flow processes in both turbines and compressors (as in nozzles and diffusers) considered here are assumed adiabatic ($q \approx 0$). This is true in practice because of proper heat insulation of the casings.

Figure 2.8 depicts the reversible and irreversible adiabatic processes in the enthalpy-entropy coordinates. The entry conditions are represented by the parameters p_1, h_1, T_1, c_1, etc. The stagnation values p_{01}, h_{01} and T_{01} are also known.

The state of the gas at the exit in an isentropic process is represented by point $2s$; various parameters at this point are p_2, h_{2s}, T_{2s}, c_{2s}, etc. On account of generation of shaft work (w_s), there is a drop in stagnation enthalpy (or temperature). However, the entropy remains constant on account of the isentropic process.

The actual expansion (irreversible adiabatic) through the turbine to the same exit pressure is represented by the line 1–2. Various parameters at this state are p_2, h_2, T_2, c_2, etc. On account of irreversibility, there is an increase in entropy. The final stagnation pressure (p_{02s} or p_{02}) cannot be compared with its initial value (p_{01}) because of work transfer.

The actual work at the turbine shaft can be determined from the difference in actual stagnation enthalpies at the entry and exit. This is shown in Fig. 2.8.

$$w_a = h_{01} - h_{02} \tag{2.105a}$$

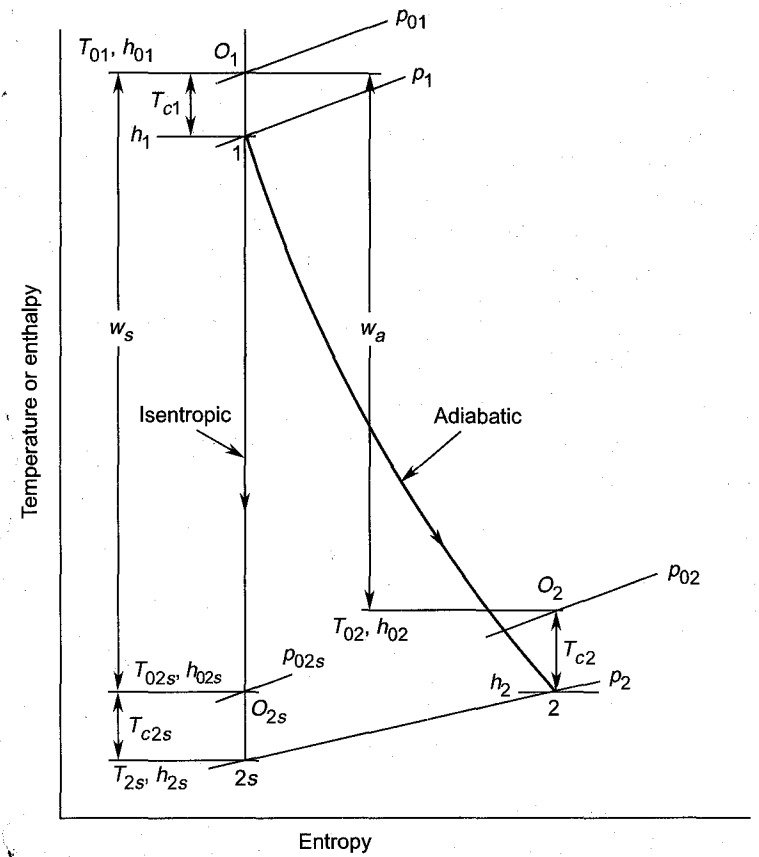

Fig. 2.8 Ideal and actual expansion processes in a turbine stage

For perfect gases,

$$w_a = c_p (T_{01} - T_{02}) \tag{2.105b}$$

The actual power can be determined by multiplying the above quantity with the mass flow rate.

2.5.1 Total-to-total Efficiency

The efficiency of a turbine is defined as the ratio of the actual work to the ideal work for the same pressure ratio ($p_r = p_1/p_2$). While the actual shaft work is something real that can be measured, the ideal work is hypothetical and depends on the manner it is defined. The ideal work (w_s) as shown in Fig. 2.8 is the work that would be obtained during the isentropic expansion of the gas from the stagnation state O_1 to state O_{2s}.

Here the kinetic energy of the gas ($c_{2s}^2/2$) is not considered as wasted because it is contained in the term h_{02s} ($h_{2s} + c_{2s}^2/2$).

$$w_s = h_{01} - h_{02s} = c_p\,(T_{01} - T_{02s}) \tag{2.106}$$

This is true for:

(a) An aircraft gas turbine which exhausts into the main propulsion nozzle; here the kinetic energy ($c_{2s}^2/2$) is a part of the energy supplied at the entry of the propulsion nozzle.

(b) A preceding stage exhausting into the following stage in a multistage turbine.

The efficiency defined on the basis of this ideal work is known as the total-to-total efficiency.

$$\eta_{tt} = \frac{\text{actual shaft work}}{\text{ideal shaft work between total conditions at entry and exit}}$$

$$\eta_{tt} = \frac{w_a}{w_s}$$

Equations (2.105) and (2.106) give

$$\eta_{tt} = \frac{h_{01} - h_{02}}{h_{01} - h_{02s}}$$

$$= \frac{T_{01} - T_{02}}{T_{01} - T_{02s}} \tag{2.107}$$

The stagnation pressure lines for p_{02s} and p_{02} are different. However, the distance between them is small. The stagnation pressure ratio is

$$p_{r0} = \frac{p_{01}}{p_{02s}} \approx \frac{p_{01}}{p_{02}} \tag{2.108}$$

$$T_{01} - T_{02s} = T_{01}\left\{1 - \frac{1}{T_{01}/T_{02s}}\right\}$$

$$T_{01} - T_{02s} = T_{01}\left\{1 - (p_{r0})^{-\frac{\gamma-1}{\gamma}}\right\}$$

This expression when substituted in Eq. (2.107) gives

$$\eta_{tt} = \frac{T_{01} - T_{02}}{T_{01}\left\{1 - (p_{r0})^{-\frac{\gamma-1}{\gamma}}\right\}} \tag{2.109}$$

For a given entry stagnation temperature, pressure ratio and efficiency the output power at the shaft is

$$W_a = \dot{m}\ c_p\ (T_{01} - T_{02})$$

$$W_a = \dot{m}\ \eta_{tt}\ c_p\ T_{01} \left\{1 - (p_{r0})^{\frac{1-\gamma}{\gamma}}\right\} \tag{2.110}$$

2.5.2 Total-to-static Efficiency

Some turbine stages exhaust into the atmosphere or in a closed space like the condensor; here the kinetic energy ($c_{2s}^2/2$) of the outgoing jet is lost because it is not used after the turbine. In such a case the ideal work is the isentropic work done between the states O_1 and $2s$.

$$w_s' = h_{01} - h_{2s} = c_p\ (T_{01} - T_{2s}) \tag{2.111}$$

The value of the actual shaft work is same as before because it does not depend on the manner of defining turbine efficiency. Therefore, total to static efficiency is given by

$$\eta_{ts} = \frac{h_{01} - h_{02}}{h_{01} - h_{2s}} = \frac{T_{01} - T_{02}}{T_{01} - T_{2s}} \tag{2.112}$$

If
$$p'_r = p_{01}/p_2 \tag{2.113}$$

$$T_{01} - T_{2s} = T_{01} \left\{1 - (p'_r)^{-\frac{\gamma-1}{\gamma}}\right\}$$

$$\eta_{ts} = \frac{T_{01} - T_{02}}{T_{01}\left\{1 - (p'_r)^{-\frac{\gamma-1}{\gamma}}\right\}} \tag{2.114}$$

Comparing the expressions for the total-to-total and total-to-static efficiencies for the same boundary conditions it can be inferred that

$$\eta_{tt} > \eta_{ts}$$

2.5.3 Finite Stage Efficiency

A stage with a finite pressure drop is a finite stage. The efficiency and work relations derived in Secs. 2.5.1 and 2.5.2 apply to a finite turbine stage.

In a multi-stage turbine along with the overall efficiency (η_T), the efficiencies (η_{s1}, η_{s2}, .) of the individual stages are important. On account of a large pressure drop and the associated thermodynamic effect, the overall efficiency is not a true index of the aerodynamic or hydraulic performance

of the machine. The same is true of a single stage with a finite pressure drop. Different stages with the same pressure ratio located in different regions in the $h - s$ plane will give different values of the work output.

Equation (2.34a) for a steady flow process is

$$dw = - v\, dp$$

This shows that for the same pressure drop, more work will be done with higher values of v; this is true in the L.P. (low pressure) stages of large multi-stage steam turbines.

Another aspect of interest here is that the stage work is proportional to the initial temperature of the gas [see Eq. (2.110)].

2.5.4 Effect of Reheat

The thermodynamic effect on the turbine efficiency can be best understood by considering a number of stages between two states 1 and 2 as shown in Fig. 2.9. The total expansion is divided into four stages of the same efficiency (η_{st}) and pressure ratio.

$$\frac{p_1}{p_x} = \frac{p_x}{p_y} = \frac{p_y}{p_z} = \frac{p_z}{p_2} \tag{2.115}$$

The overall efficiency of expansion is η_T.

Therefore, the actual work during the expansion from 1 to 2 is

$$w_a = \eta_T\, w_s \tag{2.116}$$

The values of ideal or isentropic work in the stages are Δw_{s1}, Δw_{s2}, Δw_{s3} and Δw_{s4}. Therefore, the total value of the actual work in these stages is

$$w_a = \Sigma\, \Delta w_a = \Sigma\, \eta_{st}\, \Delta w_s = \eta_{st}\, \Sigma\, \Delta w$$

$$w_a = \eta_{st}\, (\Delta w_{s1} + \Delta w_{s2} + \Delta w_{s3} + \Delta w_{s4}) \tag{2.117}$$

Equations (2.116) and (2.117) give

$$\eta_T\, w_s = \eta_{st}\, \Sigma\, \Delta w_s$$

$$\eta_T = \eta_{st}\, \frac{\Sigma \Delta w_s}{w_s} \tag{2.118}$$

The slope of the constant pressure lines on the $h - s$ plane is given by

$$\left(\frac{\partial h}{\partial s}\right)_p = T \tag{2.119}$$

Equation (2.119) shows that the constant pressure lines must diverge towards the right. Therefore, referring to Fig. 2.9,

$$\frac{\Sigma \Delta w_s}{w_s} > 1 \tag{2.120}$$

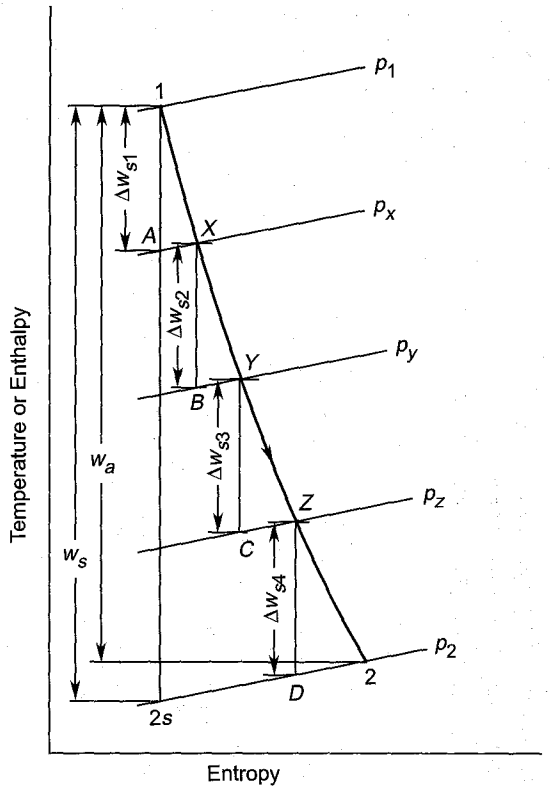

Fig. 2.9 Effect of reheating on expansion in turbine stage

This makes the overall efficiency of the turbine greater than the individual stage efficiency. Substituting Eq. (2.120) in Eq. (2.118), we get

$$\eta_T > \eta_{st} \tag{2.121}$$

The quantity $\Sigma \Delta w_s / w_s$ is known as the reheat factor and is always greater than unity.

The effect depicted by Eq. (2.121) is due to a thermodynamic effect called "reheat". This does not imply any heat transfer to the stages from outside. It is merely the reappearance of stage losses as increased enthalpy during the constant pressure heating (or reheating) processes AX, BY, CZ and D2.

2.5.5 Infinitesimal Stage Efficiency

To see the true aerodynamic performance of a stage, the concept of a small or infinitesimal stage is employed. This is an imaginary stage with an infinitesimal pressure drop and is therefore independent of the reheat effect. A finite stage can be divided into an infinite number of small stages of the same efficiencies.

An expression for the infinitesimal stage efficiency (η_p) for a perfect gas is derived here.

Figure 2.10 shows a small stage between pressures p and $(p - dp)$. This is one of the infinite number of stages between states 1 and 2 of a finite stage or a multi-stage machine.

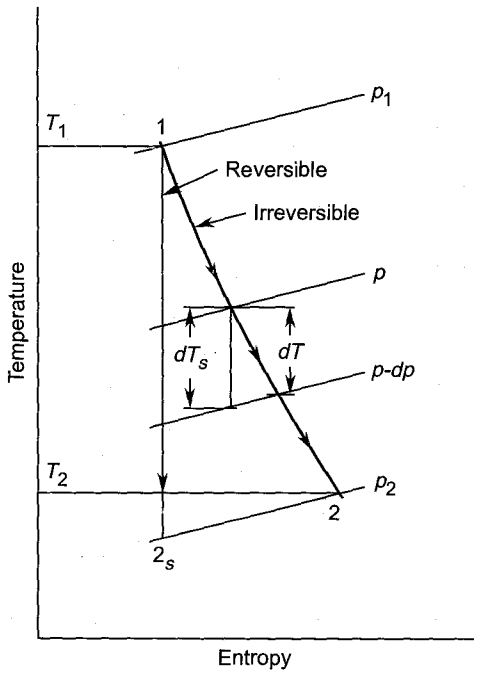

Fig. 2.10 Infinitesimal and finite expansion processes

The pressure and temperature at the entry of the small stage are p and T respectively. The isentropic and actual temperature drops are dT_s and dT respectively. Therefore, the efficiency of such a stage is

$$\eta_p = \frac{\text{actual temperature drop}}{\text{isentropic temperature drop}}$$

$$\eta_p = \frac{dT}{dT_s} \tag{2.122}$$

For infinitesimal isentropic expansion,

$$\frac{T - dT_s}{T} = \left(\frac{p - dp}{p}\right)^{\frac{\gamma-1}{\gamma}}$$

$$1 - \frac{dT_s}{T} = \left(1 - \frac{dp}{p}\right)^{\frac{\gamma-1}{\gamma}}$$

Expanding the binomial expression on the right-hand side and ignoring terms beyond the second,

$$1 - \frac{dT_s}{T} = 1 - \frac{\gamma - 1}{\gamma}\frac{dp}{p}$$

$$\frac{dT_s}{T} = \frac{\gamma - 1}{\gamma}\frac{dp}{p}$$

Substituting from Eq. (2.122) for dT_s,

$$\frac{dT}{T} = \frac{\gamma - 1}{\gamma}\eta_p \frac{dp}{p} \tag{2.123}$$

This is the differential equation valid along the actual expansion process 1-2. This on integration yields

$$\ln T + \ln \text{const.} = \ln p^{\frac{\gamma-1}{\gamma}\eta_p}$$

$$\frac{p^{\frac{\gamma-1}{\gamma}\eta_p}}{T} = \text{const.} \tag{2.124}$$

This relation defines the actual expansion line in a finite stage or a multi-stage machine between two given states 1 and 2 (Fig. 2.10).

Here the value of the infinitesimal or small stage efficiency (η_p) is constant. However, to be able to use Eq. (2.124) for a given expansion between finite states, the value of (η_p) must first be determined.

Integrating Eq. (2.123) between the given states 1 and 2,

$$\int_{T_1}^{T_2} \frac{dT}{T} = \frac{\gamma - 1}{\gamma}\eta_p \int_{p_1}^{p_2} \frac{dp}{p}$$

$$\ln\left(\frac{T_2}{T_1}\right) = \frac{\gamma - 1}{\gamma}\eta_p \ln\left(\frac{p_2}{p_1}\right)$$

$$\eta_p = \frac{\frac{\gamma}{\gamma - 1}\ln\left(\frac{T_2}{T_1}\right)}{\ln\left(\frac{p_2}{p_1}\right)} = \frac{\ln\left(\frac{T_2}{T_1}\right)}{\ln\left(\frac{T_{2s}}{T_1}\right)} \tag{2.125}$$

$$\frac{T_2}{T_1} = \left(\frac{p_2}{p_1}\right)^{\frac{\gamma-1}{\gamma}\eta_p} \tag{2.126}$$

The irreversible adiabiatic (actual) expansion process can be considered as equivalent to a polytropic process (hence the term polytropic efficiency) with index n. Thus Eq. (2.126) can be written as

$$\frac{T_2}{T_1} = \left(\frac{p_2}{p_1}\right)^{\frac{\gamma-1}{\gamma}\eta_p} = \left(\frac{p_2}{p_1}\right)^{\frac{n-1}{n}}$$

Equating the indices,

$$\frac{\gamma-1}{\gamma}\eta_p = \frac{n-1}{n}$$

$$\eta_p = \frac{n-1}{n}\,\frac{\gamma}{\gamma-1} \tag{2.127}$$

The index of expansion in the actual process is given by

$$n = \frac{\gamma}{\gamma-(\gamma-1)\eta_p} \tag{2.128}$$

When $\eta_p = 1$, $n = \gamma$. The actual expansion line coincides with the isentropic expansion and Eqs. (2.123), (2.124) and (2.126) are valid for an isentropic process.

The efficiency of a finite stage can now be expressed in terms of the small stage efficiency. Taking static values of temperature and pressure and assuming perfect gas,

$$\eta_{st} = \frac{T_1 - T_2}{T_1 - T_{2s}}$$

$$T_1 - T_2 = T_1\left(1 - \frac{T_2}{T_1}\right) = T_1\left\{1 - \frac{1}{p_r^{\frac{\gamma-1}{\gamma}\eta_p}}\right\}$$

$$T_1 - T_{2s} = T_1\left(1 - \frac{T_{2s}}{T_1}\right) = T_1\left\{1 - \frac{1}{p_r^{\frac{\gamma-1}{\gamma}}}\right\}$$

$$\eta_{st} = \frac{1 - p_r^{-\frac{\gamma-1}{\gamma}\eta_p}}{1 - p_r^{-\frac{\gamma-1}{\gamma}}} \tag{2.129a}$$

$$\eta_{st} = f(p_r,\ \eta_p) \tag{2.129b}$$

Equation (2.129a) is also applicable to a multi-stage turbine. In that case η_{st} and p_r are replaced by the overall efficiency and overall pressure ratio of the machine.

Equation (2.129a) is useful because it can predict efficiencies of various finite expansion processes with different values of the pressure ratio and small stage efficiency.

Figure 2.11 shows qualitatively the variation of the stage efficiency with the pressure ratio for various values of the small stage efficiency. The curves in the vicinity of $p_r = 1$ are shown dotted. This is because it is not possible to have a stage with $p_r = 1$. However, in a region close to $p_r = 1$, the stage efficiency has the minimum value of $\eta_{st} = \eta_p$. On account of the reheat effect, the stage efficiency is always greater than the small stage efficiency. The difference between the two efficiencies goes on increasing with the pressure ratio due to the cumulative effect of reheating.

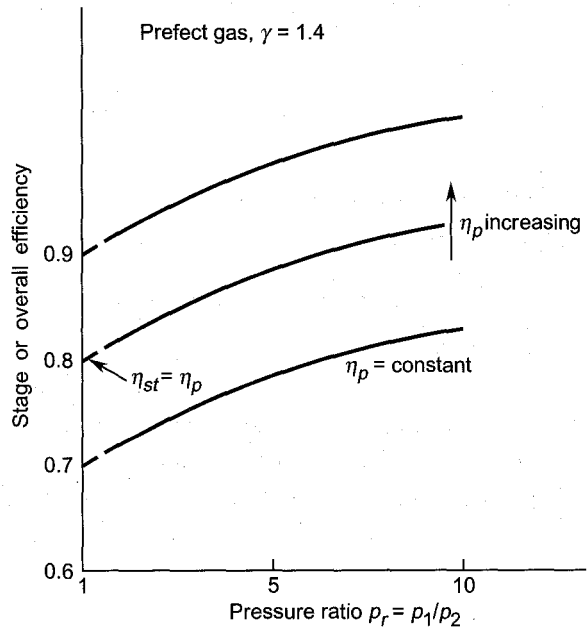

Fig. 2.11 Variation of stage efficiencies with pressure ratio at η_p = constant

In a given design η_p is the bottom line of the turbine performance.

2.5.6 Multi-stage Turbines

Thermodynamic analysis of multi-stage steam and gas turbines becomes different on account of a number of factors:

(a) While perfect gas laws can be applied in the case of gas turbine stages, they cannot be applied for all the steam turbine stages.

(b) Multi-stage steam turbines have much larger number of stages compared to those in gas turbines. In large steam turbines of 200 MW and above, the number of stages may be more than thirty. Therefore, the distribution of work in various stages is based on considerations of the overall length of the machine. It will be shown later that for a given overall pressure drop, impulse stages give the shortest length of the machine.

(c) On account of a large change in the specific volume of steam from the entry to the exit, the mean diameters of the L.P. stages are much larger than those of H.P (high pressure) stages. Since the stage work and enthalpy drop are proportional to the square of the peripheral speed of the rotor, the pressure drop in the L.P. stages will be much higher as compared to similar stages in the H.P. region.

Here some aspects of multi-stage turbines operating on a perfect gas are discussed.

2.5.7 Multi-stage Machine with Constant Stage Pressure Ratio

Let there be k stages with a constant stage pressure ratio

$$p_r = \frac{p_1}{p_2} = \frac{p_2}{p_3} = \ldots = \frac{p_i}{p_{i+1}} = \ldots = \frac{p_k}{p_{k+1}} \tag{2.130}$$

If the polytropic efficiency is η_p = constant, the efficiency of various stages is given by Eq. (2.129a) and remains constant.

The overall pressure ratio of the entire machine is given by

$$(p_r)_T = (p_r)^k = \frac{p_1}{p_{k+1}} \tag{2.131}$$

Therefore, the overall efficiency of the machine is

$$\eta_T = \frac{1-(p_r)^{\frac{1-\gamma}{\gamma} k \eta_p}}{1-(p_r)^{\frac{1-\gamma}{\gamma} k}} \tag{2.132}$$

Figure 2.12 shows the expansion of a gas in various stages of a k-stage turbine. The pressure ratio of the ith stage is p_i/p_{i+1} and that of the kth stage p_k/p_{k+1}.

The stage work is proportional to the gas temperature at its entry. Therefore, it goes on decreasing in the subsequent stages.

For the first stage,

$$\Delta T_1 = T_1 - T_2$$

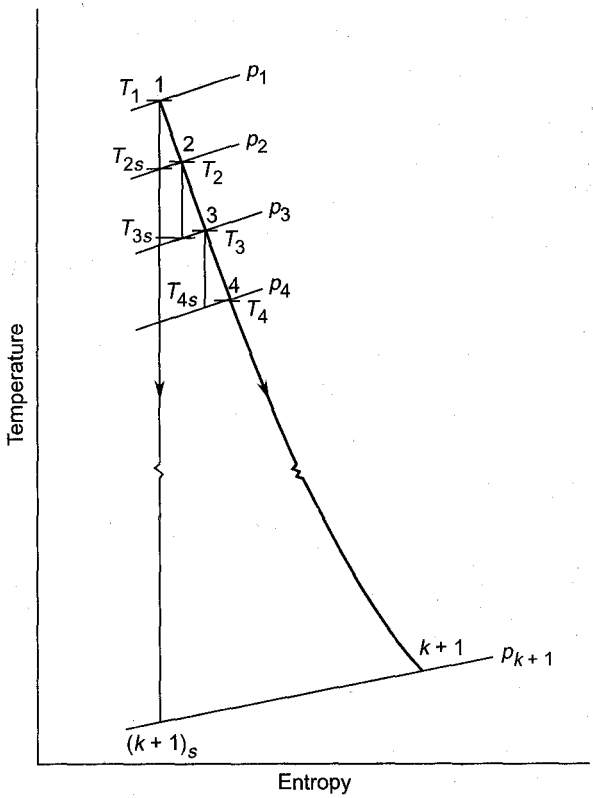

Fig. 2.12 Expansion processes in the stages of a muiti-stage turbine

$$\Delta T_1 = T_1 \left\{1 - p_r^{\frac{1-\gamma}{\gamma}\eta_p}\right\} = C\ T_1 \tag{2.133}$$

$$C = 1 - p_r^{\frac{1-\gamma}{\gamma}\eta_p} = \text{const.} \tag{2.134}$$

In the second stage,

$$\Delta T_2 = T_2 - T_3$$

$$\Delta T_2 = C\ T_2$$

But $$T_2 = T_1 - \Delta T_1 = (1 - C)\ T_1$$

Therefore,

$$\Delta T_2 = C\ (1 - C)\ T_1 \tag{2.135}$$

Similarly

$$\Delta T_3 = C\ (1 - C)^2\ T_1 \tag{2.136}$$

$$\Delta T_i = C\ (1 - C)^{i-1}\ T_1 \tag{2.137}$$

$$\Delta T_k = C\ (1 - C)^{k-1}\ T_1 \tag{2.138}$$

Thus the total actual temperature drop in the turbine is

$$(\Delta T)_T = \Delta T_1 + \Delta T_2 + \ldots + \Delta T_k$$

$$= \sum_{i=1}^{k} C(1 - C)^{i-1} T_1 \tag{2.139}$$

$$(\Delta T)_T = [1 - (1 - C)^k] T_1 \tag{2.140}$$

Substituting for C from Eq. (2.134), Eq. (2.140) becomes

$$(\Delta T)_T = \left[1 - p_r^{\frac{1-\gamma}{\gamma} k\eta}\right] T_1 \tag{2.141}$$

This relation can be obtained directly by applying Eq. (2.126) for the actual expansion line between points 1 and $k + 1$.

2.5.8 Multi-stage Machine with Constant Stage Work

If the actual work in each stage is the same, the total temperature drop $(\Delta T)_T$ is equally divided in k stages. The stage temperature drop is given by

$$(\Delta T)_{st} = \frac{1}{k} (\Delta T)_T = \frac{1}{k}\left[1 - (p_r)_T^{\frac{1-\gamma}{\gamma}\eta_p}\right] T_1 \tag{2.142}$$

This condition gives the values of the pressure ratios of various stages. For the ith stage

$$(\Delta T)_{st} = (\Delta T)_i = T_i - T_{i+1} = T_i \left[1 - \frac{1}{p_{ri}^{\frac{\gamma-1}{\gamma}\eta_p}}\right]$$

$$\left(\frac{\Delta T}{T}\right)_i = 1 - p_{ri}^{\frac{1-\gamma}{\gamma}\eta_p}$$

$$p_{ri} = \left(1 - \frac{\Delta T_i}{T_i}\right)^{\frac{\gamma}{1-\gamma}\frac{1}{\eta_p}} \tag{2.143}$$

Since all the other quantities except T_i are constant in the above equation, each subsequent stage will have a higher pressure ratio.

2.6 Work and Efficiencies in Compressor Stages

Expressions for work and various efficiencies are developed here for compressor stages. Concepts developed earlier for diffusers are also employed here, remembering the presence of shaft work.

Figure 2.13 shows a steady flow process through a turbo-compressor. The actual work supplied to the compressor from the prime mover is w_a. Due to energy transfer from the rotor or rotors to the gas (or vapour) its properties change from p_1, p_{01}, h_1, etc. to p_2, p_{02}, h_2, etc. As mentioned before, the compression process is assumed to be adiabatic.

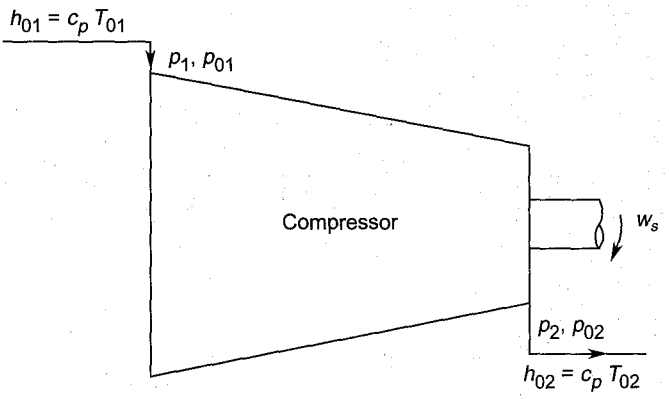

Fig. 2.13 Compression in a compressor

Figure 2.14 represents the reversible and irreversible adiabatic compression processes on the temperature-entropy coordinates. The initial state of the gas is represented by p_1, T_1, h_1, etc., the velocity of the gas is c_1. Therefore, the stagnation point O_1 is known.

The state of the gas at the exit with the isentropic work transfer (w_s) is represented by point 2*s*. Various parameters at this point are p_2, T_{2s}, h_{2s} and c_{2s}; the stagnation point corresponding to this process is O_{2s}. The entropy remains constant.

The actual compression (adiabatic) is along the process 1-2. Various parameters at the final state 2 are p_2, T_2, h_2, and c_2; the stagnation point O_2, is also known. On account of irreversibility entropy increases during the process.

The actual work (w_a) supplied during adiabatic compression is given by the energy equation between the stagnation states O_1 and O_2. Its value as shown in Fig. 2.14 is given by

$$w_a = h_{02} - h_{01} \tag{2.144a}$$

For perfect gases,

$$w_a = c_p (T_{02} - T_{01}) \tag{2.144b}$$

The actual power required is $\dot{m}\ w_a$.

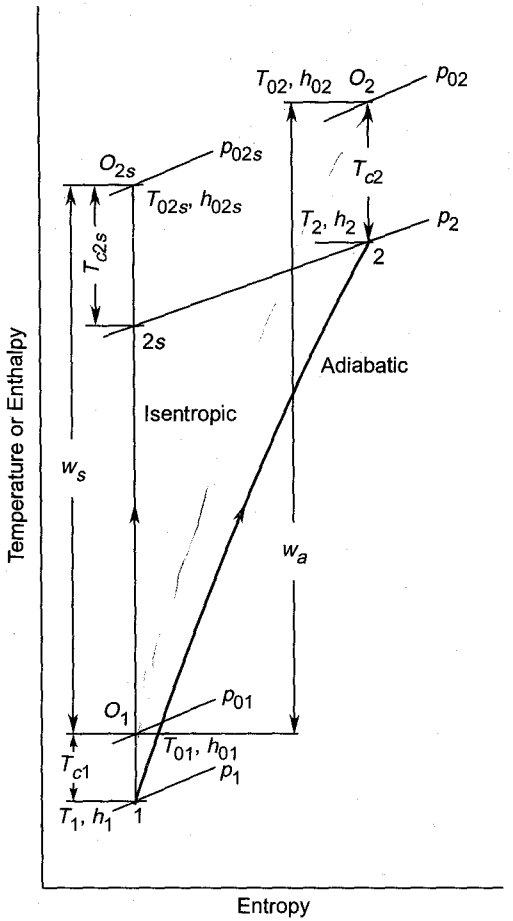

Fig. 2.14 Ideal and actual compression processes in a compressor stage

2.6.1 Total-to-total Efficiency

As explained in Sec. 2.5.1 for turbines, the actual shaft work (w_a) in a compressor is also a real quantity that can be measured. Its magnitude does not depend on its definition. In contrast to this the ideal work which is used to compare the actual work depends on the manner in which it is defined. If it is defined along the isentropic compression process between the stagnation states O_1 and O_{2s}, its value is given by

$$w_s = h_{02s} - h_{01} \tag{2.145a}$$

For perfect gases,

$$w_s = c_p (T_{02s} - T_{01}) \tag{2.145b}$$

The efficiency defined on the basis of this ideal work is the total-to-total efficiency.

$$\eta_{tt} = \frac{\text{ideal work between the stagnation states}}{\text{actual work}}$$

$$\eta_{tt} = \frac{h_{02s} - h_{01}}{h_{02} - h_{01}} = \frac{T_{02s} - T_{01}}{T_{02} - T_{01}} \tag{2.146}$$

The stagnation pressure ratio is

$$p_{r0} = \frac{p_{02s}}{p_{01}} \approx \frac{p_{02}}{p_{01}} \tag{2.147}$$

$$T_{02s} - T_{01} = T_{01}\,(p_{r0}^{\frac{\gamma-1}{\gamma}} - 1)$$

Therefore,

$$\eta_{tt} = \frac{T_{01}\,(p_{r0}^{\frac{\gamma-1}{\gamma}} - 1)}{T_{02} - T_{01}} \tag{2.148}$$

This efficiency is used in compressor stages where the gas velocities at the entry and exit are significant and the velocity temperatures T_{c1} and T_{c2s} cannot be ignored.

The shaft power required at the compressor coupling is

$$W_a = \dot{m}\ c_p\,(T_{02} - T_{01})$$

$$W_a = \dot{m}\ c_p \frac{T_{01}}{\eta_{tt}}\,(p_{r0}^{\frac{\gamma-1}{\gamma}} - 1) \tag{2.149}$$

This should be further divided by the mechanical efficiency to obtain the power of the prime mover.

2.6.2 Static-to-static Efficiency

If the gas velocities at entry and exit of a stage are almost equal, or their magnitudes are negligible, the actual and ideal works are

$$h_{02} - h_{01} = h_2 - h_1 = c_p\,(T_2 - T_1)$$

$$h_{02s} - h_{01} = h_{2s} - h_1 = c_p\,(T_{2s} - T_1)$$

An efficiency based on the above values is known as the static-to-static efficiency η_{ss}.

$$\eta_{ss} = \frac{h_{2s} - h_1}{h_2 - h_1} = \frac{T_{2s} - T_1}{T_2 - T_1} \tag{2.150}$$

$$T_{2s} - T_1 = T_1\,(p_r^{\frac{\gamma-1}{\gamma}} - 1)$$

where $p_r = p_2/p_1$ = static pressure ratio

$$\eta_{ss} = \frac{T_1 (p_r^{\frac{\gamma-1}{\gamma}} - 1)}{T_2 - T_1} \tag{2.151}$$

This expression is also applicable to a multi-stage compressor. For many applications the two efficiencies for compressors have almost identical values.

2.6.3 Finite Stage Efficiency

A compressor stage with a finite pressure rise is known as a finite stage. Efficiency and work relations derived in Secs. 2.6.1 and 2.6.2 are applicable to such a stage.

The stage work is a function of the initial temperature (T_{01} or T_1) and the pressure ratio. For the same pressure ratio, the stage requires a higher value of work with higher entry temperature.

Thus compressor stages in the higher temperature region suffer on account of this fact.

Equation (2.34a), viz. $dw = -v\,dp$, also suggests that the compression work for the same pressure rise is large at larger values of the specific volume of the gas.

The above-mentioned factors have a cumulative effective on the efficiency of a multi-stage compressor. This is explained in the following sections.

2.6.4 Effect of Preheat

To study the thermodynamic effect of multi-stage compression, a four-stage compressor is considered in Fig. 2.15. The total compression between pressures p_1 and p_2 is divided into four stages of the same pressure ratio and efficiency.

$$\frac{p_x}{p_1} = \frac{p_y}{p_x} = \frac{p_z}{p_y} = \frac{p_2}{p_z}$$

The total isentropic work from state 1 to 2s is w_s. The isentropic works in the stages are Δw_{s1}, Δw_{s2}, Δw_{s3} and Δw_{s4} as shown in Fig. 2.15.

If the overall efficiency of the compressor is η_c, the total actual work is

$$w_a = \frac{1}{\eta_c} w_s$$

This is also given by the sum of actual works in the stages.

$$w_a = \sum \Delta w_a = \sum \frac{1}{\eta_{st}} \Delta w_s = \frac{1}{\eta_{st}} \sum \Delta w_s$$

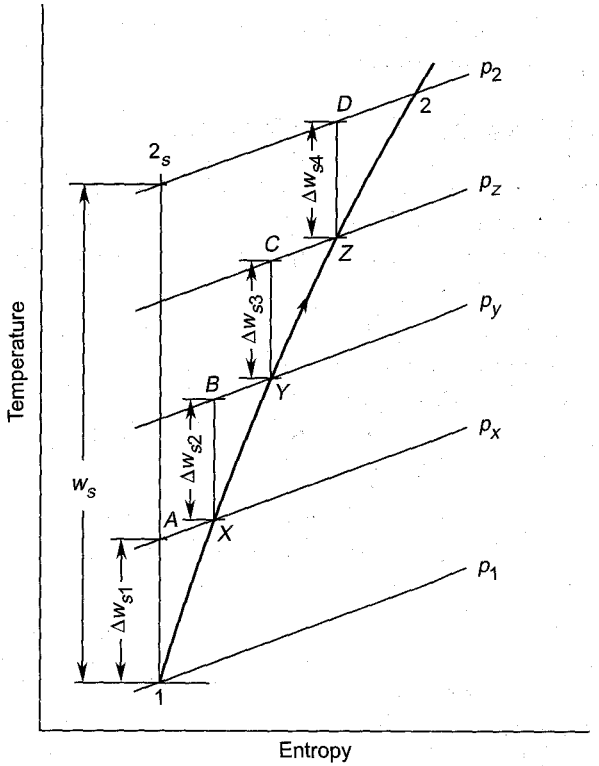

Fig. 2.15 Effect of preheating on compression in compressor stages

where $\Sigma \Delta w_s = \Delta w_{s_1} + \Delta w_{s_2} + \Delta w_{s_3} + \Delta w_{s_4}$

Equating the two values of the actual total work,

$$\eta_c = \frac{w_s}{\Sigma \Delta w_s} \eta_{st} \tag{2.152}$$

As explained before, with the aid of Eq. (2.119)

$$\frac{w_s}{\Sigma \Delta w_s} < 1 \tag{2.153}$$

This condition in Eq. (2.152) makes the value of the overall efficiency of the compressor smaller than the stage efficiency.

$$\eta_c < \eta_{st} \tag{2.154}$$

This is due to the thermodynamic effect called "pre-reheating"; the gas is not intentionally heated (pre-heated) at the end of each compression stage. The pre-reheat in small constant pressure processes AX, BY, CZ and D2 is only an internal phenomenon and the compression process still remains adiabatic.

This is a result of the reappearance of the effect of losses of the previous stage in the subsequent stage.

2.6.5 Infinitesimal Stage Efficiency

A finite compressor stage can be looked upon as made up of an infinite number of small stages (infinitesimal stages). Each of these infinitely small stages have an efficiency η_p called the small stage or the infinitesimal stage efficiency.

Equation (2.154) can be applied in this case also. Here the stage efficiency η_{st} is the overall efficiency of compression between the states 1 and 2, and η_p is the individual stage efficiency. Therefore, on the basis of discussion in the previous section, the following relation can be written:

$$\eta_{st} < \eta_p$$

The small stage efficiency, on account of the infinitesimally small pressure rise in it, is independent of the thermodynamic effect. Therefore it is, as stated before, a true measure of the aerodynamic performance of the compressor.

An expression for this efficiency is derived here for a perfect gas. Figure 2.16 shows a small stage between pressures p and $p + dp$. The changes in enthalpy or temperature between the initial and final states for isentropic and actual processes are

$$(\Delta h)_s = c_p\,(\Delta T)_s$$
$$(\Delta h) = c_p\,(\Delta T)$$

The efficiency (η_p) of the small or infinitesimal stage is given by

$$\eta_p = \frac{(dh)_s}{dh} = \frac{dT_s}{dT} \tag{2.155}$$

The final expression for η_p can be obtained by adopting the procedure of Sec. 2.5.5. However, for illustration, a different method is adopted here. This can also be used for an expansion process.

For an infinitesimal isentropic process,

$$dh_s = \frac{dp}{\rho}$$

From equation of state for a perfect gas,

$$dh_s = RT\,\frac{dp}{p} \tag{2.156}$$

In the actual infinitesimal process,

$$dh = c_p\,dT = \frac{\gamma}{\gamma - 1}\,RdT \tag{2.157}$$

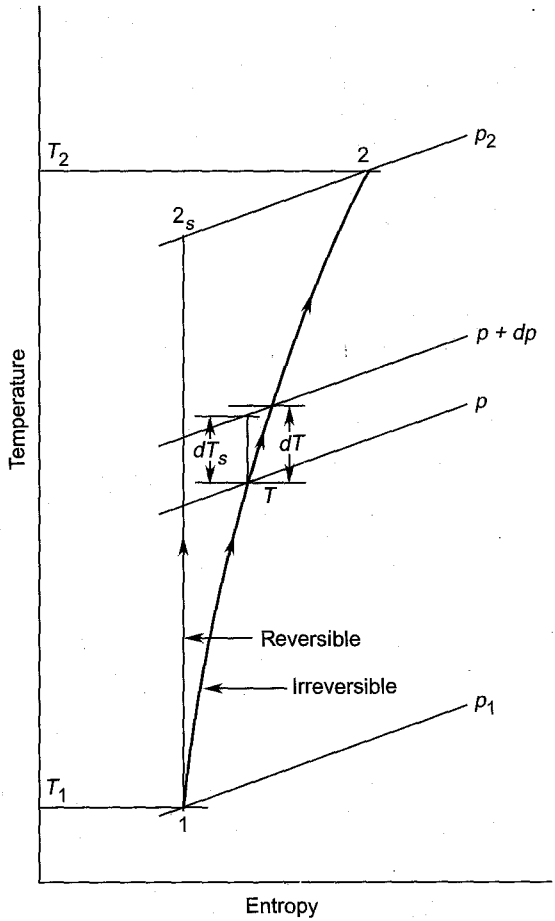

Fig. 2.16 Infinitesimal and finite compression processes

Putting Eqs. (2.156) and (2.157) in Eq. (2.155) we get

$$\eta_p = \frac{\gamma - 1}{\gamma} \frac{T}{dT} \frac{dp}{p}$$

$$\frac{dT}{T} = \frac{1}{\eta_p} \frac{\gamma - 1}{\gamma} \frac{dp}{p} \tag{2.158}$$

Equation (2.158) is applicable for the actual compression process along 1–2. On integration it gives

$$\ln p^{\frac{1}{\eta_p}\frac{\gamma-1}{\gamma}} = \ln T + \ln \text{const.}$$

$$\frac{p^{\frac{1}{\eta_p}\frac{\gamma-1}{\gamma}}}{T} = \text{const.} \tag{2.159}$$

This relation holds for an actual compression process in a finite stage or multi-stage machine. It may be noted that η_p remains constant during the compression process under consideration. Its value for the given boundary conditions is now determined.

Applying Eq. (2.159) for states 1 and 2 (Fig. 2.16),

$$\frac{p_1^{\frac{1}{\eta_p}\frac{\gamma-1}{\gamma}}}{T_1} = \frac{p_2^{\frac{1}{\eta_p}\frac{\gamma-1}{\gamma}}}{T_2}$$

$$\frac{T_2}{T_1} = \left(\frac{p_2}{p_1}\right)^{\frac{1}{\eta_p}\frac{\gamma-1}{\gamma}} \tag{2.160}$$

Taking logs on both sides and rearranging,

$$\eta_p = \frac{\frac{\gamma-1}{\gamma}\ln\left(\frac{p_2}{p_1}\right)}{\ln\left(\frac{T_2}{T_1}\right)} = \frac{\ln\left(\frac{T_{2s}}{T_1}\right)}{\ln\left(\frac{T_2}{T_1}\right)} \tag{2.161}$$

Assuming the irreversible adiabatic compression (1-2) as equivalent to a polytropic process (hence the term polytropic efficiency) with index n, Eq. (2.160) can be written as

$$\left(\frac{p_2}{p_1}\right)^{\frac{1}{\eta_p}\frac{\gamma-1}{\gamma}} = \left(\frac{p_2}{p_1}\right)^{\frac{n-1}{n}}$$

Equating the indices

$$\eta_p = \frac{\gamma-1}{\gamma}\frac{n}{n-1} \tag{2.162}$$

$$n = \frac{\gamma\eta_p}{1-\gamma(1-\eta_p)} \tag{2.163}$$

The efficiency of a finite compressor stage can be related to the small stage efficiency.

The actual temperature rise in the stage is

$$T_2 - T_1 = T_1\left(\frac{T_2}{T_1} - 1\right) = T_1\left(p_r^{\frac{1}{\eta_p}\frac{\gamma-1}{\gamma}} - 1\right)$$

Therefore, from Eq. (2.150) the stage efficiency is given by

$$\eta_{st} = \frac{p_r^{\frac{\gamma-1}{\gamma}} - 1}{p_r^{\frac{1}{\eta_p}\frac{\gamma-1}{\gamma}} - 1} \tag{2.164}$$

For a multi-stage compressor, η_{st} is replaced by the overall efficiency η_c of the compressor and p_r by the overall pressure ratio p_{rc}.

$$\eta_c = \frac{p_{rc}^{\frac{\gamma-1}{\gamma}} - 1}{p_{rc}^{\frac{1}{\eta_p}\frac{\gamma-1}{\gamma}} - 1} \tag{2.165}$$

Equations (2.164) and (2.165) can be plotted in terms of the pressure ratio for various values of η_p. Figure 2.17 shows such plots. In the vicinity of the pressure ratio $p_r \approx 1$, the stage efficiency is almost equal to the polytropic efficiency; at higher values it decreases with the pressure ratio.

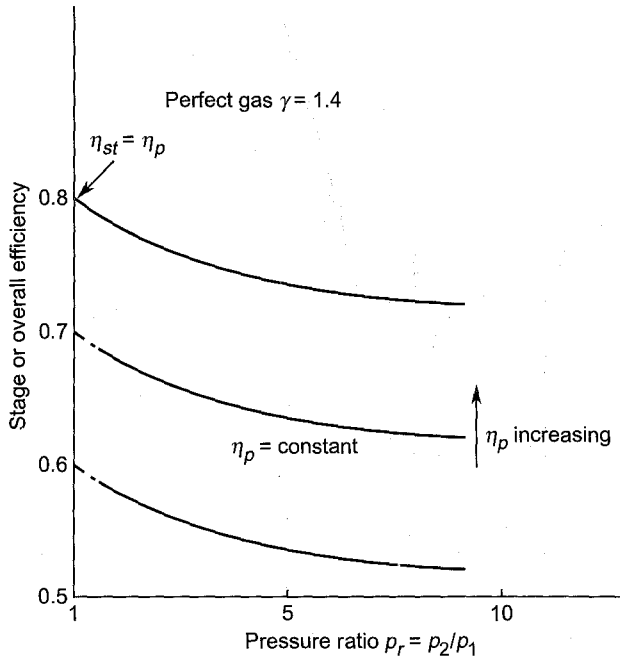

Fig. 2.17 Variation of overall efficiencies with pressure ratio at η_p = constant

For a given compressor η_p sets the upper limit of performance.

2.6.6 Multi-stage Compressors

Work and efficiency expressions for a multi-stage compressor assuming perfect gas are discussed here.

Constant stage pressure ratio

Let there be k stages. Figure 2.18 shows various stages from pressure p_1 to p_{k+1}. The reversible and irreversible compression processes are

along $1 - (k+1)_s$ and $1 - (k+1)$ respectively. For the same pressure ratio in all stages

$$p_r = \frac{p_2}{p_1} = \frac{p_3}{p_2} = \frac{p_4}{p_3} = \ldots \frac{p_{i+1}}{p_i} = \ldots = \frac{p_{k+1}}{p_k} \tag{2.166}$$

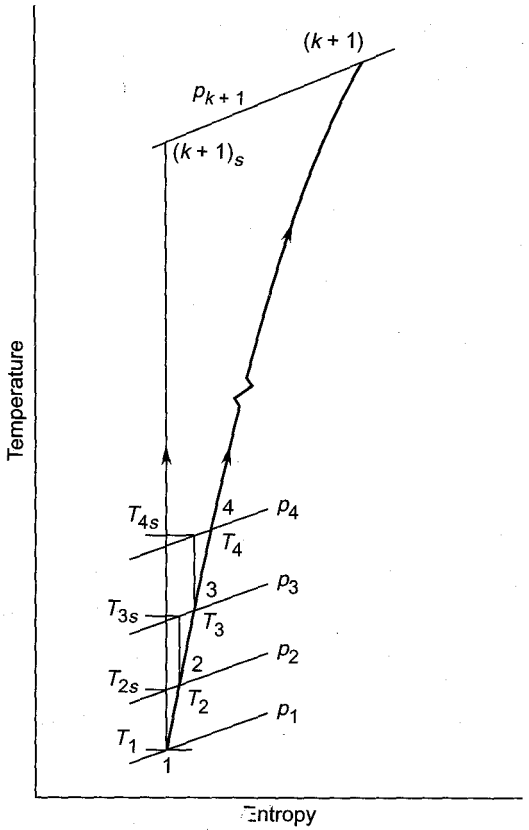

Fig. 2.18 Compression processes in the stages of a multi-stage compressor

The overall pressure ratio of the machine is

$$p_{rc} = \frac{p_{k+1}}{p_1} = p_r^k \tag{2.167}$$

Since both p_r and η_p are constants, the efficiency of all stages is same and is given by Eq. (2.164).

The overall efficiency is given by Eq. (2.165)

$$\eta_c = \frac{p_r^{\frac{\gamma-1}{\gamma}k} - 1}{p_r^{\frac{k}{\eta_p}\frac{\gamma-1}{\gamma}} - 1}$$

The stage work (temperature rise) depends on the entry temperature of each stage. Since this increases progressively, the stage work also does the same.

For the first stage,

$$\Delta T_1 = T_2 - T_1 = T_1(p_r^{\frac{1}{\eta_p}\frac{\gamma-1}{\gamma}} - 1) = CT_1 \tag{2.168a}$$

where $C = p_r^{\frac{1}{\eta_p}\frac{\gamma-1}{\gamma}} - 1 = \text{const.}$

$$\Delta T_2 = T_3 - T_2 = CT_2 = C(T_1 + CT_1)$$

$$\Delta T_2 = C\,(1 + C)T_1 \tag{2.168b}$$

Similarly,

$$\Delta T_3 = C\,(1 + C)^2\,T_1 \tag{2.169}$$

$$\Delta T_i = C\,(1 + C)^{i-1}\,T_1 \tag{2.170}$$

$$\Delta T_k = C\,(1 + C)^{k-1}\,T_1 \tag{2.171}$$

Therefore, the total temperature rise in the compressor is

$$(\Delta T)_c = \Delta T_1 + \Delta T_2 + \ldots + \Delta T_k$$

$$(\Delta T)_c = \sum_{i=1}^{k} C\,(1 + C)^{i-1}\,T_1$$

$$(\Delta T)_c = \{(1 + C)^k - 1\}T_1 \tag{2.172}$$

Substituting for C

$$(\Delta T)_c = \left(p_r^{\frac{k}{\eta_p}\frac{\gamma-1}{\gamma}} - 1\right)T \tag{2.173}$$

This is the value of the overall actual temperature rise in the machine.

Constant stage work

In a multi-stage machine the assumption of equal stage temperature rise (work) is often made.

The total temperature rise in the machine for given values of the overall pressure ratio (p_{rc}) and η_p is known for k stages. Therefore, the temperature rise per stage is

$$(\Delta T)_{st} = \frac{1}{k}\,(\Delta T)_c = \frac{1}{k}\left(p_{rc}^{\frac{1}{\eta_p}\frac{\gamma-1}{\gamma}} - 1\right)T_1 \tag{2.174}$$

The pressure ratio and hence the stage efficiency of various stages can now be found. For instance, in the ith stage

$$(\Delta T)_{st} = (\Delta T)_i = T_{i+1} - T_i = T_i\left(p_{ri}^{\frac{1}{\eta_{p\cdot}}\frac{\gamma-1}{\gamma}} - 1\right)$$

$$1 + \frac{(\Delta T)_i}{T_i} = p_{ri}^{\frac{1}{\eta_p}\frac{\gamma-1}{\gamma}}$$

The quantity on the left-hand side in this relation is known; η_p is also known. Therefore, the pressure ratio of the ith stage can be calculated.

$$p_{ri} = \left[1 + \frac{(\Delta T)_i}{T_i}\right]^{\frac{\gamma}{\gamma-1}\eta_p} \tag{2.175}$$

On account of the continuous increase in the gas temperature (T_i), the pressure ratio of the stages goes on decreasing from the L.P. end to the H.P. end.

Notation for Chapter 2

a	Velocity of sound, availability
A	Area of cross-section, availability
c	Gas velocity
c_v	Specific heat at constant volume
c_p	Specific heat at constant pressure
C	A constant
C_p	Pressure recovery coefficient
C_N	Nozzle velocity coefficient
$E = m\ e$	Energy
F	Force
$g = 9.81$ m/s^2	Acceleration due to gravity
$H = m\ h$	Enthalpy
k	Number of stages in a multi-stage machine
m	Mass
$\dot{m}$	Mass or mass-flow rate
M	Mach number
n	Index of polytropic process
p	Pressure
P	Power
$Q = m\ q$	Heat transfer
R	Gas constant
$S = m\ s$	Entropy
T	Absolute temperature
$U = m\ u$	Internal energy
$V = m\ v$	Volume
$W = m\ w$	Work
Z	Datum head

Greek symbols

$\gamma = \frac{c_p}{c_p}$	Specific heat ratio
η	Efficiency
ρ	Density

Subscripts

a	Actual or adiabatic
A	Integration over area *A*
av	Average
c	Compressor
o	Stagnation value
1	Initial
2	Final
D	Diffuser
fp	Flow process
nfp	Non-flow process
i	*i*th stage
N	Nozzle
p	Polytropic
r	Ratio
s	Isentropic or ideal
ss	Static-to-static
st	Stage
T	Turbine
ts	Total-to-static
tt	Total-to-total

Solved Examples

2.1 A nozzle expands air from $p_1 = 8.0$ bar, $T_1 = 540$ K to a pressure of 5.8 bar with an efficiency of 95%. The air is then passed through a diffuser of area ratio 4.0. The total pressure loss across the diffuser is 367 mm Hg.

Determine the efficiency of the diffuser and the velocities of air at its entry and exit. What is the static pressure at the diffuser exit?

Solution:

Nozzle

The velocity at the entry is assumed to be negligible.

$$p_r = 8/5.8 = 1.379$$

$$T_1/T_{2s} = 1.379^{0.286} = 1.096$$

$$T_{2s} = 540/1.096 = 492.7 \text{ K}$$

$$T_1 - T_2 = 0.95(540 - 492.7) = 44.935$$

$$T_2 = 540 - 44.935 = 495.065 \text{ K}$$

$$c_2 = \sqrt{2 \times 1005 \times 44.935} = 300.53 \text{ m/s } (Ans.)$$

$$\rho_2 = p_2/RT_2$$

$$\rho_2 = 5.8 \times 10^5/287 \times 495.065 = 4.08 \text{ kg/m}^3$$

Diffuser

Entry and exit are designated as 2 and 3

$$c_3A_3 = c_2A_2$$

$$c_3 = \frac{A_2}{A_3} \; c_2 = \frac{300{\cdot}53}{4} = 75.13 \text{ m/s } (Ans.)$$

Assuming the flow to be almost incompressible,

$$\eta_D = 1 - \frac{\Delta p_0}{\frac{1}{2}\rho (c_2^2 - c_3^2)}$$

$$\eta_D = 1 - \frac{2 \times 367 \times 13.6 \times 9.81}{4.08 (300.53^2 - 75.13^2)} = 0.715$$

$$\eta_D = 71.5\% \text{ (Answer)}$$

$$p_3 - p_2 = \eta_D \frac{1}{2} \rho (c_2^2 - c_3^2)$$

$$p_3 - p_2 = 0.715 \times 0.5 \times 4.08 (300.53^2 - 75.13^2)$$

$$p_3 - p_2 = 1.231 \times 10^5 \text{ N/m}^2$$

$$p_3 = 5.8 + 1.231 = 7.031 \text{ bar } (Ans.)$$

2.2 (a) A low pressure air compressor develops a pressure of 1500 mm W.G.. If the initial and final states of air are $p_1 = 1.02$ bar, $T_1 = 300$ K and $T_2 = 315$ K, determine the compressor and the infinitesimal stage efficiencies.

(b) Another compressor changes the state of air from $p_1 = 1.02$ bar, $T_1 = 300$ K to $p_2 = 2.5$ bar with an efficiency of 75 %. Determine the infinitesimal efficiency of this compressor.

Explain the large deviation in the efficiency of this compressor from that of the L.P. compressor in (*a*).

***Solution*:**

(a) $\Delta p = 1500$ mm W.G. $= 1500 \text{ kgf/m}^2$

$$\Delta p = 1500 \times 9.81 \times 10^{-5} = 0.147 \text{ bar}$$

$$p_2 = 1.02 + 0.147 = 1.167 \text{ bar}$$

$$p_2/p_1 = 1.167/1.02 = 1.144$$

$$\frac{T_{2s}}{T_1} = 1.144^{0.286} = 1.039$$

$$T_{2s} = 1.039 \times 300 = 311.7 \text{ K}$$

$$\eta_c = \frac{T_{2s} - T_1}{T_2 - T_1} = \frac{311.7 - 300}{315 - 300} = \frac{11.7}{15}$$

$$\eta_c = 78.0\% \ (Ans.)$$

$$\eta_p = \frac{\gamma - 1}{\gamma} \frac{\ln[p_2/p_1]}{\ln[T_2/T_1]}$$

$$\frac{T_2}{T_1} = \frac{315}{300} = 1.05$$

$$\eta_p = 0.286 \ \frac{\ln 1.144}{\ln 1.05} = 0.788$$

$$\eta_p = 78.8\% \ (Ans.)$$

On account of the low pressure rise in this compressor, the two efficiencies are close to each other, i.e.

$$\eta_c \approx \eta_p$$

(b) $$p_2/p_1 = 2.5/1.02 = 2.451$$

$$\frac{T_{2s}}{T_1} = 2.451^{0.286} = 1.292$$

$$T_{2s} = 1.292 \times 300 = 387.6 \text{ K}$$

$$\frac{T_{2s} - T_1}{T_2 - T_1} = \eta_c$$

$$\frac{387.6 - 300}{T_2 - T_1} = 0.75$$

$$T_2 - T_1 = 116.8$$

$$T_2 = 300 + 116.8 = 416.8 \text{ K}$$

$$T_2/T_1 = 416.8/300 = 1.389$$

$$\eta_p = 0.286 \ \frac{\ln 2.451}{\ln 1.389} = 0.78$$

$$\eta_p = 78.0\% \ (Ans.)$$

In this case, because of the higher pressure rise in the compressor, its efficiency is appreciably lower than the infinitesimal stage efficiency. This is on account of preheating.

2.3 An air compressor has eight stages of equal pressure ratio 1.35. The flow rate through the compressor and its overall efficiency are 50 kg/s and 82 per cent, respectively. If the conditions of air at entry are 1.0 bar and $t_1 = 40°C$, determine

(a) the state of air at the compressor exit,

(b) polytropic or small stage efficiency,

(c) efficiency of each stage and

(d) power required to drive the compressor assuming overall efficiency of the drive as 90%.

***Solution*:**

$$\gamma = 1.4$$

$$c_p = 1.005 \text{ kJ/kg K}$$

$$\frac{\gamma - 1}{\gamma} = 0.286$$

$$T_1 = 273 + 40 = 313 \text{ K}$$

Overall pressure ratio $p_{rc} = 1.35^8 = 11.03$

Actual temperature rise through the compressor is

$$\Delta T_c = \frac{1}{\eta_c} = \{T_{(k+1)s} - T_1\} = \frac{313}{0.82}(11.03^{0.286} - 1) = 376.75 \text{ K}$$

(a) Exit pressure and temperature are

$p_{k+1} = 11.03 \times 1 = 11.03$ bar (*Ans.*)

$T_{k+1} = 313 + 376.75 = 689.75$ K (*Ans.*)

(b) Polytropic efficiency is given by

$$\eta_p = 0.286 \ln 11.03 / \ln \left(\frac{689.75}{313}\right) = 0.871$$

$$\eta_p = 87.1\%$$

(c) Since the pressure ratio in each stage is the same, their efficiencies are also the same.

$$\eta_{st} = \frac{p_r^{\frac{\gamma-1}{\gamma}} - 1}{p_r^{\frac{1}{\eta_p}\frac{\gamma-1}{\gamma}} - 1}$$

$$\frac{1}{\eta_p}\frac{\gamma-1}{\gamma} = \frac{0.286}{0.871} = 0.328$$

$$\eta_{st} = \frac{1.35^{0.286} - 1}{1.35^{0.328} - 1} = \frac{0.0896}{0.1035}$$

$$\eta_{st} = 86.5\% \text{ (}Ans.\text{)}$$

(d) Power $$P = \frac{1}{0.9}\dot{m}c_p\,\Delta T_c$$

$$= \frac{50 \times 1.005 \times 376.75}{0.9 \times 1000}$$

$$P = 21.03 \text{ MW (Ans.)}$$

2.4 If all stages in the compressor of example 2.3 have the same temperature rise, determine the pressure ratio and efficiency of each stage. Comment on the results.

***Solution*:**

Since the actual temperature rise in each stage is the same, the pressure ratio and hence the stage efficiency of the stages will be different.

The temperature rise in the ith stage is

$$\Delta T_i = 376.75/8 = 47.09 \text{ K}$$

This remains constant but the temperature T_i at the entry of each stage varies.

$$\eta_p \frac{\gamma}{\gamma - 1} = 0.871 \times \frac{1.4}{1.4 - 1} = 3.048$$

Further calculations for the eight stages can be more conveniently done in a table.

Stage no.	T_i	$1 + \frac{\Delta T_i}{T_i}$	$p_r = \left(1 + \frac{\Delta T_i}{T_i}\right)^{\eta_p \frac{\gamma}{\gamma-1}}$	$\eta_{st} = \frac{p_r^{0.286} - 1}{p_r^{0.328} - 1}$
1	313	1.15	1.53	0.862
2	360.09	1.13	1.45	0.864
3	407.18	1.116	1.395	0.865
4	454.27	1.103	1.351	0.866
5	501.36	1.094	1.315	0.867
6	548.45	1.086	1.285	0.8672
7	595.54	1.079	1.261	0.8676
8	642.63	1.0733	1.239	0.868

It is observed from the above table that, on account of the progressively increasing values of the temperatures at the stage entries, the pressure ratios decrease and the stage efficiencies increase. The stage with the minimum pressure ratio ($i = 8$) has an efficiency nearest to the small-stage efficiency ($\eta_p = 0.871$).

2.5 The output of a three-stage gas turbine is 30 MW at the shaft coupling at an entry temperature of 1500 K. The overall pressure

ratio across the turbine is 11.0 and efficiency 88%. If the pressure ratio of each stage is the same, determine:

(a) pressure ratio of each stage,
(b) polytropic efficiency,
(c) the mass flow rate, and
(d) the efficiency and power of each stage.

The properties of the working medium are the same as of air ($\gamma = 1.4$, $c_p = 1.005$ kJ/kgK). Assume an efficiency of 91% to take into account shaft losses due to disc and bearing friction.

***Solution*:**

(a) $$p_{ri} = 11^{1/3} = 2.22 \ (Ans.)$$

(b) $$T_1 - T_2 = \eta_T (T_1 - T_{2s}) = \eta_T T_1 (1 - p_{rT}^{-0.286})$$

$$\Delta T = T_1 - T_2 = 0.88 \times 1500 \ (1 - 11^{-0.286}) = 655 \text{ K}$$

$$T_2 = 1500 - 655 = 845 \text{ K}$$

$$T_1/T_2 = 1500/845 = 1.775$$

$$\eta_p = \frac{\gamma}{\gamma - 1} \ln \left(\frac{T_1}{T_2}\right) \Big/ \ln \left(\frac{p_1}{p_2}\right)$$

$$\eta_p = 3.5 \ln 1.775 / \ln 11$$

$$\eta_p = 0.837 \ (Ans.)$$

(c) $$P = 30/0.91 = 32.96 \text{ MW}$$

$$P = \dot{m} c_p \Delta T$$

$$\dot{m} \times 1.005 \times 655 = 32960$$

$$\dot{m} = 50.07 \text{ kg/s} \ (Ans.)$$

(d) The efficiency of all stages is the same as the pressure ratio is the same.

$$\eta_{st} = \frac{1 - p_r^{\frac{1-\gamma}{\gamma} \eta_p}}{1 - p_r^{\frac{1-\gamma}{\gamma}}}$$

$$\eta_p \frac{\gamma - 1}{\gamma} = 0.837 \times 0.286 = 0.2394$$

$$\eta_{st} = \frac{1 - 2.22^{-0.2394}}{1 - 2.22^{-0.286}} = 0.1738/0.20395$$

$$\eta_{st} = 0.852 \ (Ans.)$$

The actual temperature drop in each stage is

$$\Delta T_i = T_i (1 - p_r^{\frac{1-\gamma}{\gamma}\eta_p})$$

$$\Delta T_i = T_i (1 - 2.22^{-0.2394})$$

$$\Delta T_i = 0.1738\ T_i$$

Therefore, the actual temperature drops in the stages are

$$\Delta T_1 = 0.1738 \times 1500 = 260.7 \text{ K}$$

$$\Delta T_2 = (1500 - 260.7) \times 0.1738 = 215.39 \text{ K}$$

$$\Delta T_3 = (1239.3 - 215.39) \times 0.1738 = 178 \text{ K}$$

The values of the power developed in each stage are

$$P_1 = 50.07 \times 1.005 \times .2607 = 13.1185 \text{ MW}$$

$$P_2 = 50.07 \times 1.005 \times 0.21539 = 10.8385 \text{ MW}$$

$$P_3 = 50.07 \times 1.005 \times 0.178 = 8.957 \text{ MW } (\textit{Ans.})$$

Total 32.920 MW

2.6 A gas turbine has the following data:

Inlet pressure and temperature, $p_1 = 5$ bar, $T_1 = 500$ K,

Exit pressure = 1.2 bar,

Overall turbine efficiency, $\eta_T = 0.90$,

Mass flow rate of the gas $\dot{m} = 20$ kg/s.

(a) Determine the polytropic efficiency of expansion and the power developed. Take $c_p = 1.005$ kJ/kg K, $\gamma = 1.4$.

(b) If an exhaust diffuser (area ratio = 2.5 and effeciency $\eta_D = 0.70$) is placed at the exit of the turbine calculate the static pressure rise (mm W.G.) across the diffuser and the increase in power output of the turbine. Take the velocity of gas at turbine exit as 75 m/s.

***Solution*:**

Without diffuser

(a) $$\frac{T_1}{T_{2s}} = \left(\frac{p_1}{p_2}\right)^{(\gamma-1)/\gamma} = \left(\frac{5}{1.2}\right)^{1/3.5} = 1.503$$

$$T_{2s} = T_1/1.503 = 500/1.503 = 332.67 \text{ K}$$

$$T_1 - T_{2s} = 500 - 332.67 = 167.33 \text{ K}$$

$$T_1 - T_2 = \eta_T (T_1 - T_{2s}) = 0.9 \times 167.33 = 150.6 \text{ K}$$

$$T_2 = 500 - 150.6 = 349.4 \text{ K}$$

$$T_1/T_2 = 500/349.4 = 1.431$$

$$\eta_p = \frac{\ln (T_1/T_2)}{\ln (T_1/T_{2s})} = \frac{\ln 1.431}{\ln 1.503} = \frac{0.3583}{0.4074} = 0.880 \qquad (Ans.)$$

Power output $P = \dot{m} c_p (T_1 - T_2)$

$$P = 20 \times 1.005 \times 150.6 = 3027.06 \text{ kW} \qquad (Ans.)$$

(b) With exhaust diffuser (see Fig. 2.19 and 2.20)

$$c_3 = \frac{A_2}{A_3} \times c_2 = \frac{75}{2.5} = 30 \text{ m/s}$$

$$\rho \simeq p_2/RT_2 = \frac{1.2 \times 10^5}{287 \times 349.4} = 1.196 \text{ kg/m}^3$$

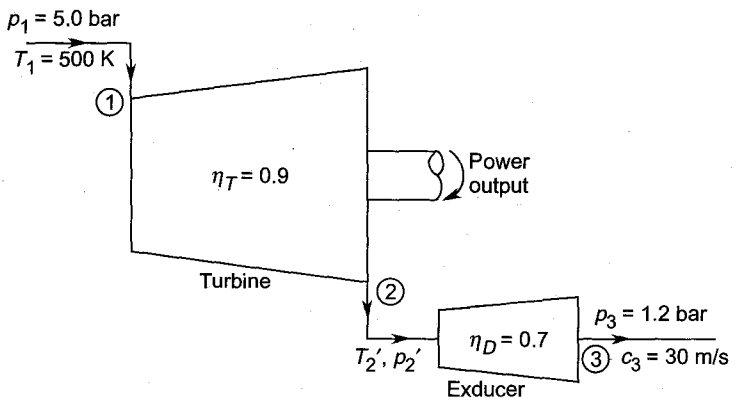

Fig. 2.19 An axial gas turbine with exhaust-diffuser (exducer)

Quantities with prime (′) refer to parameters in the presence of the diffuser.

$$\eta_D = \frac{p_3 - p'_2}{(\tfrac{1}{2})\, \rho\, ((c_2^2 - c_3^2)}$$

$$p_3 - p'_2 = \frac{1}{2}\, \rho\, (c_2^2 - c_3^2)\, \eta_D$$

$$= 0.5 \times 1.196\ (75^2 - 30^2) \times 0.7 \times 10^{-5} = 0.01979 \text{ bar}$$

Static pressure rise across the diffuser = 0.01979 bar (say 0.0198)

$$= 201.7 \text{ mm W.G.} \qquad (Ans.)$$

$$p'_2 = p_3 - 0.0198 = 1.2 - 0.0198 = 1.1802 \text{ bar}$$

$$p_1/p'_2 = 5.0/1.1802 = 4.2365$$

$$T_1/T'_{2s} = (4.2365)^{1/3.5} = 1.5106,\ T'_{2s} = 331\ K$$

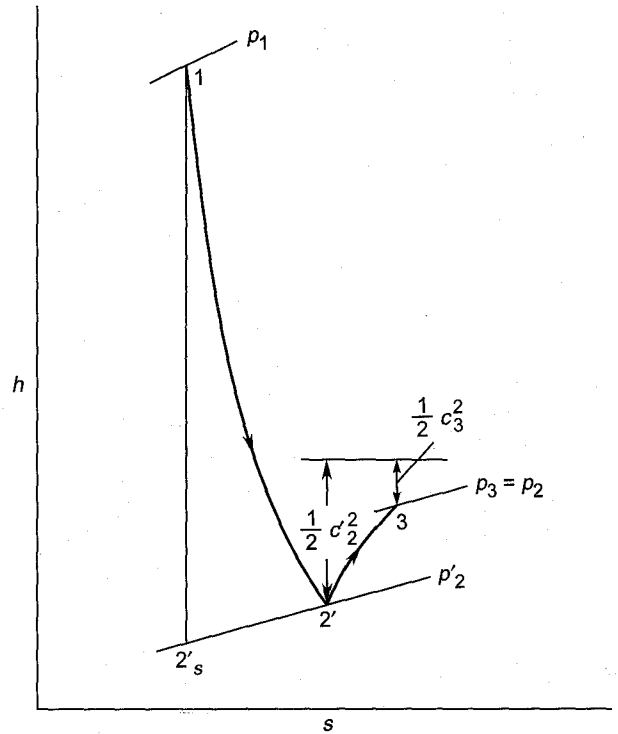

Fig. 2.20 Flow of gas through a turbine and the exhaust diffuser

$$T_1 - T'_{2s} = 169\ K$$

$$T_1 - T'_2 = 169 \times 0.9 = 152.1\ \text{K}$$

(assuming the same turbine efficiency)

$$P' = 20 \times 1.005 \times 152.1 = 3057.21\ \text{kW}$$

Increase in the power output by employing the exhaust diffuser,

$$P' - P = 3057.21 - 3027.06 = 30.15\ \text{kW} \qquad (Ans.)$$

This increase is due to the reduction in the kinetic energy in the exhaust from $\frac{1}{2}c_2^2$ to $\frac{1}{2}c_3^2$. Diffuser efficiency allows for the loss occurring in the diffuser.

It should be noted that for higher gas velocities at the turbine exhaust this gain in power output would be quite significant.

Questions and Problems

2.1 (a) Show diagrammatically on p-v coordinates the infinitesimal work for flow and non-flow processes.

(b) With the aid of these diagrams show that for these processes between two finite states:

$$w_{fp} = -\int_1^2 v\ dp = \frac{\gamma}{\gamma - 1}(p_1v_1 - p_2v_2) = h_1 - h_2$$

$$w_{nfp} = \int_1^2 p dv = \frac{1}{\gamma - 1}(p_1v_1 - p_2v_2) = u_1 - u_2$$

State the assumptions.

2.2 (a) Write down the general energy equation for a system with heat and work transfers and changes in the internal energy, kinetic energy and datum head.

(b) With the aid of this equation, show that for an adiabatic turbomachine the work transfer equals the change in stagnation enthalpy.

2.3 Show reversible and irreversible flow processes in the nozzle ring of a turbine stage on enthalpy-entropy coordinates and prove that:

(a) $\eta_N = 1 - \dfrac{\text{enthalpy loss}}{\text{ideal enthalpy drop}}$

(b) $\eta'_N = 1 - \dfrac{\text{stagnation pressure loss}}{\text{static pressure drop}}$

State the assumptions used.

2.4 Air at 2.05 bar and 417 K is expanded through a row of nozzle blades to a pressure of 1.925 bar. The stagnation pressure loss across the nozzle is measured as 10 mm Hg. Determine the efficiency of this nozzle and the velocity of air at the exit. Take c_p = 1005 J/kg K and γ = 1.4. State the assumptions used.

Ans. η_N = 89.3%; c_2 = 115.25 m/s; the flow is assumed incompressible for determining efficiency.

2.5 A gas turbine nozzle has a pressure ratio of 1.8. The initial pressure and temperature are 3.5 bar and 1050 K. The gas velocity at exit is 548 m/s. Determine the efficiency of the nozzle and the exit Mach number. Take R = 287 J/kg K, γ = 1.4.

Ans. η_N = 92%, M_2 = 0.911

2.6 Show reversible and irreversible processes in the diffuser blade ring of a turbo-compressor on enthalpy-entropy coordinates and prove that:

(*a*) $\eta_D = \dfrac{\text{static pressure rise}}{\text{change in dynamic pressure}}$

(b) $$\eta_D = \left(1 + \frac{\text{stagnation pressure loss}}{\text{static pressure rise}}\right)^{-1}$$

(c) Actual pressure recovery coefficient

$$= \eta_D \left\{1 - \frac{1}{(\text{area ratio})}\right\}$$

2.7 An air stream (ρ = 1.25 kg/m3) is decelerated from 100 m/s to 75 m/s in a diffuser giving a pressure rise of 250 mm W.G. Calculate the diffuser efficiency.

Ans. η_D = 89.7%.

2.8 Define total-to-total and total-to-static efficiencies for steam and gas turbine stages. Give two situations in each case where these efficiencies are used. Give reasons.

2.9 (a) What is infinitesimal stage efficiency in the expansion through a turbine? How is it determined?

(b) Show that the index n of polytropic expansion in a turbine of infinitesimal stage efficiency η_p is

$$n = \frac{\gamma}{\gamma - (\gamma - 1)\eta_p}$$

2.10 Prove the following relations for finite turbine stages:

(a) $$\eta_{st} = \frac{1 - p_r^{\frac{1-\gamma}{\gamma}\eta_p}}{1 - p_r^{\frac{1-\gamma}{\gamma}}} \quad \text{(single stage)}$$

(b) $$\eta_T = \frac{1 - p_r^{\frac{1-\gamma}{\gamma}k\eta_p}}{1 - p_r^{\frac{1-\gamma}{\gamma}k}} \quad (k \text{ Stages})$$

2.11 How is the efficiency η_p of an infinitesimal compression stage defined? Prove that:

(a) $p^{\frac{1}{\eta_p}\frac{\gamma-1}{\gamma}} = \text{const.} \times T$

(*b*) $$\eta_c = \frac{p_r^{\frac{\gamma-1}{\gamma}k} - 1}{p_r^{\frac{k}{\eta_p}\frac{\gamma-1}{\gamma}} - 1}$$

2.12 Explain the reheat and preheat phenomena in turbines and compressors respectively. What are their effects on the work and efficiencies in these machines?

2.13 Explain the difference between the flow processes in one-dimensional and three-dimensional nozzles. How is the efficiency of a three-dimensional nozzle defined?

2.14 Repeat Ex. 2.5 for equal power in all the stages. Determine the pressure ratio and efficiency of each stage.

Ans.

First stage $p_r = 1.929$; $\eta_{st} = 0.849$

Second stage $p_r = 2.182$; $\eta_{st} = 0.850$

Third stage $p_r = 2.611$; $\eta_{st} = 0.855$

2.15 A diffuser at the exit of a gas turbine has an area ratio of 2.0. If the static pressure at the diffuser exit is 1.013 bar and the velocity of gas 30 m/s, calculate the static pressure of the gas at the turbine exit. Take diffuser efficiency equal to 77% and density of gas as 1.25 kg/m^3 (constant). State the assumptions used.

Draw the actual and ideal diffusion processes on the h–s diagram.

(*Ans.* $p_{exit} = 1.0$ bar)

2.16 In example 2.6, if the gas velocity at turbine entry is 25 m/s, determine

(a) Total to total and total to static efficiencies when the turbine is exhausting at $p_2 = 1.2$ bar.

(b) Total to total and total to static efficiencies if the turbine is fitted with an exhaust diffuser.

(c) Total to static efficiency of the 'turbine diffuser' system considered as a single composite unit

Ans. (a) $\eta_{tt} = 89.85\%$ $\eta_{ts} = 88.35\%$

(b) $\eta_{tt} = 89.85\%$, $\eta_{ts} = 87.43\%$

(c) $\eta_{ts} = 89.3\%$

Chapter 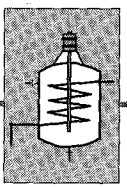 3

Gas Turbine Plants

A gas turbine plant (Fig. 3.1) consists of a turbo-compressor, combustion chamber (or heat exchanger) and turbine. The plant is started by rotating the compressor-turbine assmebly by a starting motor or any other device. When the compressor develops enough pressure to support combustion of the fuel in the combustion chamber, the hot gases can themselves drive the gas turbine, and the plant becomes self-sustaining. The turbine should develop enough power to be able to drive the compressor and load (if any). The output of the plant is the difference between the turbine work and the compressor work. The actual output at the generator terminals will be much less than this.

A majority of aircraft gas turbine plants use kerosene or gasoline whereas other plants can use natural gas, bunker oil and blast furnace gas. Coal or gasified coal can also be used in electric power generating gas turbine plants.

If the gas turbine plant is used as an aircraft engine, the net output at the turbine shaft is used to drive a propeller in a turbo-prop engine, whereas in a turbo-jet engine the turbine output equals the power required to drive the compressor. The output of such a plant is the energy in the exhaust gases which is used for jet propulsion.

The shaft power of a gas turbine plant can also be used for driving electric generators, draft fans, compressors and other industrial devices.

As will be discussed later, the combustion chamber in a large number of industrial applications is replaced by a heat exchanger.

Gas turbine plants[29-51] can be compared with steam turbine plants; the chief distinguishing features of the gas turbine plants are their high inlet gas temperatures (T_{max} > 1500 K) and lower pressures. The exhaust gas pressures of the gas turbine plants are nowhere near the considerably low pressures (≈ 22.5 mbar) employed in the condensing steam plants. This explains why it is not necessary to employ large low pressure cylinders and multiple exhaust even in large terrestrial gas turbine plants. On the other hand, when compared with the reciprocating internal combustion engine, the gas turbine has the advantage of very high flow rate, light weight and mechanical simplicity.

Component efficiencies and inlet gas temperatures were critical for the successful development of the gas turbine plant. Therefore, in the earlier stages of its development major attempts were made to improve turbine and compressor efficiencies and develop high temperature materials. At present, the component efficiencies are in excess of 85% and the turbine blade cooling has enabled the employment of gas temperatures as high as 1600 K at the inlet.

3.1 Open and Closed Circuit Plants

In the simple open circuit gas turbine plants (Fig. 3.1) atmospheric air is continuously compressed in the compressor and delivered to the combustion chamber at a high pressure. The hot gases from the combustion chamber pass out to the atmosphere after expanding through the turbine. In this arrangement since the working fluid is not restored (at station 1 in Fig. 3.1) to its initial state, technically speaking such a plant does not execute a cycle.

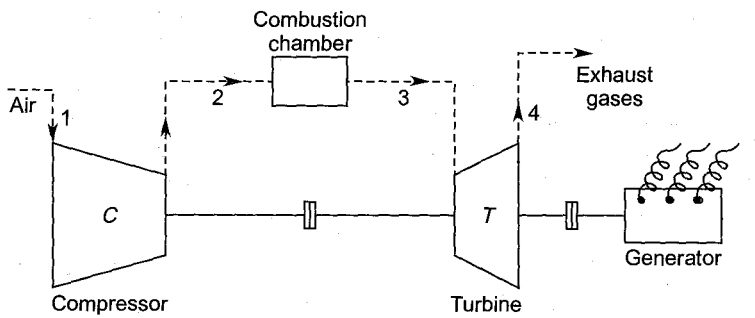

Fig. 3.1 A simple open circuit gas turbine plant

A cycle can only be executed in the closed circuit gas turbine plant shown in Fig. 3.2. Here the same working fluid (air or any other gas) circulates through its various components. Heat cannot be supplied to the working fluid by internal combustion; instead, it is supplied externally by employing a heat exchanger which replaces the combustion chamber of the open circuit plant.

A pre-cooler is included between the turbine exit and the compressor entry. This decreases the specific volume of the air or gas entering the compressor. The lower value of the specific volume reduces the compressor work ($\int v\, dp$) and its size.

The closed circuit gas turbine plant with its separate external combustion system and precooler looks like a condensing steam plant. The main differences in the two plants will be explained further in later sections. Some advantages of the closed circuit gas turbine plant are given below.

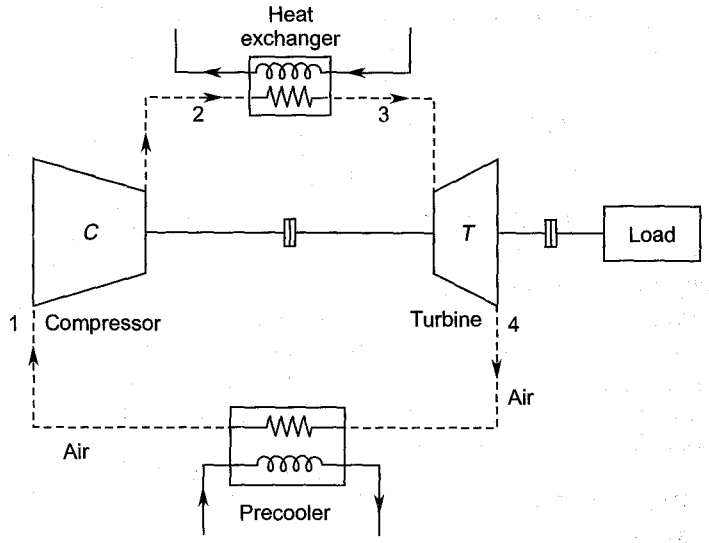

Fig. 3.2 A simple closed circuit gas turbine plant

1. Since the working fluid does not leave the plant, fluids with better thermodynamic properties other than air can be employed to derive some aero-thermodynamic advantages. For example, the velocity of sound is higher in helium which permits higher peripheral speeds of the rotor. It is inert and has a higher specific heat and thermal conductivity, resulting in a smaller heat exchanger.
2. By employing high density working fluids, the plant size for a given power can be reduced. In large plants this is a great advantage in terms of mechanical design. A higher density also provides a higher heat transfer rate.
3. The air in a conventional open circuit plant brings its own impurities which cause additional problems of blade erosion and filtration. In a closed circuit plant blade erosion due to solid particles in the air as well as in the products of combustion is absent.
4. This arrangement provides better control of the plant.

The chief disadvantage of this plant is that heat is supplied externally to the working fluid. This requires additional equipment besides being less efficient.

3.2 Gas Turbine Power Cycles

Gas turbine plants can either work on a constant pressure cycle (Joule or Brayton cycle) or a constant volume cycle (Atkinson cycle). For the purpose of theoretical analysis of the cycle, it is assumed to be executed

in a closed circuit gas turbine plant, though in practice Brayton cycle is widely employed in the open circuit plant shown in Fig. 3.1.

3.2.1 Ideal Joule Cycle

In the ideal Joule cycle the compression (1–2) and expansion (3–4) processes occurring in the compressor and turbine respectively are assumed to be isentropic. Heat addition (2–3) in the heat exchanger (combustion chamber) and rejection (4–1) occur at constant pressures. Therefore, it is also known as a constant pressure cycle. These processes, strictly speaking, occur only in the plant shown in Fig. 3.2. In Fig. 3.1 the gases at the exit of the turbine are lost into the atmosphere; therefore, the process 4–1 does not occur within the plant. Further assumptions for the ideal Joule cycle are as follows:

1. Pressure losses in the heat exchangers and the connecting passages are absent.
2. The working fluid is a perfect gas.
3. The effectiveness of the heat exchangers is 100%.

The ideal Joule cycle in the p–v and T–s planes is shown in Figs. 3.3 and 3.4 respectively. Here the suffix s is used to distin-guish between isentropic (s = constant) and adiabatic processes on the T–s diagrams in Fig. 3.4; this has been dropped in later stages. The heat is supplied during the process $2s$–3 and rejected in $4s$–1.

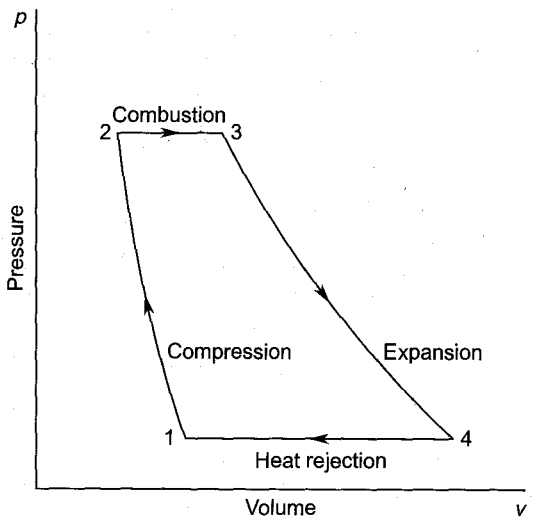

Fig. 3.3 Ideal Joule cycle in the p–v plane

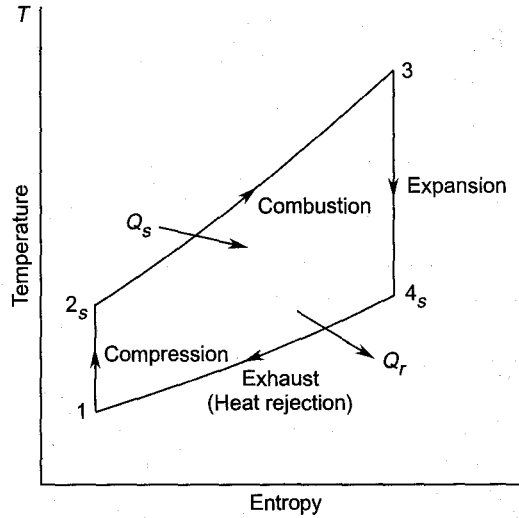

Fig. 3.4 Ideal Joule cycle in the *T–s* plane

The thermal efficiency of the air-standard or Joule cycle is given by

$$\eta_{\text{Joule}} = \frac{\text{plant output}}{\text{heat supplied}} = \frac{w_P}{Q_s}$$

Plant output is given by

$$w_P = Q_s - Q_r \tag{3.1a}$$

Therefore,

$$\eta_{\text{Joule}} = 1 - \frac{Q_r}{Q_s}$$

Referring to Fig. 3.4,

$$Q_s = c_p\,(T_3 - T_{2s})$$

$$Q_r = c_p\,(T_{4s} - T_1)$$

$$\therefore \quad w_P = c_p\,(T_3 - T_{2s}) - c_p\,(T_{4s} - T_1) \tag{3.1b}$$

$$\eta_{\text{Joule}} = 1 - \frac{T_{4s} - T_1}{T_3 - T_{2s}} \tag{3.2}$$

The temperature ratios in the isentropic processes are given by

$$t = \frac{T_{2s}}{T_1} = \frac{T_3}{T_{4s}} = \left(\frac{p_2}{p_1}\right)^{\frac{\gamma-1}{\gamma}} = \left(\frac{p_3}{p_4}\right)^{\frac{\gamma-1}{\gamma}}$$

$$= (r)^{\frac{\gamma-1}{\gamma}} \tag{3.3}$$

Equations (3.2) and (3.3) together yield

$$\eta_{\text{Joule}} = 1 - \frac{T_{4s} - T_1}{t(T_{4s} - T_1)}$$

i.e.

$$\eta_{\text{Joule}} = 1 - \frac{1}{t} = 1 - \frac{1}{r^{\frac{\gamma-1}{\gamma}}} \tag{3.4}$$

Equation (3.4) shows that the efficiency of the ideal Joule cycle increases with the pressure ratio (r) and is independent of temperature.

3.2.2 Actual Cycle

In the actual constant pressure cycle the work in the compressor and turbine is adiabatic instead of isentropic as shown in Fig. 3.5. Therefore, the compressor and turbine efficiencies are

$$\eta_C = \frac{T_{2s} - T_1}{T_2 - T_1} \tag{3.5}$$

$$\eta_T = \frac{T_3 - T_4}{T_2 - T_{4s}} \tag{3.6}$$

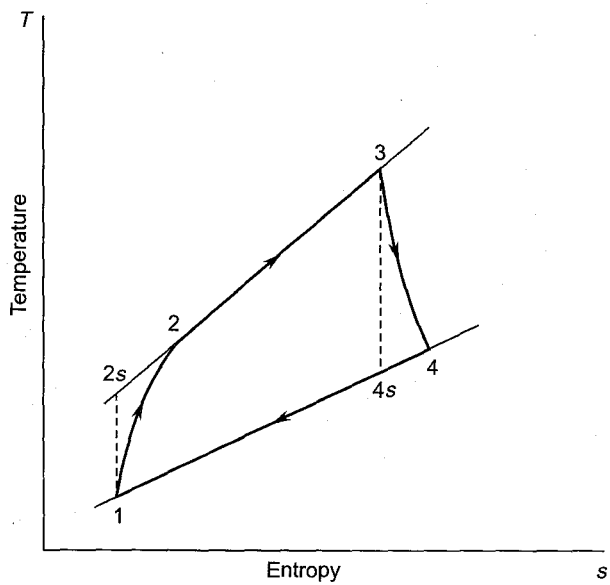

Fig. 3.5 Actual cycle without pressure losses

In the absence of pressure losses the pressure and ideal temperature ratios for the compressor and turbine are the same as before, i.e. Eq. (3.3)

is still applicable. The actual values of the turbine and compressor work are given by

$$w_T = c_p\,(T_3 - T_4) = c_p\,(T_3 - T_{4s})\,\eta_T = c_p\,\eta_T\,T_3\left(1 - \frac{T_{4s}}{T_3}\right)$$

Let the ratio of the maximum and minimum temperatures in the cycle be

$$\beta = \frac{T_3}{T_1} \tag{3.7}$$

$$w_T = \beta c_p \eta_T\,T_1\left(1 - \frac{1}{t}\right) \tag{3.8}$$

$$w_c = c_p\,(T_2 - T_1) = \frac{c_p}{\eta_c}\,(T_{2s} - T_1)$$

$$w_c = \frac{c_p}{\eta_c}\,T_1\,(t - 1) \tag{3.9}$$

The output of the plant is given by

$$w_P = w_T - w_C = \beta c_p\,\eta_T\,T_1\left(1 - \frac{1}{t}\right) - \frac{c_p}{\eta_c}\,T_1\,(t - 1)$$

$$w_P = \frac{1}{\eta_c}\,c_p\,T_1\left\{\beta\,\eta_c\,\eta_T\left(1 - \frac{1}{t}\right) - (t - 1)\right\}$$

Let $\alpha = \beta\,\eta_C\,\eta_T$ (3.10)

$$w_P = \frac{1}{\eta_c}\,c_p\,T_1\left(1 - \frac{1}{t}\right)(\alpha - t) \tag{3.11}$$

For given values of α and η_c, Eq. (3.11) can be optimized. Thus for maximum output

$$\frac{\partial}{\partial t}(w_P) = \frac{1}{\eta_c}\,c_p\,T_1\,\frac{\partial}{\partial t}\left(\alpha - \frac{\alpha}{t} - t + 1\right) = 0$$

$$t_{\text{opt}} = \sqrt{\alpha} = \sqrt{\beta\eta_c\eta_T} \tag{3.12}$$

Putting Eq. (3.12) in Eq. (3.11), we get the value of the maximum plant output

$$w_{\text{Pmax}} = \frac{1}{\eta_c}\,c_p\,T_1\left(\sqrt{\alpha} - 1\right)^2 \tag{3.13}$$

$$\eta_c\,(T_2 - T_1) = T_{2s} - T_1$$

$$T_2 = \left\{1 + \frac{1}{\eta_c}(t - 1)\right\}T_1 \tag{3.14}$$

The heat supplied is given by

$$Q_s = c_p\,(T_3 - T_2)$$

$$Q_s = \frac{1}{\eta_c}\; c_p\, T_1\, \{(\beta - 1)\;\eta_c - (t - 1)\} \tag{3.15}$$

Comparing equations (3.11) and (3.15), we get the thermal efficiency of the actual plant.

$$\eta_{th} = \frac{\left(1 - \frac{1}{t}\right)(\alpha - t)}{(\beta - 1)\eta_c - (t - 1)} \tag{3.16}$$

The thermal efficiency at the maximum plant output, by using Eq. (3.12) is given by

$$\eta'_{th} = \frac{\left(\sqrt{\alpha} - 1\right)^2}{(\beta - 1)\,\eta_c - \left(\sqrt{\alpha} - 1\right)} \tag{3.17}$$

In a real gas turbine plant (Fig. 3.6) the pressures during the processes 2–3 and 4–1 do not remain constant on account of the inherent pressure losses in both air and gas circuits. Therefore, the pressure and temperature ratios in the compressor and turbine are no longer the same. The two-fold reduction in the turbine pressure ratio reduces the plant output and

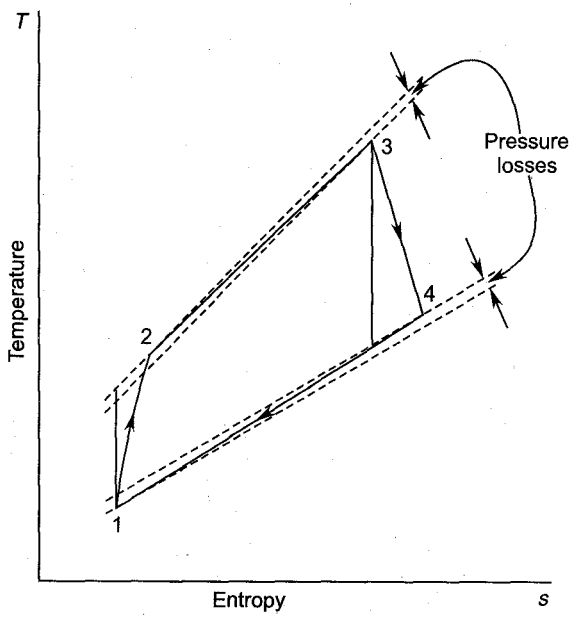

Fig. 3.6 Actual cycle with pressure losses

thermal efficiency. Besides this, the effectiveness of the heat exchangers is always less than unity.

3.2.3 Atkinson Cycle

Figure 3.7 shows the p–v diagram of a constant volume cycle known as the Atkinson cycle. The compression and expansion processes are isentropic in this cycle also. Heat addition takes place at constant volume and rejection at constant pressure. The practical difficulties in achieving constant volume heat addition and intermit-tent flow through the plant have been some of the chief hurdles in its development. For some industrial applications, this cycle has been profitably used in a combined steam and gas turbine plant.

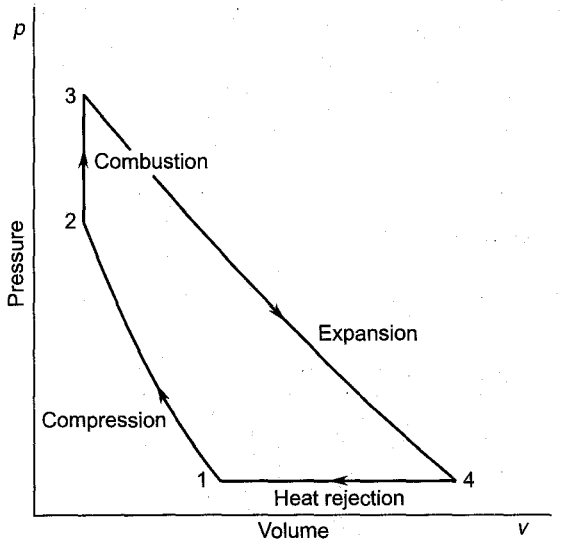

Fig. 3.7 Constant volume Atkinson cycle

Most of the modern gas turbine plants employ a number of variations of the constant pressure cycle (Joule/Brayton cycle). Therefore, further discussion in this book is restricted to only this cycle.

3.3 Improvements in the Constant Pressure Cycle

In this section methods of obtaining a higher plant output and thermal efficiency are discussed. A high plant efficiency can be obtained by employing high gas temperatures at the inlet. This is related to the development of blade materials that can withstand high temperatures.

Other methods for obtaining higher efficiencies are aimed at increasing the mean temperature of heat reception and decreasing the mean temperature of heat rejection.

3.3.1 Cycle with Exhaust Gas Heat Exchanger

The temperature of heat reception can be increased and at the same time mean temperature of heat rejection decreased by employing an exhaust gas heat exchanger as shown in Fig. 3.8. The air after compression is heated from temperature T_2 to T_5 in an exhaust gas heat exchanger. The change in temperature of the hot gas across the heat exchanger is from T_4 to T_6. For reversible transfer of heat, a contra-flow type of heat exchanger is employed. When the effectiveness of the heat exchanger is unity,

$$T_2 = T_6$$
$$T_5 = T_4 \qquad (3.18)$$

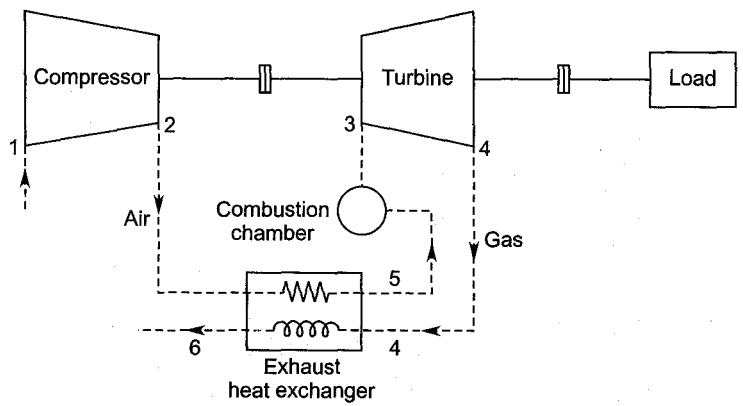

Fig. 3.8 Gas turbine plant with exhaust gas heat exchanger

Figures 3.9 and 3.10 show the ideal constant pressure cycle with heat exchange in the p–v and T–s planes.

Since the air has already been heated to a higher temperature T_5 in the heat exchanger less heat is now required to be added in the combustion chamber for the same value of maximum temperature T_3.

Referring to Fig. 3.10 and using Eqs. (3.18), heats supplied to and rejected by the plant are

$$Q_s = c_p (T_3 - T_5) = c_p (T_3 - T_4)$$
$$Q_r = c_p (T_6 - T_1) = c_p (T_2 - T_1)$$

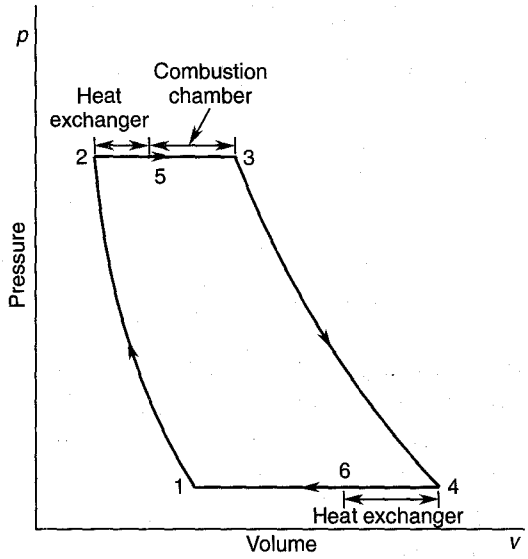

Fig. 3.9 Cycle with exhaust gas heat exchanger in the p–v plane

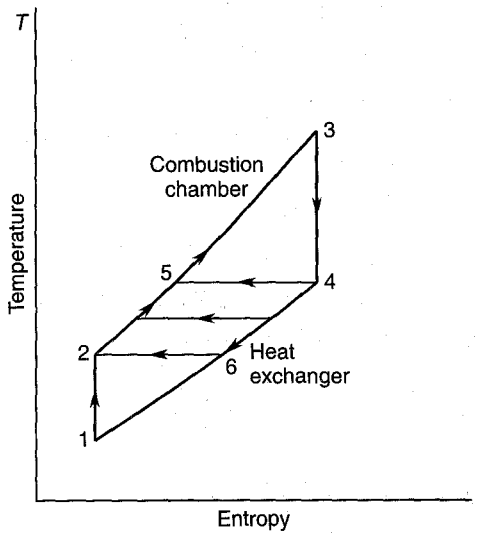

Fig. 3.10 Cycle with exhaust gas heat exchanger in the T–s plane

In an ideal closed circuit cycle, the specific heat is the same in the above two equations and remains constant. However, in a real open circuit cycle, they are different.

The thermal efficiency is given by

$$\eta_{th} = 1 - \frac{Q_r}{Q_s} = 1 - \frac{T_2 - T_1}{T_3 - T_4}$$

Using Eqs. (3.3) and (3.7), we get

$$\eta_{th} = 1 - \frac{tT_1 - T_1}{tT_4 - T_4} = 1 - \frac{T_1}{T_4}$$

$$\eta_{th} = 1 - \frac{T_3/T_4}{T_3/T_1}$$

$$\eta_{th} = 1 - \frac{t}{\beta} = 1 - \frac{(r)^{\frac{\gamma-1}{\gamma}}}{\beta} \tag{3.19}$$

Equation (3.19) shows that the efficiency of this cycle is dependent on the temperature ratio β besides the pressure ratio. For a given pressure ratio it increases with the temperature ratio β; and for a given value of β it decreases with the increase in pressure ratio.

The output of the plant is unaffected by exhaust gas heat exchange; this is shown in the following:

$$w_P = Q_s - Q_r = c_p\,(T_3 - T_4) - c_p\,(T_2 - T_1)$$
$$w_P = c_p\,(T_3 - T_2) - c_p\,(T_4 - T_1)$$

This expression is identical with Eq. (3.1b)

Effectiveness of the heat exchanger

Conditions given in Eq. (3.18) cannot be met in a real heat exchanger. The actual condition is depicted by the relations:

$$T_4 > T_5$$
$$T_6 > T_2$$

This fact is taken into account by the effectiveness or the thermal ratio of the heat exchanger which is defined by

$$\varepsilon = \frac{T_5 - T_2}{T_4 - T_2} \tag{3.20}$$

3.3.2 Cycle with Reheat

Another method of increasing the mean temperature of heat reception is to reheat the gas after it has expanded in a part of the gas turbine. By doing so the mean temperature of heat rejection is also increased, resulting in a decrease in the thermal efficiency of the plant. However, the specific output of the plant increases due to reheat.

Figure 3.11 shows a reheat gas turbine plant; the corresponding *T–s* diagram is shown in Fig. 3.12. The air compressor develops the required pressure and temperature ratios r and t during the isentropic process 1–2. Heat is supplied during the constant pressure process 2–3 after which

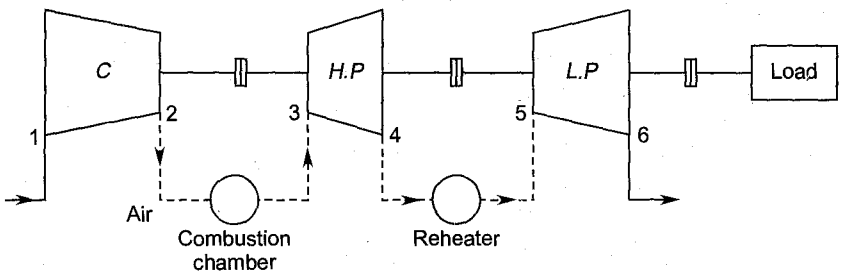

Fig. 3.11 Reheat cycle gas turbine plant

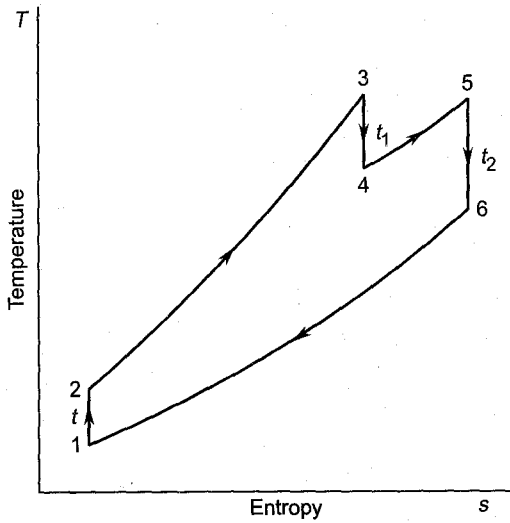

Fig. 3.12 Reheat cycle in the *T–s* plane

isentropic expansion (3–4) of the gas occurs in the high pressure turbine. The gas is heated (4–5) to its initial temperature ($T_3 = T_5$) in a reheater before its final expansion (5–6) in the low pressure turbine. The pressure and temperature ratios in the two turbines are:

$$r_1 = \frac{p_3}{p_4} \tag{3.21}$$

$$t_1 = \frac{T_3}{T_4} = \left(\frac{p_3}{p_4}\right)^{\frac{\gamma-1}{\gamma}} = r_1^{\frac{\gamma-1}{\gamma}} \tag{3.22}$$

$$r_2 = \frac{p_5}{p_6} \tag{3.23}$$

$$t_2 = \frac{T_5}{T_6} = \left(\frac{p_5}{p_6}\right)^{\frac{\gamma-1}{\gamma}} = r_2^{\frac{\gamma-1}{\gamma}} \tag{3.24}$$

For the compressor

$$r = \frac{p_2}{p_1} \tag{3.25}$$

$$t = \frac{T_2}{T_1} = \left(\frac{p_2}{p_1}\right)^{\frac{\gamma-1}{\gamma}} = r^{\frac{\gamma-1}{\gamma}} \tag{3.26}$$

Since $p_3 = p_2$, $p_4 = p_5$ and $p_6 = p_1$

$$\frac{p_2}{p_1} = \frac{p_3}{p_4}\frac{p_5}{p_6}$$

Therefore, $r = r_1 r_2$ (3.27)

$$t = t_1 t_2 \tag{3.28}$$

The total heat supplied to the plant is

$$Q_s = c_p (T_3 - T_2) + c_p (T_5 - T_4)$$

and the heat rejected is

$$Q_r = c_p (T_6 - T_1)$$

Therefore, the output of the plant is

$$w_P = Q_s - Q_r$$

$$w_P = c_p (T_3 - T_2) + c_p (T_5 - T_4) - c_p (T_6 - T_1)$$

On rearrangement,

$$w_p = c_p (T_3 - T_4) + c_p (T_5 - T_6) - c_p (T_2 - T_1) \tag{3.29}$$

This can also be obtained directly as

Plant output = work in turbines – compressor work

Since $T_3 = T_5$, Eq. (3.29) is rewritten as

$$w_P = c_p (2T_3 - T_4 - T_6 - T_2 + T_1)$$

$$w_P = \left(2\frac{T_3}{T_1} - \frac{T_4}{T_3}\frac{T_3}{T_1} - \frac{T_6}{T_5}\frac{T_3}{T_1} - \frac{T_2}{T_1} + 1\right) c_p T_1$$

Using Eqs. (3.7), (3.22), (3.24) and (3.26), we get

$$w_P = \left(2\beta - \frac{\beta}{t_1} - \frac{\beta}{t_2} - t + 1\right) c_p T_1$$

Using Eq. (3.28),

$$w_P = \left(2\beta - \frac{\beta}{t_1} - \beta\frac{t_1}{t} - t + 1\right) c_p T_1 \tag{3.30}$$

With a given overall temperature ratio (t) in the plant, the temperature ratio in only one turbine need be fixed; the other is automatically fixed by

the Eq. (3.28). The same applies to the pressure ratios [Eq. (3.27)]. Taking t_1 as a variable, its optimum value can be found from Eq. (3.30).

$$\frac{d}{dt_1} w_P = c_p T_1 \frac{d}{dt_1} \left(2\beta - \frac{\beta}{t_1} - \beta \frac{t_1}{t} - t + 1 \right) = 0$$

$$t_1 = \sqrt{t}$$

This relation in Eq. (3.28) gives

$$t_1 = t_2 = \sqrt{t} \tag{3.31}$$

The corresponding relation in terms of the pressure ratios is

$$r_1 = r_2 = \sqrt{r} \tag{3.32}$$

The heat supplied is

$$Q_s = c_p T_1 \left(\frac{T_3}{T_1} - \frac{T_2}{T_1} + \frac{T_5}{T_1} - \frac{T_4}{T_1} \right)$$

This on simplification gives

$$Q_s = c_p T_1 \left(2\beta - t - \frac{\beta}{t_1} \right) \tag{3.33}$$

Equations (3.30) and (3.33) yield

$$\eta_{th} = \frac{w_P}{Q_s} = \frac{2\beta - \beta/t_1 - \beta t_1/t - t + 1}{2\beta - t - \beta/t_1} \tag{3.34}$$

For maximum plant output, using Eq. (3.31), the efficiency expression reduces to

$$\eta'_{th} = \frac{2\beta - \frac{2\beta}{\sqrt{t}} - t + 1}{2\beta - t - \frac{\beta}{\sqrt{t}}} \tag{3.35}$$

3.3.3 Cycle with Reheat and Exhaust Heat Exchanger

It has been observed in the previous section that an increase in the specific output of the gas turbine plant is achieved by reheating at the cost of thermal efficiency. This defect can be avoided by employing exhaust heat exchange with reheat; this would give a higher specific output and thermal efficiency.

Figure 3.13 shows such a plant. The air before entering the combustion chamber receives heat from the outgoing exhaust gases in the heat exchanger. This requires less heat to be added in the combustion chamber. The gases after expansion in the H.P. turbine are again heated to their

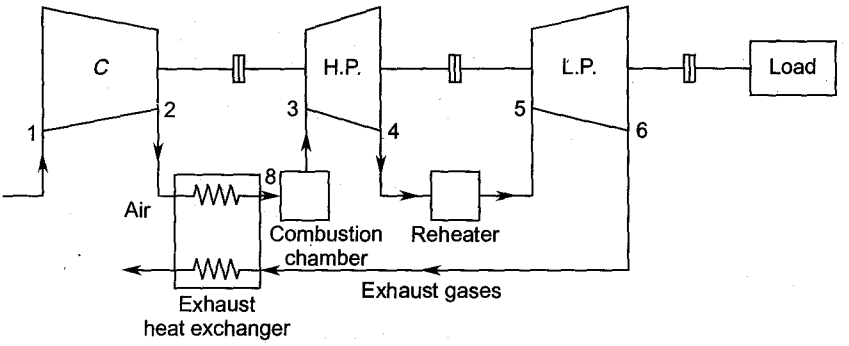

Fig. 3.13 Reheat cycle plant with exhaust heat exchanger

initial temperature ($T_3 = T_5$) before entering the L.P. turbine. The corresponding temperature-entropy diagram is shown in Fig. 3.14. Conditions stated for reheat and exhaust heat exchange cycles in Secs. 3.3.1 and 3.3.2 are also applicable here.

Therefore,
$$T_3 = T_5$$
$$T_8 = T_4 = T_6 \qquad (3.36)$$
$$T_2 = T_7$$

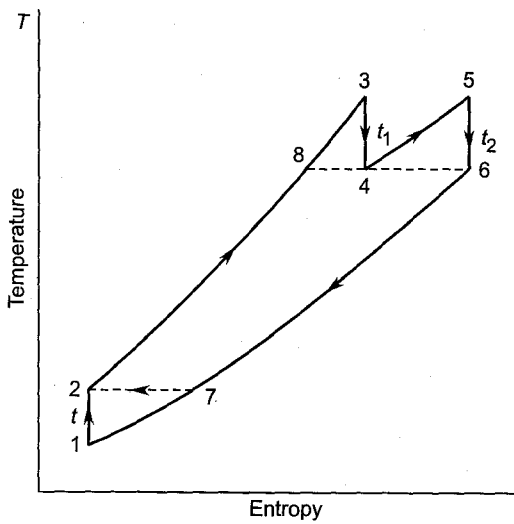

Fig. 3.14 Reheat cycle with exhaust exchanger in the *T–s* plane

Heat is supplied during the processes 8–3 and 4–5, and rejected during 7–1. Therefore,

$$Q_s = c_p (T_3 - T_8) + c_p (T_5 - T_4)$$

From Eq. (3.36)

$$Q_s = 2c_p\,(T_3 - T_4) \tag{3.37}$$

$$Q_r = c_p\,(T_7 - T_1) = c_p\,(T_2 - T_1)$$

Therefore, the plant output

$$w_P = Q_s - Q_r$$

$$w_P = 2c_p\,(T_3 - T_4) - c_p\,(T_2 - T_1) \tag{3.38}$$

Equations (3.37) and (3.38) give

$$\eta_{th} = \frac{w_P}{Q_s} = 1 - \frac{T_2 - T_1}{2(T_3 - T_4)}$$

$$\eta_{th} = 1 - \frac{T_1[(T_2/T_1) - 1]}{2T_3\,(1 - T_4/T_3)}$$

Using Eqs. (3.7), (3.22) and (3.26)

$$\eta_{th} = 1 - \frac{t - 1}{2\beta\left(1 - \frac{1}{t_1}\right)} \tag{3.39}$$

For maximum plant output conditions considered in section 3.3.2, Eq. (3.39) reduces to

$$\eta_{th} = 1 - \frac{(\sqrt{t} + 1)\sqrt{t}}{2\beta} \tag{3.40}$$

It may also be noted that expressions for plant output in Eqs. (3.30) and (3.38) are identical.

3.3.4 Cycle with Intercooling, Reheat and Exhaust Heat Exchange

The cooling of air between two stages of compression is known as intercooling. This reduces the work of compression and increases the specific output of the plant with a decrease in the thermal efficiency. The loss in efficiency due to intercooling can be remedied by employing exhaust heat exchange as in the reheat cycle.

In view of the above, it may be concluded that the best method of increasing the specific output of the plant is to employ intercooling and reheating along with exhaust heat exchange. However, this increases the bulk of the plant considerably with only a marginal gain due to intercooling. Therefore, the designers of practical gas turbine plants have little incentive to use intercooling. In contrast to this, the gains due to reheat and exhaust heat exchange are far more attractive.

Figure 3.15 shows a gas turbine plant employing intercooling, reheating and exhaust heat exchange. The air after compression in the low pressure compressor (1–2) is cooled to its initial temperature in the intercooler (2–3) before further compression in the high pressure compressor (3–4). This reduces the work in the H.P. compressor. After this the processes occurring in the rest of the plant are the same as described in the previous section.

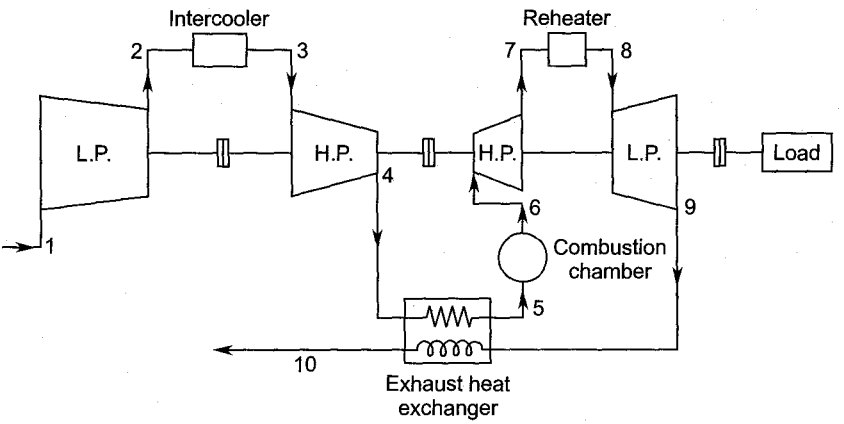

Fig. 3.15 Gas turbine plant with intercooling, reheating and exhaust heat exchange

Figure 3.16 shows a hypothetical cycle (Ericsson cycle) whose efficiency equals the efficiency of the Carnot cycle. The gas turbine plant working on this cycle employs a large number of infinitesimal compression stages with progressive intercooling; the expansion also takes place in a large number of infinitesimal stages with progressive reheating. There is perfect exhaust heat exchange, i.e. heat rejected during the constant pressure process 3–4 is fully absorbed in the constant pressure process 1–2. Thus heat reception and rejection in the cycle occur only during the constant temperature processes 2–3 (T_2 = constant) and 4–1 (T_1 = constant) respectively. Therefore, the efficiency of such a cycle is

$$\eta_{\text{Carnot}} = \frac{T_2 - T_1}{T_2} \tag{3.41}$$

Such an arrangement is only of academic interest and is not possible in practice.

3.4 Aircraft Gas Turbine Plants

Early aircrafts were flown by piston engine driven propellers. They were slow, cumbersome and had low power/weight ratio and capacity of

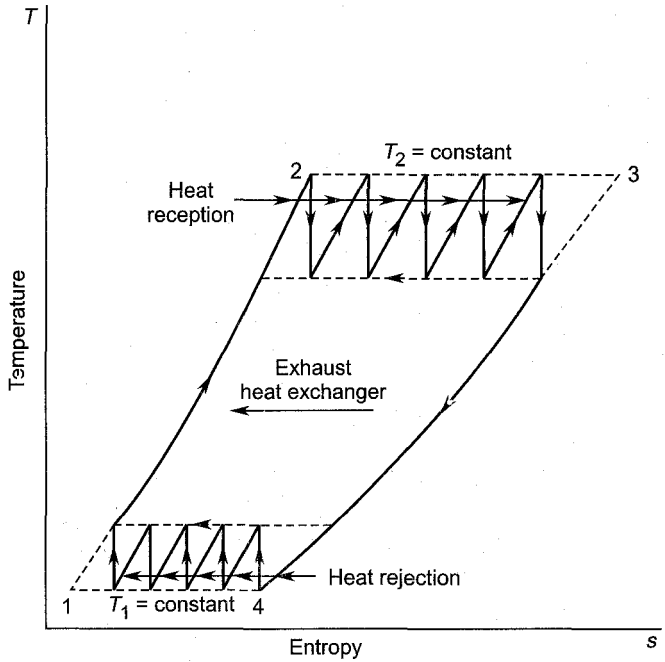

Fig. 3.16 Constant pressure cycle with a large number of inter-coolers and reheaters (Ericsson cycle)

handling gas. The late 1930s saw the successful flights of aircraft with gas turbine power plants. With the advent of this new engine, the thinking in aircraft propulsion was revolutionized. It led to higher speeds and altitudes, higher thrust/weight ratio, lower specific fuel consumption and increased reliability.

In aircraft gas turbines, the useful output of the power plant may or may not be in the form of shaft power. The gas turbine plant works entirely as a gas generator in the turbojet and turbofan engines, whereas it supplies the required shaft power to the propeller in the turboprop engine.

The gas turbine power plant[39] employed for aircraft propulsion works on the constant pressure open circuit cycle (Figs. 3.3 to 3.6) discussed in the earlier sections. An aircraft gas turbine power plant employing such a cycle is shown in Fig. 3.17. Air enters the engine at the diffuser inlet– part of the compression occurs in the diffuser and the remaining in the compressor. High pressure air from the compressor enters the combustion chamber (or chambers) as primary, secondary and tertiary air. The hot gases from the combustion chamber enter the turbine stage (or stages) which drives the compressor and propeller (if any). The hot gases leave the engine through a propelling nozzle. A part of the expansion of gases also occurs in this nozzle.

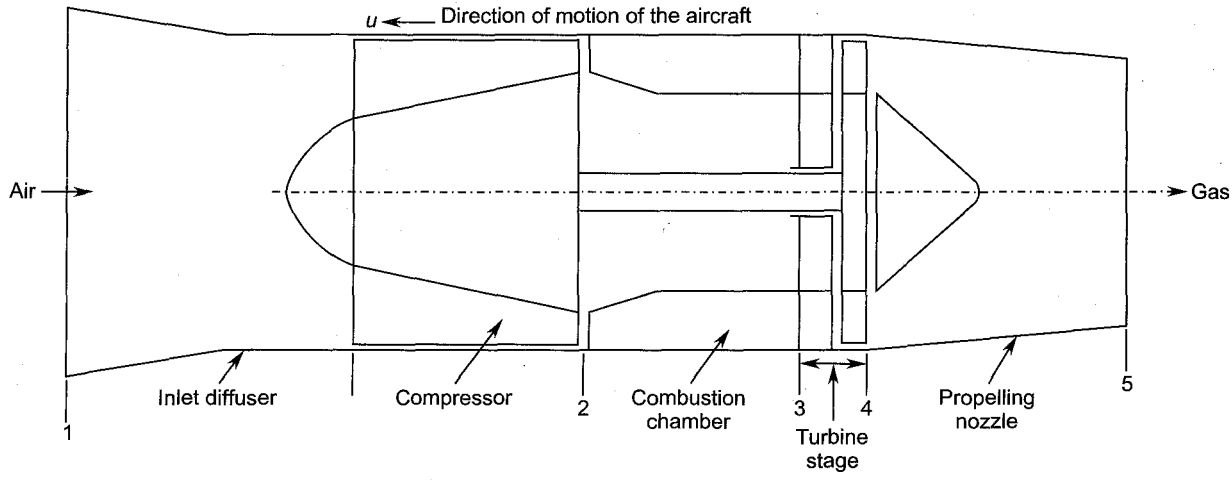

Fig. 3.17 Principal components of a turbojet engine

It is obvious that the heat rejection process cannot occur within the aircraft engine; therefore, the plant has to be an open circuit type. On account of weight considerations, intercooling, reheat and exhaust heat exchange cannot be employed. Reheat is only employed between the turbine and the propelling nozzle for obtaining thrust augmentation. This will be discussed later.

Only air breathing propulsive devices will be discussed in this section. All such engines including the piston engine require air for their working. An aircraft is propelled by the reaction of a jet of air or gas or both. These devices are:

1. Piston engine driven propeller,
2. Gas turbine driven propeller (turboprop engine),
3. Turbojet engine,
4. Turbofan engine, and
5. Ram jet.

The choice of a particular type of propulsive device (or engine) depends on the type of aircraft, its range, rate of climb, cruising speed and altitude. Piston engines have very limited applications in modern aircraft propulsion and are therefore not discussed here.

Before describing the various types of propulsive devices, a short discussion of the thrust, propulsive efficiency, specific fuel consumption etc. is given below.

3.4.1 Thrust, Specific Fuel Consumption and Propulsive Efficiency

Thrust

Figure 3.18 shows a general propulsive device moving at the speed (u) of the aircraft. The thrust (F) can be produced by accelerating either a

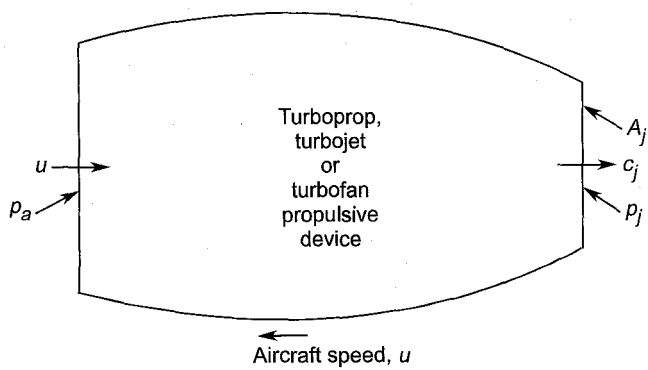

Fig. 3.18 A general propulsive device

small mass of air to a high velocity or a large mass of air to a comparatively low velocity. The change of velocity across the device (Fig. 3.18) is from u to c_j. Therefore, the steady-flow thrust due to change of momentum is

$$\dot{m}\ (c_j - u)$$

The thrust due to pressure difference on the upstream and downstream faces of the device is

$$(p_j - p_a)\ A_j$$

Therefore, the total thrust on the device is

$$F' = \dot{m}\ (c_j - u) + (p_j - p_a)\ A_j$$

For complete expansion $p_j = p_a$, the thrust for this condition is given by

$$F = \dot{m}\ (c_j - u) = \dot{m}\ u \left(\frac{c_j}{u} - 1\right) \qquad (3.42)$$

For steady-flight conditions this thrust must equal the drag force on the aircraft. It may be noted that the jet velocity c_j is always greater than the flight speed and the thrust is zero if the flight speed equals the jet speed ($u = c_j$). An increase in thrust can be obtained either by increasing the jet velocity or the mass-flow rate ($\dot{m}$) through the device. An increase in mass-flow rate requires a large-size engine with a larger frontal area which is associated with a large drag force.

The rate of work done by the thrust is given by:

Propulsive thrust power = thrust × flight speed

$$\text{Propulsive thrust power} = \dot{m}\ u\ (c_j - u) = \dot{m}u^2 \left(\frac{c_j}{u} - 1\right) \qquad (3.43)$$

Specific fuel consumption

The specific fuel consumption based on the thrust is defined as the mass of fuel required to produce a thrust of one Newton for one hour. Since it is based on thrust it is known as thrust specific fuel consumption denoted by TSFC.

$$\text{TSFC} = \frac{\dot{m}_f}{F}\ \text{(in kg/hN)} \qquad (3.44)$$

This is an index of the overall efficiency of airbreathing propulsive devices. For turboporp engines it is based on the shaft power of the engine; it is then expressed as brake specific fuel consumption (BSFC).

Propulsive efficiency

The energy supplied to the engine in the fuel is $\dot{m}_f\, Q_f$ kJ/h.

Energy output of the engine is the sum of the useful work done by the thrust and the kinetic energy in the outgoing gases. This is given by

$$\dot{m}u\ (c_j - u) + \frac{1}{2}\dot{m}(c_j - u)^2 = \frac{1}{2}\dot{m}(c_t^2 - u^2)$$

Therefore, the thermal efficiency of the engine is given by

$$\eta_{th} = \frac{\text{useful kinetic energy available for propulsion}}{\text{energy supplied to the engine}}$$

$$\eta_{th} = \frac{1}{2}\dot{m}(c_j^2 - u^2)/\dot{m}_f Q_f \tag{3.45}$$

The propulsive efficiency is defined by

$$\eta_p = \frac{\text{useful work done by the thrust}}{\text{kinetic energy available for propulsion}}$$

$$\eta_p = \frac{\dot{m}u(c_j - u)}{\dot{m}(c_j^2 - u^2)/2} \tag{3.46}$$

$$\eta_p = \frac{2u}{c_j + u} = \frac{2}{1 + (c_j/u)} \tag{3.47}$$

This is also known as Froude's efficiency. The propulsive efficiency decreases and the thrust increases as the ratio c_j/u increases. At $c_j = u$, the propulsive efficiency is unity but the thrust is zero.

Figure 3.19 gives a comparison of the efficiencies of three propulsive devices.

Overall efficiency

The overall efficiency of the propulsion device is defined by

$$\eta_o = \frac{\text{useful work done by the thrust}}{\text{energy supplied to the engine}}$$

$$\eta_o = \frac{Fu}{\dot{m}_f Q_f} = \frac{\dot{m}u(c_j - u)}{\dot{m}_f Q_f} \tag{3.48}$$

Equations (3.45), (3.46) and (3.48) yield

$$\eta_o = \eta_{th}\,\eta_p \tag{3.49}$$

Equations (3.44) and (3.48) give

$$\eta_o = \frac{u}{TSFC}\frac{1}{Q_f} \tag{3.50}$$

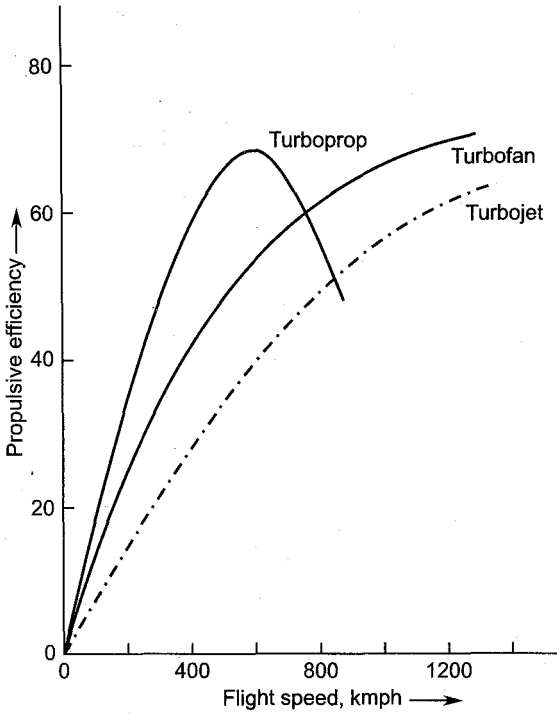

Fig. 3.19 Efficiency of various propulsive devices

Specific thrust

This is the thrust per unit flow rate of air through the device.

$$F_{sp} = \frac{F}{\dot{m}} \tag{3.51}$$

This gives an idea of the relative engine size.

Substitution of Eq. (3.51) in (3.44) gives

$$\text{TSFC} = \frac{\dot{m}_f}{\dot{m}F_{sp}} = \frac{f}{F_{sp}} \tag{3.52}$$

3.4.2 Turboprop Engine

In the turboprop system the gas turbine power plant shown in Fig. 3.17 drives a propeller at a relatively low rotational speed through a reduction gear. The turbine extracts a large proportion of the energy from the hot gases in developing the required power for driving the propeller. Therefore, the remaining energy in the exhaust gases is comparatively low. Thus the thrust due to the expanding gases in the propelling nozzle is only a small percentage ($\approx$ 10%) of the total thrust.

The large diameter propeller handles very large quantities of air with a small velocity differential. The mass of air passing through the engine is only a small fraction of the air handled by the propeller. Thus the turboprop engine can be regarded as a sort of by-pass engine with a very high by-pass ratio.

This engine provides high thrust and low TSFC at low flight speeds. In lower speed ranges, it is ideal because of its high efficiency, take-off thrust and the variable blade pitch operation.

However, the tips of the large propeller reach sonic velocity at moderate flight speeds leading to a fall in the propulsive efficiency (Fig. 3.19). Therefore, propeller engines are used only for flight Mach numbers below 0.5. An aircraft with turboprop engines must have longer landing gears.

Some details of turboprop engines are given in Sec. A.1 of Appendix A.

3.4.3 Turbojet Engine

The turbojet engine (Fig. 3.17) has already been explained briefly. It differs from the turboprop engine in that the turbine power is wholly consumed in driving the compressor; there is no shaft output power. The aircraft is wholly propelled by the jet thrust. Therefore, there is a substantial increase in the velocity of the gases as they expand in the propelling nozzle. The temperature-entropy diagram for such an engine is shown in Fig. 3.20. In this all the processes are assumed ideal. On account of the higher flight speeds, the compression (i–1) in the diffuser is substantial. Further pressure rise occurs in the compressor which may be purely axial or a combination of axial and centrifugal stages. Heat addition in the combustion chamber is represented by the constant pressure process (2–3). The expansion of the high temperature and pressure gases in the turbine stage or stages is represented by the process 3–4. further expansion in the propelling nozzle is represented by 4–5. The process 5–i does not take place inside the engine.

Figure 3.20 is also valid for a turboprop engine. However, on account of lower flight speeds and small jet thrust, the pressure changes during processes i–1 and 4–5 are comparatively small.

Since the gases at the exit of the turbine have a large amount of oxygen, more fuel can be burnt in this region for thrust augmentation. This is achieved by installing after-burners (reheater) in the jet pipe between the turbine exhaust and the propelling nozzle. A T–s diagram for such a scheme is shown in Fig. 3.21. Expansions in the turbine and the propelling nozzle are represented by 3–4 and 5–6 respectively. The reheat at constant pressure takes place during the process 4–5. Many military aircrafts employ reheat turbojet engines for their operations.

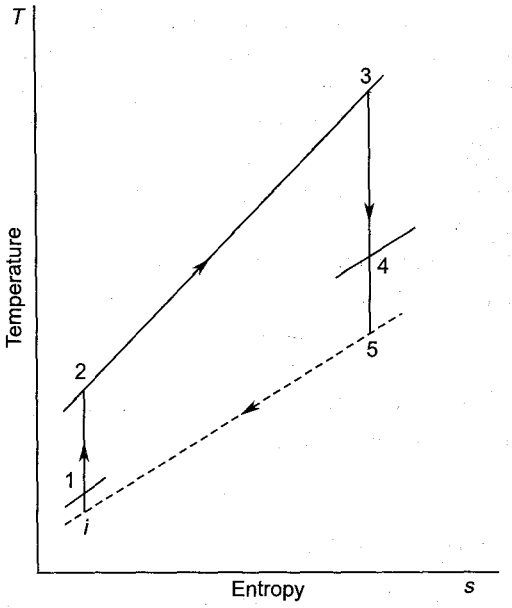

Fig. 3.20 *T–s* diagram of a turbojet engine

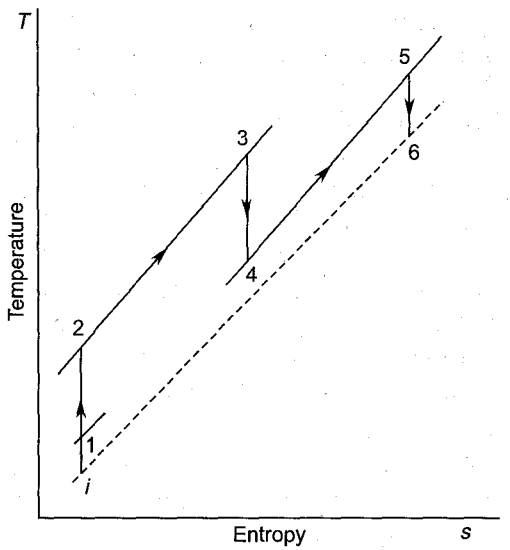

Fig. 3.21 *T–s* diagram of a turbojet engine with reheat

A turbojet engine has a relatively high specific fuel consumption at low flight Mach numbers and altitudes and requires a longer take-off roll. However, it has a low weight/thrust ratio and small frontal area.

The specifications of a typical jet engine are given in Sec. A.2 of Appendix A.

3.4.4 Turbofan Engine

In a turbofan engine[41] a large L.P. fan is driven by one of the turbine stages; unlike the turboprop, here the fan propeller is ducted. Only a part ($\dot{m}_h$) of the air from the fan is passed on to the conventional turbojet engine plant, the remaining ($\dot{m}_c$) is bypassed to the fan nozzle. The air at a slightly high pressure expands through this nozzle generating a thrust by virtue of a high flow rate with a small velocity differential.

Figure 3.22 shows the principal components of a turbofan engine. The two L.P. turbine stages drive the fan while the H.P. turbine stage drives the compressor. The air passing through the compressor, after heat addition in the combustion chamber provides all the power to drive the three-stage turbine. The hot gases leaving the last turbine stage then expand in the propelling nozzle (main nozzle) and develop thrust at a high velocity and relatively low flow rate.

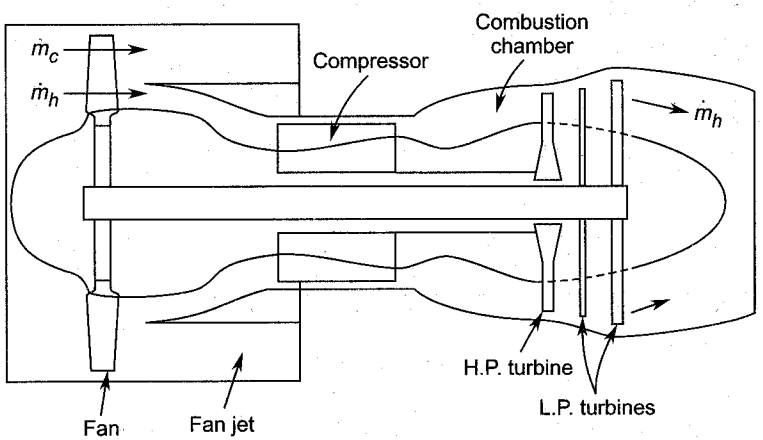

Fig. 3.22 Principal components of a turbofan engine

The total amount of air entering the fan is

$$\dot{m} = \dot{m}_c + \dot{m}_h \tag{3.53}$$

The ratio of the mass-flow rates in the cold (fan jet) and hot air jets is termed as the bypass ratio.

$$B = \frac{\dot{m}_c}{\dot{m}_h} \tag{3.54}$$

Equations (3.53) and (3.54) together give

$$\dot{m}_h = \frac{\dot{m}}{1+B} \tag{3.55}$$

$$\dot{m}_c = \frac{\dot{m}B}{1+B} \tag{3.56}$$

Assuming expansion of both the cold and hot jets to the atmospheric pressure, the application of the momentum equation gives the total thrust as

$$F = \dot{m}_c\, c_{jc} + \dot{m}_h\, c_{jh} - \dot{m}\, u$$

$$F = \frac{\dot{m}}{1+B}(B\, c_{jc} + \dot{m}_h\, c_{jh}) - \dot{m}\, u \qquad (3.57)$$

Modern bypass or turbofan engines use a bypass ratio up to a value of 8 or more. Since a large part of the total thrust is obtained by the cold jet at a low velocity, the propulsive efficiency of a turbofan engine is high (Fig. 3.19) at subsonic flight Mach numbers. This is accompanied by a considerable decrease ($\approx$ 20%) in the noise level compared to an equivalent turbojet engine.

Figure 3.23 shows a variation of the turbofan engine. Here the fan blades are an extension of the L.P. turbine rotor blades and the H.P. turbine drives the air compressor.

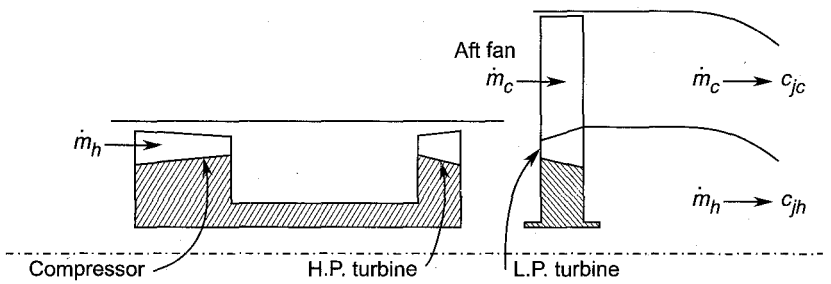

Fig. 3.23 Turbofan engine with aft fan

The specific weight and TSFC for turbofan engines are between those for the turboprop and turbojet engines; it requires a shorter take-off roll.

The principal data for a turbofan engine are given in Sec. A.3 of Appendix A.

3.4.5 Ramjet Engine

This device does not consist of a gas turbine power plant. It is included here only for a comparison with propulsive devices employing gas turbines. The compression of air takes place due to the "ram effect" at high flight Mach numbers. Therefore, the compressor and hence the driving turbine are not required. High gas temperatures can therefore be employed in the absence of the restrictions imposed by the turbine blade

material. The performance of this device is comparable with that of the turbojet engine at supersonic speeds.

Since the turbine and compressor are absent, the ramjet engine cannot be started while it is at rest. It needs a launching device.

3.4.6 Turbo-rocket Engine

As the name indicates, the turbo-rocket engine (Fig. 3.24) is a cross between the rocket motor and the turbojet engine. The turbine is driven by the gases supplied from the rocket combustion chamber which is independent of the atmospheric air. A reheater downstream of turbine replaces the combustion chamber of the conventional turbojet system. Such engines can be used to assist large aircrafts in taking off and climbing without high wing loading. Rocket-propelled aircrafts can also be used to take men and material to space stations.

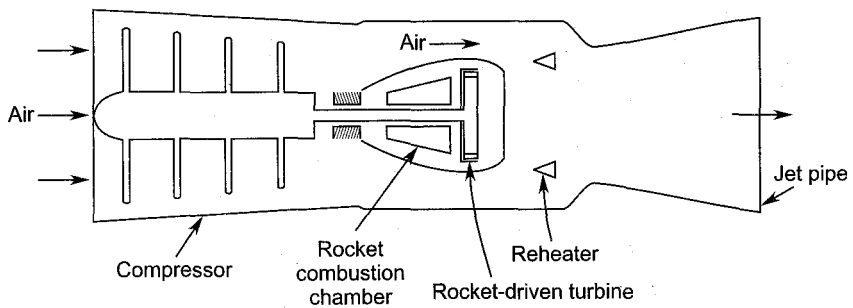

Fig. 3.24 Turbo-rocket engine

The French Mirage III aircraft (*a*) takes off on a turbojet, (*b*) employs a rocket motor for the high rate of climb, (*c*) cruises on a turbojet, (*d*) travels at a high supersonic speed for intercepting the target, and (*e*) returns on a turbojet.

3.4.7 Nuclear Aircraft Engine

Figure 3.25 shows a nuclear-powered hot air turbojet engine. The combustion chamber of the conventional turbojet engine is replaced here by a heat exchanger. A suitable coolant transfers the required amount of heat from the reactor to the air in the heat exchanger. The air compressor is driven by a hot air turbine which works here in a less hostile environment compared to gas turbines.

Section 4.7 of the steam turbine plants gives more details of the nuclear reactor.

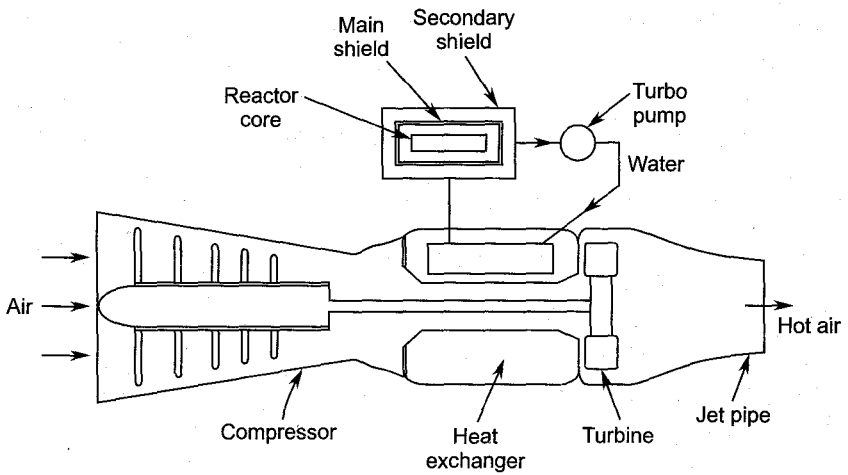

Fig. 3.25 Nuclear aircraft engine

3.5 Gas Turbines for Surface Vehicles

The problems and design features of gas turbines employed by sur-face vehicles are considerably different from those of aircraft gas turbines.

Automobiles

Attempts were made by a number of automobile manufacturing companies in various countries to perfect gas turbine engines for cars. An exhaust heat exchanger was used to improve the fuel economy. However, inspite of a high degree of technological success, the gas turbine car engine at present cannot commercially compete with the well-established piston engine. Some degree of success was achieved in the field of heavy vehicles with engines of over 200 kW. Many designs employed the combination of an axial turbine and a low pressure centrifugal compressor along with a rotary heat exchanger.

The gas turbine automobile engine is mechanically sound and pollutes the atmosphere at a lesser rate. However, it suffers from its inherent high speed, and poor part-load performance.

Railway locomotives

Long distance passenger trains have employed gas turbine locomotives in many countries. Gas turbine locomotives (with electrical transmission) can be introduced in sectors where electric traction is uneconomical.

Exhaust superchargers

Small gas turbines are also used in automobiles in another way. All large truck and railway diesel locomotive engines are supercharged. They

employ exhaust gas driven turbines (axial or inward flow radial) to drive the centrifugal air compressors (super chargers).

Hovercrafts

Commercial and naval[31,33] services are now employing an ever increasing number of air cushion crafts. They have certain advantages over marine vehicles. Gas turbine provides all the power for lift and propulsion in such crafts. In a typical 100 t U.S. design, the air cushion is generated and maintained by eight lift fans. Three marine gas turbines provide propulsion through the propellers located astern.

The world's first commercial hovertrain developed in France employs air screw propulsion and has a speed of 300 km/h. The train has two sets of six air cushions.

Hydrofoils

Hydrofoils employ the lift on an aerofoil to lift the craft above the water surface. This enables them to move at comparatively higher speeds (120 km/h). The application of gas turbines for powering hydrofoils is on a relatively small scale.

3.6 Gas Turbines for Electric Power Generation

Gas turbines are used for electric power generation in a number of ways. Some of its main advantages are ability to start quickly, lower cooling water requirement, and high temperature and low pressure of the working medium.

Aeroengines

The life of a terrestrial gas turbine between ovrhauls is 20,000-30,000 hrs. compared to 3000-7000 hrs. for aeroengines. Full advantage of the high level of design of aeroengines is taken in designing gas turbine power plants for electric power generation.

Turboprop engines with some modifications of the combustion chamber and bearings can be used to drive electric generators through reduction gears. A number of derated turbojet engines (gas generators) can supply the working gas to a separate power turbine. A large plant uses eight jet engines feeding four power turbines giving a total output of 120-140 MW. Another 100 MW single-stage gas turbine plant employs ten jet engines around the periphery of a single turbine rotor for supplying gas to its various sectors of nozzles.

Aeroengines in power stations can be brought to full-load operation from cold in a few minutes. This makes them ideal for peak load operation.

Topping plant

The temperature of the exhaust gases in a gas turbine is high. Therefore, the use of gas turbine plants in electric power stations without any heat recuperating apparatus makes them uneconomical. Some arrangements employed to recover the exhaust heat in power stations and industrial processes are discussed here and again in Sec. 4.6.

Figure 3.26 shows a gas turbine [29,30,35] as a topping plant. The gas turbine forms the high temperature loop whereas the steam plant forms the low temperature loop. The connecting link between the two loops (or cycles) is the steam boiler working on the exhaust heat of the gas turbine. The outgoing exhaust gases also heat the feed water of the steam cycle. The gas turbine, as shown here, works wholly as a gas generator for the steam plant, whereas the steam turbine drives the generator. In another arrangement the gas turbine can also drive a generator, thus contributing to the total output of the combined gas-steam plant.

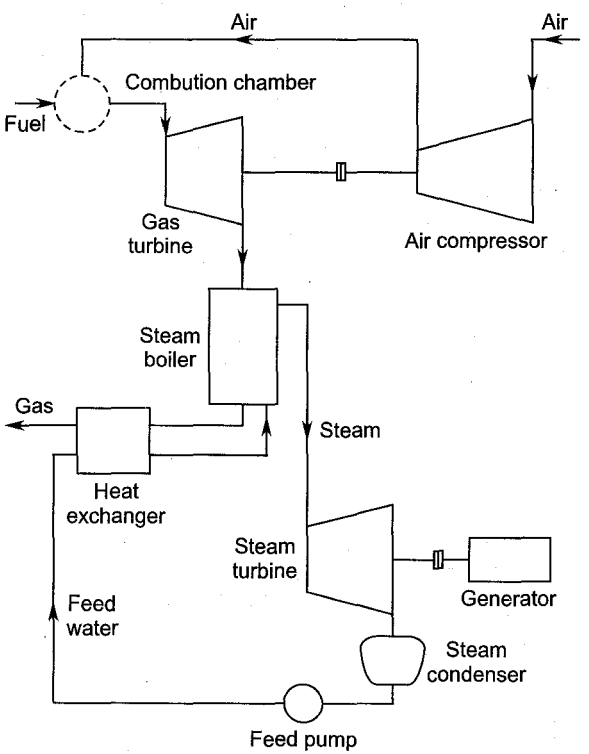

Fig. 3.26 A topping gas turbine plant (combined gas-steam plant)

Combined cycle plants are discussed in greater details in Chapter 5.

Total energy plant

Satisfying the demands of heating, cooling and electrical energy from a single source is the total energy concept. The type of fuel used in a total energy system may be liquid or gaseous and is chosen on economic considerations, availability, cost and transportation.

Figure 3.27 shows a gas turbine plant in the total energy system. The steam boiler utilizes the energy in the high temperature turbine exhaust gases. Steam can be used directly for space heating. For cooling purposes, steam is utilized in producing chilled water in an absorption chiller. The overall efficiency of the total energy plant is between 60 and 75%.

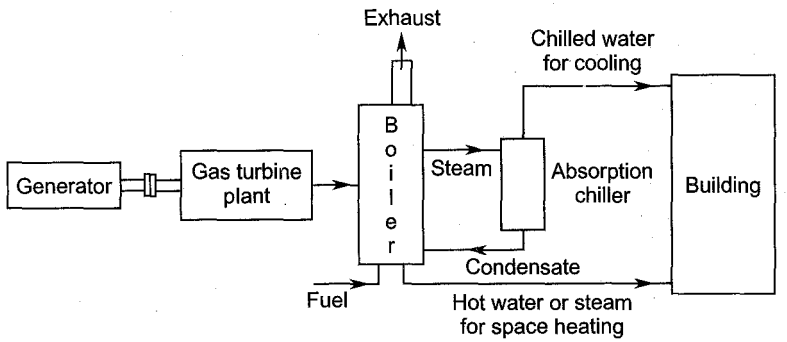

Fig. 3.27 Gas turbine plant in the total energy system

Nuclear plant

Figure 3.28 shows a closed circuit nuclear gas turbine [32,38,43] plant. Helium gas is used both as a coolant in the reactor and the working fluid in the closed circuit gas turbine plant. Helium after compression is first heated in the heat exchanger and then in the reactor. The high pressure and temperature ($p \approx$ 25-50 bar, T = 1000-1200 K) gas drives the helium turbine. The turbine drives both the compressor and the load (electric

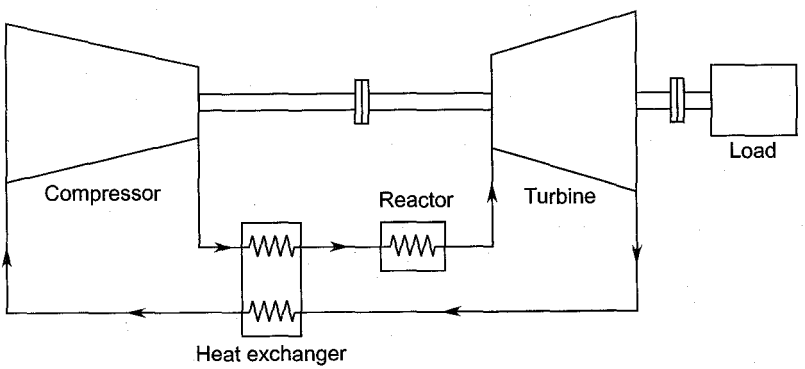

Fig. 3.28 A closed circuit nuclear gas turbine plant

generator). The details of the nuclear reactor are briefly described in Sec. 4.7.

3.7 Gas Turbines in Petro-chemical Industries

Gas turbines have special applications in a variety of industries. Some advantages of the gas turbines in these applications are:

1. A variety of fuels can be used in gas turbine plants. Some process gases (which are otherwise lost) can also be used.
2. The energy in its exhaust gases can be used in various processes.
3. They can be used conveniently for industrial utilities, such as compressed air, hot gases, steam, hot water, mechanical and electrical power.
4. It is easy to install, cheap, compact and competitive (cost-wise); it has ability to combine with other equipment.
5. Ease in speed regulation in industrial drives.

Figure 3.29 shows a gas turbine supplying preheated combustion air to boilers. The cooling of air after the blower reduces the compressor size and its work.

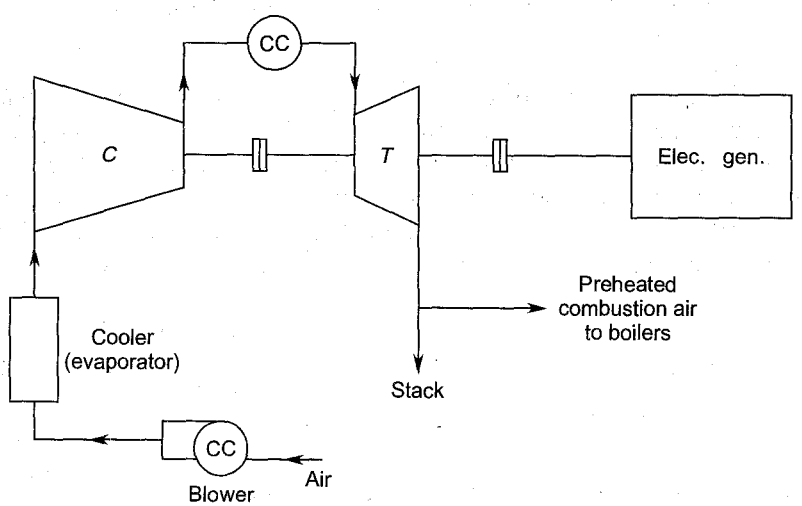

Fig. 3.29 Gas turbine supplying preheated combustion air for steam boilers

Figure 3.30 shows a gasifier supplying hot gases for an industrial process. Additional fuel is burnt in combustion chamber placed after the turbine depending on the heat requirement in the process. The hot gases,

after the process, can be further used in steam boilers. The starting turbine runs on compressed air.

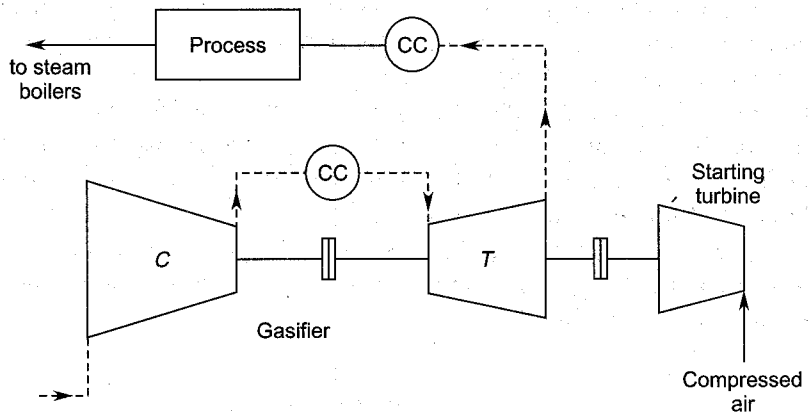

Fig. 3.30 Gasifier supplying hot gases for an industrial process

Figure 3.31 shows the application of the gas turbine and compressors in the manufacture of nitric acid. The gas turbine works on the waste heat of the process—it drives the axial and centrifugal stages of the compressor. Oxygen is removed from the high pressure air before injecting steam. A steam turbine is employed for starting the plant.

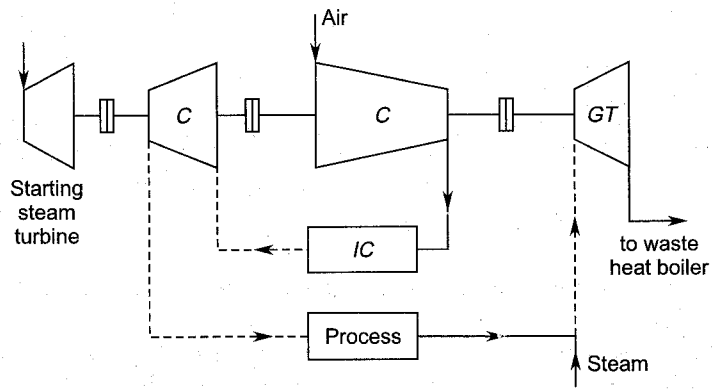

Fig. 3.31 Pressurized process used in the manufacture of nitric acid

3.8 Gas Turbines in Cryogenics

Enginneering and scientific aspects of considerably low temperature (–157°C) form the subject matter of cryogenics. Low temperatures can be obtained by:

1. Isenthalpic Joule-Thomson expansion, and
2. Isentropic expansion.

Isentropic expansion was first obtained by reciprocating expanders which had problems at very low temperatures. Rotating machines on account of high speeds (up to 6×10^5 rpm) are most suitable for this purpose. High speed turbo-expanders employing 8-16 mm diameter inward flow radial turbines give very low temperatures. Helium and hydrogen turbo-expanders do not have problems of high Mach number because of the high speed of sound.

Figure 3.32 shows the La-Fleur helium gas turbine cryogenic refrigeration system. Various processes occurring in this plant are shown in the *T-s* plane in Fig. 3.33.

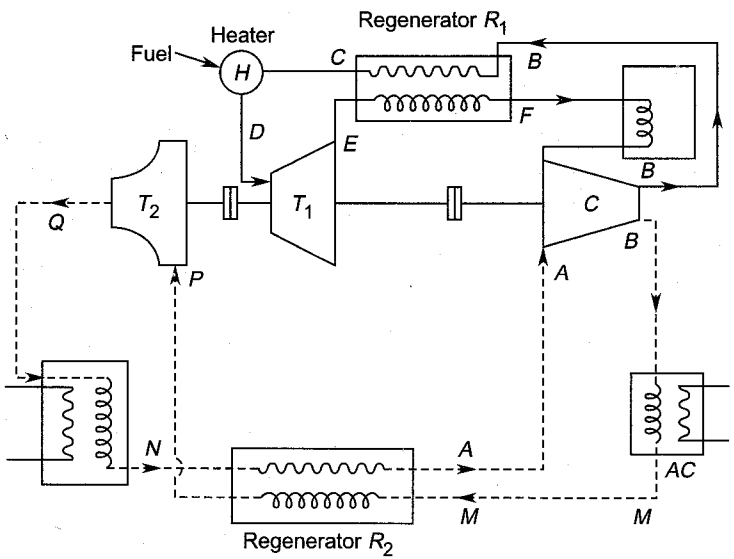

Fig. 3.32 The La-Fleur helium gas turbine refrigeration system

Helium is first compressed (AB) to a high pressure in a common compressor. At the exit of the compressor, helium is divided between the power and the refrigeration cycles.

In the closed circuit power cycle helium is passed through a regenerator (BC) before heating it by burning fuel. The heater or combustion chamber (CD) raises its temperature for doing work in the turbine (DE). The turbine power is used to drive the compressor. The exhaust from the turbine is sent back to the compressor inlet through the hot side (EF) of the regenerator and a precooler. Thus the output of the closed circuit helium gas turbine plant is the high pressure helium

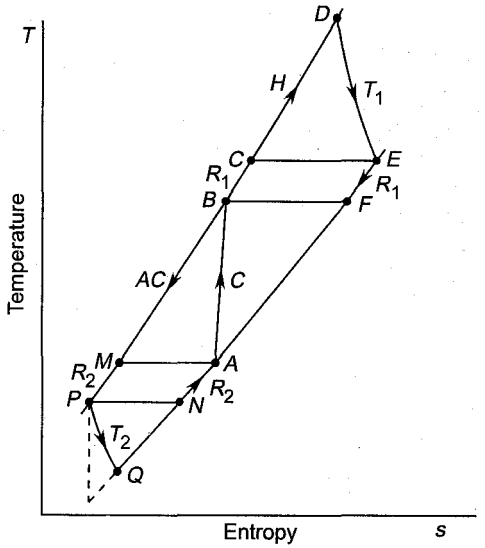

Fig. 3.33 *T–s* diagram of the La-Fleur refrigeration system

available for the refrigeration cycle. This is first cooled in the after cooler (BM) and the regenerator (MP) before expanding it in the high-speed inward flow radial cryogenic turbine (PQ). The expansion of helium in the turbine reduces it to a very low temperature. The power output of the cryogenic turbine can also be utilized in driving the helium compressor. Low temperature helium after having been used for low temperature refrigeration (QN) goes back to the compressor through the cold side of the regenerator.

3.9 Miscellaneous Applications of Gas Turbines

Only some major applications of gas turbines have been described in this chapter. The aim of this is to highlight the significance of the gas turbine as a single element in the given total system.

By virtue of the extreme simplicity and light-weight design, small gas turbines (some of them working on hot air) have found wide applications in many fields from surgery to aerospace. Small air turbines are used to operate the drills used by orthopaedic and dental surgeons. The low temperature air after expansion in these turbines is used for cooling the drilled region. Small gas turbines working on high energy fluids at low flow rates are employed in the auxiliary power units in underwater and aerospace vehicles. Gas turbine drives for turbo-pumps are used in rockets and missiles.

Other applications of gas turbines are in steel making, oil and gas pumping, marine propulsion and helicopter rotor drives.

Notation for Chapter 3

A	Area of cross-section
AC	Air cooler
B	Bypass ratio
c	Fluid velocity
C	Compressor
CC	Combustion chamber
c_p, c_v	Specific heats
F	Thrust
f	Fuel-air ratio
GT	Gas turbine
IC	Intercooler
$\dot{m}$	Mass-flow rate
p	Pressure
Q	Heat transferred or calorific value of the fuel
R	Regenerator
r	Pressure ratio
t	Temperature ratio
T	Temperature or turbine
TSFC	Thrust specific fuel consumption
u	Flight speed
v	Specific volume
w	Work

Greek Symbols

α	$= \beta\eta_C\eta_T$
β	Ratio of maximum and minimum temperatures
γ	c_p/c_v
ε	Heat exchanger effectiveness
η	Efficiency

Subscripts

a	Ambient
c	Cold
c	Compressor
f	Fuel
h	Hot

j	Jet
p	Propulsive
p	Plant
r	Rejected
s	Isentropic, supplied
sp	Specific
th	Thermal
t	Turbine
o	Overall
1	First stage or compressor entry
2	Second stage or compressor exit
3	Turbine entry
4	Turbine exit

Solved Examples

3.1 In a constant pressure cycle gas turbine plant the minimum and maximum temperatures are 50°C and 950°C respectively. If the compressor and turbine efficiencies are 0.82 and 0.87, determine for maximum power output:

(a) the pressure ratio of the turbine and compressor,

(b) the maximum power output per unit flow rate and

(c) the thermal efficiency of the plant.

Assume for both compressor and turbine $\gamma = 1.4$ and $c_p = 1.005$ kJ/kg K.

***Solution*:**

$$T_1 = 273 + 50 = 323 \text{ K}$$

$$T_3 = 273 + 950 = 1223 \text{ K}$$

$$\beta = T_3/T_1 = 1223/323 = 3.786$$

$$\alpha = \beta\eta_C\eta_T = 3.786 \times 0.82 \times 0.87 = 2.70$$

For maximum power output, the temperature ratios in the turbine and compressor are

$$t_{\text{opt}} = \sqrt{\alpha} = \sqrt{2.70} = 1.644$$

(a) In the absence of pressure losses the pressure ratio for both the turbine and compressor is

$$r = (t_{opt})^{\frac{\gamma}{\gamma-1}} = (1.644)^{3.5} = 5.697 \ (Ans.)$$

(b) $$w_{p_{max}} = \frac{1}{\eta_c} c_p T_1 (\sqrt{\alpha} - 1)^2$$

$$w_{p_{max}} = 1.005 \times 323 \ (0.644)^2/0.82$$

$$w_{p_{max}} = 164.18 \text{ kW/(kg/s)} \ (Ans.)$$

(c) The thermal efficiency of the plant for maximum power output is

$$\eta'_{th} = \frac{(\sqrt{\alpha} - 1)^2}{(\beta - 1)\eta_c - (\sqrt{\alpha} - 1)}$$

$$\eta'_{th} = \frac{0.644^2}{(3.786 - 1)0.82 - 0.644} = 0.252$$

$$\eta'_{th} = 25.2\% \ (Ans.)$$

3.2 A gas turbine plant with an exhaust heat exchanger has the following data:

Turbine and compressor pressure ratio 10.0

Minimum cycle temperature 300 K

Maximum cycle temperature 1500 K

Flow rate through turbine and compressor 10 kg/s

Thermal ratio of the heat exchanger 0.8

Turbine efficiency 85%

Compressor efficiency 82%

The mass flow of the fuel can be ignored. The properties of air and gas are about the same.

$$c_p = 1.005 \text{ kJ/kg K}, \ \gamma = 1.4$$

Determine:

(a) Power developed,

(b) Thermal efficiency of the plant and

(c) Efficiencies of the ideal Joules cycle with heat exchange and Carnot's cycle. Recalculate (*a*) and (*b*) when the thermal ratio of the heat exchanger is uniy.

***Solution*:**

Refer to Fig. 3.10.

$$T_2 - T_1 = \frac{1}{\eta_c}(T_{2s} - T_1) = \frac{T_1}{\eta_c}\left(r^{\frac{\gamma-1}{\gamma}} - 1\right)$$

$$T_2 = 300 + \frac{300}{0.82}(10^{0.286} - 1) = 640.6 \text{ K}$$

$$T_3 = 1500 \text{ K}$$

$$T_3 - T_4 = \eta_T (T_3 - T_{4s}) = \eta_T T_3 (1 - r^{-0.286})$$

$$T_4 = 1500 - 0.85 \times 1500 (1 - 10^{-0.286})$$

$$T_4 = 885 \text{ K}$$

$$\frac{T_5 - T_2}{T_4 - T_2} = 0.8$$

$$T_5 - 640.6 = 0.8 (885 - 640.6) = 195.52$$

$$T_5 = 836.12 \text{ K}$$

For the same flow rate and properties of the gases on the cold and hot sides of the heat exchanger,

$$T_5 - T_2 = T_4 - T_6$$

$$836.12 - 640.6 = 885 - T_6$$

$$T_6 = 689.48 \text{ K}$$

$$Q_s = c_p (T_3 - T_5)$$

$$Q_s = 1.005 (1500 - 836.12) = 667.2 \text{ kJ/kg}$$

$$Q_r = c_p (T_6 - T_1)$$

$$Q_r = 1.005 (689.48 - 300) = 391.43 \text{ kJ/kg}$$

(a) Power developed

$$\dot{m} w_P = \dot{m} (Q_s - Q_r)$$

$$\dot{m} w_P = 10 (667.2 - 391.43)$$

$$\dot{m} w_P = 2757.7 \text{ kW } (Ans.)$$

(b) Thermal efficiency of the plant

$$\eta_{th} = 1 - Q_r/Q_s$$

$$\eta_{th} = 1 - 391.43/667.2$$

$$\eta_{th} = 41.33\% \ (Ans.)$$

(c) The efficiency of the ideal Joule's cycle with perfect heat exchange is

$$\eta_{\text{Joule}} = 1 - \frac{1}{\beta} r^{\frac{\gamma - 1}{\gamma}}$$

$$\eta_{\text{Joule}} = 1 - \frac{1}{5}(10)^{0.286}$$

$$\eta_{\text{Joule}} = 61.36\% \ (Ans.)$$

Carnot's efficiency between temperatures 1500 K and 300 K is

$$\eta_{\text{Carnot}} = 1 - \frac{300}{1500}$$

$$\eta_{\text{Carnot}} = 80\% \ (Ans.)$$

When the thermal ratio of the heat exchanger is unity.

$$T_2 = T_6 = 640.6 \text{ K}$$

$$T_5 = T_4 = 885 \text{ K}$$

$$Q_s = c_p (T_3 - T_5)$$

$$Q_s = 1.005 (1500 - 885) = 618 \text{ kJ/kg}$$

$$Q_r = c_p (T_6 - T_1)$$

$$Q_r = 1.005 (640.6 - 300) = 342.3 \text{ kJ/kg}$$

Power developed is

$$\dot{m} (Q_s - Q_r) = 10 (618 - 342.3)$$

$$\text{Power} = 2757 \text{ kW } (Ans.)$$

This is the same as before, proving that power is not affected by the presence or performance of an exhaust heat exchanger. It is only the thermal efficiency that is affected.

$$\eta_{th} = 1 - 342.3/618$$

$$\eta_{th} = 44.6\% \ (Ans.)$$

3.3 Solve Problem 3.6 for an ideal reheat cycle with optimum reheat pressure.

Solution:

$$\beta = 5, \ r = 25$$

$$t = r^{\frac{\gamma - 1}{\gamma}} = 25^{\ 0.286} = 2.51$$

$$\sqrt{t} = \sqrt{2.51} = 1.584$$

For maximum work output

$$t_1 = t_2 = \sqrt{t} = 1.584$$

$$\dot{m} w_{p\max} = \left(2\beta - \frac{2\beta}{\sqrt{t}} - t + 1\right) mc_p T_1 = 1000$$

$$\dot{m} \times 1.005 \times 300 \left(10 - \frac{10}{1.584} - 2.51 + 1\right) = 1000$$

$$\dot{m} = 1.532 \text{ kg/s } (Ans.)$$

The thermal efficiency is given by

$$\eta_{th} = \frac{2\beta - 2\beta/\sqrt{t} - t + 1}{2\beta - t - \beta/\sqrt{t}}$$

$$\eta_{th} = \frac{2 \times 5 - 10/1.584 - 2.51 + 1}{2 \times 5 - 2.51 - 5/1.584}$$

$$\eta_{th} = 49.9\% \ (Ans.)$$

3.4 Solve Problem 3.6 for an ideal reheat cycle with optimum reheat pressure and perfect exhaust heat exchange.

***Solution*:**

The power output is unaffected by exhaust heat exchange—it only improves the thermal efficiency of the plant. For maximum plant output, it is given by

$$\eta_{th} = 1 - \frac{(\sqrt{t} + 1)\sqrt{t}}{2\beta}$$

$$\eta_{th} = 1 - \frac{(1.584 + 1)\,1.584}{2 \times 5}$$

$$\eta_{th} = 59.07\% \ (Ans.)$$

The flow rate through the plant is the same as in Ex. 3.3.

$$\dot{m} = 1.532 \text{ kg/s}$$

3.5 A gas turbine power plant has an output of 100 MW at the generator terminals. Its data is given below:

Air compressor inlet pressure and temperature $p_1 = 1.013$ bar,

$$T_1 = 310 \text{ K}$$

Compressor pressure ratio = 8.0, Efficiency $\eta_c = 0.85$,

Turbine inlet temperature = 1350 K, Efficiency $\eta_t = 0.90$,

Turbine inlet pressure = 0.98 × compressor exit pressure

Turbine exit pressure = 1.02 bar.

Calorific value of the fuel, $Q_f = 40$ MJ/kg

Combustion efficiency, $\eta_B = 0.98$,

Mechanical efficiency, $\eta_m = 0.97$,

Generator efficiency, $\eta_G = 0.98$

Take $\gamma = 1.33$, $R = 0.287$ kJ/kg K for the gas.

Determine:

(a) Gas flow rate,

(b) Fuel-air ratio,

(c) Air flow rate,

(d) Thermal efficiency of the power plant,

(e) Overall efficiency and

(f) Ideal Joule cycle efficiency.

Solution:

See figure 3.5

For air $\frac{\gamma-1}{\gamma} = \frac{1.4-1}{1.4} = \frac{1}{3.5} = 0.2857$

Air Compressor

$$\frac{T_{2s}}{T_1} = p_r^{0.2857} = 8^{.2857} = 1.811$$

$$T_2 - T_1 = \frac{T_1}{\eta_c}\left(\frac{T_{2s}}{T_1} - 1\right) = \frac{310}{0.85}(1.811 - 1) = 295.776\text{K}$$

$$T_2 = 310 + 295.776 = 605.776 \text{ K}$$

$$w_c = c_{pa}(T_2 - T_1)$$

$$w_c = 1.005 \times 295.255 = 297.255 \text{ kJ/kg}$$

Gas turbine

$$\frac{\gamma-1}{\gamma} = \frac{1.33-1}{1.33} = \frac{1}{4.03} = 0.248$$

$$c_{pg} = 1.157 \text{ kJ/kg K}$$

$$\frac{T_3}{T_{4s}} = \left(\frac{p_3}{p_4}\right)^{(\gamma-1)/\gamma}$$

$$p_3 = 0.98p_2 = 0.98 \times 8 \times 1.013 = 7.9419 \text{ bar}$$

$$\frac{p_3}{p_4} = \frac{7.9419}{1.02} = 7.786$$

$$\frac{T_3}{T_{4s}} = 7.786^{\,0.248} = 1.663$$

$$T_3 - T_4 = \eta_t T_3\left(1 - \frac{1}{T_3/T_{4s}}\right)$$

$$T_3 - T_4 = 0.9 \times 1350\left(1 - \frac{1}{1.663}\right) = 484.393\text{K}$$

$$T_4 = 1350 - 484.393 = 865.607 \text{ K}$$

$$w_t = c_{pg}(T_3 - T_4) = 1.157 \times 484.393 = 560.443 \text{ kJ/kg}$$

$$w_P = w_t - w_c = 560.443 - 297.255 = 263.187 \text{ kJ/kg}$$

$$w_g = \eta_m \times \eta_G \times w_P$$

$$w_g = 0.97 \times 0.98 \times 263.187 = 250.186 \text{ kJ/kg}$$

$$\dot{m}_g \times w_g = 100 \text{ MW}$$

(a) $$\dot{m}_g = \frac{100 \times 1000}{250 \cdot 186} = 399.703 \text{ kg/s} \quad Ans.$$

Energy balance of the combustion chamber gives

$$(\dot{m}_f Q_f)\ \eta_B = \dot{m}_g\ c_{pg}\ T_3 - \dot{m}_a . c_{pa} . T_2$$

$$\dot{m}_g = \dot{m}_a + \dot{m}_f = \left(1 + \frac{\dot{m}_f}{\dot{m}_a}\right)\ \dot{m}_a = (1 + f)\ \dot{m}_a$$

$$f . Q_f\ \eta_B = (1 + f)\ c_{pg} .\ T_3 - c_{pa} .\ T_2$$

$$40 \times 10^3 \times 0.98 \times f = (1 + f) \times 1.157 \times 1350 - 1.005 \times 605.776$$

(b) $$f = \frac{\dot{m}_f}{\dot{m}_a} = 0.0253 = \frac{1}{39.486}$$

(c) $$\dot{m}_a = \frac{\dot{m}_g}{1 + f} = \frac{399.703}{1.0253} = 389.84 \text{ kg/s}$$

$$\dot{m}_f = \dot{m}_g - \dot{m}_a = 399.703 - 387.84$$

$$\dot{m}_f = 9.863 \text{ kg /s}$$

(d) Thermal efficiency of the plant is given by

$$\eta_{th} = \frac{\text{Plant output}}{\text{Energy in the fuel}} = \frac{\dot{m}_g \times w_p}{\dot{m}_f\ Q_f}$$

$$= \frac{399.703 \times 263.187}{9.863 \times 40000} \times 100 = 26.66 \text{ per cent} \quad \text{Ans.}$$

(e) Overall efficiency is given by

$$\eta_o = \eta_m \times \eta_G \times \eta_{th}$$

$$\eta_o = 0.97 \times 0.98 \times 26.66 \qquad Ans.$$

$$\eta_o = 25.285 \text{ per cent}$$

(f) Ideal Joule cycle efficiency

$$\eta_j = 1 - \frac{1}{p_r^{(\gamma - 1)/\gamma}} = 1 - \frac{1}{8^{0.2857}}$$

$$\eta_j = 0.4478\ (44.78\%)$$

Questions and Problems

3.1 Describe with the aid of a plant layout and p–v and T–s diagrams, the working of simple closed circuit, ideal and actual constant pressure gas turbine cycles.

Mention the variables on which the efficiencies and outputs of these cycles depend.

3.2 What are the various methods employed for improving the efficiency and output of a constant pressure gas turbine plant?

3.3 Explain briefly why a constant volume cycle gas turbine plant is not as widely employed as a constant pressure type. What are its major drawbacks?

3.4 What are the advantages of a closed circuit gas turbine plant over an open circuit type? Give three practical examples where closed circuit gas turbine plants are used.

3.5 In a simple constant pressure gas turbine cycle with maximum to minimum temperature ratio β and turbine and compressor efficiencies of η_t and η_c respectively, prove that

(a) $$\frac{\text{Maximum specific work output}}{c_p T_1} = \frac{1}{\eta_c}(\sqrt{\beta \eta_c \eta_T} - 1)^2$$

(b) The thermal efficiency at maximum output is

$$\frac{\left(\sqrt{\beta \eta_c \eta_T} - 1\right)^2}{(\beta - 1)\eta_c - \left(\sqrt{\beta \eta_c \eta_T} - 1\right)}$$

(c) Determine the values in (*a*) and (*b*) for temperature ratios of 2, 3, 4, and 5 and plot them against temperature ratio.

Take $\eta_C = 75\%$ and $\eta_T = 80\%$ for all values of temperature ratio.

Ans. $(w_P)/(c_p\, T_1) = 0.012,\ 0.156,\ 0.402$ and 0.715.

$\eta_{th} = 1.37\%,\ 10.1\%,\ 17.7\%$ and 23.6%.

3.6 A small gas turbine plant has an output of 1 MW at a maximum-to-minimum temperature ratio of 5.0 and a pressure ratio of 25.0. The overall turbine and compressor efficiencies are 85% and 82% respectively. The compressor draws air at 300 K; the properties of the gas may be assumed to be the same as that of air. Determine:

(a) the mass flow through the turbine,

(b) the thermal efficiency of the plant, and

(c) the efficiencies of the reversible Joule cycle and the Carnot's cycle between the same temperatures.

Ans. $\dot{m} = 4.634$ kg/s, $\eta_{th} = 33.2\%$,

$\eta_J = 60.2\%$, $\eta_{\text{Carnot}} = 80.0\%$.

3.7 What is the pressure ratio for maximum output of the plant in Problem 3.6 Determine the corresponding values of:

(a) mass-flow rate through the turbine,

(b) thermal efficiency of the plant and

(c) the efficiencies of the reversible Joule cycle and Carnot's cycle between the same temperatures.

Ans. $r = 8.889$, $\dot{m} = 3.618$ kg/s, $\eta_J = 46.4\%$

$\eta_{\text{Carnot}} = 80\%$, $\eta_{th} = 31.1\%$

3.8 What is thermal ratio of an exhaust exchanger in a gas turbine plant? What is its effect on the power output and thermal efficiency of the plant?

3.9 **(a)** Draw an illustrative sketch of a turbojet gas turbine engine, indicating its principal parts.

(b) Show various processes occurring in the engine on a *T-s* diagram. How would it change for a reheat cycle?

3.10 Describe with the aid of illustrative sketches the working of the following aeroengines:

(a) Turbofan engine,

(b) Turbo-rocket engine and

(c) a nuclear aircraft engine.

3.11 Explain briefly how a gas turbine power plant is combined with a conventional steam plant. What are the advantages of such a scheme?

3.12 What are the main features of a gas turbine aircraft engine which differentiate it from a gas turbine plant for electric power generation?

How are the specific thrust and power output of aircraft engines improved?

3.13 How is the propulsive efficiency of an aircraft propulsion device defined?

Compare graphically the propulsive efficiencies of turboprop, turbojet, turbofan and rocket engines at various Mach numbers.

3.14 **(a)** Define specific thrust, thrust specific fuel consumption (TSFC) and bypass ratio in aeroengines.

(b) Prove that:

Overall efficiency (η_o) of a propulsion device = thermal efficiency × propulsive efficiency

$$\eta_o = \frac{\text{aircraft speed}}{\text{calorific value} \times \text{TSFC}}$$

$$\text{TSFC} = \frac{\text{fuel-air ratio}}{\text{specific thrust}}$$

3.15 If an exhaust heat exchanger (thermal ratio = 0.75) is employed in the gas turbine plant of Ex.3.5 calculate:

(a) Air-fuel ratio,
(b) Air-flow rate,
(c) Fuel flow rate, and
(d) the thermal efficiency of the plant.

Ans. (a) 49.693 (b) 391.819 kg/s
(c) 7.884 kg/s (d) 33.35 per cent.

3.16 The stagnation pressure ratio across a gas turbine stage is 2.0 and the initial and final stagnation temperatures of the gas are 600°C and 500°C respectively. The absolute velocity of the gas both at entry and exit is 120 m/s. Determine

(a) the total to total efficiency,
(b) the total to static efficiency,
(c) work done per kg of the gas, and
(d) mass flow rate of the gas to develop 10 MW.

Ans: (a) 72.5% (b) 69.5%
(c) 115.8 kJ (d) 86.6 kg/s

Chapter 4

Steam Turbine Plants

The steam turbine is one of the most important power generating turbomachines. It is the principal prime mover in the field of electric power generation. The role of the steam turbine as one of the components in the steam power plant is briefly discussed in this chapter. Some aspects of the steam turbine cycle employed in such plants are also included. The aerodynamic aspects of individual turbine stages are covered in Chapters 8 and 9.

Figure 4.1 shows the layout of a steam turbine plant. The first component of this plant is the steam boiler which raises steam at the required pressure and temperature for the turbine. The boiler receives feed water at an elevated temperature through various regenerative and heat recuperating apparatuses (not shown in Fig. 4.1). In a majority of power plants steam is superheated; in large plants it is reheated once or twice after expanding through some turbine stages.

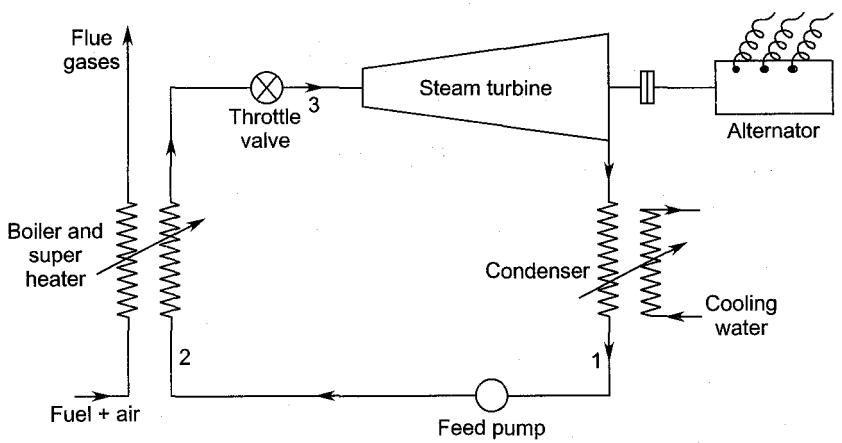

Fig. 4.1 Layout of a steam turbine plant

The air, fuel and flue gas circuit in the boiler plant consists of the burners, furnace, forced draft fan (F.D. fan), flue gas passages, induced draft fan (I.D. fan) and chimney.

Superheated steam enters the steam turbine through the governor valve. The steam turbine is invariably a multi-stage machine having one or more cylinders depending on the plant size.

The steam after expanding through the turbine condenses in the condenser at a low pressure ($p_c \approx 35$ to 70 mbar). The condensate along with the bled steam (Fig. 4.6) is pumped back to the boiler.

4.1 Types of Steam Turbines

Various types of steam turbines can be classified in the following manner:

A. On the basis of flow direction
A.1 Axial
A.2 Radial
A.3 Tangential

B. On the basis of expansion process
B.1 Impulse
B.2 Reaction
B.3 Combined impulse and reaction

C. On the basis of number of stages
C.1 Single stage
C.2 Multi-stage
Velocity compounded impulse (Curtis stages)
Pressure compounded impulse (Rateau stages)
Pressure-velocity compounded impulse (Curtis-Rateau stages)
Pressure compounded reaction (Parson's)

D. On the basis of steam entry configuration
D.1 Full admission
D.2 Partial admission
(Single or multi-arc admission)

E. On the basis of number of flows
E.1 Single flow
E.2 Double flow
E.3 Divided flow
E.4 Tandem or cross compounded

F. On the basis of relative motion of the rotor
F.1 Single rotation
F.2 Double rotation

G. On the basis of rotational speed

G.1 $N = 3000$ rpm, $f = 50$ Hz

G.2 $N = 3600$ rpm, $f = 60$ Hz

G.3 $N = 1500$ rpm

G.4 Geared units

H. On the basis of applications

H.1 Electric power generation

H.2 Industrial

H.3 Marine

I. On the basis of steam conditions

I.1 High pressure non-condensing

I.2 High pressure condensing

I.3 Back pressure

I.4 Regenerative

I.5 Reheating

I.6 Extraction

I.7 Mixed pressure

I.8 Exhaust turbine

4.2 Steam Power Cycle

Various processes occurring in a steam turbine plant are represented by the Rankine cycle. The cycle with ideal processes is known as the ideal Rankine cycle, whereas the cycle with irreversibilities is the actual Rankine cycle.

4.2.1 Ideal Rankine cycle

Figure 4.2 shows an ideal Rankine cycle in the p–v plane. The reversible adiabatic pumping of feed water from the condenser to the boiler pressure is represented by the process 1–2. The work done in the process is

$$w_P = -\int_1^2 v\,dp = -\int_1^2 dh \tag{4.1}$$

Water can be assumed to remain almost incompressible during the pumping process i.e. $v = v_w$ = constant. Therefore,

$$w_P = -(p_2 - p_1)\,v_w = -(h_2 - h_1) \tag{4.2a}$$

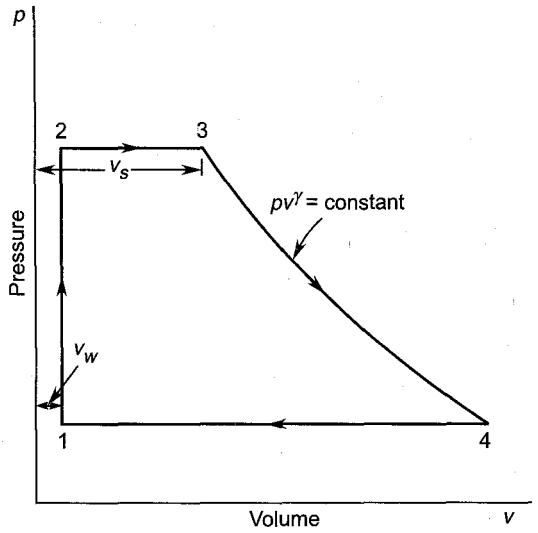

Fig. 4.2 *p–v* diagram of a Rankine cycle

The negative sign here only indicates that the work to the feed pump is supplied from out side: Therefore, it is a subtractive term. In view of this Eq. (4.2a) can also be written as

$$w_P = h_2 - h_1 \tag{4.2b}$$

Heating of the feed water up to its saturation temperature, its evaporation and superheating at constant pressure are all represented by the process 2–3. The heat supplied during this process is Q_s.

The reversible adiabatic (isentropic) expansion of steam through the turbine is represented by the process 3–4. The work done by the steam in the turbine is

$$w_T = -\int_3^4 v\,dp = \int_4^3 dh \tag{4.3}$$

$$w_T = \frac{\gamma}{\gamma - 1}(p_3 v_3 - p_4 v_4) = h_3 - h_4 \tag{4.4}$$

The condensation of steam at constant pressure is represented by the process 4–1. The heat rejected during this process is Q_r.

The corresponding temperature-entropy (*T–s*) and enthalpy-entropy (*h–s*) diagrams of the ideal Rankine cycle are shown in Figs. 4.3 and 4.4 respectively.

Referring to Fig. 4.4, the net work output of the plant is obtained from the following relations:

$$Q_s + w_P = Q_r + w_T$$

$$w_{\text{plant}} = w_T - w_P = Q_s - Q_r \tag{4.5}$$

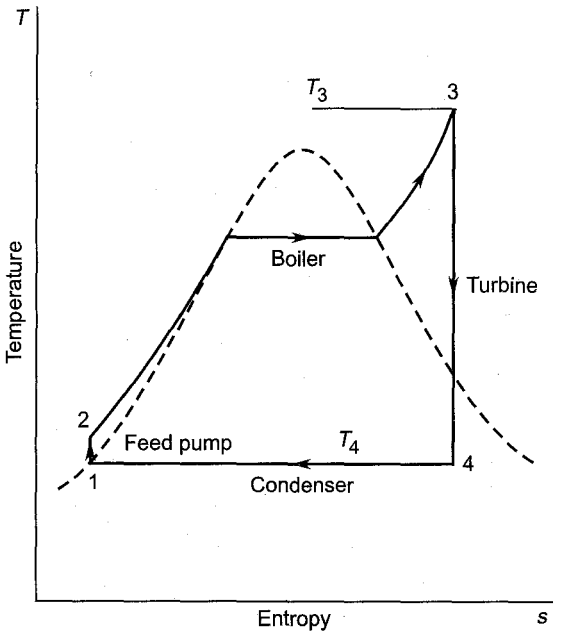

Fig. 4.3 *T–s* diagram of a Rankine cycle

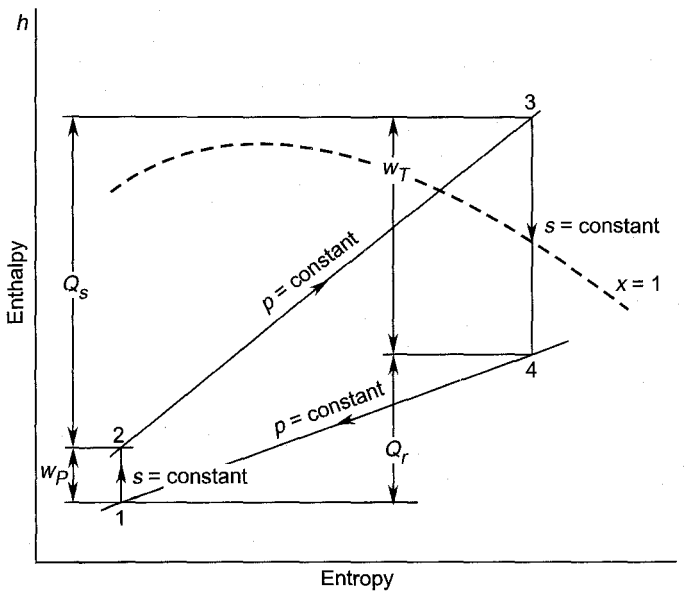

Fig. 4.4 *h–s* diagram of the ideal Rankine cycle

Putting Eqs. (4.2b) and (4.4) in Eq. (4.5), we get

$$w_{\text{plant}} = (h_3 - h_4) - (h_2 - h_1) \tag{4.6}$$

Heat supplied is

$$Q_s = h_3 - h_2$$

Therefore, the efficiency of the ideal Rankine cycle is given by

$$\eta_{\text{Rankine}} = \frac{w_{\text{plant}}}{Q_s}$$

$$\eta_{\text{Rankine}} = \frac{(h_3 - h_4) - (h_2 - h_1)}{(h_3 - h_2)}$$

$$\eta_{\text{Rankine}} = \frac{(h_3 - h_4) - (h_2 - h_1)}{(h_3 - h_1) - (h_2 - h_1)} \tag{4.7}$$

For lower pressure plants, the feed pump work $(h_2 - h_1)$ is negligible compared to other quantities in Eq. (4.7). Therefore, Eq. (4.7) is sometimes written as

$$\eta_{\text{Rankine}} = \frac{h_3 - h_4}{h_3 - h_1} \tag{4.8}$$

Rankine efficiency is the ideal thermal efficiency of the steam plant. This is never achieved and is only used as a reference value.

4.2.2 The Actual Plant Cycle

The actual plant cycle deviates from the Rankine cycle on account of pressure drops in the steam passages and irreversibilities in various components. Figure 4.5 shows the irreversible processes in the feed pump (1–2′) and the turbine (3–4′).

In view of the above the actual thermal efficiency of the plant is given by

$$\eta_{th} = \frac{\text{actual plant output}}{\text{heat supplied}}$$

$$\eta_{th} = \frac{(h_3 - h_4') - (h_2' - h_1)}{h_3 - h_2'}$$

$$\eta_{th} = \frac{(h_3 - h_4') - (h_2' - h_1)}{(h_3 - h_1) - (h_2' - h_1)} \tag{4.9}$$

The aim of the power plant designer or engineer is to obtain the value of the actual thermal efficiency close to the ideal Rankine efficiency. The efficiency ratio or the relative efficiency is an index which indicates the extent to which the above target is achieved.

$$\eta_{\text{rel}} = \eta_{th}/\eta_{\text{Rankine}}$$

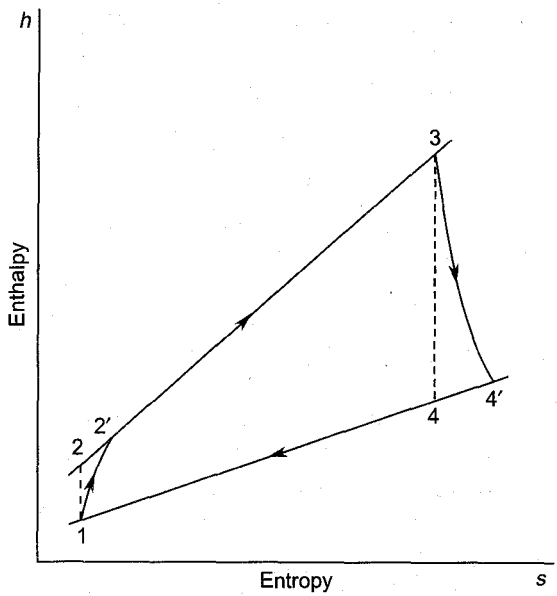

Fig. 4.5 *h–s* diagram of an actual Rankine cycle

Neglecting the quantity $(h'_2 - h_1)$, Eq. (4.9) can be rewritten as

$$\eta_{th} = \frac{h_3 - h'_4}{h_3 - h_1} \tag{4.10}$$

Equations (4.8) and (4.10) yield

$$\eta_{\text{rel}} \approx \eta'_{th}/\eta_{\text{Rankine}}$$

$$\eta_{\text{rel}} \approx \frac{h_3 - h'_4}{h_3 - h_4} = \eta_T \tag{4.11}$$

Equation (4.11) shows that the relative efficiency of a steam plant is almost equal or close to the turbine efficiency η_T.

4.3 Improvements in Plant Efficiency

The maximum and minimum temperatures of steam in the cycles (Figures 4.3, 4.4 and 4.5) discussed in the previous sections are T_3 and T_4 respectively. Therefore, the limiting value of the Carnot's efficiency is

$$\eta_{\text{Carnot}} = 1 - \frac{T_4}{T_3} \tag{4.12}$$

Therefore, the two obvious methods of improving the thermal efficiency of the plant are: (*i*) to increase the initial temperature T_3 of the steam and (*ii*) to decrease the final temperature of steam through a reduction in the exhaust or condenser pressure.

A greater insight into the improvement of the thermal efficiency of the plant can be obtained by considering the Carnot's efficiency based on the mean temperatures of heat reception (T_s) and rejection (T_r). Thus

$$\eta'_{\text{Carnot}} = 1 - \frac{T_r}{T_s} \tag{4.13}$$

Various methods for improving the thermal efficiency of the plant are briefly described below in view of the "target values" given by Eqs. (4.12) and (4.13).

4.3.1 Increase in the Initial Steam Pressure

Increase in the initial steam pressure gives a higher saturation temperature of steam below the critical value. This also increases the mean temperature of the heat reception giving a higher thermal efficiency. However, this is an indirect method of obtaining a higher steam temperature. As will be seen in later sections, the mean temperature of heat reception can also be raised by other methods without increasing the steam pressure.

The gains in thermal efficiency obtained by a large increase in the initial steam pressure in the higher ranges are of the order of 1% or less. This fact along with the disadvantage of steam becoming wet comparatively early suggests only marginal gains by increasing the steam pressure. The wet steam in the larger part of the turbine would give lower turbine stage efficiencies. This can even offset the small gain due to the higher temperature resulting from the higher steam pressure.

Along with thermodynamic considerations, the economic and mechanical design aspects of employing high steam pressures should not be ignored.

4.3.2 Increase in the Initial Steam Temperature

As explained before, it is obvious that higher thermal efficiencies can be obtained by employing higher initial temperatures of steam. This method provides appreciable gains in the thermal efficiency in contrast to other methods.

The employment of higher steam temperatures makes special technological demands on the steam boiler. The highest temperature employed in a steam plant can be taken as 566 °C. The employment of still higher temperatures will require the use of prohibitively expensive materials.

Using a higher initial temperature is useful in another way. The steam remains comparatively dry over a larger number of turbine stages; there-

fore, the efficiencies of these stages are higher. This gives a further boost to the overall thermal efficiency of the plant and decreases erosion of blades.

4.3.3 Increase in the Condenser Vacuum

The temperature T_4 at which heat is rejected can be decreased by reducing the condenser pressure or increasing its vacuum.

The condenser vacuum (or the pressure and temperature of steam inside the condenser) shows strong dependence on the inlet temperature of the cooling water. This in turn depends on the ambient temperature and the method of cooling the circulating water. In cold climates the ambient temperatures are lower which conveniently provide a low inlet temperature of the cooling water. This has resulted into comparatively lower condenser pressures ($p_c \approx 22.5$ mbar at a cooling water inlet temperature of 8°C) in power plants operating in cold climates.

In contrast to this, power plants in the hot climates of the world show generally higher condenser pressures ($p_c \approx 75-100$ mbar). This marked difference in the condenser pressures is reflected in the thermal efficiencies of the plants. Sometimes, the improvement in the efficiency may be as high as 4.5% on account of the aforementioned difference in the condenser vacuum. It is also observed that the circulating water temperature rises during the humid rainy season which decreases the condenser vacuum with a consequent decrease in the thermal efficiency.

The degree of cooiing in the condenser and hence its vacuum is strongly dependent on the rise in the cooling water temperature which is about 10°C. A further increase in the cooling of steam can be obtained by increasing the rate of circulating water and the size of the condenser. However, these parameters are tied down to the important economic aspects of the steam power plants.

Besides these factors the performance of steam ejectors affects the condenser pressure significantly.

4.3.4 Regenerative Feed Heating

The heating of feed water on its way to the steam boiler by the steam extracted at various points in the turbine is known as regenerative feed heating[60,80]. This increases the temperature of the feed water entering the boiler. The mean temperature of the heat reception is thus increased, giving a higher thermal efficiency of the plant. The gain in the thermal efficiency of some plants with a suitable number of feed heaters is about 10%. On account of this handsome gain, regenerative feed heating has

universally become an essential feature of all large steam power plants. Some other incidental advanages of feed heating are given below.

(a) Water particles escape with the bled steam through extraction belts. This reduces the moisture content in the steam thus decreasing turbine blade erosion.

(b) Owing to a reduction in the wetness of steam, the turbine stages give higher efficiencies.

(c) Steam extraction for feed heating reduces the flow rate significantly in the L.P. stages, thus allowing the blades to be shorter. This is a great advantage in large units where designing long turbine blades is very critical.

(d) Feed heating by bled steam decreases the quantity of steam reaching the condenser. This in turn reduces the size of the conderser and the cooling water requirements.

Thermal efficiency

Figure 4.6 shows three feed-water heaters I–1, I and I+1. These and other heaters (from 1 to n) receive sufficient bled steam from the turbine so as to heat the feed water to the saturation temperature corresponding to the extraction pressure. The bled steam fully condenses at its saturation temperature.

For the ith heater, the energy balance gives

Heat released by the bled steam = heat gained by the feed water

$$M_i (H_i - h_i) = m_{i-1} (h_i - h_{i-1})$$

$$M_i = \frac{h_i - h_{i-1}}{H_i - h_i} m_{i-1}$$

The mass balance for this heater gives

$$m_i = m_{i-1} + M_i$$

$$\frac{m_i}{m_{i-1}} = 1 + \frac{M_i}{m_{i-1}} = 1 + \frac{h_i - h_{i-1}}{H_i - h_i}$$

i.e.

$$\alpha_i = \frac{m_i}{m_{i-1}} = \frac{H_i - h_{i-1}}{H_i - h_i} \tag{4.14}$$

or

$$m_i = \alpha_i \cdot m_{i-1} \tag{4.15}$$

Similarly, for the $(i + 1)$th heater,

$$M_{i+1} = \frac{h_{i+1} - h_i}{H_{i+1} - h_{i+1}} m_i$$

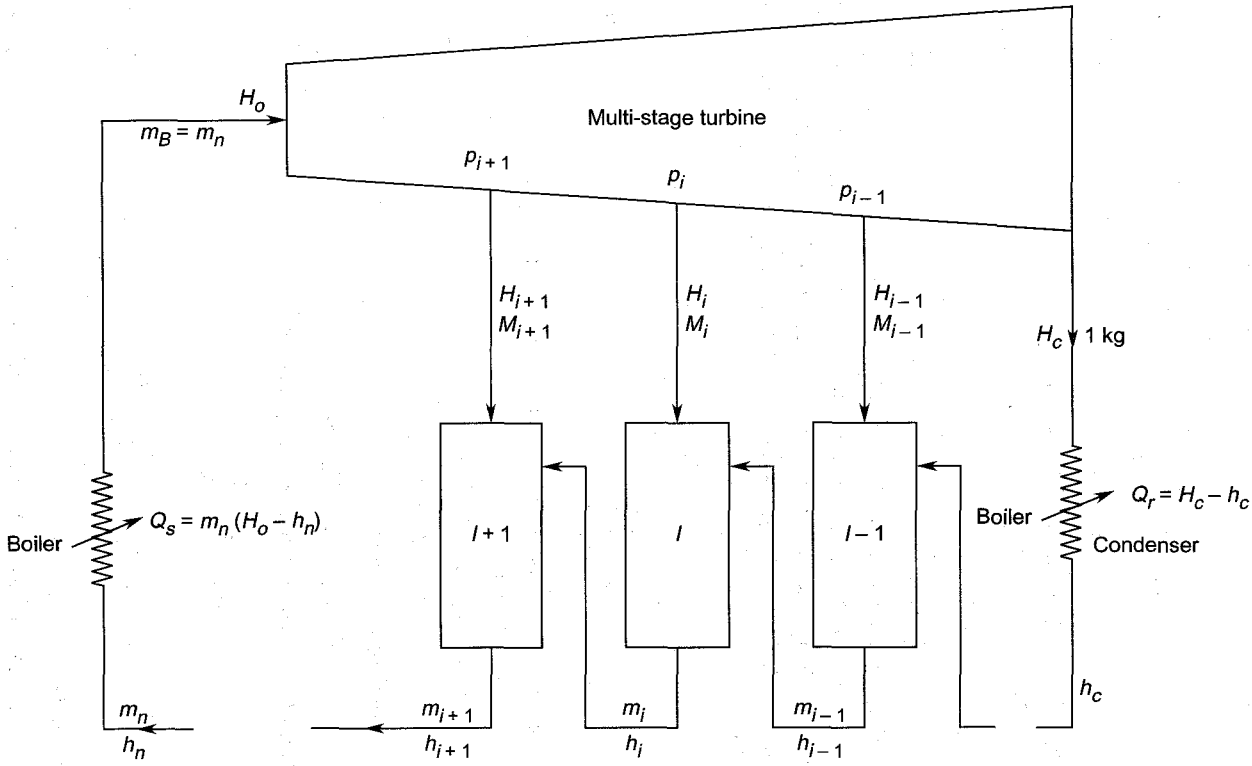

Fig. 4.6 Feed-water heating in n direct contact heaters

$$m_{i+1} = m_i + M_{i+1}$$

$$\frac{m_{i+1}}{m_i} = 1 + \frac{M_{i+1}}{m_i} = 1 + \frac{h_{i+1} - h_i}{H_{i+1} - h_{i+1}}$$

i.e.

$$\alpha_{i+1} = 1 + \frac{m_{i+1}}{m_i} = \frac{H_{i+1} - h_i}{H_{i+1} - h_{i+1}} \tag{4.16}$$

$$m_{i+1} = \alpha_{i+1}\, m_i \tag{4.17}$$

Putting Eq. (4.15) into (4.17), we get

$$m_{i+1} = \alpha_{i+1} \cdot \alpha_i \cdot m_{i-1} \tag{4.18}$$

Similarly for other heaters

$$m_{i+2} = \alpha_{i+2} \cdot \alpha_{i+1} \cdot \alpha_i \cdot m_{i-1} \tag{4.19}$$

The first heater receives one kg of water at the lowest temperature (enthalpy = h_c) from the condenser, whereas the last heater (nth) delivers $m_n = m_B$ kg of water to the boiler at an elevated temperature (enthalpy = h_n). The mass of water reaching the boiler for one kg of steam condensed is given by

$$m_B = m_n = \alpha_n \ldots \alpha_{i+2} \cdot \alpha_{i+1} \cdot \alpha_i \ldots \alpha_1$$

$$m_B = \prod_{i=1}^{i=n} \alpha_i \tag{4.20}$$

The values of various alphas are known through properties of steam as in Eqs. (4.14) and (4.16).

Heat rejected in the condenser is

$$Q_r = H_c - h_c$$

Heat supplied in the boiler

$$Q_s = m_B\,(H_0 - h_n)$$

Therefore, the thermal efficiency is given by

$$\eta_{th} = 1 - \frac{Q_r}{Q_s}$$

$$\eta_{th} = 1 - \frac{H_c - h_c}{m_B\,(H_0 - h_n)} \tag{4.21}$$

Number of feed-water heaters

The number and positions of extraction points for feed heating in a given plant depend on the number of cylinders and the mechanical convenience. The pipe work for a large number of heaters is too complicated and leads to considerable pressure losses. Sometimes a desired arrangement of

heaters is not mechanically feasible on account of the existing mechanical configuration in the given machine.

It is found that for maximum efficiency in a non-reheat cycle, the enthalpy rise is approximately the same in all the heaters and the economizer. However, the cycle efficiency does not seem to be sensitive to the distribution of the total enthalpy rise in the heaters.

In a reheat cycle the enthalpy rise in the heaters downstream of the reheat point should be greater than that in the heaters upstream of this point. This is on account of the greater heat of superheat available for the downstream heaters.

Thus if there are n heaters, the enthalpy rise in each heater is given by

$$(\Delta h)_i = \frac{h_n - h_c}{n} \tag{4.22}$$

The temperature rise per heater is

$$(\Delta t)_i = \frac{t_n - t_c}{n} \tag{4.23}$$

The maximum number of heaters employed in large plants is nine with a final feed-water temperature of about 285°C.

4.3.5 Reheating

Reheating is the process in which steam at the end of expansion in one cylinder (Fig. 4.7) is taken out to the boiler or reheater for resuperheating it. This reheated steam does more work in the next cylinder and also increases the thermal efficiency of the plant. However, the increase (or decrease) in thermal efficiency, as will be shown later, depends on the reheat pressure.

Figure 4.7 shows two reheaters, one between the H.P. and the I.P., and another between the I.P. and the L.P. cylinders. This arrangement can be used in a very large plant. On account of the mechanical complications due to intricate piping and pressure losses, more than two reheaters are not used.

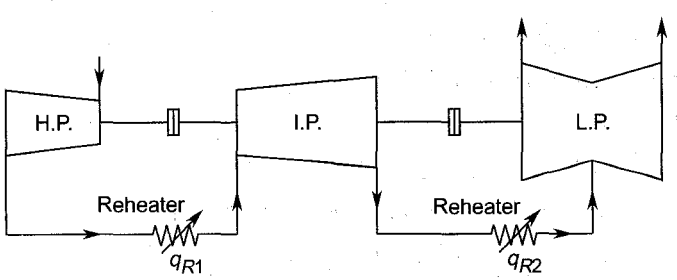

Fig. 4.7 Reheating of steam between H.P. and I.P. and L.P. cylinders

Reheating, besides increasing the mean temperature of heat reception, also increases the individual turbine stage efficiencies and decreases the erosion of turbine blades on account of the decrease in wetness.

Reheating is done at constant pressure (Fig. 4.8), but in actual practice steam undergoes a drop in pressure across the reheaters.

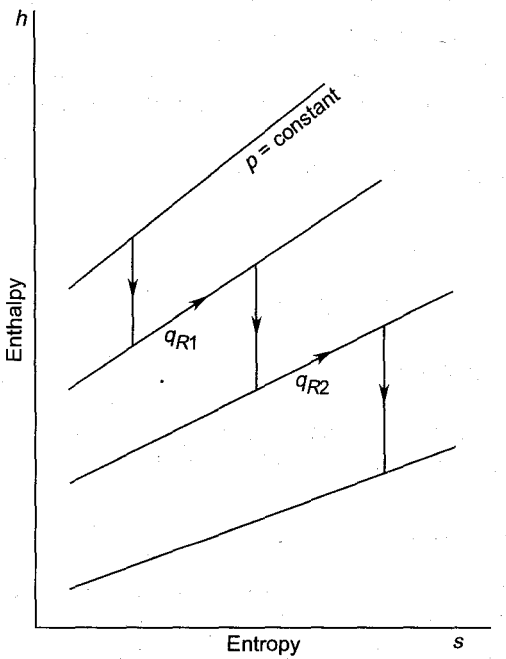

Fig. 4.8 Reheat process on *h–s* diagram

Figure 4.9 shows the Rankine cycle with single reheat without any feed-water heating. The reheat process is represented by the constant pressure line 7–5. The expansion processes before (3–7) and after (5–6) the reheat are assumed to be isentropic.

The effect of reheat is represented by the addition of the portion (4–7–5–6) to the original simple Rankine cycle shown in Fig. 4.3.

Thermal efficiency of the reheat cycle

For the non-reheat cycle 1–2–3–4,

Heat supplied, $Q_s = q_N = h_3 - h_2$

Heat rejected, $Q_r = H_4 - h_1$

The thermal efficiency of the ideal non-reheat cycle is

$$\eta_N = 1 - \frac{Q_r}{Q_s} = 1 - \frac{H_4 - h_1}{q_N}$$

$$H_4 - h_1 = (1 - \eta_N)\, q_N \qquad (4.24)$$

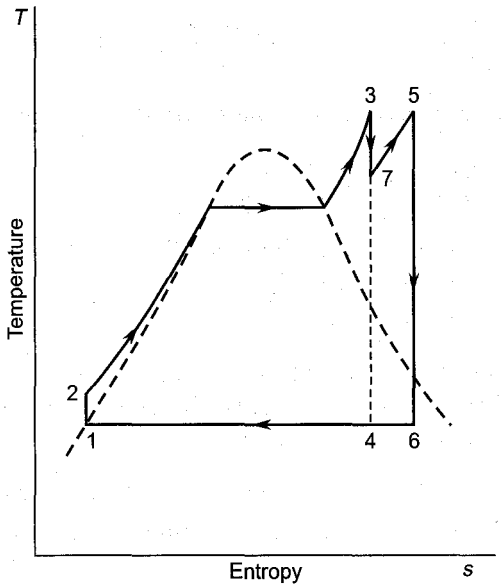

Fig. 4.9 Rankine cycle with single reheat

For the added cycle 4–7–5–6 (due to reheat),

Heat supplied, $Q'_s = H_5 - H_7 = q_R$

Heat rejected, $Q'_r = H_6 - H_4$

Therefore, the efficiency η_R of this added cycle is given by

$$\eta_R = 1 - \frac{Q'_r}{Q'_s} = 1 - \frac{H_6 - H_4}{q_R}$$

$$H_6 - H_4 = (1 - \eta_R)\, q_R \tag{4.25}$$

For the overall plant cycle 1–2–3–7–5–6–1

Heat supplied, $Q''_s = q_N + q_R$

Heat rejected, $Q''_r = H_6 - h_1$

Therefore, the thermal efficiency of the plant

$$\eta_{th} = 1 - \frac{Q_r}{Q''_s} = 1 - \frac{H_6 - h_1}{q_N + q_R}$$

$$H_6 - h_1 = (1 - \eta_{th})\,(q_N + q_R) \tag{4.26}$$

Adding Eqs. (4.24) and (4.25) and equating with Eq. (4.26),

$$(1 - \eta_R)\, q_R + (1 - \eta_N)\, q_N = (1 - \eta_{th})\,(q_N + q_R)$$

After rearrangement,

$$\eta_{th}/\eta_N = \frac{q_N + q_R\,(\eta_R/\eta_N)}{q_N + q_R}$$

$$\frac{\eta_{th}}{\eta_N} - 1 = \frac{q_N + q_R\,(\eta_R/\eta_N) - q_N - q_R}{q_N + q_R}$$

This, on further simplification and rearrangement, gives

$$\frac{\eta_{th}}{\eta_N} - 1 = \frac{\eta_R/\eta_N - 1}{1 + q_N/q_R} \tag{4.27}$$

This expression shows that the thermal efficiency of the plant will increase due to reheating only when

$$\eta_R > \eta_N$$

This will depend on the reheat pressures. At very low pressures $\eta_R < \eta_N$ the thermal efficiency would decrease with reheating. Thus there is an optimum value of the reheat pressure:

(a) (0.2 – 0.25) × initial pressure for the first reheat.

(b) (0.2 – 0.25) × first reheat pressure for the second reheat.

4.4 Heat Rate

Heat rate is defined as the number of heat units required to develop unit power output for an hour; the output is taken as one kilowatt hour. This, like the thermal efficiency, is a measure of the performance of the power plant in converting heat to useful output. Therefore, it is directly related to the thermal efficiency. The heat rate decreases with an increase in thermal efficiency. Therefore, all attmepts to increase the thermal efficiency discussed in Sec. 4.3 decrease the heat rate.

All turbine manufacturers and suppliers are required to indicate the heat rates of their machines or plants. Therefore, it is important to know the various meanings of the term.

(i) *Turbine heat rate*

The turbine heat rate is the number of heat units required to develop unit power output at the turbine coupling for an hour.

The unit output is one kilowatt hour or 3600 kJ. The thermal efficiency is

$$\eta_{th1} = \frac{\text{turbine shaft work}}{\dot{m}\,(h_3 - h_2)} \tag{4.28}$$

Here various units used are:

(a) Turbine shaft work is in kW

(b) Steam flow rate is in kg/s,

(c) $(h_3 - h_2)$ is in kJ/kg

Therefore, the turbine heat rate is

$$(HR)_T = \frac{3600}{\eta_{th1}} \text{ kJ/kWh} \tag{4.29}$$

The turbine heat rate is quoted by turbine suppliers as they are only concerned with the performance of the turbine unit.

(ii) *Turbo-generator heat rate*

Here the useful power output is considered at the generator terminals for the heat rate and thermal efficiency.

$$\eta_{th2} = \frac{\text{energy at the generator teminals}}{\dot{m}(h_3 - h_2)} \tag{4.30}$$

The turbo-generator heat rate is given by

$$(HR)_{TG} = \frac{3600}{\eta_{th2}} \tag{4.31}$$

Since $\eta_{th2} < \eta_{th1}$, the turbo-generator heat rate is higher than the turbine heat rate.

(iii) *Turbine plant heat rate*

Here the useful power output and thermal efficiency of the plant are defined by Eqs. (4.5) and (4.7) respectively. Thus, the plant heat rate is given by

$$(HR)_{\text{plant}} = \frac{3600}{\eta_{th}} \tag{4.32}$$

This is higher than the turbine heat rate.

A convenient figure to remember for heat rates is the heat rate of 9000 kJ/kWh corresponding to a thermal efficiency of 40%.

(iv) *Station heat rate*

The station heat rate takes into account the overall performance of the power station and is related to the overall efficiency (η_0) or the coal to kilowatt efficiency.

$$\eta_0 = \frac{\text{energy at the generator terminals}}{\dot{m}_f Q_f} \tag{4.33}$$

where $\dot{m}_f$ = rate of fuel used in kg/s

Q_f = calorific value of the fuel in kJ/kg

The station heat rate is given by

$$(HR)_{\text{Station}} = \frac{3600}{\eta_0} \tag{4.34}$$

The heat rates vary in a wide range with the steam conditions at the entry and exit, feed-water heating and reheat arrangements and the size of the units. Generally, a larger unit must give a lower heat rate.

The station or the overall heat rate gives a quick idea of the fuel consumption rate and the storage capacity required. Similarly the plant heat rate decides the capacity and number of boilers.

Heat rates and efficiencies for Thermal power plants are given in Appendix G.

4.5 Industrial Steam Turbines

Steam turbines which supply process steam for some industrial processes, besides generating electric power are known as industrial turbines or turbogenerators. Such turbines are used in petrochemical, sugar and paper industries. Optimum results are obtained when all or a large percentage of the total steam flow required for power generation is used as process steam.

Sometimes, the major role of a steam plant is to supply process steam and electric power is only a by-product or vice versa. Unlike power plant turbines, the low output industrial turbines can be made smaller in size by increasing the rotational speeds (N = 5000–13000 rpm). In doing so they may require reduction gear boxes for certian applications.

Figure 4.10 shows an industrial turbo-generator in which only a part of the steam at a higher pressure is used for the industrial process. This is extracted from somewhere in the high pressure region of the turbine depending on the process. The generator is driven through a reduction gear at the required speed for the desired frequency and number of poles.

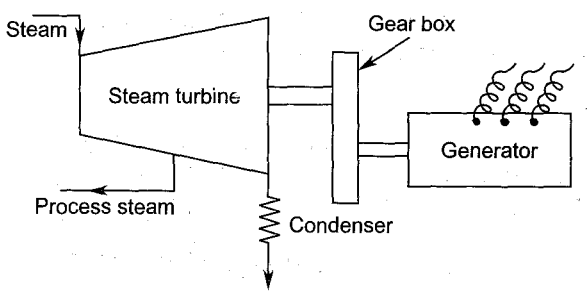

Fig. 4.10 Industrial turbo-generator

Besides supplying process steam, some turbines are required as prime movers to drive some auxiliaries in power plants and various other industries. For example, in large power plants the draft fans and feed pumps can be driven by direct coupled steam turbines instead of electric motors. Similarly, turbo-compressors in various industrial applications

can be conveniently run at the desired speeds by steam turbines. Such drives do not suffer the usual conversion losses (from mechanical to electrical and again from electrical to mechanical) and are ideal for variable speed requirements. This is much simpler compared to an equivalent variable speed drive using an electric motor.

4.6 Combined Steam and Gas Turbine Plants

In Chapter 3 on gas turbine plants and in the material covered in this chapter it is observed that, while gas turbines have the advantage of high inlet temperatures, condensing steam turbines have the unique advantage of a low exit temperature. On the other hand, the gas turbine plant efficiency suffers on account of the higher exhaust temperature and the steam turbine on account of the lower value of the maximum inlet temperature.

The combined steam and gas turbine plant[53, 54, 58, 59] combines the advantages of both gas and steam turbines without seriously suffering from their disadvantages. The combined cycle concept, in its simplest form, uses the gas turbine exhaust in raising steam which can be usefully utilized either for space heating (or cooling) or for power generation in a steam turbine.

Figure 4.11 shows a scheme of heat recovery from the gas turbine exhaust. The hot gases from the gas turbine plant supply the heat required to raise steam in the waste heat recovery boiler. A circulating pump is

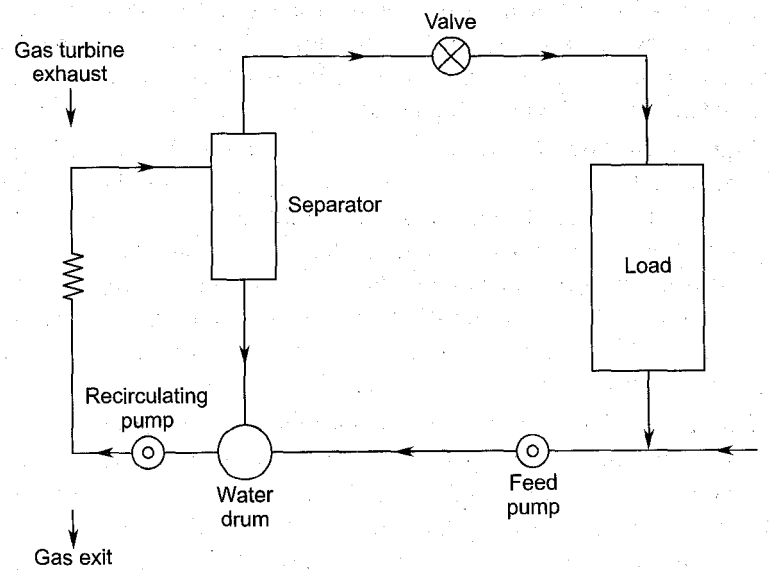

Fig. 4.11 A simple cycle for gas turbine exhaust recovery

used to increase the evaporation rate in the boiler. The moisture in the steam is separated by passing it through a separator on its way to the load.

Figure 4.12 shows the previous arrangement with an economizer. This reduces the temperature of the exhaust gases further by heating the feed water. The efficiency of this arrangement will therefore be higher.

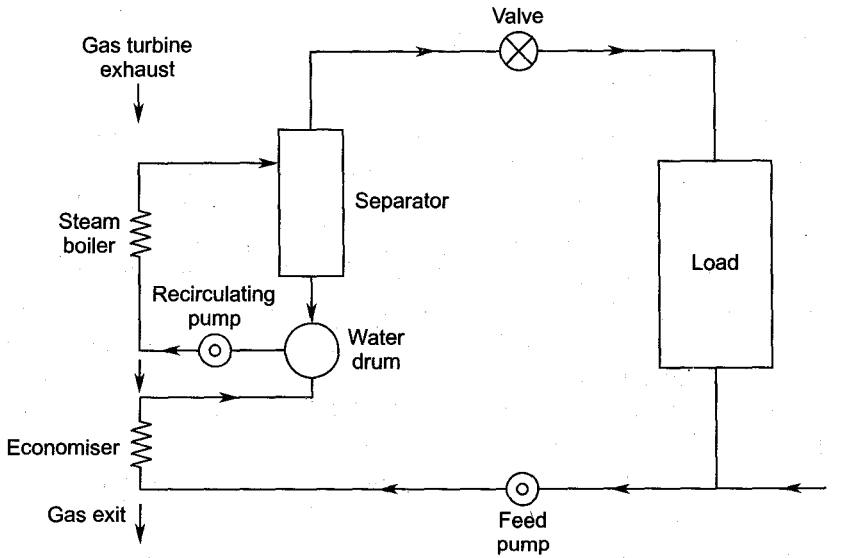

Fig. 4.12 Exhaust heat recovery with economizer

Figure 4.13 shows a further improvement over the previous two arrangements by utilizing the gas turbine exhaust in the superheater. Depending on the load requirement, additional fuel can be burnt in the superheater for achieving a higher degree of superheat.

Figure 4.14 shows the detailed layout of a combined cycle power plant. The main feature of this plant is the exhaust heat recovery boiler. The gas turbine exhaust provides the oxygen for combustion in the boiler. A part of the F.D. fan air is supplied to the boiler furnance and the rest to the air compressor. The steam plant consists of the conventional equipment. The power output available at the shafts of the steam and gas turbines are in the ratio of 80 : 20 to 60 : 40. This arrangement can give thermal efficiencies between 45 and 50 per cent.

Figure 4.15 depicts a combined plant with a supercharged boiler. The boiler combustion in this plant takes place at a much higher pressure compared to a conventional boiler. This also acts as a combustion chamber for the gas turbine plant. The gas turbine exhaust is used for feed heating in the economizer. The heating surface in this boiler is smaller than that of the conventional type. This advantage is obtained on account

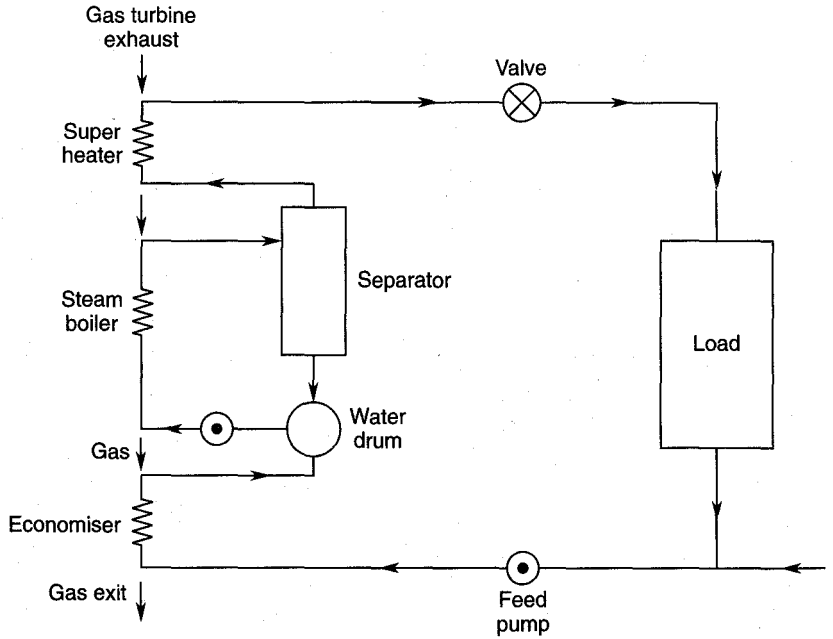

Fig. 4.13 Exhaust heat recovery with economizer and superheater

of the much higher heat transfer rate resulting from the higher pressure and temperature in the supercharged boiler furnace.

Some advantages of the combined cycle plants over the conventional steam plants are:

1. Higher thermal efficiency
2. Lower specific investment cost
3. Lower cooling water requirements
4. Possibility of using cheaper fuel.

Combined cycle plants offer a better and more practical method of using coal for a gas turbine plant. In such plants coal is first gasified and then the gases are burnt in the combustion chamber of the gas turbine plant. The high pressure air and steam required for coal gasification are drawn from the compressor and steam boiler respectively.

More details of the combined cycle plants are given in Chapter 5.

4.7 Nuclear Steam Power Plants

The gas turbine power plant employing the nuclear fission energy was described in Sec. 3.6. On account of the worldwide energy crisis, large scale power generation by nuclear steam power plants seems imperative.

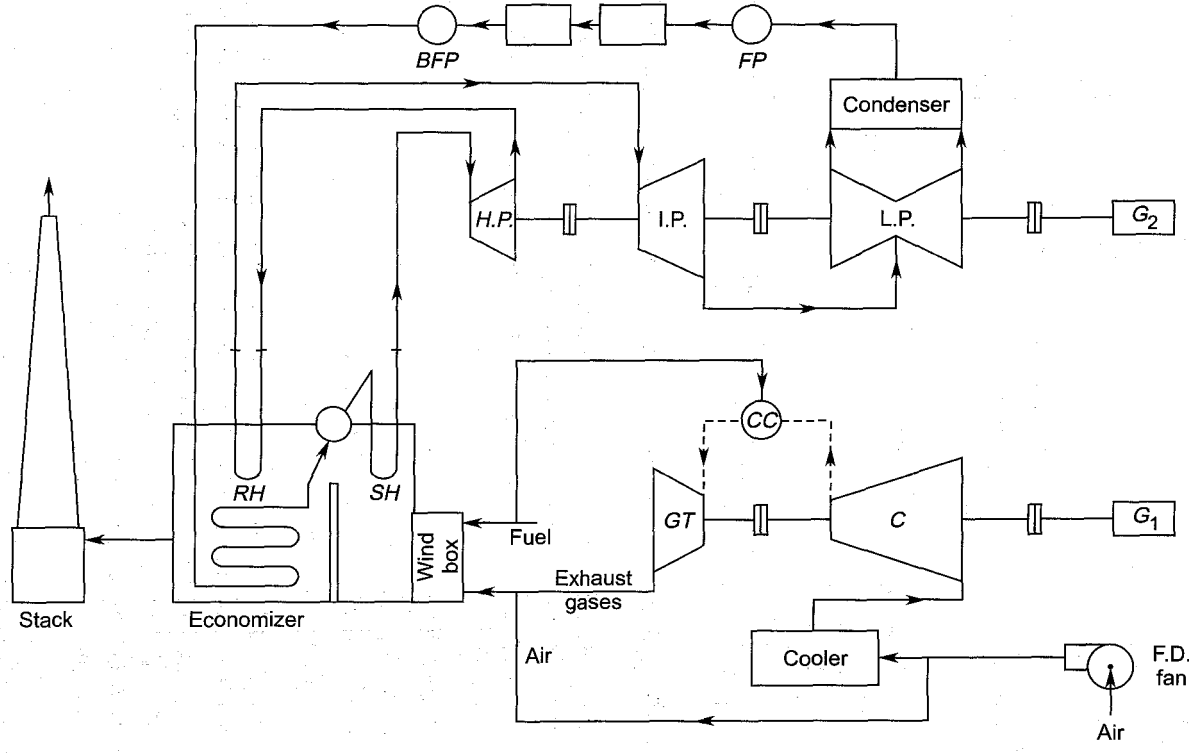

Fig. 4.14 Combined steam and gas turbine plant with exhaust heat recovery boiler (FP–feed pump, BFP–booster feed pump, GT–gas turbine, C–compressor G–generator, RH–reheater, SH–superheater, FD–forced draft)

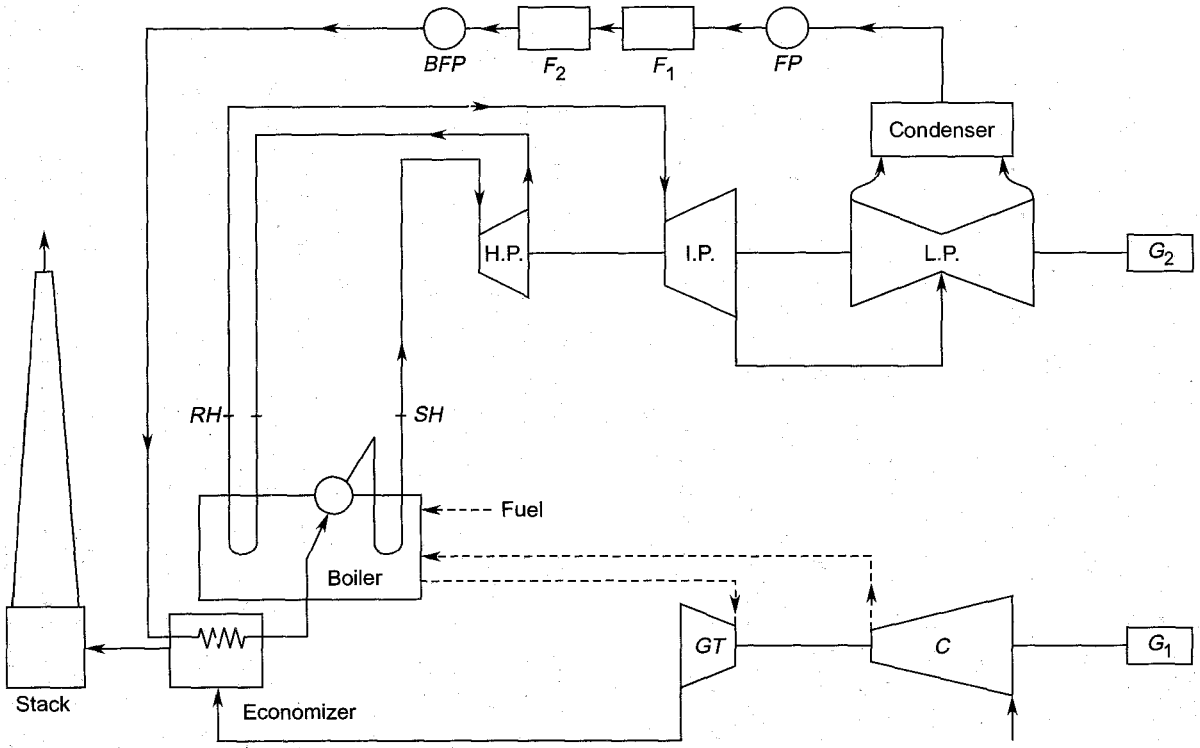

Fig. 4.15 Combined steam and gas turbine plant with supercharged boiler (FP–feed pump, BFP–booster feed pump, F–feedheaters, GT–gas turbine, C–compressor, RH–reheater, SH–superheater, G–generator)

Major efforts have been made since the 1960s to develop various types of nuclear power plants.[52, 55, 57, 67, 69]

This section deals with only those nuclear power plants in which the heat energy liberated in the power reactor is used to raise steam for conventional steam power plants. Though the capital cost of nuclear plants is much higher, their overall efficiencies ($\eta \approx 42\%$) are now comparable with the large conventional power plants.

Figure 4.16 shows a steam turbine power plant receiving its steam from a heat exchanger which in turn receives heat from the reactor. The principal components of the nuclear reactor are as follows:

(i) *The core and the fuel elements*

The nuclear fuel material must be suitable for a self-sustaining neutron chain reaction. Some nuclear fuels are U_{235}, U_{233} and plutonium 239.

The solid fuel is fabricated into various small shapes, such as plates, pins, pellets, etc; they are assembled to form fuel elements. These elements are arranged in fixed geometrical patterns to form the reactor core. A uniform rate of heat release is obtained by suitably designing the reactor core. The coolant is prevented from direct contact with the fuel material by means of coatings on the fuel element.

(ii) *Moderator*

This is a material which slows down fast neutrons quickly without absorbing them. This process is desirable because slow-moving neutrons are more effective in triggering fission than fast neutrons. The moderator material is well-distributed in the reactor core or mixed with the fuel. Graphite is one of the materials used as a moderator.

(iii) *Reflector*

A reflector is a material which has good neutron-scattering properties coupled with a low absorbing power. Therefore, when the reactor core is surrounded by this material, it reflects the neutrons back into the active core. This reduces the neutron leakage. As a result, less fuel is required to produce sufficient neutrons to sustain a chain reaction. Generally, a good moderator material is also a good reflector.

(iv) *Coolant*

Coolant is a substance (liquid or gas) which transfers the heat produced in the reactor core (Fig. 4.16) to another fluid in a heat exchanger. By virtue of continuous flow through the reactor, the coolant keeps the core temperature within the prescribed limits and prevents overheating. Some coolants are heavy water, soft water, liquid sodium, carbon dioxide and helium.

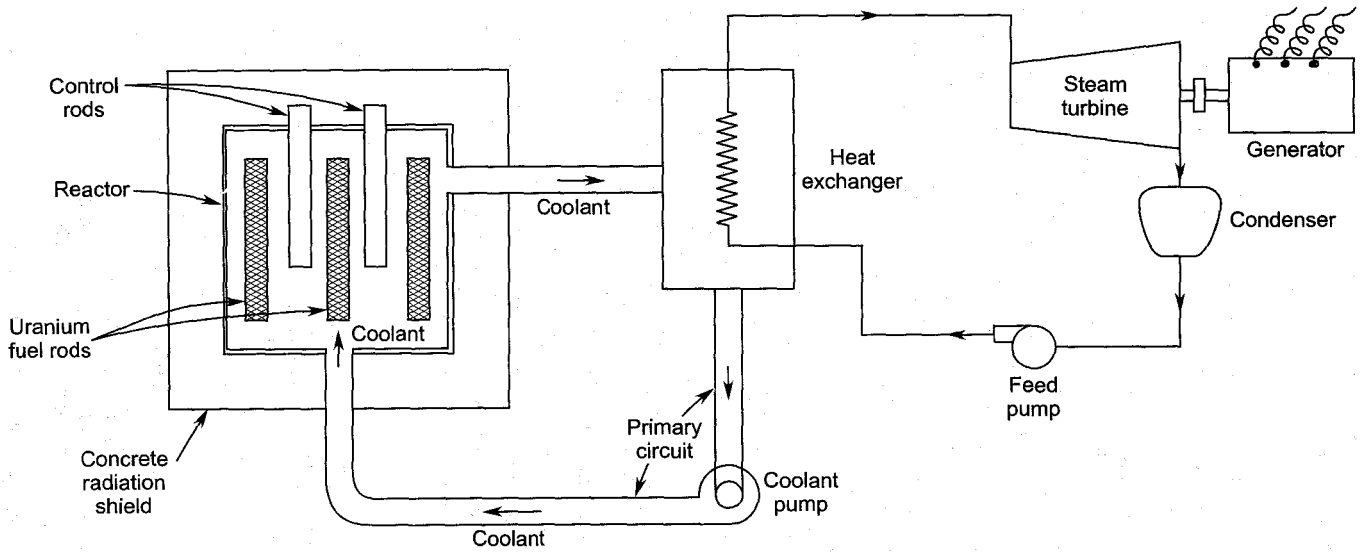

Fig. 4.16 A steam turbine power plant with a nuclear reactor

The power required by the coolant circulating pump or compressor (in the case of the gas-cooled reactor) is considerable and affects the overall efficiency significantly.

(v) *Control system*

The control mechanism in a nuclear reactor consists of the sensing elements and automatic devices which control the position of the control rods.

The sensing element measures the density of the neutron flux in the reactor and actuates the control rods to absorb excess neutrons. For a uniform rate of power generation, the rate of fission must be maintained constant. Boron and cadmium rods are used for controlling fission.

A control system, besides regulating the power output is also required to shut down the reactor in the event of an emergency. Therefore, there are two sets of control rods—one for routine power regulation and the other for emergency shut down.

(vi) *Radiation shield*

A radiation shield as shown in Fig. 4.16 surrounds the reactor to protect the personnel from radiations emitted during the fission process.

The boiling water reactor (BWR) employs the condensate of the steam plant directly as the coolant, moderator as well as the working fluid in the steam turbine. Since the pressure in the reactor is about the same as the steam pressure at the turbine inlet, this reactor is lighter than the pressurized water reactor (PWR).

The sodium-graphite reactor (SGR) has two coolant loops as shown in Fig. 4.17 Liquid sodium is used as the coolant in the primary circuit while liquid sodium-potassium in the secondary circuit. The system employs two heat exchangers as shown in Fig. 4.17.

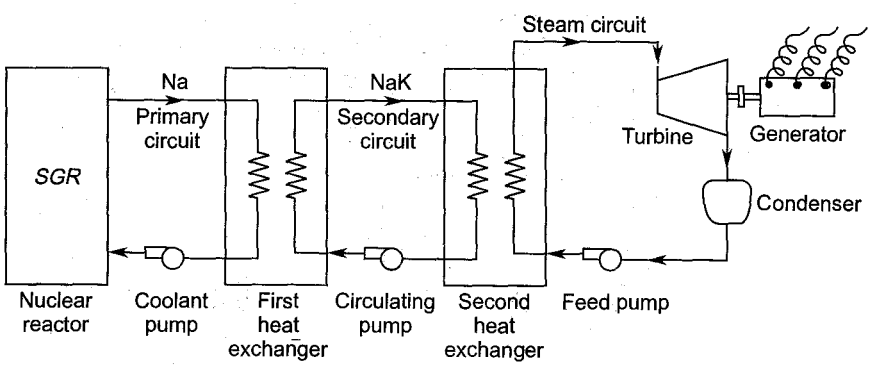

Fig. 4.17 Steam turbine plant with sodium graphite reactor (SGR)

Many other types of nuclear reactors and the concerned details which are beyond the scope of this book can be found in books on nuclear power.

Notation for Chapter 4

h	Enthalpy, enthalpy of feed water in a feed-heating cycle
Δh	Increase in enthalpy of feed water
H	Enthalpy of steam
$\dot{m}$	Mass flow rate of steam, mass of feed water
M	Mass of steam extracted for feed heating
n	number of feed-water heaters
p	Pressure of steam
q	Quantities of the heat as defined in the text
s	Entropy
t	Temperature
Δt	Increase in feed-water temperature
T	Absolute temperature
v	Specific volume
w	Specific work
HR	Heat rate

Greek Symbols

α	Ratio of the masses of the feed water leaving and entering a feed-water heater
γ	Ratio of specific heats
η	Efficiency

Subscripts

o	Turbine entry (Fig. 4.6)
1	Feed pump entry
2	Feed pump exit
3	Turbine entry
4	Turbine exit
B	Boiler
c	Condenser
i	ith feed-water heater
n	nth feed-water heater
N	Non-reheat cycle
o	Overall
P	Feed pump

r	Heat rejection
R	Reheater, reheat cycle
s	Heat reception
T	Turbine
TG	Turbine-generator
w	Water

Solved Examples

4.1 A steam power plant has the following data:

steam pressure at turbine inlet	25 bar
condenser pressure	65 mbar
turbine efficiency	78%
boiler efficiency	82%
calorific value of the fuel	26.3 MJ/kg

Assume the steam at the entry as dry.

Determine:

(a) exact and approximate Rankine efficiencies,
(b) thermal and relative efficiencies,
(c) overall efficiency,
(d) turbine and overall heat rates,
(e) steam consumption per kWh and
(f) fuel consumption per kWh.

***Solution*:**

Refer to Figs. 4.1 and 4.5

Since the efficiency of the feed pump is not given, it is assumed 100%.

Therefore, the feed pump work is

$$h_2 - h_1 = (p_2 - p_1)v_w = (25 - 0.065) \times \frac{0.001 \times 10^5}{1000}$$

$$h_2 - h_1 = 2.49 \text{ kJ/kg}$$

From steam tables at $p_c = p_1 = 0.065$ bar,

$$h_1 = 160.6 \text{ kJ/kg}$$

Therefore,

$$h_2 = 160.6 + 2.49 = 163.09 \text{ kJ/kg}$$

(a) By plotting the state points 3, 4 and 4′ on the *h–s* chart,

$$h_3 = 2800 \text{ kJ/kg}$$
$$h_4 = 1930 \text{ kJ/kg}$$

$$h_3 - h_4 = 870 \text{ kJ/kg}$$

$$h_3 - h'_4 = 0.78 \times 870 = 678.6 \text{ kJ/kg}$$

The exact Rankine efficiency is

$$\eta_{\text{Rankine}} = \frac{(h_3 - h_4) - (h_2 - h_1)}{(h_3 - h_1) - (h_2 - h_1)}$$

$$\eta_{\text{Rankine}} = \frac{870 - 2.49}{(2800 - 160.6) - 2.49} \times 100$$

$$\eta_{\text{Rankine}} = 32.89\% \ (Ans.)$$

Since the feed pump work is small, it can be ignored. Therefore, an approximate value of the Rankine efficiency is obtained by

$$\eta_{\text{Rankine}} = \frac{h_3 - h_4}{h_3 - h_1}$$

$$\eta'_{\text{Rankine}} = \frac{870 \times 100}{2800 - 160.6} = 32.96\% \ (Ans.)$$

(b) The thermal efficiency of the plant is

$$\eta'_{th} = \frac{h_3 - h'_4}{h_3 - h_1} = \frac{678.6 \times 100}{2639.4} = 25.71\% \ (Ans.)$$

$$\eta_{\text{Relative}} = \eta'_{th}/\eta'_{\text{Rankine}}$$

$$\eta_{\text{Relative}} = \frac{25.71}{32.96} \times 100 = 78.0\% \ (Ans.)$$

It is observed that the values of the turbine and relative efficiencies are identical.

(c) Overall efficiency is $\eta_o = \eta'_{th}\, \eta_B$

$$\eta_o = 25.71 \times 0.82 = 21.08\% \ (Ans.)$$

(d) Turbine heat rate is

$$(HR)_T = 3600/\eta'_{th}$$

$$(HR)_T = \frac{3600}{0.2571} = 14002.3 \text{ kJ/kWh } (Ans.)$$

Overall heat rate is

$$(HR) = \frac{3600}{\eta_o} = \frac{3600}{0.2108} = 17077.8 \text{ kJ/kWh } (Ans.)$$

(e) The steam rate ($\dot{m}$) in kg per kWh is given by

$$\dot{m}(h_3 - h'_4) = 3600$$

$$\dot{m} = \frac{3600}{678.6} = 5.305 \text{ kg/kWh } (Ans.)$$

(f) The fuel consumption per kWh is given by

$$(\dot{m}_f Q_f)\ \eta_o = 3600$$

$$\dot{m}_f = 3600/0.2108 \times 26.3 \times 1000$$

$$\dot{m}_f = 0.649 \text{ kg/kWh } (Ans.)$$

4.2 Steam expands from 160 bar, 500°C to 60 mbar in a steam turbine plant. Compare the plant efficiencies, heat rates and dryness fractions of the exhaust steam for reheat pressures of 70 bar, 50 bar and 25 bar. Assume isentropic expansion. Ignore the feed pump work.

***Solution*:**

The expansion and reheat processes for the non-reheat and the three reheat cycles have been drawn in Fig. 4.18. Figure 4.9 may also be referred to.

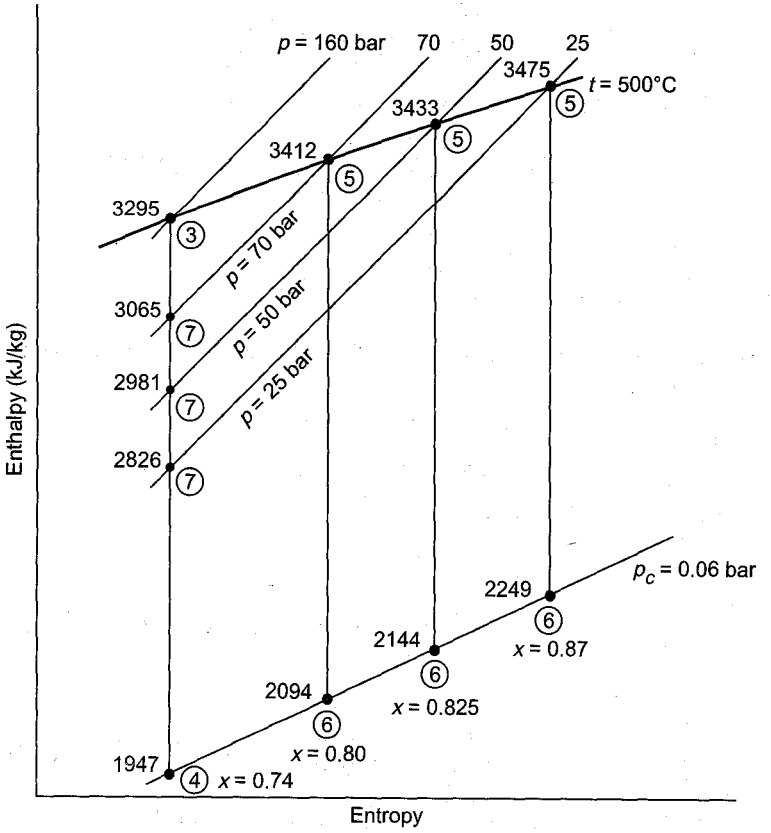

Fig. 4.18 Reheating at different pressures (Ex. 4.2)

Non-reheat cycle

The expansion line for the non-reheat cycle is 3–4. The enthalpies at these points are given on the *h–s* diagram.

The enthalpy of water at the condenser pressure from the steam tables is

$$h_c = 147 \text{ kJ/kg}$$

The heat supplied is

$$q_N = H_3 - h_c = 3295 - 147 = 3148 \text{ kJ}$$

$$\eta_N = \frac{H_3 - H_4}{H_3 - h_c} = \frac{3295 - 1947}{3148} = 0.428$$

Reheat cycles

Reheating and the subsequent expansion are represented by processes 7–5 and 5–6 respectively for the three reheat pressures given. The enthalpies of steam at points 7, 5 and 6 are given in each case.

$p = 70$ bar:

$$q_R = H_5 - H_7 = 3412 - 3065 = 347 \text{ kJ}$$

$$H_6 - H_4 = 2094 - 1947 = 147 \text{ kJ}$$

$$\eta_R = 1 - \frac{H_6 - H_4}{q_R}$$

$$\eta_R = 1 - \frac{147}{347} = 0.576$$

$$\eta_{th} = \frac{q_N + q_R\,(\eta_R/\eta_N)}{q_N + q_R}\ \eta_N$$

$$\eta_{th} = \frac{3148 + 347\,(0.576/0.428)}{3148 + 347} \times 0.428$$

$$\eta_{th} = 0.442 \quad \text{or} \quad 44.2\%$$

$$HR = 3600/\eta_{th}$$

$$HR = 3600/0.442 = 8145 \text{ kJ/kWh } (\textit{Ans.})$$

Similarly, these calculations can be done for other reheat pressures. The results of these calculations are given in the following table:

Reheat pressure	q_R	$H_6 - H_4$	η_R	η_{th}	*Heat rate*	*Final dryness fraction*
Non-reheat				0.428	8411.2	0.74
70	347	147	0.576	0.442	8145	0.80
50	452	197	0.564	0.445	8090	0.825
25	649	302	0.534	0.446	8072	0.87

4.3 A steam turbine plant employing regenerative feed heating cycle has the following data:

Steam conditions at inlet p = 82.75 bar, t = 510°C

Condenser pressure = 42 mbar

Bleed points are at pressures 22.75, 10.65, 4.35, 1.25 and 0.60 bar. The efficiencies of expansions between various pressures are 85%, 85%, 80%, 79%, 70% and 70%, respectively.

Construct the condition line for this turbine and determine:

(a) the final state of steam after expansion,

(b) mass of steam raised in the boiler per kg of steam condensed in the condenser,

(c) improvement in the thermal efficiency and heat rates due to feed heating, and

(d) decrease of steam flow to the condenser per kWh due to feed heating.

***Solution*:**

Refer to Figs. 4.6 and 4.19.

The actual state point after each expansion is obtained by the given pressure and the stage efficiency.

Actual enthalpy drop = isentropic enthalpy drop × efficiency.

Thus state points 1, 2, 3, 4, 5 and C are obtained. The temperature (or dryness fraction) of steam and enthalpies of steam and water at each point are indicated on Fig. 4.19.

Referring to Figs. 4.6 and 4.19, it may be noted that heater number one corresponds to point 5 on the condition line, heater number two to point 4, and so on.

(a) The final state at point C is

$$x = 0.875 \ (Ans.)$$

(b) The enthalpies of steam and water at various heaters are given in the following table:

Heater	$H_i - h_{i-1}$	$H_i - h_i$	$\alpha_i = \dfrac{H_i - h_{i-1}}{H_i - h_i}$
1	2510 – 121.4 = 2388.6	2510 – 360 = 2150	1.111
2	2590 – 360 = 2230	2590 – 444 = 2146	1.039
3	2730 – 444 = 2286	2730 – 612 = 2118	1.0793
4	2950 – 612 = 2338	2950 – 772 = 2178	1.0735
5	3080 – 772 = 2308	3080 – 931 = 2149	1.074

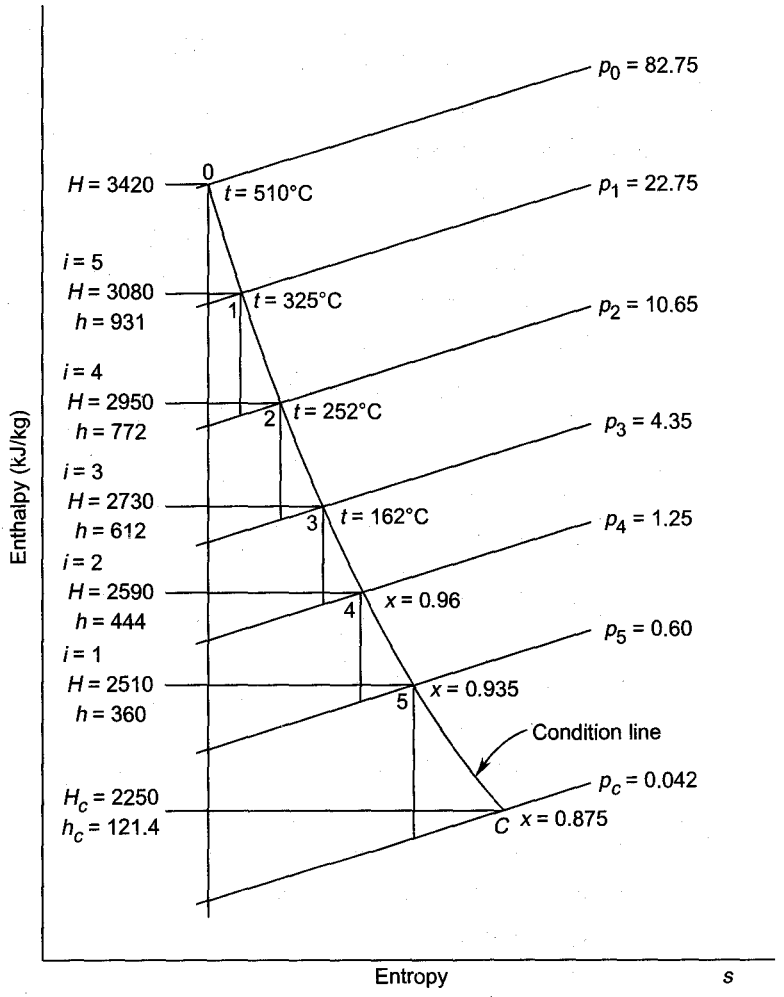

Fig. 4.19 Condition line in a regenerative feed-heating plant (Ex. 4.3)

The mass of steam raised per kg of steam reaching the condenser is given by

$$m_B = \prod_{i=1}^{i=5} \alpha_i$$

$$m_B = 1.111 \times 1.039 \times 1.0793 \times 1.0735 \times 1.074$$

$$= 1.436 \text{ kg} \qquad (Ans.)$$

(c) The thermal efficiency with feed heating is given by

$$\eta_{th} = 1 - \frac{H_c - h_c}{m_B (H_c - h_n)}$$

$$\eta_{th} = 1 - \frac{2250 - 121.4}{1.436\,(3420 - 931)} = 0.404$$

$$\eta_{th} = 40.4\%$$

The heat rate for the turbine is

$$HR_T = \frac{3600}{0.404} = 8910.9 \text{ kJ/kWh}$$

The thermal efficiency of the Rankine cycle and the heat rate without feed heating are

$$\eta_R = \frac{H_o - H_c}{H_o - h_c} = \frac{3420 - 2250}{3420 - 121.4} = 0.355$$

$$\eta_R = 35.5\%$$

The heat rate is

$$HR'_T = \frac{3600}{0.355} = 10140.8 \text{ kJ/kWh}$$

Therefore, the improvements are

$$\Delta\eta_{th} = \frac{40.4 - 35.5}{35.5} \times 100$$

$$= 12.67\% \ (Ans.)$$

$$\Delta HR_T = \frac{10140.8 - 8910.9}{10140.8} \times 100$$

$$= 12.13\% \text{ (decrease) } (Ans.)$$

(d) Heat supplied, $Q_s = m_B\,(H_o - h_n)$

$$Q_s = 1.436\ (3420 - 931) = 3574.2 \text{ kJ}$$

Heat rejected, $Q_r = H_c - h_c$

$$Q_r = 2250 - 121.4 = 2128.6 \text{ kJ}$$

Therefore, the turbine work

$$w_T = Q_s - Q_r = 3574.2 - 2128.6$$

$$= 1445.6 \text{ kJ}$$

Therefore, the turbine work per kg of steam supplied from the boiler is

$$\frac{1445.6}{1.436} = 1006.685 \text{ kJ/kg}$$

The steam flow rate per kWh is given by

$$\dot{m}\ (1006.685) = 3600$$

$$\dot{m} = 3.576 \text{ kg/kWh}$$

The steam condensed is

$$\frac{3.576}{1.436} = 2.490 \text{ kg/kWh}$$

Without feed heating, these quantities are

$$w_T = 3420 - 2250 = 1170 \text{ kJ/kg}$$

$$\dot{m} \times 1170 = 3600$$

$$\dot{m} = \frac{3600}{1170} = 3.077 \text{ kg/kWh}$$

This is the value of the steam supplied from the boiler and condensed. Thus the decrease in the steam reaching the condenser is

$$\frac{3.077 - 2.490}{3.077} \times 100 = 19\% \ (Ans.)$$

This will lead to a corresponding reduction in the cooling water flow rate and the size of the condenser.

Questions and Problems

4.1 How are steam turbines classified? Give a list of the types of steam turbines used in various applications.

4.2 How does an industrial steam turbine differ form a power plant turbine? State five points highlighting the difference.

4.3 **(a)** Draw a neat and illustrative schematic diagram of a steam turbine plant showing one reheat and five bleed points for feed heating.

(b) Show the various processes occurring in the plant on p–v, T–s and h–s coordinates.

(c) Prove that the relative efficiency of the plant is approximately equal to the turbine efficiency.

4.4 Show the locations of the F.D. and I.D. fans in a steam power plant. How do the aerothermodynamic and mechanical problems of these fans differ?

4.5 Sketch the layout of a steam turbine plant with a nuclear reactor. Describe its principal elements. What are its advantages over the conventional plant?

4.6 Explain briefly four methods which can be employed for improving the thermal efficiency of a steam turbine power plant.

4.7 Describe briefly various methods employed to recover the heat of exhaust gases from a gas turbine plant in a steam cycle.

4.8 **(a)** Prove that the thermal efficiency of a feed-heating steam power plant is given by

$$1 - \frac{\text{steam condensed per kg of steam raised}}{\text{enthalpy rise in the boiler/latent heat at condenser pressure}}$$

(b) How many feed-water heaters can be employed in a large plant? How is their number determined?

4.9 Prove that in a regenerative feed heating cycle employing n heaters the mass of steam raised in the boiler per kg. of steam condensed is

$$\prod_{i=1}^{i=n} \frac{(H_i - h_{i-1})}{(H_i - h_i)}$$

4.10 **(a)** Show a reheat cycle on the T–s and h–s diagrams.

(b) How is the reheat pressure chosen? What is its effect on the thermal efficiency of the plant?

(c) Why is the employment of more than one reheaters not popular?

4.11 Explain what is meant by the heat rates of the turbine, turbo-generator set and power station. What is the order of these values for large modern steam power stations?

4.12 Why is double-flow employed in large steam turbines? Show the layout of a three-cylinder (HP, IP and LP), single shaft steam turbine with double flow in LP cylinder.

Chapter 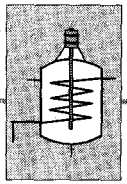 5

Combined Cycle Plants

On account of the ever-increasing demand of electric power, several new technologies have been developed during the last two decades. The thrust is mainly in the direction of increasing the efficiency of generation and the capacity of individual units and the entire power plants. New possibilities have been examined for large base load power plants, and more suitable and reliable peak load plants.

In some countries gas turbine power plants are preferred on account of the abundantly available fuel oil and natural gas. Recently large combined cycle power plants have also become popular.

The gas turbine power plant has been a late comer in the field of electric power generation. Its main disadvantages are lower thermal efficiency and capacity compared to the 'main players' in this field namely the hydro and steam turbine power plants. Attempts to improve the efficiency and output power of the gas turbine power plants by employing regeneration, intercooling and reheating result in significant pressure losses on account of longer gas flow passages; this also increases the capital and maintenance costs.

In a combined steam and gas turbine (STAG) power plant the huge loss of energy in the gas turbine exhaust is significantly reduced by utilizing its heat in a 'bottoming cycle'; here the high temperature exhaust gas transfers a large proportion of its heat to raise steam for the steam turbine power plant. Several different ways have been adopted to achieve this. The energy in the gas turbine exhaust is used during feed water heating in the economizer, and evaporation and superheating in the evaporator and superheater respectively. The ultimate aim is to obtain higher overall thermal efficiencies, which are much higher than the values obtained in the high efficiency large steam power plants.

The combined cycle plant combines the thermodynamic advantages of both the high temperature gas turbines and the lower temperature steam turbine power plants.

Generally a large proportion of the total power of the combined cycle plant is generated by the steam turbine. Several combined cycle plants employ two or more gas turbines for a single steam turbine.

5.1 The Basic Combined Cycle

As stated before in Chapters 3 and 4, the principal process in a combined gas and steam turbine cycle is the recovery of heat energy in the gas turbine exhaust by the feed water and steam in the steam turbine plant. Figure 5.1 shows the two power plant cycles, namely the Joule/Brayton cycle (gas turbine cycle) and the Rankine cycle (steam turbine cycle). The gas turbine power plant cycle (1–2–3–4–1) is the 'topping cycle; it consists of heat and work transfer processes occuring in the high temperature region. This is followed by such processes in the lower temperature region. The low temperature region has the 'bottoming cycle'—the Rankine steam cycle (a–b–c–d–e–f–a). A waste heat recovery boiler (WHRB) transfers heat energy from the high temperature gas turbine exhaust gases to water and steam used in the bottoming cycle.

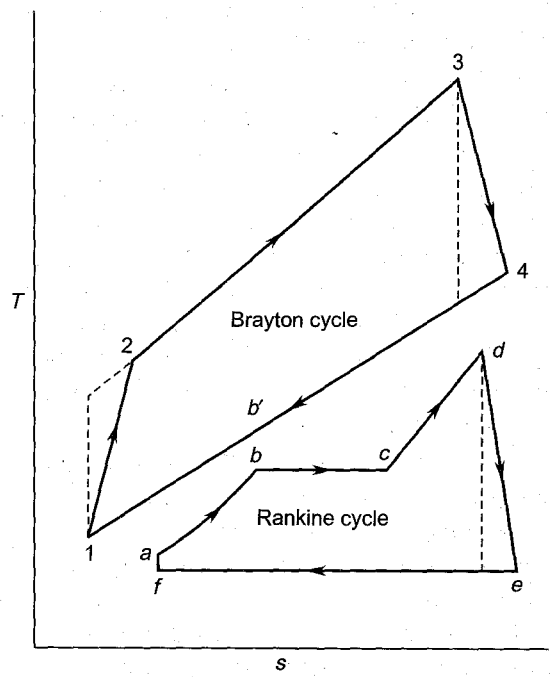

Fig. 5.1 Topping and bottoming cycles

The gas turbine exhaust gases reject heat during the constant pressure process 4–1. Part of this heat is absorbed by the feed water, and the wet and superheated steam during the processes a–b, b–c and c–d respectively.

Figure 5.2 shows the arrangement employed in the combined gas and steam turbine cycle power plant.

The gas turbine plant consists of the air compressor, combustion chamber, gas turbine and the electric generator (alternator) G.1. The corresponding

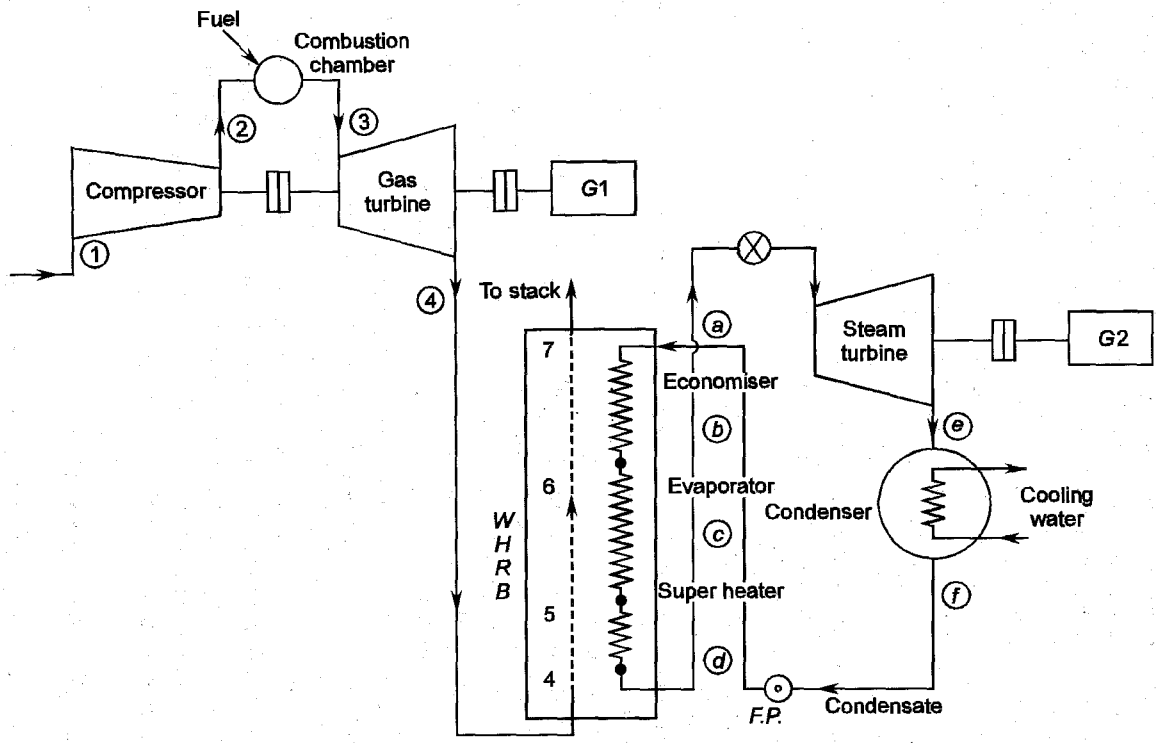

Fig. 5.2 Combined gas and steam turbine power plant

processes of compression (1–2), combustion (2–3) and expansion (3–4) are also shown in figure 5.1. It is observed in figure 5.2 that the gas turbine plant does not complete a closed cycle as depicted in figure 5.1.

The exhaust from the gas turbine passes through a heat exchanger widely known as the 'waste heat recovery boiler' (WHRB); for brevity it is also referred to as HRB. It is here that the heat energy from the gas turbine exhaust gases is transferred to the steam turbine plant; the lower temperature steam power plant consists of the WHRB, steam turbine, condenser and the electric generator G.2. The conventional feed water heaters of the turbine plant, though used are not shown in fig. 5.2. The feed pump (F.P) supplies the feed water to the economizer section (a–b) of the WHRB. After reaching the saturation temperature it absorbs the latent heat in the evaporator (b–c); the dry steam is heated to the designed temperature in the superheater (c–d) before entering the turbine.

Various stations in the gas circuit corresponding to the super-heater, evaporator and economizer sections are shown as points 4, 5, 6 and 7 respectively (refer to Fig. 5.2 and 5.10).

The exhaust flue gases leave the WHRB through the stack after supplying heat to the steam turbine power plant.

The section at which the difference in the temperatures of hot and cold fluids is minimum is known as the 'pinch point' (PP); it is given by $(T_b' - T_b)$ as shown in Fig. 5.1. It is observed that this is the difference in the temperature (T_b') of the gas turbine exhaust and the maximum temperature (T_b) (saturation temperature) of the feed water; the value of the feed water temperature (T_b) obviously depends on its pressure. This in turn, depends on the operating pressure in the steam cycle which can be fixed by the pinch point.

Figure 5.3 shows some temperature–enthalpy curves (a, b, c) for the steam turbine plant corresponding to temperature profile for the gas turbine exhaust gases. The position of the pinch-point depends on the location of the T–h curve for the exhaust gases. The magnitude of the temperature difference $(T'_b - T_b)$ differs in the different curves; therefore, the corresponding operating steam pressures will also be different. The relative sizes and the temperatures of the economizer, evaporator and the superheater will also differ for the curves a, b and c.

5.2 Steam Generators

Gas turbine power plant is thermodynamically coupled to the steam turbine plant through the waste heat recovery boiler. It receives high temperature exhaust gases from the gas turbine plant for generating steam (at the desired pressure and temperature) for driving the steam turbine. The WHRB (Fig. 5.2) is a vertical structure con-sisting of banks of water/

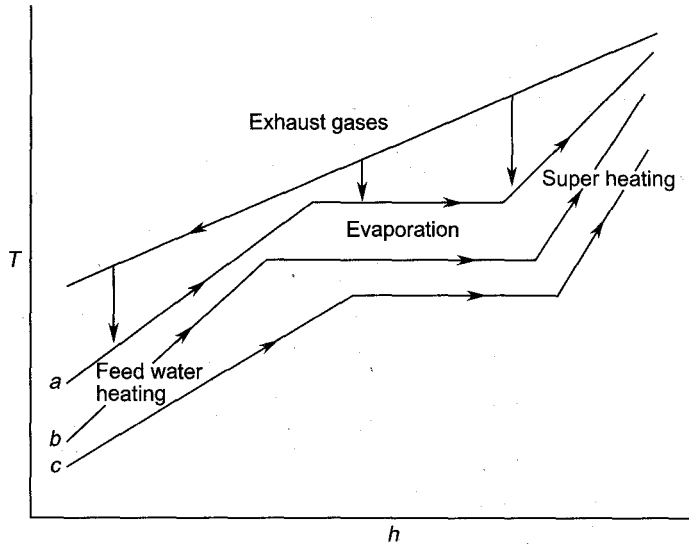

Fig. 5.3 Heat transfer from hot gases to water and steam

steam tubes in three sections comprising of the economizer, evaporator and the superheater respectively.

5.2.1 Unfired Boiler (WHRB)

The heat recovery boiler shown in Fig. 5.2 is an unfired boiler. There is no combustion of fuel in this boiler. Therefore, it does not have the fuel handling plant of the conventional steam power plant boilers. It is simply a heat exchanger. This aspect of the combined cycle plants significantly decreases the capital cost. Absence of combustion also frees the boiler operation from the problems of combustion control.

Gas turbine exhaust enters the boiler at the bottom in the super-heater section (4–5) and subsequently in the evaporator and economizer sections as it flows out from the stack.

In the water-steam circuit feed water enters the economizer at (a) and leaves at (b) after attaining saturation temperature. Then it flows through the evaporator (b–c) and the superheater (c–d).

Feed water heaters of the conventional steam power plant, pumps, water and steam drums have not been shown in Fig. 5.2 for simplicity.

When the temperature of exhaust gases entering the HRB is comparatively higher, the temperature of the gases leaving the stack may be uneconomically high. Therefore, it is desirable that more heat is recovered from the outgoing gases in the boiler. One of the methods adopted to achieve this is the employment of dual pressure boiler as shown in Fig. 5.4. Here also the arrangement is same as shown in Fig. 5.2. However, on

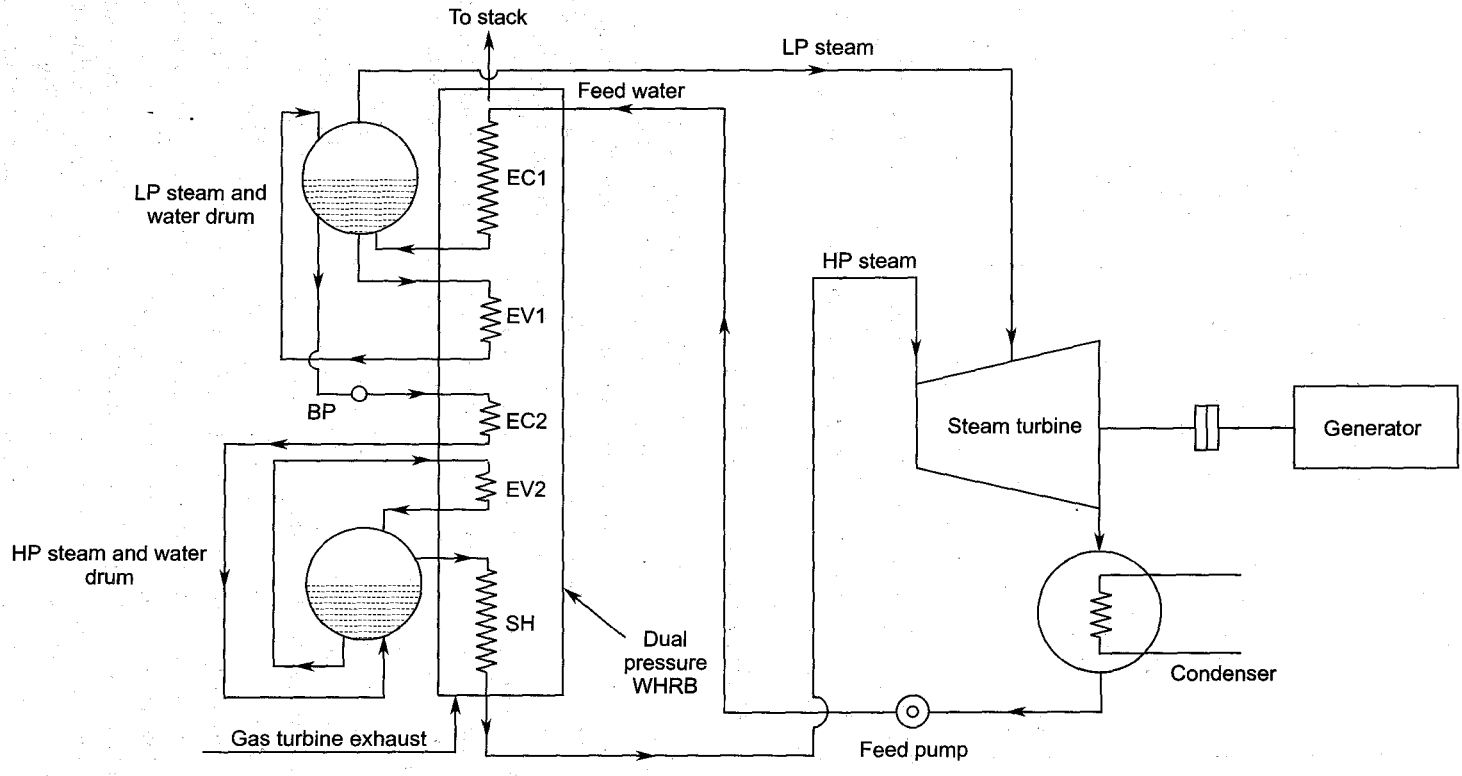

Fig. 5.4 Steam turbine plant with dual-pressure waste heat recovery boiler

account of the dual pressure, the boiler employs two separate water/steam drums. The low-pressure drum is connected to the L.P. economizer (EC.1) and the evaporator (EV.1) which are located in the lower temperature region of the heat recovery boiler. The low-pressure steam is supplied to the turbine in its L.P. stages as shown in the figure. A superheater can also be provided in the low-pressure circuit, if required.

A part of the feed water from the L.P. drum is pumped to the H.P. economizer (E.C.2) by a booster pump. This economizer heats up the water to its saturation temperature corresponding to the pressure of the high pressure steam circuit.

The saturated water enters the H.P. water/steam drum from where it flows through the H.P. evaporator (EV.2) and the superheater (SH). The H.P. economizer, evaporator and superheater are located in the higher temperature region of the boiler. The high pressure superheated steam is supplied to the turbine entry as shown.

The temperature-enthalpy curves of gas and steam for the L.P. and H.P. sections are shown in Fig. 5.5.

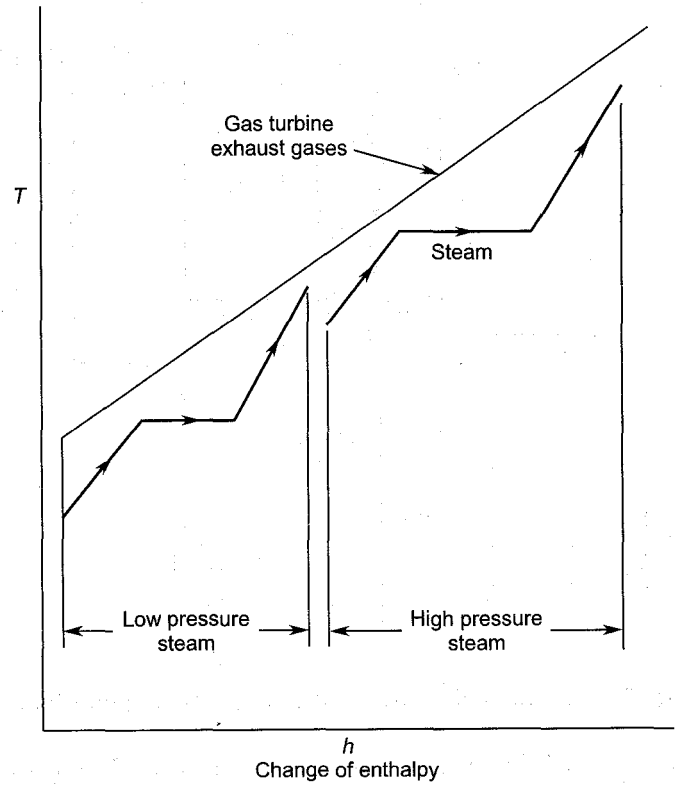

Fig. 5.5 Heat exchange in a dual-pressure waste heat recovery boiler

5.2.2 Supplementary Firing

The capacity of the unfired waste heat recovery boiler depends on the temperature and flow rate of the gas turbine exhaust; the pinch point determines the operating pressure of the steam turbine plant.

A large proportion of the combined cycle plant output is obtained from the steam turbine at comparatively higher efficiency. Some combined cycle power plants are often required to meet increased demands of power. Supplementary firing of fuel is often employed to obtain increased output of the steam power plant. More air is required for burning additional quantity of fuel during supplementary firing. This is invariably obtained by employing higher values of the air-fuel ratio in the combustion chamber of the gas turbine power plant. Thus the exhaust gases have ample air (oxygen) to support combustion of additional quantity of fuel in the WHRB. Combustion of additional fuel takes place in the gas turbine exhaust gases before they enter the unfired section of the boiler as shown in Fig. 5.6.

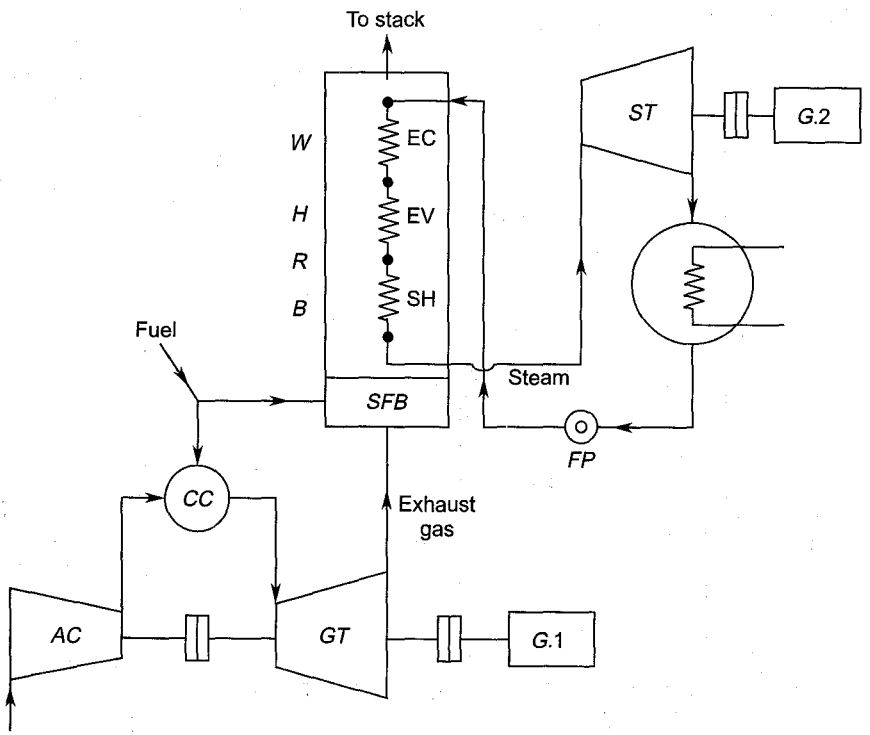

Fig. 5.6 Combined cycle plant with supplementary firing

Supplementary firing is also useful in another way. If the gas turbine plant has to operate at a reduced load, supplementary firing of the required quantity of fuel can compensate for the reduced heat input to

the waste heat recovery boiler thus maintaining its full load operation without any disturbance.

5.2.3 Supercharged Boiler

The combustion of fuel in a supercharged boiler (Fig. 5.7) takes place at a pressure which is significantly higher than the atmospheric pressure. This is done in order to achieve the expansion of the boiler flue gases (working fluid) through the gas turbine for producing work. A part of the gas turbine work is utilized to drive the air compressor which is employed to supply high pressure air to the supercharged boiler. The supercharged boiler replaces the combustion chamber of the conventional gas turbine plant. However, this boiler is much bigger in size on account of the presence of the conventional boiler components such as water tubes, steam tubes, etc. Besides this, the energy input in this boiler is much larger on account of comparatively large quantities of fuel which is burned here.

Strictly speaking the arrangement shown in Fig. 5.7 is not a 'true' combined cycle plant because here steam is not generated from the heat derived from the gas turbine exhaust.

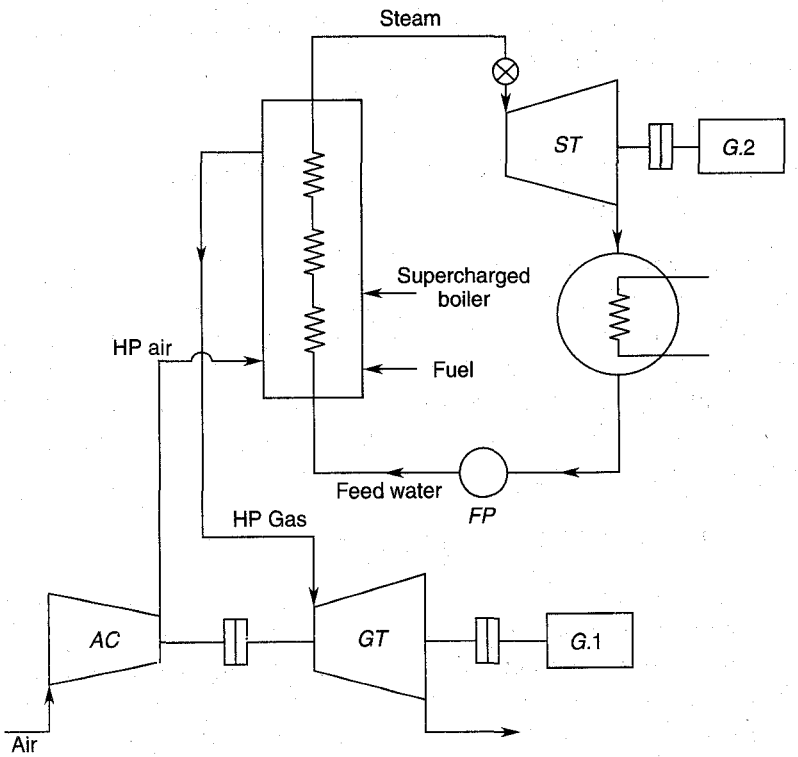

Fig. 5.7 Combined cycle plant with supercharged steam boiler

5.2.4 Coal Gasification

One of the alternatives in combined cycle plants that is considered is the use of coal as a fuel for the gas turbine plant. Here the working fluid for the gas turbine is produced from coal in a gasifier. Figure 5.8 illustrates the arrangement.

Coal gasification requires high pressure air and steam along with coal. In a combined cycle plant, both air and steam are available at the required pressure for the gasification process in the gasifier. It is not intended here to give the details of the gasifier. The figure only illustrates its integration in the combined cycle. The gas turbine plant, besides generating shaft power, supplies compressed air to the gasifier and hot gases to the WHRB. In a large plant, a separate gas turbine plant can be employed for supplying compressed air to the gasifier; the power producing gas turbine plants can employ a separate h.p. air compressor which may work in series with the gasifier compressor. Other arrangements for heat recuperation can also be employed in large plants.

Gasifiers are commercially available in various sizes. However, the range of flow rates available falls short of the usually high values required in modern gas turbine power plants.

Another aspect of gasifier application for combined cycle plants is its high capital cost. This is in sharp contrast to the role of the waste heat recovery boiler in the conventional plants.

5.3 Thermal Efficiencies and Power Output

Methods to determine the thermal efficiencies of different cycle arrangements in gas turbine and steam turbine plants have been dealt with separately in Chapters 3 and 4. In this section the two power plants are considered together for the calculation of the overall thermal efficiency and the power output. It can be seen in the layout of the combined cycle plants (as shown in Figs. 5.2, 5.4) that the two plants are thermodynamically coupled through the waste heat recovery boiler.

5.3.1 Approximate Thermal Efficiency

It is often very useful to be able to quickly calculate the overall efficiency of the combined cycle with some approximations. This is helpful in assessing the 'worth' of a given arrangement involving the location of the T–h curve for the steam cycle with respect to the given gas temperatures. Therefore, it is assumed that the gas turbine plant receives energy only in the combustion chamber and rejects it to the WHRB. Similarly the steam

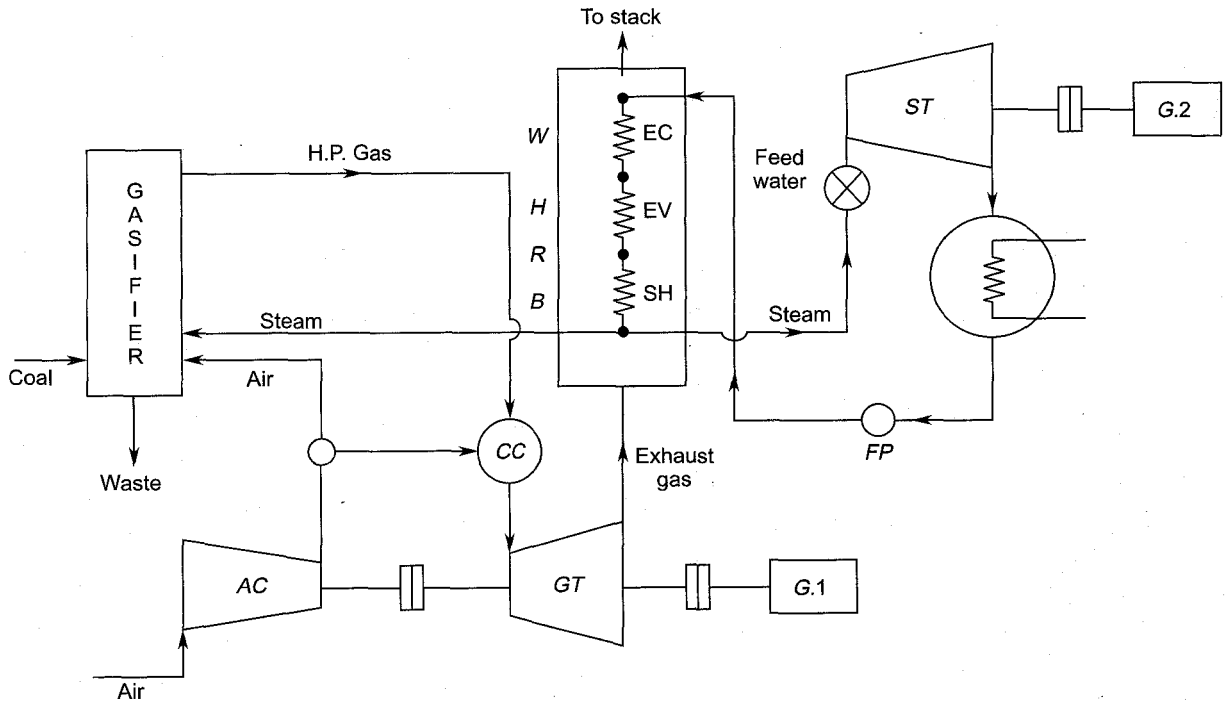

Fig. 5.8 Combined cycle plant with coal gasifier

turbine plant is assumed to receive energy only from the gas turbine exhaust rejecting energy only in the condenser. Thus the combined cycle receives energy only at one point, namely the combustion chamber and rejects energy in the condenser. The total work produced is the sum of the values of shaft work done in the gas and steam turbine plants.

In view of the above model, the energy and mass flows through the combined cycle plant are shown in Fig. 5.9. Here the heat rejected by the gas turbine plant equals the heat received (Q_{st}) by the steam plant.

Thermal efficiency of the gas turbine plant is given by

$$\eta_{gt} = \frac{\textit{heat supplied} - \textit{heat rejected}}{\textit{heat supplied}} = \frac{\textit{shaft work}}{\textit{heat supplied}}$$

$$\eta_{gt} = \frac{Q_{gt} - Q_{st}}{Q_{gt}} = 1 - \frac{Q_{st}}{Q_{gt}} = 1 - \frac{q_{st}}{q_{gt}} \qquad (5.1a)$$

$$\eta_{gt} = w_{gt}/q_{gt} \ldots\ldots \qquad (5.1b)$$

Heat supplied to the steam plant

$$q_{st} = (1 - \eta_{gt})q_{gt} \quad \ldots\ldots \qquad (5.2)$$

Thermal efficiency of the steam turbine plant is given by

$$\eta_{st} = \frac{\textit{shaft work}}{\textit{heat supplied}}$$

$$\eta_{st} = \frac{w_{st}}{q_{st}} = \frac{w_{st}}{(1-\eta_{gt})q_{gt}} \quad \ldots\ldots \qquad (5.3)$$

Therefore, for the steam turbine, shaft work per kg of the exhaust gases is given by

$$w_{st} = \eta_{st} \cdot (1 - \eta_{gt})q_{gt} \ldots\ldots\ldots \qquad (5.4)$$

Thermal efficiency of the combined cycle plant is given by

$$\eta_{gst} = \frac{w_{gt} + w_{st}}{q_{gt}} \quad \ldots \qquad (5.5)$$

$$\eta_{gst} = \frac{w_{gt}}{q_{gt}}\left(1 + \frac{w_{st}}{w_{gt}}\right) = \eta_{gt}\left(1 + \frac{w_{st}}{w_{gt}}\right) \quad \ldots \qquad (5.6)$$

Equations (5.1b) and (5.4) give

$$\frac{w_{st}}{w_{gt}} = \frac{\eta_{st}(1-\eta_{gt})}{\eta_{gt}} \qquad (5.7)$$

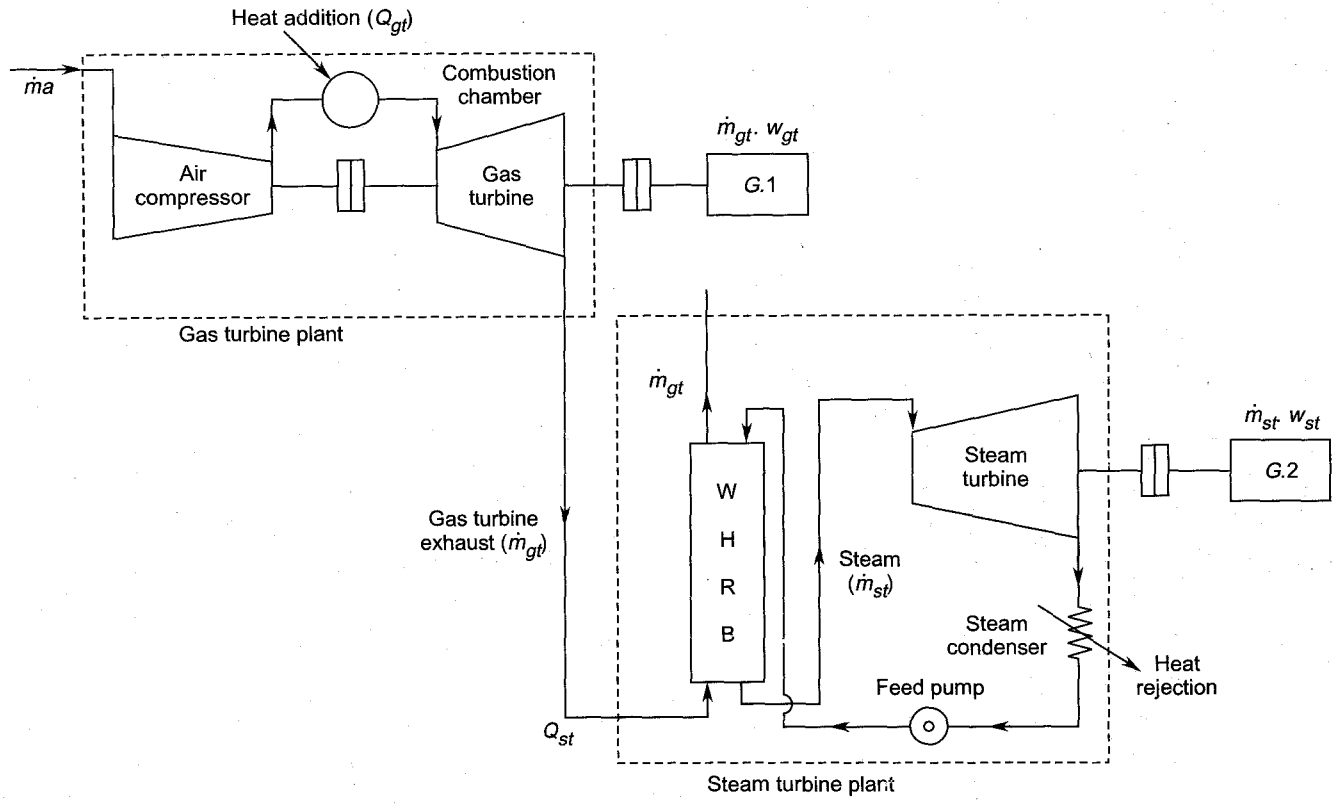

Fig. 5.9 Energy and mass flows through a combined cycle power plant

Equations (5.6) and (5.7) yield

$$\eta_{gst} = \eta_{gt} + \eta_{st}\,(1 - \eta_{gt}) \quad \text{....(5.8a)}$$

$$\eta_{gst} = \eta_{gt} + \eta_{st} - \eta_{st} \cdot \eta_{gt} \quad \text{.....(5.8b)}$$

$$\eta_{gst} = \eta_{st} + \eta_{gt}\,(1 - \eta_{st}) \quad \text{....(5.8c)}$$

$$\eta_{gst} = 1 - (1 - \eta_{gt})\,(1 - \eta_{st}) \quad \text{.....(5.8d)}$$

The actual processes of energy flow in the combined cycle plant deviate from those considered here. Therefore, this method over-estimates the performance of the combined cycle plant.

5.3.2 Power Output

Power developed in the gas turbine plant is given by

$$P_{gt} = \dot{m}_{gt}\, w_{gt} \quad (5.9)$$

$$\dot{m}_{gt} = \dot{m}_a + \dot{m}_f$$

$$\dot{m}_{gt} = \left(1 + \frac{1}{f}\right) \dot{m}_a \quad (5.10)$$

Air-fuel ratio

$$f = \frac{\dot{m}_a}{\dot{m}_f} \quad (5.11)$$

The heat supplied to the combined cycle plant is

$$Q_{gt} = \dot{m}_f \cdot Q_f \quad (5.12)$$

$$q_{gt} = \frac{\dot{m}_f}{\dot{m}_{gt}}\, Q_f$$

$$q_{gt} = \frac{1}{(1+f)} Q_f \quad (5.13)$$

Power developed in the steam turbine plant is

$$P_{st} = \dot{m}_{gt} \cdot w_{st} \quad (5.14)$$

5.3.3 Relative Flow Rates

Flow rates of gas turbine exhaust gases and steam, among other things, depend on the power outputs and the chosen temperatures in the two circuits of hot and cold streams. Temperature differences between these two streams in the different sections (Fig. 5.2) of the WHRB are shown in Fig. 5.10, following equations can be written for the energy transfer:

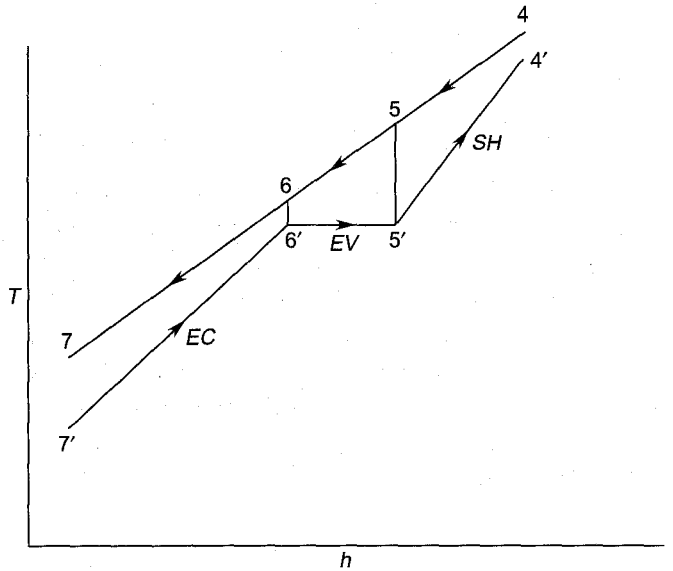

Fig. 5.10 Temperatures and enthalpies in the gas and steam circuits

Economiser:

$$\dot{m}_{gt} \cdot c_{pg} (t_6 - t_{7}) = \dot{m}_{st} (h_{6'} - h_{7'}) \tag{5.15}$$

Evaporator:

$$\dot{m}_{gt} \cdot c_{pg} (t_5 - t_6) = \dot{m}_{st} \cdot h_{fg} = \dot{m}_{st} \cdot (h_{5'} - h_{6'}) \tag{5.16}$$

Superheater:

$$\dot{m}_{gt} \cdot c_{pg} (t_4 - t_5) = \dot{m}_{st} (h_{4'} - h_{5'}) \tag{5.17}$$

Evaporator and superheater

$$\dot{m}_{gt} \cdot c_{pg} (t_4 - t_6) = \dot{m}_{st} (h_{4'} - h_{6'}) \tag{5.18}$$

$$\frac{\dot{m}_{st}}{\dot{m}_{gt}} = \frac{c_{pg} (t_4 - t_6)}{h_{4'} - h_{6'}}$$

$$= \textit{mass of steam generated per kg of exhaust gases} \tag{5.19}$$

For a chosen value of the operating steam pressure (p_s), $h_{6'}$, $h_{5'}$ and $t_{6'}$, $t_{5'}$ are known.

$$h_{6'}, h_{5'} t_{6'} = f(p_s) \tag{5.20}$$

For a given value of the pinch point

$$t_6 = t_{6'} + PP \tag{5.21}$$

Other temperatures which can be chosen are:

Steam turbine inlet temperature, $t_{4'}$,

Exhaust gas temperature in the stack, t_7,
Exhaust gas temperature t_4 at the gas turbine exit is generally known.

5.4 Fuels for Combined Cycle Plants

Gas turbines now run on a variety of fuels–solid, liquid and gaseous. Gasifiers are commercially available to gasify coal for burning in gas turbine combustion chambers. However, inadequate rate of production of the producer gas in these gasifiers may be the main hurdle, and limitation.

Coal can also be used in a supercharged boiler with fluidized-bed combustion. In such a case, high temperature and pressure flue gases from the boiler expand through the gas turbine, producing work.

Heavy fuel oils and distillates are widely used in gas turbine power plants as well as in the supplementary fired boilers for the steam turbine power plant.

Natural gas is widely used for operating a large number of big and small gas turbines as well as combined cycle power plants. Gases available in some industrial processes such as steel making can also be profitably used in gas turbines.

Closed cycle gas turbine plants use helium as the working fluid and nuclear reactors as the heat sources.

5.5 Variable Load Operation

Large steam turbine power plants are already established as base load plants. They give high performance under steady operation. Because of this, it is profitable to use combined cycle power plants also for base load operation. Therefore, it is desirable that the complementary gas turbine plant runs at a constant output.

If such a plant is required to operate at part-load, it is often convenient to decrease the output of the gas turbine/turbines feeding the heat recovery boiler and compensate the diminished heat energy in the exhaust gases by supplementary firing. In some situations one of the gas turbines (in case two or more are used) can be finally stopped if the decrease in load so demands. This allows the steam turbine and the remaining gas turbines to operate at full or near full load conditions.

In case of increased demand the output of the combined cycle plant can be increased in several ways. The steam turbine output is increased by supplementary firing. The outputs of both the gas and steam turbines can be increased by burning more fuel in the combustion chamber of the gas turbine plant.

5.6 Advantages and Disadvantages

Since the combined cycle plants offer a new technology in the field of electric power generation, it is useful if their relative position with respect to other power plants is understood.

Some of the main advantages and disadvantages are briefly described here.

5.6.1 Advantages

1. It combines the thermodynamic advantages of the high temperature gas turbine and the lower temperature steam turbine plant.
2. Superheated steam is supplied to the steam turbine without the detailed and intricate plant and machinery of the conventional steam boiler.
3. Ash and coal handling is absent.
4. It offers considerably higher efficiency and lower heat rate over a wide range of load.
5. Gas turbine part of the total plant is much easier to install. Therefore, its power is available much earlier.
6. It is easier to start (from cold) a combined cycle plant in a short time.
7. Comparatively less quantity of cooling water is required.
8. It has lower capital cost compared to the steam plant.
9. It has much lower heat rejection.
10. It is suitable for both base load and peak load.
11. Pollution from combined cycle plants is much less compared to the conventional steam or gas turbine power plants.

5.6.2 Disadvantages

1. Combined cycle plants are more complex; they require more skilled and better trained personnel in modern technologies.
2. It requires expensive fuel oil and gas.
3. Its capital cost per MW is higher than gas turbine.
4. It is less flexible in terms of fuels which can be used.

Notation for Chapter 5

AC	Air Compressor
BP	Booster Pump
CC	Combustion chamber
c_p	Specific heat at constant pressure

EC	Economizer
EV	Evaporator
FP	Feed pump
f	$= \dot{m}_a / \dot{m}_f$ Air-fuel ratio
G	Generator/alternator
GT	Gas turbine
h	Specific enthalpy
h_{fg}	Latent heat of steam
HP	High pressure
HR	Heat rate
LP	Low pressure
$\dot{m}$	Mass flow rate
p	Pressure
P	Power
PP	Pinch point
Q	Heat transferred, Calorific value
q	Heat supplied or rejected per kg of the working fluid
s	Entropy
SFB	Supplementary fired boiler
SH	Superheater
ST	Steam turbine
T	Absolute temperature
t	Temperature
w	Specific work
WHRB	Waste heat recovery boiler
x	Dyness fraction of steam
η	Efficiency

Subscripts

1, 2, 3, 4	stations shown in Fig. 5.1
4, 5, 6, 7	stations shown in Figs. 5.2 and 5.10
a	Air
c	compressor
g	Gas, dry steam
gt	Gas turbine
gst	combined gas and steam turbine plant
s	steam, saturation state
t	turbine.

Superscript

'Steam circuit

Solved Examples

5.1 A 100 MW gas turbine plant (η_{th} = 26.66%) supplies 400 kg/s of exhaust gas at 592.60°C to the heat recovery boiler of a bottoming steam power plant.

Steam is generated at a pressure of 90 bar with a pinch point of 20°C. Condenser pressure = 0.10 bar. If the gas temperature in the stack is 176°C determine

(a) capacity of the boiler in kg of steam per hour,

(b) temperature of steam at the turbine entry,

(c) steam turbine plant output and thermal efficiency and

(d) the thermal efficiency of the combined cycle plant.

Take c_{pg} = 1.157 kJ/kg for the exhaust gases and dryness fraction of steam at the turbine exit x = 0.90.

Solution:

Refer to Fig. 5.10.

(a) Heat given by the gases during process 6–7 is equal to the sensible heat received by the feed water in the economizer during process 7′–6′. Therefore,

$$\dot{m}_{gt}\, c_{pg}\, (t_6 - t_7) = \dot{m}_{st}\, (h_{6'} - h_{7'})$$

$$\frac{\dot{m}_{st}}{\dot{m}_{gt}} = \frac{c_{pg}\, (t_6 - t_7)}{h_{6'} - h_{7'}}$$

From steam tables at p = 90 bar,

$$t_{6'} = t_{5'} = 303.3°C = \text{saturation temperature}$$

$$h_{5'} - h_{6'} = h_{fg} = 1380.8\ kJ/kg$$

$$h_{5'} = 2744.6\ kJ/kg$$

$$h_{6'} = 1363.8\ kJ/kg$$

$$t_6 = t_{6'} + PP$$

$$t_6 = 303.3 + 20 = 323.3°C$$

At condenser pressure p = 0.10 *bar*, $h_{7'}$ = 191.8 *kJ/kg*

$$\frac{\dot{m}_{st}}{\dot{m}_{gt}} = \frac{1.157\,(323.3 - 176)}{1363.8 - 191.8} = 0.1454$$

Therefore, boiler capacity is

$$\dot{m}_{st} = 0.1454 \times \dot{m}_{gt}$$

$$= 0.1454 \times 400 = 58.16 \text{ kg/s}$$

$$\dot{m}_{st} = 209.376 \text{ tonnes/hr.} \qquad (Ans.)$$

(b) Energy balance for the evaporator during the process 6′–5′ (5–6) provides

$$\dot{m}_{gt} \cdot c_{pg} (t_5 - t_6) = \dot{m}_{st} (h_{5'} - h_{6'})$$

$$t_5 - t_6 = 0.1454 \times 1380.8/1.157 = 173.25$$

$$t_5 = 323.3 + 173.25 = 496.55°C$$

Similarly energy balance for the superheater (5′ – 4′) gives

$$h_{4'} - h_{5'} = \frac{\dot{m}_{gt}}{\dot{m}_{st}} c_{pg} (t_4 - t_5)$$

$$= \frac{1.157}{0.1454} (592.6 - 496.55)$$

$$= 762.1$$

$$h_{4'} = h_{5'} + 762.1 = 2744.6 + 762.1 = 3506.7 \text{ kJ/kg}$$

Steam temperature $t_{4'}$ at the turbine entry corresponding to $h_{4'}$ = 3506.7 kJ/kg (at p = 90 bar) is

$$t_{4'} = 540°C \qquad (Ans.)$$

(c) See Fig. 5.11

The actual and ideal expansion through the steam turbine is shown in fig. 5.11. Values of enthalpy at different points are shown.

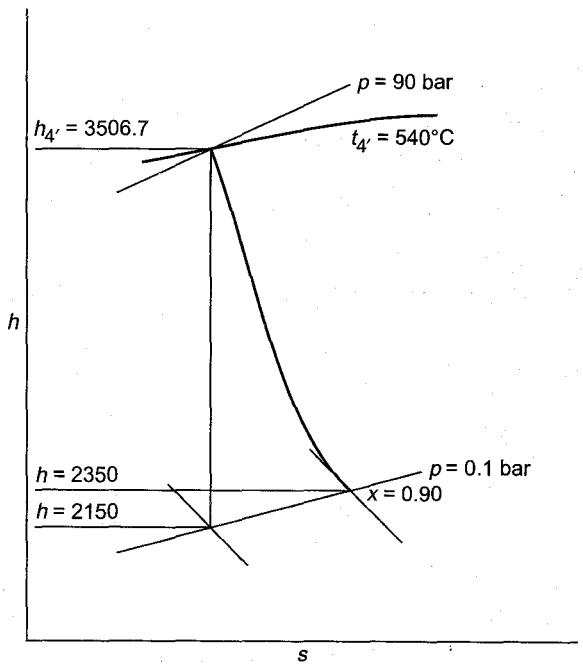

Fig. 5.11 Expansion of steam through the steam turbine (Ex. 5.1)

Specific work in the steam turbine plant is

w_{st} = actual enthalpy drop

w_{st} = 3506.7 – 2350 = 1156.7 kJ/kg of steam

w_{st} = 0.1454 × 1156.7 = 168.184 kJ/kg of gas

Power output of the steam turbine plant is

$$P_{st} = \dot{m}_{st} \cdot w_{st}$$

$$= 58.16 \times \frac{1156.7}{1000} = 67.27 \text{ MW} \qquad (Ans.)$$

Heat supplied to the steam turbine plant is

$$q_{st} = h_{4'} - h_{7'}$$

$$= 3506.7 - 191.8 = 3314.9 \text{ kJ/kg}$$

$$\eta_{st} = \frac{w_{st}}{q_{st}} = \frac{1156.7}{3314.9} \times 100 = 34.89\% \qquad (Ans.)$$

(d) Heat supplied to the combined cycle plant is

$$q_{gt} = \frac{w_{gt}}{\eta_{gt}}$$

$$\dot{m}_{gt} \cdot w_{gt} = P_{gt}$$

$$w_{gt} = P_{gt}/\dot{m}_{gt}$$

$$= 100 \times 1000/400$$

$$= 250 \text{ kJ/kg}$$

$$q_{gt} = \frac{250}{.2666} = 937.73 \text{ kJ/kg}$$

Therefore, thermal efficiency of the combined cycle plant is

$$\eta_{gst} = \frac{w_{gt} + w_{st}}{q_{gt}}$$

$$= \frac{250 + 168.184}{937.73} = 0.44595$$

$$\eta_{gst} = 44.595\% \qquad (Ans.)$$

5.2 A combined gas and steam plant develops 10 MW at the gas turbine shaft with an efficiency of 20 per cent. A steam turbine power plant (η_{st} = 32%) is operated through the WHRB which receives the turbine exhaust. Calculate:

(a) the output of the steam turbine plant,

(b) thermal efficiency of the combined cycle plant, and

(c) the overall heat rate.

Solution:

Since all the required data about the gas and steam turbines is not given calculations are based on approximations.

(a)

$$Q_{gt} = \frac{P_{gt}}{\eta_{gt}} = \frac{10 \times 1000}{0.20} = 50.000 \text{ kJ/s}$$

$$Q_{st} = (1 - \eta_{gt})Q_{gt} = (1 - 0.2) \times 50{,}000 = 40{,}000 \text{ kJ/s}$$

$$P_{st} = \eta_{st} \cdot Q_{st}$$

$$= 0.32 \times 40{,}000 = 12{,}800 \text{ kJ/s}(12.8 \text{ MW}) \quad (\textit{Ans.})$$

(b) Thermal efficiency of the combined cycle plant is given by

$$\eta_{gst} = \eta_{gt} + \eta_{st} - \eta_{gt} \cdot \eta_{st}$$

$$\eta_{gst} = 0.2 + 0.32 - 0.2 \times 0.32 = 0.456$$

$$\eta_{gst} = 45.6\% \quad (\textit{Ans.})$$

$$\eta_{gst} = \frac{10 + 12.8}{50} \times 100 = 45.6\% \ (\textit{verified})$$

(c) The heat rate of the combined cycle plant is given by

$$HR = \frac{3600}{\eta_{gst}} = \frac{3600}{.456}$$

7894.74 kJ/kWh (*Ans.*)

Question and Problems

5.1 Describe with the aid of an illustrative sketch a combined gas and steam turbine power plant working with a coal gasifier. What are the various heat recuperative methods employed to improve the thermal efficiency? What are the main disadvantages of this plant?

5.2 What is an unfired boiler? What are its limitations and advantages?

5.3 Draw a neat sketch of a dual pressure heat recovery boiler for the steam power plant in a combined cycle plant. Describe its working.

Draw the *T–h* curves for the hot gases and steam in the H.P. and L.P. circuits. Indicate the pinch points.

5.4 Write down ten advantages and five disadvantages of combined gas and steam turbine power plants.

5.5 How does a combined cycle power plant compare with gas and steam turbine plants in the following areas:

(a) Capital cost,

(b) Part-load performance,
(c) Cooling water requirements, and
(d) Environmental pollution?

Explain briefly.

5.6 Describe briefly with the aid of illustrative sketches the following in a combined cycle plant:

(a) Supplementary firing.
(b) Waste heat recovery boiler,
(c) Pinch-point,
(d) Supercharged boiler

5.7 Which fuels are generally used in combined cycle power plants?

5.8 Prove that the overall efficiency and heat rate of combined gas and steam cycle plants are given by

(a) $\eta_o = \eta_{gt} + \eta_{st} - \eta_{gt} \cdot \eta_{st}$

(b) $R_o = \dfrac{R_{gt} \times R_{st}}{R_{gt} + R_{st} - 3600}$

Here R denotes heat rate.

State the assumption used.

5.9 **(a)** Prove that the distribution of specific work (kJ/kg of gas) in the gas and steam turbine plants is approximately given by

$$\frac{w_{gt}}{w_{st}} = \frac{\eta_{gt}}{\eta_{st}\,(1-\eta_{gt})} = \textit{work ratio}$$

(b) Determine the values of the overall efficiency of the combined cycle, heat rate and work ratio for $\eta_{gt} = 26.66\%$, $\eta_{st} = 34.85\%$

(*Ans.*) $\eta_{gst} = 52.25\%$, $HR = 6890$ kJ/kWh, $\dfrac{w_{gt}}{w_{st}} = 1.043$

5.10 Gas turbine exhaust of Ex. 5.1 is employed in a waste heat recovery boiler to raise steam at $p = 66$ bar and $t = 540°C$. The steam expands to a condenser pressure of 0.1 bar and dryness fraction 0.90. Taking a pinch-point of 20°C determine.

(a) The steam boiler capacity,
(b) Temperature of the gases in the stack,
(c) Steam turbine efficiency,
(d) Steam turbine plant output and efficiency, and
(e) Efficiency of the combined cycle plant.

(*Ans.*) (a) 212 tonnes/h (b) 167.60°C
(c) 88.72% (d) 69.52 MW, 35.35%
(e) 45.2%

5.11 A combined cycle plant has the following data:

Gas turbine power output	= 70 MW
Gas turbine exhaust gas temperature	= 510°C
Steam turbine inlet pressure	= 83 bar
Steam temperature at turbine inlet	= 427°C
Condenser pressure	= 100 mm Hg
Steam turbine efficiency	= 88%
Pinch point	= 15°C
Gas turbine plant thermal efficiency	= 34.8%
Gas flow rate	= 263.61 kg/s

Determine

(a) Mass of steam generated per kg of exhaust gases,
(b) Temperature of the flue gases in the stack,
(c) Steam turbine plant output
(d) Steam turbine plant thermal efficiency,
(e) Total output and thermal efficiency of the combined cycle plant,

(*Ans.*) (a) 0.09505 kg (b) 207°C
(c) 28.223 MW (d) 35.15%
(e) 98.223 MW, η_{th} = 49.1%

5.12 In the combined cycle plant of Ex. 5.2 heat is supplied to the gas turbine at a temperature of 1350 K. Determine the flow rates of gases and the steam in the two components of the plant. Take c_{pg} = 1.157 kJ/kg K for the gases.

(*Ans.*) $\dot{m}_{gt}$ = 32.0 *kg/s* $\dot{m}_{st}$ = 32.0 kg/s

Chapter 6

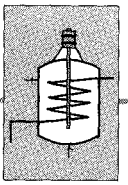

Fluid Dynamics

In this chapter we shall begin with some basic definitions used in fluid dynamics.

As stated in Chapter 2, the analysis of flow in turbomachines requires the application of Newton's second law of motion along with the equations of continuity and energy. Various forms of the energy equation were derived in Chapter 2; it will be further discussed in this chapter.

The application of Newton's second law of motion provides the equations of motion which are also known as Euler's momentum equations. These and the continuity equation have been used in the subsequent chapters. Various forms of these equations [83, 84, 94] have been summarized below.

6.1 Basic Definitions

6.1.1 Fluid

A fluid is a substance which continuously deforms when shearing forces are applied. Liquids, gases and vapours are all fluids. A non-viscous or inviscid fluid is referred to as an ideal fluid.

6.1.2 Fluid Velocity

The instantaneous velocity of the fluid particle passing through a point is known as the fluid velocity at that point.

6.1.3 Streamline

A curve in a flow field which is always tangent to the direction of flow is referred to as a streamline. These are shown in Fig. 6.1.

6.1.4 Stream Tube

A stream tube (Fig. 6.1) is an infinitesimal portion of the flow field. It is a collection of a number of streamlines forming an imaginary tube. There is no flow through the walls of a stream tube. The properties of the flow

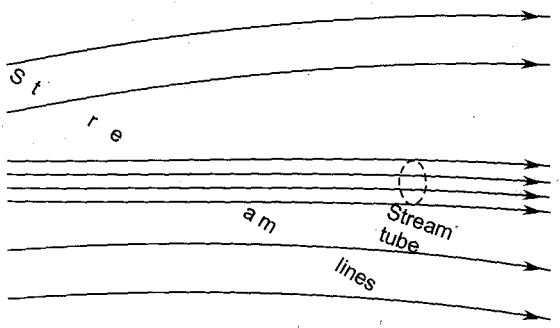

Fig. 6.1 One-dimensional flow through a stream tube

are constant across the section of a stream tube. Therefore, the flow in a stream tube is one-dimensional.

6.1.5 Incompressible Flow

If the relative change in the density of a fluid in a process is negligible, it is referred to as an incompressible process. In such a flow (or process) the fluid velocity is much smaller than the local velocity of sound in it.

The flow of gases and vapours at Mach numbers less than 0.30 can be assumed to be incompressible without much sacrifice in accuracy.

6.1.6 Compressible Flow

In compressible flows the relative changes in the fluid density are considerable and cannot be neglected. The fluid velocities in such flows are appreciable compared to the local velocity of sound. If the Mach number in a flow is higher than 0.3, it is considered to be compressible.

6.1.7 Steady Flow

A flow is known to be steady if its properties do not change with time. The shape of the stream tube does not change in steady flow. For such a flow

$$\frac{\partial c}{\partial t} = \frac{\partial p}{\partial t} = \frac{\partial T}{\partial t} = \frac{\partial \rho}{\partial t} = \frac{\partial m}{\partial t} = \ldots = 0 \qquad (6.1)$$

6.1.8 Unsteady Flow

If one or more parameters (c, p, T, ρ, m, etc.) in a flow change with time, it is known as unsteady flow.

6.1.9 Viscosity

Viscosity is the property which resists the shearing motion of two adjacent layers of the fluid.

A fluid is known as a Newtonian fluid if the relation between the shear stress and the angular deformation in it is linear. The shear stress is given by

$$\tau \propto \frac{dc}{dy}$$

$$\tau = \mu \frac{dc}{dy} \tag{6.2}$$

The constant of proportionality μ is known as the coefficient of viscosity or dynamic viscosity.

The kinematic viscosity v is the ratio of the dynamic viscosity and the density of the fluid.

$$v = \frac{\mu}{\rho} \tag{6.3}$$

All real flows experience fluid viscosity. Therefore, their behaviour is influenced by the viscous forces.

6.1.10 Inviscid Flow

If the viscosity of the fluid is assumed to be absent, the flow is referred to as inviscid flow. Such a flow glides freely over its boundaries without experiencing viscous forces.

6.1.11 Reynolds Number

The Reynolds number is the ratio of forces due to inertia and viscosity.

$$\text{Inertia force} = \rho A c^2$$

$$\text{Viscous force} = \mu c l$$

Therefore, the Reynolds number is given by

$$\text{Re} = \frac{\rho A c^2}{\mu c l}$$

where

$$l = \text{a characteristic length}$$

$$A = l^2$$

$$\frac{\mu}{\rho} = v$$

Therefore,

$$\text{Re} = \frac{\rho cl}{\mu} = \frac{cl}{\nu} \tag{6.4}$$

The value of the Reynolds number in a flow gives an idea about its nature. For example, at higher Reynolds numbers the magnitude of viscous forces is small compared to the inertia forces.

6.1.12 Mach Number

The Mach number is an index of the ratio of inertia and elastic forces. This is defined by

$$M^2 = \frac{\text{inertia force}}{\text{elastic force}} = \frac{\rho A c^2}{KA}$$

However, $K = \rho a^2$

Therefore, $$M = \frac{c}{a} \tag{6.5}$$

This relation gives another important definition of the Mach number as the ratio of the fluid velocity to the local velocity of sound. Thermodynamic relations derived in Secs. 2.2.6 to 2.2.9 demonstrate its application.

6.1.13 Laminar Flow

In laminar flow the fluid flows over a body in orderly parallel layers with no components of fluctuations in the three directions (x, y and z directions). In such a flow the surface friction force predominates and keeps the flow parallel to the surface. Other layers of flow slide on top of the other. The values of the Reynolds number in such flows are comparatively lower.

6.1.14 Turbulent Flow

At higher values of the Reynolds number, the inertia force becomes predominant and the fluid particles are no longer constrained to move in parallel layers. Such a flow experiences small fluctuation components c'_x, c'_y and c'_z in the three reference directions. These fluctuations cause continuous mixing of various layers of the flow leading to flow equalization in the major part of the flow field.

On account of different flow patterns in laminar and turbulent flow, the velocity profiles (shown in Fig. 6.2) in these are different. The nature of flow in blade passages can be identified to a great extent by the velocity profiles and the values of the Reynolds number.

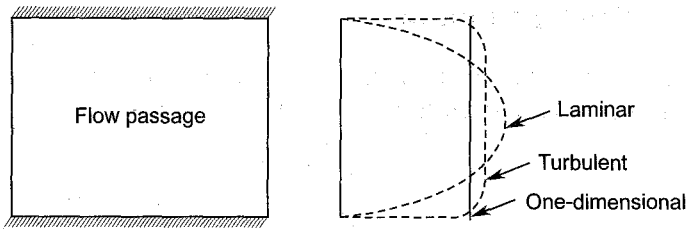

Fig. 6.2 Velocity profiles in laminar, turbulent and one-dimensional flows

6.1.15 Degree of Turbulence

The presence of small-scale fluctuations (c'_x, c'_y and c'_z) of velocity superimposed on the main flow is called turbulence. The degree of turbulence is defined by

$$\text{Degree of turbulence} = \frac{1}{c}\sqrt{\frac{1}{3}(c'^2_x + c'^2_y + c'^2_z)} \qquad (6.6)$$

6.1.16 Boundary Layer

Figure 6.3 shows the velocity profile at section A in a flow passage. The velocity of the fluid on the passage wall is zero. It develops fully to the free stream velocity c_∞ over a short distance δ from the wall. This layer of flow of thickness δ from the wall is known as the boundary layer. This exists only in a viscous flow. The boundary layer is absent in inviscid flow. The effect of viscosity is pre-dominant in this region, causing high energy losses. The boundary layer thickness decreases with an increase in the Reynolds number on account of the lower viscous forces compared to the inertia forces.

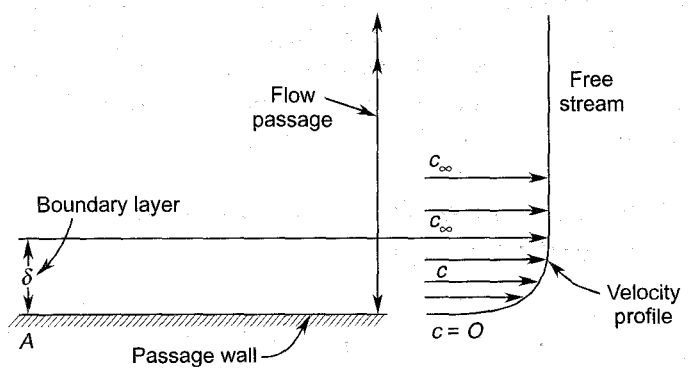

Fig. 6.3 Boundary layer and free stream regions in a flow passage

6.1.17 Friction Factor

Friction factor or the coefficient of skin friction is a measue of the frictional resistance offered to the flow. This is defined by

$$f = \frac{\tau_\omega}{\frac{1}{2}\rho c^2} \tag{6.7}$$

where f is the Fanning's coefficient of skin friction. It may be noted that Darcy's friction factor is four times the Fanning's coefficient.

6.1.18 Boundary Layer Separation

The boundary layer is the slow-moving or "tired" layer of the flow near a solid surface. When the flow occurs in the direction of static pressure rise (adverse pressure gradient), the boundary layer becomes thicker and reverses if this static pressure gradient (or the pressure hill) is too high. The leaving of the boundary layer from the surface and its reversal is known as "separation". This leads to chaotic flow, large drag and high energy losses.

In an accelerating flow, on account of the continuously decreasing static pressure, the thickening of the boundary layer is prevented; in fact, the higher inertia forces make it thinner. The available pressure drop helps in "washing down any localized thickening of the boundary layer or its separation".

The separation of boundary layer and the point of separation depend on the geometry and roughness of the surface, nature of the flow (turbulent or laminar) and Reynolds number. The laminer boundary layer gets separated earlier than the turbulent.

In order to achieve high lift and performance, it is necessary to prevent or delay the separation of the boundary layer. Two of the methods to achieve this are (*i*) sucking away the decelerated layer, and (*ii*) energizing it by injecting high energy fluid parallel to the surface. Separation can also be delayed by achieving transition of the laminar flow into the turbulent earlier.

6.2 Equations of Motion—Cartesian Coordinate System

Figure 6.4 shows a rectilinear cascade of an axial turbomachine in Cartesian coordinates. The axes of reference are X, Y and Z. The origin is located at the trailing edge of the blade at its root. The Z-axis is along the blade height, Y-axis along the blade pitch and X-axis along the axial

direction. These directions are also referred to as span-wise, pitch-wise and stream-wise directions. If it is convenient, the origin can be shifted to the leading edge also.

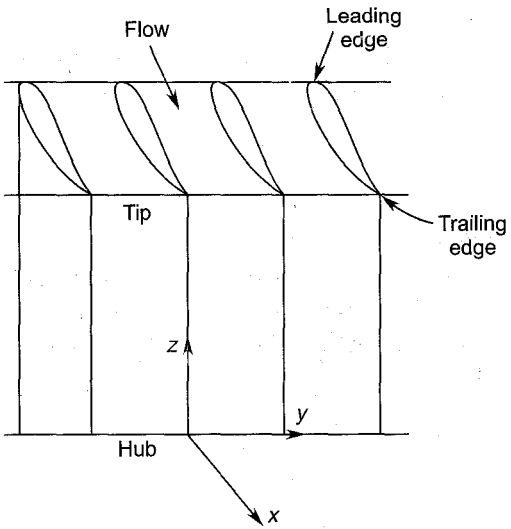

Fig. 6.4 Cartesian coordinate system

A point in the flow field through the blades is specified by its coordinates x, y and z. Various fluid dynamic parameters at this point are:

coordinates	x	y	z
velocities	c_x	c_y	c_z
vorticities	ξ	η	ζ
body forces	X	Y	Z

6.2.1 Continuity Equation

This simply states the law of conservation of mass mathematically. In three dimensions it is given by

$$\frac{\partial}{\partial x}(\rho c_x) + \frac{\partial}{\partial y}(\rho c_y) + \frac{\partial}{\partial z}(\rho c_z) + \frac{\partial \rho}{\partial t} = 0 \tag{6.8}$$

Its modified form for the following conditions are given below:

(a) *Steady flow*

There is no change in any flow parameter with time in steady flow, i.e.

$$\frac{\partial}{\partial t}\left(\quad\right) = 0$$

Therefore, for steady, three-dimensional and compressible flow,

$$\frac{\partial}{\partial x}(\rho c_x) + \frac{\partial}{\partial y}(\rho c_y) + \frac{\partial}{\partial z}(\rho c_z) = 0 \tag{6.9}$$

(b) *Incompressible flow*

The change in the fluid density is negligible in incompressible flow, i.e., $\rho \approx$ constant. Therefore,

$$\frac{\partial c_x}{\partial x} + \frac{\partial c_y}{\partial y} + \frac{\partial c_z}{\partial z} = 0 \tag{6.10}$$

(c) *Two-dimensional flow*

The flow in an infinitesimally thin slice of the flow field in the cascade shown in Fig. 6.4 will be two-dimensional; the variations in the third direction (Z-direction) are absent. Therefore, for steady, two-dimensional incompressible flow,

$$\frac{\partial c_x}{\partial x} + \frac{\partial c_y}{\partial y} = 0 \tag{6.11}$$

(d) *One-dimensional steady flow*

For one-dimensional steady flow,

$$\frac{\partial}{\partial t}\left(\quad\right) = 0, \quad \frac{\partial}{\partial y}\left(\quad\right) = 0 \text{ and } \frac{\partial}{\partial z}\left(\quad\right) = 0;$$

Therefore,

$$\frac{\partial}{\partial x}(\rho c_x) = 0$$

$$\rho A c_x = \text{const.} \tag{6.12}$$

A is the cross-sectional area prependicular to the velocity c_x.

Equation (6.12) is applicable for flow through a stream tube.

6.2.2 Momentum Equations

The momentum equation in a given direction is a mathematical statement of Newton's second law of motion. If only viscous, body and pressure forces are considered, the following equations are obtained:

$$c_x \frac{\partial c_x}{\partial x} + c_y \frac{\partial c_x}{\partial y} + c_z \frac{\partial c_x}{\partial z} + \frac{\partial c_x}{\partial t} - X + \frac{1}{\rho}\frac{\partial p}{\partial x}$$

$$= \frac{\mu}{\rho}\left(\frac{\partial^2 c_x}{\partial x^2} + \frac{\partial^2 c_x}{\partial y^2} + \frac{\partial^2 c_x}{\partial z^2}\right) \tag{6.13}$$

$$c_x \frac{\partial c_y}{\partial x} + c_y \frac{\partial c_y}{\partial y} + c_z \frac{\partial c_y}{\partial z} + \frac{\partial c_y}{\partial t} - Y + \frac{1}{\rho}\frac{\partial p}{\partial y} = \frac{\mu}{\rho}\left(\frac{\partial^2 c_y}{\partial x^2} + \frac{\partial^2 c_y}{\partial y^2} + \frac{\partial^2 c_y}{\partial z^2}\right) \tag{6.14}$$

$$c_x \frac{\partial c_z}{\partial x} + c_y \frac{\partial c_z}{\partial y} + c_z \frac{\partial c_z}{\partial z} + \frac{\partial c_z}{\partial t} - Z + \frac{1}{\rho}\frac{\partial p}{\partial z} = \frac{\mu}{\rho}\left(\frac{\partial^2 c_z}{\partial x^2} + \frac{\partial^2 c_z}{\partial y^2} + \frac{\partial^2 c_z}{\partial z^2}\right) \tag{6.15}$$

These are the well known Navier-Stokes equations for three-dimensional, unsteady and viscous flow.

(a) *Three-dimensional inviscid flow*

The above equations for non-viscous or inviscid flow reduce to the following form:

$$c_x \frac{\partial c_x}{\partial x} + c_y \frac{\partial c_x}{\partial y} + c_z \frac{\partial c_x}{\partial z} + \frac{\partial c_x}{\partial t} = X - \frac{1}{\rho}\frac{\partial p}{\partial x} \tag{6.16}$$

$$c_x \frac{\partial c_y}{\partial x} + c_y \frac{\partial c_y}{\partial y} + c_z \frac{\partial c_y}{\partial z} + \frac{\partial c_y}{\partial t} = Y - \frac{1}{\rho}\frac{\partial p}{\partial y} \tag{6.17}$$

$$c_x \frac{\partial c_z}{\partial x} + c_y \frac{\partial c_z}{\partial y} + c_z \frac{\partial c_z}{\partial z} + \frac{\partial c_z}{\partial t} = Z - \frac{1}{\rho}\frac{\partial p}{\partial z} \tag{6.18}$$

These are the three Euler's momentum equations.

(b) *Three-dimensional, inviscid and steady flow without body forces*

$$c_x \frac{\partial c_x}{\partial x} + c_y \frac{\partial c_x}{\partial y} + c_z \frac{\partial c_x}{\partial z} = -\frac{1}{\rho}\frac{\partial p}{\partial x} \tag{6.19}$$

$$c_x \frac{\partial c_y}{\partial x} + c_y \frac{\partial c_y}{\partial y} + c_z \frac{\partial c_y}{\partial z} = -\frac{1}{\rho}\frac{\partial p}{\partial y} \tag{6.20}$$

$$c_x \frac{\partial c_z}{\partial x} + c_y \frac{\partial c_z}{\partial y} + c_z \frac{\partial c_z}{\partial z} = -\frac{1}{\rho}\frac{\partial p}{\partial z} \tag{6.21}$$

6.2.3 Vorticity Components

Circulation is the line integral of velocity around a closed contour. Vorticity is the circulation per unit area. The three vorticity components in the Cartesian coordinates are

$$\xi = \frac{\partial c_z}{\partial y} - \frac{\partial c_y}{\partial z} \text{ (stream-wise vorticity)} \tag{6.22}$$

$$\eta = \frac{\partial c_x}{\partial z} - \frac{\partial c_z}{\partial x} \text{ (pitch-wise vorticity)} \tag{6.23}$$

$$\zeta = \frac{\partial c_y}{\partial x} - \frac{\partial c_x}{\partial y} \text{ (span-wise vorticity)} \tag{6.24}$$

6.2.4 The Potential Function Equation

The velocity potential function ϕ is a point function whose derivative in a given direction gives the velocity component in that direction. This function exists for an irrotational flow ($\xi = \eta = \zeta = 0$). The velocity components in terms of the potential function are

$$c_x = \frac{\partial \phi}{\partial x} \tag{6.25}$$

$$c_y = \frac{\partial \phi}{\partial y} \tag{6.26}$$

$$c_z = \frac{\partial \phi}{\partial z} \tag{6.27}$$

The differential equation for three-dimensional steady flow in terms of the potential function is

$$\left[1 - \frac{1}{a^2}\left(\frac{\partial \phi}{\partial x}\right)^2\right]\frac{\partial^2 \phi}{\partial x^2} + \left[1 - \frac{1}{a^2}\left(\frac{\partial \phi}{\partial y}\right)^2\right]\frac{\partial^2 \phi}{\partial y^2} + \left[1 - \frac{1}{a^2}\left(\frac{\partial \phi}{\partial z}\right)^2\right]\frac{\partial^2 \phi}{\partial z^2} =$$

$$\frac{2}{a^2}\left[\frac{\partial \phi}{\partial x}\frac{\partial \phi}{\partial y}\frac{\partial^2 \phi}{\partial x \partial y} - \frac{\partial \phi}{\partial y}\frac{\partial \phi}{\partial z}\frac{\partial^2 \phi}{\partial y \partial z} - \frac{\partial \phi}{\partial z}\frac{\partial \phi}{\partial x}\frac{\partial^2 \phi}{\partial z \partial x}\right] \tag{6.28}$$

In incompressible flows the fluid velocity components are small compared to the velocity of sound. Therefore, Eq. (6.28) reduces to the Laplace's equation

$$\frac{\partial^2 \phi}{\partial x^2} + \frac{\partial^2 \phi}{\partial y^2} + \frac{\partial^2 \phi}{\partial z^2} = 0 \tag{6.29}$$

For two-dimensional flow,

$$\frac{\partial^2 \phi}{\partial x^2} + \frac{\partial^2 \phi}{\partial y^2} = 0 \tag{6.30}$$

6.2.5 The Stream Function Equation

If the continuity equation for two-dimensional steady flow is satisfied, a point function called the stream function (ψ) is defined by

$$c_x = \frac{\rho_0}{\rho}\frac{\partial \psi}{\partial y} \tag{6.31}$$

$$c_y = -\frac{\rho_0}{\rho}\frac{\partial \psi}{\partial x} \tag{6.32}$$

ψ = constant lines are identical with streamlines

An equation of motion can be obtained in terms of the stream function for two-dimensional, steady and irrotational flow.

$$\left[1-\frac{1}{a^2}\left(\frac{\rho_0}{\rho}\right)^2\left(\frac{\partial \psi}{\partial y}\right)^2\right]\frac{\partial^2 \psi}{\partial x^2} + \left[1-\frac{1}{a^2}\left(\frac{\rho_0}{\rho}\right)^2\left(\frac{\partial \psi}{\partial x}\right)^2\right]\frac{\partial^2 \psi}{\partial y^2}$$

$$+\frac{2}{a^2}\left(\frac{\rho_0}{\rho}\right)^2\frac{\partial \psi}{\partial x}\frac{\partial \psi}{\partial y}\frac{\partial^2 \psi}{\partial x \partial y} = 0 \tag{6.33}$$

For incompressible flow, putting $a \approx \infty$ in Eq. (6.33),

$$\frac{\partial^2 \psi}{\partial x^2} + \frac{\partial^2 \psi}{\partial y^2} = 0 \tag{6.34}$$

Equations (6.30) and (6.34) are useful in representing two-dimensional plane flows in turbomachine flow passages. ϕ = constant and ψ = constant lines are normal to each other. Velocity and pressure distributions in a flow field can be easily derived from these equations.

6.3 Equations of Motion—Cylindrical Coordinate System

Figure 6.5 shows an annular cascade of blades in the cylindrical coordinate system[120]. The axes of reference are r (radial or spanwise direction), θ (peripheral, circumferential or tangential direction) and x (axial direction). The origin can be fixed according to convenience at the centre, hub or midheight of the cascade.

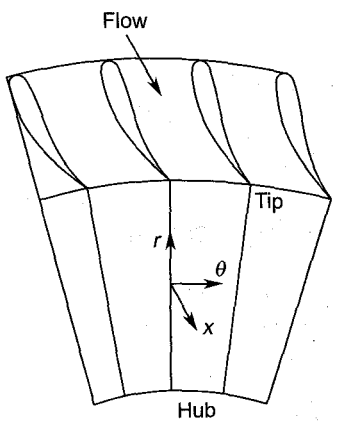

Fig. 6.5 Cylindrical coordinate system

A point in such a cascade is specified by the coordinates r, θ and x. Other parameters at this point are:

coordinates	r	θ	x
velocities	c_r	c_θ	c_x
vorticities	ξ	η	ζ
Body forces	R	Θ	X

6.3.1 Continuity Equation

The equation of continuity for three-dimensional, unsteady and compressible flow is

$$\frac{\partial}{\partial r}(\rho r c_r) + \frac{1}{r}\frac{\partial}{\partial \theta}(\rho r c_\theta) + \frac{\partial}{\partial x}(\rho r c_x) + \frac{\partial}{\partial t}(\rho r) = 0 \tag{6.35}$$

(a) *Steady flow*

$$\frac{\partial}{\partial r}(\rho r c_r) + \frac{1}{r}\frac{\partial}{\partial \theta}(\rho r c_\theta) + \frac{\partial}{\partial x}(\rho r c_x) = 0 \tag{6.36}$$

(b) *Steady and incompressible flow*

$$\frac{\partial}{\partial r}(r c_r) + \frac{1}{r}\frac{\partial}{\partial \theta}(r c_\theta) + \frac{\partial}{\partial x}(r c_x) = 0 \tag{6.37}$$

$$\frac{\partial c_r}{\partial r} + \frac{c_r}{r} + \frac{1}{r}\frac{\partial c_\theta}{\partial \theta} + \frac{\partial c_x}{\partial x} = 0 \tag{6.38}$$

(c) *Axisymmetric, incompressible and steady flow*

In an axisymmetric flow, variations in the peripheral direction (θ) are absent.

$$\frac{\partial}{\partial \theta}\left(\quad\right) = 0$$

This condition in Eq. (6.38) yields

$$\frac{\partial c_r}{\partial r} + \frac{c_r}{r} + \frac{\partial c_x}{\partial x} = 0 \tag{6.39}$$

6.3.2 Momentum Equations

The momentum equations for three-dimensional, unsteady and viscous flow in cylindrical coordinates are

$$c_r \frac{\partial c_r}{\partial r} + \frac{c_\theta}{r}\frac{\partial c_r}{\partial \theta} + c_x \frac{\partial c_r}{\partial x} - \frac{c_\theta^2}{r} + \frac{\partial c_r}{\partial t} - R + \frac{1}{\rho}\frac{\partial p}{\partial r}$$

$$= \frac{\mu}{\rho}\left(\frac{\partial^2 c_r}{\partial r^2} + \frac{1}{r}\frac{\partial c_r}{\partial r} - \frac{c_r}{r^2} + \frac{1}{r^2}\frac{\partial^2 c_r}{\partial \theta^2} - \frac{2}{r^2}\frac{\partial c_\theta}{\partial \theta} + \frac{\partial^2 c_r}{\partial x^2}\right) \tag{6.40}$$

$$c_r \frac{\partial c_\theta}{\partial r} + \frac{c_\theta}{r}\frac{\partial c_\theta}{\partial \theta} + c_x \frac{\partial c_\theta}{\partial x} + \frac{c_\theta c_r}{r} + \frac{\partial c_\theta}{\partial t} - \Theta + \frac{1}{\rho r}\frac{\partial p}{\partial \theta}$$

$$= \frac{\mu}{\rho}\left(\frac{\partial^2 c_\theta}{\partial r^2} + \frac{1}{r}\frac{\partial c_\theta}{\partial r} - \frac{c_\theta}{r^2} + \frac{1}{r^2}\frac{\partial^2 c_\theta}{\partial \theta^2} + \frac{2}{r^2}\frac{\partial c_r}{\partial \theta} + \frac{\partial^2 c_\theta}{\partial x^2}\right) \tag{6.41}$$

$$c_r \frac{\partial c_x}{\partial r} + \frac{c_\theta}{r}\frac{\partial c_x}{\partial \theta} + c_x \frac{\partial c_x}{\partial x} + \frac{\partial c_x}{\partial t} - X + \frac{1}{\rho}\frac{\partial p}{\partial x}$$

$$= \frac{\mu}{\rho}\left(\frac{\partial^2 c_x}{\partial r^2} + \frac{1}{r}\frac{\partial c_x}{\partial r} + \frac{1}{r^2}\frac{\partial^2 c_x}{\partial \theta^2} + \frac{\partial^2 c_x}{\partial x^2}\right) \tag{6.42}$$

These are the Navier-Stoke's equations.

(a) For inviscid flow, they reduce to the following Euler's momentum equations:

$$c_r \frac{\partial c_r}{\partial r} + \frac{c_\theta}{r}\frac{\partial c_r}{\partial \theta} + c_x \frac{\partial c_r}{\partial x} + \frac{\partial c_r}{\partial t} - \frac{c_\theta^2}{r} = R - \frac{1}{\rho}\frac{\partial p}{\partial r} \tag{6.43}$$

$$c_r \frac{\partial c_\theta}{\partial r} + \frac{c_\theta}{r}\frac{\partial c_\theta}{\partial \theta} + c_x \frac{\partial c_\theta}{\partial x} + \frac{\partial c_\theta}{\partial t} + \frac{c_r c_\theta}{r} = \Theta - \frac{1}{\rho r}\frac{\partial p}{\partial \theta} \tag{6.44}$$

$$c_r \frac{\partial c_x}{\partial r} + \frac{c_\theta}{r}\frac{\partial c_x}{\partial \theta} + c_x \frac{\partial c_x}{\partial x} + \frac{\partial c_x}{\partial t} = X - \frac{1}{\rho}\frac{\partial p}{\partial x} \tag{6.45}$$

(b) For three-dimensional, inviscid and steady flow in the absence of body forces, Eqs. (6.40) to (6.42) reduce to

$$c_r \frac{\partial c_r}{\partial r} + \frac{c_\theta}{r}\frac{\partial c_r}{\partial \theta} + c_x \frac{\partial c_r}{\partial x} - \frac{c_\theta^2}{r} = -\frac{1}{\rho}\frac{\partial p}{\partial r} \tag{6.46}$$

$$c_r \frac{\partial c_\theta}{\partial r} + \frac{c_\theta}{r}\frac{\partial c_\theta}{\partial x} + c_x \frac{\partial c_\theta}{\partial x} + \frac{c_r c_\theta}{r} = -\frac{1}{\rho r}\frac{\partial p}{\partial \theta} \tag{6.47}$$

$$c_r \frac{\partial c_x}{\partial r} + \frac{c_\theta}{r}\frac{\partial c_x}{\partial \theta} + c_x \frac{\partial c_x}{\partial x} = -\frac{1}{\rho}\frac{\partial p}{\partial x} \tag{6.48}$$

(c) For three-dimensional, inviscid, steady and axisymmetric flow in the absence of body forces, Eqs. (6.40) to (6.42) reduce to

$$c_r \frac{\partial c_r}{\partial r} + c_x \frac{\partial c_r}{\partial x} - \frac{c_\theta^2}{r} = -\frac{1}{\rho}\frac{\partial p}{\partial r} \tag{6.49}$$

$$c_r \frac{\partial c_\theta}{\partial r} + c_x \frac{\partial c_\theta}{\partial x} + \frac{c_r c_\theta}{r} = 0 \tag{6.50}$$

$$c_r \frac{\partial c_x}{\partial r} + c_x \frac{\partial c_x}{\partial x} = -\frac{1}{\rho}\frac{\partial p}{\partial x} \tag{6.51}$$

6.3.3 Vorticity Components

$$\xi = \frac{1}{r}\frac{\partial c_x}{\partial \theta} - \frac{\partial c_\theta}{\partial x} \tag{6.52}$$

$$\eta = \frac{\partial c_r}{\partial x} - \frac{\partial c_x}{\partial r} \tag{6.53}$$

$$\zeta = \frac{\partial c_\theta}{\partial r} - \frac{1}{r}\frac{\partial c_r}{\partial \theta} + \frac{c_\theta}{r} \tag{6.54}$$

For axisymmetric flow, Eqs. (6.52) and (6.54) reduce to

$$\xi = -\frac{\partial c_\theta}{\partial x} \tag{6.55}$$

$$\zeta = \frac{\partial c_\theta}{\partial r} + \frac{c_\theta}{r} \tag{6.56}$$

Equation (6.53) remains unaltered.

6.3.4 Potential Function Equation

The three velocity components in terms of the potential function (ϕ) in cylindrical coordinates are

$$c_r = \frac{\partial \phi}{\partial r} \tag{6.57}$$

$$c_\theta = \frac{1}{r}\frac{\partial \phi}{\partial \theta} \tag{6.58}$$

$$c_x = \frac{\partial \phi}{\partial x} \tag{6.59}$$

The flow is irrotational, i.e. $\xi = \eta = \zeta = 0$. The resulting momentum equation with these conditions is

$$\left[1 - \frac{1}{a^2}\left(\frac{\partial \phi}{\partial r}\right)^2\right]\frac{\partial^2 \phi}{\partial r^2} + \left[1 - \frac{1}{a^2 r^2}\left(\frac{\partial \phi}{\partial \theta}\right)^2\right]\frac{1}{r^2}\frac{\partial^2 \phi}{\partial \theta^2}$$
$$+ \left[1 - \frac{1}{a^2}\left(\frac{\partial \phi}{\partial x}\right)^2\right]\frac{\partial^2 \phi}{\partial x^2} + \left[1 + \frac{1}{a^2 r^2}\left(\frac{\partial \phi}{\partial \theta}\right)^2\right]\frac{1}{r}\frac{\partial \phi}{\partial r}$$
$$= \frac{2}{a^2 r^2}\left[\frac{\partial \phi}{\partial r}\frac{\partial \phi}{\partial \theta}\frac{\partial^2 \phi}{\partial r \partial \theta} + \frac{\partial \phi}{\partial \theta}\frac{\partial \phi}{\partial x}\frac{\partial^2 \phi}{\partial \theta \partial x} + \frac{r^2 \partial \phi}{\partial x}\frac{\partial \phi}{\partial r}\frac{\partial^2 \phi}{\partial x \partial r}\right] \tag{6.60}$$

For incompressible flow ($a \approx \infty$),

$$\frac{\partial^2 \phi}{\partial r^2} + \frac{1}{r^2}\frac{\partial^2 \phi}{\partial \theta^2} + \frac{\partial^2 \phi}{\partial x^2} + \frac{1}{r}\frac{\partial \phi}{\partial r} = 0 \tag{6.61}$$

For incompressible and axisymmetric flow,

$$\frac{\partial^2 \phi}{\partial r^2} + \frac{\partial^2 \phi}{\partial x^2} + \frac{1}{r}\frac{\partial \phi}{\partial r} = 0 \tag{6.62}$$

6.3.5 Stream Function Equation

The momentum equation in terms of the stream function is obtained for axisymmetric, inviscid, steady and irrotational flow. The two velocity components in terms of the stream function are

$$c_r = \frac{\rho_0}{\rho}\frac{1}{r}\frac{\partial \psi}{\partial x} \tag{6.63}$$

$$c_x = -\frac{\rho_0}{\rho}\frac{1}{r}\frac{\partial \psi}{\partial r} \tag{6.64}$$

The stream function equation is

$$\left[1 - \frac{1}{a^2 r^2}\left(\frac{\rho_0}{\rho}\right)^2 \left(\frac{\partial \psi}{\partial x}\right)\right]\frac{\partial^2 \psi}{\partial r^2} + \left[1 - \frac{1}{a^2 r^2}\left(\frac{\rho_0}{\rho}\right)^2 \left(\frac{\partial \psi}{\partial r}\right)^2\right]\frac{\partial^2 \psi}{\partial x^2}$$

$$-\frac{1}{r}\frac{\partial \psi}{\partial r} + \frac{2}{a^2 r^2}\left(\frac{\rho_0}{\rho}\right)^2 \frac{\partial \psi}{\partial r}\frac{\partial \psi}{\partial x}\frac{\partial^2 \psi}{\partial r \partial x} = 0 \tag{6.65}$$

For incompressible flow, this equation reduces to

$$\frac{\partial^2 \psi}{\partial r^2} + \frac{\partial^2 \psi}{\partial x^2} - \frac{1}{r}\frac{\partial \psi}{\partial r} = 0 \tag{6.66}$$

6.4 Equations of Motion—Natural Coordinate System

The natural system of coordinates uses the tangent to a streamline at a given point as one of the axes (s-direction) of reference. The other directions are perpendicular to the s-direction. This system of coordinates is specially useful in dealing with flows in the meridional plane of radial machines as shown in Fig. 6.6.

The momentum equations for inviscid and steady meridional flow in the absence of body forces are

$$c\frac{\partial c}{\partial s} + \frac{1}{\rho}\frac{\partial p}{\partial s} = 0 \tag{6.67}$$

$$\frac{c^2}{R} + \frac{1}{\rho}\frac{\partial p}{\partial n} = 0 \tag{6.68}$$

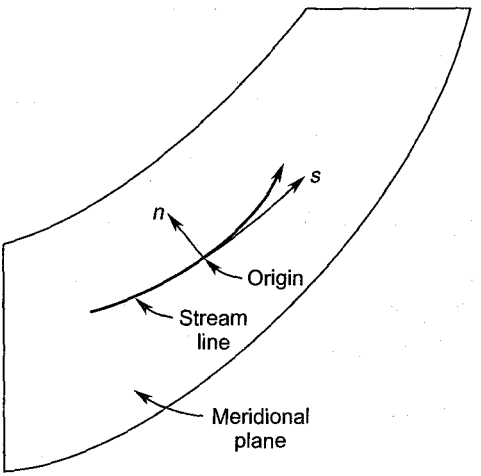

Fig. 6.6 Natural coordinate system (flow in the meridional plane of a centrifugal machine)

6.5 Further Notes on Energy Equation

The energy equation for steady adiabatic flow was derived and discussed in Sec. 2.2. In this section various other useful forms are briefly discussed.

For a perfect gas, static and stagnation enthalpies are expressed as

$$h = c_p T = \frac{\gamma}{\gamma - 1}\frac{p}{\rho} = \frac{a^2}{\gamma - 1} \tag{6.69}$$

$$h_0 = c_p T_0 = \frac{\gamma}{\gamma - 1}\frac{p_0}{\rho_0} = \frac{a_0^2}{\gamma - 1} \tag{6.70}$$

In an imaginary process gas at a given state may be assumed to expand to the absolute zero temperature ($T = 0$). In such a process the entire stagnation enthalpy is transformed into the kinetic energy of the gas. This is obviously the maximum possible value of the kinetic energy and is given by

$$h_0 = \frac{1}{2} c_{\max}^2 \tag{6.71}$$

The gas velocity at sonic conditions ($M = 1$) and the corresponding kinetic energy can be related to the stagnation enthalpy by the relation

$$h_0 = \frac{1}{2}\frac{\gamma + 1}{\gamma - 1} a^{*2} \tag{6.72}$$

Equations (6.69) to (6.72) along with Eq. (2.55) are related by the following expressions:

$$h_0 = \frac{a_0^2}{\gamma - 1} = \frac{a^2}{\gamma - 1} + \frac{1}{2} c^2 = \frac{1}{2} \frac{\gamma + 1}{\gamma - 1} a^{*2} = \frac{1}{2} c_{\max}^2 \tag{6.73}$$

$$\frac{\gamma}{\gamma - 1} \frac{p_0}{\rho_0} = \frac{\gamma}{\gamma - 1} \frac{p}{\rho} + \frac{1}{2} c^2 \tag{6.74}$$

For isentropic flow,

$$\frac{p}{\rho} = \frac{p_0}{\rho_0} \left(\frac{p}{p_0} \right)^{\frac{\gamma - 1}{\gamma}} \tag{6.75}$$

Substituting Eq. (6.75) in Eq. (6.74) gives the Bernoulli equation for isentropic compressible flow

$$\frac{\gamma}{\gamma - 1} \frac{p_0}{\rho_0} = \frac{\gamma}{\gamma - 1} \frac{p_0}{\rho_0} \left(\frac{p}{p_0} \right)^{\frac{\gamma - 1}{\gamma}} + \frac{1}{2} c^2 \tag{6.76}$$

The Bernoulli equation for incompressible flow is simply a restatement of the isentropic energy equation with constant density (ρ = constant).

The differential form of Eq. (2.55) is

$$dh + c\, dc = 0 \tag{6.77}$$

For isentropic flow

$$\frac{dp}{\rho} + c\, dc = 0 \tag{6.78}$$

The integral form of the above energy equation with ρ = constant is the familiar Bernoulli equation, viz.

$$p + \frac{1}{2} \rho c^2 = p_0 \qquad (2.66)$$

Thus for isentropic incompressible flow

$$\frac{p_0 - p}{\frac{1}{2} \rho c^2} = 1$$

For compressible isentropic flow, this is given by

$$\frac{p_0 - p}{\frac{1}{2} \rho c^2} = 1 + \frac{M^2}{4} + \frac{2 - \gamma}{24} M^4 + \ldots \tag{6.79}$$

For $\gamma = 1.4$ the value given by Eq. (6.79) is considerably higher than unity for $M > 0.3$. This may therefore be taken as the limit of incompressible flow.

6.6 Isentropic Flow through Blade Passages

For many applications, the one-dimensional isentropic flow analysis[95,104,107] gives considerable insight into a problem. For example, in this section the assumption of such a flow indicates the manner in which various flow parameters vary in turbomachine blade passages.

The continuity equation gives

$$\rho A c = \text{const.}$$

By logarithmic differentiation, this gives

$$dc = -c\left(\frac{d\rho}{\rho} + \frac{dA}{A}\right)$$

Substituting this in Eq. (6.78), we get

$$\frac{dA}{A} = \frac{dp}{\rho c^2}\left(1 - \frac{d\rho}{dp}c^2\right)$$

For isentropic process $\frac{dp}{d\rho} = a^2$, therefore,

$$\frac{dA}{A} = \frac{dp}{\rho c^2}(1 - M^2) \tag{6.80}$$

6.6.1 Accelerating Flow

Accelerating flow in blade passages is obtained by a drop in pressure, i.e. dp is negative. Therefore, Eq. (6.80) for accelerating passages gives the following three results:

For $M < 1$, dA is negative; therefore the passage must be convergent.

For $M = 1$, $dA = 0$; therefore the variation in area is absent. This occurs at the throat of a passage.

For $M > 1$, dA is positive; therefore the passage must be divergent.

6.6.2 Decelerating Flow

In a decelerating flow the velocity of gas decreases with an increase in pressure, i.e. dp is positive in Eq. (6.80). This gives the following information for the variation of area:

For $M < 1$, dA is positive; therefore the passage must be divergent.

At the throat of the passage, $M = 1$ and $dA = 0$.

For $M > 1$, dA is negative; therefore the passage must be convergent.

6.6.3 Maximum Mass-flow Parameter

The assumption of isentropic flow gives a quick estimate of the maximum possible flow rate through a passage with given stagnation conditions (p_0, T_0).

The maximum flow rate occurs at the critical pressure ratio. At this condition

$$p = p^*,\ c = c^* = a^*,\ M = 1$$

$$\frac{p^*}{p_0} = \left(\frac{2}{\gamma+1}\right)^{\frac{\gamma}{\gamma-1}} \tag{6.81}$$

The maximum mass flow rate is given by

$$\frac{\dot{m}_{\max}\sqrt{T_0}}{A^* p_0}\sqrt{\frac{R}{\gamma}} = \left(\frac{2}{\gamma+1}\right)^{\frac{\gamma+1}{2(\gamma-1)}} \tag{6.82}$$

For a given gas, γ and R remain constant. Therefore,

$$\frac{\dot{m}_{\max}\sqrt{T_0}}{A^* p_0} = \sqrt{\frac{\gamma}{R}}\left(\frac{2}{\gamma+1}\right)^{\frac{\gamma+1}{2(\gamma-1)}}$$

For air, taking $\gamma = 1.4$ and $R = 287$ J/kg K, the value of the maximum mass flow parameter is obtained.

$$\frac{\dot{m}_{\max}\sqrt{T_0}}{A^* p_0} = 0.0404 \tag{6.83}$$

where $\dot{m}_{\max}$ is in kg/s, A^* in m^2, p_0 in pascals = N/m^2 and T_0 in K.

6.7 High-speed Flows

Many turbines and compressors experience flows at high Mach numbers. The high Mach number flow gives rise to some special problems which are characteristic of only high speed flows. Most of these problems arise due to the acceleration or deceleration (to subsonic Mach numbers) of supersonic flows in blade passages; expansion and compression waves are generated which affect the nature of flow and losses in these machines.

As stated before, when the Mach number reaches unity, the flow chokes and the maximum mass flow rate is governed by Eq. (6.82).

It is well known that, in practice, a supersonic flow decelerates to subsonic through a shock wave. This may be either normal or inclined to the direction of flow. In actual practice both the types of waves exist in supersonic machines.

The shock wave is an irreversiblility and leads to stagnation pressure loss and increase in entropy.

Some important relations for these waves are summarized below.

6.7.1 Normal Shock Waves

The shock phenomenon in actual blade passages is very complicated. A normal shock wave ($\sigma = 90°$) in a turbine blade passage is shown in Fig. 6.7. The normal shock relations included in this section are for one-dimensional steady flow with constant area. The upstream (low pressure) and downstream (high pressure) sides of the shock are designated by subscripts x and y respectively.

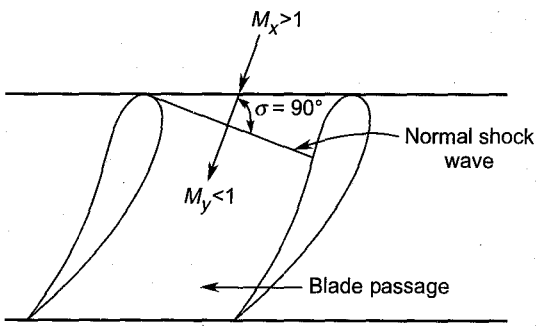

Fig. 6.7 Normal shock wave in a turbine blade passage

The velocities and critical Mach numbers are given by the following relations:

$$c_x\, c_y = a^{*2} \tag{6.84}$$

$$M_x^*\, \mathrm{M}_y^* = 1 \tag{6.85}$$

The downstream Mach number is

$$M_y^2 = \frac{\dfrac{2}{\gamma-1} + M_x^2}{\dfrac{2\gamma}{\gamma-1} M_x^2 - 1} \tag{6.86}$$

The pressure, temperature and density ratios are

$$\frac{p_y}{p_x} = \frac{2\gamma}{\gamma+1} M_x^2 - \frac{\gamma-1}{\gamma+1} \tag{6.87}$$

$$\frac{T_y}{T_x} = \frac{2(\gamma-1)\left(1+\dfrac{\gamma-1}{2} M_x^2\right)\left(\dfrac{2\gamma}{\gamma-1} M_x^2 - 1\right)}{(\gamma+1)^2\, M_x^2} \tag{6.88}$$

$$\frac{\rho_y}{\rho_x} = \frac{\left(\dfrac{\gamma+1}{2}\right) M_x^2}{1+\dfrac{\gamma-1}{2} M_x^2} \tag{6.89}$$

The Rankine-Hugoniot equation relates the density ratio across the shock to pressure ratio.

$$\frac{p_y}{p_x} = \frac{\dfrac{\gamma+1}{\gamma-1}\dfrac{\rho_y}{\rho_x} - 1}{\dfrac{\gamma+1}{\gamma-1} - \dfrac{\rho_y}{\rho_x}} \tag{6.90}$$

The stagnation pressure ratio and increase in entropy across the shock are measures of the irreversibility and losses and are given by

$$\frac{p_{0y}}{p_{0x}} = \left(\frac{\dfrac{\gamma+1}{2} M_x^2}{1 + \dfrac{\gamma-1}{2} M_x^2} \right)^{\frac{\gamma}{\gamma-1}} \Bigg/ \left(\frac{2\gamma}{\gamma+1} M_x^2 - \frac{\gamma-1}{\gamma+1} \right)^{\frac{1}{\gamma-1}} \tag{6.91}$$

$$\frac{\Delta s}{R} = \ln \left(\frac{p_{0x}}{p_{0y}} \right) \tag{6.92}$$

6.7.2 Oblique Shock Waves

As stated before, the wave angle (σ) of an oblique shock is less than 90°. The wave angle of a normal shock is 90°. Oblique shock waves may be strong or weak. The stronger shocks have wave angles nearer to 90° whereas weaker shocks have small wave angles. Oblique shocks at the leading edges of a sharp wedge and an aerofoil blade are shown in Fig. 6.8. In some flows, oblique shocks take the form of curved and conical waves.

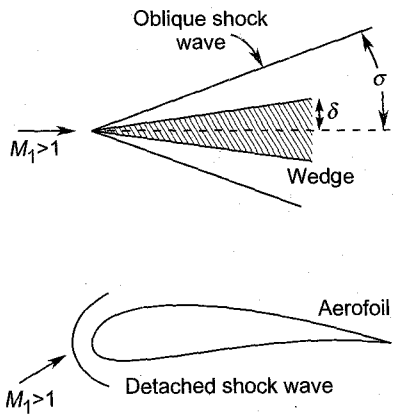

Fig. 6.8 Oblique shock waves

The wave drag on the blades, in the presence of strong shocks, is high. Therefore, the leading edges of blades in the supersonic machines must be carefully designed to keep the wave drag to a minimum.

The wave angle is a function of the wedge angle and the free stream Mach number.

$$\sigma = f(\delta, M_1)$$

$$\tan \delta = \frac{M_1^2 \sin 2\sigma - 2 \cot \sigma}{2 + M_1^2 (\gamma + \cos 2\sigma)} \tag{6.93}$$

Other parameters in the non-dimensional forms are expressed as functions of the wave angle and the free stream Mach number.

$$\frac{p_2}{p_1} = \frac{2\gamma}{\gamma + 1} M_1^2 \sin^2 \sigma - \frac{\gamma - 1}{\gamma + 1} \tag{6.94}$$

$$\frac{T_2}{T_1} = \frac{[2\gamma M_1^2 \sin^2 \sigma - (\gamma - 1)][2 + (\gamma - 1) M_1^2 \sin^2 \sigma]}{(\gamma + 1)^2 M_1^2 \sin^2 \sigma} \tag{6.95}$$

$$\frac{\rho_2}{\rho_1} = \frac{(\gamma + 1) M_1^2 \sin^2 \sigma}{2 + (\gamma - 1) M_1^2 \sin^2 \sigma} \tag{6.96}$$

$$\frac{p_{02}}{p_{01}} = \left[\frac{(\gamma + 1) M_1^2 \sin^2 \sigma}{(\gamma - 1) M_1^2 \sin^2 \sigma + 2}\right]^{\frac{\gamma}{\gamma - 1}} \times \left[\frac{\gamma + 1}{2\gamma M_1^2 \sin^2 \sigma - (\gamma - 1)}\right]^{\frac{1}{\gamma - 1}} \tag{6.97}$$

$$\frac{\Delta s}{R} = \ln \left(\frac{p_{01}}{p_{02}}\right) \tag{6.98}$$

Unlike normal shocks, the flow downstream of an oblique shock need not be always subsonic—only the normal component of the velocity vector downstream of the oblique shock need be subsonic. The downstream Mach number is given by

$$M_2^2 = \frac{2 + (\gamma - 1) M_1^2 \sin^2 \sigma}{[2\gamma M_1^2 \sin^2 \sigma - (\gamma - 1)] \sin^2 (\sigma - \delta)} \tag{6.99}$$

6.7.3 Expansion Waves

Expansion waves are generated when an initially sonic ($M = 1$) or supersonic ($M > 1$) flow is expanded by turning the passage walls away from the flow. It was shown in Sec. 6.6.1 that, for a supersonic flow, a divergent passage is required to accelerate it.

In such a flow the Prandtl-Meyer angle $\omega(M)$ gives the angle by which a wall must be deflected away from the flow to accelerate it to a given Mach number M. This is given by

$$\omega(M) = \sqrt{\frac{\gamma + 1}{\gamma - 1}} \tan^{-1} \sqrt{\frac{\gamma - 1}{\gamma + 1}(M^2 - 1)} - \tan^{-1} \sqrt{M^2 - 1} \tag{6.100}$$

The deflection (δ) of the wall required to increase the Mach number from M_1 to M_2 is

$$\delta = \omega(M_2) - \omega(M_1) \tag{6.101}$$

On account of the flattening nature of the expansion waves, they cannot coalesce into an expansion shock wave.

6.8 Aerofoil Blades

An aerofoil blade[112, 117] is a streamlined body having a thick, rounded leading edge and a thin (sometimes sharp) trailing edge. Its maximum thickness occurs somewhere near the midpoint of the chord. The backbone line lying midway between the upper and lower surfaces is known as the camber line.

When such a blade is suitably shaped and properly oriented in the flow, the force acting on it, normal to the direction of flow, is considerably larger than the force resisting its motion.

Aerofoil shapes are used for aircraft wing sections and the blades of various turbomachines.

6.8.1 Nature of Flow

When a flat plate is moved through a fluid, it experiences a resistance to its motion on account of the fluid friction on its surface. If the flow direction is parallel to its length, the force normal to the plate will be zero. However, when the plate is inclined (at an angle i) to its direction of motion, it will experience a resultant force R normal to its length. This force has a component (D) parallel to the flow and another component (L) perpendicular to it. These forces acting on such a plate are known as lift and drag forces and are shown in Fig. 6.9.

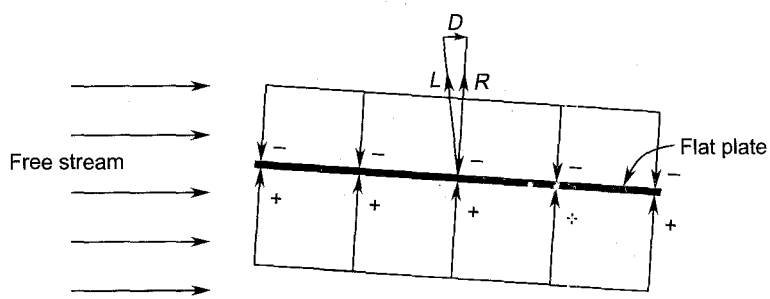

Fig. 6.9 Lift force on an inclined flat plate

The lift force arises on account of the negative and positive pressures prevailing on the upper and lower surfaces respectively. The figure depicts

only constant average values of pressures. In actual practice the pressures on the two sides will vary from the leading to the trailing edge.

When the angle (i) of attack or incidence is zero, the lift will be zero, as stated before. The lift is found to increase with incidence up to an optimum value (Fig. 6.10). Along with lift, the drag also increases. Beyond the optimum value of incidence the drag force increases very rapidly followed by a decrease in the lift force. This is obviously undesirable. The maximum drag occurs when the plate is normal ($i = 90°$) to the flow direction; the lift is zero for this position.

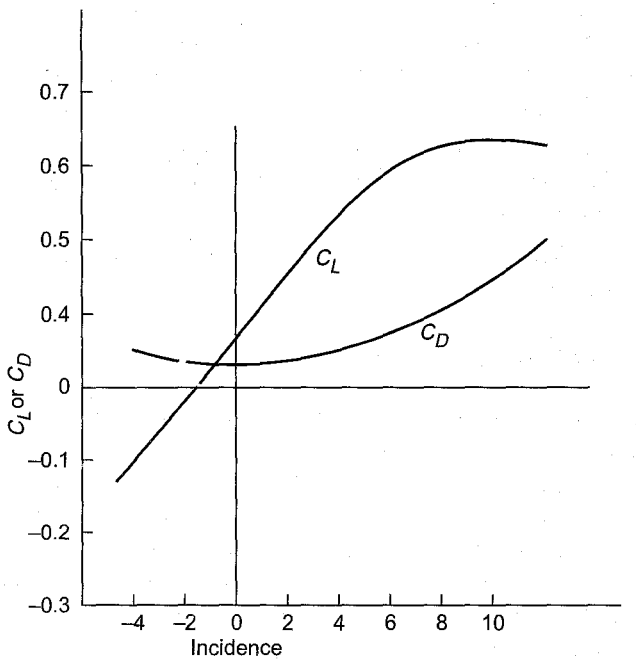

Fig. 6.10 Variation of lift and drag coefficients with incidence

In practical applications for aircraft wings and turbomachine blades, the flat plate (if used) will have to be of finite thickness. In order to achieve a high lift-drag ratio the leading edge is rounded and the blade section is tapered towards the thin trailing edge. To obtain further increase in the value of L/D, the blade is slightly curved, thus giving a curved camber line. It may be seen here that such a blade approaches a cambered aerofoil shape.

Figure 6.11 shows (a) an uncambered aerofoil blade with zero incidence, (b) an uncambered blade with incidence angle i and (c) a cambered blade with incidence. Static pressure distribution around a cambered aerofoil blade is shown in Fig. 6.12. The centrifugal force on the fluid particles on the upper (convex) side tries to move them away from the surface. This reduces the static pressure on this side below the free-stream

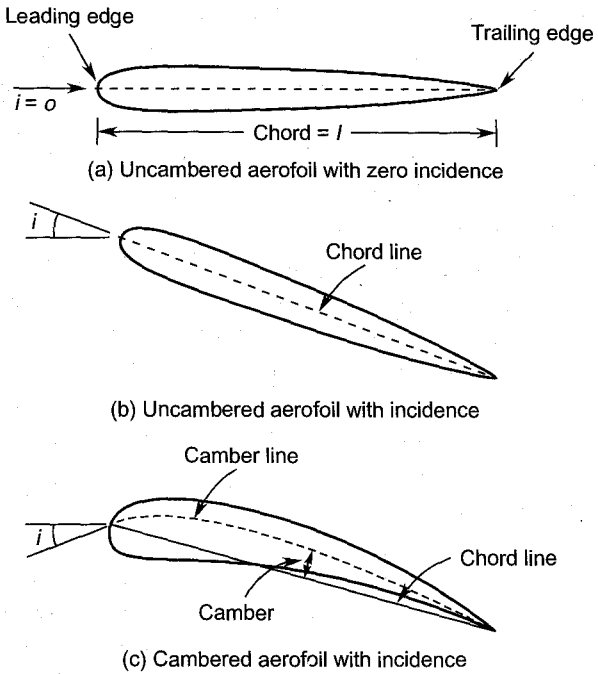

Fig. 6.11 Flow around aerofoil blades

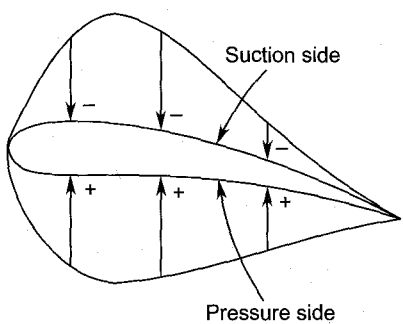

Fig. 6.12 Pressure distribution around a cambered aerofoil blade

pressure. On account of this "suction effect", the convex surface of the blade is known as the suction side. In contrast to this the centrifugal force on the lower (concave) side presses the fluid harder on the blade surface, thus increasing the static pressure above that of the free stream. Therefore, this side of the blade is known as the pressure side. On account of this phenomenon, the flow on the suction side begins accelerating along the blade chord accompanied by a deceleration on the pressure side. However, the common boundary conditions at the trailing edge require the flows on the two sides to equalize. Therefore, the accelerated flow on the suction side experiences deceleration of the flow as it approaches the

trailing edge. The already decelerated flow on the pressure side starts accelerating at some point along the chord. However, inspite of these processes, the flows coming from the two sides of the blade surface may fail to equalize.

The resultant upward force on the blade (Fig. 6.9) is the result of the cumulative effect of the positive static pressure on the pressure side and the negative pressure on the suction side.

Now the total upward force acting on the aerofoil is equal to the projected area times the pressure difference on the two sides. On an aircraft wing there is a large area available for the production of lift force. Therefore, only a small pressure difference over its aerofoil wing section will provide the required lift. This requires only a slight deflection of the approaching flow over the aircraft wings which is achieved by only slightly cambered sections.

In contrast to this, the projected areas of turbomachine blades are much smaller. Therefore, a considerable difference of static pressure between the pressure and section sides is required to provide the necessary lift or the tangential force. This can only be achieved by providing highly cambered blade sections—the blade camber in compressor blades is between those of the aircraft wings and the turbine blades.

The lift force is exerted by the fluid on the aircraft wings and the turbine rotor blades, whereas in power absorbing machines like compressors, fans and blowers, this lift force (exerted by their rotor blades on the fluid) is supplied by the torque input.

6.8.2 Coefficients of Lift and Drag

The resultant force due to the flow around an aerofoil blade acts at its centre of pressure. It has two components—lift force, normal to the flow direction (or blade chord) and the drag force parallel to the flow. These forces depend only on the density and velocity of the fluid and the blade chord.

$$L, D = f(\rho, c, l)$$

The projected area per unit length of the blade is

$$A = l \times 1$$

The lift and drag coefficients based on this area relate the dynamic pressure $\frac{1}{2}\rho c^2$ to the lift and drag forces.

$$L = C_L \frac{1}{2} \rho A c^2$$

$$D = C_D \frac{1}{2} \rho A c^2$$

Conventionally, these coefficients are expressed as

$$C_L = \frac{L}{\frac{1}{2}\rho l c^2} \tag{6.102}$$

$$C_D = \frac{D}{\frac{1}{2}\rho l c^2} \tag{6.103}$$

6.8.3 Transformation of a Circle into an Uncambered Aerofoil

Aerofoil blade shapes of various turbomachines for prescribed conditions can now be obtained by a number of mathematical methods. In this section an uncambered blade profile is obtained from a circle by employing conformal transformation.

Figure 6.13 (a) shows the Z-plane in which the origin (O) of the coordinates (r, ϕ) is shifted away by a distance eb from the centre C of a circle. In this plane a point P is described by r and ϕ. The function z is given by

$$z = x + iy = re^{i\phi} \tag{6.104}$$

The circle in the Z-plane is transformed into the ζ-plane by Zhukovsky's transformation function

$$\zeta = z + b^2/z \tag{6.105}$$

ζ is given by

$$\zeta = \xi + i\eta \tag{6.106}$$

Referring to Fig. 6.13 (a), the radius of the circle a is given by

$$a = b + eb = (1 + e)\, b \tag{6.107}$$

The triangle OPC of Fig. 6.13 (a) is shown enlarged in Fig. 6.13 (c). The angle δ is small for small values of eb. From Fig. 6.13 (c),

$$OP = r = a \cos \delta + eb \cos \phi$$

For small values of δ, $\cos \delta \approx 1$, Therefore,

$$r = a + eb \cos \phi \tag{6.108}$$

Substituting from Eq. (6.107) into Eq. (6.108),

$$r = b + eb + eb \cos \phi$$

$$\frac{r}{b} = 1 + e + e \cos \phi \tag{6.109}$$

$$\frac{b}{r} = \{1 + e\,(1 + \cos \phi)\}^{-1}$$

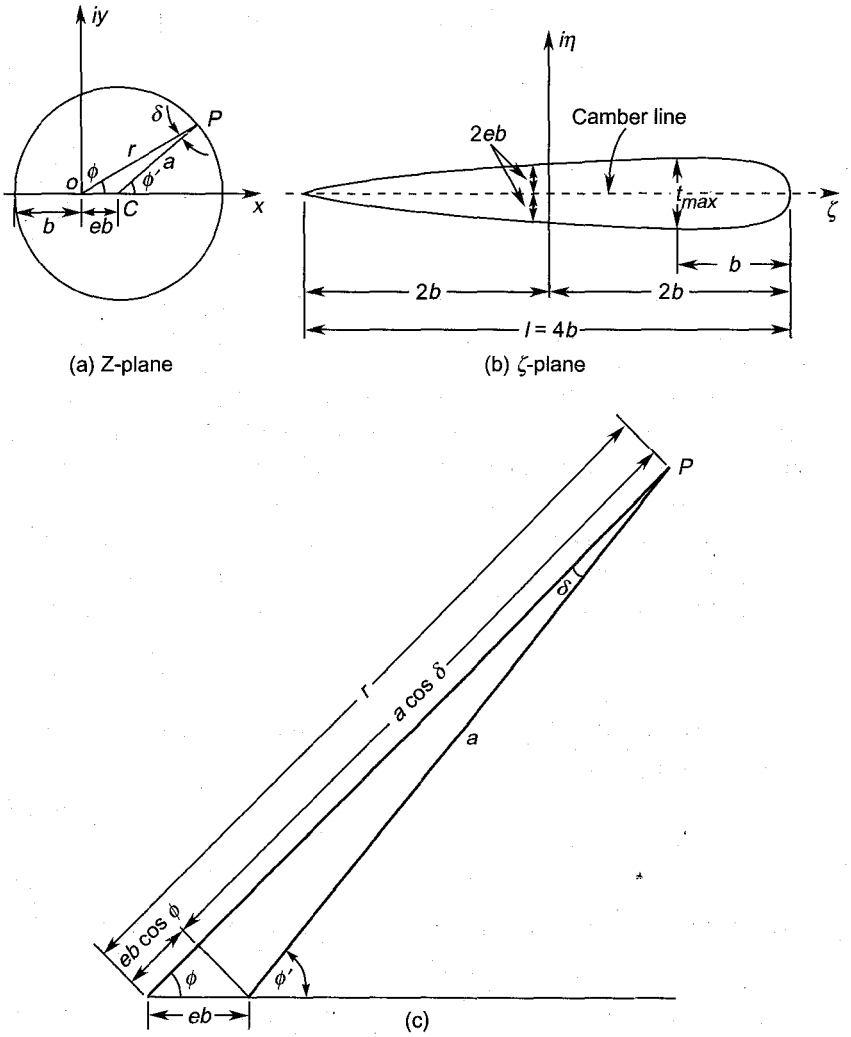

Fig. 6.13 Transformation of a circle into an uncambered aerofoil

For small values of e considering only the first two terms in the expansion of the above binomial

$$\frac{b}{r} = 1 - e - e \cos \phi \tag{6.110}$$

Substituting for z from Eq. (6.105) into Eq. (6.106),

$$\zeta = re^{i\phi} + \frac{b^2}{r} e^{-i\phi}$$

$$\zeta = r (\cos \phi + i \sin \phi) + \frac{b^2}{r} (\cos \phi - i \sin \phi)$$

Writing real and imaginary parts separately, and rearranging,

$$\zeta = b\left(\frac{r}{b} + \frac{b}{r}\right)\cos\phi + ib\left(\frac{r}{b} - \frac{b}{r}\right)\sin\phi \quad (6.111)$$

Equations (6.109) and (6.110) give

$$\frac{r}{b} + \frac{b}{r} = 2 \quad (6.112)$$

$$\frac{r}{b} - \frac{b}{r} = 2e\,(1 + \cos\phi) \quad (6.113)$$

Putting Eqs. (6.112) and (6.113) into Eq. (6.111) we get

$$\zeta = 2b\cos\phi + i\,2eb\,(1 + \cos\phi)\sin\phi \quad (6.114)$$

Comparing the real and imaginary parts in Eqs. (6.106) and (6.114),

$$\xi = 2b\cos\phi \quad (6.115)$$

$$\eta = 2\,eb\,(1 + \cos\phi)\sin\phi \quad (6.116)$$

Equations (6.115) and (6.116) give the coordinates of the aerofoil in the ζ-plane. The quantities e and b are known for a given aerofoil—angle ϕ varies from 0 to π for the upper half and 0 to $-\pi$ for the lower half. Thus for the upper half,

at $\phi = 0,\ \xi = 2b,\ \eta = 0$

$$\phi = \frac{\pi}{2},\ \xi = 0,\ \eta = 2\,eb \quad (6.117)$$

$$\phi = \pi,\ \xi = -2b,\ \eta = 0$$

and for the lower half,

at $\phi = 0,\ \xi = 2b,\ \eta = 0$

$$\phi = -\frac{\pi}{2},\ \xi = 0,\ \eta = -2\,eb \quad (6.118)$$

$$\phi = -\pi,\ \xi = -2b,\ \eta = 0$$

The chord of the blade is $4b$ as shown in Fig. 6.13(b). The values of the coordinates in Eqs. (6.117) and (6.118) show that the upper and lower curves (profiles) of the aerofoil are symmetrical.

Maximum thickness-chord ratio

From Eq. (6.116),

$$\frac{d\eta}{d\phi} = 2\,eb\,(\cos\phi + \cos^2\phi - \sin^2\phi)$$

$$\frac{d\eta}{d\phi} = 2\,eb\,(2\cos^2\phi + \cos\phi - 1)$$

For maximum thickness,

$$t_{max} = 2\eta_{max}$$

$$\frac{d\eta}{d\phi} = 2\ eb\ (2\cos^2\phi + \cos\phi - 1) = 0$$

$$2\cos^2\phi + \cos\phi - 1 = 0$$

$$(\cos\phi + 1)(2\cos\phi - 1) = 0 \qquad (6.119)$$

This equation gives the value of ϕ for maximum thickness,

(a) Taking the first root of this equation,

$$\cos\phi = -1$$

$$\phi = -\pi$$

This is inadmissible.

(b) The second root of the equation is

$$\cos\phi = 1/2$$

$$\phi = \pi/3$$

This value is admissible. Substituting this in Eq. (6.115),

$$t = t_{max} = b \qquad (6.120)$$

Equation (6.116) gives

$$t_{max} = 2\eta_{max} = 2eb\left(1 + \cos\frac{\pi}{3}\right)\sin\frac{\pi}{3}$$

$$t_{max} = 3\sqrt{3}\ eb$$

The maximum thickness-chord ratio is

$$\frac{t_{max}}{l} = \frac{t_{max}}{4b} = \frac{3}{4}\sqrt{3e}$$

$$\frac{t_{max}}{l} = 1.3\ e \qquad (6.121)$$

Equation (6.121) gives the value of e for the desired value of t_{max}/l. The maximum thickness to chord ratio is decided after taking into account the losses and the strength of the blade.

6.8.4 Transformation of a Circle into a Cambered Aerofoil

For obtaining a cambered aerofoil, the centre C of the circle is shifted both horizontally and vertically by distances eb and f respectively as shown in Fig. 6.14 (a and c). The functions z, ζ and the Zhukovsky's transformation function are still given by Eqs. (6.104), (6.106) and (6.105) respectively.

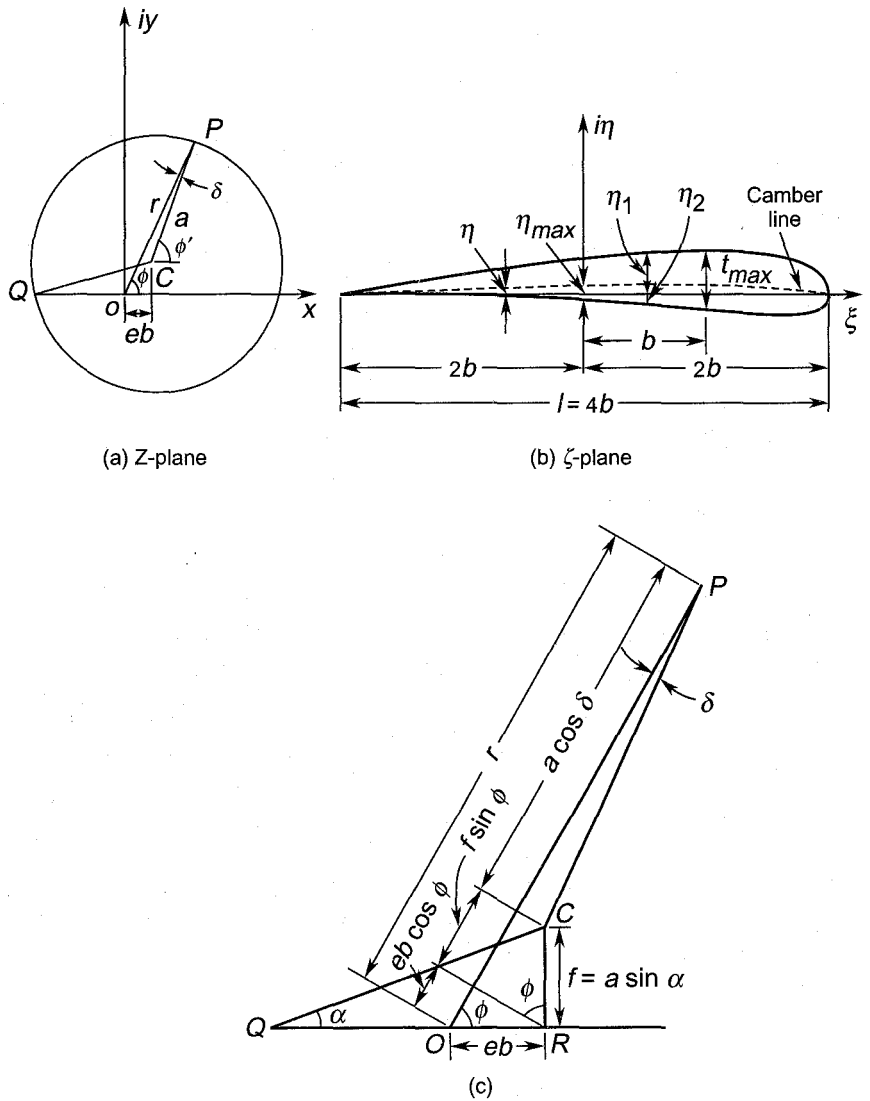

Fig. 6.14 Transformation of a circle into a cambered aerofoil

From the enlarged diagram in the Z-plane [Fig. 6.14(c)],

$$OP = r = a \cos \delta + f \sin \phi + eb \cos \phi \tag{6.122}$$

For small values of δ, $\cos \delta \approx 1$. Therefore,

$$a \cos \delta = (b + eb) \cos \delta = b + eb \tag{6.123}$$

$$f \sin \phi = (a \sin \alpha) \sin \phi = (b + eb) \sin \alpha \sin \phi$$

However, both e and a are small. Therefore,

$$\sin \alpha \approx \alpha$$

$$eb \sin \alpha \approx 0$$

$$f \sin \phi = b \alpha \sin \phi \tag{6.124}$$

Putting Eqs. (6.123) and (6.124) into Eq. (6.122), we get

$$r = b + eb + b \alpha \sin \phi + eb \cos \phi$$

$$\frac{r}{b} = 1 + e + \alpha \sin \phi + e \cos \phi \tag{6.125}$$

For small values of e,

$$\frac{b}{r} = 1 - e - \alpha \sin \phi - e \cos \phi \tag{6.126}$$

Equations (6.125) and (6.126) give

$$\frac{r}{b} + \frac{b}{r} = 2 \tag{6.127}$$

$$\frac{r}{b} - \frac{b}{r} = 2 (e + \alpha \sin \phi + e \cos \phi) \tag{6.128}$$

Equation (6.111) is applicable in this case also. Therefore, substituting from Eqs. (6.127) and (6.128) in Eq. (6.111), we have

$$\zeta = 2b \cos \phi + i\, 2b (e + \alpha \sin \phi + e \cos \phi) \sin \phi \tag{6.129}$$

Comparing the real and imaginary parts in Eqs. (6.106) and (6.129),

$$\xi = 2b \cos \phi \tag{6.130}$$

$$\eta = 2\ eb\ (1 + \cos \phi) \sin \phi + 2\alpha\, b \sin^2 \phi \tag{6.131}$$

These equations describe the profile of a cambered aerofoil shown in Fig. 6.14(b). It is observed that Eqs. (6.115) and (6.130) are identical and Eq. (6.131) reduces to Eq. (6.116) for $\alpha = 0$.

For the upper curve,

at $\phi = 0, \quad \xi = 2b, \quad \eta_1 = 0$

$$\phi = \frac{\pi}{2}, \quad \xi = 0, \quad \eta_1 = 2 (e + \alpha) b \tag{6.132}$$

$$\phi = \pi, \quad \xi = -2b, \quad \eta_1 = 0$$

For the lower curve,

at $\phi = 0, \quad \xi = 2b, \quad \eta_2 = 0$

$$\phi = -\frac{\pi}{2}, \quad \xi = 0, \quad \eta_2 = 2 (\alpha - e)\, b \tag{6.133}$$

$$\phi = -\pi, \quad \xi = -2b, \quad \eta_2 = 0$$

Equations (6.132) and (6.133) show that the aerofoil is cambered with a chord $l = 4b$.

Camber line

The camber line in the symmetrical and uncambered aerofoil coincided with the chord line (Fig. 6.13(b)). In the case of the cambered aerofoil (Fig. 6.14(b)) the camber line is displaced upwards from the chord line. Its coordinates are

$$\xi = \xi$$

$$\eta = \frac{1}{2}(\eta_1 + \eta_2)$$

For the upper curve, angle ϕ is positive. Therefore,

$$\eta_1 = 2\ eb\ (1 + \cos\ \phi)\ \sin\ \phi + 2\alpha\ b\ \sin^2\ \phi$$

For the lower curve angle ϕ is negative. Therefore,

$$\eta_2 = -\ 2eb\ (1 + \cos\ \phi)\ \sin\ \phi + 2\alpha\ b\ \sin^2\ \phi$$

Therefore,

$$\eta = 2\ \alpha\ b\ \sin^2\ \phi \tag{6.134}$$

The camber is zero for $\alpha = 0$ and it is maximum for $\phi = \pi/2$.

$$\eta_{max} = 2\alpha\ b \tag{6.135}$$

The maximum camber-to-chord ratio is

$$\frac{\eta_{max}}{4b} = \left(\frac{\eta}{l}\right)_{max} = \frac{1}{2}\ \alpha \tag{6.136}$$

It occurs at $\xi = 0$.

Maximum-thickness-chord ratio

The profile thickness is given by

$$t = \eta_1 - \eta_2$$

$$t = 4\ eb\ (1 + \cos\ \phi)\ \sin\ \phi \tag{6.137}$$

For maximum thickness (t_{max}),

$$\frac{dt}{d\phi} = 4eb\ \{(1 + \cos\ \phi)\ \cos\ \phi - \sin^2\ \phi\} = 0$$

i.e.,

$$\cos\ \phi + \cos^2\ \phi - 1 + \cos^2\ \phi = 0$$

$$2\ \cos^2\ \phi + \cos\ \phi - 1 = 0$$

This is identical with Eq. (6.119),

At $t = t_{max}$, $\phi = \pi/3$

Equation (6.137) gives

$$t_{max} = 4\ eb\left(1 + \cos\frac{\pi}{3}\right)\ \sin\ \frac{\pi}{3}$$

$$t_{max} = 3\sqrt{3}\ eb$$

The maximum-thickness chord ratio is

$$\frac{t_{max}}{l} = \frac{3}{4}\sqrt{3e}$$

$$\frac{t_{max}}{l} = 1.3\ e$$

This is identical with Eq. (6.121).

Substitution of $\phi = \pi/3$ in Eq. (6.130) gives the position of the maximum thickness section.

$$\xi_{t_{max}} = 2b \cos\frac{\pi}{3} = b$$

This result is also identical with that obtained in Eq. (6.120) for the uncambered aerofoil.

6.8.5 Velocity Distribution

With the known velocity distribution over the circular cylinder, the corresponding velocity distribution over the transformed aerofoil can be determined.

We have from Eq. (6.105)

$$\zeta = z + b^2/z$$

$$\frac{d\zeta}{dz} = 1 - \frac{b^2}{z^2} = 1 - \frac{b^2}{r^2}\, e^{-2i\phi} = 1 - \frac{b^2}{r^2}(\cos 2\phi - i \sin 2\phi)$$

$$\frac{d\zeta}{dz} = \left(1 - \frac{b^2}{r^2}\cos 2\phi\right) + i\left(\frac{b^2}{r^2}\sin 2\phi\right)$$

$$\left|\frac{d\zeta}{dz}\right| = \left\{\left(1 - \frac{b^2}{r^2}\cos 2\phi\right)^2 + \left(\frac{b^2}{r^2}\sin 2\phi\right)^2\right\}^{1/2}$$

$$\left|\frac{d\zeta}{dz}\right| = \left\{\left(1 - 2\frac{b^2}{r^2}\cos 2\phi + \frac{b^4}{r^4}\right\}^{1/2} \qquad (6.138)$$

A $\phi - \psi$ plane is defined by

$$w = \phi + i\psi$$

This is related to the function z through

$$\frac{dw}{dz} = c_x - i\, c_y = \text{velocity potential}$$

$$c_z^2 = c_x^2 + c_y^2 = \left|\frac{dw}{dz}\right|^2 \qquad (6.139)$$

Similarly the functions w and ζ are related through

$$\frac{dw}{d\zeta} = c_\xi - i\, c_\eta$$

$$c_\zeta^2 = c_\xi^2 + c_\eta^2 = \left|\frac{dw}{d\zeta}\right|^2 \tag{6.140}$$

Equations (6.139) and (6.140) give the velocity distribution (c_ζ) over the aerofoil in terms of the known velocity distribution (c_z) over the cylinder

$$\frac{c_\zeta}{c_z} = \left|\frac{dw}{d\zeta}\right| \Big/ \left|\frac{dw}{dz}\right| = \frac{1}{\left|\frac{d\zeta}{dz}\right|}$$

$$c_\zeta = c_z \Big/ \left|\frac{d\zeta}{dz}\right| \tag{6.141}$$

Putting Eq. (6.138) in Eq. (6.141) yields

$$c_\zeta = \frac{c_z}{\left\{1 - 2\frac{b^2}{r^2}\cos 2\phi + \frac{b^4}{r^4}\right\}^{1/2}} \tag{6.142}$$

More information about the above relations and detailed treatment of conformal transformation can be found in books on aerodynamics and applied mathematics.

6.9 Energy Transfer in Turbomachines

It was pointed out in Secs. 1.12 and 1.13 that, while energy transformation can occur in both stators and rotors of turbomachines, energy transfer can occur only in its moving or rotating elements, i.e. the rotors.

An expression for estimating the amount of energy transfer[6, 11, 15, 18] taking place in a turbomachine is derived below. It will be later related to the thermodynamic parameters and the boundary conditions in a machine.

Figure 6.15 shows flow through the rotor of a general turbomachine; it is shown surrounded by a control surface for writing the equation of moment of momentum. The figure also shows one of the rotor-blades along with the velocity triangles at entry (1) and exit (2). All the velocity vectors shown are in the same plane and are assumed to remain constant over the entire entry and exit sections.

The angular speed of the rotor is ω radians per second.

$$\omega = \frac{2\pi N}{60}$$

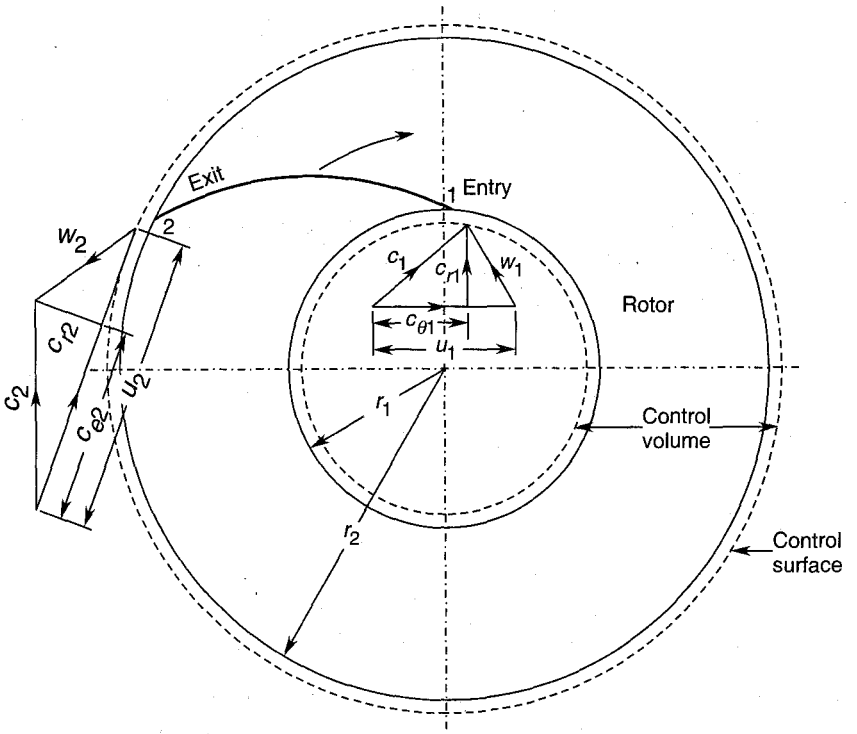

Fig. 6.15 Energy transfer during flow through a turbomachine rotor (control volume)

The peripheral velocities of the blades at the entry and exit corresponding to diameters d_1 and d_2 are

$$u_1 = \pi N d_1/60 \text{ m/s}$$

$$u_2 = \pi N d_2/60 \text{ m/s}$$

The directions of the relative velocity vectors are assumed to correspond to the rotor blade angles. The absolute velocity vectors are those which will be observed by an observer at rest, whereas the relative velocity vectors are the ones which will be observed by an observer positioned on the rotor.

The three velocity vectors c, w and u at a section (or station) are related by the simple vector equation

$$\boldsymbol{c} = \boldsymbol{u} + \boldsymbol{w}$$

The absolute velocity c at both the entry and exit has a tangential component c_θ and a radial component c_r.

The torque on the rotor (exerted by the rotor or by the fluid) is obtained by employing Newton's second law of motion for the change of moment of momentum.

In general, the algebraic sum of torques is equal to the rate of change of the moment of momentum: this is expressed mathematically by the following equation:

$$\Sigma \boldsymbol{F} \times \boldsymbol{r} = \frac{\partial}{\partial t} \int_{CV} \rho (\boldsymbol{c} \times \boldsymbol{r}) dV + \oint_{cs} \rho (\boldsymbol{c} dA)\, \boldsymbol{c} \times \boldsymbol{r} \quad (6.143a)$$

For steady flow

$$\frac{\partial}{\partial t} \int_{CV} \rho\, (\boldsymbol{c} \times \boldsymbol{r})\, dV = 0$$

Therefore,

$$\Sigma \boldsymbol{F} \times \boldsymbol{r} = \oint_{cs} \rho (\boldsymbol{c} dA)\, \boldsymbol{c} \times \boldsymbol{r} \quad (6.143b)$$

Applying this equation for steady flow through the rotor (within the control surface) shown in Fig. 6.15, we get

$$\tau = \Sigma F_\theta r = \int_{\text{exit}} (\rho\, c_n dA)\, r\, c_\theta - \int_{\text{in}} (\rho\, c_n dA)\, r\, c_\theta \quad (6.143c)$$

For writing the expression for torque only tangential components of velocity and force are considered.

The value of the infinitesimal flow rate through the control surface is given by

$$d\dot{m} = \rho\, c_n dA \quad (6.144)$$

Therefore, Eq. 6.143c gives

$$\tau = \int_{\text{exit}} r\, c_\theta\, d\dot{m} - \int_{\text{in}} r\, c_\theta\, d\dot{m} \quad (6.145a)$$

Replacing subscripts 'in' and 'exit' by 1 and 2 respectively equation (6.145a) for one-dimensional flow gives

$$\tau = r_2 c_{\theta 2}\, \dot{m}_2 - r_1 c_{\theta 1} \dot{m}_1$$

However, $\dot{m}_1 = \dot{m}_2 = \dot{m}$ = constant for steady flow.

Therefore, $$\tau_c = \dot{m}(r_2 c_{\theta 2} - r_1 c_{\theta 1}) \quad (6.145b)$$

The torque (τ_c) is exerted by the rotor blades on the fluid causing the change in the 'moment of momentum' between the entry and exit of the rotor. This happens in pumps, compressors, fans and propellers which are driven by prime movers such as electric motors, I.C. engines or turbines. The torque or work supplied by the prime mover increases the quantity $r_1 c_{\theta 1}$ to $r_2 c_{\theta 2}$. Therefore, in pressure or head producing machines,

$$r_2 c_{\theta 2} > r_1 c_{\theta 1}$$

An equal and opposite torque ($-\tau$) is exerted by the fluid on the rotor blades (Newton's third law of motion). Therefore, for turbines the value of the torque is given by

$$\tau_T = -\dot{m}\, (r_2 c_{\theta 2} - r_1 c_{\theta 1})$$

$$\tau_T = \dot{m}\ (r_1 c_{\theta 1} - r_2 c_{\theta 2}) \tag{6.146}$$

Here the work or energy transfer by the fluid to the rotor decreases the quantity $r_1 c_{\theta 1}$ to $r_2 c_{\theta 2}$. Therefore, for turbines

$$r_1 c_{\theta 1} > r_2 c_{\theta 2}$$

The rate of work done is given by

Work = torque × angular velocity of the rotor

For compressors,

$$W_c = \tau_C\, \omega = \dot{m}\ (\omega r_2 c_{\theta 2} - \omega r_1 c_{\theta 1})$$

$$W_c = \dot{m}\ (u_2 c_{\theta 2} - u_1 c_{\theta 1}) \tag{6.147a}$$

The specific work is

$$w_c = u_2 c_{\theta 2} - u_1 c_{\theta 1} \tag{6.147b}$$

Similarly, for turbines

$$W_T = \tau_T\, \omega = \dot{m}\ (u_1 c_{\theta 1} - u_2 c_{\theta 2}) \tag{6.148a}$$

$$w_T = u_1 c_{\theta 1} - u_2 c_{\theta 2} \tag{6.148b}$$

Equations (6.147) and (6.148) are also known as Euler's pump and turbine equations respectively. The differential forms of Eqs. (6.147b) and (6.148b) are

$$dw_c = d\ (uc_\theta) \tag{6.149}$$

$$dw_T = -\ d\ (uc_\theta) \tag{6.150}$$

These relations state mathematically an important fact, viz. if a turbomachine has to act as a head or pressure producing machine, its flow passages should be designed to obtain an increase in the quantity uc_θ, whereas if it is to act as a power producing machine, there must be a decrease in the quantity uc_θ between its entry and exit.

6.9.1 Forces on the Rotor Blades

The resultant force acting on a rotor blade has three components—tangential, axial and radial.

The tangential thrust is developed due to a change in the momentum of the fluid in the peripheral direction. This is the driving force on the rotor. Efforts are made in the design to obtain maximum tangential thrust for given flow conditions.

The axial thrust arises due to change of static pressure and momentum in the axial direction. This does not contribute to the motion of the rotor and has to be taken by thrust bearings. Therefore, efforts must be made to minimize it.

The radial thrust is due to changes in static pressure and momentum of the fluid in the radial direction. This also does not contribute to the motion of the rotor and must be minimized. This thrust appears as the load on the rotor shaft bearings.

6.9.2 Components of the Energy Transfer

For a better understanding of the energy transfer process in a turbomachine, Eq. (6.148b) is written here in a different form. Velocity triangles shown in Fig. 6.15 will be used for this purpose.

From the velocity triangles at the entry,

$$c_{r1}^2 = c_1^2 - c_{\theta 1}^2 = w_1^2 - (u_1 - c_{\theta 1})^2$$

This, on rearrangement, gives

$$u_1 c_{\theta 1} = \frac{1}{2}(c_1^2 + u_1^2 - w_1^2) \tag{6.151}$$

Similarly, from the velocity triangles at the exit,

$$u_2 c_{\theta 2} = \frac{1}{2}(c_2^2 + u_2^2 - w_2^2) \tag{6.152}$$

Substituting from Eqs. (6.151) and (6.152) in (6.148b), and rewriting the right-hand side as three pairs of terms,

$$w_T = \frac{1}{2}(c_1^2 - c_2^2) + \frac{1}{2}(u_1^2 - u_2^2) + \frac{1}{2}(w_2^2 - w_1^2) \tag{6.153a}$$

In the differential form,

$$dw_T = -d(uc_\theta) = -d\left(\frac{1}{2}c^2\right) - d\left(\frac{1}{2}u^2\right) + d\left(\frac{1}{2}w^2\right) \tag{6.153b}$$

Equations (6.153) show that the total energy transfer w_T or dw_T in turbines is made up of three components. Taking Eq. (6.153b), the total decrease in the quantity uc_θ through the machine is seen to be made up of a decrease in the quantities c^2 and u^2 and an increase in the quantity w^2.

The quantity $\frac{1}{2}(c_1^2 - c_2^2)$ or its differential value $\left[-d\left(\frac{1}{2}c^2\right) = -cdc\right]$ is the change in the kinetic energy of the fluid through the machine in the absolute frame of coordinates. This brings about a change in the dynamic head of the fluid through the machine.

The quantity $\frac{1}{2}(u_1^2 - u_2^2)$ is the change in the centrifugal energy of the fluid in the machine. This arises simply due to the change in the radius of rotation of the fluid. This term causes a change in the static head of the fluid through the rotor.

The quantity $\frac{1}{2}(w_2^2 - w_1^2)$ is the change in the kinetic energy of the fluid in the relative frame of coordinates. This also causes a change in the static head of the fluid across the rotor.

Energy transfer processes in a compressor can also be explained on the aforementioned lines.

6.9.3 Euler's Work

The work done by the fluid during an isentropic flow through a turbine stage with perfect guidance by its blades is the maximum work that can be expected in the stage. In such a case the deflection of the fluid through the rotor provides ideal values of the tangential velocity components $c_{\theta 1}$ and $c_{\theta 2}$.

The value of the work given by $w_T = u_1 c_{\theta 1} - u_2 c_{\theta 2}$ is the ideal work with perfect guidance by the blades. This is known as Euler's work and corresponds to the following pressure and enthalpy drops:

Euler's enthalpy drop, $$\Delta h_E = w_{ET} = u_1 c_{\theta 1} - u_2 c_{\theta 2} \tag{6.154}$$

Euler's pressure drop, $$(\Delta p)_{ET} = p_1 - p_{2E} \tag{6.155}$$

These quantities are shown in Fig. 6.16.

6.9.4 Isentropic Work

The deflection of the fluid in an actual turbine stage with isentropic flow of fluid is not the same as dictated by its blades. This is due to the imperfect guidance given by the blades to the fluid. The inability of the blade passages to provide sufficient constraint on the flow leads to lesser pressure drop and work in the stage. This will happen regardless of the fact whether the flow is reversible or irreversible. Thus in a reversible adiabatic flow with imperfect deflection, the stage work (w_{sT}) is less than the Euler's work (w_{ET}). The isentropic pressure drop is

$$(\Delta p)_{sT} = p_1 - p_{2s} = p_1 - p_{2a} \tag{6.156}$$

6.9.5 Actual Work

An actual stage with irreversible adiabatic flow produces lesser work for the same pressure drop than the isentropic work (w_{sT}) on account of losses. This work is known as the adiabatic or actual work (w_{aT}) and is lesser than the Euler's work on account of both imperfect guidance and irreversibility of the flow. Its value can also be calculated from Eq. (6.148b) provided that the actual values of the tangential velocity components are taken. Thus

$$w_{aT} = u_1 c'_{\theta 1} - u_2 c'_{\theta 2} \tag{6.157}$$

where $c'_{\theta 1}$ and $c'_{\theta 2}$ represent the actual values of the tangential velocity components.

The values of the enthalpy drop corresponding to the three kinds of turbine stage works are shown in Fig. 6.16. The final states at the end of the expansion in the three cases are represented by $2E$, $2s$, and $2a$.

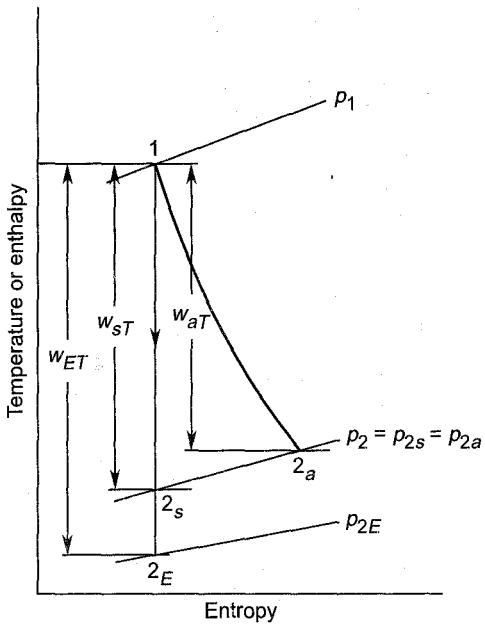

Fig. 6.16 Euler, isentropic and adiabatic works in a turbine

Eular's work (w_{EC}), isentropic work (w_{sC}) and actual work (w_{aC}) in a compressor are shown in Fig. 6.17. The Euler and the actual pressure rises are

Euler's pressure rise, $(\Delta p)_{Ec} = p_{2E} - p_1$ (6.158)

Actual pressure, rise, $(\Delta p)_{sc} = (\Delta p)_{ac} = p_2 - p_1$ (6.159)

It is seen here that, on account of the inability to fully enforce its gemoetry on the flow, the compressor stage develops a lesser pressure rise than the Euler's pressure rise during an isentropic compression process. Also, for the same pressure rise, the work required in an irreversible compression is greater than that in the reversible compression on account of losses.

Notation for Chapter 6

a	Radius of the circle, velocity of sound
A	Area

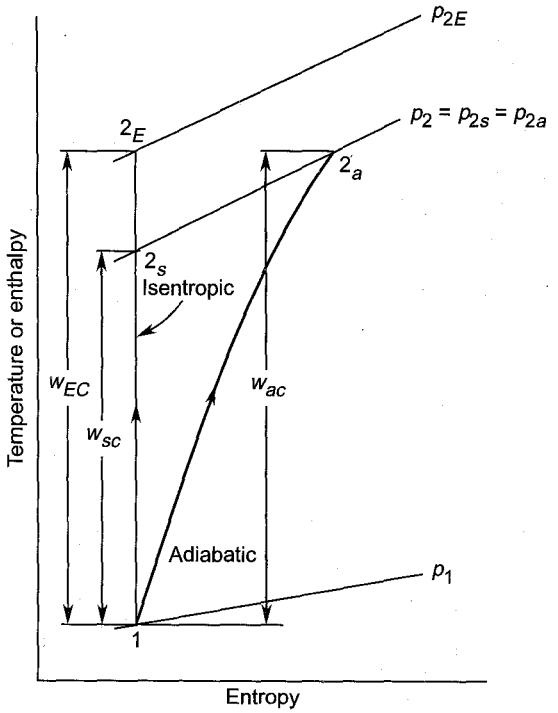

Fig. 6.17 Euler, isentropic and adiabatic works in a compressor

b	Fraction of radius a
c	Fluid velocity
C_L	Lift coefficient
C_D	Drag coefficient
d	diameter
D	Drag force
e	A factor defined in Eq. (6.107)
f	Friction factor or displacement
F	Force
h	Enthalpy
K	Bulk modulus of elasticity
l	Blade chord
L	Lift force
m	Mass, mass flow-rate
M	Mach number
n	Normal
N	Rotational speed
p	Pressure

r	Radius
R	Gas constant, radius of curvature, resultant force
Re	Reynolds number
s	Entropy
Δs	Change in entropy
t	Time, thickness
T	Temperature in Kelvin scale
u	Peripheral speed
w	Specific work, relative velocity
x, y, z	Cartesian coordinates
X, Y, Z	Body forces in Cartesian coordinates
r, θ, x	Cylindrical coordinates
R, Θ, X	Body forces in cylindrical coordinates

Greek Symbols

α	Angle shown in Fig. 6.14 (a), (b)
γ	Ratio of specific heats
δ	Boundary layer thickness, half wedge angle, angle shown in Figs. 6.13 (c) and 6.14 (a)
ξ, η, ζ	Vorticities
ξ, η	Coordinates in the ζ-plane
μ	Dynamic viscosity
ν	Kinematic viscosity
ρ	Fluid density
τ	Shear stress, torque
σ	Wave angle
ϕ	Potential function, angle shown in Figure 6.13(a)
ψ	Stream function
ω	Angular velocity

Subscripts

o	Stagnation
1	Initial, entry
2	Final, exit
∞	Free stream
a	Actual
c	Compressor
cv	Control volume
cs	Control surface
D	Drag

E	Euler's
L	Lift
max	Maximum
n	Normal to the area dA
r	Radial
s	Isentropic
T	Turbine
w	Wall
x	Axial, upstream of normal shock
y	Downstream of normal shock
z	Z-plane
θ	Tangential direction

Superscript

*	Sonic value

Solved Examples

6.1 An inward flow radial turbine has the following data:

Power	150 kW
speed	32000 rpm
outer diameter of the impeller	20 cm
inner diameter of the impeller	8 cm
absolute velocity of gas at entry	387 m/s
absolute velocity of gas at exit	193 m/s (radial)

The gas enters the impeller radially.

Construct the velocity triangles at the entry and exit of the impeller and determine:

(a) the mass-flow rate and

(b) the percentage energy transfer due to the change of radius

***Solution*:**

$$u_1 = \pi d_1 N/60 = \pi \times 0.20 \times 32000/60$$

$$u_1 = 335.1 \text{ m/s}$$

$$u_2 = (d_2/d_1)\, u_1 = \frac{8 \times 335.1}{20} = 134.04 \text{ m/s}$$

As per the given data, the velocity triangles at the entry and exit are right-angled triangles (Fig. 6.18).

The work done in the stage is

$$w_{aT} = \frac{1}{2}(c_1^2 - c_2^2) + \frac{1}{2}(w_2^2 - w_1^2) + \frac{1}{2}(u_1^2 - u_2^2)$$

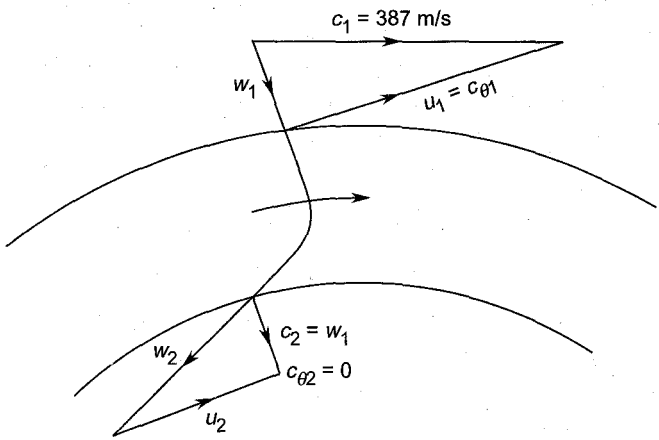

Fig. 6.18 Flow through a radial turbine (Ex. 6.1)

In the velocity triangles $w_1 = c_2$. Therefore, the above expression reduces to

$$w_{aT} = u_1^2$$

The same result is obtained from

$$w_{aT} = u_1 c_{\theta 1} - u_2 c_{\theta 2}$$

However,

$$c_{\theta 2} = 0,\ c_{\theta 1} = u_1.$$

Therefore,

$$w_{aT} = u_1^2 = \frac{335.1^2}{1000} = 112.292 \text{ kJ/kg}$$

$$\text{Power} = \dot{m} w_{aT} = 150 \text{ kW}$$

$$\dot{m} = 150/112.292 = 1.335 \text{ kg/s } (Ans.)$$

The energy transfer due to the change of radius is

$$\frac{1}{2}(u_1^2 - u_2^2) = 0.5\ (335.1^2 - 134.04^2)/1000 = 47.16 \text{ kJ/kg}$$

Therefore, the percentage of this part of the total energy transfer is

$$\frac{47.16}{112.292} \times 100 = 42.0\ (Ans.)$$

6.2 A radial-tipped blade impeller of a centrifugal blower has the following data:

speed	3000 rpm
outer diameter	40 cm
inner diameter	25 cm
impeller width at entry	8 cm
stage efficiency	70%

The absolute velocity component at the impeller entry is radial and has a magnitude of 22.67 m/s. If the radial velocity remains constant through the impeller, determine the pressure developed and the power required. Assume a constant density of air of 1.25 kg/m^3.

***Solution*:**

$$u_2 = \pi d_2 N/60 = \pi \times 0.4 \times 3000/60 = 62.83 \text{ m/s}$$

$$u_1 = 25 \times 62.83/40 = 39.27 \text{ m/s}$$

The velocity triangles are shown in Fig. 6.19. The actual work done is

$$w_{ac} = u_2 c_{\theta 2} - u_1 c_{\theta 1}$$

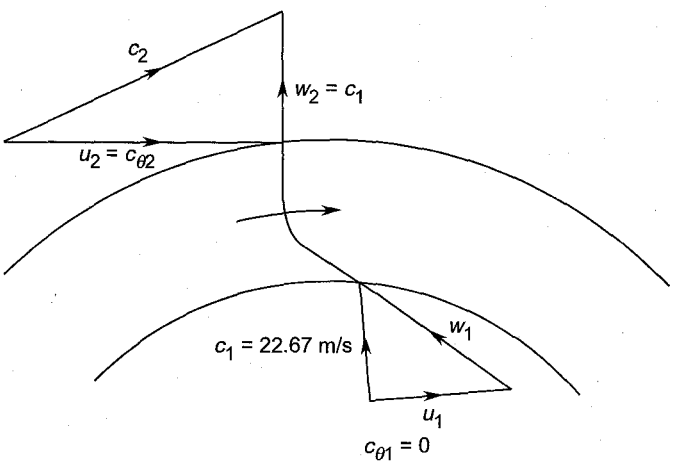

Fig. 6.19 Flow through a centrifugal blower (Ex. 6.2)

However,

$$c_{\theta 2} = u_2 \text{ and } c_{\theta 1} = 0.$$

Therefore,

$$w_{ac} = u_2^2 = (62.83)^2 = 3947.61 \text{ J/kg}$$

The ideal enthalpy change is

$$\Delta h_s = \eta_{st} w_{ac}$$

$$\Delta h_s = 0.7 \times 3947.61 = 2763.33 \text{ J/kg}$$

For isentropic flow,

$$\Delta p = \rho \Delta h_s = 1.25 \times 2763.33 = 3454.16 \text{ N/m}^2$$

$$\Delta p = 3454.16/9.81 = 352.1 \text{ kgf/m}^2$$

$$\Delta p = 352.1 \text{ mm W.G. } (Ans.)$$

Area of the impeller normal to the radial component at the entry is

$$A_1 = \pi d_1 b_1 = \pi \times 0.25 \times 0.08 = 0.0628 \text{ m}^2$$

The mass-flow rate is

$$\dot{m} = \rho c_1 A_1 = 1.25 \times 22.67 \times 0.0628 = 1.78 \text{ kg/s}$$

The power required is

$$P = \dot{m} w_{ac}$$

$$P = 1.78 \times 3.947 = 7.02 \text{ kW } (Ans.)$$

6.3 The rotor of an axial flow fan has a mean diameter of 30 cm. It runs at 1470 rpm. Its velocity triangles at entry and exit are described by the following data:

Peripheral velocity components of the absolute velocities at entry and exit are

$$c_{y1} = \frac{1}{3}u, \; c_{y2} = \frac{2}{3}u$$

(a) Draw the inlet and exit velocity triangles for the rotor and prove that the work is given by

$$w_c = \frac{1}{3}u^2$$

(b) Calculate the pressure rise (mm W.G.) taking a constant density of air, $\rho = 1.25$ kg/m^3. Notation used has its usual meaning.

***Solution*:**

(a) The velocity triangles are shown in Fig. 6.20

From Euler's compressor equation (6.147b)

$$w_c = u\,(c_{y2} - c_{y1})$$

$$w_c = u\left(\frac{2}{3}u - \frac{1}{3}u\right)$$

$$w_c = \frac{1}{3}u^2$$

(b) Since no other data about air angles and efficiency is given, the following formula is used for the pressure rise:

$$\frac{\Delta p}{\rho} = \Delta h = w_c = \frac{1}{3}\,u^2$$

$$u = \frac{\pi d N}{60} = \pi \times 0.3 \times \frac{1470}{60} = 23.091 \text{ m/s}$$

$$\Delta p = \frac{1}{3}\,\rho u^2$$

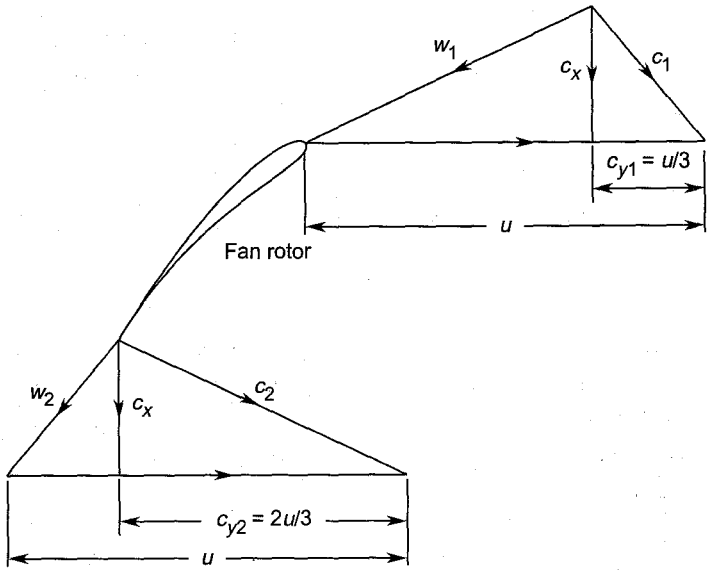

Fig. 6.20 Velocity triangles at the entry and exit of a fan rotor (Ex. 6.3)

$$= \frac{1}{3} \times 1.25 \times 23.091^2 = 222.164 \text{ N/m}^2$$

$$= 222.164/9.81 = 22.647 \text{ kgf/m}^2$$

Therefore, the pressure rise across the fan is

$$\Delta p = 22.647 \text{ mm W.G. } (\textit{Ans.})$$

Questions and Problems

6.1 Define streamlines and a stream tube. Sketch the streamlines in the flow passage of an equiangular impulse turbine blade. Map the flow from the upstream to the far downstream of such a blade channel.

6.2 Define incompressible, compressible, steady, unsteady, inviscid, viscous, laminar and turbulent flows. Give examples of each of these flows in turbomachines.

6.3 What is a boundary layer? How does it grow on the blade profile of a turbomachine? How and where is it more likely to separate on the blade surface? Illustrate with the help of sketches.

6.4 Show the streamlines in the meridional plane of a radial turbomachine. Where would you expect separation in this flow field?

6.5 Sketch a Cartesian coordinate system for a blade row of an axial flow turbomachine.

Write down continuity and momentum equations for such a system for both viscous and non-viscous flows.

6.6 Derive for incompressible, three-dimensional and irrotational flow

$$\frac{\partial^2 \phi}{\partial x^2} + \frac{\partial^2 \phi}{\partial y^2} + \frac{\partial^2 \phi}{\partial z^2} = 0$$

6.7 Sketch a cylindrical coordinate system for a blade row of an axial flow turbine. Prove that:

(a) $$\frac{\partial c_r}{\partial r} + \frac{c_r}{r} + \frac{1}{r}\frac{\partial c_\theta}{\partial \theta} + \frac{\partial c_x}{\partial x} = 0$$

(b) $$\frac{\partial c_r}{\partial r} + \frac{c_r}{r} + \frac{\partial c_x}{\partial x} = 0$$

(c) $$c_r \frac{\partial c_r}{\partial r} + c_x \frac{\partial c_r}{\partial x} - \frac{c_\theta^2}{r} = -\frac{1}{\rho}\frac{\partial p}{\partial r}$$

$$c_r \frac{\partial c_\theta}{\partial r} + c_x \frac{\partial c_\theta}{\partial x} + \frac{c_r c_\theta}{r} = 0$$

$$c_r \frac{\partial c_x}{\partial r} + c_x \frac{\partial c_x}{\partial x} = -\frac{1}{\rho}\frac{\partial p}{\partial x}$$

(d) $$\zeta = \frac{\partial c_\theta}{\partial r} + \frac{c_\theta}{r}$$

6.8 From the general equations of motion in cylindrical coordinates, prove that for incompressible, steady and axisymmetric flow

$$\frac{\partial^2 \phi}{\partial r^2} + \frac{\partial^2 \phi}{\partial x^2} + \frac{1}{r}\frac{\partial \phi}{\partial r} = 0$$

$$\frac{\partial^2 \psi}{\partial r^2} + \frac{\partial^2 \psi}{\partial x^2} - \frac{1}{r}\frac{\partial \psi}{\partial r} = 0$$

State any other assumptions made in the derivation of the above equations.

6.9 How is the maximum mass-flow rate through a turbomachine governed? Write down the well-known maximum mass-flow parameter.

6.10 Show normal and oblique shock waves in turbomachine blade passages. How are they generated? What are the advantages and disadvantages of shocks in turbomachines?

6.11 Describe the flow pattern from the leading to the trailing edge of a cambered aerofoil blade in a turbomachine. How is the lift

generated on the blade? Depict the positive and negative pressure distribution on the blade surfaces.

6.12 **(a)** Transform a circle into uncambered and cambered aerofoil sections applying Zhukovsky's transformation function

$$\zeta = z + b^2/z$$

(b) Show that:

(i) Aerofoil chord = $4b$

(ii) $\dfrac{\text{Maximum thickness}}{\text{Chord}} = 1.3 \times \text{eccentricity}$

(iii) Position of the maximum thickness section is $\frac{1}{4} \times$ chord from the leading edge.

6.13 Derive Euler's turbine and compressor equations. Hence, show that for axial machines, Euler's work is given by

$$\mp\ u\ dc_\theta$$

$$\mp\ \dot{m}\ (u_1 c_{\theta 1} - u_2 c_{\theta 2})$$

$$\mp\ \frac{1}{2}\ [(c_1^2 - c_2^2) + (w_2^2 - w_1^2)]$$

6.14 Show velocity triangles at the entry and exit of a general inward flow turbomachine.

Identify turbines and compressors from the following data for various machines:

(a) $u_1 = u_2 = 50$ m/s, $c_{y1} = 4$ m/s, $c_{y2} = 5$ m/s
(b) $c_{y1} = c_{y2} = 12$ m/s, $u_1 = 102$ m/s, $u_2 = 118$ m/s
(c) $h_{02} - h_{01} = -4$ kJ/kg
(d) $p_{02} - p_{01} = 37.5$ mm W.G.

6.15 Show Euler's, isentropic and actual values of work in turbines and compressors on h–s coordinates. Show the corresponding exit pressures in each case.

6.16 Determine Euler's, isentropic and actual values of work from the following data

(a) *Inward-flow radial turbine*

speed	24000 rpm
outer diameter of the rotor	30 cm
inner diameter of the rotor	15 cm
rotor blade angle at entry	70°
rotor blade angle at exit	25°
actual air angle at entry	75°

actual air angle at exit (from tangential direction)	35°
radial velocity at entry and exit	100 m/s
stage efficiency	91%

(*Ans.*) $w_{ET} = 160.8$ kJ/kg

$w_{ST} = 157.55$ kJ/kg

$w_{aT} = 143.62$ kJ/kg

(b) *Axial fan*

Peripheral speed	148 m/s
axial velocity component at entry and exit	35 m/s
rotor blade angle at entry	45°
rotor blade angle at exit	10°
actual air angle at entry	50°
actual air angle at exit (from axial direction)	15°
stage efficiency	82%

(*Ans.*) $w_{EC} = 4.29$ kJ/kg

$w_{sC} = 3.92$ kJ/kg

$w_{aC} = 4.785$ kJ/kg

(c) *Axial turbine*

peripheral speed	250 m/s
gas speed at nozzle exit	500 m/s
nozzle blade exit angle	70°
rotor blade exit angle	70°
actual air angle at nozzle exit	68°
actual air angle at rotor exit	62°
stage efficiency	87%

(*Ans.*) $w_{ET} = 172.4$ kJ/kg

$w_{sT} = 162.60$ kJ/kg

$w_{aT} = 141.46$ kJ/kg

6.17 If the turbine rotor in Ex. 6.1 is used for compressing air ($c_p = 1.005$ kJ/kg K, entry temperature = 300 K) what is the value of the pressure ratio obtainable with 100% efficiency? Calculate

(a) the rotor blade angle at entry, and

(b) the Mach number of the flow based on the relative velocity of air at entry.

(*Ans*) $p_r = 3.025$, $\beta_1 = 55.23°$ (from the tangential direction), M = 0.677.

Chapter 7

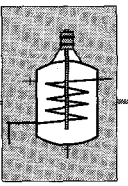

Dimensional Analysis and Performance Parameters

Dimensional analysis[6,87] of problems in turbomachines identifies the variables involved and groups them into non-dimensional quantities much lesser in number than the variables themselves. In a design problem or performance test, these non-dimensional quantities (or dimensionless parameters or numbers as they are sometimes called) are varied instead of the large number of parameters forming these groups. While the great convenience and economy in test runs provided by employing this technique is obvious, the design procedure uses these non-dimensional numbers to obtain maximum efficiency.

Some non-dimensional numbers give an idea of the type of machine and its range of operation.

The presentation of the performance of a machine is also considerably simplified by adopting non-dimensional numbers.

In this section a number of dimensionless parameters are separately developed for incompressible and compressible flow machines. Later, the preformance characteristics of only compressible flow machines (turbines, compressors, fans and blowers) are discussed employing some of these parameters. Incompressible flow machines are at places mentioned only for comparison.

7.1 Units and Dimensions

It is well known that the primary quantities are mass (M), length (L), time (T) and temperature (θ). Other quantities are derived from them.

In the S.I. system of units (System International d'units), the following units and dimensions (Table 7.1) are used for some basic variables considered in this book.

7.2 Buckingham's π-theorem

The π-theorem states that, in a given problem, if the number of variables is n, the greatest number of non-dimensional groups or dimensionless numbers (also known as π-terms) is given by

$$\pi = n - k \tag{7.1}$$

Table 7.1 Units and dimensions in S.I. units

Quantities	*Units*	*Dimensions*
Mass	kg	M
Length	m	L
Time	s	T
Temperature	°C or K	Θ
Area	m^2	L^2
Volume	m^3	L^3
Volume-flow rate	m^3/s	L^3/T
Mass-flow rate	kg/s	M/T
Velocity	m/s	L/T
Acceleration	m/s^2	L/T^2
Force (Newton, N)	kg m/s^2	ML/T^2
Pressure (Pascal, Pa)	$N/m^2 \equiv kg/ms^2$	M/LT^2
Torque	Nm ≡ kg m^2/s^2	ML^2/T^2
Heat, work, enthalpy and energy (Joules, J)	J ≡ Nm ≡ kg m^2/s^2	ML^2/T^2
Power (Watts)	J/s ≡ N m/s = kg m^2/s^3	ML^2/T^3
Dynamic viscosity	N s/m^2 ≡ kg/ms	M/LT
Density	kg/m^3	M/L^3
Kinematic viscosity	m^2/s	L^2/T
Bulk modulus of elasticity	kg/m s^2	M/LT^2
Rotational speed	revolution/s radians/s	1/T

where $k \leq m$

and m = number of primary dimensions.

Here, it will be assumed that $k = m$; this is true in a majority of situations.

Let there be three dependent variables (y_1, y_2 and y_3) and five independent variables (x_1, x_2, x_3, x_4 and x_5).

$$y_1, y_2, y_3 = f(x_1, x_2, x_3, x_4, x_5) \tag{7.2}$$

If three primary dimensions M, L and T are involved, then the theorem [Eq. (7.1)] gives

$$\pi = n - m$$
$$\pi = (3 + 5) - 3 = 5$$

Thus the number of dimensionless groups or π-terms is five. This can be expressed functionally by the following relation:

$$\pi_1, \pi_2 = f(\pi_3, \pi_4, \pi_5) \tag{7.3}$$

More dimensionless groups can be formed by a combination of the π-terms [as in Eq. (7.3)] already determined by the π-theorem.

The selection of π-terms on the two sides in Eq. (7.3) depends on the behaviour of a given machine. The terms on the right must be the control variables whose variation at will automatically "vary" terms on the left-hand side. Some control variables in turbomachine application are given below:

Table 7.2 Control variables in turbomachines

Control variables	*Turbomachines*
Mass-flow rate	Pumps, fans, blowers and compressors
Load or power output	Hydro, steam, gas and wind turbines
Speed	Pumps, fans, blowers, compressors and propellers

7.3 Principle of Similarity

The performance of an actual machine (prototype) can be predicted with the aid of simple and inexpensive tests on models. Physical conditions of a prototype can be simulated in a model by keeping the values of some dimensionless parameters (π-terms) the same in both. The following types of similarities must be satisfied.

7.3.1 Geometric Similarity

Some of the geometric variables in a turbomachine are:

blade chord (l),
blade pitch (s),
blade height (h),
rotor diameter (D), and
blade thickness (t).

For geometric similarity, the ratios of the linear dimensions and the shape of the bodies in the model and prototype are the same; the values of the individual dimensions are immaterial.

7.3.2 Kinematic Similarity

Some kinematic variables in turbomachines are:

blade velocity, ($u = \pi DN/60$),
flow velocity, (c_x or c_r),
isentropic gas velocity (c_s), and
rotational speed (ω, N).

Kinematic similarity requires that the ratios of velocities are the same in the model and prototype regardless of the individual values. This gives similar velocity triangles in both the model and prototype.

7.3.3 Dynamic Similarity

The dynamic variables affecting the performance of turbomachines are:

gas density (ρ),
dynamic viscosity (μ),
bulk modulus (K),
pressure difference (Δp),
forces (L, D, F_y, F_x) and
power (P).

In dynamic similarity, the ratios of the various forces should be the same regardless of the individual values.

Various non-dimensional numbers composed of the geometric, kinematic and dynamic variables in turbomachines are discussed in Secs. 7.4 and 7.5.

7.4 Incompressible Flow Machines

The dependent variables in incompressible flow trubomachines are usually the head (gH), power (P) and efficiently (η). These are functions of the following variables:

rotor speed (N),
rotor diameter (D)
characteristic lengths (s, l, h, etc.) or length ratios $\left(\frac{s}{l}, \frac{h}{l}, \text{etc.}\right)$
discharge (Q),
fluid density (ρ) and
fluid viscosity (μ).

Thus we have

$$gH, P, \eta = f\left(N, D, \frac{s}{l}, \frac{h}{l}, Q, \rho, \mu\right) \tag{7.4}$$

The presence of non-dimensional variables in Eq. (7.4) is not taken into account for applying the π-theorem because they are already dimensionless numbers. Thus, ignoring η, $\frac{s}{l}$ and $\frac{h}{l}$, there are seven variables ($n = 7$) and three dimensions ($m = 3$). Therefore, Eq. (7.1) gives

the number of dimensionless groups as four ($\pi = 4$). The already diminsionless variables in Eq. (7.4) remain intact in the functional equation for the dimensionless numbers. Therefore,

$$\pi_1,\ \pi_2,\ \eta = f\left(\pi_3, \pi_4, \frac{s}{l}, \frac{h}{l}\right) \tag{7.5}$$

Employing the conventional procedure (see Appendix F) for finding the dimensionless numbers, the following π-terms are obtained:

$$\pi_1 = \frac{gH}{(ND)^2} \tag{7.6}$$

$$\pi_2 = \frac{Q}{ND^3} \tag{7.7}$$

$$\pi_3 = \frac{P}{\rho N^3 D^5} \tag{7.8}$$

$$\pi_4 = \frac{\rho ND^2}{\mu} \tag{7.9}$$

The units of various quantities in these equations are given in Table 7.1.

7.4.1 Head Coefficient

The parameter $\pi_1 = \dfrac{gH}{(ND)^2}$ is known as the head coefficient. For incompressible flow, $\rho \approx$ constant. Therefore,

$$gH = \frac{\Delta p}{\rho} \tag{7.10}$$

Now $ND \propto u.$

Therefore, $$\frac{gH}{(ND)^2} \propto \frac{gH}{u^2} = \frac{\Delta p}{\rho u^2} \tag{7.11}$$

Different names are given to the quantities in Eq. (7.11). The loading coefficient is defined by

$$\psi = \frac{gH}{u^2} \tag{7.12}$$

The pressure ccefficient is given by

$$\psi' = \frac{\Delta p}{\rho u^2} \tag{7.13}$$

The two expressions in Eqs. (7.12) and (7.13) have the same value for incompressible flow machines. In some literature, the pressure coefficient is defined by

$$\psi'' = \frac{\Delta p}{\frac{1}{2}\rho u^2} \tag{7.14}$$

The above relations show that the coefficients ψ, ψ' and ψ'' are proportional to the head coefficient given by Eq. (7.6).

7.4.2 Capacity Coefficient

The parameter $\pi_2 = \dfrac{Q}{ND^3}$ is referred to as the capacity coefficient. The discharge is given by the continuity equation

$$Q = c_x A$$

The cross-sectional area A is made up of two linear dimensions which are proportional to the diameter D. Thus,

$$A \propto D^2$$

$$Q \propto c_x D^2 \tag{7.15}$$

$$ND^3 = (ND)\, D^2$$

However, $ND \propto u$, therefore,

$$ND^3 \propto uD^2 \tag{7.16}$$

Equations (7.15) and (7.16) give

$$\pi_2 \propto \frac{c_x D^2}{uD^2} \propto \frac{c_x}{u}$$

The quantity $\dfrac{c_x}{u}$ is known as the flow coefficient

$$\phi = \frac{c_x}{u} \tag{7.17}$$

It may be noted here that the capacity coefficient is proportional (and not equal) to the flow coefficient.

7.4.3 Power Coefficient

The parameter $\pi_3 = \dfrac{P}{\rho N^3 D^5}$ is known as the power coefficient. This can also be obtained by the product of the head and capacity coefficients given in Eqs. (7.6) and (7.7) respectively

$$\pi_3 = \pi_1 \pi_2$$

$$\pi_3 = \frac{gH}{(ND)^2}\frac{Q}{ND^3}$$

Power = head × mass flow rate

$$P = \rho Q\ (gH) \tag{7.18}$$

Therefore, $$\pi_3 = \frac{P}{\rho N^3 D^5}$$

which is Eq. (7.8)

7.4.4 Reynolds Number

The parameter $\pi_4 = \dfrac{\rho ND^2}{\mu}$ is proportional to the ratio of inertia and viscous forces. This is shown in the following derivation:

$$\pi_4 = \frac{\rho ND^2}{\mu} = \frac{\rho\,(ND)\,D^2}{\mu D}$$

Now $$ND \propto u \propto c$$

$$D^2 \propto A$$

$$D \propto l$$

Therefore, $$\pi_4 \propto \frac{\rho\, Au}{\mu l} \propto \frac{\rho\, Ac}{\mu l} \propto \frac{\rho\, Ac^2}{\mu cl} \tag{7.19}$$

Now ρAc^2 = inertia force

μcl = viscous force

Therefore, $$\pi_4 \propto \frac{\text{intertia force}}{\text{viscous force}}$$

This ratio is the well-known fluid dynamic parameter—the Reynolds number (Re) which has already been defined in Sec. 6.1.11.

$$\text{Re} = \frac{\rho\, Ac^2}{\mu cl} = \frac{cl}{\mu/\rho} = \frac{cl}{\nu} \tag{7.20}$$

Here the Reynolds number is based on the fluid velocity (c) and the characteristic length parameter (l). However, this need not be always in this form. These parameters can be replaced by other velocities and characteristic length parameters. For example, retaining u and D in the original expression

$$\pi_4 = \frac{(ND)\,D}{\mu/\rho} \propto \frac{uD}{\nu}$$

$$\text{Re} = \frac{uD}{\nu} \tag{7.21}$$

Equation (7.21) gives the value of a Reynolds number based on the peripheral speed and diameter of the rotor.

7.4.5 Specific Speed

As mentioned before, more dimensionless numbers can be obtained from the combination of the π-term already determined. Thus, another very useful dimensionless number (π_5) is formed by the following combination of π_1 and π_2.

$$\pi_1 = \pi_2^{1/2} / \pi_1^{3/4}$$

Substituting from Eqs. (7.6) and (7.7)

$$\pi_5 = \frac{(Q/ND^3)^{1/2}}{(gH/N^2 D^2)^{3/4}}$$

$$\pi_5 = \frac{NQ^{1/2}}{(gH)^{3/4}} \tag{7.22}$$

Here the linear dimension D has been eliminated. It is important because this suggests that Eq. (7.22) can be applied to geometrically similar machines of all sizes. This dimensionless parameter is known as the specific speed or shape parameter (N_s). Since g is constant, it is sometimes dropped; but by doing so the dimensionless nature of the π-term is not retained.

$$N_{sP} = \frac{NQ^{1/2}}{H^{3/4}} \tag{7.23}$$

(Here suffix P denotes pumps, fans and compressors).

The value of the specific speed at the maximum efficiency point is a useful guide in designing and selecting turbomachines for given conditions. Thus the use of the specific speed places various types of turbomachines in different brackets of distinct ranges. This is a very useful guide in selecting the type (axial, radial and mixed) of pumps, turbines, compressors, fans and blowers because each type has almost a well-defined range on the specific speed scale.

Another expression for the specific speed can be obtained by combining π_1 and π_3 as shown below.

$$\pi_6 = \pi_3^{1/2} / \pi_1^{5/4}$$

$$\pi_6 = \frac{(P/\rho N^3 D^5)^{1/2}}{(gH/N^2 D^2)^{5/4}}$$

$$\pi_6 = \frac{1}{\rho^{1/2}\, g^{5/4}} \frac{\sqrt{P}}{H^{5/4}}\, N \tag{7.24}$$

An expression for the power specific speed is obtained by dropping the factor $\dfrac{1}{\rho^{1/2}\, g^{5/4}}$

$$N_{sT} = \frac{\sqrt{P}}{H^{5/4}}\, N \tag{7.25}$$

(Here suffix T denotes turbines.)

Here again it must be remembered that while the expression in Eq. (7.24) is dimensionless, it is not so in Eq. (7.25).

The expressions in Eq. (7.22) or (7.23) are used for pumps, fans, blowers and compressors, whereas Eqs. (7.24) and (7.25) are employed for turbines.

In S.I. units Eqs. (7.22) and (7.24) are used for calculating the value of the specific speed. The following units are used for various quantities:

N in rps or radians per second
Q in m^3/s
g in m/s^2
H in metres
P in watts
ρ in kg/m^3

7.5 Compressible Flow Machines

Dimensional analysis for compressible flow machines [287, 411A] differs from the incompressible flow machines on account of the following factors:

1. On account of the continuously changing volume-flow rate, for a given mass-flow rate, the variable Q is replaced by the mass-flow rate ($\dot{m}$). This remains constant in steady flow.
2. The head term gH is replaced by the pressure change term (Δp_0) or the pressure ratio $p_r = p_{01}/p_{02}$. The change of specific enthalpy can also replace (gH). This is obviously the right thing to do for blowers, compressors and turbines handling compressible fluids. It is much easier to indicate the pressure difference (often in mm W.G.) developed across a blower, or a pressure ratio developed by a compressor or compresor stage.
3. The ratio (γ) of specific heats also becomes one of the independent parameters.

4. In compressible flows, elasticity of the gas is an important parameter. This is taken into account by the temperature (T_{01}) or the velocity of sound at the entry, i.e.

$$a_{01} = \sqrt{\gamma R T_{01}} \tag{7.26}$$

5. Since the values of the gas density and temperature vary in compressible flow machines, their values at the entry are taken.

In view of the above, the functional relationship [such as Eq. 7.4)] for compressible flow machines is

$$\frac{p_{01}}{p_{02}}, P, \eta = f\left(N, D, \frac{s}{l}, \frac{h}{l}, \dot{m}, \rho_{01}, \mu, \gamma, a_{01}\right) \tag{7.27}$$

In this equation, five quantities, p_{01}/p_{02}, η, $\frac{s}{l}$, $\frac{h}{l}$ and γ, are already dimensionless. Therefore, ignoring them, there are seven variables ($n = 7$) and three dimensions ($m = 3$). Thus, according to the π-theorem, there must be four more dimensionless groups or π-terms. By employing a dimensional analysis, the following groups are obtained:

$$\frac{p_{01}}{p_{02}}, \frac{P}{\rho_{01} N^3 D^5}, \eta = f\left(\frac{\rho_{01} ND^2}{\mu}, \frac{\dot{m}}{\rho_{01} N D^3}, \frac{s}{l}, \frac{h}{l}, \frac{ND}{a_{01}}, \gamma\right) \tag{7.28}$$

Various dimensionless quantities in this equation are now separately discussed in the following sections.

7.5.1 Pressure Ratio

Let $$\pi_1 = p_{01}/p_{02} \tag{7.29}$$

This dimensionless parameter is wideiy used for both turbines and compressors. If the dynamic pressures are negligible at the entry and exit, this π-term is taken as the ratio of static pressures.

In an isentropic process, the change in enthalpy (Δh_{0s}) or temperature (ΔT_{0s}) is related to the pressure ratio.

$$\frac{T_{02s}}{T_{01}} = \left(\frac{p_{02}}{p_{01}}\right)^{\frac{\gamma-1}{\gamma}} = (p_{r0})^{-\frac{\gamma-1}{\gamma}} = f(p_{r0})$$

For compressors the pressure ratio p_{02}/p_{01} (or p_2/p_1) is greater than one. Therefore, temperature rise in a compressor is given by

$$T_{02s} - T_{01} = T_{01}\left\{\left(\frac{p_{02}}{p_{01}}\right)^{\frac{\gamma-1}{\gamma}} - 1\right\}$$

$$\frac{\Delta T_{0s}}{T_{01}} = f(p_{r0}) \tag{7.30}$$

For a perfect gas,

$$c_p \frac{\Delta T_{0s}}{c_p T_{01}} = \frac{\Delta h_{0s}}{\frac{\gamma}{\gamma - 1} R T_{01}} = (\gamma - 1) \frac{\Delta h_{0s}}{a_{01}^2}$$

$$\frac{\Delta h_{0s}}{a_{01}^2} = f(p_{r0}) \tag{7.31}$$

This is also expressed as

$$\frac{\Delta h_{0s}}{N^2 D^2} = f(p_{r0}) \tag{7.32}$$

7.5.2 Dimensionless Speed Parameter

Let

$$\pi_2 = \frac{ND}{a_{01}} \tag{7.33}$$

Since the quantity ND is proportional to the peripheral speed (u) of the rotor blades, Eq. (7.33) defines a rotor blade Mach number based on the velocity of sound at the entry.

$$\pi_2 \propto \frac{u}{a_{01}}$$

$$M_{b01} = \frac{u}{a_{01}} \tag{7.34}$$

Putting Eq. (7.26) into Eq. (7.33), we get

$$\pi_2 = \frac{D}{\sqrt{\gamma R}} \frac{N}{\sqrt{T_{01}}} \tag{7.35}$$

For the same machine and gas, the factor $D/\sqrt{\gamma R}$ is constant and can therefore be dropped. Thus the conventional form of the so-called dimensionless speed parameter is obtained

$$\pi_2 \propto \frac{N}{\sqrt{T_{01}}} \tag{7.36}$$

7.5.3 Dimensionless Mass-flow Parameter

Let

$$\pi_3 = \frac{\dot{m}}{\rho_{01} N D^3} \tag{7.37}$$

π_3 is the capacity or flow coefficient. It is expressed here in a more convenient and conventional form. For a perfect gas,

$$\rho_{01} = p_{01}/RT_{01}$$

$$\pi_3 = \frac{\dot{m}RT_{01}}{p_{01}D^2\,(ND)} = \frac{\dot{m}\sqrt{RT_{01}}}{p_{01}D^2}\,\frac{\sqrt{RT_{01}}}{ND}$$

From Eq. (7.26)

$$\sqrt{RT_{01}} = a_{01}/\sqrt{\gamma}$$

Therefore,

$$\pi_3 = \left(\frac{\dot{m}\sqrt{RT_{01}}}{p_{01}D^2}\right)\left(\frac{a_{01}}{ND}\right)\left(\frac{1}{\sqrt{\gamma}}\right) \tag{7.38}$$

However, $\dfrac{ND}{a_{01}} = \pi_2$ and γ are already dimensionless groups in Eq. (7.28). Therefore yet another π-term is obtained by their combination with π_3 in Eq. (7.38). This is

$$\pi_4 = \frac{\sqrt{R}}{D^2}\,\frac{\dot{m}\sqrt{T_{01}}}{p_{01}} \tag{7.39}$$

Dropping $\sqrt{R}/D^2$ for the same machine and gas, the new dimensionless mass flow parameter is obtained in the following form:

$$\pi_4 \propto \frac{\dot{m}\sqrt{T_{01}}}{p_{01}} \tag{7.40}$$

Dimensionless mass-flow parameter in compressible flow machines also defines a "flow Mach number" (M_{x0}). In Eq. (7.39)

$$\dot{m} \propto \rho_{01}\, c_x\, D^2$$

$$p_{01} = \rho_{01}\, RT_{01}$$

Therefore,

$$\pi_4 \propto \frac{\sqrt{R}}{D^2}\,\frac{\rho_{01}\, c_x\, D^2\,\sqrt{T_{01}}}{\rho_{01}RT_{01}}$$

$$\pi_4 \propto \frac{c_x}{\sqrt{\gamma\, RT_{01}}} \propto \frac{c_x}{a_{01}} \tag{7.41}$$

The axial flow Mach number is given by

$$M_{x0} = \frac{c_x}{a_{01}} \tag{7.42}$$

The ratio of quantities in Eqs. (7.34) and (7.42) gives the flow coefficient defined earlier.

$$\phi = \frac{M_{x0}}{M_{b0}} = \frac{c_x}{u}$$

7.5.4 Power Coefficient

Let

$$\pi_5 = \frac{P}{\rho_{01} N^3 D^5} \tag{7.43}$$

$$P = \dot{m}\, c_p\, \Delta T_0 = \dot{m}\, \Delta w \tag{7.44}$$

Substituting from Eq. (7.37) for $\dot{m}$,

$$P = \pi_3 \rho_{01} ND^3\, (c_p \Delta T_0) = \pi_3 \rho_{01} ND^3\, (\Delta w) \tag{7.45}$$

Equations (7.43) and (7.45) together give

$$\pi_5 = \pi_3 \frac{c_p \Delta T_0}{N^2 D^2} = \pi_3 \frac{\Delta w}{N^2 D^2} \tag{7.46}$$

The power coefficient can now be defined in a slightly different way by combining the two π-terms in Eq. (7.46).

$$\pi_6 = \pi_5 / \pi_3$$

$$\pi_6 = \frac{c_p \Delta T_0}{N^2 D^2} = \frac{\Delta w}{N^2 D^2} \tag{7.47}$$

This is proportional to the loading coefficient [see Eq. (7.12)]

$$\psi = \frac{\Delta w}{u^2}$$

7.5.5 Reynolds Number

The other dimensionless parameter is the Reynolds number.

$$\frac{\rho_{01} ND^2}{\mu} = \frac{\rho_{01} (ND) D}{\mu} \propto \frac{\rho_{01} ul}{\mu}$$

The values of the Reynolds number in hydro turbines are much higher than the critical values. Therefore, their performance is almost independent of this parameter. This is also true in the case of a majority of large compressible flow turbines.

Reynolds number is an important parameter for small pumps, compressors, fans and blowers. Their performance improves with an increase in Reynolds number.

Other dimensionless groups in Eq. (7.28) are the pitch-chord ratio (s/l), aspect ratio (h/l) and the specific heat ratio (γ) being already dimensionless, they have remained unaltered from Eq. (7.27) to Eq. (7.28), such as the pressure ratio (p_{01}/p_{02}) and efficiency (η)

7.6 Performance of Turbines

The performance characteristic of turbines can be presented in a number of ways. Here only some of the dimensionless parameters considered earlier for compressible flow turbomachines are discussed.

Variation of the loading coefficient (ψ) with the flow coefficient (ϕ) in impulse turbine stage is shown in Fig. 7.1. This is given by

$$\frac{\Delta w}{u^2} = \frac{c_p \Delta T_0}{u^2} = f\left(\frac{c_x}{u}\right)$$

$$\psi = f(\phi)$$

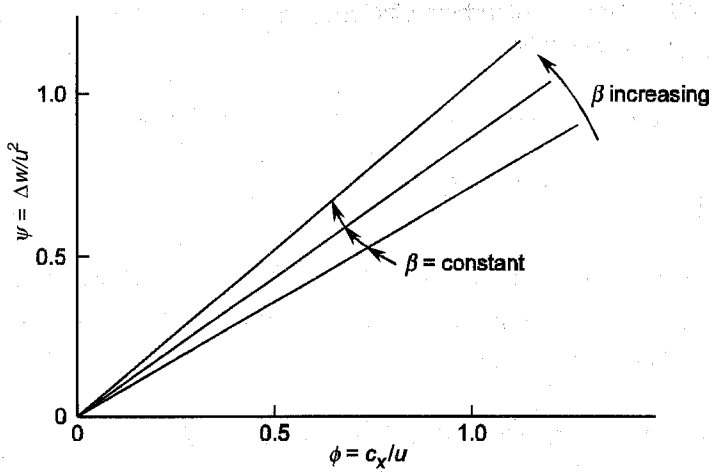

Fig. 7.1 Variation of loading coefficient with flow coefficient for an impulse turbine stage

Equiangular blades ($\beta = \beta_2 = \beta_3$) and ideal flow have been assumed in these plots. It may be seen that, for a given flow coefficient, the stage loading increases with an increase in the blade angles from the axial direction.

It can be shown that the efficiency of a turbine stage is dependent on the blade to isentropic gas speed ratio (u/c_s).

$$\eta_T = f\left(\frac{u}{c_s}\right) \tag{7.48}$$

This is shown in Fig. 7.2 for an impulse and a 50% reaction stage. The latter stage gives maximum efficiency at a higher speed ratio.

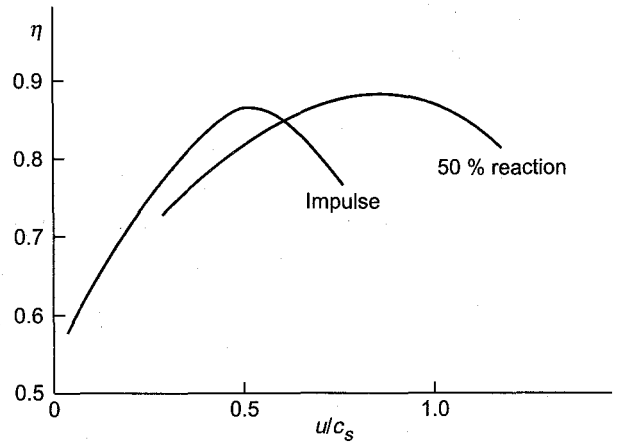

Fig. 7.2 Variation of turbine efficiency with blade to isentropic gas speed ratio

Assuming perfect gas, the performance of gas turbines is described by

$$\frac{p_{01}}{p_{02}} = f\left(\frac{\dot{m}\sqrt{T_{01}}}{p_{01}}, \frac{N}{\sqrt{T_{01}}}\right) \tag{7.49}$$

This is depicted in Fig. 7.3 for various values of the speed parameter ($N/\sqrt{T_{01}}$). The choking line shows that the turbine chokes when the flow Mach numbers become unity.

7.7 Performance of Compressors

The characteristic of a hydraulic pump expressed as a head versus capacity coefficient curve is shown in Fig. 7.4. The same characteristic for a compressible flow device (compressor) is described by the following relation:

$$\frac{p_{02}}{p_{01}} = f\left(\frac{\dot{m}\sqrt{T_{01}}}{p_{01}}, \frac{N}{\sqrt{T_{01}}}\right) \tag{7.50}$$

This is shown in Fig. 7.5. The machine will experience a surge on the positive slope slide of the characteristic curves. Therefore, a limiting line (the surge line) is drawn through points where the slope changes from negative to positive.

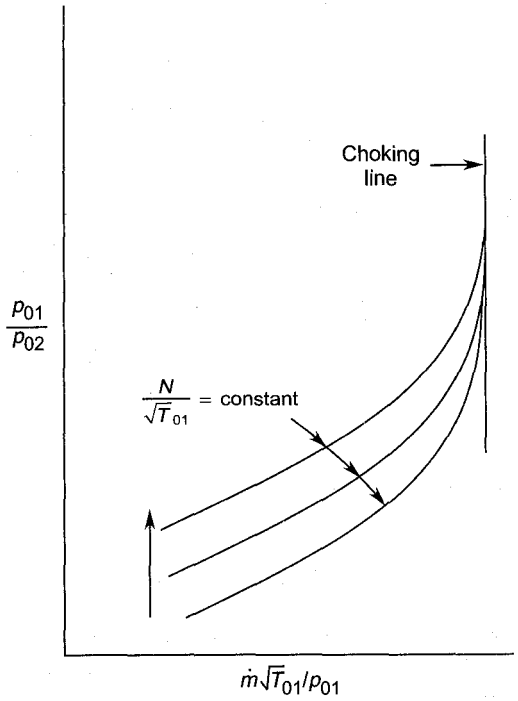

Fig. 7.3 Performance of a turbine

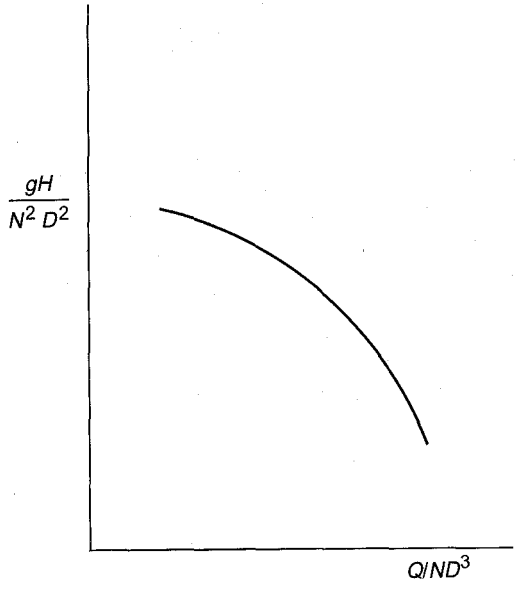

Fig. 7.4 Characteristic of a pump

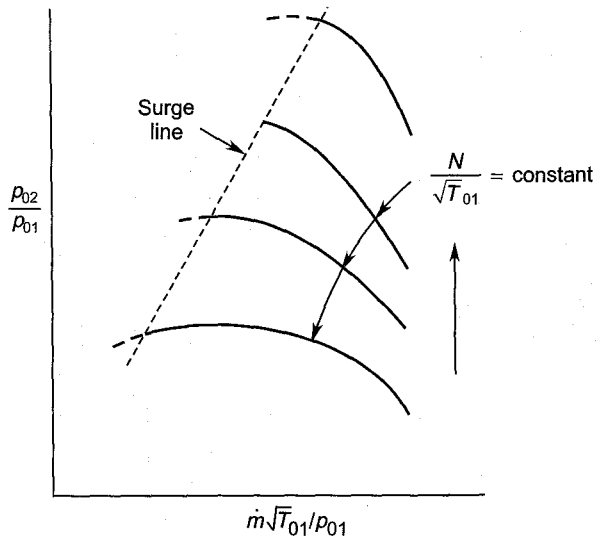

Fig. 7.5 Performance of a compressor

The stage loading or pressure coefficient for a 50% reaction stage of an axial compressor is shown in Fig. 7.6. This is the ideal curve without stage losses. The actual characteristic curve can be obtained from this by accounting for losses.

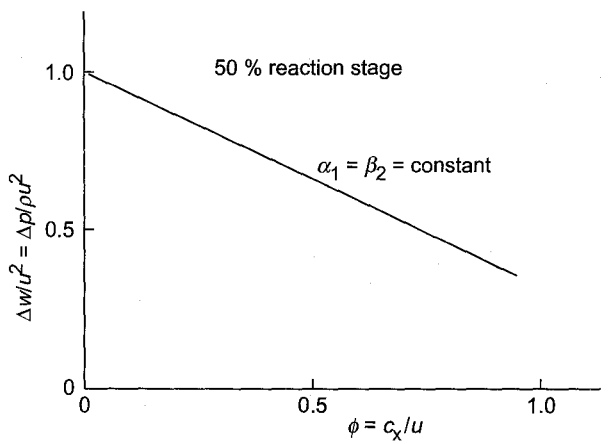

Fig. 7.6 Variation of pressure coefficient with flow coefficient for an axial flow compresor stage

Figure 7.7 compares the efficiencies and specific speed ranges of the various types of compressors. It may be seen that the rotary type positive displacement compressor has the lowest efficiency and specific speed

ranges. This is clear from the definition of the specific speed for pumps or compressors given in Eq. (7.22) or (7.23). Since this type of compressor develops comparatively higher pressure (Δp or H) and handles smaller flow rates (Q), it must have lower values of the specific speed.

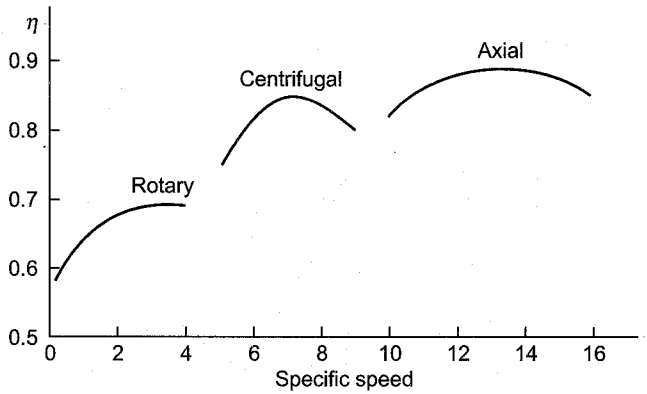

Fig. 7.7 Variation of efficiency of compressors with specific speed (types and ranges)

The axial flow stages handle very high flow rates at comparatively much lower pressures (heads). Therefore, this gives higher values of the specific speed to the axial machines. These machines have the highest efficiencies.

The centrifugal stages have efficiency and specific speed ranges between the positive displacement rotary type and the axial type.

7.8 Performance of Fans and Blowers

Like compressors, axial flow fans and blowers have higher efficiencies and operate at a higher specific speed range. This is on account of the comparatively smaller pressure rise (head developed) over the stage and higher flow rates. The centrifugal fan stages handle comparatively low flow rates and develop much higher pressures. This gives them lower specific speed and efficiency ranges.

The performance characteristics of high pressure blowers are presented and interpreted in a manner similar to compressors. However, low pressure fans and blowers are incompressible flow machines and do not show dependence on parameters related to the compressible flow effects. The characteristic of a typical axial flow fan in terms of a $\phi - \psi$ plot is shown in Fig. 7.8.

There are three types of stages in centrifugal fans: they have rotor blade outlet angles in the forward, radial and backward directions. The

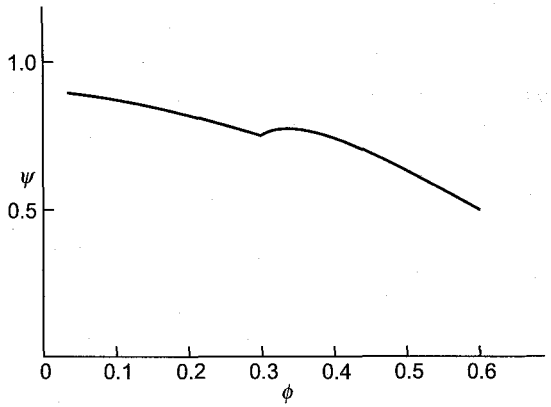

Fig. 7.8 Axial fan characteristic

performance of these types varies considerably from each other as shown in Fig. 7.9. This point is further explained in Chapter 15. A forward-swept blade impeller has the highest loading coefficient and the backward-swept type the lowest.

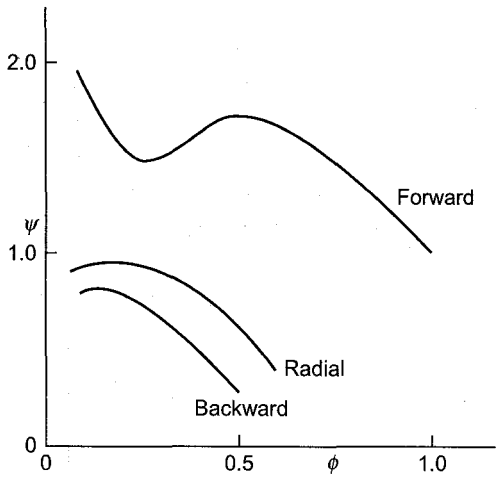

Fig. 7.9 Centrifugal fan characteristics

7.9 Performance of Cascades

A cascade, lattice or grid is formed by arranging blades of a given geometry in a rectilinear, cylindrical or any other desired pattern. The geometry of the cascade represents the geometry of the blade in an actual turbomachine stage. Thus a cascade is a geometrically similar model of a prototype, i.e. the turbomachine blade ring.

The flow behaviour of the actual blade row can be simulated in cascade tests by keeping the Reynolds number and Mach number same in both.

Various dependent and independent parameters in a cascade test are given in the following functional relation:

$\eta, C_D, C_L, \xi, Y = f(\text{Re}, M, \frac{s}{l}, \frac{h}{l}, i,$ blade profile and geometry, entry boundary layer and degree of turbulence) (7.51)

where

$$C_D = \frac{D}{\frac{1}{2}\rho Ac^2}$$

$$C_L = \frac{L}{\frac{1}{2}\rho Ac^2}$$

$$\xi = \frac{\Delta h}{\frac{1}{2}c^2}$$

$$Y = \frac{\Delta p_o}{\frac{1}{2}\rho c^2}$$

A great advantage of cascade tests is that inexpensive and convenient tests can be performed to predict very closely the performance of a given blade ring without actually "building it in metal". For example, low-speed cold air tests on wooden cascades are widely used as a tool for performance prediction of turbine and compressor blade rows.

The performance of cascades is further discussed in Chapter 8.

Notation for Chapter 7

a	Velocity of sound
A	Area, area of cross-section
c	Fluid or gas velocity
c_p	Specific heat at constant pressure
C	Coefficients
D	Rotor diameter or drag
F	Force
g	Acceleration due to gravity
h	Blade height, enthalpy

H	Head
k	Defined in Eq. (7.1)
K	Bulk modulus
l	Blade chord, length parameter
L	Dimension of length, lift
m	Mass-flow rate, number of primary dimensions
M	Dimension of mass, Mach number
n	Number of variables
N	Rotational speed
p	Pressure
Δp	Pressure difference
Δp_0	Stagnation pressure loss or difference
p_r	Pressure ratio
P	Power
Q	Volume flow rate
R	Gas constant
Re	Reynolds number
s	Blade pitch
t	Blade thickness
T	Temperature
ΔT	Temperature difference
u	Peripheral speed of the rotor blades
Δw	Specific work
x	Independent variables
y	Dependent variables
Y	Loss coefficient based on stagnation pressure loss

Greek Symbols

β	Blade angles
θ	Dimension of temperature
η	Efficiency
μ	Dynamic viscosity
ξ	Loss coefficient based on enthalpy loss
π	π-terms or their numbers
$\phi = \frac{c_x}{u}$	Flow coefficient
ψ	Loading or pressure coefficient
ρ	Density
$\gamma = c_p/c_v$	Ratio of specific heats
ν	Kinematic viscosity

ω	Rotational speed in radians
Ω	Specific speed corresponding to ω in rad/s

Subscripts

1	At entry
o	Stagnation values
b	Blade
D	Drag
L	lift
P	Pump
r	radial
s	Isentropic or specific speed
T	Turbine
x	Axial direction
y	Tangential, peripheral or circumferential direction

Solved Examples

7.1 Explain what is meant by the specific speed of a turbomachine. Derive expressions for the specific speed based on power and flow rate respectively. Calculate the specific speeds in the following cases:

(a) A 2000 kW gas turbine running at 16000 rpm for which the entry and exit conditions of the gas are:

$$T_1 = 1000 \text{ K}, \; p_1 = 50 \text{ bar and } p_2 = 25 \text{ bar.}$$

Take $c_p = 1.15$ kJ/kg K, $\gamma = 1.3$.

(b) A centrifugal compressor which develops a pressure ratio of 2.0 while running at 24000 rpm and discharging 1.5 kg/s of air.

(c) An axial compressor stage developing a pressure ratio of 1.4 and discharging 15 kg/s of air while running at 6000 rpm.

The entry conditions for both the centrifugal and axial compressor are:

$$p_1 = 1 \text{ bar and } T_1 = 300 \text{ K}$$

***Solution*:**

(a)

$$\omega = 2\pi N/60 = \frac{2\pi \times 16000}{60} = 1675.5 \text{ rad/s}$$

$$R = \frac{\gamma - 1}{\gamma} c_p = \frac{1.3 - 1}{1.3} \times 1.15 = 0.265 \text{ kJ/kg K}$$

$$\rho_1 = \frac{p_1}{RT_1}$$

$$\rho_1 = 50 \times 10^5/265 \times 1000 = 18.86 \text{ kg/m}^3$$

$$\Delta h_{os} \approx c_p (T_1 - T_{2s}) = c_p T_1 \left\{1 - \left(\frac{p_2}{p_1}\right)^{\frac{\gamma-1}{\gamma}}\right\}$$

$$\Delta h_{os} = 1150 \times 1000 \ (1 - 0.5^{0.23}) = 1.69 \times 10^5 \text{ J/kg}$$

$$\Omega = \omega \sqrt{\frac{P}{\rho}} \ (gH)^{-5/4}$$

Here $gH \equiv \Delta h_{os}$. Therefore,

$$\Omega = 1675.5 \sqrt{\frac{2000 \times 1000}{18.86}} \ (169000)^{-5/4}$$

$$\Omega = 0.159 \ (Ans.)$$

(b) For air $\gamma = 1.4$, $R = 287$ J/kg K, $c_p = 1.005$ kJ/kg K

$$\rho_1 = p_1 / RT_1 = 1 \times 10^5 / 287 \times 300 = 1.16 \text{ kg/m}^3$$

The flow rate at the entry is

$$Q = \dot{m}/\rho_1 = 1.5/1.16 = 1.293 \text{ m}^3/\text{s}$$

$$\omega = 2\pi N/60 = 2\pi \times 24000/60 = 2513.2 \text{ rad/s}$$

$$\Delta h_{os} \approx c_p (T_2 - T_1) = c_p T_1 \left\{\left(\frac{p_2}{p_1}\right)^{\frac{\gamma-1}{\gamma}} - 1\right\}$$

$$\Delta h_{os} \approx 1005 \times 300 \ (2^{0.286} - 1) = 66028.5 \text{ J/kg}$$

$$\Omega = \frac{\omega Q^{1/2}}{(gH)^{3/4}}$$

$$\Omega = 2513.2 \ \sqrt{1.293} \ /(66028.5)^{0.75}$$

$$\Omega = 0.693 \text{ (Ans.)}$$

(c)

$$Q = 15/1.16 = 12.93 \text{ m}^3/\text{s}$$

$$\omega = 2\pi \times 6000/60 = 628.3 \text{ rad/s}$$

$$\Delta h_{os} = 1005 \times 300 \ (1.4^{0.286} - 1) = 30451 \text{ J/kg}$$

$$\Omega = 628.3 \ \sqrt{12.93} \ /(30451)^{0.75}$$

$$\Omega = 0.980 \ (Ans.)$$

7.2 A fan delivers $2\text{m}^3/\text{s}$ (at 10 mm W.G.) of air while running at 1470 rpm. Determine the discharge of a geometrically similar blower

which runs at 360 rpm developing the same head. What is the specific speed of these fans?

***Solution*:**

For the first fan

$$\omega_1 = 2\pi N_1 = 2\pi \times 1470/60 = 153.94 \text{ rad/s}$$

Taking density of air as 1.25 kg/m^3, the air head is

$$H = \frac{1000}{1.25} \times \frac{1}{100} = 8 \text{ m}$$

$$\Omega = \omega \sqrt{Q} / (gH)^{0.75}$$

$$\Omega = 153.94 \sqrt{2} / (9.81 \times 8)^{0.75}$$

$$\Omega = 8.26 \ (Ans.)$$

For the same specific speed of two geometrically similar fans,

$$\frac{N_1 Q_1^{1/2}}{(gH)^{0.75}} = \frac{N_2 Q_2^{1/2}}{(gH)^{0.75}}$$

$$Q_2 = \left(\frac{N_1}{N_2}\right)^2 Q_1 = \left(\frac{1470}{360}\right)^2 \times 2$$

$$Q_2 = 33.35 \text{ m}^3/\text{s} \ (Ans.)$$

7.3 A small compressor has the following data:

Air flow rate	= 1.5778 kg/s
Pressure ratio	= 1.6
Rotational speed	= 54,000 rpm
Efficiency	= 85%

State of air at entry : p_{01} = 1.008 bar, T_{01} = 300 K

$$c_p = 1.009 \text{ kJ/kg K}$$

(a) Calculate the power required to drive this compressor.

(b) A geometrically similar compressor of three times this size is constructed. Determine for this compressor **(i)** speed **(ii)** mass flow rate **(iii)** pressure ratio and **(iv)** the power required. Assume same entry conditions and efficiency for the two compressors.

***Solution*:**

Assume kinematic and dynamic similarities between the two machines. Let subscripts 1 and 2 represent the small and large compressors respectively.

(a) Actual enthalpy rise through the compressor

$$\Delta h_{01} = c_p\,(T_{02} - T_{01})$$

$$= c_p\,\frac{T_{01}}{\eta_c}\left\{\left(\frac{p_{02}}{p_{01}}\right)^{(\gamma-1)/\gamma} - 1\right\}$$

$$= 1.009 \times \frac{300}{0.85}\,(1.6^{0.286} - 1) = 51.20 \text{ kJ/kg}$$

$$\text{Power} = \dot{m}_1\,\Delta h_{01}$$

$$= 1.5778 \times 51.20$$

$$= 80.78 \text{ kW} \qquad (\textit{Ans.})$$

(b)
$$\pi_2 = \frac{N_2\,D_2}{\sqrt{\gamma_2\,R_2\,T_{01}}} = \frac{N_1\,D_1}{\sqrt{\gamma_1\,R_1\,T_{01}}}$$

For the same working fluid $\gamma_1 = \gamma_2$, $R_1 = R_2$

Therefore, $N_2\,D_2 = N_1\,D_1$

$$N_2 = \frac{D_1}{D_2} \times N_1$$

Now $D_2 = 3D_1$

Therefore, $N_2 = \frac{1}{3}\,N_1 = \frac{1}{3} \times 54{,}000 = 18{,}000$ rpm (*Ans.*)

$$\pi_4 = \frac{\dot{m}_2\sqrt{R_2\,T_{01}}}{p_{01}\,D_2^2} = \frac{\dot{m}_1\sqrt{R_1\,T_{01}}}{p_{01}\,D_1^2}$$

for the same entry conditions in the two machines,
For the same working fluid, $R_2 = R_1$

Therefore, $\dot{m}_2 = \left(\frac{D_2}{D_1}\right)^2 \dot{m}_1$

$$\dot{m}_2 = 3^2 \times 1.5778 = 14.20 \text{ kg/s} \ (\textit{Ans.})$$

We also have for the two compressors

$$\frac{\Delta h_{02}}{(N_2\,D_2)^2} = \frac{\Delta h_{01}}{(N_1\,D_1)^2}$$

$$\Delta h_{02} = \left(\frac{N_2}{N_1} \times \frac{D_2}{D_1}\right)^2 \times \Delta h_{01}$$

$$= \left(\frac{18{,}000}{54{,}000} \times 3\right)^2 \times \Delta h_{01}$$

$$\Delta h_{02} = \Delta h_{01}$$

For the same efficiency $\eta_c = 0.85$

$$\Delta h_{0s2} = \Delta h_{0s1} = f(p_{r0})$$

Therefore, the pressure ratio of the large compressor is also 1.6.

$$\pi_5 = \frac{P_2}{\rho_{01} N_2^3 D_2^5} = \frac{P_1}{\rho_{01} N_1^3 D_1^5}$$

$$P_2 = \left(\frac{N_2}{N_1}\right)^3 \times \left(\frac{D_2}{D_1}\right)^5 \times P_1$$

$$= \left(\frac{1}{3}\right)^3 \times 3^5 \times 80.78$$

$$= 9 \times 80.78 = 727.02 \text{ kW } (Ans.)$$

It can also be calculated from —

$$P_2 = \dot{m}_2 \times \Delta h_{02} = \dot{m}_2 \times \Delta h_{01}$$

$$= 14.2 \times 51.20$$

$$= 727.04 \text{ kW (verified)}$$

7.4 A single stage gas turbine is to be designed with the following specifications:

Working gas : $\gamma = 1.33$, $R = 284.1$ J/kg K
Power output = 1.0 MW
Speed = 3000 rpm

Inlet stagnation pressure and temperature

$p_{01} = 2.5$ bar, $T_{01} = 1000$ K

Exit pressure $p_{02} = 1.0$ bar

Efficiency = 87%

(a) Determine the mass flow rate of the gas through this turbine.

(b) A model of this turbine is to be tested in the laboratory with the following parameters:

Size : One – fifth of the prototype
Working fluid : Air, $\gamma = 1.4$, $R = 287$ J/kg K
Inlet conditions : $p_{01} = 2$ bar, $T_{01} = 500$ K,
Enthalpy drop $= \frac{1}{2} \times$ enthalpy drop in the prototype

Determine for this model **(i)** speed **(ii)** mass flow rate **(iii)** power developed and **(iv)** the pressure ratio required.

Solution:

(a) For the gas $\dfrac{\gamma}{\gamma-1} = 4.0303 = \dfrac{1}{0.2481}$, $c_p = 1.145$ kJ/kg K

$$P_1 = \dot{m}_1\, c_p\, \eta\, (T_{01} - T_{02})$$

$$= \dot{m}_1\, c_p\, T_{01}\, \eta \left\{1 - \left(\frac{1}{p_{r0}}\right)^{(\gamma-1)/\gamma}\right\}$$

$$1000 = \dot{m}_1 \times 1.145 \times 1000 \times 0.87\,(1 - 2.5^{-.2481}) = 202.5\ \dot{m}_1$$

$$\dot{m}_1 = 4.938 \text{ kg/s Ans.}$$

(i) Let subscripts 1 and 2 refer to the prototype and the model.

$$\pi_1 = \frac{(\Delta h_0)_1}{N_1^2\, D_1^2} = \frac{(\Delta h_0)_2}{N_2^2\, D_2^2}$$

$$N_2 = \sqrt{\frac{(\Delta h_0)_2}{(\Delta h_0)_1}} \times \frac{D_1}{D_2} \times N_1$$

$$N_2 = \sqrt{\frac{1}{2}} \times 5 \times 3000 = 10{,}606.6 \text{ rpm} \qquad (Ans.)$$

(ii)
$$\pi_4 = \frac{\sqrt{R_1}}{D_1^2}\frac{\dot{m}_1\sqrt{T_{01}}}{p_{01}} = \frac{\sqrt{R_2}}{D_2^2}\frac{\dot{m}_2\sqrt{T_{01}}}{p_{02}}$$

$$\dot{m}_2 = \left(\frac{D_2}{D_1}\right)^2 \times \left(\frac{R_1}{R_2}\right)^{1/2} \times \left(\frac{T_{01}}{T_{02}}\right)^{1/2} \times \frac{p_{02}}{p_{01}} \times \dot{m}_1$$

$$= \left(\frac{1}{5}\right)^2 \times \left(\frac{284.1}{287}\right)^{1/2} \times \left(\frac{1000}{500}\right)^{1/2} \times \frac{2}{2.5} \times 4.938$$

$$\dot{m}_2 = 0.2223 \text{ kg/s} \qquad (Ans.)$$

(iii) $(\Delta h_0)_1 = 202.5$ kJ/kg

$$(\Delta h_0)_2 = \left(\frac{1}{2}\right)(202.5) = 101.25 \text{ kJ/kg}$$

$$P_2 = \dot{m}_2\, (\Delta h_0)_2$$

$$P_2 = 0.2223 \times 101.25 = 22.5 \text{ kW}$$

This can also be calculated from

$$\pi_5 = \left(\frac{P_1}{\rho_{01}\, N_1^3\, D_1^5}\right) = \left(\frac{P_2}{\rho_{02}\, N_2^3\, D_2^5}\right)$$

(iv) For the model, $\left(\frac{\gamma-1}{\gamma}\right) = \left(\frac{1.4-1}{1.4}\right) = 0.2857,$

$$c_p = 1.0045 \text{ kJ/kgK}$$

$$(\Delta h_0)_2 = c_p\,(T_{02} - T_{01}) = c_p\,T_{01}\left(1 - \frac{1}{p_{r0}^{.2857}}\right)$$

Substituting the values we get

$$1.0045 \times 500\,(1 - p_{ro}{}^{-0.2857}) = 101.25$$

$$p_{ro} = 2.2 \qquad (Ans.)$$

7.5 Develop the following equation for the performance of a turbo-compressor:

$$\frac{p_{02}}{p_{01}} = f\left(\frac{\dot{m}\sqrt{T_{01}}}{p_{01}}, \frac{N}{\sqrt{T_{01}}}\right)$$

Symbols used have their usual meanings.

***Solution*:**

Let the exit pressure of the compressor be expressed by the following equation:

$$p_{02} = f\,(p_{01},\ \dot{m},\ \rho_{01},\ N,\ D) \tag{1}$$

$$p_{02} = (\text{constant})\,(p_{01}{}^a \times \dot{m}^b \times \rho_{01}{}^c \times N^d \times D^e) \tag{2}$$

Substitution of the dimensions on the two sides gives

$$ML^{-1}T^{-2} = (\text{constant}) \times (ML^{-1}T^{-2})^a \times (MT^{-1})^b \times (ML^{-3})^c \times (T^{-1})^d \times L^e \tag{3}$$

Equating the indices of M, L and T on the two sides we get

$$1 = a + b + c$$

$$-1 = -a - 3c + e$$

$$-2 = -2a - b - d$$

Above equations yield

$$c = 1 - a - b \tag{4}$$

$$d = 2 - 2a - b \tag{5}$$

$$e = 2 - 2a - 3b \tag{6}$$

Substitution for the indices c, d and e in Eq.2 yields

$$p_{02} = (\text{constant})\,p_{01}{}^a \times \dot{m}^b \times \rho_{01}^{1-a-b} \times N^{2-2a-b} \times D^{2-2a-3b}$$

$$p_{02} = (\text{constant})\, p_{01}{}^{a} \times \dot{m}^{b} \times \frac{\rho_{01}}{\rho_{01}^{a}\, \rho_{01}^{b}} \times \frac{N^2}{N^{2a}\, N^{b}} \times \frac{D^2}{D^{2a}\, D^{3b}}$$

$$p_{02} = (\text{constant}) \times \left(\frac{p_{01}}{\rho_{01}\, N^2 D^2}\right)^{a} \times \left(\frac{\dot{m}}{\rho_{01}\, ND^3}\right)^{b} \times \rho_{01}\, N^2\, D^2$$

Dividing by p_{01} on both sides and simplifying

$$\frac{p_{02}}{p_{01}} = \text{constant} \times \left(\frac{p_{01}}{\rho_{01}\, N^2\, D^2}\right)^{a-1} \times \left(\frac{\dot{m}}{\rho_{01}\, ND^3}\right)^{b}$$

Therefore,

$$\frac{p_{02}}{p_{01}} = f\left(\frac{p_{01}}{\rho_{01}\, N^2\, D^2}, \frac{\dot{m}}{\rho_{01}\, ND^3}\right) \tag{7}$$

Now $\rho_{01} = \dfrac{p_{01}}{RT_{01}}$

Therefore, $\dfrac{p_{01}}{\rho_{01}\, N^2\, D^2} = \dfrac{RT_{01}}{N^2 D^2} = \dfrac{R}{D^2}\left(\dfrac{\sqrt{T_{01}}}{N}\right)^2$ (8)

For the same machine and gas $\dfrac{R}{D^2} = \text{constant}$

Therefore, $\dfrac{p_{01}}{\rho_{01}\, N^2 D^2} = \text{constant} \times \left(\dfrac{\sqrt{T_{01}}}{N}\right)^2$

Or $\dfrac{p_{01}}{\rho_{01}\, N^2 D^2} = \dfrac{\text{constant}}{(N/\sqrt{T_{01}})^2}$

This yields

$$\frac{p_{01}}{\rho_{01}\, N^2 D^2} = f\left(\frac{N}{\sqrt{T_{01}}}\right) \tag{9}$$

Similar procedure is adopted for the second term (in Eq. 7) also. Let

$$\pi_3 = \frac{\dot{m}}{\rho_{01}\, ND^3} = \frac{RT_{01}\, \dot{m}}{p_{01}\, ND^3} = \frac{\dot{m} R \sqrt{T_{01}}}{p_{01} D^3} \times \frac{\sqrt{T_{01}}}{N} \tag{10}$$

$$\pi_3 = \left(\frac{R}{D^3}\right) \times \left(\frac{1}{N/\sqrt{T_{01}}}\right) \frac{\dot{m}\sqrt{T_{01}}}{p_{01}} \tag{11}$$

For the same machine and gas $\frac{R}{D^3}$ = constant

Therefore, π_3 = constant $\times \frac{1}{N/\sqrt{T_{01}}} \times \frac{\dot{m}\sqrt{T_{01}}}{p_{01}}$

$$\frac{\dot{m}}{\rho_{01} N D^3} = f\left(\frac{N}{\sqrt{T_{01}}}, \frac{\dot{m}\sqrt{T_{01}}}{p_{01}}\right) \tag{12}$$

Substituting from equation (9) and (12) in Eq. 7 we get

$$\frac{p_{02}}{p_{01}} = f\left(\frac{N}{\sqrt{T_{01}}}, \frac{\dot{m}\sqrt{T_{01}}}{p_{01}}\right) \tag{13}$$

Note that the term $N/\sqrt{T_{01}}$ need not be repeated in equation 13 while substituting from equations 9 and 12.

Questions and Problems

7.1 What is Buckingham's π-theorem?

How many new dimensionless numbers can be formed from the variables occurring in the following relation for a turbine blade row:

$$C_D,\ C_L,\ \psi = f(N,\ D,\ M,\ \rho_1,\ \nu)$$

7.2 What are geometric, kinematic and dynamic similarities? State two governing parameters for each kind of similarity.

7.3 Determine the specific speeds of the following machines:

(a) A centrifugal air compressor

p_1 = 1 bar, t_1 = 45°C, p_2 = 1.35 bar, N = 29000 rpm,

$\dot{m}$ = 1.00 kg/s

(b) Steam turbine stage

p_1 = 98 bar, t_1 = 450°C, p_2 = 50 bar

N = 3000 rpm, $\dot{m}$ = 300 t/h

(c) Windmill

P = 1.0 kW, N = 96 rpm, Δp = 2 mm W.G.

(Ans.) (a) 1.32 (b) 0.056 (c) 9.1

7.4 What are the different variables involved in determining the performance of axial and centrifugal fans? Develop the dimension-

less parameters that are used to describe the performace of this class of turbomachines. Show graphically typical performance curves for these machines.

7.5 Show that the performance of gas turbines and compressors can be represented by the following dimensionless quantities:

$$\frac{p_{01}}{p_{02}}, \eta = f\left(\frac{\dot{m}\sqrt{T_{01}}}{p_{01}}, \frac{N}{\sqrt{T_{01}}}, \text{Re}, M\right)$$

Further show that:

$$\text{Flow coefficient} \propto \frac{\dot{m}\sqrt{T_{01}}}{p_{01}}$$

$$\text{Blade Mach number} \propto \frac{N}{\sqrt{T_{01}}}$$

7.6 Write down the expression for the dimensionless power coefficient of a turbine stage. Prove that it is proportional to the loading coefficient.

7.7 Show graphically the variation of the following dimensionless parameters:

(a) steam turbine: stage efficiency with blade to steam speed ratio,
(b) air compressor: pressure ratio with mass-flow rate,
(c) rotodynamic hydraulic pump; head with flow rate,
(d) axial flow compressor: efficiency with specific speed, and
(e) backward swept centrifugal blower: pressure coefficient with flow coefficient.

7.8 A turboblower develops 750 mm W.G. at a speed of 1480 rpm and a flow rate of 38 m^3/s. It is desired to build a small model which develops the same head at a higher speed (2940 rpm) and low discharge. Determine the specific speed and the flow rate through the model.

(*Ans.*) $\Omega = 1.42$, $Q = 9.63$ m^3/s

7.9 An inward flow radial turbine develops 238.44 kW with a flow rate of 2.0 kg/s. The density of the working fluid at entry is 2.0 kg/m^3. Rotational speed of the turbine is 30,000 rpm and efficiency 80%. Determine its dimensionless specific speed. (*Ans.*) $\Omega = 0.413$.

7.10 A fan has the following data:

Speed,	$N = 1440$ rpm
Pressure rise,	$\Delta p = 5$ cm W.G.

Flow rate of air,	$Q = 1.5$ m^3/s
Efficiency,	$\eta = 78$ per cent
Inlet pressure,	$p_1 = 1.0$ bar
Inlet temperature,	$T_1 = 290$ K.

(a) Calculate the power required to drive this fan.

(b) If this fan is taken to a high altitude place where the state of air at fan inlet is $p = 0.898$ bar, $T = 282$ K

What is the fan speed, power and volume flow rate for the same pressure rise?

(*Ans.*) (a) 0.9433 kW (b) $N = 1498.5$ rpm,
$P = 0.9815$ kW, $Q = 1.5609$ m^3/s

Chapter 8

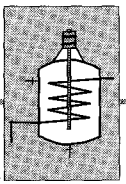

Flow Through Cascades

A row of blades representing the blade ring of an actual turbomachine is called cascade, grid, lattice or a mesh of blades. In a straight or "rectilinear cascade" the blades are arranged in a straight line. The blades can also be arranged in an annulus, thus representing an actual blade row. This arrangement is known as an "annular cascade" and is closer to the real-life situation. The aforementioned arrangements are employed for the cascades of axial-flow turbomachines.

When the flow through the ring of blades is in the radial direction (inward or outward), the arrangement is known as a radial cascade.

Before studying a particular turbine, compressor or fan stage, it will be useful to study the behaviour of flow through the blade rows of such machines. As far as such study is concerned, it is immaterial whether the flow occurs over a row of stationary blades (absolute flow) or moving blades (relative flow). The quantities that matter are flow parameters and the geometry of blade rows. Models of flows in actual machines can be constructed in stationary rows of blades (cascades) by maintaining the geometric, kinematic and dynamic similarities as far as possible.

This chapter acquaints the reader with the geometry of the individual blades and blade rows of different types of turbomachines. The main forces, viz., lift and drag, tangential and axial, that act on the blades are discussed. Some methods of studying the flow and loss mechanism and their measurement are also given.

The treatment also highlights the differences between the flows in axial and radial machines on the one hand and accelerating and decelerating flow in turbines and compressors on the other.

8.1 Two-dimensional Flow

The flow properties in a one-dimensional flow model are assumed uniform all over the entry and exit planes of the cascade. Variations in flow parameters occur only in the streamwise direction between the entry and exit planes. For such a flow only a single velocity triangle at the entry or exit represents the flow at that section. It will be observed in later sections that the assumption of one-dimensional flow in a cascade is an

over simplification of the actual flow problem. However, it is frequently employed for obtaining quick and approximate solutions of tedious problems.

The velocity (c_2) and angle (direction α_2) profiles at the exit of a cascade with one-dimensional flow are shown in Fig. 8.1 They are constant in the tangential or pitch-wise direction.

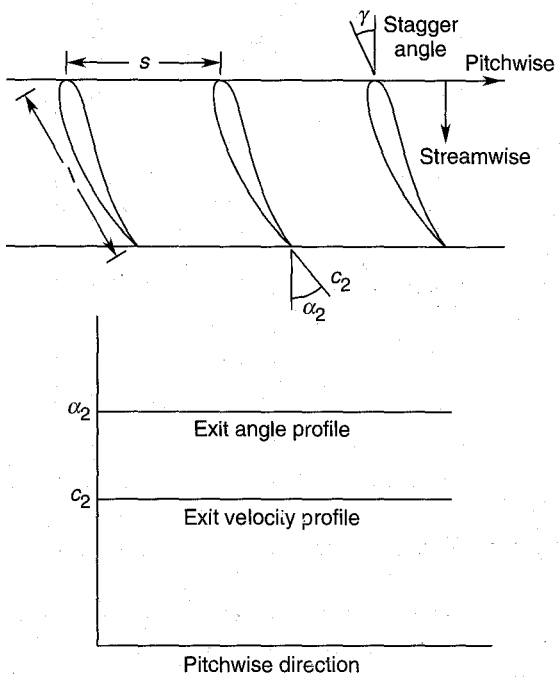

Fig. 8.1 One-dimensional flow through a cascade

The boundary layer growth on the suction and pressure sides of the blades in a real flow leads to the formation of low energy regions in the exit flow field. These are distinct separate lanes of chaotic flow with considerably low fluid velocities and the presence of vortices. These lanes are referred to as "blade wakes". The fluid velocity rises from the wake regions to a maximum in the free stream.

The exit flow angle is affected by the spacing or pitch-chord ratio and the nature of the flow. The wake flow and boundary layer separation (especially on the suction side) also considerably affect the exit angle.

The above mentioned flow phenomena distort the one-dimensional model to a flow in which there are pitchwise variations also besides the streamwise variations. Such a model is called "two-dimensional" flow model. Figure 8.2 depicts the velocity and angle profiles in the

two-dimensional flow at the exit of a cascade. In two-dimensional flow these profiles remain constant at all blade heights. The difference between Figs. 8.1 and 8.2 may be noted.

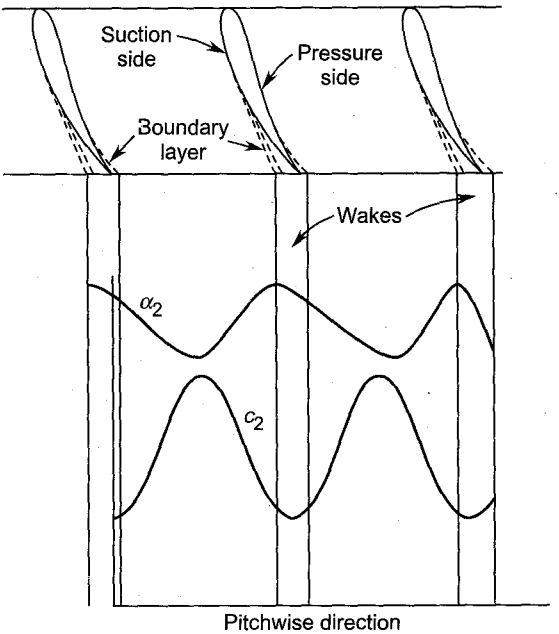

Fig. 8.2 Two-dimensional flow through a cascade

The flow in the blade passages of an actual turbomachine is three-dimensional. This is due to the rotation and growth of the boundary layers on the blade surfaces and the hub and casing of the annulus. However, to reduce a rather complex problem to a simpler one the flow is often assumed to be two-dimensional in which the variations along the blade height are ignored. In other words, such a flow is reduced to two-dimensional plane flow in which the variations in various flow parameters occur only in the streamwise and pitchwise directions.

The flow in the blade rows of axial machines with large hub-tip ratio can be approximated to the two-dimensional flow in a rectilinear cascade. Such a facility is not adequate to provide enough information on the behaviour of flow through blade row of a low hub-tip ratio.

8.2 Cascade of Blades

A cascade is constructed by assemblying a number of blades of a given shape and size at the required pitch(s) and stagger angle (γ). The assembly is then fixed on the test section of a wind tunnel (Fig. 8.3). Air

at slight pressure and near ambient temperature is blown over the cascade of blades to simulate the flow over an actual blade row in a turbomachine.

Information through cascade tests[207, 232, 237] is useful in predicting the performance of blade rows in an actual machine. These tests can also be employed in determining the optimum design of a blade row for prescribed conditions.

Both the wind tunnel[248] and the cascade can be constructed in wood. The cost of such equipment and test thereof is much lower than an actual turbomachine stage (in metal) and its testing. In a blower type of a cascade tunnel (Fig. 8.3) air is discharged into the laboratory without causing any problems to the personnel and equipment.

Blades for a cascade can be manufactured from wood, epoxy resin, glass wool, araldite or aluminium. To reduce the quantity of material and weight blades can be made hollow; this also facilitates the provision of static pressure tubes around their profiles. They can also be made by suitably bending brass, copper or perspex sheets.

If the blades are manufactured from wood, it should be of good quality (preferably teak or deodar) and perfectly seasoned. Sufficient time should be allowed for setting during their manufacture. This allows the blades to dry up and settle to their final shape and size, and minimizes any deformation after the final finish. Wooden blades should be given a hard coating of resin or some other material to make it durable.

Cast aluminium or araldite blades have a good surface finish and do not require any polishing.

Seven or more blades of equal lengths are arranged at the required pitch and stagger and then screwed between the top and bottom planks (ceiling and floor of the cascade). The length AB of the exit of the test section (Fig. 8.3) must be an exact multiple of the blade pitch(s). The inclination of the test section side walls at AB is such that the flow enters the cascade at zero incidence.

8.3 Cascade Tunnel

A wind tunnel is required to blow a jet of air (of uniform properties across the test section) over the cascade of blades. Various types of tunnels can be used for cascade testing depending on the type and range of information required. Figure 8.3 shows a blower type of a cascade tunnel. Its principal parts are the blower, diffuser, settling chamber, contraction cone and test section.

The blower can be either of the axial or centrifugal type. In the axial type (Fig. 8.3) the driving motor can either be kept in the entry duct or outside it. In a large blower the electric motor is more conveniently kept

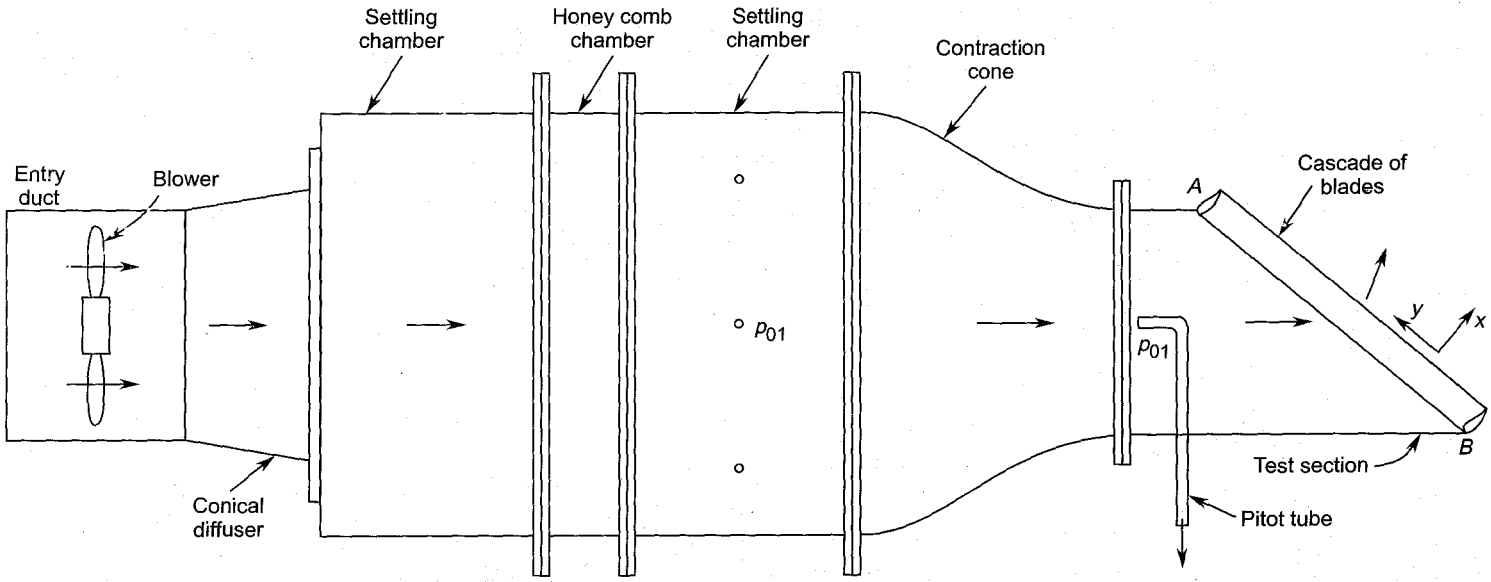

Fig. 8.3 A cascade tunnel

on the floor. It drives the blower through step-up pulleys and belts. This avoids heating up of the entering air and does not restrict the passage of air through the entry duct.

The air from the blower is supplied to the settling chamber through a short diffuser. It is more economical and practical to allow an expansion of the flow from the diffuser exit to the large settling chamber than to provide a long diffuser of a large area ratio.

On account of the large cross-sectional area (about 16 times that of the test section) of the settling chamber, the flow velocity is reduced to a small value. This and the presence of wire gauzes and honeycombs straighten the flow before it is expanded in the contraction cone.

For a rectilinear cascade, the exit of the contraction cone is rectangular or square. Both pairs of contraction walls may either converge simultaneously or the contraction may be achieved in two stages, i.e. by converging the two pairs of walls separately in two stages. This arrangement gives a large overall length. The profiles of the converging walls must be carefully designed to avoid separation and thickening of the boundary layers.

The working or test section receives a uniform stream of air from the contraction. The exit of the test section is oblique, i.e. its top and bottom walls are unequal to receive the cascade of blades in an inclined position.

To obtain a truly two-dimensional flow, a cascade of a large number of long blades is required. This is turn requires a large test section and high flow rates. These conditions are difficult to meet on account of space limitations and economic factors.

In spite of best efforts in designing a perfect contraction,[217, 244] the contraction always pours boundary layers into the test section on its four walls. Figure 8.4 shows the growth of boundary layers on the two side walls of the test section and blade passage. On account of this, the passage through the test section is further contracted leading to increased acceleration of the flow. The boundary layer on the top wall of the test section leads to stalling of flow on the topmost blade at A (Fig. 8.3). To eliminate the presence of boundary layers in the test section and blade passages it can be sucked away through porous walls specially provided for this purpose.

The disturbance in the flow in the central region of the cascade communicated due to the flow distortions at the ends A and B (Fig. 8.3) is minimized by employing a certain minimum number of blades in the cascade. It is found that a cascade of seven blades of aspect ratio (h/l) three is a good compromise.

Figure 8.5 shows a turbine blade cascade (AB) and the test section of a blower tunnel. Various quantities, such as the velocity and direction of flow are measured before and after the central region of the cascade as shown. The central blade is instrumented.

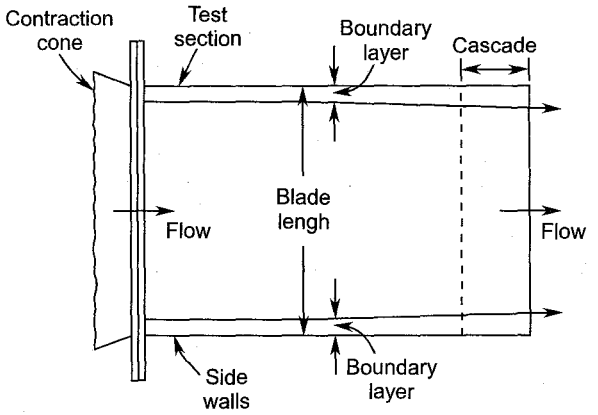

Fig. 8.4 Development of boundary layer in the test section and blade passage

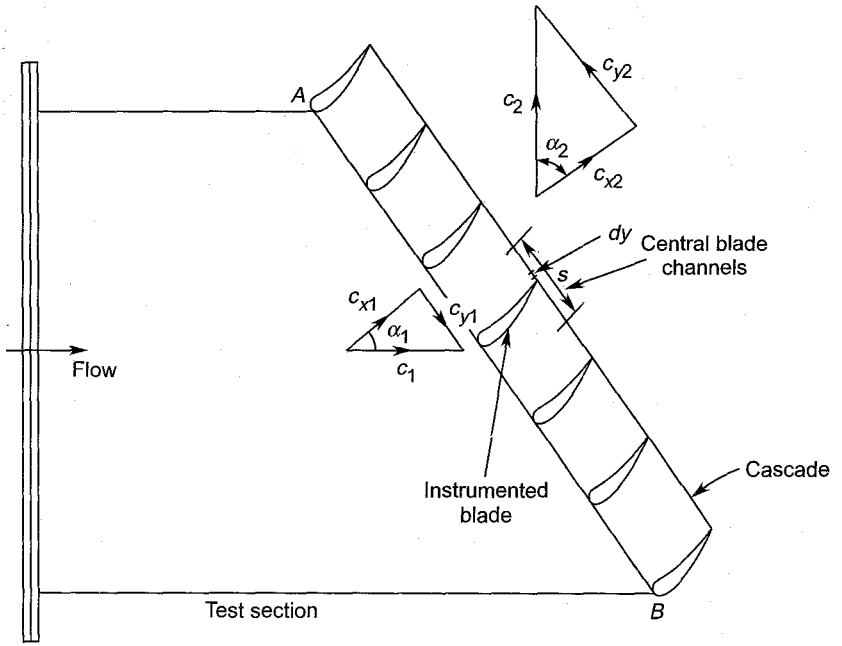

Fig. 8.5 A cascade of turbine blades

8.3.1 Measurement of Static Pressure Distribution

Figure 8.6 shows as instrumented blade. Hypodermic tubes are provided at various sections along the suction and pressure sides of the blade surface. They are closed at one end and run along the whole length of the blade. The tubes are buried inside the slots cut into the blade surface with

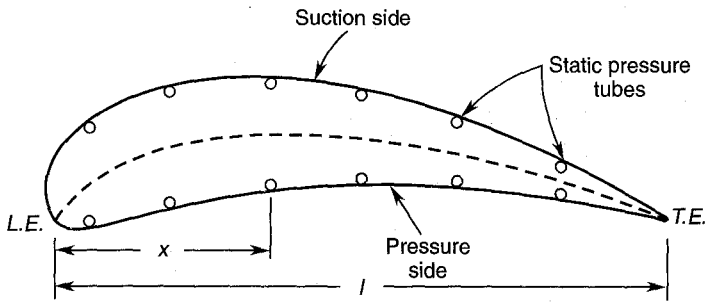

Fig. 8.6 An instrumented blade

their static holes flush with the local surface. The open ends of these tubes project out through one of the side walls of the test section. Local static pressures on the blade surface are transmitted to the manometer or any other sensitive measuring device through the open ends of the static pressure hypodermic tubes.

A typical static pressure distribution curve for a turbine blade is shown in Fig. 8.7. Local velocities on the suction and pressure sides of the blade can be deduced from this curve. Such information is useful in determining the lift on the blade and the separation point. The optimum geometry and the flow can also be obtained through such tests.

8.3.2 Upstream Traversing

Though it is expected that the flow parameters are uniform in the test section upstream of the cascade, it is preferable to check the variations of these quantities at the mid-section of the blades over at least one blade pitch (s) in the central region.

The stagnation pressure (p_{01}) measured through wall tappings (Fig. 8.3) in the settling chamber is a good reference. The losses from the settling chamber to the test section in the free stream are negligible. Therefore, the stagnation pressure measured by a pitot tube in the test section is almost equal to p_{01}. The measurement of static pressure, temperature velocity and direction is also necessary. This can easily be done by traversing a yaw meter provided with a pitot tube along the cascade (y-direction) as shown in Fig. 8.8. In a majority of cases the static pressure can be measured through a wall tapping in the test section. There is no appreciable change of temperature of the air across the cascade and can therefore be measured at any convenient point.

8.3.3 Downstream Traversing

The side walls of the test section or cascade can be extended by two or three chords to accommodate the direction and pressure measuring

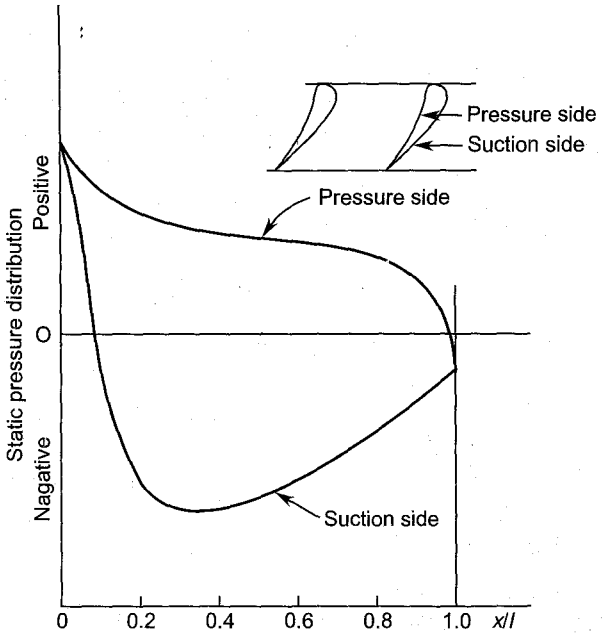

Fig. 8.7 Static pressure distribution around a turbine blade

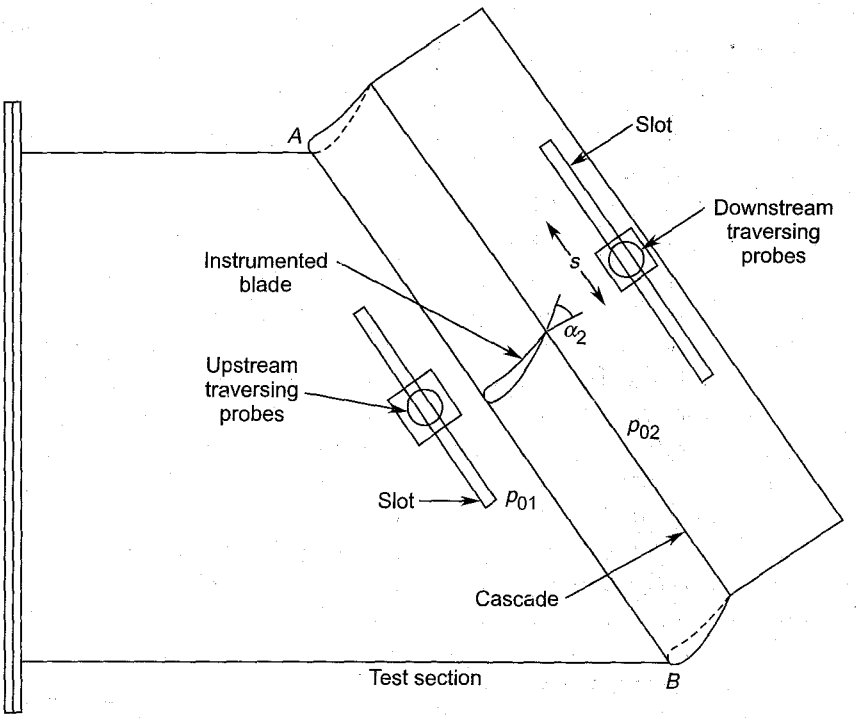

Fig. 8.8 Upstream and downstream traversing stations

instruments downstream of the cascade (Fig. 8.8). The instruments should not be traversed too close to the cascade exit. The slot (in the side wall) for traversing them is so located that their heads are one chord away from the cascade exit. Various parameters are measured at least along one or two blade pitchs as shown.

For low-speed tests ($M < 0.30$) on a blower tunnel the flow can be assumed incompressible. Therefore, the velocity of air can be obtained from the following relations:

$$\rho = p_1/RT_1 \tag{8.1}$$

$$c_1 = \sqrt{2\,(p_{01} - p_1)/\rho} \tag{8.2}$$

$$c_2 = \sqrt{2\,(p_{02} - p_2)/\rho} \tag{8.3}$$

Direction along the cascade is referred to as tangential (y-direction) and normal to it as axial (x-direction), as shown. The velocity triangles at the entry and exit of the cascade show the axial and tangential components of velocities. These are

$$\left.\begin{aligned} c_{x1} &= c_1 \cos\alpha_1 \\ c_{y1} &= c_1 \sin\alpha_1 \end{aligned}\right\} \tag{8.4}$$

$$\left.\begin{aligned} c_{x2} &= c_2 \cos\alpha_2 \\ c_{y2} &= c_2 \sin\alpha_2 \end{aligned}\right\} \tag{8.5}$$

8.3.4 Cascade Performance

The purpose of blade rows in turbomachines is to deflect the flow through desired angles. For a given entry angle, the deflection depends on the air or gas angle at the exit. This is not the same as the blade exit angle and varies along the pitch. The deflection of a real flow in a cascade occurs irreversibly, i.e. with a loss in stagnation pressure and increase in entropy.

Thus the performance of a blade row (cascade) can be obtained by measuring the exit air angle (α_2) and stagnation pressure loss (Δp_0) across it.

On account of the two-dimensional[239] nature of flow in the cascade, both α_2 and p_{02} vary in the tengential direction. Therefore, it is necessary that these values for the whole cascade are integrated into single values. This can be done by mass averaging as follows:

It is assumed that traversing is done at a number of points over one blade pitch length in the tangential direction. Each point represents an elemental distance dy along the cascade. The mass flow rate through this elemental distance dy of unit length is

$$d\dot{m} = \rho c_x dy \tag{8.6}$$

Mass-flow rate over one blade pitch

$$\dot{m} = \int_0^s \rho c_x \, dy \tag{8.7}$$

Tangential momentum of the outgoing jet

$$M_y = \int_0^s c_y \, d\dot{m}$$

Substituting from Eq. (8.6),

$$M_y = \int_0^s \rho c_x c_y \, dy \tag{8.8}$$

Axial momentum is given by

$$M_x = \int_0^s c_x \, d\dot{m}$$

$$M_x = \int_0^s \rho c_x^2 \, dy \tag{8.9}$$

The mean value of the exit air angle of the cascade is obtained from Eqs. (8.8) and (8.9).

$$\tan \bar{\alpha}_2 = \frac{M_y}{M_x}$$

$$\tan \bar{\alpha}_2 = \frac{\int_0^s \rho c_x c_y \, dy}{\int_0^s \rho c_x^2 \, dy} \tag{8.10}$$

The integrated value of the stagnation pressure loss is

$$\Delta \bar{p}_0 = \frac{\int_0^s (p_{01} - p_{02}) \, d\dot{m}}{\int_0^s d\dot{m}} \tag{8.11a}$$

Substituting from Eq. (8.6),

$$\Delta \bar{p}_0 = \frac{\int_0^s (p_{01} - p_{02}) \, \rho c_x \, dy}{\int_0^s \rho c_x \, dy} \tag{8.11b}$$

The upstream stagnation pressure is generally constant along the cascade. Therefore,

$$\Delta \bar{p}_0 = p_{01} - \frac{\int_0^s p_{02}\, \rho c_x\, dy}{\int_0^s \rho c_x dy} \tag{8.12}$$

In one-dimensional flow through the cascade Eqs. (8.10) and (8.12) reduce to

$$\tan \alpha_2 = \frac{c_y}{c_x} \tag{8.13}$$

$$\Delta p_0 = p_{01} - p_{02} \tag{8.14}$$

The values of the stagnation pressure loss in Eq. (8.12) or (8.14) are used to determine the pressure loss coefficient defined in Sec. 7.9.

$$Y = \frac{\Delta p_0}{p_{02} - p_2} = \frac{\Delta p_0}{\frac{1}{2}\rho c_2^2}$$

8.3.5 Cascade Variables

Some dependent and independent parameters for a cascade have been identified in Eq. (7.51) of Sec. 7.9. These are:

η, C_D, C_L, ξ, $Y = f$ (Re, M, s/l, h/l, blade profile and geometry, entry boundary layer, degree of turbulence)

The variation of all these parameters over a wide range in a finite test programme is obviously impossible. In developing the design of a blade row some parameters are fixed by the given conditions and a couple of others can be identified whose effects are marginal. Therefore, the variables involved can be reduced to a more practical and manageable number.

Though theoretical correlations are available for determining the optimum values of the cascade parameters, they are not yet as reliable as the information from the cascade tests. This is why cascade testing equipment and facilities have become almost an inseparable sector of all big companies which design and manufacture various types of turbines, compressors and fans.

Methods of varying the parameters shown on the right hand side of the Eq. (7.51) are briefly described here.

Reynolds number

The Reynolds number $\left(\frac{cl}{\mu/\rho}\right)$ can be varied either by varying the air velocity (c) or changing the length parameter (l) or by varying viscosity

(μ) or density (ρ). Among these, the variation of velocity is most convenient.

This is achieved by one of the following methods:

(a) by changing the speed of the blower;
(b) by throttling the flow at the blower entry; or
(c) by discharging part of the flow into the atmosphere.

If the flow is throttled at the blower entry, care should be exercised that the blower does not operate too near its unstable range of operation.

It is best to operate the blower at constant delivery conditions. Therfore, bypassing part of the blower delivery into the atmosphere is the simplest method. The bypass air should be let out well before the test section, preferably near the exit of the blower.

Mach number

In a conventional open circuit blower tunnel, the change in the Reynolds number (by a change in air velocity) is accompanied by a change in the Mach number ($M = c/a$). Independent variation of the Reynolds number and Mach number can be obtained in variable density tunnels which are not so simple as the blower tunnel.

Pitch-chord ratio

For a fixed blade chord and length of the test section, the pitch-chord ratio (s/l) can be changed by dismantling the cascade and rearranging the blades with a different pitch. For certain values of the pitch, this can disturb the matching between the end blades and the test section top and bottom walls. Continuous variation of the blade pitch without dismantling the cascade would require a very complicated mechanism.

Aspect ratio

The aspect ratio (h/l) of a cascade can be changed either by changing the blade height (length) or its chord. For a fixed geometry, the chord length (l) cannot be changed. Therefore, a variation in the aspect ratio is only achieved by varying the blade height. However, this, for a given test section, cannot be changed without changing or modifying the contraction cone and the test section. This method is very time-consuming and expensive. Therefore, a new method to vary the aspect ratio without major changes has been developed by the author.

Here the side walls of the cascade are extended as shown in Fig. 8.8. Besides these fixed walls, a pair of movable walls (thin planks of wood of the same length and breadth) are also provided which can slide along the length of the cascade as shown in Fig. 8.9. The measurements are still done at the mid-section of the blade. Thus the effective blade length (h) which governs the performance of the cascade can be varied by symmetrically moving the sliding walls towards or away from the mid-section. The

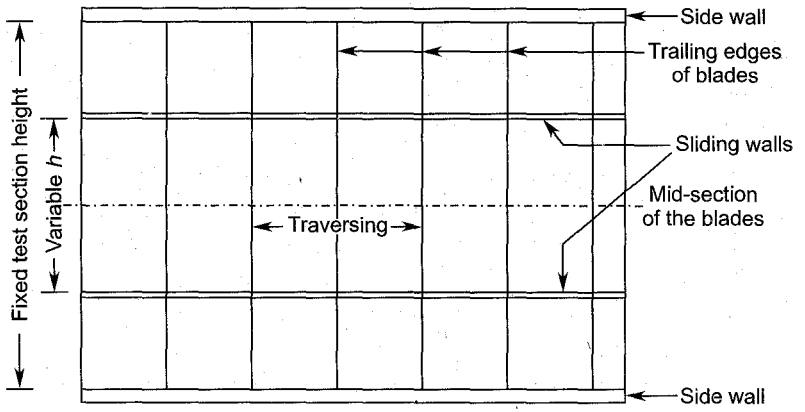

Fig. 8.9 Variable aspect ratio facility

upstream edges of the sliding walls must be sharp-edged to minimize the disturbance in the flow.

Various measuring probes pass through holes cut into the sliding walls.

Blade geometry and profile

Differnet sets of blades are required to study the effect of various blade profiles on the performance. A given set of blades can be tested for various stagger angles (γ) which can be changed without dismantling the cascade. Effects of leading and trailing edge shapes can be studied only small modifications on the same set of blades.

Boundary layer and turbulence

The effect of both the boundary layer and the degree of turbulence at the cascade entry on its performance is significant.

The thickness of the boundary layer can be varied in a number of ways. It can be changed by regulating the suction through porous walls or by varying the length of the test section.

The nature (laminar or turbulent) of the boundary layer is largely governed by the Reynolds number of the flow.

For the same value of the Reynolds number, the separation point on a given blade shows dependence on the degree of turbulence. Higher degrees of turbulence delay the separation. The effect of turbulence on the cascade flow can be studied by introducing turbulence grids (of wire, iron rods or wooden sticks) into the test section. The degree of turbulence can be varied by varying the size of the mesh or the rods, or the distance of the grid from the cascade.

Incidence

All blade rows in turbomachines have to work at some degree of incidence. The design point in a majority of machines does not correspond to zero

incidence. Besides this, the off-design performances of machines are also important because they are sometimes required to operate away from the design point also. Some methods to vary the incidence are given in the following:

(a) The incidence at the blades can be varied by turning them through the desired angle without dismantling the cascade. This is done by pivoting each blade between pins in the side walls and connecting them to a "turning mechanism" outside the cascade on one of the side walls. The mechanism can be locked for a particular position of the cascade.

(b) The degree of incidence can also be changed by introducing (or removing) a pair of wedge-shaped pieces between the side walls of the test section and the cascade. This arrangement is shown in Fig. 8.10.

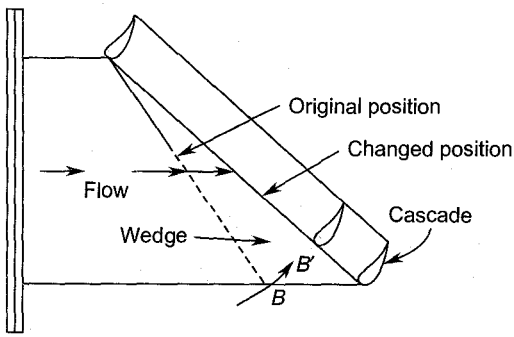

Fig. 8.10 Variation in incidence by wedges

(c) The test section can be extended by providing adjustable top and bottom walls as shown in Fig. 8.11. The cascade is then placed at

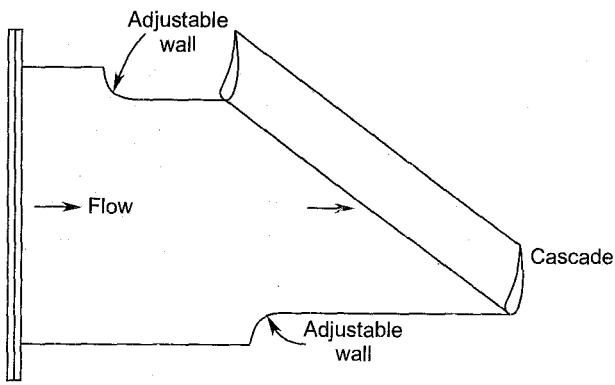

Fig. 8.11 Variation in incidence by adjustable walls

the ends of these walls. In this arrangement the incidence can be varied simply by changing the positions of the sliding walls.

The quality of flow at the cascade entry suffers by adopting this arrangement.

(d) An arrangement of continuously changing the incidence without much disturbance in the flow in shown in Fig. 8.12. The cascade is mounted on a movable box as shown. The upstream edges of the side walls of the box are arc-shaped and rest on the corresponding walls of the test section. The box is mounted on a pivot located above the test section.

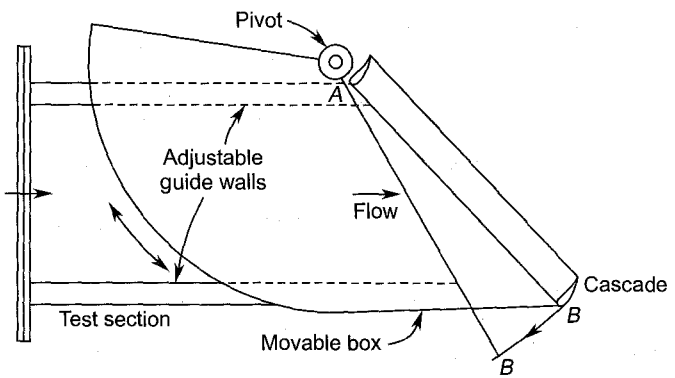

Fig. 8.12 Continuous variation of incidence

When the cascade AB is moved to the new position AB′ the end blades do not match with the top and bottom walls of the test section. A pair of adjustable guide walls is provided to guide the flow in the new position of the cascade.

8.4 Axial Turbine Cascade[219]

The development of the aerofoil-shaped turbomachine blade from simple inclined and curved plates has been discussed in detail in Sec. 6.8. A study of the nature of flow and strength considerations showed that a cambered aerofoil blade of finite thickness meets the requirements in a row of turbomachine blades.

Simple examples of transformation of circles into aerofoils have also been given. Velocity and pressure distributions and the lift and drag forces on such blades have also been briefly discussed.

8.4.1 Nomenclature

The same method is employed to specify the blade sections of axial turbines and compressors. A blade section of infinitesimal thickness is a

curved line known as "camber line" (Fig. 8.13). This forms the backbone line of a blade of finite thickness. Its shape is specified by x-y coordinates which are conventionally presented in the non-dimensional form x/l and y/l as shown in the figure. Thus they are applicable to a blade section of any chord length (l). Maximum camber $(y/l)_{max}$ and its position (a/l) are important properties.

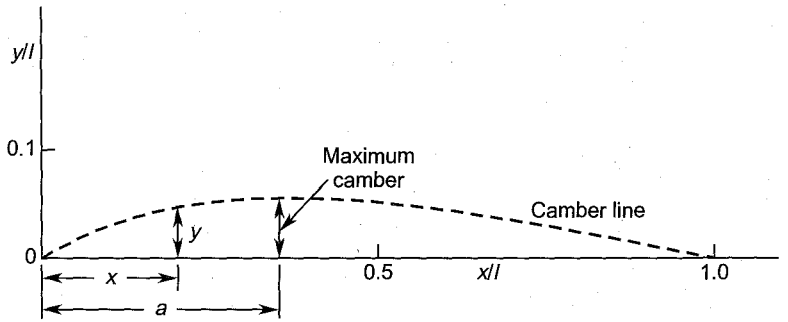

Fig. 8.13 Camber line profile

The shapes or profiles of the upper (suction) and lower (pressure) surfaces of the blades are specified by the thickness distribution along the chord or the camber line. This may be symmetrical or unsymmetrical giving a symmetrical or an unsymmetrical profile. Figure 8.14 shows the base profile of a symmetrical blade. This may be used for an actual curved blade in a cascade.

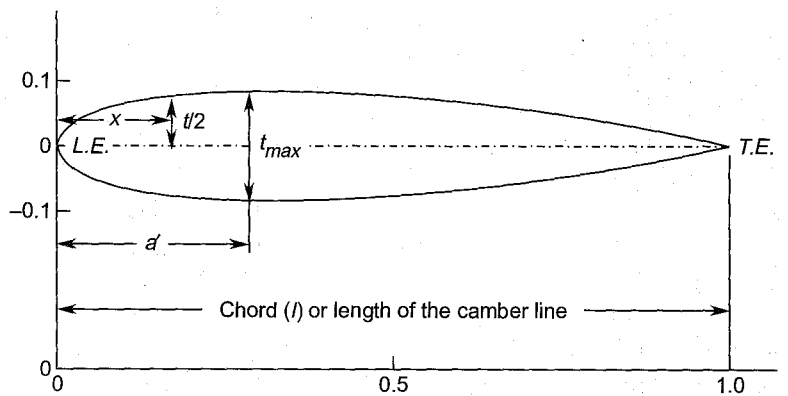

Fig. 8.14 Thickness distribution of an aerofoil (base profile)

The maximum thickness (t_{max}) of the profile and its distance (a') from the leading edge, and the shapes of the leading and trailing edges (L.E. and T.E.) are important parameters which govern the flow pattern and losses.

Appendix B gives the specifications of some turbine blade sections.

Blades of a given shape are arranged in a different manner in the cascades of turbines and compressors. The difference in the geometries is due to the accelerating and decelerating flows in turbine and compressor cascades respectively.

Figure 8.15(a) shows the camber line of a blade in such a way that the chord line coincides with the axial direction. Thus the tangents drawn on the camber line at leading (entry) and trailing (exit) edges form the camber angles χ_1 and χ_2 at the entry and exit. These are also the blade angles from the axial direction which is taken as a reference direction.

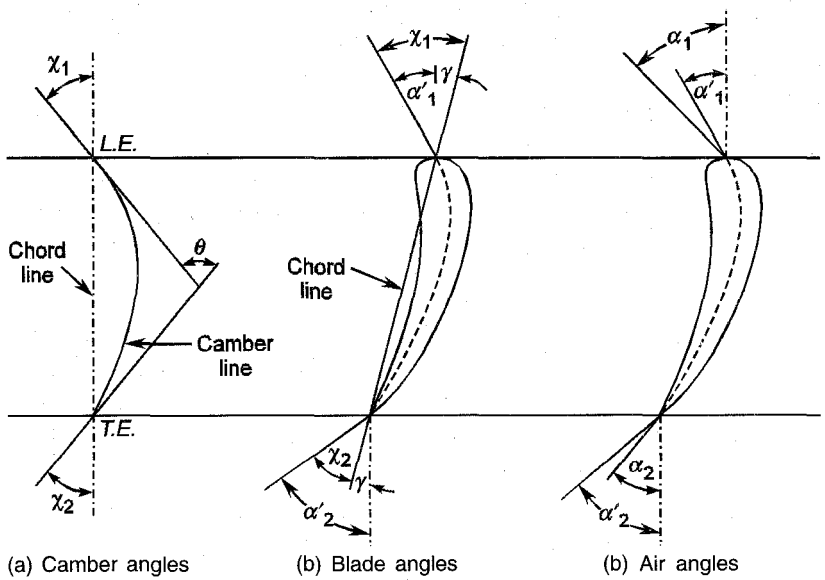

(a) Camber angles (b) Blade angles (b) Air angles

Fig. 8.15 Camber angles, blade angles and air angles

The camber angle (θ) for a given blade is the sum of the camber angles at the entry and exit.

$$\theta = \chi_1 + \chi_2 \tag{8.15}$$

The setting of blades in a turbine cascade is invariably at a stagger angle (γ) i.e. the chord lines of the blades are tilted towards the blade curvature as shown in Fig. (8.15(b)). This changes the blade angles to

$$\alpha_1' = \chi_1 - \gamma \tag{8.16}$$

$$\alpha_2' = \chi_2 + \gamma \tag{8.17}$$

Equations (8.15), (8.16) and (8.17) give

$$\theta = \chi_1 + \chi_2 = \alpha_1' + \alpha_2' \tag{8.18}$$

Figure 8.15(c) depicts the actual angles that the directions of flow make at the entry and exit of the blade. These are known as fluid, gas or air angles and are invariably different from the blade angles α_1' and α_2'.

The air angle at the entry of a cascade differs from its angle α_1' on account of the nature of flow passed on to it by the upstream blade row and the off-design operating conditions. This difference between the air angle and the blade angle is known as angle of incidence i.

$$i = \alpha_1 - \alpha_1' \tag{8.19}$$

The incidence can be positive as well as negative. Flow at a large positive incidence will lead to stalling on the suction side of the blade; this is also referred to as positive stall. Conversely, a large negative incidence is associated with negative stall, i.e. separation of flow on the pressure side of the blade.

In Sec. 8.1 it was pointed out that the actual flow in a cascade is two-dimensional. The air angles at the exit varies along the pitch on account of unequal guidance provided by the blades to the flow and the presence of wakes. Thus the exit air angle at a given point or its mean value differs from the blade angle α_1' at the exit. The difference is referred to as deviation,

$$\delta = \alpha_2' - \alpha_2 \tag{8.20}$$

Deviation in turbine cascade is relatively small. Generally, it is positive [as expressed in Eq. (8.20)] and therefore decreases the energy transfer in a moving row of blades.

Various angles defined here for a turbine cascade are shown in Fig. 8.16.

As stated before, the purpose of blade rows in turbomachines is to deflect the flow. This is measured by the deflection angle defined as the sum of the air angles at the entry and exit.

$$\varepsilon = \alpha_1 + \alpha_2 \tag{8.21}$$

Putting Eqs. (8.19) and (8.20) into Eq. (8.21), we get

$$\varepsilon = (\alpha_1' + i) + (\alpha_2' - \delta)$$

$$\varepsilon = (\alpha_1' + \alpha_2') + (i - \delta) \tag{8.22}$$

From Eq. (8.18)

$$\varepsilon = \theta + i - \delta \tag{8.23}$$

8.4.2 Velocity Triangles

The velocity triangles for one-dimensional flow (far upstream and downstream) at the entry and exit of a blade in a cascade are shown in Fig. 8.17. The velocity vectors c_1 and c_2 at the entry and exit are at air angles α_1 and α_2 respectively.

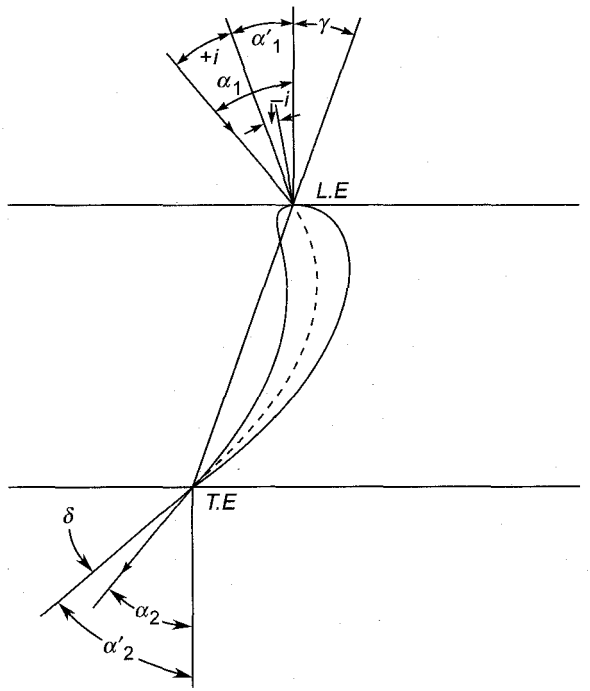

Fig. 8.16 Stagger, incidence and deviation angles

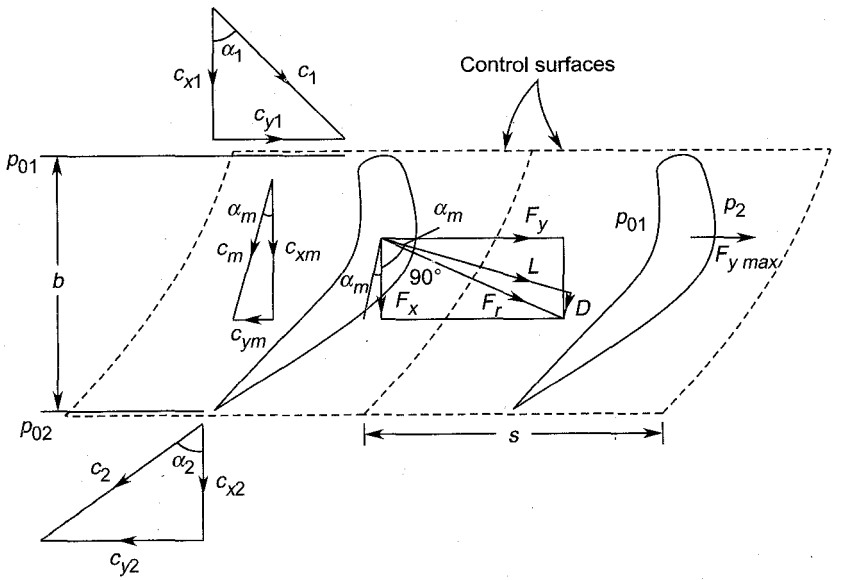

Fig. 8.17 Inlet, outlet and mean velocity triangles, and blade forces (turbine cascade)

A mean velocity triangle for the flow through the cascade is defined by the following quantities:

$$c_{xm} = \frac{1}{2}(c_{x1} + c_{x2}) \tag{8.24}$$

$$c_{ym} = \frac{1}{2}(c_{y2} - c_{y1}) \tag{8.25}$$

$$\tan \alpha_m = c_{ym}/c_{xm} \tag{8.26a}$$

For constant axial velocity,

$$\tan \alpha_m = \frac{1}{2}(\tan \alpha_2 - \tan \alpha_1) \tag{8.26b}$$

8.4.3 Blade Forces

By definitions the drag force is parallel to the direction of the mean velocity c_m and the lift normal to it as shown in Fig. 8.17. The resultant of lift and drag is the force F_r. This has another set of components F_x and F_y in the axial and tangential directions respectively. The aim of a turbine designer is to obtain the maximum value of the tangential force on the cascade with a minimum value of the axial thrust (F_x) and pressure loss Δp_0.

It may be noted that, in a turbine, the forces as shown in Fig. 8.17, are exerted by the fluid on the blade. The blade in turn exerts the same magnitude of forces in the opposite directions.

The entire cascade can be divided by the control surfaces surrounding each blade as shown in Fig. 8.17. Analysis of forces exerted on a blade can then be done by considering the flow through the control surface containing this blade.

Various relations can be written for the unit height of the blade. For simplicity, the axial velocity component and density of air are assumed to be constant across the control surface.

The continuity equation for the control surface gives

$$\dot{m} = \rho_1 c_{x1}\,(s \times 1) = \rho_2 c_{x2}\,(s \times 1)$$

But

$$\rho_1 \approx \rho_2 \approx \rho$$

$$c_{x1} = c_{x2} = c_{xm}$$

Therefore,

$$\dot{m} = \rho s c_{xm} \tag{8.27}$$

Tangential force

The tangential force on the blade is equal to the rate of change of momentum in the tangential direction.

$$F_y = \dot{m}\,\{c_{y2} - (-\,c_{y1})\}$$

$$F_y = \rho s c_{xm}\,(c_{y1} + c_{y2}) \tag{8.28a}$$

From velocity triangles

$$F_y = \rho s c_{xm}^2 (\tan \alpha_1 + \tan \alpha_2) \tag{8.28b}$$

Using exit and mean velocity triangles, the following relations are obtained:

$$F_y = \left(\frac{1}{2} \rho l c_{xm}^2\right) 2 \left(\frac{s}{l}\right) (\tan \alpha_1 + \tan \alpha_2) \tag{8.29}$$

This can be expressed in the form of dimensionless tangential force coefficients.

$$C_{Fy} = \frac{F_y}{\frac{1}{2} \rho l c_{xm}^2} = 2 \left(\frac{s}{l}\right) (\tan \alpha_1 + \tan \alpha_2) \tag{8.30}$$

$$F_y = \left(\frac{1}{2} \rho l c_2^2\right) 2 \left(\frac{s}{l}\right) \cos^2 \alpha_2 (\tan \alpha_1 + \tan \alpha_2) \tag{8.31}$$

$$C'_{Fy} = \frac{F_y}{\frac{1}{2} \rho l c_2^2} = 2 \left(\frac{s}{l}\right) \cos^2 \alpha_2 (\tan \alpha_1 + \tan \alpha_2) \tag{8.32}$$

Axial force

Generally, there is a static pressure drop across a turbine cascade. Therefore, the axial thrust is due to both the pressure difference and change of momentum in the axial direction.

$$F_x = (p_1 - p_2)\, s \times 1 + \rho\, (s \times 1)\, c_{xm}\, (c_{x1} - c_{x2})$$

For incompressible flow,

$$p_1 = p_{01} - \frac{1}{2} \rho c_1^2$$

$$p_2 = p_{02} - \frac{1}{2} \rho c_2^2$$

$$p_1 - p_2 = \frac{1}{2} \rho (c_2^2 - c_1^2) + (p_{01} - p_{02})$$

Substituting this in the expression for F_x, and assuming $c_{x1} = c_{x2}$,

$$F_x = \frac{1}{2} \rho s (c_2^2 - c_1^2) + s\, \Delta p_0$$

From the velocity triangles at the entry and exit

$$c_2^2 - c_1^2 = c_{x2}^2 + c_{y2}^2 - c_{x1}^2 - c_{y1}^2 = c_{y2}^2 - c_{y1}^2$$

$$F_x = \frac{1}{2} \rho s (c_{y2}^2 - c_{y1}^2) + \mathrm{s}\, \Delta p_0$$

$$F_x = \frac{1}{2} \rho s\, c_{xm}^2 (\tan^2 \alpha_2 - \tan^2 \alpha_1) + s\, \Delta p_0 \tag{8.33a}$$

$$F_x = \rho s c_{xm}^2 \frac{1}{2} (\tan \alpha_2 - \tan \alpha_1)(\tan \alpha_2 + \tan \alpha_1) + s \Delta p_0$$

But $\frac{1}{2} (\tan \alpha_2 - \tan \alpha_1) = \tan \alpha_m$, therefore,

$$F_x = \frac{1}{2} \rho s c_{xm}^2 \tan \alpha_m (\tan \alpha_2 + \tan \alpha_1) + s \Delta p_0 \qquad (8.33b)$$

Equation (8.33a) can also be written as

$$F_x = \left(\frac{1}{2} \rho l c_2^2\right)\left(\frac{s}{l}\right) \cos^2 \alpha_2 (\tan^2 \alpha_2 - \tan^2 \alpha_1) + s \Delta p_0 \qquad (8.33c)$$

In the dimensionless form

$$C_{Fx} = \frac{F_x}{\frac{1}{2} \rho l c_2^2} = \frac{s}{l} \cos^2 \alpha_2 (\tan^2 \alpha_2 - \tan^2 \alpha_1) + \frac{s \Delta p_0}{\frac{1}{2} \rho l c_2^2}$$

The pressure loss coefficient for the cascade is defined as

$$Y = \frac{\Delta p_0}{\frac{1}{2} \rho l c_2^2} \qquad \text{(see Sec. 7.9)}$$

Therefore, the axial thrust coefficient is

$$C_{Fx} = \frac{s}{l} \cos^2 \alpha_2 (\tan^2 \alpha_2 - \tan^2 \alpha_1) + \frac{s}{l} Y \qquad (8.34)$$

Lift force

The magnitude of lift can be obtained from the expressions for the forces in the tangential and axial directions. By resolving forces in the direction of lift (Fig. 8.17),

$$L = F_y \cos \alpha_m + F_x \sin \alpha_m$$

Substituting from Eqs. (8.28a) and (8.33b),

$$L = \rho s c_{xm}^2 (\tan \alpha_1 + \tan \alpha_2) \cos \alpha_m + \rho s c_{xm}^2 \tan \alpha_m \times (\tan \alpha_1 + \tan \alpha_2) \sin \alpha_m + s \Delta p_0 \sin \alpha_m$$

$$L = \rho s c_{xm}^2 (\tan \alpha_1 + \tan \alpha_2) \left(\cos \alpha_m + \frac{\sin^2 \alpha_m}{\cos \alpha_m}\right) + s \Delta p_0 \sin \alpha_m$$

$$L = \rho s c_{xm}^2 (\tan \alpha_1 + \tan \alpha_2) \sec \alpha_m + s \Delta p_0 \sin \alpha_m \qquad (8.35a)$$

$$L = \rho s c_m^2 \cos \alpha_m (\tan \alpha_1 + \tan \alpha_2) + s \Delta p_0 \sin \alpha_m \qquad (8.35b)$$

Equation (8.35a) can also be written as

$$L = \rho s c_{xm} \sec \alpha_m (c_{x1} \tan \alpha_1 + c_{x2} \tan \alpha_2) + s \Delta p_0 \sin \alpha_m$$

$$L = \rho s c_m (c_{y1} + c_{y2}) + s \Delta p_0 \sin \alpha_m \qquad (8.35c)$$

The lift force can be expressed in the form of the dimensionless lift coefficient (see Sec. 6.8.2).

From Eq. (8.35b),

$$L = \left(\frac{1}{2}\rho l c_m^2\right) 2 \left(\frac{s}{l}\right) \cos \alpha_m (\tan \alpha_1 + \tan \alpha_2) + s \, \Delta p_0 \sin \alpha_m$$

$$C_L = \frac{L}{\frac{1}{2}\rho l c_m^2} = \left(\frac{s}{l}\right) \cos \alpha_m (\tan \alpha_1 + \tan \alpha_2) + \frac{s}{l} \frac{\Delta p_0}{\frac{1}{2}\rho c_m^2} \sin \alpha_m \tag{8.36}$$

Drag force

The drag force is obtained by resolving the axial and tangential forces in its direction,

$$D = F_x \cos \alpha_m - F_y \sin \alpha_m$$

substituting from Eqs. (8.33b) and (8.28a),

$$D = \rho s c_{xm}^2 \tan \alpha_m (\tan \alpha_1 + \tan \alpha_2) \cos \alpha_m + s \, \Delta p_0 \cos \alpha_m - \rho s c_{xm}^2 (\tan \alpha_1 + \tan \alpha_2) \sin \alpha_m$$

After cancelling the terms,

$$D = s \, \Delta p_0 \cos \alpha_m \tag{8.37}$$

The dimensionless drag coefficient is defined by

$$C_D = \frac{D}{\frac{1}{2}\rho l c_m^2} = \left(\frac{s}{l}\right) \frac{\Delta p_0}{\frac{1}{2}\rho c_m^2} \cos \alpha_m \tag{8.38}$$

Now $c_m \cos \alpha_m = c_2 \cos \alpha_2$. Therefore,

$$\frac{\Delta p_0}{\frac{1}{2}\rho c_m^2} = \frac{\Delta p_0}{\frac{1}{2}\rho c_2^2} \frac{\cos^2 \alpha_m}{\cos^2 \alpha_2}$$

$$\frac{\Delta p_0}{\frac{1}{2}\rho c_m^2} = Y \frac{\cos^2 \alpha_m}{\cos^2 \alpha_2} \tag{8.39}$$

Substitution of Eq. (8.39) in Eq. (8.38) gives

$$C_D = \left(\frac{s}{l}\right) Y \frac{\cos^3 \alpha_m}{\cos^2 \alpha_2} \tag{8.40}$$

Putting Eq. (8.39) into Eq. (8.36), we get

$$C_L = 2 \left(\frac{s}{l}\right) \cos \alpha_m (\tan \alpha_1 + \tan \alpha_2) + \frac{s}{l} Y \frac{\cos^2 \alpha_m}{\cos^2 \alpha_2} \sin \alpha_m$$

Substitution from Eq. (8.40) yields

$$C_L = 2\left(\frac{s}{l}\right)\cos\alpha_m\,(\tan\alpha_1 + \tan\alpha_2) + C_D\tan\alpha_m \tag{8.41}$$

For reversible flow through the cascade

$\Delta p_0 = 0$, $C_D = 0$. Therefore, Eqs. (8.36) and (8.41) reduce to

$$C_L = 2\left(\frac{s}{l}\right)\cos\alpha_m\,(\tan\alpha_1 + \tan\alpha_2) \tag{8.42}$$

Equation (8.35c) for reversible flow gives

$$L = \rho c_m\,(c_{y1}s + c_{y2}s) \tag{8.43}$$

The circulation around the blade contained in the control surface (shown in Fig. 8.17) is the line integral of the velocity around the closed circuit. This is given by

$$\Gamma = c_{y1}s + c_{y2}s \tag{8.44}$$

The line integrals along the two curved branches of the circuit cancel each other.

Equations (8.43) and (8.44) give a well-known relation between the lift and the circulation

$$L = \rho c_m\,\Gamma \tag{8.45}$$

For a cascade of infinite pitch, the blade behaves as an isolated blade and Eq. (8.45) becomes Kutta-Joukowski's relation.

8.4.4 Zweifel's Criterion

Zweifel defines a tangential force coefficient [as in Eq. (8.32)] on the basis of a maximum hypothetical value.

It is assumed that a maximum tangential force on the blade is exerted in a reversible flow ($\Delta p_0 = 0$) when the pressure and suction surfaces of the blade experience uniform static pressures of p_{01} and p_2 respectively. These conditions give (see Fig. 8.17)

$$F_{y\max} = (p_{01} - p_2)\,b$$

For reversible flow,

$$p_{01} - p_2 = p_{02} - p_2 = \frac{1}{2}\rho c_2^2;\ \text{therefore,}$$

$$F_{y\max} = \frac{1}{2}\rho b c_2^2 \tag{8.46}$$

Equations (8.28a) and (8.46) yield

$$C_Z = \frac{F_y}{F_{y\max}} = 2\left(\frac{s}{b}\right)\frac{c_{xm}^2}{c_2^2}\,(\tan\alpha_1 + \tan\alpha_2)$$

For constant axial velocity

$$c_{xm}^2/c_2^2 = c_{x2}^2/c_2^2 = \cos^2\alpha_2$$

Therefore,

$$C_Z = 2\left(\frac{s}{b}\right)\cos^2\alpha_2\,(\tan\alpha_1 + \tan\alpha_2) \qquad (8.47)$$

For small blade chords, the values of the axial and actual chords are almost the same ($b \approx l$). For this condition Eqs. (8.32) and (8.47) are identical.

$$C_Z \approx C_{Fy}$$

On the basis of cascade tests, Zweifel recommends that the coefficient in Eq. (8.47) be approximately 0.80. This criterion has been used to obtain the optimum pitch-chord ratio in turbine blade rows.

8.4.5 Losses

Principal aerodynamic losses occurring in most of the turbomachines arise due to the growth of the boundary layer and its separation on the blade and passage surfaces. Others occur due to wasteful circulatory flows and the formation of shock waves. Non-uniform velocity profiles at the exit of the cascade lead to another type of loss referred to as the mixing or equalization loss.

Aerodynamic losses occurring in a turbine blade cascade [212, 273, 286] can be grouped in the following categories:

(a) *Profile loss*

As the term indicates, this loss is associated with the growth of the boundary layer on the blade profile. Separation of the boundary layer occurs when the adverse pressure gradient on the surface or surfaces becomes too steep; this increases the profile losses. The pattern of the boundary layer growth and its separation depend on the geometries of the blade and the flow. Positive and negative stall losses occur on account of increased positive or negative incidences respectively.

Generally, the suction surface of a blade is more prone to boundary layer separation. The separation point depends, besides the blade profile, on factors like the degree of turbulence, Reynolds number and the incidence.

If the flow is initially supersonic or becomes supersonic on the blade surface, additional losses occur due to the formation of shock waves resulting from the local deceleration of supersonic flow to subsonic.

(b) *Annulus loss*

The majority of blade rows in turbomachines are housed in casings. The axial turbine stage has a pair of fixed and moving blade rows.

In stationary blade rows, a loss of energy occurs due to the growth of the boundary layer on the end walls. This also occurs in the rotating row of blades but the flow on the end walls, in this case, is subjected to effects associated with the rotation of the cascade. The boundary layer on the floor (hub) of the blade passages is subjected to centrifugal force, whereas that on the ceiling (outer casing) is scrapped by the moving blades.

(c) *Secondary loss*

This loss occurs in the regions of flow near the end walls owing to the presence of unwanted circulatory or cross flows. Such secondary flows [208, 212] develop on account of turning of the flow through the blade channel in the presence of annulus wall boundary layers. Figure 8.18 depicts the pressure gradients across a blade channel and the secondary and trailing vortices. Static pressure gradients from the suction to the pressure side in the regions away from the hub and tip are represented by the curve AB. In the vicinity of the hub and tip or the end walls, the pressure gradient curve CD is not so steep on account of much lower

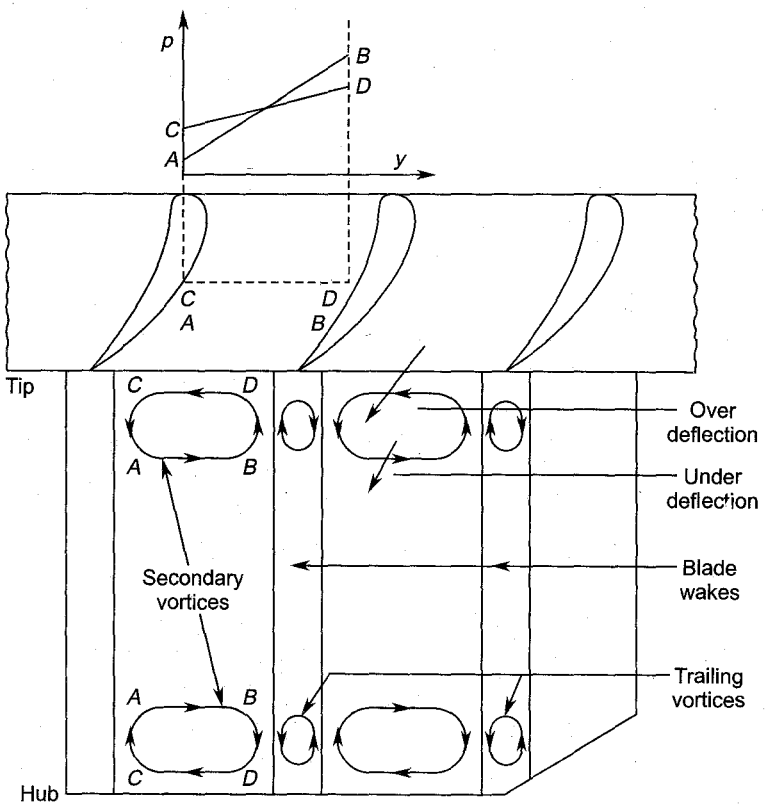

Fig. 8.18 Secondary flow in a cascade of blades

velocities due to the wall boundary layers. Thus the static pressures at the four corners of the section of flow under consideration are

$$p_B > p_D > p_C > p_A$$

These pressure differentials across the flow near the end walls give rise to circulatory flows which are superimposed on the main flow through the blade passage. As a result of this, secondary vortices in the streamwise direction are generated in the blade passages. These vortices, besides wasteful expenditure of fluid's energy, transport (DC) low energy fluid from the pressure to the suction side of the blade passage, thus increasing the possibility of an early separation of the boundary layer on the suction side. The secondary flows also distort the direction of flow in the channel. The flow nearer the hub and tip is over-deflected while that slightly away from the end walls is under-deflected as shown in Fig. 8.18.

The secondary vortices in the adjacent blade channels induce vortices in the wake regions (as shown in Fig. 8.18). These trailing vortices lead to additional losses.

It is worth observing here that the secondary flows in the cascade also affect the profile and annulus losses.

The magnitude of the loss [228, 234] due to secondary flow depends on the fraction of the passage height that is affected by this flow. Blade passages of very low height (aspect ratio) or high hub-tip ratio are likely to be fully occupied by secondary vortices as shown in Fig. 8.19(a), and experience higher secondary losses. In contrast to this longer blades (Fig. 8.19 (b)) have a large proportion of the flow free of secondary flows and therefore experience comparatively lower secondary losses.

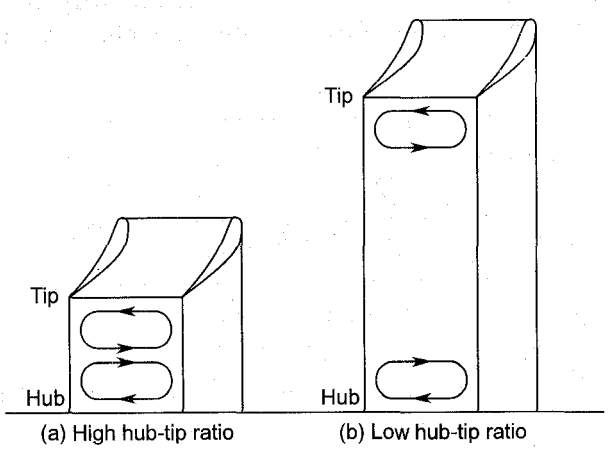

Fig. 8.19 Secondary vortices in short and long blades

If the total losses in a blade passage are measured along its height, they appear as peaks near the hub and tip on account of secondary losses. The flow in the central region which is outside the influence of secondary flows (particularly in longer blades) can be assumed to suffer only profile loss. Figure 8.20 illustrates this pattern of losses along the blade height.

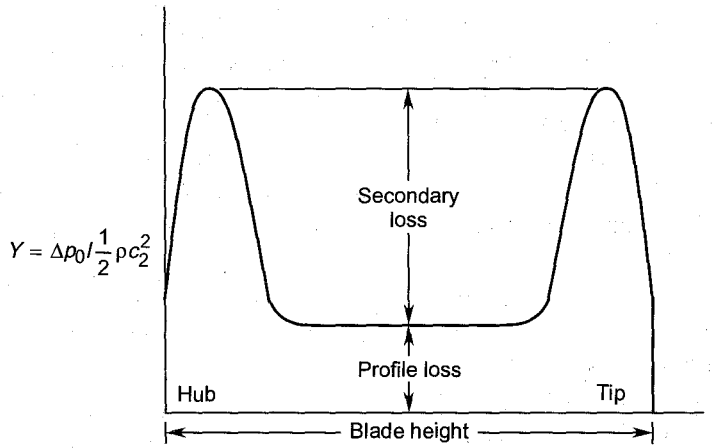

Fig. 8.20 Variation of losses along the blade height

(d) *Tip clearance loss*

This loss arises due to the clearance between a moving blade and the casing. In a turbine rotor blade ring the suction sides lead and the pressure sides trail. On account of the static pressure difference, the flow leaks from the pressure side towards the suction side as shown in Fig. 8.21. However, due to the scrapping up of the casing boundary layer by the blade tips, the scrapped up flow opposes the aforementioned tip leakage.

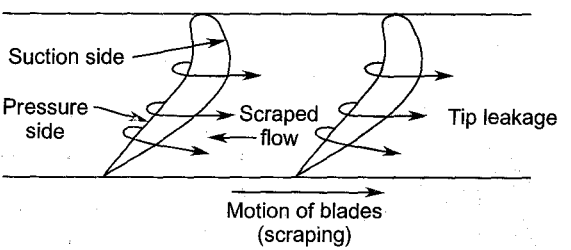

Fig. 8.21 Flow through tip clearance in a turbine cascade

The tip clearance and secondary flows are closely related to each other and it is often convenient to estimate them together.

8.4.6 Estimation of Losses

The estimation of aerodynamic losses occurring in a turbine cascade[219] is largely empirical or semi-empirical. A number of investigators have given correlations based on cascade tests. Some of these are described below.

Hawthorne's correlation [228]

The profile loss is assumed as a function of the gas deflection (ε) only

$$\xi_p = 0.025 \left[1 + \left(\frac{\varepsilon}{90}\right)^2\right] \tag{8.48}$$

The total loss is related to the profile loss and the aspect ratio (h/b) is based on the axial chord.

$$\xi = \left[1 + \frac{3.20}{h/b}\right] \xi_p \tag{8.49}$$

At $h/b = 3.20$, the total loss is twice the profile loss which is the same as the secondary loss.

$$\xi_{h/b\ =3.2} = 2\xi_p = 2\xi_s \tag{8.50}$$

For other values of the aspect ratio, the secondary loss is given by

$$\xi_s = \xi - \xi_p$$

From Eq. (8.49),

$$\xi_s = \frac{3.20}{h/b}\, \xi_p$$

Substituting from Eq. (8.48),

$$\xi_s = \frac{3.20}{h/b} \times 0.025 \left[1 + \left(\frac{\varepsilon}{90}\right)^2\right]$$

$$\xi_s = \frac{0.08}{h/b}\left[1 + \left(\frac{\varepsilon}{90}\right)^2\right] \tag{8.51}$$

For cascades of very large values of aspect ratio ($h/b \approx \infty$), the secondary loss is negligible.

Ainley's correlation [262, 263, 264]

In this correlation the profile loss at zero incidence is related to the air angles at the entry and exit, and the thickness-chord ratio.

$$Y_p\,(i = 0) = \left[Y_{p\,(\alpha 1 = 0)} + \left(\frac{\alpha_1}{\alpha_2}\right)^2 \{Y_{p\,(\alpha 1 = \alpha 2)} - Y_{p\,(\alpha 1 = 0)}\}\right]\left(5\frac{t}{l}\right)^{\alpha 1/\alpha 2} \tag{7.52}$$

This relation is applicable for both impulse and reaction blades of t/l = 0.15 to 0.25. The loss at any other incidence is then related to the incidence ratio i/i_s, where i_s is the stalling incidence. This is defined as the degree of incidence which makes the profile loss twice its value at zero incidence.

$$Y_p/Y_{p(i=0)} = f(i/i_s) \tag{8.53}$$

Figures 8.22 (a) and (b) show plots of the profile loss (at $i = 0$) against the pitch-chord ratio for nozzle and impulse blade cascades. The loss increases with the gas deflection and becomes high at low values of the pitch-chord ratio.

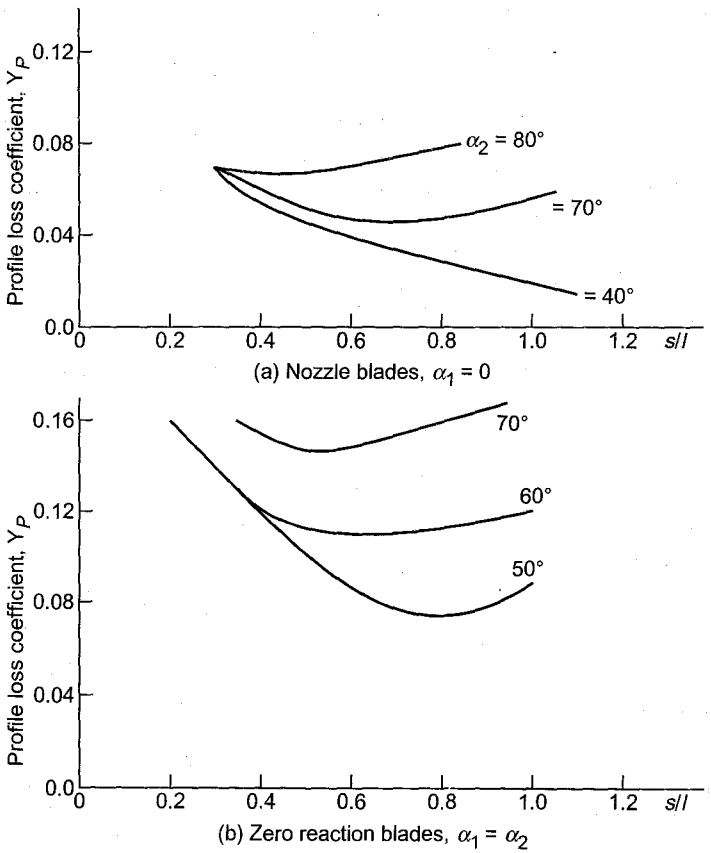

Fig. 8.22(a, b) Profile loss coefficients for turbine blades, Re = 2×10^5, $M < 0.6$, $t/l = 0.2$, $i = 0$ (From Ainley and Mathienson,[263] by courtesy of H.M.S.O., crown copyright reserved)

Figure 8.23 shows the variation of the profile loss with incidence for impulse and reaction blades. As expected, the loss is lower in reaction blades compared to the impulse type. This is due to the accelerating flow in the reaction type where the boundary layers are thinner and are less likely to separate. The losses increase rapidly in both types at higher values of positive incidence. The secondary loss is given by,

$$Y_s = \lambda \left(\frac{C_L}{s/l}\right)^2 \frac{\cos^2 \alpha_2}{\cos^3 \alpha_m} \tag{8.54}$$

$$\lambda = \frac{(A_2/A_1)^2}{1 + d_h/d_t}$$

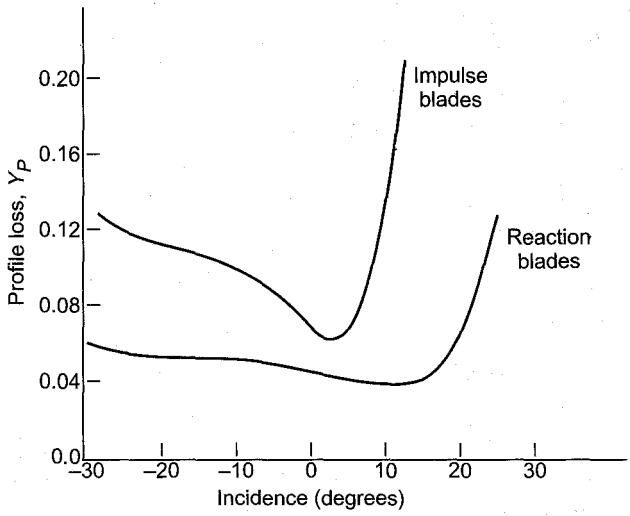

Fig. 8.23 Variation of profile loss with incidence, Re = 1.5×10^5, exit Mach number = 0.5, base profile *T*–6 (From Ainely[262] by courtesy of the Instn. of Mech. Engrs., London)

where A_1 and A_2 are the cross-sectional areas normal to the flows at the entry and exit respectively.

The loss due to the tip clearance is given by

$$Y_c = B \left(\frac{h_c}{h}\right)\left(\frac{C_L}{s/l}\right)^2 \frac{\cos^2 \alpha_2}{\cos^3 \alpha_m} \tag{8.55}$$

where $B = 0.25$ for shroud clearance and

$= 0.50$ for radial clearance

Figure 8.24 shows the variation of various aerodynamic losses with incidence in a turbine cascade.

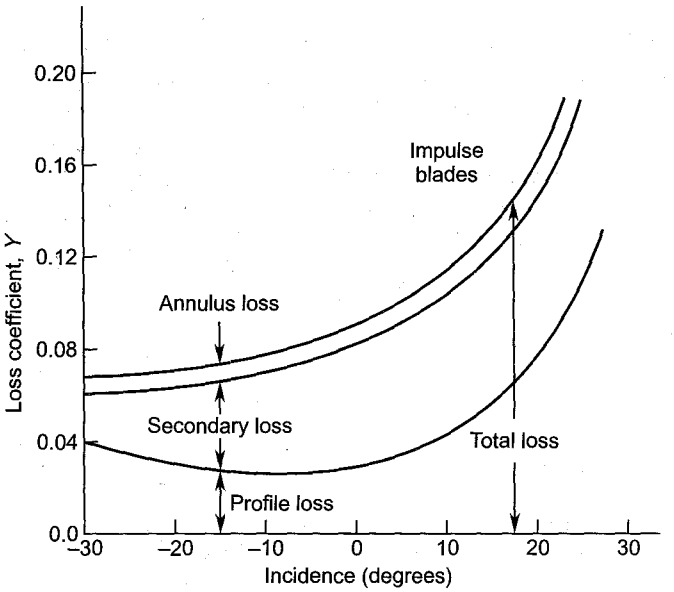

Fig. 8.24 Aerodynamic losses in a turbine blade cascade (From Ainely[262] by courtesy of the Instn. of Mech. Engrs., London)

Soderberg's correlation

The basis of this correlation [286, 287] is a nominal loss coefficient ξ^* at a Reynolds number of 10^5 and an aspect ratio of 3.0. This is valid for a cascade of blades in which the pitch-chord ratio is governed by the Zweifel's relation [Eq. (8.47)].

The nominal loss coefficient for a given maximum thickness-chord ratio is expressed as a function of the gas deflection.

$$\xi^* = f(\varepsilon) \tag{8.56}$$

Figure 8.25 shows the variation of the nominal loss coefficient with deflection for three values of the thickness-chord ratio.

The loss coefficient at a Reynolds number of 10^5 and an aspect ratio other than 3.0 is given by

$$\xi' = (1 + \xi^*)\left(0.975 + \frac{0.075}{h/b}\right) - 1 \tag{8.57}$$

This is further modified for values of the Reynolds number other than 10^5

$$\xi'' = \left(\frac{10^5}{\mathrm{Re}}\right)^{1/4} \xi' \tag{8.58}$$

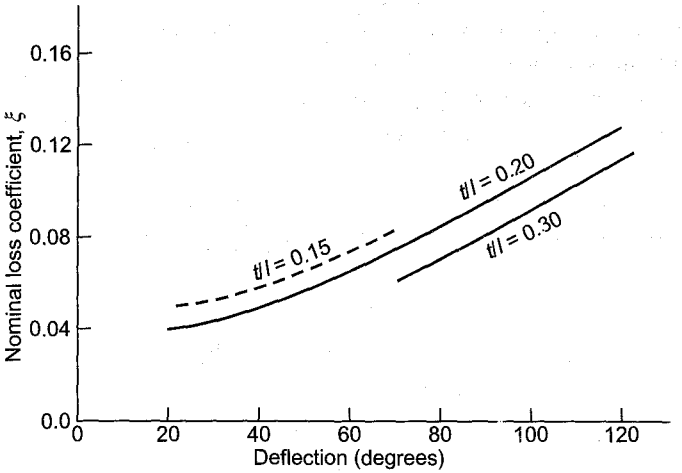

Fig. 8.25 Soderberg's nominal loss coefficient, Re = 10^5, h/b = 3.0 (From Horlock[286] by courtesy of the Pergamon Press)

The Reynolds number in Eq. (8.58) is based on the hydraulic mean diameter and fluid velocity at the exit of the blade passage.

$$d_h = \frac{2hs\cos\alpha_2}{h + s\cos\alpha_2} \tag{8.59}$$

$$\text{Re} = \frac{c_2\, d_h}{\mu/\rho} \tag{8.60}$$

Equations (8.57) and (8.58) give

$$\xi'' = \left\{(1+\xi^*)\left(0.975 + \frac{0.075}{h/b}\right) - 1\right\}\left(\frac{10^5}{\text{Re}}\right)^{1/4} \tag{8.61}$$

This is Soderberg's correlation.

8.5 Axial Compressor Cascades

A row of compressor blades deflects the incoming flow in such a manner that its static pressure increases across it. The flow therefore decelerates from a smaller to a larger cross-sectional area of a blade passage.

Since the flow occurs against a pressure hill (adverse pressure gradient), it is more likely to separate, particularly at higher rates of pressure rise. Therefore, the flow is handled more carefully in a compressor cascade. Static pressure rise in such a cascade is kept much smaller than the pressure drop in a turbine cascade.

Figure 8.26 shows a cascade of compressor blades resting on the oblique exit of the test section of a blower type wind tunnel. The static pressure distribution is obtained from the static pressure holes around the central blade. The velocities around the blade surface are obtained from the static pressure distribution. A typical velocity distribution curve is shown in Fig. 8.27.

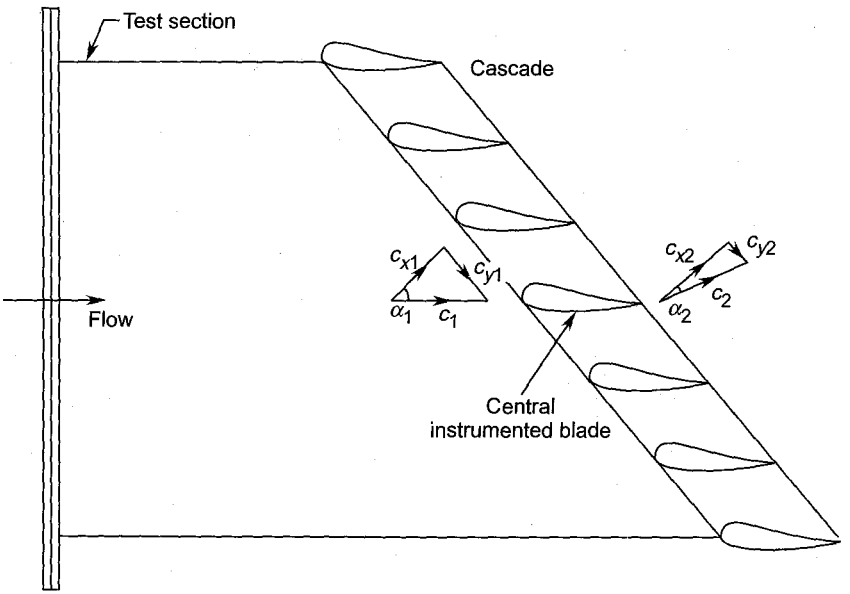

Fig. 8.26 A cascade of compressor blades

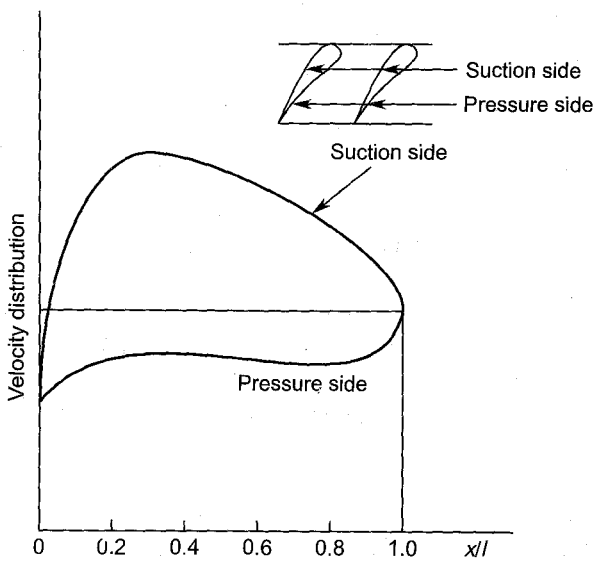

Fig. 8.27 Velocity distribution around a compressor blade

The central blade is instrumented (Fig. 8.6). The method of specifying the geometry of the individual blades and testing them is the same as described in Sec. 8.3. However, a different convention is employed here to describe the geometry of the cascade.

8.5.1 Nomenclature

There are three pairs of angles in a compressor cascade—the camber angles, blade angles and air angles. These have been explained in Sec. 8.4.1 for a turbine cascade.

Figure 8.28(a) shows a compressor blade with its chord line in the axial direction. The tangents to its camber line make angles (camber angles) χ_1 and χ_2 with the axial direction. When the blade is set at a stagger angle γ (Fig. 8.28(b)), the tangents at the entry and exit make angles of α'_1 and α'_2 with the reference axial direction. These are the blade angles.

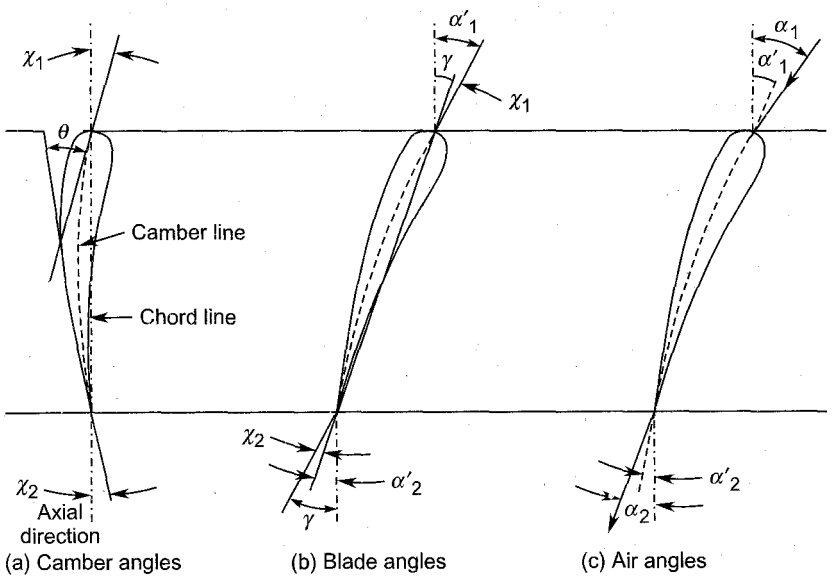

Fig. 8.28 Camber, blade and air angles

In contrast to the turbine cascade, the camber angle for the compressor cascade is defined by the following relations:

$$\theta = \chi_1 + \chi_2 = \alpha'_1 - \alpha'_2 \tag{8.62}$$

From Fig. 8.28(b),

$$\alpha'_1 = \chi_1 + \gamma \tag{8.63}$$

$$\alpha'_2 = -(\chi_2 - \gamma) \tag{8.64}$$

The air angles (α_1, α_2) are different from the blade angles (α'_1, α'_2) which depend on the nature of flow and the cascade characteristic. Fig. 8.28 (c) shows these angles.

The difference between the air and the blade angles at the entry is known as the angle of incidence.

$$i = \alpha_1 - \alpha'_1 \tag{8.65}$$

This angle can be positive or negative.

The departure of the outgoing jet from the exit blade angle can be quite large; this deviation is such that the overall deflection of the fluid through the cascade is reduced giving a lesser static pressure rise through the cascade. The deviation angle (δ) for a compressor cascade is defined as the difference between the air angle and the blade angle at exit.

$$\delta = \alpha_2 - \alpha'_2 \tag{8.66}$$

The difference between Eqs. (8.20) and (8.66) is due to the different convention used to define the stagger angle and the exit angles in compressor cascades; fluid deflection through the blades is defined as

$$\varepsilon = \alpha_1 - \alpha_2 \tag{8.67}$$

This is again different from Eq. (8.21) for turbine cascade.

Putting Eqs. (8.65) and (8.66) into Eq. (8.67) we get

$$\varepsilon = (\alpha'_1 + i) - (\alpha'_2 + \delta)$$

$$\varepsilon = (\alpha'_1 - \alpha'_2) + (i - \delta) \tag{8.68}$$

From Eq. (8.62),

$$\varepsilon = \theta + i - \delta \tag{8.69}$$

Figure 8.29 shows the various angles defined in this section for a compressor cascade. Comparison of this figure with Fig. 8.16 further explains the difference between the aforementioned angles for turbine and compressor cascades.

Appendix C gives the specifications of some compressor blade sections.

8.5.2 Velocity Triangles

Figure 8.30 shows two blades in a compressor cascade. They are enclosed in the control surfaces as shown. The velocity triangles for one-dimensional flow at the entry and exit of the control surface are shown in the figure.

Velocity vectors c_1 and c_2 at the entry and exit are at air angles α_1 and α_2 respectively. The components in axial and tangential directions are also shown. The blade heights at the entry and exit are such that the axial component of velocity remains constant.

$$c_{x1} = c_{x2} = c_{xm}$$

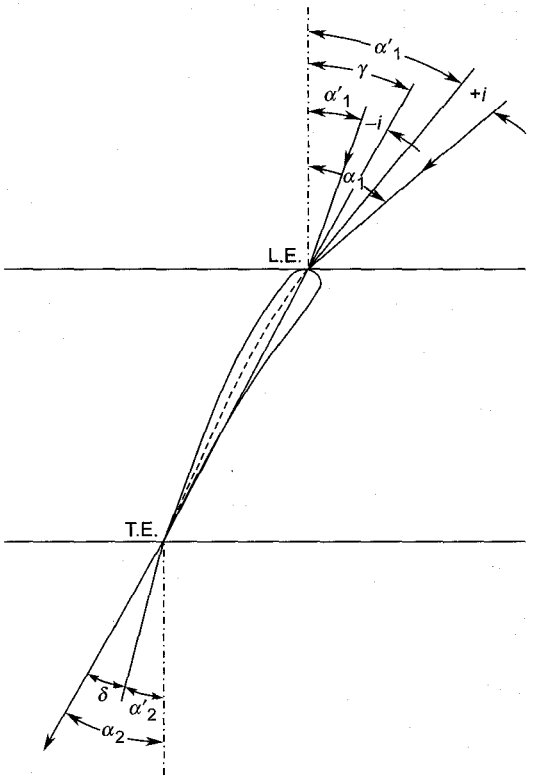

Fig. 8.29 Stagger, incidence and deviation angle

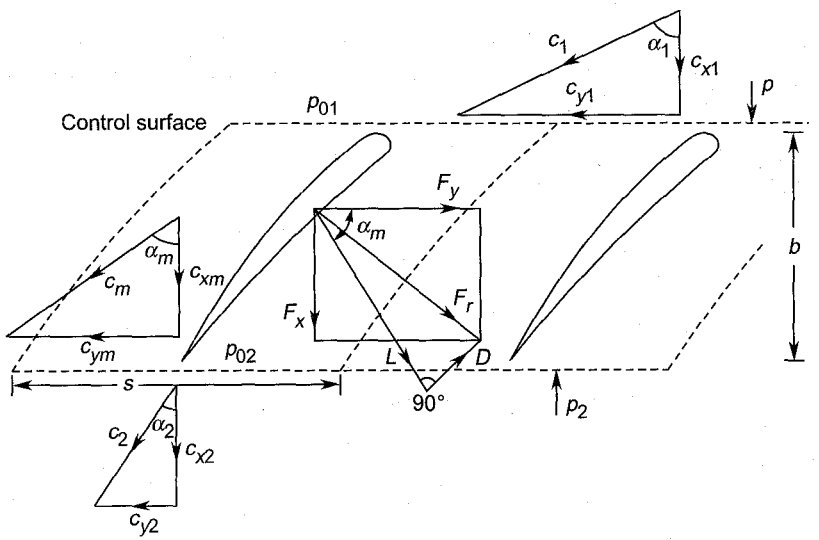

Fig. 8.30 Inlet, outlet and mean velocity triangles, and blade forces (compressor cascade)

The mean velocity triangle for flow through the blade passage is defined by the following quantities:

$$c_{xm} = \frac{1}{2}(c_{x1} + c_{x2}) \tag{8.70}$$

$$c_{ym} = \frac{1}{2}(c_{y1} + c_{y2}) \tag{8.71}$$

$$\tan \alpha_m = \frac{c_{ym}}{c_{xm}} \tag{8.72}$$

$$\tan \alpha_m = \frac{1}{2c_{xm}}(c_{y1} + c_{y2})$$

For constant axial velocity,

$$\tan \alpha_m = \frac{1}{2}\left(\frac{c_{y1}}{c_{x1}} + \frac{c_{y2}}{c_{x2}}\right)$$

$$\tan \alpha_m = \frac{1}{2}(\tan \alpha_1 + \tan \alpha_2) \tag{8.73}$$

Note the difference between Eqs. (8.71) and (8.25)

8.5.3 Blade Forces

Various forces exerted by a blade (of unit height) on the flow are shown in Fig. 8.30. The magnitudes and directions of these forces exerted by the fluid on the blade are exactly equal and opposite in direction to the forces exerted by the blade as shown in the figure.

The forces are related to the change of momentum which in turn depends on the flow rate through the control surface and the change of velocity and its direction.

The flow rate through the control surface of unit height for incompressible and steady flow is

$$\dot{m} = \rho_1 c_{x1} (s \times 1) = \rho_2 c_{x2} (s \times 1)$$

$$\dot{m} = \rho s c_{x1} = \rho s c_{x2} = \rho s c_{xm} \tag{8.74}$$

Tangential force

In a compressor cascade it is desired that the tangential force is minimum for a given rise in the static pressure. This force multiplied be the peripheral speed of the rotor blades gives the work done by the blades on the fluid.

The tangential force exerted by the fluid on one blade is

$$F_y = \dot{m}(c_{y1} - c_{y2})$$

$$F_y = \rho s c_{xm}(c_{y1} - c_{y2}) \tag{8.75}$$

From velocity triangles,

$$F_y = \rho s c_{xm}^2 (\tan \alpha_1 - \tan \alpha_2) \tag{8.76}$$

This can also be expressed in the dimensionless form as in Eqs. (8.30) or (8.32).

$$F_y = \left(\frac{1}{2} \rho l c_{xm}^2\right) 2 \left(\frac{s}{l}\right) (\tan \alpha_1 - \tan \alpha_2) \tag{8.77}$$

Therefore, the dimensionless tangential force coefficient based on the constant axial velocity c_{xm} is

$$C_{Fy} = \frac{F_y}{\frac{1}{2} \rho l c_{xm}^2} = 2 \left(\frac{s}{l}\right) (\tan \alpha_1 - \tan \alpha_2) \tag{8.78}$$

Axial force

The axial force exerted by the fluid on the blade is due to both the static pressure rise and the change of momentum in the axial direction

$$F_x = (p_2 - p_1)\, s \times 1 + \rho\, (s \times 1)\, c_{xm}\, (c_{x2} - c_{x1})$$

For constant axial velocity, the axial thrust in the upstream direction is entirely due to the pressure difference.

$$F_x = (p_2 - p_1)\, s \tag{8.79}$$

Now $p_2 - p_1 = \frac{1}{2} \rho (c_1^2 - c_2^2) - \Delta p_0$

Therefore,

$$F_x = \frac{1}{2} \rho s (c_1^2 - c_2^2) - s \Delta p_0$$

From the velocity triangles for constant axial velocity,

$c_1^2 - c_2^2 = c_{y1}^2 - c_{y2}^2$; therefore,

$$F_x = \frac{1}{2} \rho s (c_{y1}^2 - c_{y2}^2) - s \Delta p_0$$

$$F_x = \frac{1}{2} \rho s c_{xm}^2 (\tan^2 \alpha_1 - \tan^2 \alpha_2) - s \Delta p_0 \tag{8.80}$$

$$F_x = \rho s c_{xm}^2 \frac{1}{2} (\tan \alpha_1 + \tan \alpha_2) (\tan \alpha_1 - \tan \alpha_2) - s \Delta p_0$$

Substituting from Eq. (8.73),

$$F_x = \rho s c_{xm}^2 \tan \alpha_m (\tan \alpha_1 - \tan \alpha_2) - s \Delta p_0 \tag{8.81}$$

Equation (8.80) can also be written as

$$F_x = \left(\frac{1}{2} \rho l c_{xm}^2\right)\left(\frac{s}{l}\right) (\tan^2 \alpha_1 - \tan^2 \alpha_2) - s \Delta p_0$$

The dimensionless axial force coefficient is therefore,

$$C_{Fx} = \frac{F_x}{\frac{1}{2}\rho l c_{xm}^2} = \frac{s}{l}(\tan^2\alpha_1 - \tan^2\alpha_2) - \left(\frac{s}{l}\right)\frac{\Delta p_0}{\frac{1}{2}\rho c_{xm}^2} \quad (8.82)$$

Now,

$$c_{xm} = c_{x1} = c_1 \cos\alpha_1$$

$$\frac{\Delta p_0}{\frac{1}{2}\rho c_{xm}^2} = \frac{\Delta p_0}{\frac{1}{2}\rho c_1^2}\frac{1}{\cos^2\alpha_1} = \frac{\Delta p_0}{\frac{1}{2}\rho c_m^2}\frac{1}{\cos^2\alpha_m} \quad (8.83)$$

The pressure loss coefficient based on the inlet velocity is defined as

$$Y = \frac{\Delta p_0}{\frac{1}{2}\rho c_1^2}$$

Therefore,

$$\frac{\Delta p_0}{\frac{1}{2}\rho c_{xm}^2} = \frac{Y}{\cos^2\alpha_1} \quad (8.84)$$

Putting Eq. (8.84) into Eq. (8.82) yields

$$C_{Fx} = \frac{s}{l}(\tan^2\alpha_1 - \tan^2\alpha_2) - \left(\frac{s}{l}\right)\frac{Y}{\cos^2\alpha_1} \quad (8.85)$$

Lift force

By definition, the lift force on the blade is normal to the direction of the mean velocity (c_m) of flow through the blade passage.

By resolving tangential and axial forces in the direction of lift,

$L = F_y \cos\alpha_m + F_x \sin\alpha_m$ (Figure 8.30)

Substituting from Eqs. (8.76) and (8.71), we have

$$L = \rho s c_{xm}^2(\tan\alpha_1 - \tan\alpha_2)\cos\alpha_m + \rho s c_{xm}^2 \times (\tan\alpha_1 - \tan\alpha_2)\tan\alpha_m \sin\alpha_m - s\,\Delta p_0 \sin\alpha_m$$

$$L = \rho s c_{xm}^2(\tan\alpha_1 - \tan\alpha_2)\left(\cos\alpha_m + \frac{\sin^2\alpha_m}{\cos\alpha_m}\right) - s\,\Delta p_0 \sin\alpha_m$$

$$L = \rho s c_{xm}^2(\tan\alpha_1 - \tan\alpha_2)\sec\alpha_m - s\,\Delta p_0 \sin\alpha_m \quad (8.86)$$

$$L = \rho s c_m^2(\tan\alpha_1 - \tan\alpha_2)\cos\alpha_m - s\,\Delta p_0 \sin\alpha_m \quad (8.87)$$

Equation (8.86) can also be written as

$$L = \rho s c_m (c_{y1} - c_{y2}) - s\,\Delta p_0 \sin\alpha_m \quad (8.88)$$

The dimensionless lift coefficient is developed from Eq. (8.87)

$$L = \left(\frac{1}{2}\rho l c_m^2\right) 2 \left(\frac{s}{l}\right) (\tan \alpha_1 - \tan \alpha_2) \cos \alpha_m - s\, \Delta p_0 \sin \alpha_m$$

$$C_L = \frac{L}{\frac{1}{2}\rho l c_m^2} = 2 \left(\frac{s}{l}\right) (\tan \alpha_1 - \tan \alpha_2) \cos \alpha_m - \left(\frac{s}{l}\right) \frac{\Delta p_0}{\frac{1}{2}\rho c_m^2} \sin \alpha_m \tag{8.89}$$

Drag force

The drag force is parallel to the direction of mean flow. By resolving forces in this direction,

$$D = F_y \sin \alpha_m - F_x \cos \alpha_m$$

Substituting for the values of F_y and F_x,

$$D = \rho s c_{xm}^2 (\tan \alpha_1 - \tan \alpha_2) \sin \alpha_m - \rho s c_{xm}^2 (\tan \alpha_1 - \tan \alpha_2) \tan \alpha_m \cos \alpha_m + s\, \Delta p_0 \cos \alpha_m$$

After cancelling the common terms,

$$D = s\, \Delta p_0 \cos \alpha_m \tag{8.90}$$

The dimensionless drag coefficient is given by

$$C_D = \frac{D}{\frac{1}{2}\rho l c_m^2} = \left(\frac{s}{l}\right) \frac{\Delta p_0}{\frac{1}{2}\rho c_m^2} \cos \alpha_m \tag{8.91}$$

Substituting Eq. (8.83) in Eq. (8.91) gives

$$C_D = \left(\frac{s}{l}\right) \frac{\Delta p_0}{\frac{1}{2}\rho c_1^2} \frac{\cos^3 \alpha_m}{\cos^2 \alpha_1}$$

$$C_D = \left(\frac{s}{l}\right) Y \frac{\cos^3 \alpha_m}{\cos^2 \alpha_1} \tag{8.92}$$

Putting Eq. (8.91) into Eq. (8.89), we get

$$C_L = 2 \left(\frac{s}{l}\right) (\tan \alpha_1 - \tan \alpha_2) \cos \alpha_m - C_D \tan \alpha_m \tag{8.93}$$

For reversible flow through the cascade $\Delta p_0 = 0$, $C_D = 0$. Therefore, Eqs. (8.89) and (8.93) reduce to

$$C_L = 2 \left(\frac{s}{l}\right) (\tan \alpha_1 - \tan \alpha_2) \cos \alpha_m \tag{8.94}$$

Equation (8.88) for reversible flow gives

$$L = \rho s c_m (c_{y1} - c_{y2})$$

As explained for the turbine blade cascade,

$$s\,(c_{y1} - c_{y2}) = \Gamma \tag{8.95}$$

Therefore, the expression for lift is again (see Eqs. (8.44) and (8.45)) reduced to the Kutta-Joukowski's relation for an isolated aerofoil.

$$L = \rho\, c_m\, \Gamma$$

8.5.4 Static Pressure Rise

The main function of a compressor cascade is to raise the static pressure of the fluid across it. This should be achieved with minimum stagnation pressure loss or drag.

Thus the compressor cascade behaves like an adiabatic diffuser. The thermodynamics of flow through a diffuser has been discussed in detail in Sec. 2.4. Figure 2.5 depicts the ideal and actual flow processes in a diffuser.

The static pressure rise for isentropic flow is given by Eq. (2.87). This is

$$\Delta p_s = p_{2s} - p_1 = \frac{1}{2}\,\rho\,(c_1^2 - c_{2s}^2)$$

$$\Delta p_s = \frac{1}{2}\,\rho c_1^2 \left(1 - \frac{c_{2s}^2}{c_1^2}\right)$$

For incompressible flow, from Eq. (8.74),

$$c_{x1} = c_{x2}$$

$$c_1 \cos\,\alpha_1 = c_{2s} \cos\,\alpha_2$$

$$\frac{c_{2s}}{c_1} = \frac{\cos\alpha_1}{\cos\alpha_2}$$

Therefore,

$$\Delta p_s = \frac{1}{2}\,\rho c_1^2 \left(1 - \frac{\cos^2\alpha_1}{\cos^2\alpha_2}\right) \tag{8.96}$$

The pressure rise through the cascade can be expressed as a dimensionless quantity known as the pressure or pressure recovery coefficient. Thus the ideal pressure recovery coefficient for the cascade is given by

$$C_{ps} = \frac{\Delta p_s}{\frac{1}{2}\,\rho c_1^2} = 1 - \frac{\cos^2\alpha_1}{\cos^2\alpha_2} \tag{8.97}$$

For an actual flow (with the stagnation pressure loss Δp_0) the static pressure rise is given by

$$\Delta p_a = p_2 - p_1 = \Delta p_s - \Delta p_0 \text{ (see Eq. (2.90))}$$

Substituting from Eq. (8.96),

$$\Delta p_a = \frac{1}{2}\rho c_1^2\left(1-\frac{\cos^2\alpha_1}{\cos^2\alpha_2}\right)-\Delta p_0$$

Therefore, the actual pressure recovery coefficient is given by

$$C_{pa} = \frac{\Delta p_a}{\frac{1}{2}\rho c_1^2} = \left(1-\frac{\cos^2\alpha_1}{\cos^2\alpha_2}\right)-\frac{\Delta p_0}{\frac{1}{2}\rho c_1^2} \tag{8.98}$$

$$C_{pa} = C_{ps} - Y \tag{8.99}$$

The pressure recovery coefficient of a cascade is its pressure raising capacity and should not be confused with the cascade efficiency.

8.5.5 Cascade Efficiency

The efficiency of the compressor cascade is defined as the efficiency of a diffuser (see Sec. 2.4.1.). This is defined as the ratio of actual pressure rise and the isentropic pressure rise.

$$\eta_D = \frac{\Delta p_a}{\Delta p_s} = \frac{\Delta p_s - \Delta p_0}{\Delta p_s}$$

$$\eta_D = 1 - \frac{\Delta p_0}{\Delta p_s} \tag{8.100}$$

From Eq. (8.90),

$$\Delta p_0 = D/s \cos\alpha_m \tag{8.101}$$

$$\Delta p_s = \frac{1}{2}\rho\,(c_1^2 - c_2^2) = \frac{1}{2}\rho c_{xm}^2\,(\tan^2\alpha_1 - \tan^2\alpha_2)$$

$$\Delta p_s = \rho c_{xm}^2 \tan\alpha_m\,(\tan\alpha_1 - \tan\alpha_2) \tag{8.102}$$

Neglecting the second term in Eq. (8.86) as small,

$$\rho c_{xm}^2 \tan\alpha_m\,(\tan\alpha_1 - \tan\alpha_2) = \frac{L\sin\alpha_m}{s}$$

Substituting this in Eq. (8.102),

$$\Delta p_s = L\sin\alpha_m/s \tag{8.103}$$

Substituting Eqs. (8.101) and (8.103) in (8.100), we have

$$\eta_D = 1 - \frac{D}{L}\frac{1}{\sin\alpha_m\cos\alpha_m}$$

$$\eta_D = 1 - 2\,\frac{C_D}{C_L}\frac{1}{\sin 2\alpha_m} \tag{8.104}$$

Assuming C_D/C_L as constant, the optimum value of α_m can be determined. η_D is a maximum when $\sin 2\alpha_m$ is maximum. Thus the optimum value of α_m is

$$(\alpha_m)_{\text{opt}} = 45° \tag{8.105}$$

The maximum efficiency of the cascade is therefore

$$\eta_{D\max} = 1 - 2C_D/C_L \tag{8.106}$$

8.5.6 Losses and Their Estimation

The types of aerodynamic losses occurring in the compressor cascade are the same as described in Sec. 8.4.5 for the turbine cascade. Their exact nature and magnitudes are different (higher) on account of the decelerating flow in compressor cascade. Most of the theoretical methods for calculating these losses are also empirical.

The cascade losses are expressed as either pressure loss coefficients (Y) or drag coefficients (C_D). Lieblein and Roudebush [239] relate the total cascade losses to the momentum-thickness-chord ratio in the following relation:

$$Y = 2\left(\frac{\theta}{l}\right)\left(\frac{l}{s}\right)\frac{\cos^2 \alpha_1}{\cos^3 \alpha_2} \tag{8.107}$$

A large part of the blade wake is formed by the boundary layer on the suction side. The profile losses depend on the diffusion of flow on the suction side. Lieblein recommends that the diffusion ratio ($c_{\max}/c_2$) must not exceed 2.0.

An overall drag coefficient represents the total cascade losses:

$$C_D = C_{Dp} + C_{Da} + C_{Ds} \tag{8.108}$$

Quantities on the right-hand side of Eq. (8.108) represent drag coefficients corresponding to profile, annulus and secondary losses; the tip leakage loss is generally considered with the secondary loss.

The profile loss is best obtained from tests on the given cascade. This varies with incidence.

The loss due to annulus skin friction is given by

$$C_{Da} = 2f\left(\frac{s}{h}\right) \tag{8.109}$$

The friction factor for axial compressors can be taken as $f = 0.01$. Substituting this in Eq. (8.109), we get a widely-used expression:

$$C_{Da} = 0.02\left(\frac{s}{h}\right) \tag{8.110}$$

The secondary loss is given by

$$C_{Ds} = \lambda \, C_L^2 \Big/ \left(\frac{s}{l}\right) \tag{8.111}$$

Howell suggests the following relation:

$$C_{Ds} = 0.018 \; C_L^2 \tag{8.112}$$

As mentioned for turbine cascade the tip clearance between the blades and the casing causes leakage of the fluid from the pressure to the suction side of the blades. In a compressor rotor blade row the pressure side leads and the suction side trails. Therefore, the scraped up boundary layer of the casing augments the tip leakage and generates additional secondary flow. Figures 8.31 and 8.32 depict these phenomena.

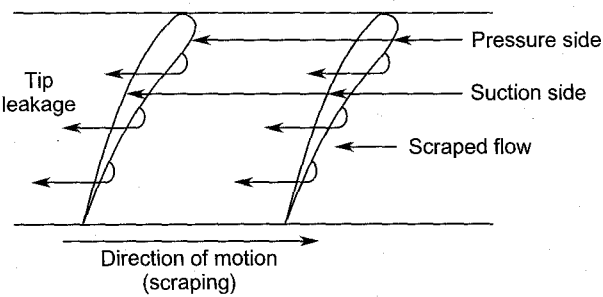

Fig. 8.31 Flow through tip clearance in a compressor cascade

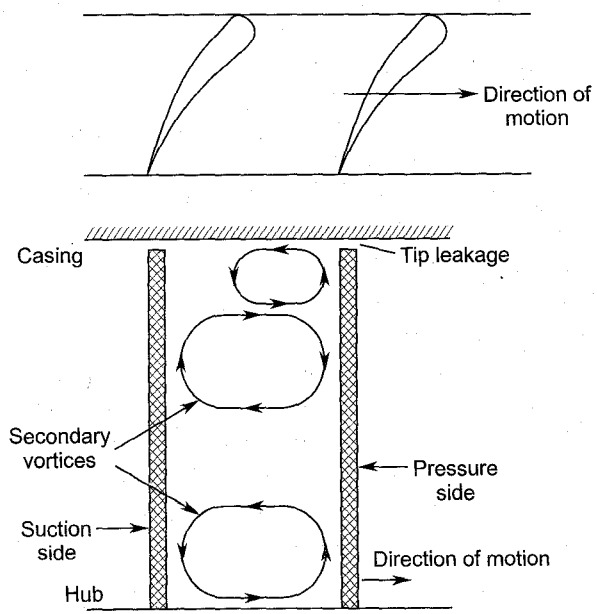

Fig. 8.32 Secondary and tip leakage flow

In compressor cascades, the profile and secondary losses are nearly of the same order (≈ 40% of the total aerodynamic losses), the remaining (≈ 20%) is the annulus loss. Fig. 8.33 shows the relative magnitudes of these losses with flow coefficient (or incidence). It is observed that the profile loss varies significantly with incidence. High loss regions at the two extremes of the total loss curve represent high cascade losses due to positive and negative stall.

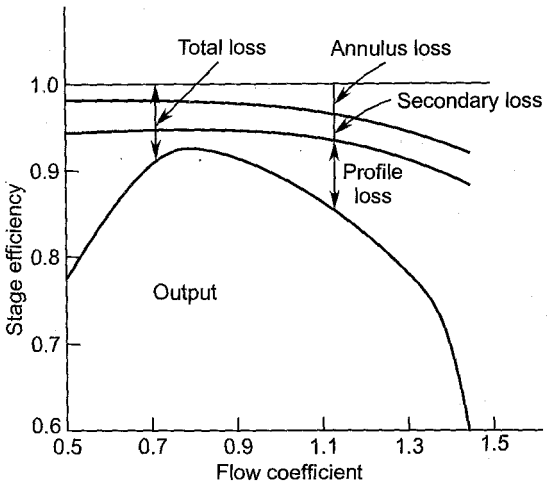

Fig. 8.33 Cascade losses in a compressor stage (From Howell,[412] by courtesy of the Instn. of Mech. Engrs., London.)

8.5.7 Howell's Correlation [412]

The static pressure rise through a compressor cascade depends on the deflection of the fluid through it. Therefore, a maximum value of the fluid deflection might appear to be desirable, but on account of stalling and the associated cascade losses, this is carefully chosen.

Howell obtains design conditions for a compressor cascade from plots of experimentally obtained values of cascade losses and deflection against incidence. Figure 8.34 shows curves for the variations of the lift coefficient, deflection angle and total pressure loss coefficient with incidence. It is observed that high losses occur at maximum values of deflection and lift coefficient. Therefore, Howell suggests that the chosen value (nominal value, ε^*) of the deflection must be fairly away from the stall point (stalling incidence i_s, deflection ε_s). Though it is difficult to specify the stall point, here it is defined as a condition at which the total cascade loss is twice its minimum value. At $i = i_s$,

$$Y_s = 2Y_{\min} \tag{8.113}$$

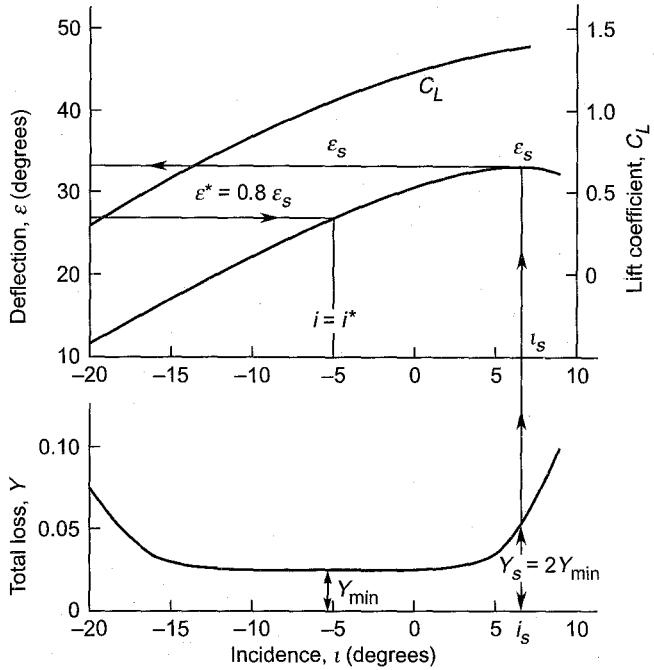

Fig. 8.34 Variation of lift, deflection and pressure loss with incidence for a compressor cascade

Howell then recommends that the nominal deflection must be 80% of the stalling deflection.

$$\varepsilon^* = 0.8\ \varepsilon_s \tag{8.114}$$

$$\varepsilon_s = 1.25\ \varepsilon^*$$

This leaves a safe margin between the chosen value of the deflection and its stalling value.

At high values of the Reynolds number, deflection is mainly a function of the degree of guidance (s/l) and the exit angle.

$$\varepsilon^* = f\left(\frac{s}{l}, \alpha_2^*\right) \tag{8.115}$$

Howell gives plots (Fig. 8.35) of the nominal deflection against exit air angles for cascades of various pitch-chord ratios. Such plots can be employed to obtain the pitch-chord ratio of a cascade with given values of deflection and the exit air angle which are decided for the required pressure rise. The following approximate expression is given to represent the plots in Fig. 8.35:

$$\tan\ \alpha_1^* - \tan\ \alpha_2^* = \frac{1.55}{1 + 1.5\ s/l} \tag{8.116}$$

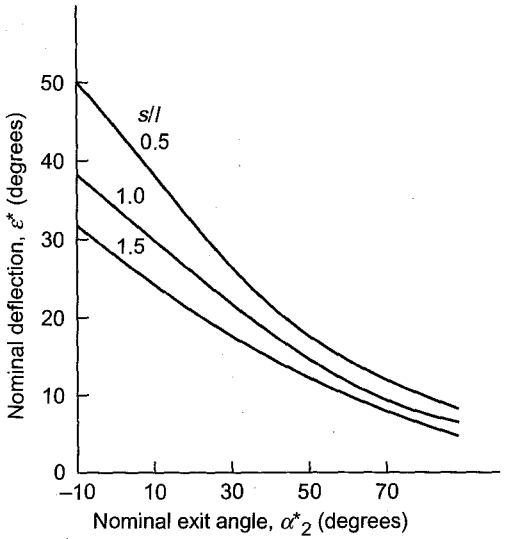

Fig. 8.35 Variation of nominal deflection with exit angle (From Howell[412], by courtesy of the Instn. of Mech. Engrs., London)

This can be used for rough calculations in the initial stages of design.

In view of the fact that large differences exist between the exit blade angles and air angles (Figs. 8.28 and 8.29), the problem of estimating deviation (δ) is important. The total deflection and the presssure rise through the cascade are significantly affected by deviation.

A large number of cascade tests have shown that deviation depends on the degree of guidance or pitch-chord ratio, blade camber, blade exit angle and the parameter a/l. Howell recommends the following relation:

$$\delta^* = m\,\theta \left(\frac{s}{l}\right)^n \tag{8.117}$$

$$m = 0.23 \left(\frac{2a}{l}\right)^2 + 0.002\ \alpha_2^* \tag{8.118}$$

$$n = \frac{1}{2} \text{ (for compressor blade cascades)}$$

For inlet guide vanes, the following values are suggested:

$$n = 1$$
$$m = 0.19$$

After obtaining the values of the deflection (ε^*) and incidence (i^*), the performance of the cascade at other values of incidence can be obtained. Howell gives the dimensionless plots (Fig. 8.36) for the deflection and drag coefficient at off-design points for a cascade.

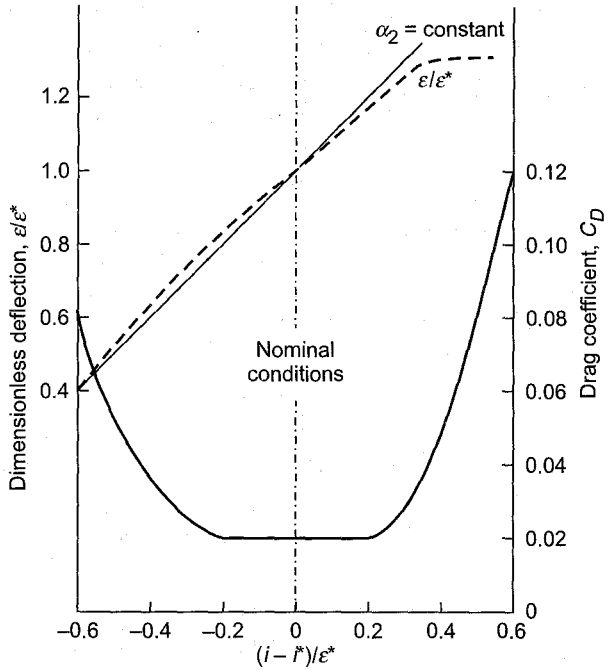

Fig. 8.36 Off-design performance of a compressor cascade (From Howell[412], by courtesy of the Instn. of Mech. Engrs., London)

8.6 Annular Cascades

If the blades are arranged in an annulus instead of a straight row (as described in Sec. 8.3 and Fig. 8.3), the arrangement is known as an annular cascade. [209, 237] The flow in such a cascade is closer to the real-life situation because it simulates three-dimensional flow occurring in actual axial flow machines.

The flow in an annular cascade is truly axisymmetric. The span-wise survey of the flow field provides useful information for both the low and high aspect ratio cascades. Tests on annular cascades are particularly useful for studying the effect of hub and casing boundary layers, secondary flows and the phenomenon of the rotating stall.

A number of arrangements can be employed to design annular tunnels. Outlines of some designs are given in the following sections.

8.6.1 Suction Type

In many situations it is more convenient to suck the air through the cascade. Figure 8.37 shows the principal parts of an annular cascade tunnel employing the suction arrangement.

A compressor or blower located downstream of the annular test section works as an exhauster. The flow over the annular cascade of blades is established by sucking air through the large outer periphery of the annular contraction. To supply air with minimum non-uniformities to the contraction, it is provided with a bell-mouthed entrance and a ring of straighteners (honeycombs) as shown.

One of the requirements of the annular cascade tunnel is to supply a swirling flow to the blades. The swirl vanes must be kept well upstream of the cascade. It is often convenient to locate the swirl vanes in a low velocity region at a larger diameter. In Fig. 8.37 adjustable swirl vanes are located in the radial section of the contraction.

The design of the contraction cone is very important for the quality of flow at the entry of the test section. The boundary layer in the test section is thinner with a large radius of curvature of the contraction walls.

Suitable arrangements for traversing the measuring instruments in the peripheral and radial directions upstream and downstream of the cascade are made.

Flow through the cascade can also be established by induction by employing high-speed annular jets instead of the exhauster. The flow from the tunnel is exhausted to the atmosphere through a diffuser and a silencer (if desired).

8.6.2 Blower Type

A blower type of annular cascade tunnel is shown in Fig. 8.38. The blower, diffuser and settling chamber are the same as in the tunnel described in Sec. 8.3 (Fig. 8.3). An annular contraction connects the cylindrical settling chamber to the annular test section. The centre body which is the hub of the annular contraction is firmly supported from the outer walls. Adjustable swirl vanes can be conveniently fixed in the annular space between the centre body and the settling chamber walls as shown in the figure.

The test section, cascade of blades and exit diffuser are arranged in the same manner as described in Sec. 8.6.1. Both the suction and blower types of annular cascades can also be arranged in a simple annulus with guide vanes (swirl vanes), the row of test blades and the axial fan; proper arrangements for upstream and downstream traversing are made as before. Such an arrangement is cheaper and occupies less space. However, the swirl vanes are too close to the test blades.

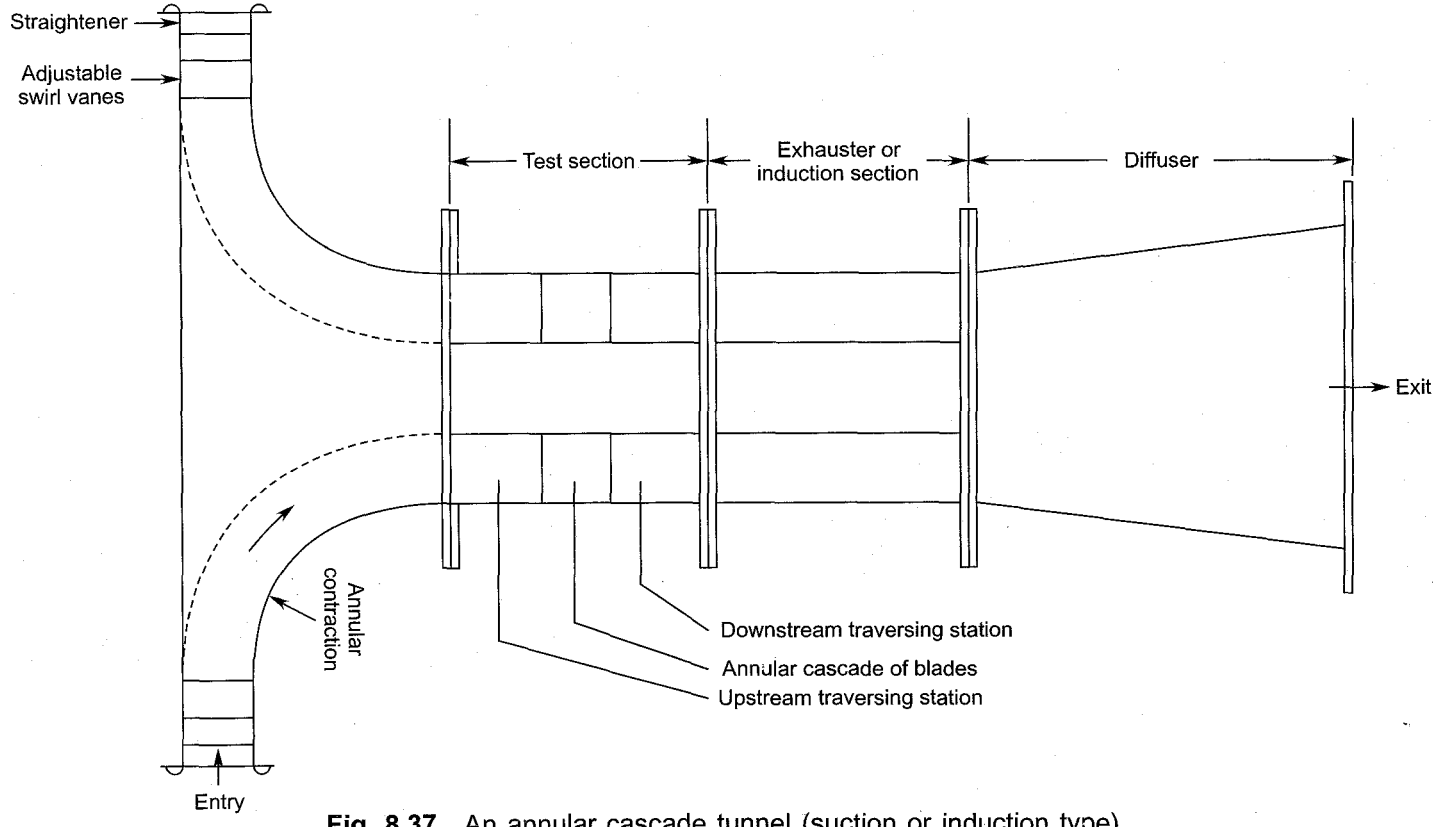

Fig. 8.37 An annular cascade tunnel (suction or induction type)

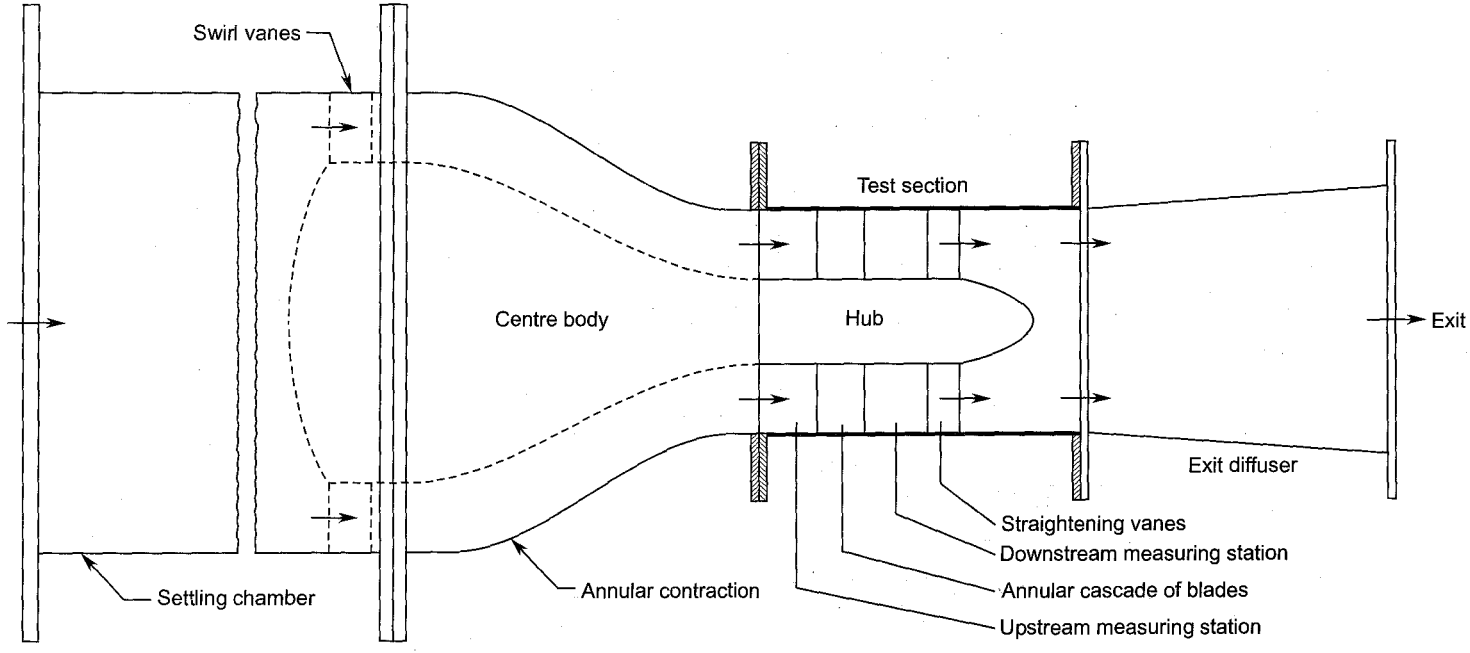

Fig. 8.38 An annular cascade tunnel (blower type)

8.7 Radial Cascades

A radial cascade [246, 258] is formed by a ring of blades arranged between two parallel, oblique or profile side walls through which the flow occurs in the radial direction. Such a facility can be used to test the performance of radial diffusing or accelerating cascades.

Data on radial cascades is very meagre compared to the vast amount of data available for cascades of axial flow machines. Cascade data on inward flow machines is almost non-existent.

8.7.1 Outward Flow

A sector of the outward flow radial cascade and the swirl generator is shown in Fig. 8.39. In a majority of applications the flow through such cascades is decelerating. Radial diffuser blade rings and the blade rows in radial compressors or blowers have been tested by employing this arrangement.

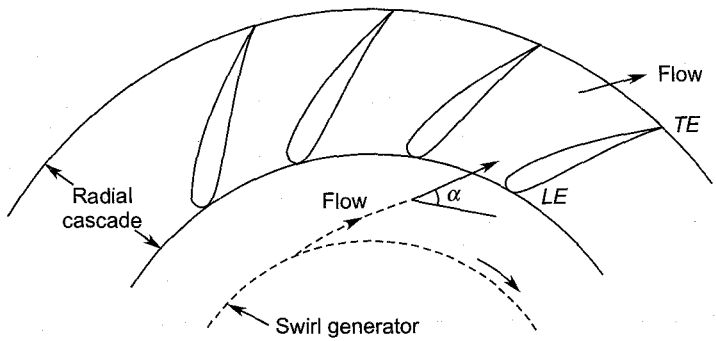

Fig. 8.39 A sector of the outward flow radial cascade and the swirl generator

Flow has to be supplied to the cascade at some angle (α) from the tangential direction. This is relatively easier in an outward flow cascade compared to an inward flow type. Swirl can be imparted to the flow either by providing guide vanes [165, 173] at a smaller radius upstream of the cascade or by some kind of a rotor. Owing to space limitations, the upstream blades pour thick wake flow into the cascade which is not desirable. The use of the bladed rotor, besides supplying wake flow, requires additional power. In contrast to this, a wire gauze swirl generator provides a swirling flow, free of wakes, and requires only small power for its drive.

The swirl generator [154, 205] shown in Fig. 8.40 is a wire gauze rotor. A ring of fine mesh wire gauze is formed by wrapping it round a disc.

Sometimes it is useful to employ two concentric wire gauzes. Wire gauzes should be selected so that the pressure loss through it is not high.

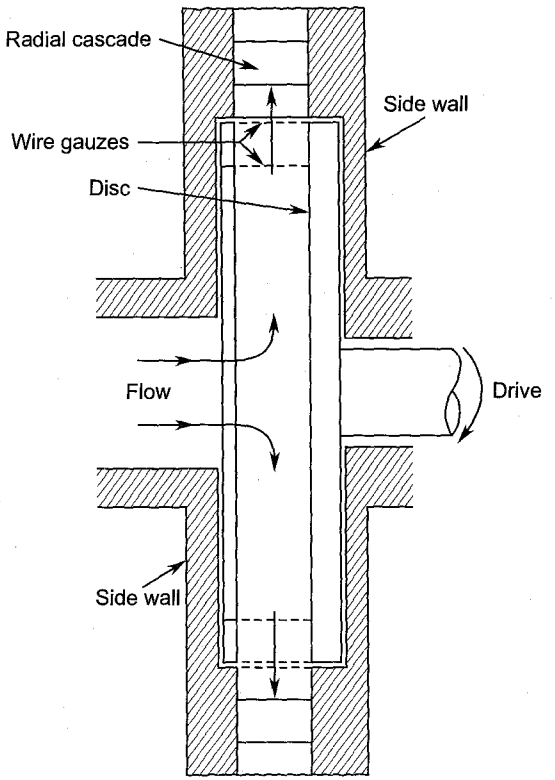

Fig. 8.40 A wire gauze swirl generator at the entry of an outward flow radial cascade

The wire gauze rotor (swirl generator) is placed at the entry of the cascade and rotated through a drive placed outside the cascade. The flow from a blower is supplied axially to the gauze rotor and turns radially outwards. It emerges out of the gauze rotor at an angle α (with the tangential direction) on account of the tangential component imparted to it by the rotating gauze.

The swirl angle (air angle at the entry to the cascade) is varied by varying the speed of the gauze rotor. The angle decreases with an increase in the rotor speed and a decrease in the flow rate. Fig. 8.41 shows the variation of the swirl angle with the rotor speed at various values of the flow rate.

Various flow parameters are measured by traversing instruments upstream and downstream of the cascade.

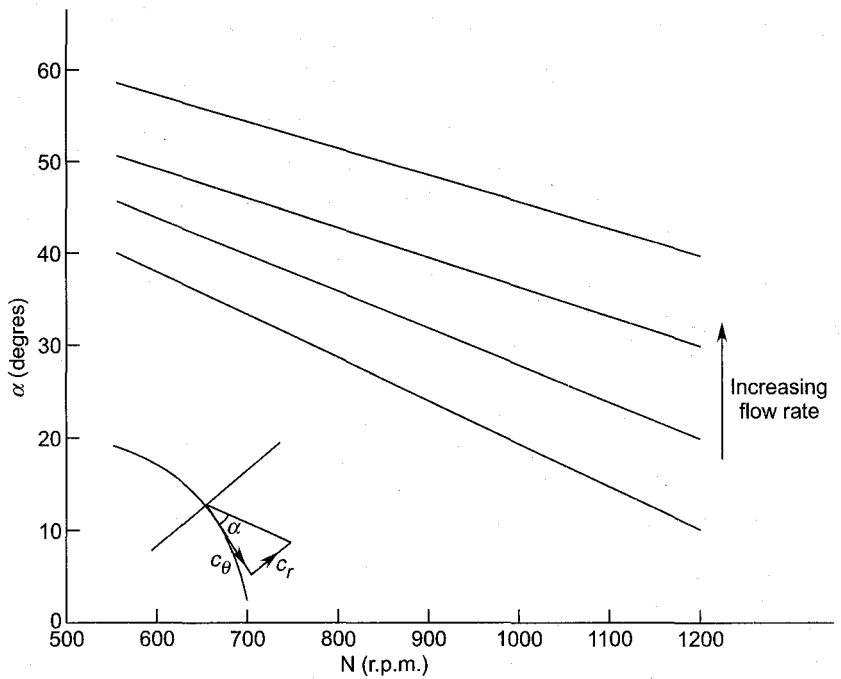

Fig. 8.41 Variation of swirl angle with the speed of swirl generator

8.7.2 Inward Flow

Figure 8.42 shows the arrangement of blades in an inward flow radial cascade. The flow is invariably accelerating in such cascades. The flow

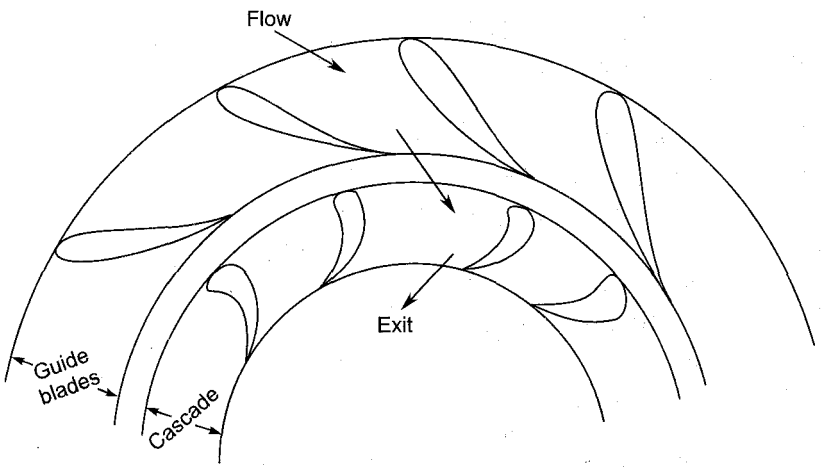

Fig. 8.42 A sector of the inward flow radial cascade and the guide blades (swirl vanes)

through the cascade can be established more conveniently by connecting the exit of the cascade to the suction of a blower or a compressor through an axial duct. This method ensures truly axisymmetric flow through the cascade. The guide blades can be set at the desired angle corresponding to the required value of the air angle at the cascade entry. This arrangement suffers from the wake flow from the guide blades.

Flow parameters are measured by traversing measuring instruments along the blade length and the pitchwise direction both at the entry and exit.

Notation for Chapter 8

a	Position of maximum camber
a'	Position of maximum thickness
A	Area of cross-section or surface area
b	Axial chord
B	Constant
c	Fluid velocity
C_D	Drag coefficient
C_{Fx}	Axial force coefficient
C_{Fy}	Tangential force coefficient
C_L	Lift coefficient
C_p	Pressure recovery coefficient
C_Z	Zweifel's coefficient
D	Drag force per unit length
f	Friction factor
F	Force
h	Enthalpy, blade height or length
h_c	Tip clearance
i	Incidence
l	Blade chord or length parameter
L	Lift force per unit length
$\dot{m}$	Mass flow rate, constant
M	Mach number, momentum
n	An index
N	Rotational speed (rpm)
p	Pressure
Re	Reynolds number
s	Blade pitch
t	Blade thickness, maximum thickness
T	Absolute temperature
x	Distance along the chord line

y	Distance along the cascade or pitch-wise direction
Y	Pressure loss coefficient

Greek symbols

α	Air angle, swirl angle
α'	Blade angle
γ	Stagger angle
δ	Deviation angle
ε	Deflection angle
η	Efficiency
θ	Camber angle, momentum thickness
λ	Constant
μ	Dynamic viscosity
ξ	Enthalpy loss coefficient
ρ	Density of fluid
Γ	Circulation
χ	Camber angle

Subscripts

o	Stagnation values
1	Upstream of the cascade
2	Downstream of the cascade
a	Actual, annulus
c	Tip clearance
D	Drag
h	Hub
L	Lift
m	Mean
min	Minimum
max	Maximum
opt	Optimum
p	Profile
r	resultant, radial
s	Isentropic, secondary, stalling
t	tip
x	Axial
y	Tangential

Superscript

*	Nominal values
–	Average values

Solved Examples

8.1 A compressor cascade has the following data:

velocity of air at entry	= 75 m/s
air angle at entry	= 48°
air angle at exit	= 25°
pitch-chord ratio	= 1.1
stagnation pressure loss	= 11 mm W.G.
density of air	= 1.25 kg/m^3

Determine loss coefficient, drag and lift coefficients, ideal and actual pressure recovery coefficients, diffuser efficiency and maximum diffuser efficiency.

***Solution*:**

$$\tan \alpha_m = \frac{1}{2} (\tan 48 + \tan 25) = 0.788$$

$$\alpha_m = 38.25°$$

$$\frac{1}{2} \rho c_1^2 = 0.5 \times 1.25 \times 75^2 = 3515.625 \text{ N/m}^2$$

$$Y = \frac{\Delta p_0}{\frac{1}{2} \rho c_1^2} = \frac{11 \times 9.81}{3515.625} = 0.0307 \text{ (}Ans.\text{)}$$

$$C_D = \left(\frac{s}{l}\right) Y \frac{\cos^3 \alpha_m}{\cos^2 \alpha_1}$$

$$C_D = 1.1 \times .0307 \cos^3 38.25 / \cos^2 48$$

$$C_D = 0.0365 \text{ (}Ans.\text{)}$$

$$C_L = 2 \left(\frac{s}{l}\right) (\tan \alpha_1 - \tan \alpha_2) \cos \alpha_m - C_D \tan \alpha_m$$

$$C_L = 2 \times 1.1 (\tan 48 - \tan 25) \cos 38.25 - .0365 \tan 38.25$$

$$C_L = 1.084 \text{ (}Ans.\text{)}$$

Ideal pressure recovery coefficient

$$C_{ps} = 1 - (\cos^2 \alpha_1 / \cos^2 \alpha_2)$$

$$C_{ps} = 1 - (\cos^2 48 / \cos^2 25) = 0.454 \text{ (}Ans.\text{)}$$

Actual pressure recovery coefficient

$$C_{pa} = C_{ps} - Y = 0.454 - 0.0307 = 0.4233 \text{ (}Ans.\text{)}$$

Diffuser efficiency $\eta_D = C_{pa}/C_{ps}$

$$\eta_D = 0.4233 / 0.454 = 0.932 \text{ (}Ans.\text{)}$$

$$\eta_{D\max} = 1 - 2\ C_D / C_L = 1 - \frac{2 \times 0.0365}{1.084}$$

$$\eta_{D\max} = 0.933\ (Ans.)$$

8.2 The data for a turbine blade row is given below:

blade entry angle	$\alpha_1' = 35°$
blade exit angle	$\alpha_2' = 55°$
incidence	$i = 5°$
deviation	$\delta = 2.5°$
maximum thickness-chord ratio	$t/l = 0.30$
aspect ratio	$h/b = 2.5$

Neglect the difference between the actual and axial chords, and the enthalpy and pressure loss coefficients. Ignore the Reynolds number effects.

Determine for this cascade:

(a) optimum pitch-chord ratio from Zweifel's relation,

(b) loss coefficient from Soderberg's and Hawthorne's relations,

(c) drag coefficient, and

(d) lift coefficient.

***Solution*:**

The air angles are:

$$\alpha_1 = \alpha_1' + i = 35 + 5 = 40°$$

$$\alpha_2 = \alpha_2' - \delta = 55 - 2.5 = 52.5°$$

(a) From Zweifel's relation [Eq. (8.47)]

$$C_z = 2 \left(\frac{s}{b}\right) \cos^2 \alpha_2\ (\tan \alpha_1 + \tan \alpha_2) = 0.8$$

$$\left(\frac{s}{b}\right) \cos^2 52.5\ (\tan 40 + \tan 52.5) = 0.4$$

This gives

$$s/b \approx s/l = 0.505\ (Ans.)$$

(b) From Soderberg's relation Eq. (8.61), ignoring the Reynolds number effect,

$$\xi''' = (1 + \xi^*) \left(0.975 + \frac{0.075}{h/b}\right) - 1$$

The deflection angle is

$$\varepsilon = \alpha_1 + \alpha_2 = 40 + 52.5 = 92.5°$$

This from Fig. (8.25) for $t/l = 0.3$ gives the nominal loss coefficient

$$\xi^* = 0.075$$

$$\xi''' = (1 + .075)\left(0.975 + \frac{0.075}{2.5}\right) - 1$$

$$\xi''' = 0.0804 \ (Ans.)$$

Hawthorne's relation (Eq. (8.48)) gives

$$\xi_p = 0.025\left[1 + \left(\frac{\varepsilon}{90}\right)^2\right]$$

$$\xi_p = 0.025\left[1 + \left(\frac{92.5}{90}\right)^2\right] = 0.0514$$

The total cascade loss coefficient is given by Eq. (8.49),

$$\xi = \left(1 + \frac{3.2}{h/b}\right)\xi_p$$

$$\xi = \left(1 + \frac{3.2}{2.5}\right) 0.0514$$

$$\xi = 0.117$$

Therefore, the average of these two values for the cascade loss is

$$Y \approx \xi_{av} = \frac{1}{2}(0.0804 + 0.117) = 0.0987$$

(c) The mean air angle is given by

$$\tan \alpha_m = \frac{1}{2}(\tan \alpha_2 - \tan \alpha_1)$$

$$\tan \alpha_m = \frac{1}{2}(\tan 52.5 - \tan 40) = 0.232$$

$$\alpha_m = 13.06°$$

The drag coefficient for the cascade is given by Eq. (8.40);

$$C_D = \frac{s}{l} Y \frac{\cos^3 \alpha_m}{\cos^2 \alpha_2}$$

$$C_D = 0.505 \times 0.0987 \frac{\cos^3 13.06}{\cos^2 52.5}$$

$$C_D = 0.124 \ (Ans.)$$

(d) The lift coefficient is given by Eq. (8.41),

$$C_L = 2\left(\frac{s}{l}\right)\cos\alpha_m\,(\tan\alpha_1 + \tan\alpha_2) + C_D\tan\alpha_m$$

$$C_L = 2 \times 0.505 \cos 13.06\,(\tan 40 + \tan 52.5) + 0.124 \tan 13.06$$

$$C_L = 2.1357 \text{ (}Ans.\text{)}$$

8.3 A compressor cascade is constructed from circular arc aerofoil blades (camber angle $\theta = 25°$) set at a stagger angle of 30° with a pitch-chord ratio of 1.0. The momentum thickness-chord ratio is 0.031. The nominal value of the incidence is 5°. Determine:

(a) the cascade blade angles,
(b) the nominal air angles,
(c) stagnation pressure loss coefficient,
(d) drag coefficient, and(e) the lift coefficient.

Solution:

(a) For a circular are camber line

$$\chi_1 = \chi_2$$

Equations (8.63) and (8.64) give

$$\alpha_1' + \alpha_2' = 2\gamma = 2 \times 30 = 60°$$

Equation (8.62) gives

$$\alpha_1' - \alpha_2' = \theta = 25°$$

Therefore, the blade angles are

$$\alpha_1' = 42.5°$$

$$\alpha_2' = 17.5° \qquad (Ans.)$$

(b) $$i^* = 5°$$

From Eq. (8.65)

$$i^* = \alpha_1^* - \alpha_1'$$

$$\alpha_1^* = \alpha_1' + i^* = 42.5 + 5$$

$$\alpha_1^* = 47.5° \text{ (}Ans.\text{)}$$

Nominal exit air angle is determined from Eq. (8.116).

$$\tan\alpha_1^* - \tan\alpha_2^* = \frac{1.55}{1 + 1.5\,s/l}$$

$$\tan\alpha_2^* = \tan\alpha_1^* - 1.55/2.5$$

$$\tan\alpha_2^* = \tan 47.5 - 0.62 = 1.091 - 0.62 = 0.471$$

$$\alpha_2^* = 25.23° \text{ (}Ans.\text{)}$$

(c) Equation (8.107) gives

$$Y = 2\left(\frac{\theta}{l}\right)\left(\frac{l}{s}\right)\frac{\cos^2 \alpha_1^*}{\cos^3 \alpha_2^*}$$

The momentum-thickness-chord ratio is given as $\theta/l = 0.031$. Therefore,

$$Y = 2 \times 0.031 \times 1 \times \frac{\cos^2 47.5}{\cos^3 25.23} = \frac{0.062 \times 0.456}{0.74}$$

$$Y = 0.0382 \ (Ans.)$$

(d) The mean air angle is

$$\tan \alpha_m = \frac{1}{2}(\tan \alpha_1 + \tan \alpha_2) \qquad \text{[Eq. (8.73)]}$$

$$\tan \alpha_m = \frac{1}{2}(\tan 47.5 + \tan 25.23) = 0.781$$

$$\alpha_m = 38°$$

$$C_D = \frac{s}{l} Y \frac{\cos^3 \alpha_m}{\cos^2 \alpha_1} \qquad \text{[Eq. (8.92)]}$$

$$C_D = 1 \times 0.0382 \ (\cos^3 38/\cos^2 47.5)$$

$$C_D = 0.041 \ (Ans.)$$

(e) $$C_L = 2\left(\frac{s}{l}\right)(\tan \alpha_1 - \tan \alpha_2) \cos \alpha_m - C_D \tan \alpha_m$$

$$C_L = 2 \times 1 \times (\tan 47.5 - \tan 25.23) \cos 38 - 0.041 \tan 38$$

$$C_L = 0.947 \ (Ans.)$$

8.4 A blower type annular cascade tunnel has 15 cm long blades on a mean diameter of 50 cm. The maximum velocity upstream of the cascade is expected to be 100 m/s. The total stagnation pressure loss in the tunnel is 10% of the dynamic head in the test section. Determine: **(a)** the total pressure developed by the blower **(b)** its discharge and **(c)** the power required to drive it. Take test section conditions as $t = 35°C$ and $p = 1.02$ bar and an overall blower efficiency of 60%.

Which type of blower do you recommend for this application?

What method do you recommend for varying the test section velocity?

***Solution*:**

$$T = 273 + 35 = 308 \text{ K}$$

$$\rho = \frac{p}{RT} = \frac{1.02 \times 10^5}{287 \times 308} = 1.154 \text{ kg/m}^3$$

(a) the stagnation pressure rise (Δp_0) across the blower less the loss equals the dynamic head in the test section.

$$\Delta p_0 - \text{loss} = \frac{1}{2}\rho c^2$$

$$\Delta p_0 - 0.1\left(\frac{1}{2}\rho c^2\right) = \frac{1}{2}\rho c^2$$

$$\Delta p_0 = 1.1 \times 0.5 \times 1.154 \times 100^2 = 6347 \text{ N/m}^2$$

$$\Delta p_0 = 6347/9.81 = 647 \text{ mm W.G. } (\textit{Ans.})$$

(b) Ignoring the blade thickness the annulus cross-sectional area is

$$A = \pi dh$$

$$A = \pi \times 0.5 \times 0.15 = 0.2356 \text{ m}^2$$

$$Q = cA = 100 \times 0.2356 = 23.56 \text{ m}^3/\text{s}$$

$$Q = 60 \times 23.56 = 1413.6 \text{ m}^3/\text{min } (\textit{Ans.})$$

(c) The power required to drive the blower is

$$P = Q\,\Delta p_0/\eta_0$$

$$P = 23.56 \times 6347/1000 \times 0.6$$

$$P = 249.2 \text{ (say 250) kW } (\textit{Ans.})$$

(d) A single stage centrifugal blower with radial blades or a multi-stage axial blower. (*Ans.*)

(e) Air can be bypassed through an exit located between the blower exit and the settling chamber.

8.5 The radial cascade in Question 8.11 requires Mach number of 0.7 in its test section (upstream of the cascade). In this case air is supplied to the tunnel by a turbo compressor of efficiency = 0.65. Determine

(a) pressure ratio of the compressor,

(b) stagnation pressure in the settling chamber,

(c) static pressure, temperature and velocity of air in the test section,

(d) mass flow rate, and

(e) the power required to drive the air compressor.

Assume isentropic flow downstream of the compressor exit. Atmospheric conditions at the compressor entry are $p_a = 1.013$ bar, $T_a = 306$ K. Take $\gamma = 1.4$ and $c_p = 1.008$ kJ/kg K for air.

***Solution*:**

Let subscripts t represent quantities in the test section, and 1 and 2 entry and exit of the compressor.

From isentropic gas tables at M = 0.7 (for $\gamma = 1.4$)

$$\frac{p_t}{p_0} = 0.721, \quad \frac{T_t}{T_0} = 0.911$$

Here, $p_{01} = p_a$, $p_{02} = p_o$ and $T_{o2} = T_o$, $T_{o1} = T_a$ Since the flow is isentropic after compressor exit, state of air in the settling chamber is same as at compressor exit. Therefore,

(a) $$\frac{p_{02}}{p_{01}} = \frac{p_{02}}{p_a} = p_r = \frac{1}{0.721} = 1.387 \ (Ans.)$$

(b) $p_{o2} = 1.387 \times p_a = 1.387 \times 1.013 = 1.405$ bar *(Ans.)*

(c) Actual temperature rise in the air compressor is

$$T_{o2} - T_{o1} = \frac{1}{\eta_c} (T_{o2s} - T_{o1}) = \frac{T_{01}}{\eta_c} (p_r^{(\gamma-1)/\gamma} - 1)$$

$$T_{o2} - T_{o1} = \frac{306}{0.65} (1.387^{0.2857} - 1) = 46.125$$

$$T_{o2} = T_{o1} + 46.125 = 306 + 46.125 = 352.125 \text{ K}$$

Now, $\frac{T_t}{T_{02}} = 0.911$, $\frac{p_t}{p_{02}} = 0.721$, therefore, test section conditions are given by

$T_t = 0.911 \times 352.125 = 320.785$ K Ans.

$p_t = 0.721 \times 1.405 = 1.013$ bar Ans.

$c_t = M_t (\gamma RT_t)^{1/2}$

$c_t = 0.7 \times (1.4 \times 288 \times 320.785)^{1/2} = 251.747$ m/s *(Ans.)*

(d) See fig. 8.41 for velocity triangle

$c_r = c_t \sin \alpha$

$c_r = 251.747 \times 0.5 = 125.87$ m/s

$$\rho_t = \frac{p_t}{RT_t} = \frac{1.013 \times 10^5}{288 \times 320.785} = 1.0965 \text{ kg/m}^3$$

$\dot{m} = \rho_t A_t c_r$

$A_t = \pi db = \pi \times .45 \times 0.1 = 0.1414 \text{ m}^3$

$\dot{m} = 1.0965 \times 125.87 \times 0.1414$

$\dot{m} = 19.515$ kg/s *(Ans.)*

(e) $P = \dot{m}\ c_p\ (T_{02} - T_{01})$

$P = 19.515 \times 1.008 \times 46.125$

$P = 907.33$ kW *(Ans.)*

Questions and Problems

8.1 Draw a neat and illustrative sketch of a straight cascade tunnel and explain its working. How is the degree of incidence varied?

8.2 (a) Explain how the mass flow weighted average values of the exit air angle and the stagnation pressure loss for a cascade are obtained experimentally?

(b) What are the various parameters that affect the losses in the cascade of blades of axial machines?

(c) Show graphically the variation of compressor cascade losses with incidence, the Reynolds number and Mach number.

8.3 Describe the working of the annular suction and the blower type cascade tunnels for axial machines. What are their advantages over the straight type?

8.4 Explain with the aid of an illustrative sketch the working of an outward flow radial cascade. How is swirling flow at different air angles supplied to such a cascade?

8.5 Show inlet, mean and outlet velocity triangles, and the lift, drag, axial and tangential forces acting on a turbine blade. Prove that:

(a) $$\frac{F_y}{\frac{1}{2}\rho l c^2} = 2\left(\frac{s}{l}\right)\cos^2\alpha_2\,(\tan\alpha_1 + \tan\alpha_2)$$

(b) $$\frac{F_x}{\frac{1}{2}\rho l c_2^2} = \frac{s}{l}\cos^2\alpha_2\,(\tan^2\alpha_2 - \tan^2\alpha_1) + \frac{s}{l}\,Y$$

(c) $$C_L = 2\left(\frac{s}{l}\right)\cos\alpha_m\,(\tan\alpha_1 + \tan\alpha_2) + \frac{s}{l}\,Y\,\frac{\cos^2\alpha_m}{\cos^2\alpha_2}\,\sin\alpha_m$$

(d) $$C_D = Y\left(\frac{s}{l}\right)\frac{\cos^3\alpha_m}{\cos^2\alpha_2}$$

(e) Tangential force/maximum tangential force

$$= 2\left(\frac{s}{b}\right)\cos^2\alpha_2\,(\tan\alpha_1 + \tan\alpha_2)$$

8.6 What is secondary flow in the axial turbine and compressor cascades? How does it lead to a loss of energy? How is it estimated?

8.7 (a) Draw a sketch of an axial flow compressor cascade. Show the stagger angle, incidence (positive and negative) and deviation angles. Prove that:

$$\varepsilon = \theta + i - \delta$$

(b) How are the nominal values of deviation and deflection for a compressor cascade obtained?

8.8 Prove the following relations for an axial compressor cascade:

(a) Pressure recovery coefficient $= 1 - \left(Y + \dfrac{\cos^2 \alpha_1}{\cos^2 \alpha_2} \right)$

(b) Cascade efficiency $= 1 - 2 \dfrac{C_D}{C_L}$ cosec $2\alpha_m$

(c) $C_L = 2 \left(\dfrac{s}{l} \right) (\tan \alpha_1 - \tan \alpha_2) \cos \alpha_m - C_D \tan \alpha_m$

(d) $C_D = Y \left(\dfrac{s}{l} \right) \dfrac{\cos^3 \alpha_m}{\cos^2 \alpha_1}$

8.9 Draw the following for axial flow compressor and turbine cascades:

(a) typical static pressure and velocity distribution curves around the blades, and

(b) velocity and direction profiles at the cascade exit.

(c) What are positive and negative stalling of turbine and compressor blades? How are they caused?

8.10 The average velocity of air at the exit of a turbine blade ($\alpha_1 = 40°$, $\alpha_2 = 65°$) cascade is 100 m/s ($\rho = 1.25$ kg/m^3). The pitch-chord ratio of the cascade is 0.91. The average loss in the stagnation pressure across the cascade is equivalent to 17.5 mm W.G.. Determine for this cascade:

(a) the pressure loss coefficient,

(b) the drag coefficient,

(c) the lift coefficient,

(d) tangential and axial force coefficients, and

(e) the pitch-chord ratio according to Zweifel's criterion.

(Ans.) (a) $Y = 0.0275$ (b) $C_D = 0.082$
(c) $C_L = 4.608$ (d) $C_{Fy} = 0.972$, $C_{Fx} = 0.656$
(e) $s/b = 0.752$.

8.11 An outward flow radial cascade is arranged between diameters of 90 cm and 45 cm, The width of the cascade at the entry is 10 cm. The maximum velocity of air at the entry of the cascade is 75 m/s at a swirl angle of 30°.

Determine the capacity of the blower and the power required to drive it; assume 7% of the head developed by the blower as lost. Take the state of air in the test section as $t = 29°C$ and $p = 1.015$ bar.

Answer: $\Delta p_0 = 360$ mm W.G., $Q = 318$ m^3/min;
$P = 30$ kW (with $\eta_0 = 62\%$).

8.12 (a) How is the mean value of the exit air angle for a cascade of blades for incompressible flow defined? Write down the formula.

(b) Data for an axial flow turbine cascade is given below:

Blade inlet angle	$= 35°$
Flow deflection	$= 91°$
Incidence	$= 4°$
Deviation	$= 3°$

Blade camber line is a circular arc : Draw three blades of this cascade and show flow angle, incidence and deviation.

Calculate:

(i) Camber angles at entry and exit,
(ii) Air angles at entry and exit,
(iii) Stagger angle of the blades
(iv) Mean flow angle through the cascade. State the assumptions used.

(*Ans.*) (i) $\chi_1 = \chi_2 = 45°$ (ii) $\alpha_1 = 39°$, $\alpha_2 = 52°$
(iii) $\gamma = 10°$ (iv) $\alpha_m = 13.23°$

8.13 The annular wind tunnel in Ex. 8.4 is modified to a ninety degree sector for reducing the power requirement. The maximum value of the Mach number at the inlet of the cascade is 0.60. Air is supplied to the tunnel by a compressor which takes in atmospheric air at $p_a = 1.013$ bar, $T_a = 306$ K. calculate

(a) pressure ratio of the compressor,
(b) stagnation pressure in the settling chamber,
(c) static pressure, temperature and velocity of air in the annular test section,
(d) mass flow rate of air, and

(e) the power required to drive the compressor,

(f) compressor power when the entire 360 degrees annulus is used.

Assume isentropic flow throughout. Take $\gamma = 1.4$ and $c_p = 1.008$ kJ/kgK for air.

(*Ans.*) (a) $p_r = 1.2775$ (b) $p_o = 1.294$ bar (c) $p = 1.013$ bar, $T = 306$ K, $c = 210.75$ m/s (d) $\dot{m} = 14.2685$ kg/s (e) $P = 319.35$ kW (f) $P = 1277.4$ kW.

Chapter 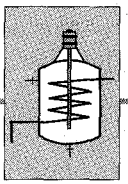 9

Axial Turbine Stages

Various aspects of work and efficencies in turbine stages were discussed in Sec. 2.5. The ideal and actual values of the turbine work and the stage efficiency were defined and the difference between the total to total and total to static efficiencies explained.

Some thermodynamic aspects of the gas and steam turbine plants were discussed in Chapters 3 and 4 respectively, without going into the aerothermodynamics of the flow processes occurring in the turbine stages.

The nature of flow through turbine blade rows (cascades) explaining the mechanism of developing tangential thrust was described in Chapter 8 (Secs. 8.1 to 8.4). Some methods of estimating the losses in blade rows were also given. However, the flow was considered to be only through stationary blade rows. The nomenclature of the individual turbine blades and their rows was introduced and the geometries of the blade rows and the flow through them also described.

This chapter deals with the aerothermodynamics[7, 287,300] of the flow in actual and complete turbine stages. The flow phenomenon occurring in rotor blade rows as observed by an observer moving with the rotor is not much different from that discussed in Sec. 8.4. Therefore, the material covered in that section is fully valid for blade rows in actual turbine stages.

In a majority of cases a velocity triangle at a given section is drawn at the mean radius of the blade row. This either represents mean values of the velocities and angles for the blade row which are obtained as explained in Chapter 8 or it is assumed that the flow is one dimensional at the section under consideration. Variations in blade and flow parameters along the blade height are considered in Sec. 9.9 on three-dimensional flow.

9.1 Stage Velocity Triangles

A brief reference to velocity triangles has been given in section 1.16. Equation (1.5) gives the method of drawing velocity triangles. The notation used here corresponds to the x-y coordinates; the suffix x

identifies components in the axial direction and the suffix y refers to the tangential direction.

Air angles in the absolute system are denoted by alpha (α), whereas those in the relative system are represented by beta (β).

Figure 9.1 gives the velocity triangles at the entry and exit of a general turbine stage. Since the stage is axial, the change in the mean diameter between its entry and exit is negligible. Therefore, the peripheral or tangential velocity (u) remains constant in the velocity triangles.

Axial and tangential components of both absolute and relative velocities are shown in the figure. Static and stagnation values of pressure and enthalpy in the absolute and relative systems are also shown.

The following useful trignometrical relations are obtained from the velocity triangles in Fig. 9.1.

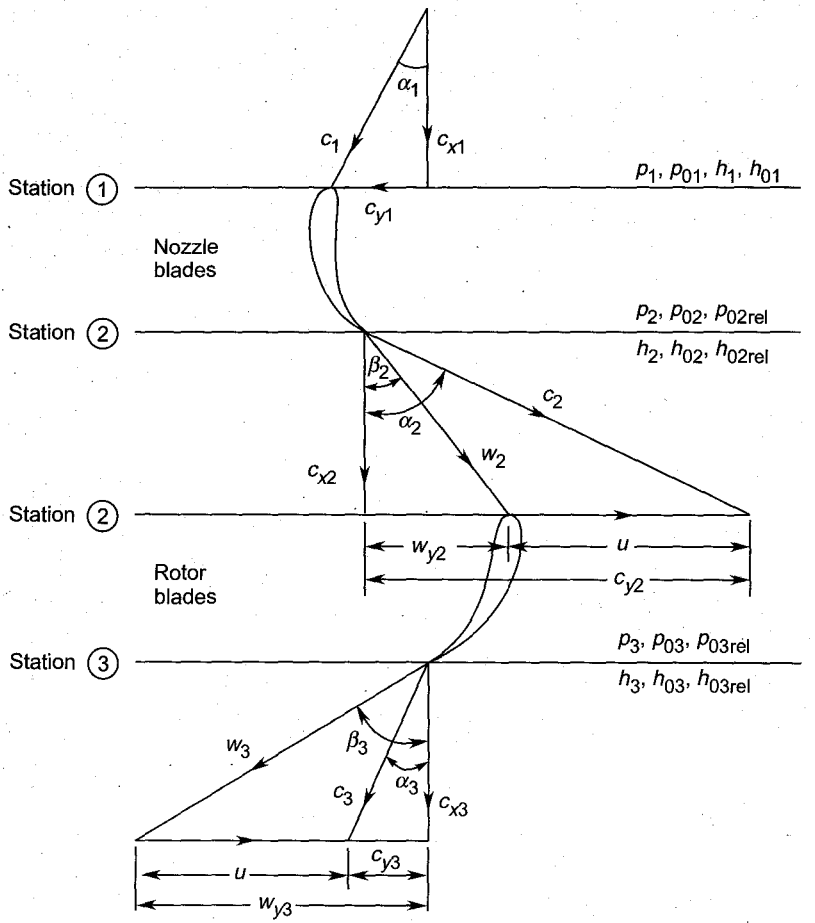

Fig. 9.1 Velocity triangles for a turbine stage

$$c_{x2} = c_2 \cos \alpha_2 = w_2 \cos \beta_2 \tag{9.1}$$

$$c_{y2} = c_2 \sin \alpha_2 = w_{y2} + u = w_2 \sin \beta_2 + u \tag{9.2}$$

$$\frac{u}{\sin(\alpha_2 - \beta_2)} = \frac{c_2}{\sin(90 + \beta_2)} = \frac{c_2}{\cos \beta_2}$$

$$\frac{u}{c_2} = \frac{\sin(\alpha_2 - \beta_2)}{\cos \beta_2} \tag{9.3}$$

$$c_{x3} = w_3 \cos \beta_3 = c_3 \cos \alpha_3 \tag{9.4}$$

$$c_{y3} = c_3 \sin \alpha_3 = w_{y3} - u = w_3 \sin \beta_3 - u \tag{9.5}$$

$$c_{y2} + c_{y3} = c_2 \sin \alpha_2 + c_3 \sin \alpha_3$$

$$c_{y2} + c_{y3} = (w_2 \sin \beta_2 + u) + (w_3 \sin \beta_3 - u)$$

$$c_{y2} + c_{y3} = w_2 \sin \beta_2 + w_3 \sin \beta_3 \tag{9.6}$$

$$c_{y2} + c_{y3} = w_{y2} + w_{y3}$$

It is often assumed that the axial velocity component remains constant through the stage. For such a condition

$$c_x = c_{x1} = c_{x2} = c_{x3}$$

$$c_x = c_1 \cos \alpha_1 = c_2 \cos \alpha_2$$

$$= w_2 \cos \beta_2 = c_3 \cos \alpha_3 = w_3 \cos \beta_3 \tag{9.7}$$

Equation (9.6) for constant axial velocity yields a useful relation:

$$\tan \alpha_2 + \tan \alpha_3 = \tan \beta_2 + \tan \beta_3 \tag{9.8}$$

9.1.1 Work

How various forces and torque are exerted on the rotor blades by the fluid flowing through them was explained in detail in Chapters 6 and 8. Though forces and torques are exerted on both stationary and moving blades alike, work can only be done on the moving rotor blades. Thus the rotor blades transfer energy from the fluid to the shaft. The differences between Euler's, isentropic and actual values of the work also have been explained in Secs. 6.9.3, 6.9.4 and 6.9.5 respectivley.

In the present system of notation, Eq. (6.148b) for the stage work in an axial turbine ($u_3 = u_2 = u$), can be written as

$$w = u \{c_{y2} - (- c_{y3})\}$$

$$w = u (c_{y2} + c_{y3})^* \tag{9.9}$$

---

* In general, Eq. (9.9) will be written with a minus sign between c_{y2} and c_{y3}. Whenever this is written with a plus sign it is implied that c_{y3} is negative.

This equation can also be expressed in another useful form.

$$w = u^2 \left(\frac{c_{y2}}{u} + \frac{c_{y3}}{u} \right) \tag{9.10}$$

The first term (c_{y2}/u) in the bracket depends on the nozzle or flixed blade angle α_2 and the ratio $\sigma = u/c_2$. The contribution of the second term (c_{y3}/u) to the work is generally small. It is also observed that the kinetic energy of the fluid leaving the stage is greater for larger values of c_{y3}. The leaving loss from the stage is minimum when $c_{y3} = 0$, i.e. when the discharge from the stage is axial $(c_3 = c_{x3})$. However, this condition gives lesser stage work as can be seen from Eqs. (9.9) and (9.10).

If the swirl at the exit of the stage is zero; i.e. $c_{y3} = 0$, Eq. (9.10) yields

$$w_{cy3=0} = \left(\frac{c_{y2}}{u} \right) u^2$$

$$w_{cy3=0} = \left(\frac{c_2 \sin \alpha_2}{u} \right) u^2$$

$$w_{cy3=0} = \left(\frac{\sin \alpha_2}{\sigma} \right) u^2 \tag{9.11}$$

9.1.2 Blade Loading and Flow Coefficients

Various dimensionless parameters for turbomachines have been developed in Chapter 7. The loading coefficient (ψ) and the flow coefficient have been defined as

$$\psi = \frac{w}{u^2} \tag{9.12}$$

$$\phi = \frac{c_x}{u} \tag{9.13}$$

Since the work in Eq. (9.12) is frequently referred to as the blade or stage work, the coefficient ψ would also be known as the blade or stage loading coefficient.

Equation (9.9) along with Eqs. (9.12) and (9.13) for constant axial velocity gives

$$\psi = \phi (\tan \alpha_2 + \tan \alpha_3) = \phi (\tan \beta_2 + \tan \beta_3) \tag{9.14}$$

The $\phi - \psi$ plots (see Sec. 7.6) are useful in comparing the performances of various stages of different sizes and geometries. This will be discussed further in later sections.

9.1.3 Blade and Stage Efficiencies

While the blade and stage works (outputs) are the same, the blade and stage efficiencies are not equal. This is because the energy inputs to the rotor blades and the stage (fixed blade ring plus the rotor) are different. The blade efficiency is also known as the utilization factor (ε) which is an index of the energy utilizing capability of the rotor blades. Thus

$$\varepsilon = \eta_b = \frac{\text{rotor blade work}}{\text{energy supplied to the rotor blades}} = \frac{w}{e_i} \tag{9.14a}$$

Section 6.9.2 gives the blade work as the sum of changes in the various kinetic energies.

$$\begin{aligned} w &= u_2 c_{y2} - u_3\, c_{y3} \\ &= \frac{1}{2}\,(c_2^2 - c_3^2) + \frac{1}{2}\,(u_2^2 - u_3^2) + \frac{1}{2}\,(w_3^2 - w_2^2) \end{aligned} \tag{9.15}$$

[see Eq. (6.153a)]

The energy supplied to the rotor blades is the absolute kinetic energy in the jet at the entry plus the kinetic energy change within the rotor blades.

$$e_i = \frac{1}{2}\,c_2^2 + \frac{1}{2}\,(w_3^2 - w_2^2) + \frac{1}{2}\,(u_2^2 - u_3^2) \tag{9.16}$$

Putting Eqs. (9.15) and (9.16) into Eq. (9.14a), we get

$$\varepsilon = \eta_b = \frac{(c_2^2 - c_3^2) + (u_2^2 - u_3^2) + (w_3^2 - w_2^2)}{c_2^2 + (w_3^2 - w_2^2) + (u_2^2 - u_3^2)} \tag{9.17}$$

For axial machines, $u = u_2 = u_3$,

$$\varepsilon = \eta_b = \frac{(c_2^2 - c_3^2) + (w_3^2 - w_2^2)}{c_2^2 + (w_3^2 - w_2^2)} \tag{9.18}$$

To avoid confusion between the blade and stage efficiencies, the term utilization factor (ε) will be used in place of blade efficiency hereafter.

A stage has been defined in Sec. 1.7. The rows of nozzle and rotor blades between stations one and two, and two and three respectively have been represented by the blades shown in Fig. 9.1.

As pointed out earlier, the stage output is the same as the rotor blade work and is given by Eqs. (9.9), (9.10) and (9.15), but the energy input to the stage is different from the input to the rotor blades. Besides this, the stage efficiency (see Sec. 2.5, Eqs. (2.107) and (2.112)) is not defined on the same lines as the utilizatin factor. The stage efficiency (η_{st}) takes into account the aerodynamic losses (Sec. 8.4.5) occurring in the fixed and moving blade rows of the stage.

9.2 Single Impulse Stage

A single stage impulse turbine is shown in Fig. 9.2. As pointed out in Sec. 1.12, there is no change in the static pressure through the rotor of an impulse machine. The variation of pressure and velocity of the fluid through the stage is also shown in Fig. 9.2.

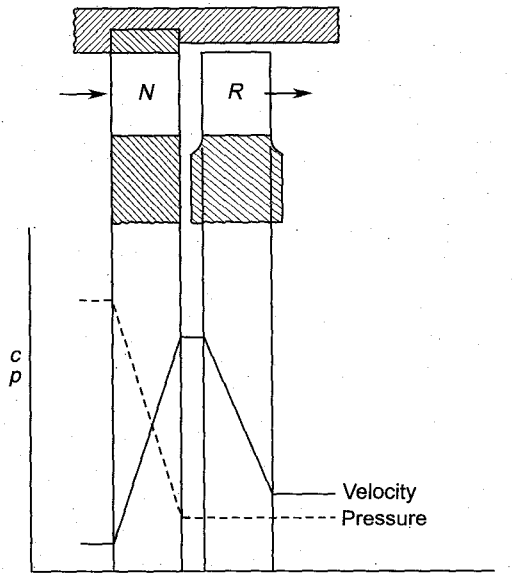

Fig. 9.2 Variation of pressure and velocity through a single stage impulse turbine

The absolute velocity of the fluid increases corresponding to the pressure drop through the nozzle blade row in which only transformation of energy occurs. The transfer of energy occurs only across the rotor blade row. Therefore, the absolute fluid velocity decreases through this as shown in the figure.

The velocity triangles for a single impulse stage are shown in Fig. 9.3 (a). In the absence of any pressure drop through the rotor blades the relative velocities at their entry and exit are the same ($w_2 = w_3$) for fricitionless flow. To obtain this condition the rotor blade angles must be equal. Therefore, the utilization factor is given by

$$\varepsilon = \frac{u\,(c_{y2} + c_{y3})}{\frac{1}{2}c_2^2}$$

Substituting from Eq. (9.6) and noting

$w_2 = w_3$, $\beta_2 = \beta_3$, we get

$$\varepsilon = 4\ uw_2 \sin \beta_2 / c_2^2$$

From the velocity triangle at the entry (Fig. 9.3 (a)),

$$\varepsilon = 4u\ (c_2 \sin \alpha_2 - u)/c_2^2$$

Putting $\sigma = u/c_2$ and rearranging,

$$\eta_b = \varepsilon = 4\ (\sigma \sin \alpha_2 - \sigma^2) \tag{9.19}$$

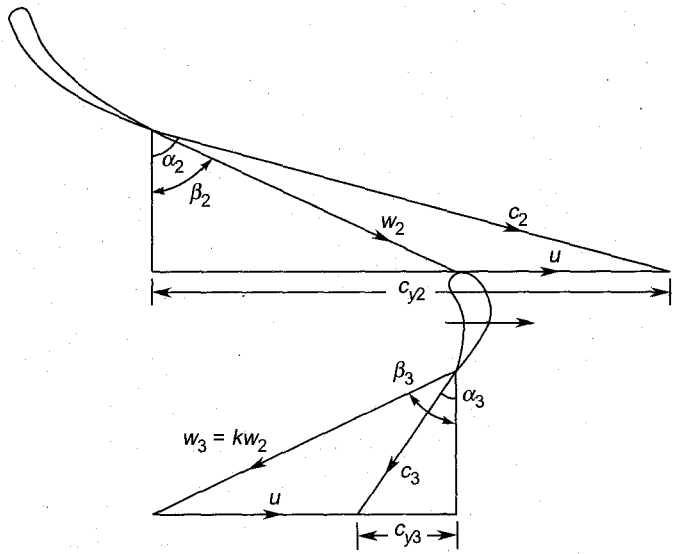

Fig. 9.3 (a) Velocity triangles for a single impulse stage with negative swirl at exit

This shows that the utilization factor is a function of the blade-to-gas speed ratio and the nozzle angle.

$$\varepsilon = f(\sigma, \alpha_2)$$

The value of σ corresponding to maximum utilization can be determined. For given value of α_2, differentiatig Eq. (9.19),

$$\frac{d\varepsilon}{d\sigma} = \sin \alpha_2 - 2\sigma = 0$$

$$\sigma_{opt} = \frac{u}{c_2} = \frac{1}{2} \sin \alpha_2 \tag{9.20}$$

$$c_2 \sin \alpha_2 = c_{y2} = 2u \tag{9.21}$$

Equations (9.2) and (9.21) give

$$w_2 \sin \beta_2 = w_3 \sin \beta_3 = u \tag{9.22}$$

Substituting this in Eq. (9.5) yields $c_{y3} = 0$. This requries the exit from the stage in the axial direction, i.e. $c_3 = c_{x3}$. This result can also be obtained by mere physical interpretation of the mechanics of flow.

Combining Eq. (9.20) and (9.11),

$$w_{cy3=0} = w_{opt} = 2\ u^2 \tag{9.23}$$

Velocity traingles to satisfy these conditions are shown in Fig. 9.3(b). The combination of Eqs. (9.19) and (9.20) gives

$$\varepsilon_{max} = \sin^2 \alpha_2 \tag{9.24}$$

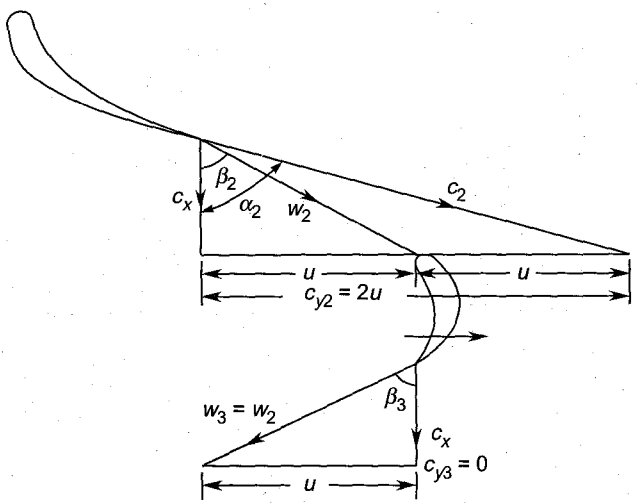

Fig. 9.3 (b) Velocity triangles for a single impulse stage with maximum utilization factor

The rotor blade angles can also be determined for these conditions

$$\tan \beta_3 = \tan \beta_2 = \frac{u}{c_2 \cos \alpha_3}$$

Substituting from Eq. (9.20),

$$\tan \beta_3 = \tan \beta_2 = \frac{1}{2} \tan \alpha_2 \tag{9.25}$$

Thus for maximum utilization factor, the rotor blade air angles are fixed by the nozzle air angle at exit.

9.3 Multi-stage Velocity-compounded Impulse

When the pressure drop available is large, it cannot all be used in one turbine stage. A single stage utilizing a large pressure drop will have an impractically high peripheral speed of its rotor. This would lead to either a larger diameter or a very high rotational speed. Therefore, machines with large pressure drops employ more than one stage.

One of the methods to employ multi-stage expansion in impulse turbines is to generate high velocity of the fluid by causing it to expand through a large pressure drop in the nozzle blade row. This high velocity fluid then transfers its energy in a number of stages by employing many rotor blade rows separated by rows of fixed guide blades. A two-stage velocity compounded impulse turbine is shown in Fig. 9.4. The decrease in the absolute velocity of the fluid across the two rotor blade rows (R_1 and R_2) is due to the energy transfer; the slight decrease in the fluid velocity through the fixed guide blades (F) is due to losses. Since the turbine is of the impulse type, the pressure of the fluid remains constant after its expansion in the nozzle blade row. Such stages are referred to as velocity or Curtis stages.

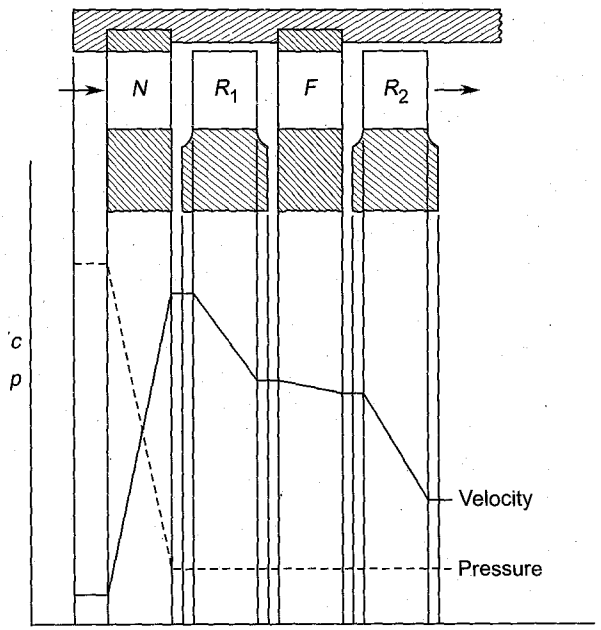

Fig. 9.4 Variation of pressure and velocity through a two-stage velocity compounded impulse trubine

Figure 9.5 shows the velocity triangles for the aforementioned turbine. For the utilization factor to be maximum, the exit from the last stage (in this case the second-stage rotor) must be in the axial direction, i.e. $\alpha'_3 = 0$ and $c'_3 = c_x$.

The following two assumptions are made for this turbine:

1. Equiangular flow through rotor and guide blades

$$\beta_2 = \beta_3;\ \alpha_3 = \alpha'_2;\ \beta'_2 = \beta'_3$$

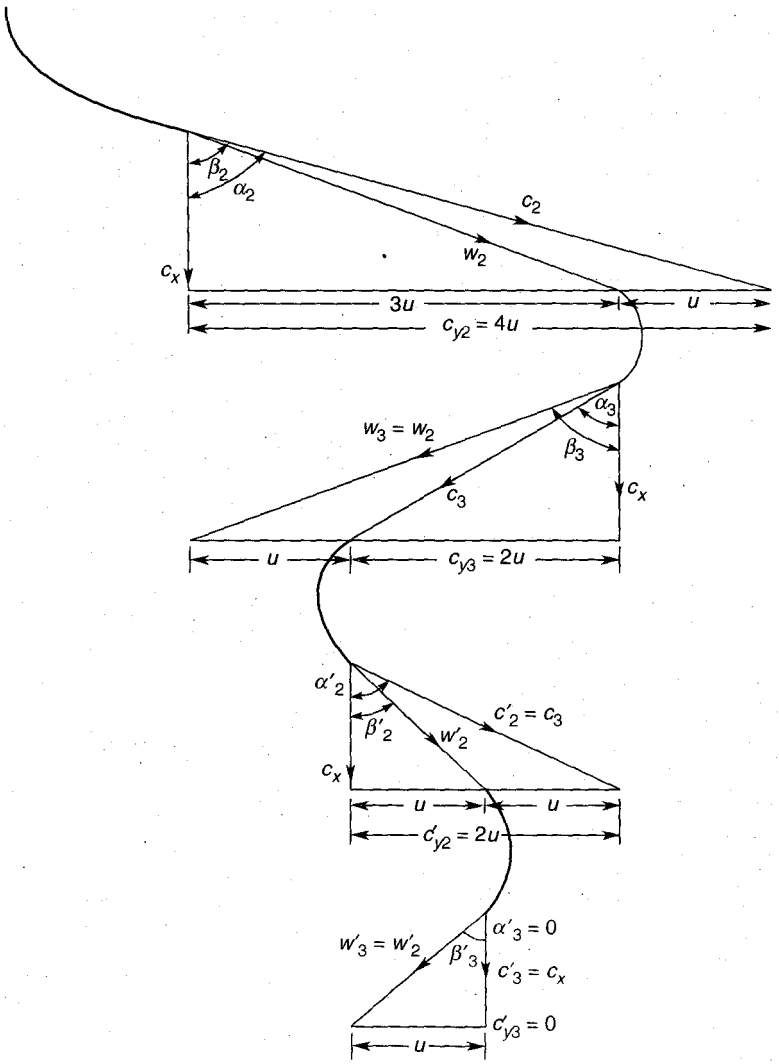

Fig. 9.5 Velocity triangles for a two-stage velocity compounded impulse turbine with maximum utilization factor

2. Frictionless flow over the blades

$$w_2 = w_3;\ c_3 = c'_2;\ w'_2 = w'_3$$

For maximum utilization factor, $c'_{y3} = 0$ and

$$u = w'_3 \sin \beta'_3 = w'_2 \sin \beta'_2 \tag{9.26}$$

$$c'_{y2} = 2u = c'_2 \sin \alpha'_2 = c_3 \sin \alpha_3 \tag{9.27}$$

$$c_{y3} = 3u = w_3 \sin \beta_3 = w_2 \sin \beta_2 \tag{9.28}$$

$$c_{y2} = c_2 \sin \alpha_2 = w_2 \sin \beta_2 + u$$

Substituting from Eq. (9.28),

$$c_2 \sin \alpha_2 = 4u$$

$$\sigma_{\text{opt.}} = u/c_2 = \frac{1}{4} \sin \alpha_2 \tag{9.29}$$

Similarly, for a three-stage velocity compounded turbine

$$\sigma_{\text{opt}} = \frac{1}{6} \sin \alpha_2$$

Thus for n velocity stages,

$$\sigma_{\text{opt}} = \frac{1}{2n} \sin \alpha_2 \tag{9.30}$$

Values of work in the first and second stages, from Eq. (9.6) are given by

$$w_I = u\,(w_2 \sin \beta_2 + w_3 \sin \beta_3)$$

$$w_{II} = u\,(w'_2 \sin \beta'_2 + w'_3 \sin \beta'_3)$$

From assumptions 1 and 2,

$$w_I = 2u w_2 \sin \beta_2$$

From Eq. (9.28)

$$w_I = 6u^2 \tag{9.31}$$

This expression can also be written directly from the velocity triangles shown in Fig. 9.5.

Similiarly Eq. (9.26) gives

$$w_{II} = 2u w'_2 \sin \beta'_2$$

$$w_{II} = 2u^2 \tag{9.32}$$

The total work of the velocity compounded impulse turbine (with two stages) is

$$w_I + w_{II} = 8u^2 \tag{9.33}$$

The expressions in Eqs. (9.31), (9.32) and (9.33) can be represented by the following general relations.

If the number of velocity stages is n with individual stages identified by $i = 1$, $i = 2, \ldots, i = n$, then the work done by the ith stage is given by

$$w_i = 2\,\{2\,(n - i) + 1\}\,u^2 \tag{9.34}$$

The total turbine work with n velocity stages is given by

$$w_T = \sum_{i=1}^{n} w_i = 2n^2\,u^2 \tag{9.35}$$

Since the turbine is of the impulse type, the input energy is equal to $\frac{1}{2} c_2^2$. Therefore, the utilization factor from Eq. (9.35) is

$$\varepsilon_{\max} = \frac{w_T}{\frac{1}{2} c_2^2} = 4n^2 \left(\frac{u}{c_2}\right)^2$$

$$\varepsilon_{\max} = 4n^2\sigma^2 \tag{9.36}$$

Equations (9.30) and (9.36) yield

$$\varepsilon_{\max} = \sin^2 \alpha_2$$

This shows that the maximum value of the utilizations factor for a given value of the nozzle angle remains unaltered with the number of velocity stages under the assumed conditions.

Values in Table 9.1 have been computed from Eqs. (9.30), (9.34), (9.35) and (9.36). It is observed that the turbine work in the velocity stages increases drastically by employing more velocity stages. This is a great advantage because the pressure of the steam (or gas) is reduced quickly. This gives a much smaller number of stages, reduces the overall turbine length and only a small part of the turbine casing is subjected to high steam pressure. However, the work in the subsequent velocity stages goes on decreasing, e.g., the third stage in the three-stage turbine only produces one-ninth of the total work. Therefore, velocity stages beyond three are of no practical value.

As stated in Sec. 1.15, the pressure ratios across gas turbines are much lower as compared to steam turbines. Therefore, the problem of reducing

Table 9.1 Values of Stage and Turbine Work, Blade-to-Gas Speed Ratio and Maximum Utillization Factor for Velocity Compounded Impulse Turbine

n	Work						σ_{opt}	ε_{max}
	$i=1$	$i=2$	$i=3$	$i=4$	$i=5$	w_T		
1	$2u^2$					$2u^2$	$\frac{1}{2}\sin\alpha_2$	$\sin^2\alpha_2$
2	$6u^2$	$2u^2$				$8u^2$	$\frac{1}{4}\sin\alpha_2$	$\sin^2\alpha_2$
3	$10u^2$	$6u^2$	$2u^2$			$18u^2$	$\frac{1}{6}\sin\alpha_2$	$\sin^2\alpha_2$
4	$14u^2$	$10u^2$	$6u^2$	$2u^2$		$32u^2$	$\frac{1}{8}\sin\alpha_2$	$\sin^2\alpha_2$
5	$18u^2$	$14u^2$	$10u^2$	$6u^2$	$2u^2$	$50u^2$	$\frac{1}{10}\sin\alpha_2$	$\sin^2\alpha_2$

the gas pressure quickly in the casings of gas turbines is not so serious. Besides this the losses in the velocity stages are higher compared to the reaction stages. Therefore, velocity staging has little to offer in the field of gas turbines except in some special applications.

9.4 Multi-stage Pressure-compounded Impulse

There are two major problems in velocity-compounded stages: (1) the nozzles have to be of the convergent-divergent type for generating high (supersonic) steam velocity. This results in a more expensive and difficult design of the nozzle blade rows; and (2) high velocity at the nozzle exit leads to higher cascade losses. Shock waves are generated if the flow is supersonic which further increase the losses.

To avoid these problems, another method of utilizing a high pressure ratio is employed in which the total pressure drop is divided into a number of impulse stages. These are known as pressure-compounded or Rateau stages. On account of the comparatively lower pressure dop, the nozzle blade rows are subsonic (M < 1). Therefore, such a stage does not suffer from the disabilities of the velocity stages. Figure 9.6 (a) shows the variation of pressure and velocity of steam through the two pressure

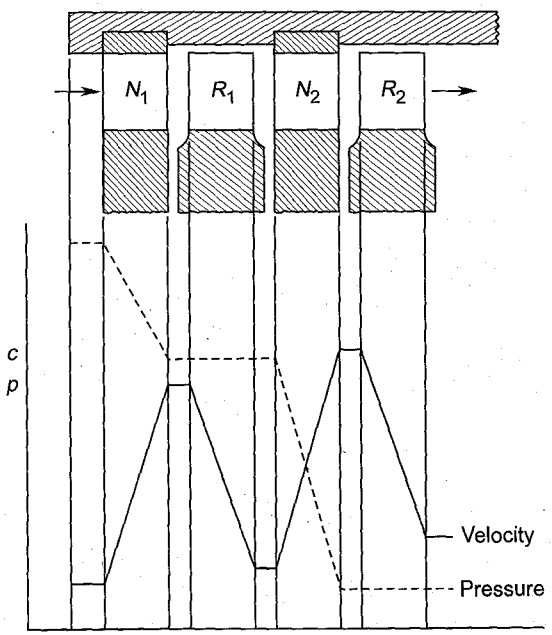

Fig. 9.6 (a) Variation of pressure and velocity through a two-stage pressure-compounded impulse turbine

stages of an impulse turbine. This is equivalent to using two stages of the type shown in Fig. 9.2 in series. Velocity triangles for two Rateau stages, each having an axial exit are shown in Fig. 9.6 (b); the nozzle blades in each stage receive flow in the axial direction.

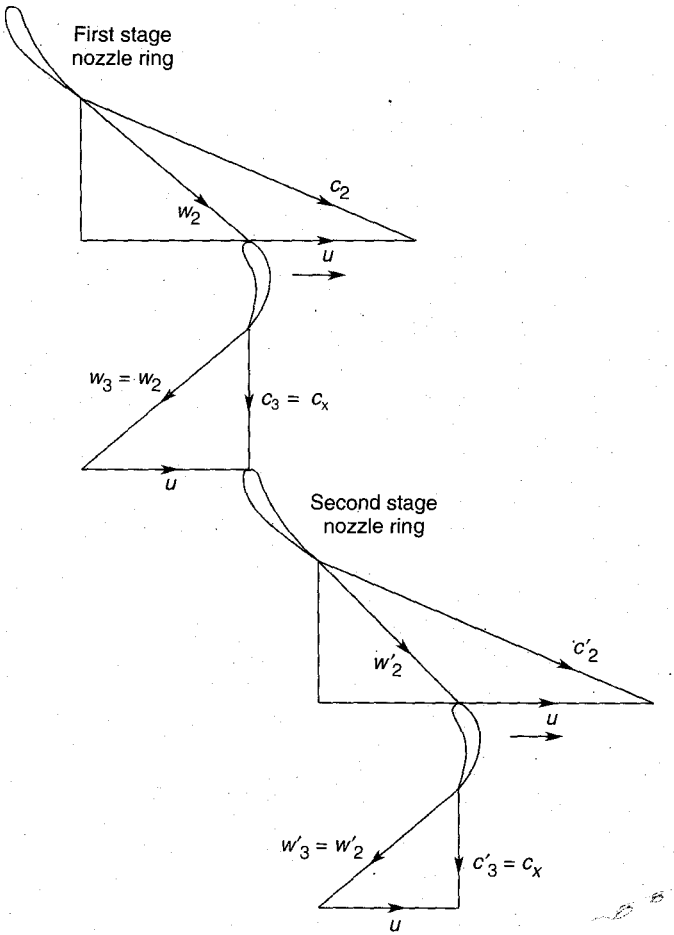

Fig. 9.6 (b) Velocity triangles for a two-stage pressure-compounded impulse turbine

Some designers employ pressure stages up to the last stage. This gives a turbine of shorter length as compared to the reaction type, with a penalty on efficiency.

9.5 Reaction Stages

A brief introduction of reaction stages and the degree of reaction is given in Sec. 1.13. Figure 9.7 shows two reaction stages and the variation of

pressure and velocity of the gas in them. The gas pressure decreases continuously over both fixed and moving rows of blades. Since the pressure drop in each stage is smaller as compared to the impulse stages, the gas velocities are relatively low. Besides this the flow is accelerating throughout. These factors make the reaction stages aerodynamically more efficient though the tip leakage loss is increased on account of the relatively higher pressure difference across the rotor blades.

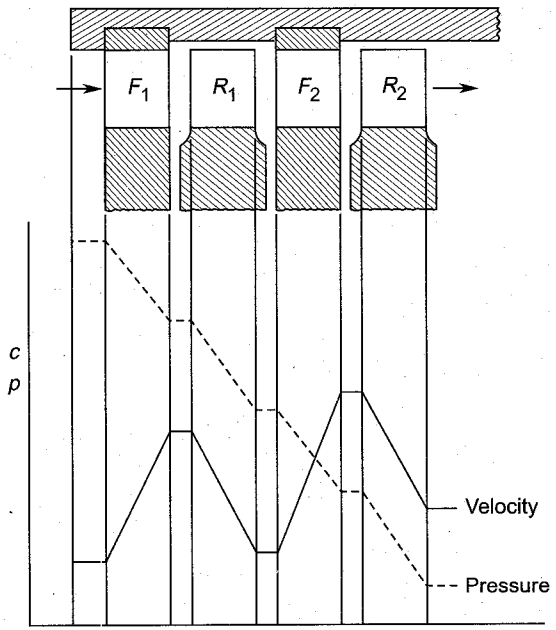

Fig. 9.7 Variation of pressure and velocity through a two-stage reaction turbine

Multi-stage reaction turbines employ a large pressure drop by dividing it to smaller values in individual stages. Thus the reaction stages are like the pressure-compounded stages (Sec. 9.4) with a new element of "reaction" introduced in them, i.e. of accelerating the flow through rotor blade rows also.

9.5.1 Enthalpy-entropy Diagram

Figure 9.8 shows the enthalpy-entropy diagram for flow through a general turbine stage with some degree of reaction. This should be studied along with the velocity triangles in Fig. 9.1. Both static and stagnation values of the pressures and enthalpies are indicated at various stations.

In general, the gas approaches the stage with a finite velocity (c_1). Therefore, the values of pressures p_1 and p_{01} and enthalpies h_1 and h_{01}

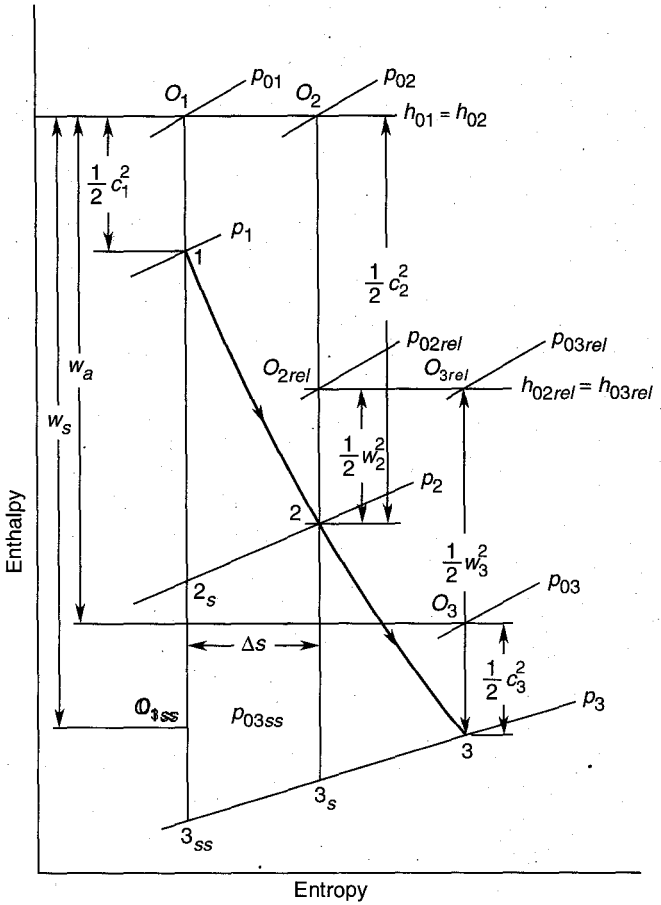

Fig. 9.8 Enthalpy-entropy diagram for flow through a turbine stage

have been differentiated. The relation between the static and stagnation values has been explained in Sec. 2.2.

The reversible adiabatic (isentropic) expansion of the gas through fixed and moving rows of blades is represented by processes 1-2*s* and 2*s*-3*ss* respectively. Stagnation points 0_1 and 0_{3ss} are defined by the following relations:

$$h_{01} = h_1 + \frac{1}{2} c_1^2 \tag{9.37}$$

$$h_{03ss} = h_{3ss} + \frac{1}{2} c_{3ss}^2 \tag{9.38}$$

The ideal work in the stage is given by

$$w_s = h_{01} - h_{03ss} = c_p (T_{01} - T_{03ss}) \tag{9.39}$$

The actual expansion process (irreversible adiabatic) is represented by the curve 1-2-3, and the actual states of the gas at the exits of the fixed and moving blades are represented by points 2 and 3 respectively. Since there is only energy transformation and no energy transfer (work) between states 1 and 2, the stagnation enthalpy remains constant.

$$h_{01} = h_{02} = h_2 + \frac{1}{2} c_2^2 \tag{9.40}$$

The loss due to irreversibility ($\Delta s = s_2 - s_{2s}$) is given by the enthalpy loss coefficient

$$\xi_N = \frac{h_2 - h_{2s}}{\frac{1}{2} c_2^2} = \frac{2c_p}{c_2^2} (T_2 - T_{2s}) \tag{9.41}$$

Various losses occurring in turbine blade cascades have already been described in Sec. 8.4.5.

The stagnation pressure loss coefficient corresponding to Eq. (9.41) is defined by

$$Y_N = \frac{p_{01} - p_{02}}{\frac{1}{2} \rho c_2^2} = \frac{(\Delta p_0)_N}{\frac{1}{2} \rho c_2^2} \tag{9.42}$$

The expansion process (2-3) in the moving blade rows represents both transformation and transfer of energy. Therefore, the difference in the absolute stagnation enthalpies at states 2 and 3 gives the actual value of the stage work.

$$w_a = h_{02} - h_{03} = h_{01} - h_{03} = c_p (T_{01} - T_{03}) \tag{9.43}$$

$$h_{03} = h_3 + \frac{1}{2} c_3^2 \tag{9.44}$$

However, to an observer moving with the rotor the relative flow appears as the absolute flow in the nozzle to a stationary observer. Therefore, for him (in the relative system) the stagnation enthalpy in the moving frame of coordinates remains constant.

$$h_{02\text{rel}} = h_{03\text{rel}}$$

$$h_2 + \frac{1}{2} w_2^2 = h_3 + \frac{1}{2} w_3^2 \tag{9.45}$$

The enthalpy and pressure losses for the moving row of blades are given by the following coefficients:

$$\xi_R = \frac{h_3 - h_{3s}}{\frac{1}{2} w_3^2} = \frac{2c_p}{w_3^2} (T_3 - T_{3s}) \tag{9.46}$$

$$Y_R = \frac{p_{02\text{rel}} - p_{03\text{rel}}}{\frac{1}{2}\rho w_3^2} = \frac{(\Delta p_0)_R}{\frac{1}{2}\rho w_3^2} \tag{9.47}$$

It can be proved that for most of the applications ($M < 1$), there is little difference between the values of the loss coefficients based on enthalpy and stagnation pressure, i.e. $\xi \approx Y$.

9.5.2 Degree of Reaction

Degree of reaction of a turbine stage can be defined in a number of ways; it can be expressed in terms of pressures, velocities, enthalpies or the flow geometry in the stage.

(a) A definition, on the basis of the isentropic change in the stage, is given by the following relation:

$$R = \frac{\text{isentropic change of enthalpy in the rotor}}{\text{isentropic change of enthalpy in the stage}}$$

$$R = \frac{\int_{3ss}^{2s} dh}{\int_{3ss}^{1} dh} = \frac{h_{2s} - h_{3ss}}{h_1 - h_{3ss}} \tag{9.48}$$

Assuming $\rho \approx$ constant, Eq. (9.48) can be transformed in terms of pressures.

Using $dh = \dfrac{dp}{\rho}$

$$R = \frac{\int_{3ss}^{2s} \frac{dp}{\rho}}{\int_{3ss}^{1} \frac{dp}{\rho}} \approx \frac{\int_{3ss}^{2s} dp}{\int_{3ss}^{1} dp}$$

$$R = \frac{p_2 - p_3}{p_1 - p_3} \tag{9.49}$$

(b) The definitions in Eqs. (9.48) and (9.49) are not widely used in practice. Since the actual enthalpy changes and work are more important for turbine stages, a definition of the degree of reaction based on these quantities is more logical and useful.

From the discussions in Sec. 6.9, it may be seen that the change through the rotor and the total change in the stage are

$$h_2 - h_3 = \frac{1}{2}(w_3^2 - w_2^2) + \frac{1}{2}(u_2^2 - u_3^2) \tag{9.50}$$

$$h_{01} - h_{03} = h_{02} - h_{03} = (u_2 c_{y2} - u_3 c_{y3}) \tag{9.51}$$

The ratio of these quantities gives another definition of the degree of reaction.

$$R = \frac{h_2 - h_3}{h_{02} - h_{03}} \tag{9.52}$$

If $c_1 \approx c_3$,

$$R = \frac{h_2 - h_3}{h_1 - h_3} \tag{9.53}$$

Equations (9.50) and (9.51) when substituted in (9.52) yield

$$R = \frac{\frac{1}{2}(w_3^2 - w_2^2) + \frac{1}{2}(u_2^2 - u_3^2)}{u_2 c_{y2} - u_3 c_{y3}} \tag{9.54}$$

For axial machines, $u_3 = u_2 = u$. Therefore, from Fig. 9.1.

$$R = \frac{w_3^2 - w_2^2}{2u(c_{y2} + c_{y3})} \tag{9.55}$$

(c) Equation (9.55) can also be expressed in terms of the geometry of flow through the stage.

From velocity triangles (Fig. 9.1),

$$w_2^2 = c_{x2}^2 + w_{y2}^2$$
$$w_3^2 = c_{x3}^2 + w_{y3}^2$$

For constant axial velocity,

$$w_3^2 - w_2^2 = w_{y3}^2 - w_{y2}^2 = c_x^2 (\tan^2 \beta_3 - \tan^2 \beta_2) \tag{9.56}$$
$$w_3^2 - w_2^2 = (w_{y3} + w_{y2})(w_{y3} - w_{y2})$$

Using Eq. (9.6) and the velocity triangles,

$$w_3^2 - w_2^2 = c_x (c_{y2} + c_{y3})(\tan \beta_3 - \tan \beta_2) \tag{9.57}$$

Equation (9.57) when put into (9.55) yields a widely used definition for the degree of reaction.

$$R = \frac{c_x}{2u}(\tan \beta_3 - \tan \beta_2) \tag{9.58}$$

But $$\phi = \frac{c_x}{u}$$

and Eq. (8.26b) gives

$$\tan \beta_m = \frac{1}{2}(\tan \beta_3 - \tan \beta_2),$$
$$R = \phi \tan \beta_m \tag{9.59}$$

Two more useful relations are obtained assuming c_x to be constant. From the velocity triangle at the entry, Eq. (9.2) can be written as

$$c_x \tan \alpha_2 = c_x \tan \beta_2 + u$$

$$\tan \beta_2 = \tan \alpha_2 - \frac{u}{c_x} \tag{9.60}$$

Eliminating $\tan \beta_2$ between Eqs. (9.58) and (9.60), and rearranging,

$$R = \frac{1}{2} + \frac{c_x}{2u} (\tan \beta_3 - \tan \alpha_2) \tag{9.61}$$

Equation (9.5) can similarly be written as

$$c_x \tan \alpha_3 = c_x \tan \beta_3 - u$$

$$\tan \beta_3 = \tan \alpha_3 + \frac{u}{c_x} \tag{9.62}$$

Equation (9.62) when substituted in (9.61) gives

$$R = 1 + \frac{c_x}{2u} (\tan \alpha_3 - \tan \alpha_2) \tag{9.63}$$

These relations will be used later.

9.5.3 Zero Degree Reaction Stages

Though a single-stage impulse turbine has already been discussed in Sec. 9.2, it is further discussed here in the light of the preceding section.

(a) Figure 9.9 shows the enthalpy-entropy diagram for reversible adiabatic expansion in an impulse stage. Expansion of the gas occurs only in the nozzle blade row and its thermodynamic state remains unchanged between stations 2 and 3. Therefore, the air *angles*, static pressure and enthalpy at the entry and exit of the rotor in this stage are the same.

$$\beta_2 = \beta_3$$

$$p_2 = p_3$$

$$h_2 = h_3$$

These conditions when put into Eqs. (9.48), (9.49), (9.52), (9.53) and (9.58) give the degree of reaction as zero. On account of the reversible nature of flow, such a stage is of no practical importance.

(b) Figure 9.10 depicts the enthalpy-entropy diagram for irreversible adiabatic expansion in an impulse stage with equal pressures at the rotor entry and exit. On account of losses, both in the nozzle and

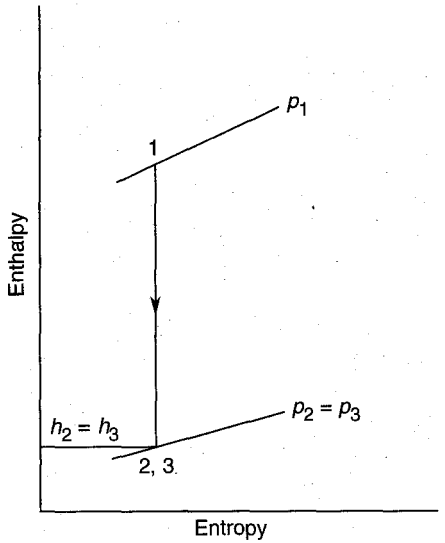

Fig. 9.9 Zero reaction or impulse stage, enthalpy-entropy diagram for reversible flow[286,287]

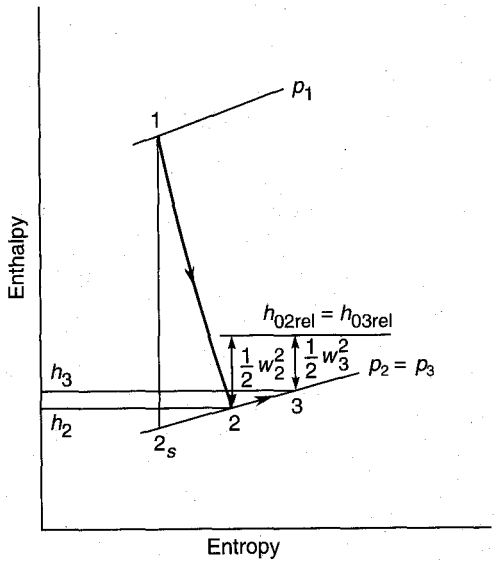

Fig. 9.10 Impulse stage (negative degree of reaction), enthalpy-entropy diagram for irreversible flow[286,287]

rotor blade rows, the gas experiences an increase in entropy. Therefore, for this stage

$$p_2 = p_3$$

$$w_2 > w_3$$

$$h_2 < h_3$$

$$\beta_2 > \beta_3$$

These conditions give the degree of reaction as negative [(Eqs. (9.52) (9.53), (9.55) and (9.58)]. However, Eq. (9.49) defines such a stage as impulse.

(c) Figure 9.11 shows the enthalpy-entropy diagram of a real (adiabatic) and a truly zero reaction stage. Here a small pressure drop in the rotor compensates for the deceleration of the flow in the rotor blades (Fig. 9.10). Thus the enthaplies and relative velocities remain constant between the rotor entry and exit.

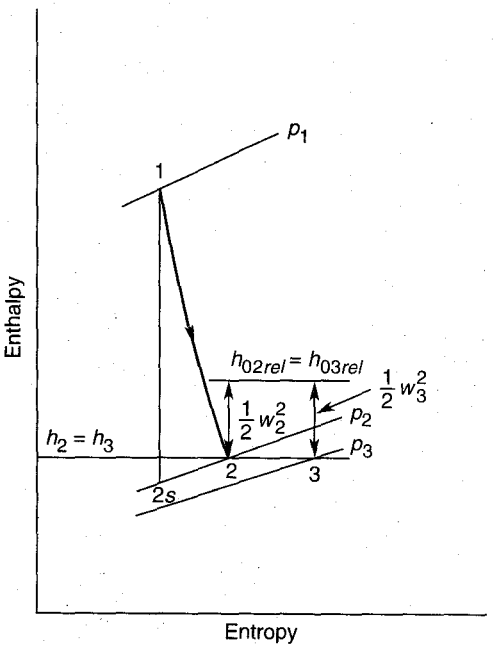

Fig. 9.11 Zero reaction stage, enthalpy-entropy diagram for irreversible flow[286,287]

Equation (9.49) for such a stage gives the value of reaction as positive, whereas Eqs. (9.52), (9.53), (9.55) and (9.58) yield $R = 0$.

9.5.4 Fifty Per Cent Reaction Stages

For fifty per cent degree of reaction, Eq. (9.53) gives

$$R = \frac{h_2 - h_3}{h_1 - h_3} = \frac{1}{2}$$

This gives equal values to the actual enthalpy drops in the fixed and rotor blade rows (Fig. 9.7).

$$h_1 - h_2 = h_2 - h_3 = \frac{1}{2}(h_1 - h_3) \tag{9.64}$$

Figure 9.12 shows the enthalpy-entropy diagram for such a stage. The flow and cascade geometries in the fixed and moving blade rows are such that they provide equal enthalpy drops. This does not imply that the pressure drops in the two rows are also the same. From Eq. (9.61)

$$\frac{1}{2} = \frac{1}{2} + \frac{c_x}{2u}(\tan \beta_3 - \tan \alpha_2)$$

$$\tan \beta_3 = \tan \alpha_2$$

$$\beta_3 = \alpha_2 \tag{9.65}$$

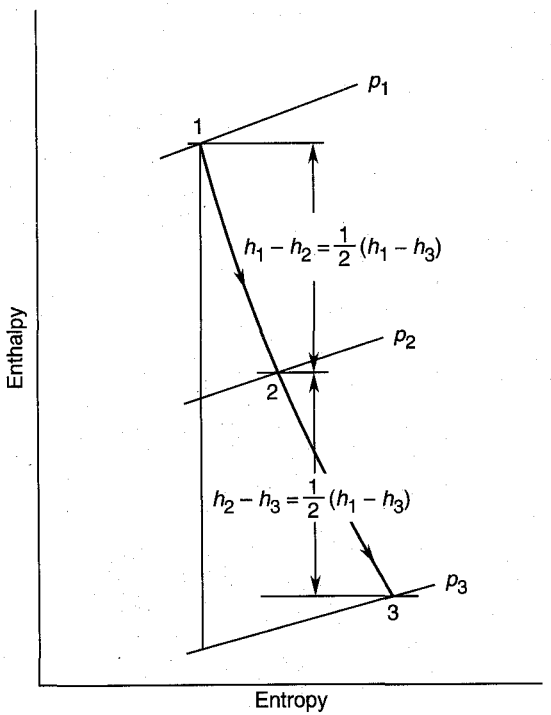

Fig. 9.12 Enthalpy-entropy diagram for a 50% reaction stage

this condition, when put into Eq. (9.8), yields

$$\tan \beta_2 = \tan \alpha_3 \tag{9.66}$$

$$\beta_2 = \alpha_3$$

Equation (9.54) for $R = \frac{1}{2}$ gives

$$\frac{1}{2}(w_3^2 - w_2^2) + \frac{1}{2}(u_2^2 - u_3^2) = \frac{1}{2}(u_2\, c_{y2} - u_3\, c_{y3})$$

For axial turbines,

$$(w_3^2 - w_2^2) = \frac{1}{2}(c_2^2 - c_3^2) + \frac{1}{2}(w_3^2 - w_2^2)$$

$$w_3^2 - w_2^2 = c_2^2 - c_3^2 \tag{9.67}$$

This with Eqs. (9.65) and (9.66) gives

$$w_3 = c_2 \tag{9.68}$$

$$w_2 = c_3$$

Thus it is observed that the velocity triangles at the entry and exit of a rotor in a fifity per cent reaction turbine are similar. These are shown in Fig. 9.13.

Utilization factor

Equation (9.68) when put into Eq. (9.18) gives the value of the utilization factor for the fifty per cent reaction stage.

$$\varepsilon = \frac{2(c_2^2 - c_3^2)}{c_2^2 + (c_2^2 - c_3^2)} = \frac{c_2^2 - c_3^2}{c_2^2 - \frac{1}{2}c_3^2}$$

$$\varepsilon = \frac{1 - c_3^2/c_2^2}{1 - c_3^2/2c_2^2} \tag{9.69}$$

From the entry velocity triangle in Fig. 9.13,

$$w_2^2 = c_2^2 + u^2 - 2\, uc_2 \cos(90 - \alpha_2)$$

$$c_3^2 = c_2^2 + u^2 - 2\, u\, c_2 \sin\alpha_2 \text{ (for } R = 1/2)$$

$$c_3^2/c_2^2 = 1 + \left(\frac{u}{c_2}\right)^2 - 2\left(\frac{u}{c_2}\right)\sin\alpha_2$$

$$\sigma = u/c_2$$

$$c_3^2/c_2^2 = 1 + \sigma^2 - 2\sigma\sin\alpha_2$$

$$1 - c_3^2/c_2^2 = 2\,\sigma\sin\alpha_2 - \sigma^2 \tag{9.70}$$

$$1 - c_3^2/2c_2^2 = \frac{1}{2}(1 + 2\sigma\sin\alpha_2 - \sigma^2) \tag{9.71}$$

Equations (9.70) and (9.71) when put into Eq. (9.69) give

$$\varepsilon = 2\left[\frac{2\,\sigma\sin\alpha_2 - \sigma^2}{1 + (2\,\sigma\sin\alpha_2 - \sigma^2)}\right]$$

$$\varepsilon = \frac{2}{1 + \dfrac{1}{2\,\sigma \sin \alpha_2 - \sigma^2}} \tag{9.72}$$

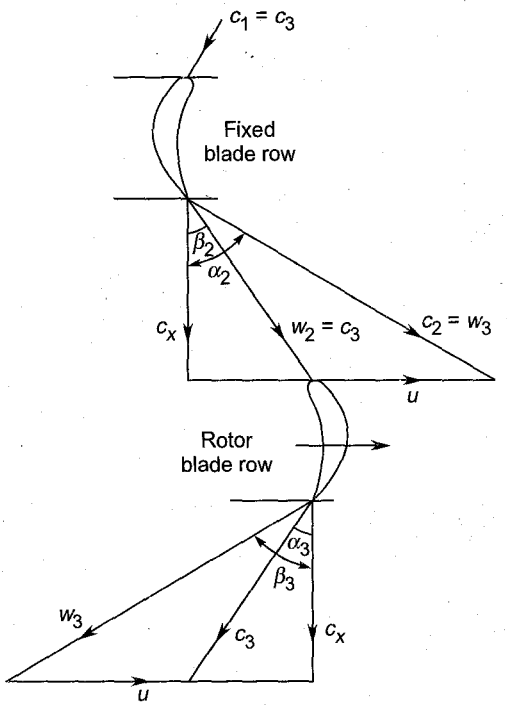

Fig. 9.13 Velocity triangles for a 50% reaction stage

The utilization factor is a maximum when the factor $(2\,\sigma \sin \alpha_2 - \sigma^2)$ is maximum.

$$\frac{d}{d\sigma}\,(2\sigma \sin \alpha_2 - \sigma^2) = 0$$

$$2 \sin \alpha_2 = 2\,\sigma$$

$$\sigma_{opt} = \frac{u}{c_2} = \sin \alpha_2 \tag{9.73}$$

This condition in Eq. (9.72) gives

$$\varepsilon_{max} = \frac{2 \sin^2 \alpha_2}{1 + \sin^2 \alpha_2} \tag{9.74}$$

Equation (9.73) gives

$$u = c_2 \sin \alpha_2 = c_{y2}$$

Since the entry and exit velocity triangles are symmetrical,

$$u = w_3 \sin \beta_3 = w_{y3}$$

These relations give right-angled velocity triangles (Fig. 9.14) at the entry and exit.

$$\beta_2 = 0$$

$$\alpha_3 = 0$$

The exit swirl is zero ($c_{y3} = 0$), i.e. the exit from the stage is axial.

The stage work for maximum utilization from Eq. (9.10) or (9.11), or direct from the velocity triangles (Fig. 9.14) is

$$w_{\text{opt}} = u^2 \tag{9.75}$$

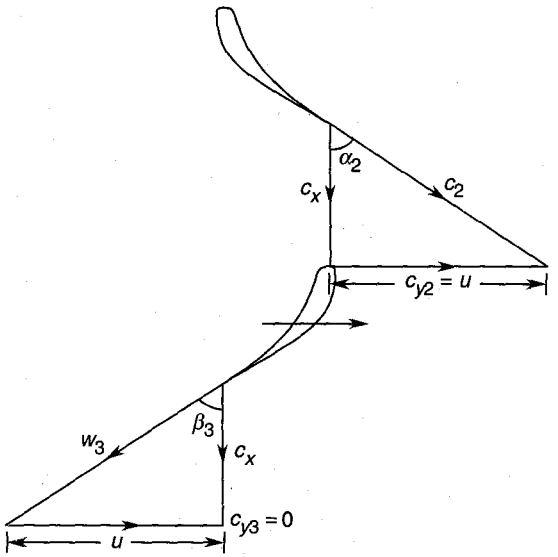

Fig. 9.14 Velocity triangles for a 50% reaction stage at maximum utilization factor

This is half of the value for a single-stage impulse and one-eighth of the two-stage velocity compounded impulse type.

Equation (9.55) can be written as

$$\frac{1}{2}(w_3^2 - w_2^2) = u(c_{y2} - c_{y3})R = \left\{\frac{1}{2}(c_2^2 - c_3^2) + \frac{1}{2}(w_3^2 - w_2^2)\right\}R$$

$$w_3^2 - w_2^2 = \frac{R}{1-R}(c_2^2 - c_3^2)$$

This, when put into Eq. (9.18), gives the utilization factor for an axial turbine as

$$\varepsilon = \frac{(c_2^2 - c_3^2)\left(1 + \dfrac{R}{1-R}\right)}{c_2^2 + \dfrac{R}{1-R}(c_2^2 - c_3^2)}$$

This, on simplification, gives a general relation between the utilization factor and the degree of reaction

$$\varepsilon = \frac{c_2^2 - c_3^2}{c_2^2 - Rc_3^2} \tag{9.76}$$

For R = 1, this equation gives indeterminate value. Therefore, Eq. (9.63) is used.

9.5.5 Hundred Per Cent Reaction

Hundred per cent degree of reaction implies that the entire change in the static properties occurs in the rotor. Equation (9.53) for this condition gives

$$R = \frac{h_2 - h_3}{h_1 - h_3} = 1$$

$$(h_1 = h_2)_{R=1} \tag{9.77}$$

Equation (9.55) gives

$$\frac{1}{2}(w_3^2 - w_2^2) = u\,(c_{y2} + c_{y3})$$

which shows that the stage work is wholly due to the change in the kinetic energy occurring in the rotor. Rewriting the quantity on the right hand side

$$\frac{1}{2}(w_3^2 - w_2^2) = \frac{1}{2}(c_2^2 - c_3^2) + \frac{1}{2}(w_3^2 - w_2^2)$$

$$(c_2 = c_3)_{R=1} \tag{9.78}$$

Further Eq. (9.63) gives

$$(\alpha_2 = \alpha_3)_{R=1} \tag{9.79}$$

These conditions give the velocity triangles as shown in Fig. 9.15. It is observed that the rotor blades are highly staggered. On account of the

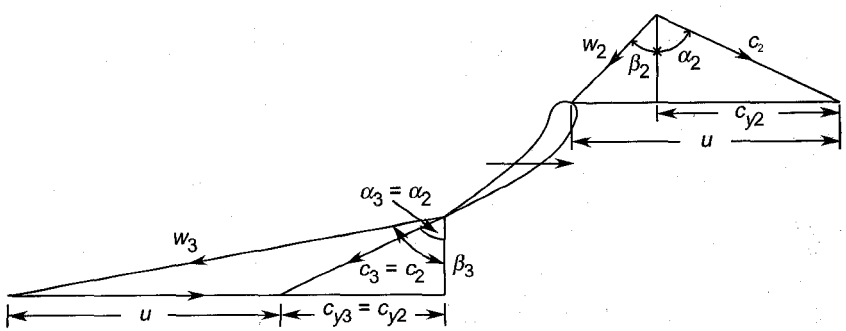

Fig. 9.15 Velocity triangles for a 100% reaction turbine stage

large difference of static pressure across the rotor and high relative velocity at its exit, the losses are relatively higher.

A stage with a degree of reaction higher than hundred per cent requires

$$h_2 > h_1$$
$$c_2 < c_1$$
$$\alpha_3 > \alpha_2$$

These conditions show that for such a stage the flow is decelerating in the nozzle or upstream fixed blades. This is obviously undesirable.

9.5.6 Negative Reaction

A negative degree of reaction in a turbine stage, (as well as $R > 100\%$) is also undesirable. For such a stage

$$h_3 > h_2 \qquad \text{[Eq.(9.52)]}$$
$$w_3 < w_2 \qquad \text{[Eq. (9.55)]}$$
$$\beta_2 > \beta_3 \qquad \text{[Eq. (9.59)]}$$

These conditions will require the diffusion of flow in the rotor blade row. Such a condition may be accepted only as a "necessary evil" in long blades where it is necessary to limit the high degree of reaction at the blade tips.

9.6 Blade-to-gas Speed Ratio

In earlier sections, we saw that the stage work and utilization factor were governed by the blade-to-gas speed ratio parameter (velocity ratio) $\sigma = u/c_2$. Its value for maximum utilization was determined for some stages. Efficiencies of the turbine stages can also be plotted against this ratio. Such plots for some impulse and reaction stages are shown in Fig. 9.16. The performance of steam turbines is often presented in this form. The curves in Fig. 9.16 also show the optimum values of the velocity ratio and the range of off-design for various types of stages. The fifty per cent reaction stage shows a wider range. Another important aspect that is depicted here is that in applications where high gas velocities (due to high pressure ratio) are unavoidable, it is advisable to employ impulse stages to achieve practical and convenient values of the size and speed of the machine.

Sometimes it is more convenient to use an isentropic velocity ratio. This is the ratio of the blade velocity and the isentropic gas velocity that would be obtained in its isentropic expansion through the stage pressure ratio.

$$\sigma_s = \frac{u}{c_s} \qquad (9.80)$$

$$\frac{1}{2} c_s^2 = h_{01} - h_{03ss} \quad \text{(Fig. 9.8)}$$

$$c_s = \sqrt{2 (h_{01} - h_{03ss})} \tag{9.81}$$

For a perfect gas,

$$c_s = \sqrt{2c_p T_{01} \left(1 - p_{r0}^{\frac{1-\gamma}{\gamma}}\right)} \tag{9.82}$$

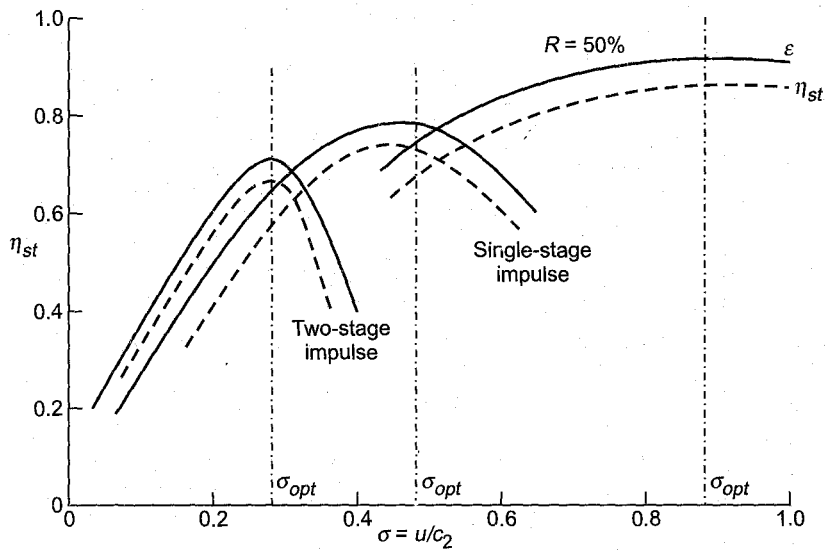

Fig. 9.16 Variation of utilization factor and stage efficiency with blade-to-gas speed ratio.

A relation between velocity ratios and the degree of reaction can be derived for isentropic flow. From Eq. (9.48),

$$R = \frac{h_{2s} - h_{3ss}}{h_1 - h_{3ss}} = 1 - \frac{h_1 - h_{2s}}{h_1 - h_{3ss}}$$

Now $$h_1 - h_{2s} \approx \frac{1}{2} c_2^2$$

$$h_1 - h_{3ss} \approx \frac{1}{2} c_s^2$$

Therefore, $$R = 1 - \frac{c_2^2}{c_s^2} = 1 - \frac{(c_2/u)^2}{(c_s/u)^2}$$

$$R = 1 - \frac{\sigma_s^2}{\sigma^2} \tag{9.83}$$

For $R = 0,\ \sigma = \sigma_s$ (9.84a)

With a nozzle efficiency η_N,

$$\sigma = \frac{1}{\sqrt{\eta_N}}\ \sigma_s \tag{9.84b}$$

For $R = \frac{1}{2}$ $\sigma = \sqrt{2}\ \sigma_s$ (9.85)

9.7 Losses and Efficiencies[264, 273, 286]

Losses occurring in turbine blade rows (stationary or moving) have been described in Sec. 8.4.5. Besides these losses, additional losses occur in an actual turbine due to disc and bearing friction.

Figure 9.17 shows the energy flow diagram for the impulse stage of an axial turbine. Numbers in brackets indicate the order of energy or loss corresponding to 100 units of isentropic work ($h_{01} - h_{03ss}$). It is seen that the energy reaching the shaft after accounting for stage cascade losses (nozzle and rotor blade aerodynamic losses) and leaving loss is about 85% of the ideal value; shaft losses are a negligible proportion of this value.

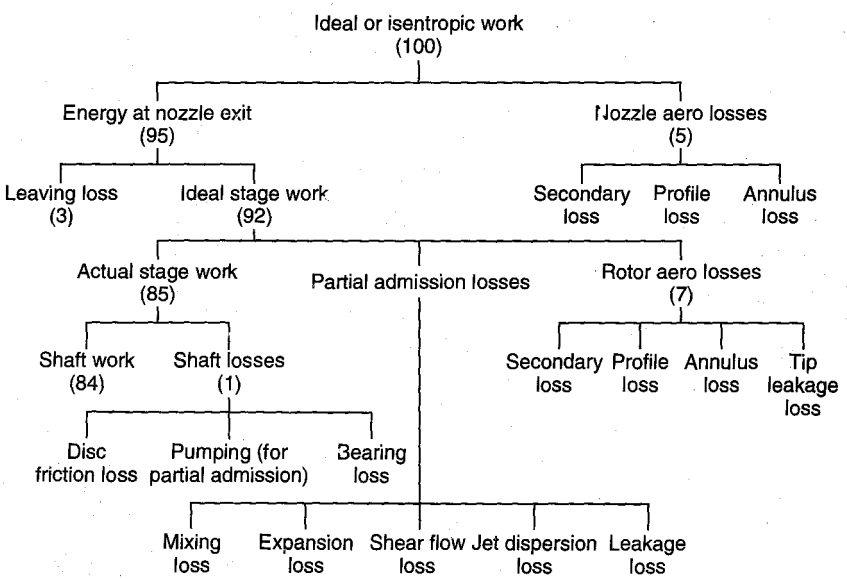

Fig. 9.17 Energy flow diagram for the impulse stage of an axial turbine

If the turbine is of the partial admission type it incurs additional losses as shown in the figure. They are discussed separately in Secs. 9.10.5 and 9.10.6.

9.7.1 Stage Losses

Stage losses are related to the flow velocities at the exits of the stationary and moving blade rows as discussed in Sec. 9.5.1. If these velocities are known, the magnitude of these losses can be determined from the knowledge of loss coefficients. The values of loss coefficients are determined either from cascade tests or theoretical correlations.

Referring to Fig. 9.8, losses in stationary or nozzle blade row are from Eq. (9.41)

$$h_2 - h_{2s} = \xi_N \frac{1}{2} c_2^2 \tag{9.86}$$

The slope of the p = constant lines on h-s coordinates is given by

$$\left(\frac{\partial h}{\partial s}\right)_p = T$$

Therefore,

$$\frac{h_2 - h_{2s}}{\Delta s} = T_2$$

$$\Delta s = \frac{1}{T_2} (h_2 - h_{2s}) \tag{9.87}$$

Similarly, assuming $T_{3s} \approx T_3$,

$$\frac{h_{3s} - h_{3ss}}{\Delta s} = T_3$$

$$h_{3s} - h_{3ss} = T_3 \, \Delta s$$

Substituting for Δs from Eq. (9.87),

$$h_{3s} - h_{3ss} = \frac{T_3}{T_2} (h_2 - h_{2s})$$

Substituting from Eq. (9.86),

$$h_{3s} - h_{3ss} = \frac{T_3}{T_2} \xi_N \frac{1}{2} c_2^2 \tag{9.88}$$

From Eq. (9.46),

$$h_3 - h_{3s} = \xi_R \frac{1}{2} w_3^2 \tag{9.89}$$

Now

$$h_3 - h_{3ss} = h_3 - h_{3s} + (h_{3s} - h_{3ss})$$

Substituting from Eqs. (9.88) and (9.89),

$$h_3 - h_{3ss} = \xi_R \frac{1}{2} w_3^2 + \frac{T_3}{T_2} \xi_N \frac{1}{2} c_2^2$$

Assuming $c_3 \approx c_{3ss}$,

$$h_{03} - h_{03ss} = h_3 - h_{3ss}$$

Therefore,

$$h_{03} - h_{03ss} = \xi_R \frac{1}{2} w_3^2 + \frac{T_3}{T_2} \xi_N \frac{1}{2} c_2^2 \tag{9.90}$$

9.7.2 Total-to-total Efficiency

Total-to-total and total-to-static efficiencies for turbines have been defined in Sec. 2.5. The total-to-total efficiency of the stage is similarly defined by

$$\eta_{tt} = \frac{\text{actual stage work}}{\text{ideal stage work between total conditions at entry and exit}}$$

$$\eta_{tt} = \frac{w_a}{w_s} = \frac{h_{01} - h_{03}}{h_{01} - h_{03ss}} = \frac{u\,(c_{y2} + c_{y3})}{h_{01} - h_{03ss}} \tag{9.91}$$

$$\eta_{tt} = \frac{h_{01} - h_{03}}{(h_{01} - h_{03}) + (h_{03} - h_{03ss})}$$

$$\eta_{tt} = \left(1 + \frac{h_{03} - h_{03ss}}{h_{01} - h_{03}}\right)^{-1}$$

Substituting from Eq. (9.90),

$$\eta_{tt} = \left(1 + \frac{\xi_R \frac{1}{2} w_3^2 + \frac{T_3}{T_2} \xi_N \frac{1}{2} c_2^2}{h_{01} - h_{03}}\right)^{-1} \tag{9.92a}$$

$$h_{01} - h_{03} = u\,(c_{y2} + c_{y3})$$

The loading coefficient as defined by Eq. (9.12) is given by

$$\psi = \frac{1}{u^2}\,(h_{01} - h_{03})$$

Therefore, $h_{01} - h_{03} = \psi u^2$

$$\eta_{tt} = \left[1 + \frac{1}{2\psi}\left(\xi_R \frac{w_3^2}{u^2} + \frac{T_3}{T_2} \xi_N \frac{c_2^2}{u^2}\right)\right]^{-1} \tag{9.92b}$$

Equation (9.92a) can also be transformed in terms of the flow coefficient and air angles.

$$\eta_{tt} = \left[1 + \frac{\xi_R\, w_3^2 + \dfrac{T_3}{T_2}\,\xi_N\, c_2^2}{2u\,(c_{y2} + c_{y3})}\right]^{-1}$$

From velocity triangles in Fig. 9.1

$$\eta_{tt} = \left[1 + \frac{\xi_R\, c_x^2 \sec^2\beta_3 + \dfrac{T_3}{T_2}\,\xi_N\, c_x^2 \sec^2\alpha_2}{2u\, c_x\,(\tan\alpha_2 + \tan\beta_3 - u/c_x)}\right]^{-1}$$

$$\eta_{tt} = \left[1 + \frac{1}{2}\,\phi^2\,\frac{\xi_R \sec^2\beta_3 + \dfrac{T_3}{T_2}\,\xi_N \sec^2\alpha_2}{\phi\,(\tan\alpha_2 + \tan\beta_3) - 1}\right]^{-1} \tag{9.92c}$$

9.7.3 Total-to-static Efficiency

The kinetic energy at the exit of a turbine stage is treated as a loss in the definition of the total-to-static efficiency.

$$\eta_{ts} = \frac{h_{01} - h_{03}}{h_{01} - h_{3ss}} \tag{9.93}$$

$$h_{01} - h_{3ss} = h_{01} - h_{03ss} + \frac{1}{2}\,c_{3ss}^2$$

Putting $c_{3ss} = c_3$,

$$h_{01} - h_{3ss} = (h_{01} - h_{03}) + (h_{03} - h_{03ss}) + \frac{1}{2}\,c_3^2 \tag{9.94}$$

Substituting this in Eq. (9.93),

$$\eta_{ts} = \frac{h_{01} - h_{03}}{(h_{01} - h_{03}) + (h_{03} - h_{03ss}) + \dfrac{1}{2}\,c_3^2}$$

$$\eta_{ts} = \left[1 + \frac{h_{03} - h_{03ss} + \dfrac{1}{2}\,c_3^2}{h_{01} - h_{03}}\right]^{-1}$$

Substituting from Eq. (9.90),

$$\eta_{ts} = \left[1 + \frac{\xi_R \frac{1}{2} w_3^2 + \frac{T_3}{T_2} \xi_N \frac{1}{2} c_2^2 + \frac{1}{2} c_3^2}{h_{01} - h_{03}}\right]^{-1} \tag{9.95a}$$

$$\eta_{ts} = \left[1 + \frac{1}{2\psi}\left(\xi_R \frac{w_3^2}{u^2} + \frac{T_3}{T_2} \xi_N \frac{c_2^2}{u^2} + \frac{c_3^2}{u^2}\right)\right] \tag{9.95b}$$

The following relation can also be derived employing velocity triangles:

$$\eta_{ts} = \left[1 + \frac{1}{2}\phi^2 \frac{\xi_R \sec^2 \beta_3 + \frac{T_3}{T_2} \xi_N \sec^2 \alpha_2 + \sec^2 \alpha_3}{\phi (\tan \alpha_2 + \tan \beta_3) - 1}\right]^{-1} \tag{9.95c}$$

It should be noted that the value of actual stage work is same in the expressions for both the efficiencies η_{tt} and η_{ts}. It is only the ideal work that differs in the two cases.

9.8 Performance Charts

Performance of various types of gas turbine stages is often presented in terms of plots of the loading coefficient (ψ) against the values of the flow coefficient (ϕ).

9.8.1 Zero Degree Reaction

Equation (9.14) for zero degree reaction ($\beta_2 = \beta_3$) gives

$$\psi = 2\phi \tan \beta_2 = 2\phi \tan \beta_3 \tag{9.96}$$

At maximum utilization factor (Fig. 9.3b),

$$\tan \beta_3 = \frac{u}{c_x} = \frac{1}{\phi}$$

Therefore,

$$\psi = 2 \tag{9.97}$$

9.8.2 Fifty Per Cent Reaction

Equation (9.60) for $R = \frac{1}{2}$ ($\alpha_2 = \beta_3$) gives

$$\tan \beta_2 = \tan \alpha_2 - \frac{u}{c_x}$$

$$\tan \beta_2 = \tan \beta_3 - \frac{1}{\phi}$$

This relation when put in Eq. (9.14) gives

$$\psi = 2\phi \tan \beta_3 - 1 = 2\phi \tan \alpha_2 - 1 \tag{9.98}$$

At maximum utilization factor (Fig. 9.14),

$$\psi = 1 \tag{9.99}$$

Equation (9.58) gives

$$R = \frac{c_x}{2u} \tan \beta_3 - \frac{c_x}{2u} \tan \beta_2$$

For axial exit from the stage,

$$\frac{c_x}{u} \tan \beta_3 = 1$$

Therefore,

$$R = \frac{1}{2} - \frac{c_x}{2u} \tan \beta_2$$

$$\frac{c_x}{u} \tan \beta_2 = 1 - 2R \tag{9.100}$$

Equation (9.14) gives

$$\psi = \frac{c_x}{u} \tan \beta_2 + \frac{c_x}{u} \tan \beta_3$$

$$\psi = \frac{c_x}{u} \tan \beta_2 + 1 = \phi \tan \beta_2 + 1 \tag{9.101}$$

This is a general equation for a stage with an axial exit. Equation (9.100) when put in Eq. (9.101) yields

$$\psi = 2\,(1 - R) \tag{9.102}$$

This for $R = 0$ and $R = 1/2$ gives the same results as in Eqs. (9.97) and (9.99) respectively. This is not valid for $R = 1$ or $R < 0$ because then the exit from the stage cannot remain axial. Equation (8.102) shows that the stage loading decreases with an increase in the degree of reaction.

Figure 9.18 shows the $\phi - \psi$ plots for various axial turbine stages.

9.9 Low Hub-tip Ratio Stages[287]

A two-dimensional approach is adequate only when the hub-tip ratio (d_h/d_t) of a stage is close to unity. However, when it is too low, the blade lengths are comparable with the mean diameter of the stage. The variations of fluid parameters along the blade height (radial direction) in such stages are considerable and therefore cannot be ignored.

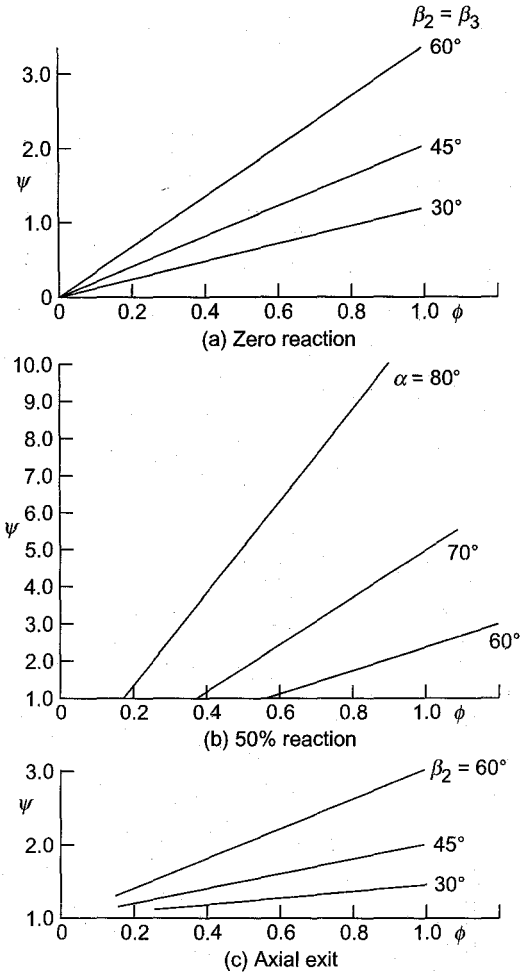

Fig. 9.18 Performance charts for various axial turbine stages

High power gas turbines require large annulus areas to pass high flow rates. Therefore, the heights of the blade rows are generally large. Similar conditions exist in the low pressure stages of large steam turbines; the hub-tip ratio in some stages is about 0.4.

To take into account the effect of varying fluid properties in the radial direction, a three-dimensional approach is required for obtaining the various stage parameters.

9.9.1 Radial Equilibrium Method[6,9,11]

Axial machine stages are often designed on the basis of the assumption of "radial equilibrium"of the flow through them. For a given value of the

radial pressure gradient $\left(\frac{dp}{dr}\right)$, a condition of the flow is assumed in which the radial component of the velocity is negligible, i.e. there is no flow occurring in the radial direction. The streamlines in such a flow do not experience any radial shift and therefore lie on coaxial cylindrical surfaces as shown in Fig. 9.19. Such a condition of the flow in an annulus is known as radial equilibrium.

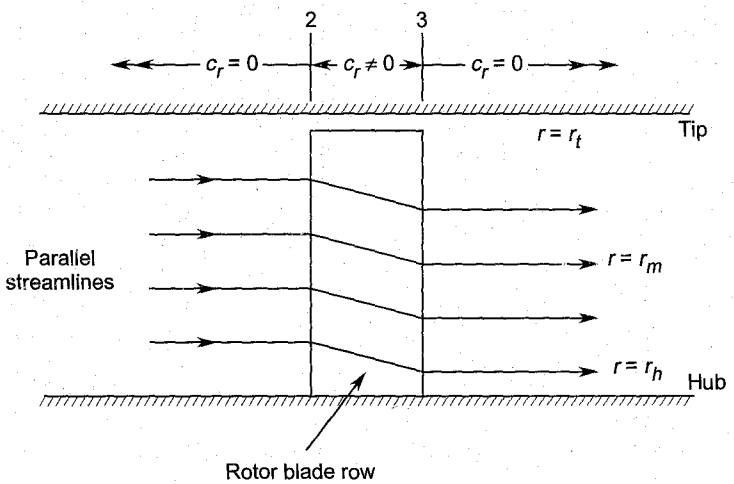

Fig. 9.19 Flow in radial equilibrium upstream and downstream of a rotor

Equations of motion for three-dimensional flow in cylindrical coordinates have been given in Sec. 6.3. Euler's momentum equation in the radial direction for axisymmetric flow is

$$c_r \frac{\partial c_r}{\partial r} + c_x \frac{\partial c_r}{\partial x} - \frac{c_\theta^2}{r} = -\frac{1}{\rho}\frac{\partial p}{\partial r} \tag{9.103}$$

As explained before, for flow in radial equilibrium

$$c_r = 0 \tag{9.104}$$

Therefore, from Eq. (9.103),

$$\frac{1}{\rho}\frac{dp}{dr} = \frac{c_\theta^2}{r} \tag{9.105}$$

Equation (9.105) gives the pressure gradient in the flow for radial equilibrium conditions. The gradient of other quantities in the radial direction can be determined through stagnation enthalpy.

$$h_0 = h + \frac{1}{2}c^2 = h + \frac{1}{2}(c_r^2 + c_\theta^2 + c_x^2)$$

For radial equilibrium,

$$h_0 = h + \frac{1}{2}(c_\theta^2 + c_x^2) \tag{9.106}$$

$$\frac{dh_0}{dr} = \frac{dh}{dr} + c_\theta \frac{dc_\theta}{dr} + c_x \frac{dc_x}{dr} \tag{9.107}$$

Entropy and enthalpy gradients can be related to the pressure gradient through

$$T\,ds = dh - \frac{1}{\rho}\,dp$$

$$T\frac{ds}{dr} = \frac{dh}{dr} - \frac{1}{\rho}\frac{dp}{dr} \tag{9.108}$$

Substituting on the right-hand side in Eq. (9.108) from Eqs. (9.105) and (9.107), and rearranging

$$c_\theta \frac{dc_\theta}{dr} + c_x \frac{dc_x}{dr} + \frac{c_\theta^2}{r} = \frac{dh_0}{dr} - \frac{Tds}{dr} \tag{9.109a}$$

This is the well-known radial equilibrium equation for axisymmetric steady flow in turbomachines.

Mathematically, this equation can be reduced to a much simpler form by assuming constant values of the stagnation enthalpy and entropy in the radial direction. This gives

$$\frac{dh_0}{dr} = 0 \qquad \text{and} \qquad T\frac{ds}{dr} = 0$$

Therefore, Eq. (9.109a) becomes

$$c_\theta \frac{dc_\theta}{dr} + c_x \frac{dc_x}{dr} + \frac{c_\theta^2}{r} = 0 \tag{9.109b}$$

$$\frac{1}{r^2}\left\{r^2\, 2c_\theta \frac{dc_\theta}{dr} + c_\theta^2\, 2r \frac{dr}{dr}\right\} + 2c_x \frac{dc_x}{dr} = 0$$

$$\frac{1}{r^2}\frac{d}{dr}(rc_\theta)^2 + \frac{d}{dr}(c_x)^2 = 0 \tag{9.109c}$$

This equation will be used in later sections for analysis of axial flow turbomachines.

A useful relation for the radial variation of the absolute velocity vector (c) and its direction is derived here from Eq. (9.109b).

$$\frac{1}{2}\frac{d}{dr}c_\theta^2 + \frac{1}{2}\frac{d}{dr}c_x^2 + \frac{c_\theta^2}{r} = 0$$

Now

$$c_\theta^2 + c_x^2 = c^2$$

$$c_\theta = c \sin \alpha$$

This can be seen from the velocity triangles of Fig. 9.1 noting that, in the present notation, $c_\theta \equiv c_y$. Therefore,

$$\frac{1}{2}\frac{d}{dr}(c_\theta^2 + c_x^2) + \frac{c_\theta^2}{r} = 0$$

$$\frac{1}{2}\frac{dc^2}{dr} + \frac{c^2 \sin^2 \alpha}{r} = 0$$

$$\frac{dc}{c} = -\sin^2 \alpha \frac{dr}{r} \tag{9.110}$$

This equation can be solved either by assuming α = constant in the radial direction or through a relation

$$\alpha = f(r) \tag{9.111}$$

The initial design of a stage is based on various parameters at the blade mid-height or the mean blade radius. The three-dimensional design procedure involves determining stage parameters at other points along the blade height. Therefore, integrating Eq. (8.110),

$$\int_{c_m}^{c} \frac{dc}{c} = \int_{r}^{r_m} \sin^2 \alpha \frac{dr}{r}$$

$$c = c_m \exp \int_{r}^{r_m} \sin^2 \alpha \frac{dr}{r} \tag{9.112}$$

This equation along with Eq. (9.111) gives the values of the absolute velocity vector (c) at various points along the blade height for a given value of c_m.

9.9.2 The Free Vortex Stage

Expressions for the three vorticity components have been given in Sec. 6.3.3. Equation (6.56) gives the axial component of vorticity for axisymmetric flow in cylindrical coordinates; this is

$$\zeta = \frac{\partial c_\theta}{\partial r} + \frac{c_\theta}{r} \tag{6.56}$$

This can also be written as

$$\zeta = \frac{1}{r}\frac{\partial}{\partial r}(rc_\theta) \tag{9.113}$$

If this component of vorticity is zero (rc_θ = const.), the resulting flow is a "free vortex" flow. By definition, in such a flow, the rotational motion of the fluid which is not acted upon by a force (by rotor blades or frictional effect) is governed by

$$rc_\theta = \text{const.} \tag{9.114a}$$

This is a convenient condition for designing blade rows of axial turbomachines. This, along with the radial equilibrium condition (Fig. 9.19) at the entry and exit of a blade row, yields its parameters along the radial direction.

Equation (9.114a) at the rotor entry and exit gives

$$r_h\, c_{\theta 2h} = r_t c_{\theta 2t} = r_m\, c_{\theta 2m} = C_2 \tag{9.114b}$$

$$r_h\, c_{\theta 3h} = r_t c_{\theta 3t} = r_m c_{\theta 3m} = C_3 \tag{9.114c}$$

Equation (9.114a) when put into Eq. (9.109c) yields another important result

$$\frac{d}{dr}\,(c_x)^2 = 0$$

From this it follows that c_x = constant along the blade height. Therefore,

$$c_{x2h} = c_{x2t} = c_{x2m} = c_{x2} \tag{9.115a}$$

$$c_{x3h} = c_{x3t} = c_{x3m} = c_{x3} \tag{9.115b}$$

Air angles

Absolute and relative air angles can now be determined at rotor entry and exit. The axial velocity across the rotor is assumed constant ($c_{x2} = c_{x3} = c_x$) as before.

Rotor entry

$$\tan \alpha_{2h} = \frac{c_{\theta 2h}}{c_x} = \frac{C_2}{r_h c_x} \tag{9.116a}$$

From Eq. (9.60)

$$\tan \beta_{2h} = \tan \alpha_{2h} - \frac{u_h}{c_x}$$

$$\tan \beta_{2h} = \frac{C_2}{r_h c_x} - \frac{u_h}{c_x} \tag{9.116b}$$

Similarly, for the tip section

$$\tan \alpha_{2t} = \frac{c_{\theta 2t}}{c_x} = \frac{C_2}{r_t c_x} \tag{9.117a}$$

$$\tan \beta_{2t} = \frac{C_2}{r_t c_x} - \frac{u_t}{c_x} \tag{9.117b}$$

Rotor exit

$$\tan \alpha_{3h} = \frac{c_{\theta 3h}}{c_x} = \frac{C_3}{r_h c_x} \tag{9.118a}$$

$$\tan \beta_{3h} = \frac{C_3}{r_h c_x} + \frac{u_h}{c_x} \tag{9.118b}$$

$$\tan \alpha_{3t} = \frac{c_{\theta 3t}}{c_x} = \frac{C_3}{r_t c_x} \tag{9.119a}$$

$$\tan \beta_{3t} = \frac{C_3}{r_t c_x} + \frac{u_t}{c_x} \tag{9.119b}$$

Variations of air angles and velocities along the blade height are shown in Figs. 9.20 and 9.21 respectively.

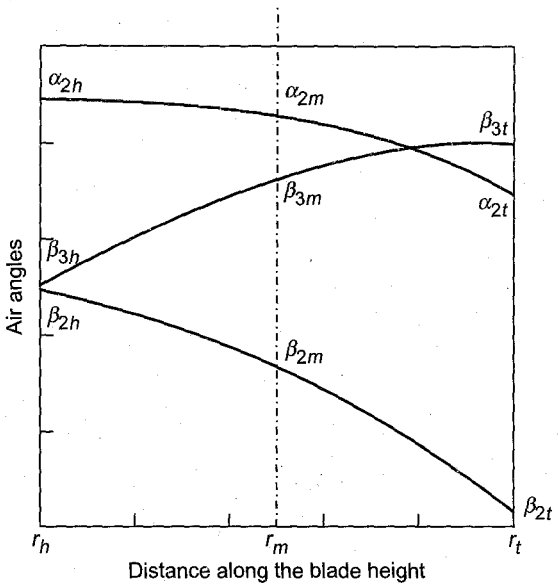

Fig. 9.20 Variation of air angles along the blade height

Specific work

At a given radial section ($r = r$) of the rotor-blade ring, the work done per kilogram of the flow from Eq. (9.9) is given by

$$w = h_{02} - h_{03} = u\,(c_{\theta 2} + c_{\theta 3})$$

The relations in Eqs. (9.114) give

$$w = \omega r \left(\frac{C_2}{r} + \frac{C_3}{r}\right)$$

$$w = h_{02} - h_{03} = \omega\,(C_2 + C_3) = \text{const.} \tag{9.120}$$

This shows that the specific work in a stage with free vortex flow in radial equilibrium remains constant at all radii. Further, if the fluid

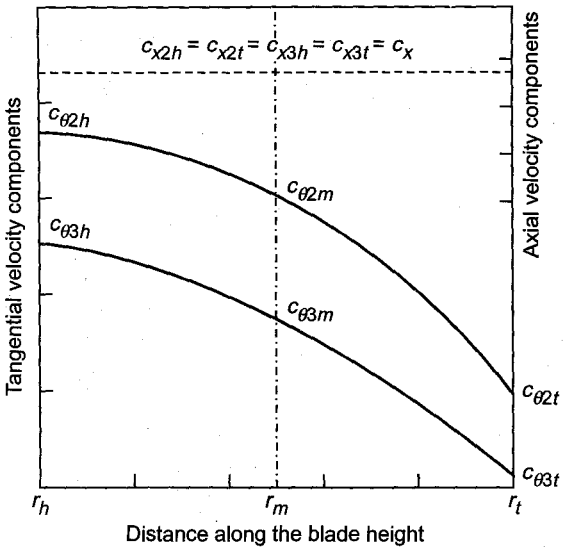

Fig. 9.21 Variation of tangential and axial velocity components along the blade height

approaching the stage has constant stagnation enthalpy (h_{01}) in the radial direction, it will remain so at the rotor entry and exit.

Degree of reaction

Since the air angles of the stage are varying along the radial direction, the degree of reaction cannot remain constant. The degree of reaction at radius r for constant axial velocity across the blade row is given by Eq. (9.58).

$$R = \frac{c_x}{2u} (\tan \beta_3 - \tan \beta_2)$$

Substituting from Eqs. (9.116b) and (9.118b) for $r = r$, we have

$$R = \frac{c_x}{2u}\left(\frac{C_3}{rc_x} + \frac{u}{c_x} - \frac{C_2}{rc_x} + \frac{u}{c_x}\right)$$

$$R = 1 + \frac{C_3 - C_2}{2ru} \tag{9.121}$$

Since a slight degree of reaction in a turbine stage is always advantageous, the hub reaction (R_h) must be kept postive as far as possible. Thus for $R = R_h$ at $r = r_h$, Eq. (9.121) gives

$$R_h = 1 + \frac{C_3 - C_2}{2r_h u_h}$$

$$C_3 - C_2 = 2 (R_h - 1) r_h u_h \tag{9.122}$$

Eliminating the constant $(C_3 - C_2)$ between Eqs. (9.121) and (9.122)

$$R = 1 + \frac{(R_h - 1)\, r_h u_h}{ru}$$

Putting $u = \omega r,\ u_h = \omega r_h$

$$R = 1 - (1 - R_h)\, \frac{r_h^2}{r^2} \tag{9.123}$$

If the hub reaction is chosen as zero,

$$R = 1 - \frac{r_h^2}{r^2} \tag{9.124}$$

Equations (9.123) and (9.124) demonstrate that the degree of reaction increases in the radial direction. Equation (9.124) shows that for zero reaction conditions at the hub, the maximum reaction (at the tip) cannot be 100%. For example, for $r_h/r_t = 0.4$ Eq. (8.124) gives $R_t = 84\%$.

Figure 9.22 shows the variation of the degree of reaction with the radius ratio (or hub-tip ratio, r_h/r_t) for various values of the hub reaction.

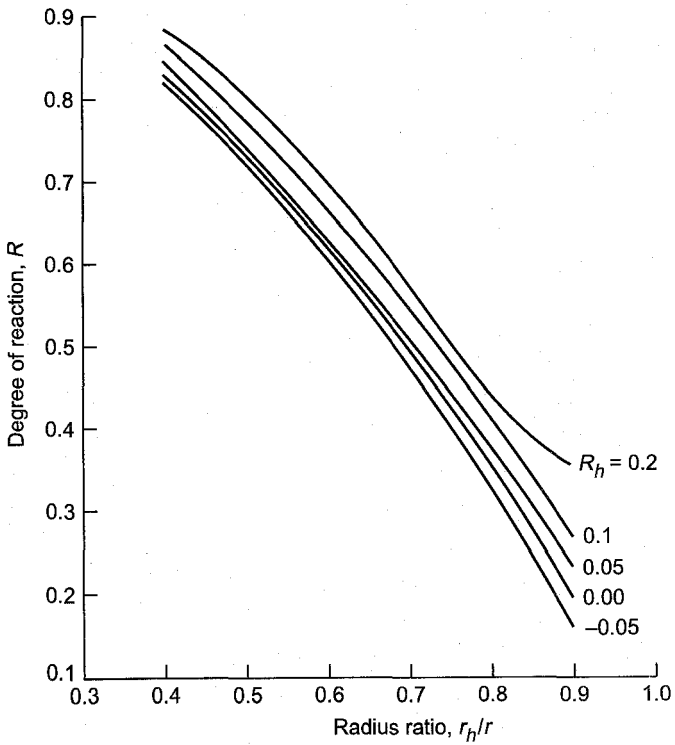

Fig. 9.22 Variation of degree of reaction with radius ratio for free vortex stage

It may be seen that the tip reaction can be kept lower by giving the hub zero or negative degree of reaction. A high reaction at the tip increases the tip leakage.

9.9.3 Constant Nozzle Angle Stage

For a constant absolute air angle, Eq. (9.112) gives

$$c = c_m \exp\left[\sin^2\alpha \int_r^{r_m} \frac{dr}{r}\right]$$

$$c = c_m \exp\left[\ln\left(\frac{r_m}{r}\right)^{\sin^2\alpha}\right]$$

$$c = c_m \left(\frac{r_m}{r}\right)^{\sin^2\alpha} \tag{9.125a}$$

The manufacture of twisted nozzle blades requires expensive production processes. Compared to them straight nozzle blades are simple and less expensive.

Equation (9.125a) at the exit of the nozzle blade row gives

$$c_2 = c_{2m}\left(\frac{r_m}{r}\right)^{\sin^2\alpha_2} \tag{9.125b}$$

This at the hub, mean, tip and general sections of the blade gives

$$c_{2h}\, r_h^{\sin^2\alpha_2} = c_{2m}\, r_m^{\sin^2\alpha_2} = c_{2t}\, r_t^{\sin^2\alpha_2} = c_2\, r^{\sin^2\alpha_2} \tag{9.126}$$

Now $c_{x2} = c_2 \cos\alpha_2$

$c_{\theta 2} = c_2 \sin\alpha_2$

Therefore, for constant value of α_2, Eq. (9.125b) gives

$$\frac{c_{x2}}{c_{x2m}} = \frac{c_{\theta 2}}{c_{\theta 2m}} = \frac{c_2}{c_{2m}} = \left(\frac{r_m}{r}\right)^{\sin^2\alpha_2} \tag{9.127}$$

Thus a turbine stage can be designed with radial equilibrium flow and a constant nozzle angle with the help of the above relations.

9.9.4 Constant Specific Mass-flow Stage

Figure 9.23 shows an infinitesimal annulus between the hub and the casing of an axial turbine stage. Its cross-sectional area and the mass flow rate through it are

$$dA = 2\pi r\, dr$$

$$d\dot{m} = \rho\, c_x\, (2\pi r dr) = \rho c_x dA$$

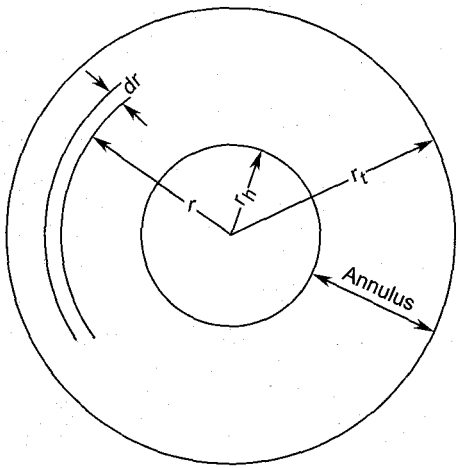

Fig. 9.23 Flow through an infinitesimal annulus in an axial turbine stage

The mass flow rate per unit area or the specific mass flow is

$$\frac{d\dot{m}}{dA} = \rho\, c_x = K_1 \tag{9.128}$$

A stage can be designed by keeping the specific mass flow constant along the blade height besides assuming the flow in radial equilibrium.

Conditions at the mean blade ring diameter are known before proceeding to calculate the various quantities along the blade height. Therefore, the constant in Eq. (9.128) is known.

$$\begin{aligned} \rho c \cos \alpha &= \rho_m\, c_m \cos\, \alpha_m = \rho_h\, c_h \cos\, \alpha_h \\ &= \rho_t c_t \cos\, \alpha_t = K_1 \end{aligned} \tag{9.129a}$$

$$\rho^2 = \frac{K_1^2}{\cos^2 \alpha} \tag{9.129b}$$

Equation (9.105) is

$$\frac{1}{2}\frac{dp}{dr} = \frac{c_\theta^2}{r}$$

$$\frac{1}{\rho}\left(\frac{dp}{d\rho}\right)_s \frac{d\rho}{dr} = \frac{c_\theta^2}{r} = \frac{c^2 \sin^2 \alpha}{r} \tag{9.130}$$

But $$\left(\frac{dp}{d\rho}\right)_s = a^2 = \gamma RT$$

and
$$\frac{T}{\rho^{\gamma-1}} = K_2 \text{ (const.)}$$
$$T = K_2 \rho^{\gamma-1}$$

Therefore,
$$\left(\frac{dp}{d\rho}\right)_s = K_2 \gamma R \rho^{\gamma-1} \tag{9.131}$$

Equation (9.131) when put into Eq. (9.130) gives
$$K_2 \gamma R \rho^{\gamma-2} \frac{d\rho}{dr} = \frac{c^2 \sin^2 \alpha}{r}$$
$$\frac{K_2 \gamma R \rho^{\gamma}}{\rho^2} \frac{d\rho}{dr} = \frac{c^2 \sin^2 \alpha}{r}$$

Substituting for ρ^2 from Eq. (9.129b)
$$\frac{K_2}{K_1^2} \gamma R \int_{\rho_m}^{\rho} \rho^{\gamma} \, d\rho = \int_{r_m}^{r} \tan^2 \alpha \frac{dr}{r}$$
$$\frac{K_2}{K_1^2} \frac{\gamma}{\gamma+1} R (\rho^{\gamma+1} - \rho_m^{\gamma+1}) = \int_{r_m}^{r} \tan^2 \alpha \frac{dr}{r}$$
$$\rho = \left[\rho_m^{\gamma+1} + \frac{\gamma+1}{\gamma} \frac{1}{R} \frac{K_1^2}{K_2} \int_{r_m}^{r} \tan^2 \alpha \frac{dr}{r} \right]^{\frac{1}{\gamma+1}} \tag{9.132}$$

Equations (9.132), (9.112) and (9.129a) are used to determine the variations in the density (ρ), velocity (c) and angle (α) respectively along the radial direction. The calculations can be done by adopting a step-by-step method for infinitesimal lengths Δr along the blade height. The value of α may be assumed constant over the small span Δr.

9.9.5 Actuator Disc Method

In an actuator disc model the blade row is assumed to be equivalent to a disc (of negligible thickness) which causes the same change in the tangential velocity or swirl component as the actual blade row. The flow is assumed in radial equilibrium ($c_r = 0$) only far upstream ($x = -\infty$) and far downstream ($x = +\infty$) of the disc. Radial components of velocity exist in regions near the disc from $x = -\infty$ to $x = +\infty$. This is shown in Fig. 9.24.

The axial velocities far upstream and far downstream of the disc are c_{x1} and c_{x2} respectively. These values from $x = -\infty$ to $x = 0$ and $x = 0$ to x

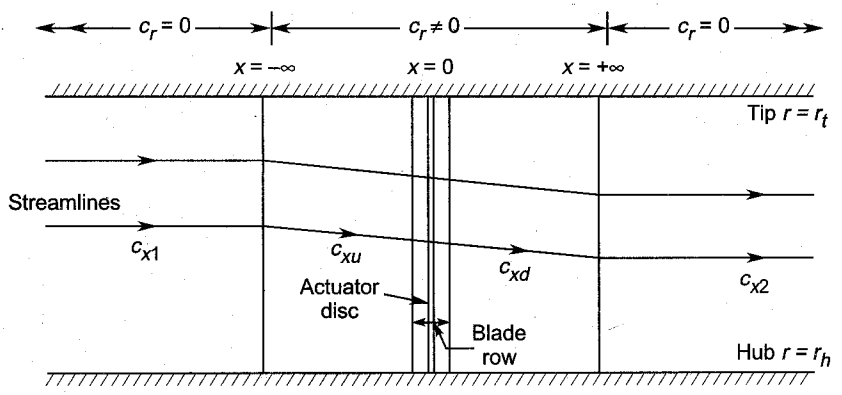

Fig. 9.24 Flow through an actuator disc

$= +\infty$ are c_{xu} and c_{xd} respectively. They vary on account of the perturbations c'_{xu} and c'_{xd}. Thus

$$c_{xu} = c_{x1} + c'_{xu} \tag{9.133a}$$

$$c_{xd} = c_{x2} + c'_{xd} \tag{9.133b}$$

An approximate expression for the axial velocity perturbations is obtained for axisymmetric and incompressible flow in which the radial shift of the streamlines is small. This is

$$c'_x = \pm \frac{1}{2}(c_{x2} - c_{x1})\, e^{\pm \pi x/h} \tag{9.134}$$

$$c'_{xu} = \frac{1}{2}(c_{x2} - c_{x1})\, e^{\pi x/h}$$

when inserted in Eq. (9.133a) gives

$$c_{xu} = c_{x1} + \frac{1}{2}(c_{x2} - c_{x1})\, e^{\pi x/h} \tag{9.135}$$

Similarly, for the downstream region

$$c'_{xd} = -\frac{1}{2}(c_{x2} - c_{x1})\, e^{-\pi x/h}$$

$$c_{xd} = c_{x2} - \frac{1}{2}(c_{x2} - c_{x1})\, e^{-\pi x/h} \tag{9.136}$$

At the disc immediately upstream or downstream ($x = 0$), Eqs. (9.135) and (9.136) give

$$c_{xu} = c_{xd} = \frac{1}{2}(c_{x1} + c_{x2}) \tag{9.137}$$

For regions far upstream and downstream, these equations yield

$$c_{xu} = c_{x1} \quad (x = -\infty)$$

$$c_{xd} = c_{x2} \quad (x = +\infty)$$

9.10 Partial Admission Turbine Stages[303 – 343]

Turbines in which the working fluid does not flow through the entire annulus (the complete 360°) of the stage are known as partial admission, partial flow or simply partial turbines.

The first stage of a high pressure steam turbine receives steam with a relatively small specific volume. Therefore, the annulus area required is small. If this small area is distributed over the complete 360°, the height of the annulus in some cases is too small (< 25 mm). The short nozzle and rotor blades thus obtained experience high cascade losses as explained in Sec. 8.4.5 (c). Therefore, to avoid this the steam is admitted over only a fraction of the annulus ($e\ \pi d$) and the blade height is correspondingly increased.

Figure 9.25 shows full and partial admission configurations. The annulus area perpendicular to the flow is

$$A = \pi d\ h_f = e\ (\pi d)\ h_p = Bh_p \tag{9.138}$$

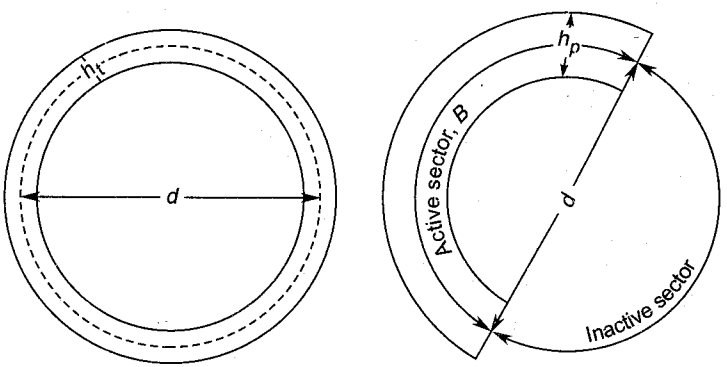

(a) Full admission (b) Partial admission

Fig. 9.25 Full and partial admission configurations

The degree of admission is defined as the ratio of the length (B) of the admission sector and the length of the entire periphery.

$$e = \frac{B}{\pi d} \tag{9.139}$$

These equations show that, by employing a suitable value of the degree of admission, the blade height in a partial admission turbine stage can be substantially increased, thereby reducing the cascade losses.

In some applications the diameter of the turbine stage is kept large, either for obtaining high torque or low rotational speed. This for a given mass-flow rate and the corresponding annulus area can lead to an

impractically small blade height. Here again the blade height can be increased by employing a certain degree of admission.

The adoption of a partial admission configuration gives rise to a new category of losses which are described in Secs. 9.10.5 and 9.10.6. Partial admission is advantageous if these losses along with other conventional cascade losses are lower than the losses of the shorter blades with full admission.

The flow in partial admission stages is unsteady, the rotor blades are subjected to large variations of forces during their passage in the active and inactive sectors of the annulus. This leads to harmful vibrations of the rotor. A partial admission configuation is only suitable for an impulse stage; in a multi-stage turbine this is invariably used only in the first stage.

Some applications are described in the following sections before discussing the flow phenomenon and losses in partial turbines.

9.10.1 Steam Turbine Governing

Partial admission of steam has been usefully employed in the governing of steam turbines. Figure 9.26 shows an arrangement employed in nozzle control governing. The admission of steam is divided by admitting it through a number of sectors (3-12), A_1, A_2, A_3, etc. These sectors govern

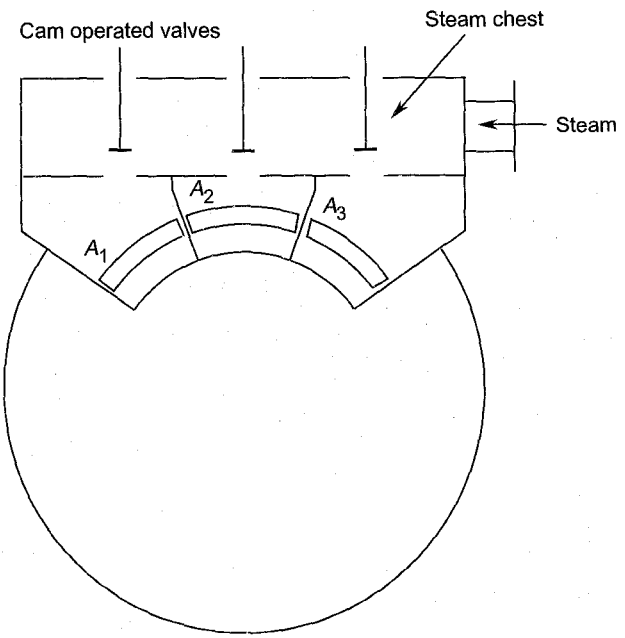

Fig. 9.26 Partial admission of steam for nozzle control governing

the flow to individual groups of nozzles. The flow rate in each group depends on the positions of the cam operated valves. The cam shaft is actuated through high pressure oil in servomotors and takes a particular angular position depending on the load.

The chief advantage of this method is that the throttling of steam is considerably reduced by employing a large number of valves and admission sectors.

The low specific volume of steam at the entry of the first stage may require only 30% or a lower degree of admission.

9.10.2 Turbo-supercharging[309,314]

Large diesel engines, specially in marine, rail and power plant applications, are generally supercharged. In a large number of such applications generally one or two centrifugal blowers driven by gas turbines (axial or radial type) are employed.

Figure 9.27 shows a four-cylinder engine supplying its exhaust gases to an axial turbine. The gases enter the turbine through three sectors of admission. This arrangement minimizes the gas dynamic interference of flows from different cylinders. Other schemes employing one or two turbo chargers can also be adopted.

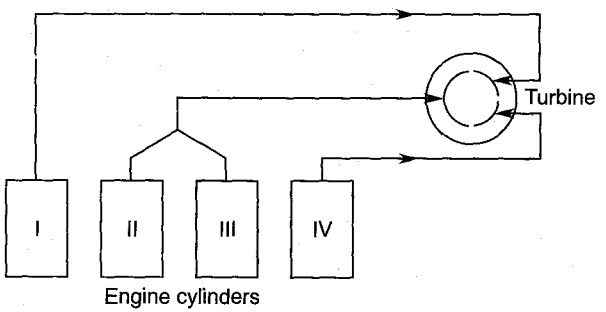

Fig. 9.27 Partial admission turbine for exhaust supercharger

9.10.3 Re-entry Turbine[303,322]

Figure 9.28 shows a re-entry turbine which is also a partial admission turbine on account of its configuration. High pressure gas or steam is expanded to a high velocity and flows through an impulse rotor in the first stage. It is then collected in a duct and reintroduced into the rotor for doing more work. Thus this turbine is a sort of velocity compounded two-or three-stage impulse type with only one rotor.

It can be seen that on account of the leakage in the peripheral direction from one sector to the other such a configuration should not be employed for reaction turbines.

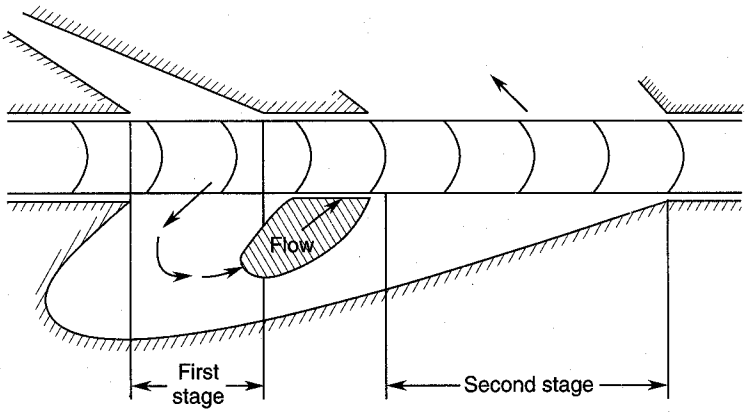

Fig. 9.28 Two stage re-entry turbine

Partial admission turbines are also used for turbo-pump drives and auxiliary power units[325,326,327] in various aerospace and underwater applications.

9.10.4 Nature of Flow

The basic difference between the flows in partial and full admission turbines is due to the presence of the "ends" of the admission sector (Fig. 9.29) in partial admission turbines. The admission arc or sector of the conventional full admission turbine is "endless". Therefore, the flow in partial turbines is significantly influenced by the end of sector effects, whereas these effects are absent in full admission turbines.

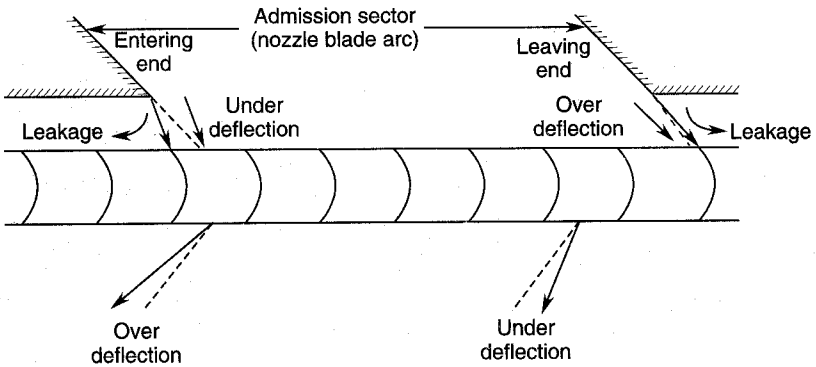

Fig. 9.29 Jet dispersion and leakage at admission sector ends[342]

In partial turbines the entire annulus is divided into active and inactive sectors as shown in Fig. 9.25. Work is done by the gas or steam on the rotor blades only when they pass across the active sector through which

the flow occurs. When the rotor blades pass through the inactive sector, they do work on the stagnant gas filling the inactive sector. The energy lost in this process is termed as pumping loss.

Besides this, as the rotor blades enter the admission sector from the inactive sector, the flow through them starts from almost stagnant conditions. This "starting of the flow" or "filling" process occurs with sudden expansion, mixing and shear. All these phenomena lead to additional cascade losses besides those occurring in conventional full admission turbines.

The flow in the blade channel leaving the admission sector also experiences some new phenomena due to the "stopping of flow" or "emptying" process. They also lead to additional losses.

On account of the admission sector, which does not cover complete 360°, the flow in it and the rotor blade rows is no longer axisymmetric. The end of sector effects communicate disturbances towards the middle of the flow field and destroy the axisymmetric nature of the flow. This leads to variations in velocity, direction and pressure along the admission sector.

For incompressible flow in the rotor blades, the pressure waves move with an excessively large velocity through the blade passages and the flow is instantaneously established through them as they enter the admission sector. In contrast to this, in compressible flows, the pressure waves move through the rotor blade passages with finite velocity. Thus, rotor blade channels move through a certain distance along the admission sector before the flow occurs at the exit.

The flow phenomena in the presence of waves is not simple. When the blades enter the admission sector, a compression wave (of some strength) descends down the channel. This is reflected from the open end as a rarefaction wave. In contrast to this, when the blade channel is cut off from the admission sector while leaving it, a rarefaction wave moves downstream which is reflected as a compression wave. This compression wave moving upstream is reflected as compression wave from the closed end.

The wave phenomenon can continue in rotor blade channels till they again enter the admission sector.

The aforementioned flow phenomena lead to two categories of additional losses[331,334,338]:

(a) end of sector losses which are additional cascade losses due to end of sector effects; and

(b) pumping losses arising from the passage of rotor blades through the inactive sector.

Disc friction loss occurs in all rotating machines. Pumping and disc friction losses are often referred to as windage losses.

The losses over and above the conventional losses of a turbine are shown in Fig. 9.17.

9.10.5 End of Sector Losses

The main cascade losses occurring at the sector ends are shown in Fig. 9.17. They are briefly described below.

(a) *Mixing loss*

When a rotor blade passage filled with stagnant gas enters the admission sector, the nozzle flow first flushes the stagnant gas before establishing a steady flow. This is a kind of "mixing" process in which the active flow from the nozzles imparts motion to the stagnant or dead gas brought by the rotor blades from the inactive to the active sector.

The acceleration of the dead gas in the rotor blade passages to the full steady flow velocity takes a finite time. During this time the rotor blades move along the admission sector by a certain distance which depends on the nozzle angle and velocity, rotor blade angles and the peripheral speed. Thus the relative flow (as observed by an observer moving with the rotor) is unsteady in front of a part of the admission sector. The development of flow through the rotor in the unsteady flow region is shown in Fig. 9.30. It should be remembered that the flow in the absolute system is steady

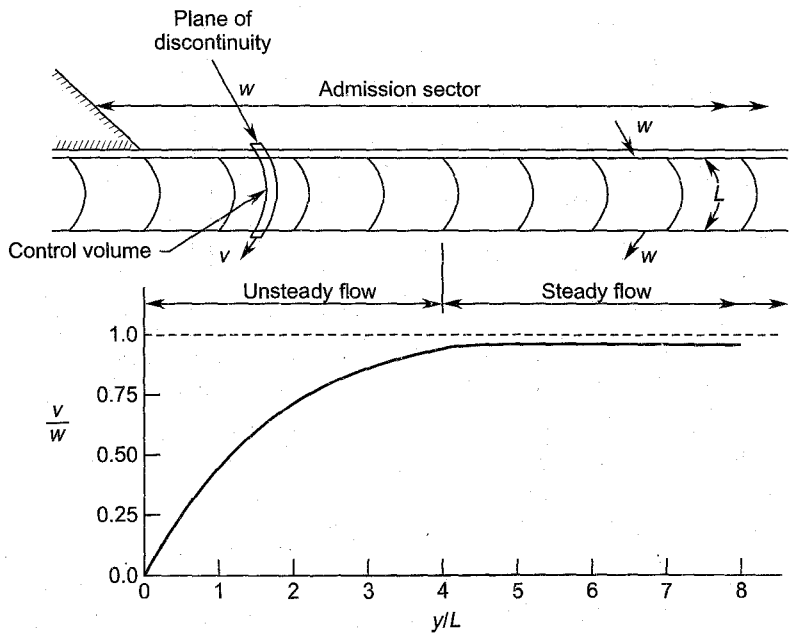

Fig. 9.30 Development of flow in a rotor blade passage of a partial admission turbine[331,337]

throughout, i.e. the velocity profile in Fig. 9.30 is constant as observed by an observer at rest.

This phenomenon of "mixing", "scavenging" or "knocking out" is accompanied by loss of energy; the mixing loss can be calculated from the velocity profile shown in Fig. 9.30.

When the active nozzle flow impinges on the stagnant gas in the rotor blade passage which enters the admission sector, static pressure at the rotor entry rises above its steady flow region value. This establishes a static pressure gradient in the peripheral direction along the admission sector. The acceleration of the gas in the rotor blade passages would depend on the magnitude of the pressure difference across them.

The static pressure rise at the rotor entry also largely depends on the axial and radial clearances. Its value may be negligible in the presence of large clearances due to "spillage" or leakage of flow from the higher to lower pressure region.

Some theoretical methods have been developed which predict the magnitude of mixing loss. They are based on the calculation of the velocity at the rotor exit in the unsteady flow region.

One such method[337] neglects the static pressure rise due to mixing at the rotor entry. This is justified on account of the sufficient spillage of the flow through the clearances. Other assumptions are:

1. inviscid and incompressible flow,
2. impulse rotor blades with constant passage area,
3. one-dimensional flow through infinitely narrow rotor blade passages, and
4. flow in the narrow curved passage (of length L) is equivalent to flow in a straight passage of the same length.

Flow at the entry and exit of the narrow rotor blade channel is shown in Fig. 9.30. It is enclosed in a control volume.

In view of the "spillage", the upstream face of the control volume is looked upon as a plane of discontinuity where the velocity of the relative flow changes from a steady value w to an unsteady value v which is a function of time (t) or the distance ($y = ut$).

The momentum equation for this model of flow through the control volume is

$$\frac{\partial}{\partial t}\,(mv)_{cv} = \int (V\,dm)_{in} - \int (V\,dm)_{out} \qquad (9.140)$$

For one-dimensional flow,

$$(mv)_{cv} = (\rho AL)v$$

$$\int (V\,dm)_{in} = \rho A w^2$$

$$\int (V\, dm)_{out} = \rho A v^2$$

Substituting these values in Eq. (9.140)

$$L \frac{dv}{dt} = w^2 - v^2$$

On integration

$$\int \frac{dt}{L} = \int \frac{dv}{w^2 - v^2} + \text{const.}$$

$$\frac{t}{L} = \frac{1}{2w} \ln \left(\frac{w+v}{w-v} \right) + \text{const.}$$

The value of the constant from the boundary conditions ($t = 0,\ v = 0$) is obtained as zero. Therefore,

$$\ln \left(\frac{w+v}{w-v} \right) = \frac{2wt}{L}$$

$$e^{2wt/L} = \frac{w+v}{w-v}$$

on further rearrangement

$$\frac{v}{w} = \frac{e^{2wt/L} - 1}{e^{2wt/L} + 1} \tag{9.141a}$$

But $y = ut$. Therefore,

$$\frac{v}{w} = \frac{e^{\frac{2w}{u}\frac{y}{L}} - 1}{e^{\frac{2w}{u}\frac{y}{L}} + 1} \tag{9.141b}$$

The following expressions for the loss coefficients have been derived from Eq. (9.141) for an impulse stage:

$$C_m = 2(1 - n)\, \eta_N\, \sigma\, [(1 - 2\sigma \sin \alpha_2 + \sigma^2) \sin \beta_2 + \sin \alpha_2 - \sigma] \tag{9.142}$$

where

$$n = 1 - \frac{2}{kt_1} + \frac{4}{kt_1 (1 + e^{kt_1})} \tag{9.143}$$

$$k = \frac{2w}{L} \qquad \text{and} \qquad ut_1 = B$$

Equation (9.142) can be reduced to a considerably simpler form by some approximations.

$$C_m = M\, \sigma_s \left(\frac{B}{L} \right)^{-1} \tag{9.144}$$

The value of the constant M is recommended as 1.73 for the usual range of operation of impulse turbine stages.

The derivations of these relations are beyond the scope of this book and can be seen in the quoted literature.

Another method[330,331] gives the following expression for the curve shown in Fig. 9.30.

$$\frac{v}{w} = \frac{1 - e^{-Ey/L}}{1 + Ce^{-Ey/L}} \tag{9.145}$$

where

$$E = \frac{w}{u} + \frac{\cos \beta_2}{\cot \alpha_2}$$

$$C = \left(1 + \frac{2u \cos \beta_2}{w \cot \alpha_2}\right)^{-1}$$

This is based on the full pressure rise (in the absence of clearances) due to mixing at the rotor entry. Therefore, it shows an underestimation of losses.

Many investigators have given formulas of the form Eq. (9.144) in which the value of the constant M also takes into account other cascade losses due to partial admission. Besides this, for relatively longer admission sectors, other losses are negligible compared to the mixing loss.

Suter and Traupel[335] suggest the following formula:

$$C_m = 0.3\ Z\ \sigma_s \left(\frac{b}{ed}\right) \tag{9.146}$$

But $b \approx L$ and $e\ (\pi d) = B$. Therefore,

$$C_m = 0.943\ Z\ \sigma_s \left(\frac{B}{L}\right)^{-1} \tag{9.147}$$

This assumes that the total loss due to mixing is proportional to the number of admission sectors if multi-arc admission is employed as in steam turbine governing.

Chupirev's formula reported by Terentiev[336] in the range σ_s = 0.35-0.55 is

$$C_m = 0.33Z\ \sigma_s \left(\frac{b}{B}\right) \frac{1}{\cos \alpha_2} \tag{9.148}$$

For $\alpha_2 = 70°$, $\cos\ \alpha_2 = 0.342$ and $\frac{b}{B} \approx \frac{L}{B}$;

Equation (9.148) reduces to

$$C_m = 0.965\ Z\ \sigma_s \left(\frac{B}{L}\right)^{-1} \tag{9.149}$$

Stenning[384] gives a formula for both mixing and full pumping losses:

$$C_m = 1.4 \left(\frac{L}{B}\right)\left(\frac{u}{c_s}\right)^2 \left(\frac{u}{c_2}\right) \frac{1}{\cos \alpha_2} \tag{9.150a}$$

But $$\sigma = \frac{u}{c_2} = \sigma_s \sqrt{\eta_N}$$

Therefore,

$$C_m = 1.4 \sec \alpha_2 \, \sigma_s^3 \left(\frac{B}{L}\right)^{-1} \tag{9.150b}$$

This expression is not rational because it takes into account the full blade pumping loss when there is no admission of the gas. The degree of admission (e) is always greater than zero and the pumping loss is proportional to $(1 - e)$.

(b) *Expansion loss*[334]

This loss arises due to the sudden expansion (or merely expansion) of the nozzle jets into the partially open rotor blade passages at the sector ends; these are shown in Fig. 9.31. Stenning has given an analysis for estimating these losses in equiangular and frictionless rotor blades of an impulse turbine stage. While considering this, he has ignored the mixing phenomenon discussed earlier.

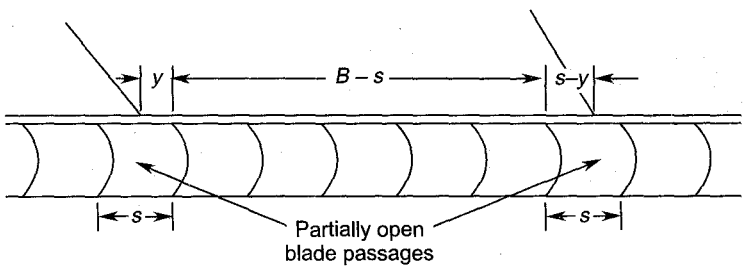

Fig. 9.31 Sudden expansion of the jets in partially open blade passages at admission sector ends[334]

If the admission sector is an exact multiple of the rotor blade pitch, the positions of the partially open blade passages at the two sector ends are as shown in Fig. 9.31. The openings of the blade passages to the admission sector are y and $s - y$ at the two ends. The corresponding expansion ratios are $\frac{s}{y}$ and $\frac{s}{s-y}$ respectively.

Referring to Fig. 9.1, the expression for the tangential force on the whole rotor is

$$F_y = w_2 \sin \beta_2 + \frac{1}{s} \int_0^s \left[\frac{y}{B}\left(\frac{y}{s}\right) + \frac{B-s}{B} + \frac{s-y}{B}\left(\frac{s-y}{s}\right) \right] \times w_3 \sin \beta_3 \, dy$$

After integration and simplification and putting

$$w_2 = w_3 \quad \text{and} \quad \beta_2 = \beta_3,$$

$$F_y = 2\left(1 - \frac{s}{6B}\right) w_2 \sin \beta_2 \tag{9.151}$$

The specific blade work is

$$F_y u = 2\left(1 - \frac{s}{6B}\right) u\, w_2 \sin \beta_2$$

From Fig. 9.1,

$$F_y u = 2\left(1 - \frac{s}{6B}\right) u\,(c_2 \sin \alpha_2 - u)$$

The blade efficiency is then given by

$$\eta_{bp} = \frac{F_y u}{\frac{1}{2} c_2^2} = \left(1 - \frac{s}{6B}\right) 4(\sigma \sin \alpha_2 - \sigma^2) \tag{9.152}$$

Substituting from Eq. (9.19),

$$\eta_{bp} = \left(1 - \frac{s}{6B}\right) \eta_b$$

Stenning recommends that, since the above expression under-estimates the losses, it can be modified to

$$\eta_{bp} = \left(1 - \frac{s}{4B}\right) \eta_b \tag{9.153}$$

The value of the factor $(1 - s/4B)$ is close to unity for large values of B/s or B/L; therefore, loss due to expansion may be ignored for values of $B/L > 10$.

(c) *Shear flow loss*

The starting of the flow in the rotor blade passages entering the admission sector is accompanied by steep velocity gradients. These gradients within the rotor blade passages are significant in the unsteady flow region (Fig. 9.30). Therefore, spanwise vortices are generated in the rotor blade passages leading to a further loss. This loss can also be looked upon as "equalization loss" of a non-uniform flow due to the significant shearing motion between various layers of flow. This phenomenon would affect the normal cascade losses of a conventional stage, but the magnitude of this loss is small compared to other losses.

(d) *Jet dispersion loss*

The direction of flows at the exits of the nozzle and rotor blades near the sector ends deviates from that in the main flow field on account of the

absence of axisymmetric flow. The jets tend to deflect away from their normal direction towards the inactive regions as shown in Fig. 9.29.

The deviation of the nozzle jets alters the incidence at the rotor entry. The incidence decreases at the entering end and increases at the leaving end. The deviation at the rotor exit decreases at the entering end and increases at the leaving end as shown in the figure. The under and over deflections of the flow may not always lead to a loss.

The dispersion of the jet at the nozzle exit can be minimized by minimizing the axial clearance between the nozzle and rotor blade rows.

(e) *Leakage loss*

The leakage of flow from the active to the inactive sector is also a consequence of the absence of axisymmetric flow conditions in the axial clearance between the nozzle and rotor blade rows. This occurs at both ends of the sector (Fig. 9.29). However, at the entering end, while on one hand it is augmented by some static pressure rise due to mixing (as explained before), on the other it is retarded by the entrained gas in the clearance space as shown in Fig. 9.32.

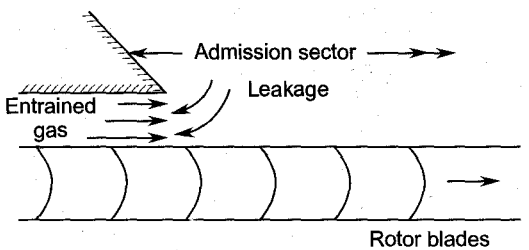

Fig. 9.32 Leakage of active flow into the inactive sector[332,340]

The leaking gas fills the inactive sector as well as flows out of the rotor doing some useful work.

(f) *Other losses*

As a rule, the partial admission configuration should not be employed for reaction stages. If it is used, then the stage will experience additional losses because of the increased leakage and varying degrees of reaction along the admission sector.

If partial admission is adopted in more than one stage, then the interstage spacing, relative sizes of the admission sectors and their relative location become additional parameters which govern losses.

9.10.6 Windage Losses

Windage losses occur in rotating machines on account of the fluid friction on the disc and the rotating blade surfaces in the inactive sector of the annulus.

The loss due to disc friction is common to both full and partial admission turbomachinery. This depends on the density of the fluid, diameter of the disc, its peripheral speed and the axial clearances between the housing and the disc. The degree of admission has no effect on this loss.

$$\text{Disc friction loss} = \text{const.} \times \rho d^2 u^3 \tag{9.154}$$

The constant takes into account the effect of housing geometry and clearances.

Since the loss due to rotor blade pumping is also found to be proportonal to the quantity $\rho d^2 u^3$, the two losses are sometimes given by a single formula.

The rotor blade pumping loss arises due to the action of rotor blades on the fluid which fills the inactive sector. Work is done by the blades on the fluid in churning gas axially (such as a compressor or fan) from one chamber to the other. This shows strong depend-ence on the geometry of the housing and the rotor blades besides the quantities mentioned earlier. For a given degree of admission (e), it is directly proportional to the quantity $(1 - e)$.

Empirical formulas suggested by some investigators are given here. The original formulas in FPS system have been converted to S.I. units.

(a) *Disc friction*

The most widely used formula for power lost in disc friction is given by Stodola[12] and later by Kerr[316]:

$$P_{df} = 1.075\ \rho d^2 u^3 \times 10^{-3}\ W \tag{9.155}$$

This takes into account the friction effects on both the sides of a single rotor disc.

(b) *Blade pumping*

The formula suggested by Stodola and Kerr for single-stage turbines with dry steam is

$$P_{bp} = 609.5\ (1 - e)\ dh^{1.5}\ \rho u^3 \times 10^{-3}\ W \tag{9.156}$$

For wet steam the increased blade pumping loss is obtained by multiplying the above value by 1.3.

Kerr gives another formula which is considered as an improvement over Eq. (9.156). It is dimensionally more rational.

$$P_{bp} = 671.5\ (1 - e) \left(\frac{h}{d}\right)^{1.5} \rho d^2 u^3 \times 10^{-3}\ W \tag{9.157}$$

Suter and Traupel[335] suggest

$$P_{bp} = 157\ (1 - e) \left(\frac{h}{d}\right) \rho d^2 u^3 \times 10^{-3}\ W \tag{9.158}$$

The formula given by Forner for unenclosed wheels is

$$P_{bp} = 123\ (1 - e) \left(\frac{h}{d}\right) \rho d^2 u^3 \times 10^{-3}\ W \tag{9.159}$$

This seems to underestimate the losses.

It is observed from the above expressions that the windage losses increase rapidly with the rotor diameter and peripheral speed. If other considerations permit, it is advantageous to use a small rotor diameter for a given peripheral speed. Table 9.2 shows comparative values of the power loss due to disc friction and blade pumping ($e = 0$).

For the sake of comparison the peripheral speed has been taken for a rotor of mean diameter 100 cm running at 3000 rpm. Rotors of smaller diameters run at proportionally higher rotational speeds.

Table 9.2 Disc Friction and Blade Pumping Losses (ρ = 1.0 kg/m^3, h/d = 0.1, and u = 157.08 m/s)

Author of the formula	*Power loss in kW*		
	d = 100 cm, N = 3000 rpm	d = 50 cm, N = 6000 rpm	d = 25 cm, N = 12000 rpm
Disc friction (Stodola)	4.165	1.042	0.261
Stodola	74.7	18.66	4.665
Kerr	82.24	20.56	5.14
Suter and Traupel	60.838	15.21	3.80
Forner	47.66	11.92	2.98

9.11 Supersonic Flow

Supersonic flow in a turbine stage affects it in a number of ways:

(a) A simple example is of a flow approaching a turbine blade at a high subsonic Mach number (say 0.80). This flow is accelerated to supersonic flow somewhere on the suction side of the blade surface. However, with subsonic exit this is followed by a deceleration process (see Sec. 6.8.1). It is well known that the supersonic flow changes to subsonic through a shock wave (Sec. 6.7) accompanied by stagnation pressure loss and increase in entropy (Eqs. (6.91) and (6.92)).

If the shock wave separates the flow from the blade surface earlier than the normal subsonic flow, there are additional losses associated with a larger region of separated flow over the blade surface.

In contrast to this there can be another situation where a shock wave reattaches a separated boundary layer to the blade surface,

thus reducing the total region of separated flow on the blade surface.

The shock waves generated in a blade passage may be normal, oblique or curved. Except the normal shock waves, the direction of flow changes after emerging from the oblique and curved shocks. Besides this, a high Mach number flow in the blade passage invariably experiences expansion waves (Mach waves) or a fan of expansion waves as shown in Fig. 9.33. The flow through such a fan expands progressively and at the same time experiences changes in its direction (see Sec. 6.7.3). The expansion waves emanating from one blade are reflected from the surface of another blade as oblique shock wave as shown in the figure. The actual wave phenomenon in the entire passage is much more complicated than this.

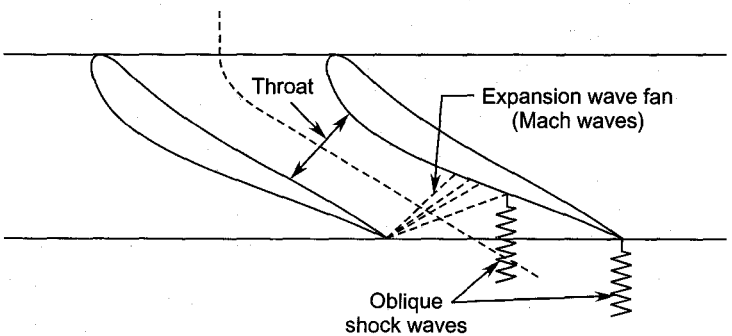

Fig. 9.33 Passage of a supersonic turbine nozzle

(b) Supersonic flow occurs in high pressure ratio Curtis and Rateau stages (Secs. 9.3 and 9.4) at the high pressure end of a large steam turbine. In a Curtis wheel the fluid velocities (Mach numbers) are high both in the nozzle and rotor blade rows.

It can be shown by gas dyanmic analysis that, when a supersonic flow approaches a sharp leading edge of the rotor blade, an attached oblique shock wave (see Sec. 6.7.2) is generated. The strength of the shock wave [Eq. (6.94)], wave angle [Eq. (6.93)] and downstream Mach number [Eq. (6.99)] depend on the upstream Mach number and the wedge angle at the leading edge of the rotor blade. However, if the leading edge is thick or blunt (as in the case of aerofoil blades), there will be a detached shock of higher strength standing upstream of the leading edge.

Thus the direction and the stagnation pressure loss (Eqs. (6.97) and (6.98)) at the leading edge in the presence of an oblique shock are decided by the wedge angle of the blade. A sharp and thin

rotor leading edge will suffer lower loss on account of a smaller wave angle and irreversibilities of lower order.

(c) Turbine stages often have high relative Mach numbers at the rotor exit. When the Mach number at the throat of the blade passage reaches the sonic value, the maximum flow through this is governed by Eq. (6.83). A further reduction of static pressure at the rotor exit does not lead to an increase in the mass-flow rate through the stage. The flow in the diverging portion of the passage will pass through a series of expansion and shock waves as explained before. Nozzle and rotor exit Mach numbers in turbines of power pack units of rockets, missiles and turbo-rocket engines are very high. Mach numbers of more than 3.0 have been used in turbine stages employing high pressure ratios.

High Mach number flows also occur in the last few stages of large steam turbines on account of relatively higher steam velocities and lower velocity of sound.

Notation for Chapter 9

a	Velocity of sound
A	Area of cross-section
b	Axial chord
B	Length of the admission sector
c	Absolute velocity of fluid
c_p	specific heat at constant pressure
C	Constant
d	Diameter
e	Degree of admission
E	Constant
F	Fixed blades
h	Enthalpy, blade height
i	Incidence, ith stage
k	Velocity coefficient, constant
K	Constant
L	Length of the blade passage
$\dot{m}$	Mass, mass flow rate
M	Mach number, constant
n	Number of velocity stages, constant
N	Revolutions per minute
p	Pressure
P	Power

r	Radius, distance in the cylindrical coordinate system
R	Degree of reaction, rotor, gas constant
s	Entropy, blade pitch
t	Time
T	Absolute temperature
u	Peripheral speed of the rotor
v	Relative velocity (unsteady)
V	Fluid velocity
w	Relative velocity (steady)
y	Distance in the tangential direction
Y	Stagnation pressure loss coefficient
Z	Number of admission sectors

Subscripts

o	Stagnation value
1	Entry to the stage, first stage
2	Exit of the nozzle or fixed blades, second stage
3	Exit of the rotor blades
I	First stage
II	Second stage
a	Actual
b	Blade
bp	Blade pumping loss
d	Downstream
df	Disc friction loss
f	Full admission
h	Hub
i	ith stage
m	Mean, mixing
max	Maximum
min	Minimum
N	Nozzle
opt	Optimum
p	Constant pressure, partial admission, profile
r	Radial
rel	Relative
R	Rotor
s,ss	Isentropic
st	Stage
t	Tip

ts	Total-to-static
tt	Total-to-total
u	Upstream
x	Axial
y, θ	Tangential

Greek symbols

α	Direction of absolute velocity vector
β	Direction of relative velocity vector, constant
γ	c_p/c_v
ε	Utilization factor
ε	Gas deflection
ζ	Axial component of vorticity
η	Efficiency
ξ	Enthalpy loss coefficient
ρ	Fluid density
σ	Blade-to-gas speed ratio
ϕ	Flow coefficient
ψ	Loading coefficient
ω	Angular speed

Solved Examples

9.1 The initial pressure and temperature of steam entering a multistage turbine (d = 100 cm, N = 3000 rpm) are 100 bar and 500° C respectively. The steam flow rate is 100 kg/s and the exit angle of the first stage nozzle blades is 70°. Assuming maximum utilization factor, determine the rotor blade angles, blade heights, power developed and the final state of steam after expansion for the following arrangements:

(a) single-stage impulse, $\eta_{st} = 0.78$,

(b) two-stage Curtis wheel, $\eta_{st} = 0.65$,

(c) two-stage Rateau wheel ($\eta_{st1} = \eta_{st2} = 0.78$) and

(d) single stage 50% reaction, $\eta_{st} = 0.85$.

State the assumptions used.

Solution:

(a) Single stage impulse (Fig. 9.3b)

Blade and air angles are assumed to be equal.

$$u = \pi\, dN/60 = \pi \times 1 \times 50 = 157.08 \text{ m/s}$$

$$\sigma_{opt} = \frac{u}{c_2} = \frac{1}{2} \sin \alpha_2 = \frac{1}{2} \sin 70 = 0.47$$

$$c_2 = 157.08/0.47 = 334.2 \text{ m/s}$$

$$c_x = c_2 \cos \alpha_2 = 334.2 \cos 70 = 114.3 \text{ m/s}$$

$$\tan \beta_2 = \tan \beta_3 = \frac{1}{2} \tan \alpha_2 = \frac{1}{2} \tan 70 = 1.3737$$

$$\beta_2 = \beta_3 = 53.95° \text{ (}Ans.\text{)}$$

$$w_{st} = 2u^2 = 2 \times 157.08^2 \times 10^{-3} \text{ kJ/kg}$$

$$w_{st} = 49.35 \text{ kW/(kg/s)}$$

$$P = \dot{m}\, w_{st} = 100 \times 49.35 \times 10^{-3}$$

$$P = 4.935 \text{ MW (}Ans.\text{)}$$

If blade heights at the rotor entry and exit are h_2 and h_3

$$h_2 = h_3 = \dot{m}/\rho\, c_x\, \pi d$$

The specific volume of steam after expansion is 0.04 m^3/kg. Therefore,

$$h_2 = h_3 = \frac{100 \times 0.04 \times 100}{114.3\, \pi \times 1} = 1.11 \text{ cm}$$

This is too small a height and would lead to excessive cascade losses. This is a case where some degree of partial admission must be employed to obtain sufficiently long blades. With 40% admission, the blade height can be increased to 1.11/0.4 = 2.78 cm. This is a reasonable value for the first stage.

The isentropic enthalpy drop in the stage (nozzles) is

$$\Delta h_s = \frac{w_{st}}{\eta_{st}} = \frac{49.35}{0.78} = 63.27 \text{ kJ/kg}$$

Figure 9.34 shows the actual and ideal expansions. The final state of the steam is

$$p = 81.5 \text{ bar}, \; t = 470 \text{ °C} \quad \text{(}Ans.\text{)}$$

(b) Two-stage Curtis wheel (Fig. 9.5)

$$\sigma_{opt} = \frac{u}{c_2} = \frac{1}{4} \sin \alpha_2 = \frac{1}{4} \sin 70 = 0.235$$

$$c_2 = 157.08/0.235 = 668.43 \text{ m/s}$$

$$c_{x2} = c_{x3} = c_2 \cos \alpha_2 = 668.43 \cos 70 = 228.6 \text{ m/s}$$

$$\tan \beta_2 = \tan \beta_3 = \frac{3u}{c_{x2}} = \frac{3 \times 157.08}{228.6} = 2.061$$

$$\beta_2 = \beta_3 = 64.12° \text{ (}Ans.\text{)}$$

$$\tan \alpha_3 = \tan \alpha'_2 = \frac{2u}{c_2 \cos \alpha_2} = \frac{2 \times 0.235}{\cos 70} = 1.374$$

$$\alpha_3 = \alpha'_2 = 54.0° \text{ (}Ans.\text{)}$$

$$\tan \beta'_2 = \tan \beta'_3 = \frac{u}{c'_{x3}} = \frac{157.38}{228.6} = 0.687$$

$$\beta'_2 = \beta'_3 = 34.5° \text{ (}Ans.\text{)}$$

$$w_{\text{I}} = 6u^2 = 6 \times 157.08^2 \times 10^{-3} = 148.04 \text{ kJ/kg}$$

$$w_{\text{II}} = 2u^2 = 2 \times 157.08^2 \times 10^{-3} = 49.35 \text{ kJ/kg}$$

$$w_{st} = w_{\text{I}} + w_{\text{II}} = 197.39 \text{ kJ/kg}$$

$$P = 100 \times 197.39 \times 10^{-3} = 19.739 \text{ MW} \quad (Ans.)$$

$$\Delta h_s = \frac{197.39}{0.65} = 303.65 \text{ kJ/kg}$$

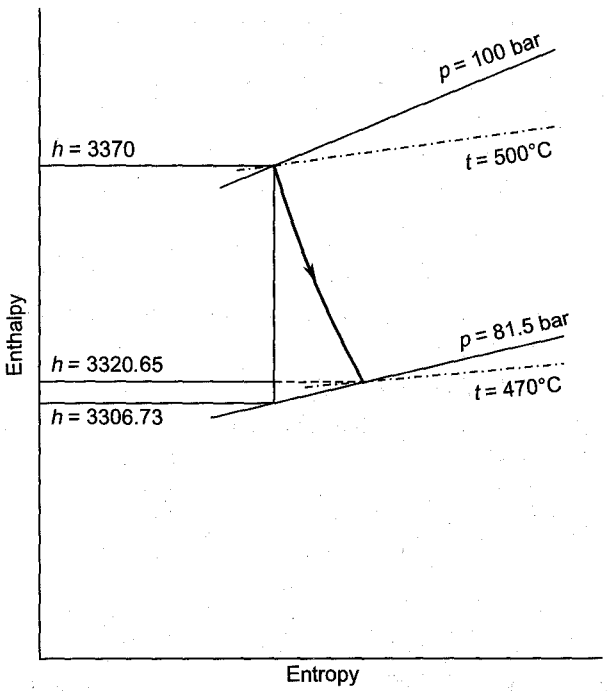

Fig. 9.34 Expansion of steam in a single-stage impulse turbine (Ex. 9.1(a))

Figure 9.35 shows the enthalpy-entropy diagram for the expansion. The final state of steam is

$$p = 27 \text{ bar}, \; t = 365°\text{C}, \; v = 0.105 \text{ m}^3/\text{kg} \quad (Ans.)$$

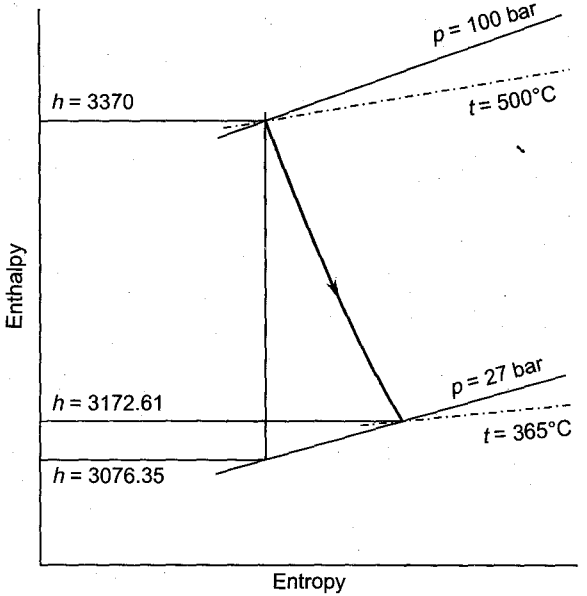

Fig. 9.35 Expansion of steam in a two-stage Curtis wheel (Ex. 9.1(b))

The rotor blade heights are

$$h = \frac{100 \times 0.105 \times 100}{228.6\,\pi \times 1} = 1.46 \text{ cm} \quad (Ans.)$$

The blade height is again small. One of the methods to increase it is to decrease the stage diameter.

(c) Two-stage Reateau wheel (Fig. 9.6b)

With the same stage diameter and velocity triangles, each stage has the same geometry as in (a), i.e.

$$\beta_2 = \beta_3 = 53.95° \quad (Ans.)$$

$$w_{st} = 2u^2 + 2u^2 = 4u^2$$

$$w_{st} = 2 \times 49.35 = 98.70 \text{ kJ/kg}$$

$$P = 100 \times 98.70 \times 10^{-3} = 9.87 \text{ MW} \quad (Ans.)$$

The *h–s* diagram is shown in Fig. 9.36. The final state of steam is

$$p = 65 \text{ bar}, \; t = 445 \text{ °C}, \; v = 0.05 \text{ m}^3/\text{kg} \quad (Ans.)$$

Rotor blade height in the first stage is 1.11 cm. For the second stage,

$$h'_2 = h'_3 = 100 \times 0.05 \times 100/114.3 \; \pi \times 1$$

$$h'_2 = h'_3 = 1.392 \text{ cm} \quad (Ans.)$$

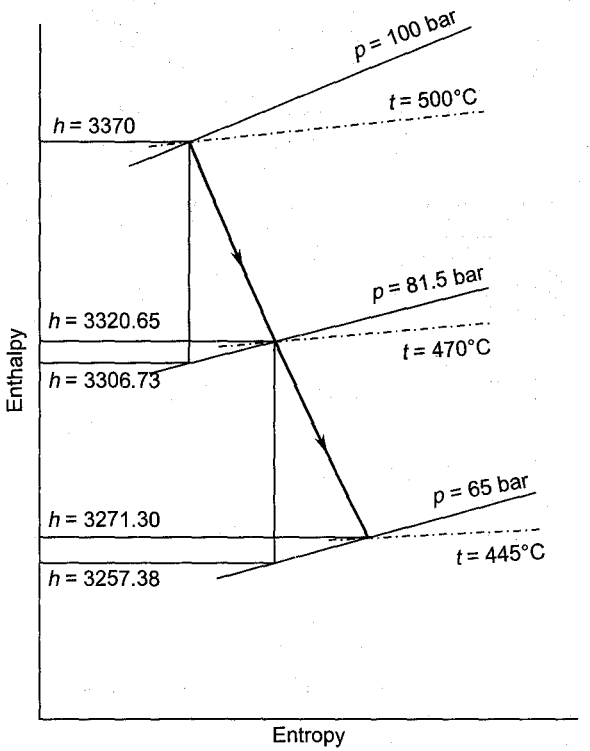

Fig. 9.36 Expansion of steam in a two-stage Rateau wheel (Ex. 9.1 (c))

(d) Single stage 50% reaction (Fig. 9.14)

$$\sigma_{opt} = \frac{u}{c_2} = \sin \alpha_2 = \sin 70 = 0.9397$$

$$c_2 = 157.08/0.9397 = 167.16 \text{ m/s}$$

$$c_{x2} = 167.16 \times \cos 70 = 57.17 \text{ m/s}$$

$$c_2 = w_3 \; ; \; \alpha_2 = \beta_3 = 70° \; ; \; \beta_2 = \alpha_3 = 0 \qquad (Ans.)$$

$$w_{st} = u^2 = 157.08^2 \times 10^{-3} = 24.67 \text{ kJ/kg}$$

$$P = 100 \times 24.67 \times 10^{-3} = 2.467 \text{ MW} \qquad (Ans.)$$

Figure 9.37 shows the h–s diagram for this stage.

$$\Delta h_s = \frac{24.67}{0.85} = 29.02 \text{ kJ}$$

The final state is given by

$$p = 90 \text{ bar}, \; t = 485°C, \; v = 0.035 \text{ m}^3/\text{kg}$$

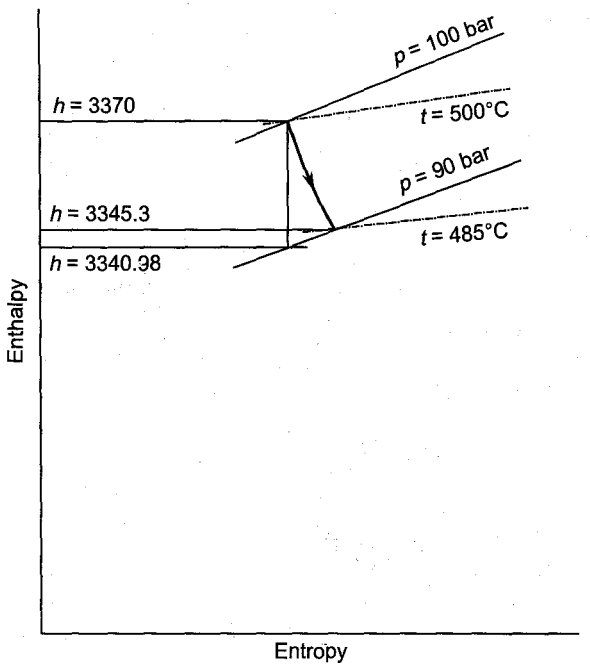

Fig. 9.37 Expansion of steam in a single-stage 50% reaction turbine (Ex. 9.1 (d))

The rotor blade height at exit is

$$h = 100 \times 0.035 \times 100/57.17 \times \pi \times 1$$

$$h = 1.948 \text{ cm} \qquad (Ans.)$$

This height is comparatively larger on account of the lower value of the axial velocity.

9.2 The data for an axial turbine stage is given below:

air angle at nozzle exit $\alpha_{2m} = 75°$
air angle at rotor entry $\beta_{2m} = 45°$
air angle at rotor exit $\beta_{3m} = 76°$
hub diameter $d_h = 450$ mm
tip diameter $d_t = 750$ mm
rotor speed $N = 6000$ rpm

Assuming radial equilibrium and free vortex flow in the stage determine for the hub, mean and tip sections:

(a) the relative and absolute air angles;
(b) degree of reaction,
(c) blade-to-gas speed ratio,
(d) specific work, and

(e) the loading coefficient.

Comment on the results.

Solution:

Refer to Fig. 9.1 and take $c_y = c_\theta$.

$$r_m = \frac{1}{2}(r_h + r_t) = 0.5\ (22.5 + 37.5) = 30 \text{ cm} = 0.3 \text{ m}$$

$$u_h = \pi d_h N = \pi \times 0.45 \times 6000/60 = 141.37 \text{ m/s}$$

$$u_m = \pi d_m N = \pi \times 0.60 \times 100 = 188.50 \text{ m/s}$$

$$u_t = \pi d_t N = \pi \times 0.75 \times 100 = 235.62 \text{ m/s}$$

Mean section

$$c_{2m} = \frac{\cos \beta_{2m}}{\sin (\alpha_{2m} - \beta_{2m})}\ u_m \qquad \text{[Eq. (9.3)]}$$

$$c_{2m} = 188.50 \cos 45/\sin (75 - 45) = 266.5 \text{ m/s}$$

$$c_{x2m} = c_{2m} \cos \alpha_{2m} = 266.5 \cos 75 = 69.0 \text{ m/s}$$

$$c_{\theta 2m} = c_{2m} \sin \alpha_{2m} = 266.5 \sin 75 = 257.42 \text{ m/s}$$

$$c_{\theta 3m} = c_{x3m} \tan \beta_{3m} - u_m$$

$$c_{\theta 3m} = 69 \tan 76 - 188.5 = 88.24 \text{ m/s}$$

$$C_2 = r_m\, c_{\theta 2m} = 0.3 \times 257.42 = 77.23 \text{ m}^2/\text{s}$$

$$C_3 = r_m\, c_{\theta 3m} = 0.3 \times 88.24 = 26.47 \text{ m}^2/\text{s}$$

For free vortex and radial equilibrium and constant axial velocity across the stage, the axial velocity is constant throughout.

$$c_x = 69.0 \text{ m/s}$$

(a) Air angles at the mean section are already given.

(b)
$$R_m = \frac{c_x}{2u_m}\ (\tan \beta_{3m} - \tan \beta_{2m}) \times 100$$

$$R_m = \frac{69.0}{2 \times 188.5}\ (\tan 76 - \tan 45) \times 100$$

$$R_m = 55.1\ \% \qquad (Ans.)$$

(c)
$$\sigma_m = u_m/c_{2m} = 188.5/266.5 = 0.707 \quad (Ans.)$$

(d)
$$w = \omega\,(C_2 + C_3) = 200\ \pi\,(77.23 + 26.47) \times 10^{-3}$$

$$w = 65.157 \text{ kJ/kg} \quad (Ans.)$$

(e)
$$\psi_m = \frac{w}{u_m^2} = \frac{65157}{188.5^2} = 1.833 \qquad (Ans.)$$

Hub section

(a) $\tan \alpha_{2h} = \dfrac{C_2}{r_h c_x} = 77.23/0.225 \times 69 = 4.975$

$\alpha_{2h} = 78.63°$ (*Ans.*)

$\tan \beta_{2h} = \tan \alpha_{2h} - u_h/c_x = 4.975 - \dfrac{141.37}{69} = 2.926$

$\beta_{2h} = 71.13°$ (*Ans.*)

$\tan \beta_{3h} = \dfrac{C_3}{r_h c_x} + \dfrac{u_h}{c_x} = \dfrac{26.47}{0.225 \times 69} + \dfrac{141.3}{69} = 3.754$

$\beta_{3h} = 75.08°$ (*Ans.*)

(b) $R_h = \dfrac{c_x}{2u_h} (\tan \beta_{3h} - \tan \beta_{2h})$

$R_h = \dfrac{69.0}{2 \times 141.37} (3.754 - 2.926) \times 100$

$R_h = 20.2\%$ (*Ans.*)

(c) $c_{2h} = c_x/\cos \alpha_{2h} = 69.0/\cos 78.63 = 350.25$ m/s

$\sigma_h = u_h/c_{2h} = 141.37/350.25 = 0.404$ (*Ans.*)

(d) $w = uc_x (\tan \beta_{2h} + \tan \beta_{3h})$

$w = 141.37 \times 69.0 (3.754 + 2.926) \times 10^{-3}$

$w = 65.160$ kJ/kg

This is the same as at the mean section.

(e) $\psi_h = w/u_h^2 = 65160/141.37^2$

$\psi_h = 3.260$ (*Ans.*)

Tip section

(a) $\tan \alpha_{2t} = \dfrac{C_2}{r_t c_x} = \dfrac{77.23}{0.375 \times 69.0} = 2.985$

$\alpha_{2t} = 71.48°$ (*Ans.*)

$\tan \beta_{2t} = \tan \alpha_{2t} - u_t/c_x = 2.985 - \dfrac{235.62}{69}$

$\tan \beta_{2t} = -0.429$

$\beta_{2t} = -23.26°$ (*Ans.*)

$\tan \beta_{3t} = \dfrac{C_3}{r_t c_x} + \dfrac{u_t}{c_x} = \dfrac{26.47}{0.375 \times 69.0} + \dfrac{235.62}{69} = 4.438$

$\beta_{3t} = 77.3°$ (*Ans.*)

(b) $$R_t = \frac{c_x}{2u_t} (\tan \beta_{3t} - \tan \beta_{2t})$$

$$R_t = \frac{69.0}{2 \times 235.62} (4.438 + 0.429) \times 100$$

$$R_t = 71.26\% \quad (Ans.)$$

(c) $$c_{2t} = c_x / \cos \alpha_{2t} = 69.0/\cos 71.48 = 217.25 \text{ m/s}$$

$$\sigma_t = u_t / c_{2t} = 235.62/217.25 = 1.085 \quad (Ans.)$$

(d) $$w = u_t c_x (\tan \beta_{2t} + \tan \beta_{3t})$$

$$w = 235.62 \times 69.0 (4.438 - 0.429) \times 10^{-3}$$

$$w = 65.17 \text{ kJ/kg (verified)}$$

(e) $$\psi_t = \frac{w}{u_t^2} = \frac{65177.4}{235.62^2} = 1.174 \quad (Ans.)$$

Various values calculated are presented in the following table for comparison:

Free vortex (positive hub reaction)

Section	α_2	β_2	β_3	R	σ	ψ
Hub	78.63	71.13	75.08	20.2	0.404	3.260
Mean	75.0	45.0	76.0	55.1	0.707	1.833
Tip	71.48	−23.26	77.3	71.26	1.085	1.174

It is observed from the table that the relative air angles at rotor entry decrease significantly towards the tip thus increasing the degree of reaction. The variations in α_2 and β_3 are not significant. The blade-to-gas speed ratio increases towards the tip and the loading coefficient decreases.

9.3 Repeat Example 9.2 for constant nozzle angle; other conditions at the mean section are

$$\alpha_{2m} = \beta_{3m} = 75°, \ \beta_{2m} = \alpha_{3m} = 0, \ R_m = 0.50.$$

Assume axial exit from the stage at all sections.

Solution:

Mean section (Fig. 9.14)

At $R_m = 0.50$, $c_{\theta 2m} = u_m = 188.5$ m/s

$$c_{xm} = u_m \cot \alpha_{2m} = 188.5/3.732 = 50.51 \text{ m/s}$$

$$c_{2m} = u_m / \sin \alpha_{2m} = 188.5/\sin 75 = 195.13 \text{ m/s}$$

$$\sigma_m = u_m / c_{2m} = 188.5/195.13 = 0.966 \quad (Ans.)$$

Specific work

$$w_m = u_m\, c_{\theta 2m} = u_m^2$$
$$w_m = 188.5^2 \times 10^{-3} \text{ kJ/kg}$$
$$w_m = 35.53 \text{ kJ/kg} \qquad (Ans.)$$
$$\psi_m = w_m/u_m^2 = 1 \qquad (Ans.)$$

Hub section

$$\sin^2 \alpha_2 = \sin^2 75 = 0.933$$

$$\frac{c_{x2h}}{c_{x2m}} = \frac{c_{\theta 2h}}{c_{\theta 2m}} = \frac{c_{2h}}{c_{2m}} = \left(\frac{r_m}{r_h}\right)^{0.933} = \left(\frac{0.3}{0.225}\right)^{0.933} = 1.308$$

$$c_{x2h} = 1.308 \times 50.51 = 66.067 \text{ m/s}$$
$$c_{\theta 2h} = 1.308 \times 188.5 = 246.56 \text{ m/s}$$
$$c_{2h} = 1.308 \times 195.13 = 255.23 \text{ m/s}$$
$$\sigma_h = u_h/c_{2h} = 141.37/255.23 = 0.554 \qquad (Ans.)$$

$$\tan \beta_{2h} = \frac{246.56 - 141.37}{66.067} = 1.592$$
$$\beta_{2h} = 57.87° \qquad (Ans.)$$
$$\tan \beta_{3h} = 141.37/66.067 = 2.14$$
$$\beta_{3h} = 65° \qquad (Ans.)$$

$$R_h = \frac{c_{xh}}{2u_h} (\tan \beta_{3h} - \tan \beta_{2h})$$

$$R_h = \frac{66.067}{2 \times 141.37} (2.14 - 1.592) \times 100$$
$$R_h = 12.8\% \qquad (Ans.)$$
$$w_h = u_h\, c_{\theta 2h} = 141.37 \times 246.56 \times 10^{-3}$$
$$w_h = 34.85 \text{ kJ/kg} \qquad (Ans.)$$
$$\psi_h = c_{\theta 2h}/u_h = 246.56/141.37$$
$$\psi_h = 1.744 \qquad (Ans.)$$

Tip section

$$\frac{c_{x2t}}{c_{x2m}} = \frac{c_{\theta 2t}}{c_{\theta 2m}} = \frac{c_{2t}}{c_{2m}} = \left(\frac{r_m}{r_t}\right)^{0.933} = \left(\frac{0.300}{0.375}\right)^{0.933} = 0.812$$

$$c_{x2t} = 0.812 \times 50.51 = 41.01 \text{ m/s}$$
$$c_{\theta 2t} = 0.812 \times 188.5 = 153.06 \text{ m/s}$$
$$c_{2t} = 0.812 \times 195.13 = 158.44 \text{ m/s}$$

$$\sigma_t = u_t/c_{2t} = 235.62/158.44 = 1.487 \qquad (Ans.)$$

$$\tan \beta_{2t} = \frac{153.06 - 235.62}{41.01} = -2.013$$

$$\beta_{2t} = -63.58° \qquad (Ans.)$$

$$\tan \beta_{3t} = \frac{235.62}{41.01} = 5.745$$

$$\beta_{3t} = 80.13° \qquad (Ans.)$$

$$R_t = \frac{41.01}{2 \times 235.62} (5.745 + 2.013) \times 100$$

$$R_t = 67.5\% \qquad (Ans.)$$

$$w_t = u_t\, c_{\theta 2t} = 235.62 \times 153.06 \times 10^{-3}$$

$$w_t = 36.06 \text{ kJ/kg} \qquad (Ans.)$$

$$\psi_t = c_{\theta 2t}/u_t = 153.06/235.62$$

$$\psi_t = 0.649 \quad (Ans.)$$

The results are summarized in the following table:

Constant nozzle angle (axial exit)

Section	α_2	β_2	β_3	R	σ	w	ψ
Hub	75	57.87	65	12.8	0.554	34.85	1.744
Mean	75	0	75	50	0.966	35.53	1.00
Tip	75	– 63.58	80.13	67.5	1.487	36.06	0.649

9.4 An axial turbine stage has the following data:

Nozzle exit air angle $\alpha_2 = 70°$

Rotor blade air angles $\beta_2 = \beta_3 = 54°$

Mean diameter of the blade rings = 1 m

Speed = 3000 rpm

Aspect ratio of the blade rows = 1.0

(a) Compute the total-to-total and total-to-satitic efficiencies.

(b) Recalculate the above values for aspect ratios of 2 and 3 and comment on the results.

Solution:

$$u = \pi\, dN/60 = \pi \times 1 \times 50 = 157.08 \text{ m/s}$$

Since $\beta_2 = \beta_3$ it is an impulse turbine stage. Therefore,

$$\sigma_{opt} = \frac{u}{c_2} = \frac{1}{2} \sin \alpha_2 = \frac{1}{2} \sin 70 = 0.47$$

$$c_2 = 157.08/0.47 = 334.2 \text{ m/s}$$

$$c_x = c_2 \cos \alpha_2 = 334.2 \cos 70 = 114.3 \text{ m/s}$$

$$\phi = c_x/u = 0.728$$

At optimum blade-to-gas speed ratio, the exit from the stage is axial, i.e.

$$\alpha_3 = 0$$

Assuming $\alpha_1 = \alpha_3 = 0$, the deflection through the nozzle blade rows is

$$\varepsilon_N = 70°$$

The rotor deflection is $\varepsilon_R = \beta_2 + \beta_3 = 54 + 54$

$$\varepsilon_R = 108°$$

The profile and total cascade losses can now be calculated from Eqs. (8.48) and 8.49)

(a) For nozzle blades ($h/b \approx 1$),

$$\xi_p = 0.025 \left[1 + \left(\frac{70}{90}\right)^2\right] = 0.04$$

$$\xi_N = \left(1 + \frac{3.2}{h/b}\right) \xi_p$$

$$\xi_N = (1 + 3.2) \times 0.04$$

$$\xi_N = 0.168$$

Similarly, for rotor blades,

$$\xi_p = 0.025 \left[1 + \left(\frac{108}{90}\right)^2\right] = 0.061$$

$$\xi_R = (1 + 3.2) \times 0.061$$

$$\xi_R = 0.256$$

From Eq. (9.92*c*)

$$\eta_{tt} = \left[1 + \frac{1}{2}\phi^2 \frac{\xi_R \sec^2 \beta_3 + \frac{T_3}{T_2} \xi_N \sec^2 \alpha_2}{\phi (\tan \alpha_2 + \tan \beta_3) - 1}\right]^{-1}$$

Assuming $T_3 \approx T_2$ which is valid in an impulse stage to a greater extent than in a reaction stage,

$$\eta_{tt} = \left[1 + 0.5 \times 0.728^2 \frac{0.256 \sec^2 54 + 0.168 \sec^2 70}{0.728 (\tan 70 + \tan 54) - 1}\right]^{-1}$$

$$\eta_{tt} = 0.782 \qquad (Ans.)$$

From Eq. (9.95c), for $T_3 \approx T_2$,

$$\eta_{ts} = \left[1 + 0.5\,\phi^2 \frac{\xi_R \sec^2 \beta_2 + \xi_N \sec^2 \alpha_2 + \sec^2 \alpha_3}{\phi\,(\tan \alpha_2 + \tan \beta_3) - 1}\right]^{-1}$$

$$\eta_{ts} = \left[1 + 0.5 \times 0.728^2 \frac{0.256 \sec^2 54 + 0.168 \sec^2 70 + \sec^2 0}{0.728\,(\tan 70 + \tan 54) - 1}\right]^{-1}$$

$$\eta_{ts} = 0.711 \qquad (Ans.)$$

(b) For aspect ratio $\approx h/b \approx 2$, the cascade losses are lower and have to be recalculated. The profile loss is assumed constant at all values of the aspect ratio.

$$\xi_N = \left(1 + \frac{3.2}{2}\right) \times 0.04 = 2.6 \times 0.04 = 0.104$$

$$\xi_R = \left(1 + \frac{3.2}{2}\right) \times 0.061 = 2.6 \times 0.061 = 0.158$$

$$\eta_{tt} = \left[1 + 0.728^2 \times 0.5 \frac{0.158 \sec^2 54 + 0.104 \sec^2 70}{0.728\,(\tan 70 + \tan 54) - 1}\right]^{-1}$$

$$\eta_{tt} = [1 + 0.1325\ (0.4573 + 0.889)]^{-1}$$

$$\eta_{tt} = 0.853 \qquad (Ans.)$$

$$\eta_{ts} = [1 + 0.1325\ (0.4573 + 0.889 + 1)]^{-1}$$

$$\eta_{ts} = 0.763 \qquad (Ans.)$$

At $h/b = 3$,

$$\xi_N = \left(1 + \frac{3.2}{3}\right) \times 0.04 = 2.067 \times .04 = 0.0827$$

$$\xi_R = \left(1 + \frac{3.2}{3}\right) \times 0.061 = 2.067 \times 0.061 = 0.1261$$

$$\eta_{tt} = [1 + 0.1325\ (0.1261 \sec^2 54 + 0.0827 \sec^2 70)]^{-1}$$

$$\eta_{tt} = 0.875 \qquad (Ans.)$$

$$\eta_{ts} = [1 + 0.1325\ (0.1261 \sec^2 54 + 0.0827 \sec^2 70 + 1)]^{-1}$$

$$\eta_{ts} = 0.7816 \qquad (Ans.)$$

Impulse stage with maximum utilization factor

Aspect ratio	η_{tt}	η_{ts}
1.0	78.20	71.10
2.0	85.30	76.30
3.0	87.50	78.46

9.5 A fifty per cent reaction stage of a gas turbine has the following data:

Entry pressure and temperature, $p_1 = 10$ bar, $T_1 = 1500$ K

Speed = 12,000 rpm,

Mass flow rate of the gas = 70 kg/s,

Stage pressure ratio and efficiency, $p_r = 2.0$, $\eta_{st} = 87\%$

Fixed and moving blade exit air angles = 60°,

Assume optimium blade to gas speed ratio. Take $\gamma = 1.4$, $c_p = 1.005$ kJ/kgK for the gas.

Determine

(a) Flow coefficent **(b)** mean diameter of the stage

(c) power developed **(d)** pressure ratio across the fixed and rotor blade rings

(e) hub-tip ratio of the rotor and **(f)** degrees of reaction at the hub and tip.

Solution:

Refer to Figures 9.8, 9.12, 9.13 and 9.14.

$$h_1 - h_3 = c_p\,(T_1 - T_{3ss})\,\eta_{st} = c_p\,T_1\left(1 - p_r^{-\frac{\gamma-1}{\gamma}}\right)\eta_{st}$$

$$h_1 - h_3 = 1.005 \times 1500\,(1 - 2^{-.286}) \times 0.87$$

$$h_1 - h_3 = 235.84 \text{ kJ/kg}$$

$$T_1 - T_3 = 234.66\text{K}$$

$$h_1 - h_2 = h_2 - h_3 = \frac{1}{2}\,(h_1 - h_3) = 117.92 \text{ kJ/kg}$$

Ignoring kinetic energy at the inlet of the fixed row of blades,

$$\frac{1}{2}\,c_2^2 = h_1 - h_2$$

$$c_2 = \sqrt{2\,(h - h_2)} = (2 \times 117920)^{1/2} = 485.63 \text{ m/s}$$

$$\frac{u}{c_2} = \sigma_{\text{opt}} = \sin\,\alpha_2 = \sin 60 = 0.866$$

$$u = 0.866 \times 485.63 = 420.56 \text{ m/s}$$

(a) $c_x = c_2 \cos 60 = 0.5\ c_2 = 0.5 \times 485.63 = 242.81$ m/s

Therefore, $\phi = \dfrac{c_x}{u} = \dfrac{242.81}{420.56} = 0.5773$ (*Ans.*)

(b) $\dfrac{\pi dN}{60} = u$

$$d = 60 \times 420.56/\pi \times 12000$$

$$d = 0.6693 \text{ m } (66.93 \text{ cm}) \qquad (Ans.)$$

(c) Power, $P = \dot{m}\, c_p \cdot (T_1 - T_3) = \dot{m}\, \Delta h$

$$P = \frac{70 \times 235.84}{1000} = 16.508 \text{ MW} \qquad (Ans.)$$

(d) $h_1 - h_{3ss} = 235.84/0.87 = 271.08$ kJ/kg

$$T_1 - T_{3ss} = \frac{271.08}{1.005} = 269.73 \text{ K}$$

Stage loss = 269.73 – 234.66 = 35.07 K

Since the blade rows in both the stator and rotor are identical the losses can also be assumed as same. Therefore,

$$T_1 - T_{2s} = T_1 - T_2 + \frac{35.07}{2} = 117.33 + 17.5 = 134.83 \text{ K};$$

$$T_1 - T_{2s} = T_1 (1 - p_r^{-.286}) = 134.83$$

$$p_{r\,(\text{stator})} = 1.387 \qquad (Ans.)$$

$$p_{r\,(\text{rotor})} = \frac{p_2}{p_3} = \frac{p_1/p_3}{p_1/p_2} = \frac{2.0}{1.387} = 1.442 \qquad (Ans.)$$

(e) For the exit of the stator or entry of the rotor

$$\rho_2 = p_2/RT_2$$

$$p_2 = \frac{10}{1.387} = 7.2 \text{ bar}$$

$$T_2 = 1500 - 117.33 = 1382.67 \text{ K}$$

$$\rho_2 = \frac{7.2 \times 10^5}{287 \times 1382.67} = 1.81 \text{ kg/m}^3$$

$$\dot{m} = \rho_2\, c_{x2}\, (\pi d l_2)$$

Assuming $c_{x2} = c_{x3} = c_x = 242.81$ m/s,

Blade height, $l_2 = \dot{m}/\rho_2\, c_x\, \pi d$

$$l_2 = 70 \times 100/1.81 \times 242.81\ \pi \times 0.6693$$

$$l_2 = 7.57 \text{ cm}$$

At the rotor exit,

$$\rho_3 = p_3/RT_3$$

$$\rho_3 = p_2/1.442 = 7.2/1.442 = 4.993 \simeq 5.0 \text{ bar}$$

$$T_3 = 1500 - 234.66 = 1265.34 \text{ K}$$

$$\rho_3 = 5 \times 10^5/287 \times 1265.34 = 1.376 \text{ kg/m}^3$$

Therefore, blade height

$$l_3 = \dot{m}/\rho_3\, c_x\, \pi d$$

$$l_3 = 70 \times 100/1.376 \times 242.81 \ \pi \times 0.6693$$

$$l_3 = 9.964 \text{ cm}$$

Therefore, the average height of the rotor blade,

$$l = \frac{l_2 + l_3}{2} = 8.762 \text{ cm}$$

The mean radius of the rotor blade ring

$$r_m = \frac{1}{2} d = \frac{1}{2} \times 66.93 = 33.46 \text{ cm}$$

Therefore, hub and tip radii are

$$r_h = r_m - \frac{l}{2} = 33.46 - \frac{8.762}{2} = 29.08 \text{ cm}$$

$$r_t = r_m + \frac{l}{2} = 33.46 + \frac{8.762}{2} = 37.841 \text{ cm}$$

This gives the hub-tip ratio of the stage as

$$\frac{r_h}{r_t} = \frac{29.08}{37.841} = 0.768 \qquad (Ans.)$$

(f) The degree of reaction along the blade height is given by Eq. 9.123,

$$R = 1 - (1 - R_h) \frac{r_h^2}{r^2}$$

Here $R_m = 0.5$ at $r_m = 33.46$ cm, therefore,

$$0.5 = 1 - (1 - R_h) \left(\frac{29.08}{33.46}\right)^2$$

$$R_h = 0.336 \ (33.6\%) \qquad (Ans.)$$

For the tip section,

$$R_t = 1 - (1 - R_h) \frac{r_h^2}{r_t^2}$$

$$R_t = (1 - .336) \ (.768)^2$$

$$R_t = 0.6078 \ (60.78\%) \qquad (Ans.)$$

Questions and Problems

9.1 Draw velocity triangles at the entry and exit for the following stages for maximum utilization factor:

(a) single-stage impulse,

(b) three-stage velocity-compounded impulse and

(c) fifty per cent reaction stage,

and show that in the absence of cascade losses the values of maximum utilization factor and work are

$$\varepsilon_{max} = \sin^2 \alpha_2$$

$$w_I = 2u^2 \text{ (single-stage impulse)}$$

$$w_{III} = 18\ u^2 \text{ (three-stage impulse)}$$

$$\left.\begin{aligned} \varepsilon_{max} &= \frac{2\sin^2 \alpha_2}{1+\sin^2 \alpha_2} \\ w &= u^2 \end{aligned}\right\} 50\% \text{ reaction}$$

9.2 (a) Why is it advantageous to have some velocity stages in the beginning of a large steam turbine? Why are more than two velocity stages not employed?

(b) What are the advantages and disadvantages of employing reaction stages from beginning to end?

9.3 Derive the following relations:

(a) For constant axial velocity through the stage,

$$\tan \alpha_2 + \tan \alpha_3 = \tan \beta_2 + \tan \beta_3$$

(b) For maximum utilization factor,

$$\sigma_{opt} = \frac{1}{2} \sin \alpha_2 \text{ (single-stage impulse)}$$

$$\sigma_{opt} = \frac{1}{2n} \sin \alpha_2 \text{ (n-stage velocity compounded)}$$

$$\sigma_{opt} = \sin \alpha_2 \text{ (50\% reaction)}$$

9.4 How is the degree of reaction of an axial turbine stage defined? Prove that:

(a) $R = \frac{1}{2}\ \phi\ (\tan \beta_3 - \tan \beta_2)$

(b) $R = 1 + \frac{1}{2}\ \phi\ (\tan \alpha_3 - \tan \alpha_2)$

(c) $R = 1 - \sigma_s^2/\sigma^2$

(d) $\psi = 2\ (1 - R)$ for axial exit

State the assumptions used.

9.5 (a) How are the loss coefficients for stationary and moving rows of blades in a turbine stage defined?

(b) How would you predict the cascade losses in a stage from its velocity triangles?

(c) Prove that the total-to-total and total-to-static efficiencies can be predicted by the following expressions:

$$\eta_{tt} = \left[1 + \frac{1}{2}\phi^2 \frac{\xi_R \sec^2 \beta_3 + \frac{T_3}{T_2}\xi_N \sec^2 \alpha_2}{\phi(\tan \alpha_2 + \tan \beta_3) - 1}\right]^{-1}$$

$$\eta_{ts} = \left[1 + \frac{1}{2}\phi^2 \frac{\xi_R \sec^2 \beta_3 + \frac{T_3}{T_2}\xi_N \sec^2 \alpha_2 + \sec^2 \alpha_3}{\phi(\tan \alpha_2 + \tan \beta_3) - 1}\right]^{-1}$$

9.6 (a) Derive the following equation for flow in the annulus of an axial flow turbomachine for radial equilibrium conditions:

$$\frac{1}{r^2}\frac{d}{dr^2}(rc_\theta)^2 + \frac{d}{dr}(c_x)^2 = 0$$

State the assumptions used

(b) Using this equation prove that the distribution of absolute velocity in the radial direction is given by

$$c/c_m = \exp \int_r^{r_m} \sin^2 \alpha \frac{dr}{r}$$

(c) For constant nozzle angle (α) show that

$$\frac{c}{c_m} = \frac{c_\theta}{c_{\theta m}} = \frac{c_x}{c_{xm}} = \left(\frac{r_m}{r}\right)^{\sin^2 \alpha}$$

9.7 What is free vortex design of a blade row? Prove for such a stage:

(a) Specific work = constant with radius

(b) $R = 1 - (1 - R_h)\left(\frac{r_h}{r}\right)^2$

9.8 What is a constant specific mass-flow stage? Prove that the density distribution in the radial direction in such a stage is given by

$$\rho = \left[\rho_m^{\gamma+1} + \frac{\gamma+1}{\gamma R}\frac{K_1^2}{K_2}\int_{r_m}^{r} \tan^2 \alpha \frac{dr}{r}\right]^{\frac{1}{\gamma+1}}$$

9.9 What is an actuator disc? How is this concept used to predict the axial velocity distribution in the actuator disc flow region? How does it differ from radial equilibrium theory?

9.10 (a) Explain the flow phenomena which differentiate supersonic and subsonic turbine stages. How are supersonic stages, compounded?

(b) Why is supersonic flow in a turbine stage avoided?

(c) What are the main advantages and disadvantages of supersonic stages compared to the subsonic stages?

9.11 (a) Why is partial admission of working gas/steam employed in some applications?

(b) Give five applications of partial admission turbines.

(c) Describe briefly the various losses which occur due to partial admission in axial turbine stages.

9.12 Repeat Ex. 9.2 if the turbine stage has the following air angles at the hub:

$$\alpha_{2h} = 70°,\ \beta_{2h} = \beta_{3h} = 54°$$

Answers are given in the following table.

Free vortex (zero hub reaction)

Section	α_2	β_2	β_3	R	σ	ψ
Hub	70	54.0	54.0	0	0.469	2.0
Mean	64.11	13.06	61.32	43.65	0.798	1.127
Tip	58.76	– 32.06	66.36	63.94	1.185	0.722

9.13 An axial turbine with constant nozzle air angle (75°) and zero reaction at the hub runs at 6000 rpm. Its hub and tip diameters are 45 and 75 cm respectively.

All sections are designed for maximum utilization factor. Assuming radial equilibrium conditions, determine for the hub, mean and tip sections:

(a) relative and absolute air angles,

(b) blade-to-gas speed ratio,

(c) degree of reaction,

(d) specific work, and

(e) the loading coefficient.

Constant nozzle angle (zero hub reaction)

Section	α_2	β_2	β_3	σ	R	w kJ/kg	ψ
Hub	75	61.81	61.81	0.483	0	39.97	2
Mean	75	25.6	72.89	0.842	42.6	40.77	1.147
Tip	75	– 51.81	78.70	1.295	62.67	41.41	0.746

9.14 Compute the total-to-total and total-to-static efficiencies of a fifty per cent reaction turbine stage at aspect ratios of 1,2 and 3 from the following data:

Nozzle blade air angle $\alpha_2 = 70°$

Mean diameter of the stage $d = 100$ cm

Speed $N = 3000$ rpm

Assume conditions corresponding to the maximum utilization factor.

Fifty per cent reaction stage with maximum utilization factor

Aspect ratio	η_{tt}	η_{ts}
1.0	84.06	79.6
2.0	89.50	84.50
3.0	91.46	86.26

9.15 Compute the total-to-total and total-to-static efficiencies for the axial turbine in Ex. 9.5. Take the aspect ratio of the blade rings as 2.0.

(*Ans.*) $\eta_{tt} = 89.29$ %, $\eta_{ts} = 77.73$ %

9.16 (a) What is relative stagnation enthalpy in an axial turbine stage? Explain briefly.

(b) Prove

$$h_{\text{orel}} = h_2 + \frac{1}{2} w_2^2 = h_3 + \frac{1}{2} w_3^2 = \text{constant}$$

9.17 Following data refer to a two-stage velocity compounded impulse turbine operating on hot air:

Flow rate = 1.0 kg/s

Mean blade diameter = 75 cm

Rotational speed = 3600 rpm

Nozzle blade angle = 80 degrees from axial direction,

Deviation = 5°

Assuming optimum utilization factor and constant axial velocity, calculate

(a) blade to gas speed ratio,

(b) utilization factor,

(c) rotor blade air angles at entry and exit in the two stages,

(d) flow coefficient,

(e) the loading coefficients in the two stages

(f) power developed separately in the two stages

(*Ans.*) (a) $\sigma = 0.241$ (b) $\varepsilon = 0.933$,
(c) $\beta_2 = \beta_3 = 70.34°$ (d) $\phi_1 = 1.07$
$\beta'_2 = \beta'_3 = 43°$
(e) $\psi_1 = 2.0$, $\psi_2 = 6.0$
(f) $P_I = 119.9$ kW, $P_{II} = 39.97$ kW

9.18 The high pressure stage of an axial turbine has the following data:
degree of reaction = 50 per cent,
exit air angle of the fixed blade ring = 70°
mean diameter of the stage = 1m
rotational speed = 3000 rpm
power developed = 5 MW

Determine

(a) blade to gas speed ratio,
(b) Utilization factor (c) flow coefficient,
(c) inlet and exit air angles for the rotor, and
(d) mass flow rate of the gas.
Assume maximum utilization factor.

(*Ans.*) (a) $\sigma = 0.9396$ (b) $\varepsilon = 0.9377$
(c) $\phi = 0.3639$ (d) $\beta_2 = 0$, $\beta_3 = 70°$,
(e) $\dot{m} = 202.64$ kg/s.

Chapter 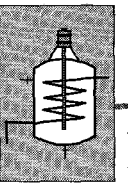 10

High Temperature (Cooled) Turbine Stages

An improvement in the Carnot's efficiency ($\eta = 1 - T_2/T_1$) of a heat engine with an increase in the temperature (T_1) at which heat is received is well known. The thermal efficiency of gas turbine plants is higher at a higher temperature of the gas at the turbine entry. Methods of achieving higher temperatures at which heat is supplied in a gas turbine plant have been discussed in Sec. 3.3.

Employment of higher gas temperatures in gas turbine plants requires materials which can withstand the effects of high temperatures. Alternatively, less expensive materials (such as low-grade steels) can be employed by cooling some components of a high temperature stage in the plant. This enables the selection of the rotor blade and disc material on the basis of ease of manufacture, such as castability, machinability and weldability.

The successful development of the gas turbine engine is a result of the developments in metallurgy which provided rotor disc and blade materials capable of withstanding high tensile stresses (1400–2100 bar) at elevated temperatures.

High temperature problems from modern gas turbine standards do not seriously affect steam turbines. Maximum temperatures ($\approx$ 840 K) employed at present in modern steam turbine plants are much lower than those used in gas turbine practice. High temperature problems of steam plants occur in steam boilers. The furnace and other high temperature regions in steam boilers are water-cooled; besides this, high temperatures of the order of 1800 K occur only in a small region of the furnace near the flame front. This is immediately reduced to about 1200 K by the introduction of secondary air. The major part of the furnace may be at an average temperature of 1000 K or lower.

The highest temperatures reached intermittently in the reciprocating internal combustion engines are in the region of 3000 K. However, the cylinder jacket cooling keeps the cylinder wall temperature to a harmless value of 500 K.

The maximum gas temperature to which the blades and the rotor discs in modern high performance gas turbines are continuously exposed is around 1600 K. Thus the high temperature problems[346,381] in gas turbines are much more serious compared to steam turbines and reciprocating internal combustion engines. This is further aggravated by the small space available for cooling and the rotation of the blades at high speeds.

10.1 Effects of High Gas Temperature

The maximum temperature (T_{max}) in a gas turbine plant cycle occurs at the entry of the first stage of the turbine. The effect of maximum cycle temperature at various values of the pressure ratio on the thermal efficiency is shown in Fig. 10.1. An increase in the pressure ratio of the plant leads to a heavier plant or an engine which is a serious disadvantage in aircraft applications. Employment of high temperatures for a given pressure ratio leads to higher thermal efficiency, high thrust-to-weight ratio and lower specific fuel consumption.

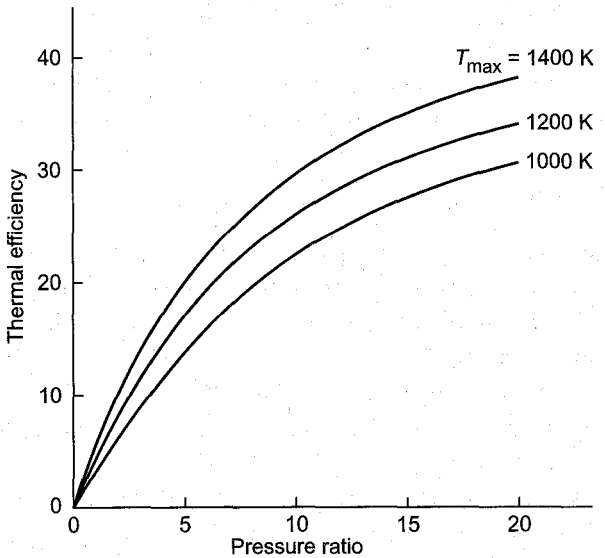

Fig. 10.1 Effect of pressure ratio and maximum temperature on the efficiency of gas turbine plants (typical curves)

Figure 10.2 shows the effect of the pressure ratio and maximum cycle temperature on the specific power output of gas turbine plants; the advantages of increasing the gas temperature are evident.

High performance supersonic turbo-jet engines require high temperatures at the turbine entry; this is only possible with air cooling of the casing,

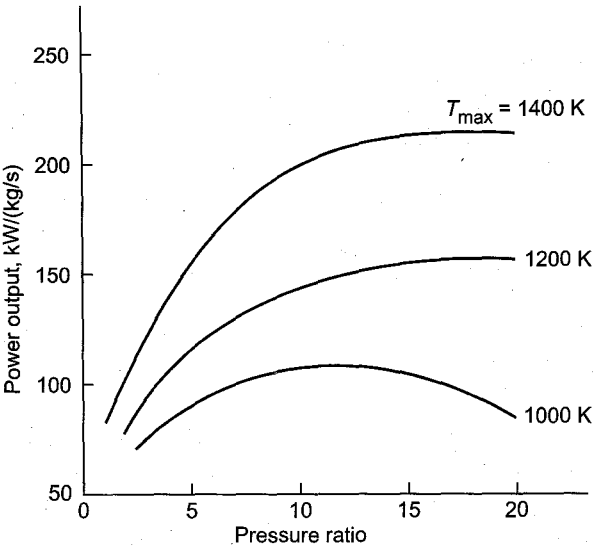

Fig. 10.2 Effect of pressure ratio and maximum temperature on the specific power output of gas turbine plants (typical curves)

nozzle and rotor blades and the rotor disc. Air cooling of these components has now become a common feature in modern turbo-jet engines.

10.2 Methods of Cooling

In order to employ high gas temperatures in gas turbine stages, it is necessary to cool the casing, nozzles, rotor blades and discs. On account of high rotational speeds and the associated stresses, cooling of the rotor blades is more critical.

Cooling of these components can be achieved either by air or liquid cooling. Liquid or water cooling, if possible, appears to be more attractive on account of the higher specific heat and possibility of evaporative cooling. However, the problems of leakage, corrosion, scale formation and choking militate against this method.

Cooling by air, besides other advantages, allows it to be discharged into the main flow without much problem. It can be tapped out from the air compressor at a suitable point. The quantity of air required for this purpose is from 1 to 3% of the main flow entering the turbine stage. Blade metal temperatures can be reduced by about 200–300 °C. By employing suitable blade materials (nickel-based alloys) now available, an average blade temperature of 800°C (1073 K) can be used. This can permit maximum gas temperatures of about 1400 K. Still higher temperatures can be employed with nickel, chromium and cobalt base alloys.

Some methods of air cooling are briefly described below.

10.2.1 Internal Cooling

Internal cooling of the blades can be achieved by passing cooling air (from the air compressor) through internal cooling passages from hub towards the blade tips. The internal passages may be circular or elliptical (Fig. 10.3a) and are distributed near the entire surface of a blade. The shapes of such blades may deviate from the optimum aerodynamic blade profile. The cooling of the blades is achieved by conduction and convection. Relatively hotter air after traversing the entire blade length in the cooling passages escapes to the main flow from the blade tips. A part of this air can be usefully utilized to blow out thick boundary layers from the suction surface of the blades.

Hollow blades can also be manufactured with a core and internal cooling passage as shown in Fig. 10.3b. Cooling air enters the leading edge region in the form of a jet and then turns towards the trailing edge. Cooling of the blade takes place due to both jet impingement (near the leading edge) and convective heat transfer.

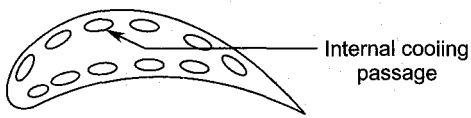

(a) Convection cooling

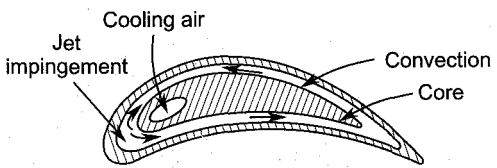

(b) Cooling by jet impingement and convection

Fig. 10.3 Internal cooling of blades

10.2.2 External Cooling

External cooling of the turbine blades is achieved in two ways. The cooling air enters the internal passages from the hub towards the tips. On its way upwards it is allowed to flow over the blade surface through a number of small orifices ($d \approx 0.5$ mm) inclined to the surface as shown in Fig. 10.4a. A series of such holes are provided at various sections of the blades along their lengths. The cooling air flowing out of these small holes forms a film

over the blade surfaces. Besides cooling the blade surface it decreases the heat transfer from the hot gases to the blade metal.

Another variation of this method is depicted in Fig. 10.4b. Here the blade surface is made of a porous wall which is equivalent to providing an infinite number of orifices as shown in Fig. 10.4a. Cooling air is forced through this porous wall which forms an envelope of a comparatively cooler boundary layer or film. This film around the blade prevents it from reaching very high temperatures. Besides this, the effusion of the coolant over the entire blade surface causes uniform cooling of the blade.

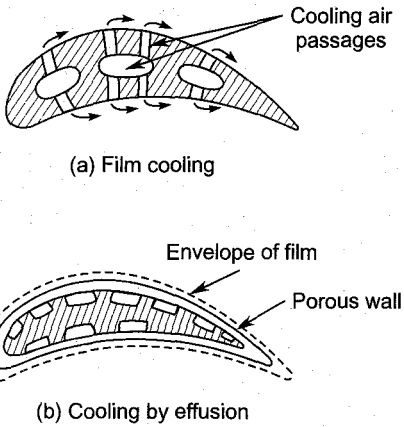

Fig. 10.4 External cooling of blades

The flow of cooling air from the internal passages to the blade surface interferes with the aerodynamics of the main flow and can lead to increased cascade losses.

10.3 High Temperature Materials

The use of high gas temperatures at the turbine entry is intimately linked with the materials[345,362] that can be used in such applications. The following properties are required in the high temperature materials employed in gas turbines:

1. high strength at the maximum possible temperature,
2. low creep rate,
3. resistance to corrosion and oxidation,
4. resistance to fatigue and
5. ease in manufacture, i.e. machinability, castability, weldability, etc.

Steel alloys[363,360] offer a number of advantages in the manufacture of gas turbine components. They generally have high percentages of nickel and chromium and can be used up to temperatures of 650°C.

Aluminium and its various alloys with their low density and workability are ideal for castings and forgings and can be used up to 260°C. Titanium and its alloys are also light and can withstand temperatures up to 550°C.

At high gas temperatures, gas turbine blades work in an atmosphere that is both corrosive and oxidizing. Therefore, for temperatures between 650°C and 950°C nickel-and chromium-based alloys are used. They have high strength and low creep combined with good ductility. The shock resistance of such alloys is also high. Cobalt alloys have high strength and resistance to oxidation up to temperatures of 1150°C.

Other alloys specially developed for gas turbine blades and discs operating at high temperatures have manganese, molybdenum, copper, columbium, silicon, tungsten, vanadium and zirconium. They are used in various proportions to obtain desired properties in the alloys.

Creep[345,349] is one of the critical factors which has to be considered while selecting the material for rotor blades in a high temperature gas turbine stage. Beyond certain temperatures (650–800°C), the blade material does not remain elastic and continues to stretch under the applied forces. If this state exists for a long time, fracture can occur. Besides this, even before the point of fracture, the elongation can exceed the radial clearance and rubbing between the blade tips and the casing may occur, leading to wreckage.

Figure 10.5 shows the development of creep in gas turbine blades. The primary, secondary and tertiary regimes of creep before fracture have been marked. Such curves for a given material at various temperatures are very useful.

10.4 Heat Exchange in a Cooled Blade

The blade temperature distribution along the blade height is a critical factor on which the thermal stresses depend. If the blade is cooled[344] by passing a coolant (air) from the hub to the tip, the blade temperature distribution depends on the variations of the temperature of the coolant from the hub to the tip.

Barnes and Fray[346] have developed expressions for the variations of the temperatures of the coolant and the blade surface along the blade height; some derivations from this are included in this section.

Figure 10.6 shows the heat exchanges between the gas and the blade, and the coolant. Properties of the blade material and its surface, the

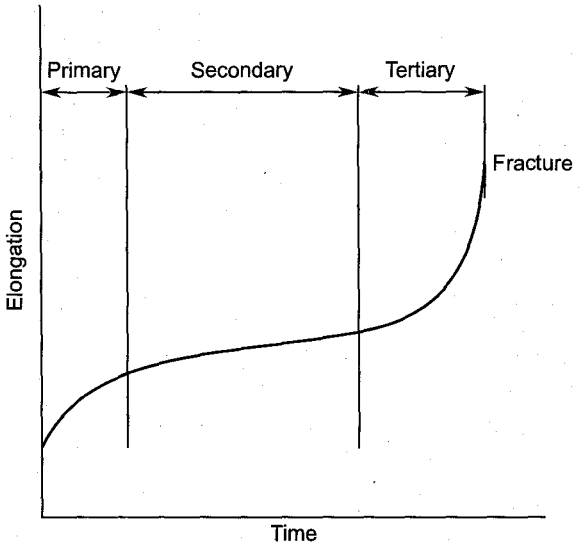

Fig. 10.5 Creep in gas turbine blades (typical curve)

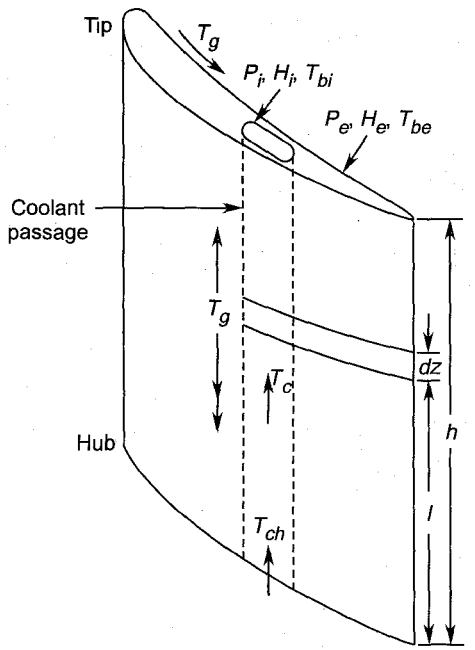

Fig. 10.6 Heat exchange in cooled blade

gas temperature (T_g) and the temperature (T_{ch}) of the coolant at the hub are known. In this, expressions for the variations of the coolant

temperature (T_c) and the internal and external blade surface temperatures (T_{bi}, T_{be}) are derived based on the following assumptions:

(a) temperature of the gas along the blade height is constant,
(b) area of cross-section of cooling passages is constant along the blade height, and
(c) heat transfer by conduction is negligible along the blade height.

The following expressions can be written for an infinitiesimal section (dz) of the blade shown in Fig. 10.6.

Heat received by the external surface of the blade from the hot gases = Heat rejected from the internal surface to the coolant

$$H_e P_e dz\,(T_g - T_{be}) = H_i P_i dz\,(T_{bi} - T_c)$$

$$T_g - T_{be} = \frac{H_i P_i}{H_e P_e}\,(T_{bi} - T_c)$$

Let $$k_1 = H_i P_i / H_e P_e \qquad (10.1)$$

Therefore, $$(T_g - T_{be}) = k_1\,(T_{bi} - T_c)$$

$$T_g - T_{be} = k_1\,[(T_g - T_c) - (T_g - T_{bi})]$$

Let $$t_{be} = T_g - T_{be} \qquad (10.2)$$

$$t_c = T_g - T_c \qquad (10.3)$$

$$t_{bi} = T_g - T_{bi} \qquad (10.4)$$

Therefore, $$t_{be} = k_1\,t_c - k_1 t_{bi} \qquad (10.5)$$

Heat transfer from the blade external surface = Heat transfer between the external and internal surfaces

$$H_e P_e\,(T_g - T_{be}) = K\,(T_{be} - T_{bi}) \qquad (10.6)$$

Let $$k_2 = K / H_e P_e$$

Therefore, $$T_g - T_{be} = k_2\,(T_{be} - T_{bi})$$

$$T_g - T_{be} = k_2\,(T_g - T_{bi}) - k_2\,(T_g - T_{be})$$

$$t_{be} = k_2 t_{bi} - k_2 t_{be}$$

$$t_{be} = \frac{k_2}{1 + k_2}\,t_{bi} \qquad (10.7)$$

Equations (10.5) and (10.7) give

$$\frac{k_2}{1 + k_2}\,t_{bi} = k_1 t_c - k_1 t_{bi}$$

$$t_{bi} = \frac{k_1 + k_1 k_2}{k_1 + k_1 k_2 + k_2}\,t_c \qquad (10.8)$$

Heat received by the coolant = Heat transfer between the internal surface and the coolant

$$\dot{m}_c\, c_p\, dT_c = H_i P_i\, dz\, (T_{bi} - T_c)$$

$$dT_c = \frac{H_i P_i}{\dot{m}_c c_p}\, (T_{bi} - T_c)\, dz$$

Let $$k_3 = H_i P_i / \dot{m}_c c_p \tag{10.9}$$

Therefore, $$dT_c = k_3\, (T_{bi} - T_c)\, dz$$

$$d\,(T_g - T_c) = [k_3(T_g - T_c) - k_3\,(T_g - T_{bi})]\, dz$$

$$-\, dt_c = (k_3 t_c - k_3 t_{bi})\, dz \tag{9.10}$$

10.4.1 Variation of Coolant Temperature

Substituting from Eq. (10.8) into Eq. (10.10),

$$-\, dt_c = k_3 \left[1 - \frac{k_1 + k_1 k_2}{k_1 + k_1 k_2 + k_2}\right] t_c\, dz$$

$$\frac{dt_c}{t_c} = -\, \frac{k_2 k_3}{k_1 + k_1 k_2 + k_2}\, dz \tag{10.11}$$

The integration is done between the following limits:

$$z = 0 \text{ to } z = z$$

$$t_c = t_{ch} \text{ to } t_c = t_c$$

$$\int_{t_{ch}}^{t_c} \frac{dt_c}{t_c} = -\int_0^z \frac{k_2 k_3}{k_1 + k_1 k_2 + k_2}\, dz \tag{10.12}$$

If the constants k_1, k_2 and k_3 are assumed invariant with z, i.e. constant along the blade height, then

$$\ln\left(\frac{t_c}{t_{ch}}\right) = k_4\, z$$

$$\frac{t_c}{t_{ch}} = \frac{T_g - T_c}{T_g - T_{ch}} = e^{-k_4 z} \tag{10.13}$$

$$k_4 = \frac{k_2 k_3}{k_1 + k_1 k_2 + k_2} \tag{10.14}$$

If the temperatures of the external and internal blade surfaces are the same ($t_b = t_{be} = t_{bi}$), Eq. (10.7) gives

$$k_2 = K = \infty$$

$$k_4 = \frac{k_3}{1 + k_1} = \frac{H_i P_i}{\dot{m}_c\, c_p \left(1 + \dfrac{H_i P_i}{H_e P_e}\right)} \tag{10.15}$$

10.4.2 Variation of Blade Surface Temperatures

Equation (10.8) gives

$$t_c = \frac{k_1 + k_1k_2 + k_2}{k_1 + k_1k_2}\, t_{bi} \tag{10.16}$$

Substituting this in Eq. (10.10)

$$-\frac{k_1 + k_1k_2 + k_2}{k_1 + k_1k_2}\, dt_{bi} = \left[\frac{k_1 + k_1k_2 + k_2}{k_1 + k_1k_2} - 1\right] k_3\, t_{bi}\, dz$$

$$\frac{dt_{bi}}{t_{bi}} = -\frac{k_2k_3}{k_1 + k_1k_2 + k_2}\, dz \tag{10.17}$$

On integration, this gives

$$\frac{t_{bi}}{t_{bih}} = \frac{T_g - T_{bi}}{T_g - T_{bih}} = e^{-k_4z} \tag{10.18}$$

Equation (10.7) gives

$$t_{bi} = \frac{1 + k_2}{k_2}\, t_{be} \tag{10.19}$$

Equation (10.19) when substituted in Eq. (10.16) gives

$$t_c = \frac{k_1 + k_1k_2 + k_2}{k_1k_2}\, t_{be} \tag{10.20}$$

Substituting from Eqs. (10.19) and (10.20) into Eq. (10.10), and simplifying

$$\frac{dt_{be}}{t_{be}} = -\frac{k_2k_3}{k_1 + k_1k_2 + k_2}\, dz \tag{10.21}$$

$$\frac{t_{be}}{t_{beh}} = \frac{T_g - T_{be}}{T_g - T_{beh}} = e^{-k_4z} \tag{10.22}$$

Equations (10.18) and (10.22) are not yet in the explicit form on account of the terms T_{bih} and T_{beh} which have to be found. Therefore, to be able to use them for determining the blade temperature distributions T_{bi} and T_{be}, they are further modified.

At the hub section, Eq. (10.8) gives

$$\frac{t_{bih}}{t_{ch}} = \frac{T_g - T_{bih}}{T_g - T_{ch}} = \frac{k_1 + k_1k_2}{k_1 + k_1k_2 + k_2} \tag{10.23}$$

The combination of Eqs. (10.18) and (10.23) gives

$$\frac{T_g - T_{bi}}{T_g - T_{ch}} = \frac{k_1 + k_1k_2}{k_1 + k_1k_2 + k_2}\, e^{-k_4z} \tag{10.24}$$

Equation (10.20) for the hub section gives

$$\frac{t_{beh}}{t_{ch}} = \frac{T_g - T_{beh}}{T_g - T_{ch}} = \frac{k_1 k_2}{k_1 + k_1 k_2 + k_2} \tag{10.25}$$

The combination of Eq. (10.22) and (10.25) yields

$$\frac{T_g - T_{be}}{T_g - T_{ch}} = \frac{k_1 k_2}{k_1 + k_1 k_2 + k_2} \; e^{-k_4 z} \tag{10.26}$$

10.4.3 Variation of Blade Relative Temperature

For $T_{bi} = T_{be} = T_b$, Eqs. (10.24) and (10.26) reduce to

$$\frac{T_g - T_b}{T_g - T_{ch}} = \frac{k_1}{1 + k_1} \; e^{-k_4 z}$$

Substituting from Eqs. (10.1) and (10.15) and rearranging an expression for the blade relative temperature is obtained.

$$\frac{T_b - T_{ch}}{T_g - T_{ch}} = 1 - \frac{\exp\left\{-\left[\dfrac{H_i P_i}{\dot{m}_c \, c_p \, (1 + H_i P_i / H_e P_e)}\right] z\right\}}{1 + H_e P_e / H_i P_i} \tag{10.27}$$

Equations (10.13) and (10.27 have been plotted in Fig. 10.7 for the variation of temperatures of the coolant and the blade along the blade height.

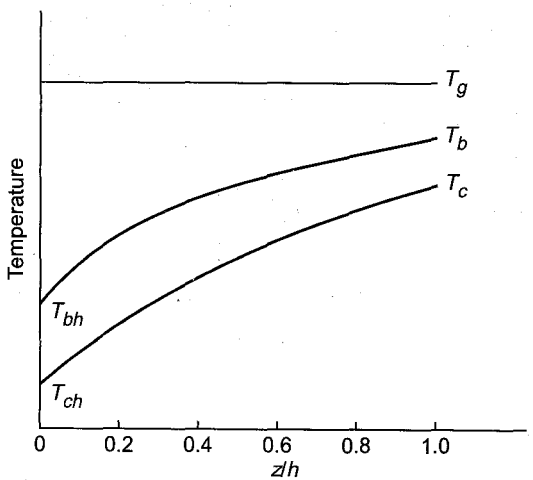

Fig. 10.7 Typical variation of blade and coolant temperatures along the blade height

The temperature of the blade in the tip region remains higher; however, it is not critical from stress considerations at that section; besides this there is some additional dissipation of heat from the tips due to radiation leading to some decrease in the blade metal temperature.

10.5 Ideal Cooled Stage[360]

Thermodynamic relations for cooled turbines have been developed by Hawthorne[360]; some basic relations are presented here.

An ideal cooled stage has reversible adiabatic flow through the blade rows accompanied by heat exchange with the coolant. The heat removed from the nozzle and rotor blade rows is q_N and q_R respectively. In the absence of this heat exchange the stage will have hundred per cent efficiency.

In this section cooling of the blades is assumed at either constant stagnation pressure (Fig. 10.8) or constant exit pressure (Fig. 10.9).

10.5.1 Work and Efficiency

The ideal work is the work in isentropic flow (0_1 to 0_{3ss}) through the stage without cooling.

$$w_s = h_{01} - h_{03ss} \tag{10.28}$$

Assuming $c_{3ss} \approx c_3$,

$$w_s = h_{01} - h_{3ss} - \frac{1}{2} c_3^2 \tag{10.29}$$

The actual work (again with isentropic flow) is less than the ideal on account of cooling.

$$w_a = h_{01} - h_{03} - (q_N + q_R) \tag{10.30}$$

The total-to-total efficiency of the ideal cooled stage is give by

$$\eta_{ci} = \frac{w_a}{w_s} = \frac{h_{01} - h_{03} - (q_N + q_R)}{h_{01} - h_{03ss}} \tag{10.31}$$

$$h_{01} + h_{03} - (q_N + q_R) = \left(h_{01} - h_{3ss} - \frac{1}{2} c_3^2\right) + (h_{3ss} - h_3 - q_N - q_R)$$

$$h_{01} - h_{03} - (q_N + q_R) = h_{01} - h_{03ss} - (h_3 - h_{3ss} + q_N + q_R)$$

Substituting in the numerator of Eq. (10.31)

$$\eta_{ci} = 1 - \frac{h_3 - h_{3ss} + q_N + q_R}{h_{01} - h_{03ss}} \tag{10.32}$$

This is a general expression for the efficiency of an ideal cooled stage and is applicable to both the type of stages shown in Figs. 10.8 and 10.9.

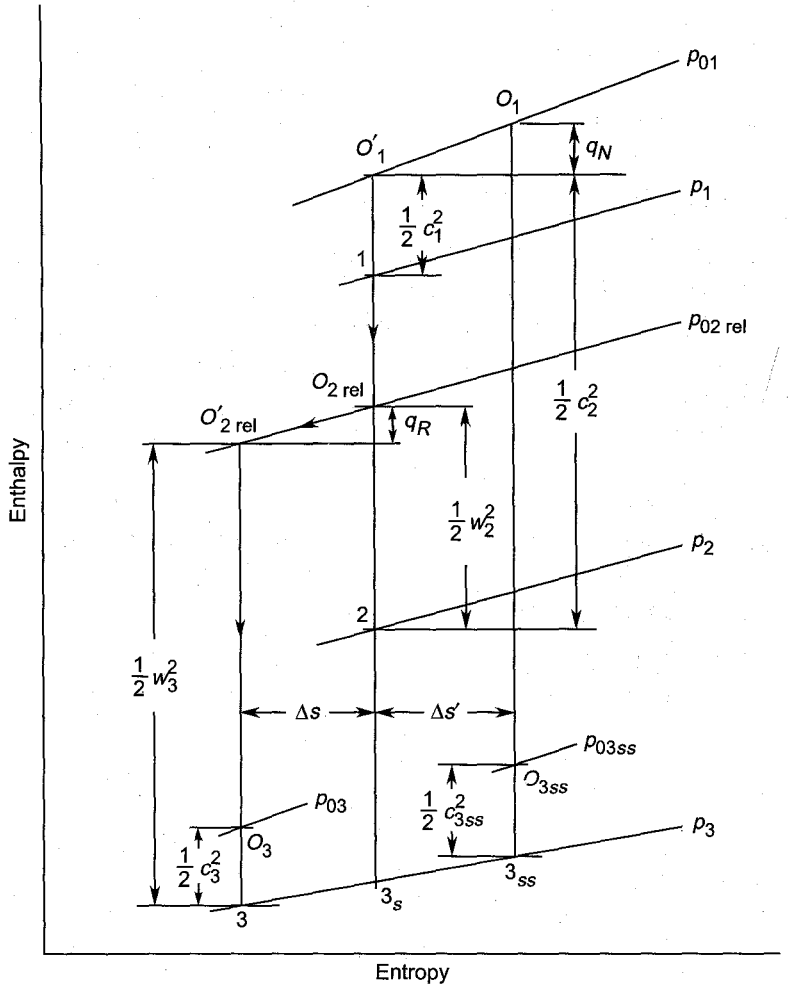

Fig. 10.8 Cooling of blade rows at constant stagnation pressure in an ideal stage

In the absence of cooling ($q_N = q_R = 0$), points 3 and 3*ss* coincide and Eq. (10.32) yields $\eta_{ci} = 1$.

Loss of work due to cooling in an ideal cooled stage is

$$\Delta w = w_s - w_a = (1 - \eta_{ci})\, w_s$$

From Eq. (10.32)

$$\Delta w = (1 - \eta_{ci})\,(h_{01} - h_{03ss})$$

$$\Delta w = h_3 - h_{3ss} + q_N + q_R \qquad (10.33)$$

The two types of ideal cooled stages are discussed separately. The cooling process in an actual cooled stage is expected to be between these models.

10.5.2 Blade Cooling at Constant Stagnation Pressure

The enthalpy-entropy diagram of an ideal turbine stage where the blade rows are assumed to be cooled at constant stagnation pressure is shown in Fig. 10.8.

The stagnation state of the gas at the entry to the stage is represented by point 0_1. On account of the heat exchange q_N during the cooling process in the nozzle row, the state shifts to $0'_1$. The stage being ideal, the expansion processes are reversible adiabatic (isentropic) both in the nozzle and rotor blade rows. The heat exchange q_R during the cooling of the rotor blades also occurs at constant stagnation pressure $p_{02\text{rel}}$.

The path of the isentropic expansion process without cooling is along $0_1 - 3ss$.

These processes should be compared with the corresponding processes shown in Fig. 9.8.

From Fig. 10.8, the slopes of the constant pressure lines p_{01} and p_3 are given by

$$\frac{h_{01} - h'_{01}}{\Delta s'} \approx T_{01}$$

$$\frac{h_{3ss} - h_{3s}}{\Delta s'} \approx T_{3s} \approx T_3$$

Combining the above expressions

$$\frac{h_{3ss} - h_{3s}}{h_{01} - h'_{01}} = \frac{T_3}{T_{01}}$$

But

$$h_{01} - h'_{01} = q_N \tag{10.34}$$

$$h_{3ss} - h_{3s} = q_N \left(\frac{T_3}{T_{01}}\right) \tag{10.35}$$

Similarly, the following relations can also be written for the slopes of the constant pressure lines:

$$\frac{h_{02\text{rel}} - h'_{02\text{rel}}}{\Delta s} \approx T_{02\text{rel}}$$

$$\frac{h_{3s} - h_3}{\Delta s} \approx T_3$$

$$\frac{h_{3s} - h_3}{h_{02\text{rel}} - h'_{02\text{rel}}} = \frac{T_3}{T_{02\text{rel}}}$$

$$h_{02\text{rel}} - h'_{02\text{rel}} = q_R \tag{10.36}$$

$$h_{3s} - h_3 = \left(\frac{T_3}{T_{02\text{rel}}}\right) q_R \tag{10.37}$$

Adding Eqs. (10.35) and (10.37)

$$h_{3ss} - h_3 = q_N \left(\frac{T_3}{T_{01}}\right) + q_R \left(\frac{T_3}{T_{02\text{rel}}}\right) \tag{10.38}$$

Equation (10.38) when substituted in Eqs. (10.32) and (10.33) yields expressions for the stage efficiency and lost work in a reversible cooled stage.

$$\eta_{ci} = 1 - \frac{q_N\,(1 - T_3/T_{01}) + q_R\,(1 - T_3/T_{02\text{rel}})}{h_{01} - h_{03ss}} \tag{10.39}$$

$$\Delta w_{ci} = q_N\,(1 - T_3/T_{01}) + q_R\,(1 - T_3/T_{02\text{rel}}) \tag{10.40}$$

10.5.3 Blade Cooling at Constant Exit Pressure

The enthalpy-entropy diagram of an ideal turbine stage where the blade rows are cooled at constant exit pressure is shown in Fig. 10.9.

The isentropic expansion in the absence of cooling is along the path $0_1 - 3ss$. The cooling of nozzle and rotor blade rows is represented by processes $2 - 2'$ and $3s - 3$. The heat exchange during these processes are

$$q_N = h_2 - h_2' \tag{10.41}$$

$$q_R = h_{3s} - h_3 \tag{10.42}$$

The expansion in the nozzle and rotor blade rows accompanied by cooling occurs along $1 - 2$ and $2' - 3s$.

The slopes of constant pressure lines p_2 and p_3 are given by the following expressions:

$$\frac{h_2 - h_2'}{\Delta s} \approx T_2$$

$$\frac{h_{3ss} - h_{3s}}{\Delta s} \approx T_3$$

$$\frac{h_{3ss} - h_{3s}}{h_2 - h_2'} = \frac{T_3}{T_2}$$

Substituting from Eq. (10.41)

$$h_{3ss} - h_{3s} = q_N \left(\frac{T_3}{T_2}\right) \tag{10.43}$$

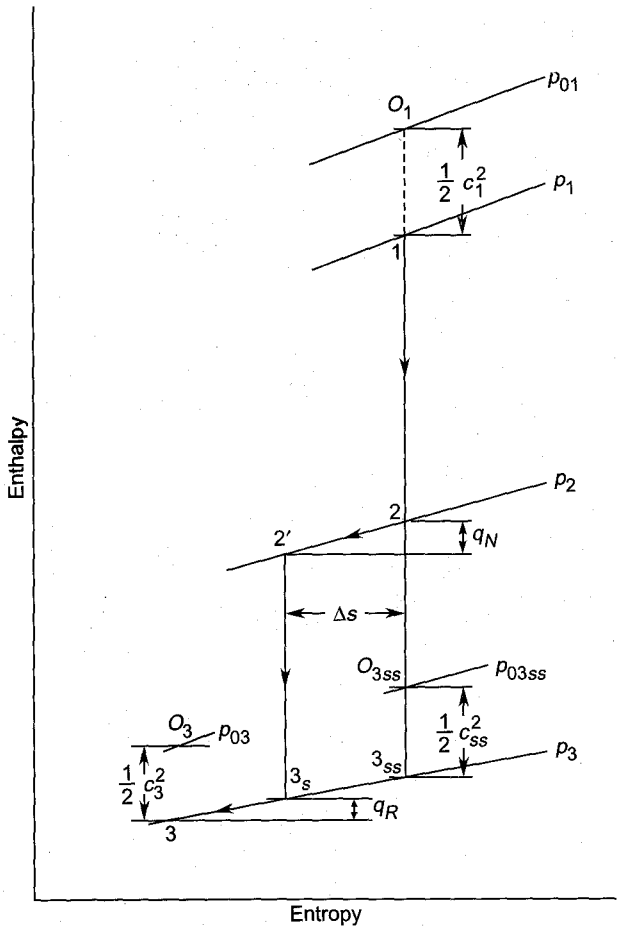

Fig. 10.9 Cooling of blade rows at constant exit pressure in an ideal stage

Adding Eqs. (10.42) and (10.43)

$$h_{3ss} - h_3 = q_R + q_N \left(\frac{T_3}{T_2}\right) \tag{9.44}$$

Substituting this value in Eqs. (10.32) and (10.33), the stage efficiency is obtained to be

$$\eta'_{ci} = 1 - \frac{q_N \left(1 - \frac{T_3}{T_2}\right)}{h_{01} - h_{03ss}} \tag{10.45}$$

and the lost work is obtained as

$$\Delta w'_{ci} = \left(1 - \frac{T_3}{T_2}\right) q_N \tag{10.46}$$

10.6 Actual Cooled Stage

In an actual cooled stage irreversible adiabatic expansion occurs in the blade rows accompanied by cooling. The efficiency of such a stage in the absence of cooling is less than hundred per cent on account of the cascade losses (Secs. 9.5.1 and 9.7.1).

The enthalpy-entropy diagram for an actual cooled stage is shown in Fig. 10.10. It may be compared with Fig. 9.8. For the sake of comparison between uncooled and cooled stages, fluid and blade velocities are assumed to be same in the two cases. As a result of this the stage work will also be the same. However, the enthalpies (temperatures) and pressures would be different.

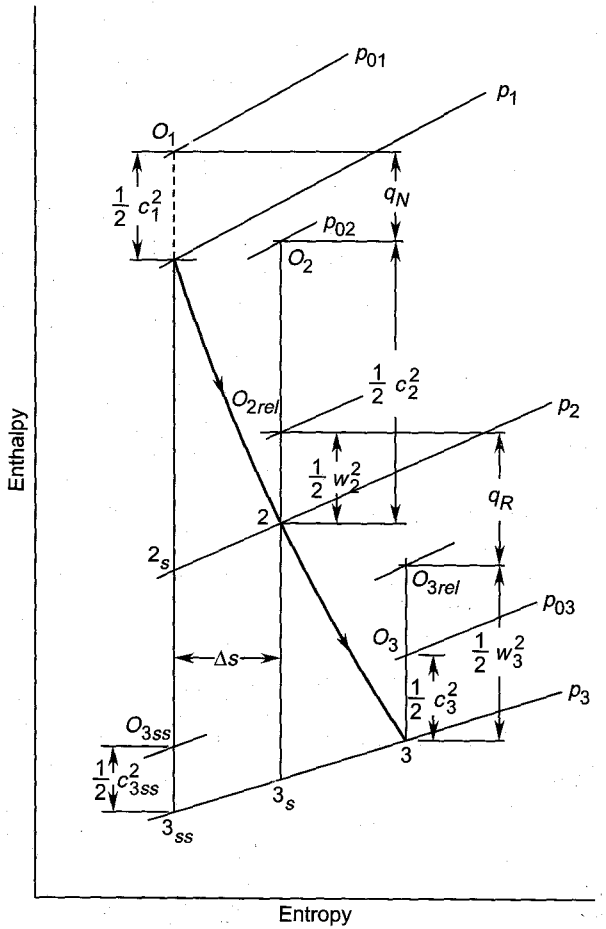

Fig. 10.10 Cooling of blade rows in an actual stage

10.6.1 Stage Efficiency

Equations (10.28) (10.30), (10.32) and (10.33) are valid here also. The cascade loss coefficients, however are a little different.

$$\xi'_N = \frac{h_2 - h_{2s}}{\frac{1}{2}c_2^2}$$

$$h_2 - h_{2s} = \frac{1}{2}\ \xi'_N\, c_2^2 \tag{10.47}$$

$$\xi'_R = \frac{h_3 - h_{3s}}{\frac{1}{2}c_3^2}$$

$$h_3 - h_{3s} = \frac{1}{2}\ \xi'_R\, w_3^2 \tag{10.48}$$

The slopes of the constant pressure lines p_2 and p_3 are

$$\frac{h_2 - h_{2s}}{\Delta s} \approx T_2$$

$$\frac{h_{3s} - h_{3ss}}{\Delta s} \approx T_{3s} \approx T_3$$

Therefore,

$$\frac{h_{3s} - h_{3ss}}{h_2 - h_{2s}} = \frac{T_3}{T_2}$$

$$h_{3s} - h_{3ss} = \frac{T_3}{T_2}\ (h_2 - h_{2s}) \tag{10.49}$$

Substituting from Eq. (10.47),

$$h_{3s} - h_{3ss} = \frac{1}{2}\ \xi'_N\, c_2^2\ \frac{T_3}{T_2} \tag{10.50}$$

Adding Eqs. (10.48) and (10.50),

$$h_3 - h_{3ss} = \frac{1}{2}\,\xi'_R w_3^2 + \frac{1}{2}\ \xi'_N\, c_2^2 \left(\frac{T_3}{T_2}\right) \tag{10.51}$$

Therefore, the loss of work in a cooled stage is

$$\begin{aligned}\Delta w_{ca} &= h_3 - h_{3ss} + q_N + q_R \\ &= \frac{1}{2}\ c_2^2 \left[\xi'_N \left(\frac{T_3}{T_2}\right) + q_N \Big/ \frac{1}{2}\, c_2^2\right] + \frac{1}{2}\ w_3^2 \left(\xi'_R + q_R \Big/ \frac{1}{2}\, w_3^2\right)\end{aligned} \tag{10.52}$$

Equation (10.32) gives the efficiency of such a stage as

$$w_a = 1 - \frac{c_2^2\left[\xi'_N\left(\frac{T_3}{T_2}\right) + q_N \Big/ \frac{1}{2}c_2^2\right] + w_3^2\left[\xi'_R + q_R \Big/ \frac{1}{2}w_3^2\right]}{2\,(h_{01} - h_{03ss})} \tag{10.53}$$

10.6.2 Stage Work

Referring to Fig. 10.10, the following relations can be written for heat exchange in the nozzle and rotor blade rows:

$$q_N = h_{01} - h_{02}$$

$$q_N = h_{01} - h_2 - \frac{1}{2}c_2^2$$

$$q_R = h_{02\text{rel}} - h_{03\text{rel}}$$

$$q_R = h_2 + \frac{1}{2}w_2^2 - h_3 - \frac{1}{2}w_3^2$$

These values, when put into Eq. (10.30), give

$$w_{ca} = h_{01} - h_{03} - \left(h_{01} - h_2 - \frac{1}{2}c_2^2\right) - \left(h_2 + \frac{1}{2}w_2^2 - h_3 - \frac{1}{2}w_3^2\right)$$

Putting $h_{03} = h_3 + \frac{1}{2}c_3^2$ and simplifying

$$w_a = \frac{1}{2}(c_2^2 - c_3^2) + \frac{1}{2}(w_3^2 - w_2^2) \tag{10.54}$$

This is only one of the forms [Eq. (6.153a) in Sec. 6.9] of the Euler's turbine equation.

Employing further geometrical relations and using velocity triangles of Fig. 9.1 Eq. (10.54) can be reduced to

$$w_{ca} = u\,(c_{y2} + c_{y3}) \tag{10.55}$$

This exercise shows that, as long as the fluid velocities are the same in a given turbine stage, cooling does not effect the stage work.

10.6.3 Decrease in Stage Efficiency

An estimation[360] of the decrease in the stage efficiency due to cooling can easily be made for the same output $(h_{01} - h_{03})$ in the cooled and uncooled states.

A general expression for the total-to-total efficiency of a turbine stage has been derived in Sec. 9.7.2. The basic relation is

$$\eta_{tt} = \left(1 - \frac{h_{03} - h_{03ss}}{h_{01} - h_{03}}\right)^{-1} \tag{10.56}$$

In this expression the values of the quantity $(h_{03} - h_{03ss})$ are different for the cooled and uncooled states.

Assuming $c_3 \approx c_{3ss}$

$$h_{03} - h_{03ss} = h_3 - h_{3ss}$$

For an uncooled stage the above expression represents the stage losses:

$$\Delta w_a = \xi_N \left(\frac{T_3}{T_2}\right) \frac{1}{2} c_2^2 + \xi_R \frac{1}{2} w_3^2 \tag{10.57}$$

The stage efficiency is given by

$$\eta_a = \left[1 + \frac{\xi_N \left(\frac{T_3}{T_2}\right) \frac{1}{2} c_2^2 + \xi_R \frac{1}{2} w_3^2}{h_{01} - h_{03}}\right]^{-1} \tag{10.58}$$

This is the same as Eq. (9.92a).

For the cooled stage the loss of work is given by Eq. (10.52). Therefore, the stage efficiency is given by

$$\eta_{ca} = \left[1 + \frac{\xi'_N \left(\frac{T'_3}{T'_2}\right) \frac{1}{2} c_2^2 + \xi'_R \frac{1}{2} w_3^2 + q_N + q_R}{h_{01} - h_{03}}\right]^{-1} \tag{10.59}$$

Here primes refer to quantities in the cooled stage. Equations (10.58) and (10.59) together give

$$\frac{1}{\eta_{ca}} - \frac{1}{\eta_a} = \frac{\left(\xi'_N \frac{T'_3}{T'_2} - \xi_N \frac{T_3}{T_2}\right) \frac{1}{2} c_2^2 + (\xi'_R - \xi_R) \frac{1}{2} w_3^2 + q_N + q_R}{h_{01} - h_{03}} \tag{10.60}$$

By expanding the binomials in Eqs. (10.58) and (10.59) and assuming

$$\xi'_N \frac{T'_3}{T'_2} = \xi_N \frac{T_3}{T_2}$$

$$\xi'_R = \xi_R$$

an approximate expression for the loss in the stage efficiency due to cooling can be obtained. This is given by

$$\Delta\eta_c = \eta_a - \eta_{ca} \approx \frac{q_N + q_R}{h_{01} - h_{03}} \tag{10.61}$$

10.6.4 Infinitesimal Stage Efficiency

An infinitesimal stage without any cooling produces work equal to dw with an isentropic enthalpy drop of dh_s through a pressure drop dp. Thus

$$\eta_p = \frac{dw}{dh_s} \tag{10.62}$$

For a perfect gas this is the same as Eq. (2.122) in Sec. 2.5.5.

An infinitesimal cooled stage (Fig. 10.11), besides producing work equal to dw, rejects heat $dq = d\,(q_N + q_R)$. Therefore, the efficiency of such a stage is defined by

$$\eta_{pc} = \frac{dw + dq}{dh_s} \tag{10.63}$$

$$\eta_{pc} = \frac{dw}{dh_s}\left(1 + \frac{dq}{dw}\right)$$

Substituting from Eq. (10.62) in Eq. (10.63)

$$\eta_{pc} = \eta_p \left(1 + \frac{dq}{dw}\right) \tag{10.64}$$

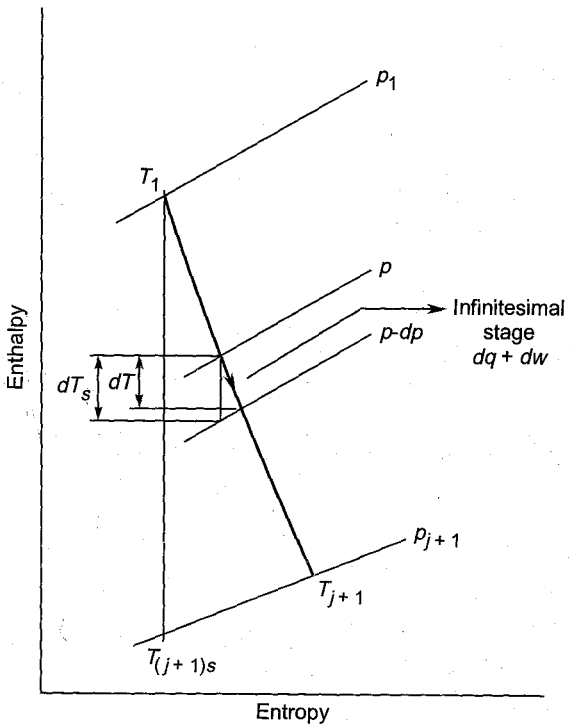

Fig. 10.11 Infinitesimal and finite expansions in a cooled turbine

Expressing Eq. (10.63) in terms of the actual and isentropic temperature drops

$$\eta_{pc} = \frac{dT}{dT_s} \tag{10.65}$$

In this equation the term dT is the actual temperature drop due to both the work done (dw) and the heat rejected (dq) in the stage. Therefore, it is not the same as Eq. (2.122).

For the infinitesimal isentropic expansion,

$$\frac{T - dT_s}{T} = \left(\frac{p - dp}{p}\right)^{\frac{\gamma-1}{\gamma}}$$

After expanding the quantity on the right-hand side, simplifying and rearranging

$$\frac{dT_s}{T} = \frac{\gamma - 1}{\gamma}\frac{dp}{p}$$

Substituting from Eq. (10.65) for dT_s

$$\frac{dT}{T} = \frac{\gamma - 1}{\gamma}\eta_{pc}\frac{dp}{p} \tag{10.66}$$

This equation defines the actual expansion line in a finite cooled stage or a multi-stage cooled turbine. On integration and rearrangement it gives

$$p^{\frac{\gamma-1}{\gamma}\eta_{pc}} = T \times \text{const.} \tag{10.67}$$

Applying this equation for states 1 and 2

$$\frac{T_2}{T_1} = \left(\frac{p_2}{p_1}\right)^{\frac{\gamma-1}{\gamma}\eta_{pc}} \tag{10.68}$$

$$\eta_{pc} = \frac{\frac{\gamma}{\gamma-1}\ln\left(\frac{T_2}{T_1}\right)}{\ln\left(\frac{p_2}{p_1}\right)} \tag{10.69}$$

10.6.5 Multi-stage Turbine Efficiency

For a known value of polytropic efficiency (η_{pc}), the efficiencies of a finite cooled stage and a multi-stage turbine can be obtained.

In a multi-stage cooled turbine (Fig. 10.11) with j stages of the same pressure ratio (p_r) the ideal and actual values of the temperature drops are

$$T_1 - T_{(j+1)s} = T_1\left[1 - \frac{T_{(j+1)s}}{T_1}\right]$$

$$T_1 - T_{(j+1)s} = T_1 \left[1 - \left(\frac{1}{p_r}\right)^{j\frac{\gamma-1}{\gamma}}\right] \tag{10.70}$$

$$T_1 - T_{j+1} = T_1 \left[1 - \frac{T_{j+1}}{T_1}\right]$$

From Eq. (10.67)

$$T_1 - T_{j+1} = T_1 \left[1 - \left(\frac{1}{p_r}\right)^{j\frac{\gamma-1}{\gamma}\eta_{pc}}\right] \tag{10.71}$$

If the total heat rejected by the turbine due to cooling is q_T, work done is w_T and the isentropic enthalpy drop Δh_{Ts}, then

$$\frac{w_T + q_T}{\Delta h_{Ts}} = \frac{w_T}{\Delta h_{Ts}}\left(1 + \frac{q_T}{w_T}\right) = \frac{T_1 - T_{j+1}}{T_1 - T_{(j+1)s}} \tag{10.72}$$

The overall efficiency of the multi-stage turbine is

$$\eta_T = \frac{w_T}{\Delta h_{Ts}} \tag{10.73}$$

Therefore, substituting from Eqs. (10.70), (10.71) and (10.73) in Eq. (10.72)

$$\eta_T\left(1 + \frac{q_T}{w_T}\right) = \frac{1 - p_r^{\,j\frac{1-\gamma}{\gamma}\eta_{pc}}}{1 - p_r^{\,j\frac{1-\gamma}{\gamma}}} \tag{10.74}$$

For a single finite cooled stage, Eq. (10.74) gives

$$\eta_{st}\left(1 + \frac{q_{st}}{w_{st}}\right) = \frac{1 - p_r^{\frac{1-\gamma}{\gamma}\eta_{pc}}}{1 - p_r^{\frac{1-\gamma}{\gamma}}} \tag{10.75}$$

Equations (10.74) and (10.75) in the absence of cooling ($\eta_{pc} = \eta_p$) give

$$\eta_T = \frac{1 - p_r^{\,j\frac{1-\gamma}{\gamma}\eta_p}}{1 - p_r^{\,j\frac{1-\gamma}{\gamma}}} \tag{10.76}$$

$$\eta_{st} = \frac{1 - p_r^{\frac{1-\gamma}{\gamma}\eta_p}}{1 - p_r^{\frac{1-\gamma}{\gamma}}} \tag{10.77}$$

These equations are identical to Eqs. (2.132) and (2.129a) respectively.

Notation for Chapter 10

c	Fluid velocity
c_p	Specific heat
h	Enthalpy, blade height
H	Heat transfer coefficient
j	Number of cooled stages
k_1, k_2, k_3, k_4	Quantities (constants) defined in the text
K	Thermal conductance of the blade material
$\dot{m}$	Mass-flow rate
p	Pressure
p_r	Pressure ratio
P	Perimeter of the heat transfer surfaces
q	Heat exchange
s	Entropy
Δs	Change in entropy
t	Temperature difference
T	Temperature
u	Peripheral speed of the rotor
w	Relative velocity of the fluid, work
Δw	Loss in stage work
z	Distance along the blade height

Greek symbols

γ	c_p / c_v
η	Efficiency
ξ	Enthalpy loss coefficient

Subscripts

o	Stagnation values
1	Entry to the stage, initial state
2	Entry to the rotor, final state
3	Exit from the stage
a	Actual
b	Blade
c	Coolant, cooled stage
ci	Ideal cooled stage
ca	Actual cooled stage
e	External surface
g	Gas
h	Blade hub

i	Internal surface, ideal
max	Maximum
N	Nozzle blade row
p	Polytropic or infinitesimal stage
rel	Relative
R	Rotor blade row
s,ss	Isentropic
st	Single stage
tt	Total-to-total
T	Multi-stage turbine

Questions and Problems

10.1 What material and aerodynamic problems arise by the use of high temperature gas in turbine stages? How are they overcome?

10.2 **(a)** What are the five most important properties which the high temperature blade material must have?

(b) Name five alloys which are commonly used for gas turbine blades, discs and casings at elevated temperature. Give the range of temperatures for each of these materials.

10.3 **(a)** Why is it desirable to employ high inlet gas temperatures in gas turbine plants for land and aeronautical applications?

(b) Explain what is the effect of high inlet temperatures on specific power output, specific thrust, plant and turbine stage efficiencies?

10.4 **(a)** Explain why and when does cooling of gas turbine blades become necessary?

(b) Why is it not necessary to cool steam turbine blades?

10.5 **(a)** Describe various methods of cooling gas turbine blades?

(b) Why is air cooling preferred to liquid cooling in aeroengines?

10.6 What is creep? How does it affect the operation of gas turbine stages at elevated temperatures?

10.7 **(a)** Starting from the fundamental equations of heat transfer, prove that the variations of the coolant and blade metal temperatures along the blade height are given by

$$\frac{T_c - T_{ch}}{T_g - T_{ch}} = 1 - e^{-C_1 z}$$

$$\frac{T_b - T_{ch}}{T_g - T_{ch}} = 1 - e^{-C_2 z}$$

State the assumptions used.

(b) Show graphically the variation of these temperatures along the blade height.

10.8 Derive the following relations for an actual cooled gas turbine stage:

(a) Lost work

$$= \frac{1}{2} c_2^2 \left[\xi'_N \left(\frac{T_3}{T_2} \right) + q_N \Big/ \frac{1}{2} c_2^2 \right] + \frac{1}{2} w_3^2 \left(\xi'_R + q_R \Big/ \frac{1}{2} w_3^2 \right)$$

(b)

$$\eta_{ca} = 1 - \frac{\text{lost work}}{\Delta h_{os}}$$

(c) Stage work

$$= \frac{1}{2} (c_2^2 - c_3^2) + \frac{1}{2} (w_3^2 - w_2^2)$$

(d) Loss of stage efficiency due to cooling

$\Delta\eta_c \approx$ heat rejected/stage work

(e) Small stage efficiency

$$\eta_{pc} = \frac{\dfrac{\gamma}{\gamma - 1} \ln \left(\dfrac{T_2}{T_1} \right)}{\ln \left(\dfrac{p_2}{p_1} \right)}$$

Chapter 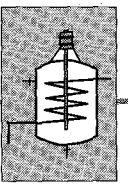 11

Axial Compressor Stages

An axial compressor[399,411A] is a pressure producing machine. The energy level of air or gas flowing through it is increased by the action of the rotor blades which exert a torque on the fluid. This torque is supplied by an external source—an electric motor or a steam or gas turbine. Besides numerous industrial applications the multistage axial compressor is the principal element of all gas turbine power plants (see Chapter 3 and 5) for land and aeronautical applications.

An axial compressor stage was defined in Sec. 1.7 and its merits discussed in Sec. 1.9. In contrast to the axial turbine stages, an axial compressor stage is a relatively low temperature and pressure machine with no serious material problems. While impulse type of stages are commonly used in turbines, these are rare in compressors except in supersonic stages.

The flow in a compressor stage is throughout decelerating as in a diffuser. In this respect the nature of flow in a compressor stage is largely identical to the diffuser flow which has been discussed in Sec. 2.4. As pointed out earlier, the blade profiles in compressor blade rows are more critical than in turbine stages. This is on account of the flow occurring against the pressure rise and the susceptibility of the flow to separation.

The arrangement of blade rows (cascades) in compressors and the nature of flow through them have been discussed at length in Sec. 8.5. Figures 8.26 to 8.36 dipict various geometrical and aerodynamic aspects of compressor blade rows and the flow through them.

This chapter deals with the aerothermodynamic analysis of flow through complete compressor stages. Methods of estimating the stage work and efficiency are given here (see Sec. 2.6). Flow problems through both long (low pressure stages) and short blades (high pressure) have been considered.

Various problems of low pressure axial compressor stages are identical to those of axial-flow fans which have been dealt with in Chapter 14. Slight amount of overlap between these chapters has been considered inevitable and tolerated. However, some aspects have been covered only in one chapter. Some striking differences that would be observed between the two chapters are the use of "multi-stages" and the term "pressure

ratio" in this chapter and "single stage fans" and "pressure rise in millimeters of water gauge" in Chapter 14.

11.1 Stage Velocity Triangles

Pressure and velocity variations through a compressor stage (with inlet guide vanes) are shown in figure 11.1(a).

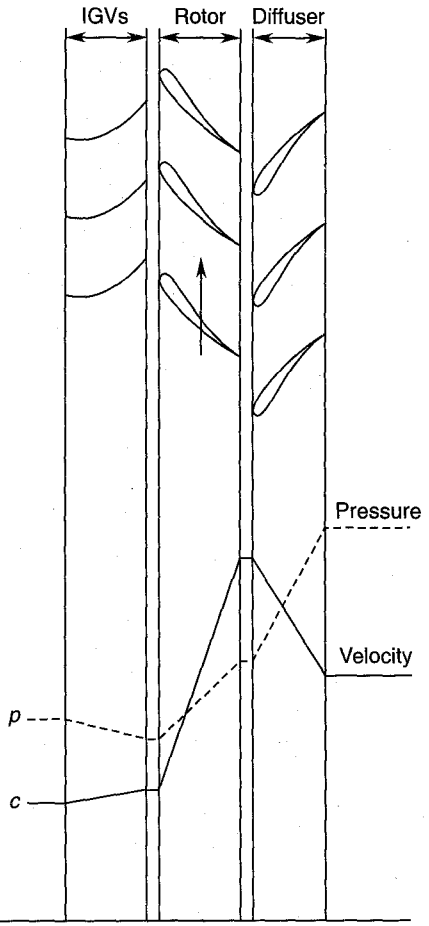

Fig. 11.1 (a) Pressure and velocity variation through a compressor stage

Velocity triangles for axial compressor stages have been briefly discussed in Chapters 1 and 8. The velocity triangles shown in Fig. 11.1(b) are for a general stage which receives air or gas with an absolute velocity c_1 and angle α_1 (from the axial direction) from the previous stage. In the case of the first stage in a multi-stage machine, the axial direction of the

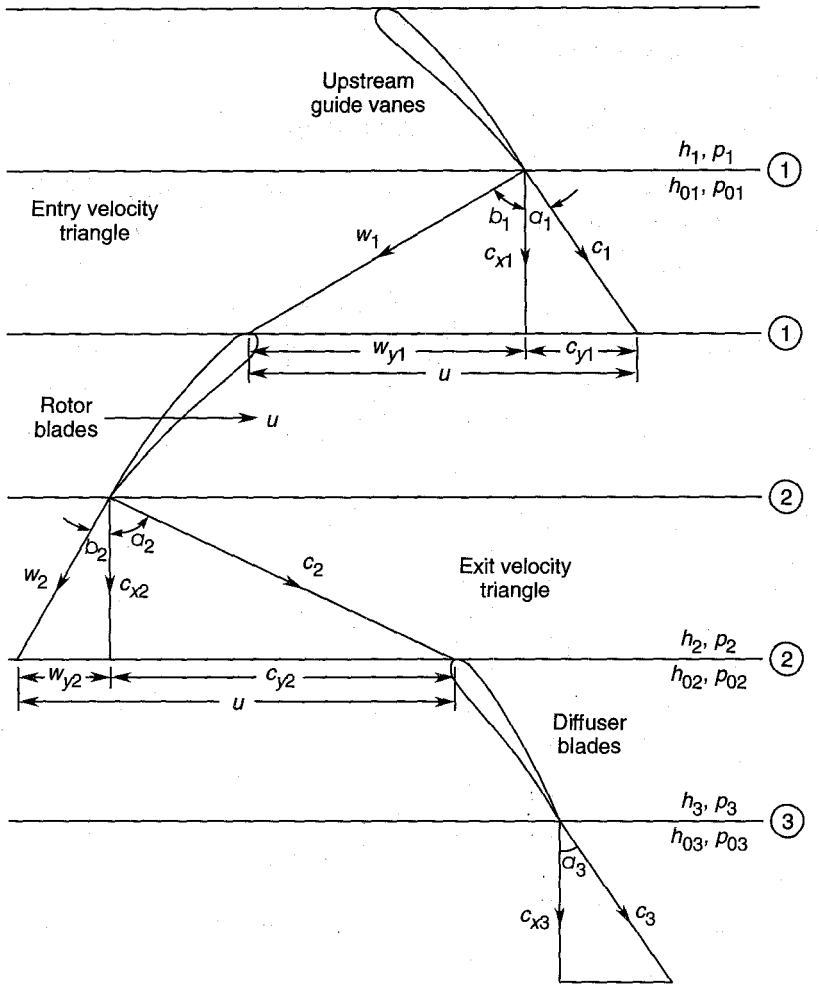

Fig. 11.1 (b) Velocity triangles for a compressor stage

approaching flow is changed to the desired direction (α_1) by providing a row of blades upstream guide vanes (UGV). Therefore, the first stage experiences additional losses arising from flow through the UGVs.

For a general stage, the entry to the rotor, exit from the rotor and the diffuser blade row (stator) are designated as stations 1, 2 and 3, respectively. The air angles in the absolute and the relative systems are denoted by α_1, α_2, α_3 and β_1, β_2 respectively. If the flow is repeated in another stage.

$$c_1 = c_3 \text{ and } \alpha_1 = \alpha_3$$

Subscripts x and y denote axial and tangential directions respectively. Thus the absolute swirl or whirl vectors c_{y1} and c_{y2} are the tangential

components of absolute velocities c_1 and c_2, respectively. Similarly, w_{y1} and w_{y2} are the tangential components of the relative velocities w_1 and w_2, respectively.

Peripheral velocity at the mean diameter of the rotor at stations 1 and 2 is taken as

$$u = u_1 \approx u_2$$

The following trignometrical relations obtained from velocity triangles (Fig. 11.1b) will be used throughout this chapter.

From velocity triangles at the entry:

$$c_{x1} = c_1 \cos \alpha_1 = w_1 \cos \beta_1 \tag{11.1}$$

$$c_{y1} = c_1 \sin \alpha_1 = c_{x1} \tan \alpha_1 \tag{11.2}$$

$$w_{y1} = w_1 \sin \beta_1 = c_{x1} \tan \beta_1 \tag{11.3}$$

$$u = c_{y1} + w_{y1} \tag{11.4a}$$

$$u = c_1 \sin \alpha_1 + w_1 \sin \beta_1 \tag{11.4b}$$

$$u = c_{x1} (\tan \alpha_1 + \tan \beta_1) \tag{11.4c}$$

From velocity triangles at the exit:

$$c_{x2} = c_2 \cos \alpha_2 = w_2 \cos \beta_2 \tag{11.5}$$

$$c_{y2} = c_2 \sin \alpha_2 = c_{x2} \tan \alpha_2 \tag{11.6}$$

$$w_{y2} = w_2 \sin \beta_2 = c_{x2} \tan \beta_2 \tag{11.7}$$

$$u = c_{y2} + w_{y2} \tag{11.8a}$$

$$u = c_2 \sin \alpha_2 + w_2 \sin \beta_2 \tag{11.8b}$$

$$u = c_{x2} (\tan \alpha_2 + \tan \beta_2) \tag{11.8c}$$

For constant axial velocity through the stage:

$$c_{x1} = c_{x2} = c_{x3} = c_x \tag{11.9}$$

$$c_x = c_1 \cos \alpha_1 = w_1 \cos \beta_1 = c_2 \cos \alpha_2 = w_2 \cos \beta_2 \tag{11.10}$$

Equations (11.4c) and (11.8c) give

$$\frac{u}{c_x} = \frac{1}{\phi} = \tan \alpha_1 + \tan \beta_1 = \tan \alpha_2 + \tan \beta_2 \tag{11.11}$$

This relation can also be presented in another form using Eqs. (11.4a) and (11.8a).

$$c_{y1} + w_{y1} = c_{y2} + w_{y2}$$

$$c_{y2} - c_{y1} = w_{y1} - w_{y2} \tag{11.12a}$$

$$c_x (\tan \alpha_2 - \tan \alpha_1) = c_x (\tan \beta_1 - \tan \beta_2) \tag{11.12b}$$

Equations 11.12 (a and b) give the change in the swirl components across the rotor blade row. For steady flow in an axial machine, this is

proportional to the torque exerted on the fluid by the rotor (Sec. 6.9, Eq. (6.145b)).

11.1.1 Work

The specific work in a compressor stage is given by Eq. (6.147b). In the present notation it is

$$w = u\,(c_{y2} - c_{y1}) \tag{11.13a}$$

Using Eq. (11.12b) it can also be expressed as

$$w = u\,c_x\,(\tan\,\alpha_2 - \tan\,\alpha_1) = u\,c_x\,(\tan\,\beta_1 - \tan\,\beta_2) \tag{11.13b}$$

If the alphas and betas are actual air angles, Eq. (11.13b) gives the actual value of the stage work. The difference between the actual, isentropic and Euler's work has already been explained in Sec. 6.9.

For axial-flow compressor ($u = u_1 = u_2$), the specific work equation identical to Eq. (6.153a) is

$$w = \frac{1}{2}\,(c_2^2 - c_1^2) + \frac{1}{2}\,(w_1^2 - w_2^2) \tag{11.13c}$$

For a desired pressure rise in a compressor, the work input should be minimized to obtain higher efficiencies. In this respect the selection of the optimum blade and flow geometries (Sec. 8.5.7) is important.

11.1.2 Blade Loading and Flow Coefficients

The blade loading coefficient for an axial compressor stage is defined as

$$\psi = \frac{w}{u^2} \tag{11.14}$$

This is a dimensionless quantity used for comparing stages of differing sizes and speeds.

Head, pressure or loading coefficients have been discused in Sec. 7.4.1. For fan applications, ψ is defined as a pressure coefficient in Eq. (14.7).

In Sec. 7.4.2 another dimensionless coefficient known as the capacity coefficient is defined. An expression for the flow coefficient is derived from this Eq. (7.17):

$$\phi = \frac{c_x}{u} \tag{11.15}$$

Equations (11.13a) and (11.13b), when put in Eq. (11.14), give successively

$$\psi = \frac{c_{y2}}{u} - \frac{c_{y1}}{u}$$

$$\psi = \phi\,(\tan\,\alpha_2 - \tan\,\alpha_1) = \phi\,(\tan\,\beta_1 - \tan\,\beta_2) \tag{11.16}$$

The performance of axial compressor stages is presented in terms of $\phi - \psi$ plots. Figure 7.6 depicts the variation of pressure coefficient (loading coefficient) with the flow coefficient for an axial compressor stage.

11.1.3 Static Pressure Rise

The main function of a compressor is to raise the static pressure of air or gas. The static pressure rise in the stage depends on the flow geometry and the speed of the rotor. The total static pressure rise across the stage is the sum of static pressure rises in the rotor and diffuser (stator) blade rows; expressions for these values are derived here assuming reversible adiabatic flow and constant axial velocity through the stage.

Further, in view of the small pressure rises over blade rows of axial compressor stages the flow is assumed incompressible, i.e. $\rho \approx$ constant.

The Bernoulli equation across the rotor blade row gives

$$p_1 + \frac{1}{2}\rho w_1^2 = p_2 + \frac{1}{2}\rho w_2^2$$

$$(\Delta p)_R = p_2 - p_1 = \frac{1}{2}\rho\,(w_1^2 - w_2^2) \tag{11.17}$$

Using velocity triangles of Fig. 11.1b,

$$w_1^2 - w_2^2 = c_{x1}^2 + w_{y1}^2 - c_{x2}^2 - w_{y2}^2 = w_{y1}^2 - w_{y2}^2$$
$$w_1^2 - w_2^2 = c_x^2\,(\tan^2\beta_1 - \tan^2\beta_2)$$

This when put in Eq. (11.17) gives the pressure rise across the rotor as

$$(\Delta p)_R = \frac{1}{2}\rho c_x^2\,(\tan^2\beta_1 - \tan^2\beta_2) \tag{11.18}$$

Similarly, the Bernoulli equation across the diffuser blade row gives

$$(\Delta p)_D = p_3 - p_2 = \frac{1}{2}\rho\,(c_2^2 - c_3^2) \tag{11.19}$$

$$(\Delta p)_D = \frac{1}{2}\rho\,(c_{y2}^2 - c_{y3}^2)$$

$$(\Delta p)_D = \frac{1}{2}\rho c_x^2\,(\tan^2\alpha_2 - \tan^2\alpha_3)$$

Assuming $\alpha_3 = \alpha_1$,

$$(\Delta p)_D = \frac{1}{2}\rho c_x^2\,(\tan^2\alpha_2 - \tan^2\alpha_1) \tag{11.20}$$

The stage pressure rise is

$$p_3 - p_1 = \Delta p_{st} = \Delta p_R + \Delta p_D$$

Substituting from Eqs. (11.18) and (11.20),

$$\Delta p_{st} = \frac{1}{2}\rho c_x^2 \{(\tan^2\beta_1 - \tan^2\beta_2) + (\tan^2\alpha_2 - \tan^2\alpha_1)\}$$

Using Eq. (11.12b)

$$\Delta p_{st} = \frac{1}{2}\rho c_x (\tan\beta_1 - \tan\beta_2)\{c_x(\tan\beta_1 + \tan\beta_2) + c_x(\tan\alpha_2 + \tan\alpha_1)\}$$

This, on rearrangement and using Eqs. (11.4c) and (11.8c), gives

$$\Delta p_{st} = \rho c_x u (\tan\beta_1 - \tan\beta_2) \tag{11.21}$$

$$\Delta p_{st} = \rho c_x u (\tan\alpha_2 - \tan\alpha_1) \tag{11.22}$$

These relations for isentropic flow can also be obtained direct from Eq. (11.13b). For such a flow, changes in pressure and enthalpy and work are related by

$$\frac{\Delta p_{st}}{\rho} = \Delta h_{st} = w \tag{11.23}$$

11.2 Enthalpy–Entropy Diagram

Figure 11.2 shows the enthalpy–entropy diagram for a general axial-flow compressor stage. Static and stagnation values of pressures and enthalpies at various stations (shown in Fig. 11.1b) have been indicated.

The stagnation state 0_1 at rotor entry in the absolute system is fixed by the pressure p_1 and velocity c_1. The isentropic flow over the rotor and diffuser blades is represented by $1–2_s$ and $2_s–3_{ss}$. The stagnation point 0_{3ss} corresponding to the final state at the end of an isentropic compression is obtained from

$$h_{03ss} = h_{3ss} + \frac{1}{2}c_{3ss}^2 \tag{11.24}$$

The irreversible adiabatic or actual compression process is represented by curve 1-2-3. Here energy transformation processes (1–2) and (2–3) in the blade rows occur with stagnation pressure loss and increase in entropy.

For the rotor blades in the relative system:

Stagnation pressure loss = $(\Delta p_0)_R = p_{01\text{rel}} - p_{02\text{rel}}$

The stagnation enthalpy remains constant.

$$\left.\begin{aligned} h_{01\text{rel}} &= h_{02\text{rel}} \\ h_1 + \frac{1}{2}w_1^2 &= h_2 + \frac{1}{2}w_2^2 \end{aligned}\right\} \tag{11.25}$$

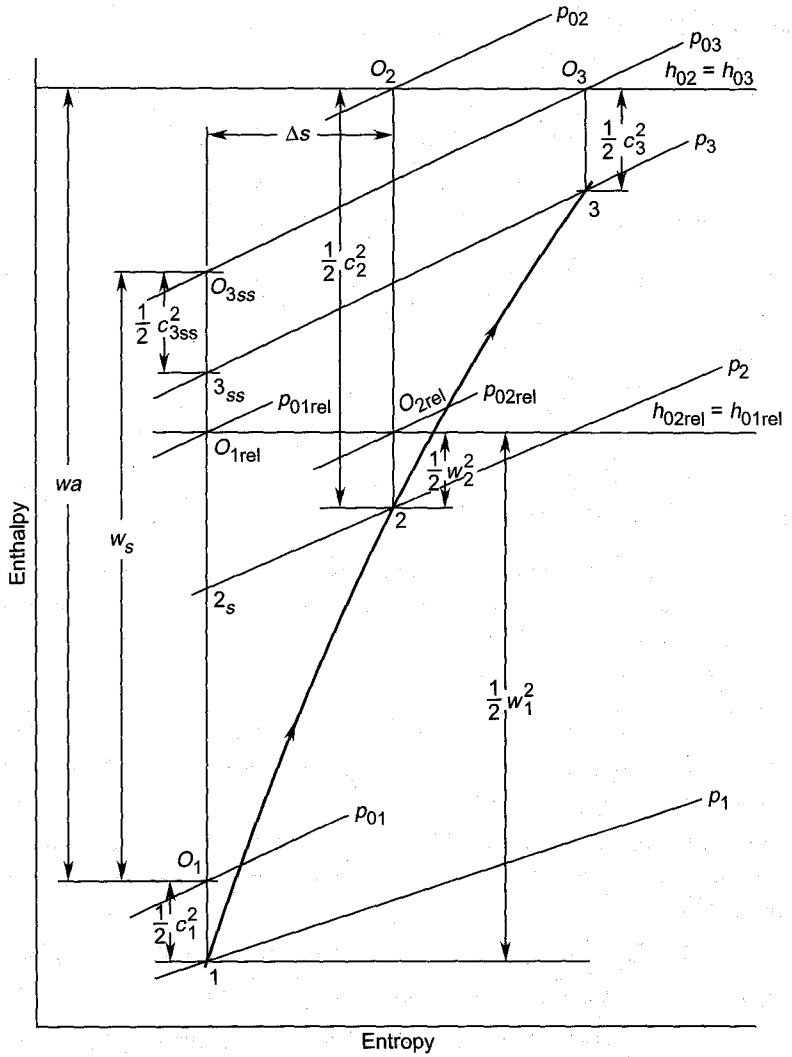

Fig. 11.2 Enthalpy-entropy diagram for flow through a compressor stage

The pressure (stagnation) and enthalpy loss coefficients are defined by

$$Y_R = \frac{(\Delta p_0)_R}{\frac{1}{2}\rho w_1^2} = \frac{p_{01\text{rel}} - p_{02\text{rel}}}{\frac{1}{2}\rho w_1^2} \tag{11.26}$$

$$\xi_R = \frac{h_2 - h_{2s}}{\frac{1}{2}w_1^2} = \frac{2\,c_p\,(T_2 - T_{2s})}{w_1^2} \tag{11.27}$$

For the diffuser blades (absolute system):

Stagnation pressure loss = $(\Delta p_0)_D = p_{02} - p_{03}$

The stagnation enthalpy remains constant.

$$\left.\begin{aligned} h_{02} &= h_{03} \\ h_2 + \frac{1}{2}c_2^2 &= h_3 + \frac{1}{2}c_3^2 \end{aligned}\right\} \tag{11.28}$$

The pressure and enthalpy loss coefficients are defined by

$$Y_D = \frac{(\Delta p_0)_D}{\frac{1}{2}\rho c_2^2} = \frac{p_{02} - p_{03}}{\frac{1}{2}\rho c_2^2} \tag{11.29}$$

$$\xi_D = \frac{h_3 - h_{3s}}{\frac{1}{2}c_2^2} = \frac{2\,c_p\,(T_3 - T_{3s})}{c_2^2} \tag{11.30}$$

11.2.1 Efficiencies

The efficiency of the compression process can now be defined on the basis of ideal (isentropic) and actual (adiabatic) processes defined in the previous section.

The ideal work in the stage is

$$w_s = h_{03ss} - h_{01} = c_p\,(T_{03ss} - T_{01}) \tag{11.31}$$

This is the minimum value of the stage work required to obtain a static pressure rise of $(\Delta p)_{st} = p_3 - p_1$

However, the actual process, on account of losses and the associated irreversibilities, will require a larger magnitude of work for the same pressure rise. This is given by

$$w_a = h_{02} - h_{01} = h_{03} - h_{01} = c_p\,(T_{03} - T_{01}) \tag{11.32}$$

Thus the total-to-total efficiency of the stage is defined by

$$\eta_{tt} = \frac{\text{ideal stage work between total conditions at entry and exit}}{\text{actual stage work}}$$

$$\eta_{tt} = \frac{w_s}{w_a} = \frac{h_{03ss} - h_{01}}{h_{03} - h_{01}} = \frac{T_{03ss} - T_{01}}{T_{03} - T_{01}} \tag{11.33}$$

The magnitude of the stage work obtained from velocity triangles with actual velocities and air angles equals the actual work. Thus Eqs. (11.13) when put into Eq. (11.32) give

$$h_{03} - h_{01} = u\,(c_{y2} - c_{y1}) \tag{11.34a}$$

$$h_{03} - h_{01} = uc_x\,(\tan\alpha_2 - \tan\alpha_1) = uc_x\,(\tan\beta_1 - \tan\beta_2) \tag{11.34b}$$

$$h_{03} - h_{01} = \frac{1}{2}\,(c_2^2 - c_1^2) + \frac{1}{2}\,(w_1^2 - w_2^2) \tag{11.34c}$$

Similarly, the actual value of the loading coefficient in Eq. (11.14) is given by

$$\psi = \frac{h_{03} - h_{01}}{u^2} = \frac{c_p\,(T_{03} - T_{01})}{u^2} \tag{11.35}$$

Equation (11.33) when put into Eq. (11.35) gives

$$\psi = \frac{h_{03ss} - h_{01}}{u^2\,\eta_{tt}} = \frac{c_p\,(T_{03ss} - T_{01})}{u^2\,\eta_{tt}} \tag{11.36}$$

Equation (11.23) is not valid for an actual flow because

$$w > \frac{(\Delta p)_{st}}{\rho}$$

For isentropic (ideal) and incompressible flow, we have from Eq. (11.31)

$$\frac{(\Delta p)_{st}}{\rho} = w_s = h_{03ss} - h_{01} = c_p\,(T_{03ss} - T_{01}) \tag{11.37}$$

With the help of this equation the following relations for the stage efficiency are obtained:

$$\eta_{tt} = \frac{(\Delta p)_{st}}{\rho\,(h_{03} - h_{01})} \tag{11.37a}$$

$$\eta_{tt} = \frac{(\Delta p)_{st}}{\rho c_p\,(T_{03} - T_{01})} \tag{11.37b}$$

$$\eta_{tt} = \frac{(\Delta p)_{st}}{\rho u\,(c_{y2} - c_{y1})} \tag{11.37c}$$

The stage pressure rise $(\Delta p)_{st}$ can easily be measured on water or mercury manometers and the actual work input can be measured through torque measuring devices. Further insight into this aspect can be obtained from the energy flow diagram given in Fig. 11.9.

If the axial velocity through the stage remains constant, then for $\alpha_1 = \alpha_3$, $c_1 = c_3$

$$\begin{aligned} h_{03} - h_{01} &= h_3 - h_1 \\ T_{03} - T_{01} &= T_3 - T_1 \end{aligned} \tag{11.38}$$

These relations are also valid approximately for small values of c_1 and c_3. Similarly, for the isentropic process

$$\begin{aligned} h_{03ss} - h_{01} &= h_{3ss} - h_1 \\ T_{03ss} - T_{01} &= T_{3ss} - T_1 \end{aligned} \tag{11.39}$$

With the help of Eqs. (11.38) and (11.39), the efficiency of the compressor stage can be defined as a static-to-static efficiency.

$$\eta_{ss} = \frac{h_{3ss} - h_1}{h_3 - h_1} = \frac{T_{3ss} - T_1}{T_3 - T_1} \tag{11.40}$$

11.2.2 Degree of Reaction

The degree of reaction prescribes the distribution of the stage pressure rise between the rotor and the diffuser blade rows. This in turn determines the cascade losses in each of these blade rows. As in axial flow turbines (Sec. 9.5.2), the degree of reaction for axial compressors can also be defined in a number of ways; it can be expressed either in terms of enthalpies, pressures or flow geometry.

(a) For a reversible stage the degree of reaction is defined as

$$R = \frac{\text{isentropic change of enthalpy in the rotor}}{\text{isentropic change of enthalpy in the stage}}$$

From Fig. 11.2 this gives

$$R = \frac{\int_1^{2s} dh}{\int_1^{3ss} dh} = \frac{h_{2s} - h_1}{h_{3ss} - h_1} \tag{11.41}$$

For isentropic flow $dh = \frac{dp}{\rho}$; therefore,

$$R = \frac{\int_1^{2s} \frac{dp}{\rho}}{\int_1^{3ss} \frac{dp}{\rho}}$$

For relatively small pressure changes flow can be assumed incompressible, i.e. $\rho \approx$ constant.

$$R = \frac{\int_1^{2s} dp}{\int_1^{3ss} dp}$$

$$R = \frac{p_2 - p_1}{p_3 - p_1} \tag{11.42}$$

In compressor applications pressures are of greater interest. Therefore, in practice the degree of reaction is more frequently defined in terms of pressures which are generally known.

(b) For a real or actual compressor stage the degree of reaction is defined as

$$R = \frac{\text{actual change of enthalpy in the rotor}}{\text{actual change of enthalpy in the stage}}$$

$$R = \frac{h_2 - h_1}{h_3 - h_1} = \frac{T_2 - T_1}{T_3 - T_1} \tag{11.43}$$

For $c_1 = c_3$, $h_3 - h_1 = h_{03} - h_{01} = u\,(c_{y2} - c_{y1})$

Equation (11.25) gives

$$h_2 - h_1 = \frac{1}{2}\,(w_1^2 - w_2^2)$$

These relations when used in Eq. (11.43) give

$$R = \frac{h_2 - h_1}{h_{03} - h_{01}} \tag{11.44a}$$

$$R = \frac{w_1^2 - w_2^2}{2u(c_{y2} - c_{y1})} \tag{11.44b}$$

This expression can be further expressed in terms of air angles.

$$R = \frac{c_x^2\,(\tan^2 \beta_1 - \tan^2 \beta_2)}{2uc_x\,(\tan \beta_1 - \tan \beta_2)}$$

$$R = \frac{1}{2}\left(\frac{c_x}{u}\right)(\tan \beta_1 + \tan \beta_2) \tag{11.44c}$$

But $\dfrac{c_x}{u} = \phi$ and $\dfrac{1}{2}\,(\tan \beta_1 + \tan \beta_2) = \tan \beta_m$

Therefore,

$$R = \phi \tan \beta_m \tag{11.44d}$$

Equation (11.44c) can be rearranged to give

$$R = \frac{1}{2}\left(\frac{c_x}{u}\right)\{(\tan \beta_1 + \tan \alpha_1) - (\tan \alpha_1 - \tan \beta_2)\}$$

From Eq. (11.11)

$$\tan \beta_1 + \tan \alpha_1 = \frac{u}{c_x}$$

Therefore,

$$R = \frac{1}{2} - \frac{1}{2}\left(\frac{c_x}{u}\right)(\tan \alpha_1 - \tan \beta_2) \tag{11.45}$$

This is a useful relation in terms of the geometry of flow and can be used to study the effect of air angles and the required cascade geometry (to provide these air angles) on the degree of reaction of an axial compressor stage.

11.2.3 Low Reaction Stages

A low reaction stage has a lesser pressure rise in its rotor compared to that in the diffuser, i.e. $(\Delta p)_R < (\Delta p)_D$. In such a stage, the quantity ($\tan \alpha_1 - \tan \beta_2$) is positive or, in other words, $\alpha_1 > \beta_2$ [Fig. 11.1b and Eq. (11.45)]. The same effect can be explained in another manner. In Eq. (11.45).

$$c_x \tan \alpha_1 = c_{y1} = u - w_{y1}$$

$$c_x \tan \beta_2 = w_{y2} = u - c_{y2}$$

Therefore, after substituting these values in Eq. (11.45)

$$R = \frac{1}{2} - \frac{1}{2}\left(\frac{c_{y1}}{u} - \frac{w_{y2}}{u}\right) \tag{11.46}$$

$$R = \frac{1}{2} - \frac{1}{2u}(c_{y2} - w_{y1}) \tag{11.47}$$

This equation relates the degree of reaction to the magnitudes of swirl or the whirl components approaching the rotor and the diffuser. Thus a low degree of reaction is obtained when the rotor blade rows remove less swirl compared to the diffuser blade rows, i.e.

$$w_{y1} < c_{y2}$$

Figure 11.3 shows the enthalpy–entropy diagram for such a stage. The swirl removing ability of a blade row is reflected in the static pressure rise across it.

In a low-degree reaction stage the diffuser blade rows are burdened by a comparatively larger static pressure rise which is not desirable for obtaining higher efficiencies.

11.2.4 Fifty Per Cent Reaction Stages

One of the ways to reduce the burden of a large pressure rise in a blade row is to divide the stage pressure rise equally between the rotor and diffuser. To approach this condition (Fig. 11.4).

$$h_2 - h_1 = h_3 - h_2 = \frac{1}{2}(h_3 - h_1) \tag{11.48}$$

This when put in Eq. (11.43) gives

$$R = \frac{1}{2} \text{ (fifty per cent reaction)}$$

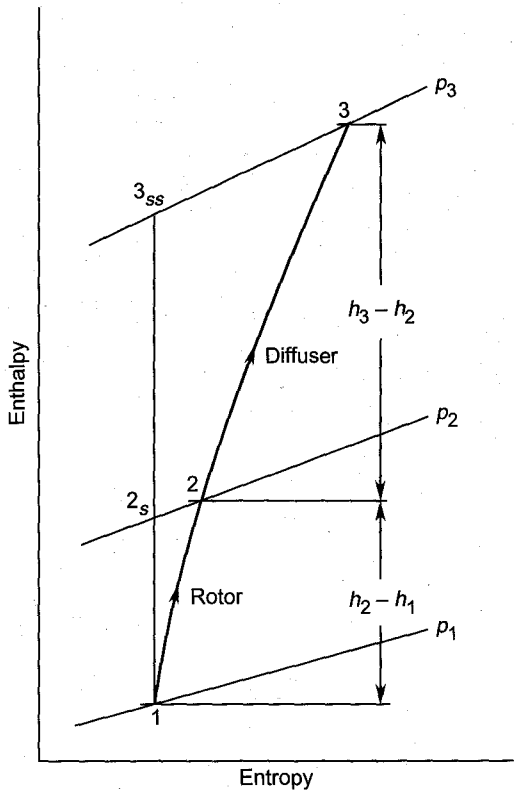

Fig. 11.3 Enthalpy-entropy diagram for flow through a low reaction stage ($R < \frac{1}{2}$)

Equation (11.44b) for $R = \dfrac{1}{2}$ gives

$$\frac{1}{2} = \frac{w_1^2 - w_2^2}{2u\,(c_{y2} - c_{y1})}$$

Substituting from Eq. (11.13c)

$$w_1^2 - w_2^2 = \frac{1}{2}\,(c_2^2 - c_1^2) + \frac{1}{2}\,(w_1^2 - w_2^2)$$

$$w_1^2 - w_2^2 = c_2^2 - c_1^2 \tag{11.49}$$

For $R = \dfrac{1}{2}$, Eq. (11.45) gives

$$\alpha_1 = \beta_2 \tag{11.50a}$$

This when substituted in Eq. (11.11) gives

$$\alpha_2 = \beta_1 \tag{11.50b}$$

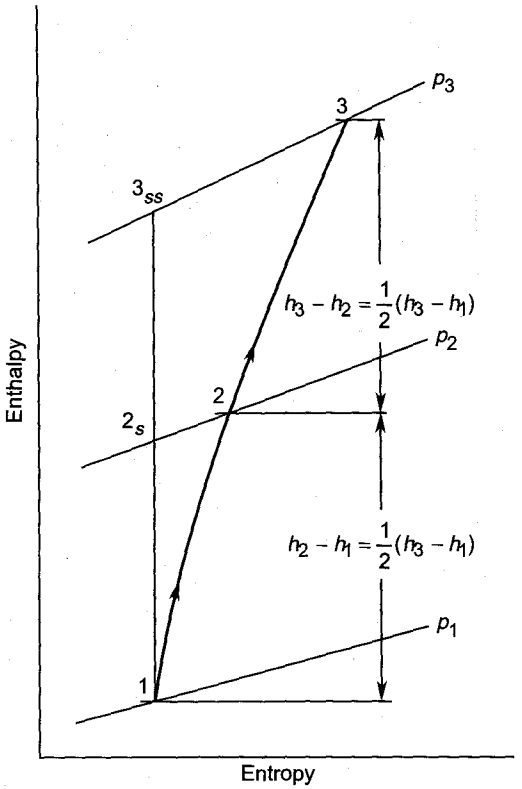

Fig. 11.4 Enthalpy-entropy diagram for a fifty per cent reaction stage

Equation (11.50) along with Eq. (11.49) yield

$$w_1 = c_2$$
$$w_2 = c_1 \tag{11.51}$$

These relations show that the velocity triangles at the entry and exit of the rotor of a fifty per cent reaction stage are symmetrical; these have been shown in Fig. 1.17. The whirl or swirl components at the entries of the rotor and diffuser blade rows are also same.

$$c_{y1} = w_{y2}$$
$$w_{y1} = c_{y2} \tag{11.52}$$

11.2.5 High Reaction Stages

The static pressure rise in the rotor of a high reaction stage is larger compared to that in the diffuser, i.e. $(\Delta p)_R > (\Delta p)_D$. For such a stage the quantity (tan α_1 – tan β_2) in Eq. (10.45) is negative, giving $R > \frac{1}{2}$.

Therefore, for such a stage

$$\beta_2 > \alpha_1$$

$$w_{y1} > c_{y2}$$

Figure 11.5 shows the velocity triangles for such a stage. It can be observed that the rotor blade row generates a higher static pressure on account of the larger magnitude of the swirl component w_{y1} at its entry. The swirl component (c_{y2}) passed on to the diffuser blade row is relatively smaller, resulting in a lower static pressure rise therein.

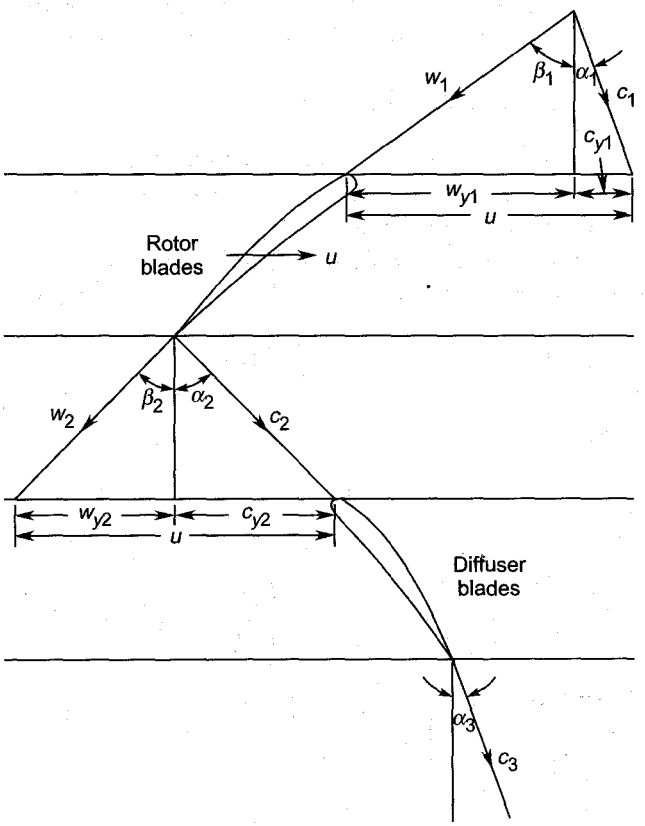

Fig. 11.5 High reaction stage ($R > \frac{1}{2}$, $\alpha_1 < \beta_2$)

Since the rotor blade rows have relatively higher efficiencies, it is advantageous to have a slightly greater pressure rise in them compared to the diffuser.

A further discussion on the various degrees of reaction of the axial fan stages has been given in Chapter 14.

11.3 Flow Through Blade Rows

After studying the geometry and thermodynamics of the flow through a compressor stage, further insight can be obtained by looking at the flow in the individual blade rows. Therefore, the two parts of the h–s diagram in Fig. 11.2 (for the stage) are redrawn in Figs. 11.6 and 11.7. The similarity between these diagrams must be noted.

Some aspects of incompressible and compressible flow through diffusers have already been discussed in Sec. 2.4.

The flow over a small pressure rise can be considered incompressible, i.e. density can be assumed to remain constant with little sacrifice in accuracy.

11.3.1 Rotor Blade Row

The flow process as observed by an observer sitting on the rotor is depicted in Fig. 11.6. The initial and final pressures are p_1 and p_2 for both isentropic and adiabatic processes.

In the isentropic process the flow will diffuse to a velocity w_{2s} giving the stagnation enthalpy and pressure as $h_{01\text{rel}}$ and $p_{01\text{rel}}$ respectively.

$$h_{2s} - h_1 = \frac{1}{\rho}(p_2 - p_1) = \frac{1}{\rho}(\Delta p)_R \tag{11.53}$$

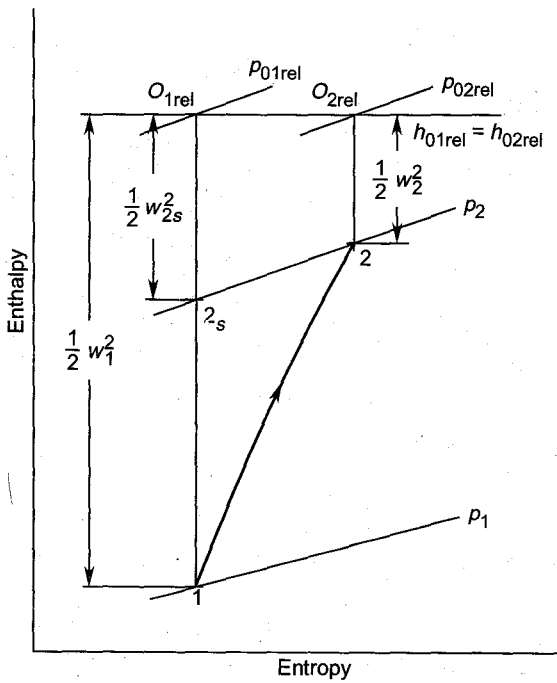

Fig. 11.6 Enthalpy-entropy diagram for flow through rotor blade row

The actual process gives the final velocity w_2 and stagnation pressure $p_{02\text{rel}}$. Here the same static pressure rise $(\Delta p)_R$ occurs with a greater change in the kinetic energy $\frac{1}{2}(w_1^2 - w_2^2)$. In the ideal or isentropic process this is

$$\frac{1}{2}(w_1^2 - w_{2s}^2) < \frac{1}{2}(w_1^2 - w_2^2)$$

This difference is due to the losses and the increase in entropy.

The efficiency of the rotor blade row can now be defined by

$$\eta_R = \frac{h_{2s} - h_1}{h_2 - h_1} = \frac{(h_2 - h_1) - (h_2 - h_{2s})}{h_2 - h_1}$$

$$\eta_R = 1 - \frac{h_2 - h_{2s}}{h_2 - h_1} \tag{11.54}$$

Assuming perfect gas and substituting from Eq. (11.27)

$$\eta_R = 1 - \frac{w_1^2}{2c_p(T_2 - T_1)}\,\xi_R \tag{11.55a}$$

$$\eta_R = 1 - \xi_R \Big/ \left(1 - \frac{w_2^2}{w_1^2}\right) \tag{11.55b}$$

The assumption of incompressible flow is not required in Eqs. (11.54) and (11.55)

$$h_2 - h_{2s} = (h_2 - h_1) - (h_{2s} - h_1)$$

For incompressible flow, substituting from Eq. (11.53)

$$h_2 - h_{2s} = \frac{1}{2}(w_1^2 - w_2^2) - \frac{1}{\rho}(p_2 - p_1)$$

$$h_2 - h_{2s} = \frac{1}{\rho}\left\{\left(p_1 + \frac{1}{2}\rho w_1^2\right) - \left(p_2 + \frac{1}{2}\rho w_2^2\right)\right\}$$

$$h_2 - h_{2s} = \frac{1}{\rho}(p_{01\text{rel}} - p_{02\text{rel}}) = \frac{(\Delta p_0)_R}{\rho} \tag{11.56}$$

Substituting this in Eq. (11.54)

$$\eta_R = 1 - \frac{(\Delta p_0)_R}{\rho(h_2 - h_1)} \tag{11.57a}$$

Substitution from Eq. (11.26) gives

$$\eta_R = 1 - Y_R \Big/ \left(1 - \frac{w_2^2}{w_1^2}\right) \tag{11.57b}$$

11.3.2 Stator Blade Row

The ideal and actual flow processes occurring in the diffuser blade row are shown in Fig. 11.7. Its efficiency is again defined as for the rotor blade row.

$$\eta_D = \frac{h_{3s} - h_2}{h_3 - h_2} = \frac{(h_3 - h_2) - (h_3 - h_{3s})}{h_3 - h_2}$$

$$\eta_D = 1 - \frac{h_3 - h_{3s}}{h_3 - h_2} \tag{11.58}$$

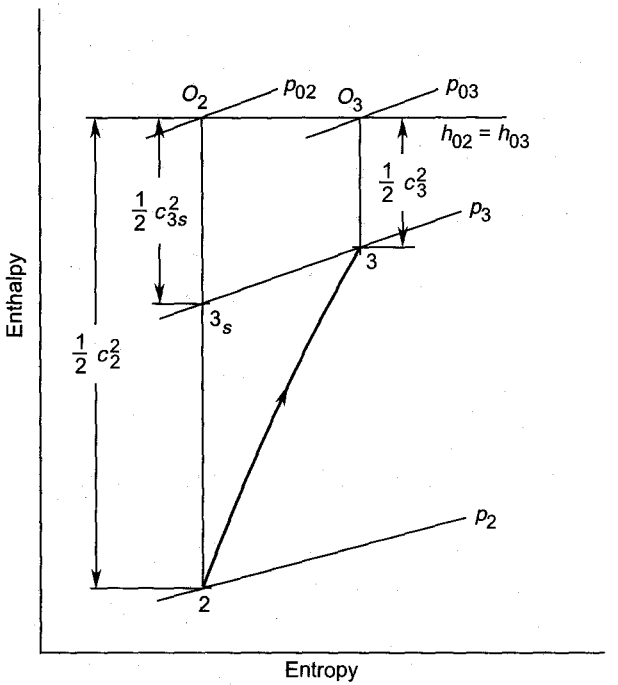

Fig. 11.7 Enthalpy-entropy diagram for flow through diffuser (stator) blade row

Substituting in terms of the enthalpy loss coefficient

$$\eta_D = 1 - \frac{c_2^2}{2c_p\,(T_3 - T_2)}\,\xi_D \tag{11.59a}$$

$$\eta_D = 1 - \xi_D \Big/ \left(1 - \frac{c_3^2}{c_2^2}\right) \tag{11.59b}$$

For incompressible flow,

$$h_3 - h_{3s} = \frac{1}{\rho}\,(p_{02} - p_{03}) = \frac{(\Delta p_0)_D}{\rho} \tag{11.60}$$

Therefore, the diffuser efficiency can be expressed in terms of the diffuser stagnation pressure loss coefficient

$$\eta_D = 1 - \frac{(\Delta p_0)_D}{\rho\,(h_3 - h_2)} \tag{11.61a}$$

$$\eta_D = 1 - Y_D \Big/ \left(1 - \frac{c_3^2}{c_2^2}\right) \tag{11.61b}$$

11.4 Stage Losses and Efficiency

Losses occurring in axial turbine and compressor cascades have been discussed in Chapter 8. Some methods of estimating these losses for compressor blade rows are given in Sec. 8.5.6. In a complete compressor, stage losses due to bearing and disc friction (shaft losses) also occur.

Cascade losses[391] depend on a number of aerodynamic and cascade geometrical parameters. Figure 11.8 shows the variation of exit air angles and losses with Reynolds number. It is observed that beyond the Reynolds number of 2×10^5, the variations are not significant.

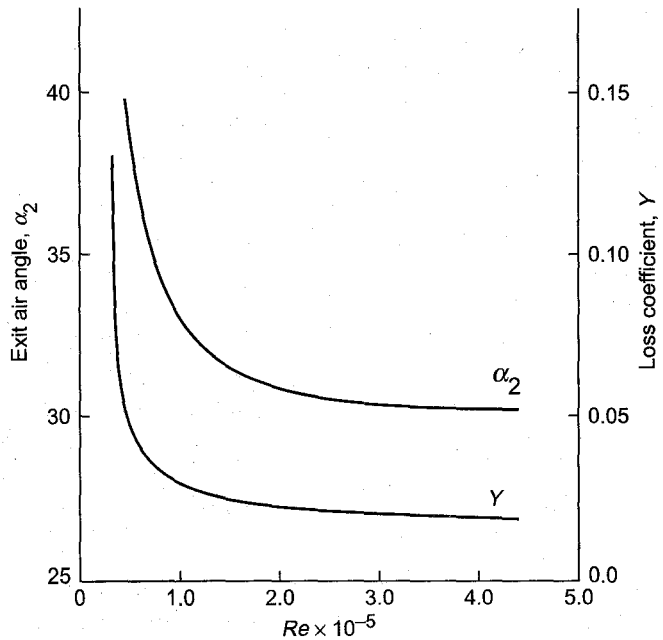

Fig. 11.8 Typical variation of exit air angles and cascade losses with Reynolds number

Figure 11.9 shows the energy flow diagram for an axial compressor stage. Figures in the brackets indicate the order of energy or loss corresponding to 100 units of energy supplied at the shaft.

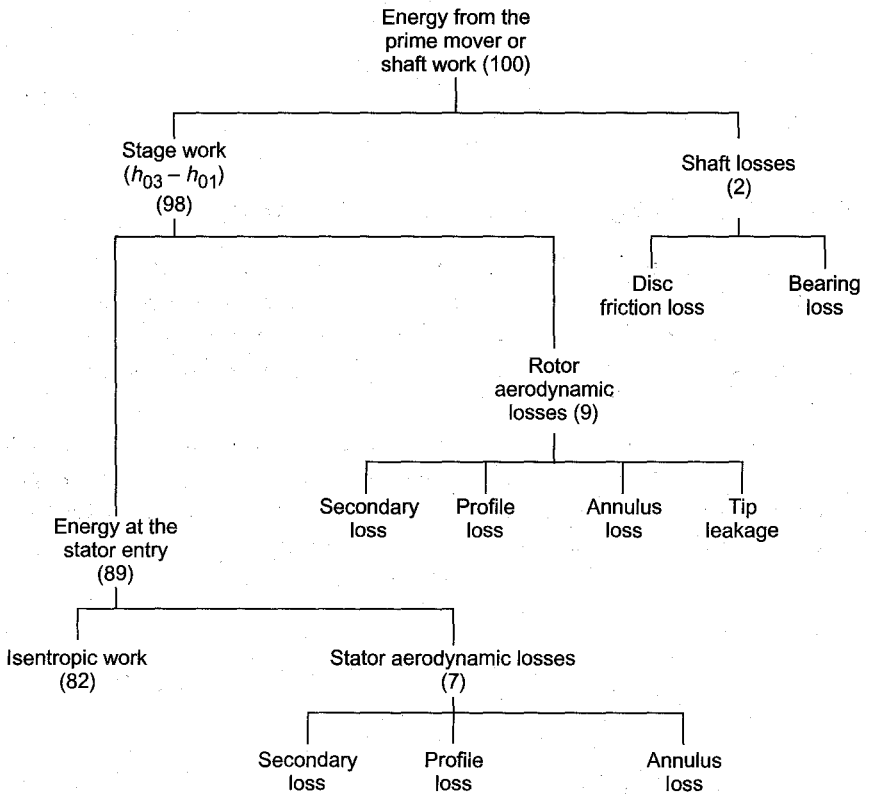

Fig. 11.9 Energy flow diagram for an axial flow compressor stage

The stage work ($h_{03} - h_{01}$) is less than the energy supplied to the shaft by the prime mover on account of bearing and disc friction losses. All the stage work does not appear as energy at the stator entry on account of aerodynamic losses in the rotor blade row. After deducting the stator (diffuser) blade row losses from the energy at its entry, the value of the ideal or isentropic work required to obtain the stage pressure rise is obtained.

The cascade losses in the rotor and stator would depend on the degree of reaction. The values shown in the the energy flow diagram are only to give an example. The ratio of the isentropic work (82) and the actual stage work (98) gives the stage efficiency, whereas the overall efficiency is directly obtained as 82%.

11.4.1 Stage Losses

It is seen from Figs. 11.2 and 11.9 that stage losses are made up of the cascade losses (see Sec. 11.2) occurring in the rotor and diffuser blade rows. The loss coefficients (Y or ξ) are proportional to the square of the entry velocities.

For incompressible flow over compressor blade rows, the pressure loss coefficient is determined by cascade tests. As stated in Sec. 9.5.1, the pressure loss coefficient (Y) can be taken as equal to the enthalpy loss coefficient (ξ) for a majority of cases.

The losses in the rotor and diffuser blade rows are now determined from Fig. 11.2 using Eqs. (11.26) and (11.27).

The slopes of the constant pressure lines p_2 and p_3 with some approximation are given by

$$\frac{h_2 - h_{2s}}{\Delta s} = T_2 \tag{11.62}$$

$$\frac{h_{3s} - h_{3ss}}{\Delta s} = T_3 \tag{11.63}$$

Eliminating Δs from these equations

$$h_{3s} - h_{3ss} = \frac{T_3}{T_2}\,(h_2 - h_{2s})$$

Substituting from Eq. (11.27)

$$h_{3s} - h_{3ss} = \frac{T_3}{T_2}\,\xi_R\,\frac{1}{2}\,w_1^2 \tag{11.64}$$

From Eq. (11.30)

$$h_3 - h_{3s} = \xi_D\,\frac{1}{2}\,c_2^2 \tag{11.65}$$

Assuming $c_3 \approx c_{3ss}$

$$h_{03} - h_{03ss} = h_3 - h_{3ss}$$

$$h_3 - h_{3ss} = (h_3 - h_{3s}) + (h_{3s} - h_{3ss})$$

Substituting from Eqs. (11.64) and (11.65)

$$h_3 - h_{3ss} = \xi_D\,\frac{1}{2}\,c_2^2 + \frac{T_3}{T_2}\,\xi_R\,\frac{1}{2}\,w_1^2 \tag{11.66a}$$

The stagnation state is represented by 0_{3ss} at the end of isentropic compression from pressure p_1 to p_3. However, due to stage losses, the actual state is represented by point 0_3 (Fig. 11.2). Therefore, the total stage losses are

$$h_{03} - h_{03s} = \xi_D\,\frac{1}{2}\,c_2^2 + \frac{T_3}{T_2}\,\xi_R\,w_1^2 \tag{11.66b}$$

11.4.2 Stage Efficiency

The total-to-total stage efficiency ($\eta_{st} = \eta_{tt}$) is given by Eq. (11.33) as

$$\eta_{st} = \frac{h_{03ss} - h_{01}}{h_{03} - h_{01}} = \frac{(h_{03} - h_{01}) - (h_{03} - h_{03ss})}{h_{03} - h_{01}}$$

$$\eta_{st} = 1 - \frac{h_{03} - h_{03ss}}{h_{03} - h_{01}} \tag{11.67}$$

Equation (11.66b) when put into Eq. (11.67) yields

$$\eta_{st} = 1 - \frac{\xi_D\, c_2^2 + \dfrac{T_3}{T_2}\, \xi_R\, w_1^2}{2\,(h_{03} - h_{01})} \tag{11.68a}$$

From velocity triangles (Fig. 11.1b), for constant axial velocity

$$c_2 = c_x \sec \alpha_2$$

$$w_1 = c_x \sec \beta_1$$

These relations along with Eq. (11.34b) give

$$\eta_{st} = 1 - \frac{\xi_D\, c_x^2 \sec^2 \alpha_2 + \dfrac{T_3}{T_2}\, \xi_R\, c_x^2 \sec^2 \beta_1}{2u\, c_x\, (\tan \beta_1 - \tan \beta_2)}$$

$$\eta_{st} = 1 - \frac{1}{2}\, \phi\, \frac{\xi_D \sec^2 \alpha_2 + \left(\dfrac{T_3}{T_2}\right) \xi_R \sec^2 \beta_1}{\tan \beta_1 - \tan \beta_2} \tag{11.68b}$$

Similar expressions in terms of pressure loss coefficients can also be derived using Eqs. (11.56) and (11.60).

$$h_2 - h_{2s} = \frac{(\Delta p_0)_R}{\rho} = \frac{1}{2}\, Y_R\, w_1^2 \tag{11.69a}$$

$$h_{3s} - h_{3ss} = \frac{T_3}{T_2}\, (h_2 - h_{2s}) = \frac{1}{2}\left(\frac{T_3}{T_2}\right) Y_R\, w_1^2 \tag{11.69b}$$

$$h_3 - h_{3s} = \frac{(\Delta p_0)_D}{\rho} = \frac{1}{2}\, Y_D\, c_2^2 \tag{11.70}$$

Therefore, the total stage losses are

$$h_{03} - h_{03ss} = \frac{1}{2}\, Y_D\, c_2^2 + \frac{1}{2}\left(\frac{T_3}{T_2}\right) Y_R\, w_1^2 \tag{11.71}$$

$$h_{03} - h_{03ss} = \frac{1}{2}\, c_x^2 \left(Y_D \sec^2 \alpha_2 + \frac{T_3}{T_2}\, Y_R \sec^2 \beta_1\right) \tag{11.72}$$

These equations when substituted in Eq. (11.67) yield

$$\eta_{st} = 1 - \frac{Y_D\, c_2^2 + \dfrac{T_3}{T_2}\, Y_R\, w_1^2}{2\,(h_{03} - h_{01})} \tag{11.73}$$

$$\eta_{st} = 1 - \frac{1}{2}\,\phi\, \frac{Y_D \sec^2 \alpha_2 + \dfrac{T_3}{T_2}\, Y_R \sec^2 \beta_1}{\tan \beta_1 - \tan \beta_2} \tag{11.74}$$

For a given geometry of the stage and flow conditions, the values of the air angles α_2, β_1 and β_2 and the loss coefficients Y_D and Y_R can be determined from cascade tests. Alternatively, these values can also be determined by empirical correlations.

11.5 Work Done Factor[412,413]

Owing to secondary flows and the growth of boundary layers on the hub and casing of the compressor annulus, the axial velocity along the blade height is far from uniform. This effect is not so prominent in the first stage of a multi-stage machine but is quite significant in the subsequent stages. Figure 11.10 depicts the axial velocity distributions in the first and last stages of a multistage axial compressor. The degrees of distortion in the axial velocity distributions will depend on the number of the stage (1st, 2nd, ..., 14th, etc.). On account of this, the axial velocity in the hub and tip regions is much less than the mean value, whereas in the central region its value is higher than the mean.

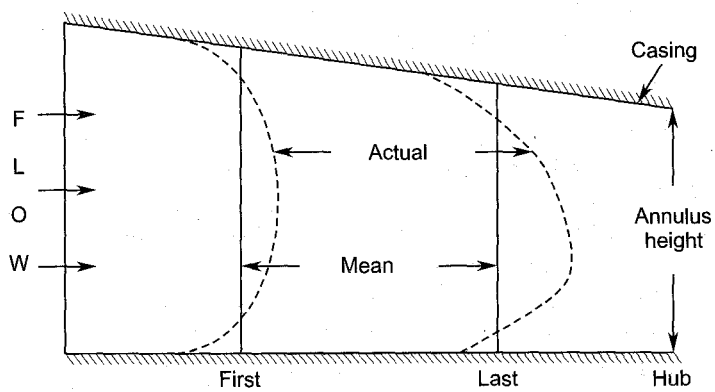

Fig. 11.10 Axial velocity distributions along the blade heights in the first and last blade rows of a multi-stage compressor (typical curves)

The effect of this phenomenon on the work absorbing capacity of the stages can be studied through Eq. (11.13b):

$$w = uc_x (\tan \beta_1 - \tan \beta_2)$$

$$w = u \{c_x (\tan \alpha_1 + \tan \beta_1) - c_x (\tan \alpha_1 + \tan \beta_2)\}$$

Substituting from Eq. (11.11)

$$w = u \{u - c_x (\tan \alpha_1 + \tan \beta_2)\} \tag{11.75}$$

The air angles β_2 and α_1 are fixed by the cascade geometry of the rotor blades and the upstream blade row. Therefore, assuming $(\tan \alpha_1 + \tan \beta_2)$ and u as constant, Eq. (11.75) relates work to the axial velocity at various sections along the blade height.

The velocity triangles of Fig. 11.1b are redrawn in Fig. 11.11 for the design value (mean value shown in Fig. 11.10), and the reduced $(c_x - \Delta c_x)$ and increased $(c_x + \Delta c_x)$ values of the axial velocity.

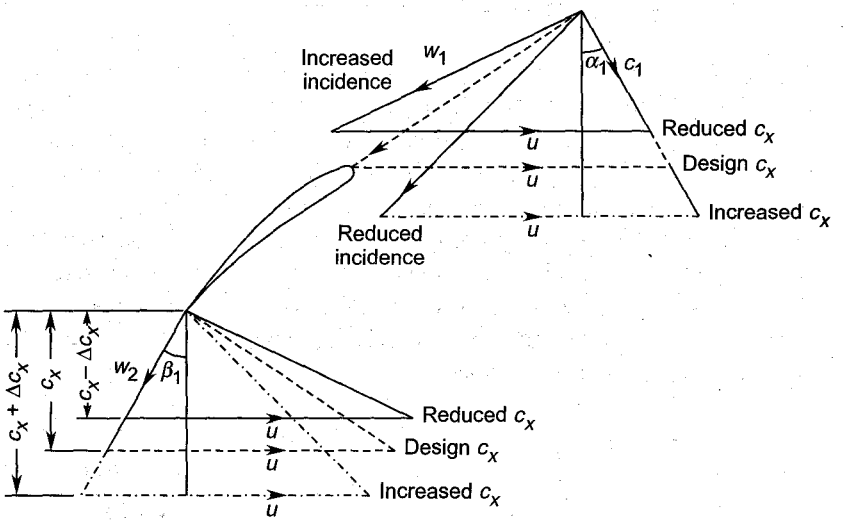

Fig. 11.11 Effect of axial velocity on the stage velocity triangles and the work

It may be seen from the velocity triangles that the work (Eqs. (11.13a) and (11.75)) decreases with an increase in the axial velocity and vice versa. Therefore, the work capacity of the stage is reduced in the central region of the annulus and increased in the hub and tip regions. However, the expected increase in the work at the hub and tip is not obtained in actual practice on account of higher losses. Therefore, the net result is that the stage work is less than that given by Euler's equation based on a constant value of the axial velocity along the blade height. This reduction in the work absorbing capaciaty of the stage is taken into account by a "workdone factor" Ω. This varies from 0.98 to 0.85 depending on the

number of stages. Therefore, the work expressions in Eqs. (11.34a) and (11.34b) are modified to

$$h_{03} - h_{01} = \Omega\, u\, (c_{y2} - c_{y1}) \tag{11.76a}$$

$$h_{03} - h_{01} = \Omega\, u\, c_x (\tan\, \alpha_2 - \tan\, \alpha_1)$$

$$= \Omega\, u\, c_x (\tan\, \beta_1 - \tan\, \beta_2) \tag{11.76b}$$

Figure 11.12 gives the mean values of the work-done factor[413] to be used for each stage in a given number of stages (shown on the X-axis).

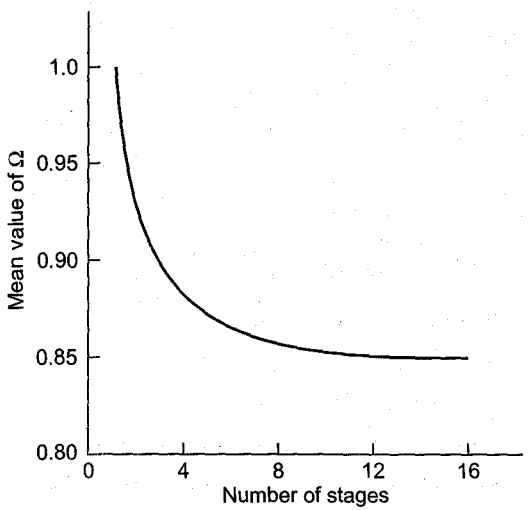

Fig. 11.12 Variation of work-done factor with number of stages of axial flow compressor (from Howell and Bonham[413], by conurtesy of the Instn. Mech. Engrs. London)

11.6 Low Hub-Tip Ratio Stages

For higher flow rates, the cross-sectional area of the low pressure stage in axial compressors must be large. This requires relatively larger mean diameters and blade heights leading to hub-tip ratios (d_h/d_t) much below unity (see Sec. 9.9).

The variation of various flow parameters in the radial direction (along the blade height) in such stages are significant and depend on the conditions imposed in their design. Some of these designs including the radial equilibrium (Sec. 9.9.1) and free vortex (Sec. 9.9.2) are discussed in the following sections.

11.6.1 Radial Equilibrium

Flow through turbine blade rows with radial equilibrium has already been discussed in Sec. 9.9.1. Equation (9.109b) is equally applicable to

compressor blade rows. However, for further understanding this equation is derived here in a different manner.

From Euler's momentum equation (6.46) for $c_r = 0$,

$$\frac{1}{\rho}\frac{dp}{dr} = \frac{c_\theta^2}{r} \tag{11.77}$$

For isentropic incompressible flow,

$$p_0 = p + \frac{1}{2}\rho c^2 = p + \frac{1}{2}\rho (c_r^2 + c_\theta^2 + c_x^2)$$

For radial equilibrium ($c_r = 0$)

$$p_0 = p + \frac{1}{2}\rho (c_\theta^2 + c_x^2) \tag{11.78}$$

$$\frac{dp_0}{dr} = \frac{dp}{dr} + \frac{1}{2}\rho \frac{d}{dr}(c_\theta^2 + c_x^2)$$

$$\frac{1}{\rho}\frac{dp_0}{dr} = \frac{1}{\rho}\frac{dp}{dr} + c_\theta \frac{dc_\theta}{dr} + c_x \frac{dc_x}{dr}$$

Substituting from Eq. (11.77)

$$c_\theta \frac{dc_\theta}{dr} + c_x \frac{dc_x}{dr} + \frac{c_\theta^2}{r} = \frac{1}{\rho}\frac{dp_0}{dr} \tag{11.79a}$$

For some conditions in the flow through compressor blade rows, the stagnation pressure can be assumed constant along the blade height, i.e.

$$\frac{dp_0}{dr} = 0$$

This condition when applied in Eq. (11.79a) gives

$$c_\theta \frac{dc_\theta}{dr} + c_x \frac{dc_x}{dr} + \frac{c_\theta^2}{r} = 0 \tag{11.79b}$$

This can be reduced to the following form:

$$\frac{1}{r^2}\frac{d}{dr}(rc_\theta)^2 + \frac{d}{dr}(c_x)^2 = 0 \tag{11.79c}$$

11.6.2 Free Vortex Flow

A free vortex turbine stage was discussed in Sec. 9.9.2. Compressor stages have also been designed for free vortex flow. This condition requires rc_θ = constant. Therefore, Eq (11.79c) gives

$$\frac{d}{dr}(c_x)^2 = 0$$

c_x = constant along the blade height

$$c_{x1h} = c_{x1t} = c_{x1m} = c_{x1} \tag{11.80a}$$

$$c_{x2h} = c_{x2t} = c_{x2m} = c_{x2} \tag{11.80b}$$

The variations of the tangential velocity components c_{θ_1} and c_{θ_2} are governed by the following relations:

$$r_h\, c_{\theta_1 h} = r_t c_{\theta_1 t} = r_m c_{\theta_1 m} = C_1 \tag{11.81a}$$

$$r_h\, c_{\theta_2 h} = r_t c_{\theta_2 t} = r_m c_{\theta_2 m} = C_2 \tag{11.81b}$$

Constants C_1 and C_2 are known from the mean section velocity triangles.

Air angles

The above relations for a free vortex stage can give air angles shown in Fig. 11.1b. Here $c_{y1} = c_{\theta 1}$ and $c_{y2} = c_{\theta 2}$.

Rotor entry

$$\tan \alpha_{1h} = \frac{c_{\theta 1h}}{c_{x1h}} = \frac{C_1}{r_h c_x} \tag{11.82a}$$

From Eq. (11.11)

$$\tan \beta_{1h} = \frac{u_h}{c_x} - \tan \alpha_{1h}$$

$$\tan \beta_{1h} = \frac{u_h}{c_x} - \frac{C_1}{r_h c_x} \tag{11.82b}$$

Similarly, for the tip section

$$\tan \alpha_{1t} = \frac{c_{\theta_1 t}}{c_{x_1 t}} - \frac{C_1}{r_t c_x} \tag{11.83a}$$

$$\tan \beta_{1t} = \frac{u_t}{c_x} - \frac{C_1}{r_t c_x} \tag{11.83b}$$

Rotor exit

$$\tan \alpha_{2h} = \frac{c_{\theta_2 h}}{c_{x_2}} = \frac{C_2}{r_h c_x} \tag{11.84a}$$

From Eq. (11.11)

$$\tan \beta_{2h} = \frac{u_h}{c_x} - \tan \alpha_{2h}$$

$$\tan \beta_{2h} = \frac{u_h}{c_x} - \frac{C_2}{r_h c_x} \tag{11.84b}$$

$$\tan \alpha_{2t} = \frac{c_{\theta_2 t}}{c_x} = \frac{C_2}{r_t c_x} \tag{11.85a}$$

$$\tan \beta_{2t} = \frac{u_t}{c_x} - \frac{C_2}{r_t c_x} \tag{11.85b}$$

Specific work

The work done per kilogram of the flow at a given radial section ($r = r$) is given by Eq. (11.13a)

$$w = h_{02} - h_{01} = u\,(c_{\theta_2} - c_{\theta_1})$$

Equation (11.81) gives

$$w = \omega r \left(\frac{C_2}{r} - \frac{C_1}{r}\right)$$

$$w = h_{02} - h_{01} = \omega\,(C_2 - C_1) = \text{const.} \tag{11.86}$$

Degree of reaction

Since the air angles in the stage are varying along the blade height, the degree of reaction must also vary. Substituting from Eqs. (11.82b) and (11.84b) in Eq. (11.44c)

$$R = \frac{1}{2}\left(\frac{c_x}{u}\right)\left(\frac{u}{c_x} - \frac{C_1}{rc_x} + \frac{u}{c_x} - \frac{C_2}{rc_x}\right)$$

$$R = 1 - \frac{C_1 + C_2}{2ur} = 1 - \frac{C_1 + C_2}{2\omega r^2} \tag{11.87}$$

If
$$K = \frac{C_1 + C_2}{2\omega} \tag{11.88}$$

$$R = 1 - \frac{K}{r^2} \tag{11.89}$$

This shows that the stage reaction in a free vortex design increases along the blade height.

Figure 11.13 shows the variation of air angles and degree of reaction along the blade height in a free vortex stage.

11.6.3 Forced Vortex Flow

In a forced vortex flow through the stage the tangential velocity component is directly proportional to the radius.

$$\frac{c_\theta}{r} = \text{const.} = C \tag{11.90}$$

This when used in the radial equilibrium flow equation (11.79c) gives

$$\frac{1}{r^2}\frac{d}{dr}\,(Cr^2)^2 + \frac{d}{dr}\,(c_x)^2 = 0$$

This on simplification yields

$$d(c_x)^2 = -\,4C^2\,r\,dr$$

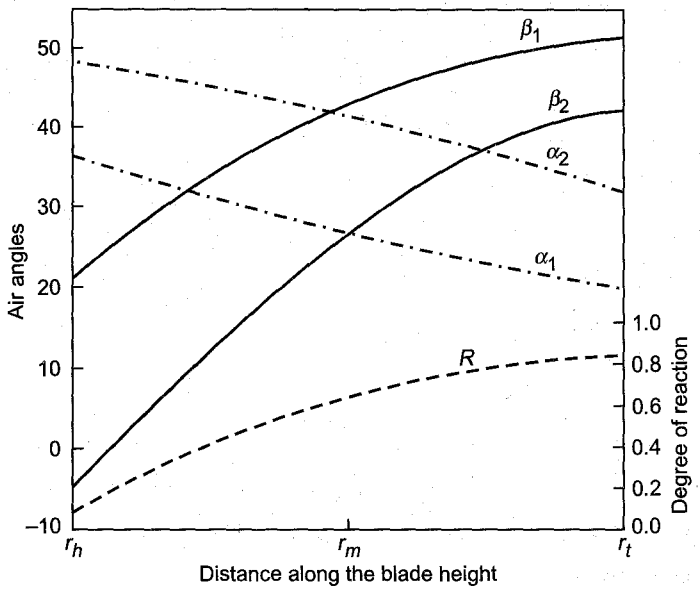

Fig. 11.13 Variation of air angles and degree of reaction along the blade height in a free-vortex stage

After integration and applying it at the rotor entry

$$c_{x1}^2 = K_1 - 2\ C_1^2\ r^2 \tag{11.91}$$

Constants C_1 and K_1 are known from conditions at the mean radius (r_m).

$$\frac{c_{\theta_1}}{r} = \frac{c_{\theta_1 h}}{r_h} = \frac{c_{\theta_1 t}}{r_t} = \frac{c_{\theta_1 m}}{r_m} = C_1 \tag{11.92}$$

$$K_1 = c_{x1m}^2 + 2C_1^2 r_m^2 \tag{11.93}$$

Thus, with known distribution of the quantities u, c_x and c_θ at the rotor entry, the velocity triangles and hence the air angles α_1 and β_1 along the blade height are known.

At the rotor exit,

$$\frac{c_{\theta_2}}{r} = \frac{c_{\theta_2 h}}{r_h} = \frac{c_{\theta_2 t}}{r_t} = \frac{c_{\theta_2 m}}{r_m} = C_2 \tag{11.94}$$

Therefore, the specific work done along the blade height is given by

$$w = h_{02} - h_{01} = \omega r\ (c_{\theta_2} - c_{\theta_1})$$

$$w = h_{02} - h_{01} = (C_2 - C_1)\ \omega r^2 \tag{11.95}$$

Now an expression (similar to (Eq. 11.91)) for the axial velocity distribution at the rotor exit can be derived assuming h_{01} = constant.

For radial equilibrium conditions,

$$c_\theta \frac{dc_\theta}{dr} + c_x \frac{dc_x}{dr} + \frac{c_\theta^2}{r} = \frac{dh_0}{dr}$$

This can be written as

$$\frac{1}{2}\frac{1}{r^2}\frac{d}{dr}(rc_\theta)^2 + \frac{1}{2}\frac{d}{dr}(c_x)^2 = \left(\frac{dh_0}{dr}\right)_2 \tag{11.96}$$

From Eq. (11.95)

$$\left(\frac{dh_0}{dr}\right)_2 = 2(C_2 - C_1)\,\omega r \tag{11.97}$$

$$\frac{1}{r^2}\frac{d}{dr}(rc_\theta)^2 = \frac{1}{r^2}\frac{d}{dr}(C_2^2\, r^4) = 4\, C_2^2\, r \tag{11.98}$$

Equations (11.97) and (11.98) when substituted in Eq. (11.96) give

$$d(c_x)^2 = 4\,[(C_2 - C_1)\,\omega r - C_2^2\, r]\, dr$$

After integration

$$c_{x2}^2 = K_2 + 2(C_2 - C_1)\,\omega r^2 - 2\, C_2^2\, r^2 \tag{11.99}$$

The new constant (K_2) of integration can again be determined from the value of c_{x_2} at the mean radius.

$$K_2 = c_{x2m}^2 - 2(C_2 - C_1)\,\omega r_m^2 + 2\, C_2^2 r_m^2 \tag{11.100}$$

Equation (11.44c) for the degree of reaction cannot be used here because at a given section $c_{x_1} \neq c_{x_2}$.

11.6.4 General Swirl Distribution

Compressor blade rows have also been designed by prescribing a general distribution of the tangential (swirl or whirl) velocity component along the blade height. The general expression is

$$c_\theta = ar^n \pm \frac{b}{r}$$

At the rotor entry,

$$c_{\theta_1} = ar^n - \frac{b}{r} \tag{11.101}$$

At the rotor exit,

$$c_{\theta_2} = ar^n + \frac{b}{r} \tag{11.102}$$

The specific work is given by

$$w = u\,(c_{\theta 2} - c_{\theta 1})$$

Substituting from Eqs. (11.101) and (11.102)

$$w = h_{02} - h_{01} = 2\omega b \tag{11.103}$$

This shows that the specific work remians constant along the blade height.

Along with the above swirl distribution the axial velocity is assumed constant for writing down the expression for the degree of reaction.

From Eq. (11.44b) and Fig. 11.1b,

$$R = \frac{w_{\theta 1}^2 - w_{\theta 2}^2}{2u\,(c_{\theta 2} - c_{\theta 1})} = \frac{(w_{\theta 1} - w_{\theta 2})\,(w_{\theta 1} + w_{\theta 2})}{2u\,(c_{\theta 2} - c_{\theta 1})}$$

From Eq. (11.12a) or Fig. 11.1b),

$$w_{\theta 1} - w_{\theta 2} = c_{\theta 2} - c_{\theta 1}$$

Therefore,

$$R = \frac{w_{\theta 1} + w_{\theta 2}}{2u} \tag{11.104a}$$

$$R = \frac{u - c_{\theta 1} + u - c_{\theta 2}}{2u}$$

$$R = 1 - \frac{c_{\theta 1} + c_{\theta 2}}{2u} \tag{11.104b}$$

Substituting from Eqs. (11.101) and (11.102)

$$R = 1 - \frac{a}{\omega}\, r^{n-1} \tag{11.105}$$

This equation is only approximately valid because it will be seen in the following sections that the axial velocity across the rotor at a given section does not remain constant.

Two cases are considered here:

(i) $n = 0$

The degree of reaction from Eq. (11.105) is

$$R = 1 - \frac{a}{\omega r} \tag{11.106}$$

and increases along the blade height. The axial velocity distribution is obtained by applying Eq. (11.79c).

At the rotor entry,

$$(rc_{\theta 1})^2 = r^2 \left(a - \frac{b}{r}\right)^2 = a^2 r^2 - 2abr + b^2$$

$$\frac{d}{dr}\,(rc_{\theta 1})^2 = 2a^2 r - 2ab$$

Substituting this in Eq. (11.79c)

$$\frac{1}{r^2}\,(2a^2\,r - 2ab)\,dr = -\,d(c_{x1})^2$$

$$c_{x1}^2 = \text{const.} + 2a^2 \int \left(\frac{b}{ar^2} - \frac{1}{r}\right) dr$$

$$c_{x1}^2 = \text{const.} - 2a^2 \left(\frac{b}{ar} + \ln r\right) \qquad (11.107)$$

At the rotor exit

$$(rc_{\theta 2})^2 = r^2 \left(a + \frac{b}{r}\right)^2 = a^2r^2 + 2abr + b^2$$

$$\frac{d}{dr}\,(rc_{\theta 2})^2 = 2a^2r + 2ab$$

Substituting this in Eq. (11.79c)

$$\frac{1}{r^2}\,(2a^2r + 2ab)\,dr = -\,d(c_{x2})^2$$

$$c_{x2}^2 = \text{const.} - 2a^2 \left(\ln r - \frac{b}{ar}\right) \qquad (11.108)$$

(ii) $n = 1$

Equation (11.105) for this condition gives

$$R = 1 - \frac{a}{\omega} \qquad (11.109)$$

Thus a stage with constant reaction is obtained. However, this is only approximately true because here also $c_{x1} \neq c_{x2}$. The axial velocity distribution is given in the following sections:

At the rotor entry

$$(rc_{\theta 1})^2 = r^2 \left(ar - \frac{b}{r}\right)^2 = a^2r^4 - 2abr^2 + b^2$$

$$\frac{1}{r^2}\frac{d}{dr}\,(rc_{\theta 1})^2 = 4a^2r - 4\frac{ab}{r}$$

$$-\,d(c_{x1})^2 = 4a^2 \left(r - \frac{b}{ar}\right) dr$$

$$c_{x1}^2 = \text{const.} - 4a^2 \int \left(r - \frac{b}{ar}\right) dr$$

$$c_{x1}^2 = \text{const.} - 4a^2 \left(\frac{1}{2}\,r^2 - \frac{b}{a}\ln r\right) \qquad (11.110)$$

At the rotor exit

$$(rc_{\theta 2})^2 = r^2 \left(ar + \frac{b}{r}\right)^2 = a^2r^4 + 2abr^2 + b^2$$

$$\frac{1}{r^2}\frac{d}{dr}(rc_{\theta 2})^2 = 4a^2r + 4\frac{ab}{r}$$

$$d(c_{x2})^2 = -4a^2\left(r + \frac{b}{ar}\right)dr$$

$$c_{x2}^2 = \text{const.} - 4a^2\left(\frac{1}{2}r^2 + \frac{b}{a}\ln r\right) \qquad (11.111)$$

The values of the constants a and b can be determined by known values of $c_{\theta 1m}$ and $c_{\theta 2m}$ at the mean radius. Similarly, the constants in Eqs. (11.107), (11.108), (11.110) and (11.111) are determined from known values of c_{x1m} and c_{x2m}.

With known values of u, $c_{\theta 1}$, c_{x1}, $c_{\theta 2}$ and c_{x2}, the air angles α_1, β_1, α_2 and β_2 along the blade height can be determined.

11.7 Supersonic and Transonic Stages

Recent developments in materials and bearing design have made higher peripheral speeds (u $\approx$ 600 m/s) possible in compressors. Higher peripheral speeds lead to supersonic fluid velocities (relative or absolute) in the blade passages which can then be employed for compression through a shock (normal or oblique) over a small axial distance.

Supersonic flow [402, 424, 431] in axial compressor stages can also occur unintentionally due to local acceleration of the flow on the blade surfaces, generally on the suction side. This happens when the inlet Mach number is in the proximity of 0.75.

When a compressor stage is intentionally designed as supersonic, the flow is supersonic in some part or parts of the stage and a significant part of the static pressure rise is obtained by compression through shock waves. A shock wave is an irreversibility and leads to an increase in entropy and stagnation pressure loss. Therefore, supersonic compressors can provide a higher pressure ratio ($\approx$ 4 – 10) in a single stage with a relatively lower efficiency ($\approx$ 75%) on account of additional losses due to shocks.

Table 11.1 gives a clear picture of the orders of pressure rise and stagnation pressure loss for some representative values of the upstream Mach numbers.

The main advantages and disadvantages are obvious from the table. Some of them are given below.

Table 11.1 Properties of flow through a normal shock ($\gamma = 1.4$)

M_1	M_2	p_2/p_1 *(advantage)*	p_{02}/p_{01} *(disadvantage)*
1.2	0.843	1.513	0.993
1.5	0.701	2.458	0.930
2.0	0.578	4.500	0.721
2.5	0.513	7.125	0.500

Advantages

1. Very high pressure ratio per stage
2. Low weight-to-power ratio
3. Small size and length of the machine
4. Higher flow rates.

Disadvantages

1. Excessive loss due to shocks
2. Early separation of the boundary layer on the suction side leading to increase in the profile and annulus losses
3. Very steep or almost vertical performance characteristic leading to unstable operation
4. Difficulty in starting
5. Excessive vibration due to instability of flow
6. Serious stress and bearing problems on account of very high peripheral speeds.

Figure 11.14 shows a supersonic compressor stage with shock in the rotor. The velocity triangles are shown in terms of the Mach numbers corresponding to the velocities. The flow approaches the stage at subsonic velocity c_1 or Mach number M_{c1}. This with a blade Mach number M_b gives a supersonic relative Mach number (M_{w1}) at the entry of rotor blades. The rotor blade passages are so designed that the entering supersonic flow is first converted to a subsonic flow through a shock and then it is subsonically diffused to a relative Mach number M_{w2}. The flow at the entry of the stator row is also subsonic. Such a stage can develop a pressure ratio of about 3.0.

Another scheme is shown in Fig. 11.15. The flow approaches both the rotor and stator at supersonic velocities. Therefore, besides subsonic diffusion, compression through shocks in both the rotor and stator is possible. This arrangement can give a very high pressure ratio (≈ 6.0) per stage.

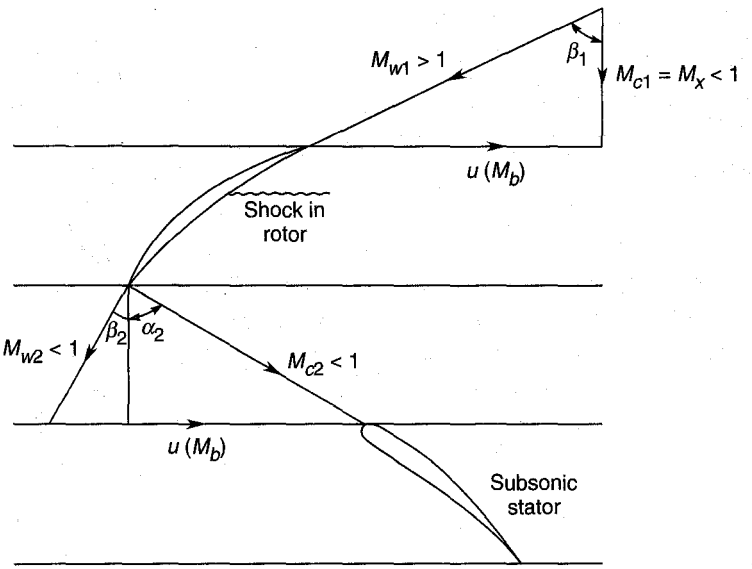

Fig. 11.14 Supersonic compressor stage with shock in the rotor ($p_r \approx 3.0$)

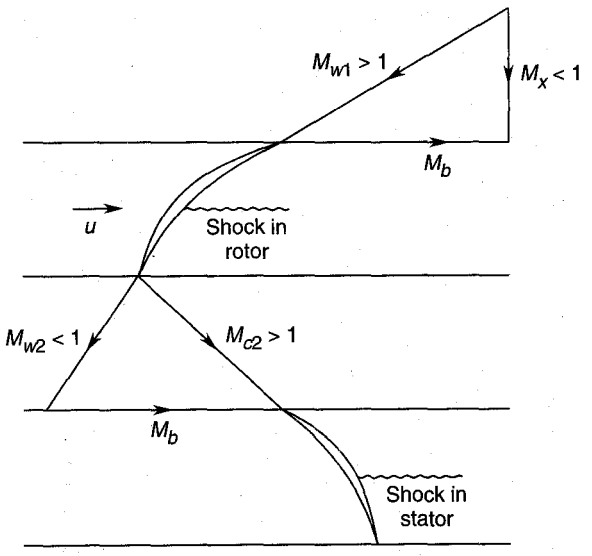

Fig. 11.15 Supersonic compressor stage with shocks in the rotor and stator ($p_r \approx 6.0$)

Other possibilities are:

(a) subsonic rotor ($M_{w1} < 1$; $M_{w2} < 1$) with shock in the stator ($M_{c2} > 1$).

(b) supersonic rotor and subsonic stator.

(c) subsonic rotor and supersonic stator.

Choking of the flow occurs if the velocities are such that the axial Mach number is unity or higher. Therefore, the velocity triangles (blade geometry) are so chosen that the axial Mach number is always less than unity.

Blades in rows receiving supersonic flow must have sharp leading edges to avoid strong detached shocks and excessive losses arising from them.

To retain some advantages of high speed compressors without suffering too much from their disadvantages, low Mach number supersonic flow or high Mach number subsonic flow can be employed. Such compressor stages are known as transonic stages[410, 421] with flow Mach numbers varying in the range 0.85 – 1.3. Such stages do not suffer from unstable flow and have relatively higher efficiencies. The flow in such stages is generally supersonic towards the tip sections of the blades.

11.8 Performance Characteristics

A brief introduction to compressor performance has been given in Sec. 7.7. The performance characteristics of axial compressors or their stages at various speeds can be presented in terms of the plots of the following parameters:

(a) *pressure rise* vs. *flow rate*,

$$\Delta p = f(Q)$$

$$\Delta p = f(\dot{m})$$

(b) *pressure ratio* vs. *non-dimensional flow rate* (Fig. 7.5),

$$\frac{p_2}{p_1} = f\left(\frac{\dot{m}\sqrt{T_{01}}}{p_{01}}\right)$$

(c) *loading coefficient* vs. *flow coefficient* (Fig. 7.6),

$$\psi = f(\phi)$$

The actual performance curve based on measured values is always below the ideal curve obtained theoretically on account of losses. This is shown in Fig. 11.16. The surge point and stable and unstable flow regimes have been explained in the following sections.

11.8.1 Off-design Operation

A compressor gives its best performance while operating at its design point, i.e. at the pressure ratio and flow rate for which it has been

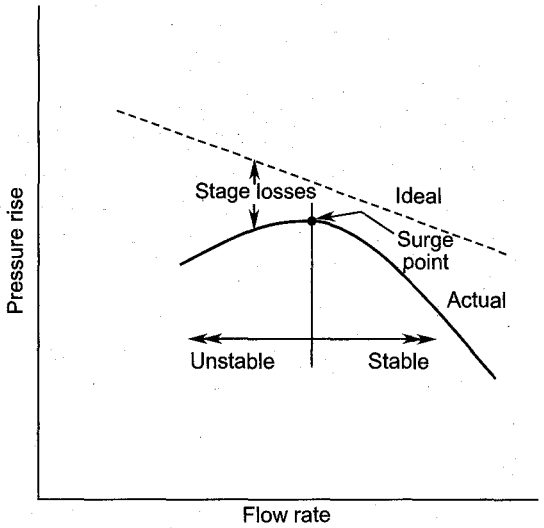

Fig. 11.16 Ideal and actual performance curves for an axial compressor

designed. However, like any other machine or system, it is also expected to operate away from the design point. Therefore, a knowledge about its behaviour at off-design operation is also necessary.

Off-design characteristic curves can be obtained theoretically from Eqs. (11.16) and (11.11).

$$\psi = \phi\,(\tan\,\alpha_2 - \tan\,\alpha_1)$$

But $\tan\,\alpha_2 = \dfrac{1}{\phi} - \tan\,\beta_2$. Therefore,

$$\psi = 1 - \phi\,(\tan\,\beta_2 + \tan\,\alpha_1) \qquad (11.112a)$$

The quantity $(\tan\,\beta_2 + \tan\,\alpha_1)$ can be assumed constant in a wide range of incidence up to the stalling value i_s. This is justified in view of small variations in the air angles at the rotor and stator exits. Therefore, writing $\alpha_1 = \alpha_3$

$$A = \tan\,\beta_2 + \tan\,\alpha_3 \qquad (11.113)$$

If the design values are identified by the superscript*, Eq. (11.112a) along with (11.113) can be written as

$$\psi^* = 1 - A\phi^* \qquad (11.112b)$$

$$A = \frac{1 - \psi^*}{\phi^*}$$

At off-design conditions

$$\psi = 1 - A\phi$$

$$\psi = 1 - (1 - \psi^*) \frac{\phi}{\phi^*} \tag{11.114}$$

This equation also gives the off-design characteristic of an axial-flow compressor. Figure 11.17 depicts theoretical characteristic curves for some values of the constant A. For positive values of A, the curves are falling, while for negative values rising characteristics are obtained. The actual curves will be modified forms of these curves on account of losses.

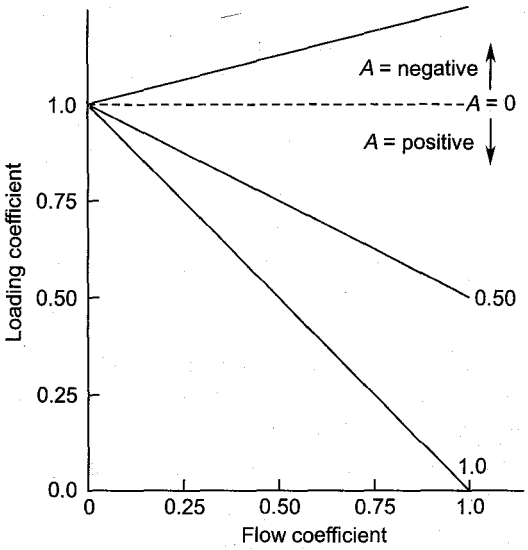

Fig. 11.17 Off-design characteristic curves for an axial compressor stage

11.8.2 Surging

Unstable flow in axial compressors can be due to the separation of flow from the blade surfaces or complete breakdown of the steady through flow. The first pehnomenon is known as stalling, whereas the second is termed as surging.[407, 437] Both these phenomena occur due to off-design conditions of operation and are aerodynamically and mechanically undesirable.

Sometimes, it is difficult to differentiate between operating conditions leading to stalling and surging. It is possible that the flow in some regions stalls without surging taking place. Surging affects the whole machine while stalling is a local phenomenon.

Some typical performance characteristic curves at different speeds (N_1, N_2, etc.) are shown in Fig. 11.18. The surge phenomenon is explained with the aid of one of the curves in this Figure. Let the operation of the

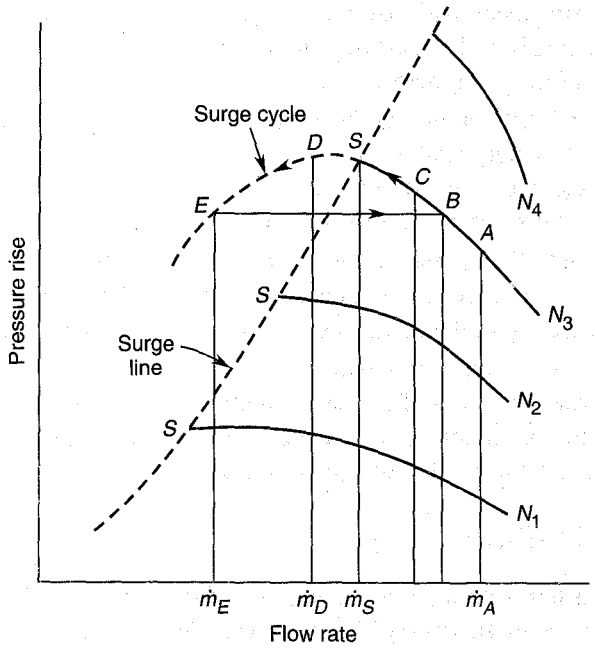

Fig. 11.18 Surging in compressors

compressor at a given instant of time be represented by point A (p_A, $\dot{m}_A$) on the characteristic curve (speed = constant = N_3). If the flow rate through the machine is reduced to $\dot{m}_B$ by closing a valve on the delivery pipe, the static pressure upstream of the valve is increased. This higher pressure (p_B) is matched with the increased delivery pressure (at B) developed by the compressor. With further throttling of the flow (to $\dot{m}_C$ and $\dot{m}_S$), the increased pressures in the delivery pipe are matched by the compressor delivery pressures at C and S on the characteristic curve.

The characteristic curve at flow rates below $\dot{m}_s$ provides lower pressure as at D and E. However, the pipe pressures due to further closure of the valve (point D) will be higher than these. This mismatching between the pipe pressure and the compressor delivery pressure can only exist for a very short time. This is because the higher pressure in the pipe will blow the air towards the compressor, thus reversing the flow leading to a complete breakdown of the normal steady flow from the compressor to the pipe. During this very short period the pressure in the pipe falls and the compressor regains its normal stable operation (say at point B) delivering higher flow rate ($\dot{m}_B$). However, the valve position still corresponds to the flow rate $\dot{m}_D$. Therefore, the compressor operating conditions return through points C and S to D. Due to the breakdown of the flow through the compressor, the pressure falls further to p_E and the entire phenomenon, i.e. the surge cycle EBCSDE is repeated again and

again. The frequency and magnitude of this to-and-fro motion of the air (surging) depend on the relative volumes of the compressor and delivery pipe, and the flow rate below $\dot{m}_s$.

Surging of the compressor leads to vibration of the entire machine which can ultimately lead to mechanical failure. Therefore, the operation of compressors on the left of the peak of the performance curve is injurious to the machine and must be avoided.

Surge points (S) on each curve corresponding to different speeds can be located and a surge line is drawn as shown in Fig. 11.18. The stable range of operation of the compressor is on the right-hand side of this line.

There is also a limit of operation on the extreme right of the characteristics when the mass-flow rate cannot be further increased due to choking. This is obviously a function of the Mach number which itself depends on the fluid velocity and its state.

11.8.3 Stalling

As stated earlier, stalling is the separation of flow from the blade surface. At low flow rates (lower axial velocities), the incidence is increased as shown in Fig. 11.11. At large values of the incidence, flow separation occurs on the suction side of the blades which is referred to as positive stalling. Negative stall is due to the separation of flow occurring on the pressure side of the blade due to large values of negative incidence. However, in a great majority of cases this is not as significant as the positive stall which is the main subject under consideration in this section.

The separation of flow on aerofoil blades has been discussed in Sec. 6.1.18. Losses in blade rows due to separation and stalling have been explained in Sec. 8.4.5.

In a high pressure ratio multi-stage compressor the axial velocity is already relatively small in the higher pressure stages on account of higher densities. In such stages a small deviation from the design point causes the incidence to exceed its stalling value and stall cells first appear near the hub and tip regions (see Sec. 11.5). The size and number of these stall cells or patches increase with the decreasing flow rates. At very low flow rates they grow larger and affect the entire blade height. Large-scale stalling of the blades causes a significant drop in the delivery pressure which can lead to the reversal of flow or surge. The stage efficiency also drops considerably on account of higher losses. The axisymmetric nature of the flow is also destroyed in the compressor annulus.

Rotating stall

Figure 11.19 shows four blades (1, 2, 3 and 4) in a compressor rotor. Owing to some distortion or non-uniformity of flow one of the blades (say

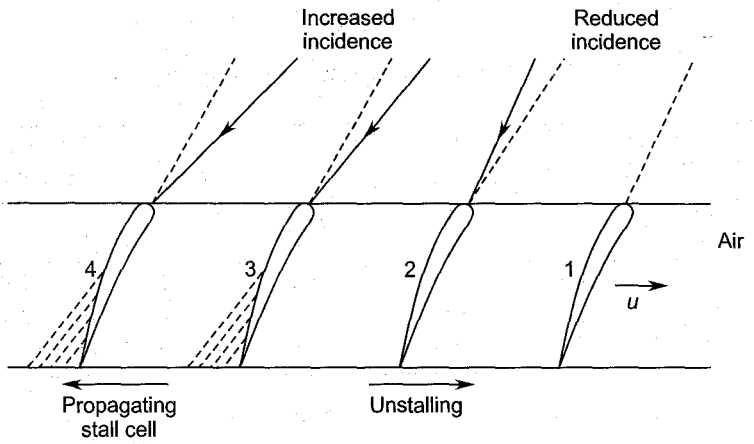

Fig. 11.19 Stall propagation in a compressor blade row

the third) receives the flow at increased incidence. This causes this blade (number three) to stall. On account of this, the passage between the third and fourth blades is blocked causing deflection of flow in the neighbouring blades. As a result, the fourth blade again receives flow at increased incidence and the second blade at decreased incidence. Therefore, stalling also occurs on the fourth blade. This progressive deflection of the flow towards the left clears the blade passages on the right on account of the decreasing incidence and the resulting unstalling. Thus the stall cells or patches move towards the left-hand side at a fraction of the blade speed. In the relative system they appear to move in a direction opposite to that of the rotor blades. However, on account of their (stall cell) lower speed as compared to that of the rotor, they move at a certain speed in the direction of the rotation in the absolute frame of coordinates.

Rotating stall cells[401,406] develop in a variety of patterns at different off-design conditions as shown in Fig. 11.20. The blades are subjected to forced vibrations on account of their passage through the stall cells at a certain frequency. The frequency and amplitude of vibrations depend on the extent of loading and unloading of the blades, and the number of stall cells. The blades can fail due to resonance. This occurs when the frequency of the passage of stall cells through a blade coincides with its natural frequency.

Both the efficiency and delivery pressure drop considerably on account of rotating stall.

Notation for Chapter 11

a	Constant
A	Constant, area of cross-section

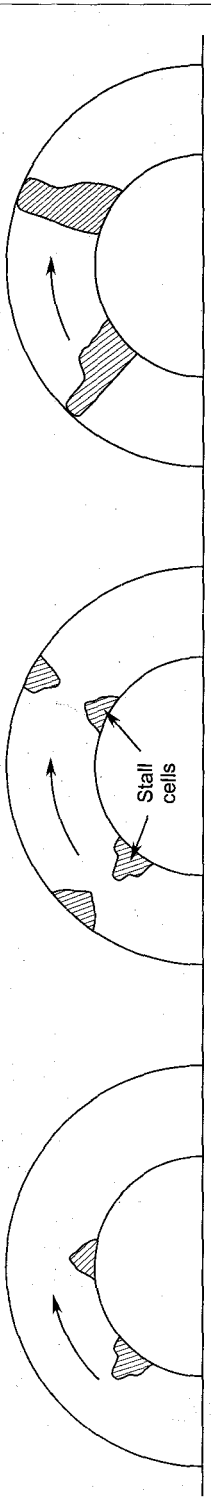

Fig. 11.20 Rotating stall cells in axial compressors

b	Constant
c	Fluid velocity
c_p	Specific heat at constant pressure
C_1, C_2	Constants
d	Diameter
h	Enthalpy
Δh	Change in enthalpy
K, K_1, K_2	Constants
$\dot{m}$	Mass-flow rate
M	Mach number
n	Index of r
N	Rotor speed
p	Pressure
Δp	Static pressure rise
Δp_0	Stagnation pressure loss
P	Power
Q	Volume-flow rate
r	Radius
R	Degree of reaction, gas constant
Re	Reynolds number
Δs	Change in entropy
T	Absolute temperature
u	Tangential or peripheral speed of the blades
w	Work, relative velocity
Y	Pressure loss coefficient

Greek Symbols

α	Air angles in the absolute system
β	Air angles in the relative system
γ	Ratio of specific heats
η	Efficiency
ξ	Enthalpy loss coefficient
ρ	Density
ϕ	Flow coefficient
ψ	Stage loading coefficient
ω	Rotational speed in rad/s
Ω	Work-done factor

Subscripts

o	Stagnation values
1	Rotor entry

2	Rotor exit
3	Stator or diffuser exit
a	Actual
b	Blade
c	Corresponding to velocity c
D	Diffuser or stator
h	Hub
m	Mean, mechanical
r	Radial
rel	Relative
R	Rotor
s,ss	Isentropic
ss	Static-to-static
st	Stage
t	Tip
tt	total-to-total
w	Corresponding to velocity *w*
x	Axial
y	Tangential
θ	Tangential

Solved Examples

11.1 An axial compressor stage has the following data:

Temperature and pressure at entry	300K, 1.0 bar
Degree of reaction	50%
Mean blade ring diameter	36 cm
Rotational speed	18000 rpm
Blade height at entry	6 cm
Air angles at rotor and stator exit	25°
Axial velocity	180m/s
Work-done factor	0.88
Stage efficiency	85%
Mechanical efficiency	96.7%

Determine: **(a)** Air angles at the rotor and stator entry, **(b)** the mass-flow rate of air, **(c)** the power required to drive the compressor, **(d)** the loading coefficient, **(e)** the pressure ratio developed by the stage and **(f)** the Mach number at the rotor entry.

***Solution*:**

$$u = \frac{\pi d N}{60} = \frac{\pi \times 0.36 \times 18000}{60} = 339.292 \text{ m/s}$$

$$\phi = \frac{c_x}{u} = \frac{180}{339.292} = 0.530$$

(a) Referring to Fig. 11.1b,

$$c_{y1} = c_x \tan \alpha_1 = 180 \tan 25 = 83.935 \text{ m/s}$$

$$w_{y1} = 339.292 - 83.935 = 255.357 \text{ m/s}$$

$$\tan \beta_1 = \frac{255.357}{180} = 1.418$$

$$\beta_1 = 54.82° \text{ (}Ans.\text{)}$$

Since the stage has 50% reaction

$$\alpha_2 = \beta_1 = 54.82°; \ \alpha_1 = \alpha_3 = \beta_2 = 25°$$

(b)
$$\rho_1 = \frac{p_1}{RT_1} = \frac{1.0 \times 10^5}{287 \times 300} = 1.161 \text{ kg/m}^3$$

$$\dot{m} = \rho_1 c_x (\pi d h_1)$$

$$\dot{m} = 1.161 \times 180 (\pi \times 0.36 \times 0.06)$$

$$\dot{m} = 14.18 \text{ kg/s (}Ans.\text{)}$$

(c) Specific work

$$w = \Omega u c_x (\tan \beta_1 - \tan \beta_2)$$

$$w = 0.88 \times 339.292 \times 180 (1.418 - 0.466)$$

$$w = 51164.15 \text{ J/kg}$$

$$P = \frac{1}{\eta_m} \dot{m} w = \frac{14.18 \times 51.164}{0.967}$$

$$P = 750 \text{ kW (}Ans.\text{)}$$

(d)
$$\psi = \frac{w}{u^2} = \frac{51164.15}{(339.292)^2} = 0.444 \text{ (}Ans.\text{)}$$

(e)
$$\Delta T_a = \frac{w}{c_p} = \frac{51164.15}{1005} = 50.91°\text{C}$$

Isentropic temperature rise

$$\Delta T_s = T_1 (p_r^{0.286} - 1) = \eta_{st} \Delta T_a = 0.85 \times 50.91$$

$$300 \ (p_r^{0.286} - 1) = 43.273$$

$$p_r^{0.286} = 1 + \frac{43.273}{300} = 1.144$$

$$p_r = 1.6 \text{ (}Ans.\text{)}$$

(f) $$w_1 = \frac{c_x}{\cos \beta_1} = \frac{180}{\cos 54.82} = \frac{180}{0.576} = 312.5 \text{ m/s}$$

The relative Mach number at the rotor blade entry

$$M_{w1} = \frac{w_1}{\sqrt{\gamma RT_1}} = \frac{312.5}{\sqrt{1.4 \times 287 \times 300}}$$

$$M_{w1} = \frac{312.5}{347.18} = 0.90$$

This Mach number will give a shock on the suction side of the rotor blade due to local acceleration and deceleration. The Mach number at the rotor blade tips will be slightly higher than this. To avoid the possibility of shocks, the maximum value of the Mach number must be kept below 0.75.

11.2 The conditions of air at the entry of an axial compressor stage are $p_1 = 768$ mm Hg and $T_1 = 314$ K. The air angles are

$$\beta_1 = 51°,\ \beta_2 = 9°,\ \alpha_1 = \alpha_3 = 7°$$

The mean diameter and peripheral speed are 50 cm and 100 m/s, respectively. Mass-flow rate through the stage is 25 kg/s; the work-done factor is 0.95 and mechanical efficiency 92%. Assuming a stage efficiency of 88% determine:

(a) air angle at the stator entry,
(b) blade height at entry and the hub-tip diameter ratio,
(c) stage loading coefficient,
(d) stage pressure ratio, and
(e) the power required to drive the stage.

***Solution*:**

$$p_1 = \frac{768}{750} = 1.024 \text{ bar}$$

$$\rho_1 = \frac{1.024 \times 10^5}{287 \times 314} = 1.136 \text{ kg/m}^3$$

(a) Equation (11.11) is

$$\tan \alpha_1 + \tan \beta_1 = \frac{u}{c_x}$$

$$\tan 7 + \tan 51 = \frac{100}{c_x} = 0.1228 + 1.2349 = 1.3577$$

$$c_x = \frac{100}{1.3577} = 73.65 \text{ m/s}$$

$$\tan \alpha_2 + \tan \beta_2 = \frac{u}{c_x}$$

$$\tan \alpha_2 + \tan 9 = \tan \alpha_2 + 0.158 = 1.3577$$

$$\tan \alpha_2 = 1.199; \quad \alpha_2 = 50.18° \ (Ans.)$$

(b) $$\dot{m} = c_x \rho_1 (\pi d h_1)$$

$$25 = 73.65 \times 1.136 \times \pi \times 0.5 \ h_1$$

$$h_1 = 0.19 \text{ m} = 19 \text{ cm} \ (Ans.)$$

$$d_t = 50 + 19 = 69 \text{ cm}$$

$$d_h = 50 - 19 = 31 \text{ cm}$$

The hub-tip ratio is

$$\frac{d_h}{d_t} = \frac{31}{69} = 0.449 \ (Ans.)$$

(c) $$w = c_p \Delta T_a = \Omega u c_x (\tan \beta_1 - \tan \beta_2)$$

$$w = 0.95 \times 100 \times 73.65 \ (1.2349 - 0.158)$$

$$w = 7534.8 \text{ J/kg}$$

$$\psi = \frac{w}{u^2} = \frac{7534.8}{100 \times 100} = 0.7535 \ (Ans.)$$

(d) $$\Delta T_a = \frac{w}{c_p} = \frac{7534.8}{1005} = 7.497°\text{C}$$

$$\Delta T_s = T_1 \ (p_r^{0.286} - 1) = \eta_{st} \Delta T_a = 0.88 \times 7.497 = 6.597$$

$$p_r^{0.286} - 1 = \frac{6.597}{314} = 0.021$$

$$p_r = (1.021)^{3.5} = 1.075 \ (Ans.)$$

Alternatively, the pressure ratio can be determined by assuming incompressible flow. From Eq. (11.37b)

$$(\Delta p)_{st} = \eta_{st} \rho w = 0.88 \times 1.136 \times 7534.8$$

$$(\Delta p)_{st} = 0.0753 \times 10^5 \text{ N/m}^2$$

$$(\Delta p)_{st} = \frac{0.0753 \times 10^5}{9.81} = 767.8 \text{ mm W.G.}$$

$$p_r = \frac{1.024 + 0.0753}{1.024} = 1.0735$$

This is a slight underestimation on account of the assumption.

(e) $$P = \frac{\dot{m} w}{\eta_m} = \frac{25 \times 7534.8}{0.92} \times 10^{-3}$$

$$P = 204.75 \text{ kW} \ (Ans.)$$

11.3 **(a)** Prove that the efficiency of a 50% reaction axial compressor stage is given by

$$\eta_{st} = 1 - \frac{\phi\, Y_R \sec^2 \beta_1}{\tan \beta_1 - \tan \beta_2}$$

(b) $\eta_{st} = \eta_D = \eta_R$

(c) In the stage of Ex. 11.1, if the loss coefficient for the blade rows is 0.09, verify the value of its efficiency.

(d) Determine the efficiencies of the rotor and diffuser blade rows.

***Solution*:**

(a) For a 50% reaction stage

$$c_1 = c_3 = w_2,\ w_1 = c_2,\ \alpha_1 = \alpha_3 = \beta_2,\ \beta_1 = \alpha_2$$

Therefore, the cascade losses in the rotor and stator blade rows are the same, i.e.

$$Y_R = Y_D = 0.09$$

For $T_3 \approx T_2$, Eq. (11.74) is

$$\eta_{st} = 1 - \frac{1}{2}\,\phi\,\frac{Y_D \sec^2 \alpha_2 + Y_R \sec^2 \beta_1}{\tan \beta_1 - \tan \beta_2}$$

$$\eta_{st} = 1 - \frac{\phi\, Y_R \sec^2 \beta_1}{\tan \beta_1 - \tan \beta_2}$$

(b)
$$\frac{c_3^2}{c_2^2} = \frac{w_2^2}{w_1^2}$$

Therefore, Eqs. (11.57b) and (11.61b) yield

$$\eta_{st} = \eta_D = \eta_R$$

(c)
$$\phi = 0.53,\ Y_R = 0.09$$

$$\alpha_2 = \beta_1 = 54.82°,\ \beta_2 = \alpha_1 = 25°$$

$$\eta_{st} = 1 - \frac{0.53 \times 0.09 \sec^2 54.82}{1.418 - 0.466} = 0.849$$

$$\eta_{st} = 84.9\%\ (Ans.)$$

This is very close to the assumed value of 85% in Ex. 11.1.

(d) From velocity triangles (Fig. 11.1b), for constant axial velocity,

$$\frac{c_3^2}{c_2^2} = \frac{c_1^2}{c_2^2} = \frac{\sec^2 \alpha_1}{\sec^2 \alpha_2} = \frac{\sec^2 25}{\sec^2 54.82} = 0.404$$

Therefore, Eq. (11.61b) becomes

$$\eta_D = \eta_R = 1 - \frac{Y_D}{1 - c_3^2/c_2^2} = 1 - \frac{0.09}{1 - 0.404} = 0.849$$

$$\eta_D = \eta_R = 84.9\% \ (Ans.)$$

In this case this is the same as η_{st}.

11.4 Assuming the data of Ex. 11.2 at the mean blade section ($r = r_m$), compute:

(a) rotor blade air angles,
(b) the flow coefficient,
(c) the degree of reaction,
(d) the specific work, and
(e) the loading coefficient at the hub, mean and tip sections. Assume free vortex flow.

***Solution*:**

Refer to Fig. 11.1b and replace the suffix y by θ to denote tangential direction.

$$\omega = \frac{u_m}{r_m} = \frac{100}{0.25} = 400 \text{ rad/s}$$

$$r_h = 0.5 \times 31 = 15.5 \text{ cm}$$

$$u_h = \omega r_h = 400 \times 0.155 = 62.0 \text{ m/s}$$

$$r_t = 0.5 \times 69 = 34.5 \text{ cm}$$

$$u_t = \omega r_t = 400 \times 0.345 = 138 \text{ m/s}$$

(a) Air angles

The air angles at the mean section are

$$\alpha_{1m} = 7°, \ \beta_{1m} = 51°, \ \beta_{2m} = 9°, \ \alpha_{2m} = 50.18°$$

$$c_{\theta 1m} = c_x \tan \alpha_{1m} = 73.65 \tan 7 = 9.04 \text{ m/s}$$

$$C_1 = r_m \, c_{\theta 1m} = 0.25 \times 9.04 = 2.26$$

$$c_{\theta 1h} = \frac{C_1}{r_h} = \frac{2.26}{0.155} = 14.58 \text{ m/s}$$

$$c_{\theta 1t} = \frac{C_1}{r_t} = \frac{2.26}{0.345} = 6.55 \text{ m/s}$$

$$\tan \alpha_{1h} = \frac{c_{\theta 1h}}{c_x} = \frac{14.58}{73.65} = 0.1978$$

$$\alpha_{1h} = 11.19°$$

$$\tan \alpha_{1t} = \frac{c_{\theta 1t}}{c_x} = \frac{6.55}{73.65} = 0.0889$$

$$\alpha_{1t} = 5.08°$$

$$\tan \beta_{1h} = \frac{u_h}{c_x} - \tan \alpha_{1h} = \frac{62.0}{73.65} - 0.1979 = 0.6439$$

$$\beta_{1h} = 32.78° \ (Ans.)$$

$$\tan \beta_{1t} = \frac{u_t}{c_x} - \tan \alpha_{1t} = \frac{138.0}{73.65} - 0.0889 = 1.7848$$

$$\beta_{1t} = 60.74° \ (Ans.)$$

$$c_{\theta 2m} = c_x \tan \alpha_{2m} = 73.65 \tan 50.18 = 88.33$$

$$C_2 = r_m \, c_{\theta 2m} = 0.25 \times 88.33 = 22.084$$

$$c_{\theta 2h} = \frac{22.084}{0.155} = 142.47 \text{ m/s}$$

$$c_{\theta 2t} = \frac{22.084}{0.345} = 64.01 \text{ m/s}$$

$$\tan \alpha_{2h} = \frac{142.47}{73.65} = 1.934$$

$$\tan \alpha_{2t} = \frac{64.01}{73.65} = 0.869$$

$$\tan \beta_{2h} = \frac{62.0}{73.65} - 1.934 = -1.092$$

$$\beta_{2h} = -47.52° \ (Ans.)$$

$$\tan \beta_{2t} = \frac{138}{73.65} - 0.869 = 1.0047$$

$$\beta_{2t} = 45.135° \ (Ans.)$$

(b) Flow coefficients

$$\phi_h = \frac{c_x}{u_h} = \frac{73.65}{62.0} = 1.188 \ (Ans.)$$

$$\phi_m = \frac{c_x}{u_m} = \frac{73.65}{100} = 0.7365 \ (Ans.)$$

$$\phi_t = \frac{c_x}{u_t} = \frac{73.65}{138} = 0.533 \ (Ans.)$$

(c) Degrees of reaction

$$R_h = \frac{1}{2} \phi_h (\tan \beta_{1h} + \tan \beta_{2h}) \times 100$$

$$R_h = 0.5 \times 1.188 \ (0.6439 - 1.092) \times 100$$

$$R_h = -26.62\% \ (Ans.)$$

$$R_m = 0.5 \times 0.7365 \ (1.2349 + 0.158) \times 100$$

$$R_m = 51.29\% \ (Ans.)$$

$$R_t = 0.5 \times 0.533 \ (1.7848 + 1.0047) \times 100$$

$$R_t = 74.34\% \ (Ans.)$$

(d) Specific work

In a free-vortex flow the specific work remains constant at all sections.

$$w = \omega \ (C_2 - C_1)$$

$$w = 400 \ (22.084 - 2.26) \times 10^{-3} \text{ kJ/kg}$$

$$w = 7.9296 \text{ kJ/kg}$$

(e) Loading coefficients

$$\psi_h = \frac{w}{u_h^2} = \frac{7929.6}{62 \times 62} = 2.063 \ (Ans.)$$

$$\psi_m = \frac{w}{u_m^2} = \frac{7929.6}{100 \times 100} = 0.793 \ (Ans.)$$

$$\psi_t = \frac{w}{u_t^2} = \frac{7929.6}{138 \times 138} = 0.416 \ (Ans.)$$

The results obtained are presented in the following table for comparison:

Free-vortex stage

Section	β_1	β_2	R	w kJ/kg	ϕ	ψ
Hub	32.78	– 47.52	– 26.62	7.93	1.188	2.063
Mean	51.0	9.0	51.29	7.93	0.7365	0.793
Tip	60.74	45.135	74.34	7.93	0.533	0.416

11.5 A forced vortex flow axial compressor stage has the same data at its mean diameter section as in Ex. 11.2. Determine **(a)** rotor blade air angles, **(b)** specific work, **(c)** loading coefficients, and **(d)** degree of reaction at the hub, mean and tip sections.

Solution:

The air angles are

$$\alpha_{1m} = 7°, \ \beta_{1m} = 51°, \ \alpha_{2m} = 50.18°, \ \beta_{2m} = 9°$$

The radii and tangential velocities are

$$r_h = 15.5 \text{ cm}, \ u_h = 62.0 \text{ m/s}$$

$$r_m = 25 \text{ cm}, \ u_m = 100 \text{ m/s}$$

$$r_t = 34.5 \text{ cm}, \; u_t = 138 \text{ m/s}$$

Angular speed $\omega = 400$ rad/s

$$c_{x1m} = c_{x2m} = c_x = 73.65 \text{ m/s}$$

(a) Air angles

$$c_{\theta 1m} = c_x \tan \alpha_{1m} = 73.65 \tan 7 = 9.04 \text{ m/s}$$

$$C_1 = \frac{c_{\theta 1m}}{r_m} = \frac{9.04}{0.25} = 36.16$$

$$c_{\theta 1h} = r_h C_1 = 0.155 \times 36.16 = 5.605 \text{ m/s}$$

$$c_{\theta 1t} = r_t C_1 = 0.345 \times 36.16 = 12.475 \text{ m/s}$$

$$c_{xm}^2 = K_1 - 2C_1^2 r_m^2$$

$$73.65^2 = K_1 - 2 \times 36.16^2 \times 0.25^2$$

$$K_1 = 5587.76$$

$$c_{x1h}^2 = K_1 - 2C_1^2 r_h^2$$

$$c_{x1h}^2 = 5587.76 - 2 \times 36.16^2 \times 0.155^2$$

$$c_{x1h} = 74.33 \text{ m/s}$$

$$c_{x1t}^2 = 5587.76 - 2 \times 36.16^2 \times 0.345^2$$

$$c_{x1t} = 72.64 \text{ m/s}$$

$$\tan \alpha_{1h} = \frac{c_{\theta 1h}}{c_{x1h}} = \frac{5.605}{74.33} = 0.0754$$

$$\tan \beta_{1h} = \frac{u_h}{c_{x1h}} - \tan \alpha_{1h} = \frac{62.0}{74.33} - 0.0754 = 0.7587$$

$$\beta_{1h} = 37.18° \; (Ans.)$$

$$\tan \alpha_{1t} = \frac{c_{\theta 1t}}{c_{x1t}} = \frac{12.475}{72.64} = 0.1717$$

$$\tan \beta_{1t} = \frac{u_t}{c_{x1t}} - \tan \alpha_{1t} = \frac{138}{72.74} - 0.1717 = 1.728$$

$$\beta_{1t} = 59.94° \; (Ans.)$$

$$c_{\theta 2m} = c_{xm} \tan \alpha_{2m} = 73.65 \tan 50.18 = 88.33$$

$$C_2 = \frac{c_{\theta 2m}}{r_m} = \frac{88.33}{0.25} = 353.32$$

$$c_{\theta 2h} = r_h C_2 = 0.155 \times 353.32 = 54.76 \text{ m/s}$$

$$c_{\theta 2t} = r_t C_2 = 0.345 \times 353.32 = 121.89 \text{ m/s}$$

$$K_2 = c_{x2m}^2 - 2 (C_2 - C_1) \omega r_m^2 + 2C_2^2 r_m^2$$

$$K_2 = 73.65^2 - 2 (353.32 - 36.16) \times 400 \times 0.25^2 + 2 \times 353.32^2 \times 0.25^2$$

$$K_2 = 5170.9$$

$$c_{x2h}^2 = K_2 + 2\,(C_2 - C_1)\,\omega r_h^2 + 2C_2^2\, r_h^2$$

$$c_{x2h}^2 = 5170.9 + 4058\; r_h^2 = 5170.9 + 4058 \times 0.155^2$$

$$c_{x2h} = 72.58 \text{ m/s}$$

$$c_{x2t}^2 = 5170.9 + 4058 \times 0.345^2 = 5653$$

$$c_{x2t} = 75.18 \text{ m/s}$$

$$\tan \alpha_{2h} = \frac{c_{\theta 2h}}{c_{x2h}} = \frac{54.76}{72.58} = 0.754$$

$$\tan \beta_{2h} = \frac{u_h}{c_{x2h}} - \tan \alpha_{2h} = \frac{62}{72.58} - 0.754 = 0.10$$

$$\beta_{2h} = 5.71° \text{ (}Ans.\text{)}$$

$$\tan \alpha_{2t} = \frac{c_{\theta 2t}}{c_{x2t}} = \frac{121.89}{75.18} = 1.621$$

$$\tan \beta_{2t} = \frac{u_t}{c_{x2t}} - \tan \alpha_{2t} = \frac{138}{75.18} - 1.621 = 0.215$$

$$\beta_{2t} = 12.1° \text{ (}Ans.\text{)}$$

(b) Specific work

$$w_h = (C_2 - C_1)\,\omega r_h^2 = 126.86\; r_h^2 \text{ kJ/kg}$$

$$w_h = 126.86 \times 0.155^2 = 3.05 \text{ kJ/kg (}Ans.\text{)}$$

$$w_m = 126.86 \times 0.25^2 = 7.93 \text{ kJ/kg (}Ans.\text{)}$$

$$w_t = 126.86 \times 0.345^2 = 15.1 \text{ kJ/kg (}Ans.\text{)}$$

(c) Loading coefficients

$$\psi_h = \frac{w_h}{u_h^2} = \frac{3050}{62 \times 62} = 0.793 \text{ (}Ans.\text{)}$$

It can be shown that the loading coefficient for a forced vortex stage remains constant along the blade height. This can be checked here.

$$\psi_m = \frac{w_m}{u_m^2} = \frac{7930}{100 \times 100} = 0.793 \text{ (}Ans.\text{)}$$

$$\psi_t = \frac{w_t}{u_t^2} = \frac{15100}{138 \times 138} = 0.793 \text{ (}Ans.\text{)}$$

(d) Degree of reaction

Since the axial velocity at a given section is varying, the degree of reaction is obtained from

$$R = \frac{w_1^2 - w_2^2}{2u\,(c_{\theta 2} - c_{\theta 1})}$$

$$R = \frac{c_{x1}^2 \sec^2 \beta_1 - c_{x2}^2 \sec^2 \beta_2}{2w}$$

At the hub section

$$R_h = \frac{74.33^2 \sec^2 37.18 - 72.58^2 \sec^2 5.71}{2 \times 3050} \times 100$$

$$R_h = 55.46\% \ (Ans.)$$

At the tip section

$$R_t = \frac{72.64^2 \sec^2 59.94 - 75.18^2 \sec^2 12.1}{2 \times 15100} \times 100$$

$$R_t = 50\% \ (Ans.)$$

The results are summarized in the following table

Forced vortex stage (variable reaction)

Section	β_1	β_2	R	w kJ/kg	ϕ	ψ
Hub	37.18	5.71	55.46	3.05	–	0.793
Mean	51.0	9.0	51.29	7.93	0.7365	0.793
Tip	59.94	12.1	50.00	15.1	–	0.793

11.6 If the stage in Ex. 11.1 is designed according to the general swirl distribution

$$c_{\theta 1} = a - \frac{b}{r}$$

$$c_{\theta 2} = a + \frac{b}{r}$$

taking the same conditions at the blade mid-height, compute air angles at the rotor entry and exit, specific work, loading coefficients and degrees of reaction at the hub, mean and tip sections.

***Solution*:**

$$c_{\theta 1m} = c_{x\,1m} \tan \alpha_{1m} = 180 \tan 25 = 83.93 \text{ m/s}$$

$$c_{\theta 2m} = c_{x\,2m} \tan \alpha_{2m} = 180 \tan 54.82 = 255.36 \text{ m/s}$$

$$a = \frac{1}{2} (c_{\theta 1m} + c_{\theta 2m}) = 0.5 \ (83.93 + 255.36)$$

$$a = 169.65$$

$$\frac{2b}{r_m} = c_{\theta 2m} - c_{\theta 1m} = 255.36 - 83.93 = 171.43$$

$$b = 0.5 \times 0.18 \times 171.43$$

$$b = 15.43$$

$$\frac{b}{a} = \frac{15.43}{169.65} = 0.09095$$

Air angles

$$c_{\theta 1h} = a - \frac{b}{r_h} = 169.65 - \frac{15.43}{0.15} = 66.78 \text{ m/s}$$

$$c_{\theta 1t} = a - \frac{b}{r_t} = 169.65 - \frac{15.43}{0.21} = 96.17 \text{ m/s}$$

$$c_{\theta 2h} = a + \frac{b}{r_h} = 169.65 + \frac{15.43}{0.15} = 272.52 \text{ m/s}$$

$$c_{\theta 2t} = a + \frac{b}{r_t} = 169.65 + \frac{15.43}{0.21} = 243.13 \text{ m/s}$$

From Eq. (11.107)

$$c_{x1m}^2 = K_1 - 2a^2 \left(\frac{b}{ar_m} + \ln r_m \right)$$

$$K_1 = 180^2 + 2 \times 169.65^2 \left(\frac{0.09095}{0.18} + \ln 0.18 \right)$$

$$K_1 = -37250$$

$$c_{x1h}^2 = -37250 - 2 \times 169.65^2 \left(\frac{0.09095}{0.15} + \ln 0.15 \right)$$

$$c_{x1h} = 192.5 \text{ m/s}$$

$$c_{x1t}^2 = -37250 - 2 \times 169.65^2 \left(\frac{0.09095}{0.21} + \ln 0.21 \right)$$

$$c_{x1t} = 166.30 \text{ m/s}$$

$$\tan \alpha_{1h} = \frac{c_{\theta 1h}}{c_{x1h}} = \frac{66.78}{192.5} = 0.347$$

$$\tan \beta_{1h} = \frac{u_h}{c_{x1h}} - \tan \alpha_{1h} = \frac{282.75}{192.5} - 0.347 = 1.1218$$

$$\beta_{1h} = 48.28° \text{ (}Ans.\text{)}$$

$$\tan \alpha_{1t} = \frac{c_{\theta 1t}}{c_{x1t}} = \frac{96.17}{166.3} = 0.578$$

$$\tan \beta_{1t} = \frac{u_t}{c_{x1t}} - \tan \alpha_{1t} = \frac{295.85}{166.3} - 0.578 = 1.802$$

$$\beta_{1t} = 60.97° \text{ (}Ans.\text{)}$$

From Eq. (11.108)

$$c_{x2m}^2 = K_2 - 2a^2 \left(\ln r_m - \frac{b}{ar_m} \right)$$

$$K_2 = 180^2 + 57562 \left(\ln 0.18 - \frac{0.09095}{0.18} \right)$$

$$K_2 = -95388$$

$$c_{x2h}^2 = -95388 - 57562\left(\ln 0.15 - \frac{0.09095}{0.15}\right)$$

$$c_{x2h} = 220.65 \text{ m/s}$$

$$c_{x2t}^2 = -95388 - 57562\left(\ln 0.21 - \frac{0.09095}{0.21}\right)$$

$$c_{x2t} = 139.3 \text{ m/s}$$

$$\tan \alpha_{2h} = \frac{c_{\theta 2h}}{c_{x2h}} = \frac{272.52}{220.65} = 1.235$$

$$\tan \beta_{2h} = \frac{u_h}{c_{x2h}} - \tan \alpha_{2h} = \frac{282.75}{220.65} - 1.235 = 0.046$$

$$\beta_{2h} = 2.65° \text{ (}Ans.\text{)}$$

$$\tan \alpha_{2t} = \frac{c_{\theta 2t}}{c_{x2t}} = \frac{243.13}{139.3} = 1.745$$

$$\tan \beta_{2t} = \frac{u_t}{c_{x2t}} - \tan \alpha_{2t} = \frac{395.85}{139.3} - 1.745 = 1.096$$

$$\beta_{2t} = 47.64° \text{ (}Ans.\text{)}$$

$$\omega = \frac{u_m}{r_m} = \frac{339.3}{0.18} = 1885 \text{ rad/s}$$

Specific work

From Eq. (11.103), the specific work is constant

$$w = 2\ \omega b$$

$$w = 2 \times 1885 \times 15.43 \times 10^{-3} \text{ kJ/kg}$$

$$w = 58.17 \text{ kJ/kg } (Ans.)$$

Loading coefficients

$$\psi_h = \frac{w}{u_h^2} = \frac{58170}{282.75^2} = 0.727 \text{ (}Ans.\text{)}$$

$$\psi_m = \frac{58170}{339.3^2} = 0.505 \text{ (}Ans.\text{)}$$

$$\psi_t = \frac{58170}{395.85^2} = 0.372 \text{ (}Ans.\text{)}$$

Degrees of reaction

Since the axial velocities at the rotor entry and exit are not the same (except at the mean section), Eqs. (11.44c) and (11.106) are not valid here. Therefore, the following equation is used:

$$R_h = \frac{1}{2w}\left(c_{x1h}^2 \sec^2 \beta_{1h} - c_{x2h}^2 \sec^2 \beta_{2h}\right)$$

$$R_h = \frac{192.5^2 \sec^2 48.28 - 220.65^2 \sec^2 2.65}{2 \times 58170} \times 100$$

$$R_h = 29.98\% \ (Ans.)$$

$$R_t = \frac{1}{2w} (c_{x1t}^2 \sec^2 \beta_{1t} - c_{x2t}^2 \sec^2 \beta_{2t})$$

$$R_t = \frac{116.3^2 \sec^2 60.97 - 139.3^2 \sec^2 47.64}{2 \times 58170} \times 100$$

$$R_t = 12.63\% \ (Ans.)$$

The results are summarized in the following table

General swirl distribution

Section	β_1	β_2	R	w kJ/kg	ϕ	ψ
Hub	48.28	2.65	29.98	58.17	–	0.727
Mean	54.82	25.0	50.0	58.17	0.530	0.505
Tip	60.97	47.64	12.63	58.17	–	0.372

11.7 The design point data for an axial compressor stage is the same as the mean section data in Ex. 11.1, i.e.

$$c_x = 180 \text{ m/s}, \ u = 339.3 \text{ m/s}, \ \alpha_1 = \beta_2 = 25°$$

Calculate the design point flow and loading coefficients. From these, compute the loading coefficients at $\phi = 0.2, 0.4, 0.6$ and 0.8.

***Solution*:**

$$\phi^* = \frac{c_x}{u} = \frac{180}{339.3} = 0.53$$

$$\tan \beta_2 + \tan \alpha_1 = 2 \tan 25 = 0.933$$

$$\psi^* = 1 - \phi^* (\tan \beta_2 + \tan \alpha_1)$$

$$\psi^* = 1 - 0.933\phi^*$$

$$\psi^* = 1 - 0.933 \times 0.53$$

$$\psi^* = 0.505 \ (Ans.)$$

At off-design points, the loading coefficients are calculated from

$$\psi = 1 - 0.933 \ \phi$$

The results are given in the following table

			Design point		
ϕ	0.2	0.4	0.53	0.6	0.8
ψ	0.813	0.626	0.505	0.439	0.253

Questions and Problems

11.1 (a) Draw a sketch of the two-stage axial flow compressor with inlet guide vanes.

(b) Draw curves indicating the variation of static pressure, temperature and absolute velocity through this compressor.

(c) Why does a compressor stage have a lower efficiency and loading factor compared to an equivalent turbine stage?

11.2 Draw velocity triangles at the entry and exit for the following axial compressor stages:

(a) $R = \frac{1}{2}$ (*b*) $R < \frac{1}{2}$ (*c*) $R > \frac{1}{2}$ (*d*) $R = 1$ (*e*) $R > 1$ (*f*) $R =$ negative

11.3 (a) Why is it necessary to employ multi-stage axial compressors to obtain moderate to high pressure ratios?

(b) What are the principal distinguishing features of the low pressure and high pressure stages from aerothermodynamic and material considerations?

11.4 Derive the following relations for an axial compressor stage with constant axial velocity.

(a) $\tan \alpha_1 + \tan \beta_1 = \tan \alpha_2 + \tan \beta_2 = \frac{u}{c_x}$

(b) $\psi = \phi (\tan \beta_1 - \tan \beta_2)$

(c) $\frac{(\Delta p)_{st}}{\rho u^2} = \phi (\tan \alpha_2 - \tan \alpha_1)$

(d) $\eta_{st} = (\Delta p)_{st}/\Omega \rho u c_x (\tan \alpha_2 - \tan \alpha_1)$

11.5 Draw the *h-s* diagram for a complete axial-flow compressor stage with $R > \frac{1}{2}$. Prove the following relations:

(a) $R = \frac{1}{2} \phi (\tan \beta_1 + \tan \beta_2) = \frac{1}{2} [1 - \phi (\tan \alpha_1 - \tan \beta_2)]$

(b) $\frac{\text{stage losses}}{\frac{1}{2} c_x^2} \approx Y_D \sec^2 \alpha_2 + Y_R \sec^2 \beta_1$

(c) $\eta_{st} \approx 1 - \frac{1}{2} \phi \frac{\xi_D \sec^2 \alpha_2 + \xi_R \sec^2 \beta_1}{\tan \beta_1 - \tan \beta_2}$

State the assumptions used.

11.6 (a) What is the work-done factor for an axial compressor stage? Why is it not employed for turbine stages?
(b) How does it vary with the number of stages?
(c) Show the axial velocity profiles along the blade height in the first and eighth stage.

11.7 (a) Describe four schemes of obtaining supersonic compression in an axial compressor stage.
(b) What are the advantages and disadvantages of supersonic stages?
(c) What is a transonic compressor stage?

11.8 What is surging in axial-flow compressors? What are its effects? Describe briefly.

11.9 (a) What is stalling in an axial compressor stage? How is it developed?
(b) What is rotating stall? Explain briefly the development of small and large stall cells in an axial compressor stage.

11.10 An axial compressor stage has a mean diameter of 60 cm and runs at 15000 rpm. If the actual temperature rise and pressure ratio developed are 30°C and 1.4 respectively, determine:

(a) the power required to drive the compressor while delivering 57 kg/s of air; assume mechanical efficiency of 86.0% and an initial temperature of 35°C,
(b) the stage loading coefficient,
(c) the stage efficiency, and
(d) the degree of reaction if the temperature at the rotor exit is 55°C.

Answer: (a) 1998.5 kW (b) 0.135
(c) 94.19% (d) 66.6%

11.11 If the loss coefficients of the stage in Ex. 11.2 ($\phi = 0.7365$, $\beta_1 = 51°$, $\beta_2 = 9°$; $\alpha_1 = 7°$, $\alpha_2 = 50.18°$) are $Y_D = 0.07$, $Y_R = 0.078$, determine the efficiencies of the diffuser and rotor blade rows and the stage.

Answer:

$$\eta_D = 88.0\%,\ \eta_R = 86.8\%,\ \eta_{st} = 87.43\%$$

11.12 An axial compressor stage has the same data as in Ex. 11.1:

$$r_h = 15 \text{ cm},\ u_h = 282.75 \text{ m/s}$$
$$r_m = 18 \text{ cm},\ u_m = 339.3 \text{ m/s}$$
$$r_t = 21 \text{ cm},\ u_t = 395.85 \text{ m/s}$$

$c_{xm} = c_{x1m} = c_{x2m} = 180$ m/s

$R_m = 50\%$, $\alpha_{2m} = \beta_{1m} = 54.82°$, $\alpha_{1m} = \beta_{2m} = 25°$

Determine rotor blade air angles, the degree of reaction, specific work, flow coefficient and loading coefficient at the hub, mean and tip sections for constant reaction.

Answer:

Forced vortex stage (constant reaction)

Section	β_1	β_2	R	$\overset{w}{\text{kJ/kg}}$	ϕ	ψ
Hub	48.0	20.08	50.0	40.376	0.677	0.505
Mean	54.82	25.0	50.0	58.17	0.530	0.505
Tip	60.97	30.54	50.0	79.17	0.417	0.505

11.13 Compute the loading coefficients for the stage in Problem 11.12 at $\phi = 0.2$, 0.4, 0.6 and 0.8. Indicate the design point values of ϕ and ψ. Plot the $\phi - \psi$ curve.

(*Ans.*)

				Design point	
ϕ	0.2	0.4	0.6	0.7365	0.8
ψ	0.944	0.887	0.831	0.793	0.775

Chapter 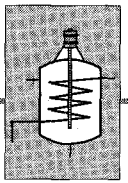 12

Centrifugal Compressor Stage

Till now only axial-flow machines have been discussed. This chapter deals with an energy absorbing and pressure producing machine of the outward flow radial type—the centrifugal compressor[439–490]. As will be seen in the various sections of this chapter the geometrical configuration of the flow and the passages is radically different from those in the axial type.

A centrifugal compressor like a pump is a head or pressure producing device. The contribution of the centrifugal energy in the total change in the energy level is significant. Section 1.10 highlights some of the special features of radial machines. From discussions given in Chapters 1 and 7 it is amply clear that a centrifugal type of compressor is suitable for low specific speed, higher pressure ratio and lower mass flow applications.

Performance-wise, the centrifugal compressor is less efficient (3-5%) than the axial type. However, a much higher pressure ratio[445,452] ($\approx$ 4.0) per stage, single-piece impeller and a wider range of stable operation are some of the attractive aspects of this type.

Besides the evolution of a perfect centrifugal pump, the developments of early supercharged aircraft reciprocating engines and later that of high output large diesel engines gave a great impetus to the development of centrifugal air compressors. These are used in large refrigeration units[462], petrochemical plants and a large variety of other industrial applications. In aircraft applications[446, 465] it is only used for small turbo-prop engines. For large turbo-jet engines, the large frontal area resulting from its application outweighs its advantages.

While the design and performance characteristics of axial compressors have been widely studied and supported by a huge mass of data acquired from cascade tests, nothing of this order is available for radial flow machines, particularly centrifugal compressors. Some methods and test facility for testing radial diffusing cascades have been described in sec. 8.7.

12.1 Elements of a Centrifugal Compressor Stage

Figures 12.1 and 12.2 show the principal elements of a centrifugal compressor stage.

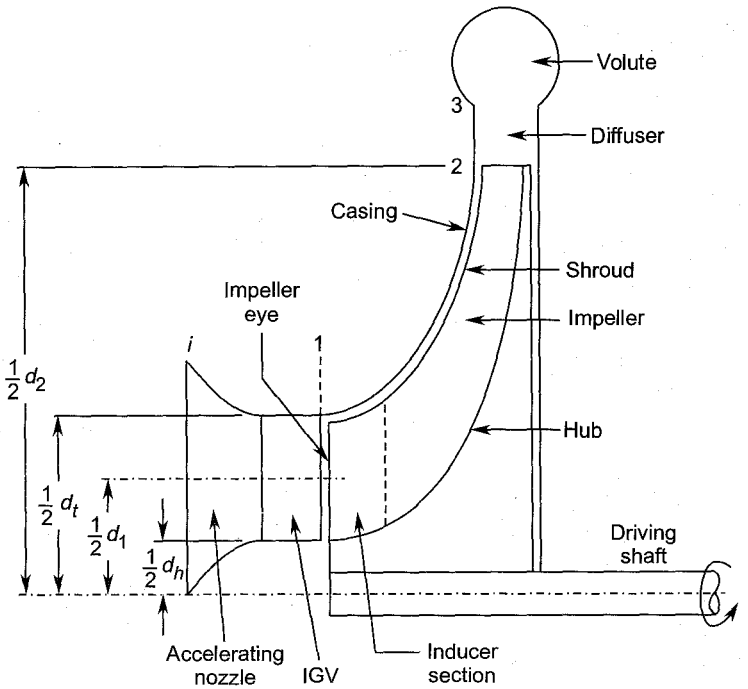

Fig. 12.1 Elements of a centrifugal compressor stage

The flow enters a three-dimensional impeller through an accelerating nozzle and a row of inlet guide vanes (IGVs). The inlet nozzle accelerates the flow from its initial conditions (at station i) to the entry of the inlet guide vanes. The IGVs direct the flow in the desired direction at the entry (station 1) of the impeller.

The impeller through its blades transfers the shaft work to the fluid and increases its energy level. It can be made in one piece consisting of both the inducer section and a largely radial portion. The inducer receives the flow between the hub and tip diameters (d_h, d_t) of the impeller eye and passes it on to the radial portion of the impeller blades. The flow approaching the impeller may be with or without swirl. The inducer section can be looked upon as an axial compressor rotor placed upstream of the radial impeller. In some designs this is made separately and then mounted on the shaft along with the radial impeller.

In a great majority of centrifugal compressors the impeller has straight radial blades after the inducer section. At high speeds, the impeller blades are subjected to high stresses which tend to straighten a curved impeller blade. Therefore, the choice of radial straight blades is more sound for higher peripheral speeds. However, in fan and blower applications (Chapter 15), on account of the relatively lower speeds, backward and forward-swept impeller blades are also used.

Unlike axial machines, the hub diameter of the radial impellers varies from the entry to the exit. The tips of the blades can be shrouded to prevent leakage, but manufacturing and other problems of the shrouded impellers have kept them open in most applications.

The impeller discharges the flow to the diffuser through a vaneless space (Fig. 12.2). Here the static pressure of the fluid rises further on account of the deceleration of the flow. The diffuser may be merely a vaneless space or may consist of a blade ring as shown in Fig. 12.2. For high performance, the design of the diffuser is as important as that of the impeller.

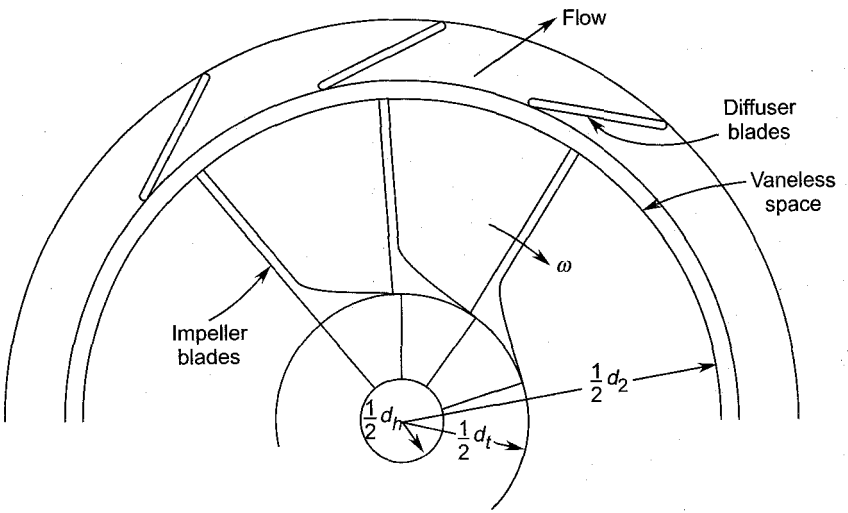

Fig. 12.2 A centrifugal compressor stage

The flow at the periphery of the diffuser is collected by a spiral casing known as the volute which discharges it through the delivery pipe.

Figure 12.3 shows a centrifugal impeller with blades located only in the radial section between diameters d_1 and d_2. To prevent high diffusion rate of the flow, the impeller blades are invariably narrower at a larger diameter ($b_2 < b_1$) as shown in the figure. The flow enters the impeller eye formed

by its hub and the casing, and then turns in the radial direction in the vaneless space between the hub and the casing upstream of the blade entry.

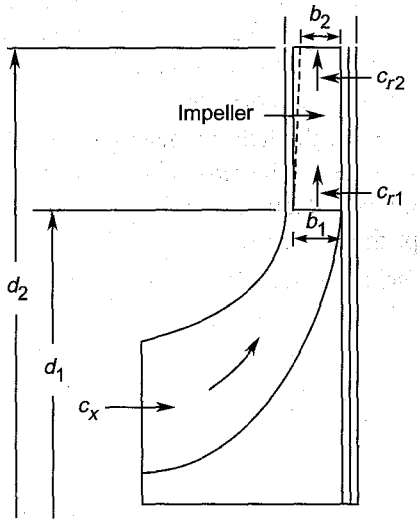

Fig. 12.3 Impeller with blades only in the radial section

12.2 Stage Velocity Triangles

The notation used here corresponds to the r, θ and x coordinate system. As per the convention for radial machines, the angles are measured from the tangential direction at a given point. The absolute and relative air angles at the entry and exit of the impeller are denoted by α_1, α_2 and β_1, β_2 respectively.

Since the change in radius between the entry and exit of the impeller is large, unlike in axial machines, the tangential velocities at these stations are different:

$$u_1 = \frac{\pi d_1 N}{60}$$

$$u_2 = \frac{\pi d_2 N}{60}$$

Entry velocity triangle

Figure 12.4 shows the flow at the entry of the inducer section of the impeller without IGVs. The absolute velocity (c_1) of the flow is axial ($\alpha_1 = 90°$) and the relative velocity (w_1) is at an angle β_1 from the tangential direction. Thus the swirl or whirl component $c_{\theta 1} = 0$.

$$\tan \beta_1 = \frac{c_1}{u_1} = \frac{c_{x1}}{u_1} \tag{12.1}$$

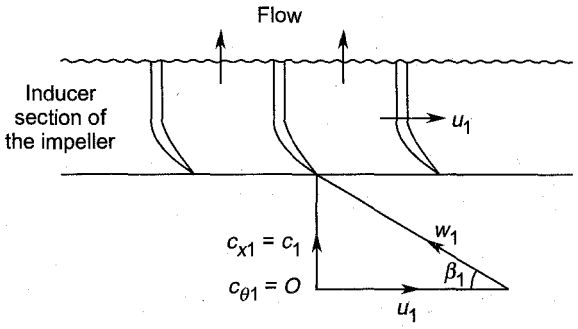

Fig. 12.4 Flow through the inducer section without inlet guide vanes

Figure 12.5 shows the flow through axially straight inducer blades in the presence of IGVs. The air angle (α_1) at the exit of the IGVs is such that it gives the direction of the relative velocity vector (w_1) as axial, i.e., $\beta_1 = 90°$. This configuration offers some manufacturing and aerodynamic advantages, viz., (i) centrifugal impellers with straight blades are much easier and cheaper to manufacture and (ii) the relative velocity (w_1) approaching the impeller is considerably reduced. In this case $\beta_1 = 90°$ and the positive swirl component is

$$c_{\theta 1} = u_1 \tag{12.2}$$

$$\tan \alpha_1 = \frac{w_1}{u_1} = \frac{c_{x1}}{u_1} \tag{12.3}$$

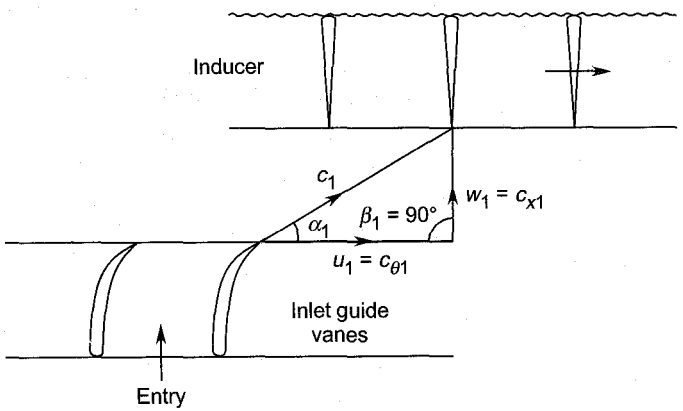

Fig. 12.5 Flow through the inducer section with inlet guide vanes

Figure 12.6 shows the entry and exit velocity triangles for impeller blades located only in the radial section. For the sake of generality, the

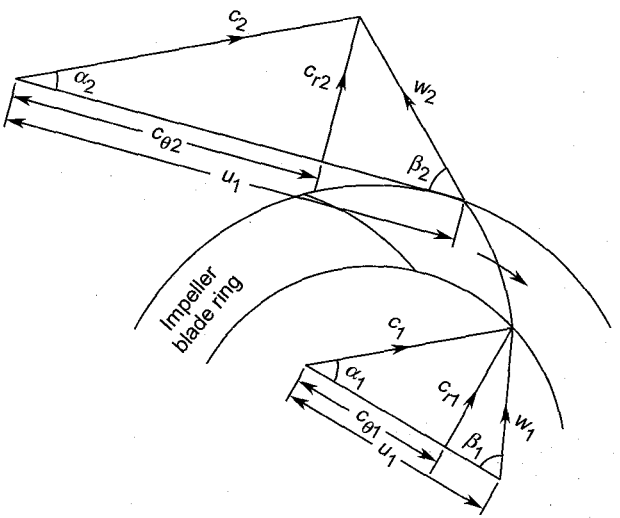

Fig. 12.6 Entry and exit velocity triangles for impeller blades only in the radial section, backward swept blades, $\beta_2 < 90°$

absolute velocity vector c_1 is shown to have a swirl component $c_{\theta 1}$. However, if there are no guide vanes, c_1 will be radial ($c_1 = c_{r1}$) and $\alpha_1 = 90°$, $c_{\theta 1} = 0$. This particular condition is expressed by "zero whirl or swirl" at the entry and would be assumed in this chapter unless mentioned otherwise.

Exit velocity triangle

The impeller blades shown in Fig. 12.6 are backward swept, i.e., $\beta_2 < 90°$. The exit velocity triangle for these blades is shown in the figure. The flow leaves the blades at a relative velocity w_2 and an air angle β_2. The absolute velocity of flow leaving the impeller is c_2 at an air angle α_2. Its tangential (swirl or whirl) component is $c_{\theta 2}$ and the radial component c_{r2}. The following relations are obtained from the velocity triangles at the entry and exit shown in Fig. 12.6:

$$c_{r1} = c_1 \sin \alpha_1 = w_1 \sin \beta_1 \tag{12.4}$$

$$c_{\theta 1} = c_1 \cos \alpha_1 = c_{r1} \cot \alpha_1 = u_1 - c_{r1} \cot \beta_1 \tag{12.5}$$

$$c_{r2} = c_2 \sin \alpha_2 = w_2 \sin \beta_2 \tag{12.6}$$

$$c_{\theta 2} = c_2 \cos \alpha_2 = c_{r2} \cot \alpha_2 = u_2 - c_{r2} \cot \beta_2 \tag{12.7}$$

Figure 12.7 shows the velocity triangles at the entry and exit of a radial-tipped impeller with blades extending into the inducer section. The velocity triangle at the entry is similar to that in Fig. 12.6; here c_{x1} replaces the velocity component c_{r1}.

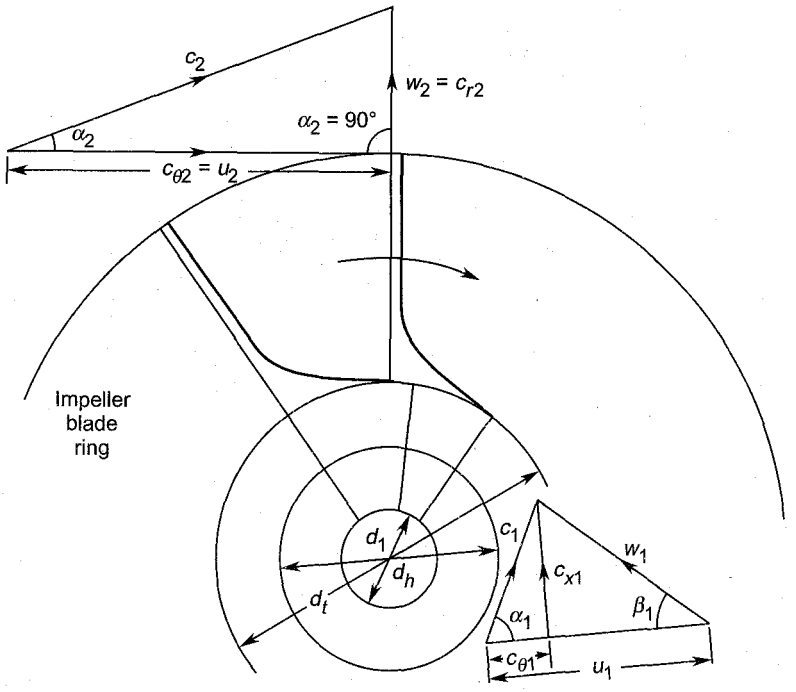

Fig. 12.7 Entry and exit velocity triangles for impeller with inducer blades, radial-tipped blades, $\beta_2 = 90°$

The exit velocity triangle here is only a special case of the triangle in Fig. 12.6 with $\beta_2 = 90°$. This condition when applied in Eqs. (12.6) and (12.7) gives

$$c_{r2} = w_2 = c_2 \sin \alpha_2 \tag{12.8}$$

$$c_{\theta 2} = c_2 \cos \alpha_2 = c_{r2} \cot \alpha_2 = u_2 \tag{12.9}$$

The mass-flow rate from the continuity equation for Figs. 12.3 and 12.6 can be written as

$$\dot{m} = \rho_1 c_{r1} \pi d_1 b_1 = \rho_2 c_{r2} \pi d_2 b_2 \tag{12.10}$$

This for Figs. (12.1) and (12.7) is

$$\dot{m} = \rho_1 c_{x1} \frac{\pi}{4} (d_t^2 - d_h^2) = \rho_2 c_{r2} \pi d_2 b_2 \tag{12.11}$$

Figure 12.8 shows the velocity triangles for forward-swept blades ($\beta_2 > 90°$) with zero swirl at the entry. It may be observed that such blades have large fluid deflection and give $c_{\theta 2} > u_2$. This increases the work capacity of the impeller and the pressure rise across it. This configuration is unsuitable for higher speeds in compressor practice and leads to higher losses. However, for fan applications such blades are used in multivane or drum-type centrifugal blowers (Sec. 15.4).

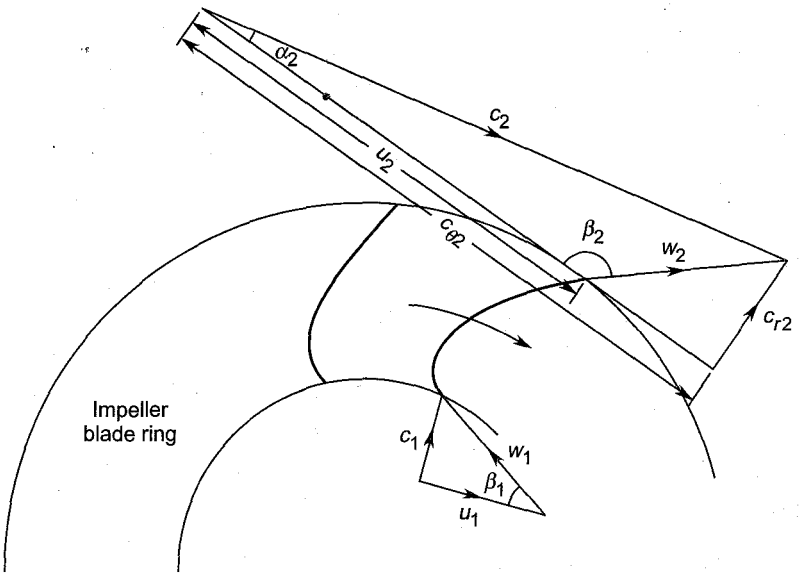

Fig. 12.8 Entry and exit velocity triangles for forward swept blades ($\beta_2 > 90°$) with zero swirl at entry

12.2.1 Stage Work

In a centrifugal compressor the peripheral velocities at the impeller entry and exit are u_1 and u_2 respectively. Therefore, the specific work or the energy transfer is

$$w = u_2 c_{\theta 2} - u_1 c_{\theta 1} \tag{12.12}$$

In this equation, if $c_{\theta 1}$ is positive (Figs. 12.5, 12.6 and 12.7), the term $u_1 c_{\theta 1}$ is subtractive. Therefore, the work and pressure rise in the stage are relatively lower. These quantities are increased by reducing $c_{\theta 1}$ to zero (Fig. 12.4) or making it negative.

In the absence of inlet guide vanes, $c_{\theta 1} = 0$. This condition will be assumed throughout in this chapter unless mentioned otherwise. Therefore, Eq. (12.12) gives

$$w = u_2 c_{\theta 2} \tag{12.13}$$

Substituting from Eq. (12.7)

$$w = u_2 (u_2 - c_{r2} \cot \beta_2)$$

The flow coefficient at the impeller exit is defined as

$$\phi_2 = \frac{c_{r2}}{u_2} \tag{12.14}$$

Therefore,

$$w = u_2^2 (1 - \phi_2 \cot \beta_2) \tag{12.15}$$

If ϕ_2 and β_2 are the actual values, the work given by Eq. (12.15) is the actual work in the stage.

The work is also given by the following form of Euler's equation:

$$w = \frac{1}{2}(c_2^2 - c_1^2) + \frac{1}{2}(w_1^2 - w_2^2) + \frac{1}{2}(u_2^2 - u_1^2) \qquad (12.16)$$

For a radial-tipped impeller with zero swirl (whirl) at the entry $\alpha_1 = 90°$, $\beta_2 = 90°$ and Eqs. (12.13) and (12.15) reduce to

$$w = u_2^2 \qquad (12.17)$$

12.2.2 Pressure Coefficient

The head, pressure or loading coefficient is defined in Sec. 7.4.1. As in earlier chapters, here also it is defined by

$$\psi = \frac{w}{u_2^2} \qquad (12.18)$$

This gives, in a dimensionless form, a measure of the pressure raising capacities of various types of centrifugal compressor impellers of different sizes running at different speeds. Equations (12.13) and (12.15) give

$$\psi = \frac{c_{\theta 2}}{u_2} \qquad (12.19a)$$

$$\psi = 1 - \phi_2 \cot \beta_2 \qquad (12.19b)$$

This expression gives the theoretical performance characteristics of impellers of different geometries. It may be noted that Eq. (12.19b) has been derived assuming zero entry swirl and no slip. Figure 12.9 shows the $\phi - \psi$ plots for forward-swept, radial and backward-swept impeller blades. The actual characteristics will be obtained by accounting for stage losses.

The backward-swept and radial blade impellers give stable characteristics. The forward-swept type gives unstable flow conditions on account of the rising characteristic as explained in Sec. 11.8.2 (Fig. 11.18).

Equations (12.19) for radial-tipped blades give

$$\psi = 1$$

12.2.3 Stage Pressure Rise

The static pressure rise in a centrifugal compressor stage occurs in the impeller, diffuser and the volute. The transfer of energy by the impeller takes place along with the energy transformation process. The pressure rise across the impeller is due to both the diffusion of the relative velocity vector w_1 to w_2 and the change in the centrifugal energy (see Sec. 6.9.2).

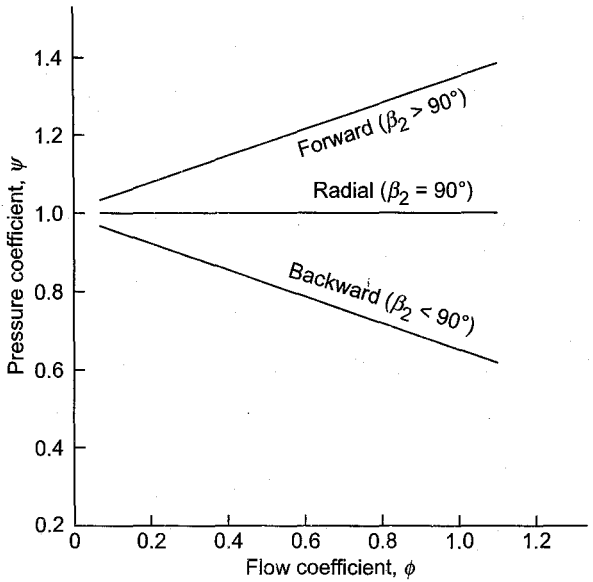

Fig. 12.9 Performance characteristics of different types of centrifugal impellers ($c_{\theta 1} = 0$, $\mu = 1$)

The static pressure rise across the diffuser and volute (if any) occurs simply due to the energy transformation processes accompanied by a significant deceleration of the flow. The initial kinetic energy (at the entry of the diffuser) is supplied by the impeller.

In this section the pressure rise (or pressure ratio) across the stage is first determined for an isentropic process.

For small values of the stage pressure rise (as in axial stages and centrifugal fans), the flow can be assumed to be incompressible. Therefore,

$$\frac{1}{\rho} \Delta p_0 = \Delta h_0 = w = u_2^2 (1 - \phi_2 \cot \beta_2)$$

$$\Delta p_0 = \rho u_2^2 (1 - \phi_2 \cot \beta_2) \tag{12.20}$$

Substituting from Eq. (12.19b)

$$\Delta p_0 = \rho \psi u_2^2 \tag{12.21}$$

However, the pressure rise in a centrifugal compressor stage is high and the change in the density of the fluid across the stage is considerable. Therefore, in most applications, the flow is not incompressible. The pressure ratio for compressible flow is obtained by the following method:

The fluid is assumed to be a perfect gas. Therefore,

$$w = \Delta h_0 = c_p (T_{02s} - T_{01})$$

$$w = c_p T_{01} \left(\frac{T_{02s}}{T_{01}} - 1 \right)$$

$$w = c_p T_{01} \left(p_{r0}^{\frac{\gamma - 1}{\gamma}} - 1 \right) \tag{12.22}$$

Substituting from Eq. (12.15)

$$c_p T_{01} \left(p_{r0}^{\frac{\gamma - 1}{\gamma}} - 1 \right) = u_2^2 (1 - \phi_2 \cot \beta_2)$$

This on rearrangement yields

$$p_{r0} = \frac{p_{02}}{p_{01}} = \left\{ 1 + (1 - \phi_2 \cot \beta_2) \frac{u_2^2}{c_p T_{01}} \right\}^{\frac{\gamma}{\gamma - 1}} \tag{12.23}$$

$$p_{r0} = \left(1 + \frac{\psi u_2^2}{c_p T_{01}} \right)^{\frac{\gamma}{\gamma - 1}} \tag{12.24}$$

12.3 Enthalpy-entropy Diagram

Figure 12.10 shows an enthalpy-entropy diagram for a centrifugal compressor stage (Figs. 12.1 and 12.2). Flow process occuring in the accelerating nozzle (i-1), impeller (1-2), diffuser (2-3) and the volute (3-4) are depicted with values of static and stagnation pressures and enthalpies.

The flow, both in the inlet nozzle and guide vanes is accelerating from static pressure p_i. On account of the losses and increase in the entropy the stagnation pressure loss is $p_{0i} - p_{01}$, but the stagnation enthalpy remains constant:

$$h_{0i} = h_{01} \tag{12.25a}$$

$$h_i + \frac{1}{2} c_i^2 = h_1 + \frac{1}{2} c_1^2 \tag{12.25b}$$

The isentropic compression is represented by the process 1-2s-4ss. This process does not suffer any stagnation pressure loss:

$$p_{02s} = p_{03ss} = p_{04ss} \tag{12.26}$$

The stagnation enthalpy remains constant.

$$h_{02s} = h_{03ss} = h_{04ss} \tag{12.27}$$

The energy transfer (and transformation) occurs only in the impeller blade passages. The actual (irreversible adiabatic) process is represented by 1-2. The stagnation enthalpies in the relative system at the impeller entry and exit are

$$h_{01\text{rel}} = h_1 + \frac{1}{2} w_1^2 \tag{12.28}$$

$$h_{02\text{rel}} = h_2 + \frac{1}{2} w_2^2 \tag{12.29}$$

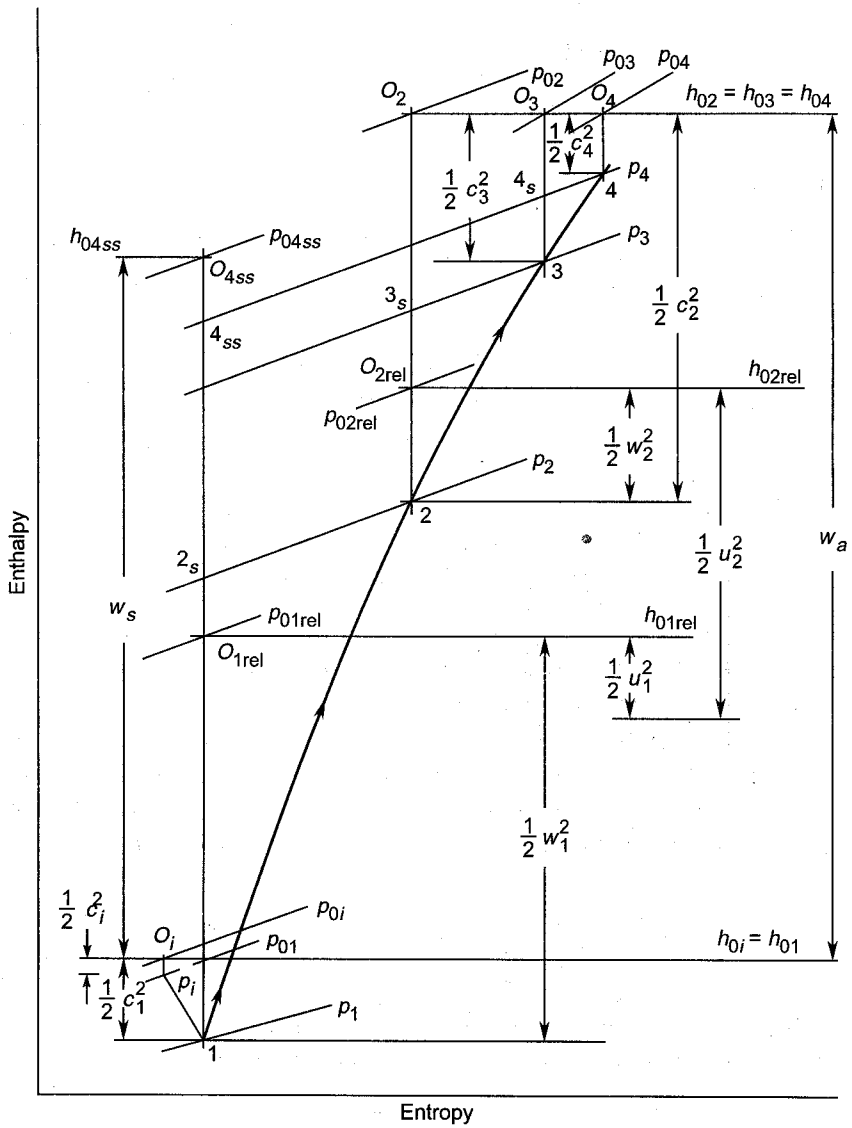

Fig. 12.10 Enthalpy-entropy diagram for flow through a centrifugal compressor stage

The corresponding stagnation pressures are $p_{01\text{rel}}$ and $p_{02\text{rel}}$.

Static pressure rise in the diffuser and the the volute occurs during the processes 2-3 and 3-4 respectively. The stagnation enthalpy remains constant from station 2 to 4 but the stagnation pressure decreases progressively.

$$h_{02} = h_{03} = h_{04} \tag{12.30}$$

$$p_{02} > p_{03} > p_{04} \tag{12.31}$$

The actual energy transfer (work) appears as the chage in the stagnation enthalpy. Therefore, from Eq. (12.16)

$$w_a = h_{02} - h_{01} = \frac{1}{2}(c_2^2 - c_1^2) + \frac{1}{2}(w_1^2 - w_2^2) + \frac{1}{2}(u_2^2 - u_1^2)$$

This on rearrangement gives

$$h_2 - h_1 + \frac{1}{2}(w_2^2 - w_1^2) - \frac{1}{2}(u_2^2 - u_1^2) = 0$$

$$\left(h_2 + \frac{1}{2}w_2^2\right) - \frac{1}{2}u_2^2 = \left(h_1 + \frac{1}{2}w_1^2\right) - \frac{1}{2}u_1^2 \qquad (12.32a)$$

$$h_{02\text{rel}} - \frac{1}{2}u_2^2 = h_{01\text{rel}} - \frac{1}{2}u_1^2 \qquad (12.32b)$$

This relation is also shown on the *h-s* diagram (Fig. 12.10).

12.3.1 Stage Efficiency

The actual work input to the stage is

$$w_a = h_{04} - h_{01} = u_2^2(1 - \phi_2 \cot \beta_2) \qquad (12.33a)$$

For a perfect gas,

$$w_a = c_p(T_{04} - T_{01}) = u_2^2(1 - \phi_2 \cot \beta_2) \qquad (12.33b)$$

The ideal work between the same static pressures p_1 and p_4 is

$$w_s = h_{04ss} - h_{01} = c_p(T_{04ss} - T_{01}) \qquad (12.34a)$$

$$w_s = c_p T_{01}\left\{\frac{T_{04ss}}{T_{01}} - 1\right\}$$

$$w_s = c_p T_{01}\{p_{r0}^{\frac{\gamma-1}{\gamma}} - 1\} \qquad (12.34b)$$

Here the stagnation pressure ratio

$$p_{r0} = \frac{p_{04ss}}{p_{01}} \approx \frac{p_{04}}{p_{01}} \qquad (12.35)$$

The last relation in Eq. (12.35) is valid for incompressible flow assuming $c_4 \approx c_{4ss}$

The ideal and actual values of the stage work are shown in Fig. 12.10. The total-to-total efficiency of the stage can now be defined by

$$\eta_{st} = \frac{w_s}{w_a} = \frac{h_{04ss} - h_{01}}{h_{04} - h_{01}} \qquad (12.36a)$$

$$\eta_{st} = \frac{c_p(T_{04ss} - T_{01})}{u_2^2(1 - \phi_2 \cot \beta_2)} \qquad (12.36b)$$

$$\eta_{st} = \frac{c_p T_{01} (p_{r0}^{\frac{\gamma-1}{\gamma}} - 1)}{u_2^2 (1 - \phi_2 \cot \beta_2)} \tag{12.36c}$$

This equation yields the pressure ratio of the stage for the given initial state of the gas and values of u_2, ϕ_2 and β_2.

$$p_{r0} = \left\{ 1 + \eta_{st} (1 - \phi_2 \cot \beta_2) \frac{u_2^2}{c_p T_{01}} \right\}^{\frac{\gamma}{\gamma-1}} \tag{12.37}$$

This is similar to Eq. (12.23) for $\eta_{st} = 1$ (reversible stage).

12.3.2 Degree of Reaction

A large proportion of energy in the gas at the impeller exit is in the form of kinetic energy. This is converted into static pressure rise by the energy transformation process in the diffuser and volute casing. The division of static pressure rise in the stage between the impeller and the stationary diffusing passages is determined by the degree of reaction. This can be defined either in terms of pressure changes or enthalpy changes in the impeller and the stationary diffusing passages. The discussions given in Secs. 9.5.2 and 11.2.2 explain various methods of defining the degree of reaction.

Expressions for the degree of reaction in this section are derived from the following definition.

$$R = \frac{\text{change in static enthalpy in the impeller}}{\text{change in stagnation enthalpy in the stage}}$$

$$R = \frac{h_2 - h_1}{h_{02} - h_{01}} \tag{12.38}$$

From Eq. (12.32a)

$$h_2 - h_1 = \frac{1}{2} (u_2^2 - w_2^2) + \frac{1}{2} (w_1^2 - u_1^2) \tag{12.39}$$

For zero swirl at the entry ($c_{\theta 1} = 0$)

$$h_{02} - h_{01} = u_2 c_{\theta 2} \tag{12.40}$$

Therefore, Eqs. (12.39) and (12.40) when put into Eq. (12.38) give

$$R = \frac{(u_2^2 - w_2^2) + (w_1^2 - u_1^2)}{2u_2 c_{\theta 2}} \tag{12.41}$$

For the constant radial velocity component.

$$c_1 = c_{r1} = c_{r2}$$

With inducer blades and zero entry swirl (Fig. 12.4),

$$c_1 = c_{x1} = c_{r2}$$

With these conditions, the following expressions are obtained from the entry and exit velocity triangles:

$$w_1^2 - u_1^2 = c_{r1}^2 = c_{r2}^2 \tag{12.42}$$

$$w_2^2 = c_{r2}^2 + (u_2 - c_{\theta 2})^2 = c_{r2}^2 + u_2^2 - 2u_2 c_{\theta 2} + c_{\theta 2}^2$$

$$u_2^2 - w_2^2 = 2u_2 c_{\theta 2} - c_{\theta 2}^2 - c_{r2}^2 \tag{12.43}$$

Equations (12.42) and (12.43), when used in Eq. (12.41), give

$$R = 1 - \frac{1}{2}\left(\frac{c_{\theta 2}}{u_2}\right) \tag{12.43a}$$

Substituting from Eq. (12.7) and rearranging

$$R = \frac{1}{2} + \frac{1}{2}\,\phi_2 \cot \beta_2 \tag{12.43b}$$

Equation (12.43b) is plotted in Fig. 12.11. The degree of reaction of the radial-tipped impeller ($\beta_2 = 90°$) remains constant at all values of the flow

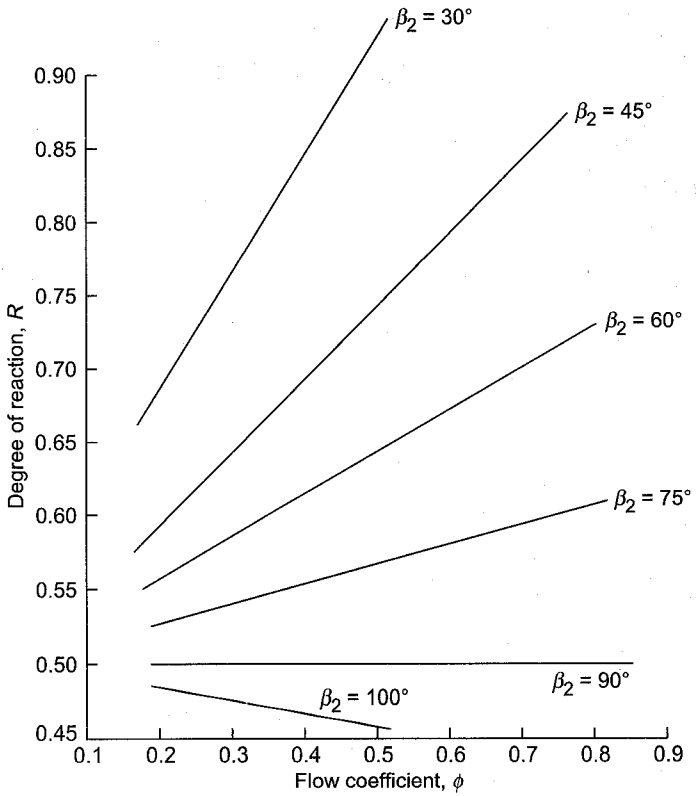

Fig. 12.11 Variation of degree of reaction with flow coefficient for various values of impeller exit air angle

coefficient. Reaction increases with flow coefficient for backward-swept impeller blades ($\beta_2 < 90°$) and decreases for forward swept type ($\beta_2 > 90°$) as shown.

From Eq. (12.19a)

$$R = 1 - \frac{1}{2}\psi \tag{12.44a}$$

$$\psi = 2(1 - R) \tag{12.44b}$$

Equation (12.44) shows that the higher the degree of reaction, the lower is the stage pressure coefficient and vice versa. This is depicted in Fig. 12.12. The backward-swept impeller blades give a higher degree of reaction and a lower pressure coefficient compared to the radial and forward-swept blades.

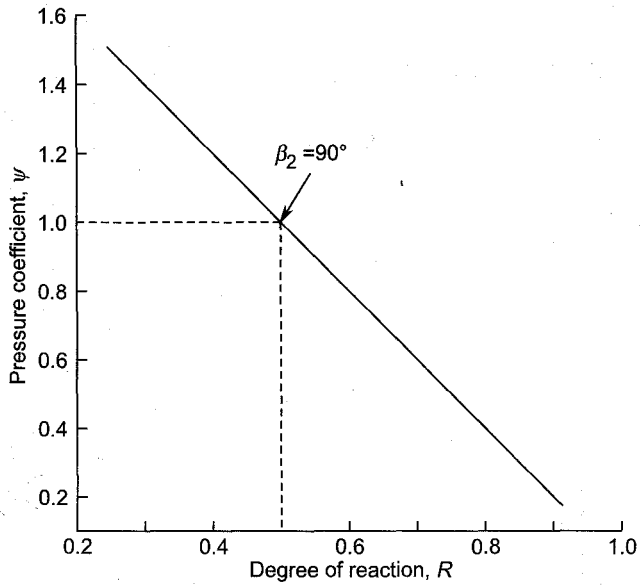

Fig. 12.12 Variation of pressure coefficient with degree of reaction

12.4 Nature of Impeller Flow

The flow pattern in the three-dimensional flow passage of the impeller of a centrifugal compressor is very complex. Various coordinate systems have been used to describe the flow field in such passages. Section 6.4 describes a natural coordinate system (Fig. 6.6).

To simplify the understanding of the flow in a radial turbo-machine the flow field can be separately considered in the radial-axial (meridional) plane (Fig. 12.13) and the vane-to-vane plane (Fig. 12.14). Further

simplification in the theoretical analysis of such a flow is obtained by assuming it to be inviscid.

12.4.1 Flow in the Meridional Plane

An infinitesimal fluid element (at radius r) in the meridional plane between the hub and the shroud is shown in Fig. 12.13. The meridional streamline passing at the centre of the element has a radius of curvature R. The meridional velocity is c_m and the velocity component in the tangential direction c_θ.

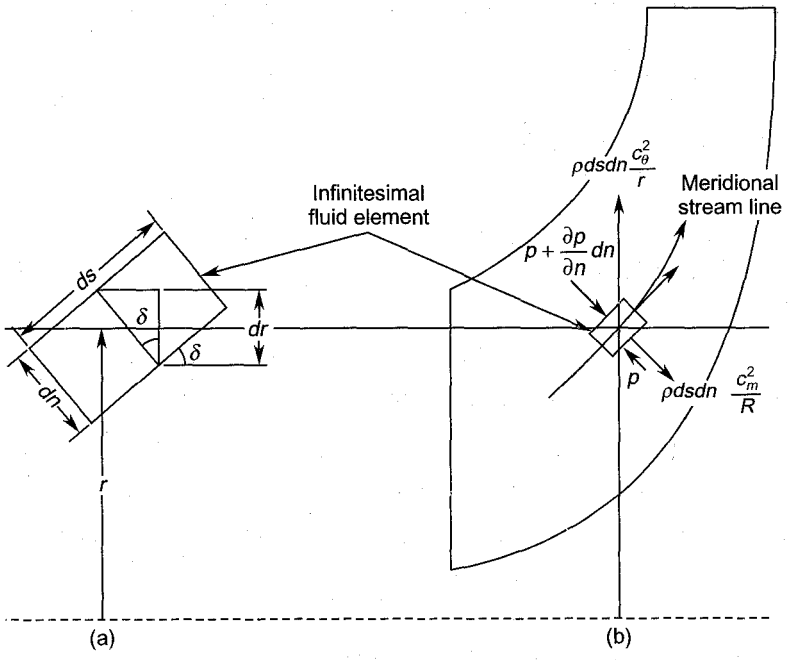

Fig. 12.13 Flow in the meridional plane

It is very convenient to study such a flow in the natural coordinate system. An expression for the meridional velocity distribution in the normal direction (n – direction) is derived here under the following assumptions:

1. isentropic and incompressible flow
2. axisymmetric flow
3. radial blades.

The thickness of the element (normal to the paper) is unity. Therefore, its volume is $ds\ dn$.

The fluid element is subjected to the centrifugal forces both due to the impeller rotation and the curvature of the meridional streamline as shown in Fig. 12.13(b).

The centrifugal force due to the tangential velocity component c_θ is

$$\rho\, ds\, dn\, \frac{c_\theta^2}{r}$$

and that due to the curvature of the streamline is

$$\rho\, ds\, dn\, \frac{c_m^2}{R}$$

Equating the forces acting on the element in the normal direction

$$p\, ds + \rho\, ds\, dn\, \frac{c_\theta^2}{r}\, \cos\, \delta = \left(p + \frac{\partial p}{\partial n}\, dn\right) ds + \rho\, ds\, dn\, \frac{c_m^2}{R}$$

This on rearrangement gives

$$\frac{1}{\rho}\frac{\partial p}{\partial n} = \frac{c_\theta^2}{r}\, \cos\, \delta - \frac{c_m^2}{R} \tag{12.45}$$

From Fig. 12.13(a)

$$\frac{\partial r}{\partial n} = \cos\, \delta \tag{12.46}$$

For axisymmetric flow and radial blades,

$$\left.\begin{aligned} c_\theta &= u = \omega r \\ c_m &= w \end{aligned}\right\} \tag{12.47}$$

Equations (12.46) and (12.47), when applied in Eq. (12.45), yield

$$\frac{1}{\rho}\frac{\partial p}{\partial n} = \omega^2 r\, \frac{\partial r}{\partial n} - \frac{w^2}{R} \tag{12.48}$$

Equation (12.32a) gives the general relation

$$h + \frac{1}{2}\, w^2 - \frac{1}{2}\, u^2 = \text{const.}$$

Differentiating and rearranging

$$dh = u\, du - w\, dw \tag{12.49}$$

For isentropic flow $dh = \dfrac{dp}{\rho}$

and $$u\, du = \omega^2 r\, dr$$

Therefore, dividing throughout by dn, Eq. (12.49) can be rewritten as

$$\frac{1}{\rho}\frac{\partial p}{\partial n} = \omega^2 r\, \frac{\partial r}{\partial n} - w\, \frac{\partial w}{\partial n} \tag{12.50}$$

Combining Eqs. (12.48) and (12.50),

$$\frac{dw}{w} = \frac{dn}{R} \tag{12.51}$$

This on integration gives

$$\ln w + \ln (\text{const.}) = \int \frac{dn}{R}$$

$$w = c_m = ke^{\int \frac{dn}{R}} \tag{12.52}$$

Equation (12.52) gives the velocity distribution in the meridional plane. The value of the constant k can be determined from the continuity equation.

The mass-flow rate through the infinitesimal stream tube of cross-sectional area $dn \times 1$ is

$$d\dot{m} = \rho\, c_m\, (2\pi r\, dn)$$

Substituting from Eq. (12.52)

$$d\dot{m} = 2\, \rho\pi r\, dn\, k \exp \int \frac{dn}{R}$$

The total mass-flow rate is obtained by integrating this from hub to the shroud.

$$\dot{m} = 2\pi k \int \left\{ \rho r \exp \int \frac{dn}{R} \right\} dn \tag{12.53}$$

12.4.2 Flow in the Vane-to-Vane Plane

Figure 12.14 shows an infinitesimally thin slice of the flow between the two backward-swept blades of an impeller. An element of the flow between two streamlines dm apart is subtended by an angle $d\theta$. The relative velocity on one side of the element is w and on the other side

$$w + \frac{\partial w}{\partial m}\, dm$$

The circulation around (anti-clockwise) this element is

$$d\Gamma = \left(w + \frac{\partial w}{\partial m} dm \right) (R + dm)\, d\theta - w\, R d\theta$$

Neglecting the product of two small quantities and substituting

$$dA = R\, d\theta\, dm$$

$$\frac{d\Gamma}{dA} = \frac{\partial w}{\partial m} + \frac{w}{R}$$

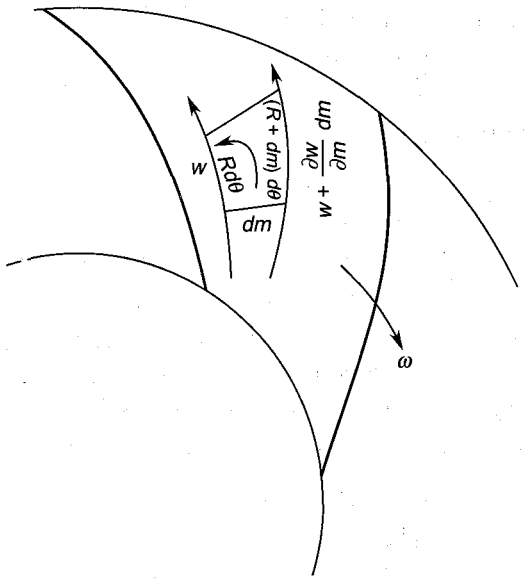

Fig. 12.14 Flow in the vane-to-vane plane

This is the vorticity in the vane-to-vane plane (see Sec. 6.3.3).

$$\xi = \frac{\partial w}{\partial m} + \frac{w}{R} \tag{12.54}$$

Helmholtz law states that the change in the absolute vorticity of an inviscid fluid with time is zero.

In the present case the fluid is assumed to enter the impeller passage without any vorticity. Therefore, if the absolute vorticity in the impeller passage (rotating with an angular velocity ω) is to be zero, the flow inside it must have a rotation of $-\omega$.

However,

$$\text{Rotation} = \frac{1}{2} \text{ vorticity}$$

$$\omega = \frac{1}{2}\xi \tag{12.55}$$

Equations (12.54) and (12.55) give

$$\frac{\partial w}{\partial m} + \frac{w}{R} = 2\omega \tag{12.56}$$

Equation (12.56) gives the velocity distribution in the vane-to-vane plane. This rotational flow in the relative system is referred to as "relative eddy". It affects the energy transfer in the impeller and hence the pressure ratio developed as discussed in the following section.

12.5 Slip Factor[455, 488, 490]

The actual velocity profiles at the impeller exit due to real flow behaviour are shown in Figs. 12.15 and 12.16. The energy transfer occurring in the

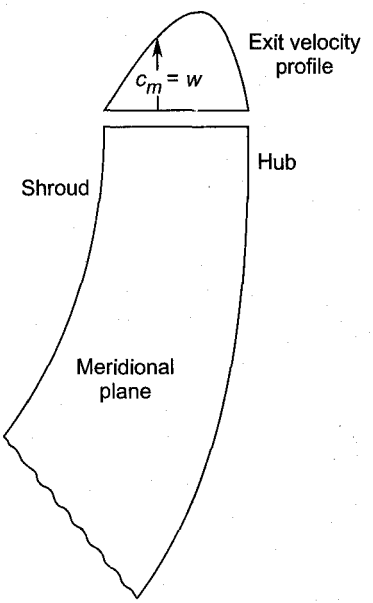

Fig. 12.15 Meridional velocity distribution at the impeller exit

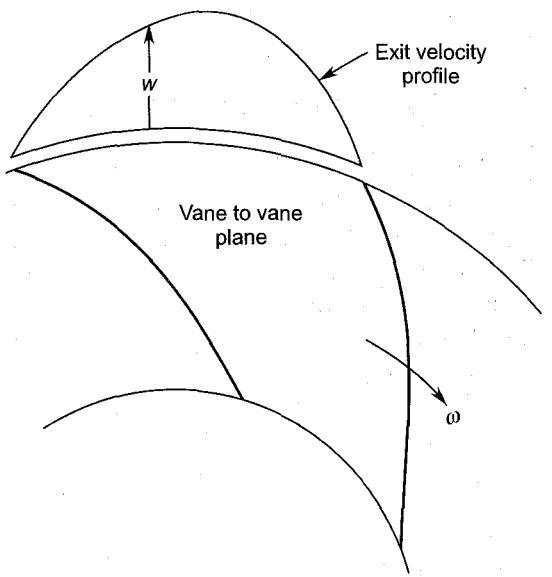

Fig. 12.16 Vane-to-vane velocity distribution at the impeller exit

impeller corresponding to these velocity profiles is less than the one that would have been obtained with one-dimensional flow.

The relative eddy mentioned earlier causes the flow in the impeller passages to deviate (Fig. 12.17) from the blade angle (β_2) at the exit to an angle β'_2, the difference being larger for a larger blade pitch or smaller number of impeller blades.

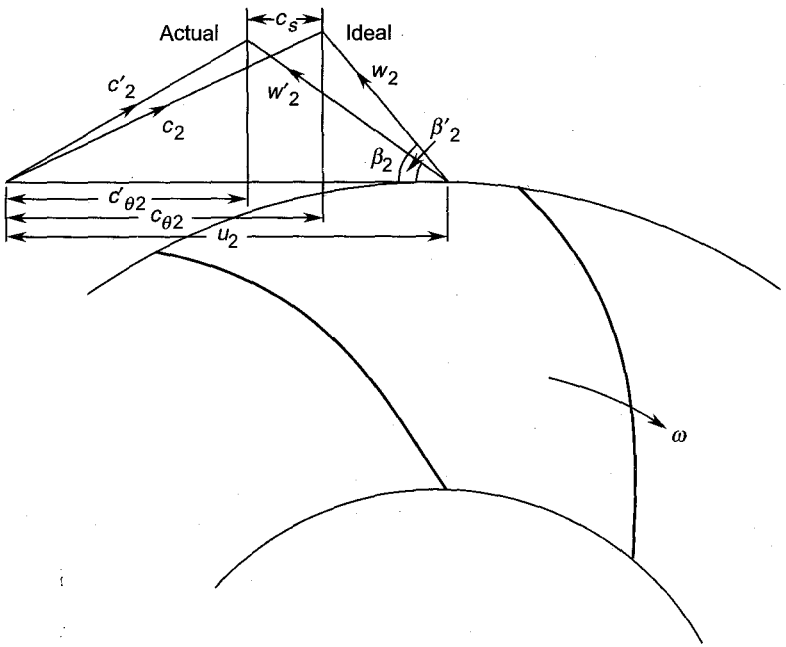

Fig. 12.17 Exit velocity triangles with and without slip

On account of the aforementioned effects, the apex of the actual velocity triangle at the impeller exit is shifted away (opposite to the direction of rotation) from the apex of the ideal velocity triangle as shown in Fig. 12.17. This phenomenon is known as slip and the shift of the apex is the slip velocity (c_s). It may be seen that, on account of the slip, the whirl component is reduced which in turn decreases the energy transfer and the pressure developed.

The ratio of the actual and ideal values of the whirl components at the exit is known as slip factor (μ)

$$\mu = \frac{c'_{\theta 2}}{c_{\theta 2}} \tag{12.57}$$

Therefore, the slip velocity is given by

$$c_s = c_{\theta 2} - c'_{\theta 2} = (1 - \mu)\, c_{\theta 2} \tag{12.58}$$

The expressions for the actual work done, pressure ratio and stage efficiency can now be rewritten with the slip factor. From Eqs. (12.13) and (12.15)

$$w = \mu\, u_2\, c_{\theta 2} = \mu\, u_2^2\, (1 - \phi_2 \cot \beta_2) \tag{12.59}$$

Similarly, Eqs. (12.36c) and (12.37) are modified to

$$\therefore \qquad \eta_{st} = \frac{c_p T_{01}\, (p_{r0}^{\frac{\gamma-1}{\gamma}} - 1)}{\mu\, u_2^2\, (1 - \phi_2 \cot \beta_2)} \tag{12.60}$$

$$p_{r0} = \left\{1 + \eta_{st}\, (1 - \phi_2 \cot \beta_2)\, \frac{\mu\, u_2^2}{c_p T_{01}}\right\}^{\frac{\gamma}{\gamma-1}} \tag{12.61}$$

The methods of determining slip factors have been suggested by various investigators. Some of them are described here briefly.

12.5.1 Stodola's Theory

Figure 12.18 depicts the model of flow with slip as suggested by Stodola[12]. The relative eddy is assumed to fill the entire exit section of the impeller passage. It is considered equivalent to the rotation of a cylinder of diameter $d = 2r$ at an angular velocity ω which is equal and opposite to that of the impeller (Sec. 12.4.2) as shown in the figure. The diameter, and hence, the tangential velocity of the cylinder, is approximately determined as follows:

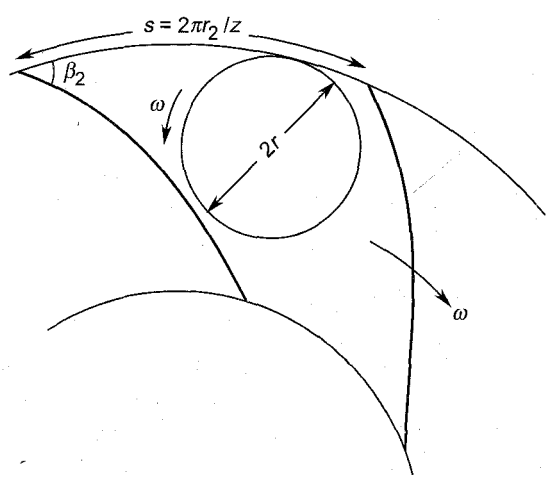

Fig. 12.18 Stodola's model of flow with slip

The blade pitch at the outer radius (r_2) of the impeller with z blades is

$$s = \frac{2\pi r_2}{z}$$

The diameter of the cylinder is

$$2r \approx s \sin \beta_2 = \frac{2\pi r_2}{z} \sin \beta_2 \tag{12.62}$$

The slip velocity is assumed to be due to rotation of the cylinder. Therefore,

$$c_s = \omega r$$

Substituting for r from Eq. (12.62)

$$c_s = \omega \frac{\pi r_2}{z} \sin \beta_2 \tag{12.63}$$

However, $u_2 = \omega r_2$. Therefore,

$$c_s = \frac{\pi}{z} u_2 \sin \beta_2 \tag{12.64}$$

Equation (12.64) when put in Eq. (12.58) gives

$$(1 - \mu)\, c_{\theta 2} = \frac{\pi}{z} u_2 \sin \beta_2$$

$$\mu = 1 - \frac{\pi}{z} \frac{u_2}{c_{\theta 2}} \sin \beta_2$$

Substituting from Eq. (12.7)

$$\mu = 1 - \frac{\pi}{z} \frac{\sin \beta_2}{1 - \phi_2 \cot \beta_2} \tag{12.65}$$

For a radial-tipped blade impeller ($\beta_2 = 90°$)

$$\mu = 1 - \frac{\pi}{z} \tag{12.66}$$

The above expressions for slip show that for a given geometry of flow the slip factor increases with the number of impeller blades. Along with this the fact that the number of impeller blades is one of the governing parameters for losses should not be lost sight of.

12.5.2 Stanitz's Method

A method based on the solution of potential flow in the impeller passages is suggested by Stanitz[800] for $\beta_2 = 45° - 90°$. The slip velociy is found to be independent of the blade exit angle and the compressibility. This is given by

$$c_s = \frac{1.98}{z} u_2 \tag{12.67}$$

$$(1 - \mu)\, c_{\theta 2} = \frac{1.98}{z}\, u_2$$

$$\mu = 1 - \frac{1.98}{z}\frac{u_2}{c_{\theta 2}}$$

$$\mu = 1 - \frac{1.98}{z\,(1 - \phi_2 \cot \beta_2)} \tag{12.68}$$

For $\beta_2 = 90°$

$$\mu = 1 - \frac{1.98}{z} \tag{12.69}$$

Equations (12.66) and (12.69) are of identical form.

12.5.3 Balje's Formula

Balje suggests an approximate formula for radial-tipped ($\beta_2 = 90°$) blade impellers:

$$\mu = \left\{1 + \frac{6.2}{z n^{2/3}}\right\}^{-1} \tag{12.70}$$

$$n = \frac{\text{impeller tip diameter}}{\text{eye tip diameter}}$$

12.6 Diffuser

The static pressure of the gas at the impeller exit is further raised by passing it through a diffuser located around the impeller periphery. The absolute velocity (c_2) of the gas at the impeller exit is high which is reduced to a lower velocity (c_3) in the diffuser as shown in the enthalpy-entropy diagram (Fig. 12.10). The amount of deceleration and the static pressure rise ($p_3 - p_2$) in the diffuser depend on the degree of reaction and the efficiency of the diffusion process. An efficient diffuser must have minimum losses ($p_{02} - p_{03}$), maximum efficiency and maximum recovery coefficient.

Expressions for the efficiency and pressure recovery coefficient have been derived in Sec. 2.4. A facility for testing the performance of a decelerating radial cascade (radial vaned diffuser) is described in Sec. 8.7.1. Diffusers in centrifugal compressors are either of the vaneless or vaned type.

12.6.1 Vaneless Diffuser

As the name indicates, the gas in a vaneless diffuser is diffused in the vaneless space around the impeller before it leaves the stage through a volute casing. In some applications the volute casing is omitted.

The gas in the vaneless diffuser gains static pressure rise simply due to the diffusion process from a smaller diameter (d_2) to a larger diameter (d_3). The corresponding areas of cross-sections in the radial direction are

$$A_2 = \pi d_2 b_2 = 2\pi r_2 b_2 \tag{12.71a}$$

$$A_3 = \pi d_3 b_3 = 2\pi r_3 b_3 \tag{12.71b}$$

Such a flow in the vaneless space is a free-vortex flow in which the angular momentum remains constant. This condition gives

$$r_2 c_{\theta 2} = r_3 c_{\theta 3} \tag{12.72}$$

The continuity equation at the entry and exit sections of the vaneless diffuser gives

$$\rho_2 c_{r2} A_2 = \rho_3 c_{r3} A_3$$

$$\rho_2 c_{r2} (2\pi r_2 b_2) = \rho_3 c_{r3} (2\pi r_3 b_3)$$

$$\rho_2 r_2 c_{r2} b_2 = \rho_3 r_3 c_{r3} b_3 \tag{12.73a}$$

For a small pressure rise across the diffuser, $\rho_2 \approx \rho_3$. Therefore,

$$r_2 c_{r2} b_2 = r_3 c_{r3} b_3 \tag{12.73b}$$

For a constant width (parallel wall) diffuser $b_2 = b_3$

$$r_2 c_{r2} = r_3 c_{r3} \tag{12.73c}$$

The absolute velocity at the diffuser exit is given by

$$c_3^2 = c_{r3}^2 + c_{\theta 3}^2 = \left(\frac{r_2}{r_3}\right)^2 (c_{r2}^2 + c_{\theta 2}^2) = \frac{r_2^2}{r_3^2} c_2^2 \tag{12.74}$$

Equations (12.72), (12.73c) and (12.74) yield

$$\frac{c_{\theta 3}}{c_{\theta 2}} = \frac{c_{r3}}{c_{r2}} = \frac{c_3}{c_2} = \frac{r_2}{r_3} \tag{12.75}$$

This relation further gives

$$\alpha_2 = \alpha_3 = \tan^{-1} \frac{c_{r2}}{c_{\theta 2}} = \tan^{-1} \frac{c_{r3}}{c_{\theta 3}} \tag{12.76}$$

It should be remembered that this equation is valid only for incompressible flow through a constant width diffuser.

Equation (12.75) clearly shows that the diffusion is directly proportional to the diameter ratio (d_3/d_2). This leads to a relatively largesized diffuser which is a serious disadvantage of the vaneless type. In some cases the overall diameter of the compressor may be impractically large. This is a serious limitation which prohibits the use of vaneless diffusers in aeronautical applications. Besides this the vaneless diffuser has a lower efficiency and can be used only for a small pressure rise.

However, for industrial applications, where large-sized compressors are acceptable, the vaneless diffuser is economical and provides a wider range of operation. Besides this, it does not suffer from blade stalling and shock waves.

12.6.2 Vaned Diffuser

For a higher pressure ratio across the radial diffuser, the diffusion process has to be achieved across a relatively shorter radial distance. This requires the application of vanes which provide greater guidance to the flow in the diffusing passages. Diffuser blade rings can be fabricated from sheet metal or cast in cambered and uncambered shapes of uniform thickness (Figs. 12.19 and 12.20). Figure 12.21 shows a diffuser ring made up of cambered aerofoil blades.

To avoid separation of flow, the divergence of the diffuser blade passages in the vaned diffuser ring can be kept small by employing a large number of vanes. However, this can lead to higher friction losses. Thus an optimum number of diffuser vanes must be employed. The divergence of the flow passages must not exceed 12 degrees.

The flow leaving the impeller has jets and wakes. When such a flow enters a large number of diffuser passages, the quality of flow entering different diffuser blade passages differs widely and some of the blades may experience flow separation leading to rotating stall and poor performance. To avoid such a possibility, it is safer to provide a smaller number of diffuser blades than that of the impeller. In some designs the number of diffuser blades is kept one-third of the number of impeller blades. This arrangement provides a diffuser passage with flows from a number of impeller blade channels. Thus the nature of flow entering various diffuser passages does not differ significantly.

Another method to prevent steep velocity gradients at the diffuser entry is to provide a small ($0.05\ d_2 - 0.1\ d_2$) vaneless space between the impeller exit and the diffuser entry as shown in Figs. 12.2 and 12.22. This allows the non-uniform impeller flow to mix out and enter the diffuser with less steep velocity profiles. Besides this the absolute velocity (Mach number) of the flow is reduced at the diffuser entry. This is a great advantage, specially if the absolute Mach number at the impeller exit is greater than unity. The supersonic flow at the impeller exit is decelerated in this vaneless space at constant angular momentum without shock.

Every diffuser blade ring is designed for given flow conditions at the entry at which optimum performance is obtained. Therefore, at off-design operations the diffuser will give poor performance on account of mismatching of the flow. In this respect a vaneless diffuser or a vaned

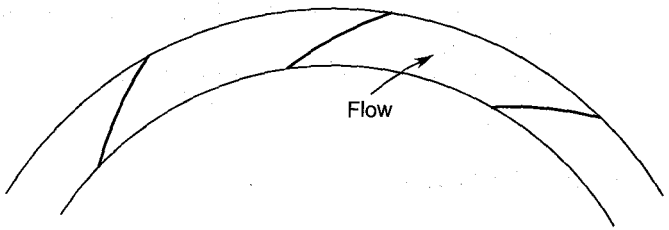

Fig. 12.19 Diffuser ring with cambered blades

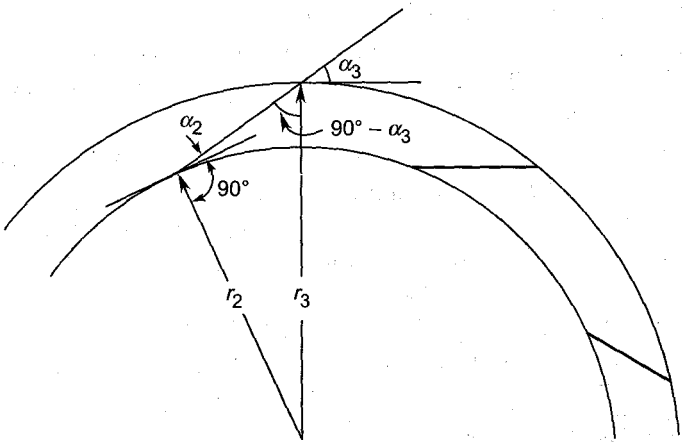

Fig. 12.20 Diffuser ring with straight (uncambered) flat blades

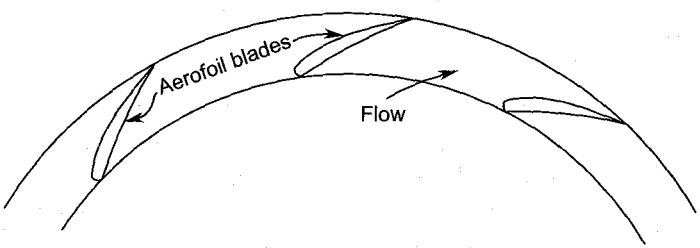

Fig. 12.21 Diffuser ring with cambered aerofoil blades

diffuser with aerofoil blades (Fig. 12.21) is better. For some applications it is possible to provide movable diffuser blades whose directions can be adjusted to suit the changed conditions at the entry.

In some designs for industrial applications, a vaneless diffuser supplies the air or gas direct to the scroll casing, whereas for aeronautical applications, various sectors of the vaned diffuser are connected to separate combustion chambers placed around the main shaft.

12.6.3 Area Ratio

Figure 12.22 shows a vaneless diverging wall diffuser. The side walls have a divergence angle of 2θ. The area ratio of such a diffuser in the radial direction is

$$A_r = \frac{A_3}{A_2} = \frac{d_3 b_3}{d_2 b_2} \tag{12.77}$$

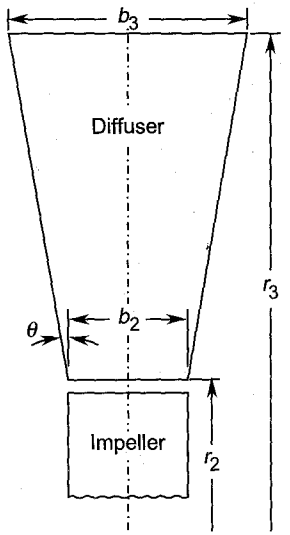

Fig. 12.22 Radial diffuser passage with diverging walls

The semi-divergence angle is given by

$$\tan\ \theta = \frac{b_3 - b_2}{2\,(r_3 - r_2)}$$

$$b_3 - b_2 = 2(r_3 - r_2)\tan\ \theta = (d_3 - d_2)\tan\ \theta$$

Now

$$\frac{b_3}{b_2} = 1 + \frac{b_3 - b_2}{b_2}$$

$$\frac{b_3}{b_2} = 1 + \frac{b_3 - b_2}{b_2}\tan\ \theta = 1 + \left\{\frac{d_3}{d_2} - 1\right\}\frac{\tan\theta}{b_2/d_2} \tag{12.78}$$

This when used in Eq. (12.77) gives

$$A_r = \frac{d_3}{d_2}\left\{1 + \left(\frac{d_3}{d_2} - 1\right)\frac{\tan\theta}{b_2/d_2}\right\} \tag{12.79a}$$

For parallel walls ($\tan \theta = 0$), this gives

$$A_r = d_3/d_2 \tag{12.79b}$$

If the diverging passage of Fig. 12.22 is fitted with straight flat blades (Fig. 12.20), the area ratio normal to the direction of flow is further increased. From Fig. 12.20,

$$\frac{r_3}{\sin(90+\alpha_2)} = \frac{r_2}{\sin(90-\alpha_3)}$$

$$\cos \alpha_3 = \frac{\cos \alpha_2}{d_3/d_2} \tag{12.80}$$

The area ratio is given by

$$A''_r = \frac{\pi d_3 b_3 \sin \alpha_3}{\pi d_2 b_2 \sin \alpha_2} = \frac{d_3 b_3}{d_2 b_2} \frac{\sqrt{1-\cos^2 \alpha_3}}{\sin \alpha_2}$$

Substituting from Eq. (12.80)

$$A'' = \frac{d_3 b_3}{d_2 b_2} \frac{1}{\sin \alpha_2} \sqrt{1-\frac{\cos^2 \alpha_2}{(d_3/d_2)^2}} \tag{12.81}$$

Substituting further from Eq. (12.78)

$$A''_r = \frac{d_3}{d_2}\left\{1+\left(\frac{d_3}{d_2}-1\right)\frac{\tan\theta}{b_2/d_2}\right\}\frac{1}{\sin\alpha_2}\sqrt{1-\frac{\cos^2\alpha_2}{(d_3/d_2)^2}} \tag{12.82}$$

Equation (12.82) shows that the area ratio of a diffuser can be increased by

(a) increasing the diameter ratio, d_3/d_2,
(b) increasing the width ratio, b_3/b_2,
(c) decreasing the leading edge vane angle, α_2
(d) various combinations of *a*, *b* and *c*.

Some typical values of these parameters are:

$$d_3/d_2 \approx 1.4 \text{ to } 1.8,$$
$$A_r = A_3/A_2 \approx 2.5 \text{ to } 3.0$$
$$\alpha_2 \approx 10 \text{ to } 20^\circ$$
$$b_2/d_2 \approx 0.025 - 0.10$$
$$\theta_{max} \approx 5^\circ$$

Figure 12.23 shows the plots of the area ratio against the diameter ratio for some diffuser configurations. It may be observed that, for a given

diameter ratio, very large values of the area ratio can be obtained by employing vaned diffusers with diverging walls.

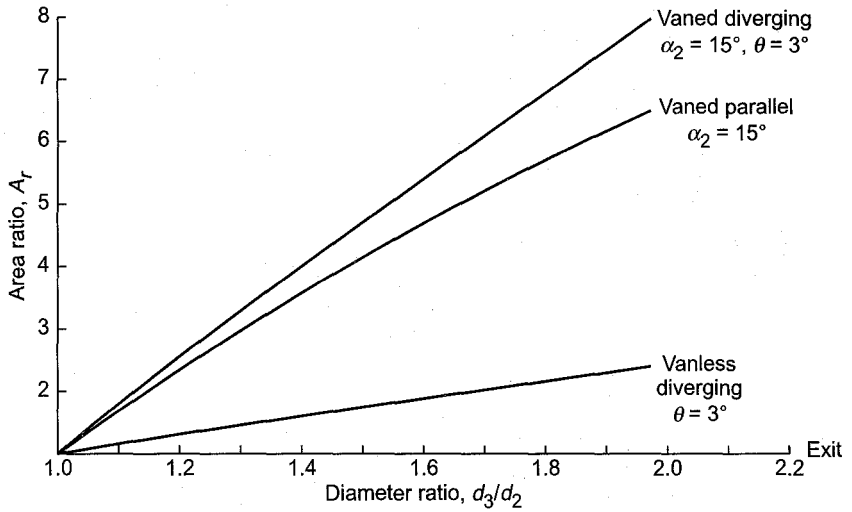

Fig. 12.23 Variation of area ratio in radial diffusers with diameter ratio

12.6.4 Mach Number at Diffuser Entry

In the absence of the vaneless space between the impeller tip and the diffuser entry, the Mach number at the diffuser entry is given by

$$M_2^2 = \frac{c_2^2}{a_2^2}$$

The flow of a perfect gas with zero whirl at the entry is considered below. From Fig. 12.6.

$$c_2^2 = c_{r2}^2 + c_{\theta 2}^2 = c_{r2}^2 + (u_2 - c_{r2} \cot \beta_2)^2$$

$$c_2^2 = u_2^2 \{\phi_2^2 + (1 - \phi_2 \cot \beta_2)^2\} \tag{12.83}$$

The velocity of sound is given by

$$a_2^2 = \gamma R T_2 + (\gamma - 1) c_p T_{01} \left(\frac{T_2}{T_{01}}\right) \tag{12.84}$$

For zero whirl at the entry,

$$h_{01} = c_p T_{01} = h_1 + \frac{1}{2} c_1^2 = h_1 + \frac{1}{2} (w_1^2 - u_1^2) \tag{12.85}$$

Equation (12.32a) gives

$$h_2 = h_1 + \frac{1}{2} (w_1^2 - u_1^2) + \frac{1}{2} (u_2^2 - w_2^2)$$

Substituting from Eq. (12.85)

$$h_2 = h_{01} + \frac{1}{2}(u_2^2 - w_2^2)$$

From Fig. 12.6, this gives

$$h_2 = h_{01} + \frac{1}{2} u^2 (1 - \phi_2^2 \operatorname{cosec}^2 \beta_2)$$

$$\frac{T_2}{T_{01}} = \frac{h_2}{h_{01}} = 1 + \frac{u_2^2}{2c_p T_{01}} (1 - \phi_2^2 \operatorname{cosec}^2 \beta_2) \tag{12.86}$$

Equations (12.84) and (12.86) give

$$a_2^2 = (\gamma - 1)\, c_p T_{01} \left\{1 + \frac{u_2^2}{2c_p T_{01}} (1 - \phi_2^2 \operatorname{cosec}^2 \beta_2)\right\} \tag{12.87}$$

Equations (12.83) and (12.87) yield

$$M_2^2 = \frac{u_2^2}{(\gamma - 1)c_p T_{01}} \times \frac{\phi_2^2 + (1 - \phi_2 \cot \beta_2)^2}{1 + \dfrac{u_2^2}{2c_p T_{01}} (1 - \phi_2^2 \operatorname{cosec}^2 \beta_2)} \tag{12.88}$$

The stagnation temperature rise ratio is

$$\frac{\Delta T_{0st}}{T_{01}} = \frac{w_{st}}{c_p T_{01}} = \frac{u_2^2}{c_p T_{01}} (1 - \phi_2 \cot \beta_2) \tag{12.89}$$

The following relation is obtained from Eqs. (12.88) and (12.89):

$$M_2 = f\left(\gamma, \frac{\Delta T_{0st}}{T_{01}}, \phi_2, \beta_2\right) \tag{12.90}$$

For a given gas and duty (fixed values of γ and $\Delta T_{0st}/T_{01}$), the impeller exit Mach number depends on ϕ_2 and β_2. To avoid the possibility of shocks, the Mach number at the diffuser entry must not be greater than 0.9. The actual value of this Mach number will be lower than that given by Eq. (12.88) due to diffusion in the vaneless space.

The deterioration of diffuser performance is significant in the presence of shocks in the flow field.

12.7 Volute Casing[608–627]

The volute or scroll casing collects and guides the flow from the diffuser or the impeller (in the absence of a diffuser). The flow is finally discharged from the volute through the delivery pipe. For high pressure centrifugal compressors or blowers, the gas from the impeller is discharged through a vaned diffuser, whereas for low pressure fans and blowers, the impeller flow is invariably collected directly by the volute since a diffuser is not required because of the relatively low pressures. Figures 12.24 and 12.25

show a volute casing along with the impeller, diffuser and vaneless spaces. The volute base circle radius (r_3) is a little larger (1.05 to 1.10 times the diffuser or impeller radius) than the impeller or diffuser exit radius. The vaneles space before volute decreases the non-uniformities and turbulence of flow entering the volute as well as noise level.

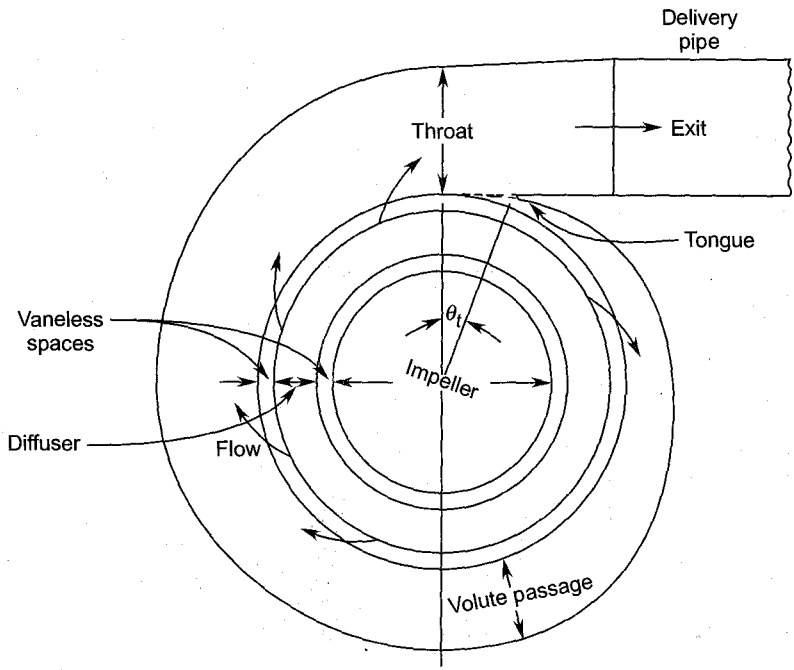

Fig. 12.24 Scroll or volute casing of a centrifugal machine

Some degree of diffusion in the volute passage is also achieved in some designs, while others operate at constant static pressure.

Different cross-sections are employed for the volute passage as shown in Fig. 12.26. The rectangular section is simple and convenient when the volute casing is fabricated from sheet metal by welding the curved wall to the two parallel side walls. While the rectangular section is very common in centrifugal blowers, the cir-cular section is widely used in compressor practice.

While, the volute performance is dependent on the quality of flow passed on to it from the impeller or diffuser, the performance of the impeller or the diffuser also depends on the environment created by the volute around them. The non-uniform pressure distribution around the impeller provided by its volute gives rise to the undesirable radial thrust and bearing pressures.

Two most widely used methods of volute design are discussed below.

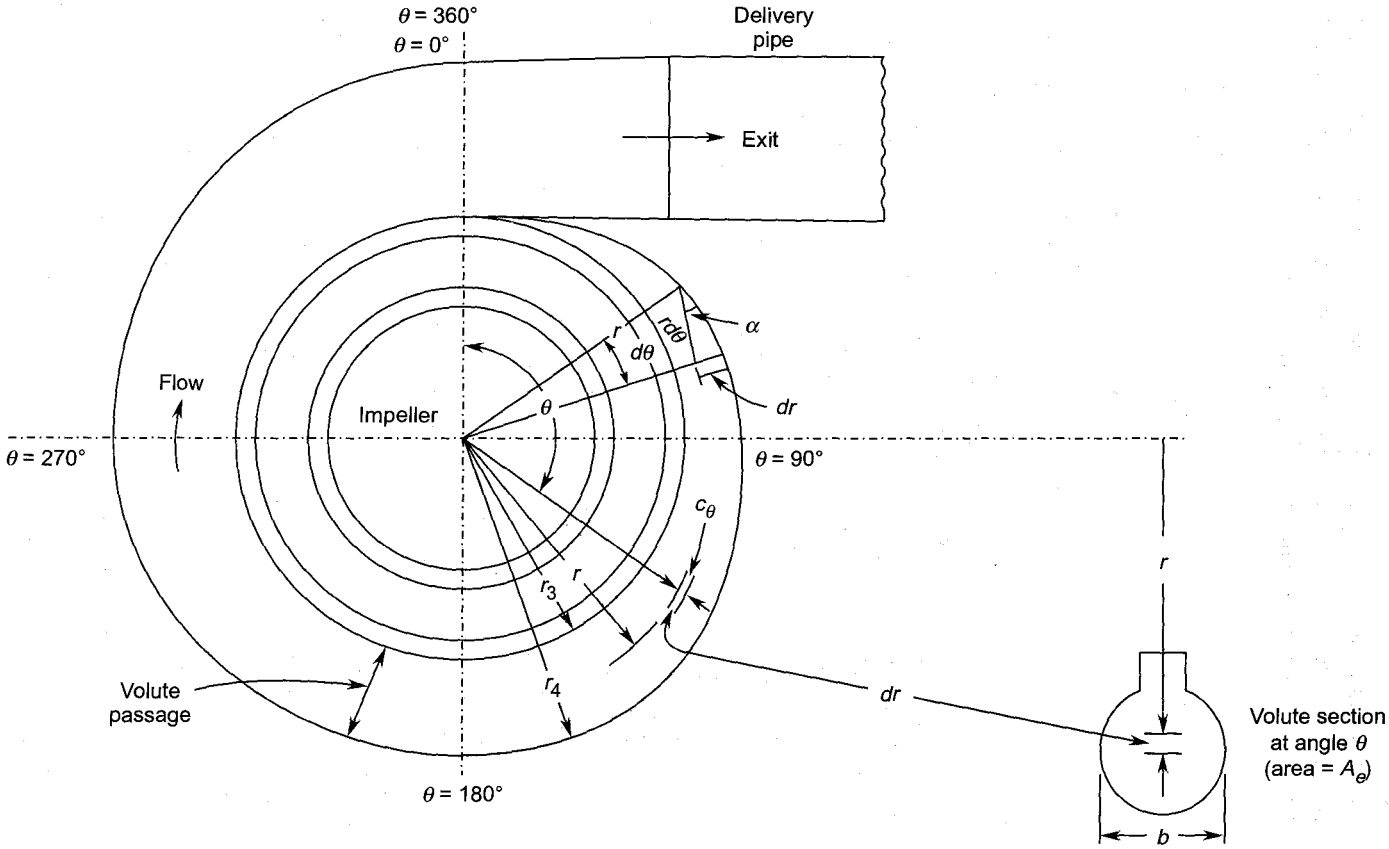

Fig. 12.25 Flow through a volute casing

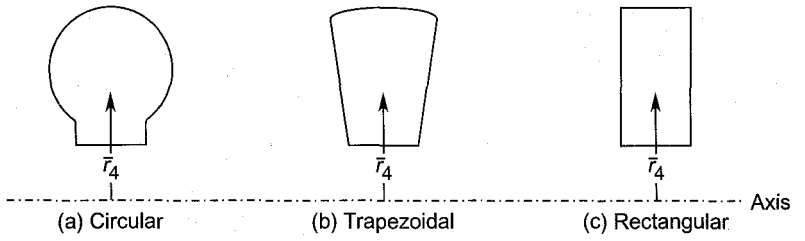

Fig. 12.26 Different cross-sections of the volute passage

12.7.1 Free Vortex Design

Here the flow through the volute passage is assumed to follow Eq. (12.72) for a free vortex flow which is

$$rc_\theta = r_2\, c_{\theta 2} = r_3 c_{\theta 3} = K$$

$$c_\theta = \frac{K}{r} \tag{12.91}$$

Equation (12.76) further shows that in such a flow for $b_3 = b_4$ the direction of the streamlines remains constant, i.e.,

$$\tan\,\alpha = \frac{c_r}{c_\theta} = \text{const.} \tag{12.92}$$

The total volume (Q) of the flow supplied by the impeller is uniformly divided at the volute base circle. Therefore, the flow rate at a section of the volute passage θ degrees away from the section at $\theta = 0°$ is

$$Q_\theta = \frac{\theta}{360}\, Q \tag{12.93}$$

The flow rate through an infinitesimal section (Fig. 12.25) of cross-section ($dr \times b_3$) is

$$dQ_\theta = c_\theta b_3\, dr$$

Substituting from Eq. (12.91),

$$dQ_\theta = Kb_3\, \frac{dr}{r}$$

For the full cross-section of the volute passage,

$$Q_\theta = Kb \int_{r_3}^{r_4} \frac{dr}{r} = Kb_3 \ln \frac{r_4}{r_3} \tag{12.94}$$

Equations (12.93) and (12.94) give

$$\ln\left(\frac{r_4}{r_3}\right) = \frac{\theta}{360}\,\frac{Q}{Kb_3}$$

For a rectangular cross-section, it is required to determine the radius (r_4) of the volute boundary from $\theta = 0°$ to $\theta = 360°$. This can be determined from

$$r_4 = r_3 \exp\left(\frac{\theta}{360}\frac{Q}{Kb_3}\right) \tag{12.95}$$

If the cross-section is not rectangular (Fig. 12.25), then the passage area (A_θ) and the radius ($\bar{r}$) of the centre of gravity of the cross-section are to be determined. Here

$$dQ_\theta = Kb\,\frac{dr}{r}$$

$$Q_\theta = K\int b\frac{dr}{r} = K\,\frac{A_\theta}{\bar{r}} \tag{12.96}$$

$$\frac{A_\theta}{\bar{r}} = \frac{\theta}{360}\frac{Q}{K} \tag{12.97}$$

The volume-flow rate (Q) can be determined from the mass-flow rate, assuming the average density of the gas in the volute passage as equal to $\rho_4 = \dfrac{p_4}{RT_4}$.

12.7.2 Constant Mean Velocity Design

For obtaining high efficiency, it is found from experience that it is necessary to maintain constant velocity of the fluid in the volute passage at the design point. This would also give uniform static pressure distribution around the impeller. In actual practice, both the velocity and pressure vary across the cross-section of the volute passage at a given section. Therefore, to be more precise, the mean velocity and pressure along the volute passage are assumed to remain constant. However, this assumption will be violated at the off-design point.

For a given value of the mean velocity (c_m), the area distribution is obtained from

$$Q_\theta = c_m A_\theta = \frac{\theta}{360}\,Q$$

Therefore,

$$A_\theta = \frac{\theta}{360}\frac{Q}{c_m} \tag{12.98}$$

For a rectangular cross-section,

$$A_\theta = b_3\,(r_4 - r_3) \tag{12.99}$$

Thus the volute radius (r_4) for given values of r_3 and b_3 can be determined.

12.7.3 Volute Tongue

Theoretically, the logarithmic curve of the volute casing begins at the impeller exit, but in practice this is not possible. If it is shifted to the base circle (Fig. 12.25) at $\theta = 0°$, a sharp-edged lip will be formed. This is known as the tongue or cut water of the volute. Its size and geometry have significant effect on the performance of the centrifugal compressors and blowers. In practice the tongue is cut back to a blunt edge and thus actually starts at $\theta = \theta_t$ (Fig. 12.24). At this point its inclination (α) must be the same as that of the streamlines. Therefore, referring to Fig. 12.25, the inclination of an elemental length of the volute boundary $r\,d\theta$ is

$$\tan \alpha = \tan \alpha_3 = \frac{dr}{r d\theta} = \text{const.}$$

$$d\theta = \frac{1}{\tan \alpha_3} \frac{dr}{r}$$

For a given radius ratio (r_3/r_3'), the angle (θ_t in radians) at which the tongue starts at the base circle is determined.

$$\theta_t = \frac{1}{\tan \alpha_3} \int_{r_3'}^{r_3} \frac{dr}{r}$$

$$\theta_t = \frac{1}{\tan \alpha_3} \ln \left(\frac{r_3}{r_3'} \right) \tag{12.100}$$

Shifting the tongue as shown above improves the performance significantly and the pressure distribution around the impeller is close to a uniform profile. Besides this, the discharge at the maximum efficiency point is also increased and the noise level decreased.

The outflow from the volute at the throat is critically affected by the location and the geometry of the tongue. It divides the flow into two streams—one that flows out and the second which reenters the volute through the gap at the tongue. If the inclination of the tongue does not conform to the flow direction shock losses and disturbed flow conditions in this area will arise. The gap between the impeller (or diffuser) and the base circle should not be too large because this increases the recirculation of the fluid and leads to additional losses.

12.8 Stage Losses[456, 487]

The power supplied to the centrifugal compressor stage is the power input at the coupling less the mechanical losses on account of the bearing, seal

and disc friction. The aerodynamic losses occurring in the stage during the flow processes from its entry to exit are taken into account by the stage efficiency. These losses result from fluid friction, separation, circulatory motion and shock wave formations. They lead to an increase in entropy and a decrease in stagnation pressure. The disc friction loss, though aerodynamic in nature, is considered along with the other shaft losses.

The nature of flow and losses occurring in centrifugal compressor stages is considerably different from those in axial compressor stages on account of different configurations of flow passages in the two types. The centrifugal stages, on account of the relatively longer flow passages and greater turning of the flow, suffer higher losses compared to the axial type. This explains the generally lower values of the efficiency of the centrifugal stages compared to the axial type.

A comparison of axial and radial stages has been given in Secs. 1.9 and 1.10. In this section different losses have been described separately on the basis of their different nature. The components of the stage in which they occur have been mentioned where necessary.

12.8.1 Friction Losses

A major portion of the losses is due to fluid friction in stationary and rotating blade passages. The flow, except in the accelerating nozzle and the inlet guide vanes is throughout decelerating. Therefore, the thickening boundary layer (see Sec. 6.1.18) separates where the adverse pressure gradient is too steep. This leads to additional losses on account of stalling and wasteful expenditure of energy in vortices. Secondary vortices develop in diffuser and volute passages.

Losses due to friction depend on the friction factor (Sec. 6.1.17), passage length and the square of the fluid velocity. Therefore, a stage with relatively longer impeller, diffuser and volute passages, and higher fluid velocities shows poor performance.

The boundary layer on the rotating surfaces is thrown away due to centrifugal force. Therefore, it is more profitable to obtain higher pressure rise by diffusion of flow in the rotating passages. Thus high degree reaction blades, like backward-swept impeller blades, give more efficient stages.

Friction losses in the accelerating nozzle and inlet guide vanes are relatively much smaller. On account of high velocities and the decelerations that follow at the leading edges of the inducer and the diffuser blades, shock waves (if present) cause additional losses. They can cause separation of the boundary layers leading to higher losses.

12.8.2 Impeller Entry Losses

In higher pressure centrifugal compressors, the radial-tipped impeller blades extend into the axial portion (Figs. 12.1 and 12.2). Thus the incoming flow is efficiently guided from the axial to the radial direction. However, in centrifugal blowers with relatively lower pressure rise, the impeller blades are located only in the radial portion (Fig. 12.3). Here the flow enters axially and turns radially in the vaneless space before entering the impeller blades. In this process the fluid suffers losses similar to those in a bend. These losses depend on the velocities c_i and c_1 (Fig. 12.10), but are small compared to other losses.

12.8.3 Shock Losses

Additional losses that occur in a row of blades in a centrifugal compressor stage on account of incidence are conventionally known as shock losses. The change of incidence itself very frequently results from the operation of the stage away from the design flow conditions. It is unfortunate that this term has come to stay in centrifugal compressors, because in the usual aerodynamic sense, a shock is a discontinuity and arises when a supersonic flow decelerates to subsonic. The shock loss referred to here has nothing of this nature.

During the off-design conditions, the flow at the entry of the impeller and diffuser blades approaches them with some degree of incidence. For instance, Fig. 12.27 depicts off-design velocity triangles at the entry of the inducer blades. At the same rotational speed, the reduced flow rate introduces positive incidence whereas negative incidence results from increased flow rate. Large incidences (specially positive), lead to flow separation, stalling and surge.

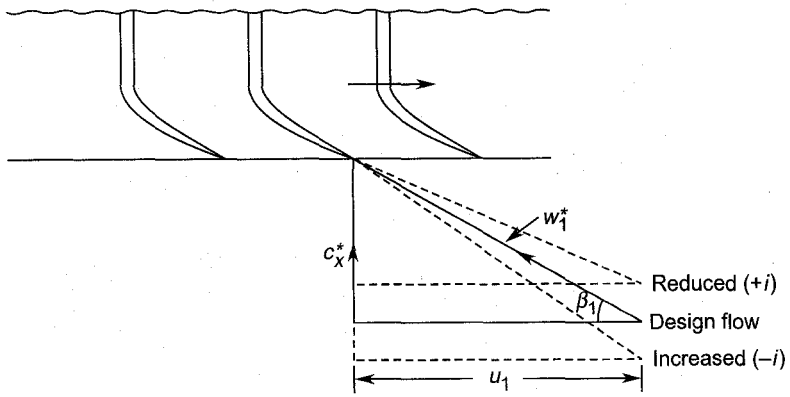

Fig. 12.27 Entry velocity triangles at off-design operation

Figure 12.28 [(a) and (b)] explains the "shock model" of flow at the impeller entry. Design point conditions are represented by the quantities β_1, w_1^*, c_x^*; off-design point values are represented by w_1 and c_x. The so-called shock loss results from the sudden change of the velocity vector w_1 to correspond to the blade angle (design point air angle) β_1 through a shock velocity component c_{sh} as shown. The actual axial velocity component during this change remains unaltered due to continuity considerations. Shock losses are proportional to the square of the shock velocity component.

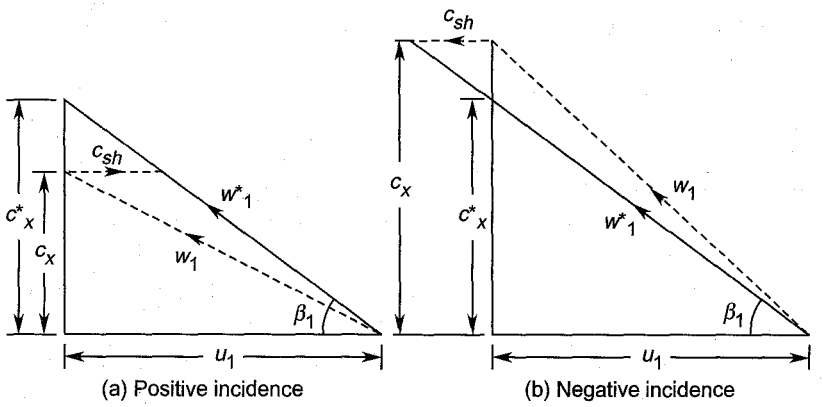

Fig. 12.28 Shock velocity (c_{sh}) (a) due to positive incidence (b) due to negative incidence

When shock losses are plotted against incidence (Fig. 12.29), it is found that they increase rapidly at large values of incidence.

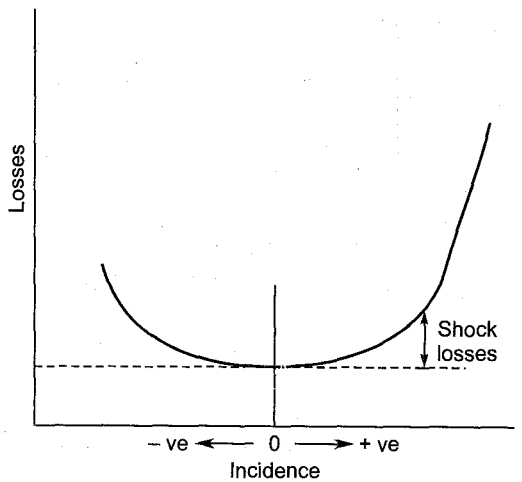

Fig. 12.29 Typical variation of shock losses with incidence

Shock losses as explained above also occur in the diffuser and volute.

12.8.4 Clearance and Leakage Losses

Certain minimum clearances are necessary between the impeller shaft and the casing, and between the outer periphery of the impeller eye and the casing (Fig. 12.1). The leakage of the gas through the shaft clearance is minimized by employing glands. For small shaft diameters with labyrinth glands, the leakage of gas is small.

On account of a higher peripheral speed and a large diameter, it is very difficult to provide sealing between the casing and the impeller eye tip. The leakage through this clearance from the impeller exit is recirculated and additional work is done on a portion of the impeller flow which does not reach the stage exit. This loss is governed by the clearance, diameter ratio (d_2/d_1) and the pressure at the impeller tip. It may by noted here that static pressure at the impeller exit is high for a higher degree of reaction.

12.9 Performance Characteristics[463, 473, 486, 489]

As discussed in Secs. 7.7 and 7.8, the performance characteristic of a centrifugal compressor or a blower at a given speed can be plotted in terms of the following quantities:

$$p_{r0} = f\left(\frac{\dot{m}\sqrt{T_{01}}}{p_{01}}\right)$$

$$\psi = f(\phi)$$

Figure 12.30 shows the theoretical and actual performance characteristics (ϕ–ψ plot) for a centrifugal stage. The actual characteristic is obtained by deducting the stage losses from the theoretical head or pressure coefficient. Therefore, the nature of the actual characteristic depends on the manner in which the stage losses vary with the operating parameters. Friction and shock losses effect the performance significantly.

As explained in Sec. 11.8, the range of stable operation is restricted by surging and choking which occur at some values of the flow coefficient peculiar to a given stage. The point corresponding to the maximum pressure and efficiency is generally close to the surge point. The basic causes and nature of unstable flow in centrifugal stages are the same as discussed in Secs. 11.8.2 and 11.8.3. However, these stages, particularly those employing a vaneless diffuser, have a wider range of stable operation. This is on account of the absence of stalling of the vaned

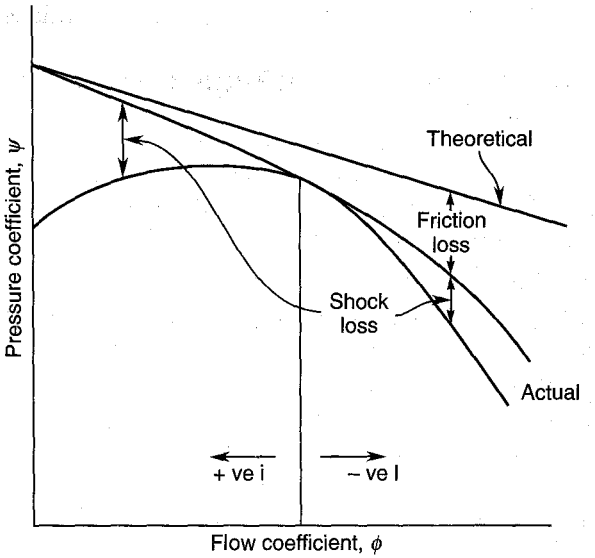

Fig. 12.30 Losses and performance characteristic of a centrifugal compressor stage

diffuser. In some centrifugal stages it has been possible to achieve stable operation on the branch of the characteristic with positive slope.

Local stalling of some inducer and diffuser blades occurs even at design point operation. Besides this, rotating stall on the lines explained in Sec. 11.8.3, would occur in both the impeller and diffuser. Surging in the centrifugal impeller is generally provoked by large-scale stalling of the diffuser blades.

Choking of the centrifugal stage occurs when the Mach number at either the inducer blades or the diffuser throat reaches unity.

Notation for Chapter 12

a	Velocity of sound
A	Area of cross-section
b	Impeller, diffuser or volute width
c	Fluid velocity
c_p	Specific heat at constant pressure
d	Diameter
h	Enthalpy
i	Incidence angle
k, K	Constants
$\dot{m}$	Mass-flow, rate, distance in the meridional plane
M	Mach number

N	Rotational speed
p	Pressure
P	Power
Q	Volume-flow rate
r	Radius
R	Gas constant, degree of reaction, radius of curvature
s	Entropy, blade pitch, distance along the streamline
T	Temperature
u	Peripheral speed
w	Relative velocity, work
z	Number of blades
n, s, m	Natural coordinates

Greek symbols

α	Air angle in the absolute system
β	Air angle in the relative system
γ	Ratio of specific heats
δ	Angle shown in Fig. 12.13
η	Efficiency
θ	Diffuser wall angle, angles shown in Figs. 12.4 and 12.25
μ	Slip factor
ξ	Vorticity, loss coefficient
Γ	Circulation
ϕ	Flow coefficient
ψ	Pressure coefficient
ω	Rotation, rotational speed in rad/s

Subscripts

o	Stagnation value
1	Entry to the impeller
2	Exit from the impeller
3	Exit from the diffuser
4	Exit from the volute
a	Actual
b	Blade
h	Hub
i	Entry to the nozzle
m	Meridional
r	Radial, ratio
rel	Relative
s	Slip

s, ss	Isentropic
sh	Shock
st	Stage
t	Tip, tongue
tt	Total-to-total
w	Corresponding to velocity w
x	Axial
*	Design values
IGVs	Inlet guide vanes
θ	Tangential, corresponding to angular position θ

Solved Examples

12.1 Air enters the inducer blades of a centrifugal compressor at p_{01} = 1.02 bar, T_{01} = 335 K. The hub and tip diameters of the impeller eye are 10 and 25 cm respectively. If the compressor runs at 7200 rpm and delivers 5.0 kg/s of air, determine the air angle at the inducer blade entry and the relative Mach number. If IGVs are used to obtain a straight inducer section, determine the air angle at the IGVs exit and the new value of the relative Mach number.

***Solution*:**

$$A = \frac{\pi}{4}(d_t^2 - d_h^2) = \frac{\pi}{4}(0.25^2 - 0.10^2) = 0.0412 \text{ m}^2$$

Both the density and the axial velocity component at the entry of the inducer are unknown. Therefore, these are determined by trial and error.

I. Let $\rho_1 \approx \frac{p_{01}}{RT_{01}} = \frac{1.02 \times 10^5}{287 \times 335} = 1.0609 \text{ kg/m}^3$

In the absence of IGVs,

$$c_1 = c_{x1} = \frac{\dot{m}}{\rho_1 A_1} = \frac{5}{1.0609 \times 0.0412} = 114.39 \text{ m/s}$$

$$\frac{c_1^2}{2c_p} = \frac{114.39^2}{2 \times 1005} = 6.51 \text{ K}$$

$$T_1 = T_{01} - \frac{c_1^2}{2c_p} = 335 - 6.51 = 328.49 \text{ K}$$

$$p_1 = p_{01}\left(\frac{T_1}{T_{01}}\right)^{\frac{\gamma}{\gamma-1}} = 1.02\left(\frac{328.49}{335}\right)^{3.5} = 0.952 \text{ bar}$$

$$\rho_1 = \frac{0.952 \times 10^5}{287 \times 328.49} = 1.01 \text{ kg/m}^3$$

The assumed value of c_{x1} can now be checked.

$$c_{x1} = 5/(1.01 \times 0.0412) = 120.16 \text{ m/s}$$

Since the diffencree is large, another trial is made.

II. Let $c_1 = c_{x1} = 123$ m/s

$$\frac{c_1^2}{2c_p} = \frac{123^2}{2 \times 1005} = 7.527 \text{ K}$$

$$T_1 = 335 - 7.527 = 327.473 \text{ K}$$

$$p_1 = \left(\frac{327.473}{335}\right)^{3.5} \times 1.02 = 0.942$$

$$\rho_1 = 0.942 \times 10^5/(287 \times 327.473) = 1.0023 \text{ kg/m}^3$$

For a check, c_{x1} is recalculated.

$$c_{x1} = 5/(1.0023 \times 0.0412) = 121 \text{ m/s}$$

This value (compared to the assumed value of 123 m/s) is acceptable. The difference is only about 1%.

$$d_1 = \frac{1}{2}(d_h + d_t) = 0.5\ (0.1 + 0.25) = 0.175 \text{ m}$$

$$u_1 = \frac{\pi d_1 N}{60} = \frac{\pi \times 0.175 \times 7200}{60} = 65.97 \text{ m/s}$$

From Fig. 12.4,

$$\tan \beta_1 = \frac{c_{x1}}{u_1} = \frac{121}{65.97} = 1.834$$

$$\beta_1 = 61.4° \ (Ans.)$$

$$w_1 = \frac{c_{x1}}{\sin \beta_1} = \frac{121}{\sin 65.97} = 137.8 \text{ m/s}$$

$$a_1 = \sqrt{\gamma R T_1} = \sqrt{1.4 \times 287 \times 327.473} = 362.737 \text{ m/s}$$

$$M_{w1} = \frac{w_1}{a_1} = \frac{137.8}{362.737} = 0.38 \ (Ans.)$$

The axial entry of the air into the inducer can be obtained by employing IGVs (Fig. 12.5). In this case

$$\alpha_1 = \tan^{-1} \frac{c_{x1}}{u_1} = 61.4° \ (Ans.)$$

$$\beta_1 = 90°$$

$$c_{x1} = w_1 = 121 \text{ m/s}$$

The new value of the relative Mach number is different on account of the changed values of w_1 and a_1.

$$c_1 = \frac{c_{x1}}{\sin \alpha_1} = \frac{121}{\sin 61.4} = 137.8 \text{ m/s}$$

$$\frac{c_1^2}{2c_p} = \frac{137.8^2}{2 \times 1005} = 9.447 \text{ K}$$

$$T_1 = 335 - 9.447 = 325.553 \text{ K}$$

$$a_1 = \sqrt{1.4 \times 287 \times 325.553} = 361.67 \text{ m/s}$$

$$M_{w1} = \frac{121}{361.67} = 0.334 \ (Ans.)$$

12.2 Determine the pressure ratio developed and the power required to drive a centrifugal air compressor (impeller diameter = 45 cm) running at 7200 rpm. Assume zero swirl at the entry and $T_{01} = 288$ K.

***Solution*:**

$$u_2 = \frac{\pi d_2 N}{60} = \frac{\pi \times 0.45 \times 7200}{60} = 169.65 \text{ m/s}$$

$$p_{r0} = \left\{1 + \frac{u_2^2}{c_p T_{01}}\right\}^{\frac{\gamma}{\gamma - 1}} = \left\{1 + \frac{169.65^2}{1005 \times 288}\right\}^{3.5}$$

$$p_{r0} = 1.393 \ (Ans.)$$

$$w = u_2^2 = \frac{169.65^2}{1000} = 28.78 \text{ kJ/kg}$$

$$P = 28.78 \text{ kW/(kg/s)} \ (Ans.)$$

12.3 A centrifugal air compressor stage has the following data:

type of impeller	radial-tipped
speed	17000 rpm
impeller tip diameter	48 cm
eye tip diameter	24 cm
eye hub diameter	12 cm
mass-flow rate	8 kg/s
slip factor	0.92
stage efficiency	0.77
entry conditions	$p_{01} = 1.05$ bar, $T_{01} = 306$ K

Determine:

(a) The air angles at the hub, mean and tip sections of the inducer, maximum Mach number at the inducer entry, total pressure ratio

developed and power required to drive the compressor without IGVs.

(b) The air angles at the hub, mean and tip sections of the IGVs at exit for axial entry to the inducer, total pressure ratio developed and the power required.

***Solution*:**

$$A = \frac{\pi}{4}(d_t^2 - d_h^2) = \frac{\pi}{4}(0.24^2 - 0.12^2) = 0.0339 \text{ m}^2$$

$$\rho_{01} = \frac{p_{01}}{RT_{01}} = \frac{1.05 \times 10^5}{287 \times 306} = 1.195 \text{ kg/m}^3$$

(a) Without IGVs (Fig. 12.4)

$$\rho_1 c_{x1} A_1 = \dot{m}$$

$$c_1 = c_{x1} = 8/(1.195 \times 0.0339) = 197.48 \text{ m/s}$$

Since the actual density will be lower than ρ_{01}, the axial velocity will be higher. Therefore, as a first trial, a value of $c_{x1} = 205$ m/s is assumed.

I.
$$\frac{c_1^2}{2c_p} = \frac{205^2}{2 \times 1005} = 20.908°\text{C}$$

$$T_1 = 306 - 20.908 = 285.092 \text{ K}$$

$$p_1 = \left(\frac{T_1}{T_{01}}\right)^{\frac{\gamma}{\gamma-1}} p_{01} = \left(\frac{285.092}{306}\right)^{3.5} \times 1.05 = 0.8196 \text{ bar}$$

$$\rho_1 = \frac{0.8196 \times 10^5}{287 \times 285.092} = 1.0 \text{ kg/m}^3$$

As a check

$$c_{x1} = 8/(1.0 \times 0.0339) = 235 \text{ m/s}$$

This is much higher than the assumed value. Therefore, another trial is required.

II. Let $c_{x1} = 240$ m/s

$$\frac{c_1^2}{2c_p} = \frac{240^2}{2 \times 1005} = 28.656°\text{C}$$

$$T_1 = 306 - 28.656 = 277.344 \text{ K}$$

$$p_1 = \left(\frac{277.344}{306}\right)^{3.5} \times 1.05 = 0.7442 \text{ bar}$$

$$\rho_1 = \frac{0.7442 \times 10^5}{287 \times 277.344} = 0.935 \text{ kg/m}^3$$

As a check

$$c_{x1} = 8/(0.935 \times 0.0339) = 252.39 \text{ m/s}$$

The difference is still large.

III. Let $c_{x1} = 262$ m/s

This gives $T_1 = 271.85$, $p_1 = 0.694$ bar,

$$\rho_1 = 0.8894 \text{ kg/m}^3$$

A cross-check gives $c_{x1} = 265.33$ m/s

This is an acceptable value.

$$d_1 = \frac{1}{2}(0.12 + 0.24) = 0.18 \text{ m}$$

$$u_{1m} = \frac{\pi d_1 N}{60} = \frac{\pi \times 0.18 \times 17000}{60} = 160.22 \text{ m/s}$$

$$u_h = \frac{12}{18} \times 160.22 = 106.8 \text{ m/s}$$

$$u_t = \frac{24}{18} \times 160.22 = 213.627 \text{ m/s}$$

$$u_2 = \frac{48}{18} \times 160.22 = 427.253 \text{ m/s}$$

Assuming the inducer blades to have free vortex flow,

$$c_{x1} = c_{x1h} = c_{x1m} = c_{x1t}$$

Therefore, the air angles are

$$\tan \beta_{1h} = \frac{c_{x1}}{u_h} = \frac{265.33}{106.8} = 2.484, \ \beta_{1h} = 68.07° \ (Ans.)$$

$$\beta_{1m} = \tan^{-1} \frac{265.33}{160.22} = 58.87° \ (Ans.)$$

$$\beta_{1t} = \tan^{-1} \frac{265.33}{213.627} = 51.16° \ (Ans.)$$

$$w_{1t} = \frac{c_{x1}}{\sin \beta_{1t}} = \frac{265.33}{\sin 51.16} = 340.65 \text{ m/s}$$

The value of the temperature T_1 corresponding to $c_{x1} = 265.33$ m/s is 270.975 K. Therefore, the acoustic velocity at the inducer entry is

$$a_1 = \sqrt{1.4 \times 287 \times 270.975} = 329.967 \text{ m/s}$$

The tip Mach number is

$$M_{1t} = \frac{w_{1t}}{a_{1t}} = \frac{340.65}{329.967} = 1.032 \ (Ans.)$$

$$\frac{p_{02}}{p_{01}} = \left\{1 + \mu\, \eta_{st}\, \frac{u_2^2}{c_p T_{01}}\right\}^{\frac{\gamma}{\gamma-1}}$$

$$p_{r0} = \frac{p_{02}}{p_{01}} = \left\{1 + \frac{0.92 \times 0.77 \times 427.253^2}{1005 \times 306}\right\}^{3.5}$$

$$p_{r0} = 3.416 \ (Ans.)$$

$$P = \dot{m}\mu\, u_2^2 = 8 \times 0.92 \times 427.253^2/1000$$

$$P = 1343.5 \text{ kW } (Ans.)$$

(b) With IGVs (Fig. 12.5)

For axial entry throughout the inducer blades the air angles at the IGVs exit are:

$$\alpha_{1h} = 68.07°$$

$$\alpha_{1m} = 58.87° \ (Ans.)$$

$$\alpha_{1t} = 51.16°$$

$$c_{x1} = w_{1h} = w_{1m} = w_{1t} = 265.33 \text{ m/s}$$

The absolute velocities and the static temperatures along the height at the inducer entry will vary. At its tip.

$$c_{1t} = \frac{w_{1t}}{\sin \alpha_{1t}} = \frac{265.33}{\sin 51.16} = 340.64 \text{ m/s}$$

$$T_{1t} = 306 - \frac{340.64^2}{2 \times 1005} = 248.27 \text{ K}$$

$$a_{1t} = \sqrt{1.4 \times 287 \times 248.27} = 315.84 \text{ m/s}$$

The relative Mach number at the tip is

$$M_{w1t} = \frac{265.33}{315.84} = 0.840 \ (Ans.)$$

$$p_{r0} = \left\{1 + \frac{\eta_{st}}{c_p T_{01}} (\mu\, u_2^2 - u_1^2)\right\}^{\frac{\gamma}{\gamma-1}}$$

$$p_{r0} = \left\{1 + \frac{0.77\,(0.92 \times 427.253^2 - 160.22^2)}{1005 \times 306}\right\}^{3.5}$$

$$p_{r0} = 2.905 \ (Ans.)$$

$$P = \dot{m}\ (\mu\, u_2^2 - u_1^2)$$

$$P = 8\ (0.92 \times 427^2 - 160.22^2)/1000$$

$$P = 1137 \text{ kW } (Ans.)$$

12.4(a) Derive an expression for the flow Mach number (M_2) at the impeller exit of a centrifugal compressor in terms of the following parameters:

$$M_2 = f\left(\frac{d_2}{d_1}, M_{b1}, \phi_2, \beta_2\right)$$

(b) In a radial-tipped blade impeller the flow coefficient ϕ_2 is 0.268 and the diameter ratio (d_2/d_1) is 2.667. The mean diameter at impeller entry is 18 cm, and speed 8000 rpm. The entry conditions of air are p_{01} = 1.0 bar and T_{01} = 293 K. Determine the blade Mach number at entry and the flow Mach number at the impeller exit.

***Solution*:**

(a) Equation (12.88) is

$$M_2^2 = \frac{u_2^2}{(\gamma-1)\,c_p T_{01}} \times \frac{\phi_2^2 + (1-\phi_2 \cot \beta_2)^2}{1 + \dfrac{u_2^2}{2\,c_p T_{01}}(1-\phi_2^2 \operatorname{cosec}^2 \beta_2)}$$

$$u_2^2 = u_1^2 \left(\frac{d_2}{d_1}\right)^2$$

$$c_p T_{01} = \frac{\gamma}{\gamma-1} RT_{01} = \frac{a_{01}^2}{\gamma-1}$$

$$\frac{u_2^2}{c_p T_{01}} = (\gamma-1)\left(\frac{d_2}{d_1}\right)^2 \frac{u_1^2}{a_{01}^2} = (\gamma-1)\left(\frac{d_2}{d_1}\right)^2 M_{b1}^2$$

Substituting this in the expression for M_2^2

$$M_2^2 = \frac{\left(\dfrac{d_2}{d_1}\right) M_{b1}^2 \{\phi_2^2 + (1-\phi_2 \cot \beta_2)^2\}}{1 + \left\{\dfrac{\gamma-1}{2}\right\}\left(\dfrac{d_2}{d_1}\right)^2 M_{b1}^2 (1-\phi_2^2 \operatorname{cosec}^2 \beta_2)}$$

(b) For radial-tipped blades $\beta_2 = 90°$

$$M_2^2 = \frac{\left(\dfrac{d_2}{d_1}\right)^2 M_{b1}^2 (1+\phi_2^2)}{1 + \dfrac{\gamma-1}{2}\left(\dfrac{d_2}{d_1}\right)^2 M_{b1}^2 (1-\phi_2^2)}$$

$$u_1 = \frac{\pi d_1 N}{60} = \pi \times 0.18 \times \frac{8000}{60} = 75.398 \text{ m/s}$$

$$M_{b1} = \frac{u_1}{\sqrt{\gamma RT_{01}}} = \frac{75.398}{\sqrt{1.4 \times 287 \times 293}} = 0.2197 \quad \textit{(Ans.)}$$

Therefore,

$$M_2^2 = \frac{(2.667 \times 0.2197)^2 (1 + 0.268^2)}{1 + \frac{1.4 - 1}{2} (2.667 \times 0.2197)^2 (1 - 0.268^2)}$$

$$M_2^2 = 0.3459$$

$$M_2 = 0.588 \ (Ans.)$$

12.5 The tangential velocity component of air at the volute base circle (r = 25 cm) is 177.5 m/s. Determine its shape and throat-to-diameter ratio for a constant width of 12 cm and discharge 5.4 m^3/s assuming:

(a) free vortex flow and

(b) constant mean velocity of 145 m/s.

***Solution*:**

(a) Free vortex flow

$$K = r_3 c_{\theta 3} = 0.25 \times 177.5 = 44.375 \ m^2/s$$

$$\frac{Q}{Kb} = \frac{5.4}{44.375 \times .12} = 1.01$$

$$r_4 = r_3 \exp \left\{ \frac{\theta}{2\pi} \frac{Q}{Kb} \right\} = 25 \exp \left\{ \frac{1.01\theta}{2\pi} \right\}$$

The volute radii at eight angular positions are given in the following table:

θ	$\pi/4$	$\pi/2$	$3\pi/4$	π	$5\pi/4$	$3\pi/2$	$7\pi/4$	2π
r_4	28.38	32.21	36.57	41.51	47.12	53.38	60.71	68.92

The length of the throat L = 68.92 – 25 = 43.92 cm

$$\frac{L}{d_3} = \frac{43.92}{50} \ 0.88 \ (Ans.)$$

(b) Constant mean velocity c_m = 145 m/s

$$A_\theta = \frac{\theta}{2\pi} \frac{Q}{c_m}$$

$$A_\theta = \frac{\theta}{2\pi} \times \frac{5.4}{145} \times 10^4 = 372.41 \left\{ \frac{\theta}{2\pi} \right\} \ cm^2$$

$$b \ (r_4 - r_3) = A_\theta$$

$$12 \ (r_4 - 25) = 372.41 \left\{ \frac{\theta}{2\pi} \right\}$$

$$r_4 = 25 + 31.03 \left\{ \frac{\theta}{2\pi} \right\} \ cm$$

The volute radii at eight angular positions are given in the following table:

θ	$\pi/4$	$\pi/2$	$3\pi/4$	π	$5\pi/4$	$3\pi/2$	$7\pi/4$	2π
r_4	28.88	32.75	36.64	40.51	44.39	48.27	52.15	56.03

$$L = 56.03 - 25 = 31.03 \text{ cm}$$

$$\frac{L}{d_3} = \frac{31.03}{50} = 0.621 \ (Ans.)$$

Questions and Problems

12.1 (a) Draw an illustrative diagram of a centrifugal compressor stage indicating the names of its principal parts.

(b) Draw sketches of the three types of impellers and the velocity triangles at their entries and exits.

12.2 (a) Why is the radial-tipped impeller most widely used in centrifugal compressor stages?

(b) Explain briefly what is the purpose of inlet guide vanes and inducer blades.

12.3 (a) What is pressure coefficient for a centrifugal compressor stage? Derive

$$\psi = 1 - \phi_2 \cot \beta_2$$

and plot ψ–ϕ_2 curves for radial, forward and backward-swept impeller blades.

(b) Prove the following for isentropic flow in a radial-tipped impeller:

$$\psi = 1$$

$$p_{r0} = \left(1 + \frac{u_2^2}{c_p T_{01}}\right)^{\frac{\gamma}{\gamma - 1}}$$

12.4 Repeat Ex. 12.2 for a stage efficiency of 0.82 and slip factor of 0.80. (*Ans.*) $p_{r0} = 1.247$, $P = 23.02$ kW

12.5 Determine the pressure ratio and power required for the compressor of Ex. 12.2 for:

(a) carbon dioxide ($\gamma = 1.29$), $c_p = 900$ J/kg K)

(b) freon-21 ($\gamma = 1.18$), $c_p = 616$ J/kg K)

Do the calculations for $\eta_{st} = 1$, $\mu = 1$, and $\eta_{st} = 0.82$, $\mu = 0.80$.

(*Ans.*)

(a) Isentropic flow, $p_{r0} = 1.597$; $P = 28.78$ kW/(kg/s);
Adiabatic flow, $p_{r0} = 1.367$; $P = 23.02$ kW/(kg/s).

(b) Isentropic flow, $p_{r0} = 2.679$, $P = 28.78$ kW/(kg/s),
Adiabatic flow, $p_{r0} = 1.94$, $P = 23.02$ kW/(kg/s).

12.6 (a) Draw the enthalpy-entropy diagram for a complete centrifugal stage showing static and stagnation values of pressure and enthalpy at various stations.

(b) Prove that:

$$h_{01\text{rel}} - \frac{1}{2} u_1^2 = h_{02\text{rel}} - \frac{1}{2} u_2^2$$

12.7 (a) What is "slip factor"? What is its effect on the flow and the pressure ratio in the stage?

(b) Give three formulas to calculate the slip factor. Derive Stodola's relation for the slip factor.

(c) A centrifugal impeller has 17 radial blades in the impeller of 45 cm diameter. The tip diameter of the eye is 25 cm. Determine the slip factor by three different formulas.
(*Ans.*) $\mu = 0.802$ (Balje); 0.883 (Stanitz); 0.815 (Stodola)

12.8 A freon centrifugal compressor has the following data:

type of impeller	radial-tipped
speed	8000 rpm
impeller tip diameter	48 cm
eye tip diameter	24 cm
eye hub diameter	12 cm
mass-flow rate	8 kg/s
slip factor	0.92
stage efficiency	0.77
entry conditions	$p_{01} = 1.0$ bar, $T_{01} = 293$ K

$R = 95$ J/kg K, $\gamma = 1.182$, $c_p = 616$ J/kg K.

Determine the axial velocity and fluid angles at the hub, mean and tip sections of the inducer, maximum Mach number at the inducer entry, total pressure ratio developed and the power required to drive the compressor without IGVs.

(*Ans.*) $c_{x1} = 72$ m/s; $\beta_{1h} = 55.08°$, $\beta_{1m} = 43.68°$, $\beta_{1t} = 35.61°$, $M_{1\max} = 0.687$, $p_{r0} = 2.60$, $P = 297.53$ kW.

12.9 Repeat problem 12.8 for air.

(*Ans.*) $c_{x1} = 283.6$ m/s; $\beta_{1h} = 79.95°$; $\beta_{1m} = 75.11°$; $\beta_{1t} = 70.48°$; $M_{1\max} = 0.939$; $p_{r0} = 1.3827$; $P = 297.53$ kW.

12.10 (a) For a low pressure ratio centrifugal stage, show that the value of the pressure ratio is approximately given by

$$p_{r0} \approx 1 + \gamma \psi \mu \eta_{st} \left(\frac{d_2}{d_1}\right)^2 M_{b1}^2$$

where M_{b1} is the blade Mach number at entry defined by u_1/a_{01}.

(b) Use this expression for calculating the pressure ratios in Problems 12.8 and 12.9.

(*Ans.*) For freon $p_{r0} = 2.03$ (Problem 12.8)

For air $p_{r0} = 1.34$ (Problem 12.9)

It may be seen that the inaccuracy is small for smaller pressure rise.

12.11 (a) How is the degrees of reaction of centrifugal stage defined? Show graphically the variation of the degree of reaction with the flow coefficient for various values of the impeller exit angle.

(b) What is the effect of reaction on the stage loading? Show it graphically.

12.12 (a) Sketch streamlines in the meridional and vane-to-vane planes of a centrifugal compressor impeller. Draw typical velocity profiles at the impeller exit from hub-to-tip and vane-to-vane.

(b) Derive the following relations for the velocities in these planes:

$$\frac{\partial w}{\partial m} + \frac{w}{R} - 2\omega = 0$$

$$w = k \exp \int \frac{dn}{R}$$

12.13 (a) In which type of centrifugal compressors and blowers are vaneless diffusers used? What are their various advantages and disadvantages?

(b) Prove the following for free vortex flow in the vaneless diffuser of a centrifugal compressor stage:

$$\frac{c_{\theta 3}}{c_{\theta 2}} = \frac{c_{r3}}{c_{r2}} = \frac{c_3}{c_2} = \frac{r_2}{r_3}$$

12.14 (a) Show a vaned diffuser for centrifugal compressor applications. What are its advantages and disadvantages compared to the vaneless type?

(b) Prove that the area ratio across a vaned diffuser of constant width, diameter ratio n and blade leading edge angle α is given by

$$(n^2 - \cos^2 \alpha_2)^{1/2} \operatorname{cosec} \alpha_2$$

12.15 (a) How do the Mach numbers at the entries of the impeller and diffuser affect the flow and efficiency of a centrifugal compressor stage? On what considerations are the limiting values of these Mach numbers decided?

(b) Prove that the Mach number at the impeller exit is given by

$$M_2^2 = \frac{M_{b1}^2 \left\{\phi_2^2 + (1 - \phi_2 \cot \beta_2)\right\} \left(\frac{d_2}{d_1}\right)^2}{1 + M_{b1}^2 (1 - \phi_2^2 \operatorname{cosec}^2 \beta_2) \left(\frac{d_2}{d_1}\right)^2 \left(\frac{\gamma - 1}{2}\right)}$$

12.16 (a) What is a free vortex volute? How is its shape determined?

(b) For a constant width (b) free vortex volute of rectangular cross-section having a base circle radius r_3, prove that its curved boundary is given by,

$$r_4 = r_3 \exp\left(\frac{\theta}{2} \frac{Q}{Kb}\right) = r_3 \exp(\theta \tan \alpha_3)$$

where K is a constant and α_3 is the direction of the streamlines entering the volute.

12.17 (a) What are the various losses occurring in a centrifugal compressor stage?

(b) Explain with the aid of velocity triangles the mechanism of shock losses (due to incidence) at the impeller and diffuser entry?

12.18 How do stalling and surging take place in centrifugal compressor stages? Suggest methods to minimize or prevent them. What is their effect on the performance?

Chapter 13

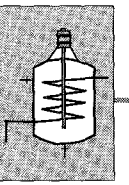

Radial Turbine Stages

A short introduction of radial turbines[491–529] was given in Sec. 1.10 (Figs. 1.11 and 1.12) where its merits and demerits were also mentioned. An inward flow radial turbine stage can be obtained by reversing the flow of a high pressure gas through a centrifugal compressor stage (Figs. 12.1 and 12.2). The high pressure gas will transfer its energy to the impeller shaft in flowing through the impeller. When compared with an axial stage, an inward-flow radial (IFR) turbine stage has a kinematic advantage, viz., the contribution of centrifugal energy of the gas flowing from a larger to a smaller radius to the total energy transfer is significant. Therefore, with the exception of the Ljungstrom turbine, most compressible flow radial turbines are inward-flow type.

The radial turbine can employ a relatively higher pressure ratio (≈ 4) per stage with lower flow rates. Thus these machines fall in the lower specific speed and power ranges. Blade root fixtures in axial machines limit their peripheral speeds, whereas a single piece rotor of a radial turbine is mechanically stronger and more reliable.

For high temperature applications rotor blade cooling (Sec. 10.2) in radial stages is not as easy as in axial turbine stages.

Variable angle nozzle blades can give higher stage efficiencies in a radial turbine stage even at off-design point operation.

IFR turbines for compressible fluids are used for a variety of applications (see section 1.19) in which the rotor diameters vary from 15 mm to 500 mm. Single stages give efficiencies of around 90 per cent.

In the family of hydro-turbines, Francis turbine is a very well known IFR turbine which generates much larger power with a relatively large impeller. Single impellers of about 10 m diameter can generate power in the neighbourhood of 500 MW. Discussion given in Sec. 1.6 explains some contrasting features between the incompressible and compressible flow turbines.

13.1 Elements of a Radial Turbine Stage

Figures 1.12, 13.1 and 13.2 show various components of an IFR turbine. When the high pressure working gas enters the turbine through a duct or

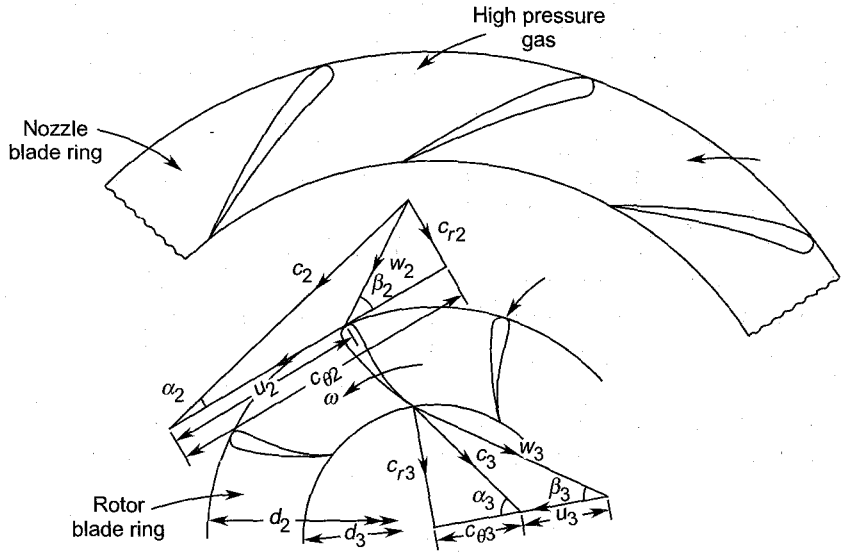

Fig. 13.1 Velocity triangles for an inward-flow radial (IFR) turbine stage with cantilever blades

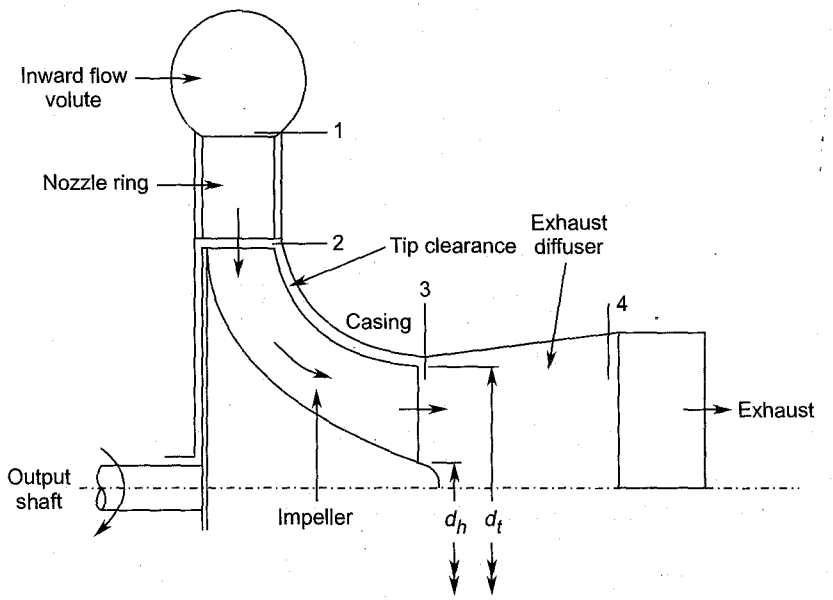

Fig. 13.2 Ninety degree inward-flow radial turbine stage

pipe, an inward-flow volute or scroll casing distributes it properly all around the nozzle ring or rotor blades. In some applications, the nozzle ring is not used and the flow receives some degree of acceleration accompanied by a static pressure drop in the volute casing.

The rotor or impeller transfers energy from the fluid to the shaft through its blades. In a great majority of cases, the blades are an integral part of the rotor disc.

While the flow has a large swirl component at the entry to the rotor, it is advantageous to allow only a small swirl component at the exit. In many designs it is close to zero.

If the kinetic energy at the rotor exit is high, a part of it can be recovered by passing the gas through an exhaust-diffuser whose action is like that of a draught tube in a hydroturbine. Some degree of swirl at the entry of the diffuser gives it higher efficiency and pressure recovery.

Figure 13.3 shows an inward mix-flow turbine. Here the rotor has no radial section. Such stages are able to use higher flow rates at high speeds and have specific speeds higher than the radial stages.

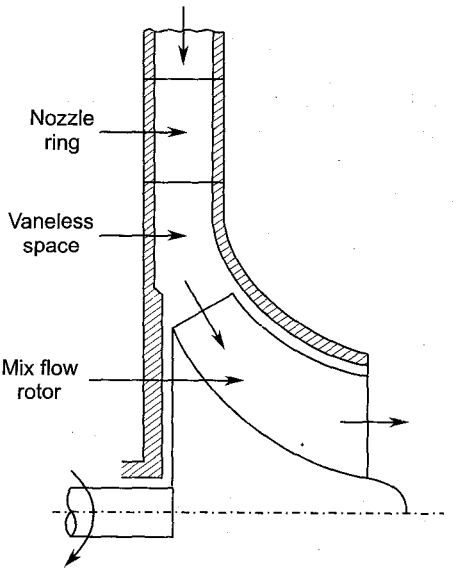

Fig. 13.3 Inward mix-flow turbine

13.2 Stage Velocity Triangles

The cylindrical coordinate system (r, θ, x) has been used for the radial machines. As per the convention, air angles are measured from the tangential direction at a given station. The notations used here are similar to those used for centrifugal compressors. Properties at the nozzle entry, rotor entry and exit are denoted by suffixes 1, 2 and 3 respectively. In the presence of an exhaust-diffuser the exit from it is represented by suffix 4.

The meridional component c_{r2} of velocity at the rotor entry is always taken here as radial, whereas at the rotor exit it has been taken to be both radial (c_{r3}) as well as axial (c_{x3}), depending on the type of the rotor.

13.2.1 Cantilever Blade IFR Turbine

Figure 13.1 shows the arrangement of blades in the nozzle ring and rotor. The rotor blades project axially outwards from a disc like a cantilever, and hence the name. For a large ratio (≈ 1.0) of the inner to outer diameter, the rotor blade ring of the cantilever type can be designed on the lines of axial-flow impulse or reaction turbine stages. The cantilever blades are located only on the radial section of the rotor flow passage. The flow leaving the rotor blades has to turn in the axial direction for exit from the turbine stage.

The radial clearance between the nozzle and rotor blade rings is small; this has been exaggerated in Fig. 13.1 only to show the velocity triangle at the rotor entry.

The radial and tangential components of the absolute velocity c_2 are c_{r2} and $c_{\theta 2}$, respectively. The relative velocity of the flow and the peripheral speed of the rotor are w_2 and u_2 respectively.

The air angle at the rotor blade entry is given by

$$\tan \beta_2 = \frac{c_{r2}}{c_{\theta 2} - u_2} = \frac{c_2 \sin \alpha_2}{c_2 \cos \alpha_2 - u_2} \tag{13.1}$$

The flow leaves the rotor with a relatively velocity w_3 at an angle β_3. The radial and tangential components of the absolute velocity c_3 are c_{r3} and $c_{\theta 3}$ respectively. The exit air angle is given by

$$\tan \beta_3 = \frac{c_{r3}}{c_{\theta 3} + u_3} = \frac{w_3 \sin \beta_3}{c_3 \cos \alpha_3 + u_3} \tag{13.2}$$

From the general Euler's equation (6.148b) for turbines, the stage work is given by

$$w = u_2 c_{\theta 2} - u_3 c_{\theta 3} \tag{13.3a}$$

By choosing the required blade angle at the rotor exit, the exit swirl or whirl component $c_{\theta 3}$ can be made zero. Then

$$w = u_2 c_{\theta 2} = u_2 c_2 \cos \alpha_2 \tag{13.3b}$$

The head or stage loading coefficient is defined by

$$\psi = \frac{w}{u_2^2} = \frac{c_{\theta_2}}{u_2} = \frac{\cos \alpha_2}{u_2 / c_2} = \phi_2 \cot \alpha_2 \tag{13.4}$$

From the velocity triangle in Fig. 13.1,

$$c_{\theta_2} = u_2 + c_{r_2} \cot \beta_2 \tag{13.5a}$$

$$\psi = 1 + \phi_2 \cot \beta_2 \tag{13.5b}$$

The continuity equation at the rotor entry and exit gives

$$\dot{m} = \rho_2 \, c_{r2} \, A_2 = \rho_3 \, c_{r3} \, A_3$$

$$\dot{m} = \rho_2 \, c_{r2} \, (\pi \, d_2 - n t_2) \, b_2 = \rho_3 \, c_{r3} \, (\pi \, d_3 - n t_3) \, b_3 \qquad (13.6)$$

The flow coefficient is defined as

$$\phi_2 = \frac{c_{r2}}{u_2} \qquad (13.7)$$

13.2.2 Ninety-degree IFR Turbine

In this design, the relatively thin blades extend from a purely radial direction ($\beta_2 = 90°$) at the entry to the axial section of the rotor. The blade angle (β'_3) at the rotor exit has some value (between zero and ninety degrees) which governs the exit swirl $c_{\theta 3}$. Strictly speaking, this is also a sort of mix flow stage.

The velocity triangles at the entry and exit of the rotor for such a stage are shown in Fig. 13.4. These are modified forms or special forms of the velocity triangles already discussed in Fig. 13.1. It may be noted that c_{r3} has been replaced by $c_{x3} = c_3$ and the discharge from the stage in the absolute system is axial, i.e., $c_{\theta 3} = 0$.

$$c_{\theta 2} = c_2 \cos \alpha_2 \qquad (13.8)$$

$$\tan \alpha_2 = \phi_2 \qquad (13.9)$$

$$\tan \beta_3 = \frac{c_{x3}}{u_3} \qquad (13.10)$$

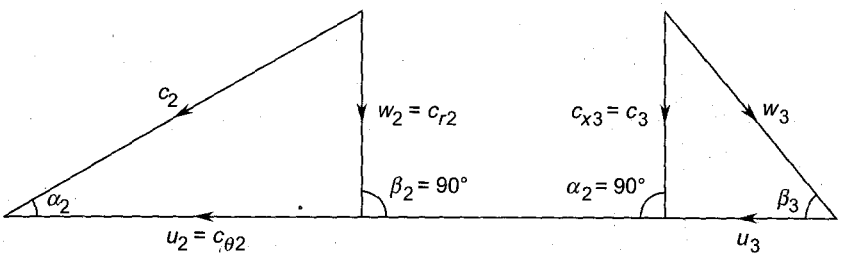

Fig. 13.4 Entry and exit velocity triangles for a ninety degree inward-flow radial turbine stage

With the assumption of zero swirl at the exit, Eq. (13.3a) gives the stage work as

$$w = u_2 \, c_{\theta 2} = u_2^2 \qquad (13.11)$$

$$\psi = 1 \qquad (13.12)$$

The continuity equation at the entry and exit of the rotor in this case gives

$$\dot{m} = \rho_2 \, c_{r2} \, (\pi \, d_2 - n t_2) \, b_2 = \rho_3 \, c_{x3} \left\{ \frac{\pi}{4} (d_t^2 - d_h^2) - n t_3 \, b_3 \right\} \quad (13.13)$$

The blade width or height at the exit is

$$b_3 = \frac{1}{2} \, (d_t - d_h)$$

13.3 Enthalpy-entropy Diagram

Figure 13.5 shows the various flow processes occuring in an IFR turbine stage on an enthalpy–entropy diagram. The stagnation state of the gas at the nozzle entry is represented by point 0_1. The gas expands adiabatically in the nozzles from a pressure p_1 to p_2 with an increase in its velocity from c_1 to c_2. Since this is an energy transformation process, the stagnation enthalpy remains constant but the stagnation pressure decreases ($p_{01} > p_{02}$) due to losses.

$$h_{01} = h_{02} \quad (13.14a)$$

$$h_1 + \frac{1}{2} \, c_1^2 = h_2 + \frac{1}{2} \, c_2^2 \quad (13.14b)$$

The isentropic process in the nozzle is represented by 1-2s which does not suffer any stagnation pressure loss. For this process

$$h_1 + \frac{1}{2} \, c_1^2 = h_{2s} + \frac{1}{2} \, c_{2s}^2 \quad (13.15)$$

The energy transfer accompanied by an energy transformation process (2-3) occurs in the rotor. Here the relative stagnation enthalpy does not remain constant on account of a radius change.

$$h_{02\text{rel}} = h_2 + \frac{1}{2} \, w_2^2 \quad (13.16a)$$

$$h_{03\text{rel}} = h_3 + \frac{1}{2} \, w_3^2 \quad (13.16b)$$

The corresponding pressures at the relative stagnation points ($0_{2\text{rel}}$ and $0_{3\text{rel}}$) are the relative stagnation pressures $p_{02\text{rel}}$ and $p_{03\text{rel}}$.

The final stagnation state is represented by the point 0_3.

$$h_{03} = h_3 + \frac{1}{2} \, w_3^2 \quad (13.17)$$

The actual energy transfer (work) is equal to the change in the actual stagnation enthalpy. Therefore, using the general Euler's equation (6.153a) for a turbine stage,

$$w_a = h_{02} - h_{03} = \frac{1}{2} \, (c_2^2 - c_3^2) + \frac{1}{2} \, (w_3^2 - w_2^2) + \frac{1}{2} \, (u_2^2 - u_3^2)$$

$$\left(h_{02} - \frac{1}{2}c_2^2\right) + \frac{1}{2}w_2^2 - \frac{1}{2}u_2^2 = \left(h_{03} - \frac{1}{2}c_3^2\right) + \frac{1}{2}w_3^2 - \frac{1}{2}u_3^2$$

$$h_2 + \frac{1}{2}w_2^2 - \frac{1}{2}u_2^2 = h_3 + \frac{1}{2}w_3^2 - \frac{1}{2}u_3^2 \qquad (13.18a)$$

$$h_{02\text{rel}} - \frac{1}{2}u_2^2 = h_{03\text{rel}} - \frac{1}{2}u_3^2 \qquad (13.18b)$$

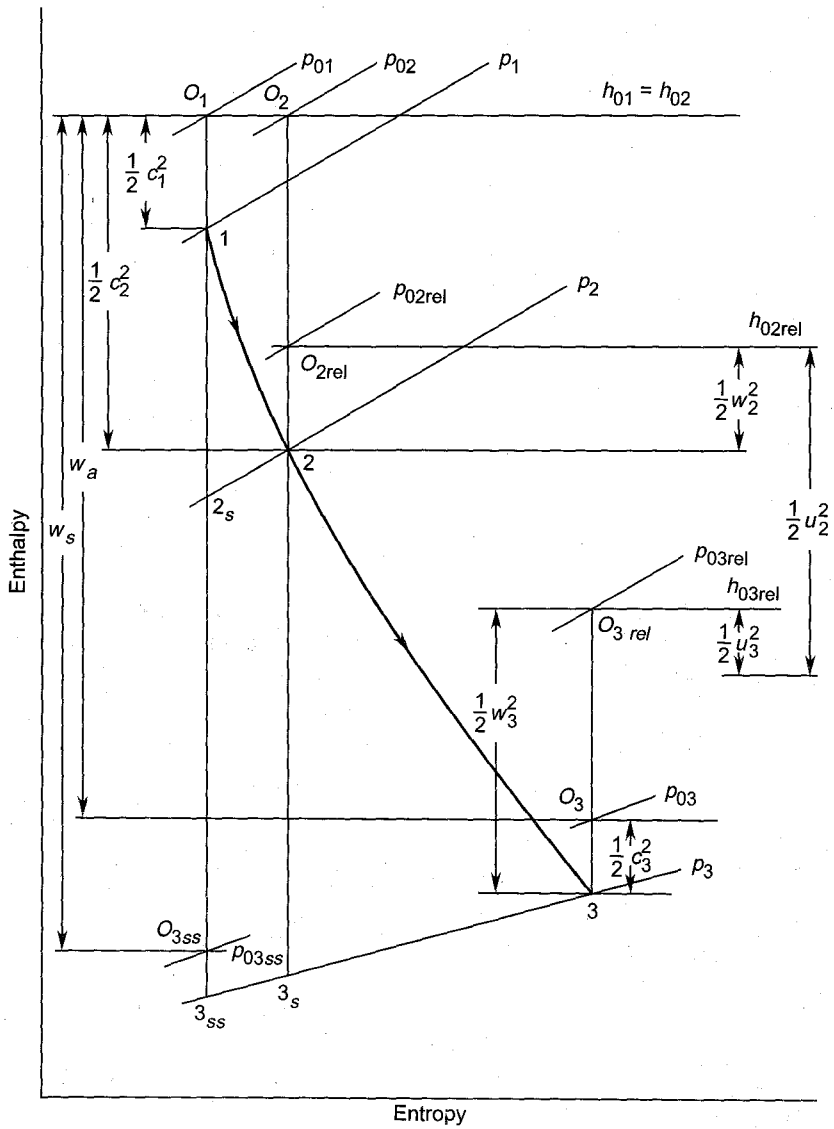

Fig. 13.5 Enthalpy-entropy diagram for flow through an IFR turbine stage

The relation between various quantities in Eq. (13.18) is depicted in Fig. 13.5.

It should be noted that Eqs. (13.18a) and (13.18b) are identical to Eqs. (12.32a and b) derived for centrifugal compressors.

13.3.1 Spouting Velocity

A reference velocity (c_0) known as the isentropic velocity, spouting velocity or stage terminal velocity is defined as that velocity which will be obtained during an isentropic expansion of the gas between the entry and exit pressures of the stage. The exit pressure may be taken as $p_{03ss} = p_{03}$ or p_3.

$$\frac{1}{2} c_0^2 = h_{01} - h_{03ss} \tag{13.19a}$$

For a perfect gas, assuming $p_{03ss} \approx p_{03}$

$$c_0 = \sqrt{2 c_p T_{01} \left\{1 - \left(\frac{p_{03}}{p_{01}}\right)^{\frac{\gamma-1}{\gamma}}\right\}} \tag{13.19b}$$

With exit pressure equal to p_3

$$\frac{1}{2} = h_{01} - h_{3ss} \tag{13.20a}$$

$$c_0 = \sqrt{2 c_p T_{01} \left\{1 - \left(\frac{p_3}{p_{01}}\right)^{\frac{\gamma-1}{\gamma}}\right\}} \tag{13.20b}$$

13.3.2 Stage Efficiency

The actual work output of the stage is

$$w_a = h_{01} - h_{03} = h_{02} - h_{03} = u_2^2 (1 + \phi_2 \cot \beta_2) = \psi u_2^2 \tag{13.21a}$$

The swirl at the exit will always be assumed to be zero ($c_{\theta 3} = 0$) in this chapter unless mentioned otherwise.

For a perfect gas,

$$w_a = c_p (T_{01} - T_{03}) = c_p (T_{02} - T_{03}) = u_2^2 (1 + \phi_2 \cot \beta_2) = \psi u_2^2 \tag{13.21b}$$

The ideal work can be defined (see Sec. 2.5) in two ways:

The ideal work (shown in Fig. 13.5) between total conditions at the entry and exit of the stage is

$$w_s = h_{01} - h_{03ss} \tag{13.22a}$$

$$w_s = c_p T_{01} \left\{1 - \left(\frac{p_{03}}{p_{01}}\right)^{\frac{\gamma-1}{\gamma}}\right\} \tag{13.22b}$$

The total-to-total efficiency is based on this value of work.

$$\eta_{tt} = \frac{w_a}{w_s} = \frac{h_{01} - h_{03}}{h_{01} - h_{03ss}} \tag{13.23a}$$

$$\eta_{tt} = \frac{u_2^2 (1 + \phi_2 \cot \beta_2)}{c_p T_{01} \left\{1 - \left(\frac{p_3}{p_{01}}\right)^{\frac{\gamma-1}{\gamma}}\right\}} = \frac{\psi u_2^2}{c_p T_{01} \left\{1 - p_{r0}^{-\frac{\gamma-1}{\gamma}}\right\}} \tag{13.23b}$$

The ideal work between total conditions at the entry and static conditions at the exit of the stage is

$$w_s = h_{01} - h_{3ss} \tag{13.24a}$$

$$w_s = c_p T_{01} \left\{1 - \left(\frac{p_3}{p_{01}}\right)^{\frac{\gamma-1}{\gamma}}\right\} \tag{13.24b}$$

The total-to-static efficiency is based on this value of work.

$$\eta_{ts} = \frac{h_{01} - h_{03}}{h_{01} - h_{3ss}} \tag{13.25a}$$

$$\eta_{ts} = \frac{u_2^2 (1 + \phi_2 \cot \beta_2)}{c_p T_{01} \left\{1 - \left(\frac{p_3}{p_{01}}\right)^{\frac{\gamma-1}{\gamma}}\right\}} = \frac{\psi u_2^2}{c_p T_{01} \left\{1 - \left(\frac{p_3}{p_{01}}\right)^{\frac{\gamma-1}{\gamma}}\right\}} \tag{13.25b}$$

13.3.3 Effect of Exhaust Diffuser

Figure 13.6 shows the enthalpy-entropy diagram for flow in an IFR turbine stage discharging through an exhaust diffuser.

The flow experiences only energy transformation across the diffuser. Therefore,

$$h_{03} = h_{04} \tag{13.26a}$$

$$h_3 + \frac{1}{2} c_3^2 = h_4 + \frac{1}{2} c_4^2 \tag{13.26b}$$

The flow suffers stagnation pressure loss $(p_{03} - p_{04})$ on account of losses.

The total-to-total and total-to-static efficiencies of the stage with the diffuser are now

$$\eta_{tt} = \frac{h_{01} - h_{03}}{h_{01} - h_{04ss}} = \frac{T_{01} - T_{03}}{T_{01} - T_{04ss}} \tag{13.27}$$

$$\eta_{ts} = \frac{h_{01} - h_{03}}{h_{01} - h_{4ss}} = \frac{T_{01} - T_{03}}{T_{01} - T_{4ss}} \tag{13.28}$$

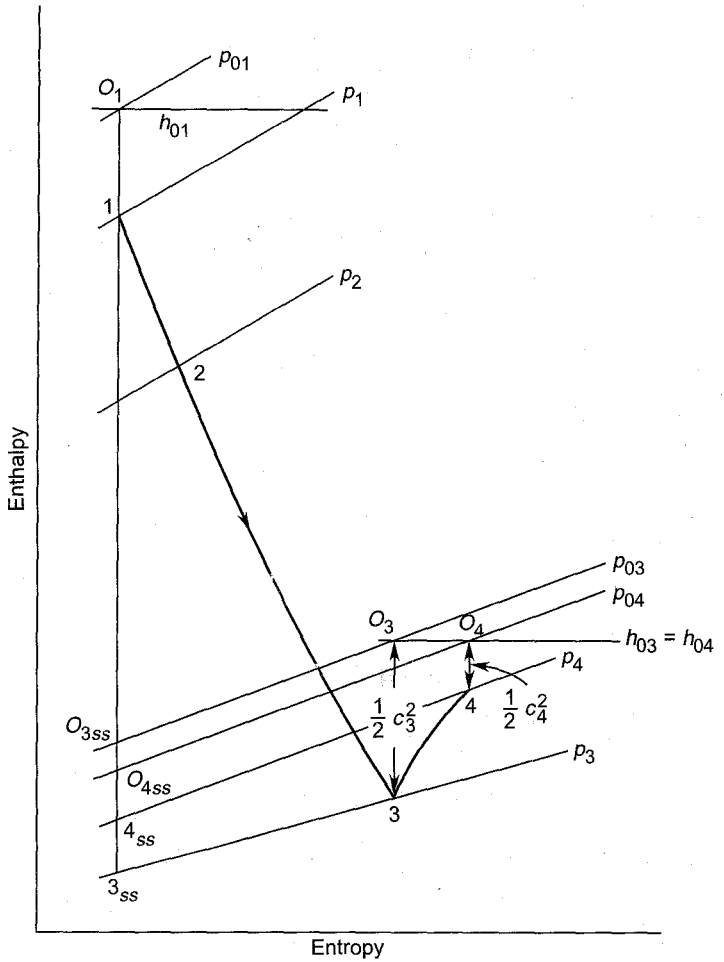

Fig. 13.6 Enthalpy-entropy diagram for flow through an IFR turbine stage with an exhaust diffuser

If the velocity at the diffuser exit is small, the two efficiencies have almost identical values.

13.3.4 Degree of Reaction

The relative pressure or enthalpy drop in the nozzle and rotor blades are determined by the degree of reaction of the stage. This is defined by

$$R = \frac{\text{static enthalpy drop in the rotor}}{\text{stagnation enthalpy drop in the stage}}$$

From the $h - s$ diagram (Fig. 13.5)

$$R = \frac{h_2 - h_3}{h_{02} - h_{03}} = \frac{T_2 - T_3}{T_{01} - T_{03}} \tag{13.29a}$$

$$R = 1 - \frac{c_2^2 - c_3^2}{2u_2 c_{\theta 2}} \tag{13.29b}$$

For constant meridional velocity component,

$$c_{r2} = c_{r3} \text{ (Fig. 13.1)}$$

$$c_{r2} = c_{x3} = c_3 \text{ (Fig. 13.3)}$$

$$c_2^2 - c_3^2 = (c_{r2}^2 + c_{\theta 2}^2) - c_{r2}^2 = c_{\theta 2}^2$$

Substituting this value in Eq. (13.29b)

$$R = 1 - \frac{c_{\theta 2}}{2u_2} \tag{13.30}$$

Substituting for $c_{\theta 2}/u_2$ from Eq. (13.4)

$$R = 1 - \frac{1}{2}\psi \tag{13.31a}$$

$$\psi = 2(1 - R) \tag{13.31b}$$

Equation (13.5b) when used in Eq. (13.31a) yields

$$R = \frac{1}{2}(1 - \phi_2 \cot \beta_2) \tag{13.31c}$$

Equations (13.31a and b) demonstrate that a highly loaded stage (high ψ) has a low degree of reaction and vice versa. The assumptions under which this statement is valid must be remembered.

Substituting from Eq. (13.18a) in the numerator of Eq. (13.29a)

$$R = \frac{\frac{1}{2}(u_2^2 - u_3^2) + \frac{1}{2}(w_3^2 - w_2^2)}{u_2 c_{\theta 2}} \tag{13.32}$$

The two quantities within the parentheses in the numerator may have the same or opposite signs. This, besides other factors, would also govern the value of reaction.

Equation (13.30) shows that the stage reaction decreases as $c_{\theta 2}$ (Fig. 13.1) increases because this results in a large proportion of the stage enthalpy drop to occur in the nozzle ring. For a given value of u_2, increased value of $c_{\theta 2}$ requires a smaller value of the air angle (β_2) at the rotor entry.

Some stages with two important values of reaction are discussed here briefly.

Impulse stage

Equation (13.30) gives for $R = 0$

$$c_{\theta 2} = 2u_2$$

$$\tan \beta_2 = \frac{c_{r2}}{u_2} = \phi_2 \tag{13.33}$$

From velocity triangles in Fig. 13.1

$$w_2^2 = u_2^2 + c_{r2}^2$$

$$w_3^2 = u_3^2 + c_{r3}^2 \text{ (for } c_{\theta 3} = 0)$$

Therefore, for $c_{r2} = c_{r3}$

$$w_3^2 - w_2^2 = -(u_2^2 - u_3^2) \tag{13.34}$$

This shows that the effect of radius change upon the degree of reaction is cancelled by the change in the relative velocity ($w_3 < w_2$).

Equation (13.31b) yields the stage loading coefficient as

$$\psi = 2 \tag{13.35}$$

This shows that an impulse IFR turbine stage is a highly loaded stage.

Fifty per cent reaction stage

Equation (13.30) for $R = \frac{1}{2}$ gives

$$\frac{1}{2} = 1 - \frac{c_{\theta 2}}{2u_2}$$

$$c_{\theta_2} = u_2$$

$$\tan \alpha_2 = \frac{c_{r2}}{u_2} = \phi_2 \text{ [Eq. (13.9)]}$$

$$\tan \beta_2 = \infty$$

$$\beta_2 = 90° \tag{13.36}$$

Equation (13.31b) gives

$$\psi = 1$$

Figure 13.7 shows the variation of the degree of reaction with flow coefficient for various values of the air angles at the rotor entry. The degree of reaction at a given flow coefficient increases with the air angle at the rotor entry; it decreases with the increase in flow coefficient for $\beta_2 < 90°$ and increases with the flow coefficient for $\beta_2 > 90°$. The degree of reaction of the fifty per cent reaction stage remains constant at all values of the flow coefficient.

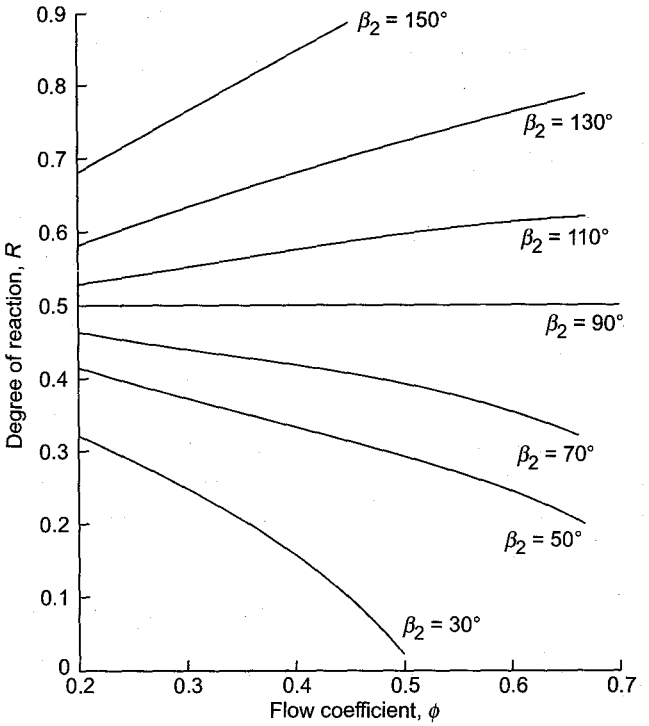

Fig. 13.7 Variation of the degree of reaction with flow coefficient and air angle at rotor entry, $c_{\theta 3} = 0$, $c_{r2} = c_{r3}$

Figure 13.8 shows the plots of the stge loading coefficient with flow coefficient for various values of β_2. Here the loading coefficient at a given flow coefficient decreases with the increase in the air angle, β_2; it increases with the flow coefficient for $\beta_2 < 90°$ and decreases with the increase in flow coefficient for $\beta_2 > 90°$.

13.4 Stage Losses[196,500]

As mentioned before, an inward-flow radial turbine stage is an inverted centrifugal compressor stage. Therefore, the nature of losses (see section 12.8) in the two machines is the same though the magnitudes differ considerably; this is on account of the accelerating flow in the turbine stage which results in lower losses.

The stage work is less than the isentropic stage enthalpy drop on account of aerodynamic losses [505,512] in the stage. The actual output at the turbine shaft is equal to the stage work minus the losses due to rotor disc and bearing friction.

The following aerodynamic losses occur in the stage:

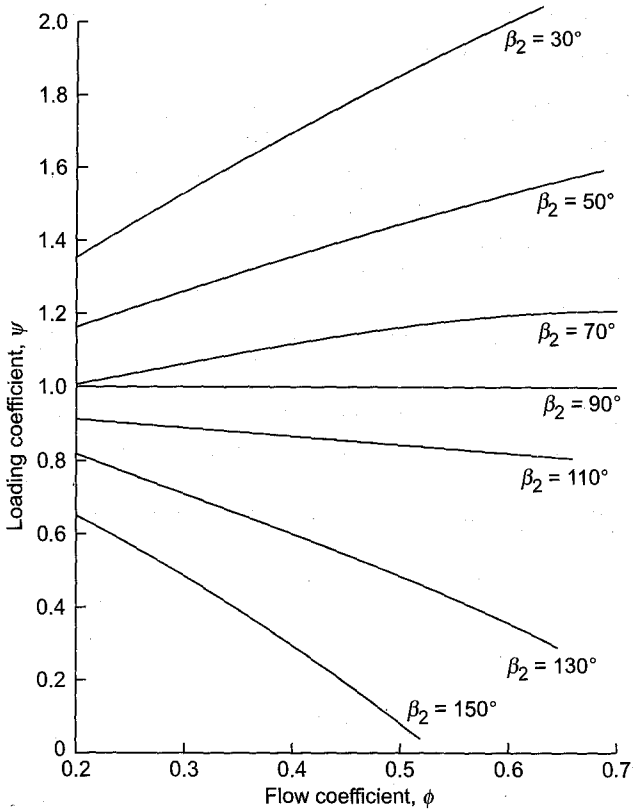

Fig. 13.8 Variation of the loading coefficient with flow coefficient and air angle at rotor entry, $c_{\theta 2} = 0$, $c_{r2} = c_{r3}$

(a) *Skin friction and separation losses in the scroll and the nozzle ring*

They depend on the geometry and the coefficient of skin friction of these components.

(b) *Skin friction and separation losses in the rotor blade channels*

These losses are also governed by the channel geometry, coefficient of skin friction and the ratio of the relative velocities w_3/w_2. In the ninety degree IFR turbine stage, the losses occurring in the radial and axial sections of the rotor are sometimes separately considered.

(c) *Skin friction and separation losses in the diffuser*

These are mainly governed by the geometry of the diffuser and the rate of diffusion.

(d) *Secondary losses*

These are due to circulatory flows developing into the various flow passages and are principally governed by the aerodynamic loading of the

blades. The main parameters governing these losses are b_2/d_2, d_3/d_2 and hub-tip ratio at the rotor exit.

(*e*) *Shock or incidence losses*

At off-design operation, there are additional losses in the nozzle and rotor blade rings on account of incidence at the leading edges of the blades. This loss is conventionally referred to as shock loss though it has nothing to do with the shock waves.

(*f*) *Tip clearance loss*

This is due to the flow over the rotor blade tips which does not contribute to the energy transfer.

Figure 13.9 shows a typical plot of rotor losses against incidence. The losses are minimum at the design point ($i = 0$). Channel losses are nearly constant with varying incidence. Shock losses increase rapidly with incidence. Secondary loss constitutes a major portion of the total losses.

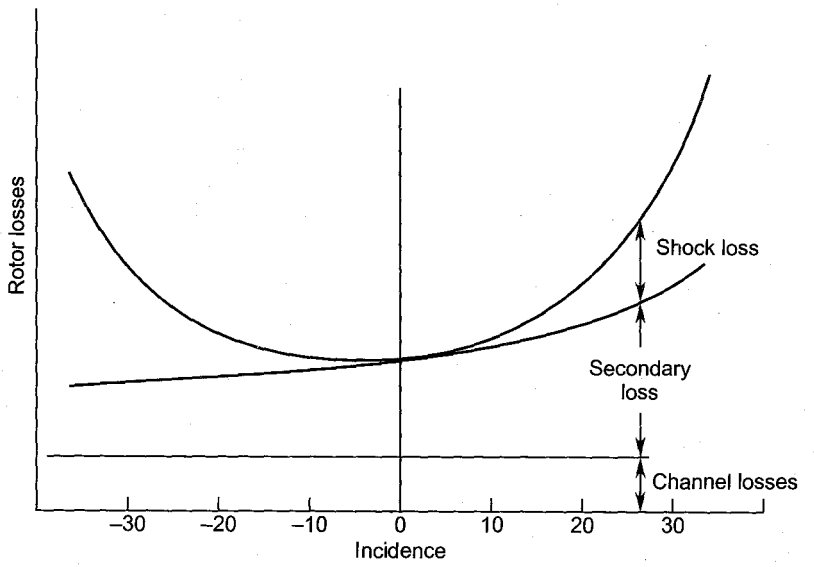

Fig. 13.9 Losses in the rotor of an IFR turbine stage (typical curve)

The losses in an IFR turbine stage can also be expressed in terms of the nozzle and rotor loss coefficients as defined for axial stages (Sec. 9.5.1).

From the enthalpy-entropy diagram (Fig. 13.5), these coefficients are

$$\xi_N = \frac{h_2 - h_{2s}}{\frac{1}{2}c_2^2} \tag{13.37}$$

$$\xi_R = \frac{h_3 - h_{3s}}{\frac{1}{2} w_3^2} \tag{13.38}$$

13.5 Performance Characteristics[501,508,514]

Various methods of presenting the performance characteristics of turbines has been discussed in Sec. 7.6.

Figure 13.8 shows the theoretical ψ–ϕ_2 plots of radial turbine stages with various values of the air angles at the rotor entry. Actual curves can be drawn either by plotting experimentally obtained values or by deducting the theoretically calculated stage losses from the ideal curves.

The actual performance can also be plotted between the quantities p_{01}/p_{03} and $\dot{m}\sqrt{T_{01}}/p_{01}$ for various values of the dimensionless speed parameter $N/\sqrt{T_{01}}$ as shown in Fig. 7.3.

12.5.1 Blade-to-gas Speed Ratio

As mentioned in Sec. 7.6 (Fig. 7.2), the performance characteristics of turbines are often presented in terms of plots between the stage efficiency and the blade-to-gas speed ratio. The blade-to-gas speed ratio can be expressed in terms of the isentropic stage terminal velocity c_0.

For an ideal or isentropic IFR turbine stage with $c_{\theta 3} = 0$ and complete recovery of the kinetic energy at the exit,

$$h_{01} - h_{03ss} = \frac{1}{2} c_0^2 = u_2 c_{\theta 2}$$

Equation (13.5a), when used in this expression, gives

$$\sigma_s = \frac{u_2}{c_0} = [2(1 + \phi_2 \cot \beta_2)]^{-1/2} \tag{13.39}$$

For $\beta_2 = 90°$

$$\sigma_s = \frac{u_2}{c_0} = \frac{1}{\sqrt{2}} = 0.707 \tag{13.40}$$

Though the above expressions have been derived for an ideal stage with simplifying assumptions, the figure in Eq. (13.40) is very close to the experimentally obtained values between 0.68 and 0.73 for maximum efficiency.

Using Eq. (13.19b) in Eq. (13.23b) and Eq. (13.20b) in Eq. (13.23b) yield

$$\eta_{st} = 2\sigma^2 (1 + \phi_2 \cot \beta_2) = 2\sigma^2 \psi \tag{13.41}$$

Equation (13.39), when used in Eq. (13.41), gives $\eta_{st} = 1$ for an isentropic stage.

Equation (13.31c) gives

$$\phi_2 \cot \beta_2 = 1 - 2R$$

This, when used in Eq. (13.41), yields another useful relation.

$$\eta_{st} = 4\sigma^2 (1 - R) \tag{13.42}$$

Figure 13.10 depicts typical curves of η_{st} versus σ for various values of the nozzle exit air angle which is generally between 11 and 25 degrees.

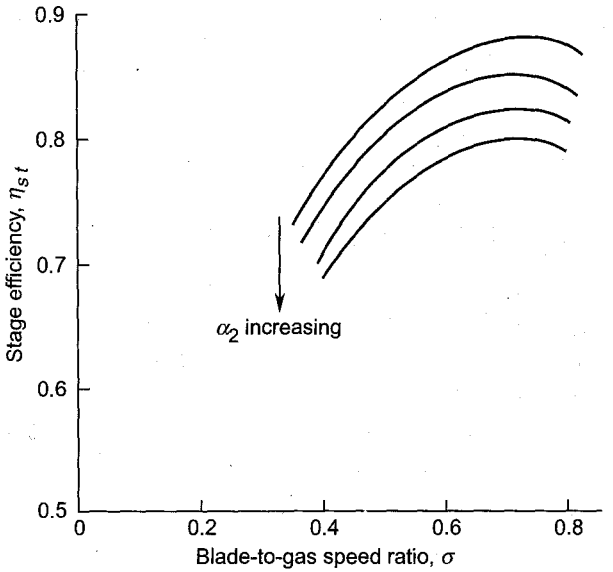

Fig. 13.10 Variation of stage efficiency of an IFR turbine with blade-to-isentropic gas speed ratio (typical curves)

13.5.2 Mach Number Limitations

The flow in a turbine stage chokes when the Mach number reaches sonic value; this can occur at the nozzle throat or anywhere in the rotor flow passage up to its exit. Besides this, the flow can reach supersonic velocities due to local acceleration in which case the deceleration (if any) to subsonic flow will result in shock waves.

Nozzle exit Mach number

The Mach number at the nozzle exit is given by

$$M_2 = \frac{c_2}{a_2} = \frac{c_2}{\sqrt{\gamma R T_2}} \tag{13.43}$$

From the velocity triangle at the entry (Fig. 13.1)

$$c_2 = u_2 (1 + \phi_2 \cot \beta_2) \sec\alpha_2 \tag{13.44}$$

$$T_2 = T_{02} - c_2^2/2c_p$$

$$T_2 = T_{02}\left[1-(\gamma-1)\frac{c_2^2}{2\gamma RT_{02}}\right]$$

Substituting for c_2 from Eq. (13.44)

$$T_2 = T_{02}\left[1-\frac{\gamma-1}{2}\left(\frac{u_2^2}{\gamma RT_{02}}\right)(1+\phi_2 \cot\beta_2)^2 \sec^2\alpha_2\right] \tag{13.45}$$

A blade Mach number based on the stagnation velocity of sound is defined as

$$M_{b0} = u_2/\sqrt{\gamma RT_{02}} \tag{13.46}$$

Substituting from Eqs. (13.44) and (13.45) in Eq. (13.43) and introducing M_{b0}

$$M_2 = \frac{M_{b0}(1+\phi_2 \cot\beta_2)\sec\alpha_2}{\left[1-\frac{\gamma-1}{2}M_{b0}^2(1+\phi_2\cot\beta_2)^2\sec^2\alpha_2\right]^{1/2}} \tag{13.47}$$

For $\beta_2 = 90°$

$$M_2 = M_{b0}\sec\alpha_2\left[1-\frac{\gamma-1}{2}M_{b0}^2\sec^2\alpha_2\right]^{-1/2} \tag{13.48}$$

Rotor exit Mach number

At the rotor exit, the highest Mach number will be corresponding to the relative velocity w_3.

$$M_{3\text{rel}} = \frac{w_3}{a_3}$$

From the exit velocity triangle (Fig. 13.3) for $c_{\theta 3} = 0$

$$M_{3\text{rel}} = \frac{u_3}{a_3}\sec\beta_3 = \frac{u_2}{a_3}\frac{d_3}{d_2}\sec\beta_3$$

$$M_{3\text{rel}} = \frac{u_2}{\sqrt{\gamma RT_3}}\frac{d_3}{d_2}\sec\beta_3 \tag{13.49}$$

$$h_{01} - h_{03} = u_2^2$$

$$h_{01} - h_3 - \frac{1}{2}c_3^2 = u_2^2$$

$$h_3 = h_{01} - u_2^2 - \frac{1}{2}u_3^2\tan^2\beta_3$$

$$c_p T_3 = c_p T_{01} - u_2^2 \left(1 + \frac{1}{2}\frac{d_3^2}{d_2^2} \tan^2 \beta_3\right)$$

$$T_3 = T_{01}\left[1 - (\gamma - 1)\frac{u_2^2}{\gamma R T_{01}}\left(1 + \frac{1}{2}\frac{d_3^2}{d_2^2}\tan^2 \beta_3\right)\right] \tag{13.50}$$

Substituting for T_3 from Eq. (13.50) in Eq. (13.49) and introducing M_{b0}

$$M_{3\text{rel}} = \frac{M_{b0}\,(d_3/d_2)\sec\beta_3}{\left[1 - (\gamma - 1)\,M_{b0}^2\left(1 + \frac{1}{2}\frac{d_3^2}{d_2^2}\tan^2\beta_3\right)\right]^{1/2}} \tag{13.51}$$

The Mach number of the absolute flow corresponding to the velocity c_3 will be lesser than $M_{3\text{rel}}$.

13.6 Outward-flow Radial Stages

In outward flow radial turbine stages, the flow of the gas or steam occurs from smaller to larger diameters. The stage consists of a pair of fixed and moving blades. The increasing area of cross-section at larger diameters accommodates the expanding gas.

This configuration did not become popular with steam and gas turbines. The only one which is employed more commonly is the Ljungstrom double rotation type shown in Fig. 1.12. It consists of rings of cantilever blades projecting from two discs rotating in opposite directions. The relative peripheral velocity of blades in the two adjacent rows, with respect to each other, is high. This gives a higher value of enthalpy drop per stage.

Figure 13.11 shows the counter rotating blade rings of a Ljungstrom turbine; each row of blades forms a stage. The velocity triangles for such stages are shown in Fig. 13.12. Various velocities at the inlet of the first stage are designated by the suffix i. The exit air angles (α) of all stages are assumed to be the same.

The relative velocity at the exit of the first stage is w_1 which along with the peripheral velocity u_1 gives the absolute velocity c_1. The relative velocity w_2 at the entry of the second stage is obtained by the vector subtraction of u_1 from c_1. Thus the exit velocity triangle of the first stage and the entry velocity triangle of the second are shown together. The same applies to the second, third and other stages.

The relative velocity at the exit from the second stage is w_3 and at the entry to the third stage is w_4. The common absolute velocity at this station is c_2.

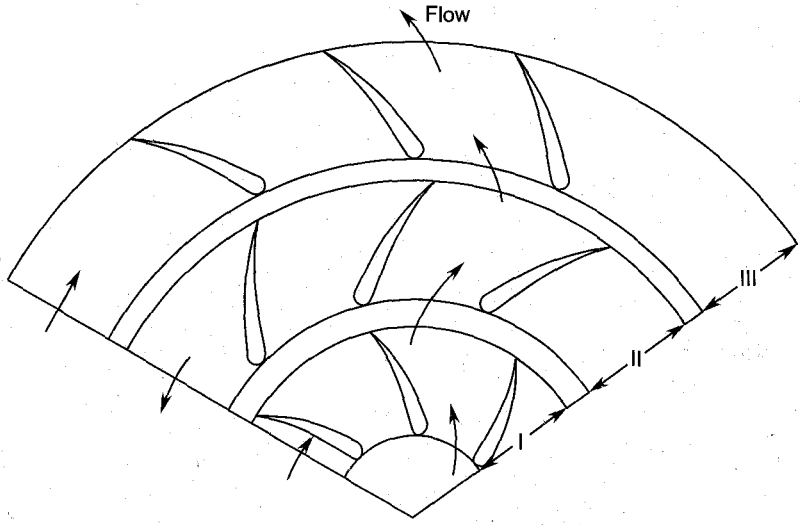

Fig. 13.11 Counter rotating blade rings of a Ljungstrom turbine

Stage work

For the purpose of analysis, the ratio of the peripheral velocity of blades and the relative velocity of flow at the exit is also assumed to be constant.

$$\sigma = \frac{u_1}{w_1} = \frac{u_2}{w_3} = \frac{u_3}{w_5} = \text{const.} \tag{13.52}$$

The first blade ring does not represent a general stage. Therefore, for the purpose of general treatment, the second or any other stage beyond this can be considered. For the second stage.

$$w = h_{01} - h_{02} = u_1\, c_{\theta 1} + u_2\, c_{\theta 2} \tag{13.53}$$

From velocity triangles

$$w = u_1\,(w_1 \cos\,\alpha - u_1) + u_2\,(w_3 \cos\,\alpha - u_2)$$

For small radial chords of the blades ($u_1 \approx u_2$) and assuming $w_1 \approx w_3$

$$w = 2u_2\,(w_3 \cos\,\alpha - u_2)$$

$$w = 2w_3^2 \left(\frac{u_2}{w_3}\cos\alpha - \frac{u_2^2}{w_3^2}\right)$$

$$w = 2w_3^2\,(\sigma \cos\,\alpha - \sigma^2) \tag{13.54}$$

The optimum value of σ for maximum work can be determined.

$$\frac{\partial w}{\partial \sigma} = 0$$

$$\cos\,\alpha - 2\,\sigma = 0$$

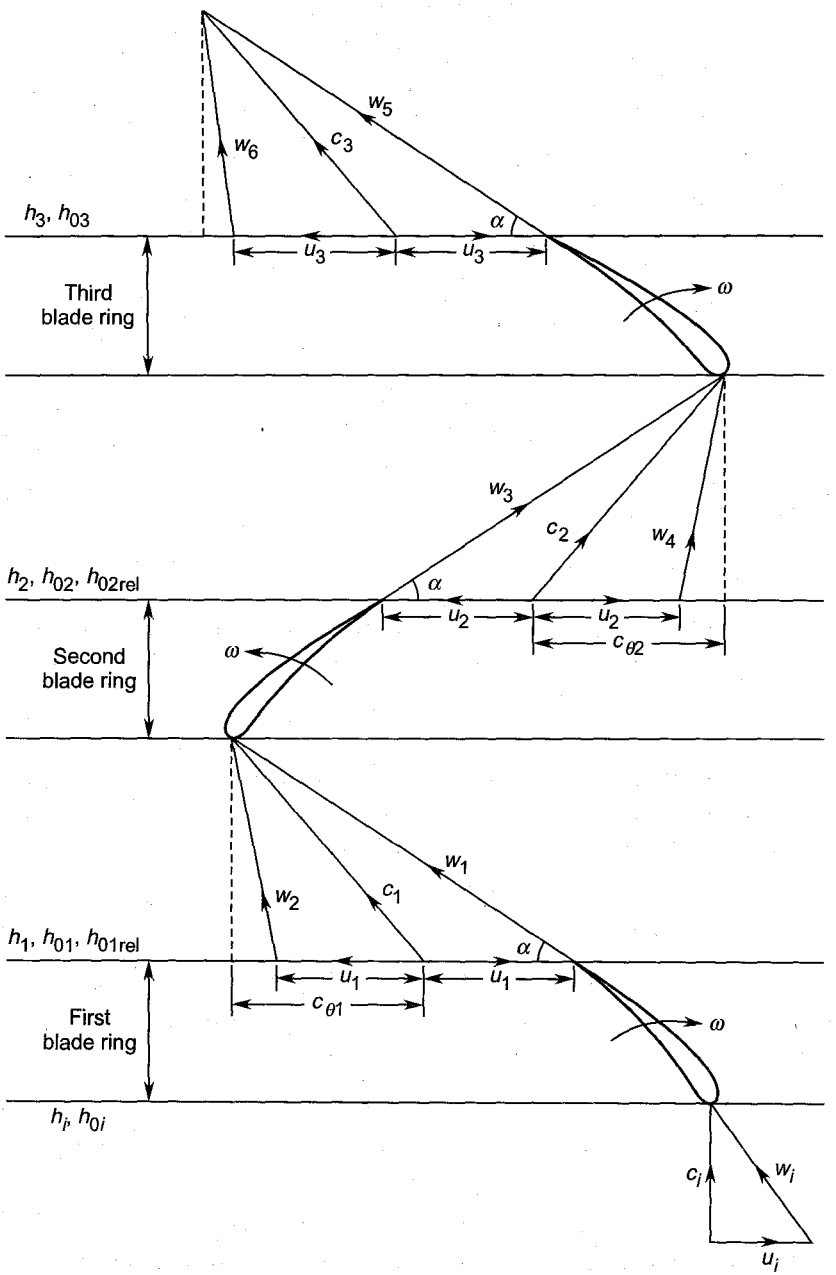

Fig. 13.12 Velocity triangles for the stages of a Ljungstrom turbine

$$\sigma_{opt} = \frac{1}{2} \cos \alpha \tag{13.55}$$

With this condition Eq. (13.52) yields

$$w_1 \cos \alpha = 2u_1 \tag{13.56a}$$

$$w_3 \cos \alpha = 2u_2 \tag{13.56b}$$

$$w_5 \cos \alpha = 2u_3 \tag{13.56c}$$

These equations show that, for maximum work condition, the air angle at the entries of the blades is 90°. The maximum work [from Eq. (13.54)] is given by

$$w_{max} = \frac{1}{2} w_3^2 \cos^2 \alpha \tag{13.57a}$$

Substituting from Eq. (13.56b)

$$w_{max} = 2u_2^2 \tag{13.57b}$$

Equations (13.55) and (13.57b) show that the outward-flow counter rotating radial stages behave like an impulse stage of the axial type [Eqs. (9.20) and (9.23)]. However, this is only an incorrect impression given by these relations. Here the equivalent or the true blade velocity is $2u_2$ on account of counter rotation. Therefore, the actual blade-to-gas speed ratio must be taken as $2u_2/w_3 = \cos \alpha$. This is the same as in the fifty per cent reaction stages of the axial type [see Eq. (9.73)]. It can also be observed that the blades of these stages for maximum work take the form of the fifty per cent reaction stages of the axial type as shown in Fig. 9.14.

Relative stagnation enthalpy

From the general Euler's turbine equation for the second stage

$$h_{01} - h_{02} = \frac{1}{2} (c_1^2 - c_2^2) + \frac{1}{2} (w_3^2 - w_2^2) + \frac{1}{2} (u_1^2 - u_2^2)$$

$$\left(h_{01} - \frac{1}{2} c_1^2\right) + \frac{1}{2} w_2^2 - \frac{1}{2} u_1^2 = \left(h_{02} - \frac{1}{2} c_2^2\right) + \frac{1}{2} w_3^2 - \frac{1}{2} u_2^2$$

$$h_1 + \frac{1}{2} w_2^2 - \frac{1}{2} u_1^2 = h_2 + \frac{1}{2} w_3^2 - \frac{1}{2} u_2^2 \tag{13.58a}$$

This, as per the notation used in Fig. 13.12, yields the well-known relation [Eq. (13.18b)] already derived for the IFR turbine stage

$$h_{01rel} - \frac{1}{2} u_1^2 = h_{02rel} - \frac{1}{2} u_2^2 \tag{13.58b}$$

It should be remembered here that the contribution of the centrifugal energy to the total energy transfer in an outward-flow radial stage is negative.

Notation for Chapter 13

a	Velocity of sound
A	Area of cross-section
b	Rotor blade width or height
c	Gas velocity
c_o	Isentropic, spouting or stage terminal velocity
c_p	Specific heat at constant pressure
d	Diameter
h	Enthalpy
i	Incidence
$\dot{m}$	Mass-flow rate
M	Mach number
n	Number of blades
N	Rotational speed
p	Pressure
p_r	Pressure ratio
P	Power
R	Degree of reaction, gas constant
t	Blade thickness
T	Absolute temperature
u	Peripheral velocity of the rotor blades
w	Relative velocity or work

Greek symbols

α	Air angles in the absolute system
β	Air angles in the relative system
γ	Ratio of specific heats
η	Efficiency
ξ	Enthalpy loss coefficient
ρ	Density
σ	Blade-to-gas speed ratio
ϕ	Flow coefficient
ψ	Loading or head coefficient

Subscripts

o	Stagnation value
1	Nozzle entry
2	Rotor entry
3	Rotor exit

4	Diffuser exit
a	Actual
b	Rotor blade
h	Hub
IFR	Inward-flow radial
N	Nozzle
opt	Optimum
r	Radial
rel	Relative
R	Rotor
s, ss	Isentropic
st	Stage
t	Tip
ts	Total-to-static
tt	Total-to-total
x	Axial
θ	Tangential

Solved Examples

13.1 A ninety degree IFR turbine stage has the following data:

total-to-static pressure ratio	$p_{01}/p_3 = 3.5$
exit pressure	1 bar
stagnation temperature at entry	650°C
blade-to-isentropic speed ratio	$\sigma = 0.66$
rotor diameter ratio	$d_3/d_2 = 0.45$
rotor speed	$N = 16000$ rpm
nozzle exit air angle	$\alpha_2 = 20°$
nozzle efficiency	$\eta_N = 0.95$
rotor width at entry	$b_2 = 5$ cm

Assuming constant meridional velocity, axial exit and that the properties of the working fluid are the same as those of air, determine the following quantities:

(a) the rotor diameter, **(b)** the rotor blade exit air angle, **(c)** the mass-flow rate, **(d)** hub and tip diameters at the rotor exit, **(e)** the power developed and **(f)** the total-to-static efficiency of the stage.

***Solution*:**

$$T_{01} = 650 + 273 = 923\text{K}$$

The isentropic gas velocity from Eq. (13.20b)

$$c_0 = \sqrt{2 \times 1005 \times 923 \,(1 - 3.5^{-0.286})}$$

$$c_0 = 747.4 \text{ m/s}$$

(a) $$u_2 = \sigma\, c_0 = 0.66 \times 747.4 = 493.284 \text{ m/s}$$

$$\pi\, d_2\, N/60 = u_2$$

$$d_2 = 60 \times 493.284/\pi \times 16000 = 0.589 \text{ m}$$

$$d_2 = 58.9 \text{ cm } (\textit{Ans.})$$

(b) $$d_3 = 0.45 \times 0.589 = 0.265 \text{ m} = 26.5 \text{ cm}$$

$$c_{r2} = u_2 \tan \alpha_2 = 493.284 \tan 20 = 179.54 \text{ m/s}$$

$$u_3 = \pi\, d_3\, N/60$$

$$u_3 = \pi \times 0.265 \times 16000/60 = 222.0 \text{ m/s}$$

$$c_3 = c_{x3} = c_{r2} = 179.54 \text{ m/s}$$

$$\tan \beta_3 = c_{x3}/u_3 = 179.54/222 = 0.8087$$

$$\beta_3 = 38.96° \ (\textit{Ans.})$$

(c) This stage has fifty per cent reaction. Therefore,

$$R = \frac{h_2 - h_3}{u_2\, c_{\theta 2}} = \frac{1}{2}$$

Assuming perfect gas $c_p\,(T_2 - T_3) = 0.5u_2^2$

$$T_2 - T_3 = 0.5 \times (493.284)^2/1005 = 121.06°\text{C}$$

$$c_p\,(T_{01} - T_{03}) = u_2^2$$

$$T_{01} - T_{03} = (493.284)^2/1005 = 242.12°\text{C}$$

$$923 - T_{03} = 242.12$$

$$T_{03} = 680.88 \text{ K}$$

$$T_3 = T_{03} - c_3^2/2\, c_p = 680.88 - \frac{(179.54)^2}{2 \times 1005}$$

$$T_3 = 664.84 \text{ K}$$

$$T_2 = 664.84 + 121.06 = 785.90 \text{ K}$$

$$c_2 = u_2/\cos \alpha_2 = 493.284/\cos 20 = 524.94 \text{ m/s}$$

$$c_p\,(T_{01} - T_{2s})\, \eta_N = \frac{1}{2} c_2^2$$

$$T_{01} - T_{2s} = 0.5 \times (524.94)^2/1005 \times 0.95$$

$$T_{01} - T_{2s} = 144.31 \text{ K}$$

The pressure ratio across the nozzle can now be determined.

$$T_{01}\,[1 - p_{rN}^{-0.286}] = 144.31$$

$$p_{01}/p_2 = \left(1 - \frac{144.31}{923}\right)^{-3.5} = 1.8135$$

$$p_{01} = 3.5\ p_3 = 3.5 \text{ bar}$$

$$p_2 = 3.5/1.8135 = 1.93 \text{ bar}$$

$$\rho_2 = p_2/R\,T_2$$

$$\rho_2 = 1.93 \times 10^5/287 \times 785.9 = 0.8556 \text{ kg/m}^3$$

Neglecting blade thickness

$$\dot{m} = \rho_2\, c_{r2}\, \pi\, d_2\, b_2$$

$$\dot{m} = 0.8556 \times 179.54 \times \pi \times 0.589 \times 0.05$$

$$\dot{m} = 14.21 \text{ kg/s } (\textit{Ans.})$$

(d)

$$\rho_3 = p_3/R\,T_3$$

$$\rho_3 = 1 \times 10^5/(287 \times 664.84) = 0.524 \text{ kg/m}^3$$

$$\rho_2\, c_{x3}\, \pi\, d_3\, b_3 = \dot{m}$$

$$b_3 = 14.21 \times 100/0.524 \times 179.54\ \pi \times 0.265$$

$$b_3 = 18.14 \text{ cm}$$

$$d_h = d_3 - b_3 = 26.5 - 18.14 = 8.36 \text{ cm } (\textit{Ans.})$$

$$d_t = d_3 + b_3 = 26.5 + 18.14 = 44.64 \text{ cm } (\textit{Ans.})$$

(e)

$$P = \dot{m}\ u_2^2/1000$$

$$P = 14.21 \times (493.284)^2/1000$$

$$P = 3457.7 \text{ kW } (\textit{Ans.})$$

(f)

$$\eta_{ts} = u_2^2/c_p\ T_{01}\left[1 - \left(\frac{p_3}{p_{01}}\right)^{0.286}\right]$$

$$\eta_{ts} = \frac{(493.284)^2}{1005 \times 923\,(1 - 3.5^{-0.286})} \times 100$$

$$\eta_{ts} = 87.11\% \ (\textit{Ans.})$$

13.2 Determine for the stage in Ex. 13.1:

(a) the nozzle exit Mach number,
(b) rotor exit relative Mach number,
(c) nozzle enthalpy loss coefficient and
(d) rotor enthalpy loss coefficient.

***Solution*:**

The blade Mach number is

$$M_{b0} = u_2/\sqrt{\gamma R T_{01}}$$

$$M_{b0} = 493.284/\sqrt{1.4 \times 287 \times 923}$$

$$M_{b0} = 0.81$$

(a)
$$M_2 = M_{b0}/\cos\ \alpha_2 \left(1 - \frac{\gamma - 1}{2} M_{b0}^2 \sec^2 \alpha_2\right)^{1/2}$$

$$M_2 = 0.81/\cos\ 20\ (1 - 0.2 \times 0.81^2 \sec^2 20)^{1/2}$$

$$M_2 = 0.934\ (Ans.)$$

This can also be found direct from the value of c_2 and T_2 already calculated in Ex. 13.1

$$a_2 = \sqrt{\gamma R T_2}$$

$$a_2 = \sqrt{1.4 \times 287 \times 785.90} = 561.938 \text{ m/s}$$

$$M_2 = 524.94/561.938 = 0.934\ (Ans.)$$

(b) The relative velocity at the rotor exit

$$w_3 = u_3/\cos\ \beta_3 = 222/\cos\ 38.96$$

$$w_3 = 285.5 \text{ m/s}$$

$$a_3 = \sqrt{1.4 \times 287 \times 664.84} = 516.848 \text{ m/s}$$

$$M_{3\text{rel}} = w_3/a_3 = 285.5/516.848$$

$$M_{3\text{rel}} = 0.55\ (Ans.)$$

This can also be found by using Eq. (13.51)

(c)
$$T_{2s} = 923 - 144.31 = 778.69 \text{ K}$$

Equation (13.37) for a perfect gas is

$$\xi_N = c_p\ (T_2 - T_{2s}) \Big/ \frac{1}{2}\ c_2^2$$

$$\xi_N = 1005\ (785.90 - 778.69)/0.5 \times 524.94^2$$

$$\xi_N = 0.1255\ (Ans.)$$

(d) The pressure ratio across the rotor is

$$p_2/p_3 = 1.93/1 = 1.93$$

$$T_2/T_{3s} = 1.93^{0.286} = 1.207$$

$$T_{3s} = 785.90/1.207 = 651.12 \text{ K}$$

Using Eq. (13.38)

$$\xi_R = c_p\,(T_3 - T_{3s}) \Big/ \frac{1}{2}\, w_3^2$$

$$\xi_R = 1005\,(664.84 - 651.12) \Big/ \frac{1}{2} \times (285.5)^2$$

$$\xi_R = 0.3383 \;(Ans.)$$

13.3 An IFR turbine impulse stage with cantilever blades has a flow coefficient of 0.4 and develops 100 kW with a total-to-total efficiency of 90% at 12000 rpm. If the flow rate of air is 1.0 kg/s at an entry temperature of 400 K, determine the rotor diameters and air angles at the entry and exit, the nozzle exit air angle and the stagnation pressure ratio across the stage.

Take $d_3 = 0.8\ d_2$, zero exit swirl and constant meridional velocity.

***Solution*:**

$$P = 2\dot{m}\ u_2^2/1000$$

$$u_2^2 = 100 \times 1000/2$$

$$u_2 = 223.606 \text{ m/s}$$

$$\pi\, d_2\, N = 60\ u_2$$

$$d_2 = \frac{60 \times 223.606 \times 100}{\pi \times 12000} = 35.588 \text{ cm } (Ans.)$$

$$d_3 = 0.8 \times 35.588 = 28.47 \text{ cm } (Ans.)$$

$$\tan \beta_2 = 0.4;\ \beta_2 = 21.80^\circ \;(Ans.)$$

$$c_{r_2} = c_{r_3} = 0.4 \times 223.606 = 89.442 \text{ m/s}$$

For an impulse stage $c_{\theta_2} = 2u_2$

$$\tan \alpha_2 = c_{r_2}/2u_2 = \frac{89.442}{2 \times 223.606}$$

$$\alpha_2 = 11.31^\circ \;(Ans.)$$

$$\left(\frac{p_{03}}{p_{01}}\right)^{0.286} = 1 - \frac{2\,u_2^2}{\eta_{tt}\, c_p\, T_{01}}$$

$$\left(\frac{p_{03}}{p_{01}}\right)^{0.286} = 1 - \frac{2 \times 223.606^2}{0.9 \times 1005 \times 400} = 0.7236$$

$$p_{01}/p_{03} = 3.10 \;(Ans.)$$

$$\tan \beta_3 = c_{r3}/u_3$$

$$u_3 = \pi \times 0.2847 \times 12000/60 = 178.88 \text{ m/s}$$

$$\tan \beta_3 = 89.442/178.88$$

$$\beta_3 = 26.56^\circ \;(Ans.)$$

Questions and Problems

13.1 Draw the sketch of a ninety degree inward-flow radial turbine stage with an exit diffuser showing its main components. What are the main advantages of this type over the other types of inward-flow gas turbines? Give its important applications.

13.2 Show the entry and exit velocity triangles for a general inward-flow radial turbine stage. Redraw them for a ninety degree IFR turbine stage. For such a stage, prove that:

(a) Power = $u_2^2 \times 10^{-3}$ kW/(kg/s)

(b) $\psi = 1$

(c) Degree of reaction = 50%

13.3 (a) Draw an enthalpy-entropy diagram for flow through an inward-flow radial turbine stage fitted with an exhaust diffuser.

(b) Prove that:

$$h_{02\text{rel}} - \frac{1}{2} u_2^2 = h_{03\text{rel}} - \frac{1}{2} u_3^2$$

13.4 (a) How is the degree of reaction of an IFR turbine stage defined?

(b) Show the entry and exit velocity triangles for impulse and fifty per cent reaction stages indicating various velocities and air angles.

(c) Prove the following relations:

$$R = 1 - \frac{c_{\theta_2}}{2u_2}$$

$$R = \frac{1}{2} (1 - \phi_2 \cot \beta_2)$$

$$\phi = 2 (1 - R)$$

State the assumptions used.

13.5 Draw and discuss briefly the following curves for an IFR turbine stage with constant meridional velocity and zero exit swirl:

(a) R vs ϕ_2

(b) R vs β_2

(c) R vs ψ

(d) ψ vs ϕ_2

(e) ψ vs β_2

13.6 What are the effects of flow Mach number on the performance of an IFR turbine stage? Derive the following expressions for a ninety degree IFR turbine stage:

(a)
$$M_2 = \frac{M_{b0}}{\cos\alpha_2 \left(1 - \frac{\gamma - 1}{2} M_{b0}^2 \sec^2 \alpha_2\right)^{1/2}}$$

$$M_{3\text{rel}} = \frac{M_{b0}\,(d_3/d_2)}{\cos\beta_3 \left[1 - (\gamma - 1)\left(1 + \frac{1}{2}\frac{d_3^2}{d_2^2} \tan^2 \beta_3\right) M_{b0}^2\right]^{1/2}}$$

13.7 (a) What is stage terminal or spouting velocity?

(b) Prove that:

$$\eta_{st} = 4\ \sigma^2\ (1 - R)$$

$$\psi = \frac{1}{2\sigma^2}\ \eta_{st}$$

$$\sigma_{\text{opt}} = 0.707$$

13.8 (a) Describe briefly the various losses occurring in an inward-flow radial turbine stage.

(b) What are the effects of the rotor entry Mach number and incidence on losses?

13.9 (a) Show the sketch of a double rotation outward flow radial steam turbine stage.

(b) Draw the entry and exit velocity triangles for a general stage and a stage with maximum energy transfer.

(c) Derive the following relations:

(i) $\sigma_{\text{opt}} = \frac{1}{2}\cos\alpha$

(ii) $w_{\max} = 2u_2^2$

(iii) $h_{0\text{rel}} - \frac{1}{2}\ u^2 = \text{const.}$

(iv) $dh = -w\ dw + u\ du$

13.10 A single stage ninety degree IFR turbine fitted with an exhaust diffuser has the following data:

overall stage pressure ratio	4.0
temperature at entry	557 K
diffuser exit pressure	1 bar
mass-flow rate of air	6.5 kg/s

flow coefficient	0.30
rotor tip diameter	42 cm
mean diameter at rotor exit	21 cm
speed	18000 rpm

Enthalpy losses in the nozzle and the rest of the stage are equal. Assuming negligible velocities at the nozzle entry and diffuser exit, determine: (*a*) the nozzle exit air angle, (*b*) the rotor width at the entry, (*c*) the power developed, (*d*) the stage efficiency, (*e*) the rotor blade height at the exit, (*f*) Mach numbers at nozzle and rotor (relative) exits and (*g*) the nozzle and rotor loss coefficients.

(*Ans.*) (*a*) $\alpha_2 = 16.699°$; (*b*) $b_2 = 2.768$ cm; (*c*) $P = 1018.48$ kW; (*d*) $\eta_{st} = 85.596$; (*e*) $b_3 = 9.433$cm; (*f*) $M_2 = 0.9489$, $M_{3rel} = 0.58$; and (*g*) $\xi_N = 0.1545$, $\xi_R = 0.4953$.

13.11 A cantilever blade type IFR turbine receives air at $p_{01} = 3$ bar, $T_{01} = 373$. Other data for this turbine are:

rotor tip diameter	50 cm
rotor exit diameter	30 cm
speed	7200 rpm
rotor blade width at entry	3 cm
air angle at rotor entry	60°
air angle at nozzle exit	25°
nozzle efficiency	97%
stage pressure ratio p_{01}/p_3	2.0

The radial velocity is constant and the swirl at the rotor exit is zero.

Determine: (a) the flow and loading coefficients, (b) the degree of reaction and stage efficiency (η_{ts}), (c) the air angle and width at the rotor exit, and (d) the mass-flow rate and power developed.

(*Ans.*) (a) $\phi_2 = 0.638$, $\psi = 1.368$; (b) $R = 31.58\%$, $\eta_{ts} = 72.13\%$; (c) $\beta_3 = 46.76°$, $b_3 = 6.476$ cm; and (d) $\dot{m} = 12.084$ kg/s, $P = 587.52$ kW.

Chapter 14

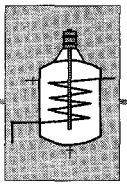

Axial Fans and Propellers

The basic purpose of a "fan" is to move a mass of gas or vapour at the desired velocity. For achieving this objective there is a slight increase in the gas pressure across the fan rotor or impeller. However, the main aim remains to move air or gas without any appreciable increase in its pressure. The total pressure developed by fans is of the order of a few millimetres of water gauge.

A "blower", which is also referred to as a "fan" in some literature, delivers the gas or air with an appreciable rise in pressure to overcome some kind of resistance in the flow. In some applications they develop pressures of the order of 1000 mm W.G. or more.

In contrast to fans and blowers, compressors (Chapters 11 and 12) develop moderate to high pressures. The pressure rise through them is conventionally expressed in terms of the pressure ratio. Some low pressure compressors are erroneously referred to as blowers.

Ceiling, table and ventilation fans are typical examples of axial fans. Forced and induced draft fans, and high draft fans used in mines, industrial furnaces and airconditioning plants are termed as blowers. Gas compression devices used in superchargers, producer gas plants and aircraft engines which are required for relatively higher pressures are known as compressors.

Fans and blowers can be either axial, centrifugal or of the mixed-flow type. A majority of low pressure machines (fans) are of the axial type, whereas a large number of high pressure machines (blowers) are of the centrifugal type.

While centrifugal machines generate higher pressures per stage at comparatively lower flow rates, axial fans and blowers handle higher flow rates at lower pressures per stage. On account of the geometrical configuration, centrifugal machines should not have many stages for obtaining higher pressures. In contrast to this, axial types can conveniently have numerous stages.

14.1 Fan Applications[542,558]

Fans and blowers are used all over the world in a wide variety of industries. Some of the important applications are in steam power stations, ventilation systems, cooling of electric motors and generators, and many industrial processes. Some of these applications are briefly described below.

14.1.1 Power Plants

Forced draft (F.D.) and induced draft (I.D.) fans are used to raise the pressure of air and flue gases necessary to overcome the draft losses in the flow passages of a steam boiler plant. The range of pressure rise is approximately from 200 to 1600 mm W.G. The forced draft fan raises the pressure of the ambient air and delivers it to the boiler furnace through the air preheater. The induced draft fan is located between the furnace and the flue gas chimney. Therefore, it works in the hostile atmosphere of high temperature (150 – 350°C) abrasive and corrosive gases. Both F.D. and I.D. fans can be either of the axial or centrifugal type, and are generally driven by electric motors. Some large fans absorb over one megawatt of power.

Small and large fans are also used for driving pulverised coal or fuel oil.

14.1.2 Cooling Towers

Large quantities of the condenser circulating water are cooled in cooling towers. The degree of cooling achieved in the cooling towers is independent of the ambient conditions (temperature and humidity). Fans for this application are generally of the large axial type, developing a low pressure rise and higher air flow rates. A typical fan of 20 m diameter developed 12 mm W.G. at about 3000 m^3/s at 75 rpm.

Cooling tower fans can also be employed as either F.D. (Fig. 14.1) or I.D. fans. The I.D. fan is located near the top of the cooling tower.

14.1.3 Cooling of Motors, Generators and Engines

Considerable quantities of heat need to be removed from internal combustion engines, and electric motors and generators. On account of the mechanical arrangement used and the magnitudes of heat transfers, forced circulation of the cooling media is almost indispensable. The cooling of the automobile jacket hot water in the radiator (Fig. 14.2) is well known. The air sucked in through the radiator cools the circulating water as well as the engine. The propeller fan is belt-driven by the engine.

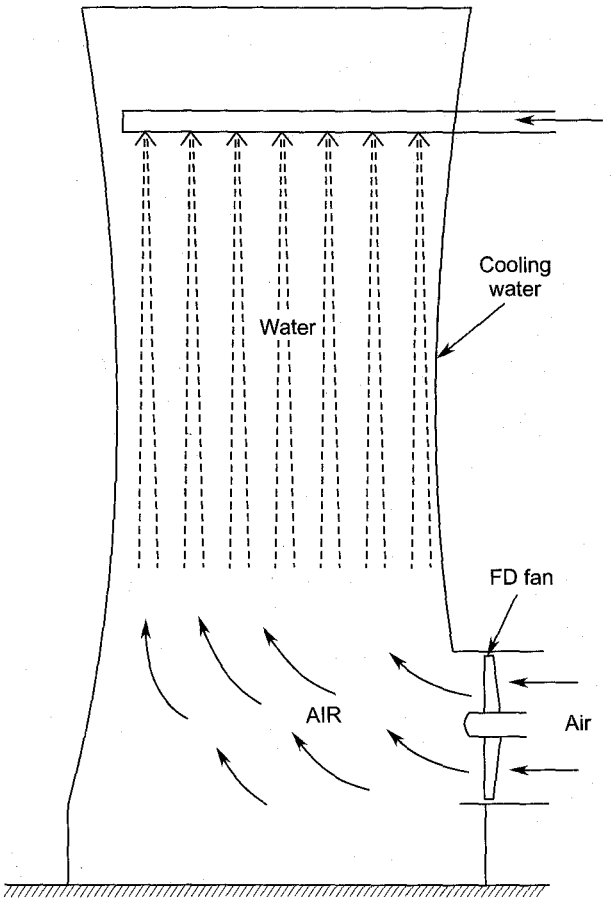

Fig. 14.1 Forced draft fan in a cooling tower

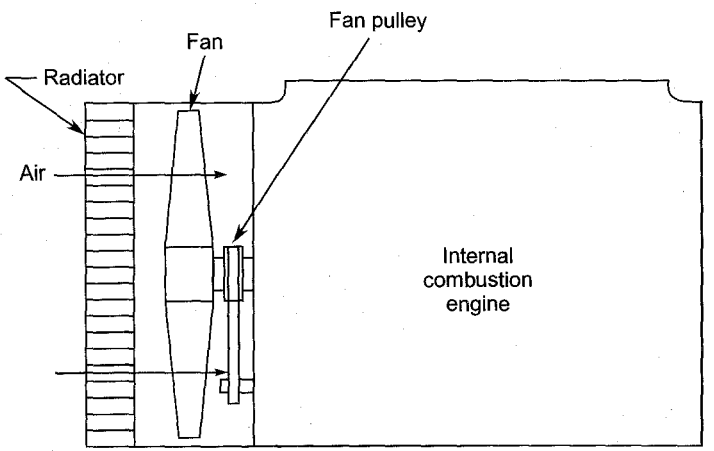

Fig. 14.2 Axial fan for engine cooling

The fans for cooling electric motors and generators are generally mounted on the extensions of their main shafts. A hydrogen-cooled sealed alternator has two axial fans at the two ends of its rotor as shown in Fig. 14.3. The fan rotor has a comparatively large number of aerofoil blades. The fans cool the windings by blowing hydrogen on them. The hydrogen in turn is cooled by circulating water. One such arrangement is shown in Fig. 14.3.

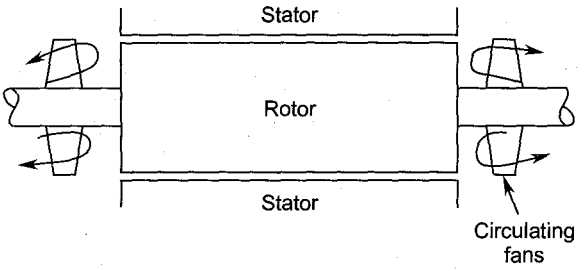

Fig. 14.3 Fans for alternator cooling

14.1.4 Air Circulation and Mine Ventilation

Fans of various ratings are used to circulate air in airconditioning systems. Besides this fans are used to circulate air in a number of other applications also, e.g. centrifugal separators, furnaces, drying equipment and cooling of electrical and optical equipment.

Fans or blowers employed for the ventilation of mines (Fig. 14.4) and tunnels are heavy-duty fans. The ratings of fans for mine ventilation can

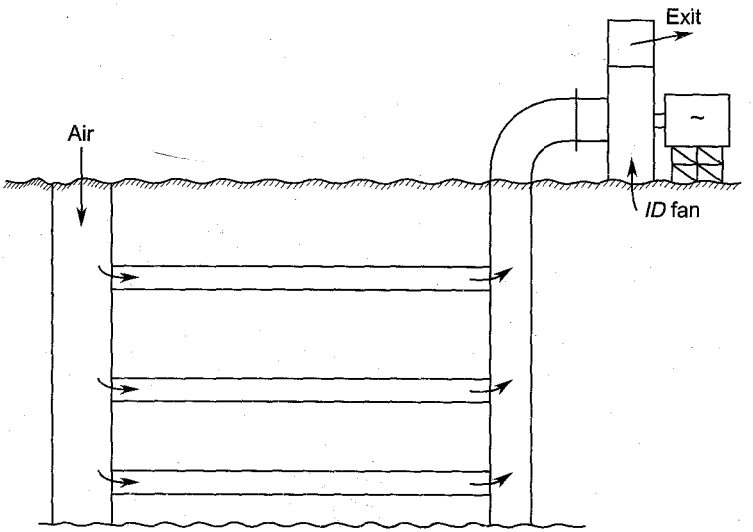

Fig. 14.4 Mine ventilation by an I.D. fan

be obtained from the number of workers in the mine and the total resistance to be overcome. Each man requires about $6m^3$ of air per minute. The resistance is of the order of 600 mm W.G. On account of the relatively higher pressure requirements, blowers of the centrifugal type are more frequently used than the axial type.

A large mine fan absorbs 2500 kW for delivering 30,000 m^3/min. of air.

14.1.5 Steel Plants

Large and small fans or blowers are employed in a number of applications in steel plants. One or more high pressure ($\Delta l \approx 1500$ mm W.G.) blowers are employed to supply blast furnace gases to the steam boilers. In such applications the impellers must withstand operation at high temperatures and speeds. Main blast furnace blowers are required to develop higher pressures ($\approx$ 3 bars), and therefore employ many centrifugal stages.

Bessemer converters employ intermittently operating blowers. The variable pressure required is achieved through variable speed electric motor drives.

The centrifugal exhauster fans in coke oven plants maintain a vacuum of about 250 mm W.G. and deliver the gases to the recovery plants at 25 mm W.G.

Other applications of fans and blowers are in pneumatic transport of granular material (pressure required $\approx$ 3000 mm W.G.), centrifugal separators, furnaces and drying equipment. The presence of miniature fans in many equipments is noticed only when they do not work properly on account of overheating.

Domestic vacuum cleaners employ three or more high speed (8000-20000 rpm) axial blowers. The power absorbed is about 100-300 W.

14.2 Axial Fans[530–560]

In its simplest form, an axial flow fan stage consists of a rotor made up of a number of blades fitted to the hub. When it is rotated by an electric motor or any other drive, a flow is established through the rotor. The action of the rotor causes an increase in the stagnation pressure of air or gas across it. A cylindrical casing encloses the rotor. It receives the flow through a well-shaped converging passage (nozzle) and discharges it through a diverging passage or diffuser as shown in Fig. 14.5. Only ducted fans are discussed in this section. Unenclosed or open fans will be discussed later in Sec. 14.5 as propellers.

The number of blades in the rotor varies from two to fifty. As in axial compressors, the flow is generally in the axial direction, Guide blades are

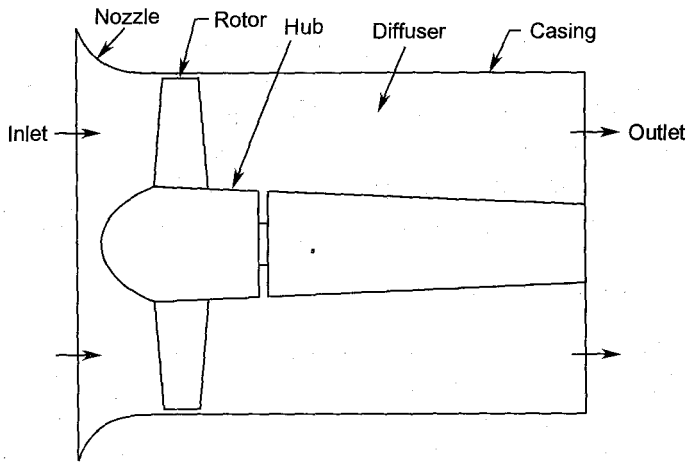

Fig. 14.5 An axial flow ducted fan without guide vanes

fixed to recover static pressure from the swirl downstream of the rotor. Many fan stages also employ guide vanes upstream of the rotor.

A large part of the material covered in Chapter 11 for axial flow compressors is also applicable for ducted axial fans. The main difference between the two classes of machines arises on account of the much lower pressures, speed and temperatures encountered in fans as compared to the compressors.

Another distinguishing feature is that, while the use of curved sheet metal blades is widespread in axial fans, they are not used in modern axial compressors which only employ well-designed aerofoil blade sections. However, many axial fans also employ aerofoil blades. The pitch-chord ratio of blades in fans is generally relatively large. When an axial fan is required to operate at varying flow conditions, its high performance can be maintained by varying the blade angle. In modern designs this variation is possible in both single and multi-stage fans while they are running.

While the axial flow fan adopts large propellers (with fewer blades) for handling considerably large quantities of air flow through small pressure differentials, there is no similar device which can be called a compressor.

14.3 Fan Stage Parameters

Some general parameters for turbomachines have been discussed in Chapters 1 and 7. Expressions for some principal fan stage parameters will be developed in the following sections. Flow has been assumed as incompressible throughout.

14.3.1 Stage Work

Velocity triangles for various types of axial fan stges are shown in Figs. 14.7, 14.8, 14.10, 14.12 and 14.14. For the sake of uniformity and clarity, the rotor entry and exit are always designated as stations 2 and 3 respectively, except in Fig. 14.14.

From Euler's equation (6.145b), the stage work is given by

$$w_{st} = u(c_{y3} - c_{y2}) \tag{14.1}$$

In an ideal case with perfect deflections and adiabatic flow, the entire work input to the rotor must appear as the stagnation enthalpy rise in air or gas.

$$(\Delta h_0)_{st} = w_{st} = u(c_{y3} - c_{y2}) \tag{14.2}$$

The mass-flow rate through the fan is

$$\dot{m} = \rho A c_x$$

$$\dot{m} = \rho \frac{\pi}{4} (d_t^2 - d_h^2) c_x \tag{14.3}$$

The power required to drive the fan is given by

$$P = \dot{m}(\Delta h_0)_{st} = \dot{m} c_p (\Delta T_0)_{st} = \dot{m} u (c_{y3} - c_{y2}) \tag{14.4}$$

If the flow velocities at the entry and exit of the stage are equal or small, the values of static and stagnation enthalpy changes are identical. The same is true for changes in pressure and temperature across the stage.

14.3.2 Stage Pressure Rise

For isentropic flow,

$$(\Delta h_0)_{st} = \frac{1}{\rho} (\Delta p_0)_{st} \tag{14.5}$$

Equations (14.2) and (14.5) give

$$(\Delta p_0)_{st} = \rho u (c_{y3} - c_{y2}) \tag{14.6}$$

This is the sum of the total change in pressure in the rotor and fixed blade rings.

14.3.3 Stage Pressure Coefficient

Using Eq. (7.14) for fan applications, the stage pressure coefficient is defined by

$$\psi = \frac{(\Delta p)_{st}}{\frac{1}{2} \rho u^2} \tag{14.7}$$

The pressure coefficient can either be based on the static pressure or stagnation pressure rise across the stage.

14.3.4 Stage Reaction

The degree of reaction for the fan is defined as the ratio of the static pressure rise in the rotor and the stagnation pressure rise over the stage.

$$R = (\Delta p)_r / (\Delta p_0)_{st} \tag{14.8}$$

The degree of reaction for fan stages can vary from zero to more than unity. This will be further discussed in this chapter.

14.3.5 Fan Efficiencies

On account of losses in the fan stage, the isentropic work is always less than the actual work input, i.e.,

$$\frac{1}{\rho}(\Delta p_0)_{st} < u(c_{y3} - c_{y2})$$

The ratio of the two quantities is known as the fan efficiency.

$$\eta_{f(\text{total})} = \frac{(\Delta p_0)_{st}}{\rho u(c_{y3} - c_{y2})} = \frac{v\,(\Delta p_0)_{st}}{u(c_{y3} - c_{y2})} \tag{14.9}$$

The actual power input to the stage is

$$P = \dot{m} u\,(c_{y3} - c_{y2}) = \frac{1}{\eta_{f\,(\text{total})}} Q\,(\Delta p_0)_{st} \tag{14.10}$$

The pressure difference across the fan stages is generally measured in terms of millimetres of water gauge (Δl).

$(\Delta p_0)_{st} = 9.81\ \Delta l\ \text{N/m}^2$; Q is in m^3/s

Taking mechanical and electrical efficiency of the drive as η_d, the overall efficiency is

$$\eta_o = \eta_d\, \eta_{f(\text{total})} \tag{14.11}$$

Therefore, the power input to the electric motor is

$$P' = \frac{1}{\eta_o} \frac{9.81 Q \Delta l}{1000}$$

$$P' = \frac{Q \Delta l}{101.94\, \eta_o} \approx \frac{Q \Delta l}{102\, \eta_o}\ \text{kW} \tag{14.12}$$

If the gas velocities at the fan entry and exit are equal or negligible, Eqs. (14.9) and (14.10) can be written as

$$\eta_{f(\text{static})} = \frac{v\,(\Delta p)_{st}}{u\,(c_{y3} - c_{y2})} \tag{14.13}$$

$$P = \frac{1}{\eta_{f\,(\text{static})}} Q\,(\Delta p)_{st} \tag{14.14}$$

Volumetric efficiency

The volumetric efficiency of a fan is defined as the ratio of the flow rates entering and leaving the fan stage.

$$\eta_v = \frac{\text{flow rate at exit}}{\text{flow rate at entry}} = \frac{Q_e}{Q_i} \tag{14.15}$$

A part of the flow which enters the fan can be recirculated between the rotor entry and exit. Thus the rotor does work on a larger quantity of fluid than is discharged by it.

14.4 Types of Axial Fan Stages

In this section various arrangements of fixed and moving blade rings in a fan stage are discussed. Expressions for pressure rise and degree of reaction are derived in each case. The axial velocity in all the stages is assumed to be constant.

$$c_x = c_{x1} = c_{x2} = c_{x3} = c_{x4}$$

The flow in all the stages enters and leaves axially. Therefore, the values of the total pressure and static pressure rise are identical.

14.4.1 Stage Without Guide Vanes

Open fans or propeller fans are examples of fans without guide vanes. A ducted fan of this type is shown in Fig. 14.5. The velocity triangles at the entry and exit of the rotor are shown in Fig. 14.10 (ignore downstream guide vanes for this type).

Since the stage under consideration here only consists of the rotor, the static pressure rise of the stage is the same as that of the rotor. Therefore, the static pressure rise in the rotor or stage is given by

$$(\Delta p)_{st} = (\Delta p)_r = \frac{1}{2}\rho(w_2^2 - w_3^2)$$

From velocity triangles (Fig. 14.10),

$$(\Delta p)_{st} = \rho u\, c_{y3} - \frac{1}{2}\rho c_{y3}^2 \tag{14.16}$$

It may be seen from this equation that on account of the non-recovery of the swirl component c_{y3} at the exit of the fan stage, the stage pressure rise is less by the amount $\frac{1}{2}\rho c_{y3}^2$. If necessary, it can be gained by turning the gas in the axial direction with the aid of downstream guide vanes as shown in Sec. 14.4.4. However, in some applications this additional pressure rise may not be required. Besides this, the provision of downstream guide vanes adds to the cost of the fan.

From Eq. (14.16),

$$(\Delta p)_{st} = \rho u^2 \left\{ \frac{c_{y3}}{u} - \frac{1}{2}\left(\frac{c_{y3}}{u}\right)^2 \right\}$$

From velocity triangles shown in Fig. 14.10, assuming constant axial velocity,

$$c_{y3} = u - c_x \tan \beta_3$$

$$\frac{c_{y3}}{u} = 1 - \frac{c_x}{u} \tan \beta_2$$

$$\frac{c_{y3}}{u} = 1 - \phi \tan \beta_3 \qquad (14.17)$$

Therefore, the static pressure rise in the rotor or stage is

$$(\Delta p)_r = (\Delta p)_{st} = \rho u^2 \left\{ 1 - \phi \tan \beta_3 - \frac{1}{2}(1 - \phi \tan \beta_3)^2 \right\}$$

$$(\Delta p)_r = (\Delta p)_{st} = \frac{1}{2} \rho u^2 (1 - \phi^2 \tan^2 \beta_3)$$

The pressure coefficient for the rotor

$$\psi_r = 1 - \phi^2 \tan^2 \beta_3 \qquad (14.18)$$

The specific work in the stage is

$$w_{st} = (\Delta h_0)_{st} = u c_{y3}$$

From Eq. (14.17),

$$w_{st} = u^2 (1 - \phi \tan \beta_3) \qquad (14.19)$$

For reversible adiabatic flow,

$$\frac{(\Delta p_o)_{st}}{\rho} = (\Delta h_0)_{st} = u c_{y3} = u^2 (1 - \phi \tan \beta_3)$$

Therefore,

$$(\Delta p_0)_{st} = \rho u^2 (1 - \phi \tan \beta_3) \qquad (14.19a)$$

$$\psi_{st} = 2(1 - \phi \tan \beta_3) \qquad (14.19b)$$

$$R = \frac{(\Delta p)_r}{(\Delta p_0)_{st}} = \frac{\psi_r}{\psi_{st}} = \frac{1}{2}(1 + \phi \tan \beta_3) \qquad (14.19c)$$

14.4.2 Stage with Upstream Guide Vanes ($R > 1$)

Figures 14.6 and 14.7 show a scheme in which upstream guide vanes (UGVs) are used to eliminate swirl at the rotor exit. The UGVs accelerate

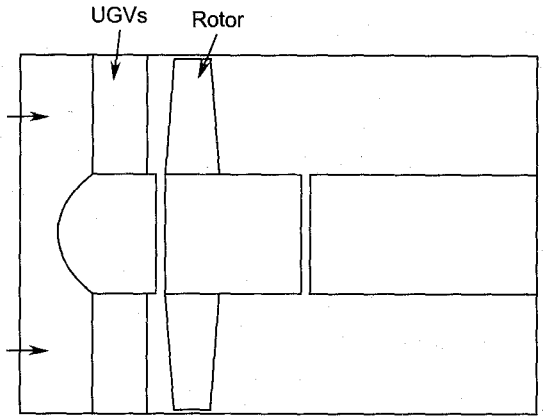

Fig. 14.6 Axial fan stage with upstream guide vanes

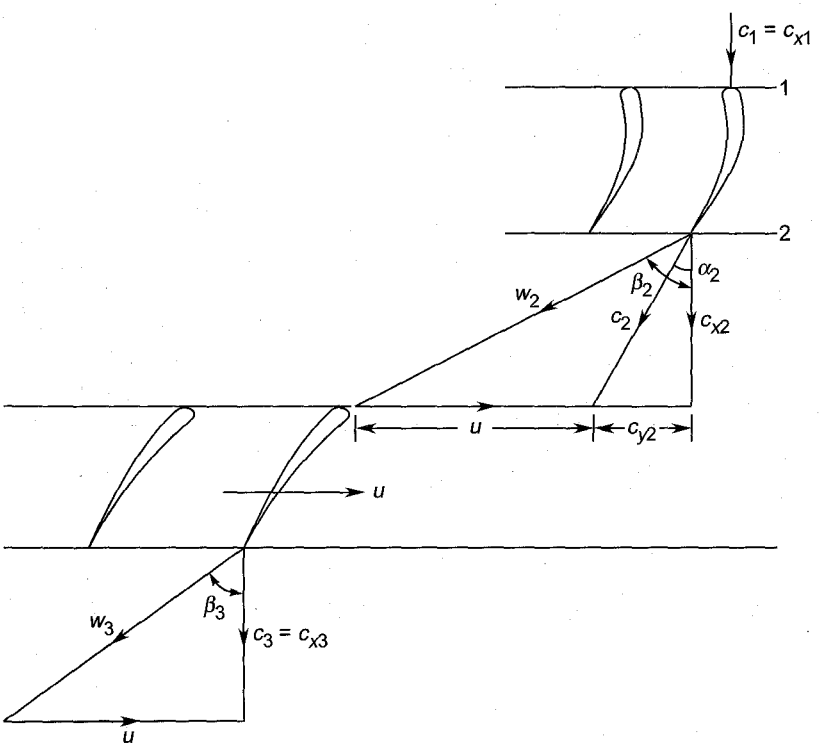

Fig. 14.7 Axial fan stage with upstream guide vanes (velocity triangles for $R > 1$)

the flow and supply the rotor with a flow having negative swirl ($- c_{y2}$). The action of the rotor cancels or removes this swirl ($c_{y3} = 0$).

From the velocity triangles shown in Fig. 14.7,

$$c_{y2} + u = c_{x2} \tan \beta_2$$

$$c_{y2} = c_x \tan \beta_2 - u = u \left(\frac{c_x}{u} \tan \beta_2 - 1 \right)$$

$$c_{y2} = u \, (\phi \tan \beta_2 - 1) \tag{14.20}$$

The stage work is

$$w_{st} = (\Delta h_0)_{st} = u \, \{c_{y3} - (- c_{y2})\}$$

$$w_{st} = (\Delta h_0)_{st} = u c_{y2}$$

Substituting from Eq. (14.20),

$$w_{st} = (\Delta h_0)_{st} = u^2 \, (\phi \tan \beta_2 - 1) \tag{14.21}$$

The stagnation pressure rise in the stage is given by Eqs. (14.5) and (14.6).

$$(\Delta p_0)_{st} = \rho \, (\Delta h_0)_{st} = \rho u c_{y2}$$

$$(\Delta p_0)_{st} = \rho u^2 \, (\phi \tan \beta_2 - 1) \tag{14.22}$$

The stage pressure coefficient is

$$\psi = \frac{(\Delta p_0)_{st}}{\frac{1}{2} \rho u^2} = 2(\phi \tan \beta_2 - 1) \tag{14.23}$$

The degree of reaction of this stage is greater than unity because of pressure drop in the UGVs. This is seen from the following derivation:

The pressure rise in the rotor is

$$(\Delta p)_r = \frac{1}{2} \rho \, (w_2^2 - w_3^2)$$

From the velocity triangles at the entry and exit (Fig. 14.7),

$$(\Delta p)_r = \frac{1}{2} \rho \, \{c_x^2 + (u + c_{y2})^2 - c_x^2 - u^2\}$$

$$(\Delta p)_r = \frac{1}{2} \rho \, (2u \, c_{y2} + c_{y2}^2) \tag{14.24}$$

The degree of reaction of the stage is

$$R = (\Delta p)_r / (\Delta p_0)_{st}$$

$$R = \frac{2u \, c_{y2} + c_{y2}^2}{2 \, u \, c_{y2}}$$

$$R = 1 + \frac{1}{2} \frac{c_{y2}}{u} \tag{14.25}$$

This shows that the degree of reaction is greater than unity.

Equations (14.20) and (14.25) give

$$R = 1 + \frac{1}{2}(\phi \tan \beta_2 - 1)$$

$$R = \frac{1}{2}(1 + \phi \tan \beta_2) \tag{14.26}$$

14.4.3 Stage with Upstream Guide Vanes $\left(R = \frac{1}{2}\right)$

Figure 14.8 shows the arrangement of blades in a fan stage of fifty per cent reaction. As in a 50% reaction axial compressor stage (Sec. 11.2.4), here also the fixed and rotating blades are symmetrical, i.e.,

$$\left.\begin{aligned} \alpha_2 &= \beta_3, \quad \beta_2 = \alpha_3 \\ c_2 &= w_3 \quad w_2 = c_3 \end{aligned}\right\} \tag{14.27}$$

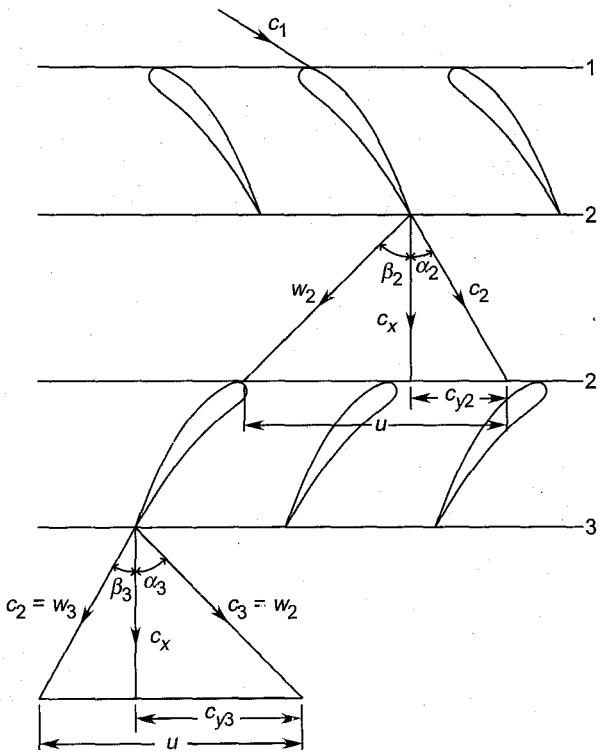

Fig. 14.8 Axial fan stage with upstream guide vanes (velocity triangles for R = 1/2)

In other words, the velocity triangles at the entry and exit are symmetrical. The pressure rise in the rotor and stator blades is the same.

$$(\Delta p)_r = \frac{1}{2}\rho(w_2^2 - w_3^2) = \frac{1}{2}\rho(c_3^2 - c_2^2) \tag{14.28}$$

$$(\Delta p_0)_{st} = \rho u(c_{y3} - c_{y2}) = \rho(w_2^2 - w_3^2) \tag{14.29}$$

From velocity triangles

$$(\Delta p_0)_{st} = \rho u(c_x \tan \alpha_3 - c_x \tan \alpha_2)$$

$$(\Delta p_0)_{st} = \rho u^2 \phi(\tan \beta_2 - \tan \beta_3) \tag{14.30}$$

The degree of reaction from Eqs. (14.28) and (14.29) is

$$R = \frac{(\Delta p)_r}{(\Delta p_0)_{st}} = \frac{1}{2}$$

The pressure coefficient from Eq. (14.30) is

$$\psi = 2\phi(\tan \beta_2 - \tan \beta_3) \tag{14.31}$$

The stage work is

$$w_{st} = u^2 \phi(\tan \beta_2 - \tan \beta_3) \tag{14.32}$$

It may be seen that the scheme depicted in Fig. 14.8 is for one of the several stages used in a multistage machine. Here the flow repeats in each stage. For example, here the absolute velocities c_1 and c_3 at the entry to and the exit from the stage are identical.

14.4.4 Stage with Downstream Guide Vanes

This arrangement is shown in Figs. 14.9 and 14.10. The rotor blades receive air in the axial direction. The absolute velocity vector (c_3) at the

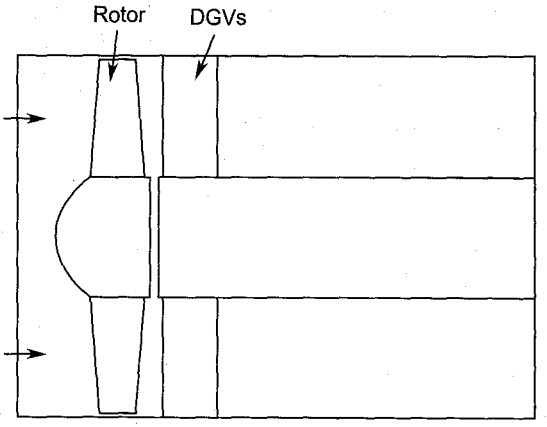

Fig. 14.9 Axial fan stage with downstream guide vanes

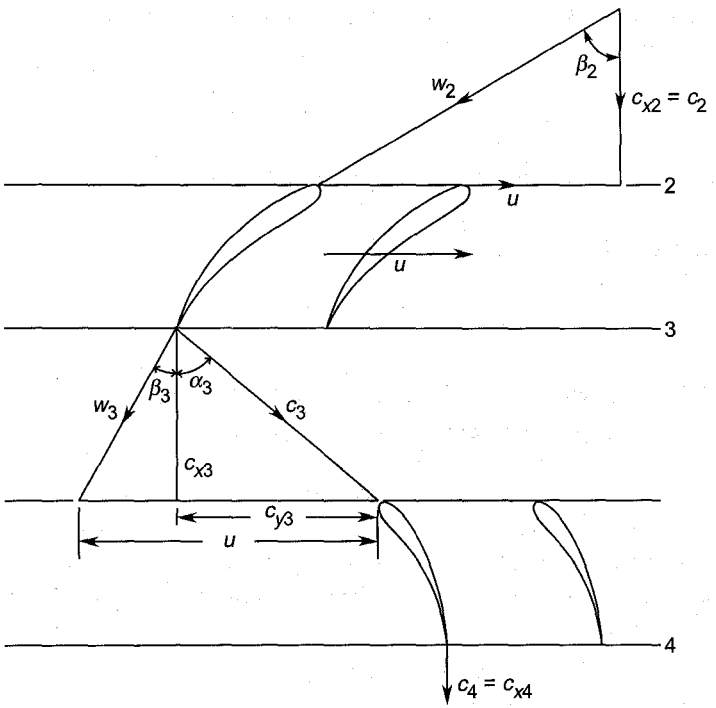

Fig. 14.10 Axial fan stage with downstream guide vanes (velocity triangles for $R < 1$).

rotor exit has a swirl component (c_{y3}) which is removed by the downstream guide vanes (DGVs) and the flow is finally discharged axially from the stage.

The swirl at the entry to the rotor is zero.

$$c_{y2} = 0$$

Most of the analysis for this stage is similar to what has already been covered in Sec. 14.4.1.

Work done in the stage is the same as in Eq. (14.19).

$$w_{st} = u\, c_{y3} = u^2\, (1 - \phi \tan \beta_3)$$

The stage pressure rise is

$$(\Delta p_0)_{st} = \rho u c_{y3} = \rho u^2\, (1 - \phi \tan \beta_3) \tag{14.33}$$

Therefore, the stage pressure coefficient

$$\psi = 2\, (1 - \phi \tan \beta_3) \tag{14.34}$$

Compare this with Eq. (14.18).

The pressure rise in the rotor is the same as given in Eq. (14.16),

$$(\Delta p)_r = \rho u c_{y3} - \frac{1}{2}\, \rho c_{y3}^2$$

Equation (14.33) when used in this relation gives the degree of reaction of the stage.

$$R = 1 - \frac{1}{2}\frac{c_{y3}}{u} \tag{14.35}$$

This relation shows that the degree of reaction of this stage is less than unity.

Equation (14.17) when put in Eq. (14.35) gives

$$R = \frac{1}{2}(1 + \phi \tan \beta_3) \tag{14.36}$$

14.4.5 Stage with Upstream and Downstream Guide Vanes

Figures 14.11 and 14.12 show a fan stage with symmetrical guide vanes upstream and downstream of the fan rotor. The pressure drop and acceleration in the UGVs are equal in magnitude to the pressure rise and deceleration in the DGVs. Therefore, the pressure rise in the rotor is identical with the stage pressure rise.

$$(\Delta p)_r = (\Delta p_0)_{st} = (\Delta p)_{st}$$

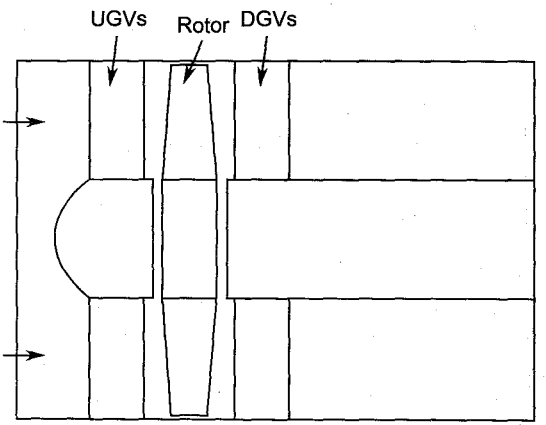

Fig. 14.11 Axial fan stage with upstream and downstream guide vanes

Thus the degree of reaction of such a stage is unity. For symmetrical UGVs and DGVs and constant axial velocity,

$$\alpha_2 = \alpha_3$$

$$c_{y2} = c_{y3} = c_x \tan \beta_2 - u$$

$$c_{y2} = c_{y3} = u(\phi \tan \beta_2 - 1) \tag{14.37}$$

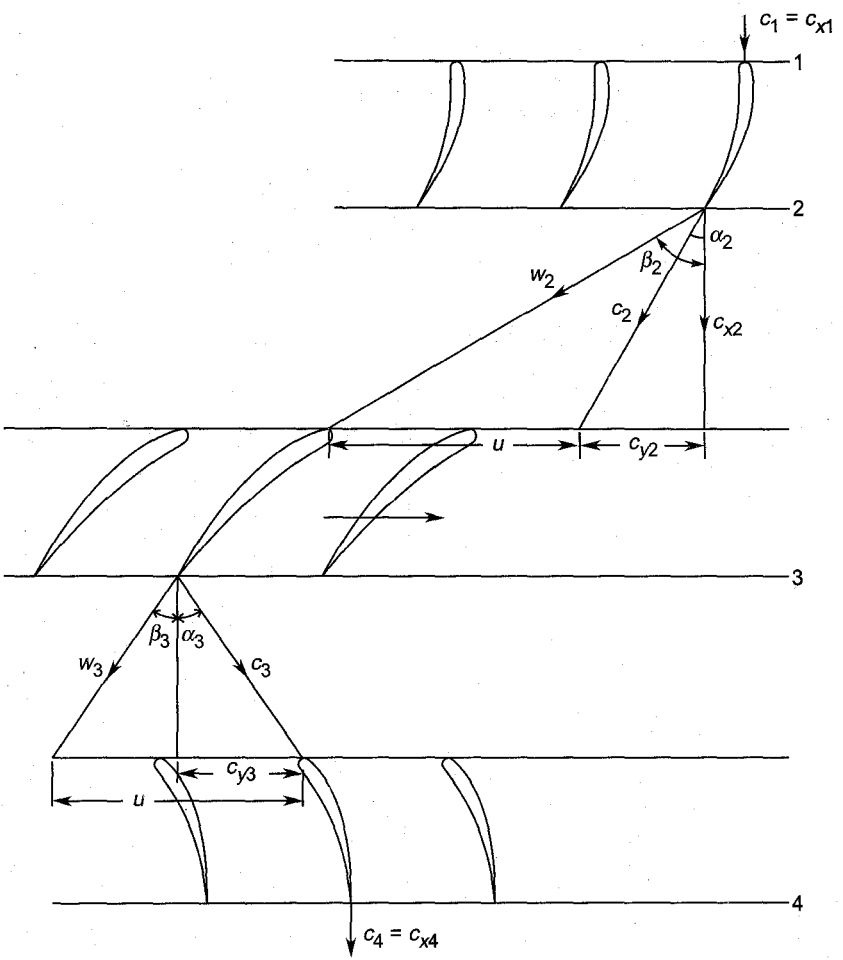

Fig. 14.12 Axial fan stage with upstream and downstream guide vanes (velocity triangles for $R = 1$)

The stage work is

$$w_{st} = (\Delta h_0)_{st} = u\{c_{y3} - (-\ c_{y2})\}$$

$$w_{st} = (\Delta h_0)_{st} = 2u\ c_{y2}$$

$$w_{st} = 2\ u^2\ (\phi \tan\ \beta_2 - 1) \tag{14.38}$$

The stage pressure rise is

$$(\Delta p)_{st} = \rho\ (\Delta h_0)_{st} = 2\ \rho\ u\ c_{y2}$$

$$(\Delta p)_{st} = 2\ \rho\ u^2\ (\phi \tan\ \beta_2 - 1) \tag{14.39}$$

The pressure coefficient is given by

$$\psi = 4\ (\phi \tan\ \beta_2 - 1) \tag{14.40}$$

The pressure rise in the rotor is

$$(\Delta p)_r = \frac{1}{2} \rho (w_2^2 - w_3^2)$$

From the velocity triangles,

$$(\Delta p)_r = \frac{1}{2} \rho \{c_x^2 + (u + c_{y2})^2 - c_x^2 - (u - c_{y3})^2$$

$$(\Delta p)_r = 2 \rho u c_{y2} = (\Delta p)_{st}$$

This again proves that the degree of reaction is unity.

14.4.6 Counter Rotating Fan Stage

Figure 14.13 shows two axial fan rotors rotating in opposite directions. The motors driving these rotors are mounted on supports provided within the casing. Such a stage gives a large pressure rise.

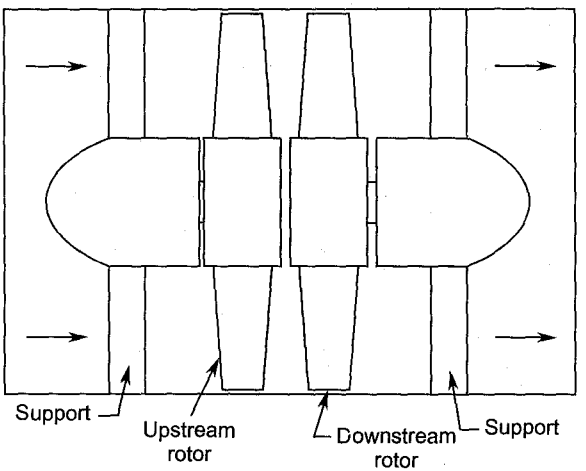

Fig. 14.13 Counter rotating axial fan stage

The velocity triangles at the entry and exit of each rotor are shown in Fig. 14.14. The entries and exits of the two rotors are at stations 1, 3 and 2, 4 respectively. Stations 2 and 3 are in fact the same, i.e., exit of the first rotor and entry of the second.

The two rotors are assumed to have the same peripheral speeds: the axial velocity is constant throughout the stage.

The upstream or the first rotor receives air axially. Therefore,

$$c_{y1} = 0$$

The air leaving the first rotor has an absolute velocity c_2 and a swirl component c_{y2}. Therefore, the work done by the first rotor is

$$w_I = u (c_{y2} - c_{y1}) = u c_{y2} \qquad (14.41)$$

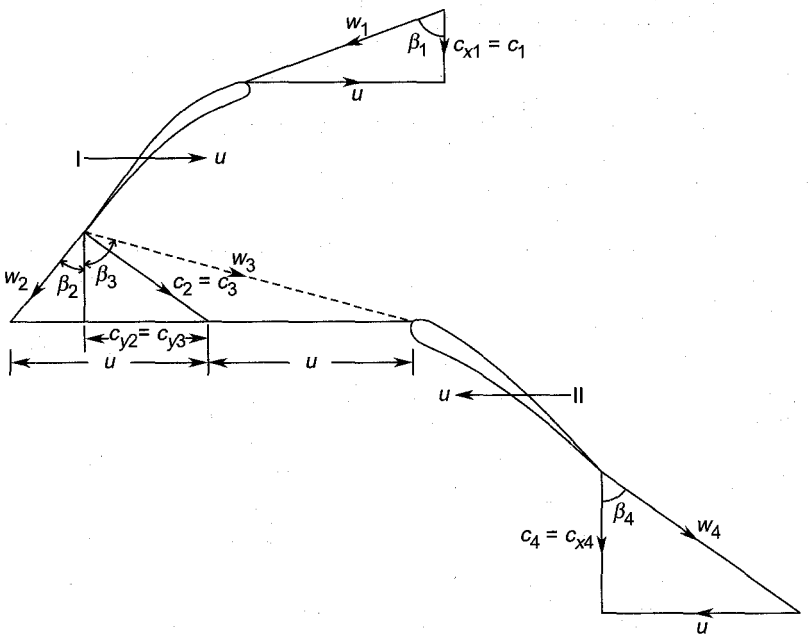

Fig. 14.14 Velocity triangles for counter rotating axial fan stage

The downstream or the second rotor receives air at an absolute velocity $c_3 = c_2$ and discharges it axially.

$$c_{y4} = 0$$

$$c_{y3} = c_{y2}$$

The velocity triangle at the exit of the first rotor is drawn together with the inlet velocity triangle for the second rotor.

Work done by the second rotor is

$$w_{II} = u \{0 - (- c_{y3})\}$$

$$w_{II} = u\, c_{y3} = u\, c_{y2} \qquad (14.42)$$

Equations (14.41) and (14.42) show that the work done and the pressure rise are the same in the two rotors. The total stage work is

$$w_{st} = w_I + w_{II} = 2\, u\, c_{y2}$$

$$w_{st} = 2\, u\, (u - c_x \tan \beta_2)$$

$$w_{st} = 2\, u^2\, (1 - \phi \tan \beta_2) \qquad (14.43)$$

The stage pressure rise is

$$(\Delta p)_{st} = 2\, \rho\, u^2\, (1 - \phi \tan \beta_2) \qquad (14.44)$$

The pressure coefficient is

$$\psi = 4\, (1 - \phi \tan \beta_2) \qquad (14.45)$$

The static pressure rises in the two rotors are

$$(\Delta p)_I = \frac{1}{2} \rho (w_1^2 - w_2^2)$$

Using the velocity triangles after some manipulation,

$$(\Delta p)_I = \rho u c_{y2} - \frac{1}{2} \rho c_{y2}^2 \tag{14.46}$$

This is identical to Eq. (14.16) for a fan stage without guide vanes.

$$(\Delta p)_{II} = \frac{1}{2} \rho (w_3^2 - w_4^2)$$

$$(\Delta p)_{II} = \rho u c_{y2} + \frac{1}{2} \rho c_{y2}^2 \tag{14.47}$$

This is identical to Eq. (14.24) for a fan stage with UGVs. In this case the first rotor blades act as UGVs.

The total static pressure rise in the stage is, from Eqs. (14.46) and (14.47),

$$(\Delta p_0)_{st} = (\Delta p)_{st} = (\Delta p)_I + (\Delta p)_{II}$$

$$(\Delta p)_{st} = 2 \rho u c_{y2}$$

This is the same as Eq. (14.44).

14.5 Propellers[549]

Propellers have much fewer (2–6) blades compared to the ducted fans discussed in the earlier sections. A large number of them are used as open or extended turbomachines. Some examples of propeller applications are in aircrafts [*see* Fig. 14.15 (Plate 1)], helicopters, hovercrafts, hydrofoils and ships.

Propellers are made of aluminium alloys or wood. Wooden propellers have been used in aircrafts, wind tunnels and cooling tower applications. They can be made of the integral blade type in which two identical blades are equally disposed about the axis of rotation. Such a rotor does not have the problems of blade root fixtures. A four-bladed propeller can be made by bolting two pairs of intergral blade propellers.

On account of the fewer blades, the rotor is unable to impose its geometry on the flow to the same extent as in rotors with many blades. Therefore, the inlet and outlet velocity triangles lose their meaning. Besides this, the rotor or propeller blades are usually very long with varying blade sections along the radius. Under these conditions a mean velocity triangle for flow only through an infinitesimal blade element is considered. The propeller blade is divided into a large number of such elements and various parameters are determined separately for each element.

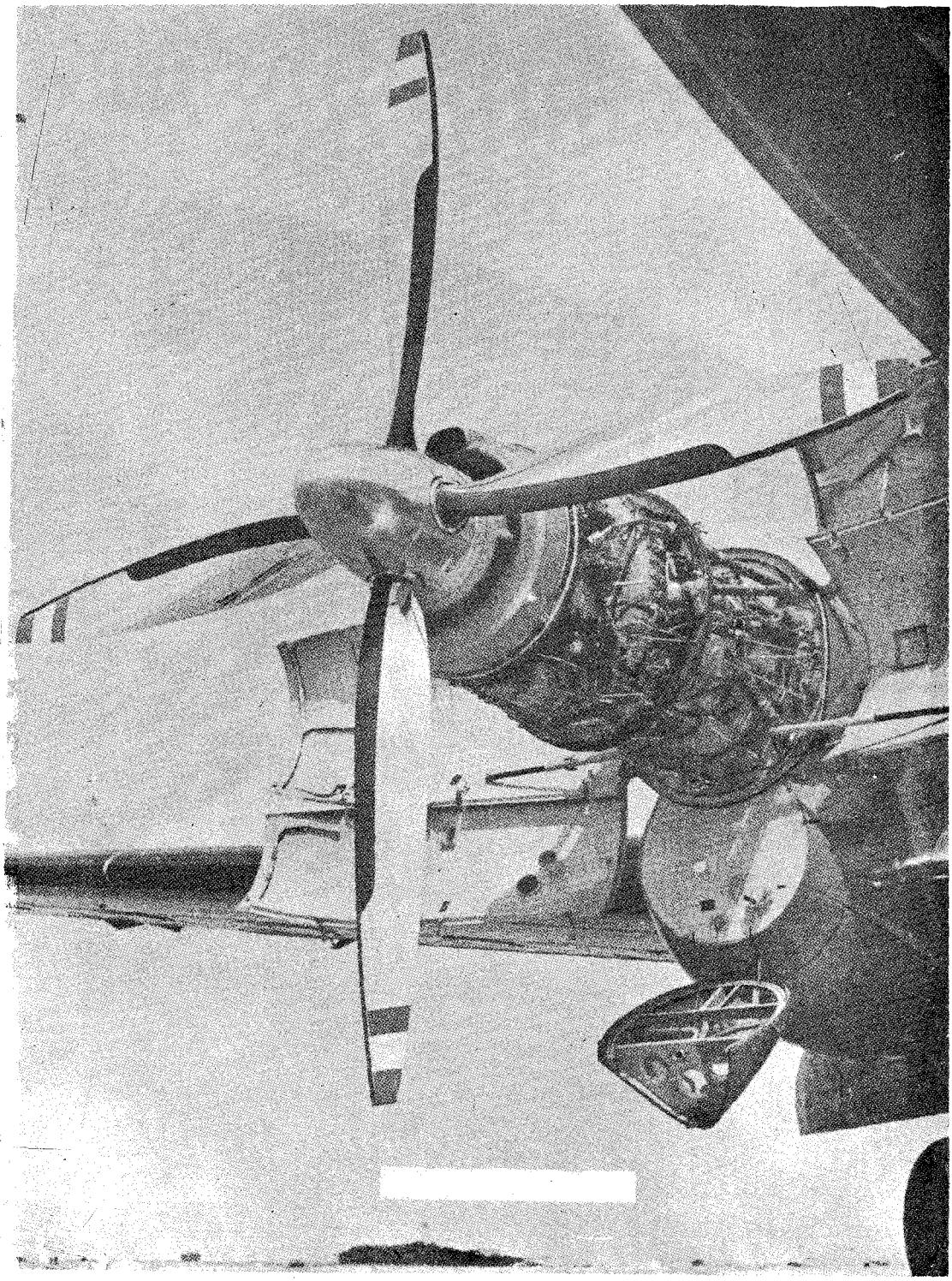

Fig. 14.15 An Aircraft Propeller

When the propeller is used for propulsion, its efficiency as a propulsion device is of interest besides power required and flow rate, etc., whereas if it is used as a fan, the parameters of interest are pressure rise, flow rate, power required and efficiency.

14.5.1 Slipstream Theory

Figure 14.16 shows the variation of pressure and velocity of air flowing through a propeller disc. This disc is assumed to have negligible thickness. The boundaries between the fluid in motion and that at rest are shown. Thus the flow is assumed to occur in an imaginary converging duct of diameter D at the disc and D_s at the exit. The entry and exit of this duct are far upstream and far downstream of the disc.

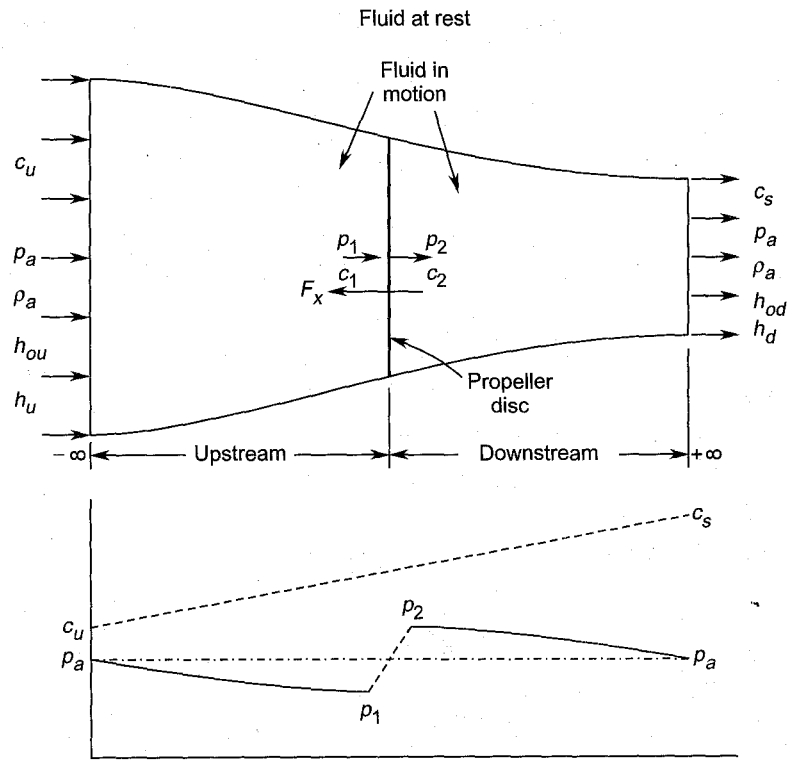

Fig. 14.16 Variation of pressure and velocity of flow through a propeller

The action of the rotating propeller accelerates the flow from a velocity c_u to the velocity of the slipstream c_s. The pressure (p_a) and density ($\rho = \rho_a$) have the same values at sections $-\infty$ and $+\infty$. However, the velocities and stagnation enthalpies are different. The velocity of flow

at the disc (c), immediately upstream (c_1) and downstream (c_2) of it are same

$$c = c_1 = c_2 \tag{14.48}$$

The area of cross-section of the disc is $A = \frac{\pi}{4} D^2$ and the mass-flow rate through it is

$$\dot{m} = \rho A c \tag{14.49}$$

The axial thrust on the disc due to change of momentum of the air through it is

$$F_x = \dot{m} (c_s - c_u) = \rho A c (c_s - c_u) \tag{14.50}$$

Applying Bernoulli equation for flows in the regions upstream and downstream of the disc

$$p_a + \frac{1}{2} \rho c_u^2 = p_1 + \frac{1}{2} \rho c^2 \tag{14.51}$$

$$p_a + \frac{1}{2} \rho c_s^2 = p_2 + \frac{1}{2} \rho c^2 \tag{14.52}$$

These equations on subtraction give

$$p_2 - p_1 = \frac{1}{2} \rho (c_s^2 - c_u^2) \tag{14.53}$$

The axial thrust due to the pressure difference across the disc is

$$F_x = A (p_2 - p_1)$$

$$F_x = \frac{1}{2} \rho A (c_s^2 - c_u^2) \tag{14.54}$$

Equations (14.50) and (14.54) yield

$$c = \frac{1}{2} (c_s + c_u) \tag{14.55}$$

A factor (less than unity) a is defined by

$$c = (1 + a) c_u \tag{14.56}$$

Equations (14.55) and (14.56) give

$$c_s = (1 + 2a) c_u \tag{14.57}$$

The change in the specific stagnation enthalpy across the disc is

$$\Delta h_0 = h_{0d} - h_{0u} = \left(h_d + \frac{1}{2} c_s^2\right) - \left(h_u + \frac{1}{2} c_u^2\right)$$

However, $h_u = h_d$. Therefore,

$$\Delta h_0 = \frac{1}{2} (c_s^2 - c_u^2) \tag{14.58}$$

Power = mass flow rate × change of stagnation enthalpy

$$P_i = \dot{m} \Delta h_0$$

Equations (14.49) and (14.58) when used in the above relation yield

$$P_i = \frac{1}{2} \rho A c (c_s^2 - c_u^2) \tag{14.59}$$

This is the ideal value of the power supplied to the propeller. The actual power will be greater than this.

If this propeller is used as a fan of discharge capacity Q developing a stagnation pressure rise of Δp_0, its power is given by

$$P_i = Q \Delta p_0$$

$$Q = A c, \Delta p_0 = \rho \Delta h_0 = \frac{1}{2} \rho (c_s^2 - c_u^2)$$

Therefore,

$$P_i = (A c) \frac{1}{2} \rho (c_s^2 - c_u^2)$$

$$P_i = \frac{1}{2} \rho A c (c_s^2 - c_u^2)$$

This is the same as Eq. (14.59).

If this propeller is employed to propel an aircraft at a speed c_u, then the useful power is $F_x c_u$. The propeller efficiency is then defined by

$$\eta_p = \frac{\text{power used in propulsion}}{\text{ideal power supplied}}$$

$$\eta_p = F_x c_u \Big/ \frac{1}{2} \rho A c (c_s^2 - c_u^2)$$

Substituting for F_x from Eq. (14.54)

$$\eta_p = c_u / c \tag{14.60}$$

Employing Eq. (14.56),

$$\eta_p = \frac{1}{1+a} \tag{14.61}$$

The continuity equation at the disc and the slipstream section gives

$$c \frac{\pi}{4} D^2 = c_s \frac{\pi}{4} D_s^2$$

$$D_s^2 = \frac{c}{c_s} D^2$$

Equations (14.56) and (14.57) give

$$c_s = \left(\frac{1+2a}{1+a} \right) c \tag{14.62}$$

Therefore,

$$D_s^2 = \left(\frac{1+a}{1+2a}\right) D^2 \tag{14.63}$$

14.5.2 Blade Element Theory[560]

Figure 14.17 shows a long blade of a propeller fan. On account of the considerable variation in the flow conditions and the blade section along the span, it is divided into a number of infinitesimal sections of small, radial thickness *dr*. The flow through such a section is assumed to be independent of the flow through other elements.

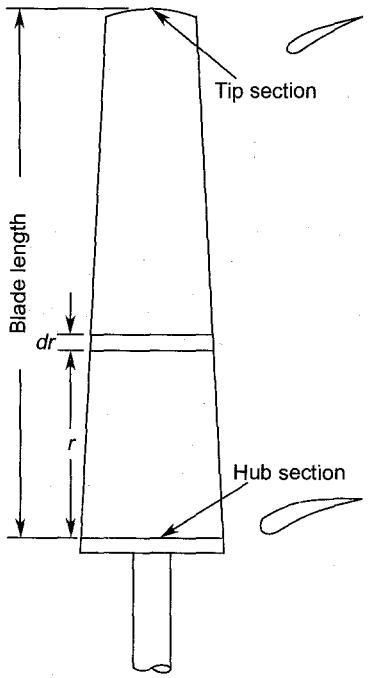

Fig. 14.17 Propeller blade with varying blade section

Velocities and blade forces for the flow through an elemental section are shown in Fig. 14.18. The flow has a mean velocity w and direction β (from the axial direction). The lift force ΔL is normal to the direction of mean flow and the drag ΔD parallel to this. This axial (ΔF_x) and tangential (ΔF_y) forces acting on the element are also shown. (ΔF_r) is the resultant force inclined at an angle ϕ to the direction of lift.

An expression for the pressure rise (Δp) across the element is now developed.

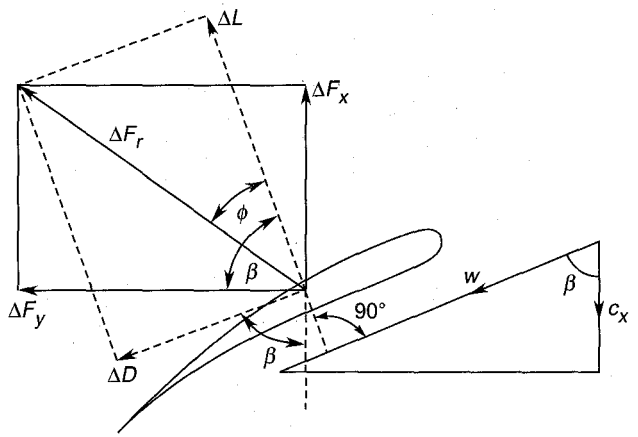

Fig. 14.18 Flow through a blade element of a propeller

Resolving the forces in the axial and tengential directions,

$$\Delta F_x = \Delta L \sin \beta - \Delta D \cos \beta \tag{14.64}$$

$$\Delta F_y = \Delta L \cos \beta + \Delta D \sin \beta \tag{14.65}$$

By definition, lift and drag forces are

$$\Delta L = \frac{1}{2} C_L \rho w^2 (ldr) \tag{14.66}$$

$$\Delta D = \frac{1}{2} C_D \rho w^2 (ldr) \tag{14.67}$$

$$\tan \phi = \frac{\Delta D}{\Delta L} = \frac{C_D}{C_L} \tag{14.68}$$

From Eqs. (14.64) and (14.68),

$$\Delta F_x = \Delta L (\sin \beta - \tan \phi \cos \beta)$$

$$\Delta F_x = \Delta L \sin (\beta - \phi)/\cos \phi$$

Substituting for ΔL from Eq. (14.66),

$$\Delta F_x = \frac{1}{2} C_L \rho w^2 (ldr) \frac{\sin (\beta - \phi)}{\cos \phi} \tag{14.69}$$

The number of blades and the spacing are related by

$$s = \frac{2\pi r}{z} \tag{14.70}$$

The total axial thrust for the elemental section of the propeller is $z\Delta F_x$. Therefore,

$$\Delta p (2 \pi r dr) = z \Delta F_x$$

Equations (14.69) and (14.70) in this relation give

$$\Delta p = \frac{1}{2} C_L \rho w^2 \left(\frac{l}{s}\right) \frac{\sin(\beta - \phi)}{\cos \phi} \tag{14.71}$$

Equation (14.68) when put into Eq. (14.71) gives

$$\Delta p = \frac{1}{2} C_D \rho w^2 \left(\frac{l}{s}\right) \frac{\sin(\beta - \phi)}{\sin \phi} \tag{14.72}$$

Now $c_x = w \cos \beta$.

Therefore, Eqs. (14.71) and (14.72) give

$$\Delta p = \frac{1}{2} C_L \rho c_x^2 \left(\frac{l}{s}\right) \frac{\sin(\beta - \phi)}{\cos^2 \beta \cos \phi} \tag{14.73}$$

$$\Delta p = \frac{1}{2} C_D \rho c_x^2 \left(\frac{l}{s}\right) \frac{\sin(\beta - \phi)}{\cos^2 \beta \sin \phi} \tag{14.74}$$

Equation (14.65) can be used to obtain the values of torque and the work for the elemental section.

14.6 Performance of Axial Fans[530,532,537]

Axial flow fans and blowers are high specific speed machines with high efficiencies. Performance curves for a typical axial fan are shown in Fig. 14.19. The efficiency and delivery pressure fall when the fan operates at higher flow rates, i.e. on the right of the point S in the stable

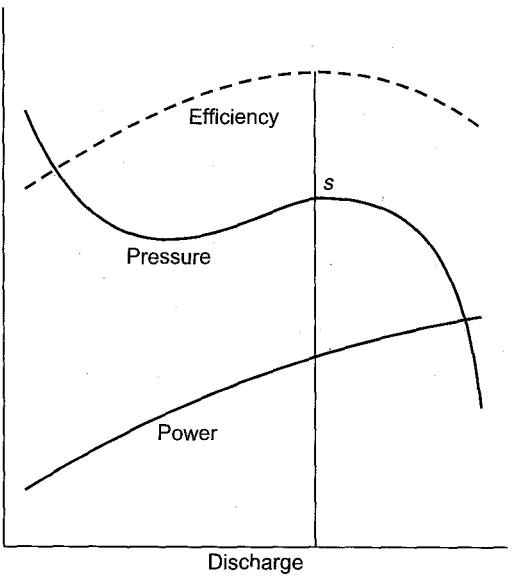

Fig. 14.19 Performance curves for axial flow fans (typical curves)

range. The flow through the fan can be varied either through a valve control or by regulating guide vanes upstream or downstream of the fan.

When the flow rate through the fan is reduced below the value corresponding to the peak (point S) of the performance curve, the flow becomes unstable. Irregularities in the flow over blade surfaces in the form of vortices, reversed and separated flows occur leading to an ultimate breakdown of flow: the fan experiences an oscillating flow. This phenomenon is known as surging and has already been discussed in Chapter 11. Such a state is accompanied with an increase in the noise level.

Fans with guide vanes are more likely to experience unstable flow. It is further observed that fans with UGVs suffer more from stalled flow than those with DGVs.

Surging can be reduced or wholly overcome by the following methods:

(a) by reducing the speed of the fan,
(b) by throttling the flow at entry,
(c) by letting off the air at exit through an automatically operated blow-off valve,
(d) by recirculating the excess air through the fan, and
(e) by employing adjustable guide vanes.

Notation for Chapter 14

a	Factor defined in Eq. (14.56)
A	Area of cross-section
c	Absolute velocity
C_D	Drag coefficient
C_L	Lift coefficient
d,D	Diameter
ΔD	Drag
F	Force
g	Acceleration due to gravity
h	Enthalpy
Δh	Change in enthalpy
H	Head
l	Blade chord
Δl	Deflection in manometer
ΔL	Lift
$\dot{m}$	Mass-flow rate
N	rpm

p	Pressure
Δp	Pressure rise
P	Power
Q	Volume-flow rate
r	Radius
R	Degree of reaction
s	Blade spacing
T	Absolute temperature
u	Peripheral speed
v	Specific volume
w	Specific work, relative velocity
z	Number of blades

Greek symbols

α	Direction of absolute velocity
β	Direction of relative velocity
η	Efficiency
ρ	Density of air or gas
ϕ	Flow coefficient or angle as shown in Fig. 14.17
ψ	Pressure coefficient
ω	Rotational speed in radians/s

Subscripts

o	Stagnation value
1	Entry to the stage
2	Rotor entry
3	Rotor exit
4	Exit of the stage
I	First rotor
II	Second rotor
a	Atmospheric
d	Downstream, drive
DGVs	Downstream guide vanes
e	Exit
f	Fan
h	Hub
i	Ideal
o	Overall
p	Propeller
r	Rotor, resultant

s	Slipstream
st	Stage
t	Tip
u	Upstream
UGVs	Upstream guide vanes
v	volumetric
x	Axial
y	Tangential

Solved Examples

14.1 An axial fan stage consisting of only a rotor has the following data:

rotor blade air angle at exit	10°
tip diameter	60 cm
hub diameter	30 cm
rotational speed	960 rpm
power required	1 kW
flow coefficient	0.245

(inlet flow conditions $p_1 = 1.02$ bar, $T_1 = 316$ K)

Determine the rotor blade angle at the entry, the flow rate, stage pressure rise, overall efficiency, degree of reaction and specific speed.

***Solution*:**

$$A = \frac{\pi}{4}(d_t^2 - d_h^2) = 0.785\,(0.6^2 - 0.3^2) = 0.212 \text{ m}^2$$

$$d = \frac{1}{2}(d_t + d_h) = \frac{1}{2}(0.6 + 0.3) = 0.45 \text{ m}$$

$$u = \pi\, dN/60 = \pi \times 0.45 \times 960/60 = 22.62 \text{ m/s}$$

$$c_x = \phi\, u = 0.245 \times 22.62 = 5.542 \text{ m/s}$$

$$Q = c_x A = 5.542 \times 0.212 = 1.175 \text{ m}^3/\text{s} \ (Ans.)$$

$$\rho = p/RT = 1.02 \times 10^5/(287 \times 316) = 1.125 \text{ kg/m}^3$$

$$(\Delta p_0)_{st} = \rho\, u^2 (1 - \phi \tan \beta_3)$$

$$= 1.125 \times 22.62^2\,(1 - 0.245 \times \tan 10)$$

$$= 550.755 \text{ N/m}^2 = \frac{550.755}{9.81} \text{ mm W.G.}$$

$$(\Delta p_0)_{st} = 56.14 \text{ mm W.G.} \ (Ans.)$$

The ideal power required to drive the fan is

$$Q\ (\Delta p_0)_{st} = 1.175 \times 550.755/1000 = 0.647 \text{ kW}$$

The overall efficiency of the fan is

$$\eta_0 = \frac{\text{ideal power}}{\text{actual power}} = \frac{0.647}{1.000} = 0.647$$

$$\eta_0 = 64.7\% \ (Ans.)$$

The blade air angle at the entry is given by

$$\tan \beta_2 = u/c_x \text{ (Fig. 14.10)}$$

$$\tan \beta_2 = 22.62/5.542 = 4.08$$

$$\beta_2 = 76.23° \ (Ans.)$$

The static pressure rise in the stage is

$$(\Delta p)_{st} = \frac{1}{2} \rho u^2 (1 - \phi^2 \tan^2 \beta_3)$$

$$(\Delta p)_{st} = 0.5 \times 1.125 \times 22.62^2 (1 - 0.245^2 \tan^2 10)$$

$$(\Delta p)_{st} = 287.27 \text{ N/m}^2 = 287.27/9.81 \text{ kgf/m}^2$$

$$(\Delta p)_r = (\Delta p)_{st} = 29.283 \text{ mm W.G.}$$

Therefore, the degree of reaction is

$$R = (\Delta p)_r / (\Delta p_0)_{st}$$

$$R = 29.283/56.14$$

$$R = 52\% \ (Ans.)$$

$$gH = 9.81 \times \frac{56.14}{1000} \times \frac{1000}{1.125} = 489.54 \text{ m}^2/\text{s}^2$$

$$\omega = 2\ \pi\ N/60 = 2\ \pi \times 960/60 = 100.53 \text{ rad/s}$$

The dimensionless specific speed is

$$\Omega = \omega Q^{1/2}/(gH)^{3/4}$$

$$\Omega = 100.53 \times 1.175^{1/2}/(489.54)^{3/4}$$

$$\Omega = 1.047 \ (Ans.)$$

14.2 Recalculate all the quantities of Ex. 14.1 with downstream guide vanes. What is the guide vane air angle at the entry?

***Solution*:**

Refer to Fig. 14.10. The axial velocity is assumed to remain constant throughout the stage. Therefore, the static pressure rise in the stage is same as the total pressure rise.

$$(\Delta p)_{st} = (\Delta p_0)_{st} = 56.14 \text{ mm W.G.}$$

The rotor blade air angles, overall efficiency, flow rate, power required and degree of reaction are the same as calculated in Ex. 14.1.

The exit angle of the DGVs is

$$\alpha_4 = 0°,$$

The entry angle is given by

$$\tan \alpha_3 = c_{y3}/c_x = \frac{1}{c_x}(u - c_x \tan \beta_3)$$

$$\tan \alpha_3 = \frac{1}{\phi} - \tan \beta_3 = \frac{1}{0.245} - \tan 10 = 3.905$$

$$\alpha_3 = 75.63° \text{ (}Ans.\text{)}$$

14.3 If the fan in Ex. 14.1 is provided with upstream guide vanes for negative swirl and the rotor blade inlet air angle is 86°, determine (i) the static pressure rise in the rotor and the stage, (ii) the stage pressure coefficient and degree of reaction, (iii) the exit air angle of the rotor blades and the UGVs and (iv) the power required if the overall efficiency of the drive is 64.7%.

***Solution*:**

Refer to Fig. 14.7. The axial velocity is assumed constant throughout the stage.

$$c_1 = c_{x1} = c_{x2} = c_{x3} = c_3 = c_x$$

The stage work is

$$w_{st} = (\Delta h_0)_{st} = u^2 (\phi \tan \beta_2 - 1)$$

$$w_{st} = 22.62^2 (0.245 \tan 86 - 1) = 1280.685 \text{ J/kg}$$

For reversible flow, the stage pressure rise is

$$(\Delta p_0)_{st} = \rho (\Delta h_0)_{st}$$

$$(\Delta p_0)_{st} = 1.125 \times 1280.685 = 1440.76 \text{ N/m}^2$$

$$(\Delta p_0)_{st} = 146.86 \text{ mm W.G.}$$

Since the velocities at the entry and exit of the stage are the same, the static and total pressure rises in the stage are same.

$$(\Delta p)_{st} = (\Delta p_0)_{st} = 146.86 \text{ mm W.G. (}Ans.\text{)}$$

The mass-flow rate through the stage is

$$\dot{m} = \rho Q = 1.125 \times 1.175 = 1.322 \text{ kg/s}$$

The power required to drive this fan is

$$\frac{\dot{m}(\Delta h_0)_{st}}{1000\,\eta_0} = \frac{1.322 \times 1280.685}{1000 \times .647} = 2.629 \text{ kW (}Ans.\text{)}$$

The stage pressure coefficient is

$$\psi = 2\ (\phi \tan \beta_2 - 1)$$

$$\psi = 2\ (0.245 \tan 86 - 1)$$

$$\psi = 5.006\ (Ans.)$$

The degree of reaction is given by

$$R = \frac{1}{2}\ (1 + \phi \tan \beta_2)$$

$$R = 0.5\ (1 + 0.245 \tan 86) = 2.25$$

$$R = 225\%\ (Ans.)$$

$$\tan \beta_3 = u/c_x = 22.62/5.542 = 4.082$$

$$\beta_3 = 76.23°\ (Ans.)$$

The UGV exit air angle is given by

$$\tan \alpha_2 = c_{y2}/c_x = \tan \beta_2 - 1/\phi$$

$$\tan \alpha_2 = \tan 86 - 1/0.245 = 10.22$$

$$\alpha_2 = 84.4°\ (Ans.)$$

The static pressure rise in the rotor is

$$(\Delta p)_r = \frac{1}{2}\ \rho\ (w_2^2 - w_3^2)$$

$$w_2 = c_{x2}/\cos \beta_2 = 5.542/\cos 86 = 79.512 \text{ m/s}$$

$$w_3 = c_{x3}/\cos \beta_3 = 5.542/\cos 76.23 = 23.285 \text{ m/s}$$

$$(\Delta p)_r = 0.5 \times 1.125\ (79.512^2 - 23.285^2)$$

$$(\Delta p)_r = 3251.25 \text{ N/m}^2 = 3251.25/9.81 \text{ kgf/m}^2$$

$$(\Delta p)_r = 331.422 \text{ mm W.G. } (Ans.)$$

The degree of reaction can be checked by this value.

$$R = (\Delta p)_r/(\Delta p_0)_{st}$$

$$R = 331.422/146.86 = 2.256 \text{ (verified)}$$

14.4 If the rotor and upstream guide blades in Ex. 14.1 are symmetrical and arranged for 50% reaction with $\beta_2 = 30°$ and $\beta_3 = 10°$ determine the stage pressure rise, pressure coefficient and power required for a fan efficiency of 80% and drive efficiency of 88%.

***Solution*:**

The stage work is given by

$$w_{st} = (\Delta h_0)_{st} = u^2\ \phi\ (\tan \beta_2 - \tan \beta_3)$$

$$w_{st} = 22.62^2 \times 0.245\ (\tan 30 - \tan 10)$$

$$w_{st} = 50.26 \text{ J/kg}$$

The overall efficiency $\eta_0 = \eta_f \times \eta_d$

$$\eta_0 = 0.8 \times 0.88 = 0.704$$

The power required to drive the fan is

$$P = \dot{m}\ (\Delta h_0)_{st}/1000\ \eta_d$$

$$P = 1.322 \times 50.26/1000 \times 0.88$$

$$P = 0.075 \text{ kW } (Ans.)$$

$$(\Delta p_0)_{st} = \eta_f \times \rho\ (\Delta h_0)_{st} = 0.8 \times 1.125 \times 50.26$$

$$(\Delta p_0)_{st} = 45.234 \text{ N/m}^2 = 45.234/9.81 \text{ kgf/m}^2$$

$$(\Delta p_0)_{st} = 4.61 \text{ mm W.G. } (Ans.)$$

The pressure coefficient of the stage is

$$\psi = 2\ \phi\ (\tan \beta_2 - \tan \beta_3)$$

$$\psi = 2 \times 0.245\ (\tan 30 - \tan 10)$$

$$\psi = 0.196\ (Ans.)$$

The motor power can also be obtained from Eq. (14.12),

$$P = \frac{Q\Delta l}{120\eta_0} \text{ kW}$$

$$P = 1.175 \times 4.61/102 \times 0.704$$

$$P = 0.075 \text{ kW (verified)}$$

14.5 If the fan of Ex. 14.4 has both UGVs and DGVs and the rotor blade air angles are $\beta_2 = 86°$ and $\beta_3 = 10°$, determine the stage pressure rise, pressure coefficient and degree of reaction. The UGVs and DGVs are mirror images of each other. Assume a fan efficiency of 85%. What is the power of the driving motor if its efficiency is 80%?

***Solution*:**

Refer to Fig. 14.12. The velocity of air at the entry and exit of the stage is the same. Since the UGVs and DGVs are mirror images of each other, the static pressure drop in the UGVs is the same as the static pressure rise in the DGVs. Therefore, the static pressure rise in the rotor is identical with the pressure rise of the stage. Thus the degree of reaction of this stage is unity or 100 per cent.

The stage work is

$$w_{st} = (\Delta h_0)_{st} = 2u^2\ (\phi \tan \beta_2 - 1)$$

$$w_{st} = 2 \times 22.62^2\ (0.245 \tan 86 - 1) = 2561.39 \text{ J/kg}$$

$$(\Delta p_0)_{st} = (\Delta p)_{st} = (\Delta p)_r = \eta_f \rho\ (\Delta h_0)_{st}$$

$$(\Delta p_0)_{st} = 0.85 \times 1.125 \times 2561.39 = 2449.3 \text{ N/m}^2$$

$$(\Delta p_0)_{st} = 249.67 \text{ mm W.G. } (Ans.)$$

$$\psi = 4(\phi \tan \beta_2 - 1)$$

$$\psi = 4(0.245 \tan 86 - 1)$$

$$\psi = 10.012 \ (Ans.)$$

The power of the electric motor is

$$P = \dot{m} w_{st}/1000\eta_d$$

$$P = 1.322 \times 2561.39/(1000 \times 0.8)$$

$$P = 4.233 \text{ kW } (Ans.)$$

14.6 The velocities far upstream and downstream of an open propeller fan (d = 50 cm) are 5 and 25 m/s, respectively. If the ambient conditions are p = 1.02 bar, t = 37 °C, determine:

(a) flow rate through the fan,

(b) total pressure developed by the fan, and

(c) the power required to drive the fan assuming the overall efficiency of the fan as 40%.

***Solution*:**

Refer to Fig. 14.16.

The area of cross-section of the propeller disc is

$$A = \frac{\pi}{4} d^2 = 0.785 \times 0.5^2 = 0.196 \text{ m}^2$$

The velocity of flow through the disc is

$$c = \frac{1}{2} (5 + 25) = 15 \text{ m/s}$$

$$\rho = \frac{p}{RT} = \frac{1.02 \times 10^5}{287 \times 310} = 1.146 \text{ kg/m}^3$$

(a) $\dot{m} = \rho Ac$

$$\dot{m} = 1.146 \times 0.196 \times 15 = 3.37 \text{ kg/s } (Ans.)$$

$$Q = 0.196 \times 15 = 2.94 \text{ m}^3/\text{s}$$

$$\Delta h_0 = \frac{1}{2} (c_s^2 - c_u^2) = 0.5 (25^2 - 5^2) = 300 \text{ J/kg}$$

(b) Pressure developed by the propeller is

$$\Delta p_0 = \rho \Delta h_0 = 1.146 \times 300 = 343.8 \text{ N/m}^2$$

$$\Delta p_0 = 343.8/9.81 = 35.04 \text{ mm W.G. } (Ans.)$$

(c) Power required is given by

$$P = \frac{\dot{m} \Delta h_0}{\eta_0 \times 1000}$$

$$P = \frac{3.37 \times 300}{0.4 \times 1000} = 2.52 \text{ kW } (Ans.)$$

Questions and Problems

14.1 Show by means of suitable diagrams the locations of I.D. and F.D. fans in cooling tower and boiler applications. What are the special advantages of axial fans in these applications?

14.2 Sketch an axial fan stage with the inlet nozzle, UGVs, DGVs and outlet diffuser. Show the variation of static pressure through such a stage. Draw the velocity triangles at the entry and exit of the impeller.

14.3 How is the volumetric efficiency of fans and blowers defined? What are the various factors which govern this efficiency?

14.4 (a) Define the degree of reaction, rotor and stage pressure coefficients and stage efficiency for fans and blowers.

(b) Prove the following relations for an axial fan stage with UGVs and DGVs:

$$(\Delta p)_{st} = 2\rho u^2 (\phi \tan \beta_2 - 1)$$

$$\psi = 4 (\phi \tan \beta_2 - 1)$$

$$R = 1$$

14.5 (a) How are the static and total efficiencies of fans defined?

(b) Show that the power required in kW to drive a fan developing a pressure equivalent to Δl mm W.G. and delivering Q m^3/s is

$$Q \, \Delta l / 102 \eta_0$$

A blower for a furnace is required to deliver 2.38 m^3/s of air at a pressure of 750 mm W.G. If the combined fan and motor efficiency is 65%, determine the power required to drive the fan. (*Ans.* 26.94 kW)

14.6 An axial ducted fan without any guide vanes has a pressure coefficient of 0.38 and delivers 3 kg/s of air at 750 rpm. Its hub and tip diameters are 25 cm and 75 cm respectively. If the conditions at the entry are p = 1.0 bar and t = 38° C, determine:

(a) air angles at the entry and exit,

(b) pressure developed in mm W.G.,

(c) fan efficiency, and

(d) power required to drive the fan if the overall efficiency of the drive is 85%.

(*Ans.*) (a) $\beta_2 = 70.84°$, $\beta_3 = 39°$, (b) 8 mm W.G.; (c) 79.3%; and (d) 325.9 watts.

14.7 A fan takes in 2.5 m^3/s of air at 1.02 bar and 42°C, and delivers it at 75 cm W.G. and 52°C. Determine the mass-flow rate through the fan, the power required to drive the fan and the static fan efficiency.

(*Ans.*) $\dot{m} = 2.82$ kg/s, $P = 28.35$ kW, and $\eta_f = 63\%$.

14.8 An axial flow blower consists of a 100-cm diameter rotor provided with DGVs which deliver the air axially. The DGVs have the same entry angle as the rotor blades. The annulus height is 15 cm and the rotor rotates at 2880 rpm. Air enters the annulus with a velocity of 30 m/s. If the blower and motor efficiencies are 85% and 78% respectively, determine:

(a) the rotor blade air angles,
(b) static pressure rise across the blower,
(c) mass-flow rate, and
(d) the power required by the driving motor.

Assume pressure and temperature at the entry of the blower as 1.02 bar and 310 K respectively.

(*Ans.*) (a) $\beta_2 = 78.75°$, $\beta_3 = 0$; (b) 225.87 cm W.G.; (c) 16.2 kg/s; and (d) 472 kW.

Chapter 15

Centrifugal Fans and Blowers

A large number of fans and blowers for high pressure applications are of the centrifugal type.[561 - 607] Figures 15.1 and 15.2 show an arrangement employed in centrifugal machines. It consists of an impeller which has blades fixed between the inner and outer diameters. The impeller can be mounted either directly on the shaft extension of the prime mover or separately on a shaft supported between two additional bearings. The latter arrangement is adopted for large blowers in which case the impeller is driven through flexible couplings.

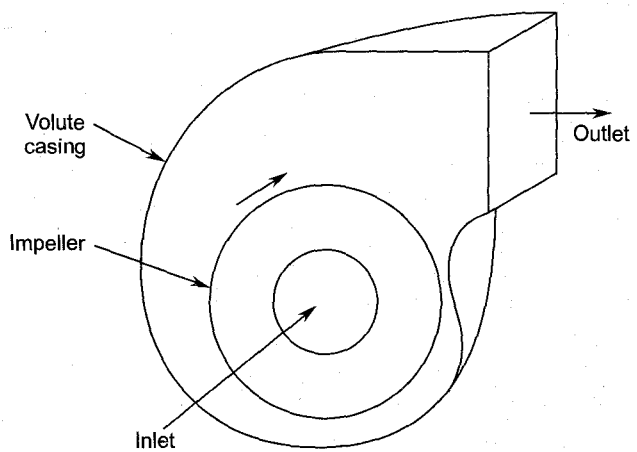

Fig. 15.1 A centrifugual fan or blower

Air or gas enters the impeller axially through the inlet nozzle which provides slight acceleration to the air before its entry to the impeller. The action of the impeller swings the gas from a smaller to a larger radius and delivers the gas at a high pressure and velocity to the casing. Thus unlike the axial type, here the centrifugal energy (see Sec. 6.9.2) also contributes to the stage pressure rise. The flow from the impeller blades is collected by a spirally-shaped casing known as scroll or volute. It delivers the air to the exit of the blower. The scroll casing can further increase the static

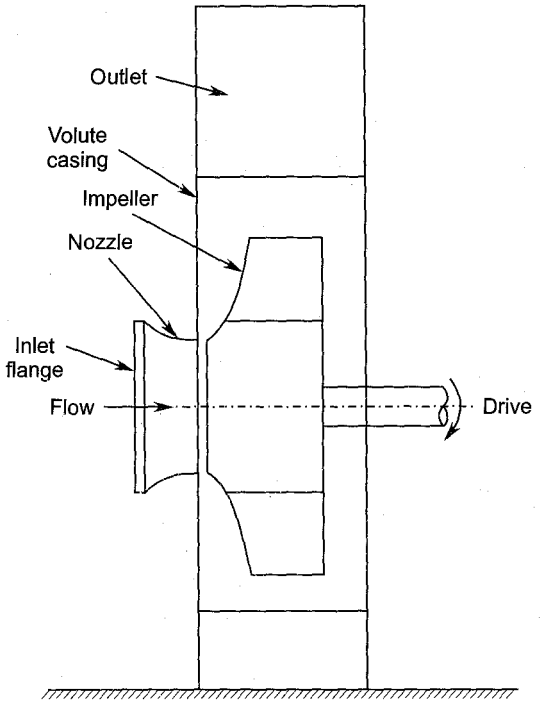

Fig. 15.2 Main components of a centrifugal blower

pressure of air. The outlet passage after the scroll can also take the form of a conical diffuser.

The centrifugal fan impeller can be fabricated by welding curved or almost straight metal blades to the two side walls (shrouds) of the rotor or it can be obtained in one piece by casting. Such an impeller is of the enclosed type. The open types of impellers have only one shroud and are open on one side. A large number of low pressure centrifugal fans are made out of thin sheet metal. The casings are invariably made of sheet metal of different thicknesses and steel reinforcing ribs on the outside. In some applications, if it is necessary to prevent leakage of the gas, suitable sealing devices are used between the shaft and the casing.

Large capacity centrifugal blowers sometimes employ double entry for the gas as shown in Fig. 15.3.

The difference between a fan, blower and compressor has already been explained in Chapter 14. Various applications have also been described briefly in that chapter. A brief discussion on radial stages is given in Sec. 1.10. Much of the material covered in Chapter 12 on centrifugal compressors is also applicable here. The principal departure in design, analysis and construction is due to the marked difference in the magnitude of the pressure rise in the two types of machines.

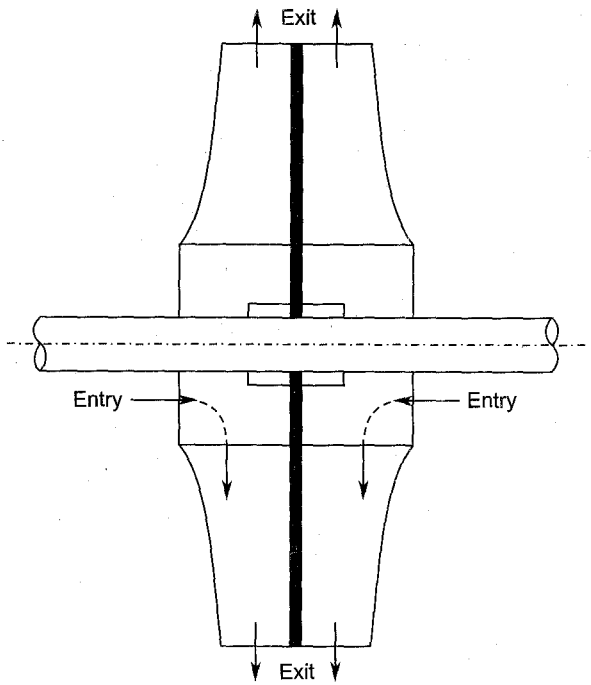

Fig. 15.3 Centrifugal impeller with double entry

15.1 Types of Centrifugal Fans

The pressure rise and flow rate in centrifugal fans depend on the peripheral speed of the impeller and blade angles. The stage losses and performance also vary with the blade geometry. The blades can be either of sheet metal of uniform thickness or of aerofoil section. Following are the main types of centrifugal fans:

15.1.1 Backward-swept Blades

Figure 15.4 shows an impeller which has backward-swept blades, i.e. the blades are inclined away from the direction of motion. Various velocity vectors and angles are shown in the velocity triangles at the entry and exit. In contrast to the axial fans, here the tangential direction is taken as the reference direction. Under ideal conditions, the directions of the relative velocity vectors w_1 and w_2 are the same as blade angles at the entry and exit.

The static pressure rise in the rotor results from the centrifugal energy and the diffusion of the relative flow. The stage work and stagnation pressure rise for a given impeller depend on the whirl or swirl components ($c_{\theta 1}$ and $c_{\theta 2}$) of the absolute velocity vectors c_1 and c_2 respectively.

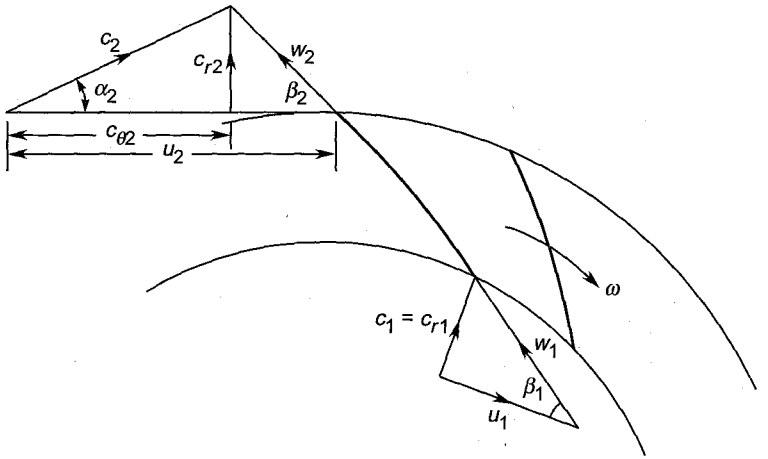

Fig. 15.4 Velocity triangles for a backward-swept blade impeller

Backward-swept blade impellers are employed for lower pressure and lower flow rates. The width to diameter ratio of such impellers is small ($b/D \approx 0.05 - 0.2$) and the number of blades employed is between 6 and 17.

15.1.2 Radial Blades

Figure 15.5 shows two arrangements for radial-tipped blade impeller. The inlet velocity triangle for the blade shape that is used in practice is shown

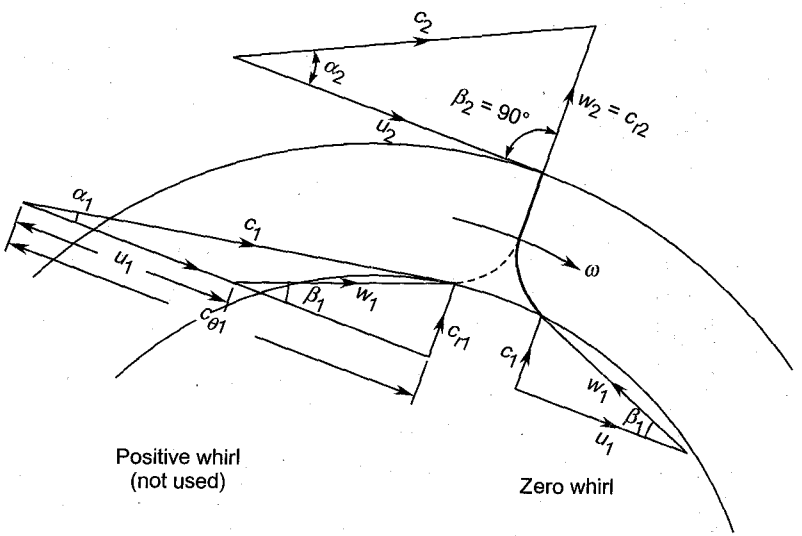

Fig. 15.5 Velocity tirangles for a radial blade impeller

on the right. This is a sort of a forward-swept radial blade and the velocity triangle is based on the absolute velocity vector c_1 which is radial. Therefore, the swirl at the entry is zero. Such a shape is simple for construction where generally only slightly bent sheet metal blades are used.

The other possibility is to employ blackward-swept radial blades. The curved part (dashed) of such a blade and the inlet velocity triangle are shown on the left. Such a fan (if designed and built) would develop a very low pressure on account of a large positive whirl component. Besides this disability, such an arrangement will require prewhirl vanes adding to the cost of the fan.

The outlet velocity triangle for both the arrangements is the same. The relative velocity w_2 is in the radial direction.

For cheap construction, the impeller blades can be kept purely radial as in the paddle type impellers. Such an impeller is unshrouded and straight radial vanes are bolted or welded on a disc which is mounted on the driving shaft. Such impellers are ideal for handling dust-laden air or gas because they are less prone to blockage, dust erosion and failure.

15.1.3 Forward-swept Blades

When the blades are inclined in the direction of motion, they are referred to as forward-swept blades. The velocity triangles at the entry and exit of such a fan are shown in Fig. 15.6. This shows the backward-swept blades of Fig. 15.4 in the forward-swept position. As a result, the inlet velocity

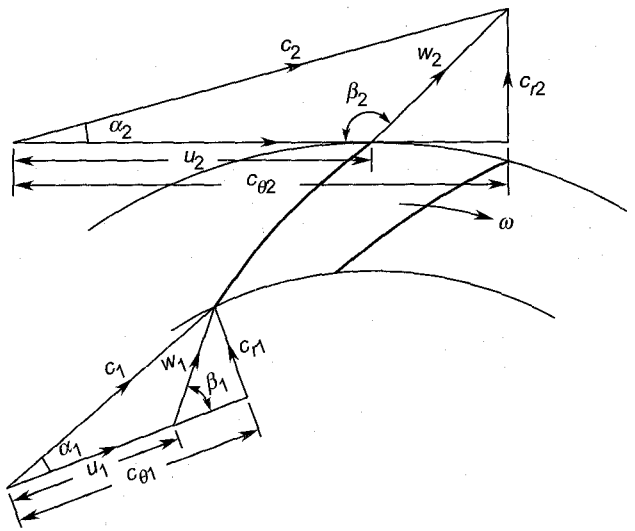

Fig. 15.6 Velocity tirangles for a forward-swept blade impeller with positive whirl

triangle again has a positive whirl component $c_{\theta 1}$. Its effect has already been explained in the previous section. Therefore, such an arrangement is not useful in practice.

The configuration of forward-swept blades that is widely used in practice is shown in Fig. 15.7. Blade tips, both at the entry and exit, point in the direction of motion. Therefore, it is possible to achieve zero whirl or swirl at the entry as in Fig. 15.4. On account of the forward-swept blade tips at the exit, the whirl component ($c_{\theta 2}$) is large, leading to a higher stage pressure rise. Such blades have a larger hub-to-tip diameter ratio which allows large area for the flow entering the stage. However, on account of the shorter length of blade passages, the number of blades required is considerably larger to be effective.

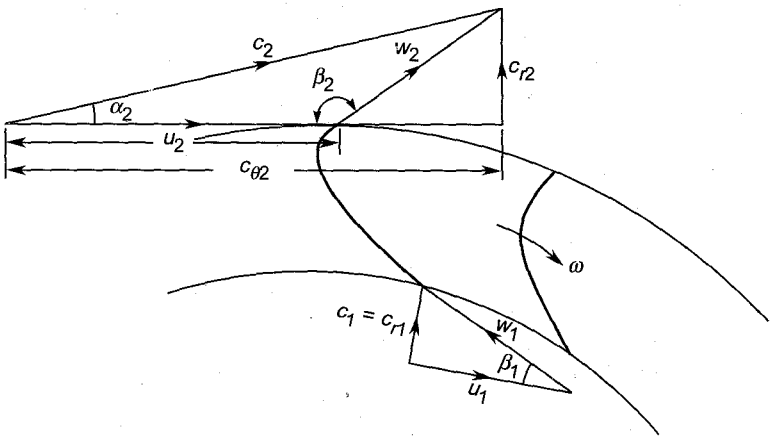

Fig. 15.7 Velocity triangles for a forward-swept blade impeller with zero whirl at entry

15.2 Centrifugal Fan Stage Parameters

In this section expressions for various parameters of a centrifugal fan or blower stage are derived. The velocity triangles shown in Figs. 15.4 to 15.7 are used for this purpose.

The mass flow rate through the impeller is given by

$$\dot{m} = \rho_1 Q_1 = \rho_2 Q_2 \tag{15.1}$$

The areas of cross-section normal to the radial velocity components c_{r1} and c_{r2} are

$$A_1 = \pi d_1 b_1 \quad \text{and} \quad A_2 = \pi d_2 b_2$$

Therefore,

$$\dot{m} = \rho_1 c_{r1} (\pi d_1 b_1) = \rho_2 c_{r2} (\pi d_2 b_2) \tag{15.2}$$

The radial components of velocities at the impeller entry and exit depend on its width at these sections. For a small pressure rise through the stage, the density change in the flow is negligible and can be assumed to be almost incompressible. Thus for constant radial velocity

$$c_{r1} = c_{r2} = c_r \tag{15.3}$$

Equation (15.2) gives

$$\dot{m} = \rho\, c_r\, (\pi\, d_1\, b_1) = \rho\, c_r\, (\pi\, d_2\, b_2)$$

$$b_1/b_2 = d_2/d_1 \tag{15.4}$$

15.2.1 Stage Work

The stage work is given by the Euler's equation

$$w_{st} = u_2\, c_{\theta 2} - u_1\, c_{\theta 1} \tag{15.5}$$

In the absence of inlet guide vanes it is reasonable to assume zero whirl or swirl at the entry. This condition gives

$$\alpha_1 = 90°,\ c_{\theta 1} = 0 \qquad \text{and} \qquad u_1\, c_{\theta 1} = 0$$

This is shown in Figs. 15.4, 15.5 and 15.7. Therefore, for constant radial velocity

$$c_1 = c_{r1} = c_{r2} = u_1 \tan \beta_1 \tag{15.6}$$

Equation (15.5) gives

$$w_{st} = u_2\, c_{\theta 2} = u_2^2 \left(\frac{c_{\theta 2}}{u_2} \right) \tag{15.7}$$

From the exit velocity triangle (Fig. 15.4),

$$u_2 - c_{\theta 2} = c_{r2} \cot \beta_2$$

$$\frac{c_{\theta 2}}{u_2} = 1 - \frac{c_{r2}}{u_2} \cot \beta_2 \tag{15.8}$$

Equations (15.7) and (15.8) yield

$$w_{st} = u_2^2\, (1 - \phi \cot \beta_2) \tag{15.9}$$

$$\frac{c_2}{\sin \beta_2} = \frac{u_2}{\sin (\alpha_2 + \beta_2)} \tag{15.10}$$

$$c_{\theta 2} = c_2 \cos \alpha_2 = \frac{u_2 \sin \beta_2 \cos \alpha_2}{\sin (\alpha_2 + \beta_2)}$$

$$\frac{c_{\theta_2}}{u_2} = \frac{\sin \beta_2 \cos \alpha_2}{\sin \alpha_2 \cos \beta_2 + \cos \alpha_2 \sin \beta_2} = \frac{\tan \beta_2}{\tan \alpha_2 + \tan \beta_2} \tag{15.11}$$

Equation (15.11) when used in Eq. (15.7) gives the stage work as

$$w_{st} = \frac{\tan \beta_2}{\tan \alpha_2 + \tan \beta_2}\, u_2^2 \tag{15.12}$$

Assuming that the flow fully obeys the geometry of the impeller blades, the specific work done in an adiabatic process is given by

$$(\Delta h_0)_{st} = w_{st} = u_2\, c_{\theta 2} = u_2^2\,(1 - \phi \cot \beta_2) \tag{15.13}$$

The power required to drive the fan is

$$P = \dot{m}\ (\Delta h_0)_{st} = \dot{m}\ c_p\ (\Delta T_0)_{st} = \dot{m}\ u_2\, c_{\theta 2} \tag{15.14}$$

15.2.2 Stage Pressure Rise

If the compression process is assumed to be reversible adiabatic (isentropic),

$$(\Delta h_0)_{st} = \frac{1}{\rho}\ (\Delta p_0)_{st}$$

Therefore,

$$(\Delta p_0)_{st} = \rho\, u_2\, c_{\theta 2} = \rho\, u_2^2\,(1 - \phi \cot \beta_2) \tag{15.15}$$

As stated before, the static pressure rise through the impeller is due to the change in the centrifugal energy and the diffusion of the relative flow. Therefore,

$$p_2 - p_1 = (\Delta p)_r = \frac{1}{2}\,\rho\,(u_2^2 - u_1^2) + \frac{1}{2}\,\rho\,(w_1^2 - w_2^2) \tag{15.16}$$

The stagnation pressure rise through the stage can also be obtained by the Euler's equation for compressors (see Sec. 6.9.2).

$$(\Delta p_0)_{st} = \frac{1}{2}\,\rho\,(u_2^2 - u_1^2) + \frac{1}{2}\,\rho\,(w_1^2 - w_2^2) + \frac{1}{2}\,\rho\,(c_2^2 - c_1^2) \tag{15.17}$$

Substituting from Eq. (14.16),

$$(\Delta p_0)_{st} = (p_2 - p_1) + \frac{1}{2}\,\rho\,(c_2^2 - c_1^2) = p_{02} - p_{01}$$

$$(\Delta p_0)_{st} = (\Delta p)_r + \frac{1}{2}\,\rho\,(c_2^2 - c_1^2) \tag{15.18}$$

15.2.3 Stage Pressure Coefficient

The stage pressure coefficient is defined by

$$\psi_{st} = (\Delta p_0)_{st} \Big/ \frac{1}{2}\,\rho u_2^2$$

From Eq.(15.15)

$$\psi_{st} = 2\frac{c_{\theta 2}}{u_2} = 2\,(1 - \phi \cot \beta_2) \tag{15.19}$$

Equation (15.11) when used in Eq. (15.19) gives

$$\psi_{st} = \frac{2 \tan \beta_2}{\tan \alpha_2 + \tan \beta_2} \tag{15.20}$$

A rotor or impeller pressure coefficient is defined by

$$\psi_r = (\Delta p)_r \Big/ \frac{1}{2} \rho u_2^2 \tag{15.21}$$

15.2.4 Stage Reaction

By definition, the degree of reaction of the fan stage is

$$R = (\Delta p)_r / (\Delta p_0)_{st}$$

This can also be expressed in terms of the pressure coefficients for the rotor and the stage.

$$R = \psi_r / \psi_{st} \tag{15.22}$$

From the velocity triangle at the entry

$$w_1^2 - u_1^2 = c_1^2$$

This when put in Eq. (15.16) gives

$$(\Delta p)_r = \frac{1}{2} \rho (u_2^2 - w_2^2 + c_1^2) \tag{15.23}$$

Equation (15.6) when applied in Eq. (15.23) gives

$$(\Delta p)_r = \frac{1}{2} \rho (u_2^2 - w_2^2 + c_{r2}^2) \tag{15.23a}$$

From the exit velocity triangle,

$$w_2^2 - c_{r2}^2 = (u_2 - c_{\theta 2})^2$$
$$u_2^2 - w_2^2 + c_{r2}^2 = u_2^2 - (u_2 - c_{\theta 2})^2$$
$$u_2^2 - w_2^2 + c_{r2}^2 = 2u_2 c_{\theta 2} - c_{\theta 2}^2$$

This expression when put into Eq. (15.23a) gives

$$(\Delta p)_r = \frac{1}{2} \rho (2u_2 c_{\theta 2} - c_{\theta 2}^2) \tag{15.24}$$

Equations (15.15) and (15.24) give the degree of reaction as

$$R = 1 - \frac{1}{2} \frac{c_{\theta 2}}{u_2} \tag{15.25}$$

Equation (15.25) gives the degree of reaction for the three types of impellers shown in Figs. 15.4, 15.5, and 15.7.

(a) Backward-swept blades ($\beta_2 < 90°$)
For backward-swept blades $c_{\theta 2}/u_2 < 1$
Therefore, the degree of reaction is always less than unity.

(b) Radial blades ($\beta_2 = 90°$)
For radial-tipped blades $c_{\theta 2} = u_2$. Therefore,

$$R = 1/2$$

(c) Forward-swept blades ($\beta_2 > 90°$)

For forward-swept blades $c_{\theta 2} > u_2$. This gives

$$R < 1/2$$

The combination of Eqs. (15.8) and (15.25) gives

$$R = \frac{1}{2} (1 + \phi \cot \beta_2) \tag{15.26}$$

A useful relation between the degree of reaction and the stage pressure coefficient can be obtained.

Equation (15.19) is

$$\frac{c_{\theta 2}}{u_2} = \frac{1}{2} \psi_{st}$$

This, in Eq. (15.25) gives

$$R = 1 - \frac{1}{4} \psi_{st} \tag{15.27}$$

$$\psi_{st} = 4 (1 - R) \tag{15.28}$$

This shows that the stage pressure coefficient decreases with increase in the degree of reaction.

15.2.5 Stage Efficiency

The actual work input to the stage is given by

$$w_{st} = u_2 \, c_{\theta 2}$$

Here $c_{\theta 2}$ is the actual value obtained in a real fan; this is less than the Eulerian value. On account of stage losses (discussed in Chapter 12) the isentropic work $\frac{1}{\rho} (\Delta p_0)_{st} = v(\Delta p_0)_{st}$ is less than the actual work ($u_2 \, c_{\theta 2}$). Therefore, the fan stage efficiency is defined by

$$\eta_{st} = (\Delta p_0)_{st} / \rho \, u_2 \, c_{\theta 2} \tag{15.29}$$

15.3 Design Parameters

Centrifugal fans and blowers, to a great extent, can be designed on the same lines as a low pressure centrifugal compressor. In fan engineering, even at the present time, many empirical and approximate relations are used to determine the various parameters. Some important aspects are discussed here briefly.

15.3.1 Impeller Size

As shown in the theoretical relations derived earlier, the peripheral speed of the impeller with a given geometry is decided by the stage pressure

rise. Therefore, for the desired value of the peripheral speed (u_2), there are various combinations of the impeller diameters and the rotational speeds. The impeller diameter and the width are also tied down to the flow rate.

On account of the much lower pressure rise in fans, their peripheral speeds are much below the maximum permissible values. Fan speeds can vary from 360 to 2940 rpm for ac motor drives at 50 c/s, though much lower speeds have been used in some applications. With other drives, considerably higher speeds can be obtained if desired.

The diameter ratio (d_1/d_2) of the impeller determines the length of the blade passages: the smaller this ratio, the longer is the blade passage. Eck[542] gives the following value for the diameter ratio:

$$d_1/d_2 \approx 1.2\ \phi^{1/3} \tag{15.30}$$

With a slight acceleration of the flow from the impeller eye to the blade entry, the following relation for the blade width to diameter ratio is recommended:

$$b_1/d_1 = 0.2 \tag{15.31}$$

Impellers with backward-swept blades are narrower, i.e. $b_1/d_1 < 0.2$.

If the rate of diffusion in a parallel wall impeller is too high, it may have to be made tapered towards the outer periphery.

15.3.2 Blade Shape

Straight or curved sheet metal blades or aerofoil-shaped blades have been used in centrifugal fans and blowers. Sheet metal blades are circular arc-shaped or of a different curve. They can either be welded or rivetted to the impeller disc.

As mentioned before, the blade exit angles depend on whether they are backward-swept, radial or for forward-swept.

The optimum blade angle at the entry is found to be about 35°.

15.3.3 Number of Blades

The number of blades in a centrifugal fan can vary from 2 to 64 depending on the application, type and size. Too few blades are unable to fully impose their geometry on the flow, whereas too many of them restrict the flow passage and lead to higher losses. Most efforts to determine the optimum number of blades have resulted in only empirical relations given below:

Eck[542] has recommended the following relation:

$$z = \frac{8.5 \sin \beta_2}{1 - d_1/d_2} \tag{15.32}$$

Pfleirderer has recommended:

$$z = 6.5 \left(\frac{d_2 + d_1}{d_2 - d_1} \right) \sin \frac{1}{2} (\beta_1 + \beta_2) \qquad (15.33)$$

From data collected for a large number of centrifugal blowers, Stepanoff[601] suggests

$$z = \frac{1}{3} \beta_2 \qquad (15.34)$$

For smaller-sized blowers, the number of blades is lesser than this.

15.3.4 Diffusers and Volutes

Static pressure is recovered from the kinetic energy of the flow at the impeller exit by diffusing the flow in a vaneless or vaned diffuser. The spiral casing as a collector of flow from the impeller or the diffuser is an essential part of the centrifugal blower.

The provision of a vaned diffuser in a blower can give a slightly higher efficiency than a blower with only a volute casing. However, for a majority of centrifugal fans and blowers, the higher cost and size that result by employing a diffuser outweigh its advantages. Therefore, most of the single stage centrifugal fan impellers discharge directly into the volute casing. Some static pressure recovery can also occur in a volute casing.

There is a small vaneless space between the impeller exit (Fig. 15.1) and the volute base circle. The base circle diameter is 1.1 to 1.2 times the impeller diameter. The volute width is 1.25 and 2.0 times the impeller width at the exit.

Volutes can be designed for constant pressure or constant average velocity. The cross-section of the volute passage may be square, reactangular, circular or trapezoidal. The fabrication of a rectangular volute from sheet metal is simple; other shapes can be cast.

15.4 Drum-type Fans

A drum or multi-vane type of a centrifugal fan is shown in Fig. 15.8. It has a large number of short-chord forward-swept blades. The hub-tip ratio of such an impeller is close to unity. On account of this, the inside diameter can be kept large giving a large inlet flow area. Therefore, such an impeller is suitable for relatively large flow rates.

Multi-vane type fans are also known as squirrel cage or Sirocco fans.

On account of the small radial depth of the blades, their number is large to be effective. Their large axial length besides being suitable for higher

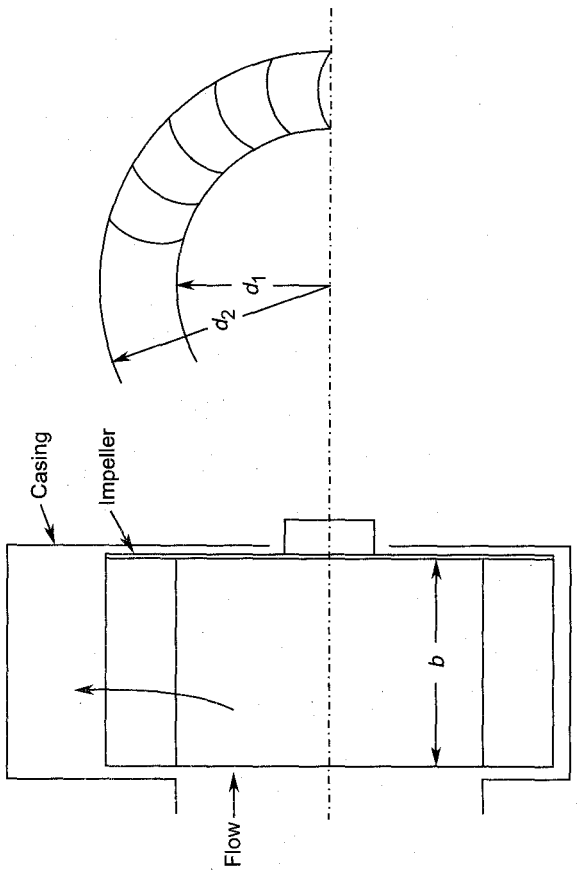

Fig. 15.8 Drum-type centrifugal fan

flow rates gives aerodynamically a more efficient impeller. The noise level of this type of fan is relatively low.

Figure 15.9 shows the three blade configurations which can be used in the impeller. The flow is assumed to enter the blades radially in all the cases, i.e. the swirl at entry is zero ($c_{\theta 1} = 0$).

For backward-swept blades as shown, $w_1 \approx w_2$ and u_2 is only a little larger than u_1. Therefore, the swirl component $c_{\theta 2}$ at the exit is small giving only a small stage pressure rise

$$\Delta p_0 = \rho\, u_2\, c_{\theta 2}$$

In radial-tipped blades $w_2 = c_{r2}$. Owing to the geometry of the blade passages, there is considerable deceleration of the flow ($w_2 < w_1$) over a short passage length. This leads to flow separation and lower efficiency.

In forward-swept blades, impeller blades of almost equal entry and exit angles ($\beta_1 \approx \beta_2$) are used to avoid deceleration of the flow leading to

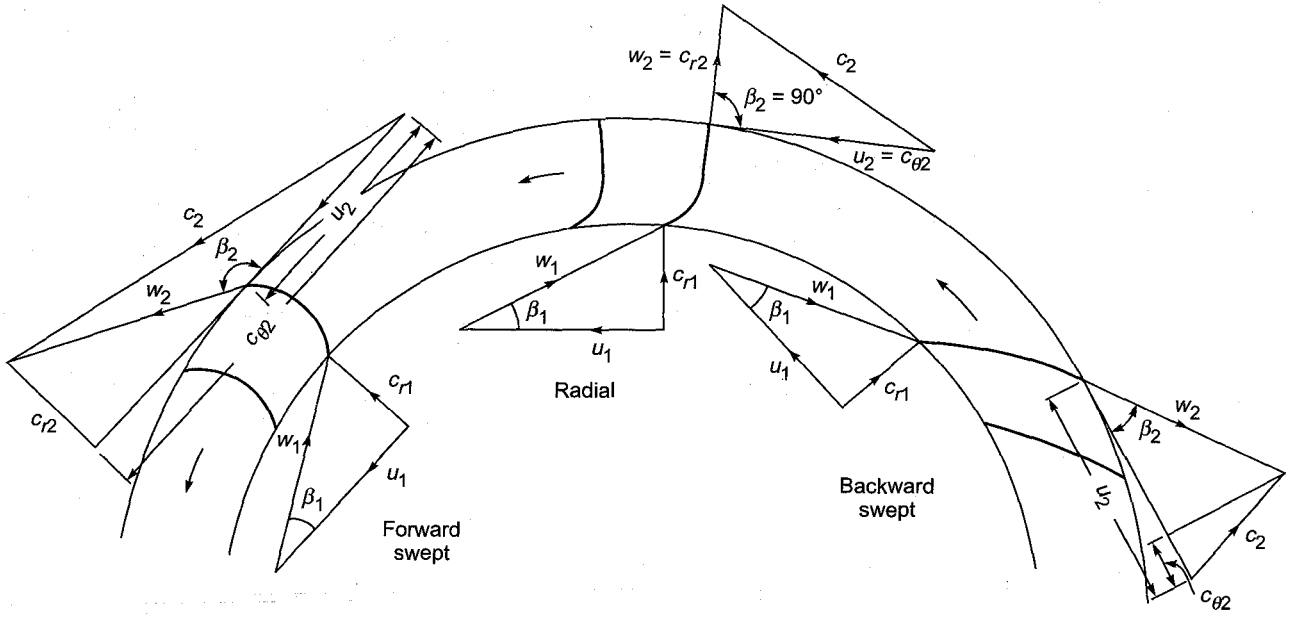

Fig. 15.9 Three-blade configurations in a drum-type centrifugal fan impeller

separation. Besides this these blades also provide a large value of $c_{\theta 2}$ giving a large stagnation pressure rise through the stage. Therefore, the drum-type centrifugal fan impellers employ only forward-swept blades.

The continuity equation at the entry and exit of the impeller gives

$$(\pi d_1 - zt_1)\, b_1\, c_{r1} = (\pi d_2 - zt_2)\, b_2\, c_{r2}$$

The flow is almost incompressible. The thickness of the impeller blades which are of thin sheet metal is negligible and the rotor width is constant ($b_1 = b_2 = b$). Therefore,

$$\frac{c_{r1}}{c_{r2}} = \frac{w_1 \sin \beta_1}{w_2 \sin \beta_2} = \frac{d_2}{d_1} \tag{15.35}$$

For $w_1 \approx w_2$,

$$\frac{d_1}{d_2} = \frac{\sin \beta_2}{\sin \beta_1} \tag{15.36}$$

The rotor blades are generally circular arcs with $\beta_1 + \beta_2 = 90°$ Therefore,

$$\sin \beta_1 = \sin (90 - \beta_2) = \cos \beta_2 \tag{15.37}$$

$$\sin \beta_2 = \sin (90 - \beta_1) = \cos \beta_1 \tag{15.38}$$

Therefore, Eqs. (15.37) and (15.38) when put into Eq. (15.36) give

$$\frac{d_1}{d_2} = \tan \beta_2 \tag{15.39}$$

$$\frac{d_2}{d_1} = \tan \beta_1 \tag{15.40}$$

Now $$c_{r2} \cot \beta_2 = \left(\frac{d_1}{d_2}\right) c_{r1} \cot (90 - \beta_1)$$

$$c_{r2} \cot \beta_2 = \frac{d_1}{d_2}\, c_{r1} \tan \beta_1$$

From the inlet velocity triangle

$$c_{r1} = u_1 \tan \beta_1$$

Therefore,

$$c_{r2} \cot \beta_2 = \frac{d_1}{d_2}\, u_1 \tan^2 \beta_1 = \left(\frac{d_1}{d_2}\right)^2 u_2 \tan^2 \beta_1$$

Substituting from Eq. (15.40),

$$c_{r2} \cot \beta_2 = u_2 \tag{15.41}$$

From the outlet velocity triangle,

$$c_{\theta 2} = u_2 + c_{r2} \cot \beta_2 = 2u_2 \tag{15.42}$$

$$\Delta p_0 = \rho\, u_2\, c_{\theta 2} = 2\, \rho\, u_2^2 \tag{15.43}$$

Therefore,

$$\psi_{st} = \frac{\Delta p_0}{\frac{1}{2}\rho u_2^2} = 4 \tag{15.44}$$

The static pressure rise across the impeller is

$$(\Delta p)_r = \frac{1}{2}\rho (w_1^2 - w_2^2) + \frac{1}{2}\rho (u_2^2 - u_1^2)$$

$$(\Delta p)_r = \frac{1}{2}\rho (c_{r1}^2 - c_{r2}^2)$$

$$(\Delta p)_r = \frac{1}{2}\rho c_{r1}^2 \left(1 - \frac{d_1^2}{d_2^2}\right) = \frac{1}{2}\rho u_1^2 \tan^2 \beta_1 \left(1 - \frac{d_1^2}{d_2^2}\right)$$

$$(\Delta p)_r = \frac{1}{2}\rho u_2^2 \left(1 - \frac{d_1^2}{d_2^2}\right) \tag{15.45}$$

Equations (15.43) and (15.45) give the degree of reaction

$$R = (\Delta p)_r/(\Delta p)_0$$

$$R = \frac{1}{4}\left(1 - \frac{d_1^2}{d_2^2}\right) \tag{15.46}$$

15.5 Partial-flow Fans

The configuration of a centrifugal fan or blower is such that the area available at the entrance is restricted on account of the inner diameter of the impeller. The outer diameter is fixed due to the maximum permissible peripheral speed and size requirements. Therefore, as pointed out earlier, a conventional centrifugal fan or blower is unsuitable for large flow rates.

15.5.1 Outward-flow Fans

Besides the disadvantage of low flow rates, the impeller width in many centrifugal fans is too small. For a given flow rate a smaller impeller width is obtained for a large diameter. Narrow impellers have relatively higher aerodynamic losses. Therefore, to increase the impeller width for achieving higher efficiency, a partial admission configuration is employed. This is done by allowing the flow to enter a wider impeller for only a part of its periphery as shown in Fig. 15.10. Such a configuration has its own disadvantages and associated losses, but an optimum combination of impeller width and degree of admission can be found.

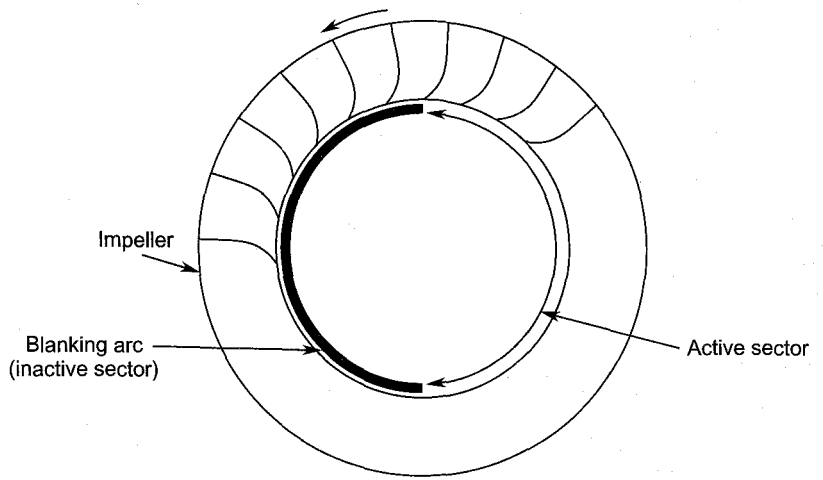

Fig. 15.10 Partial admission outward flow type radial blower

This scheme can prove very useful for a low flow rate and high pressure applications where the width of the conventional centrifugal impeller with full admission is only a few millimetres.

15.5.2 Cross-flow Fans[562,575,585]

Another method to overcome the problem of low flow rate centrifugal blowers is to employ a cross-flow configuration. Such an arrangement consists of a comparatively long impeller (generally of a relatively small diameter) closed at the two ends. The air enters the outer periphery of the impeller on one side and leaves at the other as shown in Figs. 15.11 and 15.12. The impeller housing constrains the air to flow normal to the shaft axis. Thus the air traverses the impeller blades twice: in the first stage (1–2) it crosses the impeller blade ring inwards and, in the second (3–4), in the outward direction as shown in Fig. 15.11.

It has been shown that the optimum blade shape for such a fan is the forward-swept type and the fan mainly develops a dynamic pressure, i.e. it mainly accelerates the flow from its entry to its exit. The flow decelerates in the first stage (1–2) and accelerates in the second (3–4). Such a fan can develop high pressure coefficients at comparatively lower efficiencies. Since the static pressure change in the impeller is negligible, the degree of reaction is close to zero.

Since the air does not enter over the entire periphery of the impeller, this fan is also of the partial-flow type. The cross-flow fan is also referred to as a tangential fan because in principle it is neither of the axial or radial type. The cross-flow and outward-flow types of partial-flow fans are examples of turbomachines where the flow field is not axisymmetric.

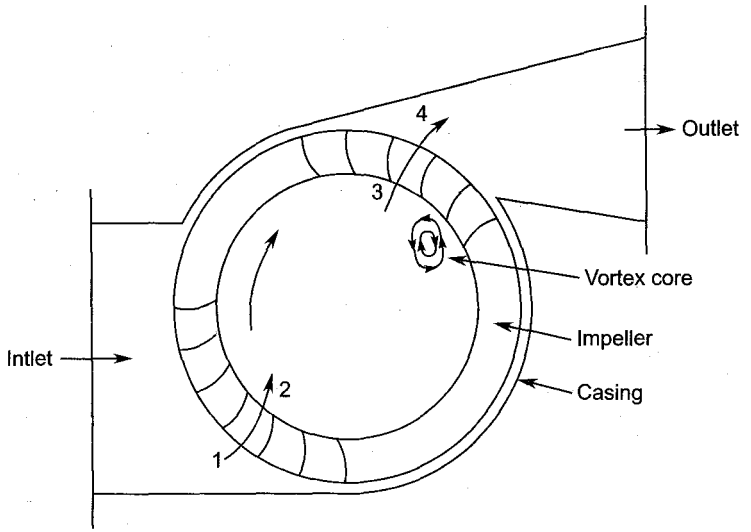

Fig. 15.11 Cross-flow fan

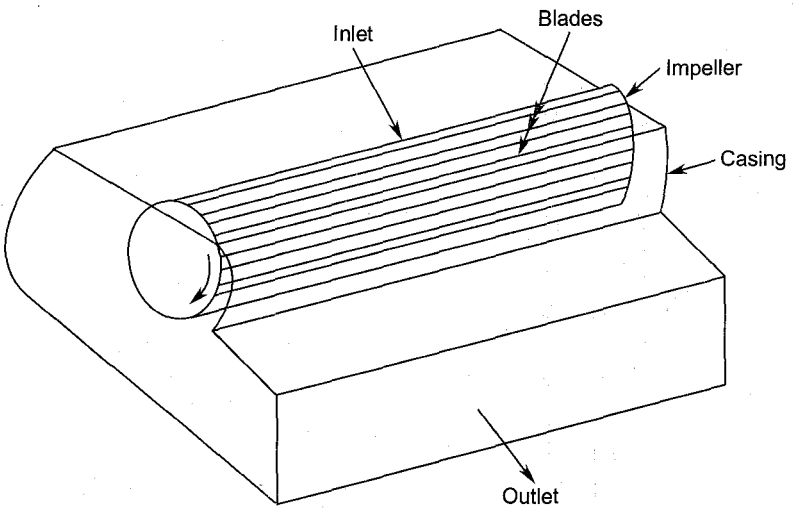

Fig. 15.12 Longitudinal view of a cross-flow fan

The design of the housing of such a fan is critical. Most efforts to improve this fan have been in optimizing the configuration of the entry, exit and housing. The role of the diffuser at the exit of this fan is very important because its static efficiency is strongly dependent on this.

The cross-flow fan is only an improved version of the paddle wheel which was employed for various applications. The cross-flow concept can also be used with a drum-type fan impeller without the casing. The air stream thus established can be used in a number of applications.

The main advantage of the cross-flow fan in that there is practically no restriction on its ability to handle high-flow rates. For a given impeller diameter, the flow rate is proportional to its length. Smaller diameter impellers can run at much higher speeds and also lead to space economy. These fans have been manufactured in both small ($d \approx 5$ cm) and large ($d \approx 280$ cm) sizes for a wide range of applications from domestic to industrial. The rectangular duct-like outlet is convenient to accommodate electric heating elements, such as in hair driers and other hot-air applications.

The flow is highly unsteady in a cross-flow fan on account of its configuration. A vortex is established (as shown in Fig. 15.11) on the inner periphery of the impeller near the exit. As a result of this, the flow at the exit is concentrated towards the vortex. The exact size and position of the vortex depend on the flow rate. The flow through the fan is largely governed by this vortex. This causes a recirculation of the flow in the vicinity of the fan exit which accounts for additional losses occurring in this fan. The shape of the casing and its distance from the impeller regulate the size and location of the vortex which in turn affects the fan efficiency.

15.6 Losses[589]

Losses occur in both the stationary as well as moving parts of the centrifugal fan stage. The basic mechanism of these losses is the same as discussed in Chapter 12 for centrifugal compressors.

By accounting for the stage losses, the actual performance of a fan or blower can be predicted from that obtained theoretically.

The various losses are briefly described below.

(a) *Impeller entry losses*

These are due to the flow at the inlet nozzle or eye and its turning from the axial to radial direction. Impeller blade losses due to friction and separation on account of a change of incidence can also be included under this head.

(b) *Leakage loss*

A clearance is required between the rotating periphery of the impeller and the casing at the entry. This leads to the leakage of some air and disturbance in the main flow field. Besides this, leakage also occurs through the clearance between the fan shaft and the casing.

(c) *Impeller losses*

These losses arise from passage friction and separation. They depend on the relative velocity, rate of diffusion and blade geometry.

(d) *Diffuser and volute losses*

Losses in the diffuser also occur due to friction and separation. At off-design conditions, there are additional losses due to incidence.

The flow from the impeller or diffuser (if used) expands to a larger cross-sectional area in the volute. This leads to losses due to eddy formation. Further losses occur due to the volute passage friction and flow separation.

(e) *Disc friction*

This is due to the viscous drag on the back surface of the impeller disc.

15.7 Fan Bearings

Fans and blowers employ simple journal bearings, ball bearings, roller bearings and self-aligning bearings. The type of bearings used depends on the fan power and speed. Bearing losses are small, sometimes negligible compared to the stage aerodynamic losses.

A fan shaft is generally stepped to accommodate and facilitate the assembly of the impeller and bearings. A small axial thrust can be taken by a thrust collar or a collar type thrust bearing.

Journal bearings are ring-oiled. The forced lubrication system requires an oil pump and an oil cooler which adds to the cost of the fan. The bearings require cooling when their temperature is higher than 150°C.

Ball bearings and roller bearings employ various types of greases for their lubrication. After suitably packing them with grease, these bearings do not require frequent attention and work satisfactrorily for long periods.

The bearing life depends on the temperature of the environment and the presence of moisture, dust and corrosive substances.

15.8 Fan Drives

Direct coupled prime movers are ideal for most fan applications. Small fan rotors are mounted on the extention of the prime mover's shaft, but large fan rotors have to be mounted on separate bearings. Shaft couplings must preferably be of the flexible type to take care of misalignments.

Some fans and blowers are belt-driven. Multi V-belt drives are widely used for large blowers. They are quiet and operate at low bearing pressure. Single V-belt drives are used for small fans and blowers. This can also be utilized as a variable speed facility by employing a variable diameter pulley. In this arrangement the distance between the two halves of the pulley is variable.

Fans and blowers can be driven by different types of electric motors and steam and gas turbines. Turbine drives are ideal for variable speed applications.

Three-phase squirrel cage induction motors are widely used for constant speed drive. Besides being cheap and rugged in construction, in the absence of moving electrical contacts they are suitable for operation when exposed to inflammable gas or dust. They maintain high efficiency and have a starting torque one and a half times the full load torque. The speeds of induction motors can be varied in a limited range by changing the frequency.

Small induction motors, from a fraction of a kilowatt to 15 kW are available in the single phase type. For constant speed applications, the squirrel cage induction motor is preferable to a dc motor, but for variable speed work, dc motors are superior to induction motors. Slip ring motors are also used for variable speeds, but they are expensive and incur high losses.

Hydraulic couplings are also used to obtain variable speeds of fans and blowers. For small loads the variable speed can be obtained by employing a magnetic coupling between the constant speed electric motor and the fan.

15.9 Fan Noise[566,580]

Noise is undesirable or unwanted sound. With a better understanding of the effects of environment on the inhabitants of dwellings and factory workers, noise has become an important subject in the design, installation and operation of fans and blowers. Fans and blowers used in various plants and machinery are major sources of factory noise. The prevention of noise in ventilation systems is equally important.

In a well-balanced and properly installed fan, the mechanical noise originating from bearings and vibration of various parts is not as prominent as the aerodynamically generated noise. The latter is due to the various flow phenomena occurring within the fan.

Noise in an open (extended turbomachine) fan rotor is generated due to the rotating pressure field.

Blade wakes are unavoidable in turbomachines. Turbulence due to wake formation contributes significantly to fan noise. As the degree of turbulence increases with the flow velocity, a higher noise level is generated at higher fan speeds. Fans with separated flows, specially at off-design operation, generate more noise on account of a higher degree of turbulence.

The main causes of aerodynamically generated noise are:

1. the flow at the entry and exit of the fan, i.e., suction and exhaust noise,
2. rotation of blades through air or gas,

3. passage of blades through wakes,
4. turbulence of air,
5. shedding of vortices from blades, and
6. separation, stalling and surging.

Some parameters on which the noise level radiated from a fan depends are: fan aerodynamic performance, duct configurations at the entry and exit, housing geometry, relative number of rotor and guide blades, magnitudes of clearances, blade thicknesses and fan speed.

The frequencies and noise levels that occur in fans and blowers are of the order of 65–8000 Hz and 60–120 dB. In comparison to these values, the approximate noise levels in bedrooms and offices are 40 and 50 dB respectively.

Some methods of reducing fan noise are:

1. operation of fans at their maximum efficiencies,
2. use of low speed and low pressure fans,
3. employment of uniform flow in ducts,
4. use of flexible fan mounting,
5. use of sound absorbing walls; ducts should also be lined by sound absorbing material,
6. use of silencers at the suction and exhaust,
7. reinforcing fan casings,
8. use of a larger clearance between the volute tongue and the rotor in centrifugal fans; the same applies to the clearance between the rotor and guide blade rings, and
9. enclosing the fan in a sound absorbing casing; the internal surface of the casing must be lined with a sound absorbing material.

15.10 Dust Erosion of Fans

Minor erosion of fan parts due to the presence of dust is quite common. However, in some applications, erosion of fan blades and casings due to dust-laden air is very serious. This is one of the causes of failure of ID fans in steam power stations.

Steam power stations cannot always burn the ideal quality of coal. Ash contents are sometimes as high as 40 per cent. Besides this, the dust-removing equipment may allow an appreciable quantity of solid particles to escape into the ID fan. This happens particularly at low temperatures. Thus the principle of "prevention is better than cure" cannot be practically applied here.

When dust particles directly hit the moving blades, they cause cracking of the blades, whereas the flow of abrasive dust through the passages causes scrapping action leading to surface erosion. Some aspects of dust erosion are given below.

(a) The worn-out blade surfaces alter the geometry of the flow far from the design. This is reflected in poor fan performance.

(b) If considerable erosion has occurred in highly stressed regions, the affected part can suddenly fail after some time.

(c) The wear of the rotor due to dust erosion is not axisymmetric. This leads to an imbalance of the rotor and increases the load on bearings.

(d) The imbalance and the resulting vibration are further increased due to the collection of dust in the pockets created by dust erosion.

Dust particles collect in the stalled regions of the fan where they erode the surface by a milling action.

In view of the erosion problems, the selection of the right type of fan is important. However, a fan which suffers least due to erosion may not always be the best choice for a given application. Dust erosion has been found to be inversely proportional to the pressure coefficient. Centrifugal types have been generally found to run without serious dust erosion problems five time longer than the axial type.

It has been found that erosion is more serious in axial type fans compared to the centrifugal type. This is due to the geometrical configuration and lower gas velocities in the centrifugal type.

Dust erosion can be minimized by:

1. employing a more efficient dust removing apparatus,
2. regulating fan speeds at part loads,
3. reducing stratification,
4. employing large and low speed fans, and
5. providing erosion shields on the blades.

Notation for Chapter 15

A	Areas of cross-section
b	Blade length or impeller width
c	Absolute fluid velocity
c_p	Specific heat at constant pressure
d, D	Diameter
g	Acceleration due to gravity

h	Enthalpy
Δh	Change in enthalpy
H	Head
$\dot{m}$	Mass-flow rate
N	Speed in rpm
p	Pressure
Δp	Pressure rise
P	Power
Q	Volume-flow rate
R	Degree of reaction, gas constant
t	Blade thickness, temperature
T	Absolute temperature
u	Tangential speed
v	Specific volume
w	Relative velocity or specific work
z	Number of rotor blades

Greek symbols

α	Direction of absolute velocity
β	Direction of relative velocity
η	Efficiency
ρ	Fluid density
ϕ	Flow coefficient
ψ	Pressure coefficient
ω	Rotational speed in rad/s

Subscripts

o	Stagnation value, overall
1	Impeller entry
2	Impeller exit
f	Fan
i	Ideal, inlet
r	Rotor or impeller, radial
st	Stage
θ	Tangential

Solved Examples

15.1 A centrifugal fan has the following data:

inner diameter of the impeller	18 cm

outer diameter of the impeller	20 cm
speed	1450 rpm

The relative and absolute velocities respectively are

at entry	20 m/s, 21 m/s
at exit	17 m/s, 25 m/s
flow rate	0.5 kg/s
motor efficiency	78%

Determine:

(a) the stage pressure rise,
(b) degree of reaction, and
(c) the power required to drive the fan.

Take density of air as 1.25 kg/m^3

***Solution*:**

$$u_1 = \pi d_1 N/60 = \frac{\pi \times 0.18 \times 1450}{60} = 13.66 \text{ m/s}$$

$$u_2 = \pi d_2 N/60 = \frac{\pi \times 0.20 \times 1450}{60} = 15.184 \text{ m/s}$$

$$\frac{1}{2}(u_2^2 - u_1^2) = 0.5\,(15.184^2 - 13.66^2) = 22.0 \text{ J/kg}$$

$$\frac{1}{2}(w_1^2 - w_2^2) = 0.5\,(20^2 - 17^2) = 55.5 \text{ J/kg}$$

$$\frac{1}{2}(c_2^2 - c_1^2) = 0.5\,(25^2 - 21^2) = 92.0 \text{ J/kg}$$

The static pressure rise in the rotor is

$$(\Delta p)_r = \frac{1}{2}\rho(u_2^2 - u_1^2) + \frac{1}{2}\rho(w_1^2 - w_2^2)$$

$$(\Delta p)_r = 1.25\,(22.0 + 55.5) = 96.875 \text{ N/m}^2$$

The total pressure rise across the stage is

$$(\Delta p_0)_{st} = \frac{1}{2}\rho\{(u_2^2 - u_1^2) + (w_1^2 - w_2^2) + (c_2^2 - c_1^2)\}$$

$$(\Delta p)_{st} = 1.25\,(22.0 + 55.5 + 92.0) = 211.875 \text{ N/m}^2$$

(a) The stage pressure rise is

$$(\Delta p_0)_{st} = 211.875/9.81 = 21.59 \text{ mm W.G. } (\textit{Ans.})$$

(b) The degree of reaction is

$$R = (\Delta p)_r/(\Delta p_0)_{st}$$

$$R = 96.875/211.875 = 0.457 \text{ (}Ans.\text{)}$$

(c) The Eulerian work is equal to the stage work,

$$w_{st} = \frac{1}{2}(u_2^2 - u_1^2) + \frac{1}{2}(w_1^2 - w_2^2) + \frac{1}{2}(c_2^2 - c_1^2)$$

$$w_{st} = 22.0 + 55.5 + 92.0 = 169.5 \text{ J/kg}$$

Therefore, the motor power required to drive the fan is

$$P = \dot{m}\, w_{st}/\eta$$

$$P = 0.5 \times 169.5/0.78 = 108.65 \text{ W } (Ans.)$$

15.2 A centrifugal blower with a radial impeller produces a pressure equivalent to 100 cm column of water. The pressure and temperature at its entry are 0.98 bar and 310 K. The electric motor driving the blower runs at 3000 rpm. The efficiencies of the fan and drive are 82% and 88% respectively. The radial velocity remains constant and has a value of $0.2u_2$. The velocity at the inlet eye is $0.4u_2$.

If the blower handles 200 m^3/min of air at the entry conditions, determine:

(a) power required by the electric motor,
(b) impeller diameter,
(c) inner diameter of the blade ring,
(d) air angle at entry,
(e) impeller widths at entry and exit,
(f) number of impeller blades, and
(g) the specific speed.

***Solution*:**

(a) Ideal power $= Q\,\Delta p_0/1000$

$$Q = 200/60 = 3.333 \text{ m}^3/\text{s}$$

$$P_i = \frac{3.333 \times 1000 \times 9.81}{1000} = 32.699 \text{ kW}$$

Actual power $= 32.699/0.82 \times 0.88$

$$P = 45.3 \text{ kW } (Ans.)$$

$$\rho = \frac{p}{RT} = \frac{0.98 \times 10^5}{287 \times 310} = 1.10 \text{ kg/m}^3$$

(b) For a radial impeller,

$$\Delta p_0/\rho\, \eta_f = u_2^2$$

$$u_2^2 = 1000 \times 9.81/1.10 \times 0.82 = 10875.83$$

$$u_2 = 104.28 \text{ m/s}$$

$$\pi\, d_2\, N/60 = u_2$$

$$d_2 = \frac{104.28 \times 60}{\pi \times 3000} = 0.664 \text{ m}$$

$$d_2 = 66.4 \text{ cm } (Ans.)$$

$$c_{r1} = c_{r2} = 0.2u_2 = 0.2 \times 104.28 = 20.856 \text{ m/s}$$

$$c_i = 0.4u_2 = 0.4 \times 104.28 = 41.71 \text{ m/s}$$

$$\left(\frac{\pi}{4} d_i^2\right) c_i = Q = 3.333 \text{ m}^3/\text{s}$$

$$d_i^2 = 3.333 \times 4/\pi \times 41.71 = 0.1017$$

$$d_i = 0.319 \text{ m} = 31.9 \text{ cm}$$

$$d_1 = d_i = 31.9 \text{ cm } (Ans.)$$

(d) $$u_1 = u_2 \left(\frac{d_1}{d_2}\right) = \frac{104.28 \times 31.9}{66.4} = 50.1 \text{ m/s}$$

$$\tan \beta_1 = \frac{c_{r1}}{u_1} = \frac{20.856}{50.1} = 0.416$$

$$\beta_1 = 22.6° \ (Ans.)$$

(e) $$c_{r1}\, (\pi\, d_1\, b_1) = Q$$

$$b_1 = Q/c_{r1}\, \pi\, d_1$$

$$b_1 = \frac{3.333 \times 100}{20.856\, \pi \times 0.319} = 15.95 \text{ cm } (Ans.)$$

$$b_2 = b_1\, d_1/d_2 = \frac{15.95 \times 31.9}{66.4} = 7.66 \text{ cm } (Ans.)$$

(f) $$z = \frac{8.5 \sin \beta_2}{1 - d_1/d_2} = \frac{8.5}{1 - 31.9/66.4} = 16.35$$

Therefore, the number of blades can be taken as seventeen, i.e.

$$z = 17 \ (Ans.)$$

(g) The head produced by the blower is

$$gH = u_2^2 = 10875.83 \text{ m}^2/\text{s}^2$$

$$\omega = \frac{2\pi\, N}{60} = \frac{2\pi \times 3000}{60} = 314.16 \text{ rad/s}$$

The specific speed is

$$\Omega = \frac{\omega \sqrt{Q}}{(gH)^{3/4}}$$

$$\Omega = \frac{314.16 \sqrt{3.333}}{(10875.83)^{3/4}} = 0.538 \ (Ans.)$$

Questions and Problems

15.1 Describe briefly with the aid of illustrative sketches five applications of centrifugal blowers.

15.2 What are the advantages and disadvantages of employing sheet metal blades in centrifugal fans and blowers? Give three applications where you would recommend their use.

15.3 How does dust erosion of centrifugal impellers occur? What is its effect on the performance?

15.4 (a) Derive an expression for the degree of reaction of a centrifugal fan or blower in terms of the flow coefficient and the impeller blade exit angle. Show graphically the variation of the degree of reaction with the exit blade angle.

(b) Show that $\psi_{st} = 4(1 - R)$

15.5 Draw inlet and outlet velocity triangles for a general centrifugal fan impeller. Show that the static pressure rise in the impeller and the degree of reaction are given by

$$(\Delta p)_r = \frac{1}{2} \rho (2 u_2 c_{\theta 2} - c_{\theta 2}^2)$$

$$R = 1 - \frac{1}{2} \frac{c_{\theta 2}}{u_2}$$

Hence, show that for an impeller with radial-tipped blades

$$(\Delta p)_r = \frac{1}{2} \rho u_2^2$$

$$R = 1/2$$

$$\psi_{st} = 2$$

15.6 What are the various methods employed to drive centrifugal blowers? State their merits. How is the impeller mounted in each case?

15.7 (a) Draw inlet and outlet velocity triangles for a radial-tipped blade impeller. Explain why the leading edges of such blades point in the direction of motion?

(b) Show that for a general centrifugal fan

$$\psi_{st} = \frac{2}{1 + \tan \alpha_2 / \tan \beta_2}$$

Hence show that

$$\psi_{st} = 2 \text{(for radial-tipped blade impeller)}$$

15.8 A centrifugal blower takes in 180 m^3/min of air at $p_1 = 1.013$ bar and $t_1 = 43°C$, and delivers it at 750 mm W.G. Taking the efficiencies of the blower and drive as 80% and 82%, respectively, determine the power required to drive the blower and the state of air at exit.

Ans.: 32.66 kW; $p_2 = 1.094$ bar; and $T_2 = 324$ K

15.9 A backward-swept centrifugal fan develops a pressure of 75 mm W.G. It has an impeller diameter of 89 cm and runs at 720 rpm. The blade air angle at tip is 39° and the width of the impeller 10 cm.

Assuming a constant radial velocity of 9.15 m/s and density of 1.2 kg/m^3, determine the fan efficiency, discharge, power required, stage reaction and pressure coefficient.

(*Ans.*) $\eta_f = 82.16\%$; $Q = 2.558$ m^3/s; $P = 2.29$ kW; $R = 66.8\%$; and $\psi_{st} = 1.328$

15.10 A backward-swept ($\beta_2 = 30°$, $d_2 = 46.6$ cm) centrifugal fan is required to deliver 3.82 m^3/s (4.29 kg/s) of air at a total pressure of 63 mm W.G. The flow coefficient at the impeller exit is 0.25 and the power supplied to the impeller is 3 kW. Determine the fan efficiency, pressure coefficient, degree of reaction and rotational speed. Would you recommend a double entry configuration for this fan?

(*Ans.*) $\eta_f = 78.7\%$; $\psi = 1.136$; $R = 71.6\%$; $N = 1440$ rpm; $b_2 = 29.7$ cm; and yes.

15.11 A fan running at 1480 rpm takes in 6 m^3/min of air at inlet conditions of $p_1 = 950$ mbar and $t_1 = 15°C$. If the fan impeller diameter is 40 cm and the blade tip air angle 20°, determine the total pressure developed by the fan and the impeller width at exit. Take the radial velocity at the exit as 0.2 times the impeller tip speed. State the assumptions used.

Ans.: $\Delta p_0 = 50.76$ mm W.G; and $b_2 = 1.28$ cm.

Chapter 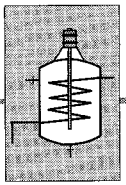 16

Wind Turbines

Wind is air in motion. Windmills or wind turbines convert the kinetic energy of wind into useful work.

It is believed that the annual wind energy available on earth is about 13×10^{12} kWh. This is equivalent to a total installed capacity of about 15 $\times 10^5$ MW or 1500 power stations each of 1000 MW capacity. While the power that could be tapped out from the vast sea of wind may be comparable with hydropower, it should be remembered that it is available in a highly diluted form. Therefore, while dams are built to exploit and regulate hydropower, there is no such parallel on the wind power scene.[628–653]

Wind had been used as a source of power in sailing ships for many centuries. The force that acted on ship's sail was later employed to turn a wheel like the water wheel which already existed. The wind-driven wheel first appeared in Persia in the seventh century A.D. By tenth century A.D., windmills were used for pumping water for irrigation and by thirteenth century A.D. for corn grinding.

The corn grinding mill was a two-storey structure; the mill stone was located in the upper storey and the lower storey consisted of a sail rotor. It consisted of six or twelve fabric sails which rotated the mill by the action of the wind. Shutters on the sails regulated the rotor speed. In 1592 A.D. the windmill was used to drive mechanical saws in Holland. A large Dutch windmill of the eighteenth century with a 30.5 m sail span developed about 7.5 kW at a wind velocity of 32 kmph.

The energy of flowing water and wind was the only natural source of mechanical power before the advent of steam and internal combustion engines. Therefore, windmills and watermills were the first prime movers which were used to do small jobs, such as corn grinding and water pumping. It is generally believed that the windmill made its appearance much later than the watermill.

The watermills had to be located on the banks of streams. Therefore, they suffered from the disadvantage of limited location. In this respect windmills had greater freedom of location. If sufficient wind velocities were available over reasonable periods, more important factors in choosing a site for the windmill would be the transportation of corn for grinding and the site for water pumping.

In both wind and water turbine plants the working fluid and its energy are freely available. Though there are no fuel costs involved, other expenditures in harnessing these forms of energy are not negligible. The capital cost of some wind power plants can be prohibitive. As in other power plants, the cost per unit of energy generated decreases as the size of the wind turbine increases.

Medium-sized (100-200 kW, d $\simeq$ 20 m) wind turbines are suitable for electric power requirements of isolated areas in hills and small islands where other sources of power may be non-existent or difficult to install and operate. The use of some form of an energy storage system can take care of the random nature of the wind energy.

Large wind power plants of capacities of a couple of megawatts can be connected to the main network fed by thermal and hydrostations. In such a system wind energy can be utilized for saving fuel and water.

Compared to other well-established sources of energy, the wind energy at present appears to be insignificant as far as the contribution to the total energy requirement is concerned. However, at a time when mankind is facing an energy crisis, every source, however small, should be tapped.

16.1 Elements of a Wind Power Plant[654–705]

A windmill or turbine is an extended turbomachine (Sec. 1.8, Fig. 1.8) operating at comparatively lower speeds. A wind turbine power plant consists of, principally, the propeller or rotor, step-up gear, an electric generator and the tail vane, all mounted on a tower or mast. The actual design will depend upon the size of the plant and its application.

Various elements of a wind turbine power plant are described here briefly.

Rotor

The shape, size and number of blades in a wind turbine rotor depend on whether it is a horizontal or vertical axis machine. The number of blades generally varies from two to twelve. A high speed rotor requires fewer blades to extract the energy from the wind stream, whereas a slow machine requires a relatively larger number of blades. Figures 16.1 to 16.3 show some types of rotors. Further details of the horizontal and vertical axis machines are discussed in Secs. 16.5 and 16.6.

In horizontal axis machines two-bladed rotors are known to have greater vibration problems compared to three blades. The blade design is based on the same lines as for axial propeller fans described in Sec. 14.5.

In wind turbine rotors blades are subjected to high and alternating stresses. Therefore, the blades must have sufficient strength and be light.

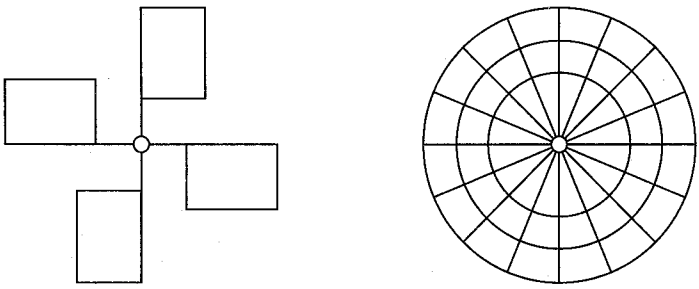

(a) Sail rotor (b) Multi-bladed rotor

Fig. 16.1 Horizontal axis windmills

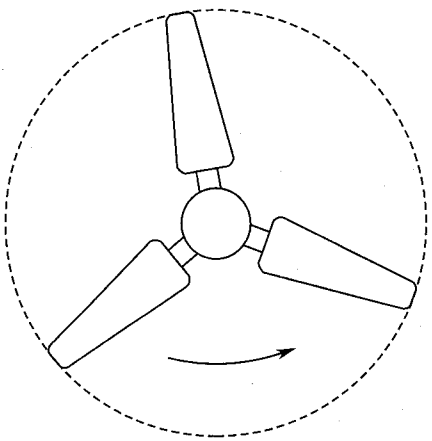

Fig. 16.2 Propeller of a horizontal axis windmill

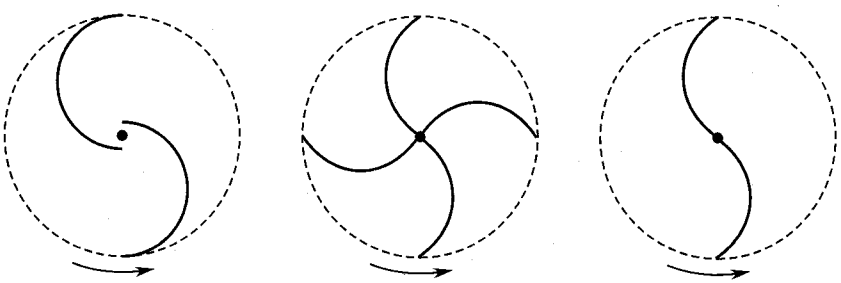

Fig. 16.3 Savonius rotors (vertical axis machines)

Thus the strength-to-density ratio of the material used is an important factor.

Wood is widely used for small high-speed machines. It has the required strength-density ratio.

Various metals and their alloys are also used. Small blades are cast. Plastic materials are now also making inroads into the manufacture of wind machines. They have high strength-density ratio, offer great ease in manufacture and are also weather resistant.

Step-up gear

On account of the great difference in rotational speeds of the wind turbine rotor (which is generally low) and the machine that it drives, a step-up gear for obtaining the required high speed is generally employed between the driving and driven shafts. This invariably takes the form of a gearing arrangement consisting of one or more gear trains. The entire gearing arrangement must have high efficiency and reliability coupled with light weight.

Belts and chains have not been employed as widely as the gearing.

Speed-regulating mechanism

From aerodynamic considerations, it is desirable to operate a wind turbine at a constant blade-to-wind speed ratio. However, in many applications a mechanism to maintain the speed of the wind turbine constant at varying wind velocities and loads is required.

A propeller type of pump and a hydraulic brake (water paddle for producing hot water) are excellent speed governers themselves. Speed regulation can be obtained for both fixed and variable pitch blades.

The mechanism for variable pitch blades is the same as that used in Kaplan hydroturbines or aircraft propellers. The variable pitch mechanism enables the rotor to operate most efficiently at varying wind velocities and in feathering during gusts.

The centrifugal force acting on the blades at speeds higher than the design is also employed to change the blade pitch. This can also be achieved by a fly-ball governor.

Electric generator

Besides driving pumps and corn grinding mills, wind turbines are now being increasingly used for driving electric generators or 'aerogenerators' as they are sometimes called. These aerogenerators are both direct and alternating current machines and are available from a capacity of a few watts to hundreds of kilowatts.

The direct current machines operate in a considerable speed range, whereas the alternating current generator with constant frequency requires constant speed.

For small isolated communities, some kind of energy storage is always required. This is best met by dc generators feeding a battery of accumulators during low load and high wind periods.

To minimize weight, aerogenerators must operate at high speeds which depend on the type of the wind turbine (blade-to-wind speed ratio) and the weight of the step-up gear.

When the speed of the wind turbine is low, multi-pole sychronous alternators are used. But the large number of poles increases the weight of the aerogenerators. However, such a machine is acceptable if it eliminates the speed-up gear by using higher blade-to-wind speed ratios.

When an alternator is directly coupled to an ac network, its speed is nearly constant. Such a generator can be designed for sufficient overload capacity to absorb the wind energy available at high wind velocities.

Orientation mechanism

A horizontal axis wind turbine requires a mechanism which turns the rotor into the wind stream. The working of the vertical axis machines does not depend on the wind direction and, therefore, an orientation mechanism is not required.

In primitive windmills the rotor was turned manually into the wind direction by a pole hanging from the tail. Modern wind turbines have sophisticated automatic mechanisms to obtain the orientation as and when required.

The simplest and most widely used method to orient small windmills in the wind direction is by employing a wind vane.

Another method is to employ an automatic direction finding and orienting mechanism. This is relatively faster.

A fan-tail whose axis of rotation is normal to the axis of the main rotor is also employed to turn the windmill into the wind stream. The cross wind drives the auxiliary rotor which in turn rotates the windmill into the wind through reduction gears. This is a slow mechanism.

Tower

All windmills have to be mounted on a stand or a tower above the ground level. Tower heights of over 250 m have been employed for obtaining high wind velocities and mounting large wind turbine rotors. Increasing the tower height, besides increasing the capital cost, also increases the maintenance cost. Therefore, the gain in the power output due to high wind velocity at a given altitude must be accurately estimated to justify the high costs. Economic and vibration problems are major factors in the design of towers for large wind turbines.

An angle iron tower of a four-sided pyramidal shape is commonly used. A similar structure constructed from metal pipings is also used. Towers have also been constructed from wood, brick and concrete.

16.2 Available Energy

The magnitude of the available energy in a wind stream during time T can be expressed by

$$E = K \int_0^T c^3 \, dt \tag{16.1}$$

The factor K depends on the density of air, and efficiency and size of the wind turbine; c is the instantaneous wind velocity.

A simple expression for power that can be generated in a wind stream of constant velocity $\bar{c}$ is written here.

The mass-flow rate in a wind stream passing through a wind turbine of swept area A is

$$\dot{m} = \rho A \, \bar{c} \tag{16.2}$$

The mean wind velocity assumed constant here for a period of time T, is given by

$$\bar{c} = \frac{1}{2} \int_0^T c \, dt \tag{16.3}$$

The kinetic energy in the wind stream is $\frac{1}{2}\bar{c}^2$ per unit flow rate. However, only a fraction of this quantity will be absorbed by a wind machine. Betz[657] of Gottingen has shown (Sec. 16.5) that the maximum energy that can be recovered from the wind is

$$\frac{16}{27}\left(\frac{1}{2}\bar{c}^2\right) = 0.593\left(\frac{1}{2}\bar{c}^2\right)$$

Therefore, the maximum power that a wind turbine can develop is

$$P_{\max} = 0.593\left(\frac{1}{2}\dot{m}\bar{c}^2\right) \tag{16.4}$$

Substituting from Eq. (16.2),

$$P_{\max} = 0.593\left(\frac{1}{2}\rho A \bar{c}^3\right) \tag{16.5a}$$

Assuming $\rho = 1.23$ kg/m^3 and expressing the power in kilowatts.

$$P_{\max} = 0.000364 \, A \, \bar{c}^3 \text{ kW} \tag{16.5b}$$

The above expression is an overestimate because of ignoring the efficiency factor. Therefore, assuming $\eta = 0.65$, this expression is modified to

$$P = 0.000237 \, A \, \bar{c}^3 \text{ kW} \tag{16.5c}$$

Writing this in terms of the propeller diameter

$$A = \frac{\pi}{4} d^2$$

$$P = 0.000186\ d^2 \bar{c}^3 \text{ kW} \qquad (16.5d)$$

Table 16.1 gives the values of power developed by propellers of various diameters at wind velocities from 10 to 50 kmph. It may be seen that the power increases more rapidly with an increase in the wind velocity than with the propeller size.

Table 16.1 Typical values of the power developed by various wind turbines at different wind velocities

($\rho = 1.23$ kg/m^3, $\eta = 0.65$)

Propeller diameter m	*Power in kW for wind velocities of*				
	10 kmph (2.78 m/s)	*20 kmph (5.56 m/s)*	*30 kmph (8.34 m/s)*	*40 kmph (11.12 m/s)*	*50 kmph (13.9 m/s)*
1	0.00355	0.0319	0.108	0.255	0.499
2	0.016	0.128	0.432	1.023	1.997
3	0.035	0.287	0.970	2.300	4.494
4	0.062	0.511	1.725	4.090	7.989
5	0.096	0.799	2.695	6.391	12.483
10	0.399	3.197	10.790	25.576	49.95
20	1.598	12.788	43.160	102.305	199.815
30	3.596	28.773	97.11	230.185	449.584
40	6.394	51.153	172.64	409.22	799.26
50	9.990	79.926	269.75	639.41	1249

A wind power plant has the maximum efficiency at its rated (design) wind velocity. However, on account of fluctuations in the wind, the efficiency will suffer.

The rated wind velocity is the lowest velocity at which the turbine develops its full power.

The minimum wind velocity below which a wind turbine would not produce useful output can be taken as 8 kmph (2.22 m/s). At the other end of the scale, wind power plants are uneconomic for wind velocities greater than 56 kmph (15.57 m/s).

Though it is difficult to prescribe the optimum propeller size for a wind turbine, it appears that the present-day technology favours diameters from 20 to 30 m.

16.3 Wind Energy Data

One of the major difficulties in exploiting wind energy is the inability to predict, even roughly, the characteristics of both the wind and the turbine in advance. This is on account of the wide variations with time during the year, location and the type of wind turbine employed. The picture is not so unpredictable with other sources of energy, including the hydro and the solar.

It would be uneconomical to install a wind power plant at a given site until encouraging wind energy data are available for it. Both long and short range records on wind behaviour (variation of velocity and direction with time, gust frequencies, velocities, durations, etc.) are required to justify the selection of a given site.

Data on wind energy can be collected and presented in numerous ways, all of which cannot be described here. There is no limit, even in the selection of stations, for wind energy surveys.

Elaborate and sophisticated wind-measuring instruments are required for generating data for the selection of a site and the design of a wind power plant. Tall masts have been used for this purpose at various prospective wind-measuring stations. Since wind power is proportional to the cube of the wind velocity, the power output of a wind turbine increases rapidly with its height above the ground. However, the cost of wind power plants and their maintenance also increase with height.

Figure 16.4 shows a typical curve depicting the variation of wind velocity with altitude. Buildings and trees cause a reduction in the wind velocity at lower altitudes. Velocity profiles at hill tops are governed by many other factors. Hill sites, specially near the sea-front, experience higher wind velocities. Isolated hills with steep and smooth slopes are ideal sites.

Very useful and basic information is obtained from records of the hourly wind velocity. Figure 16.5 shows the fluctuations of the diurnal mean wind velocity. Such curves for a given site can be plotted for various months as well as for the entire year.

The mean wind velocity is obtained from the total run (distance) of the wind during each hour. Wind velocity and power duration curves (Fig. 16.6) are also drawn from the knowledge of mean wind velocity profiles with time.

Figure 16.7 shows the variation of the annual specific output with the mean wind velocity for two wind power plants of rated mean speeds of 20 and 25 kmph. The plant corresponding to the lower value in this case runs for a longer time during the year giving a higher value of the annual specific output.

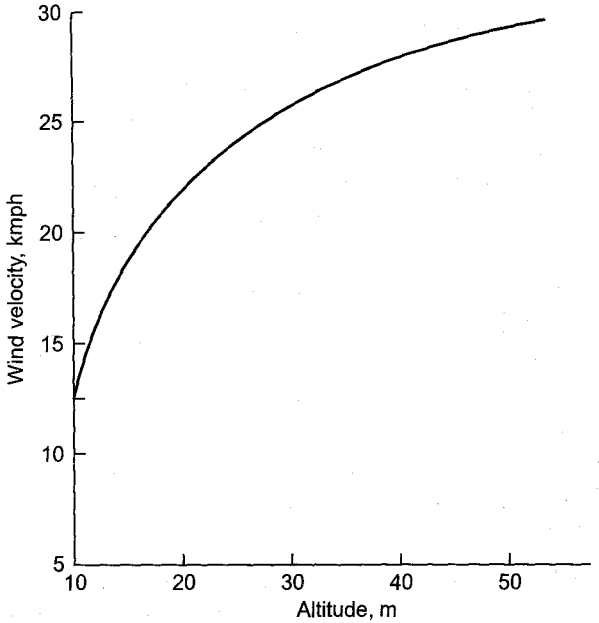

Fig. 16.4 Variation of wind velocity with height above ground (a typical curve)

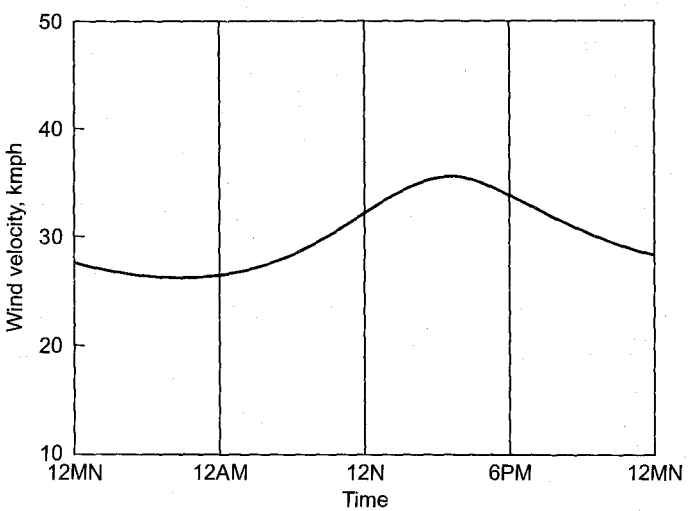

Fig. 16.5 Fluctuations in hourly wind velocity (typical curve)

Statistically, wind energy data does not vary significantly from year to year. The general characteristics of the wind at some proposed sites must be studied. Then a site with the most favourable characteristics is chosen in view of other factors discussed in the next section.

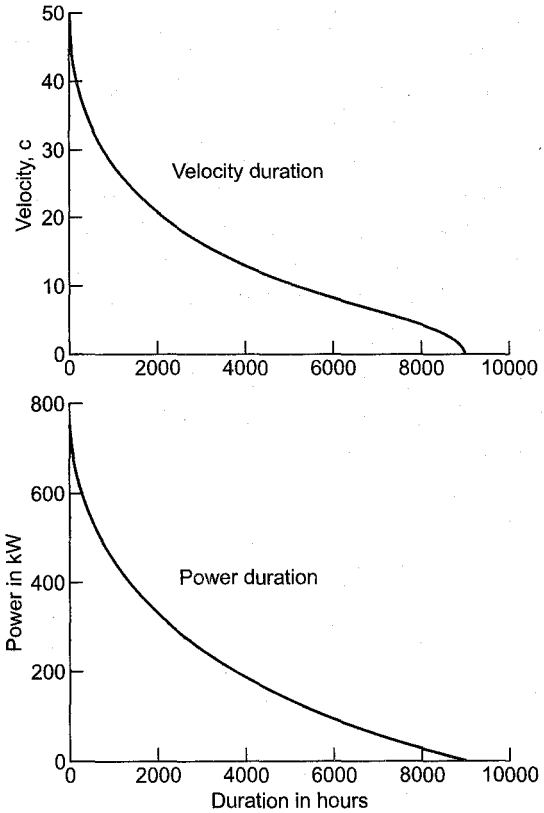

Fig. 16.6 Typical velocity and power duration curves

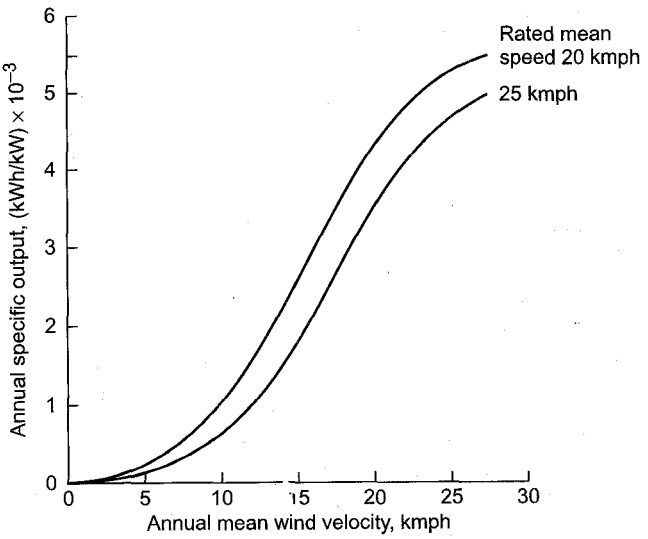

Fig. 16.7 Variation of the annual specific output with mean wind velocity (typical curves)

Besides the aforementioned factors, wind direction at a given site is also important. The 'prevailing wind' is the wind that blows more commonly in one direction than in other directions. The duration of the prevailing wind is estimated between 15 and 20 hours. Some sites experience winds consistently in one direction. Therefore, the wind machines installed at these sites need not have an orientation mechanism, leading to considerable simplification and economy.

The effect of direction on wind energy is best depicted by wind roses. Figure 16.8 shows a wind rose in which the lengths of the radial arms in various directions can represent:

(i) percentages of time during which the wind blows in various directions; sometimes the velocity range for which the percentage duration is plotted is specified, or

(ii) total run of wind in kilometres as percentages in various directions, or

(iii) wind energy in kWh/m^2.

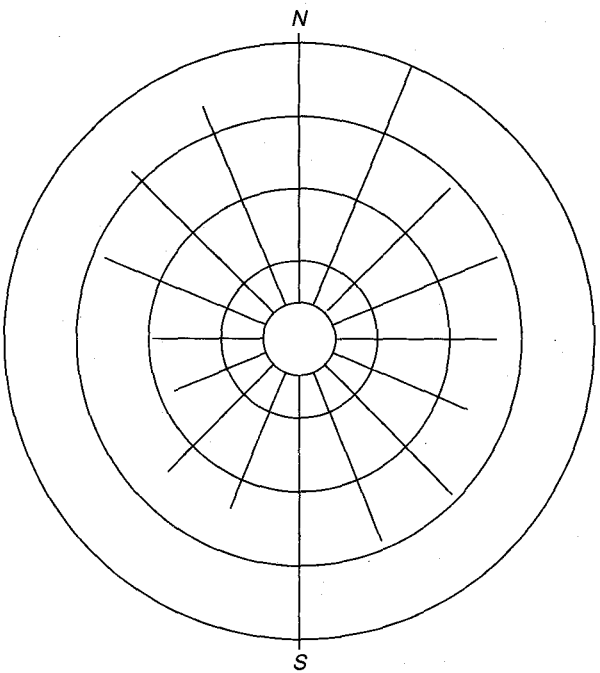

Fig. 16.8 Wind rose for wind duration, total run between specified velocities of wind energy in kWh/m^2

Diurnal, monthly and annual wind roses for a given site can provide useful information for wind energy utilization.

Gusts

A knowledge of the maximum gust velocities at the prospective wind power sites is also required to design the structures for maximum thrust.

A wind with five times the design velocity can be regarded as a gust. Maximum wind velocities of 240 kmph have been recorded. Some examples of gusts are given below:

Allahabad	159 kmph (44 m/s)
Godavari bridge	43.6 m/s
Juhu (Bombay)	45 m/s
St. Ann's Head, Pembrokshire	48.93 m/s

All wind machines must be provided with "feathering" arrangements which must stop them at wind velocities (furling velocities) likely to damage them.

Calm

Similarly, periods of calm also effect the entire wind energy system including the storage system. The wind velocity (cut in velocity) at which no useful output from the wind machine is obtained on account of low wind energy may be regarded as 8 kmph, as stated before. Periods when the wind velocities are less than 5 kmph may be regarded as "calm periods".

16.4 Selection of Site

Some important requirements for the site of a prospective wind power plant must be satisfied. A number of questions in this regard are answered by the analysis of the wind energy data collected over a long enough period.

Some of the major considerations for the selection of a site for a wind power plant are:

1. High value of the mean wind velocity.
2. Nature of surroundings: proximity of tall buildings, rocks and forests retard the wind.
3. Altitude and distance from the sea.
4. Topography.
5. Distance from the site of application, electrical load or main supply network.
6. Accessibility by rail or road; ease in construction of service road.
7. Quality of land for huge foundations.
8. Availability of local labour and building materials.

9. Possibility of installing a number of windmills in the same area. A minimum distance of eight diameters of the propeller is required downwind before the next windmill. A cluster of windmills leads to economical transmission of power and transportation of material, and maintenance.
10. Icing problems.

16.5 Horizontal Axis Wind Turbines

There is considerable similarity between the flow patterns of a propeller fan (Sec. 14.5, Fig. 14.15) and a horizontal axis wind turbine (Figs. 16.2, 16.9). The fan propeller imparts energy to the flow, whereas the wind turbine rotor absorbs energy from the wind.

In the slip stream theory the windmill rotor is considered equivalent to a disc of negligible thickness. The wind velocities far upwind and downwind of the disc are c_u and c_d. As the wind stream approaches the disc, its velocity continuously decreases accompanied by a static pressure rise. The presence of the wind turbine rotor disc develops a back pressure upwind of the disc as shown in Fig. 16.9. This causes a small pressure drop through the propeller.

The pressure and velocity variations in the region of flow near the propeller disc are shown in the figure. The pressure and velocity variations upwind and downwind of the disc are governed by the Bernoulli equation.

Expressions for the power developed and the thrust are derived here with the same assumptions as stated in Sec. 14.5.1 for propeller fans.

Power developed

The velocities at the disc and immediately upwind and downwind are the same.

$$c = c_1 = c_2 \tag{16.6}$$

The area of cross-section of the disc is

$$A = \frac{\pi}{4} d^2$$

and the mass flow rate through it is

$$\dot{m} = \rho A c \tag{16.7}$$

The axial thrust on the disc due to change of momentum of the wind through it is

$$F_x = \dot{m} (c_u - c_d) = \rho A c (c_u - c_d) \tag{16.8}$$

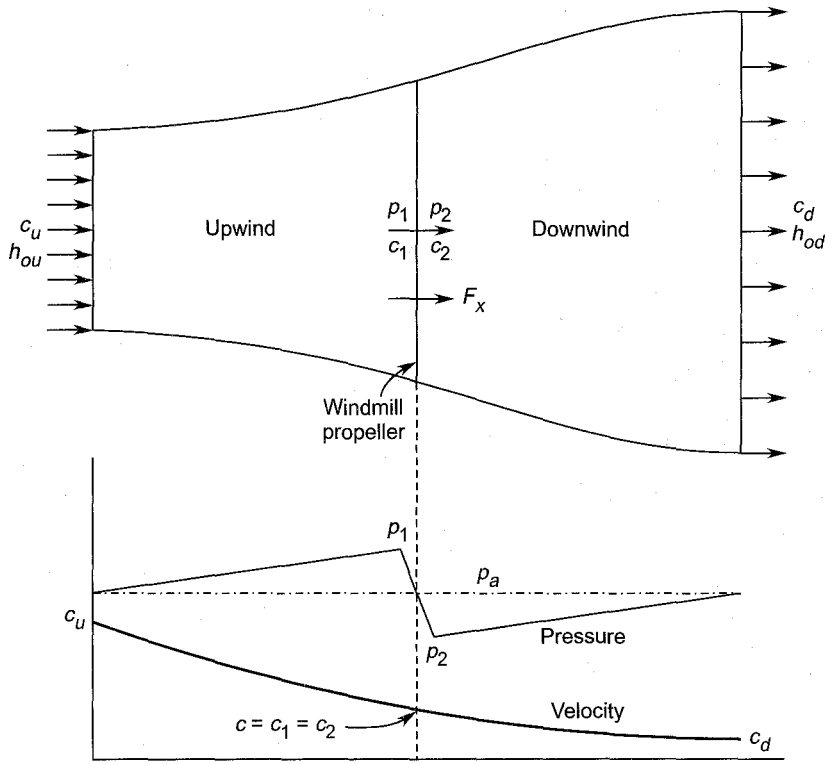

Fig. 16.9 Flow through a windmill propeller disc

From the Bernoulli equation, we have for flows upwind and downwind of the disc:

$$p_a + \frac{1}{2}\rho c_u^2 = p_1 + \frac{1}{2}\rho c^2 \tag{16.9}$$

$$p_a + \frac{1}{2}\rho c_d^2 = p_2 + \frac{1}{2}\rho c^2 \tag{16.10}$$

$$p_1 - p_2 = \frac{1}{2}\rho (c_u^2 - c_d^2) \tag{16.11}$$

The axial thrust due to the static pressure difference across the disc is

$$F_x = A (p_1 - p_2)$$

Substituting from Eq. (16.11)

$$F_x = \frac{1}{2}\rho A (c_u^2 - c_d^2) \tag{16.12}$$

Comparing Eqs. (16.8) and (16.12)

$$c = \frac{1}{2}(c_u + c_d) \tag{16.13}$$

The change in the specific stagnation enthalpy across the rotor disc is

$$\Delta h_0 = h_{0u} - h_{0d} = \left(h_u + \frac{1}{2} c_u^2\right) - \left(h_d + \frac{1}{2} c_d^2\right)$$

However, $h_u = h_d$. Therefore,

$$\Delta h_0 = \frac{1}{2} (c_u^2 - c_d^2) \tag{16.14}$$

The power absorbed (or developed) by the windmill propeller is given by
Power = mass flow rate × change in specific stagnation enthalpy.
Equations (16.7) and (16.14) give

$$P_i = \dot{m}\, \Delta h_0$$

$$P_i = \frac{1}{2} \rho A c\, (c_u^2 - c_d^2) \tag{16.15}$$

Substituting from Eq. (16.13)

$$P_i = \frac{1}{4} \rho A\, (c_u + c_d)\, (c_u^2 - c_d^2)$$

$$P_i = \frac{1}{4} \rho A\, (c_u + c_d)^2\, (c_u - c_d)$$

Let $$x = \frac{c_d}{c_u}$$

$$P_i = \frac{1}{4} \rho A\, c_u^3\, (1 + x)^2\, (1 - x) \tag{16.16}$$

For given values of ρ, A and c_u, the ideal value of the power developed is a function of the ratio x. Thus an optimum value of x can be determined.

$$\frac{\partial}{\partial x} \{(1 + x)^2\, (1 - x)\} = 0$$

$$3x^2 + 2x - 1 = 0$$

$$(x + 1)\, (3x - 1) = 0 \tag{16.17}$$

This yields two values of x of which the valid value is

$$x = \frac{c_d}{c_u} = \frac{1}{3} \tag{16.18}$$

Equation (16.18), when put into Eq. (16.13), gives

$$c = \frac{2}{3} c_u \tag{16.19}$$

Substituting from Eq. (16.18) in Eq. (16.16) and simplifying

$$P_i = \frac{8}{27} \rho A\, c_u^3 = \frac{16}{27}\left(\frac{1}{2} \rho A\, c_u^3\right) \tag{16.20}$$

This is the ideal or maximum power, ignoring the aerodynamic and mechanical losses in the wind turbine stage. The power of the upwind stream is

$$p_u = \frac{1}{2} \rho A c_u^3 \tag{16.21}$$

Thus a power coefficient for the windmill can be defined by

$$C_{P\max} = \frac{P_i}{P_u} = \frac{16}{27} = 0.593 \tag{16.22}$$

The actual power coefficient will be much lower than this value on account of losses.

Axial thrust

In the design and construction of large windmills, the axial thrust is also an important quantity. Massive structures and foundations are required for windmills subjected to a high axial thrust.

Equation (16.8) for axial thrust is

$$F_x = \rho A c (c_u - c_d)$$

Substituting from Eq. (16.13)

$$F_x = \frac{1}{2} \rho A c_u^2 (1 + x)(1 - x) \tag{16.23}$$

For maximum power (x = 1/3)

$$F_x = \frac{4}{9} \rho A c_u^2 \tag{16.24}$$

The thrust exerted during gusts will be much higher than this value. Therefore, the structural design is based on the maximum gust speed expected at a given site.

Efficiency

Horizontal axis windmills have propeller blades of considerable length with varying blade section along the length. Thus the best way to consider the power output and efficiency of such machines is to write down expressions for an infinitesimal section of the blade at a given radius, where the peripheral speed is $u = \omega r$.

Figure 16.10 shows the flow of wind through a blade element of a propeller shown in Fig. 16.2. The wind approaches the blade element axially at a velocity c. The relative velocity w is the vector difference of c and u and makes an angle ϕ with the axial direction.

The forces acting on the blade element are also shown in the figure. The resultant of lift and drag forces is F_r; the axial and tangential components of this resultant force are F_x and F_y.

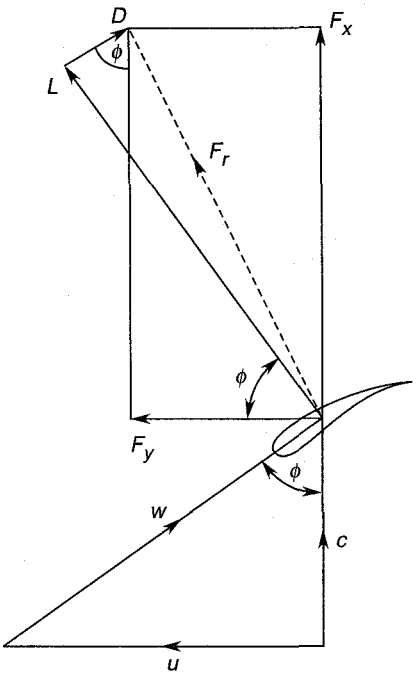

Fig. 16.10 Flow through a blade element of a windmill propeller

The velocity triangle gives the blade-to-wind velocity ratio as

$$\sigma = \frac{u}{c} = \tan \phi \tag{16.25}$$

The lift and drag forces are defined by

$$L = C_L \frac{1}{2} \rho A w^2$$

$$D = C_D \frac{1}{2} \rho A w^2$$

The lift and drag coefficients for a given element depend on the incidence, blade geometry and the Reynolds number.

By resolving forces in the axial and tangential directions

$$F_x = L \cos (90 - \phi) + D \cos \phi = L \sin \phi + D \cos \phi \tag{16.26}$$

$$F_y = L \cos \phi - D \cos (90 - \phi) = L \cos \phi - D \sin \phi \tag{16.27}$$

The efficiency of the blade element is the ratio of the rate of work done on the blade and the energy input rate.

$$\eta = \frac{F_y u}{F_x c}$$

Substituting from Eqs. (16.25), (16.26) and (16.27)

$$\eta = \frac{L\cos\phi - D\sin\phi}{L\sin\phi + D\cos\phi}\tan\phi$$

$$\eta = \frac{1 - \frac{D}{L}\tan\phi}{1 + \frac{D}{L}\cot\phi} \tag{16.28a}$$

$$\eta = \frac{1 - \frac{C_D}{C_L}\tan\phi}{1 + \frac{C_D}{C_L}\cot\phi} \tag{16.28b}$$

$$\eta = \frac{1 - \frac{C_D}{C_L}\sigma}{1 + \frac{1}{\sigma}\frac{C_D}{C_L}} \tag{16.28c}$$

Equation (16.28c) shows that the efficiency of the blade element depends on the lift-to-drag ratio and the blade-to-wind velocity ratio. The efficiency approaches unity when the lift-to-drag ratio is infinitely large.

Efficiency suffers at very low and high values of the ratio $\sigma = u/c$. Thus, in practice, there is an optimum value (σ_{opt}) for every windmill as shown in Fig. (16.11). For a constant speed machine, this ratio can be

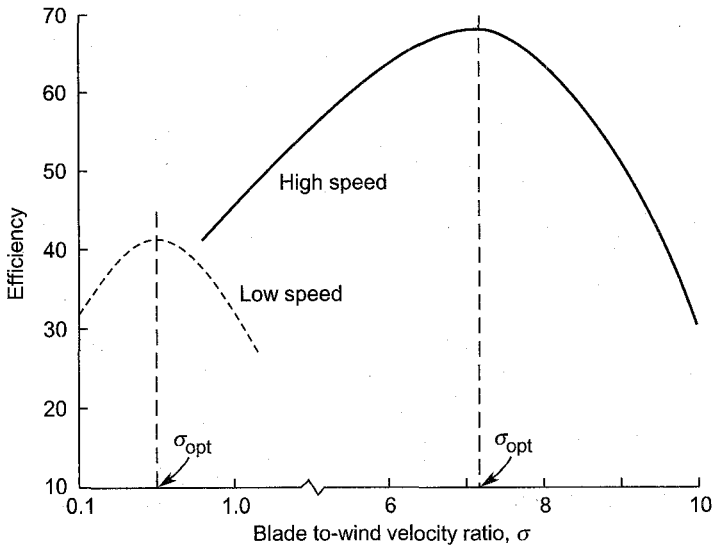

Fig. 16.11 Variation of wind turbine efficiency with blade-to-wind velocity ratio (typical curves)

maintained only at the rated mean wind velocity. However, the windmill will have to operate away from σ_{opt} at different wind velocities.

On account of a relatively very large swept area, the propeller type windmill captures a large quantity of wind energy. Besides this, it operates at higher speeds requiring a lighter step-up gear, has a higher efficiency and a higher power coefficient. The ability to vary the blade pitch when required is also a special advantage.

Horizontal axis windmills in small sizes can also be designed on the lines of a cross-flow fan (Sec. 15.5.2; Fig. 15.11) and paddle wheel. However, such machines have very poor efficiency and are mechanically unsuitable.

16.6 Vertical Axis Wind Turbines

Wind machines which generate power from the wind energy through a vertical axis rotor form a separate class of machines. Panemones, savonius rotors, cup anemometers and Darrieus turbines fall into this category.

Unlike horizontal axis machines, they do not need orientation mechanism. The torque generating surfaces move in the direction of the wind. Therefore, the blade speeds are always less than that of the wind. Thus the speeds of the vertical axis wind turbines are much lower compared to the horizontal axis type. Another limitation of this type is the movement of blades against the wind during half the revolution. Thus the rotor blades have to do work on the wind leading to a considerable reduction in the power output. This can be improved by providing a blanking arc as shown in Fig. 16.12.

For large power the rotor has to be very tall which is difficult to protect from the enormous wind pressures during gusts. Therefore, vertical axis turbines are suitable for relatively low power requirements.

Figure 16.12 shows the action of wind on a panemone. Since the wind and the blades are moving in the same direction, the relative velocity of the wind is

$$w = c - u$$

Therefore, the tangential force acting on the blades is given by

$$F_y = C_F \frac{1}{2} \rho A w^2 = C_F \frac{1}{2} \rho A (c - u)^2 \qquad (16.29)$$

C_F is a coefficient which depends on the type of blades, size of the machine, etc.

The power developed is

$$P = F_y u = C_F \frac{1}{2} \rho A (c - u)^2 u$$

$$P = C_F \frac{1}{2} \rho A c^3 (1 - \sigma)^2 \sigma \tag{16.30}$$

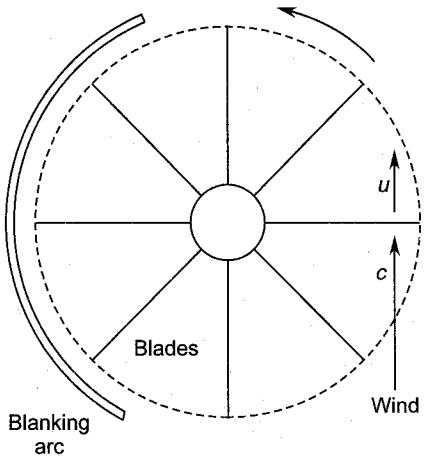

Fig. 16.12 Power generation by a vertical axis wind turbine (panemone)

The optimum value (for maximum power) of the blade-to-wind velocity ratio can be determined.

$$\frac{\partial P}{\partial \sigma} = C_F \frac{1}{2} \rho A c^3 \frac{\partial}{\partial \sigma} (\sigma - 2\sigma^2 + \sigma^3) = 0$$

$$(1 - \sigma)(1 - 3\sigma) = 0$$

This gives an optimum value of

$$\sigma_{opt} = \frac{1}{3} \tag{16.31}$$

The other value ($\sigma = 1$) is not possible.

The maximum power from Eqs. (16.31) and (16.30) is obtained as

$$P_{max} = \frac{4}{27} C_F \frac{1}{2} \rho A c^3 \tag{16.32}$$

The rate of energy input to the machine is

$$E = C_F \frac{1}{2} \rho A w^2 c$$

$$E = C_F \frac{1}{2} \rho A c^3 (1 - \sigma)^2 \tag{16.33}$$

Its value at the optimum blade-to-wind velocity ratio is

$$E_{max} = \frac{4}{9} C_F \frac{1}{2} \rho A c^3 \tag{16.34}$$

Thus for the machine considered here the maximum power coefficient is

$$C_{P\max} = \frac{1}{3} = 0.333 \tag{16.35}$$

This compared to Eq. (16.22) demonstrates the limitation of such a machine.

This is a very elementary analysis with simplifying assumptions. However, it demonstrates a marked departure from the one given for propeller type windmills in Sec. 16.5.

16.7 Wind Power Applications

In the past wind power was first used widely for corn grinding and water pumping. Then windmills were used to drive sawmills and oil extraction plants. Now wind energy is being used for a large number of other applications in areas where either electric supply is not available or fuel supplies are scarce.

A wind-driven ac generator of sufficiently large size is used to feed the main supply lines. In this application the main problem is to usefully utilize wind energy at variable velocities. Therefore, to overcome this limitation, windmills can be used to drive dc generators which generate electric power at varying voltages corresponding to the fluctuating wind velocity. This power can then be used for heating, electrolysis of water, battery charging, etc. Charged batteries and stored hydrogen and oxygen can then be used to supply energy as and when required.

Hydrogen can also be used for the manufacture of hydrochloric acid and methane gas.

Wind energy has been utilized for storing compressed air. The compressed air is used either to drive an electric generator through an air turbine or for aeration and other industrial applications.

Other applications of wind energy, specially in rural areas, are in heating of water and rural products, refrigeration and drying of agricultural products.

The success of wind power utilization schemes depends on suitable applications, energy storing methods and the overall costs involved.

Specifications of some wind machines are given in Appendix D.

16.8 Advantages and Disadvantages

Some of the main advantages and disadvantages of the wind turbine power plants are given in this section.

16.8.1 Advantages

(a) Wind turbines provide pollution free power.
(b) There is no fuel cost.
(c) Absence of transportation of fuel, its storage and handling makes the power plant very simple.
(d) Wind energy is inexhaustible.
(e) It is easy and quick to install.
(f) It is ideal for small power requirements in isolated places where other sources are absent.
(g) Wind turbines can be manufactured from a wide variety of easily available materials.
(h) Wind turbine units can be produced in large numbers in a short time.
(i) Option of wind turbines on a large scale can save fossil fuels in thermal power plants.

16.8.2 Disadvantages

(a) Wind energy is intermittent. Therefore, turbines cannot function continuously for a large part of the year.
(b) Their plant load factor is too low.
(c) Wind energy is too thinly distributed. Therefore, wind turbines are unsuitable for bulk power generation.
(d) A large number of wind turbines (wind mills) requires large areas of land and disturbs the environment.
(e) Capital cost of wind turbines is high.
(f) On account of low rotational speeds a step up gear is required for driving the electric generator.
(g) On account of widely varying wind velocity the design and operation of a constant speed wind turbine requires complicated mechanism.

Notation for Chapter 16

A	Area
c	Wind velocity
C	Coefficients
d	Diameter
D	Drag
E	Energy
F	Force
h	Enthalpy

k	Constant
K	Constant
L	Lift
$\dot{m}$	Mass-flow rate
p	Pressure
P	Power
t	Time
T	Total time
u	Tangential speed
w	Relative velocity
x	Downwind-to-upwind velocity ratio

Greek Symbols

η	Efficiency
ρ	Density of air
σ	Blade-to-wind velocity ratio
ϕ	Angle shown in Fig. 16.10
ω	Angular speed

Subscripts

o	Stagnation value
1	Immediately upstream/upwind
2	Immediately downstream/downwind
a	Atmospheric
d	Downwind
D	Drag
F	Force
i	Ideal
L	Lift
max	Maximum
opt	Optimum
P	Power
r	Resultant
u	Upwind
x	Axial
y	Tangential

➢ Solved Examples

16.1 **(a)** Determine the propeller diameter of a windmill designed to drive an aerogenerator ($\eta = 0{\cdot}95$) of 100 kW output at a rated

wind velocity of 48 kmph. Assume the mechanical and aerodynamic efficiencies of 0.90 and 0.75 respectively. Take the density of air as 1.125 kg/m^3

(b) Determine the wind velocity through the propeller disc, gauge pressures just before and after the disc, and the axial thrust corresponding to maximum power.

***Solution*:**

(a) $c_u = 48$ kmph $= 13.34$ m/s

$$P = 100 = 0.593 \times 0.7 \times 0.9 \times 0.95 \left(\frac{1}{2} \rho A c_u^3\right) \times 10^{-3}$$

$$\frac{1}{2} \rho A c_u^3 = 281.76 \times 10^3$$

Substituting the values of density and velocity

$$\frac{1}{2} \times 1.125 (13.34)^3 A = 281.76 \times 10^3$$

$$A = \frac{\pi}{4} d^2 = 211.00 \text{ m}^2$$

$$d = 16.39 \text{ m } (\textit{Ans.})$$

(b) For maximum power, the wind velocity through the propeller disc

$$c = \frac{2}{3} c_u = \frac{2}{3} \times 13.34 = 8.90 \text{ m/s } (\textit{Ans.})$$

$$p_1 - p_a = \frac{5}{8} \rho c^2 = \frac{5}{8} \times 1.125 \times 8.90^2$$

$$p_1 - p_a = 55.69 \text{ N/m}^2 = 5.68 \text{ mm W.G. } (\textit{Ans.})$$

$$p_2 - p_a = -\frac{3}{8} \rho c^2 = -\frac{3}{8} \times 1.125 \times 8.90^2$$

$$p_2 - p_a = -33.417 \text{ N/m}^2 = 3.406 \text{ mm W.G.}$$
(below atmospheric) (*Ans.*)

$$F_x = (p_1 - p_2) A$$

$$F_x = (55.69 + 33.417) \times 211.0 \times 10^{-3}$$

$$F_x = 18.80 \text{ kN } (\textit{Ans.})$$

Questions and Problems

16.1 Explain briefly the meanings of the following terms:

(i) Annual mean wind velocity

(ii) Rated wind velocity

(iii) Feathering
(iv) Cut in speed
(v) Furling speed
(vi) Velocity duration curve
(vii) Power duration curve.

16.2 What is a wind rose? Draw typical roses for the wind duration, total wind run and annual wind energy. What useful information is obtained from such roses?

16.3 (a) Draw sketches of horizontal and vertical axis wind turbines showing their main components. Explain their principle of working.

(b) State the advantages and disadvantages of the horizontal and vertical axis wind turbines.

16.4 (a) Show the variation of wind velocity and pressure in the flow field upwind and downwind of a windmill propeller.

(b) Prove that for maximum power:

(i) $c_u = \frac{3}{2} c = 3 c_d$

(ii) $P_{max} = \rho A c^3$

(iii) $F_x = \rho A c^2$

16.5 (a)Show the lift, drag, axial and tangential forces acting on the blade element of a windmill propeller. If the drag-to-lift ratio is k, show that the efficiency is given by

$$\eta = \frac{1 - k\sigma}{1 + k/\sigma}$$

Where σ = blade-to-wind velocity ratio

(b) Assuming $k = 0.01$ (constant), compute the values of efficiency for σ between 0.1 and 5, and plot a graph between η and σ.

16.6 (a) How is wind energy converted into ac electrical energy at constant and variable frequencies? How is this energy stored during low load and high wind periods? Describe three methods.

(b) What are the advantages of a dc aerogenerator over an ac type?

16.7 Describe six applications of wind energy in isolated areas far from main supply lines of fuel and power.

16.8 Show that for a vertical axis panemone type wind turbine:

(a) $C_P = \sigma$

(b) $C_{P\max} = \sigma_{\text{opt.}} = \frac{1}{3}$

(c) $P_{\max} = \frac{4}{27} C_P \left(\frac{1}{2} \rho A c^3\right)$

State the assumptions used.

16.9 A windmill with 10 m diameter propeller is designed for a rated wind velocity of 30 kmph (8.34 m/s). If its output is 10 kW, determine:

(a) overall efficiency,

(b) wind velocity through the propeller disc, and

(c) axial thrust

Assume maximum power coefficient and take air density as 1.23 kg/m^3.

(*Ans.*) (a) 60.3%

(b) 5.56 m/s

(c) 2.986 kN

Chapter 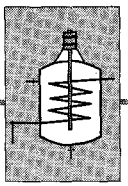 17

Solar Turbine Plants

A Solar thermal power plant works on solar energy received from solar radiation through collectors. The radiant energy from the sun is captured by solar collectors and transmitted as heat energy to a suitable working fluid such as steam, freon or helium. The energy of the working fluid in turn is converted into shaft work by the solar turbine employing one of the closed power cycles-Rankine or Brayton. A solar turbine (in short for solar thermal turbine power plant) employs Rankine cycle in the lower temperature range and Brayton cycle in the higher temperature range.

Earth receives 1.783×10^{14} kJ of solar energy per second; the energy received per square meter is 1.353 kJ/s. This varies with the distance between the sun and earth at different times of the year and the local weather. Sunshine is available for long hours during the year in tropical countries in Africa and South east Asia. India has great potential of employing solar thermal power plants for generation of electric power.

Many countries have developed solar power plants in a wide range of output from a few kilowatts to tens of megawatts. Major contraints in the development of these plants have been the size of the solar collectors required, space and high capital costs.

Another significant factor which militates against the solar power plants is the intermittent nature of solar energy. It is dependent on the weather conditions. Large and expensive solar power plants become non-operative during nights and cloudy whether. Therefore, these plant have a low load factor. In view of the aforementioned technological and economic aspects, solar power plants are not likely to make a significant contribution to the bulk power supply scenario at present. However, small contributions can ease pressure on the scarce fossil fuels—coal, gas and oil.

Solar power plants can be found attractive in remote areas such as islands and deserts where sunshine and large areas of land for solar collectors are abundantly available. Large solar plants of one megawatt capacity and above with energy storage devices can also be considered as one of the alternatives when other power plants are not available.

Now solar turbine power plants of one megawatt (and above) capacity are working in several countries such as France, Germany, Japan and the United States.

In this chapter the role of the turbine as a prime mover for generation of electricity from solar radiation is discussed. The focus is on the turbine power plant and its integration in the total system.

Only the minimum details of the collector-receiver system, storage devices and heat exchanger are included. Electric power generation through solar cells and piston engines (Stirling cycle) has not been included here.

17.1 Elements of a Solar Power Plant

A schematic block diagram of the basic components of a solar thermal power plant is shown in Fig. 17.1. The solar energy flow and losses are also depicted from the input point of solar energy to the electric power output at the generator terminals.

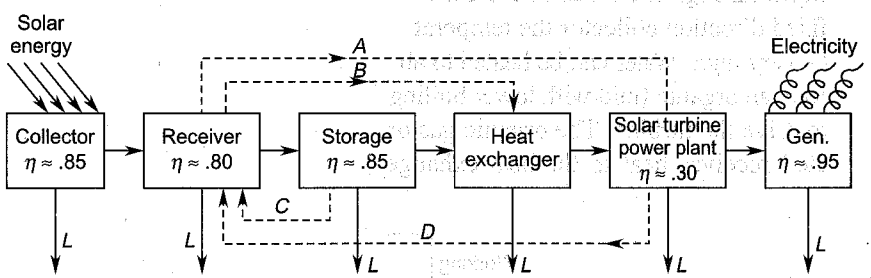

Fig. 17.1 Energy and fluid flow in a solar turbine power plant

The collector receives solar energy (radiation) and transmits it to the receiver; here the heat (solar energy) received from the collector or collectors is absorbed in a primary fluid or coolant. The thermal energy from the receiver is transferred to the heat exchanger through the primary fluid. Heat is transferred from the primary fluid to the working fluid in the heat exhanger. The working fluid produces mechanical work in an energy conversion device (piston engine or a turbine). The engine or turbine work is employed to drive the electric generator as shown in the figure. A heat exchanger is not required if the primary fluid (coolant) is same as the working fluid. In this case the working fluid flows directly to the power plant through path A.

In some solar thermal power plants an energy storage device is employed between the receiver and the turbine. This stores a part of the heat energy coming from the receiver. Working fluid flows through path B when no storage is employed. Path C represents the return of the fluid from storage device to the receiver for heating. Similarly the working fluid/coolant returns to the receiver through path D from the power plant

after doing work. Other return paths between various components for different arrangements have not been shown in the figure.

The stored heat energy is used to run the turbine in the absence of solar radiation during cloudy weather or nights. However, inclusion of the storage device adds to the capital cost and losses.

A solar turbine plant with an integral collector receiver system employing single fluid would be the cheapest and most efficient proposition.

17.1.1 Rankine Cycle Power Plant

A solar turbine power plant working on Rankine cycle is shown in Fig. 17.2 (a). The corresponding *T-s* diagram is shown in Fig. 17.2 (b). It operates with a flat-plate collector; here the receiver is an integral part of the collector. A circulating pump circulates water (coolant or primary fluid) through the tubes of the collector-receiver system. In this type of a fixed direction collector the temperature of the fluid in the receiver cannot be very high. Water can be heated to about 100°C (or slightly above). Therefore, an organic fluid with lower boiling point at a higher pressure is chosen to drive the turbine. The organic gas or vapour (freons, toluene, isobutane etc.) receives heat in the heat exhanger from the circulating hot water.

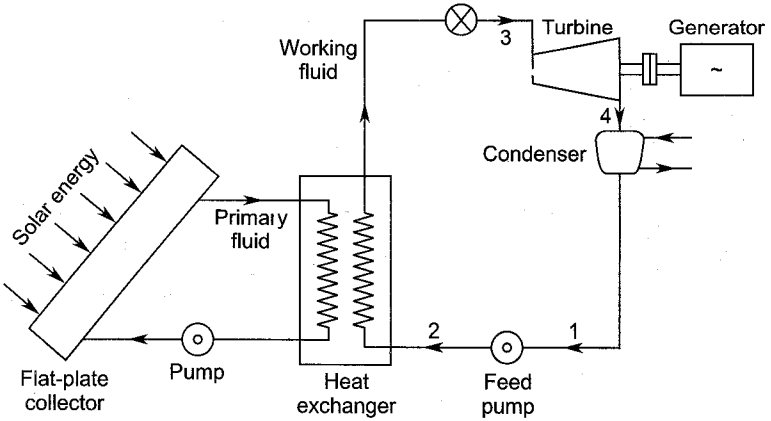

Fig. 17.2 (a) A simple solar turbine power plant (Rankine cycle)

Various thermodynamic processes occurring in this plant are shown in Fig. 17.2 (b). The feed pump raises the pressure of the working fluid from the condenser pressure ($p_1 = p_4$) to the turbine inlet pressure ($p_2 = p_3$). Heat from the primary fluid is supplied to the working fluid during the processes 2-*a*, *a*-*b* and *b*-3. Process 3-4 represents expansion of the gas or vapour through the turbine. The low pressure vapour is condensed to the liquid state in the process 4-1.

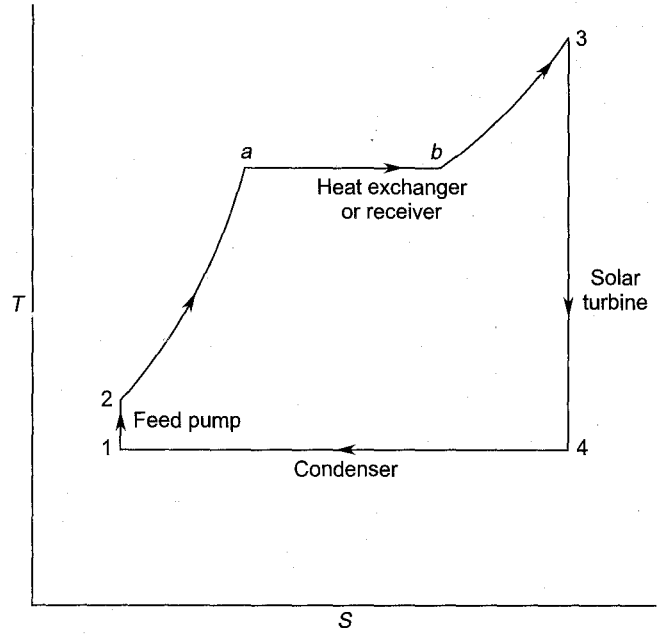

Fig. 17.2 (b) Rankine cycle for a simple solar turbine power plant

Other details of the Rankine cycle are given in chapter four on steam turbine plants.

17.1.2 Brayton Cycle Power Plants

Figure 17.3 (a) shows a closed cycle gas turbine plant working on Brayton cycle. Here the working fluid (air, helium etc.) is the same as primary fluid; it receives heat from the receiver and expands through the gas

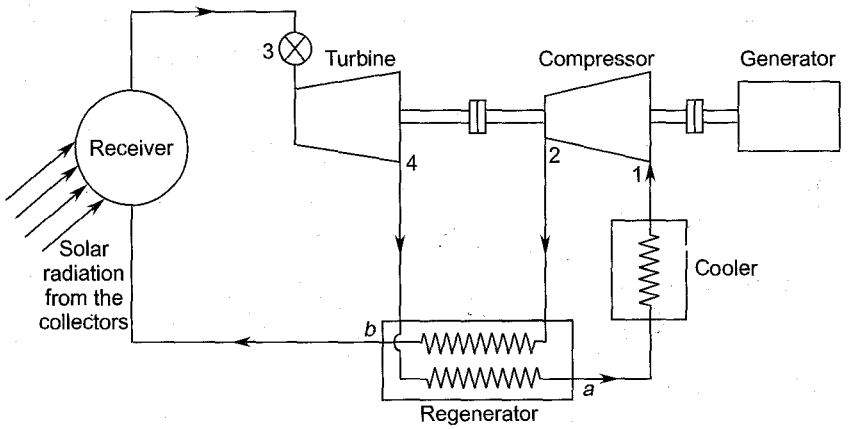

Fig. 17.3 (a) Brayton cycle solar gas turbine power plant

turbine. The low pressure exhaust is returned to the receiver at the required high pressure through the regenerator and cooler.

The *T-s* diagram (Fig. 17.3b) depicts the aforementioned thermodynamic processes in the Brayton cycle. Other details of the cycle are given in Chapter 3 on gas turbine plants.

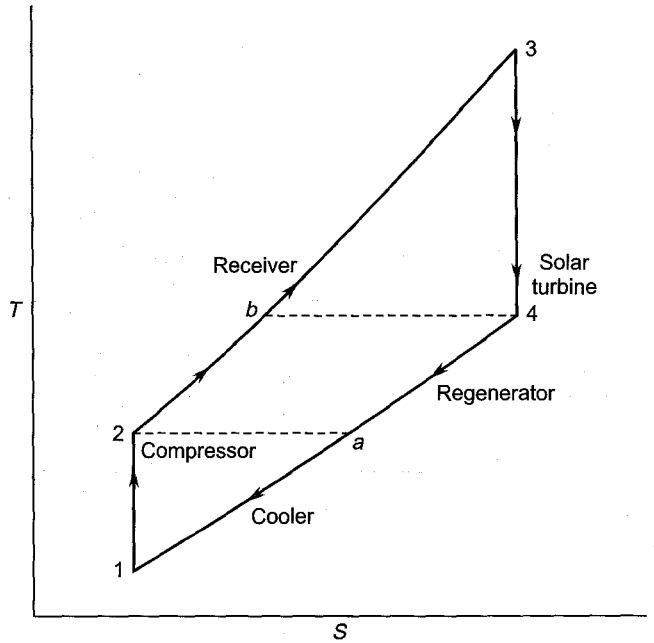

Fig. 17.3 (b) Brayton cycle for a solar gas turbine power plant

The working fluid (gas) is compressed (1-2) in the compressor for developing the pressure ratio required in the turbine. The compressed gas at pressure $p_2 = p_3$ is heated (2-3) to the required temperature in the receiver. The high temperature and pressure gas expands (3-4) in the solar gas turbine which drives the electric generator. The exhaust gas passes through a regenerator and a cooler before entering the compressor.

17.2 Solar Collectors

Any surface which receives solar radiation and transmits it to a receiver or absorber is a collector of solar energy. Its purpose is to capture solar radiation flux and transmit it to the receiver for heating a fluid. Different types of mirrors, lenses, bank of tubes and the surface of water in a pond are examples of solar collectors; they all collect solar energy through radiation.

There are several types of solar collectors. They can be classified on the basis of maximum temperature obtainable in the receiver. Thus solar collectors fall in three categories of low, medium and high temperatures; they are described briefly in the following sections with a focus on power generation. Classification on the basis of other criteria is not included in this chapter.

17.2.1 Low Temperature Collectors

A flat-plate collector (Fig. 17.2a) is an example of a low temperature collector. Here solar radiation is received by a bank of tubes mounted on a black metallic absorber plate. Besides insulation for minimising heat conduction losses, the collector tray is provided with a transparent cover of glass sheet or other material; this reduces the heat loss from the hot collector tubes. Water or some other suitable liquid is circulated through the collector tubes for absorbing solar energy as heat. The energy in the hot water (at about t_{max} = 100°C) can be used for heating or power generation (Sec. 17.1.1) in small units.

In these collectors large surfaces for collecting both direct and diffuse radiation can be obtained without employing any suntracking mechanism. A flat-plate collector receives uniform solar radiation flux over its surface. It is easy to assemble such collectors from comparatively cheaper materials. They require very little maintenance.

Energy losses in these collectors are mainly due to heat losses by conduction, convection and radiation. On account of large surface area, these losses are much higher compared to the concentrating types of collectors. Losses in flat-plate collectors are a significant proportion of the energy received by solar radiation.

The surface of water in a solar pond is also a low temperature collector. Power plants where the working fluid is heated by low temperature solar collectors suffer from very low overall efficiencies on account of the low temperature at which heat is supplied.

17.2.2 Medium Temperature Collectors

For absorbing heat at higher temperatures, solar radiation is directed on the receiver by concentrating or focusing devices such as reflecting mirrors and lenses. These concentrators are either fixed or movable. Figure 17.4 shows a parabolic mirror concentrator with the receiver at its focal point. The performance of a collector – receiver system depends, besides other factors, on the concentration ratio (CR). This is defined by

$$CR = \frac{\text{Aperture area of the concentrator}}{\text{Receiver surface area}} = \frac{A_c}{A_r} \qquad (17.1)$$

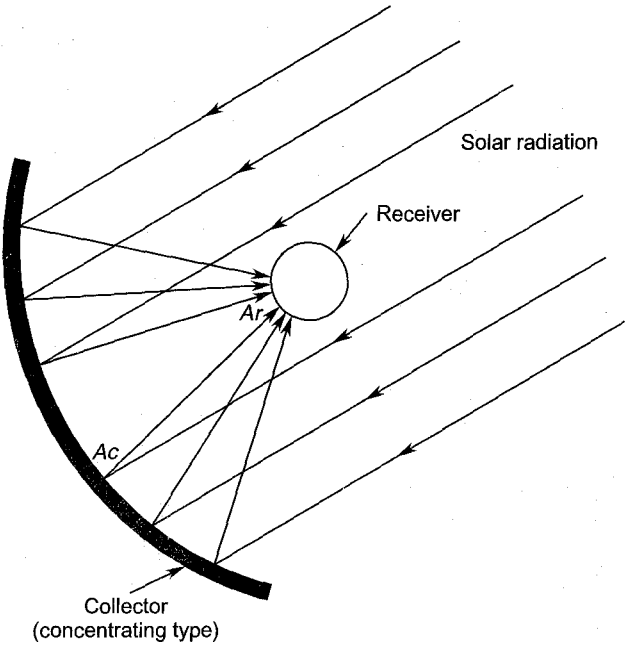

Fig. 17.4 Concentrating type collector-receiver system

Aperture and receiver areas are shown in Fig. 17.4. Higher values of concentration ratio can be obtained by employing large apertures and small receivers within practical limits. Receiver temperature increases with concentration ratio as shown in Fig. 17.5. Therefore, higher temperatures of the coolant or working fluid can be obtained in a solar power plant by employing higher values of concentration ratio. Very high

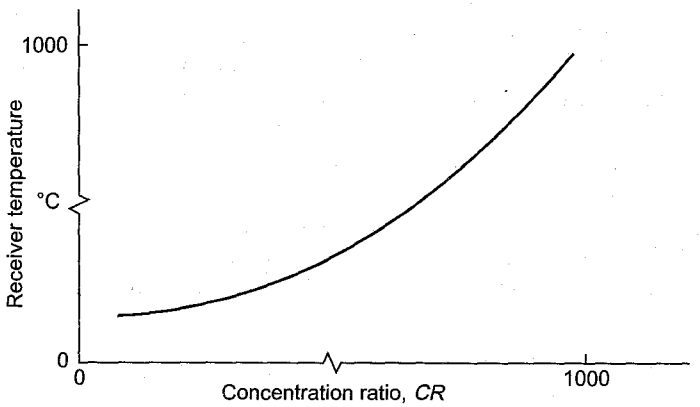

Fig. 17.5 Typical variation of receiver temperature with concentration ratio

values of concentration ratio can be obtained by employing several concentrators for a single receiver.

Optical efficiency of a solar collector can be defined by

$$\eta_0 = \frac{\text{Heat energy received by the receiver}}{\text{Incident radiation on the collector}} = \frac{Q_r}{Q_c} \tag{17.2}$$

$$Q_c = I_c A_c \tag{17.3}$$

$$\eta_0 = \frac{Q_r}{I_c \cdot A_c} \tag{17.4}$$

$$Q_r = \eta_0 I_c A_c \tag{17.5}$$

The useful heat collected or delivered to the coolant in the receiver is

$$Q_u = Q_r - \text{losses} = Q_r - L \tag{17.6}$$

The losses can be expressed through a coefficient U based on the receiver are A_r.

$$L = U A_r (T_r - T_a) \tag{17.7}$$

Equations (17.5), (17.7) in (17.6) give

$$Q_u = \eta_0 \cdot I_c \cdot A_c - U A_r (T_r - T_a) \tag{17.8}$$

The collector efficiency is defined by

$$\eta_c = \frac{\text{Useful heat received by the coolant}}{\text{Incident radiation on the collector}} = \frac{Q_u}{Q_c}$$

$$\eta_c = \frac{Q_u}{I_c \cdot A_c} \tag{17.9}$$

Equations (17.1), (17.8) and (17.9) give

$$\eta_c = \eta_0 - \frac{1}{CR}\left(\frac{UT_a}{I_c}\right)\left(\frac{T_r}{T_a} - 1\right) \tag{17.10}$$

$$\eta_c = f(CR, TR) \tag{17.11}$$

The receiver temperature (or the temperature ratio, TR) increases with the concentration ratio as shown in Fig. 17.5. Higher values of the working fluid temperature yield higher thermal efficiency of the power plant.

However, collector efficiency decreases with temperature ratio. Figure 17.6 depicts typical variation of collector efficiency for three values of the concentration ratio.

Concentrators which give receiver temperatures between 300 °C and 400 °C come under the category of medium temperature collectors. Some of them are lenses and mirrors, parabolic troughs and tubular collectors.

A compound parabolic concentrator (CPC) is shown in Fig. 17.7. The reflecting inner walls of the funnel-shaped collector are parabolic in shape. The receiver is placed at (or near) the bottom of the collector. The

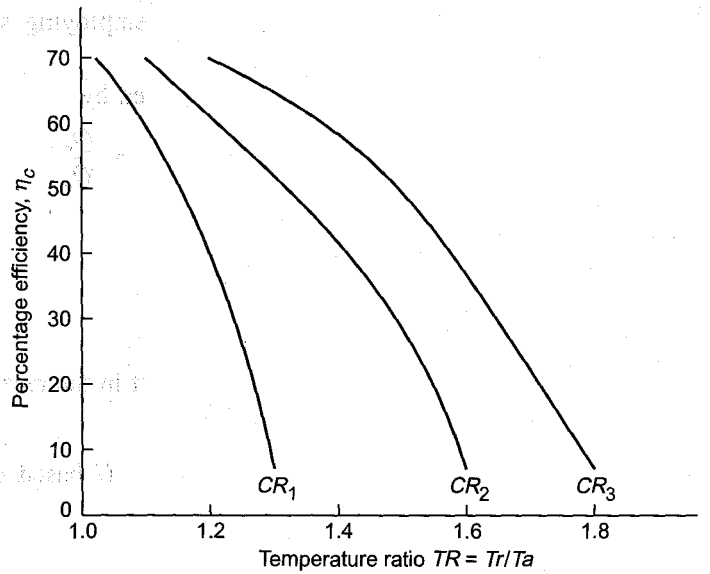

Fig. 17.6 Variation of collector efficiency with temperature ratio (typical curves)

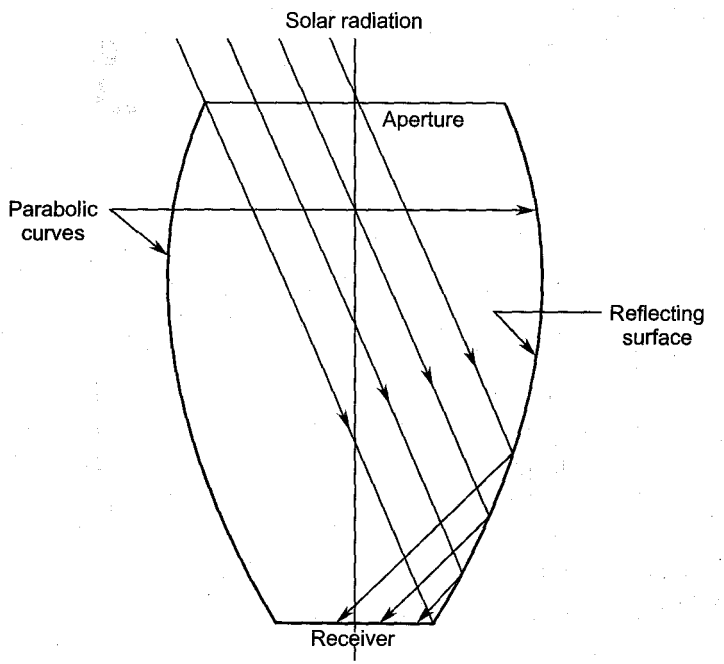

Fig. 17.7 A Compound parabolic concentrator (CPC)

incident radiation entering the aperture is directed on to the receiver surface by the reflecting surfaces. Reflection of some rays is shown in the figure.

The ratio of height and aperture along with other geometrical parameters determine the values of concentration ratio (1.5–10) and the performance of these collectors.

Fresnel lenses and mirrors are also used for obtaining medium temperatures of the coolant or the working fluid. A Fresnel lens (Fig. 17.8) is made up of several prisms each focusing the solar radiation on the receiver located at the focal point. A single large convex lens is also shown in the figure for comparison. Concentration ratio up to about 25 can be obtained for medium temperature applications.

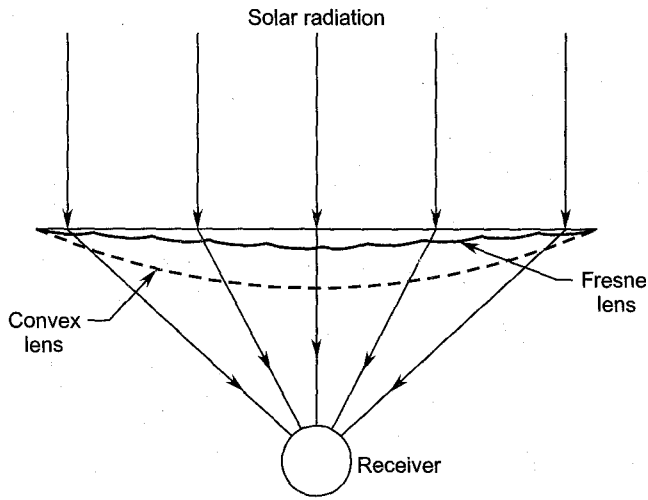

Fig. 17.8 A Fresnel lens

A Fresnel mirror is shown in Fig. 17.9; it is formed by arranging an array of plane mirror strips in a concave or plane configuration. Each strip reflects the solar radiation towards the receiver; the strips can be fixed or movable. High values of concentration ratio (CR = 50) are obtained by employing a large number mirror strips.

Figure 17.10 shows a parabolic trough collector (PTC). This is a linear focusing device. The trough has a parabolic cross-section. Solar radiation is focussed on a line by the parabolic reflecting surface. Maximum value of the concentration ratio is about 50.

The receiver is located at the focal axis of the reflector/concentrator. For increasing the coolant temperature the receiver tube in jacketed by a concentric transparent cover; this reduces the heat losses from the receiver. The coolant temperature can be further raised by evacuating the space between the receiver tube and the jacket.

Several PTCs with sun tracking device can be used for large power plants employing medium temperatures of the working fluid.

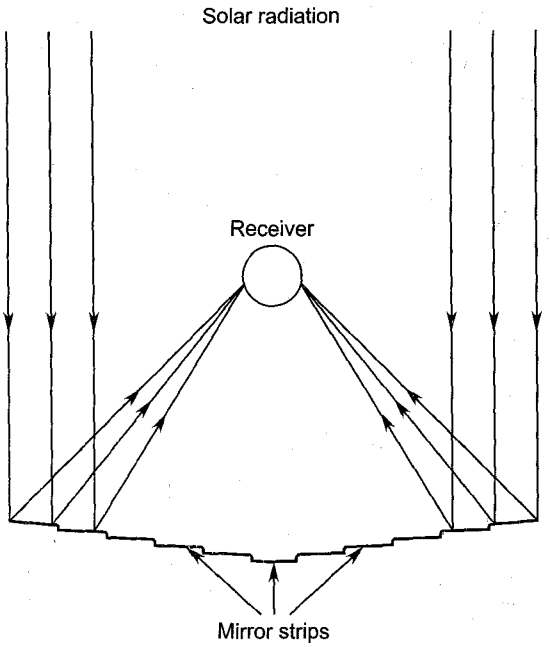

Fig. 17.9 A Fresnel reflector

Higher values of the coolant temperature can be obtained by increasing the concentration ratio and reducing the heat losses from the receiver. The tubular collector-receiver system shown in Fig. 17.11 is based on this concept. The concentric receiver tube is surrounded by a transparent casing. The lower concave surface of the annular passage acts as a reflecting surface for the inner receiver tube. Thus the coolant receives heat by the direct radiation flux incident upon the receiver surface as well as from the reflection by the lower concave surface which provides a concentration ratio of about 1.5. The heat losses from the coolant are considerably reduced by maintaining a high degree of vacuum in the annular space between the receiver tube and the transparent casing.

17.2.3 High Temperature Collectors

These are concentrating collectors which can produce receiver temperatures above 350°C. They require accurate sun tracking by employing large number of heliostats. The concentration ratio is very high (greater than 50). Central receiver systems employing a large number of heliostats have high values of concentration ratio (50-300) and temperature. They are most suitable for power generation.

Other devices for obtaining high values of concentration ratio and fluid temperatures are Fresnel lenses and mirrors, and parabolic and spherical

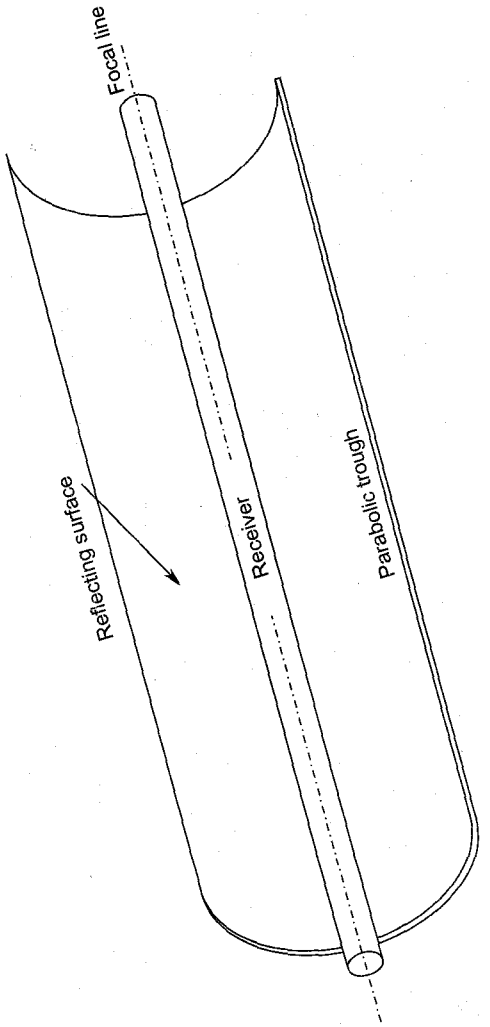

Fig. 17.10 Parabolic trough collector

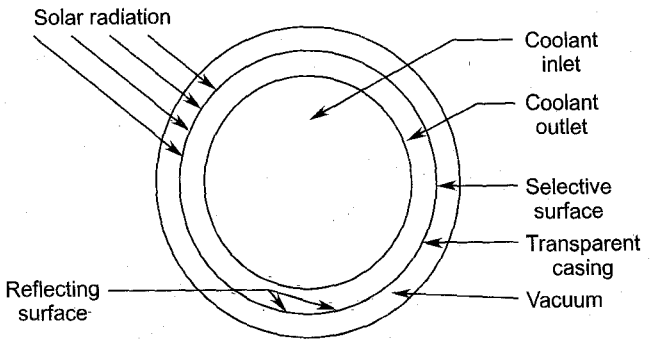

Fig. 17.11 A tubular collector-receiver

reflectors. Concentration ratio up to 3000 can be obtained with these devices. Tubular collector—receiver systems employing high vacuum in the space between the receiver and the casing can provide high fluid temperatures (400-700°C) in steam and gas turbine power plants.

17.2.4 Heliostats

On account of the changing position of the sun every day during the year, the solar radiation can neither be collected nor directed on to the receiver properly in a fixed collector-receiver system. In a central receiver system (CRS), several collectors focus the solar radiation flux on a large receiver as shown in Figs. 17.12 and 17.14. This requires that all the collectors spread over a large area (known as heliostat field) are continuously oriented towards the sun during the sunlight hours. A collector (and its steering system mounted on a stand or a tower) which continuously tracks the sun is called a heliostat. Such a collector captures the maximum possible solar radiation flux and transmits it to the receiver. This is shown in Fig. 17.12. The concentration ratio obtained by employing n heliostats focussing on a single area of the receiver is theoretically increased n times; this can give very high values of the receiver/coolant temperature. However, it should be remembered that the number of hiliostats operating at a given time is lesser than the total number installed for a receiver. With the increasing number of heliostats, the distance between some heliostats and the receiver is increased; along with this, the height of the receiver tower and the area of the heliostat field also increase. The supporting

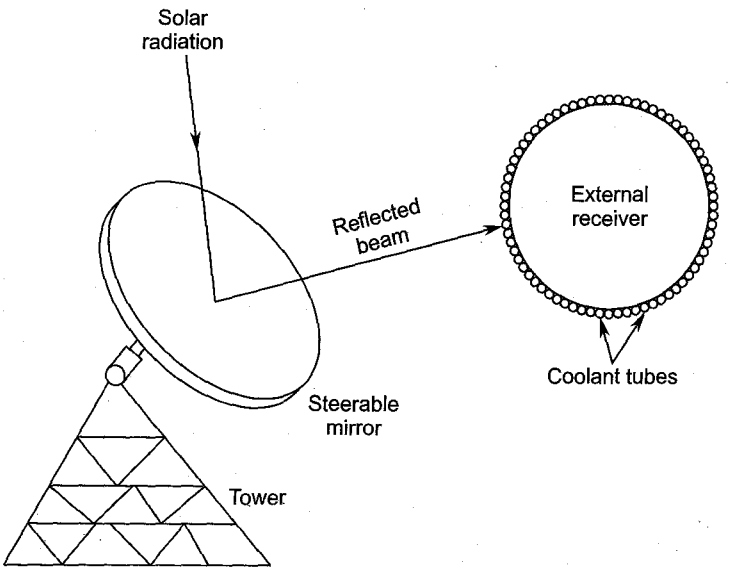

Fig. 17.12 A heliostat and an external receiver

structures of the reciever and heliostats increase the capital cost of solar turbine power plants.

The position of the individual heliostat in the field, besides other factors, depends on the geographical location of the place where they are employed. Optimisation of the layout geometry of a large number of heliostats aims at transmitting maximum heat to the receiver from the solar radiation incident upon the collectors. This requires minimum possible shadowing and blocking; the loss of energy due to scatter and absorption increases with the distance in the space between the heliostats and the receiver. The cost of the heliostat system and its operation and maintenance is a large proportion of the total cost of the power plant.

The steering system of a heliostat orients the concentrators/collectors frequently (say every fifteen minutes) according to the changing altitude angle of the sun; one or two axes drive is employed to achieve this. Besides collection and transmission of the radiation flux, the heliostats are also required to move to different modes and positions in emergency, bad weather and non-sunshine hours. Precise control of the heliostats has a significant effect on the overall efficiency of a solar power plant. A small inaccuracy in the orientation of the holiostat can cause the reflected beam to miss the target at the receiver by a large amount leading to increased energy loss. Therefore, precision electronic, hydraulic and electro-mechanical control systems are employed. Accurate sun tracking can be achieved by computer control.

17.3 Solar Receivers

The receiver absorbs heat from the solar radiation flux transmitted by the collector or collectors. The coolant or the primary fluid can be heated in the receiver to high temperatures at moderate or high pressures. The desired values of temperature and pressure of the working fluid (vapour or gas) are obtained in the heat exchanger as explained in Section 17.1. The primary fluid (coolant) can be chosen for its better thermodynamic and heat transport properties. Some fluids which are frequently used as coolants in different temperature ranges are oil, water and molten metals.

Majority of receivers for solar turbine power plants are located on high stands or towers for receiving radiation flux optimally from the collectors. Therefore, efforts are made to make the receivers and their supporting structures light and economical. This is achieved by employing coolants, which absorb heat at high temperatures and economically lower pressures. The heavier heat exchangers for higher pressures of the working fluid can be kept on the ground or the turbine floor. The relative positions of these components should take into account the pressure losses in the connecting pipes and their cost.

Heat can be absorbed in the receivers directly by the working fluid (steam, air, organic vapours, etc.). This would require the receiver pressure vessels, tubes, etc. to be designed for the working pressure of the turbine. For higher operating pressures the receiver will be very heavy and unwieldy. If steam is directly generated in the receiver, it would have to accommodate the feed water, evaporation and superheating sections.

Air, helium or organic vapours/gases employed as working fluids in solar gas turbine power plants can also be directly heated in the receiver at the desired pressure.

In some solar turbine plants the receiver is an integral part of the collector. Solar ponds and flat-plate collectors are such examples.

Majority of receivers are fixed and receive heat energy from movable or stationary collectors. However, it is sometimes more convenient to employ movable receivers with stationary collectors.

Three types of receivers will be described here briefly;

(a) External receivers,
(b) Cavity receivers and
(c) Tubular receivers.

17.3.1 External Receivers

In this type of receiver the tubes carrying the primary fluid (coolant) or the working fluid are provided on the external surface of the vertical body of the receiver as shown in Fig. 17.12; its cross-section in the horizontal plane may be polygonal or circular. The concentrators transmit the solar radiation flux on to the receiver surface. The coolant tubes on the receiver surface correspond to the water and steam tubes in the boiler of the conventional steam power plant. However, in this case the heat is supplied by the solar radiation flux instead of the hot gases.

On account of the configuration of the external receivers large arrays of heliostats around them can be employed to transmit solar radiation flux on the coolant tubes. Thus the tube-banks around the entire periphery of the receiver can receive heat energy. On account of the large number (several hundred in some cases) of concentrators their distance from the receiver is large; this requires the receiver to be placed at comparatively greater height above ground.

Since the coolant tubes are mounted on the external surface the overall size of the receiver is smaller compared to the other types. Its weight is also small which requires only lighter and cheaper structures for supporting it.

Major energy losses in receivers are on account of (a) heat losses due to conduction, convection and radiation (b) reflection and (c) spillage of

radiation flux coming from the concentrators. Losses in external receiver are higher on account of large exposed surface area.

On account of large number of concentrators employed the concentration ratio is very high (CR_{max} = 1000); this can provide fluid temperatures of the order of 500°C. Higher receiver temperatures lead to higher losses and lower collector and receiver efficiencies.

17.3.2 Cavity Receivers

Here solar energy is supplied to the coolant tubes, which are mounted on the inside surface of a large enclosure or a cavity. The radiation flux enters the cavity through one or more apertures as shown in Fig. 17.13; concentrators mounted on steerable heliostats transmit the radiation flux on to the surface of the coolant tubes through the receiver aperatures. Internal reflection of the radiation flux inside the cavity transports the heat energy to other sections of the tube bank where the radiation beam does not reach directly from the apertures.

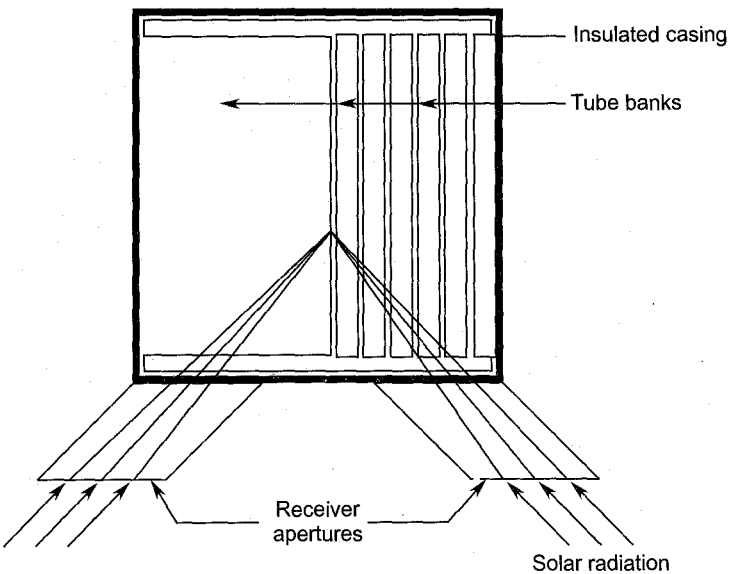

Fig. 17.13 A cavity type of solar radiation receiver

Since a large number of coolants tubes have to be accommodated inside the cavity, the overall size of a cavity type of receiver is comparatively large for a given size of the heat transfer surface. This results in a heavier receiver requiring stronger and more expensive tower.

Unlike the external type of receivers, here the concentrators can transmit the solar flux to the cavity through only a few apertures. Therefore,

a large number of heliostats cannot be employed all around the receiver. Some receivers employ a large size circular aperture at the bottom. In this case, the heliostats are arranged in a circular field and various sections of the coolant tubes receive radiation flux over large areas. If the heliostats are provided for only one (or more) aperture, it can be inclined towards them for receiving the radiation flux more efficiently. The geometry of the cavity and apertures for a given heat transfer area requires optimization.

Because of the comparatively smaller surface area in the cavity and its geometrical configuration, heat losses are less compared to the external type. Therefore, much higher values of concentration ratio and receiver temperature can be employed. Overall receiver efficiencies of more than 80 per cent have been achieved.

17.3.3 Tubular Receivers

A tubular receiver consists of a row of coaxial tubes as shown in Fig. 17.11. The outer tube is made of a transparent material which receives solar radiation. Coolant or the working fluid enters the inner tube and leaves from the annular space between the two tubes. The lower portion of the inside surface of the outer tube acts as a concentrator providing concentration values of about 1.5. Heat losses from the coaxial tube are kept considerably lower by enclosing it in a transparent concentric casing and maintaining a high vacuum in the intervening annular space as shown in the figure. Heat losses are further reduced by providing proper insulation and covering the tube-bank by a transparent sheet. This arrangement of a collector-receiver system can give fluid temperatures up to 200°C. However, much higher temperatures can be obtained if separate concentrators are employed to transmit solar flux to this type of receiver.

Several version of this concept have been employed to operate solar power plants.

17.3.4 Central Receiver System (CRS)

In this system a large number of solar collectors transmit the radiation flux to a single large size receiver for heating the coolant (or the working fluid). The high temperature coolant is then employed to supply thermal energy to the power plant through heat exchanger and the storage (if any); this is shown in Fig. 17.14. If the working fluid is directly heated in the receiver, a heat exchanger is not required. Both external and cavity types of receiver can be used in this method.

Large solar thermal power plants employ a central receiver system; this gives all the advantages of a large size boiler in terms of efficiency and economy. Power plants with CRS are known to be comparatively cheaper.

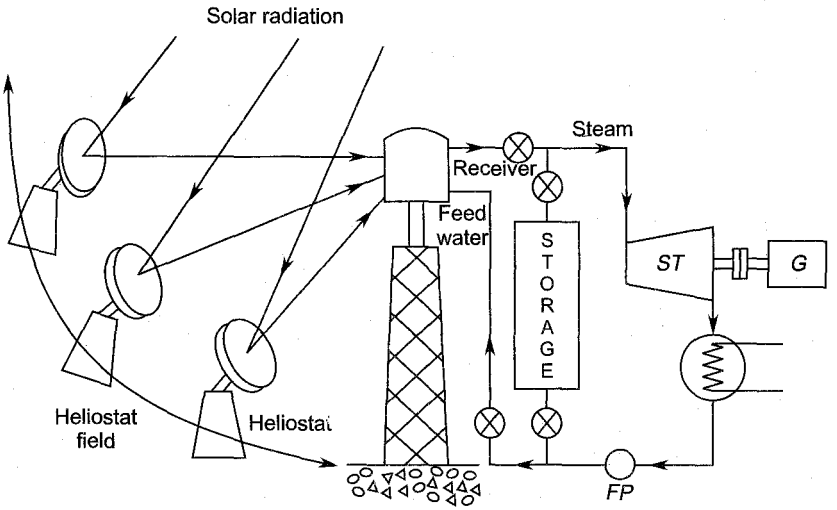

Fig. 17.14 Solar thermal power plant with a central receiver

However, this system requires large areas of land to accommodate several concentrators/heliostats. The height of the receiver tower is also large and requires strong supporting structures and foundations.

17.3.5 Distributed Receiver System (DRS)

In this system several collector-receiver modules are employed to collect solar energy in the coolant. It is then collected at a single station for transferring its heat energy to the working fluid of the power plant. Fig. 17.15 shows a block diagram of energy and fluid flow in such a system. The three collectors (C_1, C_2 and C_3) transmit solar radiation flux to their respective receivers (R_1, R_2 and R_3) where the coolant (or the working fluid) is heated separately. The high temperature coolant is then collected from these receivers and supplied to the heat exchanger where it transfers its heat energy to the working fluid. This is depicted by the Circuit A. Circuit B is employed when the coolant is also used as the working fluid. Other flow schemes can also be adopted with or without storage. Flow circuits corresponding to all possible flow schemes have not been shown and discussed here.

Various types of concentrators and receivers are employed in the individual modules of the distributed receiver system. For instance, linear, dish and compound parabolic collectors have been used in various power plants employing DRS.

A distributed system can also employ solar ponds and flat plate collector-receiver system for heating the working fluid in the lower temperature sections of the power plant.

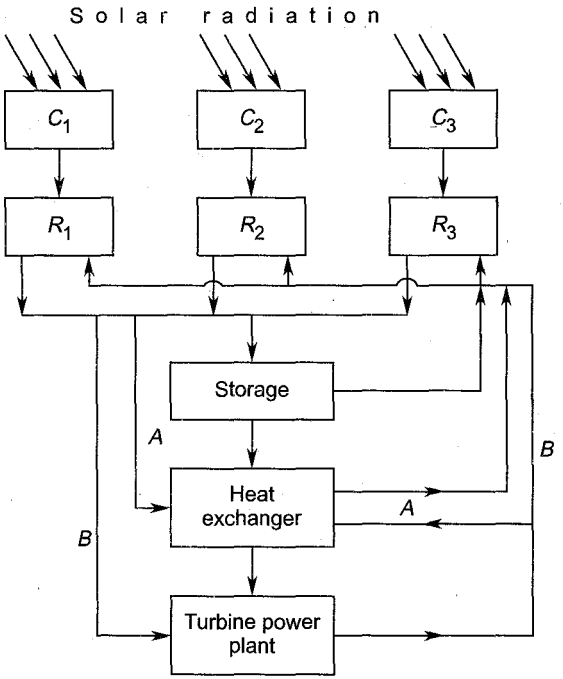

Fig. 17.15 Energy and fluid flow in a distributed receiver system

This system (DRS) can also employ several totally independent power plants with their own collector-receiver systems. In this case the generator output is small. These generators can feed their outputs to a common grid. However, gathering heat energy from several receivers and using it in one single large power plant is more common on account of its higher thermal efficiency. The long network of connecting pipes causes pressure and heat losses, which increase with the number of collector-receiver modules. This limits the use of a very large number of such modules and hence the output from such a system.

Some advantages of DRS are

1. Collector size is comparatively small.
2. Receiver height is small.
3. Distance between the collector and receiver is small
4. On account of relatively small size of the collector-receiver system wind loads are not a serious problem.
5. Land requirements are also relatively less.
6. Installation of this system takes comparatively much shorter time. Electricity is available with the installation of the first module of the DRS.

17.4 Solar Energy Storage

Solar radiation is not always available during the day. The total number of sunshine hours depends on the geographical location of the solar power plant, time of the year and local climate. Because of the intermittent nature of the solar energy, it becomes necessary to store it during sunny periods simultaneously with the generation of mechanical/electrical power. The stored energy is used for power generation when solar radiation is not available during night and the cloudy periods of the day.

Storage of solar energy for a solar thermal power plant is similar to the storage of excess water (at high head) during high discharge periods of the river in a hydro-electric power station.

A storage system for thermal energy is an essential part of a solar thermal power plant. This requires the receiver to capture much more energy from the solar collectors than required by the prime mover. The excess energy in the receiver is stored for running the power plant when solar radiation is not available. The size of the storage system depends on various factors such as the type of storage, temperatures of the coolant and the working fluid, power output and the maximum duration the power plant is required to operate without solar radiation. Some methods of storing thermal energy for the operation of thermal power plants are based on:

(a) sensible heat of solids,
(b) sensible heat of liquids,
(c) latent heat of fusion and
(d) the combination of the aforementioned phenomena.

Some important factors for employing a particular system of solar energy storage are:

(i) Physical and chemical properties of the storage medium used,
(ii) Energy density, i.e. heat energy stored per cubic meter of the storage space,
(iii) Space required,
(iv) Capital cost,
(v) Safety aspects, and
(vi) The pattern of load variation.

Energy storage for a solar thermal power plant requires huge capital investment, space and additional operating cost. The addition of energy storage element requires larger collectors and receivers. In view of this, it is necessary to evaluate the economics and operation of an alternate conventional power plant for periods when the solar power plant does not operate.

Some energy storage systems for solar power plants are briefly described in the following sections.

17.4.1 Sensible Heat Storage in Solids

In this system a portion of the heat energy of the coolant from the receiver is absorbed in a solid medium (rock, metal blocks, glass pieces, etc.) enclosed in a large space (tank). It is suitable for medium and high temperatures up to 600 °C. Heat can be supplied to the working fluid in both Rankine and Brayton cycle power plants during non-sunshine hours.

Large spaces in rock formations and disused mines can be profitably used for this purpose. Loss of stored energy through heat transfer from the enclosing walls and the top and bottom surfaces should not be too high.

Figure 17.16 shows a sensible heat storage system. During the charging process, the high temperature fluid from the receiver heats the solid packing material in the storage tank. Thus a certain amount of heat energy is stored in the tank as sensible heat of the solid medium. The amount of energy stored depends on the mass of the solid material (medium), its specific heat and the alowable temperature rise.

$$Q_{st} = m_s \cdot C_s \, (\Delta t)_s \text{ kJ} \tag{17.12}$$

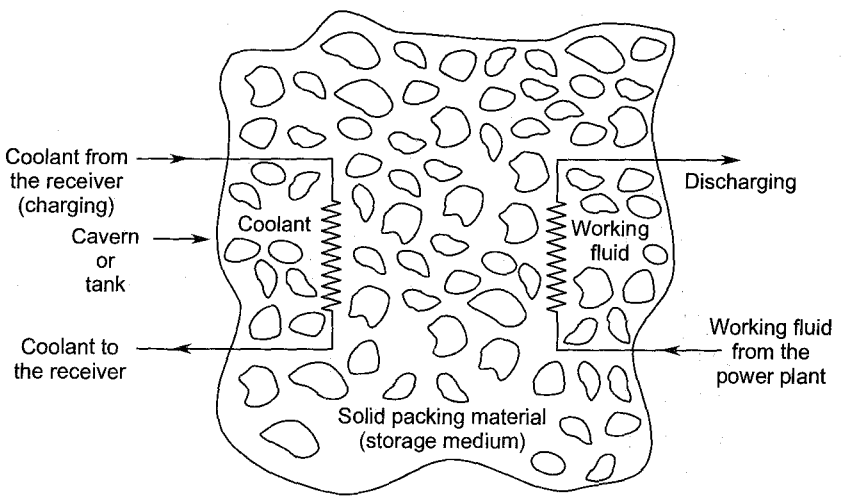

Fig. 17.16 Sensible heat storage in solids

The total mass (m_s) of the storage medium contained in the space of volume V_s depends on the density.

$$m_s = \rho_s \, V_s$$

Therefore, the energy density in storage medium is given by

$$\frac{Q_{st}}{V_s} = \rho_s \cdot C_s \, (\Delta T)_s \text{ kJ/m}^3 \tag{17.13}$$

Thus, for a given space volume heat energy stored is proportional to the density, specific heat and the temperature rise of the packing material.

Heat transfer during charging and discharging processes of the storage depends on the surface area (A_s) available. This suggests that the storage should be designed for large area to volume ratio (A_s / V_s).

The working fluid in the Rankine cycle power plant has to pass through tubes buried in the storage packing material whereas the working gas in the Brayton cycle plant can extract heat directly from the packed material. While selecting the packing material for storage it should be ensured that it will not melt or degenerate at the operating temperature of the storage.

17.4.2 Sensible Heat Storage in Liquids

Some liquids, such as water and oil, can also be used for storing heat energy as sensible heat. If the heat is stored below the boiling point of the storage medium at the ambient pressure, the container or tank is not subjected to a pressure differential. However, this can be used for heat storage only at comparatively lower temperatures.

For higher temperatures (above 100 °C), water has to be pressurized ($p = 2$ bar for $t = 120$ °C, and $p = 4.8$ bar for $t = 150$ °C) in the storage tank. Alternatively, other liquid media can be used; some of them are given here with their boiling points:

Sodium	750 °C
Hitec	540 °C
Therminol	343 °C
Oils	250 – 300 °C

The arrangement employed for liquid media is almost the same as shown in Fig. 17.16. Different combinations of tanks and pumps are employed in this storage system operating between the receiver and the turbine power plant.

A combination of solid and liquid media can also be employed for sensible heat storage.

Figure 17.17 depicts the use of a storage device for a gas turbine plant. During normal operation of the plant, a fraction of the coolant is used for charging the storage medium by partially opening the valves 3 and 4. During non-solar hours valves 1 and 2 are closed while 3 and 4 are opened; the coolant or the working fluid receives heat entirely from the

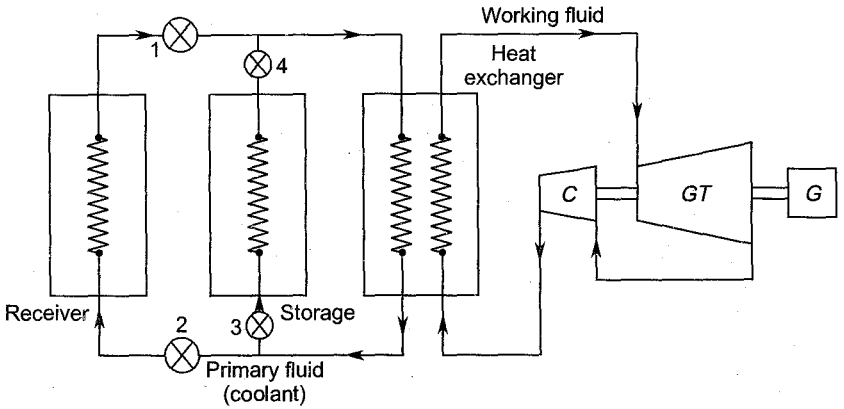

Fig. 17.17 Solar gas turbine plant with storage

storage medium. The same scheme is employed for running steam turbines as shown in Fig. 17.18. Pumps used for the coolant and the working fluid through the storage have not been shown in the figures.

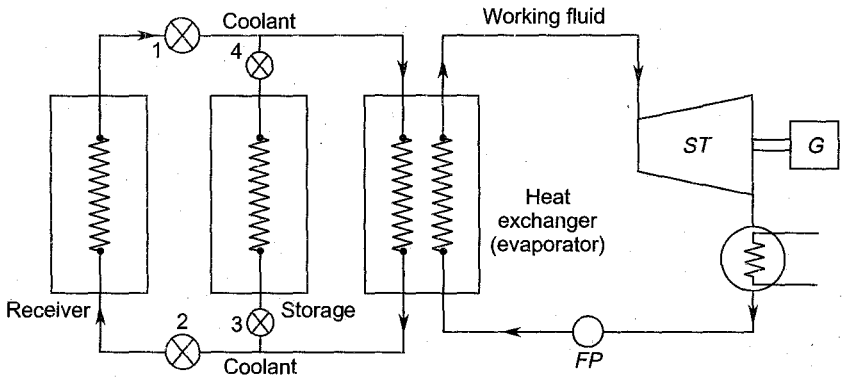

Fig. 17.18 Solar steam turbine power plant with storage device

17.4.3 Latent Heat Storage

In this system the heat storage medium (say a solid such as Lithium compounds and binary salts of Sodium) melts on receiving heat from the receiver through the coolant. Thus heat energy is stored in the medium at constant temperature (melting point of the medium) in the form of latent heat of fusion. This requires high values of latent heat of fusion, melting point and conductivity. Besides this, the material should not be very expensive, corrosive or hazardous.

The increase in volume of the medium should not be too large on melting. This aspect prevents the use of liquids on account of the enormous increase in volume during vapourization.

Compared to the large number of solids available for sensible heat storage, suitable solids for latent heat storage are not easy to find for a given application. Properties of lithium compounds, which have been used for heat storage, are given here for reference:

	Latent heat	*Melting point*
Li F	1050 kJ/kg	848 °C
Li OH	1080 kJ/kg	471 °C

A great advantage of this system of heat storage is that heat is supplied to the working fluid at constant temperature. Combined sensible and latent heat storage system can also be employed by choosing suitable media for thermal energy storage.

17.5 Solar Ponds

A solar pond (Fig. 17.19) is a large water body which is employed to receive solar energy through radiation collected by its surface. It is a collector-receiver system built into one. The heat energy is transferred from the solar pond to a suitable working fluid of low boiling point (freon, propane, toluene etc.) for driving the turbine in a Rankine cycle similar to the one shown in Fig. 17.2 (a and b); in this case the flat-plate collector is replaced by the solar pond. A large size solar pond can enable a turbine power plant to operate at constant load on account of large quantity of heat stored in it.

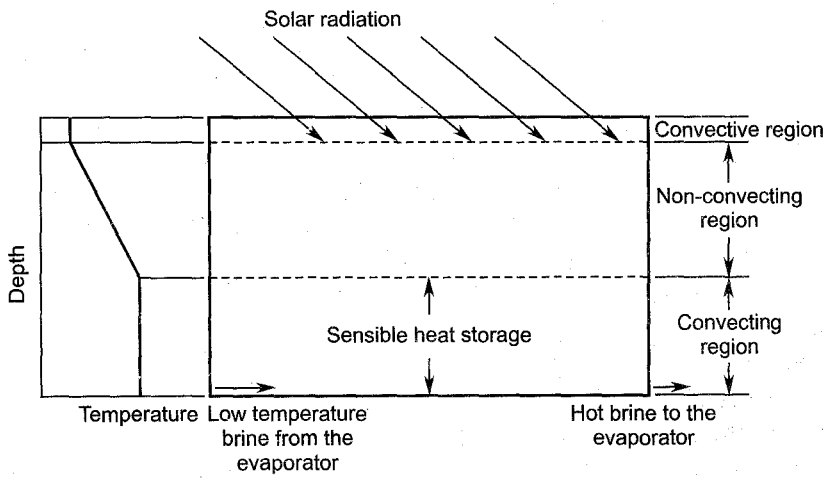

Fig. 17.19 A solar pond for power generation

The temperature in a water body whose surface is exposed to solar radiation is higher at the surface and lower at the bottom. The hotter water

remains at the top on account of its lower density. In contrast to this, if a sufficient quantity of salt (sodium chloride, magnesium chloride etc.) is added to the pond, a salinity gradient (variation of salt concentration) is established along the depth of the pond due to diffusion. Salinity is highest at the bottom and lowest at the top; this establishes a corresponding temperature gradient with temperature also increasing from top to bottom as shown in Fig. 17.19. Thus a thin layer of water at the top has minimum salinity and density. This is the convecting region. The region close to the bottom has maximum salinity and density; the temperature in this region is nearly constant. A non-convecting region separates these two convecting regions as shown in the figure. Water in this region has gradients of salinity, density and temperature.

The hot layer (convecting region) of water nearer the bottom acts as sensible heat storage. Heat is extracted from this layer by pumping hot brine to the evaporator (or heat exchanger) of the power plant where heat is supplied to the working fluid. Low temperature brine returns to the pond from the evaporator/heat exchanger.

The depth of the pond is generally between 1 and 2 meters. The sides and the bottom are treated with some sealing material for preventing or reducing leakage of water; this also decreases the heat losses. The bottom is painted black for capturing more heat energy from solar radiation.

On account of its large size, a solar pond can capture, store and supply large amounts of heat energy (at comparatively lower temperature) to a power plant. However, on account of much lower temperature (t_{max} = 100 °C) at which heat is supplied, the thermal efficiency is too low.

17.6 Solar Turbines

This section brings together the role and performance of the various components of the solar turbine power plant in terms of the turbine output and the net (overall) efficiency of the plant. The properties of the coolant and the working fluid along with the thermo-fluid parameters are discussed. Various aspects of the selection and performance of the organic vapour turbines, steam turbines and gas turbines are also dealt with briefly. Material already given in Chapters 2 to 9 is also applicable to the solar turbines used in the solar power plant.

The solar turbine output, along with the net efficiency of the plant, effects the collector-receiver size and the land area required. These factors determine the capital cost of the plant. The selection of the coolant and the working fluid are also important because they decide the major design parameters of the components of the power plant. For example, the size of the heat exchanger is larger for a small difference between the coolant and the working fluid temperatures.

Steam and gas turbines are available in a wide range of output. Their time tested and proven technology supports their selection for different solar applications. However, for low temperature collector-receiver systems, Rankine cycle organic vapour turbines are widely used in small capacities. It is profitable to employ turbine speeds of 3000 or 3600 rpm for generating electricity at a frequency of 50 or 60 cycles per second; this allows direct coupling between the turbine and the generator. If the turbine speed is higher, a reduction gear is required which leads to additional energy losses and increased cost. However, in some turbines, high rotational speeds are unavoidable.

17.6.1 Coolants and Working Fluids

As mentioned before, a coolant (or the heat transfer fluid) absorbs solar energy in the receiver as heat and transfers it to the working fluid (also known as secondary fluid) in the heat exchanger; coolants are also referred to as primary fluids. Some coolants employed in solar turbine power plants are water/steam, oils, gases, liquid metals and molten salts.

Water can be used as a coolant in both low and medium temperature power plants. Hot water from the receiver can be used to supply heat to the organic fluids in a Rankine power cycle. Steam can also be raised directly in the receiver for driving the steam turbine.

Some oils are also used in the low and medium temperature solar power plants. However, on account of decomposition the maximum oil temperature employed is about 250 °C. A serious problem of using oil in receivers and heat exchangers is its inflammability. Oil coolants are also relatively expensive.

Gases such as air, helium, argon and carbon dioxide have also been used as both coolants and working fluids over a wide range of temperatures ($t_{max} \approx 800$ °C). In this case, the receiver pressure need not always be very high. In a majority of solar power plants, coolant gas is also used as the working fluid in the turbine thus eliminating the use of the heat exchanger.

Molten salts are also used as coolants in the receivers at high temperatures. They can provide high temperatures at near ambient pressures. A slight pressure rise in the receiver is required to overcome pressure losses in the flow passages. On account of high specific heat, they are very suitable heat carriers to the heat exchanger/evaporator in the solar power plant.

Molten metals (sodium, aluminium etc.) have also been used in receivers to absorb heat at high temperatures. Both molten salts and metals require comparatively smaller receivers on account of higher densities.

Table 17.1 gives some pairs of coolants and working fluids used in solar power plants. This also gives approximate values of the maximum temperatures of the coolants and working fluids.

Table 17.1 Pairs of coolants and working fluids in solar turbine power plants

Coolant	t_{max}	*Working fluid*	t_{max}
Steam/water,	500 °C	Steam	
Pressurised water,	150 °C	R-114, R-115, Pyridine,	130 °C
Water,	100 °C	Freon, propane	
Oils	300 °C	R-113	160 °C
Calori HT-43,	216 °C	R-113, R-11,	160 °C
Gases			
Air	800 °C	Air	
Air	600 °C	Steam	550 °C
Helium,	800 °C	helium	
Carbon dioxide			
Molten salts			
Hitec,	450 °C	Steam	430 °C
(nitrates of sodium			
and potassium)	525 °C		
Molten metals			
Sodium,	550 °C	Steam	500 °C
Aluminium		Steam	

Some important considerations for selecting a coolant are:

(a) Be cheap and easily available.
(b) Be non-corrosive and non-toxic.
(c) Provide high values of heat transfer coefficient.
(d) Have low vapour pressure at high temperature.
(e) Freezing points be well below the minimum temperature that may occur in the receiver and heat exchanger.

Steam and organic vapours are used as working fluids in a large number of Rankine cycle solar turbine plants; air and helium have been used in solar gas turbines.

Some important aspects and properties of the working fluids to be considered for solar turbines are:

(a) Availability and cost,
(b) Chemical effects on the power plant components, specially on seals and bearings.

(c) Toxicity and inflammability,
(d) Freezing and boiling points,
(e) Vapour pressure,
(f) Moleculer weight, and
(g) Thermodynamic properties such as specific heat, thermal conductivity, etc.

17.6.2 Thermo-fluid Dynamic Parameters

Following equations summarise the effects of various thermo-fluid dynamic parameters on the design, performance and selection of solar turbines:

Pressure ratio, $$p_r = p_1/p_2 \tag{17.14}$$

Density, $$\rho = \frac{1}{v} = \frac{p}{RT} = \frac{W}{\mathbf{R}}\frac{p}{T} \tag{17.15}$$

Mass flow rate, $$\dot{m} = \rho A c \tag{17.16}$$

Enthalpy drop, $$\Delta h = c_p\,(\Delta T) \tag{17.17a}$$

$$\Delta h = c_p\, T_1\, \{1 - (p_r)^{\frac{1-\gamma}{\gamma}}\} \tag{17.17b}$$

Power output, $$P = \dot{m}\ (\Delta h) \tag{17.18}$$

Specific speed $$N_{st} = \frac{\sqrt{P}}{H^{5/4}}\ N \tag{17.19}$$

Reynolds number, $$\mathrm{Re} = \frac{c \times D}{\mu/\rho} \tag{17.20}$$

Mach number, $$M = \frac{c}{a} = c \times \left(\gamma \frac{\mathbf{R}}{W} T\right)^{-1/2} \tag{17.21}$$

Most of the above relations have been mentioned and discussed in earlier chapters. Chapter 7 deserves special attention in the present context.

As stated before, the type of collector-receiver system decides the temperatures of the coolant and the working fluid. The selection of the working fluid fixes the properties W, c_p, γ, R and μ. Values of enthalpy (or temperature) drop and the mass flow rate of the working fluid for a given capacity (power output) are inversely proportional to each other (Eq. 17.18). Enthalpy drop depends on the pressure ratio available (Eq. 17.17b) across the turbine. Mass flow rate is higher for a smaller value of the enthalpy drop; this offers larger flow area (Eq. 17.16) leading to longer turbine blades and lower fluid and rotor velocities. Conversely,

smaller flow rates and higher enthalpy drops give shorter blades and higher velocities which lead to higher rotor losses.

Turbine blade height can be increased by employing low density fluid for a given flow rate (Eq. 17.16).

For high values of enthalpy drop, several turbine stages are employed.

In a condensing turbine, the exit pressure (p_2) is fixed by the condenser and the cooling water temperature. For a working fluid of large specific volume (Eq. 17.15) at the turbine exit, condenser size may be impractically large.

For a given capacity and rotational speed, the specific speed of the turbine is higher for lower enthalpy drop and vice versa (Eq. 17.19). Axial flow turbines fall in the higher range of specific speed. For lower values of the specific speed, inward flow radial and partial admission turbines are other options.

Lower fluid velocity and smaller turbine size give lower values of the Reynolds number (Eq. 17.20). If it is less than 2×10^5, higher losses will occur. For higher values ($Re > 2 \times 10^5$), losses are unaffected by Reynolds number.

A higher molecular weight of the working fluid gives higher values of the Mach number (Eq. 17.21); if it is close to unity, additional losses would occur due to local acceleration and deceleration of the flow accompanied by shock waves. Higher values of the Mach number also arise due to higher fluid velocities and lower temperatures (see Eq. 17.21).

17.6.3 Organic Vapour Turbines

For lower temperatures ($t_{max} \approx 150$ °C), collector-receiver system, organic vapour turbines are employed in the solar turbine power plants. Steam and gas turbines are unsuitable for low temperature applications. Heat energy is collected in the receiver from solar radiation by hot water or oil; the relatively low temperature coolant is used to evaporate an organic fluid (freon; propane, isobutane etc.) in the heat exchanger (Fig. 17.2 a and b). The organic working fluid (vapour), having a much lower boiling point at sufficiently higher pressure, expands through the turbine.

This combination of a coolant at near ambient pressure (and comparatively lower temperature) and the working fluid at higher pressure and low temperature, enables the receiver to be lighter and comparatively cheaper. The collector and receiver efficiencies are higher on account of the lower temperature at which heat is collected from the solar radiation. Therefore, in spite of the lower thermal efficiency of the turbine power plant the net efficiency of the power plant is high, and comparable with

power plants employing steam turbines. Some organic vapour turbines show even higher efficiencies than the steam turbines in smaller capacities; their optimum rotor speeds are also lower than steam turbines.

Organic fluids for solar turbines are expensive. Therefore, organic vapour turbines are designed and manufactured as sealed units to prevent the loss of the working fluids; the working fluids are also employed for lubrication of bearings.

Some of the working fluids which have been used in organic vapour turbines are flourinol, Freon – 11, 12, 113 and 115, Isobutane, pyridine, propane and toluene.

17.6.4 Steam Turbines

Steam turbines have been employed in Rankine cycle for a large number of solar power plants of medium and large capacities. The receiver can also generate steam directly from solar radiation without an intermediate fluid or coolant; in this case the heat exchanger is not required. This is a great advantage.

However, in some plants, the receiver employs molten salts or liquid metals for higher temperatures and heat energy is transferred to the water/steam in a separate heat exchanger. Here the conventional steam boiler is replaced by the receiver or heat exchanger (Fig. 17.18).

Condensing steam turbines offer large values of pressure ratio and higher thermal efficiencies. Typical values of the pressure and temperature which have been employed in solar power plants are

Pressure	:	50 – 100 bars
Temperature	:	400 – 500 °C

Both impulse and reaction stages are used. For small values of power output and mass flow rate, impulse stages are preferable on account of the reduced leakage loss through the radial clearances. Leakage loss is considerably higher across the rotor of a reaction stage because of pressure difference. Sometimes partial admission of steam is employed in small turbines; impulse stage is also suitable for such a configuration.

If steam is generated in a storage device, lower pressure steam from the storage system is admitted through a separate valve during non-solar period. Though steam turbines have higher capital cost, their operating life is much longer.

17.6.5 Gas Turbines

Gas turbines in Brayton cycle are employed in solar power plants for higher inlet temperatures ($t_{max} \simeq 500 - 800$ °C); higher temperatures of the

working gas give higher value of the thermal efficiency. Therefore, in spite of the lower collector-receiver efficiency, the net solar power plant efficiency is comparatively higher. In a solar gas turbine power plant using air as the working fluid, the air compressor and the turbine have the same design features as in a conventional gas turbine plant; here the combustion chamber is replaced by the receiver/heat exchanger (Fig. 17.17). In some solar power plants, the working fluid is directly heated in the receiver.

The main advantages of the solar gas turbines are:

(a) Low pressure receiver/heat exchanger.
(b) Fewer stages.
(c) Lower capital cost.
(d) Absence of condenser, feed water heaters, etc.
(e) Very small cooling water requirement.

Gas turbines require expensive materials for higher gas temperatures and their operating life is relatively shorter. Since the gas temperatures in the exhaust of the gas turbines are high, employing a bottoming cycle is useful in solar turbine plants with high receiver temperatures of the order of 800 °C – 1000 °C.

On account of lower operating pressures and relatively lower values of the gas density, it is much easier to obtain higher values of the aspects ratio (longer blades); this gives much lower aerodynamic losses.

Solar gas turbine plants are not able to greatly benefit from energy storage during non-solar periods. This is because of the high temperatures of the coolant/working fluid. Storage of large quantities of heat energy at high temperatures is difficult and uneconomical.

17.6.6 Net Efficiency

Figure 17.20 depicts typical variations of the efficiencies of the collector (η_c) and the turbine power plant (η_{th}). As mentioned before, the collector efficiency decreases with the receiver temperature. The thermal efficiency (η_{th}) of the power plant increases with the inlet temperature of the working fluid. Therefore, the overall (net) efficiency (η_n) of the solar power plant varies as shown in the figure. This curve is almost flat near the maximum efficiency (η_{max}) point. In some temperature range the gain in thermal efficiency due to higher fluid temperature is offset by the significantly lower collector efficiency.

The nature of the curves shown in Fig. 17.20 would vary in different solar turbine power plants employing different collector-receiver systems and types of turbines (steam, gas and organic vapour) in various ranges of

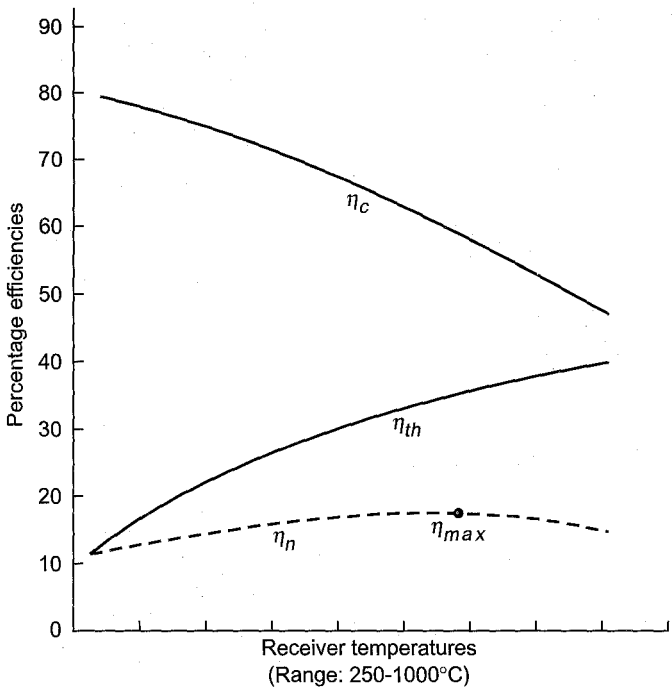

Fig. 17.20 Overall (net) efficiency of solar turbine power plants (typical curves)

the plant output. Net efficiency would be affected by factors such as pressure and temperature drops in the interconnecting passages, performance of subsystems, types of coolants and working fluids, etc.

Data suggests that the net efficiency of a large number of solar turbine power plants is between 15 and 20 per cent. In view of the wide, flat section of the net efficiency curve, economic and reliability factors take over the final choice of a system for solar turbine power plants.

17.7 Advantages and disadvantages

Some of the main advantages and disadvantages of solar turbine power plants are summarized in the following sections:

17.7.1 Advantages

1. Fuel cost is zero since solar turbine power plants do not depend on any fuel or exhaustable source of energy.
2. No extraction of fuel and transportation are required.
3. No fuel storage, processing and handling equipment are needed.

4. Large scale use of solar power plants can bring about saving in the exhaustable sources of energy such as petroleum, coal and natural gas.
5. Power is produced by solar power plants without significant environmental pollution.
6. Large solar power plants, specially those with energy storage systems, can be used in special situations when other power plants are not available.
7. Solar power plants can easily operate in remote places such as deserts and islands where large plots of land are available for solar collectors.

17.7.2 Disadvantages

1. Availability of power from solar (turbine) power plants is not continuous; it depends on sunshine.
2. For continuous supply of power it needs large heat (energy) storage systems; this adds to the already high capital cost.
3. Solar energy is very thinly distributed over the earth surface. Therefore, large surface areas are required to capture solar radiation.
4. Collection of solar energy produces large areas of shadow which can create some ecological problems.
5. Expensive sun tracking systems are required.
6. In some pressure and temperature ranges it requires special materials and expensive working fluids.
7. Its initial cost is high.
8. Solar power plants suffer from low values of plant load factor.
9. Overall efficiencies of solar turbine power plants are too low.
10. Leakage of some coolants and organic working fluids used in the power plants is a threat to life.

Notation for Chapter 17

a	Velocity of sound
A	Area of cross-section, area
c	Fluid velocity
c_p	Specific heat at constant pressure
$\text{CR} = \frac{A_c}{A_r}$	Concentration ratio

C_s	Specific heat of the solid
D	Rotor diameter
H	Head
Δh	Enthalpy drop
I	Incident solar flux
L	Losses, latent heat
m	Mass
M	Mach number
n	Number of heliostats
N	Turbine rotational speed
p	Pressure
P	Power output
Q	Heat
R	Gas constant
$\mathbf{R}$	Universal gas constant
Re	Reynolds number
T	Absolute temperature
ΔT	Temperature drop
$\text{TR} = \frac{T_r}{T_a}$	Temperature ratio
U	Heat loss coefficient
V	Volume
v	Specific volume
W	Molecular weight

Greek Symbols

γ	Ratio of specific heats
η	Efficiency
μ	Dynamic viscosity
ρ	Density

Subscripts

1	Initial
2	Final
a	Ambient
ac	Air compressor
c	Collectors/concentrators
max	Maximum value
n	Net
o	Optical

r	Receiver
s	Solid, storage medium, specific
st	storage
T	Turbine
u	Useful
th	Thermal

Questions

17.1 Draw a simple and illustrative sketch of a solar turbine power plant. Describe its working briefly.

17.2 Write down the names and chemical formulas of five working fluids besides air and steam employed in solar turbine plants.

17.3 Describe the important properties of the working fluids used in solar turbine plants.

17.4 Write down seven main advantages and five disadvantages of solar turbine plants.

17.5 What is a heliostat in a solar power plant? Describe its working.

17.6 Describe briefly three main types of solar radiation collectors. Write down their advantages and disadvantages.

17.7 What is an organic gas turbine (OGT) power plant? Describe its working with the aid of an illustrative sketch.

17.8 What is the purpose of a sun-tracking system in a solar thermal power plant? How does it work?

17.9 What is a central receiver system (CRS) in solar turbine power plant? What are its advantages and disadvantages?

17.10 Draw an illustrative diagram of a turbine power plant working in conjuction with a solar pond. Describe its working briefly.

17.11 Depict graphically the variation of

(a) temperature with depth in a saline solar pond.

(b) overall efficiency of a solar turbine plant with collector temperature.

(c) collector efficiency with temperature ratio, T_c/T_a.

17.12 What is a distributed solar thermal system for electric power generation? Explain with the aid of a sketch.

17.13 What are the various methods of thermal energy storage in solar turbine power plants? Describe one of them.

17.14 What are Fresnel lenses and mirrors? How are they used in solar power plants?

17.15 Describe the working of the following with the aid of illustrative sketches:

(a) Parabolic trough collector
(b) Compound parabolic collector
(c) Concentric turbular collector-receiver.

Appendix A
Specifications of Some Aircraft Engines

A.1 Principal Data for Turbo Prop Engines

Rolls Royce Dart (By courtesy of Rolls-Royce Limited)
[See Figs. A.1 and A.2 (Plate 2)]

Compessor	2 centrifugal
Speed	15000/1400 rpm
Compressor pressure ratio	5.6–6.35
Specific fuel consumption	0.40–0.52 kg/kWh
Engine power	1343–2238 kW
Air mass-flow	9–12.3 kg/s
Turbine stages	2–3 axial
Combustion system	7 can-type burners
Turbine entry temperature (Max)	1270 K

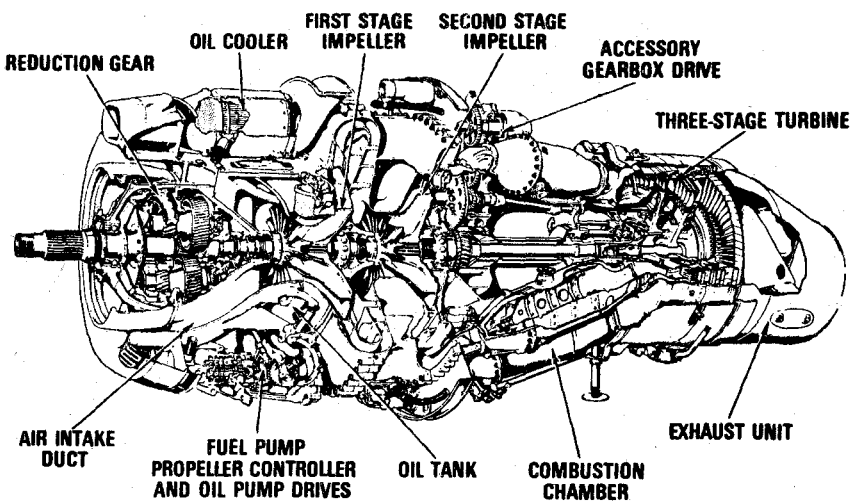

Fig. A.1 The Rolls-Royce Dart engine

PLATE 2

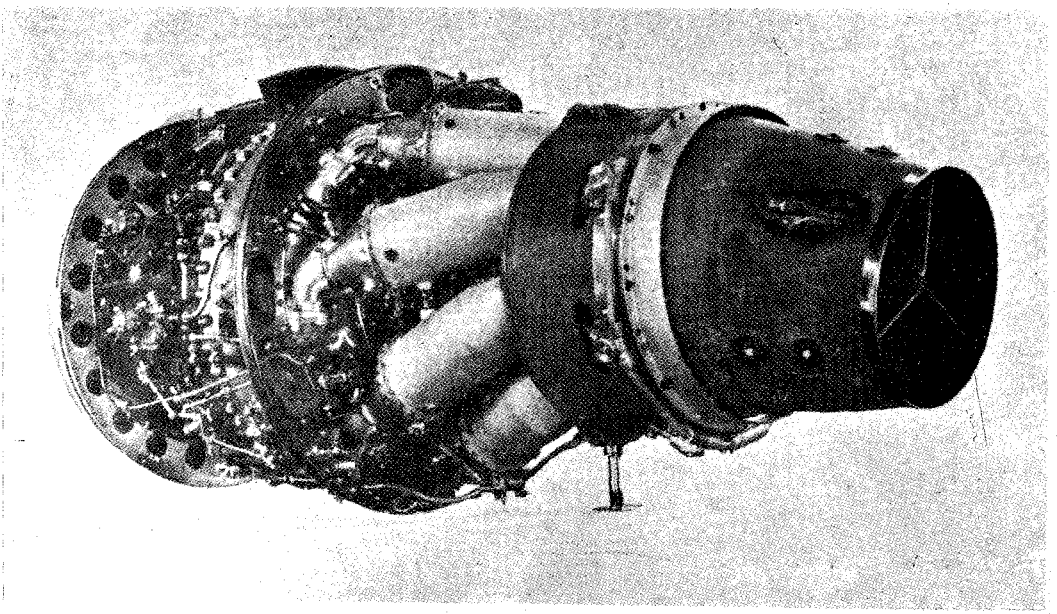

Fig. A.2 The Rolls-Royce Dart Engine

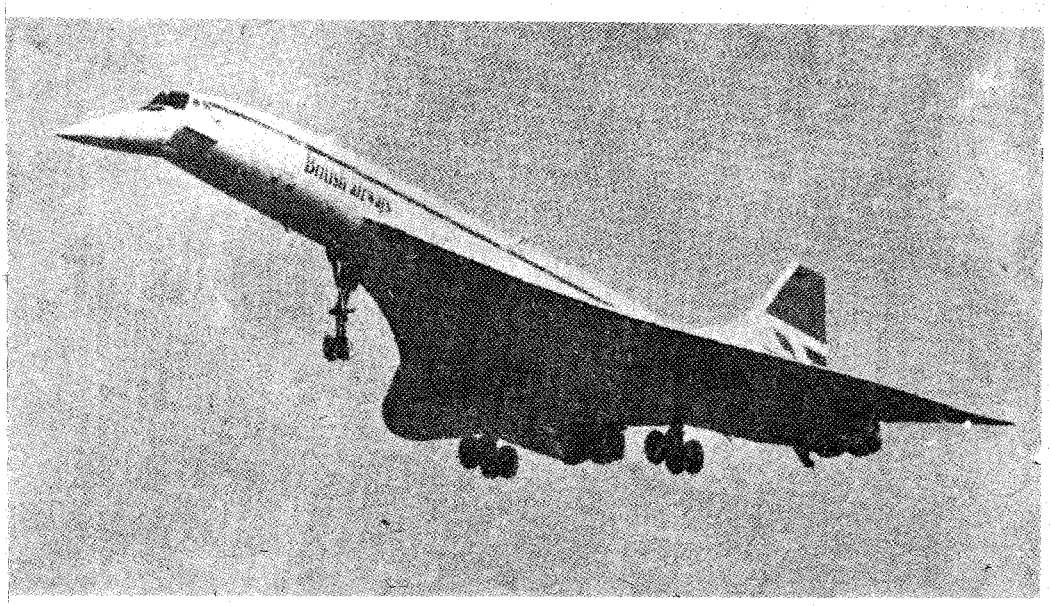

Fig. A.3 The Concorde Aircraft

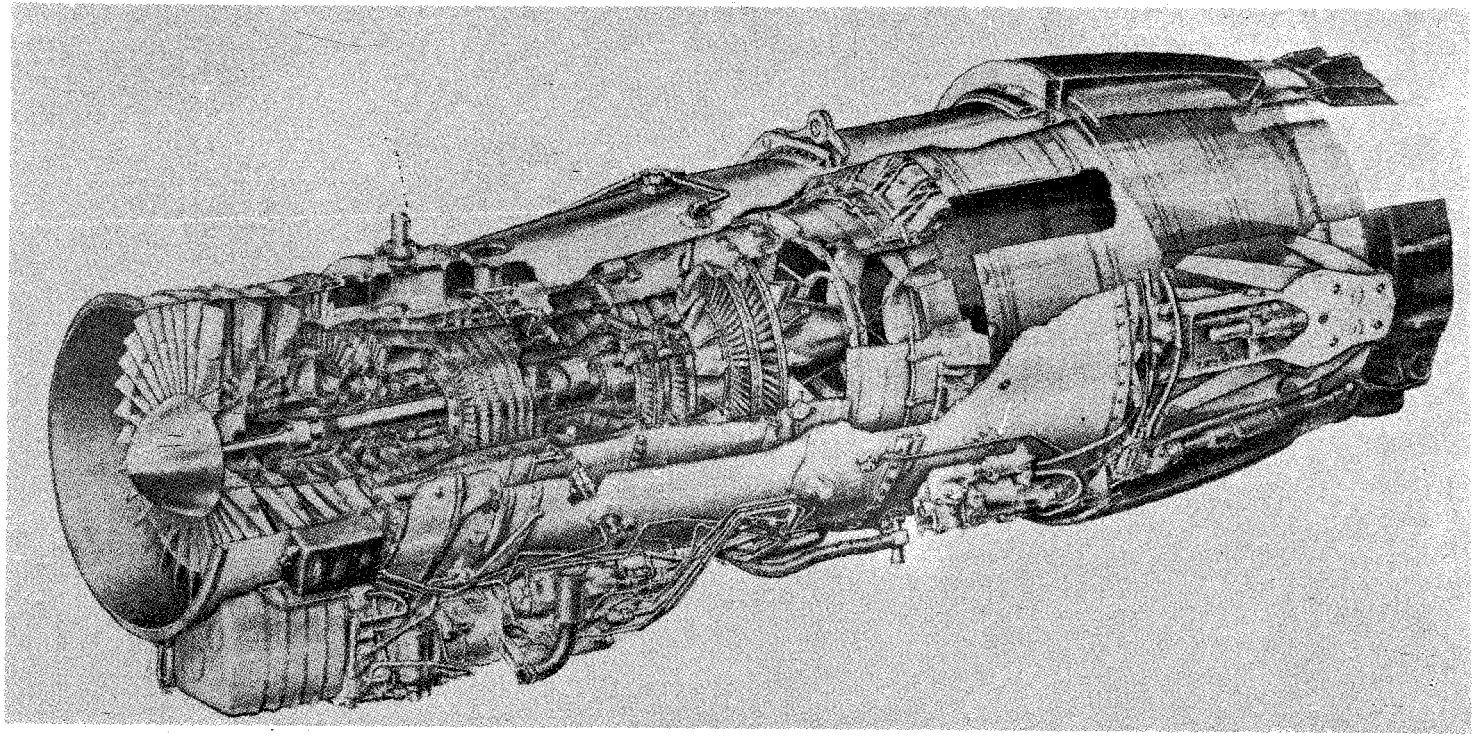

Fig. A.4 Turbo Fan Engine (Turbo-Union RB-199)

PLATE 3

Pratt and Whitney T34 (By courtesy of United Technologies)

Compressor Stages	13 axial
Pressure ratio	6.7
Speed	11000 rpm
Air mass-flow	29.5 kg/s
Combustion system	Annular type with eight combustion cones
Turbine stages	3
Specific fuel consumption	0.425 kg/kWh
Engine power	4476–5222 kW
Engine weight	1302 kg

A.2 Principal Data for a Turbojet Engine

Olympus 593 for Concorde (By courtesy of Rolls-Royce Limited)

Four Olympus 593 turbojets power the BAC/Aerospatiale Concorde aircraft [Fig. A.3 (Plate 2)], which has been designed to cruise at twice the speed of sound at altitudes up to 18288 m and to travel distances up to 6750 km without refuelling.

The engine is divided into twelve major assemblies and the exhaust into three for ease of maintenance.

Leading particulars:

Take-off thrust, including reheat	169 kN
Cruise thrust (Mach 2.0)	44.6 kN
Specific fuel consumption	33.71 mg/Ns
Pressure ratio (cruise)	11.3
Compressor stages	7 LP, 7 HP
Combustion system	Annular with vapourizing burners
Turbine stages	1 LP, 1HP
Overall length (flange-to-flange) of the engine	3810 mm
Maximum diameter	1220 mm
Intake casing diameter	1206 mm
Weight (dry engine) including primary nozzle system	3386 kg

A.3 Principal Data for a Turbofan Engine

Turbo-Union RB-199 (By courtesy of Turbo-Union Limited)

This is a three-shaft reheated turbofan engine [Fig. A.4 (Plate 3)]. It powers the twin-engined multi-role combat aircrafts (MRCA). Its main features are:

1. 3-spool layout for high performance, efficiency and flexibility,
2. Compact integral reheat system,
3. High thrust/weight ratio,
4. High thrust per unit frontal area,

5. Low fuel consumption,
6. Advanced control system,
7. Modular construction, and
8. On-condition health monitoring.

Leading particulars:

Three-shaft reheated turbofan	
Compressors	3-stage LP/3-stage IP/6-stage HP
Turbine	HP 1-stage cooled/IP 1- stage cooled/LP 2-stage
Shaft speeds	12000-19000 rpm
Thrust: class without reheat	35.5 kN
Class with reheat	71 kN
Maximum air mass-flow	over 70 kg/s
Bypass ratio	over 1
Pressure ratio	over 23
Turbine entry temperature	over 1600 K
Reheat temperature	over 1900 K
Thrust/weight ratio	over 8
Length with afterburner reheat	3.23 m
Maximum diameter	0.87 m

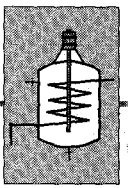

Appendix B Specifications of Some Turbine Blade Sections[262,291A]

B.1 10 C4/60 C 50

t_{max}/l = 10%
base profile C4
camber angle $\theta = 60°$
circular camber line
a/l = 50%

B.2 T 6 Aerofoil Blade

t_{max}/l = 10%
base profile T6
leading edge radius 0.12 t_{max}
trailing edge radius 0.06 t_{max}
parabolic camber line
a/l = 40%

B.3 C 90 15 A (Russian Turbine Blade Cascade)

(C) refers to stationary blade row

$$\alpha_1' = 90° \ (\alpha_1 = 70°–120°)$$
$$\alpha_2' = 15° \ (\alpha_2 = 13°–17°)$$

[A refers to subsonic cascade (M = 0.5–0.85)]

$$s/l = 0.70–0.85$$
$$\gamma = 35°–40°$$

Profile of blades is separately given.
All angles are from tangential direction.

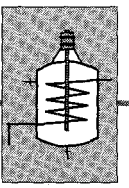

Appendix C Specifications of Some Compressor Blade Sections[213,242,412]

C.1 12C 4/35 P 30

t_{max}/l = 12%
base profile C4
camber angle θ = 35°
parabolic camber line
position of maximum camber, a/l = 30%

C.2 11C 1/45 C 50

t_{max}/l = 11%
base profile C 1
camber angle θ = 45°
circular camber line
a/l = 50%

C.3 NACA 65—(18) 10

profile shape reference number 65
lift coefficient = 1.8 (corresponding camber line)
$t_{max}/l \approx$ 10%

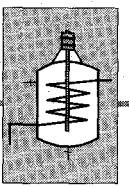

Appendix D Specifications of Some Wind Turbines*

D.1 Environmental Energies, Inc.

Wind electric battery charger

200 W, 12 V, 14 A (max.)

Wind velocity	7-23 mph
Propeller	6 ft, 2 bladed wooden
Direct driven	N = 900 rpm
Tower	10 ft.

D.2 Smith Putnam Machine, Vermont (1941-45)

1.25 MW ac power through step-up gear at 600 rpm

Propeller	175 ft (55 m), 2 bladed
Speed	28 rpm
Tower	110 ft (34 m)

D.3 Wind Works, Wisconsin, USA

Twelve footer

12V, 85 A

Wind velocity	10.2 mph (16.32 kmph)
Propeller	12 ft, 2 bladed, $N = 117$ rpm

Wind velocity		Output (W)
mph	kmph	
5	8	30
10	16	239
15	24	806
20	32	1911
25	40	3734 (max)

* (Courtesy Manufacturers).

D.4 Wind Turbine for Electric Supply to a Light House in Futaoi Island (Japan)

Wind velocity	7.5 m/s
Propeller	7 m, three-bladed, N = 65 rpm
Shaft output	2.5 kW
Generator output	2.1 kW (dc), 125 V
Battery	420 A-h

D.5 Gedser Mill (Denmark)

Wind velocity	15 m/s
Wind velocity for automatic start	5 m/s
Propeller	24 m, three-bladed, N = 30 rpm
Tower	25 m
Generator	200 kW, asynchronous 8 polar 750 rpm

Transmission between the wind turbine and the generator through a double chain drive, ratio 1 : 25.

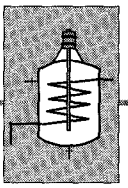

Appendix E
Principal SI Units and Their Conversion

E.1 SI Units and Dimensions

Quantity	Units	Dimensions
Length	m	L
Mass	kg	M
Time	s	T
Acceleration	m/s^2	L/T^2
Force/weight	N	ML/T^2
Torque	mN	ML^2/T^2
Pressure	N/m^2	M/LT^2
Energy/work/heat	J = Nm	ML^2/T^2
Power	Nm/s = W	ML^2/T^3

E.2 Conversion of Units

Length

1 m = 3.28 ft

1 mile = 1.609 km

1 nautical mile = 1.853 km

Area

$1\ m^2 = 10.765\ ft^2$

$1\ ft^2 = 0.093\ m^2$

Volume

$1\ m^3 = 1000$ litres $= 35.32\ ft^2$

1 litre $= 0.001\ m^3 = 0.0353\ ft^3$

1 pint = 0.568 litre

Mass

1 kg = 2.204 lb

1 lb = 0.4537 kg

1 tonne (metric) = 0.984 ton

Force

$$1\ \text{N} = 0.102\ \text{kgf} = 0.2248\ \text{lbf}$$
$$1\ \text{kgf} = 9.807\ \text{N} = 2.204\ \text{lbf}$$

Pressure

$$1\ \text{bar} = 10^5\ \text{N/m}^2 = 100\ \text{kN/m}^2 = 0.1\ \text{MN/m}^2$$
$$1\ \text{bar} = 1.0197\ \text{kgf/m}^2 = 14.504\ \text{lbf/in}^2$$
$$1\ \text{mm W.G.} = 1\ \text{kgf/m}^2 = 9.807\ \text{N/m}^2 = 0.0981\ \text{mbar}$$

Density

$$1\ \text{kg/m}^3 = 0.0625\ \text{lb/ft}^3$$
$$1\ \text{lb/ft}^3 = 16.025\ \text{kg/m}^3$$

Energy and work

$$1\ \text{Nm} = 1\ \text{J} = 0.7375\ \text{ft-lbf} = 0.102\ \text{kgf-m}$$
$$1\ \text{ft-lbf} = 0.1383\ \text{kgf-m} = 1.356\ \text{Nm}$$

Heat

$$1\ \text{kJ} = 0.9478\ \text{Btu} = 0.2388\ \text{kcal}$$
$$1\ \text{Btu} = 778\ \text{ft-Ibf} = 0.252\ \text{kcal} = 1.055\ \text{kJ}$$

Power

$$1\ \text{Nm/s} = 1\ \text{J/s} = 1\ \text{W}$$
$$1\ \text{W} = 0.7375\ \text{ft-lbf/s} = 0.102\ \text{kgf-m/s}$$
$$1\ \text{kW} = 737.5\ \text{ft-lbf/s} = 102\ \text{kgf-m/s}$$
$$1\ \text{kW} = 1.34\ \text{HP (FPS)} = 1.36\ \text{HP (metric)}$$

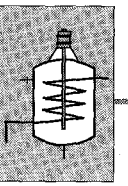

Appendix F Dimensionless Numbers for Incompressible Flow Machines

For the purpose of developing dimensionless numbers, Eq. (7.4) of Chapter 7 is rewritten as

$$P = (\text{constant})\ [(gH)^a \times Q^b \times \mu^c \times \rho^d \times N^e \times D^f] \tag{F.1}$$

Writing the dimensions on both sides of the above equation, we get

$$ML^2T^{-3} = (\text{constant})\ [(L^2T^{-2})^a \times (L^3T^{-1})^b \times (ML^{-1}T^{-1})^c \times (ML^{-3})^d \times (T^{-1})^e \times L^f] \tag{F.2}$$

Equating the indices of M, L and T on two sides, the following three equations are obtained:

$$1 = c + d \tag{F.3}$$

$$2 = 2a + 3b - c - 3d + f \tag{F.4}$$

$$-3 = -2a - b - c - e \tag{F.5}$$

Three dimensionless numbers, under the indices a, b and c, can be formed on the right hand side. Therefore, indices d, e and f are now expressed in terms of a, b and c. Equations (F.3), (F.4) and (F.5) give:

$$d = 1 - c \tag{F.6}$$

$$e = 3 - 2a - b - c \tag{F.7}$$

$$f = 5 - 2a - 3b - 2c \tag{F.8}$$

Substitution of these values in Eq. (F.1) yields

$$P = \text{constant} \times (gH)^a \times Q^b \times \mu^c \times \rho^{1-c} \times N^{3-2a-b-c} \times D^{5-2a-3b-2c}$$

$$P = \text{constant} \times (gH)^a \times Q^b \times \mu^c \times \frac{\rho}{\rho^c} \times \frac{N^3}{\left(N^2\right)^a N^b N^c} \times \frac{D^5}{\left(D^2\right)^a \left(D^3\right)^b \left(D^2\right)^c}$$

Rearrangement of the above expression in four groups with indices 1, a, b and c gives the following relations with dimensionless numbers:

$$\frac{P}{\rho N^3 D^5} = \text{constant} \left[\left(\frac{gH}{N^2 D^2} \right)^a \times \left(\frac{Q}{ND^3} \right)^b \times \left(\frac{\mu}{\rho N D^2} \right)^c \right] \tag{F.9}$$

The last term is the reciprocal of Reynolds number as shown in Sec. 7.4.4. The above equation is expressed in a more general form:

$$\frac{P}{\rho N^3 D^5} = f\left(\frac{gH}{N^2 D^2}, \frac{Q}{ND^3}, \frac{\rho ND^2}{\mu}\right) \tag{F.10}$$

Appendix G
Efficiencies and Heat Rates of Thermal Power Plants

As shown in Sec. 4.4 heat rates and efficiencies of thermal power plants are related by the following equation:

$$\text{Efficiency} = 3600/\text{Heat rate}$$

This has been used to tabulate heat rates corresponding to various values of efficiencies. The values given in Table G-1 and the plot (Fig. G-1) are applicable to all the thermal power plants—steam, gas, combined cycle solar and diesel.

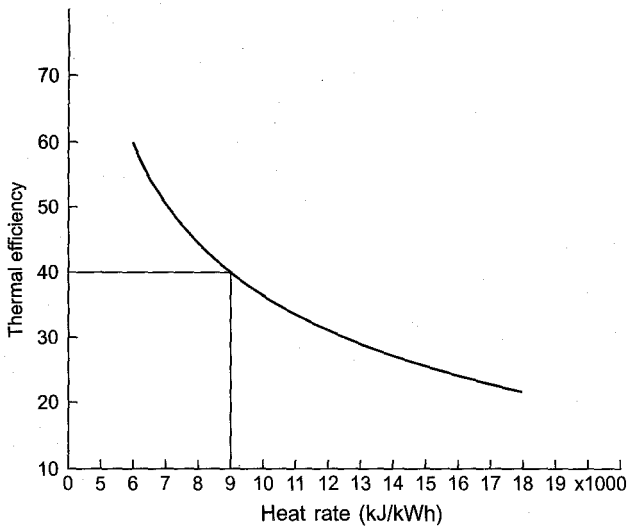

Fig. G.1 Values of thermal efficiency for thermal power plants corresponding to heat rates

Table G.1 Values of heat rate for thermal power plants corresponding to their efficiencies

Efficiency (per cent)	*Heat rate (kJ/kWh)*
20	18,000
25	14,400

Contd.

Table G.1 *Contd.*

Efficiency (per cent)	*Heat rate (kJ/kWh)*
30	12,000
35	10,285.7
40	9,000
45	8,000
50	7,200
55	6545.45
60	6,000

Chapter

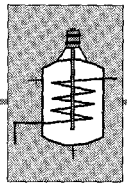

Appendix H
Specifications of a Combined Cycle Power Plant*

Some important specifications of the 817 MW Dadri combined cycle power plant are given in this appendix.

Station Capacity	2 × 408.5 = 817 MW
Each of the two units consists of two gas turbines feeding one steam turbine.	
Gas turbine output	2 × 131 = 262 MW
Steam turbine output	146.5 MW
Combined gas and steam turbine output and efficiency	408.5 MW (48.33 %)
Fuel	Main: Natural gas (from HBJ pipe line). Alternate fuel: HSD

Gas Turbine

Capacity	131.3 MW
Design inlet temperature	1060 °C
Rated speed	3000 rpm
Number of turbine stages	4
Number of compressor stages	16
Compressor pressure ratio	10.2
Mass flows rate of air (at 27 °C)	404 kg/s
Mass flow rate of exhaust gases	471.59 kg/s
Temperature of the exhaust gases at the inlet of the HRB	559.5 °C

Steam Turbine

Type	Two cylinder
Steam inlet pressure	61.75 bar
Steam inlet temperature	528.6 °C
Steam flow rate	225.9 tonnes/hr
Number of HP stages	22
Number of LP stages	7
Turbine exhaust pressure	0.1122 bar

*** By courtesy of National Thermal Power Corporation Ltd. India.**

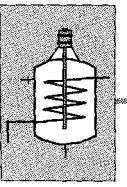

Appendix I
Technical Data for the BHEL 500 MW Steam Turbine*

Rating	500 MW
Rated speed	3000 rpm
Temperature of steam at inlet	537°C
Pressure of steam at inlet	166.716 bar (170 kgf/cm^2)
Steam flow rate	1500 tonnes/hr.
Type	Reaction
Number of cylinders	Three
High pressure	1
Intermediate pressure	1 (double flow)
Low pressure	1 (double flow)
Number of stages:	
High pressure	17
Intermediate pressure	2 × 12
Low pressure	2 × 6
Mean diameter (first stage)	1792 mm
Mean blade ring diameter (last row)	3650 mm
Height of the last blade row	1050 mm
Reheat steam temperature (between H.P. and I.P. cylinders)	537°C
Condenser pressure	0.1013 bar (0.1033 kgf/cm^2)
Mode of governing	Throttle (Electro Hydraulic)

*** Courtesy: Bharat Heavy Electricals Ltd., New Delhi, India. (Plate 4)**

PLATE 4

500 MW steam turbine-generator sets at 2000 MW Singrauli Super Thermal Power Station of NTPC—supplied and executed by BHEL, India *(Courtesy:* NTPC and BHEL, India)

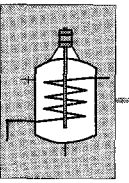

Select Bibliography

Owing to the explosion of literature in the form of books, papers, articles, etc. on the subject of "Turbines, compressors and fans", it is not found necessary to include even a small fraction of the big ocean here. The aim of compiling the present bibliography is only to acquaint the readers with the books and comparatively recent papers in the field of turbomachinery.

Since the subjects of thermodynamics, fluid mechanics, gas dynamics and aerodynamics make the foundation of the theoretical treatment of the machines discussed in this volume, some books in these areas are also included.

Various sections of the bibliography are presented approximately in the same order as the subject matter in the book. Besides this, various sections of the bibliography also acquaint the more advanced readers with the specialized areas of research in turbomachinery. Literature on both the plants, machines and their principal elements, which are the subjects of recent research, have been collected.

It is hoped that this compilation will be useful to research students and supervisors, teachers and professional engineers enquiring into various aspects of this class of machines.

Various references have been quoted by superscripts in the text where necessary.

Turbomachinery (Book)

1. Balje, O.E., *Turbomachines: A Guide to Design, Selection and Theory,* Wileys, April 1981.
2. Betz, A., *Introduction to the Theory of Flow Machines,* Pergamon Press, Oxford and London, 1966.
3. Cohen H., Rogers, G.F.C. and Saravanamuttoo, H.J.H., *Gas Turbine Theory,* (S.I. Units), 2nd edn, Longman Group Ltd., 1972.
4. Cox, H.R., *Gas Turbine Principles and Practice,* George Newnes Ltd., London, 1955.
5. Csanady, G.T., *Theory of Turbomachines,* McGraw-Hill, 1964.
6. Dixon, S.L., *Fluid Mechanics, Thermodynamics of Turbo-machinery,* 2nd edn, Pergamon Press, 1975.
7. Hawthorne, W.R. (Ed.), *Aerodynamics of Turbines and Compressors,* Vol. 10, Princeton University Press, 1964.

8. Kadambi, V. and Manohar Prasad, *An Introduction to Energy Conversion,* Vol. III—*Turbomachinery,* Wiley Eastern Ltd., 1977.
9. Kearton, W.J., *Steam Turbine Theory and Practice,* 7th edn., Pitman, London, 1958.
10. Kerrebrock, J.L., *Aircraft Engines and Gas Turbines,* The MIT Press, 1977.
11. Shepherd, D.G., *Principles of Turbomachinery,* Ninth Printing, Macmillan, 1969.
12. Stodola, A., *Steam and Gas Turbines,* Vol. I and II, McGraw-Hill, New York, 1927, Reprint, Peter Smith, New York, 1945.
13. Thomson, W.R., *Preliminary Design of Gas Turbines,* Emmott and Co. Ltd., London, 1963.
14. Traupel, W., *Thermische Turbomachinen,* 3rd edn, Springer Verlag, Berlin, 1978.
15. Vavra, M.H. *Aerothermodynamics and Flow in Turbomachines,* John Wiley and Sons, 1960.
16. Vincent, E.T., *The Theory and Design of Gas Turbines and Jet Engines,* McGraw-Hill, New York, 1950.
17. Wisclicenus, G.F., *Fluid Mechanics of Turbomachinery,* McGraw-Hill, New York, 1947.
18. Yahya, S.M., *Turbomachines,* Satya Prakashan, New Delhi, 1972.

Thermodynamics (Books)

19. Boxer, G., *Engineering Thermodynamics,* 1st edn, Macmillan, London, 1976.
20. Hatsopoulos, G.N. and Keenan, J.H., *Principles of General Thermodynamics,* John Wiley and Sons, 1965.
21. Holman, J.P., *Thermodynamics,* 2nd edn, McGraw-Hill, Kogakusha Ltd., 1974.
22. Keenan, J.H., *Thermodynamics,* John Wiley and Sons, 1941.
23. Reynolds W.C. and Perkins, H.C., *Engineering Thermodynamics,* 2nd edn, McGraw-Hill, 1977.
24. Rogers, G.F.C. and Mayhew, Y.R., *Engineering Thermodynamics, Work and Heat Transfer (S.I. Units),* 3rd edn, Longmans, Green and Co. Ltd., London, 1981.
25. Saad, M.A., *Thermodynamics for Engineers,* Prentice-Hall of India Pvt. Ltd., 1969.
26. Spalding, D.B. and Cole, E.H., *Engineering Thermodynamics,* Arnold, 1973.
27. Wark, K., *Thermodynamics,* 3rd edn, McGraw-Hall, 1977.
28. Zamansky, M.W. *et al., Basic Engineering Thermodynamics,* 2nd edn, McGraw-Hill, 1975.

Gas Turbine Plants

29. Aeberli, W.A. and Darimont, A.H., 'Automatic start-up and operation of power generating plants with a combined gas-steam cycle', *ASME paper No.* 70-GT-41, 1970.
30. Alich *et al.,* 'Suitability of low-Btu gas/combined cycle electric power generation for intermediate load service', *Combustion,* Vol. 4, 1975.
31. Armstrong, F.W. and Philpot. M.G., 'Future prospects for naval propulsion gas turbines,' *ASME paper No.* 78-GT-106, *ASME gas turbine conference and products show,* London, April 1978.
32. Bammert, K. and Bohm, E., 'High-temperature gas-cooled reactors with gas turbine', Paper No. EN-1/12, *Symposium on the technology of integrated primary circuits for power reactors,* ENEA, Paris, May 1968.
33. Bowers N.K., 'Gas turbines in the Royal Navy', *ASME J. Eng. Power,* Vol. 89, 1967.
34. Brown, D.H. and Cohn, A., 'An evaluation of steam injected combustion turbine systems' *ASME J. Eng. Power,* Paper No. 80-GT-51 Jan. 1981.
35. Bund, K. *et al.,* Combined gas/steam turbine generating plant with bituminous coal high-pressure gasification plant at the Kellermann power station', *Lunen Brennstoff-warms-kraft,* Vol. 23, No. 6, 8th World Energy Conference, 1971.
36. Corman, J.C. *et al.,* 'Energy conversion alternatives study (ECAS)', *General Electric phase II final report, NASA-CR* 134949, Vols.I-III, Cleveland, Dec. 1976.
37. Hubert, F.W.L. *et al.,* Large combined cycles for utilities', *Combustion,* Vol. I, *ASME gas turbine conference and products show,* Brussels, May 1970.
38. Hurst, J.N. and Mottram, A.W.T., 'Integrated Nuclear Gas turbines', Paper No. EN-1/41, *Symposium on the technonogy of integrated primary circuits for power reactors,* ENEA, Paris, May 1968.
39. Jackson, A.J.B., 'Some future trends in aeroengine design for subsonic transport aircraft',-*ASME J. Eng. Power,* April 1976.
40. Kehlhofer, R., 'Calculation for part-load operation of combined gas/steam turbine plants', *Brown Boveri Rev.,* 65, 10, pp 672-679, Oct. 1978.
41. Kingcombe, R.C. and Dunning, S.W., 'Design study for a fuel efficient turbofan engine', *ASME paper* No. 80-GT-141, New Orleans, March 1980.
42. Mayers, M.A. *et al.,* 'Combination gas turbine and steam turbine cycles', *ASME paper* No. 55-A-184, 1955.
43. Mcdonald, C.F. and Smith, M.J., 'Turbomachinery design considerations for nuclear HTGR-GT power plant', *ASME J. Eng. Power,* 80-GT-80, Jan. 1981.
44. Mcdonald, C.F. and Boland, C.R., 'The nuclear closed-cycle gas turbine (HTGR-GT) dry cooled commercial power plant studies', *ASME J. Eng. Power,* 80-GT-82, Jan. 1981.
45. Nabors, W.M. *et al.,* 'Bureau of mine progress in developing the coal burning gas turbine power plant', *ASME J. Eng. Power,* April 1965.

46. Osterle, J.F., 'Thermodynamic considerations in the use of gasified coal as a fuel for power conversion systems', *Frontiers of power technology conference proceedings,* Oklahoma State University, Carnegie-Mellon University, Pittsburgh, Oct. 1974.
47. Starkey, N.E., 'Long life base load service at 1600°F turbine inlet temperature', *ASME J. Eng. Power,* Jan. 1967.
48. Stasa, F.L. and Osterle, F., 'The thermodynamic performance of two combined cycle power plants integrated with two coal gasification systems', *ASME J. Eng. Power,* July 1981.
49. Traenckner, K., 'Pulverized-coal gasification Ruhrgas processes', *Trans ASME,* 1953.
50. Ushiyama, I., 'Theoretically estimating the performance of gas turbines under varying atmoshperic condition', *ASME J. Eng. Power,* Jan. 1976.
51. Yannone, R.A. and Reuther, J.F., 'Ten years of digital computer control of combustion turbines *ASME J. Engg. Power,* 80-GT-76, Jan. 1981.

Steam Turbine Plants

52. Assourd, P., 'The energy balance of a nuclear power plant' (in French), *Entropie,* 14, 83, 1978.
53. Berman, P.A. and Labonette, F.A., 'Combined-cycle plant serves intermediate system loads economically', Westinghouse Elec. Corp. Lester, Pennsylvania, 1970.
54. Berman, P.A. 'Operating concept for a 240-MW combined cycle intermediate peaking plant', *ASME paper* No. 74-GT-109, 1974.
55. 'Candu-Douglas point nuclear power station', *Nuclear Eng,* 9, 289, Aug. 1964.
56. Curren, R.M. *et al.*, 'The effect of water chemistry on the reliability of modern large steam turbines', *J. Eng. Power, Trans ASME,* 101, 3, July 1979.
57. El-Wakil, M.M., *Nuclear Energy Conversion,* Intext Educational Publishers, Scranton, Pennsylvania, 1971.
58. Flitner, D.P., 'A heavy fuel fired heat recovery steam generator for combined cycle applications', *ASME paper* No. 75-PWR-30, 1975.
59. Foster, R.W., 'Trends in combined steam gas turbine power plants in U.S.A.', *J. Eng. Power, Trans ASME,* Vol. 88, No. 4, p. 302, Oct. 1966.
60. Haywood, R.W., 'A generalized analysis of the regenerative steam cycle for a fintie number of heaters', *Proc. Instn. Mech. Engrs.,* 161, 157, 1949.
61. Heard, T.C., 'Review of a combined steam and gas turbine cycle for pipeline service' *ASME paper* No. 75-GT-51, 1975.
62. Horlock, J.H., 'The thermodynamic efficiency of the field cycle', *ASME paper* No. 57-A-44, 1957.
63. Hurlimann, R., 'On the influence of surface roughness especially of manufacturing quality on the flow losses of steam turbine blades', *VDI-Berichte,* No. 193, 1973.

64. Ileri, A. *et al.,* 'Urban utilization of waste energy from thermal-electric power plants', *ASME J. Eng. Power,* July 1976.
65. Juntgen, H. *et al.,* 'Kinetics, heat transfer and engineering aspects of coal gasification with steam using nuclear heat', *B.N.E.S. International conference,* session III, No. 12, Nov. 1974.
66. Juntgen, H. and Van Heek, K.H., 'Gasification of coal with steam using heat from HTRs', *Nuclear Eng.,* Vol. 34, No. 1, 1975.
67. Kilaparti, S.R. and Nagib, M.M., 'A combined helium and steam cycle for nuclear power generation', *ASME paper* No. 70-WA/NE-3, 1970.
68. Miller, A.J. *et. al., Use of steam-electric power plants to provide thermal energy to urban areas, ORNL-HUD*-14, Oak Ridge National Laboratory, Jan. 1971.
69. Moore, R.V. (Ed.), *Nuclear Power,* Cambridge University Press, 1971.
70. Pfenninger, H., 'Combined steam and gas turbine power stations', *Brown Boveri Rev.,* Vol. 60, No. 9, 1973.
71. Pfenninger, H., 'Coal as fuel for steam and gas turbines', *Brown Boveri Rev.,* Vol. 62, No. 10/11, 1975.
72. Reistad, G.M. amd Ileri, A., 'performance of heating and cooling systems coupled to thermal-electric power plants', *Winter annual meeting of ASME,* Nov. 1974.
73. Reinhard, K. *et al.,* 'Experience with the world's largest steam turbines', *Brown Boveri Rev.,* Vol. 63, No. 2, Feb. 1976.
74. Ringle, J.C. *et al.,* 'A systems analysis of the economic utilization of warm water discharge from power generating stations', *Oregon State University Engineering Experiment station report,* Bulletin No. 148, Nov. 1974.
75. Salisbury, J.K., *Steam turbines and their cycles,* Wileys, 1950.
76. Schadeli, R., 'The Socolie Gas-steam turbo-power station', *Sulzer Tech. Rev.,* Vol. 50, No. 4, 1968.
77. Seippel, C. and Bereuter, R., 'The theory of combined steam and gas turbine installations', *Brown Boveri Rev.,* 47, 783, 1960.
78. Speidel, L., 'Determination of the necessary surface quality and possible losses due to roughness in steam turbines', *Electrizitats wirtschaft,* Vol. 61, No. 21, 1962.
79. Van Heek, K.H. *et al.,* 'Fundamental studies on coal gasification in the utilization of thermal energy from nuclear high temperature reactors', *J. Inst. Fuel,* Vol. 46, 1973.
80. Weir, C.D., 'Optimization of heater enthalpy rises in feed-heating trains', *Proc. Instn. Mech. Engrs.* 174, 769, 1960.

Fluid Mechanics (Books)

81. Binder, R.C., *Advanced Fluid Mechanics,* Prentice-Hall, 1958.
82. Bradwhaw, P., *Experimental Fluid Mechanics,* 2nd edn, Pergamon Press, 1970.

83. Fox, J.A., *An Introduction to Engineering Fluid Mechanics,* The Macmillan Press Ltd., 1974.
84. Gibbings, J.C. *Thermomechanics, The Governing Equations,* Pergamon Press, 1970.
85. Hall, N.A., *Thermodynamics of Fluid Flow,* Prentice-Hall, 1957.
86. Howarth, L. (Ed.), *Modern Developments in Fluid Dynamics,* Oxford, 1953.
87. Hunsacker, J.C. and Rightmire, B.G., *Engineering Applications of Fluid Mechanics,* McGraw-Hill, 1947.
88. Kaufmann, W., *Fluid Mechanics,* McGraw-Hill, 1963.
89. Mcleod (Jr), E.B., *Introduction to Fluid Dynamics,* Macmillan Co., 1955.
90. Milne-Thomson, L.M., *Theoretical Hydrodynamics,* Macmillan Co., Ltd., 1960.
91. Reynolds, A.J., *Thermofluid Dynamics,* Wiley-Interscience, 1971.
92. Streeter, V.L. (Ed.), *Handbook of Fluid Dynamics,* McGraw-Hill, 1961.
93. Streeter, V.L., *Fluid Mechanics,* 5th edn, McGraw-Hill, 1971.
94. Yuan, S.W., *Foundations of Fluid Mechanics,* Prentice-Hall of India Pvt. Ltd., 1969.

Gas Dynamics (Books)

95. Cambel, A.B. and Jennings, B.H., *Gas Dynamics,* McGraw-Hill, 1958.
96. Chapman, A.J. and Walker, W.F., *Introductory Gas Dynamics,* Holt Rinehart and Winston Co., 1971.
97. Imrie, B.W., *Compressible Fluid Flow,* Butterworths, 1973.
98. Joh, J.E.A., *Gas Dynamics,* Allyn and Bacon, Boston, 1969.
99. Liepmann, H.W. and Roshko, A., *Elements of Gas Dynamics,* John Wiley and Sons, 1957.
100. Oswatitsch, K., *Gas Dynamics,* Academic Press, 1956.
101. Owczarek, J.A., *Fundamentals of Gas Dynamics,* International Text Book Co., 1964.
102. Pai, S.I., *Introduction to the Theory of Compressible Flow,* D. Van Nostrand Co., Inc., Amsterdam, 1959.
103. Rotty, R.M., *Introduction to Gas Dynamics,* John Wiley and Sons, New York, 1962.
104. Shapiro, A.H., *The Dynamics and Thermodynamics of Compressible Fluid Flow,* Vols. I and II, The Ronald Press Co., 1953.
105. Thompson, P.A., *Compressible Fluid Dynamics,* McGraw-Hill, New York, 1972.
106. Tsien, H.S., *Equations of Gas Dynamics,* Princeton University Press, 1958.
107. Yahya, S.M., *Fundamentals of Compressible Flow,* Wiley-Eastern, 1982.
108. Zucker, R.D., *Fundamentals of Gas Dynamics,* Matrix Publishers Inc., Champaign, 1977.

109. Zucrow, M.J. and Hoffman, J.D. *Gas Dynamics,* Vols. I and II, John Wiley and Sons, Inc., New York, 1977.

Aerodynamics (Books)

110. Durand, W.F. (Ed.-in-Chief), *Aerodynamic Theory,* Dover Publications, Inc., New York.

111. Dwinnell, J.H., *Principles of Aerodynamics,* McGraw-Hill, New York, 1949.

112. Glauert, H., *The Elements of Aerofoil and Airscrew Theory,* 2nd edn, Cambridge University Press, 1959.

113. Karamcheti, K., *Principles of Ideal-Fluid Aerodynamics,* John-Wiley and Sons, Inc., New York, 1966.

114. Kuethe, A.M. and Schetzer, J.D., *Foundations of Aerodynamics,* 2nd edn, John-Wiley and Sons, Inc., London, 1961.

115. Miles, E.R.C., *Supersonic Aerodynamics,* Dover Publications Inc., New York, 1950.

116. Milne-Thomson, L.M., *Theoretical Aerodynamics,* 3rd edn, Macmillan and Co. Ltd., New York, 1958.

117. Piercy, N.A.V., *Aerodynamics,* English Universities Press, London, 1955.

118. Prandtl, L. and Tietjens, O.G., *Fundamentals of Hydro and Aeromechanics,* McGraw-Hill, New York, 1934.

119. Prandtl, L. and Tietjens, O.G., *Applied Hydro and Aeromechanics,* Dover Publications, Inc., New York, 1934.

120. Rauscher, M., *Introduction to Aeronautical Dynamics,* Ist edn, John-Wiley and Sons, Inc., New York, 1953.

121. Thwaites, B. (Ed.), *Incompressible Aerodynamics,* Oxford University Press, London, 1960.

Nozzles

122. Alder, G.M., 'The numerical solution of choked and supercritical ideal gas flow through orifices and convergent conical nozzles', *J. Mech. Engg. Sci.,* 21, 3 pp 197-203, June 1979.

123. Alvi, S.H. and Sridharan, K., 'Loss characteristics of orifices and nozzles *ASME J. Fluids Eng.,* 100, 3, Sept. 1978.

124. Anderson, B.H., 'Factors which influence the analysis and design of ejector nozzles', *AIAA paper* No. 72-46, Jan. 1972.

125. Anderson, B.H., 'Computer program for calculating the field of supersonic ejector nozzles' *NASA TN D*-7601, pp 1—86, 1974.

126. Barber, R.E., 'Effect of pressure ratio on the performance of supersonic turbine nozzles', *Sundstrand Aviation Co. Report.*

127. Bobovich, A.B. *et al.,* 'Experimental investigation of asymmetric laval nozzles', *Fluid Dyn.,* 12, 2, Oct. 1977.

128. Carpenter, P.W., 'Effects of swirl on the subcritical performance of convergent nozzles *AIAA Journal,* 18, 5 (Tech. notes), May 1980.
129. Decher, R., 'Non-uniform flow through nozzles', *J. Aircr.,* 15, 7, July 1978.
130. Duganov, V.V. and Polyakov, V.V., Flow calculations in plane asymmetic nozzles in overexpanded flow regimes', *Soviet Aeronaut.,* 21, 1, 1978.
131. Keith Jr., T.G., *et al.,* 'Total pressure recovery of flared fan nozzles used as inlets', *J. Aircr.,* 16, 2, Feb. 1979.
132. Koval, M.A. and Shvets, A.I., 'Experimental investigation of sonic and supersonic anular jets', *J. Appl., Mech. Tech., Phys.,* 20, pp 456-461, Jan. 1980.
133. Kraft, H., 'Reaction tests of turbine nozzles for subsonic velocities', *Trans ASME,* 71 773, 1949.
134. Kumari, M. and Nath, G., 'Compressible boundary-layer swirling flow in nozzle and diffuser with highly cooled wall', *J. Appl. Mech., Trans ASME,* 46, June 1979.
135. Lanyuk, A.N., 'Effect of the two-dimensionality of the flow of a gas with a stepwise distribution of the total parameters on the integral characteristics of a laval nozzle', *Fluid Dyn.,* 13, 3, pp 480-483, 1978.
136. Lanyuk, A.N., 'Influence of the mixing of two flows with different total parameters in a laval nozzle on its integral characteristics', *Fluid Dyn.,* 14, 4, pp 564-569, Jan. 1980.
137. Louis, J.G. and Vanco, M.R., 'Computer program for design of two-dimensional sharp edged throat supersonic nozzle with boundary layer correction', *NASA* TM X-2343, 1971.
138. Mikhailov, V.V., 'Gas flow from a finite volume through a laval nozzle', *Fluid Dyn.,* 13, 2, Nov. 1978.
139. Nozaki, T. *et al.*, 'Reattachment flow issuing from a finite width nozzle', *Bulletin JSME,* Vol. 22, No. 165, March 1979.
140. Osborne, A.R., 'The aerodynamic performance of practical convergent-divergent nozzles with area ratio = 1.2', *NGTE Report* R 79002, Oct. 1979.
141. Osipov, I.L., 'Numerical method for constructing two-dimensional nozzles', *Fluid Dyn.,* 14, 2, pp 312-317, Sept. 1979.
142. Rogers, G.F.C. and Mayhew, Y.R., 'One-dimensional irreversible gas flow in nozzles, *Engineering,* London, 175, 355-358, 1953.
143. Senoo, Y., 'The boundary layer on the end wall of a turbine nozzle', *Trans ASME,* Vol. 80, 1958.
144. Srebnyuk, A.M., 'Experimental study of steam flow for high initial parameters of a laval nozzle (in Russian)', *Gidromekhanika,* No. 37, pp 86-91, 1978.
145. Stratford, B.S. and Sansome, G.E., 'The performance of supersonic turbine nozzles', *ARC,* R & M 3273, 1959.
146. Tagirov, R.K., 'Flow of ideal gas in tapering nozzles', *Fluid Dyn.,* 13, 2 pp 331-335, Nov. 1978.

147. Tagirov, R.K., 'Numerical investigation of the flow in axi-symmetric laval nozzles, including conditions of over-expansion with flow breakaway', *Fluid Dyn.,* 13, 3, Dec. 1978.

148. Thomas, P.D., 'Numerical method for predicting flow characteristics and performance of non-axi-symmetric nozzles—Theory', *NASA,* CR-3147, pp 109, Sept. 1979.

149. Vanco, M.R. and Goldman, L.J., 'Computer program for design of two-dimensional supersonic nozzle with sharp-edged throat', *NASA* TM X-1502, 1968.

150. Walker, C.P., 'Compressible shear flows in straight sided nozzles and diffusers', *ARC Rep.,* 23, 819, 1962.

151. Yu, A. Gostintsev and Uspenskii, O.A., 'Theory of vortical helical ideal gas flows in laval nozzles', *Fluid Dyn.,* 13, 2, Nov. 1978.

Diffusers

152. Abdelhamid, A.N. *et al.,* 'Experimental investigation of unsteady phenomena in vaneless radial diffusers', *ASME J. Eng. Power,* 101, 1, Jan. 1972.

153. Adkins, R.C., 'A short diffuser with low pressure loss', *ASME J. Fluids Eng.,* Sept. 1975.

154. Agrawal, D.P. and Yahya, S.M., 'Velocity distribution in blade-to-blade plane of a vaned radial diffuser', *Int. J. Mech. Sci.,* Vol. 23, No. 6, pp 359-366, 1981.

155. Antonia, R.A., 'Radial diffusion with swirl', *Mechanical and Chemical Engg. Transactions,* pp 127, May 1968.

156. Baade K.H., 'Unsteady flow in the vaneless diffuser of a radial compressor stage', *Proc. 4th Conf. Fluid Machinery,* pp 115-128, Budapest, 1972.

157. Baghdadi S. and McDonald, A.T., 'Performance of the vaned radial diffusers with swirling transonic flow', *ASME J. Fluids Eng.,* June 1975.

158. Baghdadi, S., 'The effect of rotor blade wakes on centrifugal compressor diffuser performance—A comparative experiment', *ASME J. Fluids Eng.,* March 1977.

159. Cockrell, D.J. and Markland, E., 'A review of incompressible diffuser flow', *Aircr. Eng.,* Vol. 35, No. 10, p. 287, Oct. 1963.

160. Dallenbach, F. and Le, N. Van, 'Supersonic diffuser for radial and mixed flow compressors', *ASME J. Basic Eng.,* pp 973-979, Dec. 1960.

161. Dean (Jr.), R.C. and Senoo, Y., 'Rotating wakes in vaneless diffusers', *ASME J. Basic Engg.,* pp 563-570, Sept. 1960.

162. Den, G.N., 'A study of vaneless diffusers with non-parallel walls', *Thermal Eng.,* 12, p. 23, 1965.

163. Den, G.N. and Tilevich, I.A., 'Gas dynamic characteristics of vaned diffusers in centrifugal compressors', *Thermal Eng.,* Vol. 13, 1966.

164. Dettmering, W., 'Flow analysis in a parallel walled diffuser', *Z. Flugwiss,* 20, Heft, 1972.

165. Emerson, D. and Horlock, J.H., 'The design of diffusers for centrifugal compressors', *ASME paper* No. 66-WA/GT-9, 1966.

166. Faulders, C.R., *An aerodynamic investigation of vaned diffusers for centrifugal compressor impellers,* Gas Turbine Laboratory, Massachusetts Institute of Technology, Boston, Jan. 1954.

167. Faulders, C.R., 'Aerodynamic design of vaned diffusers for centrifugal compressors' *ASME paper* No. 56-A-217, 1956.

168. Feil, O.G., Vane system for very wide-angle subsonic diffusers', *ASME J. Basic Eng.,* Dec. 1964.

169. Ferguson, T.B., 'One-dimensional compressible flow in a vaneless diffuser', *The Engineering,* March 1963.

170. Ferguson, T.B., 'Radial vaneless diffusers', *3rd Conf. on fluid mechanics and fluid machines,* Budapest, 1969.

171. Furuya, Y. *et al.,* 'The loss of flow in the conical diffuser with suction at the entrance' *Bulletin JSME* Vol. 9, Feb. 1966.

172. Grietzer, B.M. and Griowold, H., 'Compressor diffuser interaction with circumferential flow distortion', *J. Mech. Eng. Sci.,* Vol. 18, No. 1, 1976.

173. Hoadley, D., 'Some measurements of swirling flow in an annular diffuser', *Symposium on internal flows,* Salford Univ., U.K., April 1971.

174. Honauri, S. *et al.,* 'Investigation concerning the fluid flow in the mixed flow diffuser, *ASME paper* No. 71-GT-40, 1971.

175. Jansen, W., 'Steady fluid flow in a radial vaneless diffuser', *ASME J. Basic Eng.,* Sept. 1964.

176. Jansen, W., 'Rotating stall in a radial vaneless diffuser', *Trans ASME,* 86, series D, 750-758, 1964.

177. Johnston, J.P. and Dean, R.C., 'Losses in vaneless diffusers of centrifugal compressors and pumps', *Trans ASME,* Series A, Jan. 1966.

178. Kawaguchi, T. and Furuya, Y., 'The rotating flows in a vaneless diffuser having two parallel discs', *Bulletin JSME,* Vol. 9, No. 36, pp 711, Nov. 1966.

179. Kenney, D.P., 'A novel low-cost diffuser for high performance centrifugal compressors', *Trans ASME,* Series A, 91, 37-46, 1969.

180. Kenny, D.P., 'Supersonic radial diffusers', *AGARD lecture series,* 39, 1970.

181. Kenny, D.P., 'A comparison of high pressure ratio centrifugal compressor diffusers', *ASME paper* No. 72-GT-54, 1972.

182. Krasinske, J.S. De and Sarpal, G.S. 'A radial diffuser with a rotating boundary layer at the throat', *Trans CSME,* Vol. 1, No. 2, June 1972.

183. McDonald, A.T. *et al.,* 'Effects of swirling inlet flow on pressure recovery in conical diffusers', *AIAA Journal,* Vol. 9, 1971.

184. Moller, P.S., 'Radial flow without swirl between parallel discs' *Aeronaut. Qtly.,* Vol. 14, 1963.

185. Moller, P.S., 'Radial flow without swirl between parallel discs having both supersonic and subsonic regions', Trans ASME, Series D, *J. Basic Eng.,* p. 147, March 1966.

186. Moller, P.S., 'A radial diffuser using incompressible flow between narrowly spaced discs', *Trans ASME,* Series D, Vol. 88, March 1966.

187. Nakamura, I. *et al.*, 'Experiments on the conical diffuser performance with asymmetric uniform shear inlet flow', *Bulletin JSME,* Vol. 24, No. 190, April 1981.

188. Palani, P.N. and Gopalakrishnan, G., 'Some experiments on a radial vaned diffuser', Instn. Engrs. (India), *J. Mech Engg Div.,* 57, pp 123-125, Nov.1976.

189. Polyakov, V.Y. and Bukatykh, A.F., 'Calculation of separation-free vaneless diffusers of centrifugal compressor stages on a digital computer', *Thermal Engg.,* 16, 11, pp 40-43, Nov. 1969.

190. Reeves, G.B., 'Estimation of centrifugal compressor stability with diffuser loss-range system', *Trans ASME,* Series I, March 1977.

191. Reneau, L.R. *et al.,* 'Performance and design of straight, two-dimensional diffusers', *Trans ASME,* Series D, *J. Basic Eng.,* Vol. 89, pp 141-150, 1967.

192. Runstadler, P.W. and Dean, R.C., 'Straight channel diffuser performance at high inlet Mach numbers', *Trans ASME, J. Basic Eng.,* Vol. 91, pp 397-422, Sept. 1969.

193. Sagi, C.J. and Johnston, J.P., 'The design and performance of two-dimensional curved diffusers', *ASME paper* No. 67-PE-6., 1967.

194. Sakurai, T., 'Study on flow inside diffusers for centrifugal turbomachines', *Bulletin JSME, Rep.* 1, Vol. 14, No. 73, 1971.

195. Sakurai, T., 'Study on flow inside diffusers for centrifugal turbo-machines', *Bulletin JSME, Rep.* 2, Vol. 15, No. 79, 1972.

196. Sakurai, T., 'Study on flow inside diffusers for centrifugal turbo-machines', *Bulletin JSME, Rep.* 3, Vol. 15, No. 85, 1972.

197. Senoo, Y. and Ishida, M., 'Asymmetric flow in the vaneless diffuser of a centrifugal blower', *Proc. 2nd Int. JSME symposium on fluid machinery and fluids, Vol. 2, Fl. machinery-II,* paper 207, pp 61-69, Sept. 1972.

198. Senoo, Y. *et al.,* 'Asymmetric flow in vaneless diffusers of centrifugal blowers', *ASME J. Fluids Eng.,* March 1977.

199. Sherstyuk, A.N. *et al.,* 'A study of mixed-flow compressors with vaned diffusers', *Thermal Eng.,* Vol. 12, 1965.

200. Sherstyuk, A.N. and Kosmin, V.M., 'The effect of the slope of the vaneless diffuser walls on the characteristics of a mixed flow compressor', *Thermal Eng.,* Vol. 16, No. 8, pp 116-121, 1969.

201. Smith, V.J., 'A review of the design practice and technology of radial compressors diffusers', *ASME paper* No. 70-GT-116, 1970.

202. Sovran, G. and Klomp, E.D., 'Experimentally determined optimum geometries for rectangular diffusers with rectangular, conical or annular cross-section', *Fluid Mechanics of Internal Flow,* Ed. G. Sovran, Elsevier Pub. Co. Amsterdam, 1967.

203. Sutton, H., 'The performance and flow condition within a radial diffuser fitted with short vanes', *B.H.R.A. Rotodynamic Pumps,* 1968.
204. Waitman, B.A. *et al.,* 'Effect of inlet conditions on performance of two-dimensional subsonic diffusers', *Trans ASME,* Series D, Vol. 83, p. 349, 1961.
205. Yahya, S.M. and Gupta, R.L., 'A test rig for testing radial diffusers', *Int. J. Mech. Sci.,* Vol. 17, Pergamon Press, 1975.

Wind Tunnels and Cascades

206. Ai Xiao-Yi, (Beijing Heavy Electric Machinery Plant) 'Experiment of two-dimensional transonic turbine cascades (in Chinese)', *J. Eng. Thermophys.* Vol. 1, No. 1, Feb. 1980.
207. Balje, O.E., 'Axial cascade technology and application to flow path designs', *ASME J. Eng. Power,* Vol. 90, Series A, No. 4, Oct. 1968.
208. Belik, L., 'Secondary flows in blade cascades of axial turbomachines and the possibility of reducing its unfavourable effects', *Int. JSME symposium on fluid machinery and fluidics,* Tokyo, Sept. 1972.
209. Bettner, J.L., 'Experimental investigation in an annular cascade sector of highly loaded turbine stator blading—Vol. II: Performance of plain blade and effect of vortex generators', *NASA,* CR 1323, May 1969.
210. Bettner, J.L., 'Experimental investigation in annular cascade sector of highly loaded turbine stator blading—Vol. V: Performance of tangential jet blades', *NASA,* CR-1675, Aug. 1969.
211. Bettner, J.L., 'Summary of tests on two highly loaded turbine blade concepts in three-dimensional cascade sectors', *ASME paper 69-WA/GT-5,* 1969.
212. Came, P.M., 'Secondary loss measurements in a cascade of turbine blades', *Proc. Instn. Mech. Engrs.,* London, Conference Publication, 3, 1973.
213. Carter, A.D.S., and Hounsell, A.F., 'General performance data for aerofoils having C-1, C-2 or C-4 base profiles on circular arc camber lines', *NGTE,* M. 62, 1949.
214. Carter, A.D.S., 'Low-speed performance of related aerofoils in cascade', *ARC,* C.P. No. 29, 1950.
215. Cermak, J.E., 'Applications of wind tunnels to investigations of wind engineering problems', *AIAA J.* 17, 7, pp 679-690, July 1979.
216. Citavy, J. and Norbury, J.F., 'The effects of Reynolds number and turbulent intensity on the performance of a compressor cascade with prescribed velocity distribution', *J Mech. Eng. Sci.,* Vol. 19, 1977.
217. Cohen, M.J. and Ritchie, N.J., 'Low speed three-dimensional contraction design', *J. Roy. Aero. Society,* Vol. 66, 1962.
218. Daiguji, H. and Sakai, H., 'Finite element analysis of cascade flow with varying flow rate', *Bulletin JSME,* Vol. 21, No. 156, June 1978.
219. Deich, M.E., 'Flow of gas through turbine lattices', Translation: Tekhnicheskaia Gazodinamika, Ch. 7, *NACA,* TM 1393, 1953.

220. Dettmering, W., 'Investigation on supersonic decelerating cascades;, *Proc. V.K.I. seminar on advanced problems of turbomachines,* Brussels, March 1965.

221. Dodge, P.R., 'The use of finite difference technique to predict cascade stator and rotor deviation angles and optimum angles of attack', *ASME J. Eng. Power,* Vol. 95, 1973.

222. Dunham, J., 'A review of cascade data on secondary losses in turbines', *J. Mech. Eng. Sci.,* 12, 1970.

223. Felix, A.R., 'Summary of 65-series compressor blade low speed cascade data by use of the carpet plotting technique', *NACA,* TN, 3913, 1957.

224. Forster, V.T., 'Turbine blading development using a transonic variable density cascade wind tunnel', *Proc. Instn. Mech. Engrs.,* 1964.

225. Gahin, S.E.M. and Ferguson, T.B., 'Use of cascade data for radial vaned diffuser design', *Int. symposium on pumps in power stations,* Sept. 1966.

226. Gahin, S., 'Theoretical considerations of using rectangular cascade data for circular cascade design', *Proc. 3rd conf. fluid mechanics and fluid machinery,* Budapest, 1969.

227. Gopalakrishnan, S. and Buzzola, R., 'A numerical technique for the calculation of transonic flows in turbomachinery cascades', *ASME paper* No. 71-GT-42, 1971.

228. Hawthrone, W.R., 'Some formula for the calculation of secondary flow in cascades' *British Aero. Res. Council,* Rep. 17, 519, 1955.

229. Hawthrone, W.R., 'Methods of treating three-dimensional flows in cascades and blade rows', *Internal aerodynamics (Turbomachinery),* Instn. Mech. Engrs., 1967.

230. Heilemann, W., 'The NASA Langley 7-inch transonic cascade wind tunnel at the D.V.L. and the first results', *Advanced problems in turbomachines,* V.K.I.F.D., 1965.

231. Herrig, L.J. *et al.,* 'Systematic two-dimensional cascade tests on NACA 65-series compressor blades at low speeds', *NACA,* NT, 3916, 1957.

232. Keast, F.H., 'High speed cascade testing techniques', *Trans ASME,* 74, 685, 1952.

233. Kitmura T. *et al.,* 'Optimum operating techniques of two-stage hypersonic gun tunnel', *AIAA J.,* 16, 11, Nov. 1978.

234. Lakshminarayana, B. and Horlock, J.H., 'Review: Secondary flow and losses in cascades and axial flow turbomachines', *Int. J. Mech. Sci.,* Vol. 5, 1963.

235. Lakshminarayana, B. and Horlock, J.H., 'Effect of shear flows on outlet angle in axial compressor cascades-Methods of prediction and correlation with experiments', *J. Basic Eng.,* p. 191, March 1967.

236. Lehthaus, F., 'Computation of transonic flow through turbine cascades with a time marching method (in German)', *VDI-Forschungsheft* No. 586, 1978.

237. Lewis, R.I., 'Annular cascade wind tunnel', *Engineer,* 215, 341, London, 1963.

238. Lewis, R.I., 'Restrictive assumptions and range of validity of Schlichting's cascade analysis', *Advanced problems in turbomachines,* V.K.I. F.D., 1965.

239. Lieblein, S. and Roudebush, W.H., 'Theoretical loss relation for low-speed two-dimensional cascade flow', *NACA,* TN 3662, 1956.

240. Lieblein, S., 'Loss and stall analysis of compressor cascades', *Trans ASME,* Series D. 81, 1959.

241. Maekawa, A. *et al.*, 'Performance of rotating cascades under the inlet distortions', *Bulletin JSME,* Vol. 22, No. 165, March 1979.

242. Mellor, G., 'The 65-series cascade data', Gas turbine lab, MIT, unpublished, 1956.

243. Meyer, J.B., 'Theoretical and experimental investigations of flow downstream of two-dimensional transonic turbine cascades', *ASME paper* No. 72-GT-43, 1972.

244. Mikhail, M.N. 'Optimum design of wind tunnel contractions', *AIAA J.,* 17, 5, May 1979.

245. Nosek, S.M. and Kline, J.F., 'Two-dimensional cascade investigation of a turbine tandem blade design', *NASA* TM X-1836, 1969.

246. Pampreen, R.C., 'The use of cascade technology in centrifugal compressor vaned diffuser design', *ASME paper* 72-GT-39, March 1972.

247. Pankhurst, R.C. and Holder, D.W., *Wind Tunnel Techniques,* Sir Issac Pitman & Sons Ltd., London, 1952.

248. Pankhurst. R.C. and Bradshaw, P., 'On the design of low-speed wind tunnels', *Progress in Aero. Sci.,* Ed. D. Kuchemann and L.H.G. Sterne, Pergamon Press, Vol. 5, 1964.

249. Railly, J.W., 'A potential flow theory for separated flow in mixed flow cascades', *A.R.C.* No. 35, p. 538, 1974.

250. Railly, J.W., 'Treatment of separated flow in cascades by a source distribution', *Proc. Inst. Mech. Engrs.* Vol. 190, 35, 1976.

251. Rhoden, H.G., 'Effects of Reynolds number on the flow of air through a cascade of compressor blades', *ARC* R & M 2919, 1956.

252. Schlichting, H., 'Problems and results of investigation on cascade flow', *J. Aero Space Soc.,* March 1954.

253. Scholz, N., 'A survey of the advances in the treatment of the flow in cascades', *Internal Aerodynamics (Turbomachinery),* Instn. Mech. Engrs. Publications, 1970.

254. Shirahata, H. and Daiguji, H., 'Subsonic cascade flow analysis by a finite element method', *Bulletin JSME,* Vol. 24, No. 187, Jan. 1981.

255. Stenning, A.H. and Kriebel, A.R., 'Stall propagation in a cascade of aerofoils', *ASME paper* No. 57, 3A-29, 1957.

256. Stepanov, G.U., 'Hydrodynamics of turbomachinery cascade (in Russian)', *Gos. Izd. Phys. Mat. Lit. (Moscow).*

257. Stratford, B.S., and Sansome. G.E., 'Theory and tunnel tests of rotor blades for supersonic turbines', *ARC* R & M 3275, 1960.

258. Truscott, G.F., 'The use of cascade data in diffuser design for centrifugal pumps', *B.H.R.A.,* TN-945, March 1968.

259. Tsujimoto, Y. *et al.,* 'An analysis of viscous effects on unsteady forces on cascade blades', *Bulletin JSME,* Vol. 22, No. 165, March 1979.

260. Zhang,Yao-Ke *et al.,* 'On the solution of transonic flow of plane cascade by a time marching method', *J. Eng. Thermophys.,* Vol. 1, No. 4, Nov. 1980.

Axial Turbines

261. Agachev, R.S. and Kumirov, B.A., 'Theoretical-experimental analysis of influence of coolant discharge from perforated turbine vanes on their aerodynamic characteristics', *Sov. Aeronaut.,* 21, 1, 1978, Translated by Allerton Press Inc.

262. Ainley, D.G., 'Performance of axial flow turbines', *Proc. Instn. Mech. Engrs.,* London, 159, 1948.

263. Ainley, D.G. and Mathieson, G.C.R., 'A method of performance estimation for axial flow turbines' *A.R.C.,* R and M 2974, 1951.

264. Ainley, D.G. and Mathieson, G.C.R., 'An examination of the flow and pressure losses in blade rows of axial flow turbines', *A.R.C.,* R & M 2891, 1955.

265. Amann, C. and Sheridon, D.C., 'Comparisons of some analytical and experimental correlations of axial-flow turbine efficiency', *ASME paper* No. 67-WA/GT-6, Nov. 1967.

266. Balje, O.E., 'Axial turbine performance evaluation: Part A—loss-geometry relationship, Part B—Optimization with and without constraints', *ASME J. Eng. Power,* pp 341-360, 1968.

267. Bammert, K. and Zehner, P., 'Measurement of the four-quadrant characteristics on a multi-stage turbine', *ASME J. Eng. Power,* 102, 2, pp 316-321 April 1980.

268. Barbeau, D.R., 'The performance of vehicle gas turbines', *Trans SAE,* 76 (V), 90, 1967.

269. Boxer, E. *et al.,* 'Application of supersonic vortex flow theory to the design of supersonic compressor or turbine blade sections', *NACA,* RM L52 B06, 1952.

270. Carter, A.F. *et al.,* 'Analysis of geometry and design point performance of axial flow turbines, Pt. I: Development of the analysis method and loss coefficient correlation', *NASA,* CR-1181, Sept. 1968.

271. Chmyr, G.I., 'Integral equations for subsonic gas flow in turbines', *Sov. Appl. Mech.,* 14, 9, pp 991-997, March, 1979.

272. Deich, M.E. *et al.,* 'The effect of moving blade edge thickness on the efficiency of a supersonic turbine stage', *Thermal Eng.,* 18(10), pp 116-119, 1971.

273. Dunham, J., 'A review of cascade data on secondary losses in turbines', *J. Mech. Eng. Sci.,* Vol. 12, 1970.

274. Dunham, J. and Came, P., 'Improvements to the Ainley-Mathieson method of turbine performance prediction', *Trans ASME,* Series A, 92, 1970.

275. Evans, D.C., 'Highly loaded multi-stage fan drive turbine-velocity diagram study', *NASA,* CR-1862, 1971.

276. Evans, D.C. and Wolfmeyer, G.W., 'Highly loaded multi-stage fan drive—Plain blade configuration', *NASA,* CR-1964, 1972.

277. Fruchtman, I., 'The limit load of transonic turbine blading', *ASME paper* No. 74-GT-80, 1974.

278. Ge, Man-Chu, 'The estimation of transonic turbine at off-design conditions', *J. Eng. Thermophys.,* Vol. 1, No. 4, Nov. 1980.

279. Glassman, A.J. amd Moffit, T.P., 'New technology in turbine aerodynamics', *Proc. I turbo symposium,* Taxas, A and M Univ., Oct. 1972.

280. Glassman, A.J., 'Computer program for predicting design analysis of axial flow turbines', *NASA,* TN TND-6702, 1972.

281. Glassman, A.J. (Ed.), 'Turbine design and application', *NASA,* SP 290, Vol. (1972), Vol. II, (1973), Vol. III, (1975).

282. Haas, J.E. *et al.,* 'Cold-air performance of a tip turbine desinged to drive a lift fan, III—Effect of simulated fan leakage on turbine performance', *NASA,* TP-1109 (Jan. 1978); IV—Effect of reducing rotor tip clearance', *NASA,* TP-1126, Jan 1978.

283. Hawthorne, W.R. and Olson, W.T., *Design and Performance of Gas Turbine Power plants,* Oxford, 1960.

284. Holzapfel, I. and Meyer, F.J., 'Design and development of a low emission combustor for a car gas turbine', ASME J. Eng. Power, 101, July 1979.

285. Horlock, J.H., 'A rapid method for calculating the "off-design" performance of compressors and turbines', *Aeronaut.,* 9, 1958.

286. Horlock, J.H., 'Losses and efficiencies in axial-flow turbines', *Int. J. Mech. Sci.,* 2, 1960.

287. Horlock, J.H., *Axial Flow Turbines,* Kruger Publishing Co., 1973.

288. Johnston, I.H. and Sansome G.E., 'Tests on an experimental three stage turbine fitted with low reaction blading of unconventional form', *ARC,* R and M 3220, 1958.

289. Johnston, I.H. and Dransfield, D.C., 'The performance of highly loaded turbine stages designed for high pressure ratio', *ARC,* R and M3242, 1959.

290. Kuzmichev, R.V. and Proskuryakov, G.V. 'On the influence of short shroud on turbine stage operation', *Sov. Aeronaut.,* 22, 1, pp 90-92, 1979.

291. Lenherr, F.K. and Carter, A.F., 'Correlation of turbine blade total pressure-loss coefficients derived from achievable stage efficiency data', *ASME paper* No. 68-WA/GT-5, 1968.

291a. Markov, N.H., *Calculation of the Aerodynamic Characteristics of Turbine Blading,* Translation by Associated Technical Services, 1958.

292. Mathews, C.C., 'Measured effects of flow leakage on the performance of the GT-225 automotive gas turbine engines', *ASME J. Eng. Power,* 102, 1, 14-18 Jan. 1980.

293. Mclallin, K.L. amd Kofskey, M.G., 'Cold air performance of free power turbine designed for 112-kilowatt automotive gas turbine engine, II—Effects of variable stator-vane-chord setting angle on turbine performance', *NASA,* TM-78993, Feb. 1979.

294. Moffit, T.P. *et al.,* 'Design and cold-air test of single stage uncooled core turbine with high work output', *NASA,* TP-1680, 18 PP, June 1980.

295. Pryakhin, V.V. and Pavlovskii, A.Z., 'Experiemental investigation of the ratio between the fixed and moving blade row areas in supersonic stages', *Thermal Eng.,* Vol. 17(1), pp 129-132, 1970.

296. Rieger, N.F. and Wicks, A.L., 'Measurement of non-steady forces in three turbine stage geometries using the hydraulic analogy', *ASME J. Eng. Power,* 100, 14, Oct. 1978.

297. Smith, D.J.L. and Johnston, I.H., 'Investigations on an experimental single stage turbine of conservative design', *ARC,* R amd M 3541, 1968.

298. Stastny, M., 'Some differences in transonic flow of air and wet steam in turbine cascades', *Stro. Cas.,* 29, 3, pp 270-279, 1978.

299. Swatman, I.M. and Malohn, D.A., 'An advanced automotive gas turbine concept', *Trans SAE,* 69, 219-227, 1961; *Technical advances in gas turbine design symposium,* Instn. Mech. Engrs, 1969.

300. Thompson, W.E., 'Aerodynamics of turbines', *Proc. I turbomachinery symposium,* Texas, A and M University, Oct. 1972.

301. Topunow, A.M., Determination of optimal flow swirl at a turbine stage outlet', *Thermal Eng.,* 14, 5, pp 52-55, May 1967.

302. Yu, I. Mityushkin *et al.,* 'On axial turbine stage rotor blade twist with tangential tilt of the rotor vanes', *Sov. Aeronaut.* 22, 1, pp 99-101, 1979.

Partial Admission Turbines

303. Adams, R.G., 'The effect of Reynolds number on the performance of partial admission and re-entry axial turbines, *ASME paper* No. 65-GTP-3, 1965.

304. Berchtold, Max and Gardiner, F.J., 'The comprex, a new concept of diesel supercharging', *ASME paper* No. 58-GTP-16, 1958.

305. Buckingham, 'Windage resistance of steam turbine wheels', *Bull. Bureau. Stand. Wash.* Vol. 10, 1914.

306. Burri, H.U., 'Non-steady aerodynamics of the comprex supercharger', *ASME paper presented at the gas turbine power conference,* Washington, D.C., March 1958.

307. Deich, M.E. *et al.,* 'Investigation of double row Curtis stages with partial admission of steam', *Energomash,* Vol. 7, No. 3, 1961, English Electric Translation 559.

308. Deich, M.E. *et al.,* 'Investigation of single row partial admission stages', *Teploenergetika,* 10 (7) pp 18-21, Translation RTS 2615, 1963.

309. Dibelius, G., 'Turbocharger turbines under conditions of partial admission', Brown Boveri turbo chargers and gas turbines, CIMAC congress, London 1965.

310. Doyle, M.D.C., 'Theories for predicting partial admission losses in turbines', *J. Aerospace Sci.,* 29(4), 1962.

311. Frolov, V.V. and Ignatevskii, E.A., 'Edge losses of energy in partial admission turbine stages', *Thermal Eng.,* 18(1), pp 113-116, 1971.

312. Frolov, V.V. amd Ignatevskii, E.A., 'Calculating windage losses in a turbine stage', *Thermal Eng.,* 19(11), pp 45-49, 1972.

313. Heen, H.K. and Mann, R.W., 'The hydraulic analogy applied to non-steady two-dimensional flow in the partial admission turbines', *Trans ASME, J. Basic Eng.,* Sept. 1961.

314. Jackson, P., 'The future Doxford marine oil engine', *Trans Instn. Marine Engrs.,* 73, 1961.

315. Kentfield, J.A.C., 'An examination of pressure exchangers, equalizers and dividers', *Ph.D thesis,* London Univ., 1963.

316. Kerr, Wm, 'On turbine disc firction', *J. R. Tech. College,* Glasgow, 1 (103), 1924.

317. Klassen, H.A., 'Cold air investigation of effects of partial admission on preformace of 3.75 inch mean diameter single-stage axial-flow turbine', *NASA tech. note,* NASA TN D-4700, Aug. 1968.

318. Kohl *et al.*, 'Effect of partial admission on performance of gas turbines', *NACA,* TN 1807, 1949.

319. Korematsu, K. and Hirayama, N., 'Fundamental study on compressible transient flow and leakage in partially admitted radial flow turbines', *Proc. 2nd int. JSME symposium fluid machinery and fluidics,* Vol. 2, Sept. 1972.

320. Korematsu, K. and Hirayama, N., 'Performance estimation of partial admission turbines', *ASME paper* No. 79-GT-123, March, 1979.

321. Kroon, R.P., 'Turbine blade vibration due to partial admission', *J. Appl. Mech.,* Vol. 7, No. 4, Dec. 1940.

322. Linhardt, H.D., 'A study of high pressure ratio re-entry turbines', *Sundstrand Turbo Rep.* S/TD No. 1735, Jan. 1960.

323. Linhardt, H.D. and Silvern, D.H., *Analysis of partial admission axial impulse turbines', ARS J.,* p. 297, March 1961.

324. Macpherson, A.H., 'The use of stereo-photography and the hydraulic analogy to study compressible gas flow in a partial admission turbine', *Thesis (S.M.)* M.I.T, 1959.

325. Mann, R.W., 'Study of self contained emergency auxiliary power supplies for manned aircraft', *D.A.C.L. Rep.* No. 120, copy no. 16, M.I.T., Aug. 1958.

326. Mann, R.W., 'Fuels and prime movers for rotating auxiliary power units', *D.A.C.L. Rep.* No. 121, M.I.T., Sept. 30, 1958.

327. Mann, R.W., 'Bibiliography on missile internal power research', *Rep.* No. 128, M.I.T., June 30, 1962.

328. Nagao, Mizumachi *et al.,* 'On the partial admission gas turbines', *Trans JSME,* No. 370, 1975.

329. Nusbaum, W.J. and Wong, R.Y., 'Effect of stage spacing on performance of 3.75 inch mean diameter two-stage turbine having partial admission in the first stage', *NASA,* TN D-2335, Lewis Research Centres Cleveland, Ohio, June 1964.

330. Ohlsson, G.O., 'Partial admission, low aspect ratios and supersonic speeds in small turbines', *Thesis (Sc.D),* Dept. of Mech. Engg., M.I.T., Cambridge, Mass. 1956.

331. Ohlsson, G.O., 'Partial admission turbines', *J. Aerospace Sci.,* Vol. 29, No. 9, p. 1017, Sept. 1962.

332. Pillesbury, P.W., 'Leakage loss in the axial clearance of a partial admission turbine', *Thesis (S.M.),* M.I.T., 1957.

333. Silvern, D.H. and Balje, O.E., 'A study of high energy level, low power output turbines, *Sundstrand Turbo Rep.* S/TD No. 1195, April 9, 1958.

334. Stenning, A.H., 'Design of turbines for high energy low-power output applications', *D.A.C.L. Rep.* 79, M.I.T., 1953.

335. Suter, P. and Traupel, W., *Rep.* No. 4, The Institute of Thermal Turbines, Zurich, 1959, B.S.R.A. translation No. 917 (1960).

336. Terentiev, I.K., 'Investigation of active stages with partial admission of the working medium', *Energomash,* Vol. 6, 1960 English Electric translation No. 360.

337. Yahya, S.M., 'Transient velocity and mixing losses in axial flow turbines with partial admission', *Int. J Mech. Sci.,* Vol. 10, 1968.

338. Yahya, S.M. and Doyle, M.D.C., 'Aerodynamic losses in partial admission turbines', *Int. J. Mech. Sci.,* Vol. 11, 1969.

339. Yahya, S.M., 'Some tests on partial admission turbine cascades', *Int. J. Mech. Sci.,* Vol. 11, 1969.

340. Yahya, S.M., 'Leakage loss in steam turbine governing', *Instn. Engrs. (India),* 1969.

341. Yahya, S.M., 'Sudden expansion losses in partial admission turbine', *Instn. Engrs. (India),* 1969.

342. Yahya, S.M., 'Partial admission turbines and their problems', *Bull. Mech. Eng. Edu.,* Vol. 9, 1970.

343. Yahya, S.M. and Agarwal, D.P., 'Partial admission losses in an axial flow reaction turbine', *Instn. Engrs. (India),* 1974.

High Temperature Turbines

344. Ainley, D.G., 'Internal air-cooling for turbine blades—A general design survey', *ARC,* R and M 3405, HMSO, 1965.

345. Ammon, R.L. *et al.,* 'Creep rupture behaviour of selected turbine materials in air, ultra-high purity helium and simulated closed cycle Brayton helium working fluids', *ASME J. Eng. Power.* Vol. 103, April 1981.

346. Barnes, J.F. and Fray, D.E., 'An exprimental high temperature turbine', (No. 126), *ARC,* R and M 3405, 1965.

347. Bayley, F.J. and Priddy, W.J. 'Studies of turbulence characteristics and their effects upon heat transfer to turbine blading', *AGARD conference on heat transfer testing techniques,* paper No. 9, Brussels, 1980.

348. Behning, Frank, P. *et al.,* 'Cold-air investigation of a turbine with transpiration-cooled stator blades, III—Performance of stator with wire-mesh shell blading', *NASA,* TM X-2166, 1971.

349. Chaku, P.N. and Mcmahon Jr., C.J., 'The effect of air environment on the creep and rupture behaviour of a Nickel-base high temperature alloy', *Metall. Trans.* Vol. 5, No. 2, Feb. 1974.

350. Chauvin, J. *et al., Aerodynamic Problems in Cooled Turbine Blading Design for Small Gas Turbines,* Von Karman Institute, Belgium, Lecture series No. 15-Flow in turbines, April 1969.

351. Cheng, Ji-Rui and Wang, Bao-Guan, 'Experimental investigation of simulating impingement cooling of concave surfaces of turbine aerofoils', *J. Eng. Thermophys.,* Vol. 1, No. 2, May 1980.

352. Chupp, R.E. *et al.,* 'Evaluation of internal heat transfer coefficient for impinging cooled turbine aerofoils', *J. Aircr.,* Vol. 6, pp 203-208, 1969.

353. Colladay, R.S. and Stepka, F.S., 'Similarity constraints in testing of cooled engine parts', *NASA,* TN D-7707, June 1974.

354. Eriksen, V.L., 'Film cooling effectiveness and heat transfer with injection through holes', *NASA,* CR-72991, N72-14945, 1971.

355. Esgar, Jack B. *et al.*, 'An analysis of the capabilities and limitations of turbine air cooling methods', *NASA,* TN D-5992, 1970.

356. Fullagar, K.P.L., 'The design of aircooled turbine rotor blades', *Symposium on design and calculation of constructions subject to high temperature,* University of Delft, Sept. 1973.

357. Goldman, L.J. and Mclallim, K.L., 'Cold-air annular-cascade investigation of aerodynamic performance of core-engine cooled turbine vanes, I—Solid vane performance and facility description', *NASA,* TMX-3224, April 1975.

358. Guo, Kuan-Liang *et al.* (The Chinese Univ. of Science and Technology), 'Application of the finite element method to the solution of transient two-dimensional temperature field for air-cooled turbine blade', *J. Eng. Thermophy.,* Vol. 1, No. 2, May 1980.

359. Hanus, G.J., 'Gas film cooling of a modeled high-pressure high-temperature turbine vane with injection in the leading edge region from a single row of spanwise angled coolant holes', *Ph.D dissertation,* Mech. Engg. Dept., Purdue University, May 1976.

360. Hawthorne, W.R., 'Thermodynamics of cooled turbines, Parts I and II', *Trans ASME,* 78, 1765-81, 1956.

361. Herman Jr. W. Prust, 'Two-dimensional cold-air cascade study of a film-cooled turbine stator blade, II—Experimental results of full film cooling tests,' *NASA,* TMX-3153, 1975.

362. Herman, H. and Preece, C.M. (Eds.), *Treatise on Materials Science and Technology,* Academic Press, New York, London, 1979.

363. Kondo, T., 'Annual review of the high-temperatures metals research for VHTR', *JAERI,* Jan. 1977.

364. Lankford, James, 'Temperature-strain rate dependence of compressive strength and damage mechanisms in aluminium oxide', *J. Mat. Sci.,* 16, pp 1567-1578, 1981.

365. Lee, S.Y. *et al.,* 'Evaluation of additives for prevention of high-temperature corrosion of superalloys in gas turbines', *ASME paper* No. 73-GT-I, April 1973.

366. Lee, Jai. Sung and Chun, John. S., 'Effect of high-temperature thermo-mechanical treatment on the mechanical properties of vanadium modified AISI 4330 steel', *J. Mat. Sci.,* 16, pp 1557-1566, 1981.

367. Lemaitre, J. and Plumtree, A., 'Application of damage concepts to predict creep-fatigue failures', *J. Eng. Mat., and Technol., Trans ASME,* 101, 3, July 1979.

368. Lowell, C.E. and Probst, H.B., 'Effects of composition and testing conditions on oxidation behaviour of four cast commercial nickel-base super alloys', *NASA,* TN D-7705, 1974.

369. Lowell, C.E. *et al.,* 'Effect of sodium, potassium, magnesium, calcium and chlorine on the high-temperature corrosion of IN-100, U-700, IN-792, and MAR M-509', *J. Eng. Power, Trans ASME,* Vol. 103, April 1981.

370. Metzger, D.E. and Mitchell, J.W., 'Heat transfer from a shrouded rotating disc with film cooling', *J. Heat Transf., ASME,* 88, 1966.

371. Metzger, D.E. *et al.,* 'Impingement cooling of concave surfaces with lines of circular air jets', *ASME J. Eng. Power,* Vol. 91, pp 149-158, 1969.

372. Metzger, D.E. *et al.,* 'Impingement cooling performance of gas turbine airfoils including effects of leading edge sharpness', *ASME J. Eng. Power,* Vol. 94, pp 216-225, 1972.

373. Mills, W.J. and James, J.A., 'The fatigue-crack propagation response of two nickel-base alloys in a liquid sodium environment', *J. Eng. Mat. Technol., Trans ASME,* 101, 3, July 1979.

374. Moffit, Thomas, P. *et al.,* 'Summary of cold-air tests of a single stage turbine with various stator cooling techniques', *NASA,* TM X-52969, 1971.

375. Nouse, H. *et al.,* 'Experimental results of full scale air-cooled turbine tests', *ASME paper* No. 75-GT-116, April 1975.

376. Owen, J.M and Phadke, U.P., 'An investigation of ingress for a simple shrouded disc system with a radial outflow of coolant', *ASME paper* No. 80-GT-49, *25th ASME gas turbine conference,* New Orleans, 1980.

377. Prust Jr., H.W., 'An analytical study of the effect of coolant flow variables on the kinetic energy output of a cooled turbine blade row', *NASA,* TM X-67960, 1972.

378. Shahinian, P. and Acheter, M.R., 'Temperature and stress dependence of the atmosphere effect on a nickel-chromium alloy', *Trans ASM,* 51, 1959.

379. Sieverding, C.H. and Wilputte, Ph., 'influence of Mach numbers and end wall cooling on secondary flows in a straight nozzle cascade', *ASME J. Eng. Power,* Vol. 103, No. 2, April 1981.

380. Srtringer, J.F., 'High-temperature corrosion of aerospace alloys', *AGARD,* AG-200, Advisory group for aerospace research and development, Paris, 1975.

381. Suciu, S.N., 'High-temperature turbine design considerations', *SAE paper* No. 710462, 1971.

382. Szanca, Edward M. *et al.,* 'Cold-air investigation of a turbine with transpiration-cooled stator blades II—performance with discrete hole stator blades', *NASA,* TM X-2133, 1970.

383. Tabakoff, W. and Clevenger, W., 'Gas turbine blade heat transfer augumentation by impingement of air flowing various configurations', *ASME paper* No. 71-GT-9, 1971.

384. Tabakoff, W. and Wakeman, T., 'Test facility for material erosion at high temperature', *ASTM special technical publication,* No. 664, 1979.

385. Wall, F.J., 'Metallurgical development for 1500°F MGCR gas turbine maritime gas-cooled reactor', *Project Eng. report,* EC-193, Feb. 1964.

386. Whitney, Warren, J., 'Comparative study of mixed and isolated flow methods for cooled turbine performance analysis', *NASA,* TM X-1572, 1968.

387. Whitney, Warren, J., 'Analytical investigation of the effect of cooling air on two-stage turbine performance', *NASA,* TM X-1728, 1969.

388. Whitney, J. *et al.,* 'Cold-air investigation of a turbine for high temperature engine applications', *NASA,* TN D-3751.

Axial Compressors

389. Academia Sinica, Shenyany Aeroengine company, 'Theory, method and application of three-dimensional flow design of transonic axial-flow compressors', *J. Eng. Thermophys.,* Vol. 1, No. 1, Feb. 1980.

390. Bitterlich and Rubner, 'Theoretical and experimental investigation of the three dimensional frictional flows in an axial flow compressor stage', *Mitteilung Nr.* 74-04, des Instituts fur strahlantriebe und Turboarbeitsmaschinen der Technischen Hochschule Aachen, 1974.

391. Brown, L.E., 'Axial flow compressor and turbine loss coefficients: A comparison of several parameters', *ASME J. Eng. Power,* paper No. 72-GT-18, 1972.

392. Calvert, W.J. and Herbert, M.V., 'An inviscid-viscous interaction method to predict the blade-to-blade performance of axial compressors', *Aeronaut., Qtly.,* Vol. XXXI, Pt.3, Aug. 1980.

393. Dimmock, N.A., 'A compressor routine test code', *ARC,* R & M 3337, 1963.

394. Dixon, S.L., 'Some three dimensional effects of rotating stall', *ARC current paper* No. 609, 1962.

395. Dixon, S.L. and Horlock, J.H., 'Velocity profile development in an axial flow compressor stage', *Gas turbine collaboration committee,* paper 624, 1968.

396. Dixon, S.L., 'Secondary vorticity in axial compressor blade rows', *Fluid mechanics, acoustics and design of turbomachines,* NASA SP-304 I and II, 1974.

397. Doyle, M.D.C. *et al.,* 'Circumferential asymmetry in axial compressors', *J. Roy. Aeronaut. Soc.,* Vol. 10, pp 956-957, Oct. 1966.

398. Dunham, J., 'Non-axisymmetric flows in axial compressors', *Instn. Mech. Engrs. Monograph,* 1965.

399. Eckert, S., *Axial and Radial Compressoren,* 2nd edn., Springer, Berlin, 1961.

400. Emmons, H.W. *et al.,* 'A survey of stall propagation-experiment and theory', *Trans ASME,* Series D, 81, 1959.

401. Fabri, J., 'Rotating stall in an axial flow compressor', *Instn. Mech. Engrs., internal Aerodynamics,* pp 96-110, 1970.

402. Favrat, D. and Suter, P., 'Interaction of the rotor blade shock waves in supersonic compressors with upstream rotor vanes', *ASME J. Eng. Power,* 100, Jan. 1978.

403. Gallus, H. and Kummel, 'Secondary flows and annulus wall boundary layers in axial flow compressor and turbine stages', *AGARD conference on secondary flows in turbomachines,* CPP-214.

404. Gallus, H.E. *et al.,* 'Measurement of the rotor-stator-interaction in a subsonic axial flow compressor stage', *Symposium on aeroelasticity in turbomachines',* Paris, 18-23, Oct. 1976.

405. Gostelow, J.P. *et al.,* 'Recent developments in the aerodynamic design of axial flow compressors', *Symposium at Warwick University,* Proc. Instn. Mech. Engrs. London, 183, Pt. 3N, 1969.

406. Graham, R.W. and Prian, V.D., 'Rotating stall investigation of 0.72 hub-tip ratio single stage compressor', *NACA,* RME 53, L17a, 1954.

407. Greitzer, E.M., 'Surge and rotating stall in axial flow compressors', *ASME J. Eng. Power,* Vol. 98. No. 2, April 1976.

408. Hawthorne, W.R., 'The applicability of secondary flow analyses to the solution of internal flow problems', *Fluid Mechanics of Internal Flows,* Ed. Gino Sovran, Elsevier Publ. Co., 1967.

409. Hawthorne, W.R. and Novak, R.A., 'The aerodynamics of turbomachinery', *Annual reviews of fluid mechanics,* Vol. 1, 1969.

410. Hiroki, T. and Jshizawa. H., 'Some problems encountered in the design and development of a transonic compressor', Gas turbine paper presented at Tokyo, *Joint international gas turbine conference and products show,* 1971.

411. Horlock, J.H., 'Annulus wall boundary layers in axial compressor stages', *Trans ASME, J. Basic Eng.,* Vol. 85, 1963.

411a. Horlock, J.H., *Axial Flow Compressors,* Kruger Publishing Co., 1973.

412. Howell, A.R., 'Fluid dynamics of axial compressors', *Proc. Instn. Mech. Engrs.,* London, 153, 1945.

413. Howell, A.R. and Bonham, R.P., 'Overall and stage characteristics of axial flow compressors', *Proc. Instn. Mech. Engrs.,* London, 1963, 1950.

414. Howell, A.R. and Calvert, W.J., 'A new stage stacking method for axial flow compressor performance', *Trans ASME, J. Eng. Power,* Vol. 100, Oct. 1978.

415. Johnsen, I.A. and Bullock, R.O., 'Aerodynamic design of axial flow compressors', *NASA,* SP-36, 1965.

416. Johnston, J.P., *The effects of rotation on boundary layers in turbomachine rotors,* Report No. MD-24, Thermosciences division, Dept. of Mech. Engg., Stanford University, Stanford, California.

417. Katz, R., 'Performance of axial compressors with asymmetric inlet flows', Daniel and Guggenheim jet propulsion centre, *CALTECH Rep.* No. AFSOR-TR-58-59 AD 162, 112, June 1958.

418. Kerrebrock, J.L. and Mikolajczak, A.A., 'Intra-stator transport of rotor wakes and its effects on compressor performance', *ASME paper* No. 79-GT-39, 1970.

419. Lieblein, S., 'Experimental flow in two-dimensional cascades, Aerodynamic design of axial flow compressors', *NASA,* SP-36, 1965.

420. Masahiro, Inoue *et al.,* 'A design of axial flow compressor blades with inclined stream surface and varying axial velocity', *Bull. JSME,* Vol. 22, No. 171, Sept. 1979.

421. Mccune, J.E. and Okurounmu, O., 'Three-dimensional vortex theory of axial compressor blade rows at subsonic and transonic speeds', *AIAA. J.* Vol. 8, No. 7, July 1970.

422. Mccune, J.E. and Khawakkar, J.P., 'Lifting line theory for subsonic axial compressor rotors', *M.I.T. GTL Rep.* No. 110, July 1972.

423. Mellor, G.L. and Balsa, T.F., 'The prediction of axial compressor performance with emphasis on the effect of annulus wall boundary layers', *Agardograph,* No. 164, AGARD, 1972.

424. Mikolajezak, A.A. *et al.,* 'Comparsion for performance of supersonic blading in cascade and in compressor rotors', *ASME paper* No. 70-GT-79, 1979.

425. National Aeronautics and Space Administration, 'Aerodynamic design of axial-flow compressors', *NASA,* SP-36, 1965.

426. Pearson, H. and Mckenzie, A.B., 'Wakes in axial compressors', *J. Aero. Space Sci.,* Vol. 63, No. 583, pp 415-416, July 1959.

427. Reid, C., 'The response of axial flow compressors to intake flow distortation', *ASME paper* No. 69-GT-29, 1969.

428. Robert, F. *et al.,* 'Insight into axial compressor response to distortion', *AIAA paper* No. 68-565, 1968.

429. Sexton, M.R. *et al.,* 'Pressure measurement on the rotating blades of an axial flow compressor', *ASME paper* No. 73-GT-79, 1973.

430. Shaw, H., 'An improved blade design for axial compressor (and turbine)', *Aeronaut. J.,* Vol. 74, p. 589, 1970.

431. Simon, H. and Bohn, D., 'A comparison of theoretical and experimental investigations of two different axial supersonic compressors', *I.C.A.S. 2nd Int. symposium on air breathing engines,* Sheffield, England, March 1974.

432. Smith Jr., L.H., 'Casing boundary layers in multi-stage compressors', *Proc. symposium on flow research on blading,* Ed. L.S. Dzung, Elsevier, 1970.

433. Stenning, A.H. and Plourde, G.A., 'The attenuation of circumferential inlet distortion in the multi-stage axial compressor', AIAA paper No. 67-415, *AIAA 3rd propulsion joint specialist conf.,* Washington D-C, 17-21, July 1967.

434. Stephens, H.E., 'Supercritical aerofoil technology in compressor cascades; comparison of theoretical and experimental results', *AIAA J.* 17, 6, June 1979.

435. Swann, W.C., 'A practical method of predicting transonic compressor performance', *Trans ASME,* Series A, 83, 1961.

436. Tanaka, S. and Murata, S., 'On the partial flow rate performance of axial flow compressor and rotating stall', II report, *Bull. JSME,* Vol. 18. No. 117, March 1975.

437. Tsui, Chih-Ya *et al.,* 'An experiment to improve the surge margin by use of cascade with splitter blades', *J. Eng. Thermophys.,* Vol. 1, No. 2, May 1980.

438. Zhang, Yu-Jing, 'The performance calculation of an axial flow compressor stage', *J. Eng. Thermophys.,* Vol. 1, No. 2, May 1980.

Centrifugal Compressors

439. Balje, O.E., 'A study of design criteria and matching of turbomachines. Pt. B—Compressor and pump performance and matching of turbo components', *ASME paper* No. 60-WA-231, 1960.

440. Balje, O.E., 'Loss and flow path studies on centrifugal compressors', *Pt. I ASME paper* No. 70-FT-12a, 1970; *Pt. II ASME paper* No. 70-GT-12b, 1970.

441. Bammert, K. and Rautenberg, M., 'On the energy transfer in centrifugal compressors', *ASME paper* No. 70-GT-121, 1974.

442. Beccari, A., *Theoretical-experimental study of surging in centrifugal turbo compressor used for supercharging* (in Italian), Assoc. Tec. dell, automob., 26(10), pp 526-36, Oct. 1973.

443. Benson, R.S. and Whitfield, A., 'Application of non-steady flow in a rotating duct to pulsating flow in a centrifugal compressor', *Proc. Instn. Mech. Engrs.,* 182(Pt 3H) 184, 1967-68.

444. Boyce, M.P. and Bale, Y.S., 'Feasibility study of a radial inflow compressor', *ASME paper* No. 72-GT-52, March 1972.

445. Came, D.M., 'The current state of research and design in high pressure ratio centrifugal compressor', *ARC current paper* CP No. 1363, London, 1977.

446. Campbell, K. and Talbert, J.E., 'Some advantages and limitations of centrifugal and axial aircraft compressors', *Trans SAE,* Vol. 53, No. 10, Oct. 1945.

447. *Centrifugal Compressors and Blowers (in German) pumpen and Verdichter Inf.,* Special issue, 2, 1974.

448. Cheshire, I.J., 'The design and development of centrifugal compressors for aircraft gas turbines', *Proc. Instn. Mech. Engrs.,* 153, 426-40, 1945.

449. Csanady, G.T., 'Head correction factors for radial impellers', *Engineering,* London, 190, 1960.

450. Cyffer, M.J., 'Centrifugal compressors with rotating diffuser, Pt. 2: Diffusion at wheel exit of industrial fans and compressors (in French)', *Mechanique Materiax Electricite,* 59, June-July, Paris, 1976.

451. Dallenbach, F., 'The aerodynamic design and performance of centrifugal and mixed flow compressors', *SAE Tech. Progress Series,* Vol. 3, pp 2-30.

452. Dean Jr. Robert, C., *The Fluid Dynamic Design of Advanced Centrifugal Compressors',* TN-153, Creare, Sept. 1972.

453. Eckert, D., 'Instantaneous measurement in the jet and wake discharge flow of a centrifugal compressor impeller', *ASME J. Eng., Power,* pp 337-346, July 1975.

454. Erwin, J.R, and Vitale, N.G., *Radial Outflow Compressor-ASME Advanced Centrifugal Compressors,* 56-117, 1971.

455. Ferguson, T.B., 'Influence of friction upon the slip factor of a centrifugal compressor' *Engineer,* 213 (554C), 30 March 1962.

456. Ferguson, T.B., *The Centrifugal Compressor Stage,* Butterworth, London, 1963.

457. Groh, F.G. *et al.,* 'Evaluation of a high hub-tip ratio centrifugal compressor', *ASME paper* No. 69-WA/FE-28, 1969.

458. Gruber, J. and Litvai, E., 'An investigation of the effects caused by fluid friction in radial impellers', *Proc. 3rd conference on fluid mechanics and fluid machinery,* Akademiai Kindo, pp 241-247, Budapest, 1969.

459. Hodskinson, M.G., 'Aerodynamic investigation and design of a centrifugal compressor impeller', *Ph.D thesis,* Liverpool University, 1967.

460. Howard, J.H.G. and Osborne, C., 'Centrifugal compressor flow analysis employing a jet-wake passage flow model', *ASME paper* No. 76-FE-21, 1976.

461. Judet, De La and Combe, M.A., 'Centrifugal compressors with rotating diffuser, Pt. 1 (in French)', *Mechanique Materiax, Electricite,* Paris, June-July, 1976.

462. Kalinin, I.M. *et al.,* 'Refrigerating machines with centrifugal compressors', *Chem. Pet. Eng. (USSR).* 11(9/10) Sept. Oct. 1975.

463. Klassen, H.A., 'Performance of low pressure ratio centrifugal compressor with four diffuser designs', *NACA,* TN 7237, March 1973.

464. Koinsberg, A., 'Reasons for centrifugal compressor surging and surge control', *ASME J. Eng. Power,* paper No. 78-GT-28, 1978.

465. Kordzinski, W., 'Trends in development of the design method of aircraft engine compressors, Pt. 3—Centrifugal compressors (in Polish), *Tech. Lotnicza., Astranaut.,* 12, pp 18-26, 1972.

466. Lapina, R.P., 'Can you rerate your centrifugal compressor', *Chem. Eng. (N.Y.)* 82(2), Jan. 20, 1975.

467. Ledger, J.D. *et al.,* 'Performance characteristics of a centrifugal compressor with air injection', *Heat and Fluid Flow,* Vol. 3, No. 2 pp 105-114, Oct. 1973.

468. Mizuki, S. *et al.,* 'A study of the flow pattern within centrifugal and mixed flow impellers', *ASME paper* No. 71-GT-41, 1971.

469. Mizuki, S. *et al.,* 'Investigation concerning the blade loading of centrifugal impellers', *ASME paper* No. 74-GT-143, 1974.

470. Mizuki, S. *et al.,* 'Study on the flow mechanism within centrifugal impeller channels', *ASME paper* No. 75-GT-14, 13p. March 1975.

471. Morris, R.E. and Kenny, D.P., 'High pressure ratio centrifugal compressors for small gas turbine engines', *Advanced Centrifugal Compressors,* ASME special publication, pp 118-146, 1971.

472. Moult, E.S. and Pearson, H., 'The relative merits of centrifugal and axial compressors for aircraft gas turbines', *J. R. Aeronaut. Soc.,* 55, 1951.

473. Nashimo, T. *et al.,* 'Effect of Reynolds number on performance characteristics of centrifugal compressors with special reference to configurations of impellers', *ASME paper* No. 74-GT-59, 1974.

474. Rodgers, C., 'Variable geometry gas turbine radial compressors', *ASME paper* No. 68-GT-63, Jan. 1968.

475. Rodgers, C. and Sapiro, L., 'Design considerations for high-pressure ratio centrifugal compressor', *ASME paper* No. 72-GT-91, March 1972.

476. Rodgers, C., 'Continued development of a two-stage high pressure-ratio centrifugal compressor', USA AMRDL-TR-74-20, April 1974.

477. Sakai, T. *et al.,* 'On the slip factor of centrifugal and mixed flow impellers. *ASME paper* No. 67-WA/GT-10, 1967.

478. Schmidt *et al.,* 'The effect of Reynolds number and clearance in centrifugal compressor of a turbocharger', *Brown Boveri Rev.,* pp 453-455, Aug. 1968.

479. Schoeneck, K.A. and Hornschuch, H., 'Design concept of a high speed-high pressure ratio centrifugal compressor', *ASME paper* No. 75-Pet-4, Sept. 1975.

480. Sturge, D.P., 'Compressible flow in a centrifugal impeller with separation; a two-dimensional calculation method', *ASME paper* No. 77-WA/FE-8, 1977.

481. Tsiplenkin, G.E., 'Centrifugal compressor impeller of minimum throughout capacity', *Energomashinostroenie,* 6, 1974.

482. Van Le, N., 'Partial flow centrifugal compressors', *ASME paper* No. 61-WA-135, Winter annual meeting, 1961.

483. Vasilev, V.P. *et al.,* 'Investigation of the influence of the axial clearance on the characteristics of a centrifugal compressor', *Teploenergetika,* Vol. 16, no. 3, pp 69-72, 1969.

484. Wallace, F.J. and Whitfield, A., 'A new approach to the problem of predicting the performance of centrifugal compressors', *JSME fluid machinery and fluids symposium,* Tokyo, Sept. 1972.

485. Wallace, F.J. *et al.,* 'Computer aided design of radial and mixed flow compressors', *Comput. Aided Design,* July 1975.

486. Watanabi, I. and Sakai, T., 'Effect of the cone angle of the impeller hub of the mixed flow compressor upon performance characteristics', *SAE paper* No. 996A, 1965.

487. Whitfield, A. and Wallace, F.J., 'Study of incidence loss models in radial and mixed flow turbomachinery', *Instn. Mech. Engrs. Conference Publication,* 3, paper No. C55/73, 1973.

488. Whitfield, A., 'The slip factor of a centrifugal compressor and its variation with flow rate', *Proc. Instn. Mech. Engrs.* paper No. 32/74, 1974.

489. Whitfield, A. and Wallace, F.J., 'Performance prediction for automotive turbocharger compressors', *Proc. Instn. Mech. Engrs.* 1975.

490. Wiesner, F.J., 'A review of slip factor for centrifugal impeller', *ASME J. Eng. Power,* pp 558-572, Oct. 1967.

Radial Turbines

491. Ariga, I. *et al.,* 'Investigation concerning flow patterns within the impeller channels of radial inflow turbines with reference to the influence of splittervanes', *Int. gas turbine conf., ASME paper* No. 66-WA/FT-2, 1966.

492. Baines, N.C. *et al.,* 'Computer aided design of mixed flow turbines for turbochargers', *ASME J. Eng. Power,* 101, 3, pp 440-449, July 1979.

493. Balje, O.E., 'A study on the design criteria and matching of turbomachines', Pt. A, *ASME J. Eng. Power,* 84, 1962.

494. Baskhorne, E. *et al.,* 'Flow in nonrotating passages of radial inflow turbines', *NASA,* CR-159679, p. 104, Sept. 1979.

495. Benson, R.S. and Scrimshaw, K.H., 'An experimental investigation of non-steady flow in a radial gas turbine', *Proc. Instn. Mech. Engrs.,* 180 (Pt. 3J), 74, 1965-66.

496. Benson, R.S., 'An analysis of losses in radial gas turbine', *Proc. Instn. Mech. Engrs.,* Vol. 180 (Pt. 3J), p. 53, 1966.

497. Benson, R.S. *et al.,* 'An investigation of the losses in the rotor of a radial flow gas turbine at zero incidence under conditions of steady flow', *Proc. Instn. Mech. Engrs.,* London, 182 (Pt. 3H), 1968.

498. Benson, R.S. *et al.,* 'Flow studies in a low speed radial bladed impeller', *Proc. Instn. Mech. Engrs.,* 184 (Pt. 3G), 1969-70.

499. Benson, R.S. *et al.,* 'Calculations of the flow distribution within a radial turbine rotor', *Proc. Instn. Mech. Engrs.,* Vol. 184 (Pt. 3G), March 1970.

500. Benson, R.S., 'A review of methods for assessing loss coefficients in redial gas turbines', *Int. J. Mech. Sci.,* 12, 1970.

501. Benson, R.S., 'Prediction of performance of radial gas turbines in automotive turbochargers', *ASME paper* No. 71-GT-66, 1971.

502. Benson, R.S. *et al.,* 'Analytical and experimental studies of two-dimensional flows in a radial bladed impeller', *Int. Gas Turbine Conf. ASME paper* No. 71-GT-20, 1971.

503. Benson, R.S., 'Die Leistungseigenschaffee von Deiseniosen Radial turbines', *MTZ,* Vol. 34, No. 12, p. 417, 1973.

504. Benson, R.S. and Jackson, D.C., 'Flow studies in radial inflow turbine interspace between nozzle and rotor', *Instn. Mech. Engrs. Conference on Heat and Fluid Flow in Steam and Gas Turbine Plants,* Warwick, April 1973.

505. Bridle, E.A. and Boulter, R.A., ' A simple theory for the prediction of losses in rotors of inward radial flow turbines', *Proc. Instn. Mech. Engrs.,* 182, Pt. 3H, 1968.

506. Cartwright, W.G., 'A comparison of calculated flows in radial turbines with experiment', *ASME paper* No. 72-GT-50, 1972.

507. Cartwright, W.G., 'The determination of the static pressure and relative velocity distribution in a two-dimensional radially bladed rotor', *Instn. Mech. Engrs. Conference publication* 3, C111/73, 1973.

508. Futral, M.J. and Wasserbauer, C., 'Off-design performance prediction with experimental verification for a radial-inflow turbine', *NASA,* TN D-2621, 1965.

509. Heit, G.F. and Johnston, I.H., 'Experiments concerning the aerodynamic performance of inward radial flow turbines', *Proc. Instn. Mech. Engrs.,* London, 178, Pt. 31(ii), 1964.

510. Jamieson, A.W.H., 'The radial turbine', Ch. 9, *Gas Turbine Principles and Practice,* Ed. Sir H. Roxbee Cox, Newnes 1955.

511. Kastner, L.J. and Bhinder, F.S., 'A method for predicting the performance of a centripetal gas turbine fitted with nozzle-less volute casing', *ASME paper* No. 75-GT-65, 1975.

512. Khalil, I.M. *et al.,* 'Losses in radial inflow turbine', *ASME J. Fluid Eng.,* Vol. 98, Sept. 1976.

513. Knoernschild, E.M., 'The radial turbine for low specific speeds and low velocity factor', *ASME J. Eng. Power,* Series A, Vol. 83, No. 1, pp 1-8, Jan. 1961.

514. Kofskey, M.G. and Wasserbauer, C.A., 'Experimental performance evaluation of a radial inflow turbine over a range of specific speeds', *NASA,* TN D-3742, 1966.

515. Kosyge, H. *et al.,* 'Performance of radial inflow turbine under pulsating flow conditions', *ASME J. Eng. Power* Series A, Vol. 98, 1976.

516. Mcdonald, G.B. *et al.,* 'Measured and predicted flow near the exit of a radial-flow impeller', *ASME paper* No. 71-GT-15, March 1971.

517. *M.I.R.A. Radial Inflow Turbine—First report on aerodynamic performance tests on cold rig',* Ricardo & Co. Engrs. (1927) Ltd. Rep. No. OP 6845, Nov. 1962.

518. Mizumachi, N. *et al.,* 'A study on performance of radial turbine under unsteady flow conditions', *Rep. Institute of Industrial Sci.,* The Univ of Tokyo, 28,1, 77pp Dec. 1979.

519. Nusbaum, W.J. and Kofskey, M.G., 'Cold performance evaluation of 4.97 inch radial inflow turbine designed for single-shaft Brayton cycle space-power system', *NASA,* TN D 5090, 1969.

520. Rodgers, C., 'Efficiency and performance characteristics of radial turbines', *SAE paper* No. 660754, Oct. 1966.

521. Rodgers, C., 'A cycle analysis technique for small gas turbines', *Technical advances in gas turbine design, Proc. Instn. Mech. Engrs.,* London, 183, Pt. 3N, 1969.

522. Rohlik, H.E., 'Analytical determination of radial-inflow turbine design geometry for maximum efficiency', *NASA,* TN D 4384, 1968.

523. Swada, T., 'Investigation of radial inflow turbines', *Bull. JSME,* Vol. 13, No. 62, pp 1022-32, Aug. 1970.

524. Wallace, F.J., 'Theoretical assessment of the performance characteristics of inward-flow radial turbines', *Proc. Instn. Mech. Engrs.,* London, 172, 1958.

525. Wallace, F.J. and Blair, G.P., 'The pulsating flow performance of inward radial flow turbines', *ASME gas turbine Conf. paper* No. 65-GTP-21, Washington, 1965.

526. Wallace, F.J. *et al.,* 'Performance of inward radial flow turbines under steady flow conditions with special reference to high pressure ratio and partial admission', *Proc. Instn. Mech. Engrs.,* Vol. 184, Pt(1), No. 50, 1969-70.

527. Wallace, F.J. *et al.,* 'Performance of inward radial flow turbines under non-steady flow conditions', *Proc. Instn. Mech. Engrs.,* Vol. 184(Pt. 1), 1969-70.

528. Wasserbauer, C.A. and Glassman, A.J., 'Fortran program for predicting off-design performance of radial inflow turbines', *NASA,* TN D 8063, p.55, Sept. 1975.

529. Wood, H.J., 'Current technology of radial-inflow turbines for compressible fluids', *ASME J. Eng. Power,* 85, 1963.

Axial Fans and Propellers

530. Anon., *AMCA Fan Application Manual-Pt.* 3-A, 'Guide to the measurement of fan-system performance in the field', *AMCA* publication 203, Air moving and conditioning association. 1976.

531. Anon., *Fan Pressure and Fan Air Power where P_1 differs from P_2* ISO/TC117/SCI, Paris, 1978.

532. Anon., *ASME performance test code No. 11-Large industrial fans,* draft copy, 1979.

533. Armor, A.F., 'Computer design and analysis of turbine generator fans', *ASME paper* No. 76 WA/FE-9, 1976.

534. Bogdonoff, S.M. and Hess, E.E., 'Axial flow fan and compressor blade design data at 52.5° stagger, and further verification of cascade data by rotor tests', *NACA,* TN 1271, 1947.

535. Bogdonoff, S.M. and Harriet, E., 'Blade design data for axial flow fans and compressors', *NACA,* ACR L5 F07a, 1954.

536. Bruce, E.P., 'The ARL axial fan research fan—A new facility for investigation of time dependent flows', *ASME paper* No. 74-FE-27, 1974.

537. B.S.S. 848, Pt. 1, *Code testing of fans for general purposes excluding ceiling, desk and mine fans,* 1963.

538. Carter, A.D.S., 'Blade profiles for axial flow fans, pumps, compressors etc. *Proc. Instn. Mech. Engrs.,* 1961.

539. Cocking, B.J. and Ginder, R.B., 'The effect of an inlet flow conditioner on fan distortion tones', *AIAA paper* No. 77-1324, Oct. 1977.

540. Cumming, R.A., *et al.,* 'Highly skewed propellers', *Trans Soc. Naval Architects and Marine Engineers,* Vol. 20, 1972.

541. Cunnan, W.S. *et al.,* 'Design and performance of a 427-metre per second tip speed two-stage fan having a 2.40 pressure ratio', *NASA,* TP-1314, Oct. 1978.

542. Eck, Bruno, *Fans, Design and Operation of Centrifugal, Axial Flow and Cross-flow Fans,* Pergamon Press, 1973.

543. Fukano, T., *et al.,* 'Noise-flow characteristics of axial fans', *Trans JSME,* No. 370, 1975.

544. Fukano, T. *et al.,* 'On turbulent noise in axial fans-effects of number of blades, chord length and blade camber', *Trans JSME,* No. 375, 1976.

545. Fukano, T. *et al.,* 'Noise generated by low pressure axial flow fans' *J. Sound Vibr.* 56(2), 261-277, 1978.

546. Gelder, T.F., 'Aerodynamic performances of three fan stator design operating with rotor having tip speed of 337 m/s and pressure ratio of 1.54'. I—Experimental performance, *NASA,* TP-1610, 108 pp Feb. 1980.

547. Gerhart, P.M., 'Averaging methods for determining the performance of large fans from field measurements', *ASME J. Eng. Power,* Vol. 103, April 1981.

548. Ginder, R.B. and Cocking. B.J., 'Considerations for the design of inlet flow conditioners for static fan noise testing', *AIAA paper* No. 79-0657, March 1979.

549. Glauert, H., *The Elements of Aerofoil and Airscrew Theory,* Cambridge University Press, 1959.

550. Jaumote, A.L., 'The influence of flow distortions on axial flow fan and rotating stall', *ZAMP* 15, Vol. 2, p 116, 1964.

551. Lewis, R.I. and Yeung, E.H.C., 'Vortex shedding mechanisms in relation to tip clearance flows and losses in axial fans', *ARC,* 37359, 1977.

552. Madison, R.D., *Fan Engineering,* 5th edn, Buffalo Forge Company, New York, 1949.

553. Moore, R.D. and Reid, L., 'Aerodynamic performance of axial flow fan stage operated at nine inlet guide vans angles', *NASA,* TP-1510, 43 p. Sept. 1979.

554. Oshima, M. *et al.,* 'Blade characteristics of axial-flow propellers', *Second international JSME symposium on fluid machinery and fluidics,* Vol. 1, Tokyo, Sept. 1972.

555. Robert, S. *et al.,* 'Performance of a highly loaded two-stage axial flow fan', *NASA,* TMX-3076, 1974.

556. Urasek, D.C. *et al.,* Performance of two-stage fan with larger dampers on the first stage rotor', *NASA,* TP-1399, May 1979.

557. Van Neikerk, C.G., 'Ducted fan design theory', *J. Appl. Mech.,* 25, 1958.

558. Wallis, R.A., *Axial Flow Fans, Design and Practice,* Newnes, London, 1961.

559. Wallis, R.A., 'Optimization of axial flow fan design', *Trans Mech. and Chem. Engg.,* Instn. Engrs. Australia, Vol. MC 4, No. 1, 1968.

560. Wallis, R.A., 'A rationalized approach to blade element design, axial flow fans', *3rd Australasian conference on hydraulics and fluid mechanics,* Sydney. 1968.

Centrifugal Fans and Blowers

561. B.S.S 848, *Methods of testing fans for general purposes, including mine fans,* 1963.

562. Bush, E.H., 'Cross-flow fans—History and recent developments', *Conference on fan technology and practice,* April 1972.

563. Church, A.H. and Jagdeshlal, *Centrifugal pumps and blowers,* John Wiley & Sons, New York, 1973.

564. Daly, B.B., Fan Performance measurement, *Conference on fan technology,* April 1972.

565. Datwyler, G., 'Improvements in or relating to transverse flow fans', *U.K. Patent specification,* 988, 712, 1965.

566. Embletion, T.F.W., 'Experimental study of noise reduction in centrifugal blowers', *J. Acous. Soc. Am.,* 35, pp 700-705.

567. Fan technology and practice, *Conference Instn. Mech. Engrs.,* London, 18-19, April 1972.

568. Fujie, K., 'Study of three dimensional flow in a centrifugal blower with straight radial blades and logarithmic spiral blades in radial part only', *Bulletin JSME,* Vol. 1, No. 31958, pp 275-282.

569. Gardow, E.B., 'On the relationship between impeller exit velocity distribution and blade channel flow in a centrifugal fan', *Ph.D. thesis,* State University of New York at Buffalo, Feb. 1968.

570. Gasiorek, J.M., 'The effect of inlet clearance geometry on the performance of a centrifugal fan', *Ph.D. thesis,* University of London, 1971.

571. Gasiorek, J.M., 'The effect of inlet cone intrusion on the volumetric efficiency of a centrifugal fan', *Conference on fan technology and practice,* Instn. Mech. Engrs., London, April, 1972.

572. Gessner, F.B., 'An experimental study of centrifugal fan inlet flow and its influence on fan performance', *ASME paper* No. 67-FE-21, 1967.

573. Gopalakrishnan, G. and Arumugam, S., 'Noise pollution from centrifugal blowers', *All India Seminar on fans, blowers and compressors,* Poona, Dec. 1977.

574. Hollenberg, J.W. and Potter, J.H., 'An investigation of regenerative blowers and pumps', *ASME J. Eng. Power,* 101, 2, 147-152, May 1979.

575. Ikegami, H and Murata, S., 'A study of cross flow fans, Pt. I—A theoretical analysis', *Technology report,* Osaka University, 557, 16, 1966.

576. Iberg, H. and Sadeh, W.Z., 'Flow theory and performance of tangential fans', *Proc. Instn. Mech. Engrs.* 180, No. 19, 481, 1965-66.

577. Ishida, M. and Senoo, Y., 'On the pressure-losses due to the tip clearance of centrifugal blowers', *ASME J. Eng. Power,* Vol. 103, No. 2, April 1981.

578. Kovats, A. de and Desmur, G., *Pumps, Fans and Compressors,* Blackie and Sons, 1958.

579. Kovats, A., *Design and Performance of Centrifugal and Axial Flow Pumps and Compressors,* Pergamon Press, 1964.

580. Krishnappa, G., 'Effect of blade shape and casing geometry on noise generation from the experimental centrifugal fan', *Proc. of the 5th world conference on theory of machines and mechanisms,* 1979.

581. Krishnappa, G., 'Some experimental studies on centrifugal blower noise', *Noise Control Engineering,* March-April, 1979.

582. Laakso, H., 'Cross-flow fans with pressure coefficients $\psi > 4$' (in German), *Heiz-Luft-Haustech.,* 8, 12, 1957.

583. Matley, J. *et al., Fluid Movers, Pumps, Compressors, Fans and Blowers,* McGraw-Hill, New York, 1979.

584. Moore, A., 'The Tangential fan—Analyhsis and design', *Conference on fan technology,* Instn. Mech. Engrs. London, April 1972.

585. Murata, S. *et al.,* 'Study of cross-flow fan', *Bulletin JSME* Vol. 19, No. 129, March 1976.

586. Murata, S. *et al.,* 'A study of cross-flow fan with inner guide appratus', *Bulletin JSME,* Vol. 21, No. 154, April 1978.

587. Myles, D.J., 'A design method for mixed flow fans and pumps', *N.E.L. report* No. 177, 1965.

588. Myles, D.J., 'An investigation into the stability of mixed flow blower characteristics' *N.E.L. report* No. 252, 1966.

589. Myles, D.J., 'An ayalysis of impeller and volute losses in centrifugal fans', *Proc. Instn. Mech. Engrs.,* Vol. 184, 1969-70.

590. Neisse, W., 'Noise reduction in centrifugal fans—A literature survey', *ISVR Tech. Rep.* No. 76, June 1975.

591. Osborne, W.C., *Fans,* Pergamon Press, 1966.

592. Pampreen, R.C., 'Small turbomachinery compressor and fan aerodynamics', *Trans ASME,* Vol. 95, pp 251-256, 1973.

593. Perry, R.E., 'The operation, maintenance and repair of industrial centrifugal fans', *Barron A.S.E. Inc.,* Leeds.

594. Polikovsky, V. and Nevelson, M., 'The performance of a vaneless diffuser fan', *NACA,* TM No. 1038, 1972.
595. Porter, A.M. and Markland, E., 'A study of the cross-flow fan', *J. Mech. Eng. Sci.,* 12, 6, 1970.
596. Raj, D. and Swim, W.B., 'Measurements of the mean flow velocity and velocity fluctuations at the exit of a FC centrifugal fan rotor', *ASME J. Eng. Power,* Vol. 103, April 1981.
597. Sedille, M., *Centrifugal and Axial Fans and Compressors,* (in French), Editions Eyroller and Masson et Cie, Paris, 1973.
598. Somerling, H. and Vandevenne, J., 'The flow in the stator of a radial fan', (in Flemish), *Rev. M. Mech.,* 24, 2, pp 107-112, June 1978.
599. Spiers, R.R.M. and Whitaker, J., 'An inlet chamber test method for centrifugal fans with ducted outlets'. *NEL report* No. 457, National Engg. Laboratory, Glasgow, 1970.
600. Stepanoff, A.J. and Stahl, H.A., 'Dissimilarity laws in centrifugal pumps and blowers', *Trans ASME,* 83, Series A, 1961.
601. Stepanoff, A.J., *Theory, Design and Application of Centrifugal and Axial Flow Compressors and Fans,* John Wiley & Sons, Inc. New York.
602. Stepanoff, A.J., *Pumps and Blowers,* John Wiley and Sons, Inc., 1965.
603. Suzuki, S. *et al.,* 'Noise characteristics in partial discharge of centrifugal fans', *Bulletin JSME,* Vol. 21, No. 154, April 1978.
604. 'Tangential Fan Design', *Engineering Material and Design,* Oct. 1965.
605. Tramposch, H., 'Cross-flow fan', *ASME paper* No. 64-WA/FE 26, 1964.
606. Whitaker, J., 'Fan performance testing using inlet measuring methods', *Conference on Fan Technology,* Instn. Mech. Engrs. London, April 1972.
607. Yeo, K.W., 'Centrifugal fan noise research—A brief survey of previous literature', *Memo.* No. 143, Institute of Sound and Viberation, Southampton.

Volute Casings

608. Bassett, R.W., *Pressure Loss Tests on a Model Turbine Volute,* Div. of Mech. Engg. MET-328, NRC, Canada, Aug. 1961.
609. Bassett, R.W. and Murphy, C.L., 'Pressure loss tests on second model of turbine volute', *MET-365, test report,* NRC, Canada, Aug. 1962.
610. Bhinder, F.S., 'Investigation of flow in the nozzle-less spiral casing of radial inward flow gas turbines', Axial and radial turbomachinery, *Proc. Instn. Mech. Engrs.,* Vol. 184, Pt. 3G (ii), 1969-70.
611. Biheller, H.J., 'Radial force on the impeller of centrifugal pumps with volute, semi-volute and fully concentric casings', *ASME J. Eng. power,* Vol. 87, Series A, 1965.
612. Binder, R.C. and Knapp, R.T., 'Experimental determination of the flow characteristics in the volutes of centrifugal pumps', *Trans ASME,* 58, pp 649-663, Nov. 1936.

613. Brown, W.B. and Bradshaw, G.R., 'Design and performance of family of diffusing scrolls with mixed flow impeller and vaneless diffusers', *NACA,* R936, 1949.

614. Csanady, G.T., 'Radial forces in a pump impeller caused by a volute casing', *ASME J. Eng. Power,* p. 337, 1962.

615. Fejet, A. *et al., Study of Swirling Fluid Flows,* Aerospace research laboratory, ARL-68-0173, Oct. 1968.

616. Giraud, F.L. and Platzer, J., 'Theoretical and experimental investigations on supersonic free-vortex flow', *Gas Turbine Laboratory M.I.T. Rep* No. 36, April 1954.

617. Hamed, A. *et al.,* 'Radial turbine scroll flow', *AIAA paper* No. 77, AIAA 10th fluid and plasma dynamics, Albuque, NM, June 27-29, 1977.

618. Hamed, A. *et al.,* 'A flow study in radial inflow turbine scroll nozzle assembly', *ASME J. Fluids Eng.,* Dec. 2, 1977.

619. Iverson, H.W. *et al.,* 'Volute pressure distribution, radial force on the impeller and volute mixing losses of radial flow centrifugal pumps', *ASME J. Eng. power,* Series A, Vol. 82, pp 136-144, 1960.

620. Kettnor, P., 'Flow in the volute of radial turbomachines', *Stromungs mechanik and stromungs maschinen,* No. 3, 50-84, Dec. 1965.

621. Kind, R.J., 'Tests on tip turbine volute with circular cross-sections and gooseneck outlet', *Aeronaut. Rep.* LR-409, NRC, Canada, Oct. 1964.

622. Kovalenka, V.M., 'On the work of spiral casings in centrifugal ventilators' (in Russian) *Industrial Aerodynamics,* Moscow, Obosongiz abstracts, No. 17, pp 41-65, 1960.

623. Nechleba, M., 'The water flow in spiral casings of hydro-turbines', Acta, Techu, Naclaclatelstvi, Ceskoslevensko Akad, 5, 2, 1960.

624. Paranjpe, P., 'On the design of spiral casing for hydraulic turbines', *Escher Wyss News* 40, 1, p. 36, 1967.

625. Ruzicka, M., 'Basic potential flow in a spiral case of centrifugal compressors' (in German) *Apl. Mat. Ceskesl. Akad. Ved.,* 12, 6, pp 468-476, 1967.

626. Worster, R.C., 'The flow in volutes and its effect on centrifugal pump performance', *Proc. Instn. Mech. Engrs.,* Vol. 177, No. 31, p. 843, 1963.

627. Yadav, R. and Yahya, S.M., 'Flow visualization studies and the effect of tongue area on the performance of volute casings of centrifugal machines', *J. Mech. Sci.,* Vol. 22, Pergamon Press. 1980.

Wind Energy

628. Armstrong, J.R.C. *et al,* 'A review of the U.S. wind energy programme', *Wind Eng.,* Vol. 3, 2, 1979.

629. Best, R.W.B., 'Limits to wind power', *Energy Convers.,* Vol. 19, No. 2, 1979.

630. Black, T., 'Putting the wind to work', *Design Eng.,* Vol. 51, No. 1, Jan. 1980.

631. Bragg, G.M. and Schmidt, W.L., 'Performance matching and optimization of wind powered water pumping systems', *Energy Convers,* Vol. 19, No. 1, pp 33-39, 1979.

632. Calvert, 'Wind power in eastern Crete', *Trans. Newcomen Soc.,* U.K., Vol. XLIV, pp. 137-144, 1972.

633. Changery, M.J., 'Initial wind energy data assessment study', *Report* (NSF-RA-N-75-020) p. 131, May 1975.

634. Chen, J.M., 'Wind and solar energies in the tornado type wind energy system', *Int. J. Heat Mass Transfer,* 22, 7, pp 1159-1161, July 1979.

635. Cliff, W.C., *Wind Direction Change Criteria for Wind Turbine Design,* Richland, U.S.A., Pacific Northwest Labs., (PNL2531) 30p., Jan. 1979.

636. Elliot, D.E., 'Economic wind power', *Appl. Energy,* Vol. 1, No. 3, pp. 167-197, July 1975.

637. Extended Abstracts, *International solar energy congress,* New Delhi, 16-21, Jan. 1978.

638. Flatau, A., 'Review of power from the wind-energy research and development', *Fifth annual symposium,* Edgewood Arsenal (EO-SP-740-26), Washington D.C., March, 1974.

639. Golding, E.W., 'Wind power potentialities in India—Preliminary report', N.A.L. Bangalore, *Tech. note* No. TN-WP-7-62, July 1962.

640. Golding, E.W., *The generation of electricity by wind power,* E.F.N. Spon Ltd., London, 1976.

641. Jarass, *Wind Energy—An assessment of the technical and economic potential,* Springer-Verlag, Heidelberg, 1981.

642. Justus, C.G. *et al.,* 'Interannual and month to month variations in wind speed', *J. Appl. Meteorol.,* Vol. 18, No. 7, pp 913-920, July 1979.

643. Marsh, W.D., 'Wind energy and utilities', *Wind Power Digest,* No. 16, pp 30-36, 1979.

644. Penell, W.T., 'Siting small wind turbines', *14th Conf. on agriculture and forest meteorology,* American Meteorological Society, 1979.

645. Ramsdell, J.V., *Estimate of the Number of Large Amplitude Gusts,* Richland U.S.A, Pacific Northeast labs., (P.N.L 2508) 54p., March 1978.

646. Reed, J.W., *An Analysis of the Potential of Wind Energy Conversion Systems,* Albuquerque, U.S.A, Sandia Labs (Sand 78 2099C), 1979.

647. Renne, D.S., 'Wind characteristics for agricultural wind energy applications', *14th Conference on agriculture and forest meteorology,* U.S.A, Am. Met. Soc., Session 4, 1979.

648. Taylor, R.H., 'Wind power: The potential lies off shore', *Electr. Re (London),* Vol. 203, No. 20, Nov. 1978.

649. Vries, O. de, *Fluid Dynamic Aspects of Wind Energy Conversion,* Nevilly Sur. Seine, France, NATO, (AGARD-AG-243), July 1979.

650. Wilson, D.G., *Windmill Development by Model Testing in Water,* Inter. Soc. Energy conversion Engg., paper 759147, pp 981-986, IEEE, New York, 1975.

651. Wendell, E.H., 'Wind power potential in the Pacific North West', Citizens' forum on potential energy sources, *Proc. Portland State Univ.,* pp 7-24, Portland, 1975.

652. 'Wind Power for City Dwellers', *Wind Power Digest,* No. 16, pp 18-28, 1979.

653. 'Wind Power', *Proc. U.N. Conf. on new sources of energy,* Vol. 7, U.N., New York, Aug. 1961.

(a) Frankiel, 'Wind flow over hills in relation to wind power utilization'.
(b) Ramakrishnan and Venkiteshwaran, 'Wind power sources of India with particular reference to wind distribution'.
(c) Lange, 'Some aspects of site selection for wind power plants in mountainous terrain'.
(d) Golding, E.W., 'Studies of wind behaviour and investigation of suitable sites for wind driven plants'.
(e) Santorini, 'Considerations on a natural aspect of the harnessing of wind power'.
(f) Arnfred, 'Developments and potential improvements in wind power utilization'.

Wind Turbines

654. Auld, H.E. and Lodde, P.F, *A Study of Foundation/Anchor Requirements for Prototype Vertical Axis Wind Turbines,* Albuquerque, U.S.A, Sandia Labs (SAND 78 7046, Feb. 1979)

655. Base, T.F., 'Effect of atmospheric turbulence on windmill performance', Hydrogen Economy, *Miami Energy (THEME) Conf. Proc.,* Pt. A, pp 87-105, March, 1974.

656. Bergey, K.H. Excerpts from 'Wind power potential from the United States', *Energie,* Vol. 1, No. 2, May 1975.

657. Betz, A., 'Windmills in the light of modern research', *NACA-Tech. Rep.* No. 474, 1928.

658. Blackwell, B.F. *et al., Wind Tunnel Performance Data for the Darrieus Wind Turbine with NACA 0012 Blades',* SAND 76-0130, 1976.

659. Blackwell, B.F. and Reis, G.E., 'Blade shape for a Troposkein type of vertical-axis wind turbine', *Sandia Laboratories energy report* SLA-74-0154, April 1974.

660. Coulter, P.E., 'Aerogenerator for electricities from the wind', *Energie,* Vol. 2, No. 2, pp 8-11, April 1976.

661. 'Direct acting windmill', *A report of the work done at the National Aeronautical Laboratory,* Bangalore, March 1974.

662. Gilbert, B.L., and Foreman, K.M., 'Experimental demonstration of the diffuser augumented wind turbine concept', *J. Energy,* 3, 4, pp 235-240, July/Aug. 1979.

663. Glasgow, J.C. and Robbins, W.H., *Utility Operational Experience on the NASA/DOE/Mod-OA 200 kW Wind Turbine,* (NASA TM 79084) Washington D.C., U.S.A, 1979.

664. Goiling, G. and Robert, J., 'Tilting at windmills', *Electron Power,* Vol. 22, No. 6, pp 347-351, June 1976.

665. Govinda Raju, S.P. *et al.,* 'Some windmill rotors for use in a rural environ-ment', *Rep. FMI,* Dept. of Aero. Engg. Indian Institute of Science, Bangalore, Jan. 1976.

666. Harner, K.I. *et al.,* 'Wind turbine generator control', *Brit. Pat. Appl.* 2023237 A, Appl. June 15, 1979.

667. Herter, E., 'Wind turbine', *Brit. Pat. Appl.* 2008202A, Appl. Oct. 12, 1978, Publ. May 1979.

668. Hinrichsen, E.N., *Induction and Synchronous Machines for Vertical Axis Wind Turbines,* Albuquerque, U.S.A, Sandia Labs (Sand 79 7017) June 1979.

669. Hunnicutt, C.L. *et al.,* 'An operating 200 kW horizontal axis wind turbine', *NASA,* TM-79034, Washington, D.C., 1978.

670. Jayadev, T.S., 'Wind powered electric utility plants', *ASME J. Eng. Industry,* Vol. 98, sec. B No. 1, pp 293-296, Feb. 1976.

671. Johnson, Craig, C., 'Economical design of wind generation plants', *IEEE Trans Aerosp. Electron, Syst.* VAE-12, No. 3, pp 316-330, May 1976.

672. Johnson, C.C. and Smith, R.T., 'Dynamics of wind generators on electric unit network', *IEEE Trans-Aerosp. Electron Syst.,* VAE-12, No. 4, pp. 483-493, July 1976.

673. Lapin, E.E., 'Theoretical performance of vertical axis wind turbines', *ASME paper* No. 75-WA/Ener-1, Nov-Dec. 1975.

674. Lewis, R.I. *et al.*, 'A theory and experimental investigation of ducted wind turbines', *Wind Eng.,* Vol. 1, No. 2, pp 104-125, Multi-Science Publishing Co., 1977.

675. Lewis, R.I., 'A simple theory for the straight bladed vertical axis wind turbine', *Technol., Ire.,* Aug. 1978.

676. Lewis, R.I. and Cheng, K.Y., 'A performance analysis for horizontal axis wind turbines applicable to variable pitch or airbrake control', *Wind Eng.,* Vol. 4, No. 4, 1980.

677. Lysen, E.H. *et al.,* 'Savonius rotors for water-pumping', Amersfoort, *The Netherlands steering committee on wind-energy for developing countries,* June 1978.

678. Manser, B.Z. and Jones, C.N. 'Power from wind and sea—The forgotten panemone', Thermo-fluids conference: Energy transportation, storage and conversion, Brisbane, Australia, Dec. 1975.

679. Mercadiar, Y., 'Method of calculating the geometry and the performance of a high-speed wind turbine' (in French), *Wind Eng.,* Vol. 2, No. 1, 1978.

680. Musgrove, P.J., 'The variable geometry vertical-axis windmill', *Int. symposium on wind energy systems,* Cambridge, paper C7-87/100, Sept. 1976.

681. Ottosen, G.O., 'Improvements in windmills', *Brit. Pat.* Spec. 1560 064, Publ. Jan. 1980.

682. Paraschivolu, I. and Bilgen, E., 'Free vortex from a wing for wind turbine system', *J. Energy,* Vol. 3, No. 3, pp 190-192, May-June 1979.

683. Pershing, B.M., 'Performance of windmills in a closely spaced array', *J. Energy,* Vol. 3, No. 3, pp 145-150, May-June, 1979.

684. Pontin, G., 'Electrical machinery for windmills', *Electr. Rev. (London).,* Vol. 203, No. 20, Nov. 1978.

685. *Proceedings: Vertical-axis wind turbine technology workshop,* ERDA, Sandia laboratory, Sand 76-5586, 1976.

686. Rangi, R.S. *et al.,* 'Wind power and the vertical axis wind turbine developed at the NRC, DME/NAE', *Quarterly Bulletin* No. 1974(2) Ottawa, July 1974.

687. Robbins, W.H. and Thomas, R.L., 'Large horizontal axis wind turbine development', *NASA* TM 791 74, Washington D.C, USA, 1979.

688. Shankar, P.N., 'On the aerodynamic performance of a class of vertical axis windmills *NAL Rep.,* Bangalore, July 1975.

689. Shutis, J.K., 'Optimum selection of a wind turbine generator system', *J. Energy,* Vol. 3, No. 3, pp 145-150, May-June 1979.

690. 'Simplicity means economy for windmill design', *Mach., Des.,* Vol. 51, No. 28, Dec. 1979.

691. South, P. and Rangi, R.S., 'The performance and economics of the vertical axis wind turbine developed at the N.R.C, Canada', *Annual meeting of the Pacific Northwest region of the American Society of Agricultural Engineers,* Calgary, Alberta, Oct. 10-12, 1973.

692. South, P. and Rangi, R.S., Preliminary tests of a high speed vertical axis windmill model', *N.R.C. Canada,* LTR, LA, 74, 1974.

693. South, P. and Rangi, R.S., 'An experimental investigation of a 12-ft diameter high speed vertical axis wind turbine', *N.R.C. Canada,* Rep. No. LTR-LA-166, 1975.

694. Strickland, J.H. *et al.,* 'A vortex model of the Darrieus turbine: An analytical and experimental study', *J. Fluids Eng., Trans ASME,* 101, 4, Dec. 1979.

695. *Survey of Solar Energy Products and Services,* U.S. Govt. Printing Office, Washington, 1975.

696. Templin, R.J., 'Aerodynamic performance theory for the vertical axis wind turbine', *N.R.C Rep.,* LTR-LA-160-NAE, Canada, Ottawa, 1974.

697. Thomas, R. *et al.,* 'Plans and status of the NASA-Lewis research centre wind energy project', *Energy Tech. Conf. 2nd Proc.* pp 290-314, Washington, D.C., May 1975.

698. Thomas, R.L. and Donovon, R.M., 'Large wind turbine generators', *NASA,* TM 73767, Washington D.C., U.S.A., March 1978.

699. Thomson, T.A., 'The theoretical performance of a straight bladed vertical axis wind turbine', *Aero. tech. note* 7802, Sydney University, Australia, Jan. 1978.

700. Vinayagalingam, T., 'The pedal wind turbine', *J. Energy,* 3, 4, 254-256 (Tech. notes), July/Aug. 1979.

701. Walters, R.E. *et al.*, 'Innovative wind machines', *West Virginia University Rep.,* No. TR-50, 1976.

702. Wilson, R.E. and Lissaman, P.B.S., 'Applied aerodynamics of wind power machines', *Oregon State Univ. Rep. for NSF Grant,* GI-41840, May 1974.

703. Wind Energy Utilization., 'A bibliography with abstracts cumulative volume 1944-1974', NM Univ., Technol Appl. Cent. Albuquerque, TAC/W75-700/WSF/RA/N-75-061, April, 1975, *Wind Power.*

704. *Proc. of the U.N. conf. of new sources of energy,* Vol. 7, U.N., New York, Aug. 1961.

(a) Juul, 'Economy and operation of wind power plants'.

(b) Nilkantan *et al.,* 'Windmill types considered suitable for large scale use in India'.

(c) Walker, 'Utilization of random power with particular reference to small-scale power plants'.

(d) Hutter, 'The aerodynamic design layout of wing blades of wind turbines with high tip-speed ratio'.

705. Worsteli, M.H., 'Aerodynamic performance of the 17 metre diameter Darrieus wind turbine', Albuquerque, U.S.A, Sandia labs. (SAND 78 1737), Jan. 1979.

Instrumentation and Measurement in Turbomachinery

706. Acharyo, M., 'On the measurement of turbulent fluctuations in high speed flow using hot wires and hot films', *NASA,* TM 78535, Washington D.C, Nov. 1978.

707. Asanuma (Ed.), 'Flow visualization', *Proc. Instn. Symp. of flow visualization,* Oct. 1977, Tokyo, Japan, Hemisphere Publishing, Washington, D.C., 1979.

708. Bammert, K. *et al.,* 'Unsteady flow measurements in centrifugal compressors', *Atomkernenergie,* 27(4), pp. 217-229, 1976.

709. Bessling, H. and Hinz. T., 'Gravimetric investigation of the particle number density distribution function in the high speed cascade wind tunnel for laseranemometry measurements' (in German), *DFVLR*-FB79-12, p. 38, 1979.

710. Bouis, X., 'Optical measurements in flows, Applications to wind tunnels and engine test stands' (in French), Office National d'Etudes et de Recherches Aerospatials, *Note Technique* No. 1978-5, p. 42, 1978.

711. Boutier, A. *et al., Operational Two-Dimensional Laser Velocimeter for Various Wind Tunnel Measurements,* Chatillion, France Office Nat D' etudes et de Recherches Aerosptials, 1978.

712. Bradshaw, P. and Johnson, R.F., 'Turbulence measurements with hot wire anemometer', *NPL notes on applied science,* No. 33, H.M.S.O., London, 1963.

713. Brayer, D.W. *et al.,* 'Pressure probes selected for three-dimensional flow measurements', *ARC,* RM, 3037, 1958.

714. Brayer, D.W. and Pankhurst, R.C., *Pressure Probe Methods for Determining Wind Speed and Flow Direction,* H.M.S.O., London, 1971.

715. Dau, K. *et al.,* 'Two probes for the measurement of the complete velocity in subsonic flow', *Aeronaut. J.,* p. 1066, Vol. 72, 1968.

716. Dolan, F.X. and Runstadler Jr., P.W., 'Design development and test of a laser velocimeter for a small 8:1 pressure ratio centrifugal compressor', *NASA,* CR-134781, March 1979.

717. Dunkar, R. and Strinning, P., 'Flow velocity measurements inside of a transonic axial compressor rotor by means of an optional technique and compared with blade-to-blade calculations' *3rd ISABE symposium,* Munich 1976.

718. Eckardt, D., 'Application of dynamic measurement techniques for unsteady flow investigations in centrifugal compressors', Advanced radial compressors (Von Karman Institute for fluid dynamics, Belgium), *Lecture series* 66, 1974.

719. Fabri, J., 'Flow visualization in compressors', Advanced techniques in turbomachines, *V.K.I. lecture series* 78, April 1975.

720. Ferguson, T.B. and Al-Shamma, K.A., 'Wedge-type pitot-static probes', *BHRA* SP 919, 1967.

721. Ferguson, T.B. *et al.,* 'The effect of leading edge geometry on the performance of wedge type pitot-static yaw-meters, *Trans Measurement and Control,* paper 5-74, Vol. 7, April 1974.

722. Gallus, H.E., 'Results of measurements of the unsteady flow in axial subsonic and supersonic compressor stages', *Conf. on unsteady phenomena in turbomachinery,* Preprint No. 177, AGARD, Monterey/ California, 1975.

723. Gallus, H.E. *et al.,* 'Measurements of the quasi-steady and unsteady flow effects in a supersonic compressor stage', *ASME paper* No. 77-GT-13, 1977.

724. Gettelmam, C.C. and Kause, L., 'Characteristics of a wedge with various holder configurations', *NACA,* R & ME 51G09, 1951.

725. Gorton, C.A. and Lakshminarayana, B., 'A method of measuring the three-dimensional mean flow and turbulence quantities inside a rotating turbomachinery passage', *J. Eng. power, Trans ASME,* Series A, Vol. 98, No. 3, April, 1976.

726. Grahek, E. *et al.,* 'Application of the laser droppler anemometer to indust-rial problems', D.I.S.A. Inf. No. 25 Feb. 1980; Group of single-stage axial flow compressor test (Tsinghua University), 'Some problems of the press-ure measurement in the single-stage axial flow compressor test', *J. Eng. Thermophys.,* Vol. 1, No. 3, Aug. 1980.

727. Head, M.R. *et al.,* 'The Preston tube as a means of mesuring skin friction', *J. Fluid Mech.,* 14, 1962.

728. Howard, J.H.G. and Kittmer, C.W., 'Measured passage velocities in a radial impeller with shrouded and unshrouded configuration', *J. Eng. Power, Trans ASME,* Series A, 97, 1975.

729. Howells Jr., R.W., 'Experimental and analytical investigation of three-dimensional inviscid effects in turbomachinery', *Tech. Memo.* TM 4-161, Penn. State Univ. May 1974.

730. Howells, R. and Lakshminarayana, B., *Instrumentation for Measuring Steady-State Static Pressure on a Rotating Blade in the Axial Flow Research Fan',* The Penn. State Univ. Applied research laboratory, TM 74-201, June 25, 1974.

731. Kielbasa, J. and Smolarski, A.Z., 'Interaction of two hot-wire probes placed perpendicularly to the flow velocity vector', *Bull. Acad Pol. Sci. Maths. Astron. Phys.,* 26, 10, 1978.

732. Laufer, J., 'New trends in experimental turbulence research', *Ann. Rev. Fluid Mech.,* Vol. 7, p. 307, 1975.

733. Lorenszi, A. and Scarsi, G., 'A theoretical investigation on the measurement of the average velocity of a fluid in steady and nonsteady motions' (in Italian), *Termotecnica,* 32, 12, pp. 648-656, Dec. 1978.

734. Maki, H. and Ikeda, Y., 'Measurement of pulsating flow rate by means of float-area type flow', *Bull. JSME,* Vol. 24, No. 189, March 1981.

735. Meyer, C.A. and Benedict, R.P., 'Instrumentation for axial flow compressor research', *Trans ASME,* 74, 1327, 1952.

736. Morris, R.E., 'Multiple head instruments for aerodynamic measurement, *Engineer,* 212, London, 1961, 315.

737. Nishioka, M., 'The characteristics of Hot-wire probe and construction of a linearized constant temperature anemometer', *Bull. JSME,* Vol. 16, No. 102, Dec. 1973.

738. O'Brien, W.F. and Moses, H.L., 'Instrumentation for flow measurement in turbomachine rotors', *ASME paper* No. 72-GT-55, 1972.

739. O'Brien, W.F. *et al.,* 'A multichannel telemetry system for flow research on turbomachine rotors', *ASME paper* No. 74-GT-112, 1974.

740. Owen, J.M. and Pincombe, J.R., 'Velocity measurements inside a rotating cylindrical cavity with a radial outflow of fluids', *J. Fluid Mech.,* 99, 111, 1980.

741. Ower, E. and Pankhurst, R.C., *The Measurement of Air Flow,* Pergamon Press, Oxford, 1966.

742. Perry, J.H., *Calibration and Comparison of Cobra Probe and Hot-Wire Anemometer for Flow Measurements in Turbomachinery,* CSIRO, TRI, Div. of Mech. Engg., 1974.

743. Presser, K.H., 'Air flow measurement by means of the compensation method', (in German), Tech. *Mess.,* 46, 5, May 1979.

744. Purtell, L.P, *Low Velocity Performance of a Bronze Bearing Vane Anemometer,* Bureau Standards, NBSIR 78-1433, Feb. 1978.

745. Rasmussen, C.G. and Madsen, B.B., 'Hot-wire and Hot-film anemometry', *NASA,* TM 75143, May 1979.

746. Rimmer, R.J. and Bassett, R.W., A small propeller-type anemometer for use in automotive radiator air flow measurement', *NRC* (LTR-ENG-85), Aug. 1978.

747. Roberts, W.B. and Slovisky, J.A., 'Location and magnitude of cascade shock loss by high-speed smoke utilization', *AIAA J.* 17, 11, pp. 1270-1272 (Tech. notes), Nov. 1979.

748. School, R., 'A laser dual-beam method for flow measurements in turbomachines', *ASME paper* No. 74-GT-157, 1974.

749. Shaw, R. *et al.,* 'Measurements of turbulence in the Liverpool University turbomachinery wind tunnels and compressor', *ARC,* 26486, 1964.

750. Stevens, S.J. and Fry, P., 'Measurement of the boundary layer growth in annular diffusers', *J. Aircr.,* p. 73, 1973.

751. Takei, Y. *et al., Measurement of Pressure on a Blade of Propeller Model,* Ship Research Institute, No. 55, March 1979.

752. Thompson, H.D. and Stevenson, W.H., *Laser Velocimetry and Particle Sizing,* D.C. Hemisphere Publishing, Washington, D.C., 1979.

753. Verholek, M.G. and Ekstrom, P.A., *Remote Wind Measurements with a New Microprocessor Based Accumulator Device,* Richland, U.S.A, Pacific Northwest Labs, (P.N.L. 2515), p 26, April 1978.

754. Weyer, H. and Schodl, R., 'Development and testing of techniques for oscillating pressure measurements especially suitable for experimental work in turbomachenery', *ASME paper* No. 71-FE-28, 1971.

Theoretical Analysis of Flows in Turbomachinery

755. Aboltin, E.V. and Zaichenko, E.N., 'Calculation of the potential flow of a gas in a centrifugal compressor diffuser without guide vanes', (in Russian) *N.A.M.I., Proc.,* 138, 1972.

756. Argyris, J.H. *et al.,* 'Two and three-dimensional flow using finite elements', *Aeronaut. J.,* Nov. 1969.

757. Bosman, C. and Marsh, H., 'An improved method for calculating the flow in turbomachines, including a consistent loss model', *J. Mech. Eng. Sci.,* Vol. 16, 1974.

758. Bosman, C. and Al-Shaarawi, M.A.I., 'Quasi-three dimensional numerical solution of flow in turbomachines', *ASME paper* 76-FE-23, April 1976.

759. Daneshyar, M. *et al.,* 'Prediction of annulus wall boundary layers in axial flow turbomachines', *AGARDograph* No. 164, AGARD, 1972.

760. Davis, W.R. and Miller, D.A.J., 'A comparison of the matrix and streamline curvature method of axial flow turbomachinery analysis from users point of view', *ASME paper* No. 74-WA/GT-4, Nov. 1974.

761. Davis, W.R., 'A general finite difference technique for the compressible flow in the meridional plane of centrifugal turbomachinery', *ASME paper* No. 75-GT-121, 1975.

762. Dean Jr., R.C. *et al.,* 'Fluid mechanic analysis of high-pressure ratio centrifugal compressor data', *USA AV LABS Rep.* 69-76, Feb. 1970.

763. Dean Jr., R.C., 'On the unresolved fluid dynamics of the centrifugal compressor: in advanced centrifugal compressors', *ASME special publication,* pp. 1-55, 1971.

764. Frost, D.H., 'A streamline curvature throughflow computer program for analysing the flow through axial flow-turbomachines', *ARC,* R & M 3687, 1972.

765. Gallus, H.E., 'Survey of the techniques in computation and measurement of the unsteady flow in turbomachines', *Proc. 5th Conf. on Fluid Machinery,* p. 335/349, Budapest, 1975.

766. Gostelow, J.P., 'Potential flow through cascades, extensions to an exact theory', *ARC,* CP 808, 1964.

767. Hamrick, J.T. *et al.,* 'Method of analysis for compressible flow through mixed-flow centrifugal impellers of arbitrary design', *NACA,* Rep. 1082, 1952.

768. Hatton, A.P. and Wolley, N.H., 'Viscous flow in turbomachine blade passages', *Instn. Mech. Engrs. Conf.—Heat and fluid flow in steam and gas turbine plants,* Univ. of Warwick, April 1973.

769. Hawthorne, W.R. and Horlock, J.H., 'Actuator disc theory of the incompressible flow in axial compressors', *Proc. instn. Mech. Engrs.,* London, 176, 1962.

770. Hawthrone, W.R. and Novak, R.A., 'The aerodynamics of turbomachinery', *Ann. Rev. Fluid Mech.,* Vol. 1, 1969.

771. Horlock, J.H., 'On entropy production in adiabatic flow in turbomachines', *J. Basic Eng. Trans,* ASME, 1971.

772. Horlock, J.H. and Perkins, H.J., 'Aerodynamic analysis of turbomachinery', *GEC J. Sci. Technol.,* Vol. 41, No. 2 and 3, 1974.

773. Jansen, W., 'A method for calculating the flow in a centrifugal impeller when entropy gradients are present', Instn. Mech. Engrs., *Internal Aerodynamics (Turbomachinery),* 1970.

774. Japiske, D., 'Progress in numerical techniques', *J. Fluid Eng.,* pp. 592-606, Dec. 1976.

775. Katsanis, T., 'Use of arbitrary quasi-orthogonals for calculating flow distribution in the meridional plane of a turbomachine', *NASA,* TN D2546, 1964.

776. Katsanis, T., 'A computer program of calculating velocities and stream-lines for two-dimensional flow in axial blade rows', *NASA,* TN D-3762, 1967.

777. Kastsanis, T., 'Computer program for calculating velocities and stream-lines on a blade-to-blade stream surface of a turbomachine', *NASA,* TN, D-4525, 1968.

778. Kastsanis, T., 'Quasi three-dimensional calculation of velocities in turbomachine blade rows', *ASME paper* No. 72-WA/G7-7, Nov. 1972.

779. Krimerman, Y. and Adler, D., 'The complete three dimensional calculation of the compressible flow field in turbo-impellers', *J. Mech. Eng. Sci.,* Vol. 20, No. 3, 1978.

780. Lakshminarayana, B. and Horlock, J.H., 'Review: Secondary flows and losses in cascades and axial-flow turbomachines', *Int. J. Mech. Sci.,* Vol. 5, 1963.

781. Lakshminarayana, B., 'Methods of predicting the tip clearance effects in axial flow turbomachinery', *J. Basic Eng., Trans ASME,* pp. 467-482, Sept. 1970.

782. Lewis, R.I. and Fairbairn, G.W., 'Analysis of the through flow relative eddy of mixed flow turbomachines', *Int. J. Mech. Sci.,* Vol. 22, pp. 535-549, 1980.

783. Marsh, H., 'A digital computer program for the through flow fluid mechanics on an arbitrary turbomachine using a matrix method', *ARC,* R & M 3509, 1968.

784. Marsh, H. and Merryweather, H., 'The calculation of subsonic and supersonic flow in nozzle', *Salford Univ. Conf. on internal flow, paper* No. 22, April 1971.

785. Mellor, G., A combined theoretical and empirical method of axial compressor cascade prediction', *ASME paper* No. 72-WA/GT-5, Nov. 1972.

786. Novak, R.A., 'Streamline curvature computing procedure for fluid flow problem', *J. Eng. Power, Trans ASME,* Vol. 89, 1967.

787. Novak, R.A., 'Streamline curvature analysis of compressible and high Mach number cascade flows', *J. Mech. Eng. Sci.,* Vol. 13, No. 5, pp 344-57, 1971.

788. Novak, R.A., *Axisymmetric Computing System for Axial Flow Turbomachinery, Sec. 29-The mean Stream Sheet Momentum Continuity Solution Techniques for Turbomachinery,* Iowa State Univ. 15-25, July 1975.

789. Perkins, H.J. and Horlock, J.H., 'Computation of flows in turbomachines', *Finite Element Methods in Flow Problems,* 1974.

790. Preston, J.H., 'A simple approach to the theory of secondary flows', *Aeronaut, Qtly.* 5 (pt. 3), 1953.

791. Quemard, P.C. and Michel, R., 'Definition and application of means for predicting shear turbulent flows in turbomachines', *ASME paper* No. 76-GT-67, 1976.

792. Schilhansi, M.J., 'Three-dimensional theory of incompressible and inviscid flow through mixed-flow turbomachines', *Trans ASME, J. Eng. Power,* Oct. 1965.

793. Senoo, Y. and Nakase, Y., 'An analysis of flow through a mixed-flow impeller', *Trans ASME, J. Eng. Power,* Jan 1972.

794. Smith, K.J. and Hamrick, J.T., 'A rapid approximate method for the design of the shroud profile of centrifugal impellers of given blade shape', *NACA,* TN 3399, 1955.

795. Smith Jr., L.H., 'The radial equilibrium equation of turbomachinery', *Trans ASME,* Series A, 88, 1966.

796. Smith, D.J.L. and Barnes, J.F., 'Calculation of fluid motion in axial flow turbomachines', *ASME paper* No. 68-GT-12, March 1968.

797. Smith, D.J.L. and Frost, D.H., 'Calculation of the flow past turbomachine blades', *Proc. Instn. Mech. Engrs.,* 184 (Pt. 3G), 1969-70.

798. Smith, D.L.J., 'Computer solutions of Wu's equation for compressible flow through turbomachines', *NASA,* SP-304, 1974.

799. Stanitz, J.D. and Prian, V.D., 'A rapid approximate method for determining velocity distribution on impeller blades of centrifugal compressors', *NACA,* TN 2421, 1951.

800. Stanitz, J.D., 'Some theoretical aerodynamic investigations of impellers in radial and mixed flow centrifugal compressors', *Trans ASME,* 74, 4, 1952.

801. Verba, A., 'Method of singularities for computing the velocity distribution in a radial impeller', *ACTA Technica,* 1961.

802. Vernon, R.J., 'An analysis of the error involved in unrolling the flow field in turbine problem', Mitt. Aus. Dem. Inst. Aerodynamik (ETH Zurich) *Rep.* 23, Verlag Leeman, Zurich, 1957.

803. Wilkinson, D.H., 'Stability, convergence and accuracy of two-dimensional streamline curvature method using quasi-orthogonals', *Proc. Instn. Mech. Engrs.,* 184(Pt. 3G), 1969-70.

804. Wu, C.H., 'A general theory of three-dimensional flow in subsonic and supersonic turbomachines of axial, radial and mixed-flow types', *NACA,* TN-2604, 1952.

Miscellaneous Topics

805. Adachi, T., *et al.,* 'Study on the secondary flow in the downstream of a moving blade row in an axial flow fan', *Bull. JSME,* Vol. 24, No. 188, Feb. 1981.

806. Agarwal, D.P., 'Some studies on flow through radial vaned diffusers', *Ph.D. thesis,* Indian Institute of Technology, Delhi, 1978.

807. Anand, Ashok K., 'An experimental and theoretical investigation of three-dimensional turbulent boundary layers inside the passage of a turbomachinery rotor', *Ph.D. thesis,* Pennsylvania State Univ., 1976.

808. Baskharone, Erian Aziz, 'A new approach to turbomachinery flow analysis using the finite element method', *Doctoral thesis,* Univ. of Cincinnati, 1979.

809. Butler, J.L. and Wagner, J.H., 'An improved method of calibration and use of a three sensor hot-wire probe in turbomachinery flows', *AIAA paper* No. 82-0195, Jan. 1982.

810. Caruthers, John Everett, 'Theoretical analysis of unsteady supersonic flow around harmonically oscillating turbofan cascades', *Doctoral thesis* Georgia Inst. of Tech., 1976.

811. Cegielski, John M. Jr., 'Low energy gas utilization combustion gas turbines', *Doctoral thesis,* Univ. of Wyoming, 1973.

812. Clevenger, W.B. Jr. 'Trajectories of erosive particles in radial inflow turbines', *Doctoral thesis,* Univ. of Cincinnati, 1974.

813. Davino, R. and Lakshminarayana, B., 'Characteristics of mean velocity at the annulus wall region at the exit of a turbomachinery passage', *AIAA paper* No. 81-0068, *AIAA* J. March, 1982.

814. Duffie, J.A. and Beckman, W.A., *Solar energy thermal processes,* John Wiley, New York, 1974.

815. Gorton, C.A., and Lakshminarayana, B., 'Analytical and experimental study of the three-dimensional mean flow and turbulence characteristics inside the passages of an axial flow inducer', *NASA,* CR 3333, Nov. 1980.

816. Gourdon, C. *et al.,* 'Triple hot-wire probe calibration in water', *DISA information* No. 26, Feb. 1981.

817. Grant, George K., 'A model to predict erosion in turbomachinery due to solid particles in particulated flow', *Doctoral thesis,* Univ. of Cincinnati, 1973.

818. Greenwood, S.W., 'Turbojet engine performance at high turbine entry temperatures with transpiration cooled turbine blading', *Doctoral thesis,* Univ. of Maryland, 1977.

819. Gupta, R.L., 'Performance of radial flow vaneless diffusers with diverging walls', *Ph.D. thesis,* Indian Institute of Technology, Delhi, 1974.

820. Haider, S.Z., 'Effect of partial admission on the performance of a centrifugal blower', *Ph.D. thesis,* Indian Institute of Technology, Delhi, 1979.

821. Isaac, J.J. and Paranjpe, P.A., 'Thermodynamic optimization of Rankine cycle terrestrial solar power systems employing flat-plate collector', *Tech. Memo.* No. NAL/PR-UN-103. 1/78, Banglore, Jan. 1978.

822. Isaac, J.J. and Paranjpe, P.A., *Cycle Optimization for a Solar Turbopack,* NAL TM-PR-UN-O-103.1-78, Bangalore, April, 1978.

823. Ito, Sadasnko, 'Film cooling and aerodynamic loss in a gas turbine cascade', *Doctoral thesis,* Univ. of Minnesota, 1976.

824. Khalil, Ihab. Mohammad, 'A study of viscous flow in turbomachines', *Doctoral thesis,* Univ. of Cincinnati, 1978.

825. Lakshminarayana, B., 'Techniques for aerodynamic and turbulence measurements in turbomachinery rotors', *ASME J. Eng. Power,* Vol. 103, April 1981.

826. Lakshminarayana, B., Davino, R. and Pouagare, M., 'Three-dimensional flow field in the tip region of a compressor rotor passage', Pt. 1 (Mean velocity), *ASME paper* No. 82-GT-11, 1982; Pt. 2 (Turbulence properties), *ASME paper* No. 82-GT-234, 1982.

827. Lakshminarayana, B., 'Three sensor hot-wire/film technique for three-dimensional mean and turbulence flow field measurement', *J. Measur. Tech. Aerosol. Fluid Mech. Res.,* Jan-March, 1982.

828. McFarland, E.R., 'An investigation of the aerodynamic performance of film-cooled turbine blades', *Doctoral thesis,* Univ. of Cincinnati, 1976.

829. Murthy, M.V.A. and Paranjpe, P.A., *Turbine test facility of propulsion division,* NAL. TM PR 101/1, Bangalore, 1977.

830. Murthy, M.V.A. and Paranjpe, P.A., *Test facility for performance evaluation of model turbine stages,* NAL TM PR 101/2-77, Bangalore, Oct. 1977.

831. Murugesan, K. and Railly, J.W., 'Pure design method for aerofoils in cascade', *J. Mech. Eng. Sci.* Vol. 11, Nov. 5, Instn. Mech Engrs., Oct. 1969.

832. Pai, B.R. *et al., Development of gas turbine combustor operating on gasified coal: Test results on modified Avon combustor at atmospheric pressure,* NAL TM PR-203, 1/78, Aug. 1978.

833. Pai, B.R. and Abbey, D.K., *Development of a gas turbine operating on sludge gas: Test results of modified part 514/7 combustor studies,* NAL TM PR oh-121. 1/81, Bangalore, Feb. 1981.

834. Prince, T.C., 'Prediction of transonic inviscid steady flow in cascades by finite element methods', *Doctoral thesis,* Univ. of Cincinnati, 1976.

835. Raj. R., 'On the investigation of cascade and turbomachinery rotor wake characteristics' *Doctoral thesis,* Pennsylvania State Univ., 1974.

836. Ramachandra, M.S., Recalibration of the Ava wedge probe and its applications for evaluation of cascade wake measurements, DFLR-AVA 251 75 A 31.

837. Ramachandra, M.S. *et al.*, Design of contraction for the transonic cascade tunnel, NAL'TM-PR-324.2/72, Bangalore, March 1976.

838. Ramachandra, M.S. *et al.*, 'The NAL transonic cascade tunnels', Int. congress on instrumentation in aerospace simulation facilities, Dayton, Ohio, USA, 1981.

839. Sankaranarayanan, S. *et al.*, 'Experimental investigation of a developmental turbine', VI national conf. on fl. mechanics and fl. power, IIT Kanpur, Dec. 1975.

840. Sankaranarayanan, S. and Paranjpe, P.A., 'Application of turbopack in solar energy system', Paper No. 0078, Int. solar energy conference, Delhi, Jan. 1978.

841. Singh, K. and Murugesan, K., Design of a highly loaded turbine stage, NAL TM PR 103.1/74, Bangalore, Jan. 1974.

842. Taber, H. and Bronicki, 'Small turbine for solar energy power package', Paper No. 5/54, UN Conference—New sources of energy, April 1961.

843. Tewari, S.K. *et al.*, Design of foundation for turbine research rig, NAL TM PR 321/2, Bangalore, 1970.

844. Trilokinath, 'Flow investigation in the volute casings of inward-flow radial turbines', *Ph.D. thesis*, Indian Institute of Technology, Delhi, 1980.

845. Venkatrayulu, N. *et al.*, 'Some investigations on off-design performance of an axial flow fan', *Ph.D. thesis*, Indian Institute of Technology, Madras, June 1974.

846. Venkatrayulu, N. *et al.*, 'Some experimental investigations on the improvement of off-design performance of a single stage axial flow fan', Int. Symposium on air breathing engines, Munich, March 1976.

847. Venkatrayulu, N., 'On secondary flow losses in bends', Research report, Cambridge University, Engg. Deptt. Cambridge, 1976.
848. Venkatrayulu, N. *et al.*, 'Influence of freely rotating inlet guide blades on the return flows and stable operating range of an axial flow fan', Tran ASME, J. Eng. Power, Vol. 122, Jan. 1980.
849. Walker, S.N., 'Performance and optimum design analysis/computation for propeller type wind turbines', *Doctoral thesis*, Oregon State Univ., 1976.
850. Yadav, R., 'Analysis of flow through volute casings of centrifugal machines', *Ph.D. thesis*, Indian Institute of Technology, Delhi, 1977.

Abbreviations

The following is a list of abbreviations used in the above bibliography:

Aeronaut. Qtly.	Aeronautical Quarterly
AGARD	Advisory Group for Aeronautical Research and Development
AIAA	American Institute of Aeronautics and Astronautics
AMCA	Air Moving and Conditioning Association
ARC	Aeronautical Research Council
ARS	American Rocket Society
ASME	American Society of Mechanical Engineers
ASTM	American Society for Testing and Materials
BHRA	British Hydro Research Association
BNES	British Nuclear Engineering Society
Brit. Pat	British Patent
BSRA	British Ship Research Association
BSS	British Standard Specifications
Bull.	Bulletin
Chem. Engg.	Chemical Engineering
CP	Current Papers
CR	Current Reports
CSIRO	Commonwealth Scientific and Industrial Research Organization
CSME	Canadian Society of Mechanical Engineers
DACL	Dynamic Analysis and Control Laboratory
Fluid Dyn.	Fluid Dynamics
GEC	General Electric Company
GT	Gas Turbine
HMSO	Her Majesty's Stationery Office
IEEE	Institute of Electrical and Electronic Engineers
Int. J. Mech. Sci	Internal Journal of Mechanical Sciences
ISVR	Institute of Sound and Vibration Research
J. Aero. Sci.	Journal of Aeronautical Sciences

J. Aerospace Sci.	Journal of Aerospace Sciences
J. Aircr.	Journal of Aircrafts
J. Appl. Mech.	Journal of Applied Mechanics
J. Appl. Meteorol.	Journal of Applied Meteorology
J. Basic Eng.	Journal of Basic Engineering
J. Eng. Mat. Technol.	Journal of Engineering Materials and Technology
J. Eng. Power	Journal of Engineering for Power
J. Eng. Thermophy.	Journal of Engineering and Thermophysics
J. Fluids Eng.	Journal of Fluids Engineering
J. Fluid Mech.	Journal of Fluid Mechanics
J. Mat. Sci.	Journal of Material Science
J. Mech. Eng. Sci.	Journal of Mechanical Engineering Science
J. Roy. Aero. Society	Journal of Royal Aeronautical Society
JSME	Japan Society of Mechanical Engineers
MIT	Massachusetts Institute of Technology
NACA	National Advisory Committee for Aeronautics
NASA	National Aeronautics and Space Administration
NAL	National Aeronautical Laboratory
NEL	National Engineering Laboratory
NGTE	National Gas Turbine Establishment
NRC	National Research Council
ONERA	Office National d'Etudes et de Recherches
Proc. Instn. Mech. Engrs.	Proceedings of the Institution of Mechanical Engineers
R and M	Reports and Memoranda
RTS	Russian Translation Service
SAE	Society of Automotive Engineers
Sov. Appl. Mech.	Soviet Applied Mechanics
Sov. Aeronaut.	Soviet Aeronautics
TM	Technical Memoranda
TN	Technical Notes
TR	Technical Reports
Trans	Transactions
VDI	Verein Deutscher Ingenieure
VKI	Von-Karman Institute
Wind Eng.	Wind Engineering
ZAMM	Zeitschrift fur angewandte Mathematik und Mechanik

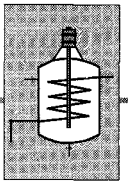

Supplementary Bibliography

Abdelhamid, A.N., "Experimental investigations of unsteady phenomenon in vaneless diffusers", *ASME paper no.* 78-GT-23, 1978

Abdelhamid, A.N., "Analysis of rotating stall in vaneless diffusers of centrifugal compressors", *ASME paper no.* 80-GT-184.

Abdelhamid, A.N., "Effects of vaneless diffuser geometry on flow instability in centrifugal compressor systems", *ASME paper no.* 81-GT-18

Abdullah, S. and Henderson, R.E., "Improved approach to the streamline curvature method in turbomachinery", *ASME J. of Fl. Engg.,* Vol.109, Sept, 1987.

Adenubi, S.O., "Performance and flow regimes of annular diffusers with axial turbomachine discharge inlet conditions", Trans. *ASME, J. of Fl. Engg.,* June 1976.

Adler. D., "Status of centrifugal impeller aerodynamics", Pt-II, Trans ASME, *J. of Engg. for Power*, 1979.

Adler, D and Levy. Y. "A laser-Doppler investigation of the flow inside a back swept, closed centrifugal impeller," *J. Mech. Eng. Sci*, 21(1), 1979.

Ariga, I. *et al.*, "The effect of inlet distortion on the performance characteristics of a centrifugal compressor," *Trans., ASME, J. of Engg. for Power*, 1983.

Arnold, D.G. and Balje, O.E., "High temperature potential of uncooled radial turbines," *Trans. ASME*, 100(2), 294, April 1978.

Asanuma, T., "Review of flow visualization techniques in Japan," *Proc. Ist International symposium on flow visualization*, Tokyo, Oct. 1977

Atkins, M.J., "Secondary losses and end wall profile in a turbine cascade," *Proc. Instn. Mech. Engrs., Turbomachinery-efficiency prediction and improvement*, No. C/255/87, 1987

Balje, O.E, "A flow model for centrifugal compressor rotors," *Trans. ASME*, 100(1), 148, January 1978

Bammert, K. *et al.*, "Matching of turbo-components described by the example of impeller and diffuser in a centrifugal compressor," *Trans. ASME, J. Engg. for Power*, Vol.102, July 1980

Bammert, K. Jansen, M. and Rautenberg, M., "On the influence of the diffuser inlet shape on the performance of a centrifugal compressor stage," *ASME paper no*: 83-GT-9, 1983

Bannister, R.L. *et al.*, "Developing a direct coal fired combined cycle," *Mech. Engg.*, Dec. 1992

Becker, B. and Schetter, B., "Gas turbines above 150 MW for integrated coal gasification combined cycle (IGCC)," *Trans. ASME, J. of Engg. for Gas turbines and Power*, Vol. 114, Oct. 1992.

Bhinder, F. S., "Development and application of performance prediction method for straight rectangular diffusers," *Trans. ASME, J. Engg. Power*, Vol. 105, Jan. 1983.

Bindon, J.P. and Morphis, G., "The development of axial turbine leakage loss for two profiled tip geometries using linear cascade data," *Trans. ASME, J. of Turbomechinery*, Vol. 114, 1992

Binsley, R.L and Boynton, H.L., "Aerodynamic design and verification of a two-stage turbine with a supersonic first stage," *J. of Engg. for Power, Trans. ASME*, 100(2), 197, April 1978.

Blair, L.W. and Russo, C.J., "Compact diffusers for centrifugal compressor," *J. Aircr.*, Vol. 19. No.1, Jan.1982.

Bolton, A.N., "Pressure pulsation and rotating stall in centrifugal fans." *Proc. Instn. Mech. Engrs.*, C115/75, 1975.

Bolton, A.N. and Margetts, E.J., "The influence of impedence on fan sound power," *Proc. Inst. Mech. Engrs.*, C124/84, 1984.

Bosman, C., "Analytical theory of three-dimensional flow in centrifugal compressors," *J. Mech. Eng. Sci., I. Mech. Engrs.*, Vol. 23, No.4, 1981.

Boyce, M.P., "*Gas turbine hand book*," Gulf Publishing Company, Houston, Texas, 1982.

Brownell, R.B. *et al.*, "Flow visualization in a laboratory vaned diffuser," *Jr. of Heat and Fl. flow*, Vol. 8, No.1, March 1987.

Csendes, Z.J., "A Fortran programme to generate finite difference formulas," *Int. J. for Numerical Methods in Engg.*, Vol.9, 1975.

Cai, R., "A summary of developments of the mean streamline method in China, *Trans. ASME, J. Eng. for Power*, 1983 (ASME paper no 83-GT-11)

Casey, M.V., "A computational geometry for the blades and internal flow channels of centrifugal compressors," *ASME Transactions, J. Engg. for Power*, Vol.105, April 1983.

Casey, M.V. and Roth., "A streamline curvature through flow method of radial turbocompressors," *Proc. Computationl Methods in Turbomachinery, Instn. Mech. Engrs.*, London, C57/84, 1984.

Casey, M.V., "Effect of Reynolds number on the efficiency of centrifugal compressor stages," *ASME Jr. of Engg. for Gas turbine and Power*, Vol. 107, April 1985.

Colantioni, S. and Braembussch, R.V.D., "*Optimization of a transsonic and supersonic phenomenon in turbomechines*, Munchen, Sept. 1986.

Clements, W.W. and Artt.D.W., "The influence of diffuser channel geometry on the flow range and efficiencey of a centrifugal compressor," *Proc. Instn. Mech. Engrs.*, Vol. 201, No. A2, 1987.

Coladipeitro, R. *et al.*, "Effect of inlet flow conditions on the performance of equiangular annular diffusers," *Trans. Canadian Society of Mech. Engg.* Vol.3, No.2, 1975

Cassar, B.F.J. *et al.*, "Rotating stall in uniform and non-uniform flow," *Trans. ASME J. of Engg. for Power*, Vol. 102, 1980

Cory, T.W.T., "The effect of inlet conditions on the performance of a high specific speed centrifugal fan," *Proc. Instn. Mech. Engrs.*, C68/84, 1984

Daiguji, H., "A finite element method for analysing the 3-D flow in turbo machines," *Finite Element Flow Analysis*, Ed. Kawai, T, University of Tokyo Press, July 1982

Daiguji, H. "Finite element analysis for 3-D compressible potential flow in turbomechinery," *Proc. Int. Gas Turbine Congress*, Tokyo, 1983

Daiguji, H. "Numerical analysis of 3-D potential flow in centrifugal turbomachines," *Bulletin of the JSME*, Vol.26, No.219, Sept. 1983.

Dean, R.C. Jr., "The fluid dynamic design of advanced centrifugal compressors," Creare Inc. TN-244, July 1976.

Deconinck, H. and Hirsch Ch., "Finite element methods for transonic blade to blade calculation in turbomachines," ASME paper no. 81-GT-5

Denton, J.D., "A time marching method for two and three-dimensional blade to blade flows," *ARC, R and M No.* 3775, Oct.1974

Dovzhik, S.A. and Kartavenko, V.M., "Measurement of the efficiency of annular ducts and exhaust nozzles of axial turbomachines," *Fluid Mechanics-Soviet Research*, Vol.4, no.4, July-Aug. 1975

Duggins, R.K, "Research note: Conical diffusers with annular injection," *J.Mech. Engg. Sci.*, 1975

Dutton, J.C. *et al.*, "Flow field and performance measurements in a vaned radial diffuser," *ASME J. of Fl. Engg.*, Vol. 108, June 1986

Eckardt, D. "Detail flow investigation within a high speed centrifugal compressor impeller," *Trans. ASME J. Fl Engg.* Vol.98, 1976

Eckardt, D. "Jet-wake mixing in the diffuser entry region of a high-speed centrifugal compressor," *Proc. joint sym. on design and operation of fluid machinery*, Colorado State University, June 1978.

Eckardt, D. "Investigation of disturbed flow pattern within and at the dischrage from a highly loaded centrifugal compressor," Institute fiir Luftstrahlantriebe, Porz-Wahn, 1975

Eckardt, D. "Instantaneous measurements in the jet-wake discharge flow of centrifugal compressor impeller," *J. of Eng. for Power*, Trans. ASME, 97(3), 337, July 1975

Elder, R.L. and Gill, M.E., "A discussion on the factors affecting surge in centrifugal compressors," *Trans. ASME J. of Engg. for Gas Turbine and Power*, Vol. 107, 1985

Eckhardt, D. "Investigation of the jet-wake regime behind a highly loaded centrifugal compressor rotor," DFVLR research rep. DLR-FB 77-32 Koln, Germany, 1977

Elgammal, A.H. amd Elkersh, A.M., "A method for predicting annular diffuser performance with swirling inlet flow," *J. Mech. Eng. Sci., Instn. Mech. Engrs.* Vol. 23, No. 3, 1981.

Farokhi, S., "Analysis of tip clearance loss is axial; flow turbines," *J. of Propulsion*, Vol.4, 1988

Fisher, F.B. "Development of vaned diffuser compressor for heavy duty diesel engine turbo-charger," *I. Mech. Engrs.*, C-108/86, 1986

Fringe, P. and Van Den Braembussche, R., "Distinction between different types of impeller and diffuser rotating stall in a centrifugal compressor with vaneless diffuser," *Trans. ASME, J. of Gas Turbine and Power*, Vol.106, 1984.

Fowler, H. S., "The influence of blade profile and slots on the performance of a centrifugal impeller," *NRC Canada*, No. 18123 ME248, 1980

Fry, A.T., "On fan application of noise attenuations," *Proc. Instn. Mech. Engrs. C* 123/84, 1984

Furuya, Y. *et al.*, "On the characteristics of the two-dimensional diffusers with suction through parallel porous side walls," *Memoirs of the Faculty of Engg.*, Nagoya Univ., Vol-29. No.2, 1977

Fringe, P. and Braembussche, R.V.D., "A theoretical model for rotating stall in a vaneless diffuser of a centrifugal compressor," Paper no. 84-GT-204, *29th Int. Gas turbine conference and exhibition*, Amsterdam, June 1984.

Fletcher, C.A.J., "A comparison of finite element and finite difference solutions of the one and two-dimensional Burger' equations," *J. of Computational Physics*, Vol.51, No.1, July 1983

Fischer, E. H. and Inoue, M. "A study of diffuser-rotor interaction in a centrifugal compressor," *J. Mech. Engg. Sci.*, Vol. 23, No.3, 1981

Ginevskiy, A.S. *et al.*, "Aerodynamic performance of flat diffusers with no flow separation," *Fluid Mechanics-Soviet Research, Vol.4, No.3*, May/June 1975

Gogolev *et al.*, "Study of flow swirl influence on axi-radial diffuser effectiveness," *Soviet Aeronautics, Vol.19, No.*1, 1976

Gooble, S.M. *et al.*, "An experimental investigation of the effect of incidence on the two dimensional performance of an axial turbine cascade," ISABE-89-7019, 1989

Goulas, A. and Baker, R.C., "Flow in centrifugal compressor impellers: A hub-to-shroud solution," *J. Mech. Engg.. Sci.*- Vol.22, 1980

Govardhan, M., "Secondary flows and losses in an annular turbine cascade," Ph.D thesis, I.I.T. Madras, 1984

Govardhan, M. and Sastri, SRK., "Flow Studies through a linear turbine cascade with a large tip clearance," *Instn. Engrs. (India)*, 1998

Graham, J.A.H., "Investigation of a tip clearance cascade in a water analogy rig," *Trans. A.S.M.E., J. of Engg; for Gas turbine and Power*, Vol.108, 1986

Greitzer, E.M. and Griswold, H.R., "Compressor-diffuser interaction with circumferential flow distortion," *J. Mech. Engg. Sci*, Vol.18, no.1, 1976

Harada, H., "Performance characteristics of shrouded and unshrouded impellers of centrifugal compressor," *Trans. ASME, J. of Eng. for Gas Turbine and power*, Vol.107, 1985

Harrison, "Interction of tip clearance flows in a linear turbine cascade," *Trans. A.S.M.E., J. of Turbomachinery*, Vol.112, 1989

Harsha, P.T. and Glassman, H.N., "Analysis of turbulent unseperated flow in subsonic diffusers," *A.S.M.E. paper No.*76-FE-26 (Trans. ASME, J. Fl. Engg., June, 1976

Henssler, H.D. and Bhinder, F.S., "The influence of scaling on the performance of a small centrifugal compressor," *Proc. Instn. Mech. Engr.*, C186/77, 1977

Heyes, F.J.G. *et al.*, "The effect of blade tip geometry on the tip leakage flow in axial turbine cascade," *Trans. A.S.M.E., J. of Turbomachinery*, Vol.114, 1992

Hirayama, N., "Recent research on the flow though turbine blade rows," *Int. J. of JSME*, Vol.30, 1987

Hoffmann, J. A., "Effects of free-stream turbulence on diffuser performance," *Trans. ASME, J. Fl.* Eng. Sept. 1981

Horlock, J.H, "*Combined cycle plants*," Pergamon Press, 1992

Howard, J.H.G. and Kittner, C.W., "Measured passage velocities in a radial impeller with shrouded and unshrouded configurations,". *Trans. ASME J. of Eng. for power*, 1975

Imaichi, K. *et al.*, "A two-dimensional analysis of the interaction effect of radial impeller in volute casing," *Proc. IAHR Symposium*. Tokyo, 1980

Inoue, M. and Cumspty,. N.A., "Experimental study of centrifugal impeller discharge in vaneless and vaned diffusers," *ASME J. of Engg. for gas turbine and power*, Vol.106, April 1984

Iwanaga, K. *et al.*, "The construction of 700 MW units with advanced steam conditions" *Proc. Instn. Mech. Engrs.* Vol. 205, 1991

Japikse, D. and Pampreen, R, "Annular diffuser proformance for an automotive gas turbine," *Trans. ASME, J. Eng. for Power*, Vol.101, No.3, July 1979

Japikse, D., "A new diffuser mapping technique," Pt-1: Studies in component performance," *ASME J. of Fl. Engg.*, Vol.108 June 1986

Johnson, M.W. and Moore, J. "The influence of flow rate on the wake in a centrifugal impeller," *Trans. ASME J. of Eng.-for Power*, Vol. 105, 1983

Johnson, M.W. and Moore, J., "Secondary flow mixing losses in a centrifugal impeller," *Trans. ASME J. of Engg. for Power*, Vol.105, 1983

Jones, M.G., "The performance of a 6.5 pressure ratio centrifugal compressor having a radially-vaned impeller," *ARC report* C.P. No.1385, Sept. 1976

Juhasz, A.J., "Effect of wall edge suction on the performance of a short annular dump diffuser with exit passage flow resistance," *NASA* TM X-3221,

Juhasz, A.J. and Smith, J.M., "Performance characteristics of two annular dump diffusers using suction-stablized-vortex flow control," *NASA* TM-73857, 1978

Juhasz, A.J. and Smith, J.M., "Performance of high area-ratio annular dump diffuser using suction-stablized vortex flow control," *NASA* TM X-3535, 1977

Juhasz, A.J., "Effect of wall suction on performance of a short annular diffuser at inlet Mach numbers upto 0.5," *NASA* TM X-3302, Oct. 1975

Kamal, W.A. and Livesey, J.L., "Prediction of diffuser flow and performance following a normal wave-turbulent boundary layer interaction," *Proc. of Symposium on Turbulent Shear flows*," Univ. Park, Pennsylvania, April 1977.

Kamal, W.A. and Livesey, J.L., "Diffuser inlet flow structure following a shock-boundary layer interaction, Pt. I, *AIAA Journal*, 1979

Kamal, W.A. and Livesey, J.L., "The dependence of conical diffuser performance on inlet flow conditions Pt. II," *AIAA Journal,* 1979

Kachhara, N.L. *et al.*, "An initial approach to the design of very wide angle axisymmetric diffusers with gauzes to achieve uniform outlet velocity profiles," *Trans ASME, J. Fl Engg.* 1977

Kano, F *et al.*, "Aerodynamic performance of large centrifugal compressors," *ASME J. of Eng. for Power*, Vol. 104, Oct. 1982

Kawal, T. *et al.*, "Secondary flow control and loss reduction in a turbine cascade using end-wall fences," *Int. J. of JSME*, Vol.32, 1989

Kenny, D.P., "A novel correlation of centrifugal compressor performance for off-design prediction," *AIAA/SAE/ASME Fifteenth Joint Propulsion Conference*, paper no. 79-1159, Las Vegas, Navada, June 1979

Kikuyama *et al.*, "Flows and pressure recovery in a rotating diffuser," *Bull JSME*, Vol.26, Jan. 1983.

Klassen, H.A., "Effect of inducer inlet and diffuser throat area on performance of a low-pressure ratio swept back centrifugal compressor," *NASA* TMX-3148, Lewis Research Centre, Jan. 1975.

Klein, A., "Review: Effects of inlet conditions on conical-diffuser performance," *Trans. ASME, J. Fl. Engg.* Vol.103, June 1981

Kosuge, H. *et al.*, "A consideration concerning stall and surge limitations within centrifugal compressor," *Trans. ASME J. of Eng for Power*, Vol.104, 1982

Krain, H., "A study of centrifugal impeller and diffuser flow," *ASME J. of Eng. for Power*, Vol.103, Oct.1981

Kubo, T and Murata, S., "Unsteady flow phenomenon in centrifugal fans," *Bull. J.S.M.E.*, Vol.19, 1976

Laskaris, T.E., "Finite-element analysis for three-dimensional potential flow in turbomachines," *AIAA Journal*, Vol.16, no.7, July 1978

Linder, P., "Aerodynamic tests on centrifugal process compressors: Influence of diffuser diameter ratio, axial stage pitch and impeller cut back," *ASME J. of Eng. for Power*, Vol. 105, Oct. 1983

Livesey, J.L. *et al.*, "Compressible conical diffuser flow using the energy deficit boundary layer method," *J. Mech. Eng. Sci.*, No.4, 1975

Lohmann, R.P. *et al.*, "Swirling flow through annular diffusers with conical walls," *Trans. ASME, J. Fl. Engg.*, Vol.101, June 1979

Ludtke, K., "Aerodynamic tests on centrifugal process-compressors: The influence of vaneless diffuser shape," *ASME J. of Eng. for Power*, Vol.105, Oct. 1983.

Mashimo, T *et al.*, "Effects of Raynolds number on performance characteristics of a centrifugal compressor with special reference to configurations of impellers," *ASME J. of Eng. for Power*, Vol.97, July 1975

Mc Donald, P.W., "The computation of transonic flow through two-dimensional gas turbine cascade," *ASME paper* No. 71-GT-89

Metallikov, S.M. *et al.*, "Experimental investigation of diffusers of contrifugal compressors," *Teploenergetika*, 17(9), 68-70, 1970

Metallikov, S.M. *et al.*, "An investigation of radial diffusers with transonic velocity of the approach flow," *Teploenergetika*, 20(10), 64-70, 1973

Mishina, H. and Gyobu, I., "Performance investigation of large capacity centrifugal compressors," *ASME paper* No. 78-GT-3

Mizuki, S. *et al*, "A study on the flow mechanism within centrifugal impeller channels," *ASME conference on Gas Turbines and Product Show*, Texas, March, 1975

Mizuki, S. *et al.*, "Investigations concerning rotating stall and surge phenomenon within centrifugal compressor channels," *Trans. ASME, paper* No. 78-GT9, 1978

Moffat, R.J. "Contribution to the theory of single-sample uncertainty analysis," AFSOR-HTTM *conference on Complex Turbulent Flows Sept., 1981. Revised Report, Thermoscience Division*, Stanford Univ., Feb.1982

Moffat, R.J., "Using uncertainty analysis in the planning of an experiement," *Trans. ASME, J. of Fl. Eng. Vol.107*, June 1985

Nelson, C.D. *et al.*, "The disign and performance of axially symmetrical contoured wall diffusers employing suction boundary layer control," *Trans. ASME, J. of Engg. for Power*, 1975

Osborne, C. *et al.*, "Aerodynamic and mechnical design of an 8:1 pressure ratio centrifugal compressor," *Creare Inc.*, Hanover, April 1975

Osborne, C., "Turbocharger compressor design and development," *Creare* TN-263, July 1979

Parnpreen, R.C., "Small turbomachinery compressor and fan aerodynamics," J. of Eng. for Power, *Trans. ASME, Series A*, July 1973

Peacock, R.E., "*Turbomachinery tip-gas aerodynamics*," a review, ISABE-89, 7056, 1989

Philbert, M. and Fertin, G., "Schlieren systems for flow visualization in axial and radial flow compressors, *ASME J. of Eng. for Power*, Vol.97, April 1975

Povinelli, L.A., "Experimental and analytical investigation of axismmetric diffusers," *AIAA Journal*, Vol. 9, 1976

Raj, D. and Swin., W.B., "Measurement of mean flow velocity and velocity fluctuations at the exit of the FC centrifugal fan rotor," *Trans. ASME J. of Eng. for Power*, 1981

Rodgers, C., "Impeller stability as influenced by diffusion limitations," *ASME Gas turbine and Fl. Eng. conference*, March 1976

Rodgers, C. and Mnew, H. "Experiments with a model free rotating vaneless diffuser," *J. of Eng. for Power, Trans. ASME*, 97(2), 231, April 1975

Rodgers, C. "Static pressure recovery characteristics of some radial vaneless diffusers," *Canadian Aeronautics and Space Journal*, Vol.10, No.1, March 1984

Russo, C.J. and Blair, L.W., "Effects of size and Reynolds number on centrifugal diffuser performance," *ASME paper No.* 81-GT-8, 1981

Sapiro, L., "Effect of impeller extended shrouds on centrifugal compressor performance as a function of specific speed," *Trans. ASME J, of Eng. for Power*, Vol.105, 1983

Senoo, Y. and Ishida, M., "Behaviour of severely asymmetric flow in a vaneless diffuser," ASME J. of Eng. for Power, Vol.97, July 1975.

Senoo, Y and Nishi, M, "Decelerating rate parameter and algebraic prediction of turbulent boundary layer." *Trans. ASME, J. of Fl. Engg.*, June 1977

Senoo, Y. *et al.*, "Swirl flow in conical diffusers," *Bull. of JSMF*, Vol.21, No.151, June 1978.

Senoo, Y. *et al.*, "Low-solidity cascade diffusers for wide flow range centrifugal blowers," *Int. J. of Turbo and Jet Engines*, 3, 1986

Shallan, M.R.A. and Shabaka, I.M.M; "An experimental investigation of the swirling flow performance of an annular diffuser at low speed," *ASME paper* No.75-WA/FE-17, 1975

Shamim, M. *et al.*, "Comparison of performance of radial vaneless and vaned diffusers with diverging walls of area ratio 4.5," *J. of Thermal Eng., ISME*, Vol.2, No.2, 1981

Sharma, O.P. and Butler, T.L., "Predictions of end-wall losses and secondary flows in axial flow turbine cascades," *Trans. A.S.M.E. J. of Turbomachinery*, Vol.109, 1987.

Sherstyuk, A.N. and Sokolov, A.I., "*Meridional profiling of vaneless diffusers*," Thermal Engineering, 13(2), 1966

Sihaie, A.M.E and Nassar, M.H., "The effects of variation of diffuser design on the performance of centrifugal compressor," *Proc. of Int. Congress on Air Breathing Engines*, Paris, June 1983.

Simon, H. and Bulskamper, A. "On the evaluation of Reynolds number and relative surface roughness effects on centrifugal compressor performance based on systematic experimental investigations," *ASME J. of Eng. for Gas Turbines and Power*, Vol.106, April 1984

Smith, J.M. and Juhasz, A.J., "Performance of a short annular dump diffuser using suction-stablized vortices at inlet Mach. numbers to O.41," *NASA*, TP-1194, 1978

Steidel, R. and Weiss, H., "Performance test of a bladeless turbine for geothermal applications," Lawrence Livermore Laboratory, *UCID*-17068, March 1976.

Stevens, S.J. and Williams, G.J., "The influence of inlet conditions on the performance of annular diffusers," *Trans. ASME, J. of Fl. Engg.*, Vol. 102, Sept. 1980

Suzuki, S. and Ugai, Y., "Study on high specific speed airfoil fans," *Bull. JSME,* Vol. 20, 1977

Suzuki, S. *et al.*, "Noise characteristics in partial discharge of centrifugal fans," *Bull. JSME*, Vol. 21, 1978.

Teipel, I. and Wiedermann, A. "The influence of different geometries of a vaned diffuser on pressure distribution in the centrifugal compressor," *Int. J. of Turbojet* Engines, 2, 1985

Toyoma. K. *et al.*, "An experimental study of surge in centrifugal compressor," *ASME Gas turbine and Fluid Engg. conference*, March 1976

Tsurusaki, H. *et al.*, "A study on the rotating stall in vaneless diffusers of centrifugal fans: first report-Rotational speeds of stall cells, critical inlet flow angle," *JSME Int. Journal*, Vol.30, No. 260, 1987.

Utgikar, P.S. *et al.*, "Performance of a flat plate radial bladed rotor for producing swirl," *Proc. Twelfth National Conference on Fl. Mechs. and Fl. Power*, I.I.T, Delhi, Dec. 1983

Utgikar, P.S. *et al.*, "Effect of number of vanes on the performance of a diverging wall vaned radial diffuser," *Sixth ISME Conference*, Delhi, Jan. 1985

Utgikar, P.S., "Investigation on vaned radial diffusers with diverging walls," *Ph.D Thesis*, I.I.T, New Delhi, India, March 1985.

Utgikar, P.S. *et al.*, "Some studies on diverging wall varying aspect ratio vaned radial diffusers for centrifugal compressors," *Proc. 13th National Conf. on Fl. Mechanics and Fl. Power*, REC, Trichi, India, 1984.

Verdonk, G. "Theoretical and experimental investigation of the flow at the inlet of the vaned diffuser for a high pressure ratio centrifugal compressor," *V.K.I for Fluid Dynamics*, Tech. Note 125, March 1978

Verdonk, G. "Vaned diffuser inlet flow conditions for high pressure ratio centrifugal compressor," *ASME paper* No. 78-GR-50, 1978

Vijaya Raghavan, S.B. and Kavanagh, P., "Effect of free-stream turbulence, Reynolds number and incidence on axial turbine cascade performance," *A.S.M.E. paper* no. 88-GT-15, 1988

Walker, P.J. and Hesketh, J.A., "Design of low-reaction steam turbine blades," *Proc. Instn. Engrs.* Vol.213, Part C, 1998

Wallis, R.A., "Annular diffusers of radius ratio 0.5 for axial-flow fans," *CSIRO, Div. of Mech. Engg.* Tech. Rep. TR4, 1975

Welsh, M.C. *et al.*, "Straight walled annular diffusers for 0.5 boss-ratio flow fans," *Thermofluids Conference*, Hobart, Dec. 1976

Whitefield, A. and Bains, N.C., "*Design of Radail Turbomachines.*" Longman Scientific and Technical,

Wilkinson, D.H. "Calculation of blade-to-Blade flow in a turbomachine by streamline curvature method," *ARC, R and M No.* 3704, 1972

Wiesner, F.J., "A new appraisal of Reynolds number effects on centrifugal compressor performance," *ASME J. of Eng. for power*, Vol-101, July 1979

Wright, T. "Centrifugal fan performance with inlet clearances," *Trans. ASME J. of Engg. G.T and Power*, Vol. 106, 1984

Wright, T. *et al.*, "Centrifugal fan performance with distorted inflows," *Trans. ASME J. of Engg. G.T and Power*, Vol. 106, 1984

Wright, T. *et al.*, "Flow in centrifugal fan impeller at off-design conditions," *Trans. ASME J. of Engg. G.T and Power*, Vol. 106, 1984

Yamamoto, A and Nouse, H., "Effect of incidence on Three Dimensional flows in a linear turbine cascade," *Trans. A.S.M.E, J. of Turbomechinery*, Vol.110, 1989

Yang, T. and Nelson, C.D., "Griffith diffusers," *Trans. ASME, J. Fl. Eng.*, Vol. 101. Dec. 1979

Yaras, M.I. and Sjolander, S.A., "Prediction of Tip leakage losses in axial turbines," *Trans. ASME, J. of Turbomachinary*, Vol. 114, 1992

Ying Kang, Z. and Sjolander, S.A. "Effect of geometry on the performance of radial vaneless diffusers." *ASME paper* no. 87-GT-169, 1987

Yoshinaga, Y. *et al.*, "A study of performance improvement for high specific speed centrifugal compressors by using diffusers with half guide vanes," *ASME J. of Fl. Eng.* Vol.109, Dec. 1987

Yoshinaga, Y. *et al.*, "Aerodynamic performance of a centrifugal compressor with vaned diffuser," *ASME J. of Fl. Eng.* Vol.102, Dec. 1980

Yoshinaga, Y. *et al.*, "A study of aerodynamic performance of diffusers of centrifugal compressors," *Bulletin, JSME*, Vol.28, Aug. 1985

SOLAR POWER PLANTS

Bannister, P. and Mayer, I.F., "Development of solar thermal receiver studies for the white cliffs Solar Thermal Power Plants, Vol. 119 No.1, *ASME Jr.* of Solar Energy Engg, Feb. 1997.

Beale, William, T, "Solar powered engine for electric power generation," *Energy Information Dissemination Program*, Okhlahoma State University, Dec.17, 1980.

Bettleson, K. W. "Solar Power Tower design guide: solar thermal central receiver system, a source of electricity and/or process heat", *SAND* 81-2005, April, 1981, Sandia National laboratories, Livermore, California.

Burnger, A. and Hollands, K. "Back of plate heat transfer in unglazed perforated collectors operated under Non-uniform air flow conditions," Presented at *the 22nd Annual Conference of the Solar Energy Society of Canada, Inc.*, Ontario, Canada, June 1996.

Donald Rapp. "*Solar energy*". Prentice Hall, Inc. 1981.

Dymond, C.; Kutscher, C. "A Computer Design Model for Transpired Solar Collector System", Presented at the ASME International Solar Energy Conference. Also accepted for Publication in the journal of Solar, Engg. March 1995.

Dayan, M.; Beekman, W. and Klein, S. "Analysis of Serpentine collectors in low flow systems." *American Solar Energy Society*, 1998.

Gretz, J. *et al.*, "*Thermomechanical solar power plants*," D. Reidel Publishing Co. Dordrecht, Holland, 1985.

Karm, J, *et al.*, "The DIAPR: A High-Pressure, High-Temperature Solar Receiver" Vol.119, No. 1, *ASME, Jr. of solar energy Engg.* (Feb.1997).

Kleis S.J., Haoming Li, and J. Shi., "A gradient maintenance technique for seawater solar ponds" Vol. 119, Number 1 : *ASME Jr. of Solar Energy Engg.* (Feb.1997).

Kreider, J. F. and Krieth, F., "*Solar energy hand book.*" Mc Graw-Hill Book Company, 1981, New York.

Kreith, Frank and Kreider, Jan. F., "*Principles of solar engineering*," 1978, Hemisphere, Washington, D.C.

Kuo, S.C. *et al.*, "Parametric analysis of power conversion systems for central receiver power generation," *ASME paper* 78-WA/So 1-2, ASME Winter Meeting, San Francisco, California, Dec. 10-15, 1978.

Kutscher C. and, Christensen, C. and, Barker, G. "Unglazed transpired solar collector: An Analytical Model and test results." *Proceedings of the Biennial Congress of the International Solar Energy Society*, August 1991.

Kutscher, C. and, Christensen, C. and, Barker, B. "Unglazed transpired solar collectors: heat loss theory." *ASME Journal of Solar Energy Engineering*, Aug.1993.

Marion, W. and Willox, S. "Solar radiation data manual for flat-plate and concentrating Collectors." *NREL*/TP-463-5607. golden, Co: National Renewable Energy Laboratory, 252p., 1994.

Meaburn, A. and Hughes F.M. "Feedforward control of solar thermal power plants" Vol.119, No. 1: *ASME of Solar Energy Engg.* (Feb., 1997).

Muratova, T.M. and Teplykov, D.I., "Experimental SES-5 nonsteady state conditions of operation of the solar steam generator." Geliotekhnika, Vol.24, No.5, 1988.

Myers, John D., *Solar applications in industry and commerce* New Jersey: Prentice Hall, 1984.

Palz. W., "*Solar electricity*", Butterworth, 1978.

Powell, C.J. *et al.*, "Dynamic conversion of solar generated heat into electricity," *NASA* report CR-134724, 1974.

Proceedings, International Symposim CNRS/CEE Solar Power Systems, Marseilles, 1980.

Proceeding, *Ispra course solar thermal power generation*," Sept., 1979. Elsevier Sequola, S.A, Lausanne.

Segal, A. and Epstein, M., "Modeling of solar receiver for cracking of liquid petroleum gas" Vol. 119, No.1: *ASME J. of Solar Energy Engg.* (Feb. 1997).

Shi, J. *et al.*, "Gradient-zone erosion in seawater solar ponds" Vol.119, No.1: *ASME Jr. of Solar Energy Engg.* (Feb. 1997).

Solar Thermal Central Receiver Systems, Proceedings Held At Konstanz, F.R. Germany; June 23-27, *1986 International Workshop on Solar Thermal Central Receiver System:3:* Konstanz, F.R. Germany; 1986 Berlin: Springer-Verlag, 1986.

Sukhatme, S.P., Solar Energy: *Principles of thermal collection and storage, New Delhi*, McGraw-Hill, 1984.

Stine William B. and R.W. Harrigan, "*Solar energy fundamentals and design with computer applications*," A Wiley-Interscience Publication, John Wiley and Sons, 1985.

Winter, Francis DE (ed.,) *Solar collectors, energy storage and materials, London*: MIT Press, 1990.

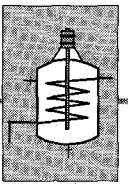

Index

TURBINES COMPRESSORS AND FANS

SECOND EDITION

Turbomachines, which comprise of turbines, compressors and fans are now being used in electric power generation, aircraft propulsion and a wide variety of medium and heavy industries. These important class of machines need a special emphasis in light of the future developments namely "2000 MW steam turbines" and "turbo-jet airlines" flying between major cities.

Turbines, compressors and fans is a self-contained treatise on the theory, design and applications of turbomachines. The book deals with the use of turbomachines in air handling, power generation, aircraft propulsion and several industrial applications. It covers the basic principle of working and theory of all kinds of turbomachines. In addition the book covers the fundamentals and discusses:

- The role of individual turbomachines in a plant
- Dimensional analysis and flow through cascades
- Fans, blowers, high-temperature turbine stages and wind turbines

The revised edition of this book includes chapters on:

- Combined Cycle Plants
- Solar Turbine Plants
- Also numerous solved examples, questions and problems have been added.

With this comprehensive coverage, the book would be of immense use to design and research engineers in the areas of aerospace, power plants, supercharged IC engines, industrial fans, blowers and compressors. It will also serve as a valuable reference for students of mechanical and aerospace engineering.

Prof S M YAHYA is Emeritus Fellow at the Indian Institute of Technology, Delhi. A Ph D from the University of Liverpool (England), he has been a visiting fellow at the Imperial College, London and the University of Cambridge.

Prof Yahya has vast teaching and research experience in turbomachinery and power plants. He has organised and coordinated several professional course programmes for post-graduate students and practising engineers. He has also designed and started Masters' Programmes in turbomachinery and power generation technology at IIT Delhi. Prior to the present assignment, Prof Yahya was professor and head of the Mechanical Engineering Department and NTPC-Chair Professor. He also served as Pro Vice-Chancellor of the Aligarh Muslim University for one year (1991-92).

He has supervised several Ph D and M Tech dissertations. Besides numerous publications in India and abroad, he has also authored four books—*Turbomachines (1972), Elementary Gas Dynamics (1973), Gas Tables (1978)* and *Fundamentals of Compressible Flow (1982).*

PHOTOGRAPHS:

Front Cover

- Compressor and gas turbine rotors under assembly at BHEL-Hyderabad, India — *Courtesy: BHEL, India*

Back Cover

- Double-flow L.P. turbine rotor at the Over-Speed Vacuum Balancing Tunnel—a unique facility at BHEL, Haridwar, India — *Courtesy: BHEL, India*
- 500 MW steam turbine-generator sets at 2000 MW Singrauli Super Thermal Power Station of NTPC—supplied and executed by BHEL, India — *Courtesy: NTPC & BHEL, India*

Visit us at www.tatamcgrawhill.com

ISBN 0-07-042039-4

9 780070 420397

Tata McGraw-Hill

A Division of The McGraw·Hill Companies

TURBINES COMPRESSORS AND FANS

SECOND EDITION

YAHYA

TATA McGRAW HILL